PROCEEDINGS
OF THE
WEDNESDAY SLIDE
CONFERENCE 2022-2023

JOINT PATHOLOGY CENTER
VETERINARY PATHOLOGY SERVICE
SILVER SPRING, MD 20910

This work reflects a collaborative effort by a team of professionals from around the world who believe in open access to education and the stewardship of veterinary pathology. This year, we transitioned to digital distribution of WSC cases, and this move is another step toward removing barriers to participation in the conference and the widest dissemination of results. On behalf of the Joint Pathology Center, I would like to extend immense gratitude to all the contributors who submitted cases to the 2022-2023 Wednesday Slide Conference and who remained flexible during our digital transition.

Throughout this conference year, the following veterinary pathologists lent their time and expertise by moderating for Wednesday Slide Conference: Corrie Brown, Erica Barkei, Jeremy Bearss, Kelsey Fiddes, Bruce Williams, Rob Kim, Francisco Uzal, Charles Bradley, Don Meuten, Joseph Anderson, Elise LaDouceur, Alicia Moreau, John Cullen, Sarah Cudd, Cory Brayton, Julianna Lee, Eric Lee, Kali Holder, Jo Lynne Raymond, Keith Koistinen, Daniel Finnegan, Patricia Pesavento, Jey Koehler, and Rachel Neto. Thank you all for making this year a success!

The Joint Pathology Center's military and civilian staff and residents make an undertaking like this possible. I would like to personally thank Dr. Bruce Williams for leading the WSC program and for his mentorship; Ms. Casey Wood for her excellent communication and attention to detail; Ms. Kenenya Gathers for accessioning and organizing cases; and Ms. Stacey Tamer providing special and immunohistochemical stain support.

Finally, I would like to thank my husband, Robin, and daughter, Zelda. I love you both and could not have completed this year without your support.

Sarah Sulkosky, DVM
2022-2023 WSC Coordinator

Case	JPC No.	Slide ID No.	Species	Tissue	Lesion/condition	Page
Conference 1 - August 17, 2022						
1	4120173	N-178/18	Sheep	Lung	Ovine progressive adenocarcinoma / Jaagsiekte Sheep Retrovirus	8
2	4156027	20202	Sheep	Esophagus	Esophageal myofiber degeneration / Bluetongue Virus	13
3	4165838	N-298/20	Ox	Lung	Caseonecrotic bronchopneumonia / *Mycoplasma bovis*	19
4	4101206	D15-048236	Ox	Esophagus	Necroulcerative esophagitis / Bovine viral diarrhea virus	27
Conference 2 - August 24, 2022						
1	4166941	P21-0286	Pig	Brain	Granulomatous encephalitis / *Mycobacterium avium hominissuis*	34
2	4117035	17-15645	Dog	Eye	Idiopathic necrotizing scleritis	38
3	4166546	672918	Dog	Spinal cord	Intravascular lymphoma and embolus	42
4	4140673	2019 NHP JPC Case 1	Rhesus macaque	Ileum	Intestinal adenocarcinoma	47
Conference 3 - August 31, 2022						
1	4168535	21N055	Mouse	Lung, liver, gall bladder	Acidophilic macrophage pneumonia, extramedullary hematopoiesis, and epithelial hyalinosis	53
2	4168471	21N045	Mouse	Heart, haired skin	Atherosclerosis, ulcerative dermatitis	57
3	4167359	D21-010259	Cat	Lung	Necrosuppurative and histiocytic pneumonia / *Neisseria* sp.	62
4	4170017	NP-20-0000570	Chicken	Small intestine, pancreas	Lymphoproliferative disease (Marek's Disease)	67
Conference 4 - September 14, 2022						
1	4066375	15041635	Alpaca	Lung	Granulomatous pneumonia / *Histoplasma capsulatum*	74
2	4163165	17934	Cat	Haired skin, liver	Cholangiocarcinoma and paraneoplastic alopecia	78
3	4169524	N-086-21	Hedgehog	Haired skin	Poxviral dermatitis	84
4	4168074	50607	Cat	Stomach	Verminous gastritis / *Ollulanis tricuspis*	89
Conference 5 - September 21, 2022						
1	4152800	D19-013690	Dog	Colon	Histiocytic ulcerative colitis	95
2	4135353	19V04893	Mink	Lung	Fibrinosuppurative bronchopneumonia / *Pseudomonas aeruginosa*	99
3	4101488	A	Ferret	Small intestine	Proliferative enteritis / *Lawsonia intracellularis*	104
4	4066917	XGL1315B	Dog	Lung	Pulmonary hyalinosis	110
Conference 6 - September 28, 2022						
1	4182279	22-432	Ox	Adrenal gland	Necrotizing adrenalitis / Bovine herpesvirus 1	114

Case	JPC No.	Slide ID No.	Species	Tissue	Lesion/condition	Page
2	4117379	18H9445	Dog	Cerebrum	GM1 gangliosidosis	119
3	4152966	469477	Cat	Brain	Pyogranulomatous encephalitis / Feline coronavirus (FIP)	126
4	4153144	19920 C33	Hedgehog	Oral and nasal cavities	Squamous cell carcinoma	133
Conference 7 - October 5, 2022						
1	4166549	20211	Ox	Abomasum	Necrotizing abomasitis / *Candida alibcans, Aspergillus* spp, Muocraceae, and bovine adenovirus-4	138
2	4068725	A15-10090	Goat	Liver	Necrosuppurative hepatitis / *Listeria monocytogenes*	144
3	4166548	20212	Ox	Liver	Hepatitis / *Salmonella enterica* subsp. *enterica* Dublin	148
4	4153531	P305-20	Ox	Ileum	Enteropathogenic *E. coli*	154
Conference 8 - October 12, 2022						
1	4168137	19B2865	Ox	Haired skin	X-linked hypohidrotic ectodermal dysplasia	161
2	4168023	N2021-78	Hedgehog	Haired skin	Disseminated trichophytosis	165
3	4166821	Case #2	Cat	Haired skin	Sebaceous adenitis	171
4	4117062	2016-1178(INIA 15-029)	Dog	Haired skin	Prototheca	175
Conference 9 - November 2, 2022						
1	4142167	HSRL-425	Dog	Lymph node	Metastatic urothelial cell carcinoma	182
2	4170046	3.201E+11	Dog	Thyroid	Hurthle cell carcinoma	187
3	4166125	2005 35	Dog	Bile duct	Carcinoid (neuroendocrine carcinoma)	192
4	4155465	19-015167	Dog	Adrenal gland	Pheochromocytoma	196
Conference 10 - November 9, 2022						
1	4154919	20-30209	Goat	Liver and lung	Necrotizing hepatitis and pneumonia / Caprine hepatitis virus 1	204
2	4160775	322057	Cat	Spinal cord	Necrotizing myelitis / *Toxoplasma gondii*	209
3	4179969	21V123-21	Rabbit	Uterus	Uterine venous aneurysm, cystic endometrial hyperplasia	212
4	4085020	CASE 2	Dog	Uterus	Eosinophilic endometritis and myometritis	216
Conference 11 - November 30, 2022						
1	4181856	74275	Octopus	Gill	Coccidiosis	225
2	4168081	C202370081	Crab	Apron, caparapce, limb, gill	Black spot shell disease	228
3	4085108	2	Tortoise	Liver	Necrotizing hepatitis / *Entamoeba* sp.	232

Case	JPC No.	Slide ID No.	Species	Tissue	Lesion/condition	Page
4	4183634	13310-A 10	Crawl cay boa	Intestine	Lymphoma	238
Conference 12 - December 7, 2022						
1	4179906	20-0135-87	Goat	Kidney	Chronic glomerulonephritis	245
2	4168028	19-44685	Dog	Kidney, lung	Renal amyloidosis and pulmonary mineralization	249
3	4181849	F22-54493	Ox	Kidney	Acute tubular necrosis / oak toxicosis	253
4	4165968	21V-257-1	Cat	Kidney	Polyarteritis nodosa	258
Conference 13 - December 14, 2022						
1	4154566	20-0424A	Goat	Liver	Acute hepatic necrosis / *Trema tomentosa* toxicity	263
2	4139466	86/866	Ox	Liver	Chronic hepatic degeneration / *Lantana camara* toxicity	267
3	4136403	19-004799	Dog	Liver	Biliary atresia	271
4	4167234	N21-34	Hamster	Liver	Polycystic liver disease	277
Conference 14 - 4 January 2023						
1	4182699	T7562/21	Cat	Lymph node	Hodgkins-like lymphoma	283
2	4169456	16610	Rabbit	Haired skin	Erythema multiforme	288
3	4153949	19-034733	Dog	Skeletal muscle	Muscular dystrophy	293
4	4181065	018829B	Dog	Vertebra	Multiple myeloma	300
Conference 15 - 11 January 2023						
1	4182586	21N140	Rat	Small and large intestine	Radiation induced gastrointestinal syndrome	306
2	4128010	18N095-2	Mouse	Liver	Microvascular dysplasia	313
3	4118170	18-1152	Rat	Kidney	Nephroblastoma	317
4	4167864	1235813-013	Rat	Kidney	Nephroblastematosis	322
Conference 16 - 18 January 2023						
1	4183636	22-H40121	Snow Leopard	Lung	Interstitial pneumonia / SARS-CoV2 with pyogranulomatous fungal pneumonia	327
2	4181139	D21-031185	Bobcat	Ileum, mesenteric lymph node	Necrotizing ileitis / *Francisella tularensis*	333
3	4154914	19-0278	Cat	Spleen	Histiocytic and neutrophilic splenitis / *Klebsiella pneumoniae*	339
4	4136501	18014E	African Green Monkey	Stomach	Gastrointestinal stromal tumor	342
Conference 17 - 25 January 2023						
1	4181858	N-002-21	Pig	Lung	Arteritis and interstitial pneumonia / Porcine circovirus-3	349
2	4118014	P1487-17	Dog	Lung	Bronchointerstitial pneumonia/ Canine distemper virus	354

Case	JPC No.	Slide ID No.	Species	Tissue	Lesion/condition	Page
3	4168075	50562	Dog	Brain	Lymphohistiocytic encephalitis / Canine distemper virus	359
4	4137574	N-061/19	Dog	Kidney	Granulomatous nephritis / *Mycobacterium tuberculosis*	369
Conference 18 - 1 February 2023						
1	4161431	HB6504	Goitered Gazelle	Lung	Necrotizing bronchopneumonia / Peste des petits ruminants	377
2	4182648	65530	Grant's Gazelle	Liver	Necrotizing hepatitis / *Chlamydia pecorum*	381
3	4182644	L21 5287 G	Bald Eagle	Lung, panceras, skeletal muscle	Systemic sarcocystosis	385
4	4117381	S-9111	Striped Hyena	Haired skin	Glomus tumor	390
Conference 19 - 8 February 2023						
1	4118021	15-081037	Dog	Lung, Aorta	Chemodectoma and pulmonary adenocarcinoma	396
2	4186709	X-18712-21	Rabbit	Eye	Uveitis / *Encephalitozoon cuniculi*	402
3	4166942	H21-0433	Cat	Eye	Melanoma	406
4	4182583	NC-21-1573	Dog	Lung	Alveolitis / *Pneumocystis*	410
Conference 20 - 15 February 2023						
1	4154916	H19-002678	Goat	Cerebrum	Enzootic ataxia	416
2	4085016	WSC-2016-2	Ox	Brain	Lead toxicity	420
3	4136394	18-1765	Rat	Brain	Neuronal necrosis due to status epilepticus	424
4	4167230	P2263-20	Dog	Brain	Vascular necrosis due to phenethylamine toxicosis	430
Conference 21 - 29 March 2023						
1	4136165	50237	Dog	Brain	Granular cell tumor	436
2	4182281	152370-21	Dog	Urinary bladder	Malakoplakia	441
3	4166996	18-001	Dog	Lymph node	Nodal plexiform vasculopathy	445
4	4087118	15-516	Dog	Lung	Congenital pulmonary airway malformation	450
Conference 22 - 12 April 2023						
1	4118307	04705	Ox	Oral mucosa	Malignant catarrhal fever / Ovine gammaherpesvirus 2	457
2	4152223	19-2277	Cat	Lung	Pulmonary endarteritis / *Dirofilaria immitis*	463
3	4167357	D19-042303B	Dog	Brain	Encephalitis / Canine Adenovirus 1	469
4	4182289	22-104	Mink	Lung	Interstitial pneumonia / Aleutian mink disease	474
Conference 23 - 19 April 2023						
1	4181059	2021901437	Dog	Eye	Orbital meningioma	480

Case	JPC No.	Slide ID No.	Species	Tissue	Lesion/condition	Page
2	4181067	128036	Cat	Spinal cord	Gemistocytic astrocytoma	484
3	4181847	S342/20	Cat	Spinal cord	Leptomeningeal oligodendrogliomatosis	489
4	4182862	N21-434/7	Dog	Cerebellum	Cerebellar granuloprival degeneration	496
Conference 24 - 26 April 2023						
1	4186714	220953721	Ox	Coxofemoral joint	Congenital *Ureaplasma* arthritis	502
2	4162085	V164/20	Dog	Joint capsule	Synovial myxoma	505
3	4152965	469361	Ox	Mandible	Ossifying fibroma	509
4	4184464	N-155-21	Pig	Maxilla	Fibrous osteodystrophy	514
Conference 25 -10 May 2023						
1	4084740	15C20652	Dog	Epididymis	Systemic reactive histiocytosis	523
2	4166820	S-00-2021-1	Cat	Lung	Pulmonary langerhans cell histiocytosis	527
3	4153752	WSC CASE1	Dog	Eye	Ocular osteosarcoma	532
4	4116582	281/10	Ox	Eye	*Besnoitia besnoiti*	536

Joint Pathology Center
Veterinary Pathology Services

WEDNESDAY SLIDE CONFERENCE 2022-2023

Conference #1 17 August 2022

CASE I:

Signalment:
6 year-old. Female. Roya Bilbilitana. Ovine (*Ovis orientalis aries*)

History:
The animal presented with respiratory distress to the clinical service for ruminants (*Servicio Clínico de Rumiantes* – SCRUM) of the University of Zaragoza. The animal came from a herd of 1300 sheep and seven of them presented the same clinical signs. At clinical examination, the animal showed tachypnea and abundant foamy fluid flowing from the nostrils.

Gross Pathology:
Prior to post-mortem examination, educational computed tomography (CT) scans were recorded of the thorax and evinced multiple nodules throughout the cranioventral area of the pulmonary parenchyma. At necropsy, the sheep was in poor body condition. Lungs presented a bilateral consolidation of the anterior lobes and the ventral area of the posterior ones. Lung weight was three times higher in comparison with a normal lung. There was abundant fluid in the trachea and bronchi.

Laboratory Results:
No laboratory findings reported.

Microscopic Description:
Lung. Expanding and substituting up to 70% of the pulmonary parenchyma there is a multilobulated, non-encapsulated, well-demarcated, moderately cellular and expansive neoplasm that compress adjacent airways and alveoli. Neoplastic cells form acini, tubuli and rare papillae, supported by a moderate amount of fibrovascular stroma that are multifocally expanded by dense mature collagen and fibrocytes (scirrhous reaction). Cells are polygonal to columnar, 10-15 µm; show distinct cell borders, occasional apical cilia, a moderate amount of finely granular eosinophilic cytoplasm, a round to oval 7-12 µm basally located nuclei with coarsely

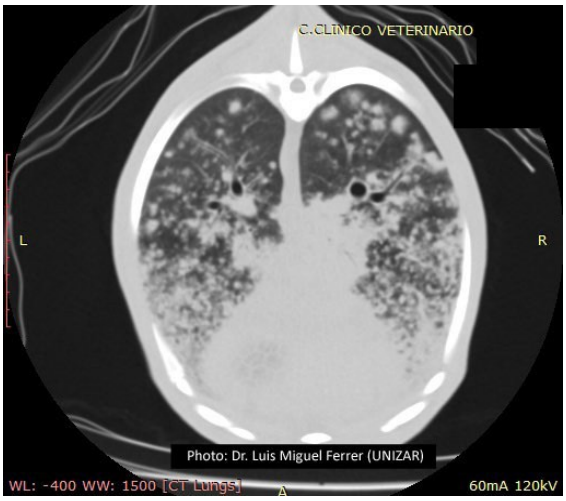

Figure 1-1. Lung, sheep. A CT scan of the anterior lung field demonstrates numerous coalescing nodular opacities. (Photo courtesy of: Universidad de Zaragoza Departamento de Pathologia Animal, https://patologiaanimal.unizar.es.)

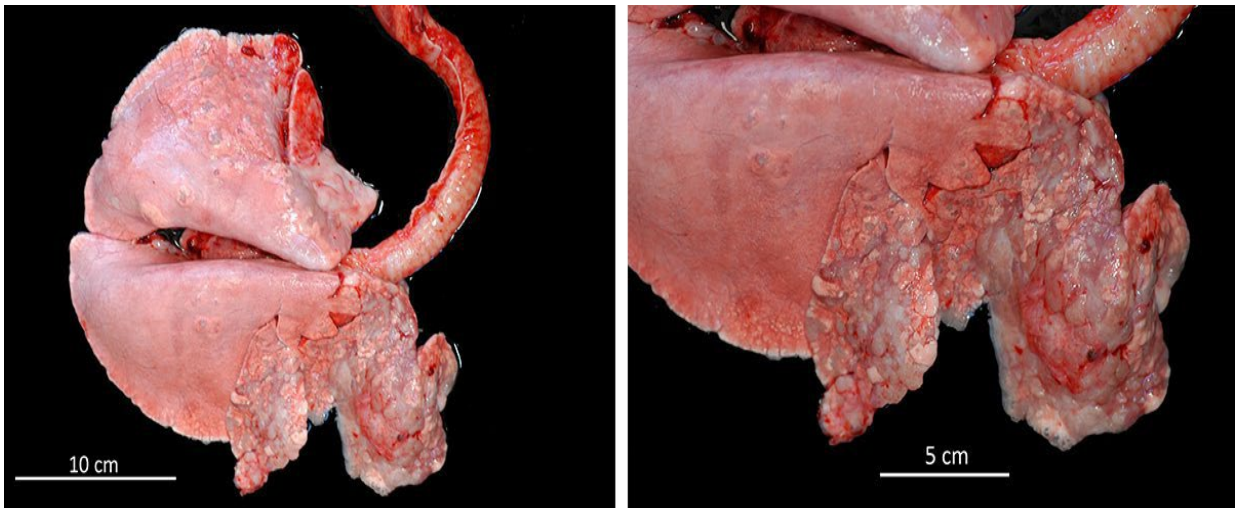

Figure 1-2. Lung, sheep. There is bilateral cranioventral lung lobe consolidation. (Photo courtesy of: Universidad de Zaragoza Departamento de Pathologia Animal, https://patologiaanimal.unizar.es.)

stippled chromatin and 1-2 visible nucleoli. There is moderate anisocytosis and anisokaryosis and less than one mitotic figure per 1 HPF (0.237 mm^2). Multifocally, within the peritumoral non-affected parenchyma, there are intra-alveolar sheets of foamy alveolar macrophages (alveolar histiocytosis). There are intra and peritumoral aggregates of lymphocytes, plasma cells and less histiocytes as well as dense aggregates of viable and degenerated neutrophils within some tumoral acini. There are multifocal areas of alveolar edema, emphysema and prominent peribronchial lymphoid follicles (BALT hyperplasia).

Contributor's Morphologic Diagnoses:
Lung. Adenocarcinoma

Condition: Ovine Pulmonary Adenocarcinoma / Jaagsiekte / Pulmonary adenomatosis

Cause: Ovine betaretrovirus

Contributor's Comment:
This is the classical form of the Ovine Pulmonary Adenocarcinoma (OPA), also called Sheep Pulmonary Adenomatosis (SPA). This contagious pulmonary tumor is caused by an exogenous betaretrovirus, Jaagsiekte sheep retrovirus (JSRV), that target respiratory epithelial cells, mainly bronchiolar club cells and alveolar type II pneumocytes.[8]

There are two forms of presentation of the tumor. Classical OPA usually affects cranioventral pulmonary lobes that become solid, grey or light purple and which bronchiole are filled by abundant alveolar fluid.[5] The tumor usually progress leading to respiratory embarrassment of the animal, that is evinced by dyspnea, tachypnea, exercise intolerance and, in severe cases, marked movement of the abdominal wall (abdominal lift). On the other hand, the Atypical OPA is compound of solitary or aggregated white hard nodules. There is no production of alveolar fluid and lesion do not progress so it usually remains subclinical and is a necropsy finding.

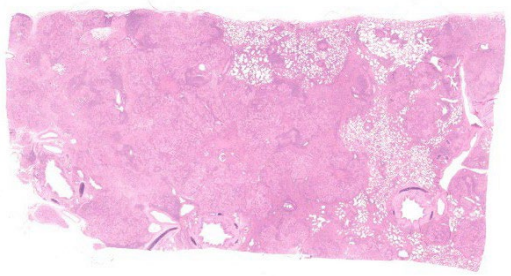

Figure 1-3. Lung, sheep. At subgross magnification, 90% of the section is effaced by coalescing neoplastic nodules. (HE, 7X)

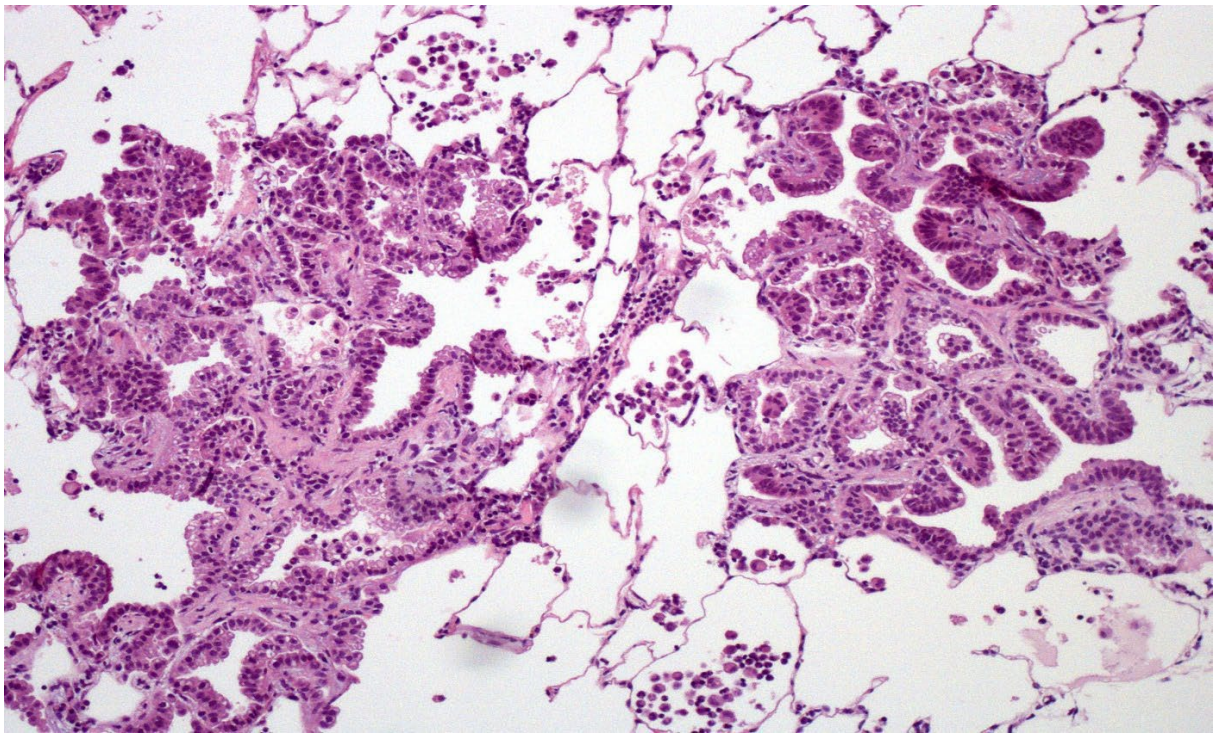

Figure 1-4. Lung, sheep. The lepidic form of growth, in which neoplastic cells extend outward along alveolar septa is best seen in less affected areas of the section. (Photo courtesy of: Universidad de Zaragoza Departamento de Pathologia Animal, https://patologiaanimal.unizar.es.) (HE, 100X)

Microscopically, both forms are characterized by a lepidic cell pattern that can become papillary or acinar in certain areas. Classical form is usually more invasive whereas atypical form is well demarcated and surrounded by prominent infiltrate of lymphocytes and plasma cells.[6,12] Metastasis to regional lymph nodes may occur in 10% of animals affected by the classical form but dissemination to other organs is extremely rare.

Pathogenesis of the tumor is not fully understood but envelope protein has been shown to induce tumor in mice.[8] The development of the classical or the atypical form seems to stem from the host immune response. Atypical forms contain more intratumoral CD4 and CD8 T-cell subsets as well as higher MHC Class II receptor expression in the tumor cells.[11] It has been thought that JSRV could be lined with the induction of human lung adenocarcinoma, however new studies discard this hypothesis.[6]

Transformed epithelial respiratory cells are the major sites for viral replication but JSRV can also be found in lung fluid and lymphoid tissues.[4] The virus is mainly transmitted by the respiratory route and close contact between animals plays a crucial role.[12]

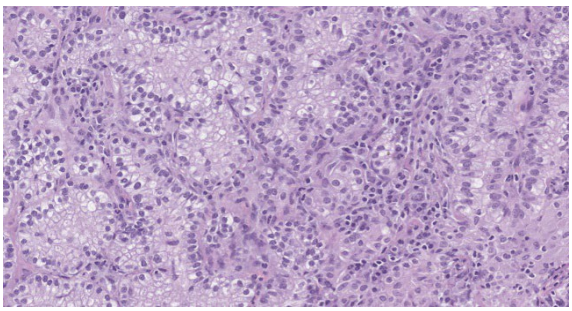

Figure 1-5. Lung, sheep. Most of the section is solidly cellular with alveoli lined by neoplastic columnar epithelium which fills the lumen and effaces normal alveolar architecture. (HE, 314X)

Retroviruses that Induce Tumors in Animals – Adapted from Fenner's Veterinary Virology.[10]		
Genus	**Species**	**Syndrome**
Alpharetrovirus	Avian leukosis virus	Leukosis (lymphoma, leukemia), nephroblastoma in fowl
	Rous sarcoma virus	Sarcoma in fowl
	Avian myeloblastosis virus	Myeloblastosis in fowl
Betaretrovirus	Mouse mammary tumor virus	Mammary carcinoma in fowl
	Mason-Pfizer monkey virus	Sarcoma and immunodeficiency disease in monkeys
	Ovine pulmonary adenocarcinoma virus (Jaagsiekte virus)	Pulmonary adenocarcinoma in sheep
	Enzootic nasal tumor virus	Enzootic nasal adenocarcinoma in sheep and goats
Gammaretrovirus	Feline leukemia virus	Leukemia in cats
	Feline sarcoma virus	Sarcoma in cats
	Murine leukemia and sarcoma viruses	Leukemia, lymphoma, and sarcoma in mice
Deltaretrovirus	Avian reticuloendotheliosis virus	Reticuloendotheliosis in fowl
	Bovine leukemia virus	Leukemia (B cell lymphoma) in cattle

Table 1-1

Perinatal transmission via colostrum and milk is also possible.[1] Most lambs become infected at very early age but only a minority (5-20%) develop OPA and they usually do between 2 and 4 years of age, evincing a long incubation period.[5] Resistance to infection increases with age due to the decrease of the proliferation rate of type II pneumocytes in adults.

The main differential diagnosis of the classic form of OPA is Maedi or ovine progressive pneumonia. This disease also presents as chronic progressive respiratory problems. However, there is no fluid production and the gross appearance is that of uncollapsed lungs and diffuse interstitial pneumonia. Gross appearance of classical OPA could be easily confused by chronic bronchopneumonia. Goats can also suffer from OPA but the incidence is lower.[8] The transmission of the tumor between both species is possible although rare. Cattle and other animals are resistant.

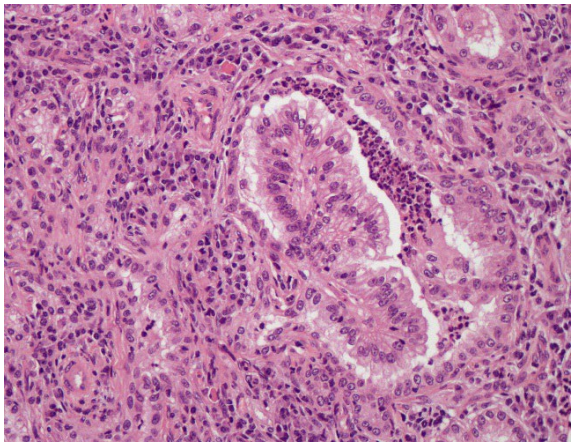

Figure 1-6. Lung, sheep. Occasionally, neoplastic epithelium extends outward into ectatic alveoli, forming papillary projections into the lumen, which is partially filled by a neutrophilic exudate. (Photo courtesy of: Universidad de Zaragoza Departamento de Pathologia Animal, https://patologiaanimal.unizar.es.) (HE, 400X)

Another betaretrovirus infection in sheep is Enzootic Nasal Tumor; however, both tumors are rarely seen in the same animal.

Contributing Institution:
Universidad de Zaragoza. Departamento de Patología Animal
https://patologiaanimal.unizar.es/

JPC Diagnosis:
Lung: Pulmonary adenocarcinoma.

JPC Comment:
The contributor provides an excellent overview of both the classical and atypical forms of ovine pulmonary adenocarcinoma.

Jaagsiekte is an Afrikaans term meaning "chase sickness", and refers to the exacerbation of clinical signs from the stresses and physical demands of herding.[9] The disease was originally described in South Africa in the 1800's and is now seen regularly in South America, Africa, Europe, Africa, and Asia.[2,9] The disease has not been documented in Australia.[2] In Iceland, a major outbreak in the 1930's affected up to 30% of the nation's sheep population and was eradicated by widespread culling and strict isolation measures.[6]

Antemortem diagnosis of OPA can be challenging. Sheep do not produce a humoral response to viral infection, so no serological tests are available. [8] PCR for pro-viral DNA in peripheral blood has low sensitivity for an individual animal (11%) but may be useful in monitoring at the flock level.[6,8] Bronchoalveolar lavage fluid is more sensitive for PCR testing, however it is an impractical test to employ in the field.[6] Thoracic ultrasound has also been described but has low sensitivity for lesions found deeper within the lungs and a high false positive rate. In a recent survey of sheep in the UK, only 24% of animals diagnosed with OPA via ultrasound were positive on histologic and IHC examination.[3]

As the contributor stated, the gross appearance of OPA can mimic that of chronic bronchopneumonia, and in one study of OPA in abattoirs in Ireland, there was a 89% false-positive rate for diagnosis of OPA based on gross lesions alone.[6] Histologic examination improves diagnostic rates, however confirmatory IHC or RT-PCR may be needed to rule out the less common non-JSRV associated pulmonary adenocarcinoma or to diagnose OPA masked by concurrent disease (i.e. bronchopneumonia).[6]

Table 1-1, adapted from Fenner's Veterinary Virology, summarizes the major retroviruses

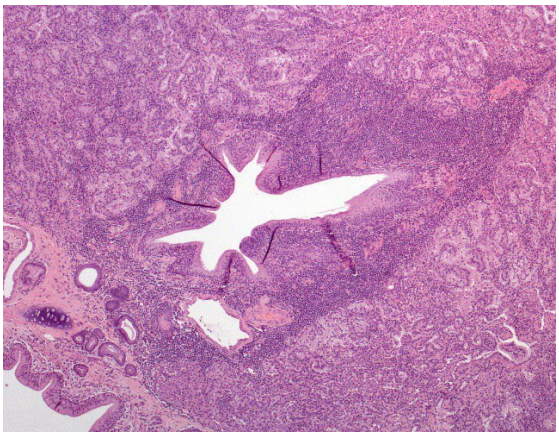

Figure 1-7. Lung, sheep. There is marked BALT hyperplasia. (Photo courtesy of: Universidad de Zaragoza Departamento de Pathologia Animal, https://patologia-animal.unizar.es.) (HE, 200X)

that induce neoplasia in animals. Both the enzootic nasal tumor retroviruses and JSRV are classified as a *trans*-activating retroviruses as neoplastic transformation stems from expression of the viral *env* gene, compared to *cis*-acting retroviruses that alter expression of the host proto-oncogenes. [10]

During the conference, the moderator, Dr. Corrie Brown from the University of Georgia, described clinical and pathologic features of the cases she has seen during her work overseas, including the wheelbarrow test. Lifting an affected animal's hindlimbs like a wheelbarrow will cause frothy fluid pour from the nostrils; this is secondary to agonal reflux of high-protein pulmonary edema. Dr. Brown also reminded conference participants of the impact this diagnosis can have on small farmers in low-income countries: if one animal is affected, the farmer will invariably lose more of their herd – and a significant portion of their livelihood.

References:

1. Borobia M, De Las Heras M, Ramos JJ, et al. Jaagsiekte Sheep Retrovirus Can Reach Peyer's Patches and Mesenteric

Lymph Nodes of Lambs Nursed by Infected Mothers. Vet Pathol.; 2016; 53(6):1172-1179.
2. Caswell JL, Williams KJ. The respiratory system. In: Maxie MG, ed. Jubb, Kennedy, and Palmer's Pathology of Domestic Animals. 6th ed. Vol 2. Philadelphia, PA: Elsevier Saunders; 2016: 559-562.
3. Davies P, Strugnell B, Waine K, et al. To scan or not to scan? Efficacy of transthoracic ultrasonography for ovine pulmonary adenocarcinoma screening in a large commercial UK sheep flock. Vet Rec. 2022; e1578.
4. De Las Heras M, De Martino A, Borobia M, et al. Solitary Tumours Associated with Jaagsiekte Retrovirus in Sheep are Heterogeneous and Contain Cells Expressing Markers Identifying Progenitor Cells in Lung Repair. J Comp Pathol; 2014; 150:138–147.
5. Griffiths DJ, Martineau HM, Cousens C. Pathology and Pathogenesis of Ovine Pulmonary Adenocarcinoma. J Comp Pathol. 2014; 142:260–283.
6. Lee AM, Wolfe A, Casside JP, et al. First confirmation by PCR of Jaagsiekte sheep retrovirus in Ireland and prevalence of ovine pulmonary adenocarcinoma in adult sheep at slaughter. Ir Vet J. 2017;70(33): 1-12.
7. Miller AD, De Las Heras M, Yu J, et al. Evidence against a role for jaagsiekte sheep retrovirus in human lung cancer. Retrovirology. 2017; 14:3
8. Monot M, Archer F, Gomes M, Mornex J-F, Leroux C. Advances in the study of transmissible respiratory tumours in small ruminants. Vet Microbiol. 2015; 181:170–177.
9. Murphy B. Chapter 14 – Retroviruses. In: MacLachlan NJ, Dubovi EJ eds. Fenner's Veterinary Virology. 5th ed. Boston, MA: Academic Press, 2017: 269-298.
10. Niewiesk S, Oglesbee M. Chapter 3 – Pathogenesis of Viral Infections and Diseases. In: MacLachlan NJ, Dubovi EJ eds. Fenner's Veterinary Virology. 5th ed. Boston, MA: Academic Press, 2017: 47 – 78.
11. Sharp JM, De Las Heras M. Contagious respiratory tumours. In: Aitken ID, editor. Diseases of Sheep. Fourth Edition. Oxford (UK): Blackwell Publishing; 2007. 211–217.
12. Summers C, Benito A, Ortin A, et al. The distribution of immune cells in the lungs of classical and atypical ovine pulmonary adenocarcinoma. Vet Immunol Immunopathol. 2012; 146:1–7.

CASE II:

Signalment:
32-month-old, female, cross- corriedale sheep (*Ovis aries*)

History:
This ewe showed depression, dysphagia, nasal discharge, coughing, and drooling. Two days prior to death, she developed a high fever, constant salivation and head drooping. There were no vesicular formation or ulcers in the oral cavity. Subsequently, the sheep died, and was autopsied in the next morning. No animals had been introduced on this farm for three years.

Gross Pathology:
The lung presented bilaterally dark red in color with a firm consistency and did not collapse after the thorax was opened. The respiratory tract was filled with yellowish-white foamy materials. The gastrointestinal tract was dark red in color throughout.

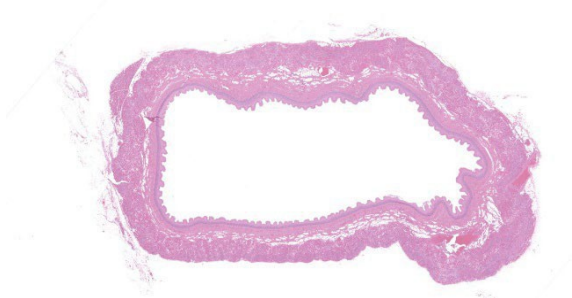

Figure 2-1. Esophagus, sheep. There is diffuse thinning of the esophageal muscle, and the section appears flaccid and partially collapsed. (HE, 8X)

Laboratory Results:
The gene of Bluetongue virus (serotype 21) was detected from the blood samples by reverse transcription-polymerase chain reaction (RT-PCR).

Any bacterial pathogens were not detected from major organs examined. Postmortem testing of hepatic selenium and Vitamin E concentrations reveal levels as adequate.

Microscopic Description:
Upper esophagus: The histologic lesion is mainly in the muscle layer as multifocal muscle fiber degeneration and necrosis, and the epithelial layer is intact. Degenerate and necrotic muscle fibers are fragmented with loss of cross striations, and hyalinized homogenous sarcoplasm. There is infiltration of prominent macrophages, a few lymphocytes and plasma cells between affected muscle fibers. The necrotic areas are replaced by a variable amount of collagens and fibroblasts. The regenerative change of myofibers characterized by a row of nuclei, centralized nuclei and basophilic cytoplasm frequently appears adjacent to affected region. Small blood vessels are occasionally lined by hypertrophied endothelial cells or disrupted endothelium with scattered pyknotic or karyorrhectic nuclei.

Contributor's Morphologic Diagnosis:
Esophagus: Multifocal myofiber degeneration and necrosis, moderate, with mild fibrosis and regeneration.

Contributor's Comment:
This slide presents a typical case of Bluetongue (BT) with muscle fiber degeneration and necrosis, and a vascular lesion. The muscle lesion also showed regenerative changes

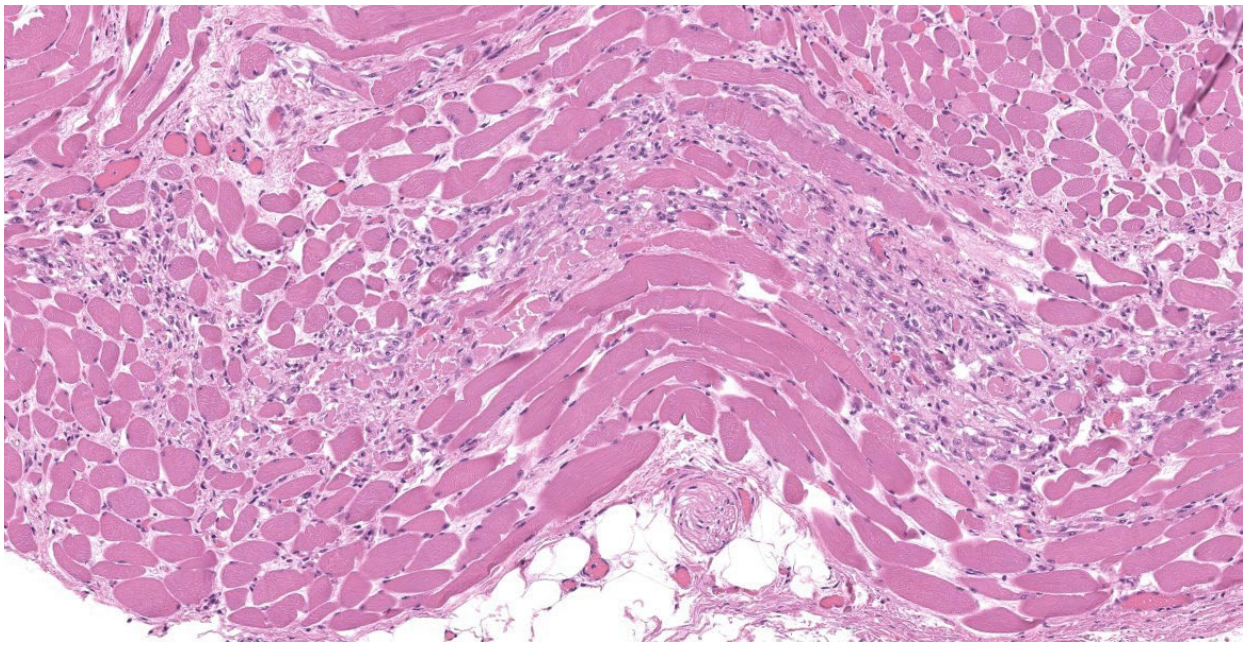

Figure 2-2. Esophagus, sheep. There are multifocal areas of myofiber degeneration and necrosis and replacement fibrosis. (HE, 314X)

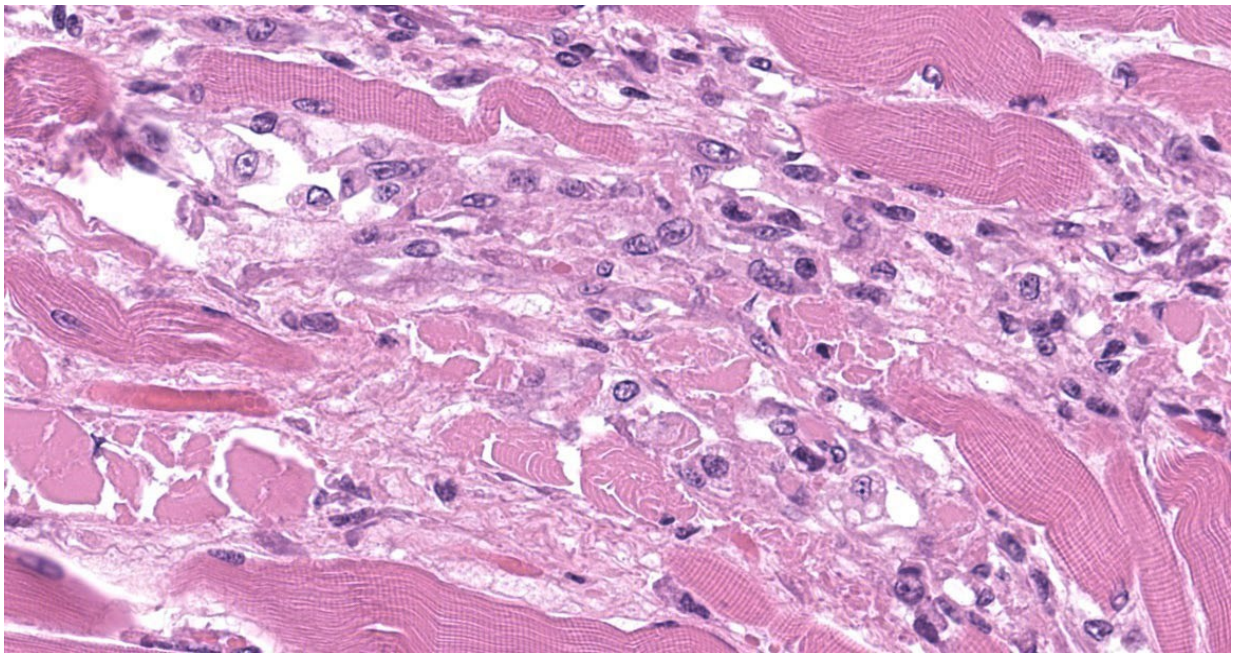

Figure 2-3. Esophagus, sheep. Higher magnification of an area of myofiber degeneration and necrosis with infiltration by macrophages and replacement fibrosis. (HE, 614X

including basophilic myoblasts, myotubes and fibrovascular response. These findings indicate that 1-2 weeks have elapsed since lesion formation. This is consistent with that the ewe died about a week after the onset of clinical symptoms.

BT is an infectious, non-contagious, vector-borne viral disease that affects wild and domestic ruminants.[14] The disease is caused by Bluetongue virus (BTV), family Reoviridae, the prototype virus for genus Orbivirus.[1] At least 27 or more distinct BTV serotypes were defined.[4,12] The virus is essentially transmitted by *Culicoides* biting midges among susceptible animals, however vertical transmission and horizontal transmission have also been reported. [2,13,16,21] BTV infection has been reported from worldwide including tropical, subtropical and some temperate regions, and the global distribution of the virus is consistent with the distribution of competent insect vectors and appropriate climatic conditions.[15]

Among domestic ruminants, clinical BT cases mainly occur in sheep. Clinical manifestations of the disease vary widely depending on the type and strain of infected virus, rearing factors and breed. Other species including cattle and goat are typically asymptomatic or subclinical, although specific BTV strains such as serotype 1 and 8, currently circulating in Europe, can induce severe disease in these animals. [5,10,23] BT in sheep causes severe hemorrhagic syndrome characterized by fever, edema, hemorrhages, dyspnea, mucosal erosions and ulcerations, muscle necrosis, and coronitis.[6,20]These symptoms are generally reflect viral kinetics.

After *Culicoides* insect bites, BTV first replicates in the regional lymph nodes, then it spreads to other organs including lung, lymph nodes and spleen. BTV demonstrates a tropism for a variety of cell types, including dendritic cells, mononuclear phagocytic cells, activated lymphocytes and endothelial cells. [9,11,22] The virus replication in endothelial cells directory induce degenerate, necrotic, and hyperplasic changes in the endo-

thelium, which result in increased of vascular permeability and causing edema, congestion, hemorrhage, thrombosis and necrosis. Additionally, the inflammatory and vasoactive mediators released by BTV infected cells have been proposed as responsible for worsening of endothelial dysfunction and vascular damage.[14]

Pulmonary lesions such as edema and hemorrhage are important change observed in almost all BT in sheep.[14] Greater susceptibility to BTV replication is reported in endothelial cells of respiratory micro-vesicular system.[7,8] Moreover, aspiration pneumonia is frequently observed as a result of aspiration of regurgitated food content followed by paralysis of the esophagus due to muscle necrosis induced by virus induced vascular damage.[3]

The differential diagnosis of BT in sheep should be done in conjunction with other diseases that cause edema, hemorrhage and epithelial damage.[3] The type of lesion and its distribution in affected animals can support development of BT diagnosis. The differential diagnosis includes foot-and-mouth disease, vesicular stomatitis, peste des petits ruminants, contagious ecthyma, sheep pox and photosentisation.[19,25] The initial lesion of BT is similar to foot-and-mouth disease. However, foot-and-mouth disease lesions are vesicular, whereas BT lesions are hemorrhagic and edematous. Vesicular stomatitis is also a disease that can be mistaken for BT. Since the lesion findings are similar to those of foot-and-mouth disease, the same criteria can be used to make a diagnosis. In the case of peste des petits ruminants, extensive gastrointestinal mucosal lesions are impressive, and may be concentrated in lymphoid tissues, such as Peyer's patches. In the case of contagious ecthyma and sheep pox, histopathology revealed proliferative lesion and intracytoplasmic inclusion body in epithelial layers. Photosensitization is also included in differential diagnosis. The absence of hemorrhage and erosions in the oral cavity, in addition to the generalized nature of the skin lesions, and their association with non-pigmented areas of the skin may be helpful for diagnosis. In addition, lesions such as myonecrosis in BT may mimic nutritional muscular dystrophy due to vitamin E and selenium deficiency. It is important that the clinical history and lesions be confined to the muscle for the differential diagnosis.

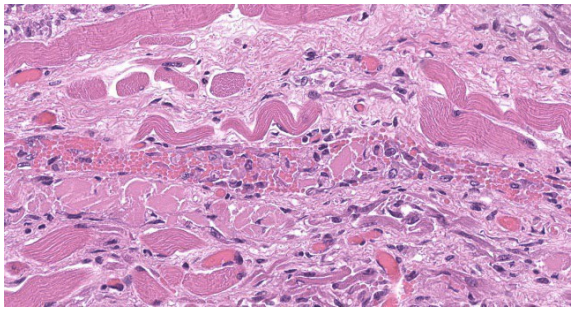

Figure 2-4. Esophagus, sheep. There is segmental loss of endothelium, multiple non-occlusive thrombi, and perivascular hemorrhage within rare vessels in the muscular layers. (HE, 670X)

Contributing Institution:
National Institute of Animal Health,
National Agriculture and Food Research Organization (NARO)
3-1-5 Kannondai, Tsukuba, Ibaraki 3050856, Japan

JPC Diagnosis:
Esophagus: Myocyte degeneration, necrosis, and regeneration, circumferential, multifocal to coalescing, moderate, with replacement fibrosis and multifocal vasculitis.

JPC Comment:
The contributor provides an excellent overview of the pathogenesis, clinical signs, and differential diagnoses for bluetongue virus (BTV) infections.

While phylodynamic models estimate that BTV has been circulating in ruminants for over a millennium, the first documented

cases occurred in South Africa in the nineteenth century, and in 1902, the term malarial catarrhal fever was used to describe the disease. Once a viral etiology was uncovered in 1905, the disease became known by its current and similarly descriptive name, which denotes the cyanosis most visible on the swollen tongue. The disease slowly spread through tropical climates during the first half of the twentieth century, and has now also been reported in Australia, the Americas, Asia, and Europe with serious economic consequences.[4] Ongoing geographic spread of this arbovirus can be partially attributed to changing environmental conditions and subsequent expansion of the *Culicoides* vector habitat.[17,18]

BTV is a segmented dsRNA virus that encodes seven structural (VP 1-7) and five nonstructural (NS 1-4) proteins.[17] VP7 is the most conserved protein and the basis for most seroconversion assays.[18] As the contributor describes, there are at least 27 serotypes of BTV, and this diversity is due to high variability of VP2, segment re-assortment during infection with multiple strains, and genetic drift.[17,18] There is little cross-protection between serotypes.[18] Recently, several atypical serotypes of BTV have been identified which are associated with asymptomatic to mild infections in small ruminants only and at least one of these serotypes (BTV-25) is associated with persistent infection.[18]

After initial infection, the BTV causes a biphasic viremia, with the initial spike in viral replication reduced by an interferon response.[18] BTV affects multiple lymphoid populations early during viremia, producing transient immunosuppression and increased susceptibility to secondary infections.[18] During the second and third week, adaptive immune responses begin effectively controlling infection with expansion of CD8+ T-cells and CD21+ B cells inducing seroconversion against VP7. In some cases, the virus may persist by evading these adaptive immune responses. BTV can disrupt the function of follicular dendritic cells, delaying antibody production by B cells and decreasing T cell responsiveness through unknown mechanisms.[18] Ongoing research into BTV dynamics and immune evasion will be critical in understanding and controlling this important disease.

Conference participants discussed esophageal hyperkeratosis and potential causes in this case. Orthokeratotic hyperkeratosis in the esophagus can occur in an anorectic animal as keratinized squamous epithelial cells are not removed by passing ingesta.[24] Alternatively, parakeratotic hyperkeratosis may occur with reactive epithelial hyperplasia from epithelial injury.[24]

References:

1. Attoui H, Maan S, Anthony SJ, Mertens PPC. Bluetongue virus, other orbiviruses and other reoviruses: Their relationships and taxonomy. In: *Bluetongue*. 1st ed. London, UK: Academic Press; 2009:23–52.
2. Backx A, Heutink R, van Rooij E, van Rijn P. Transplacental and oral transmission of wild-type bluetongue virus serotype 8 in cattle after experimental infection. *Vet Microbiol*. 2009;138:235–243.
3. Bianchi RM, Panziera W, Faccin TC, et al. Clinical, pathological and epidemiological aspects of outbreaks of bluetongue disease in sheep in the central region of Rio Grande do Sul. *Pesqui Vet Bras*. 2017;37:1443–1452.
4. Bumbarov V, Golender N, Jenckel M, et al. Characterization of bluetongue virus serotype 28. *Transbound Emerg Dis*. 2020;67:171–182.
5. Dal Pozzo F, De Clercq K, Guyot H, et al. Experimental reproduction of bluetongue virus serotype 8 clinical disease

in calves. *Vet Microbiol*. 2009;136:352–358.
6. Darpel KE, Batten CA, Veronesi E, et al. Clinical signs and pathology shown by British sheep and cattle infected with bluetongue virus serotype 8 derived from the 2006 outbreak in northern Europe. *Vet Rec*. 2007;161:253–261.
7. DeMaula CD, Jutila MA, Wilson DW, MacLachlan NJ. Infection kinetics, prostacyclin release and cytokine-mediated modulation of the mechanism of cell death during bluetongue virus infection of cultured ovine and bovine pulmonary artery and lung microvascular endothelial cells. *J Gen Virol*. 2001;82:787–794.
8. DeMaula CD, Leutenegger CM, Jutila MA, MacLachlan NJ. Bluetongue virus-induced activation of primary bovine lung microvascular endothelial cells. *Vet Immunol Immunopathol*. 2002;86:147–157.
9. Drew CP, Heller MC, Mayo C, Watson JL, MacLachlan NJ. Bluetongue virus infection activates bovine monocyte-derived macrophages and pulmonary artery endothelial cells. *Vet Immunol Immunopathol*. 2010;136:292–296.
10. Fabiana DP, Claude S, Etienne T. Bovine infection with bluetongue virus with special emphasis on European serotype 8. *Vet J*. 2009;182:142–151.
11. Hemati B, Contreras V, Urien C, et al. Bluetongue Virus Targets Conventional Dendritic Cells in Skin Lymph. *J Virol*. 2009;83:8789–8799.
12. Jenckel M, Emmanuel B, Schulz C, et al. Complete coding genome sequence of putative novel bluetongue virus serotype 27. *Genome Announc*. 2015;3(2):e00016-15.
13. Koenraadt CJM, Balenghien T, Carpenter S, et al. Bluetongue, Schmallenberg - what is next? Culicoides-borne viral diseases in the 21st century. Vol. 10, *BMC Vet Res*. 2014;10:77.
14. Maclachlan NJ, Drew CP, Darpel KE, Worwa G. The Pathology and Pathogenesis of Bluetongue. *J Comp Pathol*. 2009;141:1–16.
15. Maclachlan NJ, Mayo CE, Daniels PW, Savini G, Zientara S, Gibbs EPJ. Bluetongue. *OIE Rev Sci Tech*. 2015;34:329–340.
16. Menzies FD, McCullough SJ, McKeown IM, et al. Evidence for transplacental and contact transmission of bluetongue virus in cattle. *Vet Rec*. 2008;163:203–209.
17. Rivera NA, Varga C, Ruder MG, et al. Bluetongue and Epizootic Hemorrhagic Disease in the United States of America at the Wildlife-Livestock Interface. *Pathogens*. 2021;10: 1-21.
18. Rodriguez-Martin D, Louloudes-Lazaro A, Avia M, Martin V, Rojas JM, Sevilla N. The Interplay between Bluetongue Virus Infections and Adaptive Immunity. *Viruses*. 2021;13: 1-17.
19. Rojas JM, Rodríguez-Martín D, Martín V, Sevilla N. Diagnosing bluetongue virus in domestic ruminants: current perspectives. *Vet Med Res Reports*. 2019;10:17–27.
20. Schulz C, Sailleau C, Bréard E, et al. Experimental infection of sheep, goats and cattle with a bluetongue virus serotype 4 field strain from Bulgaria, 2014. *Transbound Emerg Dis*. 2018;65:e243–e250.
21. Sluijs MTW van der, Schroer-Joosten DPH, Fid-Fourkour A, et al. Transplacental transmission of bluetongue virus serotype 1 and serotype 8 in sheep: *Virological and pathological findings*. PLoS One. 2013; 8(12): e81429.
22. Stott JL, Blanchard-Channell M, Scibienski RJ, Stott ML. Interaction of bluetongue virus with bovine lymphocytes. *J Gen Virol*. 1990;71:363–368.

23. Toussaint JF, Vandenbussche F, Mast J, et al. Bluetongue in northern Europe. *Vet Rec*. 2006;159:327.
24. Uzal FA, Plattner BL, Hostetter JM. Alimentary System. In: Maxie GM, ed. Vol. 2, *Jubb, Kennedy, and Palmer's pathology of domestic animals*. St. Louis, Missouri: Elsevier, Inc; 2016:31.
25. Williamson S, Woodger N, Darpel K. Differential diagnosis of bluetongue in cattle and sheep. *In Pract*. 2008;30:242–251.

CASE III:

Signalment:
10-month-old calf, female, Limousine, Bovine (*Bos taurus taurus).*

History:
A flock of 70 calves enters the feedlot at the beginning of August 2020. Soon after, these animals began to suffer severe problems (such as conjunctivitis, dyspnea and sudden deaths) that lasts until November. Before death, the animal suffered severe dyspnea for a week.

Gross Pathology:
Lung: cranioventral to caudal chronic, severe, pulmonary consolidation with multifocal to coalescing, well-demarcated and variably sized pale yellow and slightly raised nodules (caseonecrotic bronchopneumonia). On cut, these lesions with caseous material extend through parenchyma and appear within distended airways, such in small bronchioles and alveoli, accompanied by areas of hemorrhage. Along the dorsal aspect of the lung, there was a severe emphysematous distension and thickening of lobular septae (interstitial emphysema). On cut surfaces, these septae appeared thickened and edematous with small gas bubbles admixed.

Laboratory Results:
PCR positive for *Mycoplasma bovis*.

See Table 3-1

Microscopic Description:
Lung: a lesion of inflammatory origin is diffusely obliterating respiratory spaces throughout the whole section of the lung, with extensive multifocally necrotizing coalescing foci centered mainly in bronchioles and alveoli. These foci are composed by an eosinophilic material with a mild admixed cellular debris delimited by a variable number of devitalized leukocytes that maintain cellular figures (ghost-like remnants of leukocytes) and a small number of active macrophages with scattered lymphocytes and some fibroblasts (caseonecrotic centers). Other bronchioles and alveoli are obliterated by high number of viable neutrophils (initial lesions). Sometimes they have multifocal mineralized areas and have multiple distributed clusters of basophilic cocci to coccobacilli bacterial colonies mainly at the periphery, but also ad mixed with the caseonecrotic debris. Occasionally, there are also inside, foreign bodies most compatible with inhaled vegetable structures or hair.

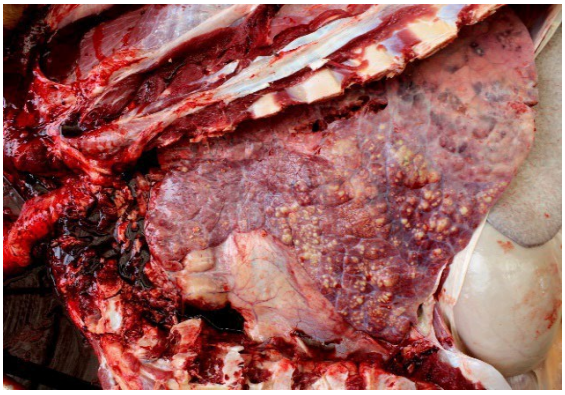

Figure 3-1. Lung, ox. There is marked consolidation and scattered caseonecrotic nodules within all but caudal lung fields. (Photo courtesy of: Universidad de Zaragoza. Departamento de Patología Animal Web: https://patologiaanimal.unizar.es)

Sometimes, these exogenous particles contain bacterial colonies or are mineralized. There are small, scattered foci with leukocytes with streaming hyperchromatic to smudgy nuclei fill the alveoli (oat cells) with fibrin, edema and necrotic karyorrhectic debris with no centers of caseous necrosis. Main bronchi epithelium is hyperplasic with some degenerative changes, individual apoptotic cells and mild submucosal lymphoplasmacytic infiltrate and reactive BALT. In the rest of pulmonary parenchyma alveolar septa are thickened by a marked hyperplasia of pneumocytes type II, macrophages, neutrophils, red blood cells and some fibrin thrombi. Alveolar spaces have areas containing eosinophilic and fibrillar agglomerated substance (polymerized fibrin) and unsettled areas of homogenous eosinophilic clear fluid (edema). Others have severely number of macrophages sometimes phagocytizing fibrin and occasional multinucleated cell of 2-7 nuclei. Some arterioles and small arteries within the parenchymal tissue have extended walls with muscular layer hypertrophy and fibrin deposition. Other major arteries present intraluminal thrombi and some mononuclear inflammatory cells. Pleura and pulmonary septa around main arteries are distended by

SAMPLE	TEST	AGENT	RESULT
Fresh lung	Culture and mass spectrometry technology (MALDI-TOF)	*Mannheimia haemolytica*	Positive ++
Fresh lung	Culture and mass spectrometry technology (MALDI-TOF)	*Trueperella pyogenes*	Positive +++
Fresh lung	Culture and mass spectrometry technology (MALDI-TOF)	*Escherichia coli*	Positive +++
Pool of 2 samples of fresh lung	Real time PCR	*Pestivirus*	Positive
Pool of 2 samples of fresh lung	Real time PCR	*IBR*	Positive
Pool of 2 samples of fresh lung	Real time PCR	*Parainfluenza 3*	Positive
Pool of 2 samples of fresh lung	Real time PCR	*BRSV*	Negative
Pool of 2 samples of fresh lung	Real time PCR	*Bovine coronavirus*	Negative
Pool of 2 samples of fresh lung	**Real time PCR**	***Mycoplasma bovis***	**Positive**
Pool of 2 samples of fresh lung	Real time PCR	*Pasteurella multocida*	Positive
Pool of 2 samples of fresh lung	Real time PCR	*Mannheimia haemolytica*	Positive
Pool of 2 samples of fresh lung	Real time PCR	*Histophilus somni*	Negative
Pool of 2 samples of fresh lung	Real time PCR	*Birbestenia trehalosi*	Negative

Table 3-1

edema and some mononuclear cells that also distend some lymphatic vessels.

Contributor's Morphologic Diagnoses:
Lung: Severe chronic multifocal to coalescing caseonecrotic and necrotic bronchopneumonia with intralesional colonies of bacterial cocci.

Lung: Diffuse interstitial pneumonia with pneumocytes type II hyperplasia, fibrin and interlobular edema.

Contributor's Comment:
Mycoplasmas were discovered for the first time by the team of Pasteur, Nocard and Roux in 1898, when the first report of mycoplasmosis was released [35]. This mycoplasma was isolated from a cattle and was compatible with the current *Mycoplasma mycoides* subsp *mycoides* (formerly known as *M. mycoides* subsp. *mycoides* ¨small colony¨). At that time mycoplasma organisms were known as *pleuropneumonia like-organisms (PPLO)* for being the causative agent of contagious bovine pleuropneumonia (CBPP) [33,35]. Nowadays these microbes belong to the genus *Mycoplasma spp.* and the class Mollicutes, which

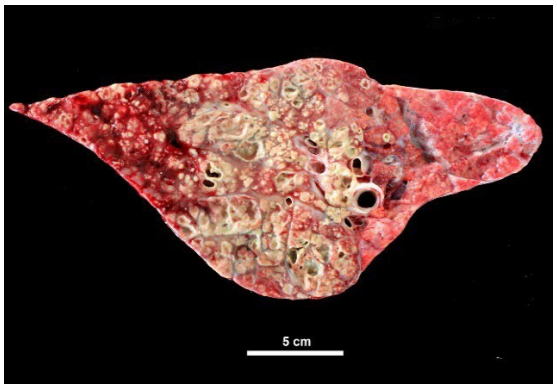

Figure 3-2. Lung, ox. On cut section, there is consolidation (left), áreas of caseating and cavitating necrosis (center), and some partially aerated, less affected lung (right). (Photo courtesy of: Universidad de Zaragoza. Departamento de Patología Animal
Web: https://patologiaanimal.unizar.es)

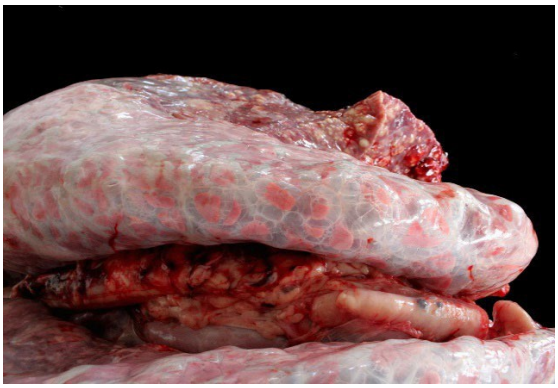

Figure 3-3. Lung, ox. On gross inspection of caudal lung lobes, there is marked interlobular emphysema. (Photo courtesy of: Universidad de Zaragoza. Departamento de Patología Animal
Web: https://patologiaanimal.unizar.es)

differ from other bacteria by their small genomes (580-2220 Kb) and no cell wall [44]. Mycoplasmas are highly contagious organisms and their virulent spread throughout Europe and the world during middle 19th century by cattle trade is well documented. The infection was controlled by "stamping out" policies, persisting in African countries during 20th century [14,36].

Currently *Mycoplasma bovis* is one of the major causative agents of bovine mycoplasmosis [7,8] and is also consider a major player in bovine respiratory disease complex (BRD) [3]. It was first isolated in 1961 in the United States [13], since then, has been turned to be the one of the more pathogenic species of the genus *Mycoplasma* [9]. This has not been enough to implement restrictions on cattle movement related to *M. bovis* [37]. *M. bovis* has a well-known economic, productivity, welfare and health impact in dairy and beef cattle worldwide [32], particularly on the North America and more recently in continental Europe [1]. This impact is due to the frequent chronicity of the infection [10,12,32], the increasingly unresponsiveness to most treatments due to antibiotic resistance and this chronicity [28,31] and the variety of clinical manifestations includ-

ing most commonly bronchopneumonia[2,8,11,16,18,19,42], otitis media[16,27], mastitis[1,6,8,15,20,32,36,43] and arthritis/tenosynovitis[19,42]. Other less consistent manifestations include urogenital disorders (metritis, abortion, infertility, endometritis, salpingitis, reduction of conception rate, seminal vesiculitis, epididymitis and orchitis in bulls) [6,11,23], meningitis[4], keratoconjunctivitis [2,29], decubital abscesses [26] and endocarditis[25].

The incubation period is difficult to define because it varies with the age and these clinical and pathological effects [9]. The clinical expression of these manifestations is highly variable and there are individuals without clinical symptoms in which the organism is isolated from the upper respiratory tract (URT). Thus, the presence *M. bovis* not always result in disease [21,32,43]. As "Trojan horses", these asymptomatic individuals are the leading cause of introduction of *M. bovis* into disease-free herds and the maintenance of infection. These animals can shed the bacteria intermittently from a few months to several months or even years [11,32]. Probably, this particular case and the flock were naïve at the moment of entry to the chronic infected feedlot. In fact, stressors related to immunosuppression such as transportation, entry of a new animal, overcrowding and weaning increase the shedding of the bacteria [9,12,32,37].

The mammary gland and the mucosa of the upper respiratory tract (URT) have been

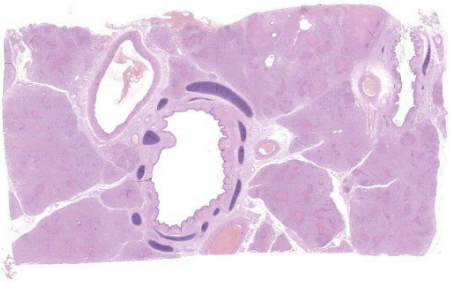

Figure 3-4. Lung, ox. There is diffuse consolidation of the entire section with loss of normal architecture. (HE, 5X).

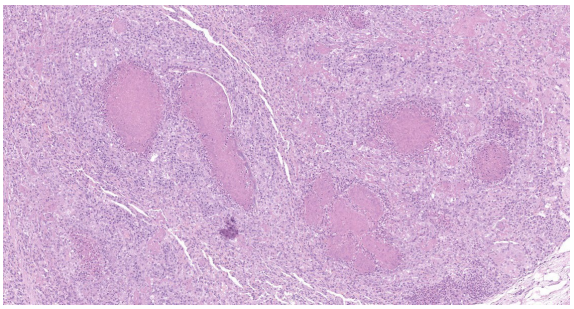

Figure 3-5. Lung, ox. Airways are filled and effaced by abundant brightly eosinophilic cellular debris which extends through the walls and is contained with multiple layers of fibrous connective tissue. (HE, 86X)

shown to be the most serious sites of persistence and transmission. It is transmitted through secretions of the UPR, through milk, from udder to udder, by ingestion and inhalation of aerosols in the case of the calf and through close contact between animals. Infrequently, colostrum, genital secretions, and fomites are a source of infection [11,13,21,32,37]. The possible intrauterine route has also been discussed [22].

Endowed with some proposed virulent mechanisms, *M. bovis* evades the host immune response resulting in chronic infections [9]. However, the pathogenesis is not fully understood and this and other molecular mechanisms involved are still under study[7]. Great advances have been made in this regard with the improvement of genetic techniques, such as the complete sequencing of the *M.bovis* genome [34,45]. Certain high-frequency rearrangements of its genome give it an ability to variably express the surface Vsp lipoprotein and avoid the host immune response. Other mechanisms are adhesion to host cells with adhesins, through surface Vsp, or even metabolic enzymes such as a-enolase, NADH oxidase, TrmFO protein and the in vitro discovered fructose 1,6-biphosphate aldolase and methylenetetrahydrofolate-tRNA-(uracil-5-)-methyltransferase. *M. bovis* has nucleases (such as MBOVPG45, MnuA and MBOV_RS02825) that can destroy NETs and also cause macrophage apoptosis. Other

form of immunologic evasion would be by intracellular infection of epithelial cells, red blood cells and circulating immune cells [9,37]. The formation of a protective biofilm continue to be studied [9,32,37] and Vsp not only mediates adherence, but strongly induces immune response through activation of TLR2 and IL-1β production [9]. The production of H2O2 as part of its virulence is suspected [9,37].

The most common gross lesions described for *M. bovis* are those observed in this case characterized by cranioventral lung consolidation and multifocal to coalescing caseonecrotic nodules that varies from pinpoint to several centimeters. They are well-demarcated, coalescing, circular, white, dry, crumbly, bulging from the pleural or cut surfaces of the lung. In addition, these nodules are delimited by areas of reddened, collapsed and consolidated lung, and the majority of nodules can be better observed with a cut through the parenchyma. Normally, these lesions are bilateral and can affect the 20% to 90% of the lung in severe cases, extending from cranioventral lobes to medial and even with relative sparing of the caudal and dorsal aspects of the caudal lobes. The key feature of this diagnosis is the friable caseous nature of the lesions, but sometimes can appeared liquefied with a suppurative consistence because secondary contamination of nodules with other bacteria (such as *Trueperella pyogenes*) [11,12]. Occasionally we can also observe foci of coagulative necrosis that differ from caseonecrotic nodules, because they are irregular in shape, red tan, non-friable and not raised [11]. The secondary interstitial emphysema observed in the dorsal aspect of the lung may be associated with the "*one-way valve effect*" of pulmonary exudates and/or the high pressure of air within the lung caused by the severe dyspnea [30]. Infection with *M. bovis* by itself could be involved as a neutrophils elastase has been related with emphysema [17,30] and *M. bovis* can induce greater secretion of theses proteases by neutrophils [24].

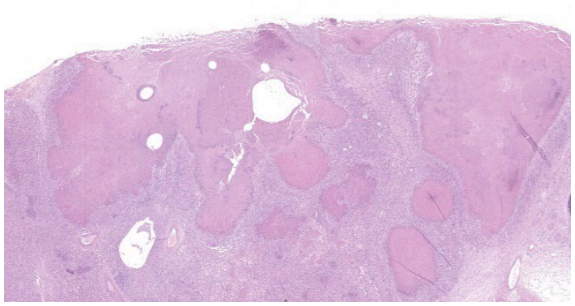

Figure 3-6. Lung, ox. In some lobules, effaced airways have coalesced in to large foci of necrosis, some of which have cavitations within the necrotic debris. (HE, 21X)

Histologic lesions include four main patterns of lesions: caseonecrotic bronchopneumonia (most common), bronchopneumonia with foci of coagulation necrosis, suppurative bronchopneumonia without necrosis and chronic bronchopneumonia with abscessation. Caseonecrotic nodules are distinctive lesions with caseous necrosis that fill small bronchioles, alveoli or interlobular septa. As we could observed on tissue section, in the earliest lesions, leukocytes are within the airways, but undergo a distinctive form of necrosis maintaining their ghost-like cellular outlines, having hypereosinophilic cytoplasm with inapparent or fragmented nuclei. The respiratory epithelium appeared eroded and this nodules are delimited by layers of necrotic cells with pyknotic nuclei, macrophages, lymphocytes and fibroblasts [11,12].

Coagulative necrosis could coexist and complicate lesions. We could observe scattered patterns of this necrosis in which bronchiolar or alveolar structure remains visible. *M. bovis* could be related with those patterns sometimes, but they are indistinguishable from *Mannheimia haemolytica*. The suspicion of *Mannheimia haemolytica* coinfection was confirmed by PCR and its presence could be related with those areas of the so called "*oat*

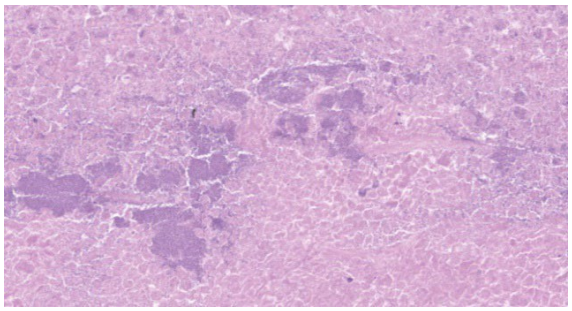

Figure 3-7. Lung, ox. In larger areas of suppuration, there are large colonies of bacilli consistent with Trueperella. (HE, 670X)

cells", that are not expected in mycoplasmosis [11]; elongated hyperchromatic cells, with the appearance of being perforated and smudged. This is a result of the activity of the typical ruminant specific *Mannheimia haemolytica* leukotoxin (Lkt), which induces multiple transmembrane pores in the macrophages membrane at a high concentration, and induces bovine cells to undergo respiratory burst and release of inflammatory mediators and cytokines at a sublytic concentrations [5,40]. In fact, bacterial coinfections with mycoplasma are common in cases of pneumonia [18,19,32,42] and even otitis [27,32]. On one occasion, *M. bovis* was isolated from 82% of feedlot calves with fibrinosuppurative pneumonia from which *Mannheimia haemolytica* was isolated. [19,32]. Other bacteria such as *Pasteurella multocida* (isolated in this case) or *Histophilus somni* have been described [9,13,18,37], so bacterial culture should be done in order to identify coinfective organisms. Mycoplasma exhibits a very slow growth up to 10 days in culture, which is why PCR is the preferred method for confirming the pathogen [36]. Concomitant infections with other viruses such as bovine viral diarrhea virus (BVDV), Infectious bovine rhinothracheitis virus (IBRV) and Bovine parainfluenza 3 virus (bPI-(3)V) were detected. The relationships with viral coinfections and Mycoplasma is less clear [34], but these and other viruses including BRSV (Bovine respiratory syncytial virus), bovine adenoviruses (BdVs) or bovine coronavirus (BCV) have been isolated. These viruses have been frequently detected with *M. bovis* and their possible synergistic role in the disease has been extensively discussed [9,10,18,32,37,42]. However, it exists some discrepancies about it [38].

Recently, *M. bovis*, which had been anecdotally described in North American bison from 2000, was finally detected in an outbreak affecting bisons of all ages. In this case, *M. bovis* bison strain (most probably a host-adapted variant) showed different genetics to that isolated from cattle and, unlike bovines, the organism was the primary agent of a process that had a mortality of up to 45% [37,39].

Contributing Institution:
Universidad de Zaragoza. Departamento de Patología Animal
https://patologiaanimal.unizar.es

JPC Diagnosis:
Lung: Pneumonia, fibrinosuppurative, caseating and necrotizing, diffuse, severe, with bronchiectasis and colonies of coccobacilli.

JPC Comment:
The contributor provides a thorough report on the pulmonary manifestation of *Mycoplasma bovis* as well as the history, virulence factors, control, and ongoing research for this economically important disease. During the conference, the moderator emphasized the importance of the mucociliary apparatus in protecting the lung and described a list of pathogens which can cause dysfunction, including *Mycoplasma, Bordetella*, viruses, and dehydration. Mucociliary apparatus dysfunction is an important part of the pathogenesis of bovine respiratory disease complex, a disease which costs $1B USD annually in the United States alone.

As the contributor mentions, *M. bovis* can cause a spectrum of diseases, and a brief review of the other most common manifestations is worthwhile. Within the host, *Mycoplasma bovis* bacteremia results in hematogenous spread to other sites and can lead to mastitis, otitis, and arthritis.[13,32] Mastitis may be the result of udder-to-udder transmission or spread from other primary sites of infection and can affect dairy cows in all life stages, including dry cows.[32] The infection varies from subclinical to severe with multiple quarters affected and results in fibrinosuppurative to caseonecrotic mastitis.

Otitis media due to *M. bovis* tends to affect dairy and beef calves two to four months of age.[27,32] Infection may be unilateral or bilateral, and most affected calves have concurrent *M. bovis* pneumonia. Initial stages are characterized by ear pain and head shaking. As the disease progresses, animals may become febrile, and involvement of the facial nerve can cause drooping of the ear and ptosis. Severe infections may progress to the inner ear and possible meninges, resulting in dysfunction of the vestibulocochlear nerve and glossopharyngeal nerve.[32] Histologically, the otitis is characterized by suppurative inflammation with extensive bony lysis.[27]

Arthritis due to *M. bovis* frequently occurs in concert with pneumonia or mastitis and is a feature of chronic pneumonia and polyarthritis syndrome (CPPS) described in feedlot cattle.[32] Clinical signs are typical of a septic arthritis, and large high-movement joints such as the hips and stifle tend to be affected. Severe cases are characterized by fibrinosuppurative arthritis with synovial hyperplasia, erosion of articular cartilage, and extension of edema, necrosis, and fibrosis into the periarticular tissues.[19,32]

References:

1. Aebi M, Bodmer M, Frey J, Pilo P. Herd-specific strains of Mycoplasma bovis in outbreaks of mycoplasmal mastitis and pneumonia. *Vet Microbiol*. 2012;157:363–368.
2. Alberti A, Addis MF, Chessa B, et al. Molecular and antigenic characterization of a Mycoplasma bovis strain causing an outbreak of infectious keratoconjunctivitis. *J Vet Diagnostic Investig*. 2006;18:41–51.
3. Arcangioli MA, Duet A, Meyer G, et al. The role of Mycoplasma bovis in bovine respiratory disease outbreaks in veal calf feedlots. *Vet J*. 2008;177:89–93.
4. Ayling R, Nicholas R, Hogg R, et al. Mycoplasma bovis isolated from brain tissue of calves. *Vet Rec*. 2005;156:391–392.
5. Benz R, Piselli C, Potter AA. Channel formation by LktA of Mannheimia (Pasteurella) haemolytica in lipid bilayer membranes and comparison of channel properties with other RTX-Cytolysins. *Toxins (Basel)*. 2019;11:16.
6. Biddle MK, Fox LK, Evans MA, Gay CC. Pulsed-field gel electrophoresis patterns of Mycoplasma isolates from various body sites in dairy cattle with Mycoplasma mastitis. *J Am Vet Med Assoc*. 2005;227:455–459.
7. Bürgi N, Josi C, Bürki S, Schweizer M, Pilo P. Mycoplasma bovis co-infection with bovine viral diarrhea virus in bovine macrophages. *Vet Res*. 2018;49.
8. Bürki S, Frey J, Pilo P. Virulence, persistence and dissemination of Mycoplasma bovis. Vol. 179, *Veterinary Microbiology*. 2015:8.
9. Calcutt MJ, Lysnyansky I, Sachse K, Fox LK, Nicholas RAJ, Ayling RD. Gap analysis of Mycoplasma bovis disease, diagnosis and control: An aid to identify future development requirements. *Transbound Emerg Dis*. 2018;65.

10. Caswell JL, Williams WJ. Respiratory System. In: Maxie GM, ed. Vol. 2, *Jubb, Kennedy, and Palmer's pathology of domestic animals*. St. Louis, Missouri: Elsevier, Inc; 2016:465–591.
11. Caswell JL, Archambault M. Mycoplasma bovis pneumonia in cattle. *Anim Heal Res Rev*. 2007;8:161–186.
12. Caswell JL, Bateman KG, Cai HY, Castillo-Alcala F. Mycoplasma bovis in respiratory disease of feedlot cattle. Vol. 26, *Veterinary Clinics of North America - Food Animal Practice*. 2010:
13. Dudek K, Szacawa E. Mycoplasma bovis infections: Occurrence, diagnosis and control,. Vol. 9, *Pathogens*. 2020:640.
14. Dupuy V, Manso-Silván L, Barbe V, et al. Evolutionary history of contagious bovine pleuropneumonia using next generation sequencing of Mycoplasma mycoides Subsp. mycoides 'Small Colony'. *PLoS One*. 2012;7:9.
15. Fox LK. Prevalence, incidence and risk factors of heifer mastitis. *Vet Microbiol*. 2009;134:82–88.
16. Francoz D, Fecteau G, Desrochers A, Fortin M. Otitis media in dairy calves: A retrospective study of 15 cases (1987 to 2002). *Can Vet J*. 2004;45:661–666.
17. Fujie K, Shinguh Y, Yamazaki A, Hatanaka H, Okamoto M, Okuhara M. Inhibition of elastase-induced acute inflammation and pulmonary emphysema in hamsters by a novel neutrophil elastase inhibitor FR901277. *Inflamm Res*. 1999;48:160–167.
18. Fulton RW, Blood KS, Panciera RJ, et al. Lung pathology and infectious agents in fatal feedlot pneumonias and relationship with mortality, disease onset, and treatments. *J Vet Diagnostic Investig*. 2009;21:464–477.
19. Gagea MI, Bateman KG, Shanahan RA, et al. Naturally occurring Mycoplasma bovis-associated pneumonia and polyarthritis in feedlot beef calves. *J Vet Diagnostic Investig*. 2006;18:29–40.
20. Hale HH, Helmboldt CF, Plastridge WN, Stula EF. Bovine mastitis caused by a Mycoplasma species. *Cornell Vet*. 1962 Oct;52:582–591.
21. Hazelton MS, Sheehy PA, Bosward KL, et al. Short communication: Shedding of Mycoplasma bovis and antibody responses in cows recently diagnosed with clinical infection. *J Dairy Sci*. 2018;101:584–589.
22. Hermeyer K, Peters M, Brügmann M, Jacobsen B, Hewicker-Trautwein M. Demonstration of Mycoplasma bovis by immunohistochemistry and in situ hybridization in an aborted bovine fetus and neonatal calf. *J Vet Diagnostic Investig*. 2012;24:364–369.
23. Hirth RS, Nielsen SW, Plastridge WN. Bovine Salpingo-oophoritis Produced with Semen Containing a Mycoplasma. *Vet Pathol*. 1966;3:616–632.
24. Jimbo S, Suleman M, Maina T, Prysliak T, Mulongo M, Perez-Casal J. Effect of Mycoplasma bovis on bovine neutrophils. *Vet Immunol Immunopathol*. 2017;188:27–33.
25. Kanda T, Tanaka S, Suwanruengsri M, et al. Bovine Endocarditis Associated with Mycoplasma bovis. *J Comp Pathol*. 2019;171.
26. Kinde H, Daft BM, Walker RL, Charlton BR, Petty R. Mycoplasma bovis associated with decubital abscesses in Holstein calves. *J Vet Diagnostic Investig*. 1993;5:194–197.
27. Lamm CG, Munson L, Thurmond MC, Barr BC, George LW. Mycoplasma otitis in California calves. *J Vet Diagnostic Investig*. 2004;16:397–402.
28. Ledger L, Eidt J, Cai HY. Identification of antimicrobial resistance-associated genes through whole genome sequencing of mycoplasma bovis isolates with

different antimicrobial resistances. *Pathogens*. 2020;9:588.
29. Levisohn S, Garazi S, Gerchman I, Brenner J. Diagnosis of a mixed mycoplasma infection associated with a severe outbreak of bovine pinkeye in young calves. *J Vet Diagnostic Investig*. 2004;16:579–581.
30. López A, Martinson SA. Respiratory System, Mediastinum, and Pleurae. In: Zachary FJ, ed. *Pathologic Basis of Veterinary Disease Expert Consult*. St. Louis, Missouri: Elsevier Inc.; 2017:471–560.
31. Lysnyansky I, Ayling RD. Mycoplasma bovis: Mechanisms of resistance and trends in antimicrobial susceptibility. *Front Microbiol*. 2016;7.
32. Maunsell FP, Woolums AR, Francoz D, et al. Mycoplasma bovis infections in cattle. *J Vet Intern Med*. 2011;25:772–783.
33. Morowitz HJ. When PPLO became mycoplasma. *American Scientist*. 2011;99:102–105.
34. Nicholas RAJ. Bovine mycoplasmosis: Silent and deadly. *Vet Rec*. 2011;168:459–462.
35. Nocard, Roux. The microbe of pleuropneumonia. *Clin Infect Dis*. 1990;12:354–358.
36. Parker AM, Sheehy PA, Hazelton MS, Bosward KL, House JK. A review of mycoplasma diagnostics in cattle. Vol. 32, *Journal of Veterinary Internal Medicine*. 2018:
37. Perez-Casal J. Pathogenesis and Virulence of Mycoplasma bovis. *Vet Clin North Am - Food Anim Pract*. 2020;36:269–278.
38. Prysliak T, Van Der Merwe J, Lawman Z, et al. Respiratory disease caused by Mycoplasma bovis is enhanced by exposure to bovine herpes virus 1 (BHV-1) but not to bovine viral diarrhea virus (BVDV) type 2. *Can Vet J*. 2011;52.
39. Register KB, Olsen SC, Sacco RE, et al. Relative virulence in bison and cattle of bison-associated genotypes of Mycoplasma bovis. *Vet Microbiol*. 2018;222:55–63.
40. Singh K, Ritchey JW, Confer AW. Mannheimia haemolytica: Bacterial-host interactions in bovine Pneumonia. *Vet Pathol*. 2011;48:338–348.
41. Stalheim OHV, Page LA. Naturally occurring and experimentally induced mycoplasmal arthritis of cattle. *J Clin Microbiol*. 1975;2:165–168.
42. Stipkovits L, Ripley P, Varga J, Pálfi V. Clinical study of the disease of calves associated with Mycoplasma bovis infection. *Acta Vet Hung*. 2000;48.
43. Thomas A, Ball H, Dizier I, et al. Isolation of Mycoplasma species from the lower respiratory tract of healthy cattle and cattle with respiratory disease in Belgium. *Vet Rec*. 2002;151:472–476.
44. Weisburg WG, Tully JG, Rose DL, et al. A phylogenetic analysis of the mycoplasmas: Basis for their classification. *J Bacteriol*. 1989;171:6455–6467.
45. Wise KS, Calcutt MJ, Foecking MF, et al. Complete genome sequence of Mycoplasma bovis type strain PG45 (ATCC 25523). Vol. 79, *Infection and Immunity*. 2011:982–983.

CASE IV:

Signalment:
6-month-old, Aberdeen-Angus bull calf (*Bos taurus or domesticus*)

History:
The clinical signs prior to death included diarrhea, snotty nose, and a low body temperature (99-100 F˚). The calf had been vaccinated 2 weeks prior with a vaccine containing a modified-live Bovine Viral Diarrhea Virus (BVDV).

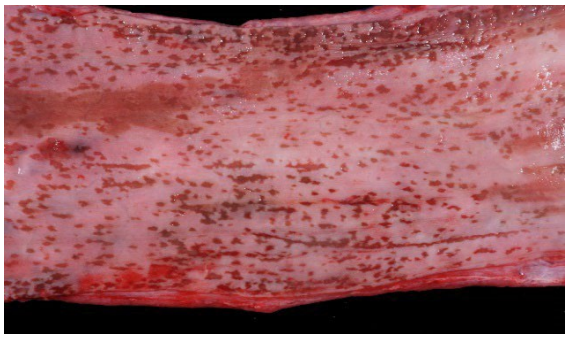

Figure 4-1. Esophagus, ox. There are multifocal to coalescing, approximately linear erosions/ulcers widely disseminated on the esophageal mucosa. (Photo courtesy of: Veterinary Diagnostic Laboratory, University of Minnesota, www.vdl@umn.edu)

Gross Pathology:
Alimentary system – At the rostral aspect of the hard palate and at the margins of the buccal mucosa, there were multifocal to coalescing, 5-10mm diameter, dark red, slightly depressed regions with partial to complete loss of the mucosa (erosions and ulcers) as well as multifocal pinpoint erosions/ulcers at the junction of the hard and soft palate. There were numerous, multifocal to coalescing, approximately linear, 1-3mm x 5-10mm, slightly depressed erosions/ulcers that were widely disseminated along the entire length of the mucosal aspect of the esophagus. The abomasal mucosa was diffusely red with numerous, 2-5mm dark red to black erosions/ulcers widely disseminated throughout the mucosal surface affecting approximately 20-30% of the surface area. The small intestinal mucosa was reddened. Multifocally and widely disseminated throughout the mucosal surface of the small intestine, there were small numbers of 3mm diameter, black foci. The colonic and rectal mucosa had multiple red approximately linear regions. There was a large amount of soft to watery intestinal contents.

Laboratory Results:
Molecular Diagnostics: Tissue homogenate was positive for BVDV by PCR.

Microscopic Description:
Esophagus – Multifocally, there is partial to complete loss and sloughing of the epithelium (erosion and ulceration) with replacement by necrotic cellular debris, few neutrophils, a small amount of fibrin, few erythrocytes, and occasional bacterial colonies. The adjacent epithelial cells are often swollen and pale (ballooning degeneration) or are shrunken, deeply eosinophilic with pyknotic to karyorrhectic nuclei (necrosis). Multifocally in other regions, the epithelium is degenerate to necrotic. There are small numbers of neutrophils infiltrating the remaining epithelium (transmigration) and occasionally extending into the underlying submucosa forming microabscesses. The mucosal and submucosal blood vessels are congested.

Contributor's Morphologic Diagnosis:
Esophagus – necroulcerative esophagitis, multifocal to coalescing, marked, acute with few neutrophils and rare microabscesses.

Contributor's Comment:
Bovine viral diarrhea virus (BVDV) is an RNA virus that most commonly causes disease in cattle, but it, or closely related viruses, can infect most even-toed ungulates including swine and camelids. [14] BVDV (BVDV-1 and BVDV-2) is in the genus *Pestivirus* (fam-

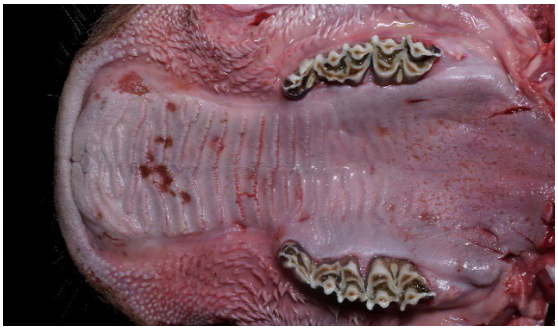

Figure 4-2. Hard palate, ox. Within the oral cavity, there were multifocal to coalescing erosions/ulcers on the hard palate, buccal mucosa, and extending into the soft palate. (Photo courtesy of: Veterinary Diagnostic Laboratory, University of Minnesota, www.vdl@umn.edu)

ily Flaviviridae) which also includes Classical swine fever virus and Border disease virus.[14] BVDV has two biotypes including both a noncytopathic (NCP) and cytopathic (CP) form.[14] Additionally, there is a more recently identified species of pestivirus which has been classified as BVDV-3, also known as HoBi-like or atypical pestivirus.[14]

There are multiple varying clinical presentations of BVDV in juvenile to adult cattle ranging from mild clinical signs (fever, anorexia, lethargy) to severe clinical signs and death.[14] A severe acute form of BVDV is termed BVD type 2 (often caused by BVDV-2) and presents with a fever, sudden death, diarrhea, or pneumonia.[14] A thrombocytopenic form of BVDV has been described.[14] These varying forms are not mutually exclusive and often present with overlap. Fetal infections, which vary clinically by time of gestation, can occur when an immunocompetent, seronegative dam is infected. If the dam is infected during approximately the first 4 months of gestation by a NCP form of BVDV that crosses the placenta, the fetus may die leading to resorption, mummification, abortion, develop congenital abnormalities, or survive leading to birth of a persistently infected (PI) calf (typically 42-125 days gestation).[8,14,16]

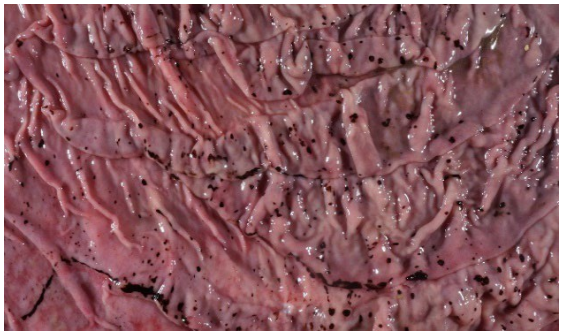

Figure 4-3. Abomasum, ox. There were multifocal dark red to black erosions/ulcers widely disseminated throughout the abomasal mucosa. (Photo courtesy of: Veterinary Diagnostic Laboratory, University of Minnesota, www.vdl@umn.edu)

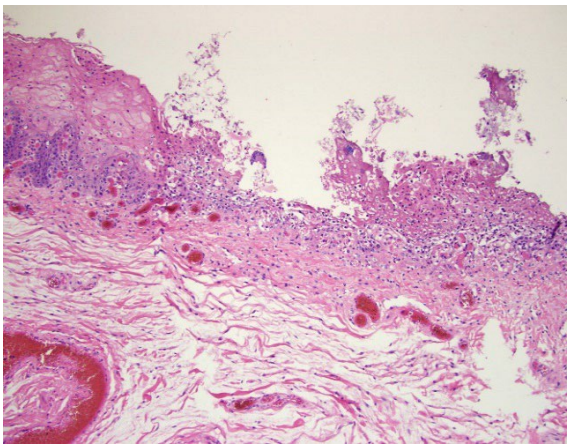

Figure 4-4. Esophagus, ox. Esophagus – Focally, there is loss of the epithelium (ulceration) with replacement by a small amount of cellular debris and few bacteria. There is degeneration and necrosis of the adjacent epithelial cells with infiltration by few neutrophils. (Photo courtesy of: Veterinary Diagnostic Laboratory, University of Minnesota, www.vdl@umn.edu) (HE 200X)

At birth PI calves can appear completely normal or have non-specific clinical signs (poor doing, rough hair coat), or are undersized. PI calves remain viremic throughout life and shed large amounts of virus.[14] Due to the timeframe of fetal infection and immune system development, these calves are seronegative but antigen positive, and viral antigen can be identified with immunohistochemistry in a variety of tissues.[14] PI calves must be differentiated from acutely infected calves by the absence of lesions in the presence of antigenic positivity.[14] PI calves are vulnerable to mucosal disease.[14]

Mucosal disease is a syndrome whereby PI calves become infected with a CP biotype that is similar to the NCP biotype of original fetal infection or when the NCP biotype of the persistent infection mutates.[14] Evidence has shown that vaccination with a modified-live BVDV can also lead to mucosal disease in PI calves.[14] Due to the immunotolerance created by the timing of the fetal infection, the calf is unable to elicit an immune response to the CP BVDV leading to an overwhelming infection and destruction of mucosal epithelial cells.[8,14,16]

Histopathologic features of mucosal disease and acute BVDV include epithelial necrosis with erosions and ulcerations throughout the alimentary tract often including esophagus, rumen, reticulum, abomasum, and intestine.[14] The most characteristic histopathologic features of BVDV are found in the intestine and include destruction of the crypts of Lieberkühn with luminal dilation by mucus along with lysis of the Peyer's patches and associated overlying mucosal inflammation.[14] Differential etiologies for the histologic findings of epithelial necrosis with erosions and ulceration in the alimentary tract include malignant catarrhal fever, rinderpest, and vesicular diseases; however, the intestinal changes are only similar in rinderpest.[8,14] Osteopetrosis has also been identified in PI calves.[15]

Due to the economic importance of BVDV, there have been a few recent studies completed to streamline diagnosis and understand pathogenesis and lesions. As PI animals are the main concern for spread of disease, better detection strategies for rapid identification were warranted. According to Brodersen, the use of ear notches with immunohistochemistry has enabled quick identification of PI animals to assist with on-farm control strategies.[4] As previously described, mucosal disease typically affects the entire alimentary tract; however, a recent report describes a mucosal disease outbreak with lesions restricted to the upper alimentary tract and skin (interdigital) with no lesions in the intestine, which may pose a challenge when differentiating from vesicular diseases.[3] In order to more fully understand the pathogenesis of mucosal disease, varying apoptotic pathways were evaluated by Hilbe et al.[10] It was found that caspase-3 and caspase-9 (intrinsic pathway) are more strongly expressed in mucosal disease lesions while caspase-8 (extrinsic pathway) was not.[10]

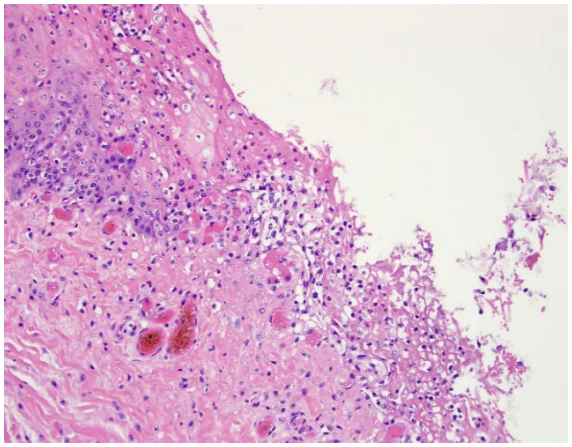

Figure 4-5. Esophagus, ox. Esophagus – The epithelial cells are degenerate to necrotic with infiltration and transmigration of few neutrophils. (Photo courtesy of: Veterinary Diagnostic Laboratory, University of Minnesota, www.vdl@umn.edu) (HE 400X)

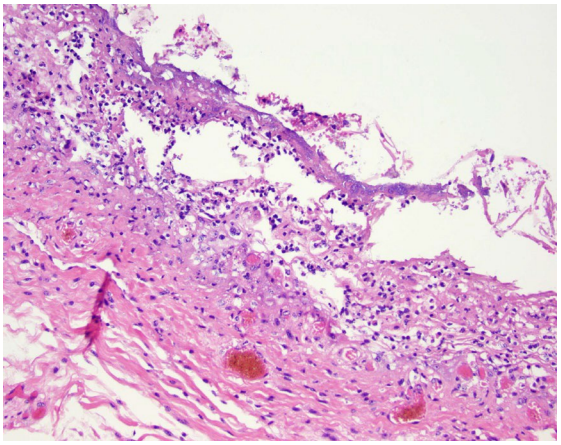

Figure 4-6. Esophagus, ox. There is sloughing of the epithelium. There is epithelial infiltration by few neutrophils and superficial bacterial colonies. (Photo courtesy of: Veterinary Diagnostic Laboratory, University of Minnesota, www.vdl@umn.edu) (HE 400X)

Contributing Institution:
Veterinary Diagnostic Laboratory, University of Minnesota, www.vdl@umn.edu

JPC Diagnosis:
Esophagus: Esophagitis, ulcerative, acute, multifocal.

JPC Comment:
Bovine viral diarrhea was first described as a new disease of cattle in 1946 by researchers

in New York. Subsequent work in cell cultures allowed for isolation of the virus and vaccine development in the 1960s.[6] The proclivity of the virus to survive in culture and the spread of the infection in pregnant cows lead to contamination of numerous ruminant cell cultures uncovered in the 1980s. Viral contamination of cell cultures can occur through the addition of infected fetal bovine serum or, less commonly, by using infected bovine fetal tissue for the initial culture.[2,9] Such viral contamination compromises research studies and in several instances has led to contamination of vaccine stocks in both veterinary patients and humans. Early poliovirus vaccines produced on rhesus monkey kidney cell cultures were contaminated with simian polyomavirus SV40, a virus endemic to rhesus macaques and carcinogenic in humans.[5] This led to widespread exposure of the human population between 1955 and 1963 and even later in some countries. Strict controls on international trade have been implemented and new improved protocols require irradiation of serum prior to addition to cell cultures.[9] Additionally, technological advances now allow for detection and sequencing of all nucleic acids within a culture.[9] It was through these detection methods that HoBi-like pestivirus (HoBiPeV) was first identified in 2004 when it was isolated from contaminated bovine fetal serum from Brazil.[11]

As the contributor described, bovine viral diarrhea virus has two traditional genotypes, BVDV-1 and BVDV-2. HoBiPeV can cause the produce the same spectrum of disease as the typical BVDV genotypes and has now been reported in South America, Europe, and Asia.[1,11] In a recent report of HoBi-like pestivirus in feedlot steer in Argentina, the virus was associated with bronchointerstitial pneumonia in one animal and fibrinosuppurative bronchopneumonia in another animal coinfected with *Mannheimia hemolytica*.[11] This report is suggestive of HoBiPeV's role in development of bovine respiratory disease complex, similar to that of BVDV. This study also demonstrated HoBiPeV's potential cross-reactivity against BVDV immunohistochemical stains, which is attributed to the highly-conserved viral glycoprotein GP48 present in all three species. Current antigenic and serologic tests are less or ineffective at detecting HoBiPeV, and there is limited cross protection between strains in commercially available BVDV vaccines.[7,11]

Since 2000, the list of known pestiviruses has grown to include several additional pathogens of cloven-hoofed animals, including atypical porcine pestivirus and Bungowannah virus in pigs, Aydin-like pestivirus in sheep and goats, and pronghorn antelope vi-

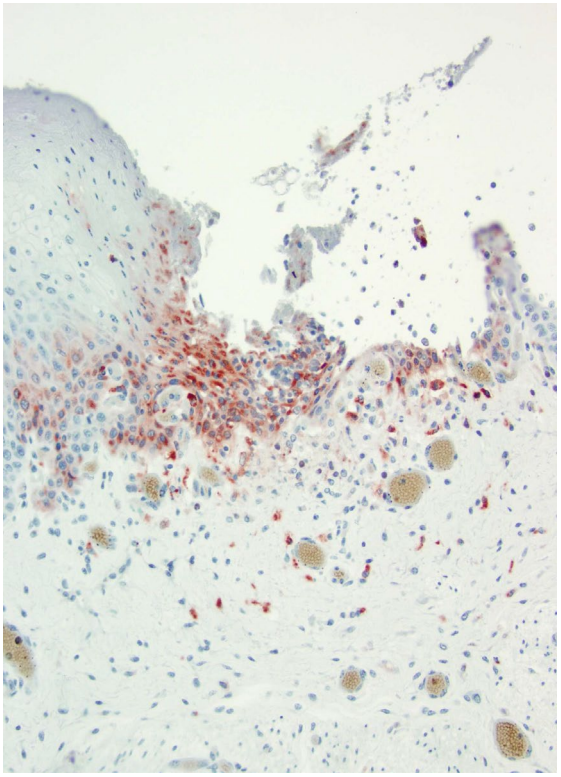

Figure 4-7. Esophagus, ox There is strong intracytoplasmic BVDV immunoreactivity of numerous epithelial cells and few inflammatory cells within an affected region of esophagus (Photo courtesy of: Veterinary Diagnostic Laboratory, University of Minnesota, www.vdl@umn.edu) (anti-BVDV, 400X)

rus. Additionally, a number novel pestiviruses of questionable pathogenicity have been isolated from non-ungulate species, including pangolins, rodents, bats, and harbor porpoises.[12] With this growing list, there is a proposed revision of Pestivirus taxonomy, with each species denoted by a single letter. Under the new taxonomy, BVDV-1 is designated Pestivirus A, BVDV-2 is Pestivirus B, and HoBiPeV is Pestivirus H.[13]

References:

1. Balasuriya UBR, Reisen W. Chapter 29 – Flaviviruses. In: MacLachlan NJ, Dubovi EJ eds. *Fenner's Veterinary Virology*. 5th ed. Boston, MA: Academic Press, 2017: 525-546.
2. Barrat-Boyes S. Golde WT. Chapter 4 – Antiviral Immunity and Virus Vaccines. In: MacLachlan NJ, Dubovi EJ eds. *Fenner's Veterinary Virology*. 5th ed. Boston, MA: Academic Press, 2017: 79-104.
3. Bianchi MV, Konradt G, de Souza SO, et al. Natural Outbreak of BVDV-1d-Induced Mucosal Disease Lacking Intestinal Lesions. *Vet Pathol*. 2017;54:242-248.
4. Brodersen BW. Bovine Viral Diarrhea Virus Infections: Manifestations of Infection and Recent Advances in Understanding Pathogenesis and Control. *Vet Pathol*. 2014;51:453-464.
5. Carbone M, Gazdar A, Butel JS. SV40 and human mesothelioma. *Transl Lung Cancer Res*. 2020 Feb;9(Suppl 1):S47-S59.
6. Coffey LL. Chapter 1 – The Nature of Viruses. In: MacLachlan NJ, Dubovi EJ eds. *Fenner's Veterinary Virology*. 5th ed. Boston, MA: Academic Press, 2017:1-16.
7. Decaro N. HoBi-Like Pestivirus and Reproductive Disorders. *Frontiers in Vet Sci.* 2020;7:1-5.
8. Gelberg HB. Alimentary System and the Peritoneum, Omentum, Mesentery, and Peritoneal Cavity. In: Zachary JF. *Pathologic Basis of Veterinary Disease. 6*th ed. St. Louis, MO: Elsevier; 2017: 395-397.
9. Heidner H. Chapter 2 – Virus Replication. In: MacLachlan NJ, Dubovi EJ eds. *Fenner's Veterinary Virology*. 5th ed. Boston, MA: Academic Press, 2017:17-46.
10. Hilbe M, Girao V, Bachofen C, et al. Apoptosis in Bovine Viral Diarrhea Virus (BVDV)-Induced Mucosal Disease Lesions: A Histological, Immunohistological, and Virological Investigation. *Vet Pathol*. 2012;50:46-55.
11. Margineda CA, Ferreyra FM, Masnyj F, et al. HoBi-like pestivirus in 2 cases of fatal respiratory disease of feedlot cattle in Argentina. *J Vet Diagn Invest.* 2022; 34(4):693-698.
12. Postel A, Smith DB, Becher P. Proposed Update to the Taxonomy of Pestiviruses: Eight Additional Species within the Genus *Pestivirus*, Family *Flaviviridae*. *Viruses*. 2021 Aug 4;13(8):1542.
13. Smith DB, Meyers G, Bukh J, et al. Proposed revision to the taxonomy of the genus *Pestivirus*, family *Flaviviridae*. *J. Gen. Virol.* 2017;**98**:2106–2112.
14. Uzal FA, Plattner BL, and Hostetter JM. Alimentary System. In: Maxie MG. *Jubb, Kennedy, and Palmer's Pathology of Domestic Animals*. 6th ed. Missouri: Elsevier, 2016: Vol 2: 122-139.
15. Webb BT, Norrdin RW, Smirnova NP, et al. Bovine Viral Diarrhea Virus Cyclically Impairs Long Bone Trabecular Modeling in Experimental Persistently Infected Fetuses. *Vet Pathol*. 2012;49:930-940.
16. Zachary JF. Mechanisms of Microbial infections. In: Zachary JF. *Pathologic Basis of Veterinary Disease.* 6th ed. St. Louis, MO: Elsevier; 2017: 200-201.

WSC 2022-2023 Self-assessment.
Conference 1

1. True or false? All cases of ovine pulmonary carcinoma caused by retrovirus eventually become clinical.
    a. True
    b. False

2. Which is the most common cause of spread of ovine pulmonary adenocarcinoma in sheep?
    a. Colostrum
    b. Biting insects
    c. Traumatic inoculation
    d. Respiratory droplet transmission from close contact

3. Which of the following is the vector for bluetongue in sheep?
    a. Ticks
    b. Mosquitoes
    c. Snails
    d. Biting midges

4. In the ox, a site of persistence and transmission of *Mycoplasma bovis* is:
    a. Lower respiratory tract
    b. Tonsils
    c. External ear
    d. Mammary gland

5. True or false. Mucosal disease is initiated by the infection of a bovine fetus between 42 and 125 with a cytopathic strain of bone pestivirus.?
    a. True
    b. False

Please email your completed assessment for grading to Dr. Bruce Williams at bruce.h.williams12.civ@mail.mil. Passing score is 80%. This program (RACE program 33611) is approved by the AAVSB RACE to offer a total of 0.5 CE Credits, with a maximum of 12.5 CE Credits being available to any individual Veterinary Medical Professionals for the 2019-2020 Wednesday Slide Conference. This RACE approval is for the subject matter categories of: SCIENTIFIC using the delivery method of NONINTERACTIVE DISTANCE. This approval is valid in jurisdictions which recognize AAVSB RACE.

Joint Pathology Center
Veterinary Pathology Services

WEDNESDAY SLIDE CONFERENCE 2022-2023

Conference #2 — 24 August 2022

CASE I:

Signalment:
A three-year-old female pot-bellied pig (*Sus scrofa domesticus*)

History:
Two-week history of intermittent pelvic limb lameness and abnormal mentation. Brought to the Veterinary Teaching Hospital unable to ambulate in rear. Neuro exam w/CT scan indicated multiple cerebellar masses. Owner elected euthanasia due to deteriorating neurological condition of patient and poor prognosis.

Gross Pathology:
Brain: The gyri and sulci are flattened throughout the cerebrum. When removed the cerebrum leaks a large amount of clear cerebrospinal fluid and the cerebrum flattens. The cerebellum is cone-shaped and pushed out the foramen magnum. The vermis is flattened and has loss of detail. After fixation the brain is sectioned. The lateral ventricles are severely dilated and the gray and white matter of the cerebrum compressed. There are several pale tan nodules that distort the cerebellum.

Laboratory Results:
Scrolls were cut from formalin-fixed, paraffin embedded blocks of cerebellum. DNA was extracted using the Qiagen QIAmp DNA FFPE Tissue kit according to the manufacturer's directions. Extracted DNA was amplified using forward and reverse primers for the 16S-23S rRNA gene spacer as published.[1] The amplicon was submitted for Sanger sequencing with the product submitted for a BLAST search. The sequence had highest identity (99.63%) with *Mycobacterium avium* subsp. *hominissuis*.

Microscopic Description:
Cerebellum: The cerebellar gray and white matter are effaced by large, unencapsulated, compressive nodules composed of large numbers of epithelioid macrophages and multinucleate giant cells with peripheral nuclei. There are smaller numbers of neutrophils, lymphocytes and eosinophils scattered

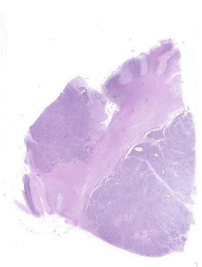

Figure 1-1. Cerebellum, pig. Approximately 50% of the cerebellar architecture is effaced by a large inflammatory exudate. (HE, 3X)

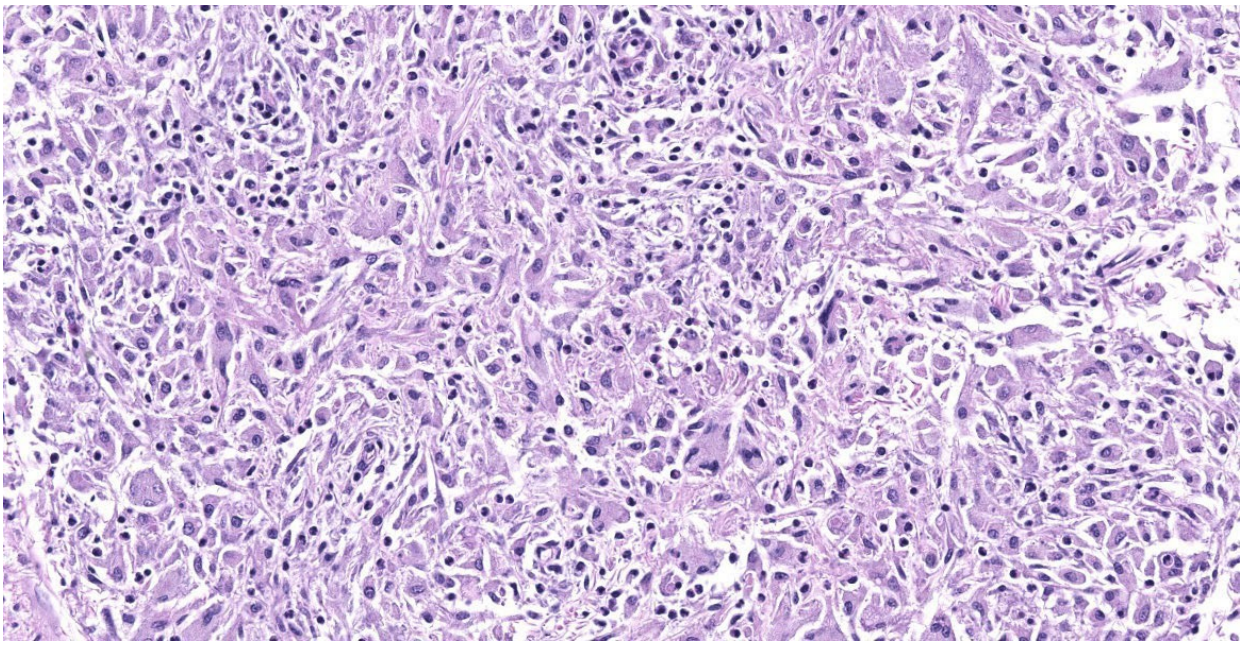

Figure 1-2. Cerebellum, pig. The inflammatory focus is composed of innumerable epithelioid macrophages and multinucleated giant cell macrophages. (HE, 283X)

within the nodules. Some of the larger cells have slight heterogeneity of the eosinophilic cytoplasm. Staining with acid fast stain reveals large numbers of bacilli with in the cytoplasm of macrophages and multinucleate giant cells. Large clusters of lymphocytes and plasma cells surround medium-caliber blood vessels.

Contributor's Morphologic Diagnoses:
Brain:

1. Granulomas, multifocal, chronic, severe, cerebellum with intralesional acid fast bacteria
2. Hydrocephalus, diffuse, severe with cerebellar coning

Contributor's Comment:
At the time of necropsy, cerebellar neoplasia was the primary differential based on MRI and gross findings of space occupying masses that compressed cerebral spinal fluid flow and led to secondary hydrocephalus. On histologic review, granulomatous inflammation was identified and slight granularity of the cytoplasm of epithelioid macrophages and multinucleate giant cells suggested intracellular organisms. Small bacilli consistent with mycobacteria were confirmed with acid-fast staining. Because there was no fresh tissue for culture, the organisms were identified using PCR and Sanger sequencing.[7] *Mycobacterium avium* subsp. *hominissuis* was identified. Deep sequencing was attempted, but host nucleic acid predominated and no reads corresponding to mycobacteria were identified.

Mycobacteria are acid-fast, non-motile, non-spore forming, intracellular, aerobic bacilli. *Mycobacterium avium* subsp. *hominisuis* is a

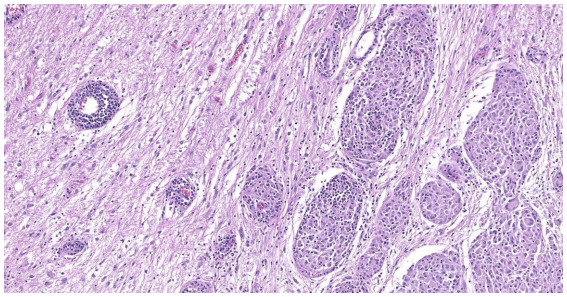

Figure 1-3. Cerebellum, pig. At the advancing edge of the focus of granulomatous inflammation, macrophages, lymphocytes, and plasma cells, in varying concentrations, expanded the perivascular space. (HE, 347X)

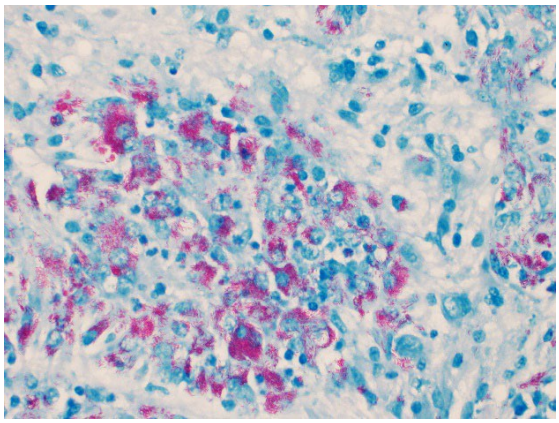

Figure 1-4. Cerebellum, pig. An acid-fast stain demonstrates innumerable bacilli in macrophages. (Fite-Faraco, 400X)

member of the *M. avium* complex (MAC) as compared to other mycobacteria in the *M. tuberculosis* complex with members such as *M. bovis, M. tuberculosis,* and *M. microti*. MAC is primarily composed of *M. avium* subspecies and *M. intracellulare* and are commonly found in fresh and salt water as well as soil.[9] Infections are typically associated with immunocompromise in the mammalian host and are typically not contagious. *M. avium* subspecies *hominissuis* is most frequently isolated from humans and pigs as suggested by the nomenclature.

While reports of mycobacterial lymphadenitis are common and worldwide,[9] to our knowledge, the only report of mycobacteriosis in pot-bellied pigs is a single case report of *M. kansasii*, another member of MAC.[8] That case report, as well as reports in other porcine species, typically present as disseminated disease with colonization and inflammation most prominent in lung and lymph nodes.[3] This case is unusual in that the granulomas and organisms were only identified in the cerebellum without lymphadenitis or lesions in thoracic or abdominal tissues. There was no indication of underlying disease or immunocompromise.

Contributing Institution:
Virginia Maryland College of Veterinary Medicine.
205 Duck Pond Dr
Blacksburg, VA 24061
https://vetmed.vt.edu/departments/biomedical-sciences-and-pathobiology.html

JPC Diagnosis:
Cerebellum: Meningoencephalitis, granulomatous, multifocal to coalescing, severe, with innumerable intrahistiocytic bacilli.

JPC Comment:
Conference participants discussed differentials for granulomatous disease in this case, including mycobacterial and fungal infections. During the pre-conference lecture, the moderator, LTC Erica Barkei, described a case of *Mycobacterium tuberculosis* she diagnosed in a rhesus macaque; the paucibacillary lesions in that case provided a striking contrast to the abundant acid fast bacteria in the multibacillary granulomas seen in this case. The moderator explained that the mycolic acid within cell walls impart the acid-fast character of mycobacteria, though they can also be weakly gram-positive, as demonstrated with B&H staining in this case.

Bacteria of the family *Mycobacteriaceae* may be classified according to the spectrum of disease they cause or their ability to grow in culture. The tuberculous group is composed of closely related zoonotic obligate pathogens *M. tuberculosis*, *M. bovis,* and *M. microti*.[5,6] Tuberculous mycobacteria elicit a

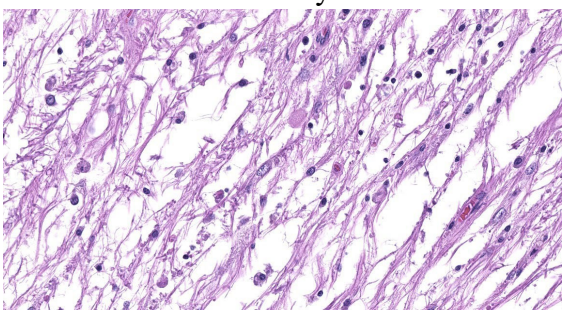

Figure 1-5. Cerebellum, pig. There are numerous dilated myelin sheaths, spheroids, and Gitter cells in the white matter at the advancing edge of the inflammatory focus. (PAS, 40X)

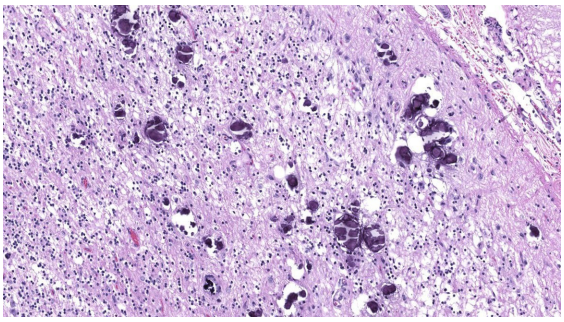

Figure 1-6. Cerebellum, pig. Vessels within the cerebellar folia, primarily in the molecular layer, but also in the meninges contain luminal or mural crystalline mineral. (HE, 156X)

Th1 response, where interferon gamma stimulates cell mediated immunity and the increased bactericidal activity of macrophages results in few bacteria within lesions. IFN-gamma also leads to secondary tissue damage, with granuloma formation or potentially caseous necrosis.[2]

Another group of obligate pathogens is the leprosy group, which includes *M. lepraemurium* and *M. visibilis*.[5] In humans, leprosy may incite a tuberculoid (Th1) response, as previously described, or a lepromatous response, in which there is a weak Th1 response and variable Th2 response. In these cases, there is weak cell-mediated immunity, abundant bacteria within lesions, and potential production of non-protective antibodies which lead to antigen-antibody complex deposition.[2]

The nontuberculous group includes, among others, the *M. avium* complex (MAC) with subspecies *avium, sylvaticum, paratuberculosis,* and *hominissuis*.[1] As the contributor mentioned, MAC bacteria are environmental opportunistic pathogens and infection is generally localized to the skin unless there is concurrent immunocompromise.[5] MAC bacteria grow slowly in culture but lesions in animals contain generally contain abundant bacteria.[5] Other nontuberculous mycobacteria which grow rapidly in culture can cause atypical mycobacteriosis, particularly in cats. The lesions similarly depend on the immune status of the animal and vary from chronic panniculitis, granulomatous pneumonia, to systemic disease in immunosuppressed animals.[5] Few bacteria are found within the lesions of atypical mycobacteriosis.[5]

In general, poultry and swine are considered more susceptible to MAC, whereas dogs, cats, and domestic rabbits are more resistant.[1,3] Literature on primary *M. avium hominissuis* (MAH) in domestic animals is sparse; however a couple of recent reports have described MAH infection in a cat and a rabbit without evidence of underlying immunosuppression. The feline case involved a young cat with chronic neurologic signs, pyogranulomatous meningoencephalitis, and generalized granulomatous lymphadenitis with abundant acid-fast bacteria found in multiple organ systems.[4] The rabbit had a focal fibrinonecrotic ulceration within the cecum characterized by granulomatous inflammation, multinucleated giant cells, and intra- and extra-cellular acid-fast bacteria.[1] Granulomatous inflammation was also observed in the spleen, liver, lungs, and cecal lymph node, and only the enlarged cecal lymph node contained bacteria, which were scant. In both the cases, *M. avium* subsp. *hominissuis* was identified.[1,4]

References:

1. Bertram CA, Barth SA, Clockner B, et a. Intestinal *Mycobacterium avium* Infection in Pet Dwarf Rabbits (*Oryctolagus cuniculus*). *J. Comp Path.* 2020; 180:73-78.
2. Frank KM, McAdam AJ. Infectious Diseases. In: Kumar V, Abbas AK, Aster JC, eds. *Robins & Cotran Pathologic Bases of Disease*. 10th ed. Philadelphia, PA: Elsevier, Inc; 2021: 339-404.
3. Greene CE, Gunn-Moore DA. Mycobacterial Infections: Infections Caused by

Slow-growing Mycobacteria. In: Greene CE, ed. *Infectious Diseases of the Dog and Cat*. 4th ed. St. Louis, MO: Elsevier Saunders; 2012: 495-513.
4. Madarame H, Saito M, Ogiara K, et al. *Mycobacterium avium* subsp. *hominissuis* meningoencephalitis in a cat. *Vet Micro*. 2017; 204:43-45.
5. Mauldin EA, Peters-Kennedy A. Integumentary System. In: Maxie MG, ed. *Jubb, Kennedy, and Palmer's Pathology of Domestic Animals*. Vol 1. 6th ed. Philadelphia, PA: Elsevier Saunders; 2016: 639-641.
6. Pekkarinen H, Airas N, Savolainen LE, et a. Non-tuberculous Mycobacteria can Cause Disseminated Mycobacteriosis in Cats. *J Comp Path*. 2018; 160:1-9.
7. Roth A, Reischl U, Streubel A, et al. Novel diagnostic algorithm for identification of mycobacteria using genus-specific amplification of the 16S-23S rRNA gene spacer and restriction endonucleases. *J Clin Microbiol*. 2000:38: 1094-1104.
8. Schafbuch R, Tinkler S, Lim CK, et al. Disseminated mycobacteriosis caused by Mycobacterium kansasii in a pot-bellied pig. *J Vet Diagn Invest*. 2018:30: 646-650.
9. Thorel MF, Huchzermeyer HF, Michel AL. *Mycobacterium avium* and *Mycobacterium intracellulare* infection in mammals. *Rev Sci Tech*. 2001:20: 204-218.

CASE II:

Signalment:
11-yr-old, F/S, Canine, Labrador cross

History:
The dog was diagnosed with suspected immune-mediated keratitis 2 months prior. The dog did very well with treatment for 1.5 months but developed prominent thickening of the scleral wall and infiltrative keratitis laterally. A computed topography (CT) scan also showed severe thickening of the scleral wall without extraorbital irregularities. Due to pain, blindness and now a failure to respond to treatment, enucleation was performed.

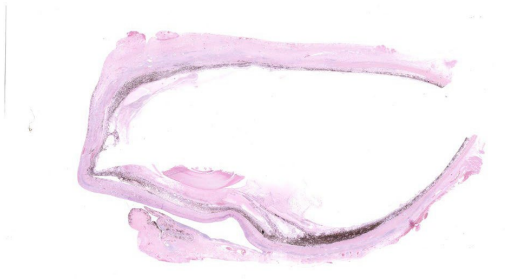

Figure 2-1. Globe, dog. A tangential section of the globe is presented for examination, with one iris leaflet, one fragment of the lens, no retina, and no optic nerve present in the section. There is an inflammatory exudate within the cornea, uvea, choroid, and sclera, and a hemorrhagic inflammatory within the anterior segment. (HE, 5X)

Gross Pathology:
The right eye was submitted, and no obvious mass was observed in parasagittal bisections.

Laboratory Results:
No laboratory findings reported.

Microscopic Description:
Right eye: The corneal stroma is infiltrated by large numbers of lymphocytes and plasma cells with fewer neutrophils, small amounts of extracellular melanin pigment and scattered melanophages. The stroma has significant corneal neovascularization, and at the limbus, some corneal epithelial cells have intraepithelial melanin pigment. The remainder of the corneal epithelium is irregularly hyperplastic or eroded, and there are small numbers of interepithelial neutrophils and scattered apoptotic epithelial cells. The sclera is markedly thickened and broadly infiltrated by abundant macrophages, neutrophils, plasma cells, and lymphocytes accompanied by small amounts of necrotic cellular debris and many, large lymphoid aggregates. The scleral

collagen is separated in areas (collagenolysis). The basement membrane separating the choroid and sclera is often obscured by inflammation, which extends into the choroid and vitreous chamber, and aggregates of melanocytes infiltrate the sclera. Multifocal scleral vessel walls are infiltrated by the inflammation (vasculitis), and one vessel is filled with organized fibrin (thrombus). The retina is detached, but obvious tomb-stoning of underlying pigmented epithelium is not apparent (possible artifactual retinal detachment). In addition to abundant large foamy macrophages and neutrophils within the vitreous chamber, there are also aggregates of erythrocytes, fibrin and flocculent eosinophilic material. The iris and ciliary body are expanded by similar inflammation and the anterior iris epithelium is covered by a 2-5 cell layer thick fibrovascular membrane (preiridal fibrovascular membrane), which is adhered to the cornea (anterior synechia) and spreads across the entirety of Descemet's membrane. Additionally, the posterior iris is adhered to the lens (posterior synechia; lens is not within provided sections). The iridocorneal filtration angle and uveal trabecular meshwork are unapparent due to the anterior synechiae, and infiltration by inflammatory cells. The conjunctival propria has multifocal to coalescing aggregates of lymphocytes and plasma cells, generally superficial and periadnexal.

Special stains: No organisms were detected in serial sections stained with Fite's acid fast or Grocott's methenamine silver stains.

Contributor's Morphologic Diagnoses:

1. Scleritis, histiocytic, neutrophilic, lymphoplasmacytic and necrotizing, chronic, severe, with vasculitis, choroiditis, endophthalmitis, anterior uveitis, anterior and posterior synechiae, and closure of the iridocorneal filtration angle
2. Keratitis and conjunctivitis, lymphoplasmacytic, chronic, moderate, with corneal erosion and neovascularization

Contributor's Comment:

The histologic features are compatible with granulomatous/necrotizing scleritis. Not all submitted slides show all the histologic changes (e.g. retina and lens are absent in most slides), and the audience is urged to focus on the scleral, corneal and uveal changes.

Idiopathic necrotizing/ granulomatous scleritis is a condition manifested as a bilateral, progressive, inflammatory disease of the sclera and cornea that induces significant uveitis, most commonly in dogs, but has been diagnosed in a cat and 2 birds.[4,5] Grossly, the affected area of sclera is usually thickened and solid white, representing the granulomatous infiltrate. The histologic lesions of granulomatous scleritis are characterized by vasculitis, collagen degeneration/collagenolysis, granulomatous inflammation (histiocytes/tissue macrophages) and perivascular lymphoplasmacytic aggregation.[2,4,5] There may be a suppurative component, or in chronic scleritis, a lymphoplasmacytic component may predominate. Less commonly, the sclera may be thin and have dramatic staphylomas associated with a more lymphocyte-rich infiltrate. Retinal detachment is a possible sequela to granulomatous/necrotizing scleritis. A diagnosis of scleritis in one eye implies that the second eye is at risk of developing scleritis. Idiopathic canine necrotizing scleritis shares similar histopathologic features with non-necrotizing scleritis (trauma or foreign-body related) and episcleritis, but these diseases are generally unilateral.[5]

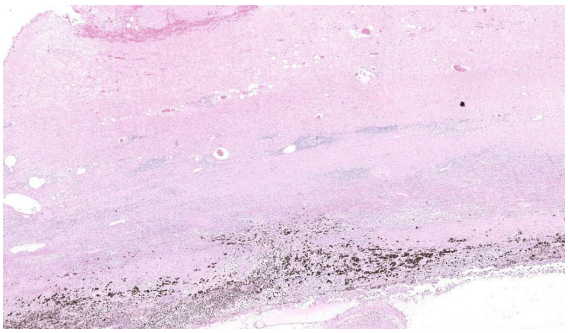

Figure 2-2. Globe, dog. There is no visible division between the sclera and uvea and uveal melanocytes have migrated into the sclera. (HE, 154X)

In humans, granulomatous scleritis has been associated with other autoimmune conditions such as rheumatoid arthritis, systemic lupus erythematosus, Wegener's granulomatosis, inflammatory bowel disease and Reiter's syndrome, but this has not been a consistent feature of reported canine cases.[2,5,7,10-13] In humans, necrotizing scleritis is regarded as a type III hypersensitivity reaction (immune complexes), as well as combined with a type IV hypersensitivity.[1,3,6] The condition in dogs is thought to be immune-mediated, and one study demonstrated IgG deposition within blood vessel walls in one dog, suggestive of an immune-complex component (type III hypersensitivity).[2] A primary type IV hypersensitivity was proposed, in addition to an underlying type III hypersensitivity, based on vascular/perivascular granulomatous to lymphoplasmacytic inflammation. This study described a prominent population of T lymphocytes, and proposed that CD4+ T lymphocytes are responsible for the tissue destruction in this disease. However, another study described a mixed population of lymphocytes (B lymphocytes predominated), which may also support the type III sensitivity involvement theory.[4] Response to medical therapy with corticosteroids (topical, systemic) or other immunomodulators such as azathioprine have been reported and also supports an immune-mediated etiology, but relapses and complications resulting in blindness occur frequently. Since little is known about the pathogenesis of idiopathic necrotizing scleritis in dogs, and there are few, somewhat contrasting reports in the literature, comparing the disease to human scleritis may not be appropriate.

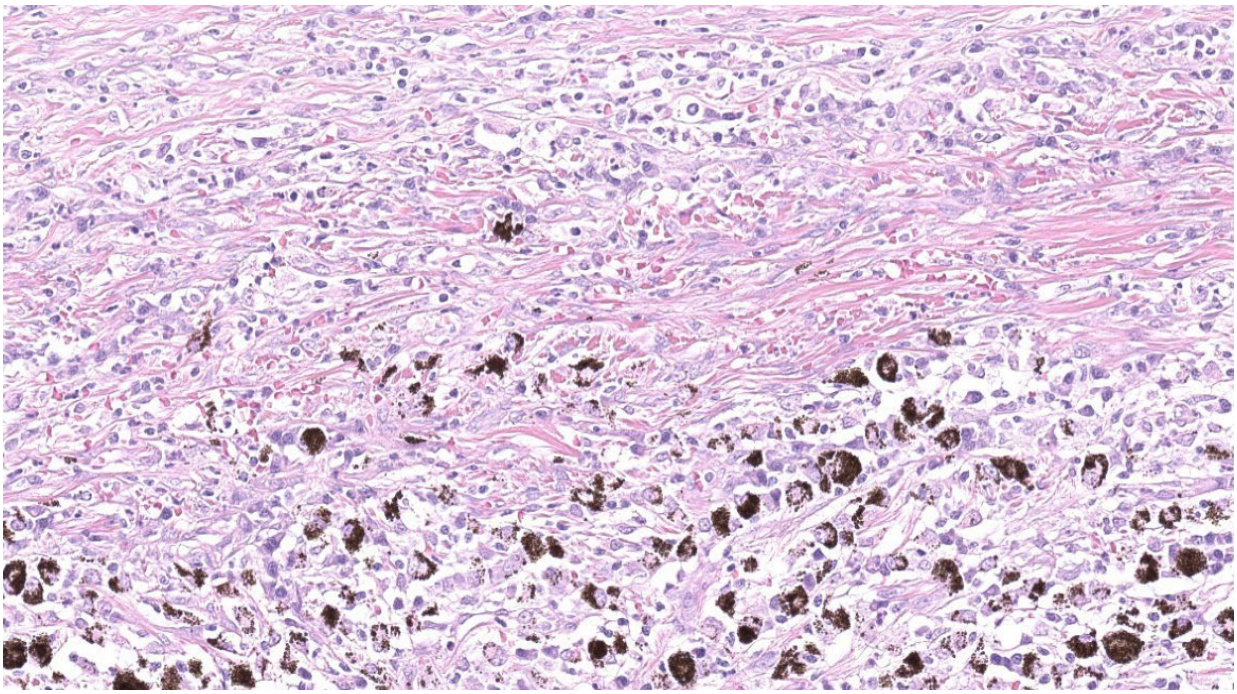

Figure 2-3. Globe, dog. There is infiltration of innumerable macrophages separating scleral collagen and migration of uveal melanophages into the sclera. (HE, 381X)

Contributing Institution:
Washington Animal Disease Diagnostic Lab
College of Veterinary Medicine, Washington State University
http://waddl.vetmed.wsu.edu/

JPC Diagnosis:
1. Eye: Scleritis, collagenolytic, lymphoplasmacytic, chronic, diffuse, severe, with keratitis, panuveitis, anterior synechia, fibrovascular membranes, and hyphema.
2. Conjunctiva: Conjunctivitis and dacryoadenitis, lymphoplasmacytic, chronic, multifocal, moderate.

JPC Comment:
This case provides a classic example of the relatively rare condition necrotizing granulomatous scleritis, and the contributor succinctly describes this condition in veterinary species as well as similar diseases in humans. Two differential diagnoses that may be considered during clinical and histopathologic examination are episcleritis and non-necrotizing granulomatous scleritis. Additional differential diagnoses for granulomatous disease include bacterial, acid-fast, and fungal infections, which were not observed on special stains in this case.

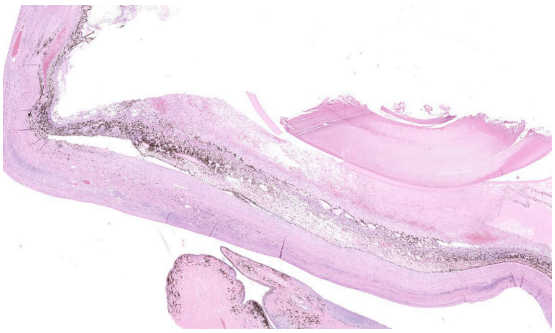

Figure 2-4. Globe, dog. There is occlusion of the drainage angle and adhesion of the iris leaflet to the choroid. The iris leaflet is expanded by edema and numerous macrophages, and there is a thin pre-iridal fibrovascular membrane. Numerous inflammatory cells, hemorrhage, and fibrin adhere to the posterior surface of the iris. (HE, 14X)

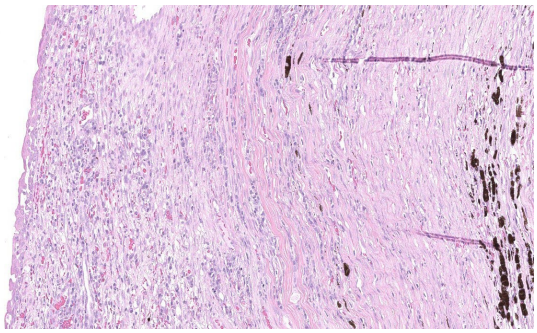

Figure 2-5. Globe, dog. The cornea is infiltrated by large numbers of macrophages. There is proliferation of vessel within the corneal stroma and mild squamous hyperplasia of the central corneal epithelium. (HE, 190X)

Episcleritis can occur secondary to severe intraocular or systemic disease, or may be a primary condition, such as in nodular granulomatous episcleritis (NGE), an inflammatory disease affecting the episcleral and adjacent conjunctiva.[6] NGE is more common and has a slower onset than necrotizing granulomatous scleritis. Single or multiple nonpainful elevated fleshy masses develop near the limbus or nictitating membrane and may extend into the adjacent cornea. A recent report described three cases of atypical NGE where the inflammatory infiltrate was limited to the corneal stroma and did not extend into the episclera or conjunctiva; the histologic appearance otherwise was consistent with NGE.[9] Severe cases of NGE may cause exophthalmos.[14] While both nodular granulomatous episcleritis and necrotizing granulomatous scleritis feature histiocytes admixed with lymphocytes and plasma cells, the episcleritis nodules are discrete (compared to the invasive nature of necrotizing scleritis) and lack collagenolysis.[15]

Non-necrotizing granulomatous scleritis also lacks the collagenolysis and perivascular necrosis seen with the necrotizing version of the disease. Additionally, chronic cases may feature fibrosis or formation of cystic spaces, and in general, it is generally milder than its necrotizing counterpart.[8,14] Otherwise, non-necrotizing granulomatous scleritis causes a

similar spectrum of clinical signs, including ocular pain, and can infiltrate to other structures in the eye, causing keratitis, uveitis, and choroiditis, as seen in this case.

References:

1. Akpek EK. Necrotizing Scleritis: Diagnosis and therapy. The Ocular Immunology and Uveitis Foundation. 1994; I(3). Accessed May 25, 2018. https://uveitis.org/wp-content/uploads/2017/05/necrotizing_scleritis_diagnosis_therapy.pdf
2. Day MJ, Mould JR, Carter WJ. An immunohistochemical investigation of canine idiopathic granulomatous scleritis. *Vet Ophthalmol*. 2008;11(1):11-7.
3. De la Maza MS, Tauber J, Foster CS. Immunological considerations of the sclera. In: *The sclera*. New York, NY: Springer; 2012: 33-58.
4. Denk N, Sandmeyer LS, Lim CC, Bauer BS, Grahn BH. A retrospective study of the clinical, histological, and immunohistochemical manifestations of 5 dogs originally diagnosed histologically as necrotizing scleritis. *Vet Ophthalmol*. 2012;15(2):102-9.
5. Dubielzig RR, Ketring K, McLellan GJ, and Albert DM. Diseases of the Cornea and Sclera. In: *Veterinary Ocular Pathology: a comparative review*. Philadelphia, PA: Saunders Elsevier; 2010: 201-243.
6. Gan, YK, Ahmad SS, Alexander SM, Samsudin A. Acute anterior necrotizing scleritis: A case report. *J Acute Dis*. 2016:5(5): 439-41.
7. Ghanchi FD, Rembacken BJ. Inflammatory bowel disease and the eye. *Surv Ophthalmol*. 2003;48(6):663-676.
8. Grahn BH, Sandmeyer LS. Canine Episcleritis, Nodular Episclerokeratitis, Scleritis, and Necrotic Scleritis. *Vet Clin Small Anim*. 2008; 38:291-308.
9. Hamzianpour N, Heinrich C, Gareth Jones R, et al. Clinical and pathological findings in three dogs with a corneocentric presentation of nodular granulomatous episcleritis. *Vet Ophth*. 2019: 1-9.
10. Harper SL, Letko E, Samson CM, Zafirakis P, et al. Wegener's granulomatosis: the relationship between ocular and systemic disease. *J Rheumatol*. 2001;28(5):1025-32.
11. Heiligenhaus A, Dutt JE, Foster CS. Histology and immunopathology of systemic lupus erythematosus affecting the conjunctiva. *Eye (Lond).*1996; 10(4):425-32.
12. Kiss S, Letko E, Qamruddin S, Baltatzis S, Foster CS. Long-term progression, prognosis, and treatment of patients with recurrent ocular manifestations of Reiter's syndrome. *Ophthalmology*. 2003;110(9):1764-9.
13. Reddy SC, Rao UR. Ocular complications of adult rheumatoid arthritis. *Rheumatol Int*. 1996;16(2):49-52.
14. Whitley RD, Hamor RE. Diseases and Surgery of the Canine Cornea and Sclera. In: Gelatt KN, ed. *Veterinary Ophthalmology.* Vol 1. 6th ed. Hoboken, NJ: Wiley Blackwell; 2021.1153-1155.
15. Wilcock BP, Njaa BL. Special Senses. In: Maxie MG, ed. *Jubb, Kennedy, and Palmer's Pathology of Domestic Animals*. Vol 1. 6th ed. Philadelphia, PA: Elsevier Saunders; 2016: 407-508.

CASE III:

Signalment:

Tissue from a 9-year-old neutered female German Shepherd dog (*Canis lupus familiaris)*

History:

The patient was presented for bilateral hind limb ataxia. MRI showed an intramedullary spinal cord lesion at L 4-5. Additional masses on the body wall found with ultrasound. Specimens of spleen and mammary gland samples were submitted in addition to spinal

cord, and were diagnosed as nodular lymphoid hyperplasia and benign mixed mammary tumor (not shown).

Gross Pathology:
Several cross-sections of lumbar spinal cord contained soft, reddish brown, tissue affecting the gray matter bilaterally.

Laboratory Results:
No laboratory findings reported.

Microscopic Description:
Much of the spinal cord gray matter and the ventrolateral white matter are soft and malacic. The tissue architecture is obliterated, with endothelial hypertrophy and hyperplasia of remaining blood vessels. Gitter cells fill some of the tissue spaces. The ventral spinal artery is obliterated by a large lumenal thrombus. It and the arteries extending up along the ventral median fissure are blocked by large round cells. Wallerian degeneration affected much of the ventral white matter. Cells are characterized by scant amphophilic cytoplasm and a large cleaved to reniform nuclei. The chromatin is arranged in coarse, irregular clumps; nuclear outlines are very irregular. Intravascular mitoses are present in the population. These cells are not present in smaller blood vessels. A less severely affected section of spinal cord has ventral white matter Wallerian degeneration, with a smaller ventral spinal artery filled with organisms. Two of the spinal nerves are degenerate and inflamed, with several radicular vessels being blocked (not shown). Lymphoplasmacytic inflammation occurs in the meninges and in perivascular cuffs near malacic spinal cord (also in affected roots). Intravascular tumor cells are immunohistochemically CD3 positive, demonstrated along cell membranes.

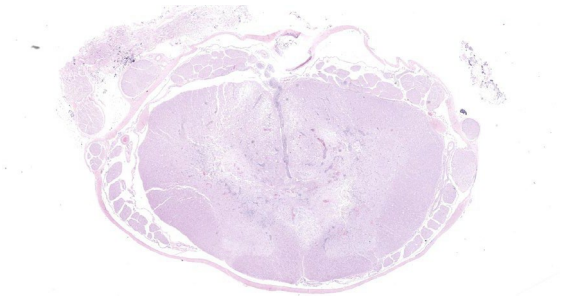

Figure 3-1. Spinal cord, dog. One section of spinal cord with numerous spinal nerve roots is submitted for examination. There are multiple areas of pallor, representing malacia, in the grey matter; in the white matter they are located primarily in the dorsal and ventral funiculi (HE, 7X)

Contributor's Morphologic Diagnoses:

1. Myelomalacia with ventral spinal and radicular artery tumor embolism
2. Intravascular lymphoma

Contributor's Comment:
At first glance the distribution of the spinal cord lesions brings to mind fibrocartilaginous embolism (FCE), due to the commonality of affected blood vessels (primarily the ventral spinal artery and branches, with infarction of the spinal gray matter.[3,6] However, both arteries and veins have been reported affected in FCE, while arteries and arterioles are affected in this case.

The presence of neoplastic cells in the ventral spinal artery and its branches is consistent with a diagnosis of large cell lymphoma, a tumor restricted to growth in the lumens of small- to intermediate-sized vessels.[7] This tumor would be described as the so-called classic form, with involvement primarily in the organ of presentation (usually brain or skin). A hemophagocytic syndrome-associated form can also occur in which patients present with multi-organ failure.[12] In humans, neoplastic cells express B cell markers (such as CD20 or CD79a). T-cell tumors are much less common,[14] but do occur. In people, neoplastic growth can occasionally extend across vascular walls, as in a few areas in this dog,

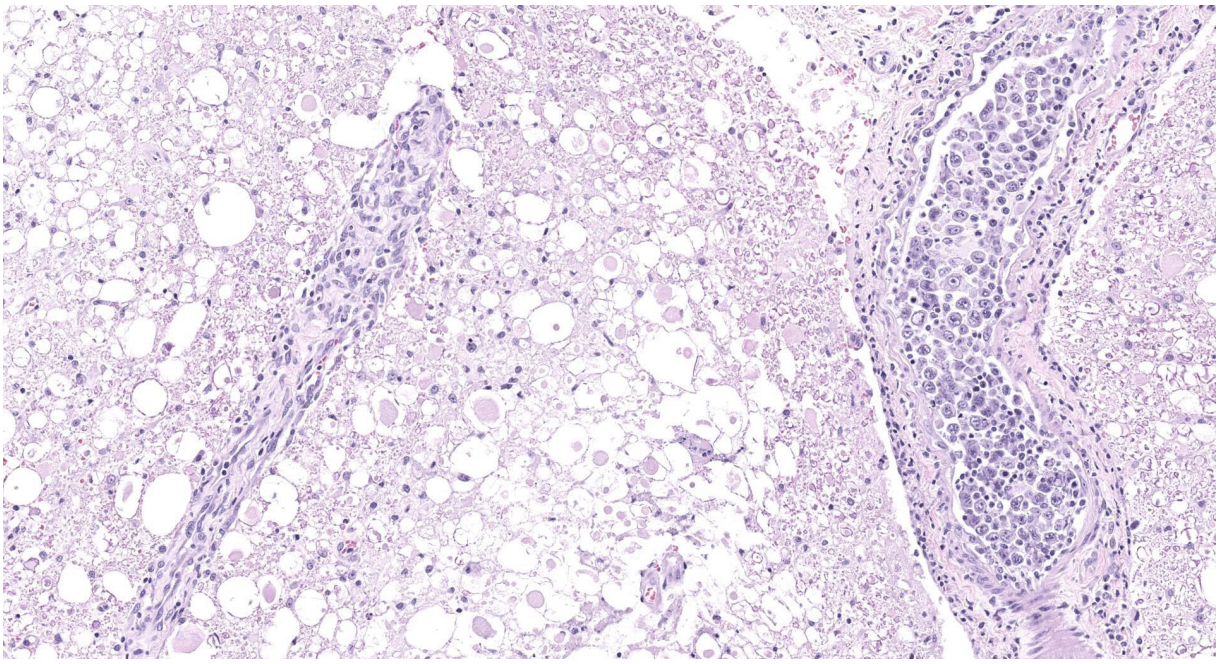

Figure 3-2. Spinal cord, dog. Meningeal and parenchymal vessels contain pleomorphic neoplastic lymphocytes. Vessel walls contain histiocytes, lymphocytes and plasma cells, and the adventitia is multifocally bounded by plump fibroblasts. Within the adjacent white matter, there are numerous dilated myelin sheaths, spheroids, myelin debris, and Gitter cells. (HE, 174X)

and can be mistaken for primary parenchymal lymphoma. T cell intravascular lymphomas are rare in humans and have been reported in dogs.[2,5,11] A tally of immunohistochemistry of intravascular lymphomas in 2 case series [2,5] revealed 11 T cell, 4 B cell and 10 Non-T non-B cell tumors. Most human tumor are of B cell origin.[7]

The intravascular location of tumor cells leads to thrombosis and infarction, which are responsible for clinical signs. Intravascular B cell lymphomas in people lack expression of surface adhesion molecules (e.g. cd29 and ICAM 1). Tumor cells proliferate within the blood vessels without being able to exit them, potentially occluding them and causing ischemia without tissue invasion. Cells also lack the expression of matrix metalloproteinase (MMP) 2 and MMP9 involved in the extravascular invasion of other lymphomas. Therefore, intravascular growth is associated with the inability of intravascular lymphoma cells to infiltrate extravascular tissues.[12]

Contributing Institution:
University of Missouri
https://vmdl.missouri.edu/

JPC Diagnosis:
1. Spinal cord, meningeal and parenchymal vessels: Intravascular lymphoma.
2. Spinal cord: Myelomalacia, multifocal to coalescing, moderate to marked, with thrombosis.

JPC Comment:
Historically, intravascular lymphoma in humans was known by the name malignant angioendotheliomatosis due to the unique histologic appearance mimicking proliferation of endothelial cells; however, clinical, immunohistochemical, ultrastructural, and therapeutic studies revealed the disease to be an angiotropic form of lymphoma.[4] In 1988, a case of angioendotheliomatosis in an adult German shorthaired pointer was also confirmed to be angiotropic lymphoma through ultrastructural and immunofluorescence investigation.[4] Since then, this disease has been reported

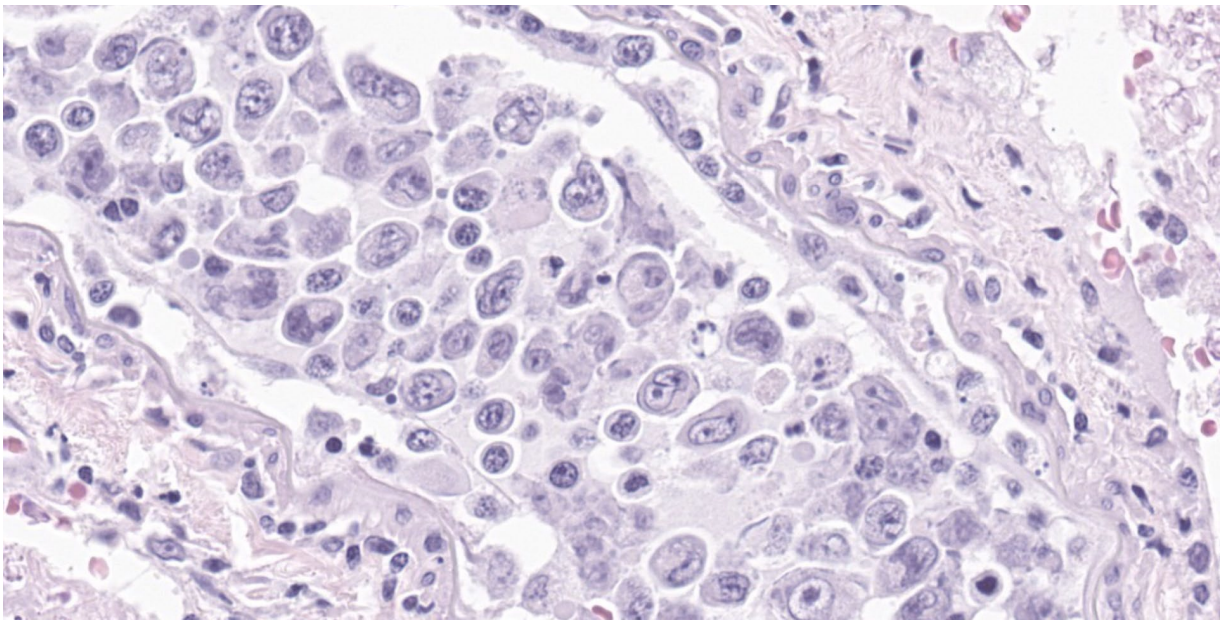

Figure 3-3. Spinal cord, dog. High magnification of neoplastic intravascular lymphocytes. There is moderate pleomorphism, and occasional apoptosis. (HE, 194X)

rarely in dogs, and even more rarely in cats and horses.[10]

Intravascular lymphoma most frequently affects the central nervous system and is characterized by rapidly progressive neurologic signs secondary to infarction with death occurring within weeks of initial clinical signs. Diagnosis is always made post-mortem. Rarely, neoplastic cells have been observed ante-mortem on peripheral blood smears or in cavitary effusions; however, even in these cases, refining the diagnosis beyond round cell neoplasm was not possible until post-mortem histopathology.[10,13] Differential diagnoses on histopathology include other round cell neoplasms which form a cuff around blood vessels, vaccine reactions, or systemic reactive angioendotheliomatosis.[15]

As the contributor described, neoplastic lymphocytes appear unable to exit blood vessels in this condition, and studies in human and veterinary patients illustrate altered expression of clusters of differentiation (CD) markers. In humans, neoplastic cells of intravascular lymphoma lack CD11a, 18, and 29 expression.[10]A study of canine intravascular lymphoma found that there was decreased CD29 expression and increased CD44 expression compared to canine primary/metastatic CNS lymphoma.[5] Some of these markers are critical during the leukocyte adhesion cascade and delivery of inflammatory cells to sites of inflammation.

Briefly, the leukocyte adhesion cascade has five steps which are partially propelled by cytokines: margination, rolling, integrin activation, stable adhesion, and transendothelial

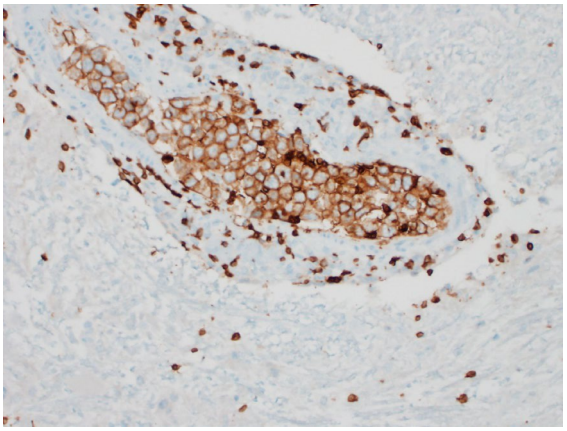

Figure 3-4. Spinal cord, dog. Neoplastic lymphocytes within meningeal vessels demonstrate strong membranous immunoreactivity for CD3. (anti-CD3, 400X)

migration.[1,9] Selectins are adhesion molecules which cause marginated leukocytes to slow and begin rolling, and integrins are adhesion molecules which then enforce firm adhesions between endothelial cells and leukocytes. CD11a/18 is the β2 integrin LFA-1 which binds intercellular adhesion molecules (ICAM) 1 and 2 (CD 54 and 102, respectively) on the endothelium during stable adhesion.[9] CD29 is found in β1 integrins (such as VLA-4) which facilitate leukocyte adhesion and transendothelial migration.[1,9] The previously noted alterations in expression of these markers in intravascular lymphoma provide some insight into the intravascular growth and lack of extravasation seen in this neoplasm.

References:

1. Ackermann MR. Inflammation and Healing. In: Zachary JF, ed. *Pathologic Basis of Veterinary Disease*. 7th ed. St. Louis, MO: Mosby Elsevier; 2021:104-170.
2. Bush WW, Throop JL, McManus PM, et al. Intravascular lymphoma involving the central and peripheral nervous systems in a dog. *J Am Anim Hosp Assoc*. 2003;39(1):90-96.
3. Cauzinille L, Kornegay JN. Fibrocartilaginous embolism of the spinal cord in dogs: review of 36 histologically confirmed cases and retrospective study of 26 suspected cases. *J Vet Intern Med*. 1996;10(4):241-245.
4. Dargent FJ, Fox LE, Anderson WI. Neoplastic angioendotheliomatosis in a dog: an angiotropic lymphoma. *Cornell Vet.* 1988; 78(3): 253-62.
5. Degl'Innocenti S, Camera ND, Falzone C, et al. Canine Cerebral Intravascular Lymphoma: Neuropathological and Immunohistochemical Findings. *Vet Pathol*. 2019;56(2):239-243.
6. Griffiths IR, Barker J, Palmer AC. Cholesterol masses in association with spinal cord infarction due to intervertebral disc emboli. *Acta Neuropathol*. 1975 Oct 27;33(1):85-88.
7. Grimm KE, O'Malley DP. Aggressive B cell lymphomas in the 2017 revised WHO classification of tumors of hematopoietic and lymphoid tissues. *Ann Diagn Pathol*. 2019;38:6-10.
8. Kawai S, Okuda T, Fukui A, et al. Intravascular Lymphoma Presenting as a Cavernous Sinus Tumor. *Intern Med*. 2019;58:2085-2089.
9. Kuman V, Abbas AK, Aster JC, eds. Inflammation and Repair. In: *Robbins & Cotran Pathologic Basis of Disease.* 10th ed. Philadelphia, PA: Elsevier, Inc; 2021: 71-114.
10. Lane LV, Allison RW, Rizzi TR, et al. Canine intravascular lymphoma with overt leukemia. *Veterinary Clinical Pathology.* 2012; 41(1): 84-91.
11. McDonough SP, Van Winkle TJ, Valentine BA, et al. Clinicopathological and immunophenotypical features of canine intravascular lymphoma (malignant angioendotheliomatosis). *J Comp Pathol*. 2002; 126(4):277-88.
12. Poropatich K, Dittmann D, Chen YH, et al. A Small Case Series of Intravascular Large B-Cell Lymphoma with Unexpected Findings: Subset of Cases with Concomitant Extravascular Central Nervous System (CNS) Involvement Mimicking Primary CNS Lymphoma. *J Pathol Transl Med*. 2017;51(3):284-291.
13. Ridge L, Swinney G. Angiotropic intravascular lymphosarcoma presenting as bi-cavity effusion in a dog. *Australian Veterinary Journal.* 2204; 82(1): 616-618.
14. Setoyama M, Mizoguchi S, Orikawa T, et al. A case of intravascular malignant lymphomatosis (angiotropic large-cell lymphoma) presenting memory T cell phenotype and its expression of adhesion molecules. *J Dermatol*. 1992;19(5):263-9.

15. Valli VE, Bienzle D, Meuten DJ. Tumors of the Hemolymphatic System. In: Meuten DJ, ed. *Tumors in Domestic Animals.* 5th ed. Ames, IO: John Wiley & Sons, Inc; 2017: 203-321.

CASE IV:

Signalment:
19-year-old intact female rhesus macaque (*Macaca mulatta*)

History:
Several week history of inappetence, weight loss, and chronic non-regenerative hypochromic and microcytic anemia.

Gross Pathology:
The abdominal cavity contained ~1 liter of serosanguinous fluid. The mesentery and abdominal visceral serosa contain too numerous to count, multifocal-to-coalescing, pale tan-to-white, slightly raised, firm coalescing nodules ranging from 1-4 millimeters in diameter. The distal 2 cm of the ileum and proximal 1 cm of the paired ceca and colon are infiltrated and effaced by a poorly demarcated, highly infiltrative neoplasm. On cut surface, the lumen of the distal ileum is severely stenotic, with loss of normal intestinal mural stratification.

Laboratory Results:
Repeated CBC results indicated a chronic progressive hypochromic and microcytic non- anemia.
See Table 4-1

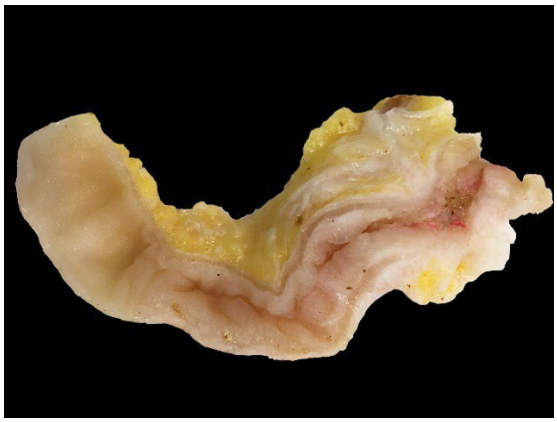

Figure 4-1. Ileum, rhesus macaque On cut surface, the lumen of the distal ileum is severely stenotic, with loss of normal intestinal mural stratification (Photo courtesy of: Boston University School of Medicine, National Emerging Infectious Diseases Laboratory http://www.bu.edu/neidl/)

Microscopic Description:
Distal ileum: In the sections submitted the submucosa, muscularis and serosa are multifocally effaced by an unencapsulated, poorly circumscribed, low-to-moderately cellular, infiltrative, highly pleomorphic epithelial neoplasm. Neoplastic cells are cuboidal-to-columnar and form both tubules and acini, with occasional formation of variably sized mucinous lakes surrounded by dense fibrous connective tissue stroma (desmoplasia). Formation of signet ring cells (epithelial cell with a large, clear cytoplasmic vacuole that peripheralizes the nucleus) is occasionally observed. Stroma is infiltrated by lymphocytes and lesser numbers of histiocytes. Neoplastic cells exhibit marked anisocytosis and anisokaryosis, have variably distinct cells borders and a moderate amount of granular, eosinophilic cytoplasm. Nuclei are round to oval with one or two distinct nucleoli. The

Table 4-1: CBC Parameters		
WBC (K/uL)	13.6	7.72–9.17
RBC (M/uL)	5.3	6.24–6.73
HGB 9G/dL)	5.7	12.03–12.95
HCT (%)	22.2	41.90–44.77
MCV (fL)	42	66.02–68.02
MCH (pg)	10.8	18.84–19.81
MCHC (g/dL)	25.7	28.32–29.29
Reticulocyte (%)	4.9	1.44+/-0.46
Absolute Reticulocyte (K/uL)	260	79.8+/-24.3
Nucleated RBC (/100 WBC)	None seen	

Figure 4-2. Mesentery, rhesus macaque The mesentery and abdominal visceral serosa contain too numerous to count, multifocal-to-coalescing, pale tan-to-white, slightly raised, firm coalescing nodules ranging from 1-4 millimeters in diameter. (Photo courtesy of: Boston University School of Medicine, National Emerging Infectious Diseases Laboratory (http://www.bu.edu/neidl/)

mitotic rate ranges from 1-4/HPF. Transmurally lymphatics are markedly ectatic (lymphangiectasia) as indicated by large clear spaces neoplastic cells display cytoplasmic immunoreactivity to pancytokeratin supportive of epithelial origin.

Mesentery: Similar neoplastic epithelial cells as described infiltrating the wall of the ileum efface and expand the mesentery, with scattered patches of retained adipocytes and mesenteric blood vessels.

Contributor's Morphologic Diagnosis:
Ileocecocolic junction adenocarcinoma (scirrhous, mucus producing) with lymphangiectasia, and abdominal carcinomatosis

Contributor's Comment:
In humans, gastrointestinal carcinomas are relatively common, but most of these arise in the colon and rectum with only a small percentage in the small intestine and ileum.[1] Furthermore, large intestinal neoplasia in the rhesus macaque is believed to be significantly different from that in humans due to the absence of polyp formation, although there are similarities in histologic appearance and immunohistochemical characteristics.[1] In contrast, the ileocolic junction is considered a common site for intestinal adenocarcinomas in aged rhesus macaques and has also be described in the duodenum, jejunum, distal ileum, cecum, and colon.[1,5,10] Cotton-top marmosets are unique among NHPs as they often develop adenocarcinomas in response to chronic inflammation of the colon, including the cecum–colon, and rectum.[1] The most commonly reported site of metastasis of intestinal adenocarcinoma in NHPs is the regional mesentery lymph nodes, with colonic and thoracic lymph nodes, peritoneum, diaphragm, intercostal muscles, kidneys, adrenal glands, liver, lung, and spleen also having been reported.[1,5] Representative specimens of the mesentery and intestinal neoplasm were the only tissues submitted for histopathologic examination from this case and thus we cannot rule out the possibility of previously described metastatic locations.

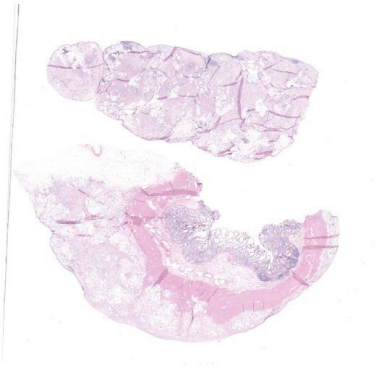

Figure 4-3. Ileum and mesentery, rhesus macaque. A section of ileum is presented with marked expansion of the submucosa and serosa at subgross magnification. There is loss of normal mesenteric architecture as well. (HE, 0.4X)

Surgical excision with intestinal resection and anastomosis remains the preferred treatment for intestinal adenocarcinoma in rhesus macaques. In a review article of the WNPRC breeding colony, 12% (3 of 25) of animals with surgical resection of intestinal adenocarcinomas were alive, with a mean survival time of 1.5 years.[1] The other 22 of 25 animals were euthanized due to deterioration of clinical health. Following necropsy of these animals, surgical excision was determined to be curative in 55% (12 of 22) of cases with no gross or histologic evidence of recurrence at the time of necropsy.

This case of ileocecocolonic adenocarcinoma is particularly impressive given that there was severe mesenteric and peritoneal seeding (carcinomatosis) that resulted in occlusion of lymphatics and subsequent lymphangiectasia. Neither a serum iron concentration or a fecal occult blood test were conducted in this case, but it is reasonable to attribute the chronic microcytic hypochromic anemia to a combination of G.I. hemorrhage, chronic inflammation resulting in sequestration of iron stores, as well as malabsorption due to the lymphangiectasia.

Contributing Institution:
Boston University School of Medicine, National Emerging Infectious Diseases Laboratory (http://www.bu.edu/neidl/)

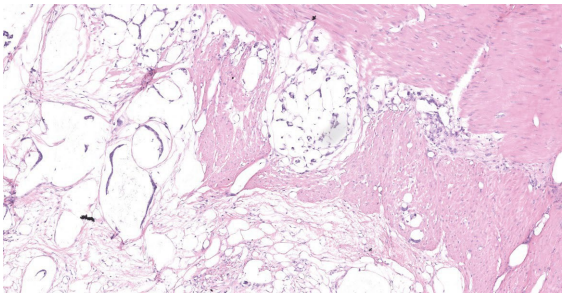

Figure 4-4. Ileum, rhesus macaque. The wall is transmurally infiltrated in this image, the outer longitudinal layer of the muscularis and the serosa by nests of neoplastic intestinal epithelium which produce abundant mucus. (HE, 94X)

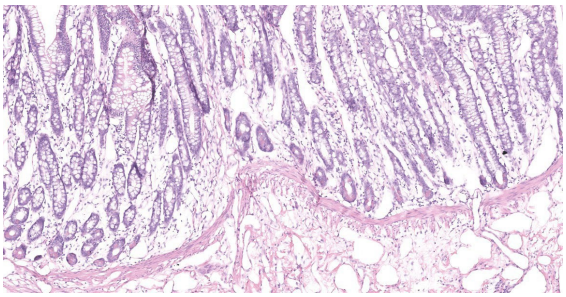

Figure 4-5. Ileum, rhesus macaque. The lamina propria and submucosa are markedly expanded by mucus-producing neoplastic epithelium. (HE, 94X)

JPC Diagnoses:
Ileocecocolic junction and mesentery: Mucinous adenocarcinoma.

JPC Comment:
Ileocecocolic adenocarcinoma is the most common gastrointestinal neoplasm in rhesus macaques and has also been reported in Japanese and cynomolgus macaques.[9] Clinical signs include weight loss, inappetence, bloating, hematochezia, and decreased fecal volume. Grossly, the annular appearance of intestinal adenocarcinoma may mimic chronic cicatrizing ulcerative colitis, an uncommon condition in macaques which also affects the cecum and colon and causes distension of the proximal intestinal segments.[6] These neoplasms invade transmurally and incite a pronounced desmoplastic response.[9] Prominent infiltrates of lymphocytes within and surrounding the tumor may be present.[4] In the mucinous subtype, which accounts for 25% of colonic adenocarcinomas in rhesus macaques, neoplastic cells produce abundant mucin which may impart a bubbly appearance grossly; histologically, neoplastic cells may accumulate mucin intracellularly, producing the signet ring appearance, or they may produce extracellular lakes of mucin which cause attenuation of surrounding cells.[4,6,10]

As the contributor stated, ileocecal/colonic adenocarcinomas in rhesus macaques differ from similar neoplasms in humans by the lack of polyp formation; however, a recent study suggests that at least one colony of rhesus macaques may be a suitable model for a certain type of hereditary colorectal cancer in humans.[4] Lynch syndrome, which can cause hereditary nonpolyposis colorectal cancer (HNPCC) in humans, is characterized by damage in any of the DNA mismatch repair (MMR) genes MSH2, MLH1, MSH6, or PMS2. [4] Humans with Lynch syndrome have higher risks of various neoplasms at a younger age, including neoplasms of the colon, endometrium, stomach, and small intestine. [4] Lynch syndrome can be diagnosed through identification of microsatellite instability, a phenomenon where unrepaired DNA errors occur in certain short repetitive DNA segments (microsatellites) due to MMR gene defects. Additionally, immunohistochemical staining can illustrate decreased reactivity of the MMR proteins in neoplastic cells. In a study of 60 spontaneous cases of colorectal cancer in one closed colony of rhesus macaques, 17 of 20 tested animals lacked MLH1 and PMS2 immunoreactivity, and 6 of 9 tested animals demonstrated microsatellite instability.[4] Whole genome sequencing also revealed strong association of colorectal cancer and mutations in MLH1 and MSH6 genes.[4] This study indicates that this colony of rhesus macaques could potentially supply investigative avenues for a human disease where current animal models are lacking. [4]

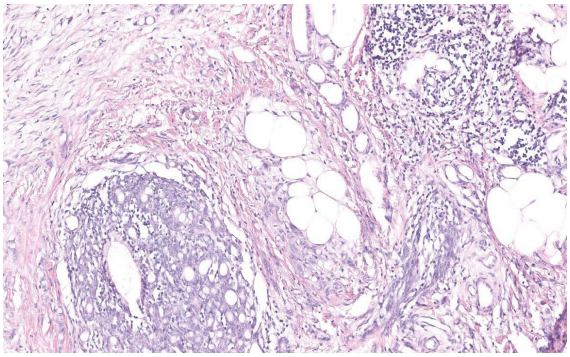

Figure 4-6. Mesentery, rhesus macaque. The mesentery is effaced by infiltrating, mucus-producing epithelial cells. (HE, 175X)

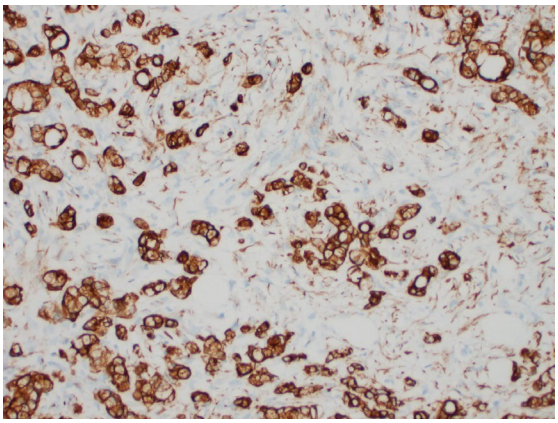

Figure 4-7. Mesentery, rhesus macaque. Neoplastic epithelial cells are strongly immunopositive for cytokeratin. (anti AE1/AE3, 400X)

References:

1. Beart RW, et al. Management and survival of patients with adenocarcinoma of the colon and rectum: a national survey of the Commission on Cancer. *J Am Coll Surg*. 1995; 181(3): 225-36.
2. Chalifoux LV, Bronson RT. Colonic adenocarcinoma associated with chronic colitis in cotton top marmosets, Saguinus oedipus. *Gastroenterology*. 1981; 80(5 pt 1): 942-946.
3. DePaoli A, McClure HM. Gastrointestinal neoplasms in nonhuman primates: a review and report of eleven new cases. *Vet Pathol.* 1982; 19 (Suppl 7): 104-125.
4. Dray BK, Raveendran M, Harris RA. Mismatch repair gene mutations lead to lynch syndrome colorectal cancer in rhesus macaques. *Genes & Cancer*. 2018; 9(3-4): 142-152.
5. Harbison CE, et al. Immunohistochemical Characterization of Large Intestinal Adenocarcinoma in the Rhesus Macaque (*Macaca mulatta*). *Vet Pathol*. 2015; 52(4): 732-40.
6. Johnson AL, Keesler RI, Lewis AD, Reader JR, Laing ST. Common and Not-So-Common Pathologic Findings of the

Gastrointestinal Tract of Rhesus and Cynomolgus Macaques. *Tox Pathol*. 2002; 50(5): 638-659.
7. Kerrick GP, Brownstein DG. Metastatic large intestinal adenocarcinoma in two rhesus macaques (*Macaca mulatta*). *Contemp Top Lab Anim Sci*. 2000; 39(4): 40-42.
8. Lang CD, et al. Adenocarcinoma of the ileocolic junction and multifocal hepatic sarcomas in an aged rhesus macaque (*Macaca mulatta*). *Comp Med*. 2013. 63(4): 361-366.
9. Miller AD. Neoplasia and Proliferative Disorders of Nonhuman Primates. In: Abee CR, Mansfied K, Tardif S, Morris T, eds. *Nonhuman Primates in Biomedical Research: Diseases*. Vol 2. 2nd ed. Waltham, MA: Elsevier; 2012: 325-356.
10. Simmons HA. Age-Associated Pathology in Rhesus Macaques (*Macaca mulatta*). *Vet Pathol*. 2016; 53(2): 399-416.

WSC 2022-2023 Self-Assessment
Conference 2

1. The most common form of inflammation associated with *M. avium var. hominisuis* in swine?
    a. Eosinophilic
    b. Granulomatous
    c. Suppurative
    d. Lymphoplasmacytic

2. Which of the following is not seen in granulomatous scleritis in dogs?
    a. Vasculitis
    b. Lymphoplasmacytic perivascular infiltrates
    c. Collagenolysis
    d. Mineralization

3. True or false? Intravascular lymphomas in dogs are most commonly of T-cell origin.
    a. True
    b. False

4. True or false. Neoplastic cells in intravascular lymphomas are unable to emigrate from vessels.
    a. True
    b. False

5. The most common site of metastasis of intestinal adenocarcinoma in rhesus monkeys is which of the following ?
    a. Regional lymph nodes
    b. Liver
    c. Spleen
    d. Bone

Please email your completed assessment for grading to Dr. Bruce Williams at bruce.h.williams12.civ@health.mil. Passing score is 80%. This program (RACE program 33611) is approved by the AAVSB RACE to offer a total of 0.5 CE Credits, with a maximum of 12.5 CE Credits being available to any individual Veterinary Medical Professionals for the 2019-2020 Wednesday Slide Conference. This RACE approval is for the subject matter categories of: SCIENTIFIC using the delivery method of NONINTERACTIVE DISTANCE. This approval is valid in jurisdictions which recognize AAVSB RACE.

Joint Pathology Center
Veterinary Pathology Services

WEDNESDAY SLIDE CONFERENCE 2022-2023

Conference #3 — 31 August 2022

CASE I:

Signalment:
2-year-old, male, C57/BL6 CuZnSOD wild type (*Mus musculus*)

History:
This mouse recently arrived at the facility and was housed in quarantine. Two days after arrival the mouse presented clinically with abdominal distension. On physical examination, a large abdominal mass was palpated, and humane euthanasia was elected.

Gross Pathology:
The mouse was in fair body condition (BCS 2.5/5). The lungs were mottled with patchy pale yellow to pink foci. Within the abdomen, there were three encapsulated masses associated with the mesentery that ranged in size from 0.5-2cm in diameter (gross photo, black asterisks). On cut section, the masses were abscessed. The liver and the spleen were diffusely enlarged.

Laboratory Results:
No laboratory findings reported.

Microscopic Description:
Throughout all lung lobes there are multifocal to coalescing inflammatory infiltrates filling alveolar spaces. Inflammatory infiltrates are primarily composed of large plump macrophages and multinucleated giant cells admixed with eosinophils and fewer lymphocytes, plasma cells, and neutrophils. Macrophages and multinucleated giant cells contain abundant intracytoplasmic brightly eosinophilic partially refractile acicular to rectangular crystals admixed with homogenous eosinophilic hyalinized material. Crystals and hyaline are also present within in the extracellular space. There are perivascular and peribronchiolar lymphoplasmacytic cuffs.

In the section of liver, there is marked proliferation of myeloid precursors primarily surrounding portal regions. Myeloid precursors

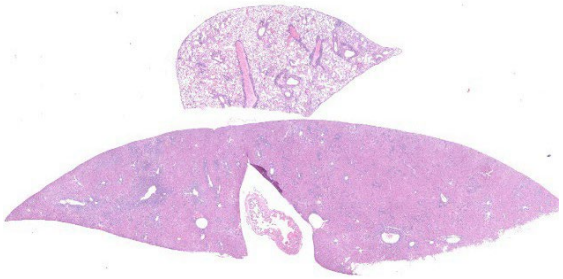

Figure 1-1. Lung, liver, mouse. A section of lung and liver are submitted for examination. At subgross magnification, there is diffuse expansion of peribronchiolar and perivascular areas by a cellular infiltrate and a focally extensive area of subpleural inflammation; the liver demonstrates expansion of portal areas and focally extensive thickening of the gallbladder mucosa. (HE, 7X)

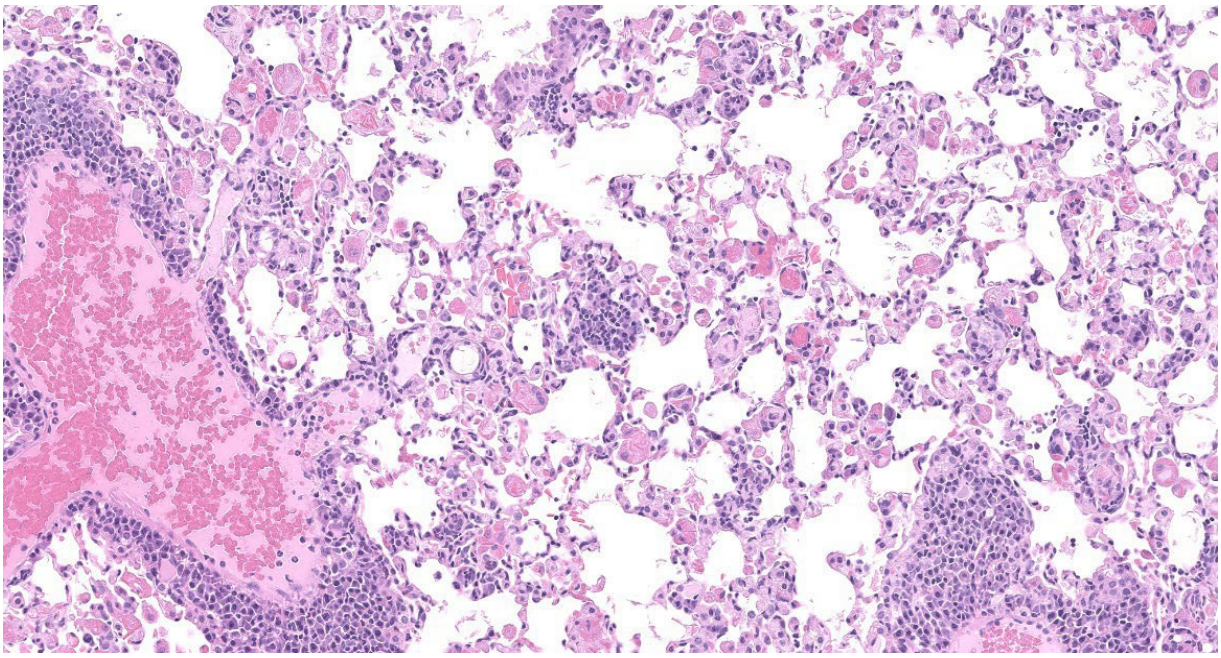

Figure 1-2. Lung, mouse. Alveolar lumina contain scattered aggregates of swollen eosinophilic macrophages and occasional large extracellular eosinophilic crystals; there are numerous plasma cells and fewer lymphocytes and macrophages in perivascular areas. (HE, 181X)

infiltrate into the parenchyma and bridge adjacent portal tracts. Hepatic cords are attenuated. The biliary and gall bladder epithelium are expanded by intracytoplasmic eosinophilic hyalinized material. There are acicular and rectangular crystals within the gall bladder.

Contributor's Morphologic Diagnoses:
Lung: Eosinophilic and granulomatous pneumonia, chronic, severe, with eosinophilic crystals.
Liver and spleen: Myeloid hyperplasia, marked, diffuse.
Bile ducts/gall bladder: Epithelial hyalinosis, marked, multifocal.

Contributor's Comment:
Eosinophilic crystalline pneumonia (ECP), also known as acidophilic macrophage pneumonia, is a common age-related background lesion in C57/BL6 and 129/Sv mice and in many of their knockout and transgenic derivatives.[5,7,9] This lesion can be exacerbated during concurrent pulmonary disease, and has been reported in association with systemic infectious, neoplastic, hypersensitivity, and lymphoproliferative disorders.[5] Eosinophilic crystals are derived from macrophages and are primarily composed of iron, alpha-1 antitrypsin, immunoglobulin, and granulocyte breakdown products.[2,6] In addition to accumulation within macrophages and the lung, this protein can also accumulate within epithelial cells of the pancreas, stomach, liver and gallbladder, and the olfactory epithelium.[2,4] Of note, in addition to ECP and epithelial hyalinosis, this mouse also had multiple abdominal abscesses and myeloid hyperplasia in the spleen, kidney, and liver. Thus, it was determined that the severe ECP in this case was likely due to age and exacerbated by chronic systemic inflammation.

Contributing Institution:
In Vivo Animal Core, University of Michigan, Unit for Laboratory Animal Medicine
https://animalcare.umich.edu/business-services/vivo-animal-core
ulam-ivac@umich.edu

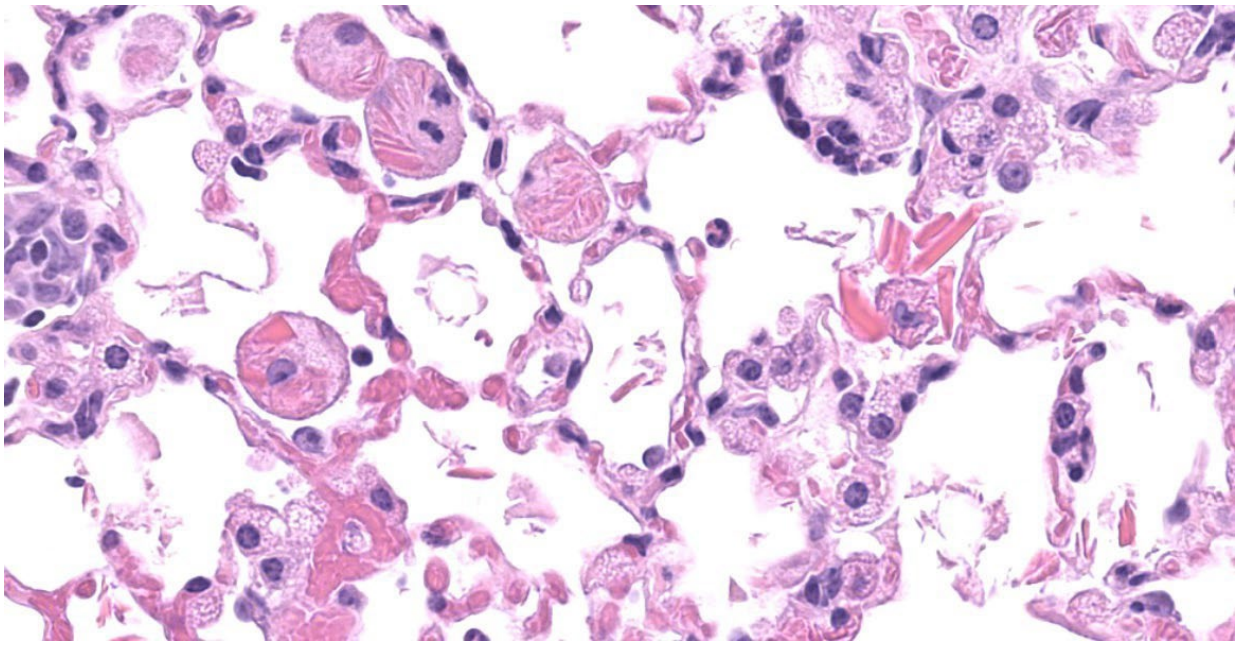

Figure 1-3. Lung, mouse. Macrophages contain large oblong to needle-shaped eosinophilic crystals within their cytoplasm; similar crystals are also freely present in the alveolar lumina. (HE, 715X)

JPC Diagnoses:

1. Lung: Alveolitis, granulomatous, diffuse, moderate, with intrahistiocytic and extracellular eosinophilic crystals and perivascular plasmacytosis.
2. Liver, gallbladder: Biliary epithelial hyalinosis and extracellular crystals, diffuse, severe.
3. Liver: Extramedullary hematopoiesis, diffuse, severe.

JPC Comment:

As the contributor mentions, eosinophilic crystalline pneumonia occurs regularly in aged B6 mice and has a more rapid onset in the moth-eaten phenotype of B6 mice.[2] Moth-eaten strains have a deficiency of Shp1, a protein tyrosine phosphatase involved in the immune signaling pathways of multiple hematopoietic cell types, due to a spontaneous mutation of Ptpn6.[1] In the lung, Shp1 deficiency is associated with the rapid accumulation of eosinophilic crystals within pulmonary macrophages, while in the skin, Shp1 deficiency results in neutrophilic inflammation and dendritic-cell driven autoimmunity producing chronic dermatitis and alopecia, the basis of the "moth-eaten" designation.[1,10] Other strains which are predisposed to hyalinosis include female CYP1A2-null mice and female 129S4/SvJae mice, with one study documenting hyalinosis of the glandular stomach in over 95% and 45% of these strains, respectively.[10] These mice had grossly visible plaque-like lesions in the cardia; histologically, there was disorganization, hyperplasia, and hyalinization of gastric epithelial cells and abundant extracellular eosinophilic crystals.[10]

Grossly, ECP causes firm pale tan lesions in the lung which fail to collapse.[8] Affected

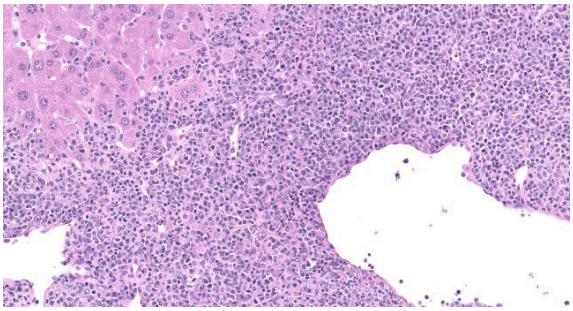

Figure 1-4. Liver, mouse. There is marked extramedullary hematopoiesis within perivascular areas on the liver. (HE, 247X)

gallbladders may have mural thickening and opacification with bile duct fibrosis.[10]

In addition to the components listed by the contributor, eosinophilic crystals contain Ym1 (eosinophilic chemotactic factor) and Ym2, two closely related chitinases with different patterns of distribution throughout the body.[2,10] Pulmonary lesions primarily contain Ym1, and other organ systems contain a mixture of both Ym1 and Ym2.[2]

Differential diagnoses for ECP include pulmonary histiocytosis, which typically occurs in the subpleural regions, or alveolar lipoproteinosis, may contain granular eosinophilic material (surfactant) and scattered macrophages.[2] Hemorrhage can lead to extracellular hemoglobin crystal formation.[2,3] Eosinophilic crystals have also been seen in particulate inhalation studies, *Cryptococcus neoformans* infections in mice, and some dietary toxicity and drug studies in rats.[3]

References:

1. Abram CL, Roberge GL, Pao LI, Neel BG, Lowell CA. Distinct roles for neutrophils and dendritic cells in inflammation and autoimmunity in motheaten mice. *Immunity*. 2013;38: 489-501.
2. Barthold SW, Griffey SM, Percy DH. Pathology of Laboratory Rodents and Rabbits. 4th ed. Ames, IO: Wiley Blackwell; 2016: 3,94-95,100.

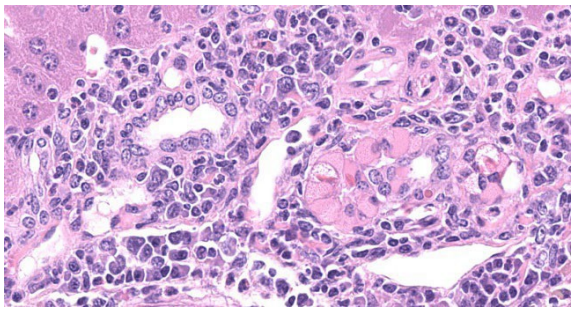

Figure 1-5. Liver, mouse. Multifocally, biliary epithelium in portal areas is markedly swollen with eosinophilic cytoplasmic granules. (HE, 720X)

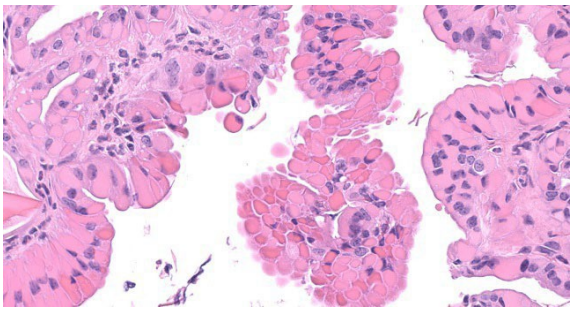

Figure 1-6. Gallbladder, mouse. Gallbladder epithelium is segmentally expanded by epithelium with pink to bright red cytoplasmic granules. (HE, 520X)

3. Cesta MF, Dixon D, Herbert RA, Staska LM. Lung – Crystals. US Department of Health and Human Services National Toxicology Program Nonneoplastic Lesion Atlas. Accessed 11 August 2022. https://ntp.niehs.nih.gov/nnl/respiratory/lung/crystal/index.htm
4. Giannetti N, Moyse E, Ducray A, et al. Accumulation of Ym1/2 protein in the mouse olfactory epithelium during regeneration and aging. *Neuroscience*. 2004;123: 907-917.
5. Hoenerhoff MJ, Starost MF, Ward JM. Eosinophilic crystalline pneumonia as a major cause of death in 129S4/SvJae mice. *Vet Pathol*. 2006;43(5).
6. Klug JJ, Snyder JM. Eosinophilic crystalline pneumonia, an age-related lesion in mice. *Aging Pathobiol Ther*. 2020;2: 232-233.
7. Murray AB, Luz A. Acidophilic Macrophage Pneumonia in Laboratory Mice. *Vet Pathol*. 1990;27(4).
8. Pettan-Brewer C, Treuting PM. Practical pathology of aging mice. *Pathobiol Aging Age Relat Dis*. 2011;1.
9. Radaelli E, Castiglioni V, Recordati C, et al. The Pathology of Aging 129S6/SvEv-Tac Mice. *Vet Pathol*. 2016;53(2): 477-492.
10. Ward JM, Yoon M, Anver MA, et al. Hyalinosis and Ym1/Ym2 Gene Expression in the Stomach and Respiratory Tract of 129S4/SvJae and Wild-Type and

CYP1A2-Null B6,129 Mice. *Am J Pathol.* 2001; 158(1):323-332.
11. Zhao T, Su Z, Li Y, Zhang X, You Q. Chitinase-3 like-protein-1 function and its role in diseases. *Signal Transduct Target Ther*. 2020;5: 201.

CASE II:

Signalment:
18-month-old male, *Apoe*^{tm1Unc} KO on C57BL/6 background (*Mus musculus*)

History:
This mouse was part of an atherosclerosis study and was transitioned to a Western high fat diet at 3-months of age. At 15-months, the mouse became pruritic and developed ulcerative dermatitis that wax and waned despite treatment. Humane euthanasia was elected at 18-months.

Gross Pathology:
The mouse was overly conditioned with a body condition score of 5/5. On external examination, there were deep skin erosions and ulcers on the right flank and left right forelimb that ranged in size from 1-4mm in diameter. The liver was diffusely enlarged and friable. The submandibular and renal lymph nodes were enlarged. The remainder of the postmortem examination was within normal limits.

Laboratory Results:

Figure 2-1. Heart and pinna, mouse. At subgross magnification, the pinna wall is markedly expanded and normal architecture is lost. (HE, 7X)

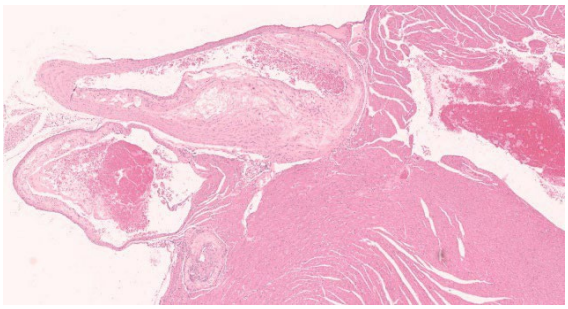

Figure 2-2. Heart base, mouse. The walls of the aorta, pulmonary artery and a subjacent coronary artery are segmentally to circumferentially expanded by lipid, forming clear clefts within the tunica intima and media. The lumen of the coronary artery is recanalized. (HE, 35X)

No laboratory findings reported.

Microscopic Description:
The aorta and pulmonary artery are segmentally narrowed due to luminal expansion by atherosclerotic subintimal plaques. Subintimal plaques occasionally extend into the tunica media and are composed of diffuse aggregates of acicular cholesterol cleft, plump foamy macrophages, multinucleated giant cells, and lymphocytes. There are rare foci of dystrophic mineralization and fibrosis.

In multiple sections of skin, the epidermis is necrotic and ulcerated and the dermis is expanded by granulation tissue which supports abundant acicular cholesterol clefts, plump foamy macrophages, multinucleated giant cells, and fewer lymphocytes and plasma cells. Inflammation and cholesterol deposits extend from the superficial dermis into the deep muscular layers and subcutis. Inflammation occasionally encompasses nerve bundles and skeletal muscle myofibers are atrophied. Adjacent to the ulcers the epidermis is acanthotic and there are superficial serocellular crusts.

Contributor's Morphologic Diagnoses:
Heart (pulmonary artery, aorta, and vessels): Atherosclerosis, segmental, moderate.
Skin: Ulcerative dermatitis with dermal xanthomatosis, chronic, multifocal, severe.

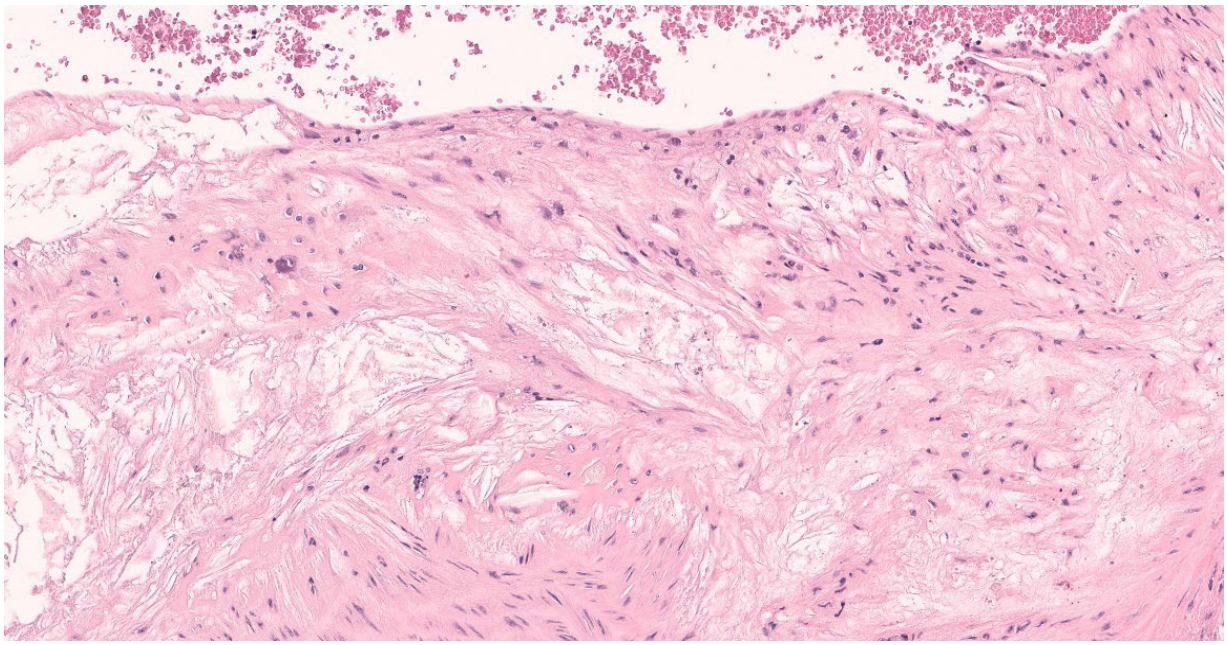

Figure 2-3. Aorta, mouse. There is marked disorganization of the aortic tunica intima and media. The wall is expanded by clefts of lipid and there is loss of the tunica intima, marked smooth muscle disarray, and fibrosis. (HE, 163X)

Contributor's Comment:

Apolipoprotein E deficient ($ApoE^{-/-}$) mice are useful for the study of mechanisms underlying cardiovascular disease and atherosclerosis, fat metabolism, and neurodegenerative diseases.[3,8,16] ApoE is a structural component of lipoproteins that regulates lipid homeostasis and facilitates lipid transport. It functions as a ligand in the transport of many lipid products, such as cholesterol and fat-soluble vitamins, between cells and tissue.

Hypercholesterolemia is the primary clinical pathology finding characteristic of $ApoE^{-/-}$ mice.[20] Subsequently, atherosclerosis and multicentric xanthomas (lipid mass-like accumulations) are well-recognized phenotypes of this model. Indeed, $ApoE^{-/-}$ mice can develop pre-atherosclerotic lesions, such as subintimal fatty streaks, in the proximal aorta as early as 3-months of age.[16] Of interest to the current case, chronic hypercholesterolemia can alter epidermal lipid composition which may impair innate immune defense barriers of the skin which is associated with foam cell deposition in the dermis in both humans and in mice.[1,9] Further, $ApoE^{-/-}$ mice fed a hypercholesterolemic diet exhibited xanthomatosis in many organs with a predilection for the subcutaneous and peritendinous tissues, similar to the skin lesions presented in this case. However, the ulcerative epidermal component in this mouse is somewhat unique.[18] Given the C57/BL6 background idiopathic ulcerative dermatitis (UD), a commonly reported entity associated with pruritis in aging C57/BL6 mice, was considered as a top differential clinically. Indeed, wild type C57/BL6 mice fed a high-fat diet had worsened UD lesions compared to mice on standard rodent chow.[5] In this case, it is suspected the implementation of a high fat diet exacerbated the lipogranulomatous dermal lesion and the presence of inflammation around nerve bundles may have contributed to the pruritis and subsequent ulcerative dermatitis noted clinically; however, initial UD may have also played a primary role. In conclusion, the clinical and histopathologic features of both ulcerative dermatitis and dermal xanthomatosis were considered in this case. The underlying etiologies of the skin lesion

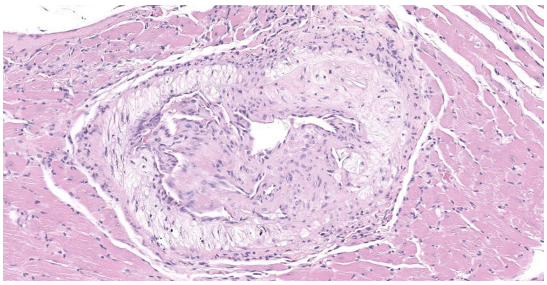

Figure 2-4. Coronary artery, mouse. Similar changes are present in the wall of the coronary artery. Smooth muscle cells also contain cytoplasmic lipid. There is recanalization of the lumen with marked fibrosis of the tunica intima. (HE, 226X)

are thought to be driven by the genotype and further potentiated by both the high fat diet and UD.

Contributing Institution:
In Vivo Animal Core, University of Michigan, Unit for Laboratory Animal Medicine
https://animalcare.umich.edu/business-services/vivo-animal-core
ulam-ivac@umich.edu

JPC Diagnoses:
1. Heart, arteries: Atherosclerosis, multifocal, marked.
2. Heart, left ventricle: Fibrosis, subendocardial, multifocal, mild to moderate, with cardiomyocyte degeneration and loss.
3. Ear pinna: Dermatitis, xanthogranulomatous, diffuse, marked with multifocal epidermal ulceration.

JPC Comment:
The term xanthoma is derived from *xanthos*, the Greek word for yellow.[19] Xanthomas have been reported in numerous veterinary species and are relatively common in birds, less common in cats, and rare in dogs, horses, amphibians, and reptiles.[13,14,15,17,19] Of the avian species, older psittacines are the most commonly affected, and lesions may occur in the skin of the abdomen, wings, and eyelids, with rare involvement of internal organs such as the bone marrow, liver, and ventriculus.[15,17] In birds, dermal xanthomas are variably inflamed, often pruritic nodular masses that lead to self-mutilation. Chronic irritation, trauma, and high fat/high cholesterol diets are associated with xanthoma development in birds. In mammals, xanthomas may also be caused by high lipid diets, defective lipid metabolism, or underlying endocrine dysfunction (such as diabetes mellitus, hypothyroidism, hypoadrenocorticism, and pituitary pars intermedia dysfunction in horses).[19] In dogs, a rare but striking form of xanthoma can occur in the eye secondary to the previously listed causes or lens-induced uveitis; grossly, affected eyes may be filled with yellow-tan material.[7]

Xanthomas in the central nervous system can lead to neurologic signs secondary to compression of adjacent parenchyma. In dogs, xanthogranulomas have rarely been reported in the sellar region. One recent report described xanthogranuloma intimately associated with a functional pituitary adenoma in a dog with hyperadrenocorticism and hypoparathyroidism; while the clinical signs in this case were attributed to the functional pituitary adenoma, another report described neurologic changes including aggression, seizures, and proprioceptive deficits due to compression by a xanthogranuloma in the pituitary region of a poodle with hyperadrenocorticism and hypothyroidism.[2] A similar lesion, termed cholesteatoma, occurs in the choroid plexus of older horses secondary to recurrent mild hemorrhage.[11] Large cholesteatomas obstruct the flow of cerebrospinal fluid causing secondary hydrocephalus.[11]

Buildup of lipid, lipid-laden macrophages, and cholesterol crystals in the tunica intima of large arteries, as demonstrated in this case, is termed atherosclerosis. Atherosclerosis is one of the most important diseases of humans

and is a leading cause of mortality due to resulting myocardial infarction, cerebral infarction, aneurysm, and peripheral vascular disease. The complex pathogenesis involves a combination of hypercholesterolemia, endothelial dysfunction, and chronic inflammation.[12] Intimal plaques occur in areas of turbulent blood flow and endothelial dysfunction and are initially composed of lipid-laden smooth muscle cells and macrophages. Extracellular oxidized LDL (generated by reactive oxygen species from previously activated macrophages) and phagocytosed cholesterol and fatty acids stimulate inflammasome formation, IL-1 production, and further activation of macrophages and T cells, perpetuating the inflammation. Cytokines and growth factors stimulate smooth muscle proliferation and collagen production, expanding the intimal plaque and creating a fibrous cap on the luminal surface. The plaque contains a core of lipid, lipid-laden cells, and possibly mineral, and if the fibrous cap is unstable and ruptures, this material is released into the vessel, causing thrombosis with vessel occlusion or embolization. Alternatively, outward pressure of the growing plaque can weaken the tunica media, resulting in aneurysm. Chronic atherosclerosis can also lead to gradual stenosis in smaller arteries, such as the coronary arteries, eventually resulting in tissue ischemia.

Clinical atherosclerosis in veterinary species is exceedingly rare, which creates a challenge when searching for animal models in this important human disease. Chickens, parrots, rabbits, pigs, and primates are susceptible to atherosclerosis, and while cats are generally considered atheroresistant, a recent report described clinical atherosclerosis in two related Korat breed cats with progressive cardiovascular failure.[6] The histologic lesions were nearly identical to those seen in humans, and both had chronic myocarditis and fibrosis likely secondary to coronary artery stenosis and myocardial ischemia. In experimental models, pigs, rabbits, non-human primates, and mice are currently used, with the mouse being the most popular model in part due to its relative low cost and ease of genetic manipulation.[4] ApoE or LDL deficient mouse models have provided tremendous insight

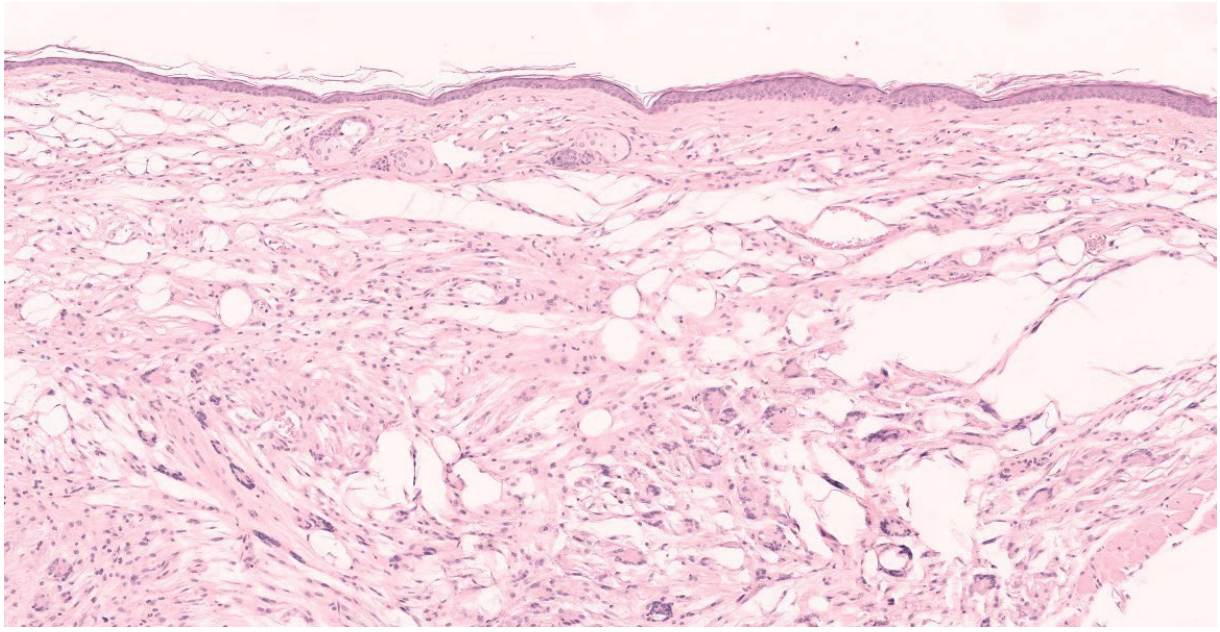

Figure 2-5. Pinna, mouse. The dermis is markedly expanded by acicular lipid either free in the tissue or surrounded by multinucleated giant cell macrophages. (HE, 98X)

into atherogenesis, but even they do not perfectly recapitulate the human disease, as they lack coronary stenosis and plaque instability.[4]

References:

1. Bedja D, Yan W, Lad V, et al. Inhibition of glycosphingolipid synthesis reverses skin inflammation and hair loss in ApoE−/− mice fed western diet. *Sci Rep.* 2018;8(1).
2. Fernandez-Gallego A, Del-Pozo J, Boag A, Maxwell S, Perez-Acino J. Xanthogranulomatous Pituitary Adenoma in a Dog with Typical Hyperadrenocorticism. *J Comp Pathol*. 2020;180**:** 115-121.
3. Gao J, Katagiri H, Ishigaki Y, et al. Involvement of apolipoprotein E in excess fat accumulation and insulin resistance. *Diabetes.* 2007;56(1).
4. Getz GS, Reardon CA. Animal models of atherosclerosis. *Arterioscler Thromb Vasc Biol*. 2012;32**:** 1104-1115.
5. Hampton AL, Aslam MN, Naik MK, et al. Ulcerative dermatitis in C57BL/6NCrl mice on a low-fat or high-fat diet with or without a mineralized red-algae supplement. *J Am Assoc Lab Anim Sci*. 2015;54(5).
6. Karkamo V, Airas N, Linden J, et al. Severe Spontaneous Atherosclerosis in Two Korat Breed Cats is Comparable to Human Atherosclerosis. *J Comp Pathol*. 2021;188**:** 52-61.
7. Labelle P. The Eye. In: Zachary JF, ed. *Pathologic Basis of Veterinary Disease*. 7th ed. St. Louis, MO: Elsevier, Inc; 2021: 1429.
8. Lewandowski CT, Maldonado Weng J, LaDu MJ. Alzheimer's disease pathology in APOE transgenic mouse models: The Who, What, When, Where, Why, and How. Neurobiol Dis. 2020;139. doi:10.1016/j.nbd.2020.104811
9. Martins Cardoso R, Creemers E, Absalah S, et al. Hypercholesterolemia in young adult APOE −/− mice alters epidermal lipid composition and impairs barrier function. Biochim Biophys Acta - Mol Cell Biol Lipids. 2019;1864(7).
10. Mitchell RN, Halushka MK. Blood Vessels. In: Kumar V, Abbas AK, Aster JC, eds. *Robins & Cotran Pathologic Basis of Disease*. 10th ed. Philadelphia, PA: Elsevier, Inc; 2021: 493-504.
11. Miller AD, Porter BF. Nervous System. In: Zachary JF, ed. *Pathologic Basis of Veterinary Disease*. 7th ed. St. Louis, MO: Elsevier, Inc; 2021: 966.
12. Oakes SA. Cell Injury, Cell Death, and Adaptations. In: Kumar V, Abbas AK, Aster JC, eds. *Robins & Cotran Pathologic Basis of Disease*. 10th ed. Philadelphia, PA: Elsevier, Inc; 2021: 62-63.
13. Origgi FC. Lacertilia. In: Terio KA, McAloose D, St. Leger J, edgs. *Pathology of Wildlife and Zoo Animals.* Cambridge, MA: Elsevier, Inc: 2018: 879.
14. Pessier AP. Amphibia. In: Terio KA, McAloose D, St. Leger J, edgs. *Pathology of Wildlife and Zoo Animals.* Cambridge, MA: Elsevier, Inc: 2018: 927.
15. Reavill DR, Dorrestein G. Psittacines, Coliiformes, Musophagiformes, Cuculiformes. In: Terio KA, McAloose D, St. Leger J, edgs. *Pathology of Wildlife and Zoo Animals.* Cambridge, MA: Elsevier, Inc: 2018: 782.
16. Reddick RL, Zhang SH, Maeda N. Atherosclerosis in mice lacking Apo E - Evaluation of lesional development and progression. *Arterioscler Thromb Vasc Biol*. 1994;14(1).
17. Schmidt RE, Reavill DR, Phalen DN. *Pathology of Pet and Aviary Birds*. 2nd ed. Ames, IO: John Wiley & Sons, Inc; 2015. 73, 116, 194, 260, 264.
18. van Ree JH, Gijbels MJJ, van den Broek WJAA, Hofker MH, Havekes LM. Atypical xanthomatosis in apolipoprotein E-

deficient mice after cholesterol feeding. Atherosclerosis. 1995;112(2).
19. Welle MM, Linder KE. The Integument. In: Zachary JF, ed. *Pathologic Basis of Veterinary Disease*. 7th ed. St. Louis, MO: Elsevier, Inc; 2021: 1190, 1219.
20. Zhang SH, Reddick RL, Piedrahita JA, Maeda N. Spontaneous hypercholesterolemia and arterial lesions in mice lacking apolipoprotein E. *Science* (80-). 1992;258(5081).

CASE III:

Signalment:
2 year old, female intact, Domestic Shorthair cat (*Felis catus*)

History:
This cat presented to the primary veterinarian following acute decline at home over the previous 24 hours, characterized by acute inappetence, lethargy, labored breathing, an enlarged left submandibular lymph node, abnormal urination and defecation, and hiding behavior. The cat had been acting normally prior to the decline and no vomiting, diarrhea, coughing or sneezing were noted. The cat was indoor only and had been previously vaccinated but was not up to date. It was living with three more cats, none of whom displayed abnormal clinical signs. On physical examination, the cat was lethargic, bradycardic (130 beats/min), and tachypneic (90 breaths/min) with an audible wheeze and increased abdominal effort. The left submandibular lymph node was markedly enlarged to approximately 2 cm in diameter, while the remaining peripheral lymph nodes palpated normal. The cat was afebrile and had no obvious oral lesions.

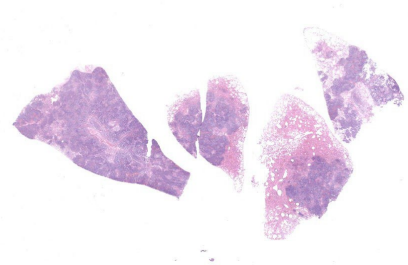

Figure 3-1. Multiple sections of lung are submitted for examination, with up to 100% effacement of pulmonary architecture by a dense cellular infiltrate. (HE, 7X)

A complete blood count (CBC) and blood smear revealed a marked leukopenia, driven by marked neutropenia and lymphopenia. FeLV and FIV testing was negative. Thoracic radiographs revealed multiple nodular soft tissue opacities throughout the lung fields, ranging in size from 0.2 cm to greater than 1.0 cm. Advanced pulmonary metastatic disease was suspected, with bacterial or fungal granuloma considered less likely.

The cat was euthanized due to the need for aggressive intervention and a guarded prognosis.

Gross Pathology:
Affecting approximately 60-70% of the total surface area of the lungs were numerous, occasionally coalescing, well demarcated, raised, slightly firm, irregularly circular, beige to dark brown masses surrounded by a thin beige rim. The masses ranged from 0.4 cm to 1.9 cm in diameter, extended deep into the lung parenchyma, and had a bulging, granular appearance on cut surface. Overall, the lungs were mottled red to dark red, wet, heavy, and oozed a small to moderate amount of red, clear, watery fluid and a small amount of pink-tinged froth on cut section. There were multiple, friable, weak adhesions between the lung lobes and the adjacent mediastinum and costal pleura. Sections of lung containing the irregularly circular nodules sank in formalin.

Laboratory Results:
Special stains:

Gram stain: The coccobacilli were Gram negative.
Bacteriology: Aerobic culture of the lungs yielded *Neisseria* sp. (predominant, 3+) and *Pasteurella* sp. (mixed, 2+) based on MALDI-TOF analysis.

Microscopic Description:
Slide B: Lungs – Widely-disseminated throughout all representative sections, affecting approximately 60-80% of the parenchyma, there are numerous, variably well demarcated nodules characterized by marked infiltration of the alveolar lumina, airways, and interstitium by degenerate and non-degenerate neutrophils admixed with abundant fibrin and large numbers of foamy macrophages. Within affected areas, alveolar septa are pale and indistinct to completely lost and replaced by large amounts of fibrin and proteinaceous and karyorrhectic debris (coagulative to lytic necrosis). Scattered bronchioles exhibit similar coagulative to lytic necrosis, with widespread sloughing and/or absence of bronchiolar epithelium. Numerous, large clusters of extracellular and occasionally intra-neutrophilic and intra-histiocytic, basophilic, approximately 1um, coccobacilli are scattered throughout areas of inflammation and necrosis. Moderate to large numbers of extravasated erythrocytes are present in the alveolar lumina, airways, and interstitium multifocally (hemorrhage). Bronchiolar lumina are variably filled by large numbers of degenerate and non-degenerate neutrophils and macrophages, moderate numbers of sloughed epithelial cells, moderate numbers of coccobacilli, and large amounts of fibrin and cytoplasmic and nuclear debris. Blood vessels within nodules occasionally contain partially-occlusive to fully-occlusivethrombi

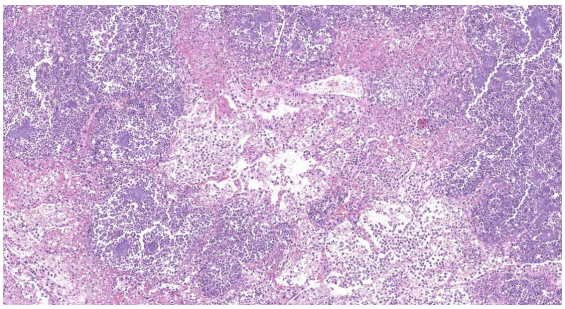

Figure 3-2. Lung, cat. There is extensive necrosis of the pulmonary parenchyma with septal necrosis, and filling of alveoli with fibrin, innumerable necrotic and viable neutropils, and large bacterial colonies. (HE, 108)

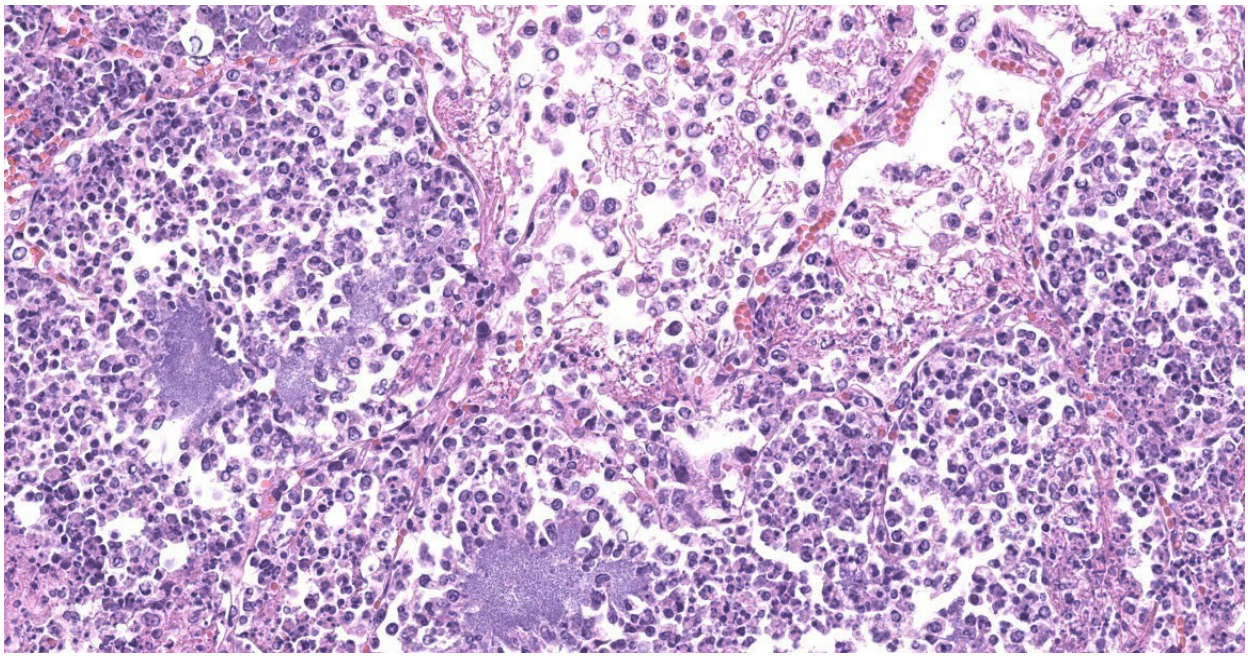

Figure 3-3. Lung, cat. Higher magnification of necrotic pulmonary parenchyma and alveolar contents. (HE, 367X)

with admixed degenerate and non-degenerate neutrophils and rare bacteria. The alveolar lumina between the nodules are filled by homogenous, eosinophilic material (edema) and contain small to moderate numbers of neutrophils and macrophages. Multifocally, mesothelial cells are plump (reactive) and the pleura is mildly to moderately thickened by small to moderate numbers of neutrophils and macrophages, and small amounts of fibrin and cellular debris.

Contributor's Morphologic Diagnoses:

1. Lungs:
   a. Pneumonia, necro-suppurative and histiocytic, multifocal, marked, acute with intralesional, intraneutrophilic, and intrahistiocytic bacteria, bronchitis, pleuritis, hemorrhage, and bacterial emboli.
   b. Alveolar edema, diffuse, marked, acute

Contributor's Comment:

Lower respiratory tract infection is an uncommon cause of morbidity and mortality in cats. Lower respiratory tract infections are often difficult to diagnose clinically due to nonspecific or inconsistent clinical, hematologic, and radiographic findings and concomitant respiratory or systemic pathology.[6] Reported infectious causes associated with feline pneumonia include bacteria, viruses, fungi, protozoa, rickettsia, and parasites, with *Bordetella bronchiseptica*, *Pasteurella* sp., *Mycoplasma* sp., *Streptococcus* sp., and *Escherichia coli* considered the most common bacterial agents. [6]

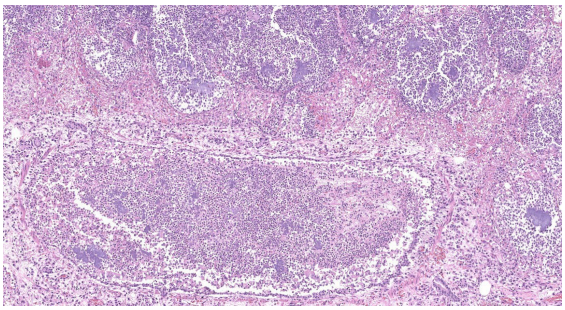

Figure 3-4. Lung, cat. Airways contain refluxed inflammatory cells and bacterial colonies. There is necrosis of airway epithelium and extension of inflammation into the peribronchiolar tissue. (HE, 367X)

Neisseria sp. bacteria are small, gram negative, coccobacilli, ecologically similar to *Pasteurella* sp. In human medicine, they are known as the causative agents of the sexually transmitted infection gonorrhea (*N. gonorrhoeae*), a form of bacterial meningitis (*N. meningitidis*), and uncommonly seen as secondary infection following feline and canine bite wounds (*N. animaloris* and *N. zoodegmatis*).[7,9] *Neisseria* sp. have been isolated as commensal flora from the oral cavity of healthy cats and dogs but are also a seldom reported cause of feline pneumonia.[6,7,9] Feline *Neisseria sp.* pneumonia was first described in 3 domestic cats in 1973, and sporadically thereafter in cases involving further domestic cats, a tiger cub, a lion, and Chinese leopard cats.[5,8,10,11]

Cases of feline *Neisseria* sp. pneumonia are most commonly reported in adult cats, who present with variable clinical signs including acute depression, dehydration, respiratory distress, salivation, or sudden death.[3,6,8,10,11] Antemortem diagnostic testing results are also variable, with the most consistent finding being discrete, multifocal nodular densities and/or lung consolidation on thoracic radiographs.[6,8] Gross lesions consist of widespread, white to tan nodules scattered throughout the lung parenchyma, while the disease is histologically characterized by marked, multifocal, necrosuppurative and histiocytic, nodular pneumonia with abundant intralesional bacteria.[5,8,10,11]

While relatively unique, the reported radiographic, gross, and histologic findings are not considered pathognomonic for this entity without ancillary testing. Similar radiographic patterns have been reported in neoplasia and uncommonly secondary to other infectious causes, including but not limited to

Yersinia pestis, *Cryptococcus neoformans*, *Toxoplasma gondii*, *Mycoplasma* sp., *Mycobacterium* sp., and rarely other bacterial, fungal or parasitic causes.[3,6] While both *Neisseria* sp. and *Pasteurella* sp. bacteria were cultured from the lung in this case, *Pasteurella* sp. were considered less likely to be causing the primary disease, as these bacteria are common in the oral cavity and airways in healthy adult cats, are not uncommonly reported in mixed growth from feline pneumonia, and are generally associated with a suppurative bronchopneumonia when causing opportunistic lower respiratory tract disease.[2] In addition, multiple historic cases of feline nodular, necrosuppurative pneumonia, both in the literature and at our institution, have yielded pure growth of *Neisseria* sp. on aerobic culture.

The pathogenesis of feline *Neisseria* sp. pneumonia is not clear, but given the distribution and vascular bacterial emboli, is considered most likely secondary to hematogenous spread, potentially from the oral cavity.[8,11] The reason for the rare and severe nature of the disease given the oral commensal nature of some *Neisseria* species is not understood. One proposed mechanism is that chronic infection circumvents the host immune response, leading to a period of asymptomatic bacteremia and hematogenous spread to locations that favor survival and growth, with subsequent severe disease.[9] Immunosuppression has been hypothesized as a potential causative factor for pathogenesis in previous case reports, however, while this case exhibited marked neutropenia and lymphopenia, there was no evidence of other pathogenic processes leading to immunosuppression within the history, clinical, gross, or histologic findings.[5]

Unfortunately, prognosis is poor in *Neisseria* sp. pneumonia cases, with decline and death generally within hours to days of onset of clinical signs, and only a single case report of successful feline *Neisseria* sp. pneumonia treatment.[6]

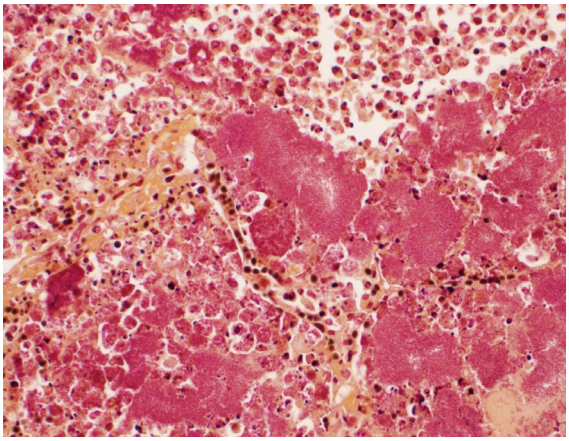

Figure 3-5. Lung, cat. Bacterial colonies are composed of large colonies of gram-negative cocci. (Brown-Hopps, 400X)

Contributing Institution:
Drs. Chris Bolt and Arno Wuenschmann
Minnesota Veterinary Diagnostic Laboratory
and Department of Population Medicine
University of Minnesota
1333 Gortner Ave.
St. Paul, MN 55108
www.vdl.umn.edu

JPC Diagnosis:
Lung: Pneumonia, necrotizing and fibrinosuppurative, diffuse, severe with thrombosis and large colonies of extracellular and intracellular cocci.

JPC Comment:
Neisseria animaloris and *Neisseria zoodegmatus* were previously known as Centers for Disease Control (CDC) Group Eugonic Fermenters (EF) 4a and 4b, respectively, until they were determined to belong to the *Neisseria* genus in 2006.[13] As the contributor states, *Neisseria* sp. are commensal organisms of the oral cavity of dogs and cats, and in addition to infrequently causing pneumonia, can rarely cause subcutaneous infections

of the neck and facial regions in cats. One report described a young adult Russian Blue cat with a submandibular mass characterized by necrosis, purulent inflammation, and fibrosis secondary to *Neisseria animaloris* (EF-4a at the time).[1] In a separate report, a young adult domestic short hair cat developed subcutaneous swelling over the bridge of the nose due to pyogranulomatous inflammation and *Neisseria* sp infection.[4] Routine stains did not illustrate bacteria in the first case; however, in the second case, gram-negative, non-acid-fast coccobacilli with a PAS-positive capsule were identified within macrophages. Both cases responded to debulking and antibiotic therapy, and traumatic inoculation from penetrating injury were suspected to be the initial cause of infection.[1,4]

As the contributor mentioned, *N. meningitidis* and *N. gonorrhoeae* are significant pathogens in humans. While most Gram-negative bacteria use siderophores to obtain iron, pathogenic (non-commensal) *Neisseria* species have evolved a unique mechanism to extract iron from host serum transferrin (TF), the predominant mammalian transport protein for iron.[12] The bacterial transferrin receptor consists of two parts: TF-binding protein B (TbpB, a surface lipoprotein), which initially harnesses TF, and TF-binding protein A (Tbp A, a TonB-dependent transporter), which removes and transports ferric acid into the bacteria through a conformationally-active pore.[12] While the majority of research on Tbps has been conducted in Neisseria species, similar receptors have been found in Pasteurellaceae and Moraxellaceae species, including *Actinobacillus pleuropneumoniae* and *Histophilus somni*.[12] Bacterial Tbp activity appears to be host-species specific and increases pathogen virulence within the host.

References:

1. Baral RM, Catt MJ, Soon L, et al. Successful treatment of a localized CDC group EF-4a infection in a cat. *J Feline Med Surg*. 2017;9(1):67-71.
2. Bart, M et al. Feline Infectious Pneumonia: A Short Literature Review and a Retrospective Immunohistological Study on the Involvement of Chlamydia spp. and Distemper Virus. *The Veterinary Journal.* 2000; 159:220-230.
3. Carniel F et al. What Is Your Diagnosis? *J Am Vet Med Assoc*. 2020; 257(4):375-377.
4. Carr SV, Martin PA, Keyes L, Tong LJ, Talbot JJ, Muscatello G, Barrs VR. Nasofacial infection in a cat due to a novel bacterium in *Neisseriaceae*. *JFMS Open Rep.* 2015;1(2):1-5.
5. Ceyssens et al. Necrotizing Pneumonia in Cats Associated with Infection of EF-4a Bacteria. *J Vet Med*. 1989; 36(4):314-316.
6. Foster S, Martin P. Lower Respiratory Tract Infections in Cats - Reaching beyond empirical therapy. *J Feline Med Surg.* 2011; 13(5):313-332.
7. Heydecke A et al. Human wound infections caused by *Neisseria animaloris* and *Neisseria zoodegmatis*, former CDC Group EF-4a and EF-4b. *Infection Ecology and Epidemiology.* 2013; 3: 20312.
8. Jang SS et al. Focal Necrotizing Pneumonia in Cats Associated with a Gram Negative Eugonic Fermenting Bacterium. *Cornell Vet*. 1973; 63:446-454
9. Liu G et al. Non-Pathogenic *Neisseria*: members of an abundant, multi-habitat, diverse genus. *Microbiology*. 2015; 161:1297-1312
10. Lloyd J, Allen JG. The isolation of Group EF-4 bacteria from a case of granulomatous pneumonia in a tiger cub. *Aust Vet J.* 1980; 56(8):399–400.
11. Perry AW, Schlingman DW. Pneumonia Associated with Eugonic Fermenter-4 Bacteria in Two Chinese Leopard Cats. *Can Vet J*. 1988; 29(11): 921-922.

12. Pogouste AK, Morales TF. Iron acquisition through the bacterial transferrin receptor. *Crit Rev Biochem Mol Biol.* 2017: 52(3):314-326.
13. Vandamme P, Holmes B, Bercovier H, Coenye T. Classification of Centers for Disease Control Group Eugonic Fermeter (EF)-4a as *Neisseria animaloris* sp. nov. and *Neisseria zoodegmatis* sp. nov, respectively. *Int J Syst Evol Microbiol.* 2006:56(Pt8):1801-1805.

CASE IV:

Signalment:
1-year-old female Wyandotte chicken (*Gallus gallus*)

History:
This chicken was lethargic, diarrheic and was losing weight. She was found laterally recumbent with her right leg extended behind her and the left leg curled underneath her. Coelomocentesis revealed yellow coelomic fluid. Euthanasia was elected, and the carcass was received for examination. This chicken was part of a small backyard flock of 16 chickens.

Gross Pathology:
The chicken was in poor body condition with scant visceral fat and moderate pectoral muscle atrophy. There was approximately 100 mL of yellow, turbid, watery fluid within the coelomic cavity. Multifocally throughout the walls of the small intestine and large intestine, and occasionally extending into the lumen, were dozens of semi-firm, pale tan-yellow nodules which ranged from 0.3 to 2 cm in diameter. On cut section, these nodules were pale tan and bulged slightly. The mesentery was tan and diffusely moderately thickened.

Laboratory Results:
Qualitative fecal analysis: Few *Capillaria* sp. eggs, few *Heterakis* sp. eggs, few coccidial oocysts

Microscopic Description:
Small intestine: Diffusely expanding and effacing the serosa of the small intestine and the surrounding mesentery is a poorly demarcated, highly cellular proliferation of neoplastic round cells. Neoplastic cells are arranged in sheets and supported by collagenous stroma. Neoplastic cells are round with distinct cell borders and have small to moderate amounts of eosinophilic cytoplasm. Nuclei are round, finely stippled to vesiculate and have 1-3 nucleoli. There is moderate anisocytosis and anisokaryosis and 43 mitoses in 10 high-power fields (400x). Multifocally, neoplastic cells infiltrate the small intestinal muscularis and submucosa. The adjacent pancreas is extensively obscured to effaced by similar neoplastic cells.

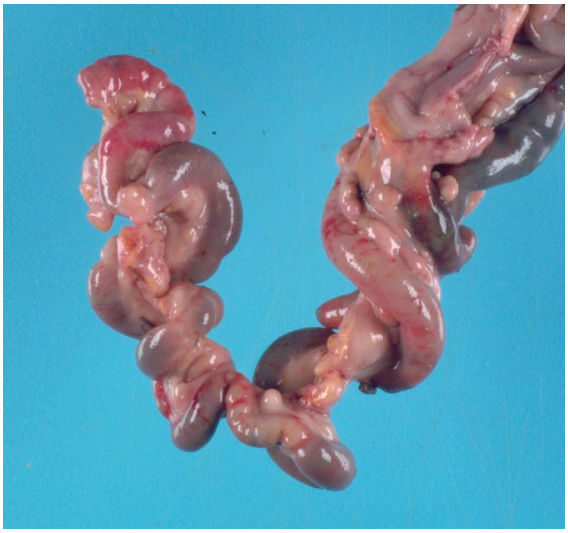

Figure 4-1. Small intestine, chicken. There are dozens of multifocal to coalescing semi-firm, tan-yellow, 0.3-2 cm diameter nodules throughout the walls of the small intestine, mesentery and pancreas. (Photo courtesy of NIH Comparative Biomedical Scientist Training Program, National Cancer Institute, https://nih-cbstp.nci.nih.gov/)

Immunohistochemistry:
The neoplastic round cells within the small intestine, mesentery and pancreas exhibit strong perimembranous immunoreactivity for CD3, strong nuclear immunoreactivity for Meq and are not immunoreactive for BLA.36.

Contributor's Morphologic Diagnoses:
Small intestine: T-cell lymphoma
Pancreas: T-cell lymphoma

Contributor's Comment:
The histopathologic findings are consistent with visceral lymphoma, which in this case was immunohistochemically confirmed as Marek's disease using antibodies directed against the Marek's disease virus Meq protein.

Marek's disease (MD) in chickens occurs upon inhalation of gallid alphaherpesvirus-2, a cell-associated alphaherpesvirus with lymphotropic properties similar to gammaherpesviruses.[13] Marek's disease virus (MDV) is a member of the genus Mardivirus and are divided into three serotypes: Gallid herpesvirus 2 (MDV-1), Gallid herpesvirus 3 (MDV-2), and Meleagrid herpesvirus 1 (MDV-3). Of these three serotypes, only MDV-1 causes disease in chickens.[13,15] Strains of MDV are classified into four pathotypes based on their virulence, referred to as mild (m), virulent (v), very virulent (vv)

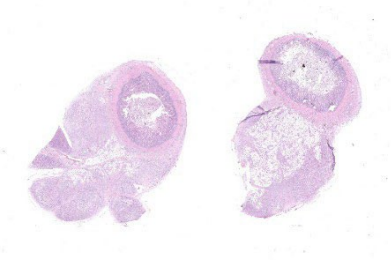

Figure 4-2. Small intestine and mesentery. Two sections of intestine and mesentery (one with pancreas) are submitted for examination. At subgross, the mesentery and intestine contain a dense cellular exudate. (HE, 5X)

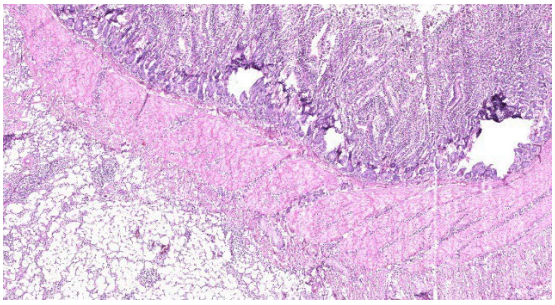

Figure 4-3. Small intestine and mesentery. A moderately cellular round cell neoplasm transmurally infiltrates the intestine and extends into the adjacent mesentery. (HE, 49X)

and very virulent plus (vv+) strains.[1,13] The m strains can cause mild neurological disease, the v and vv strains can cause lymphomas, and the vv+ strains can cause fatality with severe brain edema and tumors in unvaccinated and vaccinated chickens.[1,15]

Previously, MDV posed a serious economic threat causing up to 60% mortality in layer flocks, and currently exists in all poultry-producing countries.[2,13,14] Despite the more recent advent and widespread use of a live-attenuated vaccine, sporadic losses still occur on individual farms, and the disease is still a concern in poultry flocks.[13] Concerns of the vaccine selecting for MDV strains of higher virulence also exist, as MDV vaccines prevent clinical signs but do not prevent virus replication and shedding in vaccinated chickens.[1,14] Nearly all chickens can be infected by MDV and develop tumors, and turkeys, quail, and pheasants are also susceptible to infection and disease.[13] Marek's disease outbreaks may occur in unvaccinated chickens as young as 3-4 weeks, although most serious cases begin after 8-9 weeks of age.[13]

The pathogenesis of MDV infection in vivo is divided into four stages.[15] In the early cytolytic phase, B cells undergo cytolytic infection.[15] In the latency phase, MDV infects CD4+ and CD8+ T-cells.[15] Following MDV reactivation in CD4+ T-cells, a late cytolytic

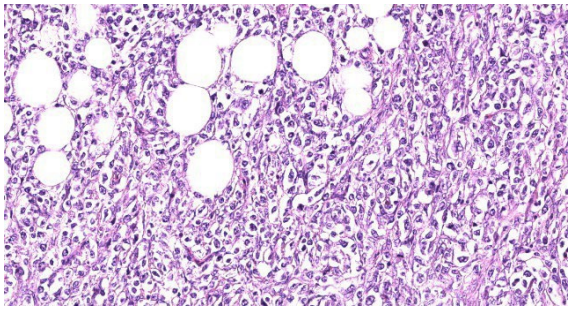

Figure 4-4. Mesentery, chicken. Neoplastic cells infiltrate and efface the mesentery. (HE, 381X)

and immunosuppressive phase is initiated.[15] Finally, the transformation phase occurs and is characterized by the development of CD4+ T-cell lymphomas.[15]

Marek's disease can manifest as distinct lymphoproliferativesyndromes, such as lymphomas, cutaneous leukosis, atherosclerosis, early mortality, cytolytic syndromes, immunosuppression, and lymphoproliferation in the eyes and CNS as well as peripheral nerves resulting in "fowl paralysis".[13] Gross lesions associated with MD may include unilaterally gray or yellow, edematous, and enlarged peripheral nerves, such as the sciatic and brachial nerves, which may be 2 to 3 times normal size.[13] Lymphomas may also occur in virtually all visceral organs, including the mesentery, intestine, pancreas, kidney, liver, spleen, bursa of Fabricius, thymus, iris ("gray eye"), feather follicles, heart, muscle and gonads, particularly the ovary.[13] Visceral tu mors may appear as gray or yellow firm nodules or diffuse organ enlargements.[13] In this case, differential diagnoses for the gross lesions would include avian tuberculosis or Hjarre's disease (coligranuloma), which were later ruled-out with microscopic examination.

Microscopic lesions within visceral organs correspond to proliferations of monomorphic neoplastic small to large T-cells, lymphoblasts and mononuclear inflammatory infiltrates.[13] Within peripheral nerves, lymphoproliferative lesions are separated into types A and B.[3,13] Type A lesions are neoplastic and consist of T-cells and fewer B-cells.[3,13] Type B lesions are inflammatory and are characterized by mononuclear cell infiltrates composed of small lymphocytes and plasma cells and fewer macrophages.[3,13]

In the current case, only lymphoma affecting visceral organs was appreciated. In addition to infiltrating and obliterating the intestinal walls, mesentery, and pancreas, similar neoplastic lymphocytes extensively effaced the ovary and infiltrated the splenic capsule.

The primary differential diagnoses for lymphoma in chickens include Marek's disease, and the retroviruses avian leukosis virus (ALV) and reticuloendothelial virus (REV).[7,13] Immunophenotyping with T- and B-cell markers can help to distinguish between MDV and ALV, as MDV commonly induces T-cell lymphomas, while ALV induces B-cell lymphomas.[7] In the current case, neoplastic cells exhibited strong perimembranous labeling for the T-cell marker CD3 and were negative for the B-cell marker BLA.36. PCR may also be used to identify the presence of MDV.[6,7,11]

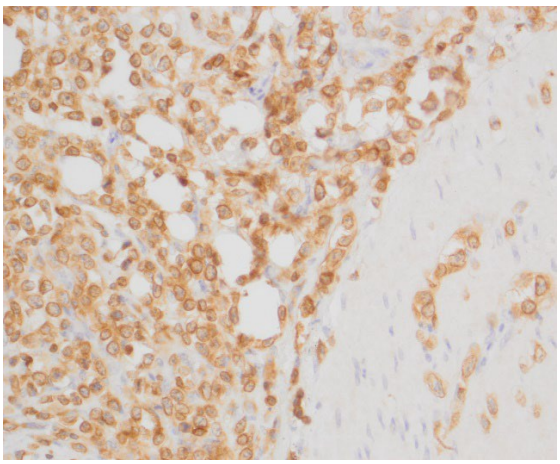

Figure 4-5. Small intestine, chicken. Neoplastic lymphocytes exhibit strong perimembranous immunoreactivity for CD3 (anti-CD3, 400X). (Photo courtesy of NIH Comparative Biomedical Scientist Training Program, National Cancer Institute, https://nih-cbstp.nci.nih.gov/)

In addition, immunohistochemistry using antibodies directed against the MDV-specific viral antigens Meq and pp38 can be used to help confirm a diagnosis of MD. Meq (Marek's EcoQ) is a leucine zipper regulatory protein similar to the Fos and Jun oncoproteins, and has been demonstrated to be critical to MD oncogenesis.[10,14] The functions of Meq include DNA binding, chromatin remodeling and regulation of transcription.[14] Meq can form homodimers or heterodimers with proto-oncoproteins, such as c-Myc, c-Fos, ATF and c-Jun. Meq can also bind to and sequester RB, p53 and cyclin-dependent kinase 2 (CDK2), leading to dysregulated cell-cycle control and the oncogenic transformation of T-cells.[14] The exact biological function of pp38 is currently unknown, but has been associated with lymphoid tropism, oncogenicity, reactivation from latency, viral replication in the early lytic phase and maintenance of transformation in MDV-infected tumor cells.[8] Meq has been shown to be the only viral antigen consistently expressed, but pp38 positive cells may also be observed.[7] In our case, the neoplastic T-cells exhibited strong nuclear immunoreactivity for Meq but were not immunoreactive for pp38.

Contributing Institution:
NIH Comparative Biomedical Scientist Training Program, National Cancer Institute
https://nih-cbstp.nci.nih.gov/

JPC Diagnoses:
1. Small intestine, mesentery, pancreas: Lymphoma.
2. Small intestine, lumen: Cestode adult.

JPC Comment:
In 1907, Hungarian veterinarian Jozsef Marek described a syndrome of polyneuritis in chickens termed fowl paralysis and now known as Marek's disease.[1] In 1967, the herpesviral etiology was discovered. Observations that the virus spread via indirect contact and remained infectious in the environment for months led to further research into the transmission of the virus, and in 1970, Calnek et al. described enveloped herpesvirus particles in the feather follicular epithelium that were infectious to and produced Marek's disease in other chickens.[4] Since then, cell-free virions produced in the feather follicle epithelium and shed in feathers and dander of infected birds have been recognized as the source of horizontal transmission.

The economic impact of Marek's disease is estimated to be up to $2B USD annually, with losses stemming from decreased productivity, immunosuppression leading to comorbidities, and aesthetic condemnation at slaughter.[1,5,12] As such, tremendous research has gone into developing prevention and control methods, and there are currently three main lines of effort: selecting for genetically resistant chickens, improving biosecurity to prevent spread between flocks, and vaccination. Several Marek's disease virus (MDV) vaccinations have been developed, including a vaccine using herpesvirus of turkeys and attenuated MDV strains SB1 and CVI988.[5]

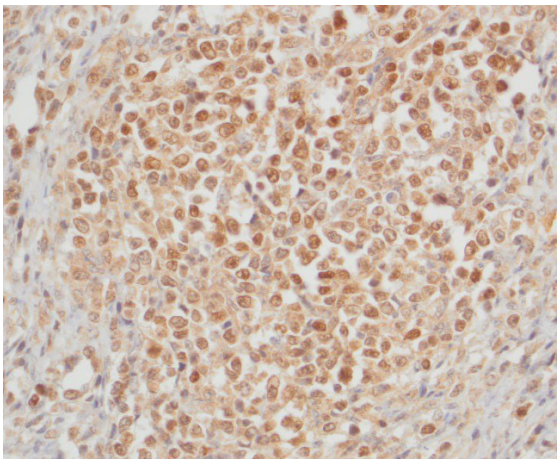

Figure 4-6. Small intestine, chicken. Neoplastic lymphocytes exhibit nuclear immunoreactivity for Meq (anti-Meq, 400X). (Photo courtesy of NIH Comparative Biomedical Scientist Training Program, National Cancer Institute, https://nih-cbstp.nci.nih.gov/)

While these vaccines are generally effective in preventing clinical disease in vaccinated birds, they do not produce sterile immunity, and vaccinated birds can still be infected and shed the virus. This has selected for and supported the spread of more virulent strains of MDV that would, in unvaccinated populations, be self-limiting in scope due to their high mortality rates. [1,5,12]

Recent research has uncovered one key component of MDV transmission: conserved herpesvirus protein kinase (CHPK).[9] CHPKs are encoded by all members of the Herpesviridae family and support a variety of functions throughout viral infection stages (such as nuclear egress and viral DNA replication).[9] In MDV, CHPK is not required for cell-to-cell transmission or progression of clinical disease, but it is specifically required for horizontal transmission.[9] Recent studies indicate that CPHK is most likely integral for production of cell-free virions, as mutated CPHK results in defects in the viral replication pathway in feather follicular epithelium, but CPHK's role in establishing infections in new individuals has not been ruled out.[9] In either case, this research provides insight into the horizontal transmission of MDV which has yet to be overcome by vaccination strategies.

References:

1. Bertzbach LD, Conradie AM, You Y, Kaufer BB. Latest insights into Marek's disease virus pathogenesis and tumorigenesis. *Cancers*. 2020;12(3):647.
2. Boodhoo N, Gurung A, Sharif S, Behboudi S. Marek's disease in chickens: a review with focus on immunology. *Veterinary research*. 2016;47(1):1-9.
3. Burgess SC, Basaran BH, Davison TF. Resistance to Marek's disease herpesvirus-induced lymphoma is multiphasic and dependent on host genotype. *Veterinary Pathology*. 2001;38(2):129-42.
4. Calnek BW, Adldinger HK, Kahn DE. Feather follicle epithelium: A source of enveloped and infectious cell-free herpesvirus from Marek's disease. *Avian Dis.* 1970; 14:219-233.
5. Davidson I. Out of Sight, but Not Out of Mind: Aspects of the Avian Oncogenic Herpesvirus, Marek's Disease Virus. *Animals*. 2020; 10: 1319-1332.
6. Gimeno IM, Dunn JR, Cortes AL, El-Gohary AE, Silva RF. Detection and differentiation of CVI988 (Rispens vaccine) from other serotype 1 Marek's disease viruses. *Avian diseases*. 2014;58(2):232-43.
7. Gimeno IM, Witter RL, Fadly AM, Silva RF. Novel criteria for the diagnosis of Marek's disease virus-induced lymphomas. *Avian Pathology*. 2005;34(4):332-40.
8. Gimeno IM, Witter RL, Hunt HD, Reddy SM, Lee LF, Silva RF: The pp38 Gene of Marek´s Disease Virus (MDV) Is Necessary for Cytolytic Infection of B Cells and Maintenance of the Transformed State but Not for Cytolytic Infection of the Feather Follicle Epithelium and Horizontal Spread of MDV. *Journal of Virology* 2005;79(7):4545-4549.
9. Krieter A, Ponnuraj N, Jarosinski KW. Expression of the Conserved Herpesvirus Protein Kinase (CHPK) of Marek's Disease Alphaherpesvirus in the Skin Reveals a Mechanistic Improtance for CHPK during Interindividual Spread in Chickens. *J Virol*. 2020; 95(5):1-12.
10. Lupiani B, Lee LF, Cui X, Gimeno I, Anderson A, Morgan RW, Silva RF, Witter RL, Kung HJ, Reddy SM. Marek's disease virus-encoded Meq gene is involved in transformation of lymphocytes but is dispensable for replication. *Proceedings of the National Academy of Sciences*. 2004;101(32):11815-20.
11. Mete A, Gharpure R, Pitesky ME, Famini D, Sverlow K, Dunn J. Marek's disease in

backyard chickens, a study of pathologic findings and viral loads in tumorous and nontumorous birds. *Avian diseases*. 2016;60(4):826-36.
12. Nair V. Spotlight on avian pathology: Marek's Disease. *Avian Path.* 2018; 47(5):440-442.
13. Nair V, Gimeno I, Dunn J. Neoplastic diseases: Marek's disease. In: Swayne DE, ed. *Diseases of Poultry*. 14th ed. Wyley-Blackwell. 2020.
14. Osterrieder N, Kamil JP, Schumacher D, Tischer BK, Trapp S. Marek's disease virus: from miasma to model. *Nature Reviews Microbiology*. 2006;4(4):283-94.
15. Shi MY, Li M, Wang WW, Deng QM, Li QH, Gao YL, Wang PK, Huang T, Wei P. The emergence of a vv+ MDV can break through the protections provided by the current vaccines. *Viruses*. 2020;12(9):1048.

WSC 2022-2023 Self-assessment.
Conference 3

1. The most common form of inflammation associated with *M. avium var. hominisuis* in swine?
    a. Eosinophilic
    b. Granulomatous
    c. Suppurative
    d. Lymphoplasmacytic

2. Which of the following is not seen in granulomatous scleritis in dogs?
    a. Vasculitis
    b. Lymphoplasmacytic perivascular infiltrates
    c. Collagenolysis
    d. Mineralization

3. True or false? Intravascular lymphomas in dogs are most commonly of T-cell origin.
    a. True
    b. False

4. True or false. Neoplastic cells in intravascular lymphomas are unable to emigrate from vessels.
    a. True
    b. False

5. The most common site of metastasis of intestinal adenocarcinoma in rhesus monkeys is which of the following ?
    a. Regional lymph nodes
    b. Liver
    c. Spleen
    d. Bone

Please email your completed assessment for grading to Dr. Bruce Williams at bruce.h.williams12.civ@mail.mil. Passing score is 80%. This program (RACE program 33611) is approved by the AAVSB RACE to offer a total of 0.5 CE Credits, with a maximum of 12.5 CE Credits being available to any individual Veterinary Medical Professionals for the 2019-2020 Wednesday Slide Conference. This RACE approval is for the subject matter categories of: SCIENTIFIC using the delivery method of NONINTERACTIVE DISTANCE. This approval is valid in jurisdictions which recognize AAVSB RACE.

Joint Pathology Center
Veterinary Pathology Services

WEDNESDAY SLIDE CONFERENCE 2022-2023

Conference #4 — 14 September 2022

CASE I:

Signalment:
14-year-old intact female Alpaca (*Vicugna pacos*)

History:
Per attending veterinarian: "Presented with hypernatremia, mild azotemia, decreased albumin, treated last week with IV fluids, electrolytes. Suspect bilateral polycystic kidney disease."

Gross Pathology:
The peritoneal, pleural and pericardial cavities contained approximately 2 L, 1.5 L and 10 mL of clear, yellow watery fluid with scant fibrin strands. The pleural surfaces of the lung lobes contain scant, scattered fibrin strands. The lungs are diffusely wet, heavy and meaty and did not collapse when the chest cavity was opened. The lungs contain enumerable, individual to coalescing nodules ranging from 0.2 cm-2 cm. The nodules are firm and white; some of the larger nodules contain central caseous material.

Laboratory Results:
No laboratory findings reported.

Microscopic Description:
The open alveolar architecture of the lung is nearly diffusely effaced secondary to alveolar filling by numerous macrophages, epithelio id macrophages and fewer multinucleated giant cells, lymphocytes and plasma cells. Randomly scattered conspicuous aggregates of neutrophils (intact and degenerate) randomly interrupt the otherwise monotonous infiltr ate by macrophages. When visible, alveolar septa are thickened by congestion approximately 2X expected. Many of the macrophages contain numerous yeast organisms; the yeast organisms were characterized by a 1.0 µm, round to crescent-shaped yeast body surrounded by a variably-sized (1.0-2.0 µm) halo.

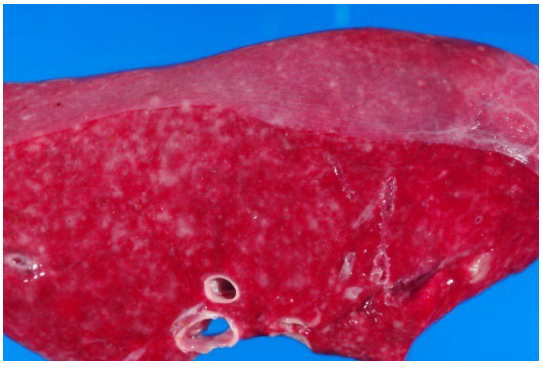

Figure 1-1. Lung, alpaca. The lung is heavy, meaty, does not collapse, and contains numerous white foci measuring 0.2-2.0 cm scattered throughout all lobes. (Photo courtesy of: Department of Veterinary Pathobiology & the Oklahoma Animal Disease Diagnostic Laboratory, Center for Veterinary Health Sciences, Oklahoma State University, www.cvhs.okstate.edu)

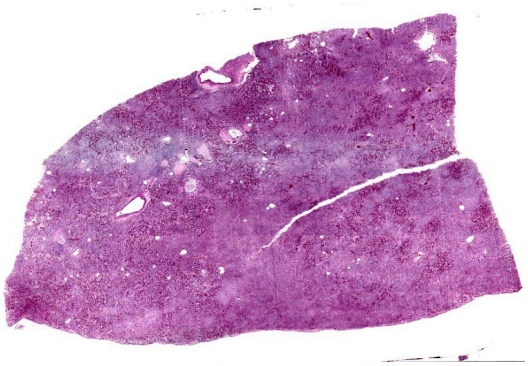

Figure 1-2. Lung, alpaca. There is diffuse consolidation of all lobules within the submitted section of lung. (HE, 5X)

In addition to the lung (provided), sections of the liver and spleen also contained randomly distributed aggregates of macrophages (some with epithelioid morphology and multinuc leated giant cells) containing yeast organisms similar to that described in the lung.

Contributor's Morphologic Diagnoses:
Syndrome: Disseminated histoplasmosis

1. Severe, diffuse, granulomatous pneumonia with myriad intralesional yeast organisms consistent with *Histoplasma capsulatum*.
2. Severe, multifocal, granuloma to us splenitis with myriad intralesio nal yeast organisms consistent with *Histoplasma capsulatum*.
3. Severe, multifocal, granuloma to us hepatitis myriad intralesional yeast organisms consistent with *Histoplasma capsulatum*.

Contributor's Comment:
This patient originally presented with a history and clinical diagnosis of renal disease. The severe pneumonia, as well as other lesions secondary to histoplasmosis, were a surprise finding at necropsy. After the fact query of the attending veterinarian did not reveal any mention of clinical signs of respiratory disease.

Our institution has a respectable caseload of llamas/alpacas; however, disseminated histoplasmosis has not before been seen, even as an etiology for pneumonias. A literat ure search revealed a single case report of pulmonary histoplasmosis in a llama.[11] The patient in that report had been recently imported from Bolivia seven months prior; however,

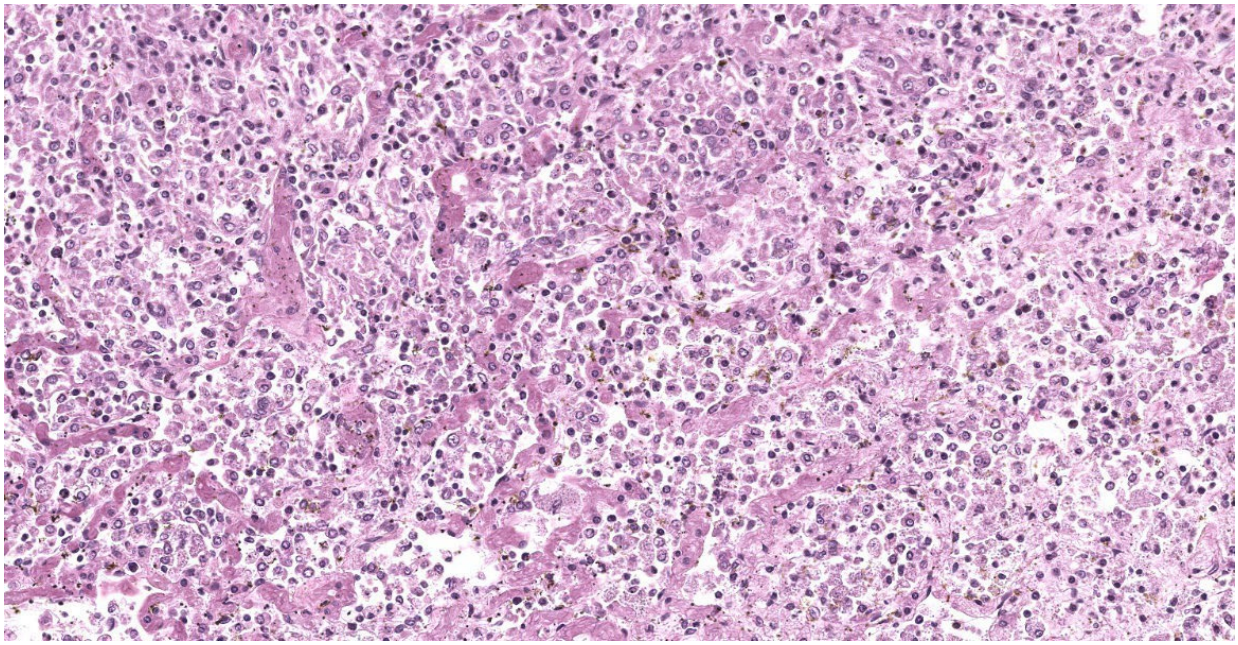

Figure 1-3. Lung, alpaca. Alveoli are filled to bursting with macrophages. At right, alveoli have ruptured and alveolar septa are no longer visible. (HE, 247X)

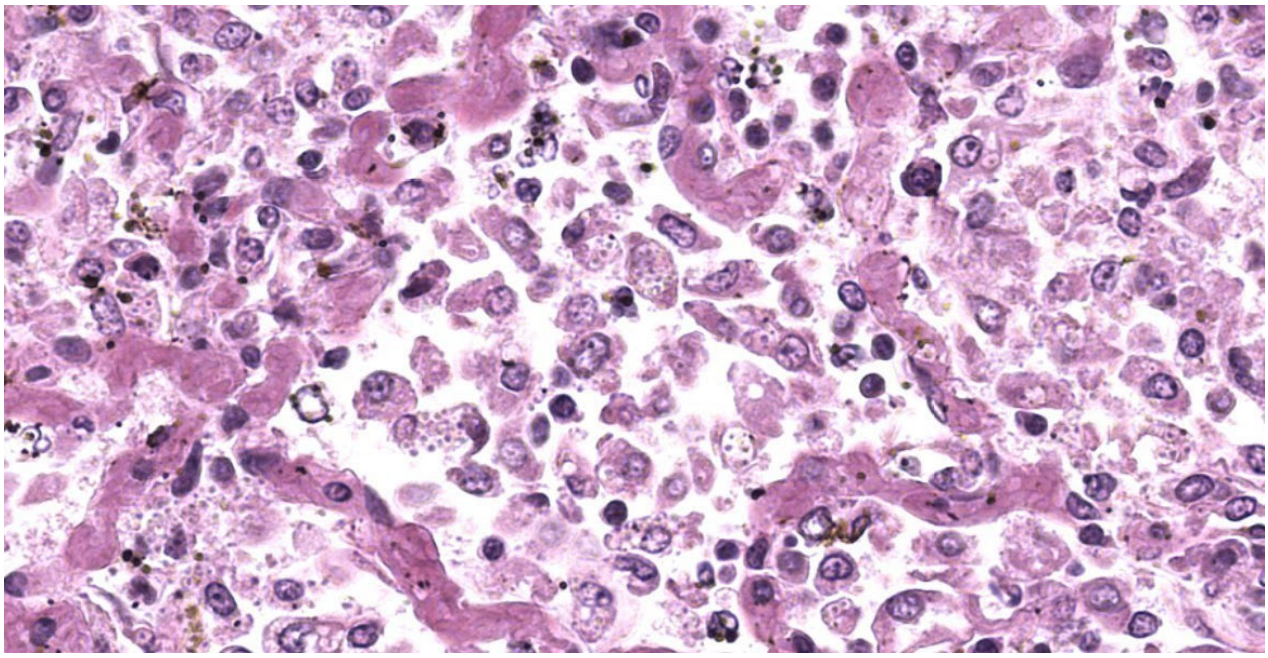

Figure 1-4. Lung, alpaca. Intra-alveolar macrophages contain numerous 2-4 µm round yeasts within their cytoplasm. (HE, 817X)

the patient in this report had spent its entire life in the United States.

Histoplasma capsulatum is a dimorphic fungus commonly found in soil that has been contaminated with bird feces or bat guano.[1] Within the United States, histoplasmosis is most common in the Mississippi, Missouri and Ohio river valleys; however, infect io ns are certainly not uncommon elsewhere in the Midwest.[5] The organism exists in the soil as a mold producing infective microconidia.[1] When inhaled, the microconidia convert to yeast forms that replicate within phagolysosomes of the pulmonary mononuclear-pha g-ocytic system.[1,6] From this initial pulmonar y infection, the organism disseminates into other organs by hematogenous (spleen, liver) or lymphatic (lymph node) routes.

Contributing Institution:
Department of Veterinary Pathobiology &
The Oklahoma Animal Disease Diagnost ic Laboratory
Center for Veterinary Health Sciences
Oklahoma State University
www.cvhs.okstate.edu

JPC Diagnosis:
Lung: Pneumonia, granulomatous, diffuse, severe with numerous intrahistiocytic yeasts.

JPC Comment:
During the conference, participants discussed the similar histologic morphology of this entity to *Sporothrix schenkii,* and that definit ive diagnosis may require speciation through culture, PCR, or IHC.

Histoplasma capsulatum subs. *capsulatum* infects a wide variety of mammals (includ ing humans) and birds, and most infections are likely subclinical or mild due to effective adaptive immunity involving cytokine-med i-ated macrophage killing and T-cell response.[9] Overt pulmonary or disseminated infections may occur if the animal is exposed to a large dose of infectious microconidia or is immunosuppressed.[1, 9] Dogs and cats are most commonly affected by clinical disease, but a plethora of reports demonstrate that disseminated histoplasmosis can occur in many species, including goats and raccoons, or as seen in this case, an alpaca.[8, 2] Even if an effective immune response is generated, yeast

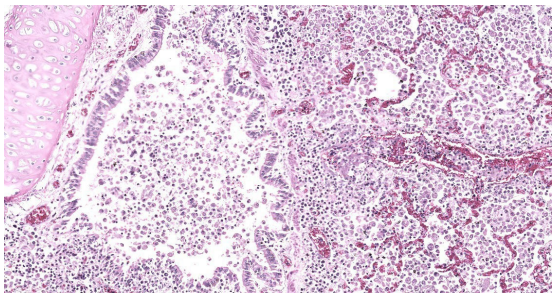

Figure 1-5. Lung, alpaca. Airways (in this case, a bronchiole) are filled with refluxed inflammatory exudate from surrounding alveoli. (HE, 159X)

may enter a state of dormancy and re-emerge when the animal becomes immunocomp romised.[1,9] In disseminated infections, *Histoplasma* travels in phagocytic cells to other organs with high concentrations of phagocytes, such as lymph nodes, gastrointestinal tract, spleen, and liver. Spread to the adrenal glands, skin, eye, and bone is also possible.[9]

In most cases, the host develops an appropriate adaptive immune response which controls and eliminates the *Histoplasma* infection. In immunocompetent hosts, the Th1 response is critical in controlling infection.[6] Innate cells initially produce IL-12, which stimulates the production of IFN-gamma mostly by CD4+ T cells.[6] IFN-gamma has a wide range of effects including activation of macrophages, stimulation of intracellular nitric oxide production by macrophages, and regulation of iron and zinc availability.[6] T cells also produce TNF-alpha, which further stimulates nitric oxide production, chemokine production, and increased INF-gamma production.[6] TNF-alpha also restricts expansion and traffick ing of regulatory T cells and signals for apoptosis.[6] These proinflammatory cytokines stimulate expression of CCR5, the receptor for chemokines CCL3, CCL4, and CCL5, all of which become upregulated during *Histoplasma* infection.[6] CCR5 activation leads to influx of additional inflammatory cells.[6] These cytokines also activate macrophages to produce microbe-killing agents such as reactive oxygen species (ROS).[12]

The NADPH-oxidase system produces many of these reactive oxygen species, includ ing superoxide, hydroxyl, and peroxide, to neutralize and destroy microbes, and *Histoplasma* has evolved a few tricks to resist ROS destruction. *H. capsulatum* produces two catalases, CatB (M-antigen) and CatP, which create a layered defense by neutralizing extracellular and intracellular ROS, respectively.[12] *H. capsulatum* also produces superoxide dismutases, such as extracellular Sod3 and intracellular Sod1, which add to these defenses.[12] Other mechanisms that *Histoplasma* has evolved to evade non-oxidative host defenses include producing anti-inflamma tory IL-4, melanin, and substances which increase intracellular pH.[1]

Other pathogenic *H. capsulatum* species include *H. capsulatum* var. *farciminosum* (HCF) and *H. capsulatum* var. *duboisii* (HCD). HCF, or equine histoplasmos is, causes epizootic lymphangitis (pseudoglanders) in horses and mules.[7] The yeast enters open wounds in the skin and causes swollen lymphatics and chronic, progressive, ulcerative nodules that drain and scar.[7] Less commonly, HCF can cause rhinitis, sinusit is, pneumonia, or keratoconjunctivitis.[7] *H. capsulatum* var. *duboisii* causes African histo-

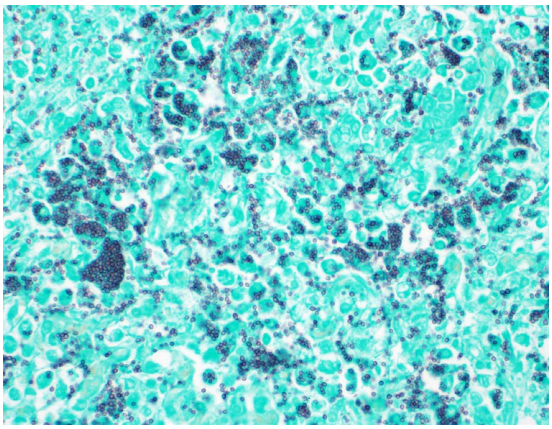

Figure 1-6. Lung, alpaca. A silver stain demonstrates the numerous yeasts present within macrophages . (Gomori methenamine silver, 400X)

plasmosis, which is characterized by granulomatous inflammation within the skin and bone of baboons and humans, though disseminated disease can also occur.[3] A recent report described granulomatous gingivitis due to HCD infection in three baboons.[4]

References:

1. Brömel C, Green CE. Histoplasmosis. In: *Infectious diseases of the dog and cat*. 4th ed. St. Louis, MO, USA: Saunders; 2012: 614-621.
2. Clotheir KA, Villaneuva M, Torain A, Reinl S, Barr B. Disseminated histoplasmosis in two juvenile raccoons (*Procyon lotor*) from a nonendemic region of the United States. *Jour Vet Diag Invest*. 2014; 26(2):297-301.
3. Hensel M, Hoffman AR, Gonzales M, Owston MA, Dick EJ. Phylogenic analysis of *Histoplasma capsulatum* var *duboisii* in baboons from archived formalin-fixed, paraffin embedded tissues. *Medical Mycology*. 2019; 57:256-259.
4. Johannigman TA, Gonzalez O, Dutton JW, Kumar S, Dick EJ. Gingival histoplasmosis: An atypical presentation of African Histoplasmosis in three baboons (*Papio spp)*. *J Med Primatol.* 2020; 49(1): 47-51.
5. Kauffman CA. Histoplasmosis: a clinica l and laboratory update. *Clin Microbiol Rev.* 2007; **20**:115-132.
6. Kroetz DN, Deepe GS. The role of cytokines and chemokines in *Histoplasma capsulatum* infection. *Cytokine*. 2012; 58:112-117.
7. Robinson WF, Robinson NA. Cardiovascular System. In: Maxie MG, ed. *Jubb, Kennedy, and Palmer's Pathology of Domestic Animals.* Vol 3. 6th ed. Philade l-phia, PA: Elsevier Saunders; 2016: 97-98.
8. Schlemmer SN, Fratzke AP, Gibbons P, et al. Histoplasmosis and multicent r ic lymphoma in a Nubian goat. *Journ Vet Diag Invest*. 2019; 31(5): 770-773.
9. Valli VEO, Kiupel M, Bienzle D. Hematopoietic System. In: Maxie MG, ed. *Jubb, Kennedy, and Palmer's Pathology of Domestic Animals.* Vol 3. 6th ed. Philadelphia, PA: Elsevier Saunders; 2016: 186-187.
10. Woods JP. Knocking on the right door and making a comfortable home: *Histoplasma capsulatum* intracellular pathogenesis. *Curr Opinion in Microbiol.* 2003; 6:327-331.
11. Woolums AR, DeNicola DB, Rhyan JC, Murphy DA, Kazacos KR, Jenkins SJ, Kaufman L, Thronburg M. Pulmonar y histoplasmosis in a llama. *J Vet Diagn Invest.* 1995; **7**:567-569.
12. Youseff BH, Holbrook ED, Smolnyck i KA, Rappleye CA. Extracellular Superoxide Dismutase Protects *Histoplasma* Yeast Cells from Host-Derived Oxidative Stress. *PLoS Pathog.* 2012; 8(5): e1002713.

CASE II:

Signalment:

Twelve-year-old, neutered female, domestic shorthair cat (*Felis catus*)

History:

The cat presented with a two month history of anorexia and weight loss. On presentation there was severe alopecia and erythema on the ventral thorax, abdomen, neck, perineum and also extended to the medial aspect of the legs to the paws. The periocular and ear pinna skin also presented with a similar change. Due to the characteristic shiny or gliste ning appearance of the skin, feline paraneoplastic alopecia was initially suspected. Ultrasound examination was performed with mult ip le masses detected in the liver and small hypoechoic nodule associated with the small intestinal, pancreas and peritoneum (neoplasia

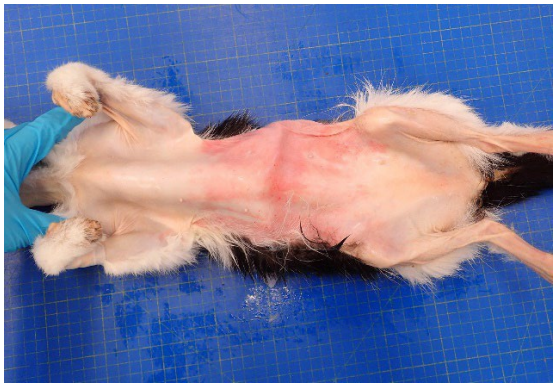

Figure 2-1. Haired skin, cat. Ventral and lateral abdominal skin and that of the extremities is severely alopecic with a glistening and shiny appearance. (Photo courtesy of: University of Liverpool, Institute of Infection, Veterinary and Ecological Sciences, Department of Veterinary Anatomy, Physiology and Pathology , Leahurst campus, Chester High Road, Neston, CH64 7TE, United Kingdom)

considered most likely). As the masses were widespread and the prognosis was poor, the animal was euthanized.

Gross Pathology:

The skin from the sternal to the inguinal regions, extending to the medial antebrachia and to the posterior extremities and partially the lateral abdominal regions, was severely alopecic with a glistening and shiny appearance. Throughout the alopecic skin, poorly demarcated pale red areas (erythema) and rare pale brown crusts were also present. Both periocular and perinasal areas were partially alopecic with increased amount of crusts. The right metatarsal paw pad and the right ventral tarsus showed multifocal ulcers. In the liver, scattered throughout all hepatic lobes, there were multifocal to coalescing, 0.2 to 2 cm in diameter, well demarcated, firm, pale tan nodules showing occasional central umbilication.

Laboratory Results:

No laboratory findings reported.

Microscopic Description:

Haired skin (abdomen)**:** Throughout a multifocally mildly hyperplastic epidermis there are multifocal areas of: intracellular edema, spongiosis, and parakeratosis. In rare foci (not present in all slides), the epidermis is restricted to 1-2, poorly defined, thin layers (epidermal atrophy). The hair follicles are diffusely and markedly reduced in size (atrophy and miniaturization) and contain rare intraluminal eosinophilic tricholemmal keratin (telogen). Adjacent to the atrophied follic les, variably atrophic sebaceous glands and commonly dilated apocrine glands are found. The dermis shows multifocal edema, with mild perivascular to interstitial accumulation of neutrophils, mast cells and extravasated erythrocytes (hemorrhage). Numerous deep dermal and subcutaneous lymphatic vessels (not present in all slides) are markedly dilated by intraluminal accumulation of concentrically arranged, homogenous and acellular eosinophilic material (likely proteinaceous lymph) and rare foamy (activated) macrophages.

Liver: Multifocally infiltrating and effacing the liver, there is a well demarcated, densely cellular, infiltrative and non-capsulated neoplastic proliferation. It is composed of confluent small islands, ribbons and nests of neoplastic cells showing occasionally central

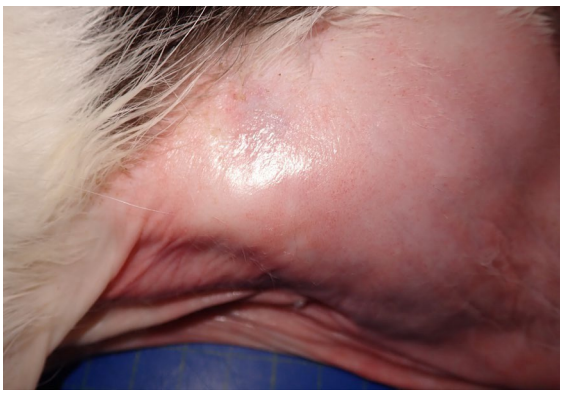

Figure 2-2. Haired skin, cat. Close examination of the shiny appearance to the epilated skin. (Photo courtesy of: University of Liverpool, Institute of Infection, Veterinary and Ecological Sciences, Department of Veterinary Anatomy, Physiology and Pathology, Leahurst campus, Chester High Road, Neston, CH64 7TE, United Kingdom)

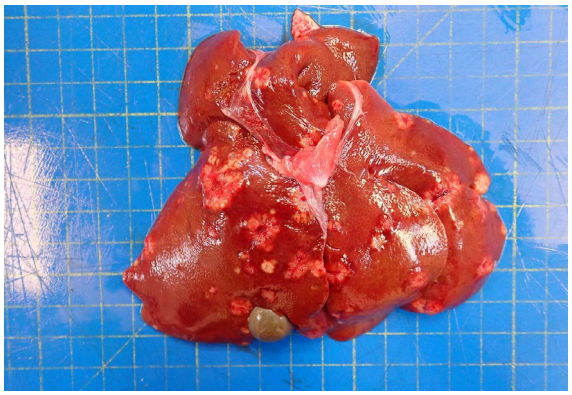

Figure 2-3. Liver, cat. Umbilicated neoplasms are present within all hepatic lobes. (Photo courtesy of: University of Liverpool, Institute of Infection, Veterinary and Ecological Sciences, Department of Veterinary Anatomy, Physiology and Pathology, Leahurst campus, Chester High Road, Neston, CH64 7TE, United Kingdom)

necrotic cores (comedonecrosis) and separated by moderate amount of edematous eosinophilic fibrovascular tissue (desmoplasia). Neoplastic cells are polygonal, variably sized 15-40 µm in length, showing indistinct cell borders, a moderate amount of eosinophilic fibrillary cytoplasm and a single, oval nucleus, bearing vesicular chromatin and 1-2 prominent nucleoli. Anisocytosis and anisokaryosis are moderate and 6 mitoses are observed in 10 HPF (40x objective). Neoplastic islands are also occasionally observed within blood vessels (tumor emboli). Embedded within the fibroblastic stroma, there are hemorrhages and scattered small compressed hepatocytes (compression atrophy). These hepatocytes occasionally have intracytoplasmic finely granular dark brown to green pigment (likely lipofuscin). Centrilobular hepatocytes shows frequently intracytoplasmic lipofuscin (geriatric finding).

Contributor's Morphologic Diagnoses:

Haired skin – severe bilateral ventrally-oriented symmetrical alopecia with glistening appearance with multifocal erythema and crusts.

Haired Skin – Mild multifocal to diffuse epidermal hyperplasia, with miniaturized and atrophic telogen hair follicles and multifocal parakeratotic hyperkeratosis

Haired skin – mild perivascular to interstitial neutrophilic and mastocytic dermatitis, with dermal edema

Liver – cholangiocarcinoma

Contributor's Comment:

The present case was characterized by widespread ventrally oriented bilateral and symmetrical alopecia revealing a shiny and glistening skin, in conjunction with multiple hepatic masses, extending to the pancreas. Histological examination revealed a widespread epidermal thickening with smaller hair follicles, containing very rare trichilemmal keratin. There was also a hepatic carcinoma, whose origin is most compatible with a cholangiocarcinoma. Based on the present findings, a diagnosis of feline paraneoplastic alopecia was made.

Feline paraneoplastic alopecia (FPA) is an infrequent but characteristic cutaneous disorder and has been reported in feline patients with a variety of neoplasms. Usually, FPA manifests between 7 and 16 years of age. It is classically associated with pancreatic carcinomas and bile duct carcinomas; nevertheless, other tumors such as hepatocellular carcinoma,[4]

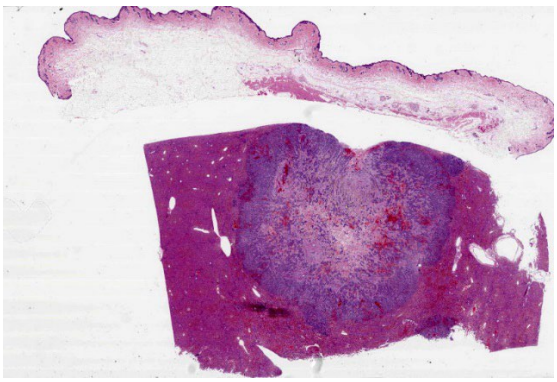

Figure 2-4. Haired skin and liver, cat. A section of haired skin (top) and liver (bottom) are submitted for examination. At subgross magnification, the haired skin has a remarkably paucity of follicles and adnexa, and a large multinodular neoplasm is present within the liver. (HE, 7X)

metastasizing intestinal carcinoma,[3] pancreatic neuro-endocrine and hepatosplenic plasma cell tumor[1] have been associated with this condition.

The characteristic glistening appearance with the mild epidermal hyperplasia and the severe atrophy and miniaturization of the hair follicles are considered key elements in the diagnosis. The skin is shiny, inelastic but not fragile, in contrast to that in hyperadrenocorticism: the latter is characterized by atrophic and telogenized hair follicles with epidermal atrophy rather than the hyperplasia observed in this case.

In FPA, it is reported that the stratum corneum is often missing, likely due to excessive grooming (although a clear evidence for this is lacking). This change, together with the patchy parakeratosis, is what is considered to give the spectacular shiny appearance. In the present case, both parakeratosis and absence of stratum corneum are present and alternating one with the other. Although the stratum corneum is often absent, the absence of the granular layer of the epidermis is inconsistently reported in the FPA reports.[4]

As in other reported FPA cases,[6] crusting, in association with *Malassezia* sp. proliferation was observed in the ear pinna skin but not in the submitted skin sample, and there was also paw pads fissuring and ulceration.

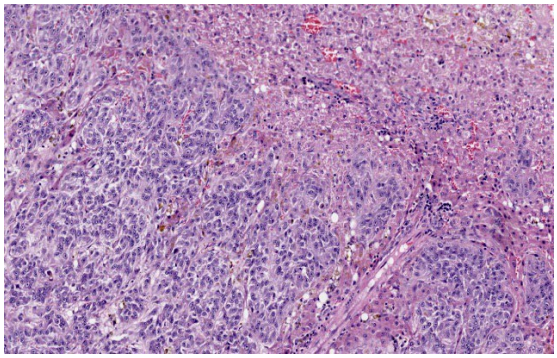

Figure 2-5. Liver, cat. The neoplasm is composed of nests, islands, and trabeculae of epithelial cells on a moderately dense fibrous stroma. (HE, 35X)

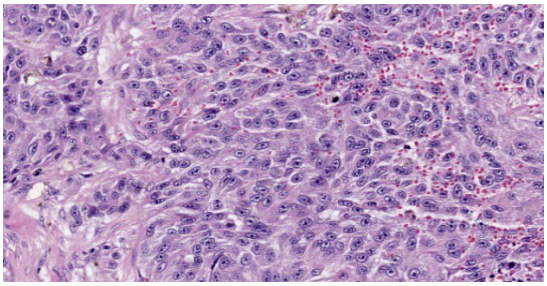

Figure 2-6. Liver, cat. High magnification of neoplastic cells. (HE, 381X)

Adnexae are usually normal or mildly atrophic. In the present case, normal sebaceous glands were intermixed with mildly atrophic ones. The apocrine glands, instead, were diffusely dilated and lined by flattened epithelial cells exhibiting evident suprabasilar cleft-like changes, compatible with either a genuine supra-basilar vacuolar degeneration or artefact.

Another unreported and striking finding was the presence of eosinophilic acellular (Congo red-negative) material in the deep lymphatic vessels, possibly suggestive of a protein rich fluid. There was some discussion about the origin of this change, as they could represent dilated mammary glands/ducts lined by very atrophic epithelial cells.

The hepatic neoplasia was cytologically and behaviorally malignant and consistent with an epithelial origin (i.e. carcinoma). The nodule in the pancreas showed an overlapping morphology with hepatic one, complicating the identification of the origin of the neoplasm. According to the bigger size of the hepatic masses and the histomorphology, a bile duct carcinoma (cholangiocarcinoma) is believed to be more likely. Nevertheless, other tumors, including exocrine pancreatic carcinoma or neuroendocrine pancreatic carcinoma cannot be fully excluded.

The pathogenesis of this cutaneous lesion has not been understood, due to its relative rarity. Considering that all the FPA-related tumors

reported show a variable neoplastic invasio n of the liver, it can be hypothesized that some hepatic metabolic derangement are responsible of the cutaneous disorder.

Contributing Institution:
University of Liverpool, Institute of Infection, Veterinary and Ecological Sciences Department of Veterinary Anatomy, Physiology and Pathology
Leahurst campus
Chester High Road, Neston,
CH64 7TE,
United Kingdom

JPC Diagnosis:
1. Liver: Carcinoma, poorly differentiated.
2. Haired skin, epidermis and adnexa: Atrophy, diffuse, severe, with telogenization of follicles.

JPC Comment:
The contributor lists two differential diagnoses that were discussed by conference participants: pancreatic carcinoma and neuroendocrine tumor. Participants could not definitively determine the cell of origin based on H&E and thus favored the diagnosis of poorly differentiated carcinoma. Additionally, participants remarked on the hepatic stellate cell (Ito cell) hyperplasia present

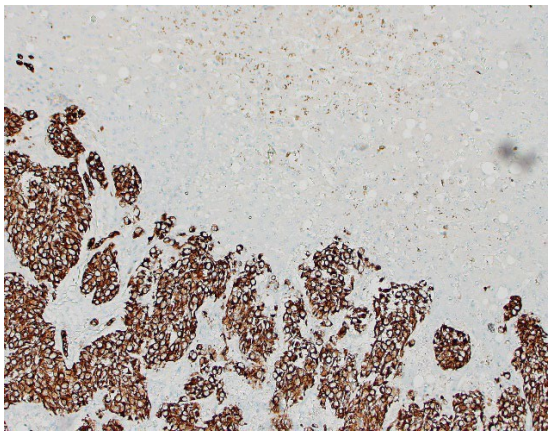

Figure 2-7. Liver, cat. Neoplastic cells are strongly positive for cytokeratins (AE1/AE3, 400X)

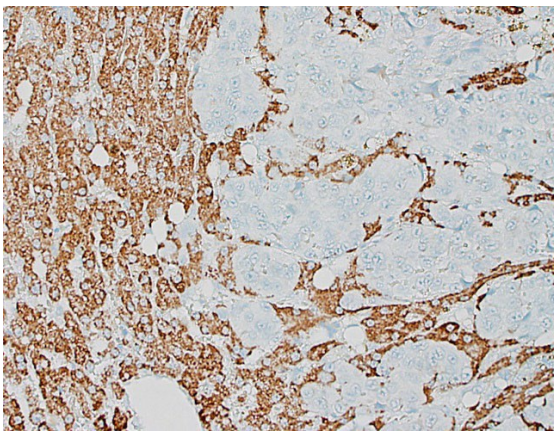

Figure 2-8. Liver, cat. Neoplastic cells are immunonegative for Hep-Par1, a hepatocyte stain. (anti Hep-par1, 400X)

throughout the liver, which may have been secondary to or unrelated to the neoplasm.

This case is a classic example of paraneoplastic syndrome: the manifestation of a disease in a separate organ system secondary to malignancy elsewhere in the body. While paraneoplastic syndromes in the integume n tary system are uncommon in animals, several distinct conditions have been reported.[1] Since integumentary lesions are easily detected by owners and often precede signs of the primary malignancy, paraneoplastic syndromes are frequently the reason for init ia l presentation of the patient.

Exfoliative dermatitis is another example of paraneoplastic syndrome causing alopecia in cats. This syndrome occurs secondary to thymomas in cats, rarely in rabbits, and anecdotally in a dog, though spontaneous (non-neoplastic) cases occur in cats as well.[5,7] Grossly, there is patchy to diffuse scaling and alopecia, with accumulation of brown waxy material around the claws and mucocutaneo us junctions.[5] Histologically, there is variable lymphocytic interface dermatitis and mural folliculitis with orthokeratotic hyperkeratosis, hydropic degeneration of keratinocytes, and decreased to absent sebaceous glands. [5, 7]

Paraneoplastic pemphigus has rarely been reported in dogs, a cat, and a horse and have occurred secondary to sarcomas and thymic lymphomas.[1,5,7] This is a rapidly progressive, severe condition characterized by blistering, erosions, and ulcerations at the mucocuta neous junctions and on mucosal surfaces. Histologically, the syndrome shares features of pemphigus vulgaris, with suprabasilar acantholysis, and erythema multiforme, with a cell-rich lymphohystiocytic interface derma- titis.[5, 7]

Necrolytic migratory erythema, also known as superficial necrolytic dermatitis or hepatocutaneous syndrome, occurs in dogs and rarely in cats secondary to glucagonoma and certain non-neoplastic conditions like diabetes mellitus and hepatic disease.[1, 5, 7] In cats, the condition has also been reported secondary to pancreatic carcinoma, hepatic carcinoid, and lymphoma.[7] Grossly, there is scaling and alopecia with erythema, blistering, and ulceration around the face, pinnae, and pressure points (i.e. elbows). The paw pads are frequently thickened and fissured.[1, 5, 7] Histologically, there is diffuse parakeratotic hyperkeratosis, severe hydropic degeneration and acanthosis within the superfic ia l stratum spinosum, and hyperplasia in the deeper stratum spinosum and stratum basale, imparting a distinct red, white, and blue striped appearance, and there is minimal inflammation.[5, 7]

Nodular dermatofibrosis is another paraneoplastic syndrome of the skin which occurs in German shepherd dogs and occasionally other large breed dogs in conjunction with renal cysts, renal cystadenocarcinomas, and uterine leiomyo- mas.[1, 5] These manifest as multifocal, slow-growing, nodular collagenous hamartomas typically in the subcutis and dermis of the extremities.[1, 5] Other reported paraneoplastic syndromes affecting the skin include necrotizing panniculitis (secondary to pancreatic neoplasia or pancreatitis in dogs, cats, and horses), cutaneous flushing (secondary to pheochromocytomas in dogs), and generalized pruritus (secondary to lymphoma in dogs and horses).[1, 5]

References:

1. Bergman PJ. Paraneoplastic Syndromes. In: Withrow SJ, Vail DM, Page RL, eds: *Withrow and MacEwen's Small Animal Clinical Oncology*. 5th ed. St. Louis, MO: Elsevier Saunders; 2013: 89-90.
2. Caporali C, Albanese F, Binanti D, Abramo F. Two cases of feline paraneoplastic alopecia associated with a neuroendocrine pancreatic neoplasia and a hepatosplenic plasma cell tumour. *Vet Dermatol*. 2016;**27**:508-e137
3. Grandt LM, Roethig A, Schroeder S, et al. Feline paraneoplastic alopecia associated with metastasising intestinal carcinoma. *JFMS Open Rep*. 2015:2055116915621582.
4. Marconato L, Albanese F, Viacava P, Marchetti V, Abramo F. Paraneoplastic alopecia associated with hepatocellular carcinoma in a cat. *Vet Dermatol*. 2007 ;**18**:267-71.
5. Mauldin EA, Peters-Kennedy J. Integumentary System. In: Maxie MG, ed. *Jubb, Kennedy, and Palmer's Pathology of Domestic Animals*. Vol 1. St. Louis, MO: Elsevier. 2016; 586, 603, 691-693.
6. Turek MM. Cutaneous paraneoplastic syndromes in dogs and cats: a review of the literature. *Vet Dermatol*. 2003;**14**:279-96.
7. Welle MM, Linder KE. The Integument. In: Zachary JF, ed. *Pathologic Basis of Veterinary Disease.* 7th ed. St. Louis, MO: Elsevier. 2022: 1209, 1255, 1261.

CASE III:

Signalment:
Adult (unknown age), female, Brazilian hedgehog/Brazilian porcupine (*Coendou prehensilis*)

History:
This porcupine was captured in a transitio nal region (native forest area on the outskirts of a small town) and sent to the Veterinary Hospital (UFMT) quite dehydrated and with swollen and wrinkled skin on its head. The animal received support treatment, but died the next day.

Gross Pathology:
The animal was submitted to necropsy and showed good conservation status. On the skin of the head (ear, periocular region, lateral face, muzzle and submandibular region), and in the perigenital region there were papules with irregular coalescing plaques, separated by superficial to deep grooves and moderately erythematous. These changes in the periocular region caused eyelid slit occlusion, blocking the view of the eyeball. Additionally, in the nasal and perioral plane region, there were yellowish crusts and a slight superficial erosion of the skin. In the internal examination, no significa nt alterations were observed.

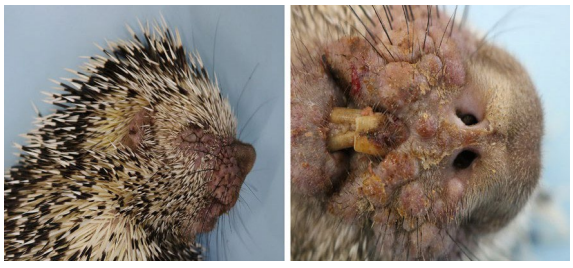

Figure 3-1. Haired skin, Brazilian hedgehog. Plaques of thickened crusted skin coalesce over the face of this hedgehog. (Photo courtesy of Universidade Federal de Mato Grosso, Faculdade de Medicina Veterinária, Hospital Veterinário, Laboratório de Patologia Veterinária, https:// www.ufmt.br/ufmt/site/, Av. Fernando Corrê a da Costa, nº 2367 - Bairro Boa Esperança. Cuiabá, Brasil - MT - 78060-900)

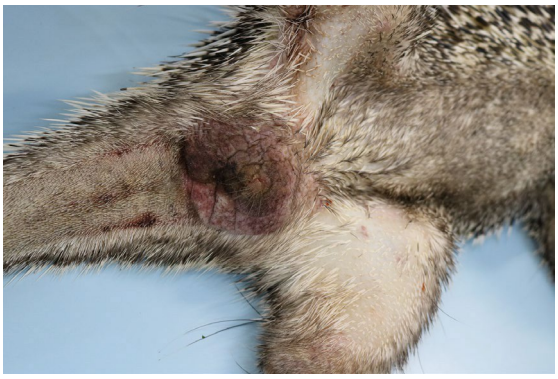

Figure 3-2. Haired skin, Brazilian porcupine. Similar plaques are present on the genitalia as well. (Photo courtesy of Universidade Federal de Mato Grosso, Faculdade de Medicina Veterinária, Hospital Veterinário, Laboratório de Patologia Veterinária, https:// www.ufmt.br/ufmt/site/, Av. Fernando Corrêa da Costa, nº 2367 - Bairro Boa Esperança. Cuiabá, Brasil- MT - 78060-900)

Laboratory Results:
A pan-pox universal PCR practice was performed[9] and subsequent amplico m sequencing, revealing 100% identity with the Brazilian porcupinepox virus (BPoPV).

Microscopic Description:
In the skin section, there are epidermal and hair follicles epithelial sheathing with intense proliferation and thickening (acanthosis). In the epidermis, interdigitations towards the dermis (rete pegs) are frequent. Multifoca l ly, keratinocytes show intracytoplasmic edema and vacuolization (ballooning degeneratio n). Intercellular edema and mild to moderate, random, multifocal acantholysis are also seen, mainly at the basal and spinous layers, and are often keratinocytes with round/oval, eosinophilic, intracytoplasmic inclus io n (Bollinger bodies). In the epidermis and hair follicles, there are multifocal areas of necrosis associated with moderate to severe neutrophil infiltration. There is a diffuse and moderate thickening of the stratum corneum in the epidermis, in which cell contours and finely elongated nuclei are seen, interspersed or paved with basophilic coccoid bacterial colonies (Brown & Hopps methods: gram

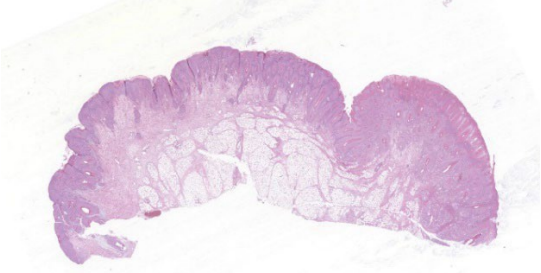

Figure 3-3. Haired skin, Brazilian porcupine. A single section of haired skin is submitted for examination. At subgross magnification, there is diffuse marked epidermal hyperplasia. (HE, 7X)

positive), associated with cellular debris of neutrophils and keratinocytes. In the dermis, from the dermic-epidermic junction to the adipose panniculus there is an infiltra t io n composed of lymphocytes, plasma cells and in multifocal to coalescent areas along with mononucleated inflammatory cells that present distended and eosinophilic cytoplasm with peripheral nucleus. Connective tissue fibers are separated (edema) with a discrete myxoid appearance, especially in the superficial dermis.

Contributor's Morphologic Diagnoses:

1. **Hairy skin, vulva:** Proliferat ive, necrotic, multifocal to coalescent epidermitis with parakeratotic hyperkeratosis, intracytoplasmic inclus io n bodies in keratinocytes and intraepider mal and follicular pustules.
2. **Hairy skin, vulva:** Diffuse, accentuated, and subacute lymphohistiocytic dermatitis.

Contributor's Comment:

Poxvirus is one of the largest and most complex known viruses. It is a double-stranded DNA virus which comprises a wide variety of susceptible species (vertebrates and invertebrates). Historically, it has as its main representative the variola virus (VARV), which causes human smallpox, the most devastating infectious disease in history.[3,11] In the present case, the morphological findings observed in this Brazilian porcupine (*Coendou prehensilis*) are consistent with an infection caused by a new genus of poxviruses belonging to the family Poxviridae, subfamily Chordopox-virinae. The first report of this infect io n occurred in 2019 in Brazil, in a free-living Brazilian porcupine that had lesions characteristic of poxvirus infection (There are approximately 1000 km of distance between the case reported by Hora in 2019 and this case). As it is phylogenetica l ly distinct from the other poxviruses previously reported, this poxvirus was named Brazilian Porcupinepox Virus (BPoPV).[6]

Brazilian porcupine (OC) is an arboreal rodent belonging to the Erethizont idae family, found in forests and riparian areas in several South American countries. This animal is more frequently observed in Brazil, where in the last two years have been reports of OC showing characteristic clinical signs of poxvirus infection, associated with high mortality. This situation increased the alert regarding the risk and threat to the conservation of this species.[6]

Macroscopically, the lesions are characterized by wrinkling, thickening and skin erythema of the head, limbs, and genitals.[6] Initially, these lesions appear as papules that coalesce and transform into plaques. Microscopically, the lesions occur mainly at the mucocutaneous junction, and are characterized by prolifera t ive (hyperplasia and hyperkeratosis) and degenerative (ballooning degeneration and intercellular edema) changes in keratinocytes with visualization of intracytoplas m ic eosinophilic viral inclusions.[6] These macroscopic and microscopic changes were also seen in this case and are typically related to poxvirus infection.[11]

Other rodents and also lagomorphs are also susceptible to poxvirus infections, but with

clinical manifestations, different from those presented by porcupines. Among them, myxomatosis in rabbits stands out, a fatal disease caused by the myxoma virus (MYXV), a leporipoxvirus belonging to the Poxviridae family that is antigenically associated with the rabbit fibroma virus. [1,4] It is characterized by the presence of cutaneous nodules (myxomas) around the eyes, nose, mouth, ears and genitalia. It can also present in the amyxomatous (respiratory) form, with different degrees of severity.[1,6] Microscopically, skin lesions consist of proliferation of stellate mesenchymal cells surrounded by a mucinous matrix. Intracytoplasmic inclusions are also observed in various cell types, as well as hyperplasia and/or degeneration in keratinocytes.[8]

Another member of the Poxviridae family is the rabbit fibroma virus (Shope), initially considered a benign disease, however, it can cause high morbidity and mortality in newborn animals. It is characterized by flat, mobile subcutaneous nodules that occur mainly on the limbs, feet, ears, muzzle and around the eyes, regressing spontaneously within a few months. Microscopic examination of skin lesions reveals proliferation of mesenchymal cells that become stellate or ovoid with multifocal areas of necrosis and inflammatory infiltrates of mononuclear and polymorphonuclear cells.[8]

Squirrel fibromatosis (SF) is caused by a poxvirus of the genus Leporipoxvirus, subfamily Chordopoxvirinae, and is also closely associated with rabbit fibroma virus. It has been described in red squirrels (*Tamiasciurus hudsonicus*), gray squirrels (*Sciurus carolinensis*) and fox squirrels (*Sciurus niger*). Macroscopically, the disease is characterized by firm, alopecic dermal nodules. Microscopically, typical poxviral lesions, epidermal hyperplasia, ballooning degeneration and intracytoplasmic inclusion bodies are observed, and the proliferation of atypical fibroblasts in the superficial dermis makes it distinct from other infections.[2]

It has been reported in pygmy mice proliferative epidermal lesions on the tail and paws caused by a poxvirus. Lesions appeared

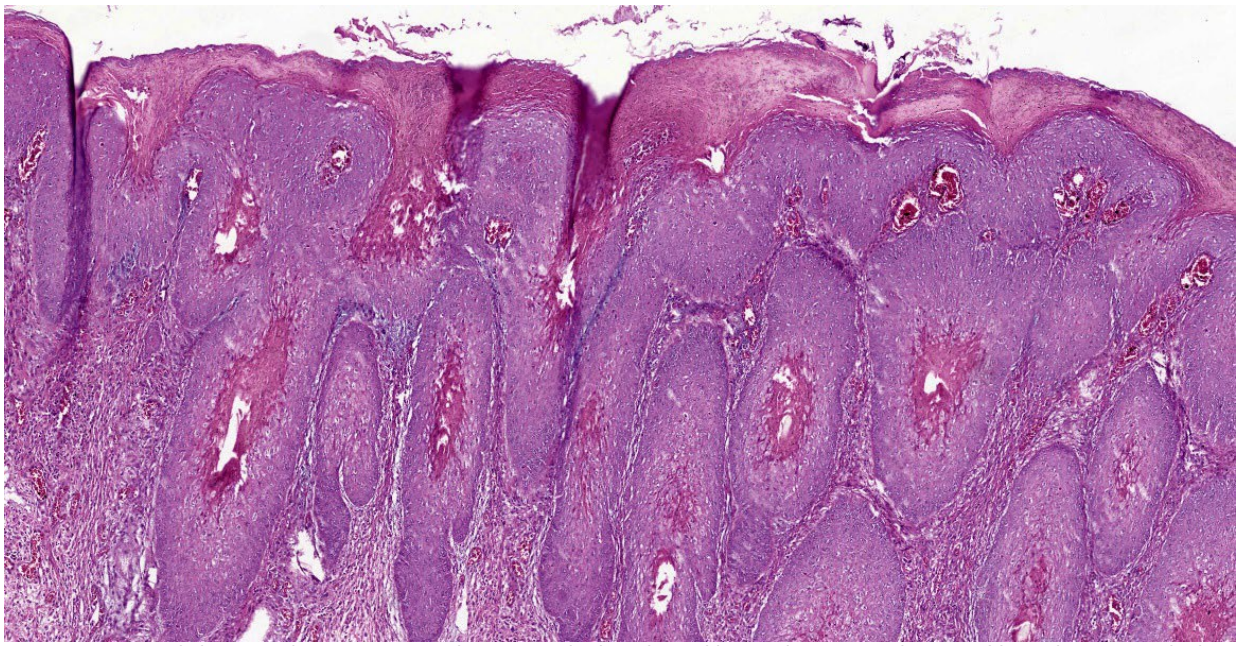

Figure 3-4. Haired skin, Brazilian porcupine. There is marked epidermal hyperplasia, acanthosis and hyperkeratosis which extends down into follicular ostia. (HE, 55X)

as firm, irregular, and pedunculated masses. On microscopic examination, the epidermis presents orthokeratotic and parakeratotic hyperkeratosis, ballooning degeneration of keratinocytes, and intracytoplas m ic eosinophilic viral inclusions. Molecular analyzes identified that this poxvirus did not belong to any recognized genus until March 2018, this new species being called Brazospox virus,[5] therefore molecular methods play a fundamental role in the identification and monitoring of the propagation of new poxviruses in wild animals, allowing warnings about the risk and emergence of diseases that represent risks to the conservation of species, especially those that are threatened.

Contributing Institution:
Universidade Federal de Mato Grosso, Faculdade de Medicina Veterinária, Hospital Veterinário, Laboratório de Patologia Veterinária, https:// www.ufmt.br/ufmt/site/, Av. Fernando Corrêa da Costa, nº 2367 - Bairro Boa Esperança. Cuiabá, Brasil - MT - 78060-900

JPC Diagnosis:
Haired skin, epithelium: Hyperplasia, diffuse, severe, with ballooning degeneratio n, necrosis, and intracytoplasmic viral inclusions.

JPC Comment:
The contributor provides both an informa t ive example of the novel Brazilian porcupine poxvirus and a broad overview of the *Leporipoxvirus* genus. These viruses all belong to the subfamily Chordopoxvirinae, or poxviruses which infect vertebrates.[6] There are ten genera and several newer unclassified viruses within this subfamily.[6] The *Orthopoxvirus* genus contains several poxviruses which are zoonotic or pathogenic to humans, including both the historically devastating and now eradicated variola virus (smallpo x)

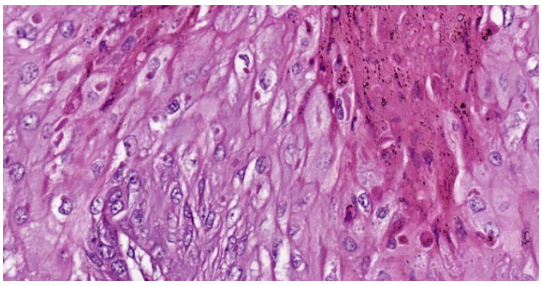

Figure 3-5. Haired skin, Brazilian porcupine. Numerous keratinocytes, often displaying ballooning degenerative changes, contain 2-4 um round intracytoplasmic viral inclusions. (HE, 663X)

and the newer emerging public health threat, monkeypox virus.[6, 12, 16]

Smallpox has affected the human population for millennia, with evidence of smallpox lesions in Egyptian mummies from 1186-1070 BC.[12] Smallpox is estimated to have caused 400,000 deaths annually in Europe in the eighteenth century and up to 4 million deaths in the Aztec and Incan empires after introduction of the virus to the Americas.[12] Initial vaccines were developed in the eighteenth century, and after a widespread eradication campaign, the World Health Organization declared the disease eradicated in the late 1970s.[16] Importantly, smallpox has a very narrow host range and lacks an animal reservoir, which made it susceptible to eradication strategies and contrasts with the wide host range of monkeypox virus.[12]

Monkeypox virus was first identified in cynomologous macaques imported from Africa into Copenhagen, Denmark in 1958.[12, 16] This discovery lead to the somewhat inaccurate naming of the virus, whose largest known reservoir is rodents.[16] Monkeypox infections have been documented in a wide range of animals, including numerous species of mice and rats, prairie dogs, hedgehogs, opossums, wild boar, several monkey and macaque species, orangutans, chimpanzees, and gorillas.[12] The first report of infection in

a human occurred in 1970 in the Democratic Republic of Congo (previously Zaire). Humans can be infected from direct or indirect contact with animals, such as bites, scratches, and the hunting of small animals for bushmeat.[16]

After 1970, case rates slowly increased in Central and West Africa.[16] Some of this spread is attributed to waning population immunity after termination of smallpox vaccination campaigns, which had offered cross protection against other orthopox-viruse s; other factors include increased interactio n with wildlife, civil unrest, and population dynamics.[16] Sporadic outbreaks outside of Africa occurred due to import of infected animals (United States in 2003) and international travel (UK and Israel in 2018).[16]

The current monkeypox outbreak began in May 2022 and has been designated as a public health emergency of international concern by the World Health Organization.[1, 18] As of September 2, 2022, 51,163 laboratory confirmed cases and 17 deaths have been reported in 102 countries around the world.[1] Transmission occurs through large respiratory droplets and direct contact with skin lesions, and over 95% of reported cases are in men who have sex with men.[1, 18] Clinica l signs include fever and lymphadenopat hy, with painful skin lesions such as papules, pustules, and ulcers most commonly found in the anogenital area, trunk and limbs, or face.[18]

In the current outbreak, only one case of monkeypox to date has been reported in a companion animal.[14,17] A four year old male Italian greyhound living in a household with two humans infected monkeypox developed mucocutaneous pustules and ulcers.[17] Swabs from the skin lesions were PCR positive for monkeypox and showed 100% homology with the virus isolated from one of the human owners.[17]

References:

1. 2022 Monkeypox Outbreak: Global Trends. World Health Organization. September 2, 2022. Accessed September 4, 2022. https://worldhealthorg.shinyapps.io/mpx_global/
2. Abade dos Santos, FA; Carvalho, CL; Pinto, A. et al. Detection of Recombina nt Hare Myxoma Virus in Wild Rabbits (Oryctolagus cuniculus algirus). *Viruses*. 2020, 12:1127.
3. Bangari DS, Miller MA, Stevenson GW et al. Cutaneous and systemic poxviral disease in red (*Tamiasciurus hudsonicus*) and gray (*Sciurus carolinensis*) squirrels. Vet Pathol. 2009,46(4):667-72.
4. Barrett, JW, McFadden, G. Origin and Evolution of Poxviruses. In: Domingo, E, Parrish, CR, Holland, JJ. Origin and *Evolution of Viruses*. Academic Press. 2008:431-446.
5. Bertagnoli S, Marchandeau S. Myxomatosis. *Rev Sci Tech*. 2015; 34(2):549-56.
6. Delhon GA. Poxviridae. In: MacLachlan NJ, Dubovi AJ, eds. *Fenner's Veterinary Virology*. 5th ed. New York, NY: Elsevier. 2017; 157-174.
7. Hodo CL, Mauldin MR, Light JE et al. Novel Poxvirus in Proliferative Lesions of Wild Rodents in East Central Texas, USA. *Emerg Infect Dis*. 2018;24(6):1069-1072.
8. Hora AS, Taniwaki SA, Martins NB, et al. Genomic Analysis of Novel Poxvirus Brazilian Porcupinepox Virus, Brazil, 2019. *Emerg Infect Dis.* 2021:(4): 1177-1180.
9. Hughes AL, Irausquin S, Friedman R. The evolutionary biology of poxviruses. Infect Genet Evol. 2010 Jan;10(1):50-9.

10. Krogstad AP, Simpson JE, Korte SW. Viral diseases of the rabbit. *Vet Clin North Am Exot Anim Pract.* 2005;8(1):123-38.
11. Li Y, Meyer H, Zhao H, et al. GC content-based pan-pox universal PCR assays for poxvirus detection. *J Clin Microbiol*. 2010;48(1):268-276.
12. MacNeill AL. Comparative Pathology of Zoonotic Orthopoxviruses. *Pathogens*. 2022; 11(8):892-914.
13. Marinho-Filho, J., & Emmons, L. 2016. *Coendou prehensilis*. *The IUCN Red List of Threatened Species* 2016: e.T101228458A22214580. https://dx.doi.org/10.2305/IUCN.UK.2016-2.RLTS.T101228458A22214580.en. Downloaded on 28 July 2021.
14. Monkeypox in Animals. Centers for Disease Control and Prevention. August 17, 2022. Accessed September 4, 2022. https://www.cdc.gov/poxvirus/monkeypox/veterinarian/monkeypox- in-animals.html
15. Oliveira JS, Figueiredo PO, Costa GB, et al. Vaccinia Virus Natural Infections in: Brazil: The Good, the Bad, and the Ugly. *Vírus*. 2017; 9(11):340.
16. Peterson E, Koopmans M, Yinka-Ogunleye A, Ihekweazu C, Zumla A. Human Monkeypox Epidemiologic and Clinical Characteristics, Diagnosis, and Prevention. Infect *Dis Clin N Am.* 2019; 33: 1027-1043.
17. Seang S, Burrel S, Todesco E, et al. Evidence of human-to-dog transmission of monkeypox virus. *The Lancet.* 2022; 500(10353):658-659.
18. Thornhill JP, Barkati S, Walmsley S, et a. Monkeypox Virus Infection in Humans across 16 Countries – April-June 2022. *The New England Journal of Medicine*. 2022;387(8):679-691.

CASE IV:

Signalment:
17-year-old, female spayed, domestic short-hair cat (*Felis catus*)

History:
The patient presented for evaluation of progressive weight loss and inappetence. Recent increase in seizure activity. Newly diagnosed pulmonary mass, presumptive pulmonar y carcinoma. Historical small cell lympho ma, chronic rhinitis, hyperthyroidism, acute cerebral infarction.

Clinical Diagnosis:
1. Historical acute cerebral infarction
2. Stable small cell lymphoma
3. Pulmonary carcinoma
4. Hyperthyroidism
5. Chronic idiopathic rhinitis
6. Acute exacerbation of neurologic signs
7. Progressive weight loss - metastatic disease

Gross Pathology:
The mucosa of the body of the stomach is markedly expanded by irregular, cobble- stone-like thickening of the gastric rugae (rule out neoplasia vs proliferative gastritis vs lymphofollicular hyperplasia. The irregular mucosal thickening up to 2.5 mm can be appreciated within the mucosa upon sectioning of the fixed tissue.

Laboratory Results:
Abdominal ultrasound of the stomach was normal.

Microscopic Description:
Two sections of gastric wall from the body/pylorus of the stomach are examined. The mucosa is highly folded and increased in thickness, measuring up to 2 mm. The thickened mucosa comprises increased numbers of

gastric pits lined by abundant mucus containing epithelial cells (mucus neck cells) which are typically lined by a single epithelial cell, but multifocally pile up to 2-3 cell layers thick. Chief and parietal cells are present but comprise a minority of the mucosal area. There are increased numbers of inflammatory cells throughout the lamina propria, with ectatic gastric glands and frequent glandular and luminal nematode parasites. Nematode parasites range from 20-30 um in diameter, with regularly arranged, evenly spaced cuticular spicules. These parasites have platymyarian-meromyarian musculature, a pseudocoelom with a large intestine composed of few multinucleated cells and reproductive structures. Moderately increased amounts of fibrous connective tissue are noted throughout the lamina propria, sometimes concentrically surrounding and separating glands that contain nematode parasites. Inflammation consists of predominantly lymphocytes with fewer plasma cells, macrophages and eosinophils throughout the lamina propria. Lymphocyte aggregates are occasionally present without formation of follicular structures. Multifocally, ectatic gastric glands contain sloughed cells and necrotic cell debris with occasional nematode parasites. The lining glandular epithelium of these dilated glands is multifocally attenuated. The submucosa

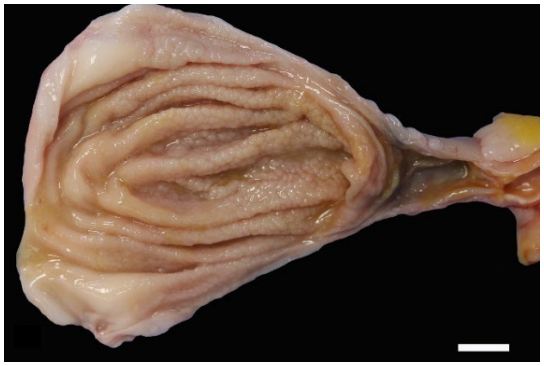

Figure 4-1. Stomach, cat. The mucosa of the body of the stomach is markedly expanded by irregular, cobblestone-like thickening of the gastric rugae (Photo courtesy of Animal Medical Center, 510 East 62nd St. New York, NY 10065, www.amcny.org)

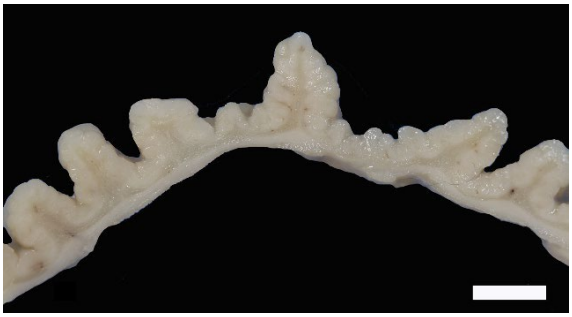

Figure 4-2. Stomach, cat. A cross-section of the gastric mucosa is irregularly thickened up to 2.5mm. (Photo courtesy of Animal Medical Center, 510 East 62nd St. New York, NY 10065, www.amcny.org)

contains adipose tissue (within normal limits for spp).

Contributor's Morphologic Diagnoses:
Stomach: Gastritis, proliferative, lymphocytic, chronic, marked with fibrosis, luminal and glandular nematode parasites (morphology consistent with *Ollulanis tricuspis*)

Contributor's Comment:
The grossly identified cobblestone-like thickening of the stomach mucosa corresponds with proliferative gastritis and nematode parasitism. Numerous nematode parasites observed throughout the mucosa were histologically consistent with trichostronglyes, for which *Ollulanus tricuspis* is given primary consideration.[6] Confirmatory ancillary tests were not performed. *Ollulanis tricuspis* is a small (0.7-1.0 mm length) trichostrongl yid nematode with worldwide distribution.[4] This parasite is typically found in the stomach of domestic cats but has been reported in large, non-domestic felids (including captive cheetah, tigers, lions and cougars), dogs, red foxes and pigs.[2,4,5,7,10] *Ollulanis tricuspis* has a direct life cycle, transmitted by ingestion of infected vomitus.[2,4,5,7-10] No paratenic or intermediate hosts have been identified.[5] *O. tricuspis* is larviparous, third stage (L3) larvae developing in the uterus. L3s eliminated in the vomitus are thought to be infective and can remain viable for up to 12 days. A single sample of vomitus can contain 0 to greater

than 170 parasites.[5,7] Feral and colony-raised cats may have a higher likelihood of being infected due to the concentration of numerous cats in a small area.[9] It has been suggested that infected long-haired cats are more likely to transmit the parasite because of more frequent vomiting due to a higher tendency to develop gastric trichobezoars.[8,9]

Infection with this parasite is frequently incidental.[4] The parasite is thought to increase gastric mucus production.[7] Clinical signs, when present include anorexia, weight loss and intermittent vomiting, however heavy infections can cause severe gastritis, neoplastic transformation and rarely death.[4,10] Vomiting has been reported as the most common clinical sign.[4] This patient had multiple concurrent comorbidities, some of which could also present with vomiting (e.g. intestinal small cell lymphoma), however, gastrointest inal signs were not listed as a prominent clinica l concern in the historical summary. Despite the large numbers of parasites and prominence of the gastric mucosal proliferation, infection with this parasite was most likely incidental.

In felids with *O. tricuspis* parasitism, the gross appearance of the stomach can vary, depending upon the severity of the infect io n, ranging from macroscopically normal to grossly evident gastritis with mucosal hyperplasia and rugal thickening.[8] In one study,

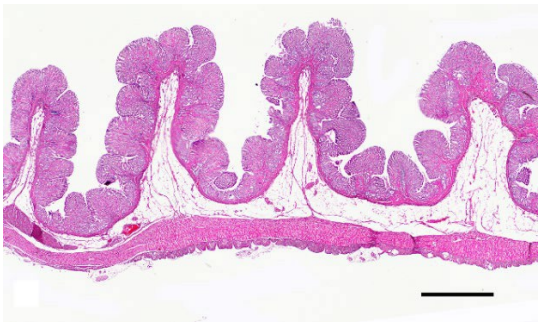

Figure 4-3. Stomach cat. The mucosa is highly folded and increased in thickness, measuring up to 2 mm. (Photo courtesy of Animal Medical Center, 510 East 62nd St. New York, NY 10065, www.amcny.org)(HE, 100X)

only 1 of 26 cats infected with *O. tricuspis* had grossly visible gastric lesions.[9] Reported histologic lesions include mucosal hyperplasia, mucosal erosion, fibrosis, increased mucosal lymphoid aggregates (some of which display large germinal centers) and increased globule leukocytes.[7,8,9,12] In this case, gastritis predominantly comprised lymphocytes with lymphocyte aggregates but no formation of follicular structures. Increased globule leukocytes were not observed. Mucosal proliferation is attributed to hyperplasia of mucus containing epithelial cells of the gastric pits. Parasites were generally observed within gastric glands as well as the gastric lumen. Fibrosis was also noted, sometimes concentrically surrounding glands with luminal parasites. Fibrosis was more promine nt in the deeper portions of the stomach, just superficial to the muscularis mucosa, as has been previously reported.[8]

Other nematode parasites reported in the stomach of cats include *Gnathostoma* sp, *Cylicospirura* felineus, *Physaloptera*, *Cyathospirura* sp, *Aleurostrongylus abstrusus*, *Spirocerca lupi*, *Aonchotheca putorii*, other *Trichostronglyus* spp and oxyurids of prey animals (e.g. mice).[4,5,12] The demonstratio n of regular cuticular spicules is considered a key distinguishing morphologic feature of adult *O. tricuspis*.[4,6,9] These small parasites can be easily overlooked (both at postmortem examination and clinical examination of vomitus), thus the occurrence may be underestimated, as parasites or eggs are not typically present in feces.[4] Adult *O. tricuspis* usually die due to the high pH of the small intestine and are digested before excretion into the feces.[5] Small worm burdens may lead to difficultly observing or identifying parasites in histologic samples. In studies involving postmortem examination of stomach samples, worms were only identified in half the cats with *O. tricuspis* in three histologic sections, however, all cats had inflammatory changes

consistent with *O. tricuspis* infection.[9] Thus, pathologists should carefully ev-
aluate samples of gastric mucosa in which the typical histologic features of *O. tricuspis* infection are observed. A differential diagnosis in captive cheetah is infection with gastric spiral bacteria (*Helicobacter* spp) which can chronic gastritis.[5] Antemortem methods of diagnosing infections with this parasite include antemortem gastric washings or gastric mucosal scrapings in addition to obtaining endoscopic biopsies. Postmortem peptic digestion of stomach samples can also be performed.[5,7]

Contributing Institution:
Animal Medical Center, 510 East 62nd St. New York, NY 10065, www.amcny.org

JPC Diagnosis:
Stomach, pylorus: Gastritis, proliferat ive, chronic, diffuse, moderate, with mucous neck cell hyperplasia, glandular atrophy, and luminal and intraglandular trichostrongyle adults and larvae.

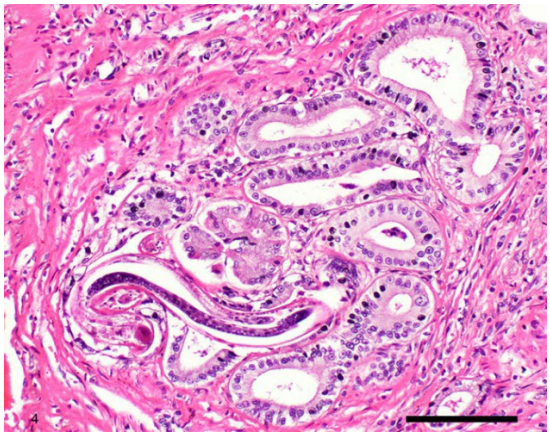

Figure 4-4. Stomach cat. Gastric glands in the deeper mucosa are surrounded by fibrous connective tissue, contain low numbers of a mixed inflammatory population, and cross sections of adult trichostrongyle nematodes. (Photo courtesy of Animal Medical Center, 510 East 62nd St. New York, NY 10065, www.amcny.org) (HE, 400X)

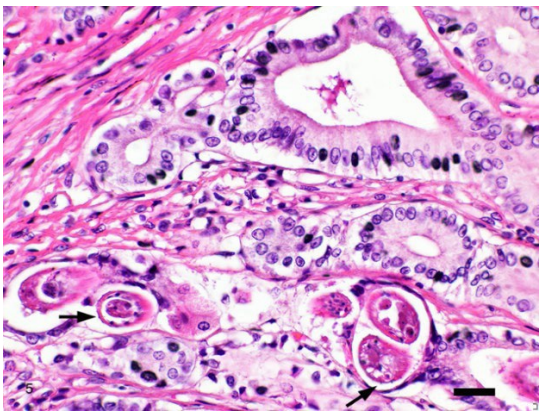

Figure 4-5. Stomach, cat. Cross sections of the nematodes demonstrate evenly spaced cuticular ridges (arrow) and platymyarian-meromyarian musculature. (Photo courtesy of Animal Medical Center, 510 East 62nd St. New York, NY 10065, www.amcny.org) (HE, 400X)

JPC Comment:
The contributor provides a thorough report on this nematode in the stomach of cats. As the contributor mentions, low *O. tricuspis* burdens can make histopathologic examination an insensitive means of detection of the parasite, and the absence of parasites in histologic sections may lead pathologis ts searching for other differentials. One rare nonparasitic differential which causes simi- lar histologic lesions is chronic hypertrophic gastritis, or Ménétrier's-like disease. In this condition, gastric rugae are diffusely thickened with variable cystic glandular dilation.[1, 11] Histologically, there is mucous cell hyperplasia and atrophy of the oxyntic glands coupled with a mononuclear infiltrate within the mucosa.[1, 11] While Ménétrier's disease and its canine equivalent are rarely reported, there is only a single report of a similar condition in a cat.[1] The patient was a young adult domestic shorthair cat with a history of chronic weight loss and increased appetite.[1] Gastric biopsies showed mucosal hypertrophy with variable cystic glandular dilation, glandular atrophy, fibrosis, and lymphoplasmacytic inflammation.[1] While no evidence of parasitism was observed on histology, the patient in this report was euthanized without necropsy,

so the authors were unable to conduct ancillary testing to rule out *O. tricuspis*. [1]

As the contributor mentions, *Ollulanis* nematodes and eggs are rarely found in feces; thus, a few unique methods can be used to detect infection. Antemortem diagnosis typically involves cytologic examination of gastric fluid collected through gastric lavage or induction of emesis.[3] The specimen is centrifuged or filtered through a Baermann apparatus prior to cytologic examination, which has an estimated sensitivity of 70%.[3] In postmortem specimens, rice-grain sized scrapings collected from various areas of the gastric mucosa are mixed with saline (and KOH if needed) and examined cytologically.[3] Peptide-digestion can also be conducted, but is more laborious and involves everting and soaking the entire stomach in pepsin digestion fluid at 37 degrees Celsius for up to 8 hours and examining the sediment for nematodes.[3]

References:

1. Barker EN, Holdsworth AS, Hibbert A, Brown PJ, Hayward NJ. Hyperplastic and fibrosing gastropathy resembling Ménétrier disease in a cat. *JFMS Open Rep.* 2019;5(2)1-7.
2. Bell AG. *Ollulanus tricuspis* in a cat colony. N Z Vet J. 1984 Jun;32(6):85-7.
3. Bowman DB, Hendrix CM, Lindsay DS, Barr SC. *Feline Clinical Parasitology*. Ames, IO: Iowa State University Press. 2002; 263.
4. Cecchi R, Wills SJ, Dean R et al. Demonstration of *Ollulanis tricuspis* in the stomach of domestic cats by biopsy. *J Comp Pathol* 2006. 134:374-77.
5. Collett MG, Pomroy WE, Guilford WG, et al. Gastric *Ollulanus tricuspis* infection identified in captive cheetahs (Acinonyx jubatus) with chronic vomiting. *J S Afr Vet Assoc.* 2000 Dec;71(4):251-5.
6. Gardiner CH, Poynton SL. *An Atlas of Metazoan Parasites in Animal Tissues*. Washington, DC: Armed Forces Institute of Pathology;1999:22-26.
7. Guy, P A. *Ollulanis tricuspis* in domestic cats – prevalence and methods of postmortem diagnosis. *New Zealand Vet J.* 1984. 32(6):81-84.
8. Hargis AM, Prieur DJ, Blanchard JL. Prevalence, lesions and different ia l diagnosis of *Ollulanis tricuspis* infection in cats. *Vet Pathol.* 1983. 20:71-79.
9. Hargis, A M, Prieur DJ, Blanchard JL, et al. Chronic fibrosing gastrit is associated with *Ollulanus tricuspis* in a cat. *Vet Pathol* 1982. 19: 320-323.
10. Kato D, Oishi M, Ohno K, et al. The first report of the ante-mortem diagnosis of *Ollulanis tricuspis* infect io n in two dogs. J Vet Med Sci. 2015. 77(11):1499-1502.
11. Uzal FA, Plannter BL, Hostetter JM. Alimentary System. In: Maxie MG, ed. *Jubb, Kennedy, and Palmer's Pathology of Domestic Animals*. Vol 2. 6th ed. St. Louis, MO: Elsevier. 2013; 53.
12. Veterinary Systemic Pathology Online:https://www.ask-jpc.org/vspo/show_page.php?id=ejYyVGcraFE3alY5cGF-WeXJtdVVzZz09

WSC 2022-2023 Self-assessment.
Conference 4

1. Which of the following forms is inhaled by a susceptible host, initiating an infection with *Histoplasma capsulatum*?
    a. Aelurospores
    b. Hyphae
    c. Yeasts
    d. Microconidia

2. Neoplasms of which of the following has not been associated with paraneoplastic alopecia in cats?
    a. Liver
    b. Lung
    c. Intestine
    d. Neuroendocrine system

3. Hair follicles in cats with paraneoplastic alopecia are present in which stage?.
    a. Anagen
    b. Catagen
    c. Telogen

4. Which of the following is a characteristic change in keratinocytes following poxviral infection?.
    a. Ballooning degeneration
    b. Apoptosis
    c. Dysplasia
    d. Dyskeratosis

5. *Ollulanus tricuspis* is transmitted via?
    a. Respiratory secretions
    b. Wounds
    c. Feces
    d. Vomit

Please email your completed assessment for grading to Dr. Bruce Williams at bruce.h.williams12.civ@mail.mil. Passing score is 80%. This program (RACE program 33611) is approved by the AAVSB RACE to offer a total of 0.5 CE Credits, with a maximum of 12.5 CE Credits being available to any individual Veterinary Medical Professionals for the 2019-2020 Wednesday Slide Conference. This RACE approval is for the subject matter categories of: SCIENTIFIC using the delivery method of NONINTERACTIVE DISTANCE. This approval is valid in jurisdictions which recognize AAVSB RACE.

Joint Pathology Center
Veterinary Pathology Services

WEDNESDAY SLIDE CONFERENCE 2022-2023

Conference #5 21 September 2022

CASE I:

Signalment:
15-month-old, female, French bulldog, *Canis lupus familiaris*

History:
Fifteen month old French bulldog with chronic diarrhea for months that occasionally contained blood but not always. Some weight loss with a current BCS 4.5/10. Fecal smear was positive for giardia. Treated with fenbendazole / metronidazole. No more blood reported in stools but still chronic diarrhea. The dog was euthanized and the necropsy revealed a very thickened large intestine and distal small intestine. Owner says they have had other dogs with similar symptoms without any successful treatment.

Laboratory Results:
No laboratory findings reported.

Microscopic Description:
Within the submitted and examined sections of colon the mucosa and underlying submucosa is markedly expanded by a dense infiltrate composed of large numbers of macrophages admixed with lesser numbers of neutrophils, lymphocytes, and plasma cells. These macrophages often contain abundant vacuolated cytoplasm with karyorrhectic debris and rare intracytoplasmic basophilic rod-shaped bacteria. There is also multifocal to coalescing ulceration of the mucosa that varies from superficial to nearly full thickness. The deep mucosa and submucosa underlying the most severely affected areas contains increased numbers of neutrophils. The colonic glands are mildly hyperplastic with evidence of regeneration including piling of glandular epithelium, karyomegaly, increased cyto-

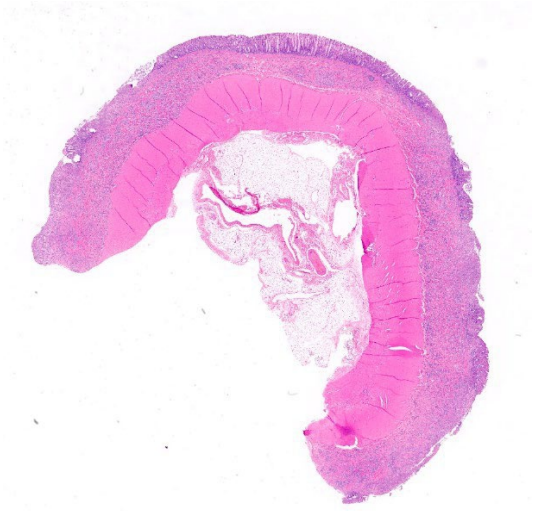

Figure 1-1. Colon, French bulldog. Multifocal ulceration and erosion of the colonic mucosa along with an expanded submucosa with marked increased cellularity. (HE, 5X) (Photo courtesy of: Kansas State Veterinary Diagnostic Laboratory (KSVDL), http://ww.ksvdl.org/)

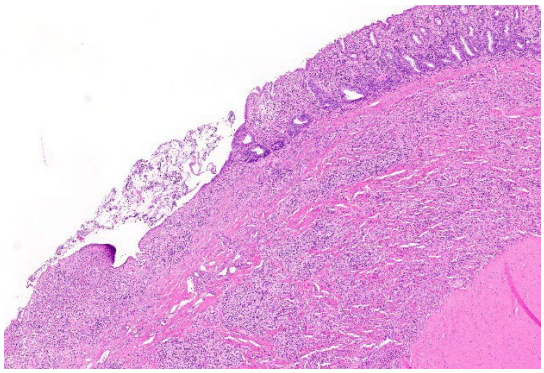

Figure 1-2. Colon, French bulldog. Area of mucosal ulceration with underlying diffuse infiltration of the submucosa. The adjacent intact mucosa is also expanded by a marked cellular infiltrate. (HE, 40X) (Photo courtesy of: Kansas State Veterinary Diagnostic Laboratory (KSVDL), http://ww.ksvdl.org/)

plasmic basophilia, and frequent mitotic figures. Occasionally these glands contain small numbers of intraluminal spirochete-like organisms.

The macrophages present within the mucosa and submucosa contain frequent PAS positive material within their cytoplasm.

Contributor's Morphologic Diagnoses:
Colon: Histiocytic and ulcerative colitis, multifocal to coalescing, severe

Contributor's Comment:
Histiocytic ulcerative colitis (HUC), also known as granulomatous colitis (GC), is a chronic enteropathy of dogs that was first reported in 1965.[15] It is histologically characterized by marked infiltration of the colonic mucosa and submucosa by large, periodic acid-Schiff (PAS)-positive macrophages; these are typically accompanied by mucosal ulceration, loss of goblet cells[8], and infiltrates of lymphocytes, plasma cells, and neutrophils.[1,13,15] Histopathological demonstration of macrophages with intracytoplasmic PAS positive material has been accepted as the pathognomonic feature of HUC[4,10] and the PAS positive material is considered to be glycoprotein from bacterial cell walls.[9]

Although this condition has nonspecific gross lesions, findings in previously reported cases include reduction in the colonic length, eccentric thickening of the intestinal wall, and

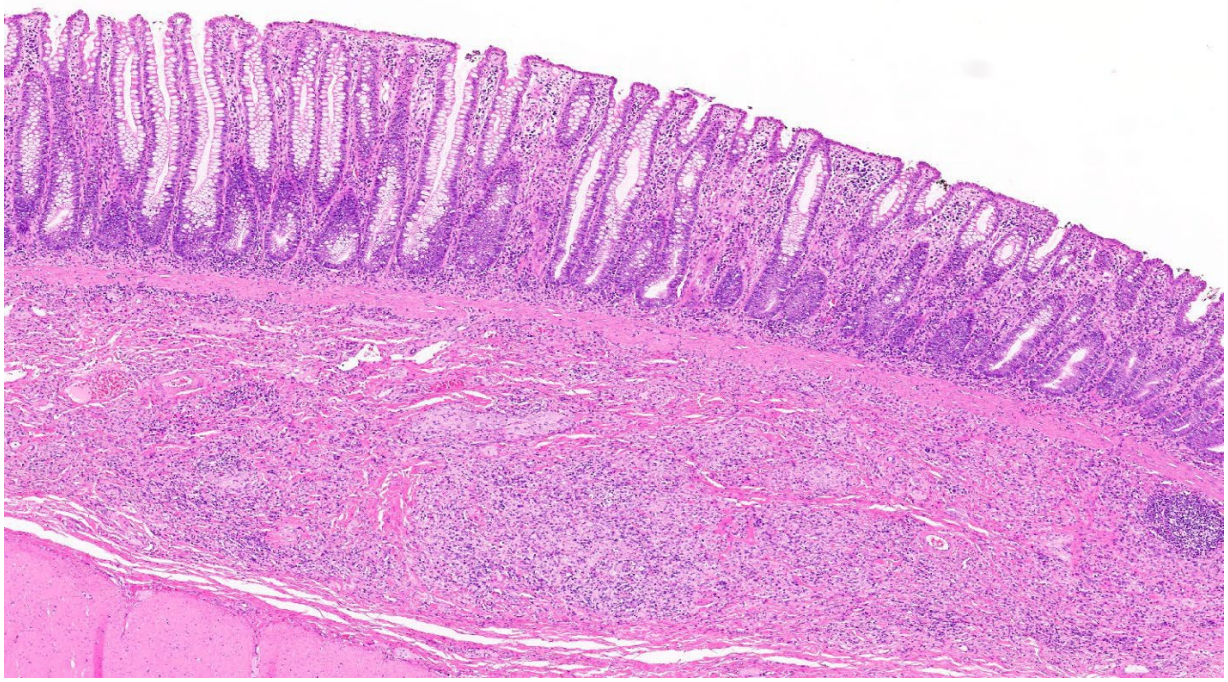

Figure 1-3. Colon, French bulldog. Intact mucosa with glandular hyperplasia and a cellular infiltrate within the lamina propria and submucosa. (HE, 4.5X) (Photo courtesy of: Kansas State Veterinary Diagnostic Laboratory (KSVDL), http://ww.ksvdl.org/)

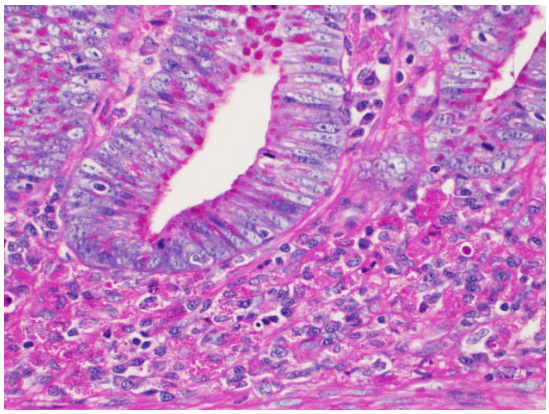

Figure 1-4. Colon, French bulldog. Eosinophilic intracytoplasmic material is contained within histiocytes in the lamina propria. (PAS, 400X)

multifocal to coalescing areas of ulceration that can be present in the colon, cecum and rectum.[2,4,14] Clinical features include chronic diarrhea, increased frequency of defecation, and feces that are soft, tan, granular, glistening, and sometimes or always contain blood. Affected dogs are afebrile and late in disease often develop dehydration with weight loss.[16]

HUC has been described most commonly in young Boxers and French Bulldogs, although it has been sporadically reported in a variety of other breeds; Mastiff, Alaskan Malamute, Doberman Pincher, American Staffordshire Terrier[1], and Beagle.[2,13,14] It has also rarely been reported in cats, including a Persian-crossbred and two domestic shorthaired cats.[6,9,15]

HUC was previously regarded as an idiopathic immune-mediated disease[14], and although the exact cause and pathogenesis are still not well understood, recent reports have identified *Escherichia coli* in both canine[1,2,5,7,8,11] and feline cases.[6,9] In both species, clinical remission as well as histologic resolution has been described after eradication of the invasive *E. coli* by use of antibiotics including Enrofloxicin.[8,9] The response to these treatments varies by case and antibacterial resistance, especially to enrofloxacin, can affect the outcome with nonresponsive or refractory cases.[14] Thus, the regression of clinical and histologic lesions suggest that *E. coli* has a critical role in the development of HUC.[9] The predisposition of Boxers to HUC is thought to be due to a heritable anomaly that confers susceptibility to the invasion and persistence of an adherent and invasive group of *E. coli.*[1] The rarity of disease in cats may suggest variation in hereditary and host susceptibility to *E coli*-induced HUC between dogs and cats.[9]

Contributing Institution:
Kansas State Veterinary Diagnostic Laboratory (KSVDL)
http://ww.ksvdl.org/

JPC Diagnosis:
Colon: Colitis, histiocytic and ulcerative, diffuse, marked, with glandular hyperplasia.

JPC Comment:
While the presence of PAS-positive cytoplasmic material in macrophages on histopathology is virtually pathognomonic for histiocytic ulcerative colitis, fluorescent in-situ hybridization (FISH) is the definitive diagnostic test for identifying *E. coli* in this condition.[3, 8, 12] This technique uses fluorescent probes to specifically target and hybridize with *E. coli*

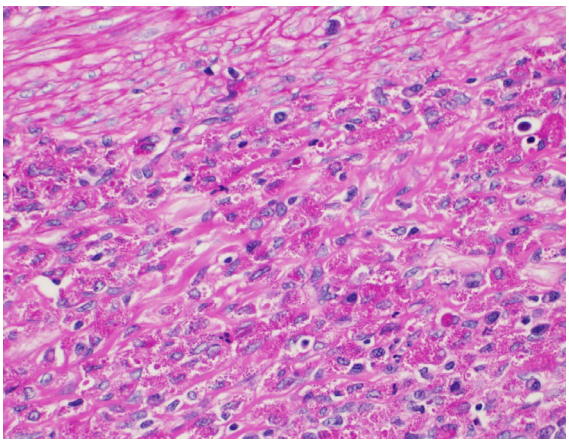

Figure 1-5. Colon, French bulldog. Eosinophilic intracytoplasmic material is contained within histiocytes in the submucosa. (PAS, 40X)

16S ribosomal rDNA, thus enabling identification and localization of the bacteria within HUC lesions.[8] In addition to allowing direct observation of *E. coli* within macrophages, FISH has several methodological advantages: it can be conducted on formalin-fixed paraffin-embedded sections, it is not confounded by normal flora present in the colon, and it can detect multiple bacterial species at once.[12]

Two recent reports have described the correlation of histologic and cytologic findings in two dogs with HUC.[3, 12] Both dogs had a history of chronic diarrhea and hematochezia and were painful with thickened, irregular mucosa on rectal exam.[3, 12] Rectal scrapings in both dogs revealed mixed inflammation and occasionally macrophages contained pink cytoplasmic granules or phagocytosed bacteria.[3, 12] In one case, the pink cytoplasmic material was confirmed to be PAS-positive.[3] In both cases, HUC was confirmed with histopathology and FISH.[3, 12] These are the first published reports of cytologic findings of HUC, so the sensitivity and specificity of rectal scrapings for this condition is unknown.[12] The results suggest, however, that cytologic examination may be helpful as an initial test for guiding further diagnostics, particularly since it is non-invasive, economical for owners, and does not require a specialized laboratory for analysis.

References:

1. Argenta FF, de Souza SO, Meirelles, LS, et al. Histiocytic ulcerative colitis in an American Staffordshire Terrier. *J Comp Path*. 2018;165:40-44.
2. Carvallo FR, Kerlin R, Fredette C, et al. Histiocytic typhlocolitis in two colony Beagle dogs. *Exp Toxicol Pathol* 2015;67:219–221.
3. Conrado FO, Jones EA, Graham EA, Simpson KW, Craft WF, Beatty SSK. Cytologic, histopathologic, and clinical features of granulomatous colitis in a French bulldog. *Vet Clin Pathol.* 2021;00:1-7.
4. German AJ, Hall EJ, Kelly DF, Watson ADJ, Day MJ. An immunohistochemical study of histiocytic ulcerative colitis of Boxer dogs. *J Comp Path*. 2000;122:163-175.
5. Hostutler RA, Luria BJ, Johnson SE, Weisbrode SE, Sherding RG, Jaeger JQ, et al. Antibiotic-responsive histiocytic ulcerative colitis in 9 dogs. *J Vet Intern Med*. 2004;18:499-504.
6. Leal RO, Simpson K, Fine M, Husson J, Hernandez J. Granulomatous colitis: more than a canine disease? A case of *Escherichia coli*-associated granulomatous colitis in an adult cat. *J Feline Med Surg.* 2017;3:1-5.
7. Manchester AC, Hill S, Sabatino B, et al. Association between granulomatous colitis in French Bulldogs and invasive *Escherichia coli* and response to fluoroquinolone antimicrobials. *J Vet Intern Med* 2013;27:56–61.
8. Mansfield CS, James FE, Craven M, Davies DR, OHara AJ, Nicholls PK, et al. Remission of Histioytic ulcerative colitis in boxer dogs correlates with eradication of invasive intramucosal *Escherichia coli. J Vet Intern Med.* 2009;23:964-969.
9. Matsumoto I, Nakashima Ko, Morita H, Kasahara K, Kataoka O, Uchida K. Escherichia coli-induced granulomatous colitis in a cat. *J Feline Med Surg*. 2019;5:1-5.
10. Nolte A, Junginger J, Baum B, et al. Heterogeneity of macrophages in canine histiocytic ulcerative colitis. *Innate Immun* 2017;23:228–239.
11. Simpson KW, Dogan B, Rishniw M, et al. Adherent and invasive *Escherichia coli* is associated with granulomatous colitis in boxer dogs. *Infect Immun* 2006;74:4778–4792.

12. Sims CS, Nagle J, Tolbert MK, Anderson K, Linder K, Neel J. Correlation of cytology to histology in a case of granulomatous colitis in a Boxer dog. *Vet Clin Pathol.* 2022:50(Suppl.1):83-87.
13. Stokes JE, Kruger JM, Mullaney T, Holan K, Schall W. Histiocytic ulcerative colitis in three non-boxer dogs. *J Am Anim Hosp Assoc.* 2001;37:461-465.
14. Uzal FA, Plattner BL, Hostetter JM. Alimentary system. In: Maxie MG, ed. *Jubb, Kennedy and Palmer's Pathology of Domestic Animals.* Vol. 2. 6th ed. Philadelphia, PA: Elsevier. 2016:97-98.
15. Van Kruiningen HJ and Dobbins WO 3rd. Feline histiocytic colitis. A case report with electron microscopy. *Vet Pathol.* 1979;16:215–222.
16. Van Kruiningen HJ, Montali RJ, Strandberg JD, Kirk RW. A granulomatous colitis of dogs with histologic resemblance to Whipple's disease. *Path Vet.* 1965;2:521-544.

CASE II:

Signalment:
Two 6-month-old, black, American mink (*Neovison vison*), one male and one female.

History:
A farm of approximately 50,000 all black, American mink experienced increased mortality within two shelters. Approximately 15-20 animals died over the course of two days, with two submitted for necropsy.

Gross Pathology:
Two reportedly six-month-old, black mink weighing 1.9 kg (female) and 2.4 kg (male) were necropsied. The bodies of both were in good condition (BCS 3/5) and postmortem autolysis was moderate. The lungs in both animals were diffusely firm and mottled bright red to purple with areas of paler color. At least one section of lung from both animals sank in formalin; other sections floated.

Laboratory Results:
Black mink, female, lung tissue, Aerobic culture: 4+ *Pseudomonas aeruginosa*.

Black mink, male, lung tissue, Aerobic culture: 4+ *Pseudomonas aeruginosa* - sensitivity performed on female, see Table 2-1.

Microscopic Description:
Lung. Sections of lung in which there is diffuse, coagulative necrosis and suppurative inflammation effacing up to 90% of the pulmonary parenchyma. These areas contain necrotic cell debris, seroproteinaceous fluid, neutrophils and myriad clusters of small, gram-negative bacteria. In nearby alveoli, there is intraalveolar hemorrhage. Several bronchioles are occluded or partially occluded by aggregates of fibrin and neutrophils, and cell debris.

Contributor's Morphologic Diagnoses:
Lung: Bronchopneumonia, severe, acute, diffuse, hemorrhagic, fibrinosuppurative.

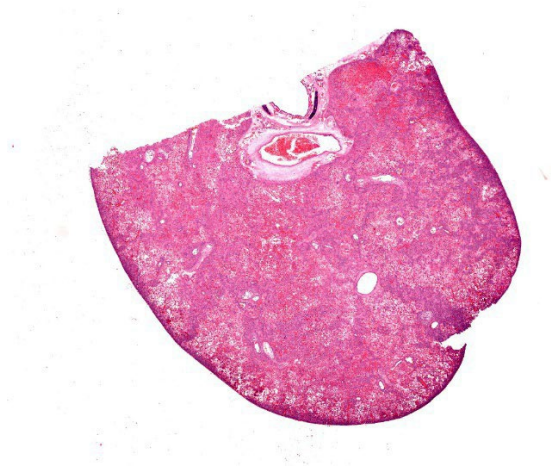

Figure 2-1. Lung, mink. A single, diffusely consolidated section of lung is submitted for examination. (HE, 5X)

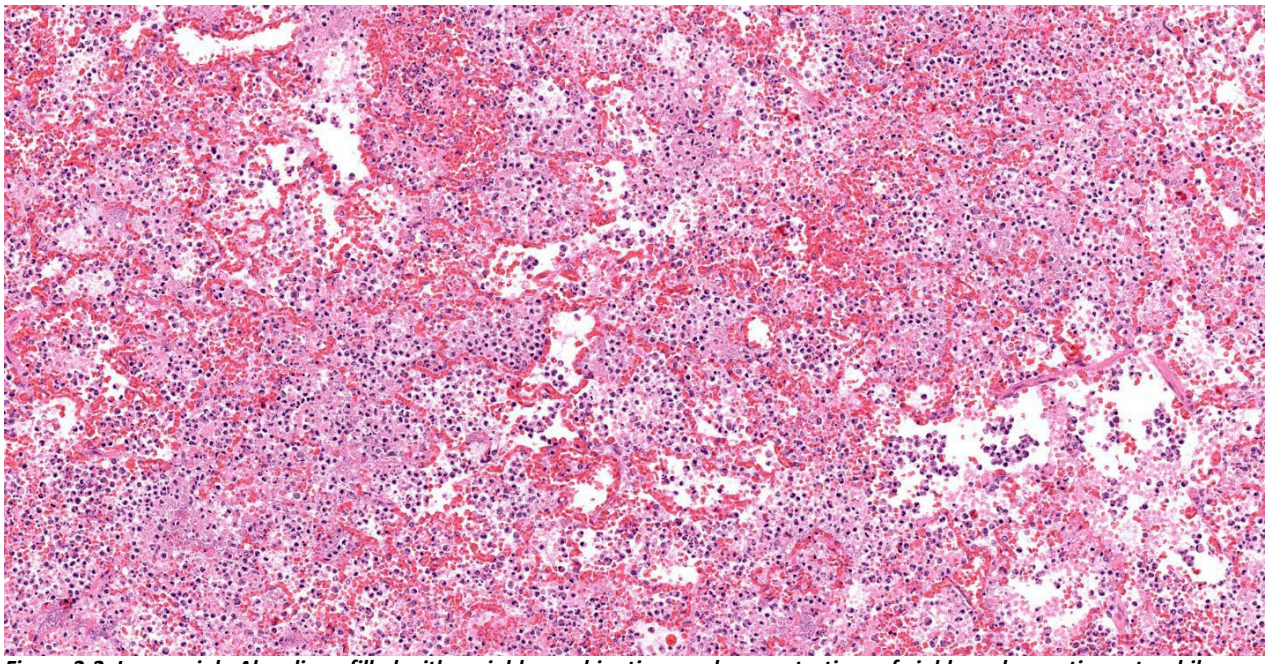

Figure 2-2. Lung, mink. Alveoli are filled with variable combinations and concentrations of viable and necrotic neutrophils, fewer macrophages, cellular debris, fibrin, and edema, and innumerable bacterial rods. (HE, 154X)

Contributor's Comment:

Pseudomonas aeruginosa is a known cause of contagious, hemorrhagic bronchopneumonia in farmed mink, although most mustelids are susceptible.[4] It was first described in 1953.[10] It is a seasonal disease most commonly seen in September to November. It is often acute and fatal and some mink can be found with blood around the nostril and mouth without previous signs of illness.[17,18] Experimentally, the organism can be carried in the nasal cavity without causing disease. There are various serotypes and genotypes and many of these form biofilms.[14,19] Also, numerous vaccines and other therapeutic strategies have been investigated.[8] In one study, Phage YH30 delivered intranasally reduced disease severity.[7] Antibiotic resistance is common in *Pseudomonas* spp. and can vary geographically and temporally; antibiotic resistance and sensitivities seen here are different than those previously reported.[14] Outbreaks of hemorrhagic pneumonia have been associated with hemolytic *Escherichia coli* infection as well.[16]

ANTIBIOTIC	MIC (µG/ML)	INTERPRETATION
AMIKACIN	< 1.000 µg/ml	Sensitive
AMOXICILLIN/CLAVULANIC ACID	>64.000 µg/ml	Resistant
AMPICILLIN	>48.000 µg/ml	Resistant
CEFPODOXIME	>64.000 µg/ml	Resistant
CEPHALOTHIN	>128.000 µg/ml	Resistant
CHLORAMPHENICOL	32.0 µg/ml	Intermediate
CLINDAMYCIN	>12.000 µg/ml	Resistant
ENROFLOXACIN	0.4 µg/ml	Sensitive
GENTAMICIN	1.5 µg/ml	Sensitive
IMIPENEM	< 0.750 µg/ml	Sensitive
MARBOFLOXACIN		Sensitive
ORBIFLOXACIN	2.0 µg/ml	Intermediate
TETRACYCLINE	16.0 µg/ml	Resistant
TMP/SULFA	>12.000 µg/ml	Resistant
TOBRAMYCIN	< 0.380 µg/ml	Sensitive

Table 2-1

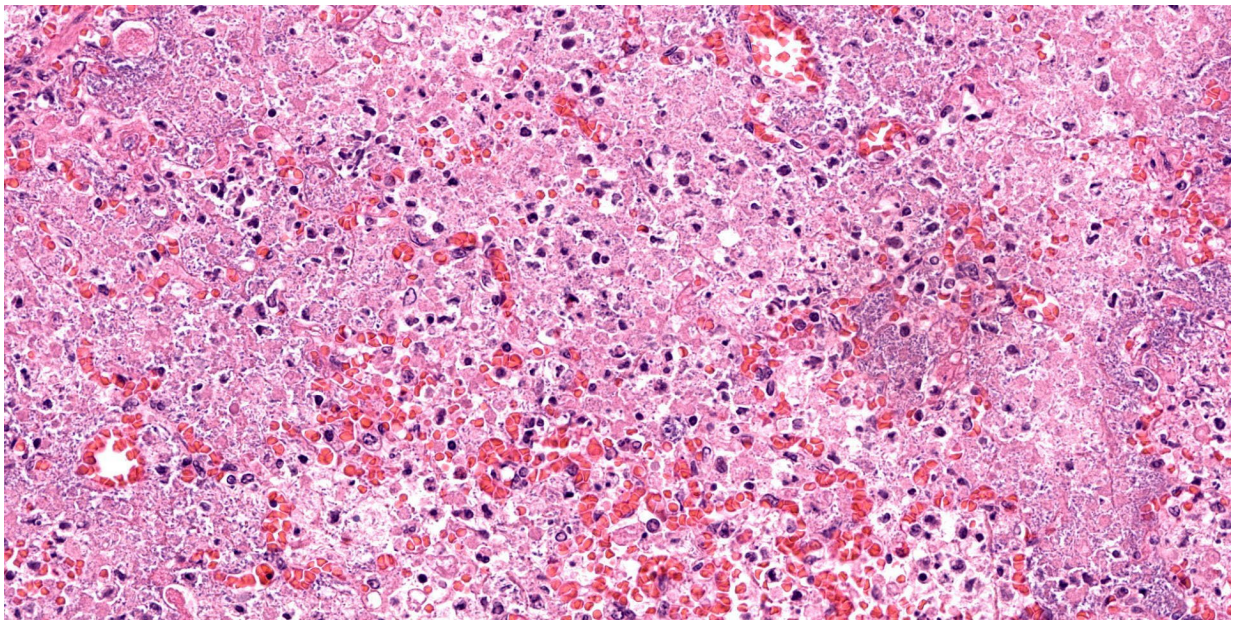

Figure 2-3. Lung, mink. There are areas of septal necrosis scattered throughout the section. Septa are discontinuous with multifocal hemorrhage and exuded fibrin, not to mention the large numbers of bacilli within the expanded alveoli. (HE, 381X)

Contributing Institution:
Oregon State University, Carlson College of Veterinary Medicine, Veterinary Diagnostic Laboratory
https://vetmed.oregonstate.edu/diagnostic

JPC Diagnosis:
Lung: Pneumonia, fibrinosuppurative, diffuse, severe, with septal necrosis, vasculitis and innumerable perivascular and alveolar bacilli.

JPC Comment:
Jubb, Kennedy, and Palmer's Pathology of Domestic Animals delineates four main morphologic types of pneumonia: bronchopneumonia, interstitial pneumonia, bronchointerstitial pneumonia, and embolic pneumonia.[2]

Bronchopneumonia is caused by aerogenous delivery of bacteria to the terminal bronchioles, causing the hallmark lesion of an exudate at the broncho-alveolar junction.[2] Exudates can be found in the bronchi, bronchioles, and alveoli, but the bronchiolar epithelium is typically normal.[2] The distribution is typically cranioventral, and affected lobes are firm.[2] Bronchopneumonia may be caused by opportunistic pathogens during times of immunosuppression, impaired pulmonary defenses (i.e. viral or *Mycoplasma* infection), or exposure to overwhelming numbers of bacteria. [2]

Interstitial pneumonia is characterized by inflammation and damage within the alveolar septae and the adjacent terminal bronchioles.[2] Interstitial pneumonia commonly features diffuse alveolar damage, or damage to pneumocytes and/or alveolar capillary endothelial cells.[2] Acutely, this leads to exudation and hyaline membrane formation followed by type II pneumocyte hyperplasia, all of which interfere with gas exchange.[2] Pulmonary fibrosis follows in the chronic phase of interstitial pneumonia.[2] Grossly, affected lungs will fail to deflate and may have rib imprints and a rubbery texture.[2] There are many subtypes and causes interstitial pneumonia, which include viral infections, inhalation of toxic gases or fumes, ingestion of certain toxins, ascarid larval migration, sepsis, and disseminated intravascular coagulation.[2] In bronchinterstitial pneumonia, there is bronchiolar damage and necrosis in addition to the

diffuse alveolar damage characteristic of interstitial pneumonia.[2]

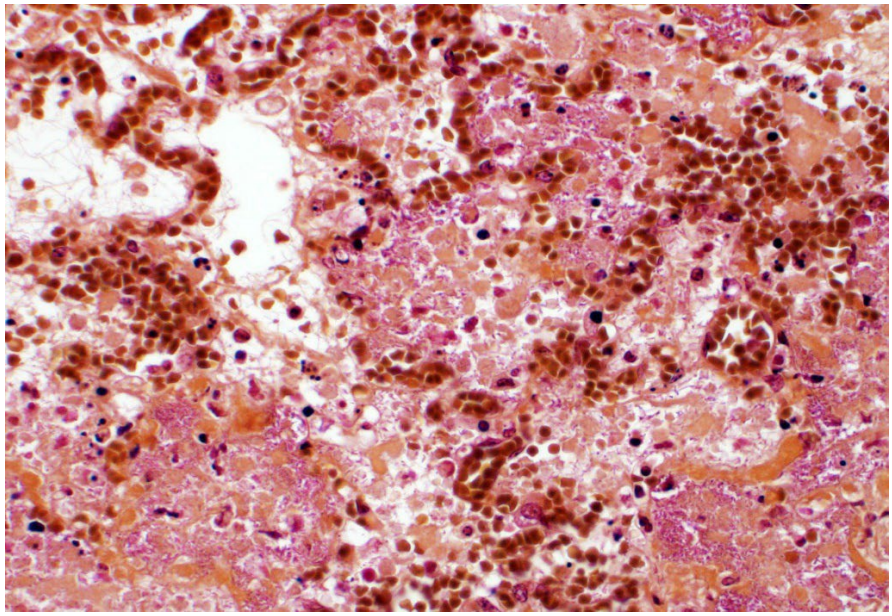

Figure 2-4. Lung, mink. The large numbers of bacilli within the alveoli stain positively as gram negative on a tissue Gram stain. (Brown and Hopps, 400X)

Embolic pneumonias are caused by hematogenous showering of bacterial (or inflammatory) emboli from a nidus of infection resulting in multifocal lesions throughout all lung lobes.[2,12] Embolic pneumonia frequently features pulmonary abscess formation.[2] While abscesses can also occur in bronchopneumonia, the cranioventral distribution distinguishes it from embolic pneumonia.[2] Possible sources of emboli include hepatic abscesses, omphalophlebitis, or endocarditis, and embolic pneumonia has been described secondary to *Pseudomonas aeruginosa* in a puppy with necrotizing enteritis.[12]

The distribution of histologic lesions led to spirited discussion among conference participants regarding the correct morphologic classification of this pneumonia. The pathogenesis of *Pseudomonas* pneumonia in mink is supports a diagnosis of bronchopneumonia, with aerogenous delivery of bacteria to the lower airways.[12] In this case, however, much of the necrosis and bacterial colonies are centered on blood vessels, leading a few participants to consider embolic pneumonia as a morphologic pattern. The contributor did not describe any possible nidus of infection in this case, and perivascular localization of bacteria is characteristic in *Pseudomonas* pneumonias of both mink and rats.[16] Since the pathogenesis and histologic appearance do not fit into one precise category, participants decided not to further subtype the morphologic diagnosis beyond pneumonia.

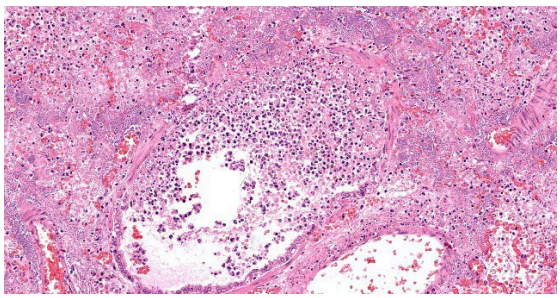

Figure 2-5. Lung, mink. Airways contain aggregates of neutrophils which infiltrate segmental areas of mural necrosis and loss of epithelium. (HE, 385X)

Pseudomonas aeruginosa is typically an opportunistic pathogen which causes disease in immunocompromised animals or animals with surgical implants.[11] The bacteria thrives in moist environments, such as water bottles in laboratory animal enclosures, and gains entry through the gastrointestinal tract or by penetrating inflamed or injured oronasal mucosa or intertriginous skin.[1,11] In immunocompromised mice and rats, infection can lead to bacteremia and gram-negative septicemia with vasculitis, thrombosis, and necrosis in multiple organs, including the lung, liver, spleen, and kidneys.[1] The bacteria can also lead to deep pyoderma, septic arthritis,

discospondylitis, otitis, and a number of other conditions.[1,6,11] Due to the bacteria's propensity for moist environments, improperly chlorinated pools and hot tubs can harbor *P. aeruginosa*, and human skin can be inoculated by abrasive surfaces, resulting in two self-limiting but painful conditions: acute folliculitis and pseudomonas hot-foot syndrome (nodules of suppurative inflammation on the hands and feet).[5]

The pathogenicity of *P. aeruginosa* is determined by a number of virulence factors, including exotoxins which are toxic to macrophages and epithelial cells, a type III secretion system for injecting proteins directly into cells, elastase which destroys pulmonary microbe clearance mechanisms like mucin, and immunomodulatory alkaline protease A.[11,15] *P. aeruginosa* also produces two relatively unique virulence factors: pyocyanin, a redox metabolite, and pyoverdine, a siderophore.[9] These virulence factors are pigments that can impart a blue-green discoloration to superficial infections.[9] Rabbits with moist dermatitis and *P. aeruginosa* develop blue-green tinged fur.[12] In humans, *Pseudomonas* can cause green nail and green foot syndromes, and, when associated with intertrigo, causes blue-green staining of undergarments.[9] Indeed, when *P. aeruginosa* was first cultured from blue-green pus in superficial wounds in the 1880's, it was aptly dubbed *Bacillus pyocyaneus*, or "bacteria of blue pus".[19] The current name also references this distinctive hue: aerugo is Latin for copper rust, which is characteristically green.[19]

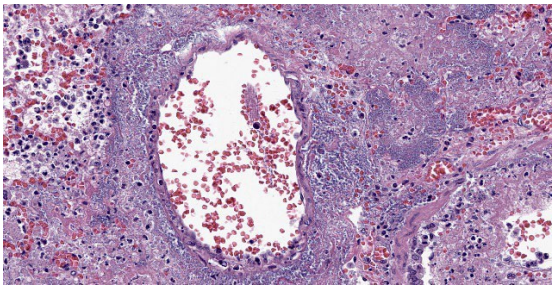

Figure 2-6. Lung, mink. Vessel adventitia is markedly expanded by bacilli which fill adjacent alveoli as well. (HE, 375X)

References:

1. Barthold SW, Griffey SM, Percy DH. *Pathology of Laboratory Rodents and Rabbits*. 4th ed. Ames, IO: John Wiley & Sons, Inc. 2016; 66, 143.
2. Caswell JL, Williams KJ. Respiratory System. In: *Jubb, Kennedy, and Palmer's Pathology of Domestic Animals.* Vol 2. 6th ed. St. Louis, MO: Elsevier. 2016; 500-520.
3. Cole LK. Otitis Externa. In: Greene CE, ed. *Infectious Disease of the Dog and Cat*. 4th ed. St. Louis, MO: Elsevier Saunder. 2012; 886-891.
4. Fernandez-Moran J. Chapter 49: Mestelidae. *Zoo and Wild Animal Medicine.* Fowler ME and Miller RE, eds. Saunders: St. Louis, MO. 501-516, 2003.
5. Fiorillo L, Zucker M, Sawyer D, Lin AN. The Pseudomonas Hot-Foot Syndrome. *The New England Journal of Medicine.* 2001; 354:335-338.
6. Greene CE, Bennett D. Musculoskeletal Infections. In: Greene CE, ed. *Infectious Disease of the Dog and Cat.* 4th ed. St. Louis, MO: Elsevier Saunder. 2012; 892-915.
7. Gu J, Li X, Yang M, Du C, Cui Z, Gong P, Xia F, Song J, Zhang L, Li J, Yu C, Sun C, Feng X, Lei L, Han W. Therapeutic effect of Pseudomonas aeruginosa phage YH30 on mink hemorrhagic pneumonia. *Vet Microbiol.* 190:5-11, 2016.
8. Homma JY, Abe C, Yanagawa R, Noda H. Effectiveness of immunization with multicomponent vaccines in protection against hemorrhagic pneumonia due to Pseudomonas aeruginosa infection in mink. *Rev Infect Dis.* 5 Suppl 5:S858-66, 1983.

9. Kaya TI, Delialioglu N, Yazici AC, Tursen U, Ikizoglu G. Medical Pearl: Blue underpants sign – A diagnostic clue for Pseudomonas aeruginosa intertrigo of the groin. *J Am Acad Dermatol.* 2005; 53(5): 869-871.
10. Knox B. Pseudomonas aeruginosa som årsag til enzootiske infektioner hos mink (Pseudomonas aeruginosa as the cause of enzootic infections in mink). *Nord Vet Med.* 5:731, 1953.
11. Koenig Amie. Gram-Negative Bacterial Infections. In: Greene CE, ed. *Infectious Disease of the Dog and Cat.* 4th ed. St. Louis, MO: Elsevier Saunder. 2012; 349-354.
12. Lopez A, Martinson SA. Respiratory System, Thoracic Cavities, Mediastinum, and Pleura. In: Zachary JF, ed. *Pathologic Basis of Veterinary Disease.*7th ed. St. Louis, MO: Eslevier. 2022; 581-591.
13. O'Donoghue PN, Whatley BF. Pseudomonas aeruginosa in Rabbit Fur. *Laboratory Animals.* 1971; 5:251-255.
14. Qi J, Li L, Du Y, Wang S, Wang J, Luo Y, Che J, Lu J, Liu H, Hu G, Li J, Gong Y, Wang G, Hu M, Shiganyan, Liu Y. The identification, typing, and antimicrobial susceptibility of Pseudomonas aeruginosa isolated from mink with hemorrhagic pneumonia. *Vet Microbiol* 70(3-4):456-61, 2014.
15. Qian Zhu, Hui Peng, Han Li et al. Serotypes and virulence genes of Pseudomonas aeruginosa isolated from mink and its pathogenicity in mink. *Microbial Pathogenesis*. 2020; 139:1-5.
16. Salomonsen CM, Boye M, Høiby N, Jensen TH, Hammer AS: Comparison of histological lesions in mink with acute hemorrhagic pneumonia associated with Pseudomonas aeruginosa or Escherichia coli. *Can J Vet Res.* 77(3):199-204, 2013.
17. Salomonsen CM, Chriél M, Jensen TH, Rangstrup-Christensen L, Høiby N, Hammer AS. Effect of infectious dose and season on development of hemorrhagic pneumonia in mink caused by Pseudomonas aeruginosa. *Can J Vet Res*. Jul;77(3):221-5,2013.
18. Shimizu T, Homma JY, Aoyama T, Onoera T, Noda H. Virulence of Pseudomonas aeruginosa and spontaneous spread of Pseudomonas pneumonia in a mink ranch. *Infect Immun.*10:16–20, 1974.
19. Villavicencio RT. The History of Blue Pus. *J Am Coll Surg*. 1998: 187(2): 212-216.
20. Zhao Y, Guo L, Li J, Fang B, Huang X. Molecular epidemiology, antimicrobial susceptibility, and pulsed-field gel electrophoresis phenotyping of *Pseudomonas aeruginosa* isolates from mink. *Can J Vet Res.* 2018; 82(4): 256-263.

CASE III:

Signalment:
Five year old intact male ferret (*Mustela putorius furo*), mustelid.

History:
This is the second ferret from a rescue facility to present to the referring veterinarian in a severely debilitated state, emaciated, dehydrated and hypothermic. The ferret was euthanized.

Gross Pathology:
This male ferret was in emaciated body condition, with a poor, sparse hair coat and hair loss of the distal tail. Internally, there were still some subcutaneous adipose stores in the inguinal fatpad, around the kidneys and in the mesentery, however there was generalized

muscle wasting. The heart was globose. The adrenal glands were small and symmetrical. Small intestinal content was scant, and there were soft dark brown feces in the colon.

Laboratory Results:
No laboratory findings reported.

Microscopic Description:
Small intestine: Diffusely throughout the section, there is villus blunting and fusion with loss of goblet cells and marked cryptal epithelial hyperplasia, characterized by elongated and tortuous crypts lined by tall columnar epithelial cells with abundant lightly eosinophilic cytoplasm and elongate vesicular nuclei. The crypt epithelium is disorganized and occasionally piles up to five cells thick at the base of the crypts. There is frequent single cell death within the mucosal epithelium, characterized by individualized and hypereosinophilic enterocytes with fragmented or condensed nuclei; mitotic figures are also frequent. Occasional crypt lumens are dilated, lined by attenuated low columnar to cuboidal epithelium, and contain necrotic cellular debris or mucinous fluid. The lamina propria and submucosa are variably expanded by clusters of lymphocytes, plasma cells and macrophages. The villus epithelium is predominantly intact, multifocally attenuated at the surface, and contains scattered apicomplexan organisms of various life stages, including meronts, macrogametocytes, microgametocytes and occasional oocysts visible within the luminal debris.

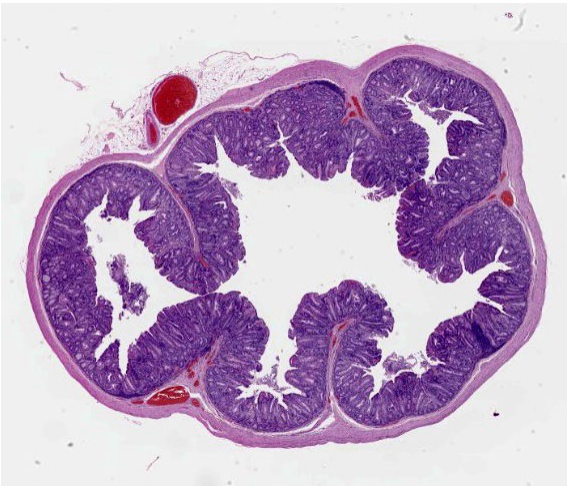

Figure 3-1. Colon, ferret. One section of colon with marked thickened and rugose mucosa is submitted for examination. (HE, 7X)

Warthin Starry silver stains of the intestine reveal numerous argyrophilic curved small (approximately 5 x 1 micron) bacilli concentrated in the apical cytoplasm of hyperplastic mucosal epithelial cells. Immunohistochemistry was performed using a polyclonal antibody to *Lawsonia intracellularis*, confirming the identity of the bacteria.

DNA was extracted from the frozen intestine and from formalin-fixed paraffin-embedded tissue scrolls. PCR was conducted to amplify short regions of the nuclear 18S rDNA (231 bp) and mitochondrial cytochrome c oxidase subunit I (COI) (512 bp). PCR and sequencing of the resulting amplicons identified the coccidia present as *Eimeria furonis*. In addition, measurement of 6 oocysts observed in the intestinal content averaged 12.1 x 10.6 µm with a shape index of 1.14. These measurements are also consistent with the dimensions of oocysts of *E. furonis*.

Contributor's Morphologic Diagnoses:
Enteritis, proliferative, chronic, moderate with villus atrophy, crypt abscesses and numerous argyrophilic intraepithelial bacilli (*Lawsonia intracellularis*), and intralesional coccidia (*Eimeria furonis)*

Contributor's Comment:
The debilitated state of this adult ferret is associated with concurrent infection by *Lawsonia intracellularis* and the coccidian parasite, *Eimeria furonis*.

The histologic lesions in this case are dominated by changes due to infection by *Lawsonia intracellularis*. *L.* intracellularis is a

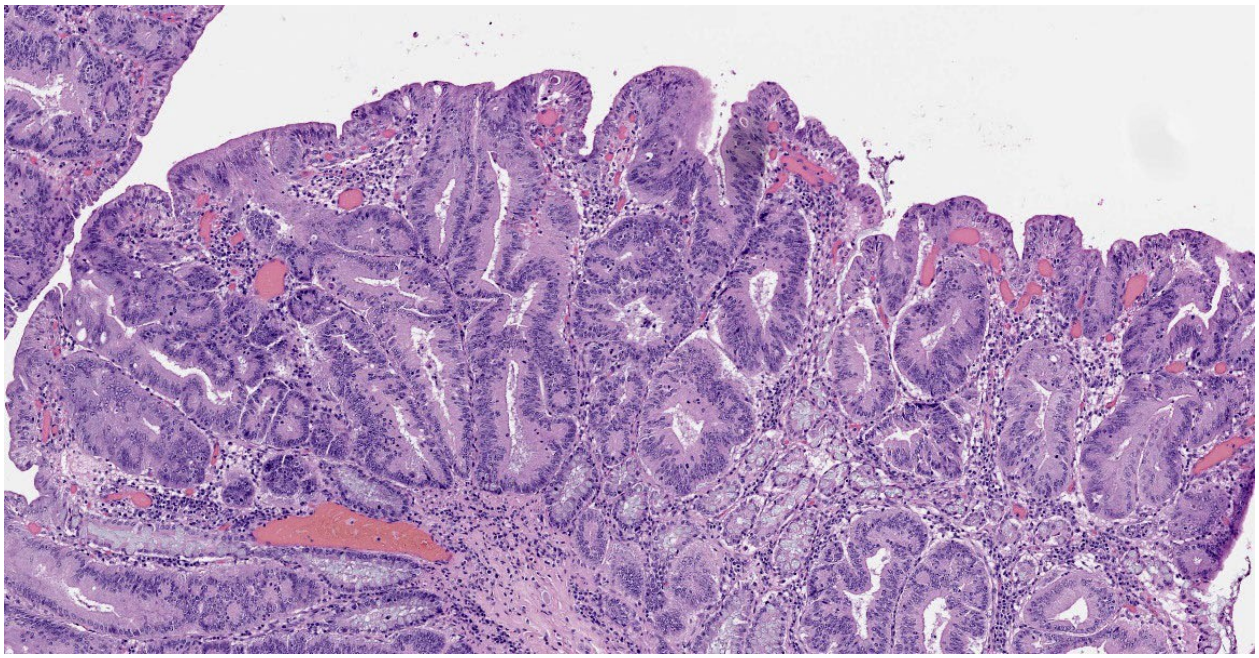

Figure 3-2. Colon, ferret. Colonic glands are hyperplastic and lack goblet cells. Hypercellularity is evident in the lamina propria. (HE, 60X)

gram-negative, non-spore-forming, microaerophilic, curved rod, and is an obligate intracellular pathogen. It is the etiologic agent of proliferative enteropathy (PE), characterized clinically by diarrhea associated with loss of functional mucosal surface area, as well as wasting due to protein-losing enteropathy. Histologically, PE is characterized by thickening of the distal small and/or large intestinal mucosa due to crypt enterocyte infection and proliferation. PE is an important endemic disease in swine herds and is also becoming an important disease of horses, predominantly weanling foals, worldwide. However, the bacterium can cause disease in a broad host range including donkeys, hamsters, rabbits, ferrets, foxes, dogs, rats, sheep, deer, emus, ostriches, nonhuman primates and guinea pigs.[6] There are some differences in clinical and pathologic presentation of disease among affected species. Mucosal hyperplasia is characteristic of PE in all species, however the type and extent of associated inflammatory reactions vary and may depend on host-specific differences.[6] The bacterium infects intestinal crypt cells, causing alterations in host gene expression resulting in induction of cell proliferation and mucosal thickening, as well as inhibition of secretory goblet cell and absorptive enterocyte differentiation leading to altered mucosal integrity.[2] These changes are associated with simultaneous induction of Notch-1 signalling and attenuation of B-catenin/Wnt pathways.[2]

Several species of coccidia have been reported to infect the intestinal tract of the ferret, including *Isospora laidlawi*, *I. eversmanni*, *Eimeria ictidea*, *E. furonis,* and *E. vision*. *Emeria hiepei* also has been reported to infect the biliary epithelium. *E. furonis* is the most commonly identified species, and is generally associated with subclinical infections. *E. furonis* infects the small intestinal and rectal epithelium although there is a single case report of infection of the epithelium of hepatic bile ducts and gallbladder.[5] Speciation of *Eimeria* is based on differentiating characteristics including host affected, specific location of the parasite within the host, and organism size and shape. This *Eimeria* species has approximately 12.8 x 12.0 µm diameter, roughly spherical oocysts containing

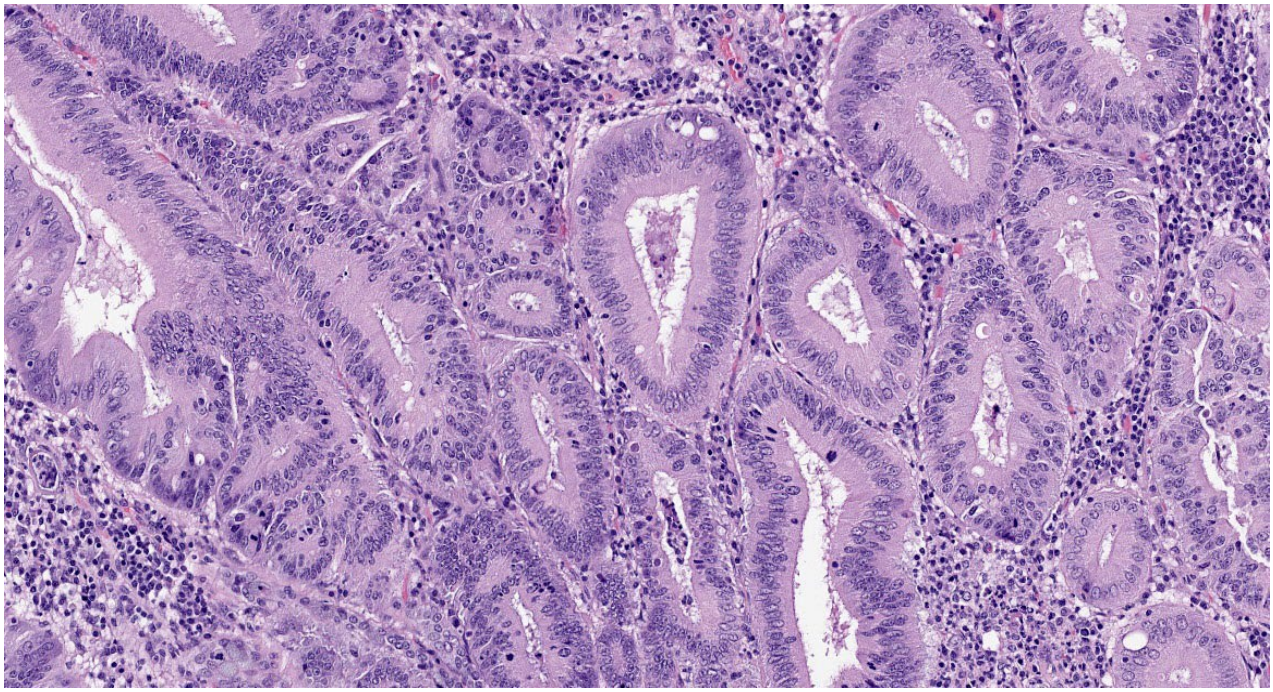

Figure 3-3. Colon, ferret. Colonic glands are tortuous with cellular basophilia, nuclear crowding, and numerous mitotic figures. Goblet cells are absent. (HE, 194X)

4 sporocysts each with 2 sporozoites. By comparison, *E. ictidea*, a closely related species, has oocysts measuring 23 x 17.5 µm. Laboratory identification can be assisted by sporulating viable oocysts from fresh feces in the laboratory, or using molecular techniques.[1]

Although historically rarely associated with clinical disease in ferrets, a recent report by Sledge et al. documents severe outbreaks of enteric coccidiosis due to *E. furonis* in three ferret rescue shelters, a situation similar to the case described here.[5] Clinical signs in these groups of affected animals included foul-smelling diarrheic feces, melena, lethargy, weight loss, dehydration, anorexia and weakness. In one of the reported outbreaks in a shelter population of 42 ferrets, greater than half were clinically affected and 7 died, while in a second group of 63 ferrets, 13 died and at least 21 additional animals displayed clinical signs but recovered. No other co-pathogens were discovered in these groups in this study. The authors suggest that high population density and the dynamic population structure of these groups, with regular introductions of newly rescued or adopted naïve animals may have predisposed to outbreak situations. Diagnosis can be challenging, as shedding of oocysts may be intermittent and may occur in low enough numbers to be not easily detected by routine fecal examination.

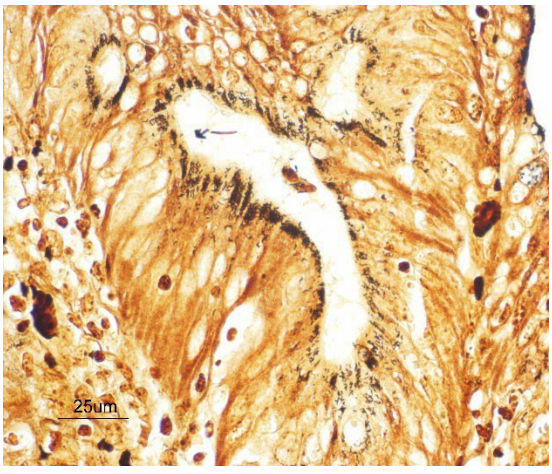

Figure 3-5. Colon, ferret. Warthin Starry silver stains of the intestine reveal numerous argyrophilic curved small bacilli concentrated in the apical cytoplasm of hyperplastic mucosal epithelial cells. (WS, 600X) (Photo courtesy of: Animal Health Laboratory, University of Guelph, Guelph, Ontario, Canada http://ahl.uoguelph.ca)

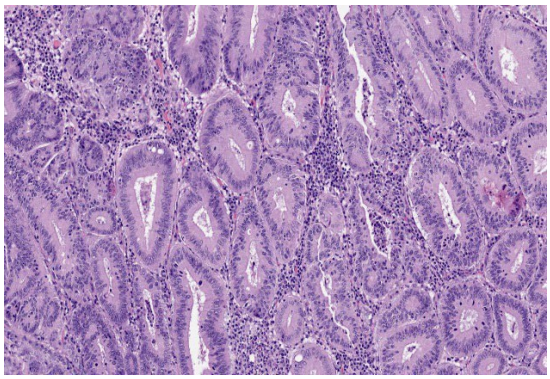

Figure 3-4. Colon ferret. Glands occasionally contain necrotic epithelial cells admixed with few neutrophils and cellular debris (crypt abscesses). The lamina propria is expanded by moderate numbers of neutrophils, lymphocytes and plasma cells. (HE, 194X)

Contributing Institution:
Animal Health Laboratory, University of Guelph, Guelph, Ontario, Canada
http://ahl.uoguelph.ca

JPC Diagnosis:
1. Colon: Colitis, proliferative, diffuse, severe with decreased goblet cells.
2. Colon: Intraepithelial apicomplexan schizonts, gamonts, and oocysts, few.

JPC Comment:
Proliferative enteropathy is an economically important disease of swine production, with an estimated 96% of farms affected and a lost production cost of US $1 to $5 for every clinically affected pig.[7] In swine, *Lawsonia intracellularis* infection can cause an acute hemorrhagic enteropathy; in chronic cases, it can cause proliferative intestinal adenomatosis or, in cases of secondary infection, can progress to necrotic enteritis.[7] Pigs are infected through ingestion of the bacteria, which survive the acidic environment of the stomach and, once in the intestine, use polar flagella to reach the enterocytes.[3, 7] The exact mechanism by which the bacteria enters enterocytes is unknown but may be mediated by a type III secretion system (T3SS).[7] The bacteria proliferates by binary fission in the apical cytoplasm of infected cells.[7] Spread of infection between enterocytes occurs mainly when infected progenitor cells giving rise to infected progeny; however, cell-rupture and liberation of bacteria can also lead to infection of neighboring enterocytes.[3, 7]

There are still many unknowns regarding pathogenesis of proliferative enteropathy, as the obligate intracellular and microaerophilic nature of *L. intracellularis* hinders research efforts.[9] A recent study in yeast identified a potential effector protein, named LI1035, injected by the bacteria's T3SS that may target the MAPK system and affect cell growth.[9] Another study demonstrated that *L. intracellularis* can survive and possibly proliferate in porcine macrophages in vitro.[3]

A recent in vivo study in pigs uncovered the possible mechanisms behind mucosal hyperplasia and inhibition of goblet cell differentiation.[2] As the contributor mentions, the cell signaling pathways β-catenin/WNT and Notch are complex intracellular mechanisms which control homeostasis and differentiation of enterocytes. Wnt-1 interaction with

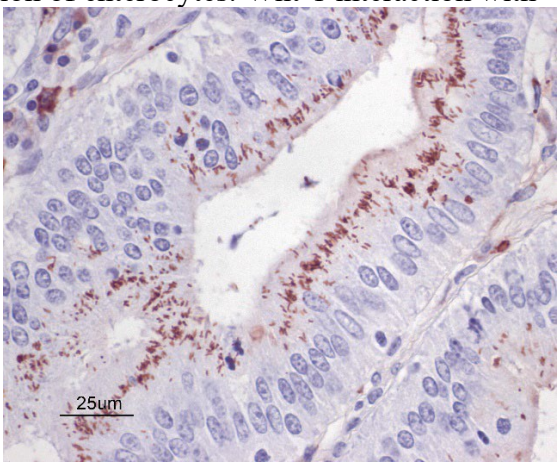

Figure 3-6. Colon, ferret. Curved small bacilli in the apical cytoplasm of enterocytes detected using a polyclonal antibody to Lawsonia intracellularis. (anti-L. intracellulare, 40X) (Photo courtesy of: Animal Health Laboratory, University of Guelph, Guelph, Ontario, Canada http://ahl.uoguelph.ca)

the membrane-bound Frizzled receptors prevents auto-phosphorylation of cytoplasmic β-catenin, which then migrates to the nucleus and induces gene expression associated with proliferation of intestinal stem cells, the precursor to transit-amplifying progenitor cells.[2, 4] Separately, Notch receptor activation leads to translocation of the Notch receptor intracellular domain (NICD) into the nucleus, which stimulates gene expression that drives progenitor cell differentiation into an absorptive enterocyte and suppresses differentiation into the secretory phenotype (i.e. goblet cell).[2] Huan et. al demonstrated that *L. intracellularis* infection was associated with increased levels of NICD1 and decreased levels of goblet-cell associated *ATOH1* and *MUC2.* Their study also demonstrated increased cytomembranous (and thus decreased nuclear signaling) of β-catenin, which in mice induces proliferation of progenitor cells.[2] This study provides a glimpse into the uncertain yet costly pathogenesis of *L. intracellularis* infections.

References:

1. Abe N et al. First record of *Eimeria furonis* infection in a ferret, Japan, with notes on the usefulness of partial small subunit ribosomal RNA gene sequencing analysis for discriminating among *Eimeria* species. Parasitol Res 2008; 103:967-970.
2. Huan YW, Bengtsson RJ, MacIntyre N, et al. *Lawsonia intracellularis* exploits β-catenin/Wnt and Notch signalling pathways during infection of intestinal crypt to alter cell homeostasis and promote cell proliferation. *PLoS ONE*. 2017;12(3):1-21.
3. Pereira CER, Resende TP, Armien AG, et al. Survival of *Lawsonia intracellularis* in porcine peripheral blood monocyte-derived macrophages. *PLoS ONE*. 2020;15(7):1-10.
4. Silva-Garcia O, Valdez-Alarcon JJ, Baizabal-Aguirre VM. Wnt/β-catenin Signaling as a Molecular Target by Pathogenic Bacteria. *Frontiers in Immunology*. 2019: 10(2135), 1-14.
5. Sledge DG et al. Outbreaks of severe enteric disease associated with *Eimeria furonis* infection in ferrets (*Mustela putorius furo*) of 3 densely populated groups. J Am Vet Med Assoc 2011; 239: 1584-1588.
6. Vannucci FA and Gebhart CJ. Recent advances in understanding the pathogenesis of *Lawsonia intracellularis* infections. Vet Pathol 2014; 51:465-477.
7. Vannucci FA, Gebhart CJ, McOrist S. Proliferative Enteropathy. In: Zimmerman JJ, Karriker LA, et al, eds. *Diseases of Swine*. 11th ed. Hoboken, NJ: John Wiley & Sons, Inc. 2019: 898-911.
8. Williams BH, Chimes MJ, Gardiner CH. Biliary coccidiosis in a ferret (*Mustela putorius furo*). Vet Pathol 1996; 33: 437-439.
9. Yang L Lai F, He L, et al. LI1035, a putative effector secreted by *Lawsonia intracellularis,* targets the MAPK pathway and regulates actin organization in yeast and mammalian cells. *Veterinary Microbiology*. 2019; 235:127-135.
10. Gu J, Li X, Yang M, Du C, Cui Z, Gong P, Xia F, Song J, Zhang L, Li J, Yu C, Sun C, Feng X, Lei L, Han W. Therapeutic effect of Pseudomonas aeruginosa phage YH30 on mink hemorrhagic pneumonia. *Vet Microbiol.* 190:5-11, 2016.

CASE IV:

Signalment:
5 year, 2 month old female Beagle dog (*Canis familiaris*)

History:
A multiparous female from a breeding colony was noted to have bilaterally elevated nictitating membranes and a body temperature of 99.8 °F. No other clinical signs were noted. Two days later the dog was found moribund and was humanely euthanized. Approximately 5 years prior to this episode, the dog had been treated for respiratory disease (pneumonia).

Gross Pathology:
The animal was in good body condition with copious fat deposits. Caudal lung lobes contained multiple, gray brown, 0.5 - 1 cm diameter subpleural nodules. Stomach contents were dark brown with flecks. Small areas of petechiation and yellow chyme-like material were noted in the duodenal mucosa and lumen respectively. No other gross lesions were noted.

Laboratory Results:
No laboratory findings reported.

Microscopic Description:
Lung: In one or more subpleural or apical foci, alveoli are filled with macrophages, multinucleate giant cells, and amorphous pale gray-brown material; small accumulations of amorphous material are often within multinucleate giant cells. Some alveoli contain only amorphous material (without inflammatory cells). Alveolar septa are thickened by fibrous connective tissue and infiltrated by varying numbers of mononuclear inflammatory cells. Amorphous material is strongly PAS positive, and exhibits birefringent peripheral radial striation under polarized light.

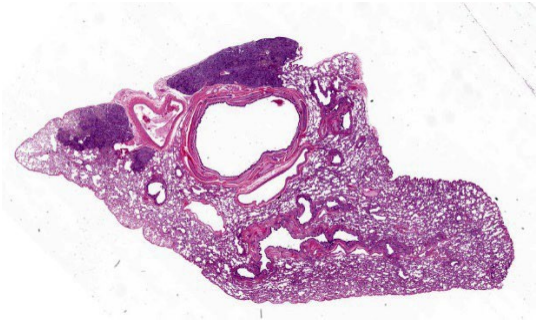

Figure 4-1. Lung, dog. In approximately 15% of the slide, subpleural alveoli are consolidated (HE, 5X)

Contributor's Morphologic Diagnoses:
Pneumonia, granulomatous, multifocal, chronic, with intralesional hyaline material.

Contributor's Comment:
Pulmonary hyalinosis is considered an incidental finding in older dogs characterized by intraalveolar accumulations of intracellular and extracellular amorphous or laminated, amphophilic, PAS-positive material and an accompanying macrophage and multinucleate giant cell response.[2] Scientific literature concerning this condition is sparse. Although the initial report of "pulmonary granulomas associated with PAS-positive bodies" found a greater incidence in brachycephalic dogs,[1] others reported the lesion in laboratory beagles exposed to ionizing radiation.[4]

Contributing Institution:
Covance Laboratories, Inc, Madison, Wisconsin, USA.

http://www.covance.com/industry-solutions/drug-development/services/safety-assessment/nonclinical-pathology-services.html

JPC Diagnosis:
Lung: Pneumonia, granulomatous, multifocal, moderate, with abundant intraalveolar and intrahistiocytic anisotropic hyaline material (Billups bodies).

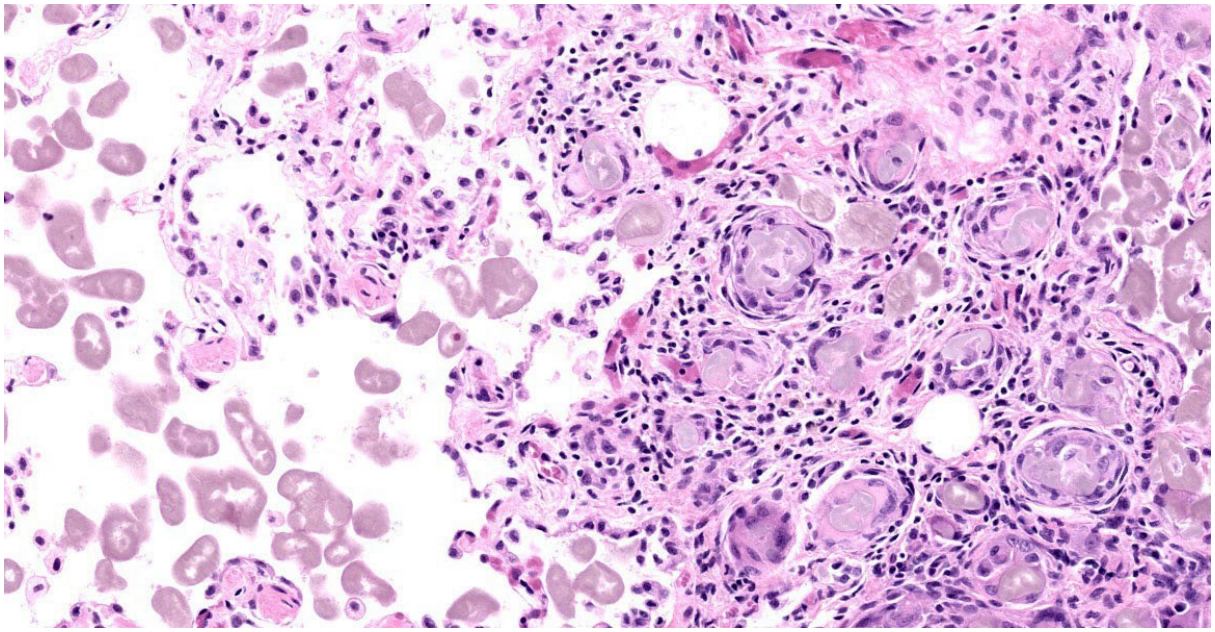

Figure 4-2. Lung dog. Aggregates of amphophilic protein are present within alveoli (left) and in large areas of the lung; they have been surrounded and engulfed by macrophages within affected alveoli. Alveolar septa are expanded by fibrosis and moderate numbers of macrophages, lymphocytes, and plasma cells. (HE, 258X)

JPC Comment:

This disease was first described by Dr. Leonard Billups and Dr. FM Garner in a manuscript published in *Veterinary Pathology* in 1972. Dr. Billups had a long career as an esteemed Army Officer and accomplished veterinary pathologist. He was a Vietnam veteran, completed his residency in veterinary pathology at the Armed Forces Institute of Pathology in 1969, and retired as a colonel (O-6) in 1995. After retiring from active duty, he served as an associate professor of pathology and Dean of Administrative Services at Tuskegee University College of Veterinary Medicine from 1995-2009. Dr. Billups is remembered within our organization as a consummate professional, officer, and academic who ignited a passion for veterinary pathology in many of his students.

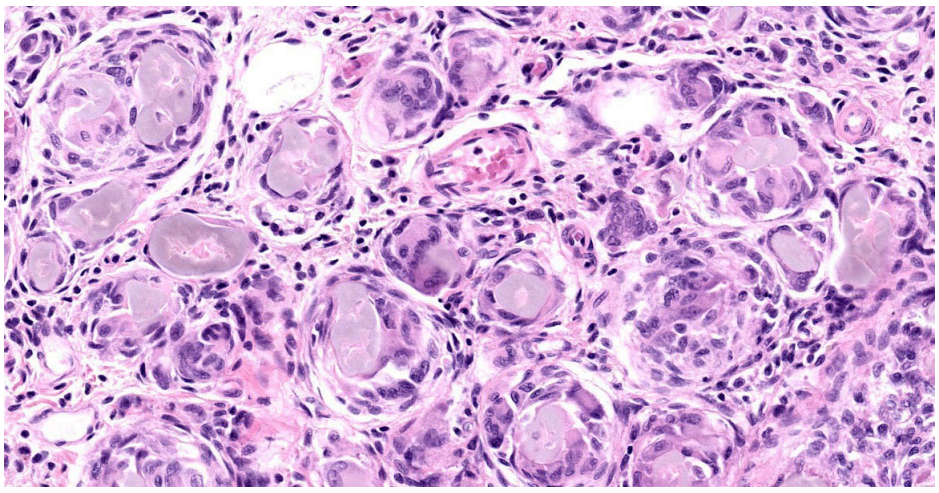

Figure 4-3. Lung dog. Higher magnification of granulomatous inflammation surrounding intra-alveolar protein. (HE, 381X)

As the contributor states, literature on pulmonary hyalinosis is sparse. While not fully understood, this abnormal alveolar material may accumulate due to increased production of an endogenous substance or decreased mucociliary clearance or impaired macrophagic breakdown

of endogenous or exogenous substances.[5] In addition to being PAS positive, the hyaline material has been reported to be diastase resistant, positive for oil red-O, blue when stained with crystal violet, and negative for GMS, Giemsa, Prussian blue, and Congo red.[1, 4, 5]

Pulmonary hyalinosis (PH) has recently been reported in captive sugar gliders and an inbred strain of laboratory rabbits.[3, 5] In a retrospective review of sugar glider necropsies, pulmonary hyalinosis was identified in 6 animals from 18 autopsies with lung tissue available; the animals were of various ages, with two considered young, and PH was considered the cause of death in one animal.[5] In a separate study, the lesion was identified as an incidental finding in 8 of 13 aging audiogenic EIII/JC strain rabbits (which develop seizures after auditory stimuli).[3] In this report, type II pneumocyte hyperplasia was frequently noted.[3] The material was also immunoreactive for surfactant protein-A (SPA) antibody, a finding that had not been evaluated in previous reports on PH.[3] The authors pre ferred the term surfactant pneumonia as it more accurately described the etiology and avoids confusion with the epithelial hyalinosis observed in laboratory mice.[3]

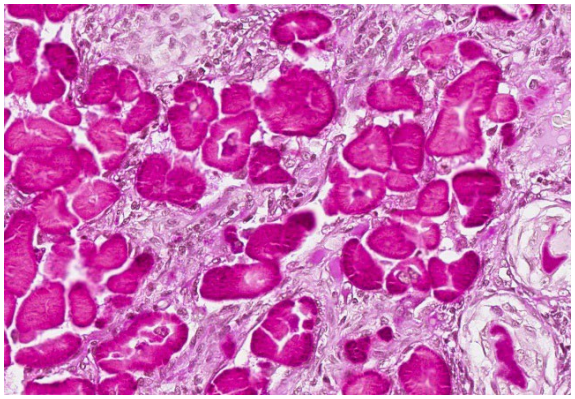

Figure 4-4. Lung, dog. Intra-alveolar protein is PAS-positive. (PAS, 400X) (Photo courtesy of Covance Laboratories, Inc, Madison, Wisconsin, USA, http://www.covance.com/industry-solutions/drug-development/services/safety-assessment/nonclinical-pathology-services.html)

References:

1. Billups, LH, Liu, SK, Kelly, DF, Garner, GM. Pulmonary granulomas associated with PAS-positive bodies in brachycephalic dogs. *Vet Pathol.* 1972;9:294-300.
2. Caswell JL, Williams KJ. Respiratory System. In: *Jubb, Kennedy, and Palmer's Pathology of Domestic Animals*. 5th ed. Vol 2. 2007:572-573.
3. Cooper TK, Griffith JW, Chroneos ZC, et al. Spontaneous Lung Lesions in Aging Laboratory Rabbits (*Oryctolagus cuniculus*). *Vet Pathol.* 2017; 54(1):178-187.
4. Dagle, G., Filipy, R., Adee, R., and Stuart, B. Pulmonary Hyalinosis in Dogs. *Vet Pathol*. 1976;13:138-142.
5. Sokol SA, Agnew DW, Lewis AD, Southard TL, Miller AD. Pulmonary hyalinosis in captive sugar gliders (*Petaurus breviceps*). *J Vet Diag Invest.* 2017;29(5):691-695.

WSC 2022-2023 Self-assessment.
Conference 5.

1. Which of the following is the cause of histiocytic ulcerative colitis in the dog?
    a. *Mycobacterium avium*
    b. *Salmonella enteritidis*
    c. Proteus vulgaris
    d. E. coli

2. In addition to Pseudomonas aeruginosa, which of the following has been identified as causing hemorrhagic pneumonia in mink?
    a. *Proteus vulgaris*
    b. *E. coli*
    c. *Salmonella typhimurium*
    d. *Staphylococcus intermedius*
3. True or false? Infection with *Lawsonia intracellularis* impairs differentiation of absortive enterocytes.
    a. True
    b. False

4. *Eimeria furonis* has also been identified in which of the following organs in mustelids?
    a. Gallbladder
    b. Urinary bladder
    c. Lens
    d. Spleen

5. The amphophilic protein in pulmonary hyalinosis in the dog stains positively with which of the following?
    a. Gomori methenamine
    b. Periodic acid Schiff
    c. Colloidal iron
    d. Phosphotungstic acid hematoxylin

Please email your completed assessment for grading to Dr. Bruce Williams at bruce.h.williams12.civ@mail.mil. Passing score is 80%. This program (RACE program 33611) is approved by the AAVSB RACE to offer a total of 0.5 CE Credits, with a maximum of 12.5 CE Credits being available to any individual Veterinary Medical Professionals for the 2019-2020 Wednesday Slide Conference. This RACE approval is for the subject matter categories of: SCIENTIFIC using the delivery method of NONINTERACTIVE DISTANCE. This approval is valid in jurisdictions which recognize AAVSB RACE.

Joint Pathology Center
Veterinary Pathology Services

WEDNESDAY SLIDE CONFERENCE 2022-2023

Conference #6 — 28 September 2022

CASE I:

Signalment:
2-week-old, male castrated, Angus calf (*Bos taurus*)

History:
Ocular opacity, ocular and nasal discharge, foam coming out mouth and nose, dehydration, abdominal distention, dyspnea.

Gross Pathology:
The body is in fair nutritional and postmortem condition. Multiple joints contain small amounts of fibrin. Across the mucosal surface of the larynx and trachea, there are loosely adherent, multifocal to coalescing, slightly raised, moist, tan plaques. The lungs are diffusely dark, wet, and slightly firm. Randomly distributed throughout all lung lobes are 50-100 targetoid, ~0.2 cm diameter nodules that range from tan to dark red. The myocardium heart is slightly mottled and pale. There is mild splenic enlargement and congestion of the renal medullary regions/vessels. The umbilicus is markedly thickened by fibrous tissue (chronic omphalitis). Bilaterally, the umbilical artery lumens persist and are mildly distended with opaque, brown, slightly viscous fluid (interpreted as omphaloateritis).

Laboratory Results:
PCR Results: Lung tissue tested:
Bovine coronavirus - negative
Bovine herpes virus 1 – positive (CT value = 21.77)
Bovine parainfluenza 3 – negative
Bovine syncytial virus - negative
Bovine Viral Diarrhea - negative
Influenza D virus – negative
Malignant Catarrhal Fever – negative
Mycoplasma bovis – negative

Immunohistochemistry Results: Adrenal gland:
BHV-1– positive staining (within foci of necrosis)

Aerobic Culture Results: Lung and liver:

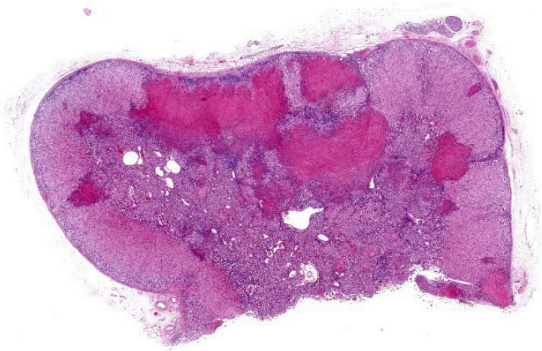

Figure 1-1. Adrenal gland, ox. A section of adrenal gland is submitted for examination. There are extensive areas of necrosis, primarily within the cortex, but which may extend into the medulla. (HE, 5X)

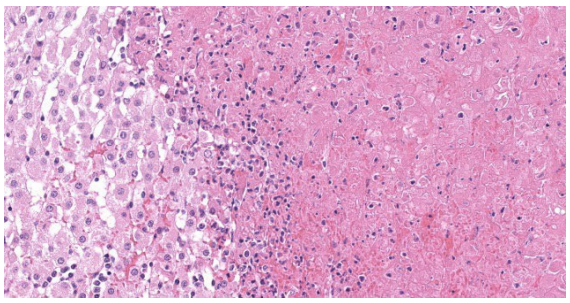

Figure 1-2. Adrenal gland, ox. Areas of necrosis are large coagulative in nature, but are undergoing lytic change, with infiltration of neutrophils admixed with cellular debris. (HE, 304X)

1+ *Pseudomonas aeruginosa*, *Staphylococcus sciur*i and *E. coli* (postmortem overgrowth)

Microscopic Description:
Adrenal gland: Scattered throughout the section, affecting both cortical and medullary regions, there are multifocal, random, variably sized, discrete areas of acute lytic necrosis affecting approximately 40% of the examined section. The foci of necrosis and inflammation are characterized by hypereosinophilic accumulations of necrotic cellular debris, acute hemorrhage, fibrin exudation, and infiltration by degenerating neutrophils and fewer mononuclear cells. Intact adrenal cortical and medullary cells bordering the foci of necrosis frequently show marginalization of nuclear chromatin and variably frequent, 2-4 µm diameter, eosinophilic to amphophilic intranuclear inclusion bodies that are either surrounded by a clear halo or fill the nucleus. Infrequent multinucleate syncytial cells are noted at the margins of necrosis/inflammation. Similar mixtures of degenerate neutrophils and fewer mononuclear cells surround and variably infiltrate the adrenal capsule as well as associated vessels with nerves and ganglia being less affected. Subtle degeneration and lipid-vacuole loss is noted in the surrounding adipose tissue.

Immunohistochemical staining for bovine herpesvirus 1 reveals abundant positive dark brown cytoplasmic and membrane staining associated with the foci of necrosis and virus-infected cells.

Contributor's Morphologic Diagnoses:
Adrenal gland: Adrenalitis, necrotizing, random, acute with eosinophilic intranuclear inclusion bodies (consistent with bovine herpesvirus 1 adrenalitis)

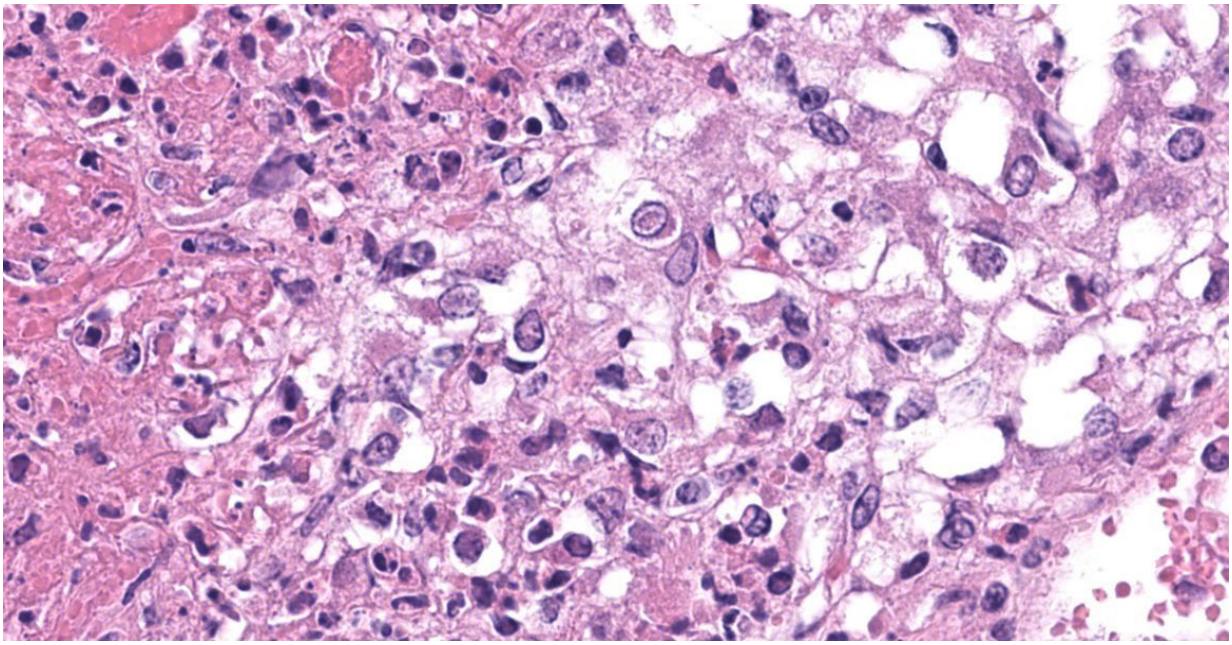

Figure 1-3. Adrenal gland, ox. Adrenocortical cells at the periphery of the necrotic areas contain a single eosinophilic intranuclear viral inclusion that peripheralizes chromatin. (HE, 590X)

Contributor's Comment:
Bovine herpesvirus 1 (BHV-1; Alphaherpesvirinae) infects a wide range of animals, including cattle, sheep, goats, llamas, swine, water buffalo, mustelids, and rabbits.[2] The virus is widespread among cattle populations and is the cause of the following clinical disease patterns: infectious bovine rhinotracheitis (IBR), keratoconjunctivitis, bronchointerstitial pneumonia, abortion, encephalitis, systemic herpesvirus infection in young calves, and pustular vulvovaginitis or balanoposthitis in unvaccinated/naive cattle.[2, 4] Routine vaccination has reduced the incidence of BHV-1 infections in both dairy and beef animals but stress, or steroid treatment, may result in reactivation of latent virus infections.[4]

Respiratory infections usually involve the upper respiratory tract (nasal mucosa and muzzle inflamed) and lungs and can vary from subclinical to severe infections. Young animals may also develop keratoconjunctivitis with or without upper respiratory disease, while young adult animals may also develop pustular vulvovaginitis or balanoposthitis when infected BHV-1.[4]

Disseminated/systemic infections with multiple organ involvement have also been identified and well documented in neonatal calves and fetuses infected with BHV-1.[1, 5, 8, 14, 11] Lesions in affected neonates and fetuses have been reported to involve the upper respiratory tract, lungs, oral cavity, esophagus, rumen, liver, kidney, spleen, as well as adrenal gland,[1, 5, 8, 14] with enteritis and encephalitis being observed in some clinical cases.[1, 5, 14] In this case, the calf age and lesion distribution best fits with the systemic form of BHV-1 infection in young calves.

The adrenal lesions are consistent with those previously reported in systemic herpesvirus infection and are characterized as multifocal random foci of necrosis range from coagulative to lytic) accompanied by infiltration with scattered degenerate neutrophils.[1,12] Like other reports, occasional eosinophilic intranuclear viral inclusion bodies and syncytial cells are observed amongst the necrotic cells as well as within intact virus-infected cells bordering foci of necrosis.[1, 2, 12] As Moeller Jr. and others (2013) noted, microscopic le-

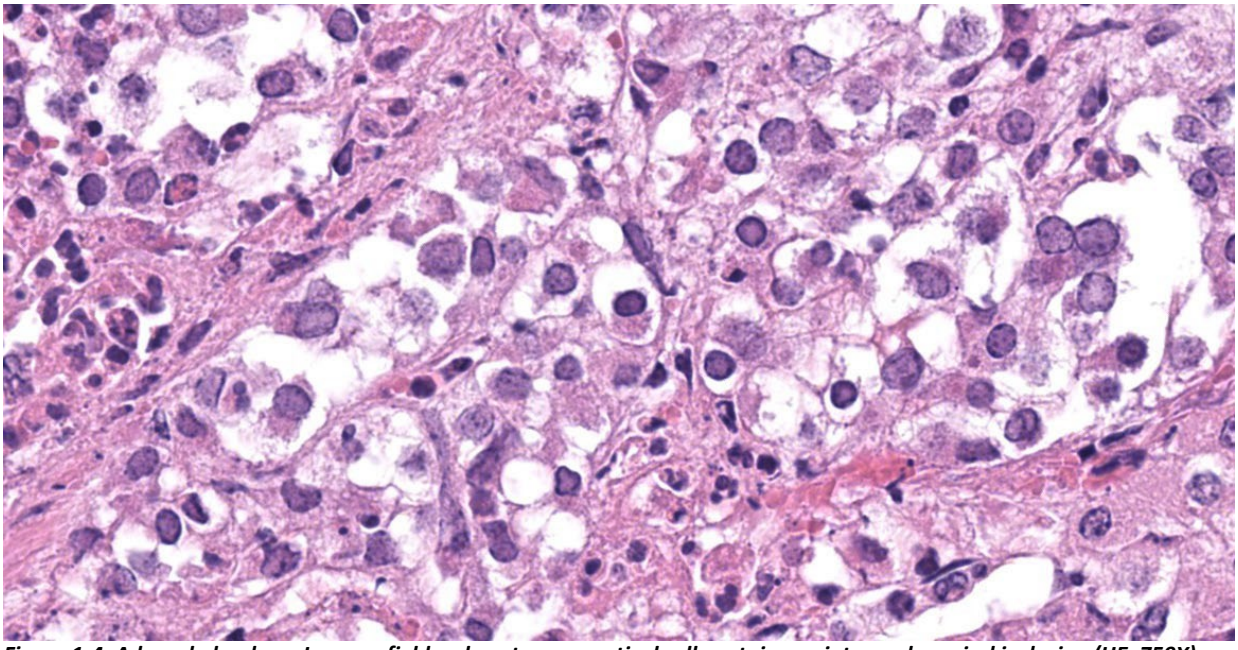

Figure 1-4. Adrenal gland, ox. In some fields, almost every cortical cell contains an intranuclear viral inclusion (HE, 759X)

sions associated with neonatal BHV-1 infection may be confined to the adrenal gland only (29/62 animals examined had adrenal lesions only) and the diagnosis may be missed if adrenal gland is not sampled during postmortem examination.[12]

The source of BHV-1 transmission from infected dams to calves may occur in utero (late gestation) or during parturition and can result in fetal abortion or systemic disease in neonatal or suckling calves (up to 1 month of age; clinical disease following a 2–6-day incubation period).[2, 11, 12] Reactivation of latent infections or activation of modified live vaccine strain virus may also be linked to environmental stressors and/or immunosuppression (e.g., inadequate colostrum intact) have been shown to contribute to the expression of clinical disease in calves and cattle infected BHV-1.[1, 9, 10] A limited vaccination history of dams and potential inadequate colostrum intact may account for the development of systemic disease in this calf.

Contributing Institution:
Department of Veterinary Clinical and Diagnostic Sciences with the Faculty of Veterinary Medicine, University of Calgary.

JPC Diagnosis:
Adrenal gland: Adrenalitis, necrohemorrhagic, multifocal to coalescing, moderate, with intranuclear viral inclusions and viral syncytia.

JPC Comment:
Bovine herpesvirus-1 is a double-stranded DNA virus which was first isolated in 1956.[3] There are three subtypes, BHV 1.1, 1.2a, and 1.2b, which have slight variations in clinical presentation, pathogenicity, and geographic distribution.[6] All subtypes can cause infectious bovine rhinotracheitis which is the most common presentation in feedlot cattle. BHV-1 is similar to *Mycoplasma bovis*, as seen in Conference 1 Case 3 earlier this year, in that it can damage host respiratory defense mechanisms and predispose to secondary bacterial invaders, culminating in bovine respiratory disease complex (shipping fever), an economically important disease which costs at least $1 billion annually in the United States alone.[7]

BHV lacks tissue tropism and can infect a wide range of cells, as illustrated in this case of systemic disease. BHV-1 attaches to the cell surface using envelope proteins gB and gC, interacts with the intercellular adhesion molecule Nectin-1 using envelope protein gD, and enters the cell after viral and cell membrane fusion.[6] The virus can spread directly between cells without cell lysis using a variety of other glycoproteins and can spread systemically through a cell-associated viremia.[3,6,13] BHV-1 can also spread through rupture of infected cells. The virus induces production of "virus host shut off" (vhs) protein, so named because it disables cellular protein synthesis, compromises membrane stability, and ultimately results in cell necrosis.[3] Virus particles liberated from ruptured cells can subsequently infect adjacent cells.[3] In the airways, necrosis of epithelial cells disrupts the mucociliary apparatus, preventing clearance of inhaled particles and allowing bacterial deposition within the lungs.[3] Additional, the virus can replicate in endothelial cells, causing vascular damage and ischemia. Confer-

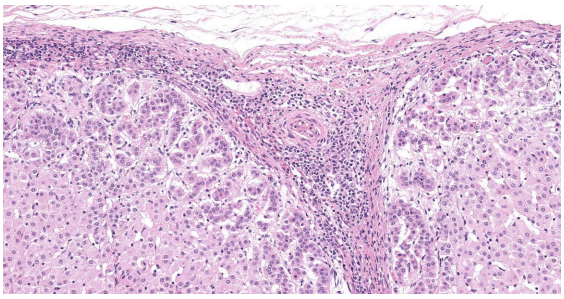

Figure 1-5. Adrenal gland, ox. There are aggregates of lymphocytes and macrophages in the capsule, often overlying areas of necrosis deeper in the cortex. (HE, 150X)

ence participants remarked on the lack of viral inclusions in the endothelium in this case, which was surprising given the degree of necrosis in the section.

BHV-1 also induces a transient immunosuppression through a variety of mechanisms. Viral infection induces apoptosis of CD4+ T cells and impairs CD8+ CTL function by inhibiting antigen processing and repressing MCHI expression.[6] The vhs protein inhibits MHCII expression. Finally, viral bICP0 gene activity inhibits interferon gamma production by inhibiting interferon regulatory factor (IRF) 7 and stimulating proteosomic destruction of IRF3.[6]

Latency and recrudescence are a hallmark of herpesviral infection and make control and eradication of BHV-1 difficult.[3,13] After initial infection, BHV-1 spreads between cells and ultimately enters the peripheral nervous system.[3] In respiratory infections, the virus becomes latent in the trigeminal ganglion, while genital infections result in latency in the sciatic nerve.[13] Latency in other organs, including the tonsils, lymph nodes, blood, and spleen, has also been documented.[6] Latent infection and recrudescence are controlled by a few viral proteins and the host immune system.[6] The latency-related (LR) gene is active early in infection of neurons and helps inhibits neuronal apoptosis, productive infection, and bICP0 expression.[6] Active cell-mediated immunity also enforces latency, and CD8+ T cells which persist in the infected ganglia produce IFN-gamma and may induce cytotoxicity to reduce viral spread.[6] Stress (i.e. from shipping or introduction into a new herd) or administration of corticosteroids is associated with reduced LR expression, active viral replication, and recrudescence. [6]

References:

1. Bryan LA, Fenton RA, Misra V, Haines DM. Fatal, generalized bovine herpesvirus type-1 infection associated with a modified-live infectious bovine rhinotracheitis parainfluenza-3 vaccine administered to neonatal calves. *Can Vet J*. 1994;35: 223-228.
2. Caswell JL, Williams KJ. Chapter 5 - Respiratory System. In: Maxie MG, ed. *Jubb, Kennedy & Palmer's Pathology of Domestic Animals:* Volume 2. 6th ed. Philadelphia, PA: Elsevier Saunders; 2016:465-591, e464.
3. Ellis JA. Update on viral pathogenesis in BRD. *Animal Health Research Reviews.* 2010; 10(2):149-153.
4. Graham DA. Bovine herpes virus-1 (BoHV-1) in cattle-a review with emphasis on reproductive impacts and the emergence of infection in Ireland and the United Kingdom. *Ir Vet J*. 2013;66: 15.
5. Hill BD, Hill MW, Chung YS, Whittle RJ. Meningoencephalitis in calves due to bovine herpesvirus type 1 infection. *Aust Vet J*. 1984;61: 242-243.
6. Jones C, Chowdhury S. A review of the biology of bovine herpesvirus type 1 (BHV-1), its role as a cofactor in the bovine respiratory disease complex and development of improved vaccines. *Animal Health Research Reviews*. 2008; 8(2):187-205.
7. Jones C, Chowdhury. Bovine Herpesvirus Type 1 (BHV-1) is an Important cofactor in the Bovine Respiratory Disease Complex. *Vet Clin Food Anim.* 2010; 26:303-321.
8. Kennedy PC, Richards WPC. The Pathology of Abortion Caused by the Virus of Infectious Bovine Rhinotracheitis. *Pathologia veterinaria*. 1964;1: 7-17.

9. Mechor GD, Rousseaux CG, Radostits OM, Babiuk LA, Petrie L. Protection of newborn calves against fatal multisystemic infectious bovine rhinotracheitis by feeding colostrum from vaccinated cows. *Can J Vet Res*. 1987;51: 452-459.
10. Meyer G, Lemaire M, Ros C, et al. Comparative pathogenesis of acute and latent infections of calves with bovine herpesvirus types 1 and 5. *Arch Virol.* 2001;146: 633-652.
11. Miller RB, Smith MW, Lawson KF. Some lesions observed in calves born to cows exposed to the virus of infectious bovine rhinotracheitis in the last trimester of gestation. *Can J Comp Med.* 1978;42: 438-445.
12. Moeller RB, Adaska J, Reynolds J, Blanchard PC. Systemic Bovine herpesvirus 1 infections in neonatal dairy calves. *Jour Vet Diag Invest*. 2013;25: 136-141.
13. Osterrieder K. Herpesvirales. In: MacLachlan NJ, Dubovi EJ, eds. *Fenner's Veterinary Virology.* 5th ed. Cambridge, MA: Elsevier. 2017; 194-195, 199-201.
14. Penny CD, Sargison ND, Howie F, Nettleton PF, Schock A. Upper respiratory disease and encephalitis in neonatal beef calves caused by bovine herpesvirus type 1. *Veterinary Record.* 2002;151: 89-91.

CASE II:

Signalment:
0.5 years old, male, golden retriever (*Canis familiaris*)

History:
This dog was purchased through a breeder at 7 weeks of age. At around 4 months of age, the dog started having uncontrolled watery−mucoid diarrhea that was large volume and frequent. He was placed on metronidazole and Proviable and needed to stay on the medication, as diarrhea would return when the drugs were not used. The dog was diagnosed with carpal flexure deformity at 3 months of age. Radiographs of the cervical spine and hips revealed mild hip dysplasia and shortened distal cervical vertebral bodies. The dog developed urinary accidents (normal volume) at home. On presentation to Iowa State University Teaching Hospital, the dog had lateral strabismus, vertical nystagmus, ataxia that was worse in hind limbs with normal reflexes and placement and hopping, head tremor, and rectal mucosa felt very irregular on rectal palpation. The owner did not allow many additional tests; only creatine kinase, which was mildly increased at 378, and blood smear which showed possible granules in lymphocytes. The dog's condition deteriorated over a week and was euthanized.

Gross Pathology:
Small intestine: A small number (approximately 10) of 2−5 cm in length and 2 mm in

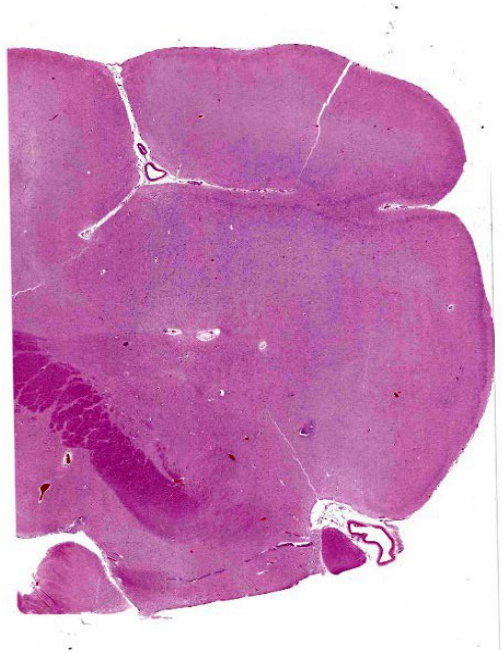

Figure 2-1. Cerebrum, dog. A single section of cerebrum is submitted for examination; there is no visible lesion at subgross magnification. (HE, 7X)

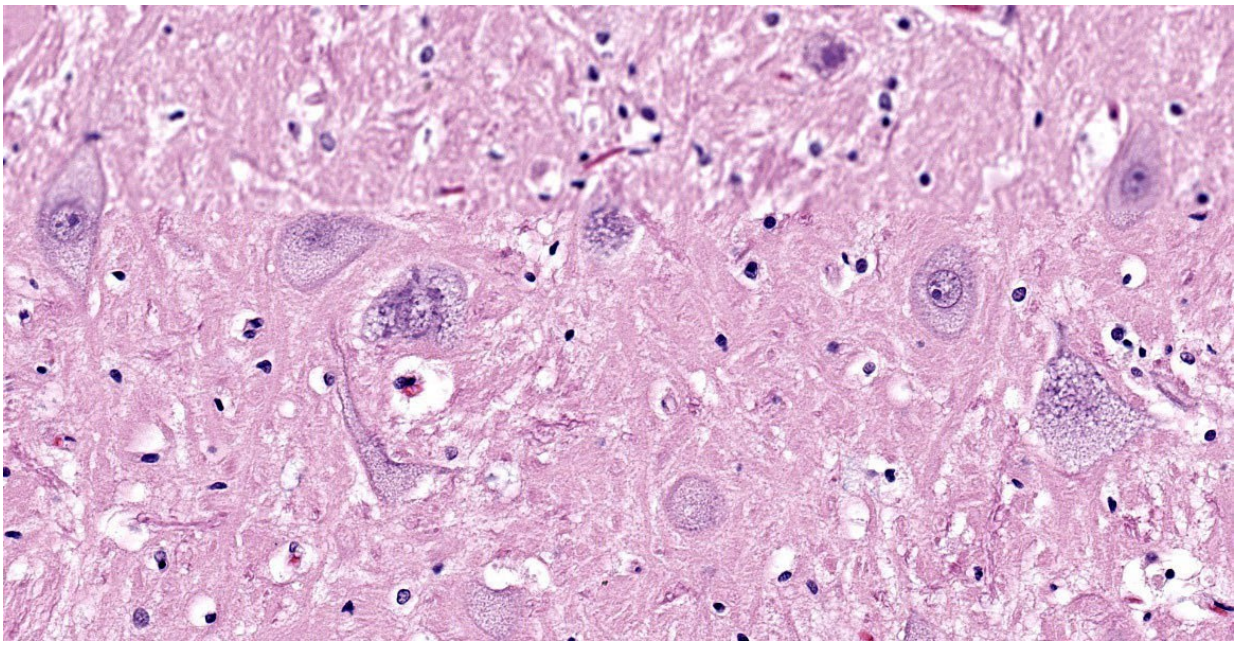

Figure 2-2. Cerebrum, dog. Diffusely, neurons are swollen by an accumulation of cytoplasm vacuoles which disperses Nissl substance. (HE, 381X)

diameter, white, elongate nematodes with tapered ends (roundworms) were present multifocally within the small intestinal lumen.

Laboratory Results:
Hepatic beta-hexosaminidase (*Hex*) An enzyme activity in the liver was elevated.

Microscopic Description:
Brain (cerebral cortex at the level of internal capsule): Diffusely, neurons are moderate to markedly expanded by microvacuolated cytoplasm, which often peripheralizes the nucleus and occasionally extends into and expands proximal processes. Infrequently, neurons also contain larger vacuoles up to 8 microns in diameter. Microglia are subjectively increased in number. There is rare neuronal necrosis, and rare blood vessels are cuffed by few lymphocytes. White matter is mildly vacuolated with occasional spheroids and few vacuolated cells (small neuron or astrocyte morphology). The caudate nucleus is regionally hypercellular with vascular proliferation and gliosis − extant neurons are similarly vacuolated.

Other findings:
Spinal cord (Slides not submitted): All spinal cord segments are similarly affected. Diffusely, neurons are variably expanded by abundant finely vacuolated cytoplasm, which often peripheralizes the nucleus and Nissl substance. Multifocal neurons contain larger vacuoles, up to 8 microns in diameter, containing pale eosinophilic material. Some neurons contain both foamy microvacuolated cytoplasm and larger vacuoles. Glia appears unaffected. White matter and nerve rootlets contain scattered dilated and often empty axon sheaths. Meninges, blood vessels − no specific pathologic findings.

Eye (Slides not submitted): Retinal ganglion cells are similarly enlarged and vacuolated with margination of the nucleus.

Duodenum and colon (Slides not submitted): Myenteric and submucosal plexus neurons occasionally appear enlarged with microvacuolated clear to eosinophilic cytoplasm with marginated nuclei.

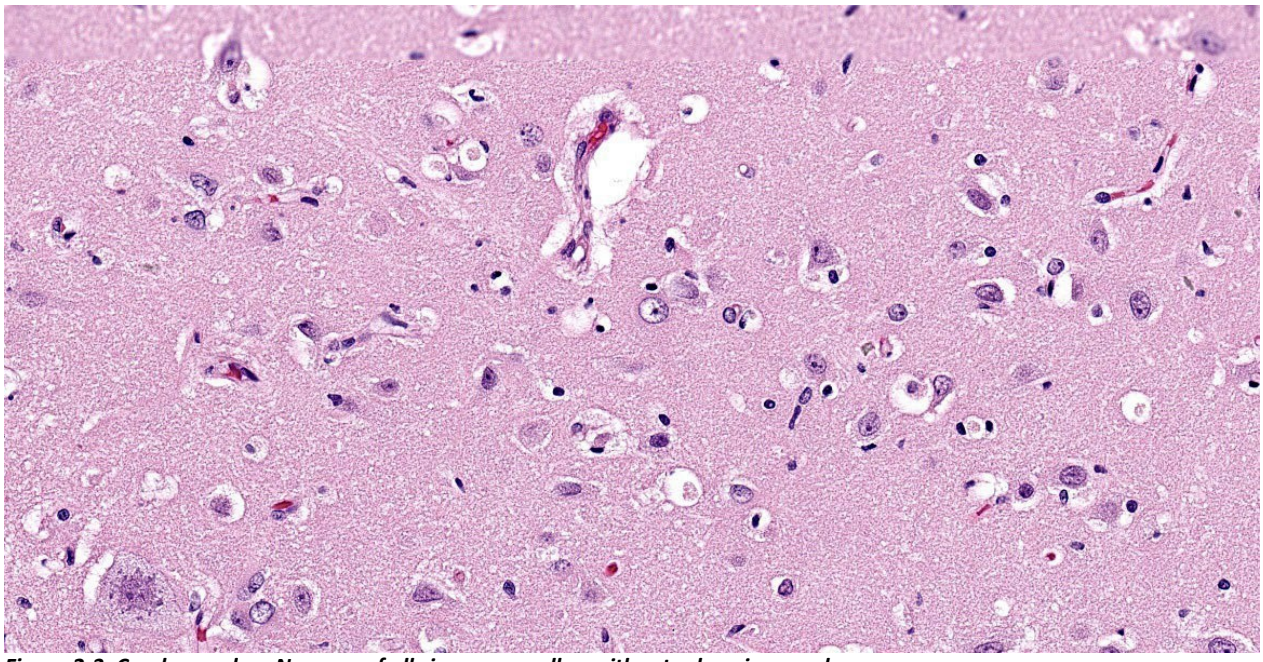

Figure 2-3. Cerebrum, dog. Neurons of all sizes are swollen with cytoplasmic vacuoles

Urinary bladder (Slides not submitted): Ganglion cells within the bladder wall are similarly enlarged and vacuolated.

Mesenteric ganglion (Slides not submitted): Ganglion cells are markedly distended by similar microvaculated cytoplasm as described above.

Contributor's Morphologic Diagnoses:
Cerebral cortex: Neuronal cytoplasmic vacuolation, diffuse, moderate to severe.

Table 2-1: Select sphingolipidoses

Name		Protein defect		Ultrastructural feature of vacuole	Histological features
GM1 gangliosidosis		beta-galactosidase		Lamellar	Vacuoles in neurons, astrocytes, endothelial cells, retinal cells, hepatocytes, and Kupffer cells
GM2 gangliosidosis	B variant (Tay-Sachs disease)	beta-hexosaminidase (Hex)	Alpha subunit of Hex A	Lamellar	Vacuoles in neurons and retinal ganglion cells
	O variant (Sandhoff disease)		Beta subunit of Hex A and B		
	AB variant	Activator protein			
Sphingomyelinosis (Niemann-Pick disease)		Sphingomyelinase		Lamellar	Vacuoles in macrophages and parenchymal cells in many tissues
		Cholesterol transporter			
Galactocerebrosidosis (galactosylceramide lipidosis, globoid cell leukodystrophy, Krabbe disease)		Beta-galactocerebrosidase		Tubular	Vacuoles in oligodendrocytes, Schwann cells, macrophages, globoid cells, with demyelination
Glucocerebrosidosis (glucosylceramidosis, Gaucher disease)		Glucocerebrosidase		Tubular	Vacuoles in neurons, macrophages, Gaucher cells in the spleen, lymph nodes, liver, and bone marrow

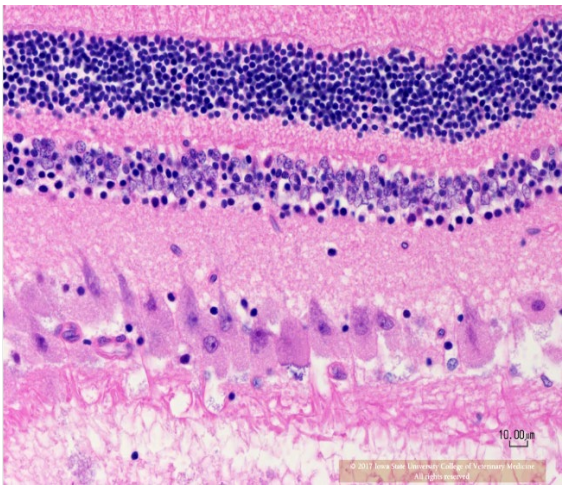

Figure 2-4. Retina, dog. Ganglion cells of the retina are markedly dilated due to an accumulation of clear vacuoles within the cytoplasm. (HE, 400X) (Photo courtesy of: Department of Veterinary Pathology, College of Veterinary Medicine, Iowa State University, https://vetmed.iastate.edu/vpath)

Spinal cord, mesenteric ganglia: Neuronal cytoplasmic vacuolation, diffuse, moderate to severe.

Retina: Retinal ganglion cell vacuolation, cytoplasmic, diffuse, moderate.

Contributor's Comment:
Microscopic changes in this dog were consistent with a lysosomal storage disease (LSD). Vacuolation was predominantly, if not solely, intraneuronal affecting the central, autonomic nervous systems, and retina. The vacuoles were positive for luxol fast blue (myelin stain) but negative for PAS stain, indicating the inclusions are composed predominately of lipid. Ultrastructural examination of the affected neurons revealed that the vacuoles contain concentric lamellated inclusions which are most consistent with the GM1 and GM2 gangliosidoses or sphingomyelinosis.

Sphingolipidoses are characterized by genetic defects in catabolism of glycosphingolipids which are normal components of cell membranes and extracellular matrix. In animals, based on protein defects, there are at least five important types, including GM1 gangliosidosis, GM2 gangliosidosis, sphingomyelinosis, galactocerebrosidosis, and glucocerebrosidosis (table 2-1)[5–7]. These protein defects lead to impaired function of lysosomal enzymes themselves or proteins assisting lysosomal enzymes in substrate processing. Ultrastructurally, the inclusions in GM1 and GM2 gangliosidoses and sphingomyelinosis reveal whorls and laminar arrangements, while the inclusions in galactocerebrosidosis and glucocerebrosidosis are characterized by long tortuous and twisted tubules.

GM1 gangliosidosis results from the deficiency of beta-galactosidase and shows accumulation of glycolipids and oligosaccharides in many cell types and tissues, including neurons, astrocytes, retinal cells, hepatocytes, Kupffer cells, and endothelial cells in different tissues. Canine GM1 gangliosidosis has an autosomal recessive pattern of inheritance.[25] Different breeds reveal variable defects in the *GLB1* (Galactosidase, beta 1) gene. In Portuguese Water Dogs, a G→A mutation in exon 2 results in an Arg→His amino acid substitution.[22] In Shiba Inu dogs,

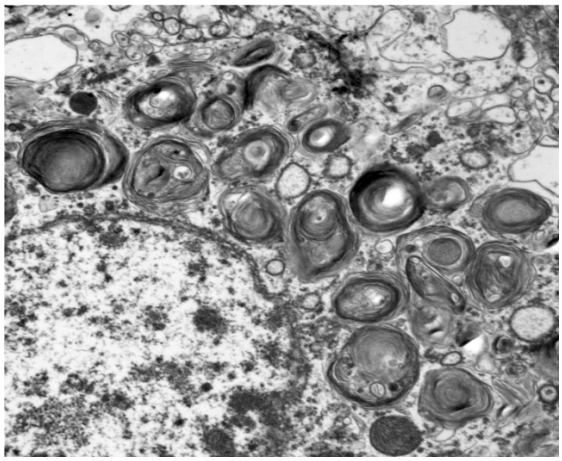

Figure 2-5. Thalamus, dog. Numerous lysosomes with lamellated contents populate the cytoplasm of a thalamic neuron. (TEM, 15,000X). (Photo courtesy of: Department of Veterinary Pathology, College of Veterinary Medicine, Iowa State University, https://vetmed.iastate.edu/vpath)

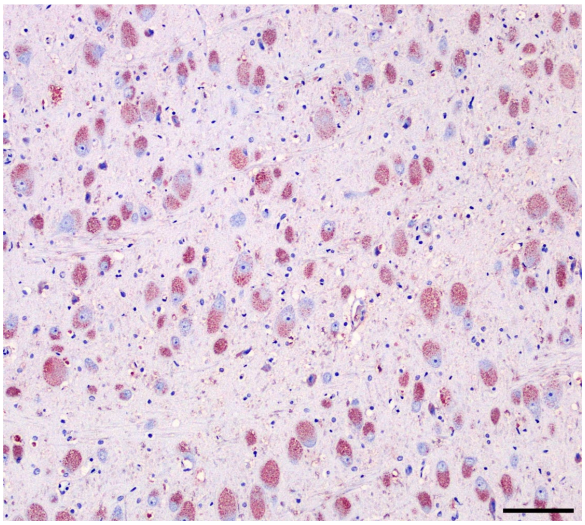

Figure 2-6. Cerebrum, dog. Vacuolated neurons stain strongly immunopositive with cholera toxin subunit B. (anti CTSB, 200X) (Photo courtesy of: Department of Veterinary Pathology, College of Veterinary Medicine, Iowa State University, https://vetmed.iastate.edu/vpath)

the mutation is a deletion of C nucleotide 1668 in exon 15.[23] Alaskan huskies reveal 19-bp duplication in exon 15 of *GLB1*. [12, 13] Due to similar genetic defects, clinical signs, and lesions, dogs are considered as a suitable animal model of human GM1 gangliosidosis. [1, 8, 11, 22] In humans, GM1 gangliosidosis is divided into three types: type 1 (infantile), type 2 (late infantile/juvenile), and type 3 (adult). Except for the English springer spaniel, other canine breeds are comparable with the late infantile/juvenile form (Table 2-2).[24] In this form, these dogs show progressive clinical nervous signs accompanied by possible skeletal abnormality and hepatosplenomegaly.

In this dog, elevated *Hex*A activity ruled out B and O variants of GM2 gangliosidosis. Strong signal of cholera toxin subunit B in the cytoplasm of vacuolated neurons demonstrated the presences of GM1 ganglioside, potentially implicating GM1 gangliosidosis as the disease entity affecting the patient.[9] However, GM1 ganglioside can also accumulate secondarily in other lysosomal storage diseases.[19] Assay for enzyme deficiency or genetic analysis of the *GLB1* gene is necessary for a definitive diagnosis of GM1 gangliosidosis. In this case, whole genome sequencing revealed a missense mutation in *GLB1* resulting in a C→A substitution at exon 3. Additionally, beta galactosidase activity was significantly decreased in brain white matter, gray matter and liver. Activity levels of neuraminidase and protective protein/cathepsin A (PPCA) were normal. Taken together, these results are consistent with GM1 gangliosidosis, novel in the Golden Retriever breed, and most comparable to the late infantile/juvenile form in humans.

Table 2-2：Comparison of human and canine GM1 gangliosidosis

Human	Features	Dog
Type 1 (infantile)	Dwarfism, facial distortion, bone deformities, hepatosplenomegaly, seizures, vision loss (early), startled response to sound	English Springer Spaniel[3]
Type 2 (late infantile / juvenile)	Bone deformities+/-, hepatosplenomegaly+/-, seizures, ataxia, spasticity, vision loss (late), startled response to sound	German Shorthair Pointer[9], Beagle/Mixed-breed[14,15], Portuguese Water Dog[2], Shiba Inu[18], Alaskan husky[13]
Type 3 (adult)	Ataxia, spasticity	

Contributing Institution:
Department of Veterinary Pathology
College of Veterinary Medicine
Iowa State University
https://vetmed.iastate.edu/vpath

JPC Diagnosis:
Cerebrum, neurons: Vacuolation, cytoplasmic, diffuse, moderate, with mild gliosis.

JPC Comment:
Gangliosides have been studied extensively due to their role in gangliosidosis and the altered levels found in various neurodegenerative disorders such as Alzheimer's disease.[21] Gangliosides are a diverse group of molecules synthesized in the endoplasmic reticulum and Golgi apparatus. While found throughout

the body, they are concentrated in the nervous system, residing in lipid rafts on the external plasma membrane surface of neuronal cells and synapses.[21] Ganglioside prevalence changes with age; in humans, for instance, GM1 concentration increases until adulthood and gradually decreases in old age.[21] While elevated concentration of gangliosides can cause severe disease, in certain conditions, gangliosides can have neurotrophic or neuroprotective effects.[21] Human trials, for instance, have demonstrated that exogenous GM1 helped alleviate neurotoxicity associated with chemotherapy.[21]

In addition to various breeds of dogs, gangliosidoses have been reported in cats, sheep, cattle, pigs American black bears, and emus.[4,15] In sheep, GM1 gangliosidosis has been reported in the Suffolk (type 1) and Romney (types 1, 2, and 3) breeds; in cats, it has been documented in Siamese, Korat, and mixed breed cats.[18,20]

Muthupalani et al. described seven young free-ranging American black bears in New England with poor body condition and variable neurologic symptoms including tremors, ataxia, and hypermetria. The animals had few vacuolated mononuclear cells and neutrophils on blood smear and cerebral atrophy with enlarged ventricles and prominent sulci on necropsy. [15] Eosinophilic vacuoles were present in neurons, retinal ganglion cells, renal proximal tubular epithelium, chondrocytes, and hepatocytes; the vacuoles in the neurons and retina were blue on Luxol fast blue staining. [15] Enzymatic testing revealed drastically decreased beta galactosidase activity compared to the control, and gene sequencing identified a missense mutation Y348H on exon 10 in the GLB1 gene. [15] These findings were consistent with GM1-gangliosidosis. [15]

Bermudez et al described two adolescent emu hatchmates with progressive neurologic signs had similar vacuoles reported in neurons of the cerebrum, brainstem, cerebellum, spinal and autonomic ganglia, and retina. [4] GM1 and GM3 levels were up to 25 times higher than controls, and decreased beta-galactosidase activity; these findings were all consistent with gangliosidosis.[4] This was the first documented report of a neuronal storage disease in avian species outside of Lafora body neuropathy.

References:

1. Ahern-RindellAJ, KretzKA, O'BrienJS. Comparison of the canine and human acid beta-galactosidase gene. *Am J Med Genet*. 1996 May 17 [cited 2018 May 27];63:340–345.
2. AlroyJ, OrgadU, DeGasperiR, et al. Canine GM1-gangliosidosis. A clinical, morphologic, histochemical, and biochemical comparison of two different models. *Am J Pathol*. 1992;140:675–689.
3. AlroyJ, OrgadU, UcciAA, et al. Neurovisceral and skeletal GM1-gangliosidosis in dogs with beta-galactosidase deficiency. *Science*. 1985 Aug 2 [cited 2018 May 27];229:470–472.
4. Bermudez AJ, Johnson GC, Vanier MT, et al. Gangliosidosis in Emus (Dromaius novaehollandiae). *Avian Diseases*. 1995; 39:292-303.
5. CantileC, Youssef S. Nervous System. In: Maxi MG, ed. *Jubb, Kennedy, and Palmer's Pathology of Domestic Animals.* Vol 1. 6th ed. Philadelphia, PA: Elsevier Saunders. 2016:287–288.
6. Cheville NF. Metabolic and Storage Diseases. In: *Ultrastructural Pathology The Comparative Cellular Basis of Disease*. Wiley-Blackwell; 2009:856–861.

7. GilmanS. Lysosomal disorders of the nervous system. In: *Neurobiology of Disease*. Elsevier; 2011:1–9.
8. HubertJJ, O 'brienJS. Dog and human acid beta-D-galactosidases are structurally similar. *Biochem J*. 1983;213:473–478.
9. IwamasaT, OhshitaT, NashiroK, IwanagaM. Demonstration of GM1-ganglioside in nervous system in generalized GM1-gangliosidosis using cholera toxin B subunit. *Acta Neuropathol*. 1987 [cited 2018 May 27];73:357–360.
10. Karbe E, Schiefer B. Familial Amaurotic Idiocy in Male German Shorthair Pointers. *Pathol Vet.* 1967; 4(3):223-32. [cited 2018 May 27].
11. Kaye EM, Alroy J, Raghavan SS, et al. Dysmyelinogenesis in animal model of GM1 gangliosidosis. *Pediatr Neurol*. 1992 [cited 2018 May 27];8:255–261.
12. KreutzerR, KreutzerM, PröpstingMJ, et al. Insights into post-translational processing of β-galactosidase in an animal model resembling late infantile human GM1-gangliosidosis. *J Cell Mol Med.* 2008;12:1661–1671.
13. Kreutzer R, Leeb T, Müller G, Moritz A, Baumgärtner W. A duplication in the canine β-galactosidase gene GLB1 causes exon skipping and GM1-gangliosidosis in Alaskan huskies. *Genetics*. 2005;170:1857–1861.
14. Lldinger SA, Oritz AM, Urbriggen AZ, Irchhof NK, Ewell AS, Aumga WB. GM 1 -gangliosidosis in Alaskan Huskies : Clinical and Pathologic Findings. *Vet Pathol.* 2001; 38(3); 281–290.
15. Muthupalani S, Torres PA, Wang BC, et al. GM1-gangliosidosis in American black bears: Clinical, pathological biochemical, and molecular genetic characterization.*Mol Genet Metab.* 2014; 111(4): 513-521.
16. Read DH, Harrington DD, Keenana TW, Hinsman EJ. Neuronal-visceral GM1 gangliosidosis in a dog with beta-galactosidase deficiency. *Science*. 1976 Oct 22 [cited 2018 May 27];194:442–445.
17. RodriguezM, O'BrienJS, GarrettRS, PowellHC. Canine GM1 gangliosidosis. An ultrastructural and biochemical study. *J Neuropathol Exp Neurol*. 1982 Nov [cited 2018 May 27];41:618–629.
18. Ryder SJ, Simmons MM. A lysosomal storage disease of Romney sheep that resembles human type 3 GM1 gangliosidosis. *Acta Neuropathol*. 2001; 101:225-228. Mol Genet Metab. 2014; 111:513-521.
19. Satoh H, Yamato O, Asano T, Yamasaki M, Maede Y. Increased concentration of G M1 -ganglioside in cerebrospinal fluid in dogs with GM1- and GM2-gangliosidoses and its clinical application for diagnosis. *J Vet Diagn Invest.* 2004;16:223–226.
20. Uddin MM, Hossain MA, Rahman MM, et a. Identification of Bagladeshi Cats with GM1 Gangliosidosis caused by the c.1448>C Mutation of the Feline GLB1 Gene: Case Study. *J Vet Med Sci.* 2013; 75(3):395-397.
21. Vasques JF, de Jesus Goncalves RG, da Silva-Junior AJ, Martins RS, Gubert F, Mendez-Otero R. Gangliosides in nervous system development, regeneration, and pathologies. *Neural Regeneration Research*. 2023: 18(1): 81-86.
22. WangZH, ZengB, ShibuyaH, et al. Isolation and characterization of the normal canine beta-galactosidase gene and its mutation in a dog model

of GM1-gangliosidosis. *J Inherit Metab Dis.* 2000;23:593–606.
23. Yamato O, Endoh D, Kobayashi A, et al. A novel mutation in the gene for canine acid beta-galactosidase that causes GM1-gangliosidosis in Shiba dogs. *J Inherit Metab Dis.* 2002 Oct [cited 2018 May 27];25:525–526.
24. YamatoO, MasuokaY, YonemuraM, et al. Clinical and clinico-pathologic characteristics of Shiba dogs with a deficiency of lysosomal acid beta-galactosidase: a canine model of human GM1 gangliosidosis. *J Vet Med Sci.* 2003;65:213–217.
25. Yamato O, Ochiai K, Masuoka Y, et al. GM1 gangliosidosis in shiba dogs. *Vet Rec.* 2000;146:493–496.

CASE III:

Signalment:
8-month old, male, Birman cat (*Felis catus*)

History:
Animal referred to the Neurology Unit of the Small Animal Hospital (School of Veterinary Medicine, University of Glasgow) with a 3 month history of hind limb weakness and hyporexia.

On clinical examination, the animal showed weakness in all limbs and urinary incontinence.

Clinical chemistry Hyperglobulinaemia, hyperproteinaemia.

Neurological examination revealed mild right sided head tilt, tremors of the head, CP severely delayed right side, tetra-ataxia and tetraparesis. Spinal and cranial nerve reflexes were normal.

MRI investigation identified ventriculomegaly, perivascular and white matter extensive oedema.

The owners elected euthanasia and authorised postmortem collection of the brain for histological evaluation.

Gross Pathology:
Upon dissection of the fixed brain, there is moderate bilateral dilation of the ventricles, with accumulation of moderate amount of pale translucent gelatinous fluid.

Laboratory Results:
Immunohistochemistry for Feline Coronavirus (FCoV) confirmed the presence of FCoV antigen within the cytoplasm of macrophages in the inflammatory infiltrates.

Microscopic Description:
Section of brain at the level of the thalamus. Bilaterally affecting the lateral ventricles there are diffuse inflammatory changes effac-

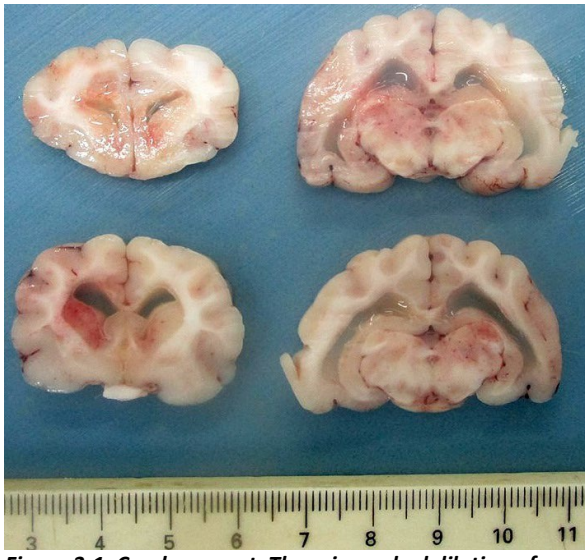

Figure 3-1. Cerebrum, cat. There is marked dilation of ventricles which contain a gelatinous exudate. (Photo courtesy of: Division of Pathology, Public Health and Disease Investigation, Veterinary Diagnostic Services, School of Veterinary Medicine, College of Medical, Veterinary and Life Sciences, University of Glasgow (Garscube Campus), 464 Bearsden Road, Glasgow G61 1QH, Scotland, https://www.gla.ac.uk/schools/vet/cad/)

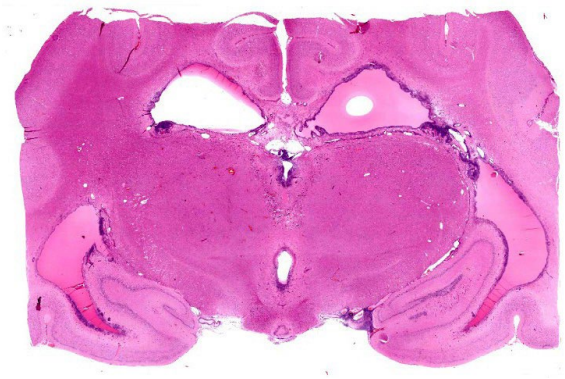

Figure 3-2. Diencephalon, cat. A section of cerebrum at the level of the diencephalon is submitted for examination. There is marked periventricular inflammation and the dilated ventricles contain a protein rich exudate. (HE, 5X)

ing the ependymal lining and variably extending into the subependymal neuropil. Inflammation is dominated by macrophages admixed with scattered neutrophils, and variable numbers of plasma cells, and lymphocytes. Multifocal perivascular (cuffs up to 5 layers) and in some instances mural inflammatory infiltrates dominated by lymphocytes and plasma cells and variable numbers of macrophages affect small to medium sized vessels (venules) in the periventricular neuroparenchyma. Bilaterally the periventricular neuroparenchyma medial to the upper portion of the ventricles is partially effaced by accumulation of eosinophilic proteinaceous fluid with associated sparse infiltration of foamy macrophages admixed with lymphocytes and plasma cells. Multifocally, the periventricular grey and white matter is irregularly vacuolated (spongy change) with few scattered spheroids.

Bilaterally, the lateral ventricles are distended by moderate to large amounts of eosinophilic proteinaceous fluid.

Multifocally, within the hippocampus, in both the pyramidal and molecular layers, there are numerous deposits of coarse globular to laminar basophilic material (mineralisation) variably obliterating the wall and lumen of small capillary vessels and in some instances apparently associated with neurones.

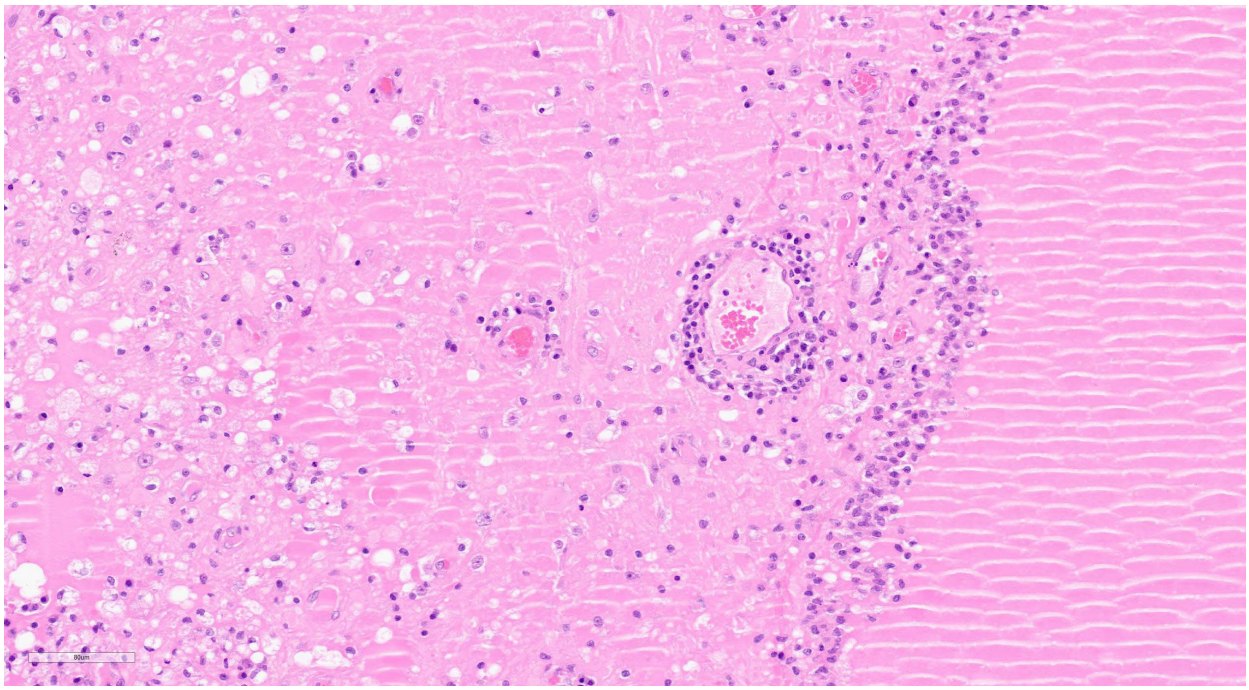

Figure 3-3. Diencephalon, cat. The ventricle contains a protein rich exudate. Numerous lymphocytes, macrophages, and neutrophils infiltrate the ventricle, ependyma, and periventricular white matter. Similar inflammatory cells are present within the walls and perivascularly within the periventricular veins. The periventricular white matter is spongiotic. (HE, 284X)

Table 3-1: coronaviruses affecting different species and their associated disease/lesions

Animal species	Virus	Associated disease/lesions	References
Feline	Feline infectious peritonitis virus (FIPV)	Multisystemic granulomatous/pyogranulomatous disease with vasculitis, serositis, meningoencephalitis, uveitis/ophthalmitis	12,14,22,23
	Feline enteric coronavirus (FECV)	Enteritis with diarrhoea in kittens	19
Canine	Canine Coronavirus (CCV)	Nonfatal enteritis in puppies	2,4
Ferret	Ferret enteric coronavirus (FRECV)	Epizootic catarrhal enteritis	24
	Ferret systemic coronavirus (FRSCV)	Systemic pyogranulomatous inflammation similar to FIP in cats	5,7
Bovine	Bovine coronavirus (BCV)	Severe diarrhoea and respiratory disease in calves and diarrhoea (winter dysentery) in adults	1,15
Mouse	Mouse hepatitis virus (MHV)	Enteritis, hepatitis and demyelinating encephalomyelitis	3
Porcine	Porcine endemic diarrhoea virus (PEDV)	Atrophic enteritis in neonatal piglets	10
	Porcine hemagglutinating encephalomyelitis virus (PHEV)	Lymphoplasmacytic perivascular cuffing in the brain, and stomach muscularis and submucosa	13
	Transmissible gastroenteritis virus (TGEV)	Enteritis with diarrhoea	11
Rat	Rat coronavirus (RCV)	Rhinitis, tracheitis, pneumonitis in young rats	17,21
	Rat sialodacryoadenitis virus (SDAV)	Sialoadenitis, dacryoadenitis, rhinitis, tracheitis, bronchitis/bronchiolitis and alveolitis	21,25
Chickens	Avian infectious bronchitis virus (IBV)	Tracheobronchitis, nephritis	9
Turkeys	Turkey coronavirus (TCV)/Bluecomb virus	Enteritis, cyanosis, severe growth depression	8
Humans	Middle East respiratory syndrome coronavirus (MERS-CoV)	Mild respiratory illness to severe pneumonia and multi-organ failure	16
	Severe acute respiratory syndrome coronavirus (SARS-CoV)	Severe acute respiratory syndrome	20
	Severe acute respiratory syndrome coronavirus 2 (SARS-CoV-2)	Severe acute respiratory syndrome / COVID-19	26,27

In the leptomeninges on the ventral aspect of the thalamus there is variable mild to moderate infiltration of lymphocytes, macrophages, neutrophils plasma cells with sparse and perivascular distribution and moderate necrosis. Immunohistochemistry for Feline Coronavirus (FCoV) confirmed the presence of FCoV antigen within the cytoplasm of macrophages in the inflammatory infiltrates.

Note:
Due to availability of material in the original samples, the slides have been prepared from two different tissue blocks. Inflammatory changes in the leptomeninges ventral to the thalamus are mild in one section and more prominent in the other section. In the latter section, mineralisation is also variably present in the periventricular neuroparenchyma in the thalamus.

Contributor's Morphologic Diagnoses:
Brain: periventricular encephalitis, granulomatous/pyogranulomatous and lymphoplasmacytic, chronic extensive marked.
Meningitis, pyogranulomatous necrotising and lymphoplasmacytic, chronic multifocal moderate.
Hippocampus, capillary vessels and neurones, mineralisation, multifocal moderate.

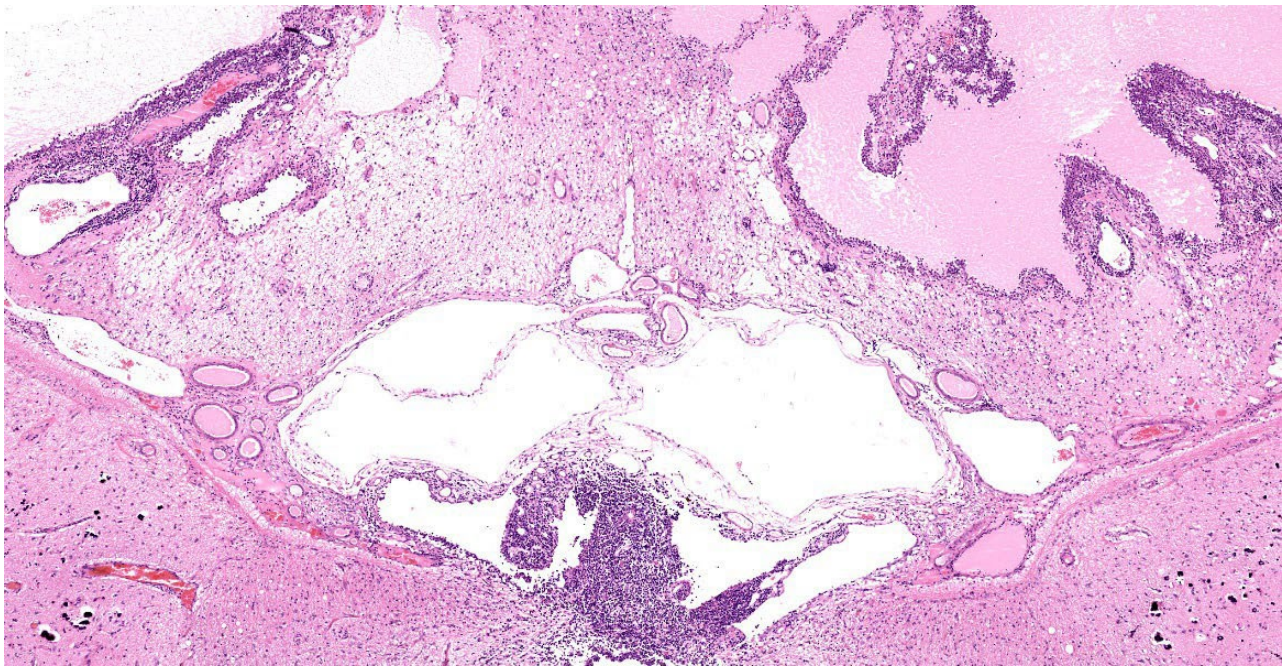

Figure 3-4. Diencephalon, cat. There is marked edema of the periventricular white matter and tela choroidea. The choroid plexus of the third ventricle is expanded by lymphocytes, neutrophils and macrophages and similar inflammation bordering the ventricular ependyma and veins. (HE, 43X)

Contributor's Comment:

Feline coronaviruses (FCoVs) are pleomorphic, enveloped, single-stranded positive sense RNA viruses that belong to the family *Coronaviridae*, order Nidovirales, and genus Alphacoronavirus, species Alphacoronavirus 1.[13] FCoVs occur as 2 biological pathotypes: feline enteric coronavirus (FECV), defined as the ''ubiquitous enteric biotype,'' and feline infectious peritonitis virus (FIPV), the ''virulent biotype" that causes FIP in individual cats.[13, 25] FCoVs can also be divided into two antigenically distinct serotypes (I and II) based on cell culture cytopathic effect and other features, and type I FCoV are more frequently associated with FIP than type II FCoV.[25] Given their close genetic relationship, the viral strains are serologically indistinguishable and difficult to differentiate by routine laboratory testing, making an accurate clinical diagnosis of FIP often difficult.[24] FCoVs are ubiquitous in cats, but the disease FIP is sporadic, and purebred, young, intact male cats appear to be more susceptible.[25] It is transmitted via the faecal-oral route and primarily infect enterocytes.[13] Whereas FECVs replicate mainly in intestinal epithelium and are shed in faeces, FIPVs replicate efficiently in monocytes and induce systemic disease. The host's genetics and immune system also play important roles.[13, 25]

FIP is characterized by fibrinous serositis, with protein-rich effusions in the body cavities of affected cats (effusive or "wet" FIP), as well as granulomatous-necrotising lesions, periphlebitis, and granulomatous and pyogranulomatous inflammatory lesions in several organs, especially, liver, kidney, spleen, leptomeninges, and eyes (non-effusive or "dry" FIP)[16] However, mixed forms are probably common.[25]

Lesions in the CNS are typically oriented toward the surface and target the leptomeninges, ependyma, choroid plexus, and neuroparenchyma.[24] The presence of eosinophilic proteinaceous material within the lateral ventricles observed in this case is interpreted as hydrocephalus, which is a common secondary gross finding described in cases of FIP.[20,

[24, 25] Inflammation within or around the ventricular system may lead to obstruction of cerebrospinal fluid and cause secondary hydrocephalus.[24]

It can be speculated that the presence of multifocal mineral deposits within the hippocampus is a consequence of hypercalcaemia in this cat, which has been reported in association with a few infectious diseases featuring granulomatous inflammation (including FIP). Macrophages can synthesize calcitriol from calcidiol without any negative feedback regulation, thus leading to hypercalcaemia and subsequently metastatic mineralisation.[6]

Contributing Institution:
Division of Pathology, Public Health and Disease Investigation
Veterinary Diagnostic Services
School of Veterinary Medicine
College of Medical, Veterinary and Life Sciences
University of Glasgow (Garscube Campus)
464 Bearsden Road
Glasgow G61 1QH, Scotland
https://www.gla.ac.uk/schools/vet/cad/

JPC Diagnosis:
Diencephalon: Ventriculitis, pyogranulomatous and lymphoplasmacytic, diffuse, severe, with hydrocephalus, phlebitis, choroid plexitis, periventricular necrosis and edema, meningitis, and mineralization.

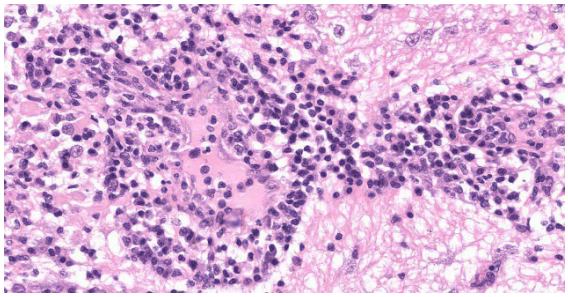

Figure 3-5. Diencephalon, cat. There are lymphocytes, macrophages, and fewer plasma cells within walls off veins which infiltrate the surrounding perivascular parenchyma. (HE, 505X)

JPC Comment:
Neurologic manifestations of feline infectious peritonitis have three general distribution patterns as described by Rissi: diffuse leptomeningitis; rhombencephalitis (or inflammation of the brainstem/cerebellum); and periventricular encephalitis, which is demonstrated in this case and was the most prevalent form in Rissi's study of 26 cats affected by FIP in the central nervous system.

Feline coronavirus (FCoV) is extremely common in domestic cats, and it's estimated that 25% of cats in single cat households and over 75% of cats within multi-cat households are infected.[9] Of those infected, anywhere from 1 to 12% may develop FIP.[9,14] As an RNA-virus, FCoV is prone to replication errors, and a mutation within the spike protein likely accounts for the ability of FIP to infect monocytes and macrophages and cause systemic infection.[14] The spike protein has two subunits, S1 (receptor binding) and S2 (fusion), and a proteolytic cleavage site which, when cleaved, results in activation of the spike protein.[14] In a study of 11 cats with FIP, unique mutations were consistently found in the S1/S2 cleavage site, which the authors speculate may make the protein more susceptible to cleavage by other enzymes.[14]

The internal mutation theory is the most widely accepted model of FIP pathogenesis and asserts that, in each patient, FCoV spontaneously mutates into the pathogenic non-contagious FIP.[9] A variation of the internal mutation theory called the circulating virulent and avirulent theory asserts that certain strains are more likely to induce FIP, which may explain periodic clusters of FIP cases.[9,14] Such a case series was documented in four cats from a single household who succumbed to FIP after being displaced due to a house fire and surrendered to a shelter. [9] The three cats which had viral genetic sequencing each

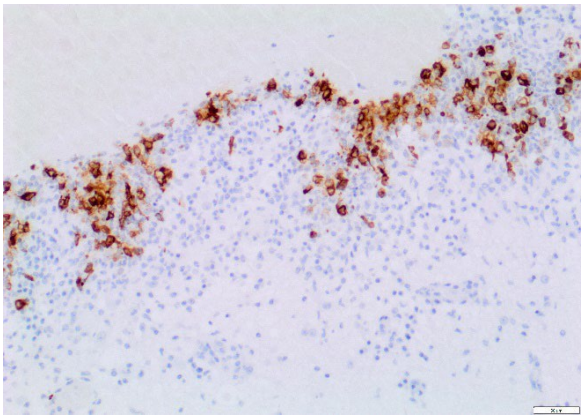

Figure 3-6. Diencephalon, cat. Large numbers of macrophages in the ependymal and periventricular inflammatory infiltrates demonstrate strong cytoplasmic staining for feline coronaviurs (FCoV) antigen. (anti-feline coronavirus, 400X)

had different mutation profiles within the *S1/S2* gene. [9] The authors concluded that these cats likely had a unique FCoV strain prone to FIP-mutation, and the mutations in each cat may have been precipitated by significant physiologic stress. [9]

Finally, rare cases of horizontal transmission have also been reported. At one Taiwanese shelter, 13 cats (28% of the population) succumbed to FIP over a one year time period.[26] All cats were infected with type II FCoV, and the viruses all had identical *S* gene mutations.[26] Those infected later in the year had additional unique mutations in the *3c* gene indicating ongoing mutation.[26] Additionally, the type II FCoV associated with FIP was isolated from both the feces and oronasal and conjunctival samples from infected cats, indicating horizontal transmission was likely responsible for the spread of the virus within the shelter.[26]

References:

1. Bok M, Alassia M, Frank F, Vega CG, Wigdorovitz A, Parreño V. Passive immunity to control Bovine coronavirus diarrhea in a dairy herd in Argentina. *Rev Arg Microb*. 2018;50:23–30.
2. Buonavoglia C, Decaro N, Martella V, et al. Canine Coronavirus Highly Pathogenic for Dogs. *Emerg Infect Dis.* 2006;12:492–494.
3. Compton SR, Ball-Goodrich LJ, Johnson LK, Johnson EA, Paturzo FX, Macy JD. Pathogenesis of Enterotropic Mouse Hepatitis Virus in Immunocompetent and Immunodeficient Mice. *Comp Med*. 2004;54:681-689.
4. Decaro N, Buonavoglia C. An update on canine coronaviruses: Viral evolution and pathobiology. *Vet Microb*. 2008;132:221–234.
5. Doria-Torra G, Vidaña B, Ramis A, Amarilla SP, Martínez J. Coronavirus Infection in Ferrets: Antigen Distribution and Inflammatory Response. *Vet Pathol.* 2016;53:1180–1186.
6. Finch NC. Hypercalcaemia in cats: The complexities of calcium regulation and associated clinical challenges. *J Feline Med Surg.* 2016;18:387–399.
7. Garner MM, Ramsell K, Morera N, et al. Clinicopathologic Features of a Systemic Coronavirus-Associated Disease Resembling Feline Infectious Peritonitis in the Domestic Ferret (Mustela putorius). *Vet Pathol*. 2008;45:236–246.
8. Guy JS. Turkey coronavirus is more closely related to avian infectious bronchitis virus than to mammalian coronaviruses: A review. *Avian Pathol.* 2000;29:207–212.
9. Healey EA, Andre NM, Miller AD, Whitaker GR, Berliner EA. Outbreak of feline infectious peritonitis (FIP) in shelter-housed cats: molecular analysis of the feline coronavirus S1/S2 cleavage site consistent with a 'circulating virulent-avirulent theory' of FIP pathogenesis. *JFMS Open Rep.* 2022. 8(1):1-8.

10. Ignjatovic J, Sapats S. Avian infectious bronchitis virus. *Rev Sci Tech*. 2000;19:493-508.
11. Jung K, Saif LJ. Porcine epidemic diarrhea virus infection: Etiology, epidemiology, pathogenesis and immunoprophylaxis. *Vet J.* 2015;204:134–143.
12. Kim SH, Kim IJ, Pyo HM, Tark D-S, Song JY, Hyun BH. Multiplex real-time RT-PCR for the simultaneous detection and quantification of transmissible gastroenteritis virus and porcine epidemic diarrhea virus. *J Virol Methods.* 2007;146:172–177.
13. Kipar A, Meli ML. Feline Infectious Peritonitis: Still an Enigma? *Vet Pathol.* 2014;51:505–526.
14. Licitra BN, Millet JK, Regan AD, et al. Mutation in Spike Protein Cleavage Site and Pathogenesis of Feline Coronavirus. *Em Infect Dis*. 2013;19(7):1066-1073.
15. Mora-Díaz JC, Piñeyro PE, Houston E, Zimmerman J, Giménez-Lirola LG. Porcine Hemagglutinating Encephalomyelitis Virus: A Review. *Front Vet Sci.* 2019;6:53.
16. Myrrha LW, Silva FMF, Peternelli EF de O, Junior AS, Resende M, Almeida MR de. The Paradox of Feline Coronavirus Pathogenesis: A Review. *Adv Virol*. 2011;2011:1–8.
17. Oma VS, Tråvén M, Alenius S, Myrmel M, Stokstad M. Bovine coronavirus in naturally and experimentally exposed calves; viral shedding and the potential for transmission. *Virol J*. 2016;13:100.
18. Omrani AS, Al-Tawfiq JA, Memish ZA. Middle East respiratory syndrome coronavirus (MERS-CoV): animal to human interaction. *Pathog Glob Health.* 2015;109:354–362.
19. Parker JC, Cross SS, Rowe WP. Rat coronavirus (RCV): A prevalent, naturally occurring pneumotropic virus of rats. *Archiv Gesamte Virusforschung*. 1970;31:293–302.
20. Pedersen NC, Allen CE, Lyons LA. Pathogenesis of feline enteric coronavirus infection. *J Feline Med Surg*. 2008;10:529–541.
21. Pedersen NC. A review of feline infectious peritonitis virus infection: 1963–2008. *J Feline Med Surg*. 2009;11:225–258.
22. Peiris JSM, Guan Y, Yuen KY. Severe acute respiratory syndrome. *Nat Med.* 2004;10:S88–S97.
23. Percy DH, Barthold DW. Chapter 2: Rat. In: *Pathology of Laboratory Rodents and Rabbits.* Wiley Blackwell; 2016:125-127.
24. Rissi DR. A retrospective study of the neuropathology and diagnosis of naturally occurring feline infectious peritonitis. *J Vet Diagn Invest*. 2018;30:392–399.
25. Uzal FA, Blattner BL, Hostetter JM. Alimentary System. In: Maxie MG, ed. *Jubb, Kennedy & Palmer´s Pathology of Domestic Animals.* Vol. 2. 6th ed. Philadelphia, PA: Elsevier Saunders; 2016:253-255.
26. Wang YT, Su BL, Hseih LE, Chueh LL. An outbreak of feline infectious peritonitis in a Taiwanese shelter: epidemiologic and molecular evidence for horizontal transmission of a novel type II feline coronavirus. *Vet Res*. 2013; 44(57):1-9.
27. Wise AG, Kiupel M, Maes RK. Molecular characterization of a novel coronavirus associated with epizootic catarrhal enteritis (ECE) in ferrets. *Virology*. 2006;349:164–174.
28. Yoo D, Pei Y, Christie N, Cooper M. Primary Structure of the Sialodacryoadenitis Virus Genome: Sequence of

the Structural-Protein Region and Its Application for Differential Diagnosis. *Clin Diagn Lab Immunol.* 2000;7:568–573.

29. Zhang Y-Z, Holmes EC. A Genomic Perspective on the Origin and Emergence of SARS-CoV-2. *Cell.* 2020;181:223–227.

30. Zhou P, Yang X-L, Wang X-G, et al. A pneumonia outbreak associated with a new coronavirus of probable bat origin. *Nature.* 2020;579:270–273.

CASE IV:

Signalment:
4 year old, female, African pygmy hedgehog (*Atelerix albiventris)*

History:
A progressive mass was noted on the right side of the mouth, resulting in halitosis, tooth mobility, exophthalmus, scale loss, anorexia and weight loss. This was refractory to antibiotics (enrofloxacin) and anti-inflammatories (Meloxicam).

Gross Pathology:
Around the maxillary dental arcade was a poorly demarcated, firm, multilobulated, off-white to tan mass; within the oral cavity, this

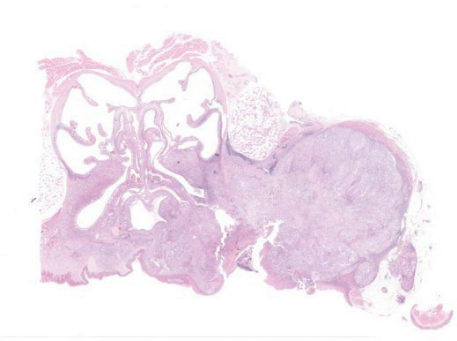

Figure 4-1. Cross section of head, hedgehog. An infiltrative neoplasm arises from the oral cavity and effaces the bones and soft tissues of the face and infiltrates the sinuses dorsally. (HE, 5X)

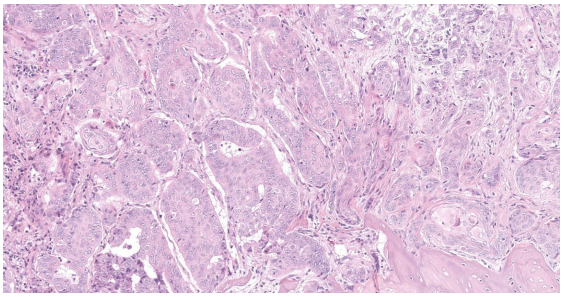

Figure 4-2. Head, hedgehog. Neoplastic squamous epithelium is arranged in nests, cords and trabeculae, and keratinizes poorly within the center of nests. (HE, 170)

was approximately up to 25 mm x 14 mm x 12 mm. The surface was ulcerated and only one molar tooth remained, which was very loose. There was a focal area of ulceration of the hard palate (up to 5 mm x 4 mm). The left maxillary dental arcade was missing several cheek teeth and the remaining teeth were loose. On transverse sectioning of the skull, the mass extended dorsally, replacing much of the right side musculature and the maxillary bone, and extending medially, invading the right nasal cavity (the maximum size of the mass was ~25 mm x 14 mm x 20 mm).

Laboratory Results:
No reported laboratory results.

Microscopic Description:
The tissue is markedly effaced and replaced by a poorly demarcated proliferation of atypical squamous epithelial cells arranged in variably sized cords, trabeculae and nests. Individual cells are oval to polygonal, with variably distinct cell borders and a moderate amount of eosinophilic cytoplasm. They have oval to polygonal, hypochromatic, vesicular nuclei, with one or multiple prominent nucleoli. There is moderate anisocytosis and marked anisokaryosis, and frequent binucleate and multinucleate cells. Atypical cells often palisade around the margin of lobules, and central cells often undergo abrupt keratinisation (hypereosinophilic cells with poorly discernible nuclei) or are markedly swollen. There are occasional individualised necrotic

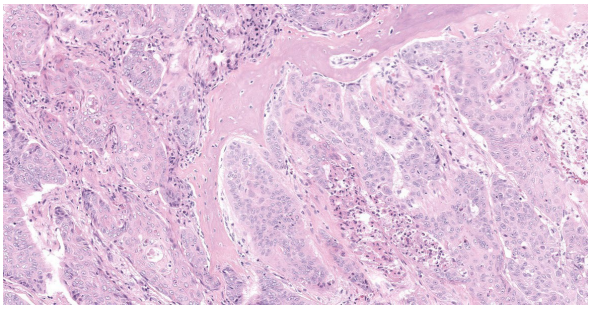

Figure 4-3. Head, hedgehog. Neoplastic cells effaced facial bones. (HE, 170X)

cells (hypereosinophilic cells with karyorrhectic or pyknotic nuclei), clusters of necrotic cells with infiltrates of neutrophils, or apoptotic cells (shrunken cells with pyknotic nuclei). The mucosal surface is thinned (eroded), lost (ulcerated) or is degenerate, with marked vacuolated keratinocytes (ballooning degeneration). The subepithelial tissue contains moderate number of lymphocytes, plasma cells and fewer granulocytes.

Contributor's Morphologic Diagnoses:
Oral squamous cell carcinoma.

Contributor's Comment:
Oral squamous cell carcinomas (SCCs) are commonly diagnosed in the African pygmy hedgehog, and are the third most common neoplasm in this species, presenting with clinical signs including tooth mobility, edentulism and gingivitis.[11] Oral SCCs in African pygmy hedgehogs have been previously described as commonly locally infiltrative with rare metastases, though metastases to distant sites have been reported.[5] In addition to oral SCCs, cutaneous SCCs have also been described in African pygmy hedgehogs.[2] There are few studies characterizing oral SCCs in African pygmy hedgehogs.

Oral squamous cell carcinomas have been characterized in greater detail in other domestic animals, and is the most common oral tumor in cats and the second most prevalent in dogs.[14] These present frequently on the tongue and gingiva, with local invasion, bone invasion and a variable survival, with the greatest mean survival time (MST) following removal of invaded bone.[7] Canine SCCs have been classified further into Conventional (82.1% of cases), Papillary and Basaloid (5.95%), Adenosquamous (3.6%) and spindle cell SCCs (2.4%).[8] However, there is little data to determine variance in prognosis for these different histological subtypes.[7] In any case, spread of oral SCCs to local lymph nodes often occurs late in the disease process[4] and local reoccurrence is the most common form of treatment failure.[12]

Currently, the pathogenesis of oral SCCs is thought to be following long term epithelial hyperplasia from chronic gingivitis irritation.[14] In dogs though there may be a tentative link with canine oral papillomavirus (CPV-1) producing papillomas which undergo malignant transformation.[13] In humans, multiple factors have been implicated in the development of oral SCCs including environmental factors such as tobacco consumption, alcohol consumption and chronic inflammation which leads to dysplasia of the local area and multiple alterations to tumor suppressor genes (p16, $p14^{ARF}$, FHIT, RSSFIA and p53) leading to "field cancerization" and development of SCCs.[1] "Field cancerization" refers to a theory based on the frequent observation of epithelial dysplasia at the periphery of human invasive oral cancers in situations of chronic exposure to carcinogenic insult, which may leads to increased risk of malignant transformation in the entire area affected by the insult.

Contributing Institution:
Easter Bush Pathology – Royal (Dick) School of Veterinary Studies. https://www.ed.ac.uk/vet/services/easter-bush-pathology

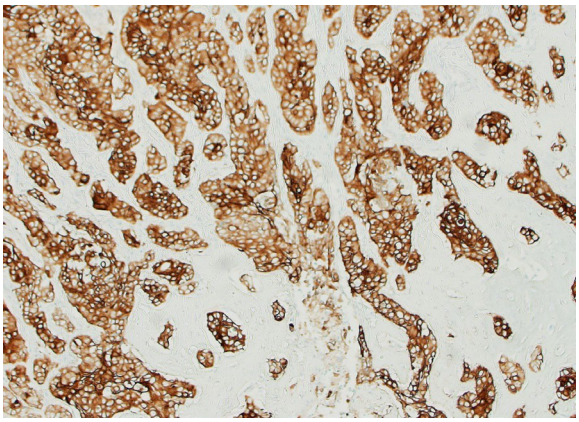

Figure 4-4. Head, hedgehog. Neoplastic cells demonstrate strong immunopositivity for cytokeratin. (anti-AE1/AE3, 400X)

JPC Diagnosis:
Cross section of head: Squamous cell carcinoma.

JPC Comment:
With the growing popularity of hedgehogs as pets, numerous retrospective studies have described the prevalence of neoplasia within captive populations, each with slightly different results. In a study of pet hedgehogs in the US, the most common neoplasms were mammary neoplasia, lymphoma, and oral squamous cell carcinoma.[11] In a study in Japan, the most common neoplasms were endometrial stromal tumor, fibrosarcoma, and mammary neoplasms.[9] In a study of 63 hedgehogs from the Tai Pei Zoo, the three most common neoplasms were oral squamous cell carcinoma, lymphoma, and pulmonary adenocarcinoma.[10] The authors speculated that geographic variability may be due to in-breeding of closed populations due to movement restrictions imposed due to the species' susceptibility to foot and mouth disease.[10]

A study of captive hedgehogs in Chile focused specifically on oral masses found that 17 of 27 oral masses were squamous cell carcinoma. These neoplasms were generally ulcerated (13 cases) and occurred most commonly (12 cases) in the caudal aspect of the right maxilla.[3] Gingival hyperplasia was the second most common diagnosis (8 cases). Gingival hyperplasia was found in varied location, manifested as pedunculated or sessile masses, and was non-ulcerated.[3]

Hedgehogs are one of a few non-cloven hooved species which can be naturally infected by foot and mouth disease virus. During a series of in England in the 1940s, several infected wild hedgehogs were found with vesicles on the feet, and researchers subsequently demonstrated that cattle could experimentally infect hedgehogs.[6] The authors concluded that hedgehogs had some role in spreading infection between cattle.[6]

References:

1. Choi, S. & Myers, J. N. Molecular pathogenesis of oral squamous cell carcinoma: Implications for therapy. *J. Dent. Res.* 87, 14–32 (2008).
2. Couture, É. L., Langlois, I., Santamaria-Bouvier, A. & Benoit-Biancamano, M. O. Cutaneous squamous cell carcinoma in an African pygmy hedgehog (Atelerix albiventris). *Can. Vet. J.* 56, 1275–1278 (2015).
3. Del Aguila G, Torres C, Carvallo FR, Gonzolaz CM, Cifuentes FF. Oral masses in African pygmy hedgehogs. *Jour Vet Diag Invest*. 2019; 31(6): 864-867.
4. Grimes, J. A. et al. Histologic evaluation of mandibular and medial retropharyngeal lymph nodes during staging of oral malignant melanoma and squamous cell carcinoma in dogs. *J. Am. Vet. Med. Assoc.* 254, 938–943 (2019).
5. Heatley, J., Mualdin, G. & Cho, D. A Review of Neoplasia in the Captive African Hedgehog (). *Semin. Avian Exot. Pet Med.* 14, 182–192 (2005).

6. McLaughlan JD, Henderson WM. The occurrence of foot-and-mouth disease in the hedgehog under natural conditions. *J Hyg (Lond).* 1947; 45(4): 474-479.
7. Meuten D.J. *Tumors in domestic animals.* 5th ed. Ames, IO: John Wiley & Sons, Inc. 2002.
8. Nemec, A., Murphy, B., Kass, P. H. & Verstraete, F. J. M. Histological Subtypes of Oral Non-tonsillar Squamous Cell Carcinoma in Dogs. *J. Comp. Pathol.* 147, 111–120 (2012).
9. Okada K, Kondo H, Sumi A, Kagawa Y. A retrospective study of disease incidence in African pygmy hedgehogs (*Atelerix albiventris*).
10. Pei-Chi H, Jane-Fang Y, Lih-CHiann W. A Retrospective Study of the Medical status on 63 African Hedgehogs (*Atelerix albiventris*) at the Taipei Zoo from 2003 to 2011. *J Exot Pet Med*. 2015; 24:105-111.
11. Raymond, J. T. & Garner, M. M. Spontaneous tumours in captive African hedgehogs (Atelerix albiventris): A retrospective study. *J. Comp. Pathol.* 124, 128–133 (2001).
12. Riggs, J. et al. Outcomes following surgical excision or surgical excision combined with adjunctive, hypofractionated radiotherapy in dogs with oral squamous cell carcinoma or fibrosarcoma. *J. Am. Vet. Med. Assoc.* 253, 73–83 (2018).
13. Thaiwong, T. et al. Malignant transformation of canine oral papillomavirus (CPV1)-associated papillomas in dogs: An emerging concern? *Papillomavirus Res.* 6, 83–89 (2018).
14. Uzal F, Plattmer B. Alimentary System. In: Maxie MG, ed. *Jubb, Kennedy and Palmer's Pathology of Domestic Animals*. Vol 2. 6th ed. Philadelphia, PA: Elsevier Saunders. 2016: 25–26.

WSC 2022-2023 Self-assessment.
Conference 6

1. Which of the following is the cause of histiocytic ulcerative colitis in the dog?
    a. *Mycobacterium avium*
    b. *Salmonella enteritidis*
    c. Proteus vulgaris
    d. E. coli

2. Which of the following tests is most specific for identifying GM-1 gandgliosidosis in the dog?
    a. Electron microscopy
    b. PAS
    c. Luxol fast blue
    d. Cholera toxin subunit B

3. Which of the following is characterized by tubular inclusions within cytoplasmic vacuoles?
    a. GM1-gangliosidosis
    b. GM2-gangliosidosis
    c. Sphingomyelinosis
    d. Globoid cell leukodystrophy

4. True or false? Feline infectious coronaviruses replicate efficiently in monocytes.
    a. True
    b. False

5. True or false? Chronic periodontal disease is considered to be the most likely cause for development of oral squamous cell carcinomas in animals.
    a. True
    b. False

Please email your completed assessment for grading to Dr. Bruce Williams at bruce.h.williams12.civ@mail.mil. Passing score is 80%. This program (RACE program 33611) is approved by the AAVSB RACE to offer a total of 0.5 CE Credits, with a maximum of 12.5 CE Credits being available to any individual Veterinary Medical Professionals for the 2019-2020 Wednesday Slide Conference. This RACE approval is for the subject matter categories of: SCIENTIFIC using the delivery method of NONINTERACTIVE DISTANCE. This approval is valid in jurisdictions which recognize AAVSB RACE.

Joint Pathology Center
Veterinary Pathology Services

WEDNESDAY SLIDE CONFERENCE 2022-2023

Conference #7 5 October 2022

CASE I:

Signalment:
A 17-day-old, male, Japanese Black, bovine

History:
A Japanese black male calf was born at full-term. The calf weighted 30 kg and received colostrum. The calf presented with fever (40 ℃), cough, nasal discharge, poor suckling, wobbler, and bilateral ocular cloudiness on day 4 of life, after which he developed astasia. On day 5 of life, the calf became recumbent and presented with dizziness and nystagmus. The calf was treated with medications such as antibiotics, non-steroid anti-inflammatory drugs, and vitamin B1, but he died on day 17 of life.

Gross Pathology:
Multiple white nodules with dark red edges and a diameter of 1 - 3 cm were found scattered in the peritoneum, including the spleen, stomach, and diaphragm. Many white nodules were also observed in the liver serosa and parenchyma. The surface of the forestomach mucosa was covered with a gray-yellowish caseous substance. Multiple erosions and ulcers were observed in the forestomach and the abomasum. The abomasum mucosa was extensively dark red. The calf had an increased volume of the cerebrospinal fluid, which was muddy; thymic hypoplasia; and persistent urachus.

Laboratory Results:
Bacteriological examination: Yeast-like fungi were isolated from the samples collected from the liver, kidney, lung, brain, and cerebrospinal fluid, which were identified as *Candida albicans* (99.12%) on sequence analysis of the ITS region.

Virological examination: Bovine adenovirus (BAdV) type 4 was detected on the PCR for BAdV and sequence analysis of DNA extracted from paraffin-embedded sections of the liver, reticulum, and ileocecal colon.

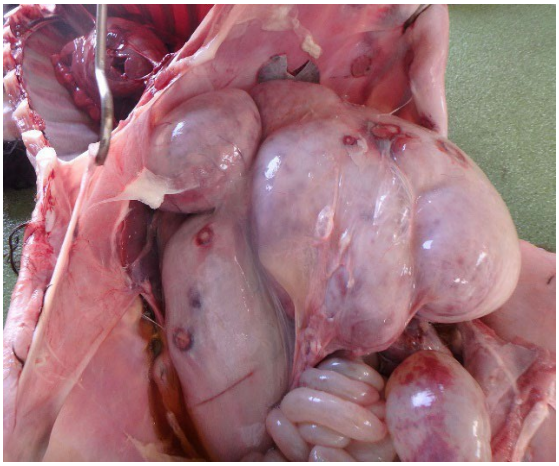

Figure 1-1. Abdominal viscera, ox. Numerous 1-3mm white nodules with a hemorrhagic border are scattered along the serosa of the gastrointestinal tract. (Photo courtesy of: National Institute of Animal Health, National Institute of Animal Health, National Agriculture and Food Research Organization (NARO), 3-1-5Kannondai, Tsukuba, Ibaraki 3050856, Japan, (WSC ID95), http://www.naro.affrc.go.jp/english/niah/index.html)

Microscopic Description:
Multiple extensive necroses were observed from the mucosal epithelium to the submucosal tissue of the abomasum. In the necrotic area, typical structures were replaced by hemorrhage, acidophilic cell debris, and mostly necrotic infiltrated neutrophils. Numerous thrombi were observed in small-to-medium blood vessels from the lamina propria to the submucosa. Numerous fungal hyphae were found in the necrotic lesions. Presence of fungi was also found in thrombi and on the walls of blood vessels. The submucosa was highly edematous, with numerous neutrophil infiltrations, mild macrophage infiltrations, and presence of fibrin. Grocott's staining and PAS reaction revealed the presence of multiple species of fungi in the lesion. On the mucosal surface, a large number of yeasts and pseudohyphae were found mixed with inflammatory cells and cell debris. A large number of hyphae were found from the necrotic area to the submucosa. They were 5-8 μm wide, non-parallel, thin walled, and irregularly branched and had no septum. Such hyphae had also infiltrated the thrombus and walls of blood vessels. In some areas, these hyphae were mixed with pseudohyphae, which invaded the blood vessels. In the submucosa adjacent to these areas, a large number of hyphae were focally observed in the blood vessels, blood vessel walls, and surrounding tissues. They had slightly thicker walls; were 4-5 μm wide, parallel, and sharply branched; and contained septum. Immunohistochemically, these fungi reacted positively to anti-*Candida* (Biogenesis, UK), anti-*Rhizomucor* (Clone Mab-WSSA-RA-1, DAKO, USA), and anti-*Aspergillus* (Clone Mab-WF-AF-1, DAKO, USA) antibodies, respectively.

Furthermore, amphoteric-to-basophilic Cowdry A-type or full-type intranuclear inclusion bodies were observed in endothelial cells of most blood vessels. Electron microscopy of vascular endothelial cells revealed adenovirus-like particles with a diameter of approximately 80 nm, consistent with intranuclear inclusion bodies.

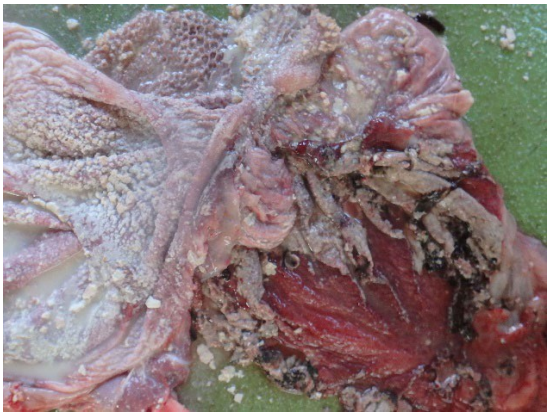

Figure 1-2. Abomasum, ox. The mucosa of the abomasum is partially covered by a fibrinonecrotic membrane. (Photo courtesy of: National Institute of Animal Health, National Institute of Animal Health, National Agriculture and Food Research Organization (NARO), 3-1-5Kannondai, Tsukuba, Ibaraki 3050856, Japan, (WSC ID95), http://www.naro.affrc.go.jp/english/niah/index.html)

In the forestomach, severe hyperkeratosis or parakeratosis, mild-to-moderate erosion of the epithelium, and intoraepithelial accumulation of neutrophils (microabscesses) were observed. A large number of anti-*Candida* antibody-positive yeasts and pseudohyphae were observed in these lesions. In addition, numerous thrombi and extensive necrosis of the surrounding tissues were also observed in the rumen submucosa. In the necrotic tissue and blood vessels, anti-*Aspergillus* antibody-positive hyphae were observed. Anti-*Aspergillus* antibody-positive hyphae were also observed in the serosa. In other regions, a large number of anti-*Rhizomucor* antibody-positive hyphae in the vascular wall and necrotic foci of the lamina propria were observed. There were numerous viral intranuclear inclusion bodies in the vascular endothelium of the forestomach. In the ileum, swelling of vascular endothelial cells, presence of

thrombi with numerous intranuclear inclusions scattered from the lamina propria to the submucosa, and necrosis with hemorrhage were widely observed.

Many focal necroses or granulomas with mild hemorrhage were scattered in the brain and the spinal cord. A large number of anti-*Candida* antibody-positive pseudohyphae were observed in these lesions. Mild mononuclear cell infiltration was observed in the meninges, and one mycotic granulomatosis was observed in the choroid plexus. Intranuclear inclusion bodies were rarely observed in vascular endothelial cells.

Focal extensive necrosis with thrombosis was observed in the liver. Many hyphae that reacted against the anti-*Aspergillus* antibody were observed in thrombi and vascular wall. Furthermore, numerous focal necroses with anti-*Candida* antibody-positive pseudohyphae were randomly scattered. In addition, a number of intranuclear inclusion bodies were found in the endothelium or hepatocytes. A few anti-*Candida* antibody-positive pseudohyphae were observed around small vessels in the kidney, heart, and lung.

In the thymus, there was severe depletion of lymphocytes in both the cortex and medulla.

Contributor's Morphologic Diagnoses:
Abomasum: abomasitis, necrotizing, severe with vasculitis, vascular thrombosis, numerous multiple species of fungi, and viral intranuclear inclusion bodies

Etiology: *Candida albicans*, *Aspergillus* spp., Mucoraceae, and BAdV type 4

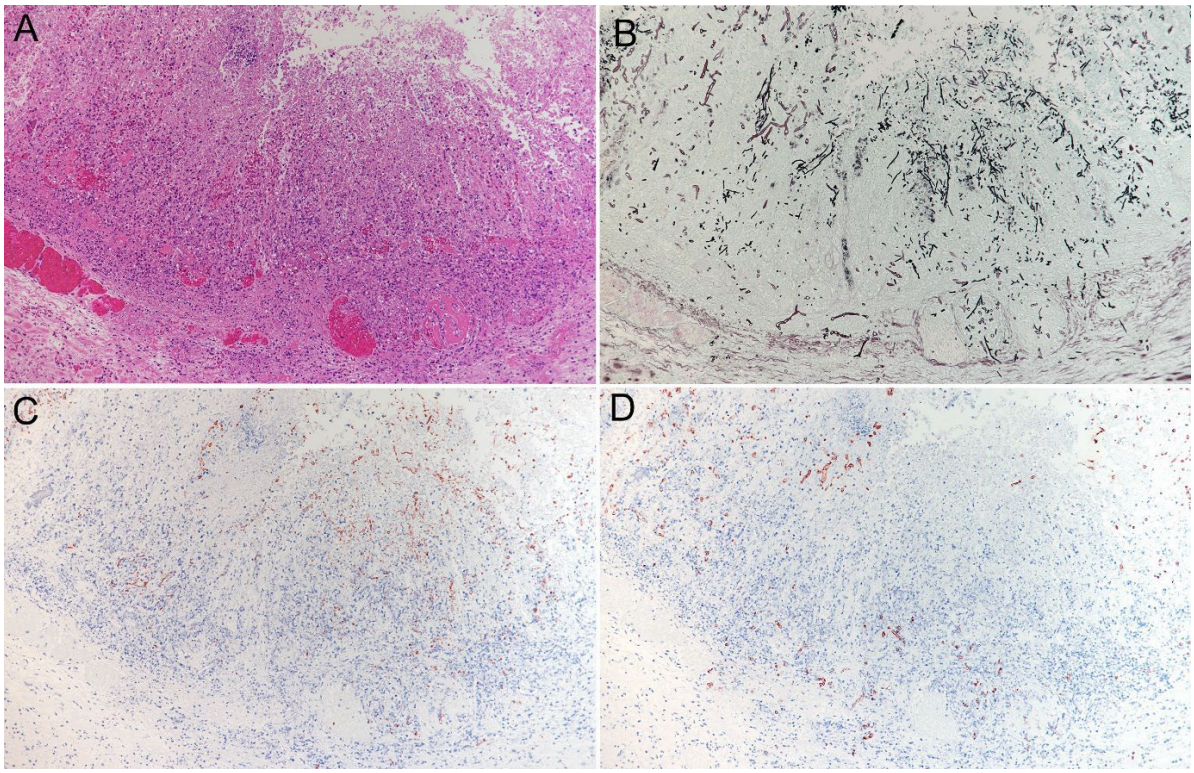

Figure 1-3. Abomasum, ox. A) There are multifocal areas of full-thickness necrosis of the abomasal mucosa. B) A Grocott methenamine silver stain highlights multiple fungal morphologies within the areas of necrosis. C) Some of the fungal hyphae are immunopositive for antibodies directed against Candida sp. D) Some of the fungal hyphae are immunopositive for antibodies directed at Rhizomucor. (Photo courtesy of: National Institute of Animal Health, National Institute of Animal Health, National Agriculture and Food Research Organization (NARO), 3-1-5Kannondai, Tsukuba, Ibaraki 3050856, Japan, (WSC ID95), http://www.naro.affrc.go.jp/english/niah/index.html)

Contributor's Comment:
In this case, fungal lesions caused by *C. albicans* were systemically disseminated in many organs. Co-infection with *Aspergillus* spp. and Mucoraceae was observed in fungal lesions of the gastrointestinal tract and liver. Systemic BAdV type 4 infection was also observed.

Deep-seated mycosis is a fungal infection that forms lesions in the internal organs or subcutaneous tissue. In cattle, mastitis, endometritis, ulcerative gastroenteritis, pneumonia, and abortion have been reported.[16] Deep-seated mycosis occurs in animals with weakened immunity, and the main causative fungi are *Candida* spp., *Aspergillu*s spp., and Mucoraceae,[2,4,7,15,16] either alone[1,5,6,12] or in combination[2,3,14]. In cattle with deep-seated mycosis, co-infection with two types of fungi[3,13,14] and mixed infection with fungi and protozoa have been reported.[13] Many cases of systemically disseminated mycosis in cattle caused by Mucoraceae, resulting in infection of central nervous system tissues, have been reported.[1,4-6,12,13] In contrast, a few cases of central nervous system lesions caused by *Aspergillus* spp.,[3] without the presence of *Candida* spp. have been reported. In the present case, co-infection with three species of fungi was observed. *C. albicans* was identified as the causative fungi for lesions systemically disseminated to multiple organs, especially meningoencephalomyelitis.

A large number of *Aspergillus* spp. hyphae were observed in the liver, rumen, and abomasum, and a large number of Mucoraceae hyphae were observed in the rumen and abomasum. Both fungi were associated with thrombosis, vasculitis, and extensive necrotic lesions. Numerous yeasts and pseudohyphae of *C. albicans* were observed in the hyperkeratotic and parakeratotic mucosal epithelium and superficial lamina propria lesions of the forestomach, and they were not mixed with other fungi. However, in the abomasum, pseudohyphae of *C. albicans* were observed in the necrotic foci mixed with Mucoraceae hyphae along with invasion into the deep mucosa or blood vessels. These findings suggest that *C. albicans* was disseminated systemically through necrosis and vascular lesions caused by Mucoraceae in the abomasum.

On the other hand, viral intranuclear inclusion bodies were observed in vascular endothelial cells throughout the body, such as in the gastrointestinal tract, liver, and brain. Electron microscopy and sequence analysis of DNA extracted from FFPE samples showed that the inclusion bodies were BAdV type 4. BAdV disease is caused by BAdV belonging to the Mastadenovirus genus or the Atadenovirus genus of the Adenoviridae family.[18] It is mainly characterized by respiratory and digestive diseases. BAdVs are commonly isolated from the feces of healthy cattle,[11] which are rarely onset by BAdV alone. There are 10 serotypes of BAdV, and BAdV type 7 is highly pathogenic, [18] causing severe hemorrhagic diarrhea and calf frailty syndrome. Only a few cases of BAdV disease have been reported in Japan.[8,9] BAdV type 4 was identified only in one of these case via bovine testis cell culture.[8] Gastric erosion, ulcers, and hemorrhagic colitis have been reported in previous cases of BAdV infection.[17,18] In the present case, mucosal necrosis without fungal infection was observed in the ileum. It was suggested that BAdV type 4 injured blood vessels and induced gastrointestinal lesions. Furthermore, it was considered that *C. albicans* entered the bloodstream and invaded the parenchyma of the brain and liver through the vascular walls systemically damaged by the virus, causing inflammation or necrosis.

In addition, thymic hypoplasia, which was observed in the present case, may have contributed to these systemic infections.

Many cases of zygomycosis are angioinvasive and disseminated systemically.[1,5,6] However, no systemic dissemination of Mucoraceae was observed in the present case, probably because the calf developed fatal meningoencephalomyelitis due to *C. albicans* before the dissemination of Mucoracease.

Contributing Institution:
National Institute of Animal Health, National Institute of Animal Health, National Agriculture and Food Research Organization (NARO)
3-1-5Kannondai, Tsukuba, Ibaraki 3050856, Japan
(WSC ID95)
http://www.naro.affrc.go.jp/english/niah/index.html

JPC Diagnosis:
1. Abomasum: Abomasitis, necrotizing, multifocal to coalescing, marked, with vasculitis, thrombosis, and numerous mucosal and submucosal fungal pseudohyphae, hyphae, and yeasts.
2. Abomasum, vessels: Vasculitis, necrotizing, multifocal, moderate with endothelial intranuclear viral inclusions.

JPC Comment:
The contributor has provided an excellent example of an endotheliotropic virus causing vascular damage, creating a permissive environment for the growth and invasion of multiple opportunistic fungal organisms, and setting the stage for systemic spread of *Candida albicans*. A remarkably versatile fungus, *C. albicans* has evolved numerous mechanisms of pathogenicity and adaptability that enable it to spread and cause disease in a wide range of host tissues.

C. albicans has three main morphologies: yeast, hypha, and pseudohypha. The yeast form exists at a lower pH and generally higher density than the hyphal form and is associated with fungal dissemination, whereas the hyphal form tends to invade tissue. A number of adhesins, including agglutinin-like sequence (Als) 3 and hyphal wall protein (Hwp) 1, facilitate adherence to tissue and formation of antibiotic and immunoresistant biofilms. *C. albicans* has two methods of invading cells. Surface integrins (including Als3) can interact with host ligands (such as E-cadherin) to stimulate endocytosis; or it can actively penetrate the cell through methods not fully elucidated.[10]

In order to survive in a variety of tissues with varied nutrient availability, *C. albicans* has developed metabolic adaptability. Glycolysis is its major source of energy in tissues rich in glucose (blood) or glycogen (liver), but in phagocytic cells such as macrophages, the fungus subsists on lipids and amino acids using gluconeogenesis and, later, the glyoxylate cycle. In other tissues, the fungus secretes proteases and subsists on liberated amino acids. [10]

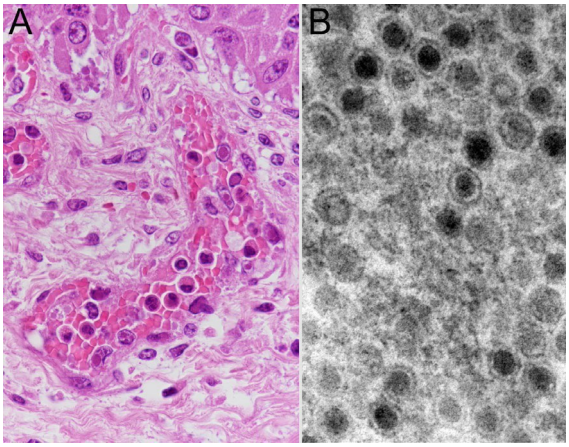

Figure 1-4. Abomasum, ox. A) Endothelial cells occasionally are swollen and contain a karyomegalic eosinophilic intranuclear viral inclusion with varying degrees of halo formation. B) Transmission electron microscopy of the affected nuclei demonstrates 80nm adenovirus-like particles. (Photo courtesy of: National Institute of Animal Health, National Institute of Animal Health, National Agriculture and Food Research Organization (NARO), 3-1-5Kannondai, Tsukuba, Ibaraki 3050856, Japan, (WSC ID95), http://www.naro.affrc.go.jp/english/niah/index.html)

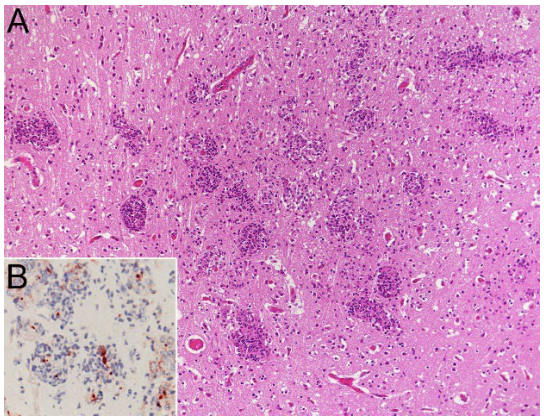

Figure 1-5. Brain, ox. A) The brain contained numerous foci of granulomatous inflammation. B) Within these foci, a large number of anti-Candida antibody-positive pseudohyphae are present. (Photo courtesy of: National Institute of Animal Health, National Institute of Animal Health, National Agriculture and Food Research Organization (NARO), 3-1-5Kannondai, Tsukuba, Ibaraki 3050856, Japan, (WSC ID95), http://www.naro.affrc.go.jp/english/niah/index.html)

Interestingly, amino acid absorption indicates a less permissive environment, and, in response, the yeast will actively secret ammonia to stimulate its own pH receptors and induce hyphal formation. The pH is detected using surface receptors Dfg16 and Rim21 which act through Rim101 transcription factor to mediate various cellular responses. In addition to switching morphologies, the fungus can respond to change in pH by altering expression of cell wall beta glycosidases Phr1 and Phr2 to maintain virulence in neutral-alkaline and acidic pHs, respectively.[10]

C. albicans has evolved a few mechanisms to obtain iron, another key nutrient for survival. While it does not produce its own siderophores, *C. albicans* absorbs iron from the siderophores of other microbes using the transporter Sit1. Alternatively, it can use Als3 to acquire iron from host ferritin and transferrin, or it may acquire iron from hemoglobin and heme using a variety of proteins.[10]

The moderator, Dr. Francisco (Paco) Uzal, discussed differentials for this case and highlighted the fact that bovine adenovirus 1 can cause identical clinical signs and intranuclear inclusion bodies as BAdV-4. In general, however, gastrointestinal disease caused by adenoviruses in cattle is rare.

References:

1. Bianchi RM, Vielmo A, Schwertz CI et al. Fatal systemic *Mortierella wolfii* infection in a neonatal calf in southern Brazil. *Cienc Rural*. 2020;50(1):1-5.
2. Chihaya Y, Furusawa Y, Okada H, Matukawa k, Matsui Y. Pathological Studies on Systemic mycoses in Calves. *J Vet Med Sci*. 1991;53（6）:1051-1058.
3. Chihaya Y, Matsukawa K, Furusawa Y, Hatta Y, Okada H, Arisawa K. Disseminated aspergillosis with lesions in the central nervous system in a calf. *Jpn J Vet Sci*. 1988;50 (1):131-137.
4. Chihaya Y, Okada H, Matsukawa K, Matsui Y. Disseminated mycoses in cattle. A study on nine autopsy cases. *J Vet Med Sci*. 1992;54（3）:485-491.
5. Curtis B, Hollinger C, Lim A, Kiupel M. Embolic mycotic encephalitis in a cow following *Mortierella wolfii* infection of a surgery site. *J Vet Diagn Invest*. 2017;29(5):725–728.
6. Davies JL, Ngeleka M, Wobeser GA. Systemic infection with *Mortierella wolfii* following abortion in a cow. *Can Vet J*. 2010;51:1391–1393.
7. Matsui Y, Matsukawa K, Okada M, Chihaya Y, Kikuchi M. Bovine abortion by mycotic infection in Japan, particulaly isolation and identification of *Aspergillus fumigatus* and histopathological observations. *Jap J Zootech Sci*. 1977;48(9):481-488.
8. Matumoto M, Inaba Y, Tanaka Y, Sato K, Ito H, Omori T. Serological typing of bovine adenovirus, Nagano and Fukuroi, as type 4 and new type 6. *Jpn J Microbiol*. 1969;13(1):131-132.

9. Matumoto M, Inaba Y, Tanaka Y, Sato K, Ito H, Omori T. New Serological type 7 of bovine adenovirus. *Jpn J Microbiol*. 1970;14(5):430-431.
10. Mayer FL, Wilson D, Hube N. *Candida albicans* pathogenicity mechanisms. *Virulence.* 2013; 4(2): 119-128.
11. Motes CM, Casares PC, Hundesa A, Martín M, Girones R. Detection of bovine and porcine adenoviruses for tracing the source of fecal contamination. *Appl Environ Microbiol*. 2004;70 (3):1448-1454.
12. Munday JS, Laven RA, Orbell GMB, Pandey SK. Meningoencephalitis in an adult cow due to *Mortierella wolfii*. *J Vet Diagn Invest*. 2006;18:619–622.
13. Nakagawa M, Hasegawa K, Suda H, Hiramune T. Bovine cerebellar zygomycosis : a case report. *J Vet Med Sci*. 1986;48（4）:809-812.
14. Riet -Correa F, Krockenberger M, Dantas AFM, Oliveira DM. Bovine cryptococcal meningoencephalitis. *J Vet Diagn Invest*. 2011;23（5）:1056-60.
15. Saini P, Singh M, Kumar P. Fungal endometritis in bovines. *Open Vet J.* 2019;9(1):94-98.
16. Seyedmousavi S, Bosco SMG, Hoog SM, et al. Fungal infections in animals: a patchwork of different situations. *Med Mycol*. 2018;56:165-187.
17. Thompson KG, Thomson GW, Henry JN. Alimentary tract manifestations of bovine adenovirus infections. *Can Vet J*. 1981;22:68-71.
18. Uzai FA, Plattner BL, Hostetter JM. Alimentary System. In: Maxie MG ed. *Jubb. Kennedy, and Palmer's Pathology of Domestic Animals*. 6th ed. Vol.2 Elsevier; 2016:143-144.

CASE II:

Signalment:
6-month old, male (intact), pygmy goat
Capra aegagrus hircus

History:
The goat was euthanized following several days of diarrhea and a 24-hour period of "mental inappropriateness." No additional history was provided.

Gross Pathology:
The liver was enlarged, with 1 mm, soft, white, foci widely disseminated throughout capsular and cut surfaces. A focal, 1 cm in diameter ulcer was present in the abomasum near the pylorus, with adhered margins and subadjacent, firm, pale tan thickening of the wall (fibrosis).

Laboratory Results:
FA negative for rabies
FA positive, brain and liver, for *Listeria monocytogenes*
Aerobic culture, very light growth unidentified Gram-negative bacterium, enrichment broth culture negative for *L. monocytogenes*

Microscopic Description:
Hepatocytes are uniformly small, forming thin cords accentuated by moderate sinusoidal congestion. The parenchyma contains

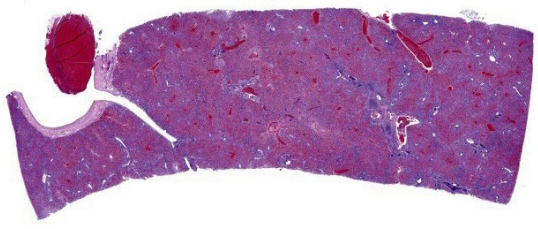

Figure 2-1. Liver, goat. One section of liver is submitted for examination. At subgross magnification, portal areas are outlined by biliary hyperplasia and a cellular infiltrate which occasionally fills bile ducts. There is diffuse edema of the connective tissue surrounding the gallbladder. (HE, 9X)

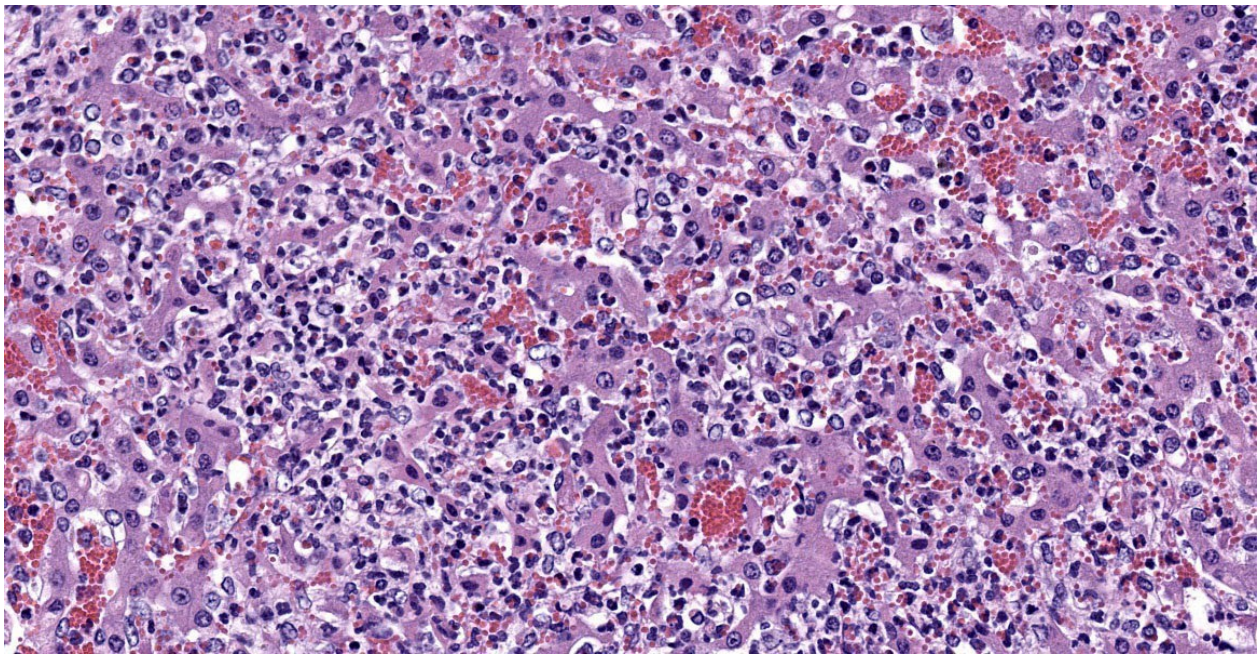

Figure 2-2. Liver, goat. Foci of lytic necrosis are scattered through the section. These areas contain large numbers of neutrophils which efface hepatocytes and fill adjacent sinusoids. (HE, 381X)

multifocal to coalescing, irregular, well-demarcated, variably sized, randomly distributed foci of hepatocellular degeneration and necrosis infiltrated by moderate to large numbers of predominantly neutrophils. There is widespread expansion of periportal areas by mixtures of edema, fibroplasia, proliferating bile ducts, and mixed inflammatory infiltrates predominated by lymphocytes and plasma cells, with smaller numbers of neutrophils. Biliary hyperplasia frequently links adjacent portal areas. Primarily larger bile ducts are ectatic, with lumens distended by large numbers of neutrophils, necrotic cellular debris and occasional unsporulated coccidial oocysts. The epithelium of affected bile ducts is variably attenuated, to degenerate or necrotic. Many cells have vacuolated cytoplasm that contains small coccidial meronts with merozoites, macrogametes, microgametes and developing oocysts. The lumens of some bile ducts and sinusoids contain microcolonies of small bacterial rods.

Contributor's Morphologic Diagnoses:
Liver: Necrosuppurative hepatitis, acute, multifocal to coalescing, severe, with severe suppurative cholangitis, lymphoplasmacytic pericholangitis, marked biliary hyperplasia and multiple coccidial stages

Contributor's Comment:
Gross and microscopic findings are consistent with listeriosis, a global disease of humans and other animals caused by the opportunistic, Gram-positive, intracellular bacterium, *Listeria monocytogenes*. Infection was confirmed by positive fluorescent antibody staining of the brain and liver. The environmentally resistant bacterium is widely distributed in soil, vegetation and in animals.[1] Large numbers are present in ruminant feces and it is frequently isolated from normal tissues.[2] In humans, transmission usually occurs through the consumption of contaminated food, rarely from infected animals to humans, between humans, and in utero. In foods, it survives processing technologies relying on acidic or salty conditions and can multiply at low temperatures.[1] Encephalitis in ruminants

is often associated with heavy silage feeding.[2]

Cell mediated immune responses are related to intracellular replication and have been recently reviewed, as have strategies used by the bacterium to exploit host molecular mechanisms, including translocation from cell to cell. [3,4,5] In mammalian hosts, three disease syndromes occur in relation to the bacteria's ability to cross intestinal, feto-placental and blood brain barriers. It can also survive in bile and induce biliary tract infection.[6] Infection of the pregnant uterus results in abortion and frequently lethal neonatal disease. Encephalitis usually occurs in adults and is typified by microabscess formation in the brainstem. Ascending infection of the trigeminal nerve follows trauma to the oral mucosa. Septicemia, with coagulative necrosis and abscess formation occurs mainly in the livers of neonates and young juveniles following disruption of the intestinal mucosal barrier and translocation of bacteria to the submucosa and vasculature. Focal infections can include the conjunctiva, skin, mammary glands, heart, arteries, spleen, lymph nodes, joints, bone, and fascia.[1,2]

In addition to its biliary presence, severe intestinal coccidiosis, a common cause of diarrhea in confined young goats, may have compromised the intestinal mucosa, providing a portal of entry for *L. monocytogenes* into the portal circulation. Similar changes, including hepatic necrosis, biliary hyperplasia, periportal fibrosis and lymphocytic inflammation have been reported in association with hepatic coccidiosis, caused by an *Eimeria* sp., in a goat.[7]

Contributing Institution:
www.vet.uga.edu/VPP

JPC Diagnosis:
Liver: Cholangiohepatitis, suppurative and lymphoplasmacytic, chronic, diffuse, marked, with biliary hyperplasia and numerous apicomplexan meronts, gamonts, and oocysts.

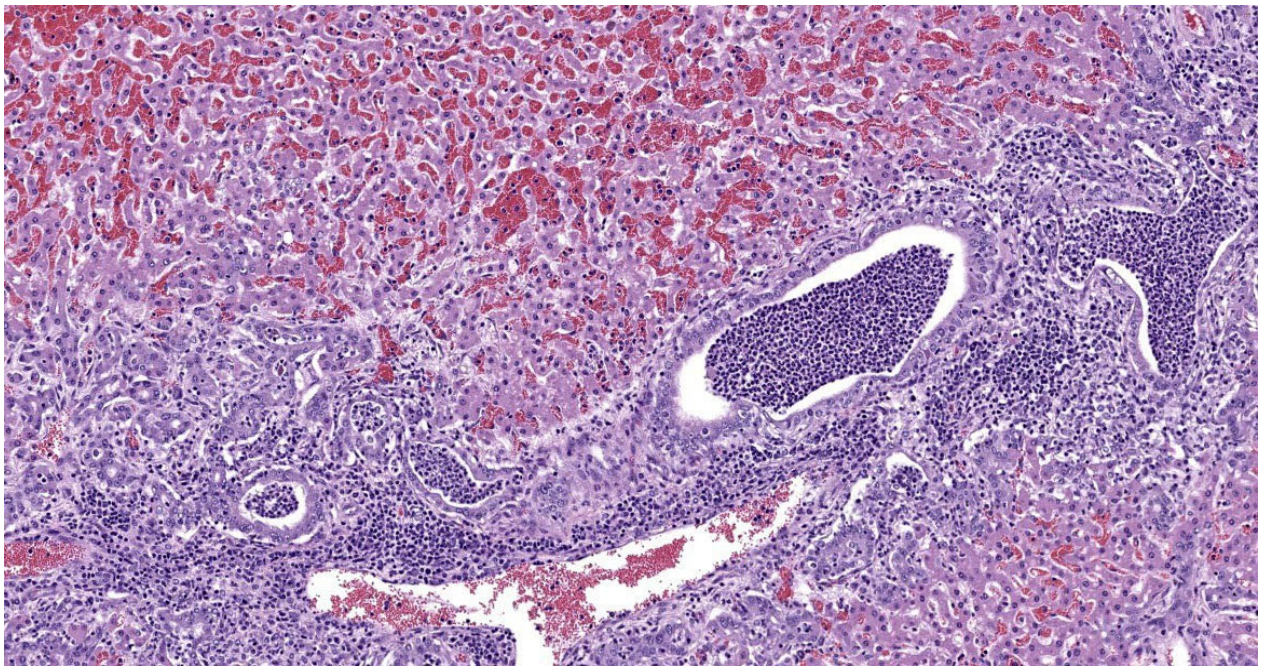

Figure 2-3. Liver, goat. Within portal areas, the lumen of bile ducts are filled with numerous viable and degenerate neutrophils and cellular debris but lining epithelium is intact. There are numerous lymphocytes and plasma cells surrounding ducts. Profound biliary hyperplasia extends well beyond the limiting plate. (HE, 130X)

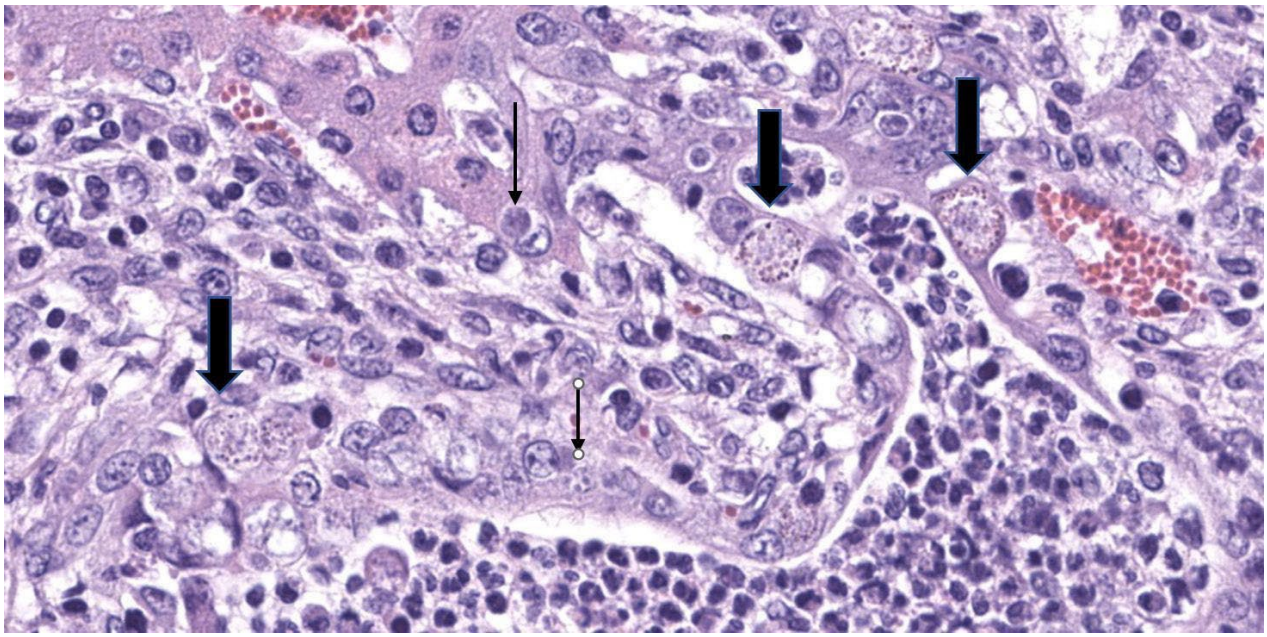

Figure 2-4. Liver, goat. Coccidial meronts, schizonts (small arrows) and gamonts (large arrows) are present within he biliary epithelium. (HE, 623X)

JPC Comment:

Listeria monocytogenes was first described 101 years ago in a human patient and in animal species a few years later. There are 13 serovars, with three serovars (1/2a, 1/2b, 4b) being the most commonly isolated in clinical disease. As the contributor mentions, the bacterium is ubiquitous in the environment, but pathogenic serotypes have frequently been isolated from wild animals, suggesting a possible wild reservoir.[2]

At physiologic temperatures, *L. monocytogenes* actively expresses positive regulatory factor A (PrfA), allowing it to switch from an environmental to an infective lifestyle. A number of virulence factors are then expressed, including internalin A and B (InlA and InlB). These bind to non-phagocytic cell membrane receptors such as E-cadherin and induce receptor-mediated endocytosis. Alternatively, *L. monocytogenes* can be directly phagocytosed by phagocytic cells. Within the cytoplasmic vacuole, listeriolysin O, phospholipase A, and phospholipase B create membrane pores which allow the bacteria to escape in the cytoplasm and begin replicating. Recent evidence has also shown that the bacteria can actually remain and replicate slowly within the vacuoles. Once in the cytosol, the actin assembly-inducing protein causes the cytoskeleton to rearrange, forming actin comet-tails which propel the bacteria around the cytoplasm or into an adjacent cell.[2]

While ocular, cutaneous, and many rhombencephalic infections are initiated via traumatic inoculation, the method with which *L. monocytogenes* establishes enteric infection in ruminants is still somewhat a mystery. In mice, InlA, InlB, and *Listeria* adhesion protein (LAP) enable the bacteria to translocate the mucosa with minimal host reaction. Ruminants are frequently asymptomatically infected, but in clinically affected animals bacterial infection of myocytes leads to neutrophilic inflammation focused on the muscularis mucosa. In subsequent bacteremia, *L. monocytogenes* spreads to the spleen and liver, causing random hepatocellular necrosis, pyogranulomas, and periportal inflammation. Bacteremic spread can also spread to the placenta, causing fetoplacental infection, or to the udder, causing mastitis (though masti-

tis may also occur through direct inoculation). [2] The moderator and conference participants discussed the possibility that this case originated as a fetoplacental infection in which the fetus survived.

In monogastrics, blood-borne bacteria (either extracellular or in leukocytes) can cross the blood-brain barrier, causing meningitis or meningoencephalitis. In ruminants, the bacteria follows a different route of infection, crossing oral mucosa or skin, traveling up the axons of the cranial nerves, and establishing infection in the brainstem, causing rhombencephalitis.[2] For additional information on the neurologic manifestation of *L. monocytogenes* in ruminants, we recommend reviewing WSC 21-22, Conference 12, Case 2, which featured listerial rhombencephalitis in a lamb.

The moderator and conference participants considered the distribution of hepatocellular necrosis in this case and agreed the majority of necrosis is affecting the periportal region, thus included under the umbrella of suppurative cholangiohepatitis.

References:

1. Allerberger F, Wagner M. Listeriosis: a resurgent foodborne infection. *Clinical Microbiology and Infection.* 2009; 16:16-23.
2. Bagatella S, Tavares-Gomes L, Oevermann A. *Listeria monocytogenes* at the interface between ruminants and humans: A comparative pathology and pathogenesis review. *Vet Pathol*. 2022; 59(2):186-210.
3. Charlier C, Fevre C, Travier L, et al. *Listeria monocytogenes*-associated biliary tract infections. *Medicine*. 2014; 93:1-11.
4. Cossart P. Illuminating the landscape of host-pathogen interactions with the bacterium *Listeria monocytogenes*. *PNAS*. 2011; 108:19484-19491.
5. Cossart P, Lebreton A. A trip in the "new microbiology" with the bacterial pathogen Listeria monocytogenes. *FEBS Letters*. 2014; 588: 2437-2445.
6. Maxie MG, Youssef S. Nervous System. In: Maxie MG, ed. *Jubb, Kennedy and Palmer's Pathology of Domestic Animals*. 5th ed. Philadelphia, PA: Elsevier Saunders; 2007: 281-457.
7. Schafer KA, Stevenson W, Kazacoa KR. Hepatic coccidiosis associated with hepatic necrosis in a goat. *Vet Pathol*. 1995; 32:723-727.
8. Stavru F, Archambaud C, Cossart P. Cell biology and immunology of *Listeria monocytogenes* infections: novel insights. *Immunological Reviews*. 2011; 240:160-184.

CASE III:

Signalment:
67-day old, male, Holstein, bovine (*Bos taurus*)

History:
The calf was transferred to a farm for fattening at 7-days old. The calf did not receive any vaccinations and developed respiratory signs, including coughing; the condition worsened despite antibacterial treatment with oxytetracycline. The calf was euthanized at the age of 67-day old due to anorexia and respiratory distress.

Gross Pathology:
At necropsy, the liver was swollen and faded in color, with multiple, micro-yellow-white foci on the cut surface. The lungs showed hepatization in the anterior and middle lobes and regression failure in the posterior lobes.

Multiple petechiae and white foci were detected in the renal cortex. The spleen was congested and swollen. The growth of rumen papillae was poor, and the contents were muddy with an acidic odor. The pulmonary hilum, hepatic hilum, and mesenteric lymph nodes were edematous and swollen.

Laboratory Results:
Bacterial colonies morphologically and biochemically consistent with *Salmonella enterica* were isolated from the liver, spleen, kidney, lung, pulmonary hilar, and mesenteric lymph nodes by direct culture, and formed the whole blood, rumen, and cecal contents in an enriched culture. The isolates were identified as *S. enterica* subsp. *enterica* by 16S rDNA sequencing and serotyped as *Salmonella* Dublin (serotype O9: g, p :-). The isolates contained the *invA* and *spvC* genes. No virological examination was performed.

Microscopic Description:
Severe multifocal hepatic necrosis and paratyphoid nodules were observed and characterized by histiocytic, lymphocytic, and neutrophil infiltration. Infiltration of lymphocytes and plasma cells was also detected in Glisson's capsule. A hyaline thrombus was observed in the central vein. In the kidney, severe multifocal pyogranulomatous interstitial nephritis was detected with hemorrhage. Similar lesions were found in the spleen and lung interstitium, as well as in the submucosa of the rumen, ileum, and cecum. Immunostaining for anti-*Salmonella* O9 rabbit serum showed positivity in the cytoplasm of macrophages in the hepatic lesions.

Contributor's Morphologic Diagnoses:
Liver: hepatitis, multifocal, necrotizing, histiocytic, lymphocytic and neutrophilic, paratyphoid nodules, *Salmonella enterica* subsp. *enterica* Dublin, *Bos taurus*, bovine

Contributor's Comment:
Salmonellosis is a zoonotic, enteric, or multisystemic disease, distributed worldwide.[1, 3, 6,7,9-11] This infection causes huge economic losses to the food animal industry. *Salmonella* spp. are rod-shaped, gram-negative, facultatively anaerobic bacteria belonging to the *Enterobacteriaceae* family.[4] The genus *Salmonella* includes more than 2,500 serotypes within two species: *S. enterica* (more than 2,400 serotypes) and *Salmonella bongori* (20 serotypes).[4,10] *S. enterica* is a major pathogen that can infect numerous animal species, in addition to humans.10

Some *Salmonella* serotypes have particular host predilections. *S.* Dublin, *Salmonella* Choleraesuis, and *Salmonella* Gallinarum preferentially infect cattle, pigs, and chickens, respectively.[4,9,10] *Salmonella* Typhi and *Salmonella* Paratyphi infect only humans, causing typhoid fever. In contrast, *Salmonella* Typhimurium and *Salmonella* Enteritidis can infect a wide range of host species.

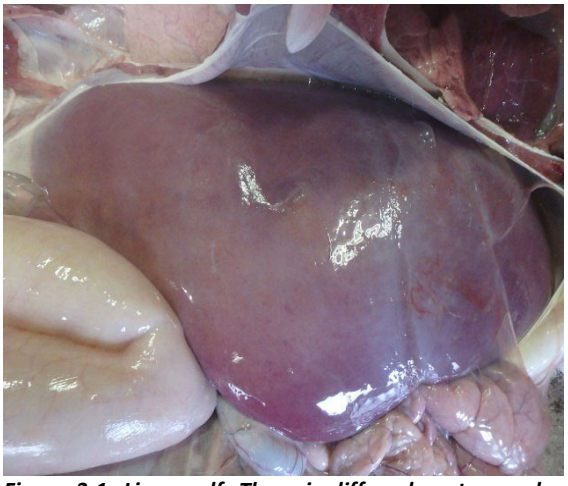

Figure 3-1. Liver, calf. There is diffuse hepatomegaly with rounded edges. (Photo courtesy of: National Institute of Animal Health, National Institute of Animal Health, National Agriculture and Food Research Organization (NARO), 3-1-5Kannondai, Tsukuba, Ibaraki 3050856, Japan, (WSC ID95), http://www.naro.affrc.go.jp/english/niah/index.html)

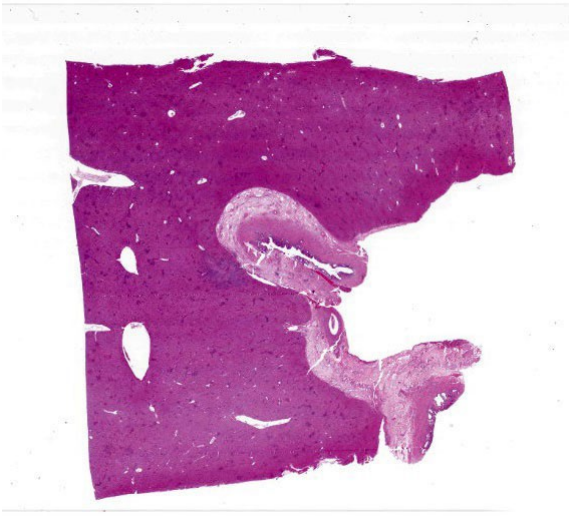

Figure 3-2. Liver, calf. One section of liver and gallbladder is submitted for examination. At subgross magnification, there is moderate edema of the connective tissue surrounding the gallbladder. (HE, 8X)

Bovine salmonellosis is caused predominantly by *S.* Dublin and *S.* Typhimurium;[1,4] however, other serotypes are also capable of causing infection in cattle.[1,4] In adult cattle, *S.* Dublin infection is common, and can be asymptomatic or characterized by abortion in pregnant cows. *S.* Dublin infection is also associated with fever, reduced milk production, and mild-to-moderate diarrhea. The affected animals shed *S.* Dublin intermittently, leading to sporadic or repeated outbreaks of disease in the herd.[10] In calves, *S.* Dublin is associated with systemic infections, which can result in meningoencephalitis, polyarthritis, hepatitis, cholecystitis, pneumonia, splenitis, and lymphadenitis occasionally in the absence of diarrhea.[4,10,11] Recently, pyelonephritis, urocystitis, ureteritis, and gangrene of the distal extremities have also been reported in calves.[3,7,12]

Conversely, *S.* Typhimurium causes enteritis and marked acute exudative diarrhea in young calves less than 2 months of age.[4] Fever, anorexia, prominent diarrhea, and dehydration, which are secondary to acute necrotizing enteritis, are found in bovine *S.* Typhimurium infections. Disease severity and lethality were inversely proportional to the age of the affected calves. The feces are often watery, with variable amounts of mucus, fragments of the intestinal mucosa, or blood clots. Abortion is uncommon in *S.* Typhimurium infections.[10]

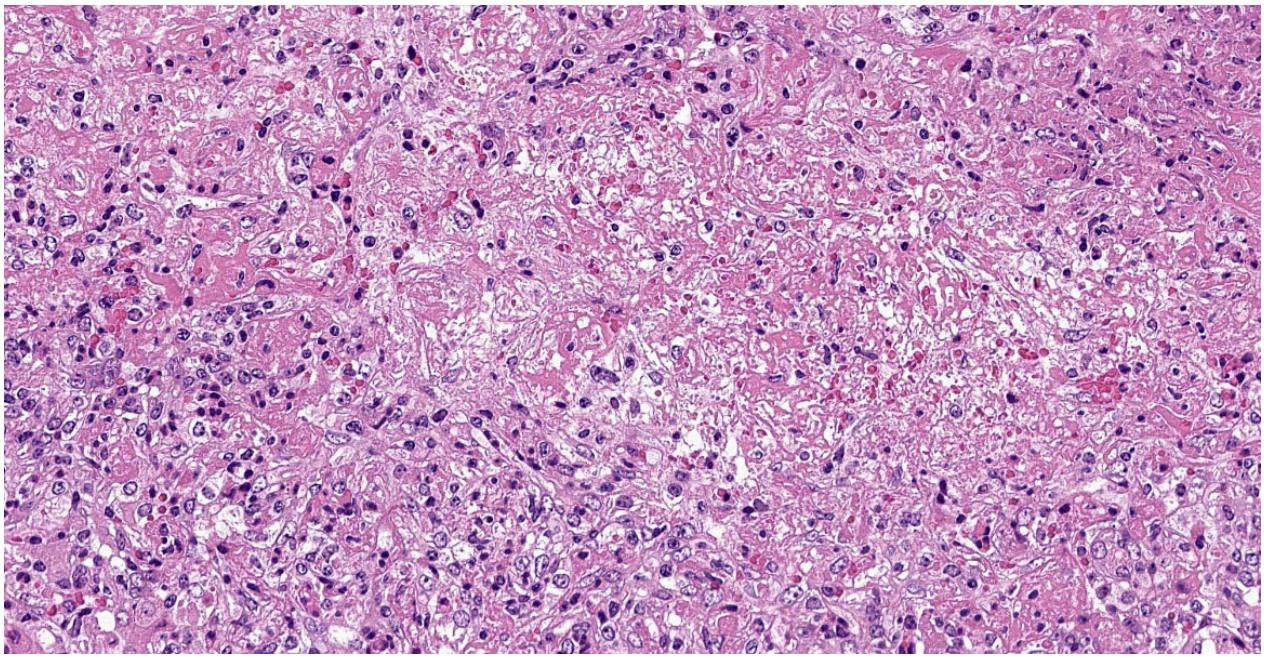

Figure 3-3. Liver, calf. In proximity to the gallbladder, there is a large focus of hepatocellular necrosis and loss with stromal collapse. There is infiltration of macrophages peripherally and fewer lymphocytes. (HE, 367X)

The diagnosis of septicemic salmonellosis is based on clinical and pathological findings and confirmed through microbiological culture and identification of *S.* Dublin by the polymerase chain reaction technique.[6] *S.* Dublin was identified by culture, 16S rDNA sequencing and serotyping. On immunohistochemical examination, *Salmonella* O9 antigen was detected in the lesions. The pathological and bacterial findings in this case were consistent with septicemic salmonellosis.[11]

Oral transmission can occur via the feces, contaminated food, water, or milk/colostrum. The emergence of multidrug-resistant strains is beginning to limit treatment options.[1,5,15]

Contributing Institution:
National Institute of Animal Health,
National Agriculture and Food Research Organization (NARO)
3-1-5Kannondai, Tsukuba, Ibaraki 305-0856, Japan
(WSC ID95)
http://www.naro.affrc.go.jp/english/niah/index.html

JPC Diagnosis:
1. Liver: Hepatitis, necrotizing, multifocal, random, marked (paratyphoid nodules), with vasculitis and thrombosis.
2. Bile duct, adventitia: Edema, diffuse, moderate.

JPC Comment:
It is hypothesized that there were three major steps in the evolution of *Salmonella enterica* subsp. *enterica* from its common ancestor with *Escherichia coli.*[1] The first step involved acquisition of *Salmonella* pathogenicity island (SPI-1), which is present in all *Salmonella* species and encodes virulence factors important in establishing an intestinal infection. [1] The second step involved acquisition of *Salmonella* pathogenicity island 2 (SPI-2), which is present in *S. enterica* but lacking in *S. bongori.* [1] The last jump involved expansion of the host range from ectothermic vertebrates to bird and mammals, and the bacteria may have developed the ability to survive within macrophages as a mechanism to overcome the robust gastrointestinal defense mechanisms in this new host range.[1]

As the contributor describes, different serotypes of *Salmonella enterica* subsp. *enterica* have different host ranges and spectra of disease. *Unrestricted* serotypes, including Typhimurium and Enteritidis, tend to cause enteritis in young animals in a wide range of species. *Host-adapted* serotypes, such as Dublin and Cholerasuis, can cause either enteritis or systemic disease in their specific species.[14] *Host-restricted* serotypes, including Typhi, Gallinarum, and Abortisuis, tend to cause systemic infection with minimal to no enteritis in their specific species.[14]

Table 3-1. Examples of host adapted and restricted *Salmonella enterica* subsp. *enterica* serotypes. Adapted from Uzzau et al, 2000.

	Serotype	Natural host	Other hosts (rare)
Host-adapted	Cholerasuis	Swine	Human
Host-adapted	Dublin	Bovine	Human, ovine
Host-restricted	Typhi	Human	-
Host-restricted	Paratyphi A, C	Human	-
Host-restricted	Sendai	Human	-
Host-restricted	Abortusovis	Ovine	-
Host-restricted	Gallinarum	Poultry	-
Host-restricted	Typhisuis	Swine	-
Host-restricted	Abortisequi	Equine	-

Typically, bacteria which are highly adapted to a host have evolved to cause a minimal to tolerable level of disease, allowing for host survival and spread of bacterial infection.[1] *S. enterica* is unique in that high adaptation corresponds to higher virulence within the host, which mathematic models suggest has favored the development of the carrier state.[1] The success of this strategy is evidenced by the proverbial disease carrier, Typhoid Mary, who harbored *S.* Typhi in a gallstone and spread the infection to numerous individuals while working as a cook in the early 1900s.[8]

Salmonella possesses flagella which enable motility and uses fimbriae to adhere to the mucosal epithelial cells.[13] A type III secretion system allows injection of effector proteins into the cytoplasm. [13] The bacteria is engulfed into a vacuole via receptor-mediated endocytosis or by entering through the intercellular junction complex. [13] LPS on the cell wall resists host defense mechanisms (such as opsonization) and stimulates prostaglandin synthesis. In cases of enteritis, diarrhea occurs as a result of enterocyte loss, prostaglandin E2-induced hypersecretion, and leakage from damaged mucosa. [13]

In systemic salmonellosis, the bacteria invades and survives within macrophages, producing bacteremia and septicemia.[13] *S.* Dublin is unique in that it can also survive extracellularly and spread free within lymphatic

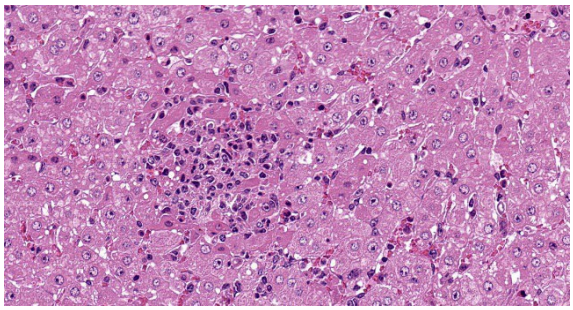

Figure 3-4. Liver, calf. Smaller foci of necrosis are infiltrated by macrophages (paratyphoid nodules). (HE, 459X)

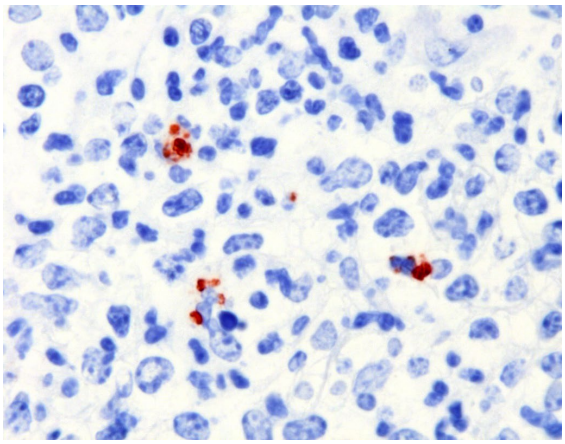

Figure 3-5. Liver, calf. Macrophages within necrotic lesions demonstrate immunopositivity with antisera against Salmonella sp. (anti-Salmonella, 400X) (Photo courtesy of: National Institute of Animal Health, National Institute of Animal Health, National Agriculture and Food Research Organization (NARO), 3-1-5Kannondai, Tsukuba, Ibaraki 3050856, Japan, (WSC ID95), http://www.naro.affrc.go.jp/english/niah/index.html)

fluid.[13] Once in systemic circulation, bacteria are removed by fixed macrophages throughout the body, including in the liver, spleen, kidney, and bone marrow, producing paratyphoid granulomas as seen in this case.[13] In severe cases, septicemia may be fatal. [13]

As the contributor describes, *S.* Dublin causes severe acute disease in calves characterized by endotoxemia with depression, respiratory distress, and death. In a recent review of 57 infected Holstein calves less than 6 months of age, the most consistent lesions were neutrophilic infiltrates in the alveolar capillaries and septa and necrosuppurative and histiocytic hepatitis with paratyphoid granulomas.[11] In approximately half of the cases, neutrophilic infiltrates were observed in the lymph nodes and marginal zone of the spleen.[11] Key features which differentiated *S.* Dublin from systemic *E. coli* infection were paratyphoid nodules in the liver and age, with *E. coli* endotoxemia primarily affecting calves less than two weeks of age and *S.* Dublin affecting older calves.[11]

The moderator provided a general rule of thumb for two gross necropsy findings highly suggestive of *S.* Dublin infection in calves: icterus and gall bladder edema with mucosal pseudomembrane formation.

References:

1. Baumler AJ, Tsolis RM, Ficht TA, Adams LG. Evolution of Host Adaptation in *Salmonella enterica*. *Infection and Immunity.* 1998: 4579-4587.
2. Casaux ML, Caffarena RD, Schild CO, Giannitti F, Riet-Correa F, Fraga M: Antibiotic resistance in *Salmonella enterica* isolated from dairy calves in Uruguay. *Braz J Microbiol.* 2019; **50**(4):1139-1144.
3. Costa RA, Casaux ML, Caffarena RD, Macías-Rioseco M, Schild CO, Fraga M, Riet-Correa F, Giannitti F: Urocystitis and ureteritis in Holstein calves with septicaemia caused by *Salmonella enterica* serotype Dublin. *J Comp Pathol.* 2018; **164**:32-36.
4. Costa LF, Paixão TA, Tsolis RM, Bäumler AJ, Santos RL: Salmonellosis in cattle: advantages of being an experimental model. *Res Vet Sci.* 2012; **93**(1):1-6.
5. Estevez MB, Casaux ML, Fraga M, Faccio R, Alborés S: Biogenic silver nanoparticles as a strategy in the fight against multi-resistant *Salmonella enterica* isolated from dairy calves. *Front Bioeng Biotechnol.* 2021; **9**:644014.
6. Guizelini CC, Tutija JF, Morais DR, Bacha FB, Ramos CAN, Leal CRB, Zaquetti ME, Lemos RAA: Outbreak investigation of septicemic salmonellosis in calves. *J Infect Dev Ctries.* 2020; **14**(1):104-108.
7. Loeb E, Toussaint MJ, Rutten VP, Koeman JP: Dry gangrene of the extremities in calves associated with *Salmonella* dublin infection; a possible immune-mediated reaction. *J Comp Pathol.* 2006; **134**(4):366-369.
8. Marineli F, Tsoucalas G, Karamanou M, Androustous G. Mary Mllon (1869-1938) and the history of typhoid fever. *Ann Gastroenterol.* 2013; 26(2): 132-134.
9. Meneguzzi M, Pissetti C, Rebelatto R, Trachsel J, Kuchiishi SS, Reis AT, Guedes RMC, Leão JA, Reichen C, Kich JD: Re-emergence of salmonellosis in hog farms: outbreak and bacteriological characterization. *Microorganisms*. 2021; **9**(5):947.
10. Nielsen LR: Review of pathogenesis and diagnostic methods of immediate relevance for epidemiology and control of *Salmonella* Dublin in cattle. *Vet Microbiol.* 2013; **162**(1):1-9.
11. Pecoraro HL, Thompson B, Duhamel GE: Histopathology case definition of naturally acquired *Salmonella enterica* serovar Dublin infection in young Holstein cattle in the northeastern United States. *J Vet Diagn Invest.* 2017; **29**(6):860-864.
12. Taghipur Bazargani T, Khodakaram-Tafti A, Ashrafi I, Abbassi AM: Giant hydronephrosis and secondary pyelonephritis induced by *Salmonella* Dublin in a Holstein calf. *Iran J Vet Res.* 2015; **16**(1):114-116.
13. Uzal FA, Plattner BL, Hostetter JM. Alimentary system. In: Maxie MG, ed. *Jubb, Kennedy and Palmer's Pathology of Domestic Animals*. Vol 2. 6th ed. Philadelphia, PA: Elsevier Saunders; 2016: 167-176.
13. Uzzau S, Brown DJ, Wallis T, et al. Host adapted serotypes of *Salmonella enterica*. *Epidemiol Infect.* 2000 (125): 229-255.
14. Wang X, Biswas S, Paudyal N, Pan H, Li X, Fang W, Yue M: Antibiotic resistance in *Salmonella* Typhimurium isolates recovered from the food chain through na-

tional antimicrobial resistance monitoring system between 1996 and 2016. *Front Microbiol.* 2019; **10**:985.

CASE IV:

Signalment:
4 day-old, female, Belgian blue x Holstein, Bos Taurus, cattle/bovine.

History:
This calf was from a 100 head dairy farm with a few weeks history of diarrhea in neonatal calves; diarrheal episodes were also observed in a few older calves and heifers. As the diarrhea resolved within a few days with no or only supportive treatment, the cause was not thoroughly investigated, although coprological examinations revealed *Cryptosporidium*. However, as four diarrheic calves had died in the previous week, the veterinarian submitted an untreated dead calf to our diagnostic laboratory. The same herd had experienced *Salmonella Dublin*-associated disease 5 years before.

Gross Pathology:
The calf was submitted partially frozen. Body condition was assessed as good. The perineal region was covered with abundant feces. There was marked bilateral enophtalmos and the subcutaneous tissues were "sticky", consistent with dehydration. The thymus was moderately atrophied. Intestinal contents in the distal half of the small intestine, the cecum and spiral colon were not abundant, but they were liquid, pinkish to brownish with small clumps of fibrin-like material. The intestinal mucosa was hard to assess due to freezing/thawing, but there was no evidence of hyperemia, necrosis or fibrinous pseudomembranes. There was some milk in the rumen ("ruminal drinking"), but contents and mucosa of the gastric compartments were otherwise normal.

Laboratory Results:
Bacteriology: ileum and colon: ++++ non-hemolytic *E. coli* that were eae+, but F5-, STa-, Stx1- and Stx2- (3/3 colonies tested → EPEC). Negative for *Salmonella*. Virology: PCR negative for BCoV (coronavirus), type A rotavirus and BVDV. Parasitology: only a few *Cryptosporidium* oocysts were detected.

Microscopic Description:
This is a section of ileum; there is variability among slides (either one of two sections) and moderate post-mortem changes, mostly desquamation. Multifocally, short bacilli are adherent to the villous enterocytes' brush border, sometimes intimately with basophilia (bacteria) and palisading, and/or a scalloped epithelial surface. A Gram stain showed the bacilli to be Gram-negative (slide not provided). Similar lesions were present in the middle and distal jejunum and rarely in the colon. Associated changes vary from a few scattered luminal neutrophils to a luminal mass of fibrin, neutrophils and debris; in the latter case, there are a few capillaries with fibrin thrombi in the lamina propria. There is moderate lymphoid depletion in Peyer's patches.

Contributor's Morphologic Diagnoses:
Ileum, villous epithelium: intimately adherent bacilli with attaching and effacing morphology and minimal enteritis (consistent with EPEC infection)

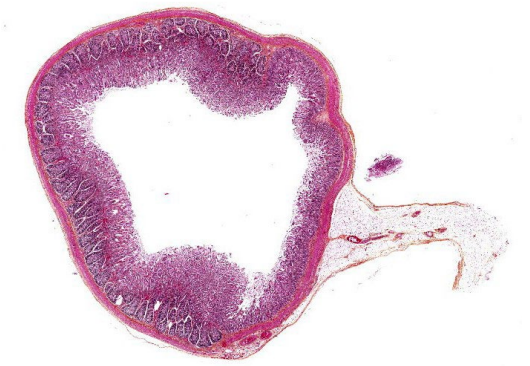

Figure 4-1. Ileum, calf. A single section of ileum is submitted for examination. (HE, 5X)

Contributor's Comment:
Based on the typical attaching and effacing intestinal lesions, the bacteriological results, and the absence of another cause, the diarrhea in this case was attributed to EPEC (*enteropathogenic E. coli*) infection, which is unusual as although EPEC infection is not infrequent in calves, it is rarely diagnosed as the main or sole cause of diarrhea. Although not conspicuous in examined sections, it was assumed that microulcerations were present and responsible for the fibrinosuppurative exudate seen grossly and in one of the sections. The Gram stain was done to be sure the bacteria were not enteroadherent cocci (e.g. *Enterococcus durans*), a rare cause of diarrhea in calves and piglets.

In humans, diarrheagenic *E. coli* (DEC) can be classified into six major classes, or pathotypes: enterotoxigenic *E. coli* (ETEC), enteropathogenic *E.coli* (EPEC), enterohemorrhagic E. coli (EHEC), enteroinvasive E.coli (EIEC), enteroaggregative E. coli (EAEC) and diffusely adherent *E. coli* (DAEC).[1,4,9] Another pathotype, adherent invasive *E.coli* (AIEC), has been proposed to be involved in inflammatory bowel disease (Crohn's disease; ulcerative colitis).[1,7] Of these pathotypes, only ETEC is a significant cause of diarrhea in domestic animals, especially in piglets and calves,[9,11] except in rabbits in which EPEC is a major cause of diarrhea;[14] EPECs in humans primarily involves children, especially infants, in developing countries.[4] Domestic animals, especially ruminants, are mostly reservoirs for EHECs, but EHECs can occasionally cause diarrhea in some species. The other pathotypes (EIEC, EAEC and DAEC) have not to our knowledge been reported in natural disease in domestic animals and will not be discussed further. ETECs, EPECs and EHECs are defined by virulence factors, have histopathologic characteristics (type and localization), and are associated with typical clinical signs; these categories

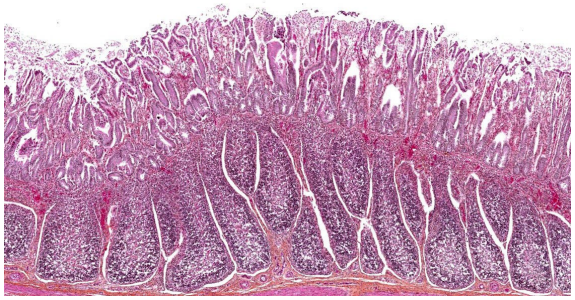

Figure 4-2. Ileum, calf. There is mild autolysis of this section, hampering evaluation of villar length. There is mild depletion of the underlying Peyer's patch. (HE, 38X)

are not mutually exclusive and some strains overlap pathotypes.[4]

ETECs are able to colonize the small intestinal villous enterocytes through one or more fimbriae and produce one or more enterotoxin that cause secretory diarrhea, which is watery and profuse.[1,11] On light microscopy, bacilli are seen close to the apical portion of the villous enterocytes and are typically not associated with significant morphologic or inflammatory changes except in piglets in which mostly F4+ strains can occasionally cause a hemorrhagic gastroenteritis, possibly due to endotoxic shock.[2,11]

EPECs and the vast majority of EHECs cause a characteristic lesion known as "attaching and effacing" (AE) and are thus collectively known as attaching and effacing *E. coli* (AEEC).[1, 9,11,12] AEEC lesions have described in humans/primates, rabbits, pigs, small ruminants, dogs, cats and birds (broiler chickens and turkeys).[6,12]This lesion is characterized at the light microscopic level by a colonization that is more intimate than for ETECs and associated with morphologic/degenerative changes in colonized enterocytes; bacteria in well-established lesions can be seen as coccobacilli, which are often more basophilic, in the brush border. Villous and cryptal epithelium in the small and/or large intestine can be involved. Colonized enterocytes eventually appear rounded-up, giving

the epithelium a scalloped surface, and ultimately die and slough; if enterocyte loss is marked, villous atrophy/fusion, erosions and superficial ulcerations may be observed, with secondary inflammatory changes.[1,11,12] Electron microscopic AEEC lesions are characterized by intimate attachment of the bacteria to the enterocytes' apical cytoplasmic membrane, often with a cup-shaped actin "pedestal" in the underlying cytoplasm, and effacement of the microvilli.[12] The genes responsible for the attaching and effacing lesion are located on the "locus of enterocyte attachment" (LEE), a large pathogenicity island; the LEE includes the eae (intimin) and, except in EHECs and "atypical" EPECs, bfp (bundle-forming pili) genes; detection of the eae gene is used for molecular identification of AEEC strains. The genesis of AE lesions essentially goes through four stages: 1) initial non-intimate attachment (bfp in typical EPECs; other fimbriae in atypical EPECs and in EHECs), 2) translocation of bacterial proteins, including Tir (translocated intimin receptor), into the enterocyte's cytosol, 3) intimate attachment mediated by intimin, which binds to Tir, with underlying cytoskeletal reorganization (actin pedestal) and 4) invasion of bacteria into the cytoplasm (free or within vacuoles).[4, 12] Attaching and effacing lesions are not restricted to AEEC. *Citrobacter rodentium* causes transmissible murine colonic hyperplasia in mice (one strain of *Citrobacter rodentium* had previously been called mouse-pathogenic *E.coli*), and *Escherichia albertii* is emerging as a new human diarrheagenic bacterium (including some misidentified as atypical EPECs) and avian pathogen; both produce AE lesions via the LEE genes.[1,8,13]

In contrast to EPECs, EHECs produce shigatoxins from either or both Stx1 and Stx2 families/groups; although EHECs have other potential virulence factors, this is the defining characteristic that separates EHECs from EPECs.[1,4,9] EHECs are included in the shigatoxin-producing *E. coli* pathotype (STEC),[1] and STEC and EHEC are sometimes used interchangeably, which is not correct as some STEC strains are neither AE nor diarrheagenic (e.g. Stx2e-producing in porcine edema disease).[9] Some STEC strains are LEE-negative (and thus not AE), but produce

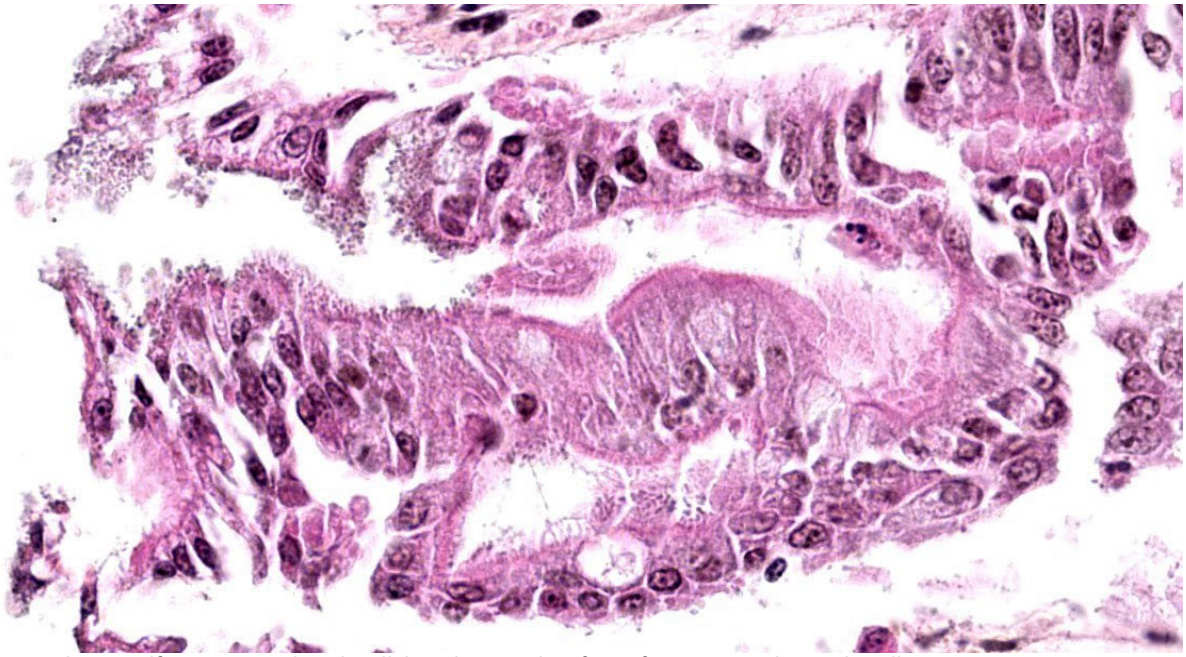

Figure 4-3. Ileum, calf. Numerous short bacilli line the apical surface of enterocytes lining the villar enterocytes.

hemorrhagic colitis and HUS, and are thus considered EHECs.[1,9] Shigatoxins bind and cause damage to enterocytes and vascular endothelial cells (mostly intestinal and renal). Damage to renal endothelial cells is the basis of a thrombotic microangiopathy known as hemolytic uremic syndrome (HUS), which is a potentially lethal complication of EHEC infection in humans;[1] HUS-like lesions have been reported in animals, but were not associated with EHEC-induced hemorrhagic colitis. EPEC-induced diarrhea in humans and other animals varies from mild to marked and may be variably blood-tinged if epithelial damage is extensive. The pathogenesis of EPEC-induced diarrhea does not involve toxin production and the exact mechanism is uncertain. Diarrhea is assumed to be due mainly to maldigestion (loss of brush border enzymes) and malabsorption (loss of absorptive surface), thus osmotic in nature, and dependent on lesion extent; alteration of water and ion channels due to the AE lesion may also be involved.[1,11] EHEC-induced diarrhea in humans varies from mild, with only AE lesions, to severe with hemorrhagic colitis (or ileocolitis) and variably HUS; the best known and studied serotype associated with the latter is O157:H7.[1] In other animals, EHEC-induced diarrhea has only been reported, to our knowledge, in calves and a goat.[9,11,12] In calves, lesions are essentially similar to those in humans, but are generally less severe and not associated with HUS.[9,11,12] This has been ascribed to the lack of Stx receptors in bovine endothelial cells; however, Stx does bind to bovine enterocytes and causes epithelial damage.[9]

The main causes of diarrhea in young calves are *E. coli*, type A rotavirus, bovine coronavirus, *Cryptosporidium parvum* and *Salmonella enterica* subsp. *enterica* (mainly serovars Typhimurium and Dublin).[11] With regards to *E. coli*, the overwhelming majority of cases are due to F5+ Sta+ ETECs and are seen as a profuse watery diarrhea in the first 7-10 days of life.[9,10] EPECs and EHECs have been isolated from feces of diarrheic and normal calves, usually 1-5 weeks of age (i.e. older than for ETECs);[9,11] their importance in calf diarrhea is not clear. In autopsy cases, both EPECs and EHECs have been shown to cause diarrhea/enterocolitis in calves, but are much less frequently involved than ETECs and are often associated with other diarrheagenic agents. Clinically, the disease ranges from mild diarrhea to, mostly with EHECs, dysenteric (variably hemorrhagic). In our laboratory, EPECs is rarely diagnosed as the main or sole cause of diarrhea in calves and piglets, usually in immunocompromised animals.

Contributing Institution:
Faculty of veterinary medicine, Université de Montréal. Website: http://www.med-vet.umontreal.ca

JPC Diagnosis:
Small intestine: Enterocyte degeneration, acute, multifocal, moderate, with villar blunting and numerous attached apical coccobacilli.

JPC Comment:
The contributor provides an outstanding explanation of attaching and effacing pathogens, *E. coli* classifications, and differential diagnoses for this case. At the heart of the attaching and effacing activity is a type 3 secretion system (T3SS) that allows the bacteria to inject virulence proteins (effectors) into the host cell cytoplasm. The T3SS is encoded in the LEE, as described by the contributor, which is highly conserved in all attaching-effacing pathogens.[3] Also known as an injectisome, the T3SS contains a syringe shaped structure with a central channel which accommodates translocation of unfolded proteins, and each EPEC cell is estimated to have

twelve needle complexes.[3] Injection of effectors into the host cytosol enables the bacteria to modify host actin cytoskeleton, interfere with ion transport, and prevent formation of microtubules.[3]

Gram-negative bacteria have six dedicated secretion systems, numbered I through VI, which vary in structure and substances which can be transported. T1SS, found in bacteria such as *Vibrio cholerae* and *Serratia marcescens,* can transport substances across two membranes, the inner and outer bacterial membranes, in one step.[5] Types IV and VI can transfer substances across three membranes: both bacterial membranes and one additional host membrane.[5] T4SS is capable of transporting DNA and proteins, and is found in *Brucella suis, Helicobacter pylori*, and *Neisseria gonorrheae,* among others.[5] T6SS, found in *V. cholerea* and *Pseudomonas aeruginosa,* may transfer effectors into host cells but may also be used to secrete substrates into the environment for bacterial communication and competition.[5]

T2SS and T5SS are isolated to the outer bacterial membrane. T2SS is found in most Gram-negative bacteria and transfers folded proteins from the periplasm to the extracellular space.[5] T5SS is unique in that the substrates are auotransporters, forming their own channels in the outer membrane.[5] This system requires proteins in the periplasm to be unfolded prior to secretion, and most of the substrates are virulence factors such as toxins or receptor-binding proteins.[5] Examples include YadA from *Yersinia enterocolitica* and IcsA of *Shigella flexneri.*[5] From assisting with adhesion to secreting toxic effectors, these secretion systems play important roles in pathogenesis of various gram-negative infections.

References:

1. Croxen MA, Law RJ, Scholz R, et al. Recent advances in understanding enteric pathogenic *Escherichia coli*. *Clin Microbiol Rev.* 2013;26(4):822-80.
2. Faubert C, Drolet R. Hemorrhagic gastroenteritis caused by *Escherichia coli* in piglets: Clinical, pathological and microbiological findings. *Can Vet J.* 1992;33(4):251-6.
3. Gaytan MO, Martinez-Santos VI, Soto E, Gonzalez-Pedrajo Bertha. Type Three Secretion system in Attaching and Effacing Pathogens. *Front Cell Infect Microbiol.* 2016; 6(129):1-25.
4. Gomes TA, Elias WP, Scaletsky IC, et al. Diarrheagenic *Escherichia coli*. *Braz J Microbiol*. 2016; 47 (Suppl 1):3-30.
5. Green ER, Mecsas J. Bacterial Secretion Systems – An overview. *Microbiol Spectr.* 2016. 4(1): 1-19.
6. Janke BH, Francis DH, Collins JE, et al. Attaching and effacing *Escherichia coli* infections in calves, pigs, lambs, and dogs. *J Vet Diagn Invest*. 1989;1(1):6-11.
7. Lee JG, Han DS, Jo SV, et al. Characteristics and pathogenic role of adherent-invasive Escherichia coli in inflammatory bowel disease: Potential impact on clinical outcomes. *PLoS One*. 2019;14(4): 1-14.
8. Luperchio SA, Newman JV, Dangler CA, et al. *Citrobacter rodentium*, the causative agent of transmissible murine colonic hyperplasia, exhibits clonality: synonymy of C. rodentium and mouse-pathogenic Escherichia coli. *J Clin Microbiol*. 2000;38(12):4343-50.
9. Moxley RA, Smith DR. Attaching-effacing *Escherichia coli* infections in cattle. *Vet Clin North Am Food Anim Pract.* 2010;26(1):29-56.
10. Ngeleka M, Godson D, Vanier G, et al. Frequency of *Escherichia coli* virotypes in calf diarrhea and intestinal morpho-

logic changes associated with these virotypes or other diarrheagenic pathogens. *J Vet Diagn Invest*. 2019;31(4):611-615.
11. Uzal FA, Plattner BL, Hostetter JM. Alimentary system.In: *Jubb, Kennedy, and Palmer's Pathology of domestic animals*. Vol 2. 6th ed. St.Louis, MO: Elsevier. 2016; 1-257.
12. Wales AD, Woodward MJ, Pearson GR. Attaching-effacing bacteria in animals. *J Comp Pathol.* 2005;132(1):1-26.
13. Yamamoto D, Hernandes RT, Liberatore AM, et al. *Escherichia albertii*, a novel human enteropathogen, colonizes rat enterocytes and translocates to extra-intestinal sites. *PLoS One*. 2017;12(2):1-16.

WSC 2022-2023 Self-assessment.
Conference 7

1. Which of the following is the cause of severe hemorrhagic diarrhea in calves?
    a. Bovine adenovirus-1
    b. Bovine adenovirus-4
    c. Bovine adenovirus-7
    d. Bovine adenovirus-8

2. Which of the cranial nerves is involved in listerial encephalitis?
    a. Facial
    b. Trigeminal
    c. Hypoglossal
    d. Auditory

3. Which of the following is NOT a classic form of listeriosis in ruminant?
    a. Abortion
    b. Enteritis
    c. Encephalitis
    d. Septicemia

4. True or false? *Salmonella dublin* may cause abortion in pregnant cows.
    a. True
    b. False

5. Which of the following forms of pathogenic *E. coli* has not been reported in natural disease in domestic species?
    a. Diffuse-adherent E. coli
    b. Enterotoxigenic E. coli
    c. Enteropathogenic E. coli
    d. Enterohemorrhagic E. coli

Please email your completed assessment for grading to Dr. Bruce Williams at bruce.h.williams12.civ@mail.mil. Passing score is 80%. This program (RACE program 33611) is approved by the AAVSB RACE to offer a total of 0.5 CE Credits, with a maximum of 12.5 CE Credits being available to any individual Veterinary Medical Professionals for the 2019-2020 Wednesday Slide Conference. This RACE approval is for the subject matter categories of: SCIENTIFIC using the delivery method of NONINTERACTIVE DISTANCE. This approval is valid in jurisdictions which recognize AAVSB RACE.

Joint Pathology Center
Veterinary Pathology Services

WEDNESDAY SLIDE CONFERENCE 2022-2023

Conference #8 12 October 2022

CASE I:

Signalment:
10-day-old Red Angus-Simmental calf (*Bos Taurus*) bovine

History:
Over a period of 8 years (2013–2021) a total of six Red Angus-Simmental bull calves were born alive full term with hypotrichosis and oligodontia on a ranch in the Nebraska panhandle, USA. According to the attending veterinarian, the calves appeared almost completely alopecic. Animals tended to die in the first week of life, probably related to being born in spring with associated cold temperatures. The owners kept one calf (current case) alive by housing him indoors, wrapped in an insulated coat. A skin sample was taken to exclude inter-uterine infection with bovine viral diarrhea virus (BVDV), with negative results. The calf was alert and nursed normally. He was euthanized at 10 days of postnatal life in order to characterize cutaneous lesions and to establish whether lesions were present elsewhere, particularly in respiratory tract and oral cavity.

Gross Pathology:
The calf was almost completely devoid of large, guard-type hairs at birth, excepting distal parts of the limbs and tail, eyelids, chin and tragus. Vibrissae were present on the muzzle and chin. Short fine hairs consistent with undercoat were present over the trunk, neck, head and upper two thirds of the limbs. The nasolabial plate was flat and dry. All incisors were absent grossly, a finding that was confirmed radiographically. According to the owner and the attending veterinarian, the other five affected bull calves had a similar phenotype, including the absence of visible teeth. Hooves were unremarkable. Obvious ocular lesions were absent.

Laboratory Results:
A biopsy of aural skin was negative for bovine viral diarrhea virus by antigen ELISA.

Microscopic Description:
Haired skin-subcutis from flank. There is a complete absence of large caliber hair folli-

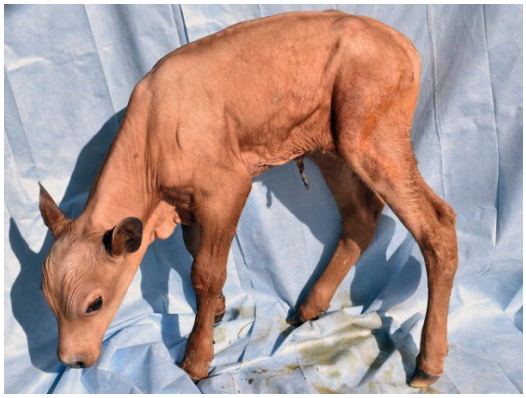

Figure 1-1. Presentation, calf. The calf is partially alopecic with no large guard-type hairs, excepting distal parts of the limbs and tail, eyelids, chin and tragus. Vibrissae were present on the muzzle and chin. The nasolabial labial plate is dry. (Photo courtesy of: Wyoming State Veterinary Laboratory; 1174 Snowy Range Road; Laramie; WY 82070; http://www.uwyo.edu/wyovet/)

cles containing medullated hair shafts. Existing follicles are uniformly small (diameter of 35 - 40 µm) and contain non-medullated, lightly pigmented hairs of unremarkable appearance. Each follicle retains a normal relationship with apocrine glands, arrector pili, and sebaceous glands. There is a mild diffuse lymphohistiocytic inflammation in upper dermis.

Contributor's Morphologic Diagnoses:
1. Severe diffuse congenital hypotrichosis, with absence of primary hair follicles.
2. Mild diffuse superficial lymphohistiocytic dermatitis.

Contributor's Comment:
In addition to hypotrichosis, the affected calf had oligodontia with only 12 deciduous teeth, all of which were unerupted or barely erupted premolars at the time of euthanasia. The calf also lacked nasolabial, tracheal and bronchial-bronchiolar glands. Analysis at the Institute of Genetics in the University of Bern identified a 53 kb deletion in the X chromosome, including part of the *EDA* gene and all of *AWAT2*. Partial deletion of *EDA* is the likely basis for this form of hypotrichosis-oligodontia.[8]

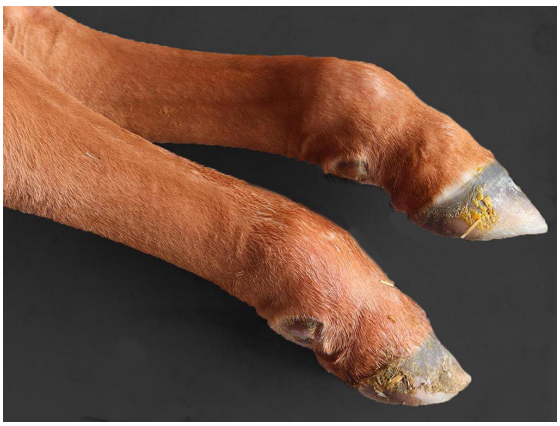

Figure 1-2. Legs, calf. Short fine hairs consistent with undercoat were present over the trunk, neck, head and upper two thirds of the limbs. (Photo courtesy of: Wyoming State Veterinary Laboratory; 1174 Snowy Range Road; Laramie; WY 82070; http://www.uwyo.edu/wyovet/)

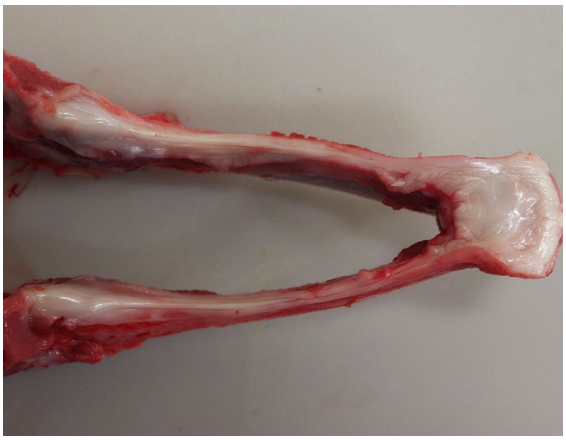

Figure 1-3. Mandible, calf. Incisors and cheek teeth are absent. (Photo courtesy of: Wyoming State Veterinary Laboratory; 1174 Snowy Range Road; Laramie; WY 82070; http://www.uwyo.edu/wyovet/)

This combination of lesions involving hair follicles, teeth and aplasia of selected glands indicates an ectodermal dysplasia.[5] Mutation in *EDA*, marked reduction in large (developmentally first-formed) hair follicles containing medullated hairs, restriction of the disorder to bull calves, and the lesions in non-cutaneous tissues is consistent with an X-linked disease. This is reported sporadically in Holstein and Holstein Friesian cattle, Japanese Black cattle, and crossbred cattle. Currently most of the published reports document one or more affected calves in commercial herds in Europe.[9] Affected calves die or are killed early in post-natal life. Some can be kept alive when fed a chopped diet after they begin to ruminate, combined with protection from weather extremes. Currently 9 episodes of the bovine condition have been documented.[9] The causative abnormality in *EDA* varies. Investigators report various small or gross deletions, insertions, inversions, splicing, and nonsense (stop-gain) mutations. The resultant phenotype is remarkably uniform, based on published accounts. Similar forms of ectodermal dysplasia due to *EDA* variants are reported in dogs, mice, and people.[3] *AWAT2* encodes an enzyme in the diacylglycerol

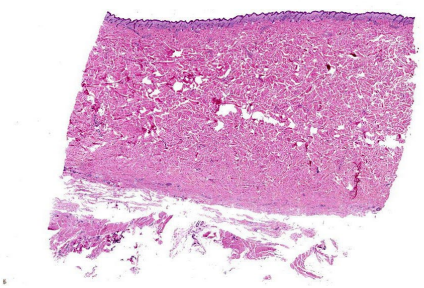

Figure 1-4. Haired skin, calf. The epidermis and superficial dermis are markedly thinned (hypoplasia). (HE, 5X)

acyltransferase family. The enzyme produces wax esters as part of the normal lipid metabolism of skin, primarily in sebocytes. The submitter did not recognize a lesion in sebaceous glands of affected calves.

This bovine ectodermal dysplasia corresponds to X-linked hypohidrotic ectodermal dysplasia-1 in human subjects (ECTD1)(OMIM 305100).[10,13] *EDA* codes for ectodysplasin, a member of the TNF-related ligand family which mediate epithelial-mesenchymal interactions during fetal development, including formation of ectodermal appendages.[11] Use of the term ECTD has been proposed for calves with analogous mutations in *EDA*.[3]

Unlike affected people and mice, there is no simple way to assess the function of sweat glands in neonatal calves. There is disagreement about whether sweat glands in affected calves are histologically normal. The submitter compared sweat glands from affected calves to those in unaffected calves from the source herd and there was no obvious difference.

Affected human patients have a triad of signs comprising sparse hair (hypotrichosis), abnormal or missing teeth (anodontia or hypodontia), and anhidrosis/hypohidrosis. Medical complications in affected people are hyperthermia due to inability to sweat normally, and recurrent respiratory infections. Affected children can be treated successfully using antenatal injections of recombinant ectodysplastin.[12] Treatment was also successful two animal models of ECTD-like syndromes (*Tabby* mice; dogs).[4,6]

It is diagnostically useful to check for oligodontia in calves with marked congenital hypotrichosis, since its presence narrows differential considerations regarding etiology. Calves that are bald at birth will be obvious to owners. It is common for veterinarians to be contacted about such calves. The first question is generally: could this be inherited? Non-genetic causes of congenital hypotrichosis exist, such as transplacental bovine diarrhea virus infection (excluded here), maternal iodine deficiency, and adenohypophyseal hypoplasia. Neonatal calves that present with hypotrichosis, oligodontia and a smooth dry nasal plate should prompt consideration of an inherited abnormally in the EDA molecular pathway. The defect most commonly involves *EDA* itself. Mutations may affect other genes in the pathway (i.e., *EDAR*, *EDARADD* or*TRAF6*), resulting in a similar phenotype.[11]

Mild changes affecting teeth, hair and sweat glands occurs in some mothers of children with ECTD1, but are generally subtle. Investigation of similar changes in carrier carriers and calves is limited.

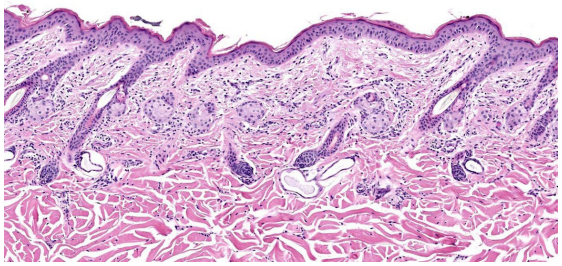

Figure 1-5. Haired skin. The epidermis is hypoplastic, with one cell for each of the basal layer, stratum spongiosum, and stratum corneum. All follicles are in telogen. Hair shafts within telogen follicles are thin with no medulla; deeper telogen follicles are twisted. Sebaceous glands are normal, and there are few lymphocytes and plasma cells within the dermis. (HE, 200X)

Contributing Institution:
Wyoming State Veterinary Laboratory; 1174 Snowy Range Road; Laramie; WY 82070; http://www.uwyo.edu/wyovet/

JPC Diagnosis:
1. Haired skin: Hypotrichosis, diffuse, severe with trichodysplasia.
2. Haired skin: Dermatitis, lymphohistiocytic, superficial and perivascular, mild.

JPC Comment:
This week's moderator, Dr. Charles Bradley from the University of Pennsylvania, emphasized that it is not possible based on histopathologic examination alone to rule out non-genetic causes of hypotrichosis. Other differentials in calves which be considered include iodine deficiency; toxins (*Veratrum album* in Japanese cattle), adenohypophyseal hypoplasia in Guernsey and Jersey cattle, and intrauterine infection with bovine pestivirus (bovine viral diarrhea virus; ruled out in this case using ELISA testing).

Currently, there are nine X-linked *EDA* mutations causing ectodermal dysplasia in various breeds of cattle.[1] Additionally, there is one documented autosomal recessive mutation in the *EDA* receptor gene associated with ectodermal dysplasia in Charolais cattle.[8]

Humans, mice, and cattle with ectodermal dysplasia may lack of normal glands of the respiratory tract, such as bronchial and bronchiolar glands, which compromises mucociliary clearance and predisposes affected animals to respiratory infections, including sinusitis and pneumonia.[1,7,8] Additionally, EDA is crucial for the development and function of lacrimal and Meibomian glands, corneal homeostasis, and corneal wound healing, and recurrent conjunctivitis has been documented in dogs with ectodermal dysplasia and EDA-deficient mice.[1,7,8]

Recently, it has been reported that several mice and rat strains with EDA deficiency also have significant Zymbal's gland hypoplasia, with fewer hair follicles and smaller sebaceous glands in the external ear canal.[2] Affected rodents have increased prevalence of otitis externa, and the authors concluded this was likely due to sebum deficiency.[2] Strains with Zymbal's gland hypoplasia included EDA-deficient mice, EDA receptor (EDAR) deficient mice, and EDAR-associated death domain (EDARADD) deficient rats.[2] The EDA-deficient mice and EDARADD deficient rats were also predisposed to otitis media due to deficiency of nasopharyngeal submucosal glands associated with the auditory tube.[2]

References:

1. Capuzzello G, Jacinto JCP, Hafliger IM, et al. A large deletion encompassing exon 2 of the *ectodysplasin A* (*EDA*) gene in a British blue crossbred calf with hypohidrotic ectodermal dysplasia. *Acta Veterinaria Scandinavica*. 2022; 64(23):1-8.
2. Del-Pozo, Headon DJ, Glover JD, et al. The EDA deficient mouse has Zymbal's gland hypoplasia and acute otitis externa. *Dis Model Mech*. 2022; 15(3):1-31.
3. Drögemüller C, Distl O, Leeb T. X-linked anhidrotic ectodermal dysplasia (*ED1*) in men, mice, and cattle. *Genet Sel Evol.* 2003;35: S137-145.
4. Gaide O, Schneider P. Permanent correction of an inherited ectodermal dysplasia with recombinant EDA. *Nat Med*. 2003;9:614-618.
5. Hargis AM, Ginn PE. The integument. In: Zachary JF, McGavin MD, eds. *Pathologic Basis of Veterinary Disease*. 5th ed. Elsevier Inc. 2012.
6. Mauldin EA, Gaide O, Schneider P, Casal ML. Neonatal treatment with recombinant ectodysplasin prevents respiratory disease in dogs with X-linked ectodermal

dysplasia. *Am J Med Genet A*. 2009;149A:2045-2049.
7. Moura E, Rotenberg IS, Pimap CT. X-Linked hypohydrotic ectodermal dysplasia - General features and dental abnormalities in affected dogs compared with human dental abnormalities. *Top Companion Anim Med.* 2019, 35, 11-17.
8. O'Toole D, Häfliger IM, Leuthard F, et al: 2021, X-linked hypohidrotic ectodermal dysplasia in crossbred beef cattle due to a large deletion in *EDA*. *Animals (MDPI*). 2021;11:657.
9. OMIA - Online Mendelian Inheritance in Animals database search engine. Accessed 27 May 2021. https://www.omia.org/home/
10. OMIM – Online Mendelian Inheritance in Man database search engine. Accessed 27 May 2021. https://www.omim.org/about
11. Sadier A, Viriot L, Pantalacci S, Laudet V. The ectodysplasin pathway: from diseases to adaptations. *Trends Genet*. 2014;30:24–31.
12. Schneider H, Faschingbauer F, Schuepbach-Mallepell S, et al. Prenatal correction of X-linked hypohidrotic ectodermal dysplasia. *N Engl J Med*. 2018;378:1604-1610.
13. Wright JT, Fete M, Schneider H, et al. Ectodermal dysplasias: Classification and organization by phenotype, genotype and molecular pathway. *Am J Med Genet*. 2019, 179, 442-447.

CASE II:

Signalment:
3 year, 7 month old female four-toed hedgehog (*Atelerix albiventris*)

History:
This adult female hedgehog had a brief (2-3 day) history of reduced appetite and unsteady gait before being found dead.

Gross Pathology:
Gross examination revealed a large, solitary, well-demarcated, 1.3 cm x 1.2 cm x 1.8 cm mass in the left axillary region, approximately 0.2 cm lateral to the second left teat. An approximately 3.0 cm x 1.0 cm x 0.4 cm segment of the mass projected cranially through the subcutis, adjoining the axillary lymph node. On cut section, the mass was firm and tan with coalescing red segments. The skin overlying the mass was partially alopecic and hyperkeratotic, while the skin of the pinnae and dorsum exhibited moderate hyperkeratosis and flaking. Internally, two, approximately 2 mm diameter, tan, firm nodules were present in the dorsal aspect of the right lung and there was enlargement of a dorsocranial mediastinal lymph node (1.2 cm x 0.4 cm x 0.3 cm) which was mottled red and tan. Moderate thoracic effusion, approximately 2-3 ml of brown translucent fluid, was present. The spleen was mildly enlarged (5.6 cm x 1.5 cm x 0.4 cm) and diffusely dark purple.

Laboratory Results:
PCR targeting the ITS2 region of the fungal genome (5.8S – 28S), performed on FFPE tissue from the axillary mass, amplified two bands. The first, a 256 bp sequence, was 97.6% identical to GenBank No.

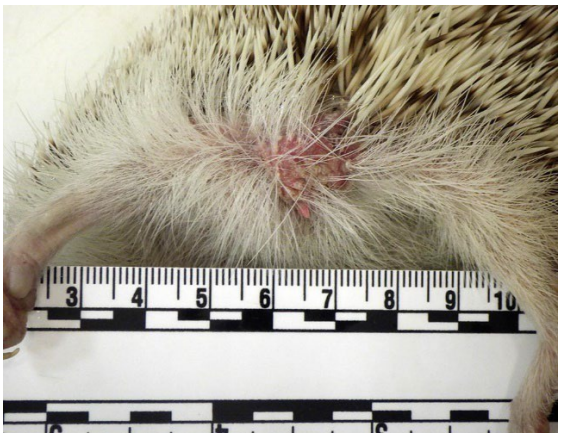

Figure 2-1. Axilla, hedgehog. There is a 1.3 cm nodule within the axillary subcutis. (Photo courtesy of: Wildlife Conservation Society, Zoological Health Program; https://oneworldonehealth.wcs.org; www.wcs.org)

NR_149340, *Trichophyton erinacei* strain ATCC 28443 (Blastn analysis, NCBI). Analysis of this sequence using the ISHAM (International Society for Human and Animal Mycology) Barcoding Database (https://its.mycologylab.org/; accessed June 2021) revealed this sequence to be greater than 99.4% identical to two strains of *T. erinacei*. 367 bp of trimmed DNA sequence was also obtained, and Blastn analysis showed this sequence to be 100% identical to several isolates of *Malassezia restricta*, including GenBank No. EU915456.

Microscopic Description:

Axillary Skin: Markedly expanding and effacing the subcutis, and multifocally effacing skeletal muscle and extending into the dermis is a densely cellular inflammatory infiltrate. The infiltrate is composed of loose nodules of neutrophils, macrophages and multinucleated giant cells with occasional eosinophils, surrounded by a rim of epithelioid macrophages and a thin band of fibrous connective tissue (pyogranulomas). There is multifocal lysis of leukocytes within the center of some pyogranulomas. Similar inflammatory cells, accompanied by lymphocytes, plasma cells and scattered eosinophils and mast cells, fill the space between nodules, leaving little more than small islands of remnant adipose. Within pyogranulomas and within the cytoplasm of scattered multinucleated giant cells are low to moderate numbers of fungal elements. Round to ovoid yeast-like structures ranging in diameter from approximately 5

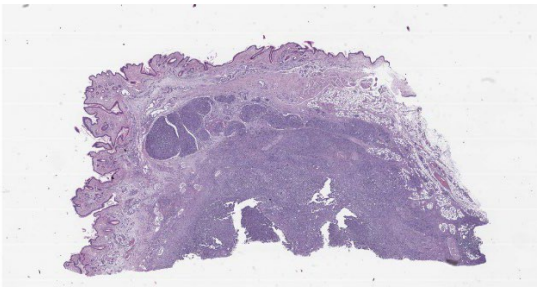

Figure 2-2. Haired skin, hedgehog. There is an extensive focus of pyogranulomatous inflammation within the deep dermis and subcutis. (HE, 12X)

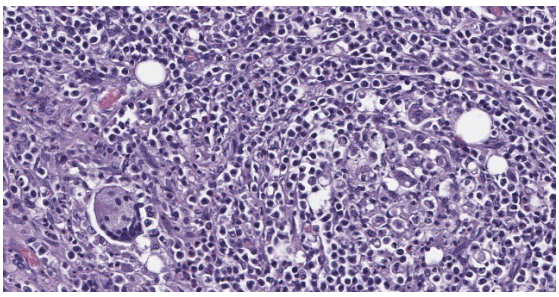

Figure 2-3. Haired skin, hedgehog. The inflammatory nodule is composed of innumerable neutrophils, macrophages, lymphocytes, and plasma cells, with numerous multinucleated macrophages including some ranging up to 60um, enmeshed in strands of collagen. (HE, 376X)

µm up to approximately 15 µm in diameter which display occasional budding and often form tight clusters and knots are most prevalent. Rare elongate cytoplasmic protrusions are present and some yeast-like structures have thick, refractile capsules with an internal granular appearance. Chains of round or more elongate yeast-like structures, each individual unit separated from the next by septation with a waist-like indentation, are also present, as are branching true hyphae. A dense fibrous capsule which contains relatively few lymphocytes and plasma cells multifocally separates the inflammation from the surrounding tissue. In some areas, inflammation extends into the superficial dermis, where higher numbers of eosinophils and mast cells are present. Clear space (edema), pale basophilic granular material and/or inflammatory cells expand lymphatic vessels throughout the dermis. Endothelial cells lining vessels in areas of inflammation are enlarged with prominent nuclei with open chromatin. Degeneration, necrosis and regeneration are present in the inflamed skeletal muscle deep to the dermis. The overlying epidermis exhibits mild orthokeratotic hyperkeratosis and there are scattered aggregates of yeast within the keratin (approximately 3 µm diameter).

Contributor's Morphologic Diagnoses:
Skin, axillary: Cellulitis, dermatitis, pyogranulomatous to mixed, chronic, locally extensive, marked, with intralesional and intracorneal fungal elements.
Skin, axillary: Hyperkeratosis, orthokeratotic, chronic, diffuse, mild, with intracorneal yeast

Contributor's Comment:
Systemic fungal infection identified in this four-toed hedgehog (*Atelerix albiventris*) was most severe in the left axillary subcutis, where a large inflammatory mass was present, but also involved the lungs and multiple lymph nodes. Histology of the lungs and lymph nodes was similar to that described in the axillary region, with the additional findings of bronchiolitis and vasculitis in the lung, and vasculitis and rare intralesional bacteria (gram-negative bacilli) in the lymph nodes. Fungi within lesions were largely round to ovoid yeast-like forms of varying size, with occasional thick capsules and internal granularity, and multifocally forming chains. The appearance was somewhat reminiscent of *Blastomyces* species. Branching hyphae and chains of more elongate structures, representing abnormal arthroconidiation or pseudohyphae were also present, as were rare elongate structures similar to germ tubes. PAS and GMS staining markedly enhanced visualization of fungi. Pan-fungal PCR utilizing primers targeting the ITS2 region amplified two separate and discrete bands, both of which were sequenced and were consistent with *Trichophyton erinacei* and *Malassezia restricta*, respectively; *T. erinacei* was suspected to be the primary etiology.

Trichophyton erinacei, formerly *T. mentagrophytes* var. *erinacei* and of the *T. benhamiae* complex, is a common isolate from hedgehog skin, with both clinical disease and subclinical carrier states being identified in

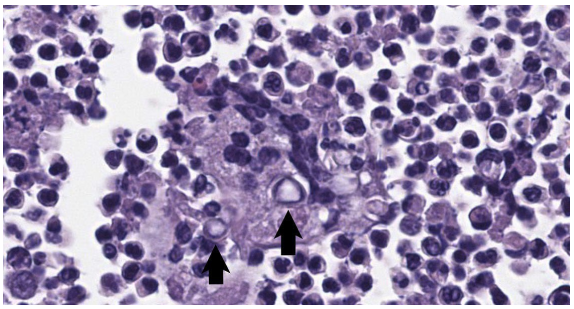

Figure 2-4. Haired skin, hedgehog. Macrophages and multinucleated cells often contain phagocytized 8-14 µm yeasts (arrows). A pseudohypha or germ tube is present adjacent to the yeast at left. (HE, 576X)

free-ranging and pet European (*Erinaceus europaeus*) and four-toed hedgehogs.[1] In one study investigating dermatophytosis in European hedgehogs at a wildlife center in France, over 79% of the *T. erinacei* culture-positive animals were asymptomatic and overall 20% of animals without skin disease were culture positive for *T. erinacei*.[7] When present, disease associated with *T. erinacei* in hedgehogs presents with scaling, crusting and alopecia, including loss of spines; the head is often the focus of infection.[1,2,7] While the histologic appearance of dermatophytosis in hedgehogs is not well described, it is expected to consist of fungal hyphae limited to the keratin layers and the hair/spine shafts, with mild inflammation and proliferative changes to include epidermal hyperplasia and hyperkeratosis, as described in other species.[5,9] In addition to the large axillary inflammatory mass, this patient had a focal area of fungal dermatitis on the foot which was reddened grossly (no flaking or crusting) and histologically exhibited orthokeratotic hyperkeratosis with intracorneal hyphae. This was interpreted as a potential second, more typical, area of *T. erinacei* dermatomycosis, although fungal identification was not pursued at this site.

Dermatophytosis is relatively common in both domestic animals and humans. It is caused by keratinophilic fungi, typically belonging to one of three genera: *Trichophyton*, *Epidermophyton* and *Microsporum*.[3,9] Der-

matophyte species are further classified according to natural history; these categories include the zoophilic species which primarily infect animals but can be transmitted to humans, the anthropophilic species which primarily infect humans, and the geophilic species which are typically found in the soil but can also infect animals and humans.[3,9] *Trichophyton erinacei* is an example of a zoophilic dermatophyte, and one that may be considered an emerging pathogen based on increases in human and pet infections.[2] Dermatophytes can be readily transmitted between animals and between animals and humans via direct contact with infected animals or indirect exposure to shed hairs (made brittle and easily broken by infection) and desquamated keratin containing infective spores.[9] While normal, intact skin resists infection, minimal damage to the epidermis can predispose to infection.[3] As alluded to above, the typical presentation consists of superficial lesions with fungi restricted to the stratum corneum of the epidermis and hair follicles and/or the hair shafts themselves. Deep infection by dermatophytes is rare in humans but can be prominent in animals, and includes both kerion (solitary inflammatory nodules, often with draining tracts) and pseudomycetoma (subcutaneous inflammatory nodules). Development of deep infection can result from implantation or furunculosis of affected follicles.[9]

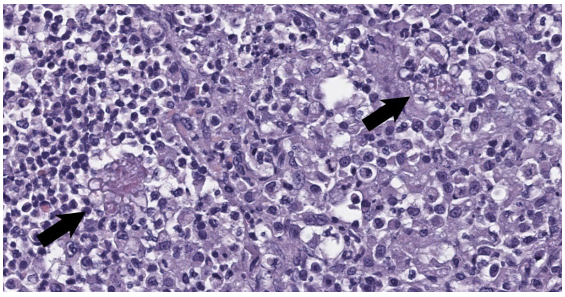

Figure 2-5. Haired skin, hedgehog. Clusters of 8-14 µm yeasts and pseudohyphae are scattered throughout the inflammatory nodules (arrows). (HE, 576X)

Deep and/or systemic/disseminated trichophytosis in hedgehogs due to *T. erinacei* has not been described. In the sections examined from this case, folliculitis was not observed, nor was there specific evidence of furunculosis, such as hair or keratin within lesions. The presence of eosinophils, most notably in the dermis, was suggestive of furunculosis, however, and this remains a possibility, especially given the apparent chronicity of the case. One of the most interesting features in this case was the fungal morphology. *Trichophyton* species are typically hyphal when found superficially[5] and morphologic forms like those seen in the current case have not been described with *T. erinacei*. However, *T. rubrosum*-associated deep mycoses in humans can contain atypical forms of the fungus, including *Blastomyces*-like yeast forms as seen here, as well as short, thickened hyphal fragments and arthroconidia.[8,10,11,12] Descriptions of atypical dermatophyte morphology have to date been restricted to immunocompromised patients, in whom deep dermatophytoses are typically described, and have been limited to *T. rubrosum* in humans. While immune compromise was not confirmed in this hedgehog, marked lymphoid depletion in the spleen could indicate some degree of underlying immunodeficiency; the bone marrow was unremarkable. As in humans, superficial dermatophytosis was suspected to precede the deep infection in this hedgehog and more typical fungal hyphae were identified within the stratum corneum via GMS staining.

Malassezia restricta, identified via PCR, was considered an incidental finding. This is a yeast that is part of the normal skin flora of humans and for which there are no descriptions of abnormal morphologies, or hyphal elements, in tissue. Yeast were present on the surface of the skin which may have been responsible for the positive PCR result. Confirmation of the fungal species within the

deep lesions would require immunohistochemistry, in-situ hybridization or other advanced diagnostic modalities, none of which were pursued in this case.

Additional findings of note in this hedgehog included vacuolation in brain and spinal cord, predominantly affecting the white matter in the latter with more generalized distribution in the brain. This was similar to lesions described with "wobbly hedgehog syndrome (WHS)," a somewhat common idiopathic condition in hedgehogs and WHS could have contributed to those signs. This was a slightly unusual case in that WHS clinical signs are typically insidious in onset, rather than the acute onset in the current case, and other causes of vacuolation were not ruled out. It is possible that this lesion was incidental and the perceived neurologic signs the result of patient weakness and debilitation due to systemic fungal disease. There was also acute renal tubular degeneration and necrosis attributed to pulmonary disease and tissue hypoxia, and chronic hepatic and biliary changes suggestive of prior biliary obstruction.

This case highlighted the importance of ancillary testing for fungal disease, including culture and/or molecular diagnostics, rather than reliance on tissue fungal morphology alone.

Contributing Institution:
Wildlife Conservation Society, Zoological Health Program;

- https://oneworldonehealth.wcs.org
- www.wcs.org

JPC Diagnosis:
Haired skin: Dermatitis and cellulitis, pyogranulomatous, focally extensive, severe, with numerous fungi.
Haired skin: Hyperkeratosis, orthokeratotic, diffuse, mild, with superficial yeast.

JPC Comment:
The contributor provides a thorough report of *Tricophyton erinacei* infection in hedgehogs. Similar to *T. erinacei*, hedgehogs have a high prevalence of *mecC*-methicillin resistant *S.* aureus (MRSA), with carriage rates of 60-64% in various studies in wild European hedgehogs (*Europeaus erineaus*).[4] The *mecC* gene encodes penicillin-binding protein 2c (PBP2c) and confers resistance to most beta-lactam antibiotics. Most *mecC*-MRSA infections occur in Europe, and it was initially isolated in bulk milk tanks and human infections in Europe.[4] Dairy cattle were thought to be the reservoir, and it was believed that administration of beta-lactam antibiotics selected for resistant bacteria.[4,6] While recent studies confirm that antibiotic exposure has indeed selected for *mecC*-MRSA resistance, a different antibiotic source has been incriminated: the cohabitant *T. erinacei*.

Penicillin-producing dermatophytes and penicillin-resistant *S. aureus* were first documented in hedgehogs in the 1960s, and it was recently demonstrated that *T. erinacei* from wild hedgehogs encodes and expresses the same antibiotic-encoding genes as *Penicillium chrysogenum*, with some isolates actively producing benzylpenicillin.[4] A subsequent *in vitro* study showed that the fungus has greater growth inhibition on *mecC*-deleted MRSA mutants compared to *mecC*-

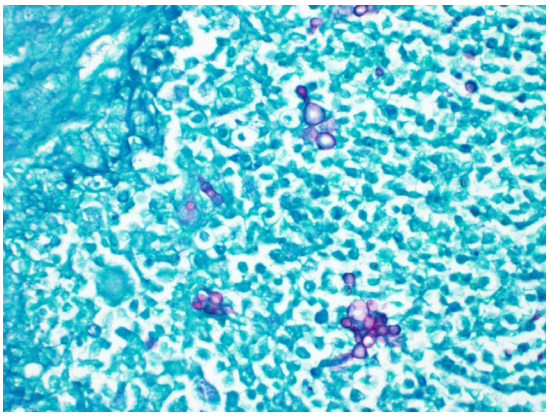

Figure 2-6. Haired skin, hedgehog. Yeasts form pseudohyphae and multidirectional chains. (PAS, 400X)

MRSA.[6] These results strongly suggest that *T. erinacei* has imposed a selective pressure on *S. aureus* which favors resistance. Furthermore, phylogenetic studies have indicated that resistance of many *mecC*-MRSA lineages was acquired prior to the modern use of antibiotics. This is supported by the fact that *T. erinacei* isolates from hedgehogs in New Zealand have produced the same antibiotic resistance in *mecC*-MRSA, and these hedgehogs were imported from Europe in the 1800s.[6]

There is wide diversity but geographic clustering of *mecC*-MRSA isolates in hedgehogs.[4] Most isolates lack the genetic variations required to infect humans and cattle, implying that methicillin-resistance did not originate in these other species.[6] Furthermore, human and hedgehog isolates within the same geographic region have similar patterns of genetic variation.[6] Coupling these facts with the high prevalence of *mecC*-MRSA in hedgehogs, researchers have concluded that hedgehogs are the natural reservoir for *mecC*-MRSA, and, for this strain, antibiotic resistance developed due to selective pressure from *T. erinacei* and predates medical use of antibiotics.[6]

References:

1. Abarca ML, Castella G, Martorell J, Cabanes FJ. *Trichophyton erinacei* in pet hedgehogs in Spain: Occurrence and revision of its taxonomic status. *Med Mycol*. 2017;55:164-172.
2. Cmokova A, Kolarik M, Dobias R, et al. Resolving the taxonomy of emerging zoonotic pathogens in the *Trichophyton benhamiae* complex. *Fungal Diversity*. 2020;104:333-387.
3. Donnelly TM, Rush EM, Lackner PA. Ringworm in small exotic pets. *Sem Av Ex Pet Med*. 2000;9:82-93.
4. Dube F, Soderlund R, Salomonsson ML, Troell K, Borjesson S. Benzylpenicillin-producing *Trichophyton erinacei* and methicillin resistant *Stapylococcus aureus* carrying the *mecC* gene on European hedgehogs – A pilot study. *BMC Microbiology.* 2021; 21:212-222.
5. Gregory MW, English MP. *Arthroderma benhamiae* infection in the Central African hedgehog, *Erinaceus albiventris*, and a report of a human case. *Mycopathologia*. 1975;55:143-147.
6. Larsen J, Raisen CL, Ba X, et al. Emergence of methicillin resistance predates the clinical use of antibiotics. *Nature*. 2022; 602:135-141.
7. Le Barzic C, Cmokova A, Denaes C, et al. Detection and control of dermatophytosis in wild European hedgehogs (*Erinaceus europaeus*) admitted to a French wildlife rehabilitation centre. *J Fungi*. 2021;7:74-87.
8. Lillis JV, Dawson ES, Chang R, White CR. Disseminated dermal *Trichophyton rubrum* infection – an expression of dermatophyte dimorphism? *J Cutan Pathol*. 2010;37:1168-1169.
9. Mauldin EA, Peters-Kennedy J. Integumentary system. In: Maxie, MG, ed. *Jubb, Kennedy and Palmer's Pathology of Domestic Animals Volume 1*. 6th ed. Elsevier; 2016.
10. Nir-Paz R, Elinav H, Pierard GE, et al. Deep infection by *Trichophyton rubrum* in an immunocompromised patient. *J Clin Microbiol*. 2003;41:5298-5301.
11. Squeo RF, Beer R, Silvers D, Weitzman I, Grossman M. Invasive *Trichophyton rubrum* resembling blastomycosis infection in the immunocompromised host. *J Am Acad Dermatol*. 1998;39:379-380.
12. Talebi-Liasi F, Shinohara MM. Invasive *Trichophyton rubrum* mimicking blastomycosis in a patient with solid organ transplant. *J Cutan Pathol*. 2017;44:798-800.

CASE III:

Signalment:
5-year-old spayed female European Shorthair cat (*Felis catus*)

History:
The cat had a chronic history of diffuse exfoliative dermatitis with multifocal alopecia, in particular in the region of head, trunk and limbs with scaling, hair casts, flakes, easy detachable hairs and moderate itching.

Based on clinical history the main differential diagnoses were: demodicosis, dermato-phytosis, exfoliative dermatitis (thymoma associated or not), and sebaceous adenitis.

Gross Pathology:
Four skin biopsies (8 mm punch and surgical scissors excision) were performed at the level of the neck (right side), costate, right thigh.

Laboratory Results:
Microbiology: negative.
Deep skin scraping: negative.
PAS stain: negative.

Microscopic Description:
Haired skin. Haired skin is affected by a moderate inflammatory change involving hair follicles and obscuring sebaceous glands. Follicular walls are transmurally infiltrated, mainly in the region of isthmus and extending to the other portions, by a high number of lymphocytes and a lower number of macrophages and rare neutrophils. Keratinocytes of the outer root sheath frequently have vacuolated cytoplasm and rarely are shrunk-en, hypereosinophilic with pyknotic nuclei (apoptosis). In the superficial dermis a mild perivascular to interstitial inflammatory infiltrate composed, in a similar amount, of mast cells, lymphocytes, plasma cells and eosinophils is present associated with scant interstitial edema.

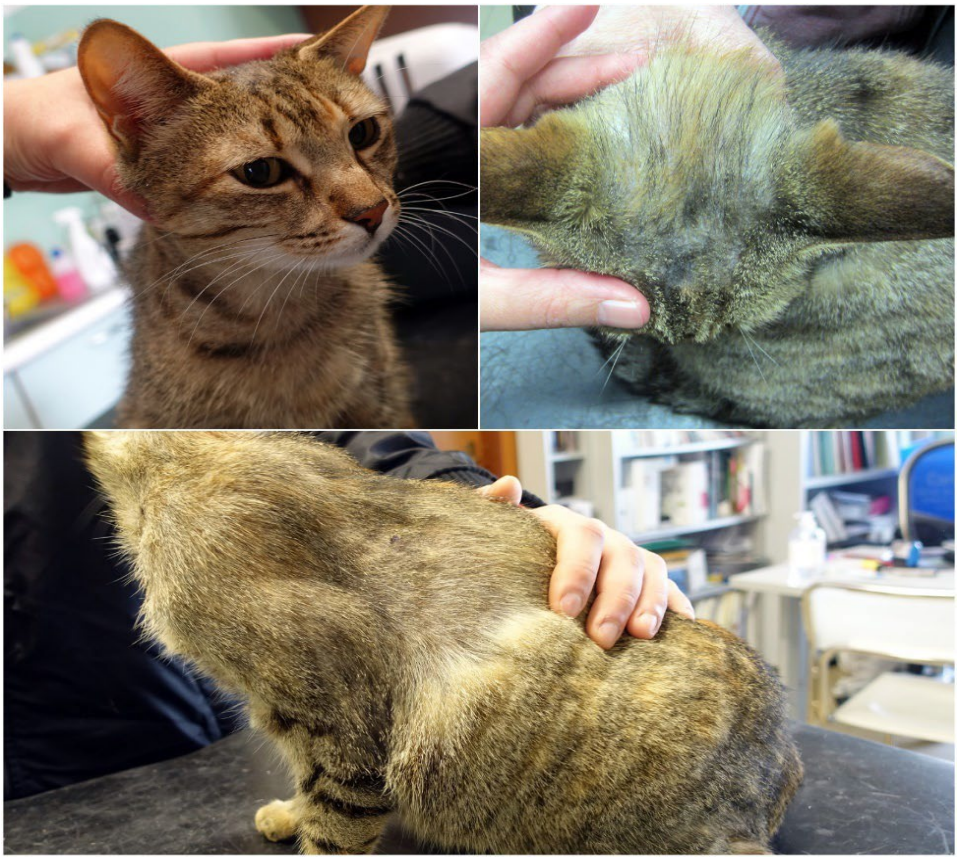

Figure 3-1. Presentation, cat. "Lola" has patchy alopecia, especially on the head and flank.on the head and flank. (Photo courtesy of: San Marco Veterinary Clinic and Laboratory, Pathology division, Viale dell'Industria 3, 35030, Veggiano (PD), Italy, https://www.clinicaveterinari-asanmarco.it/))

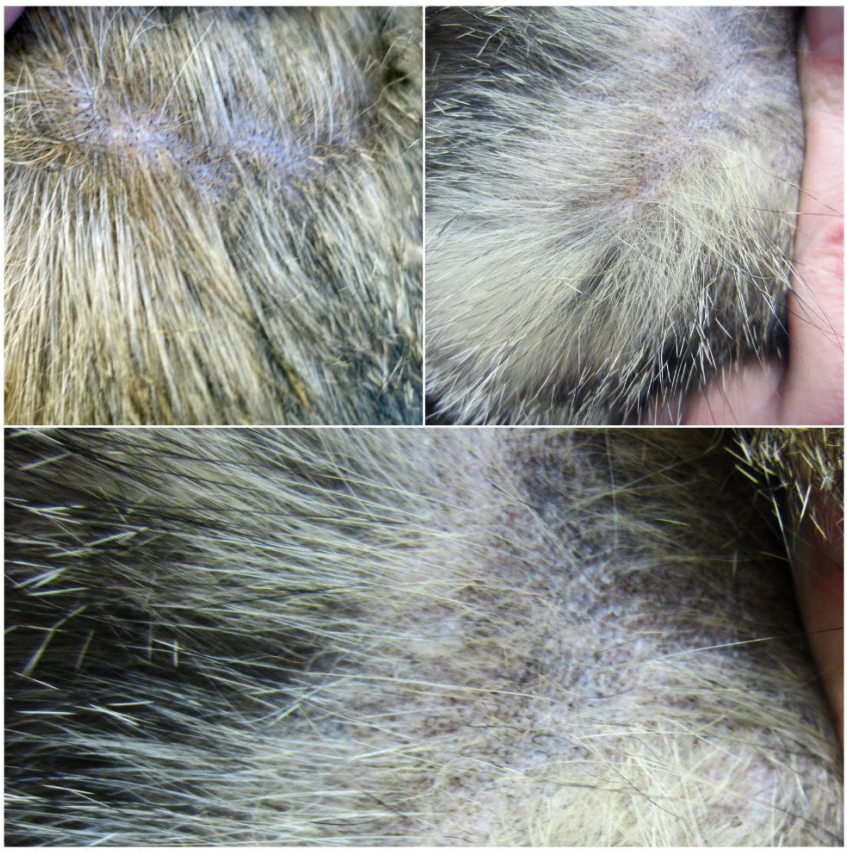

Figure 3-2. Presentation, cat. Hairs are easily detached, and there is skin flaking and hair casts. (Photo courtesy of: San Marco Veterinary Clinic and Laboratory, Pathology division, Viale dell'Industria 3, 35030, Veggiano (PD), Italy, https://www.clinicaveterinariasanmarco.it/)

Contributor's Morphologic Diagnoses:
Haired skin:
-moderate chronic lymphocytic mural folliculitis with loss of sebaceous glands
-mild perivascular to interstitial superficial dermatitis lymphoplasmacytic, with mast cells and eosinophils

Contributor's Comment:
Histopathological findings are consistent with a sebaceous adenitis associated with mural folliculitis. Sebaceous adenitis is an uncommon disease in dogs and rabbits and extremely rare in cats.

Sebaceous adenitis in dogs, although it has idiopathic origin, in standard poodles and akitas can be inherited through an autosomal recessive gene with variable expression. Hypothesis made for its pathogenesis include a cornification disorder, a cell-mediated destruction of sebaceous glands, an anatomic defect in sebaceous glands leading to lipid leakage and a foreign body response, and a metabolic defect in lipid metabolism leading to a cornification abnor-mality and sebaceous gland destruction.[1,3,6]

Histology of canine sebaceous adenitis varies depending on the duration of disease and the breed affected. In the early stages histological lesions are characterized by a granulomatous to pyo-granulomatous inflammation targeting the sebaceous glands while, in the chronic stage, which are more frequently submitted to laboratories, appears in an almost total loss of sebaceous glands. Severe epidermal orthokeratotic hyperkeratosis and follicular keratosis are invariably present. In Standard Poodles, the late stage of disease may be characterized by follicular atrophy and an absence of sebaceous glands, while in Vizslas inflammation

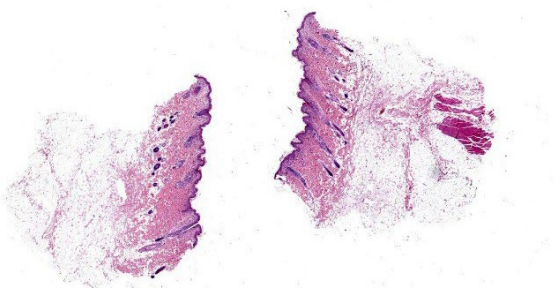

Figure 3-3. Haired skin, cat. Two sections of haired skin are submitted for examination. (HE, 14X)

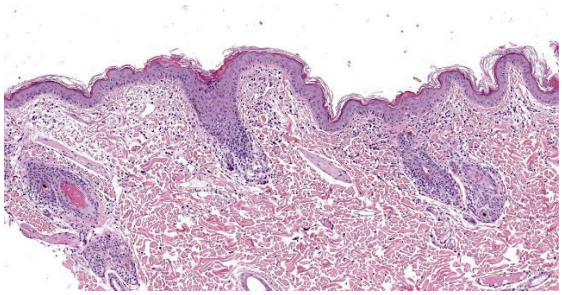

Figure 3-4. Haired skin, cat. Each follicle is infiltrated by numerous lymphocytes. (HE, 108X)

is more consistently prominent at all stages of the disease and the main differential diagnosis, in this case, is leishmaniasis.[1,3]

In rabbits, in addition to what is described in dogs, an interface dermatitis and an interface folliculitis are often present, suggesting that sebaceous adenitis may be only one aspect of a more generalized disorder.[10]

In cats, it is rarely described and it occurs as a chronic progressive disease with non-itchy scaling, crusting, alopecia and skin depigmentation in regions of the face, cervical and trunk which are the same features found in the case described except for pruritus. The latter has been described to be related to secondary infections and/or *Malassezia* spp. overgrowth.[2,4,6]

In our case, the definitive diagnosis was established histologically. The main lesions were the loss of sebaceous glands and a mural folliculitis, prominent in the isthmic region. The former is frequently described in sebaceous adenitis in different species; the latter is a reaction pattern of cats that has been associated with several diseases, included sebaceous adenitis but also with allergic dermatoses.[7] In this case, once dermatophytosis and demodicosis were excluded with special stains, negative cultures and deep skin scraping, histological lesions associated with clinical presentation led to the diagnosis of sebaceous adenitis with mural folliculitis. Treatments proposed include cyclosporin therapy; in one case, topical fatty acid supplementation was also reported.[2,4] Our case improved quickly with a cyclosporin therapy.

Contributing Institution:
San Marco Veterinary Clinic and Laboratory Pathology division
Viale dell'Industria 3, 35030
Veggiano (PD), Italy
https://www.clinicaveterinariasanmarco.it/

JPC Diagnosis:
1. Haired skin: Sebaceous adenitis, lymphocytic, diffuse, marked with sebaceous gland loss and multifocal mural folliculitis.
2. Haired skin: Dermatitis, mastocytic and eosinophilic, superficial and perivascular, mild.

JPC Comment:
One hallmark gross lesion of sebaceous adenitis is the follicular cast, as demonstrated in figure 3-2, which appear grossly as flaky concretions surrounding the bases of hair shafts, though this is less common in short haired dogs.[9]

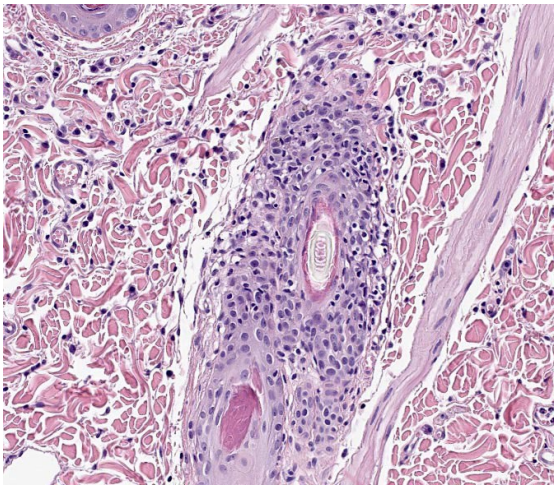

Figure 3-5. Haired skin, cat. Lymphocytes efface sebaceous glands and infiltrate the outer root sheath of the follicular infundibulum. (HE, 357X)

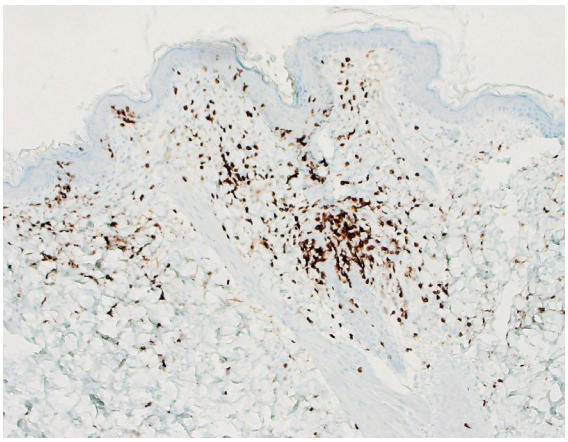

Figure 3-6. Haired skin, cat. Lymphocytes infiltrating follicles and adnexa demonstrate strong cytoplasmic immunopositivity for CD-3. (anti-CD3, 200X)

As the contributor mentioned, a main gross differential in this cat is exfoliative dermatitis. Histologically, the mural folliculitis of exfoliative dermatitis is focused on the infundibulum and isthmus and is frequently accompanied by secondary sebaceous adenitis or absence of sebaceous glands, which may mimic sebaceous adenitis.[9] Exfoliative dermatitis can be differentiated, however, by its variable lymphocytic interface dermatitis with hydropic degeneration of basal keratinocytes, suprabasilar keratinocyte apoptosis, and orthokeratotic hyperkeratosis.[9]

Standard poodles are predisposed to a sebaceous adenitis, in addition to a few other autoimmune diseases, including primary hypoadrenocorticism. This high incidence of these two diseases have been linked to an artificial genetic bottleneck which occurred in the mid 20th century resulting from the closed breed registry and intensive breeding of a handful of show-winning dogs, including Sir Gay, Wycliffe Jacqueline, Bel Tor, Carillon, and a few other dogs with equally grandiose names. [5] A study of pedigrees and DLA (MHC) markers in standard poodles from the US, Canada, and Europe showed that this mid-century bottleneck decreased genetic diversity within 70% of the standard poodle population and concentrated the genetic polymorphisms underlying sebaceous adenitis and primary adrenocorticism. [5] Geneticists recommend careful mate selection based on pedigree and genetic testing to improve the diversity within the breed and decrease incidence of disease within this breed.[5] As there is no currently available DNA test for sebaceous adenitis, the Orthopedic Foundation for Animals (OFA) recommends histologic evaluation of biopsies every 1 to 2 years in breeding animals greater than 12 months of age to assist in removing affected animals from the breeding population.[8]

References:

1. Bardagì M, Fondevila D, Zanna G et al. Histopathological differences between canine idiopathic sebaceous adenitis and canine leishmaniosis with sebaceous adenitis. *Veterinary Dermatology*. 2010; 21: 159-165.
2. Glos K, von Bomhard W, Bettenay S et al. Sebaceous adenitis and mural folliculitis in a cat responsive to topical fatty acid supplementation. *Veterinary Dermatology*. 2016; 11:57-60.
3. Gross TL et al. *Skin diseases of the dog and cat*. Second edition. Blackwell Publishing; 2005.
4. Noli C, Toma S. Three cases of immune-mediated adnexal skin disease treated with cyclosporine. *Veterinary Dermatology*. 2006;17: 85–92.
5. Pederson NC, Brucker L, Tessier NG, et al. The effect of genetic bottlenecks and inbreeding on the incidence of two major autoimmune diseases in standard poodles, sebaceous adenitis and Addison's disease. *Canine Genetics and Epidemiology*. 2015 (2):14-32.
6. Possebom J, de Farias MR, de Assunção DL et al. Sebaceous Adenitis in a Cat. *Acta Scientiae Veterinariae*. 2015; 43:1-5.
7. Rosenberg AS, Scott DW, Hollis N et al. Infiltrative lymphocytic mural folliculitis: a histopathological reaction pattern in

skin-biopsy specimens from cats with allergic skin disease. *Journal of Feline Medicine and Surgery*. 2010; 12: 80-85.
8. Sebaceous adenitis. OFA. Accessed October 12, 2022. https://ofa.org/diseases/other-phenotypic-evaluations/sebaceous-adenitis/
9. Welle MW, Linder KE. The Integument. In: Zachary JF, ed. *Pathologic Basis of Veterinary Disease.* St. Louis, MO: Elsevier. 2022; 1246-1247,1261.
10. White SD, Linder KE, Shultheiss P et al. Sebaceous adenitis in four domestic rabbits. *Veterinary Dermatology*. 2000; 11: 53-60.

CASE IV:

Signalment:
4-year-old, intact male, mix breed canine (*Canis lupus familiaris*)

History:
A 4-year-old, intact male, medium-sized (~15 Kg of body weight), mix breed dog was presented to the veterinary clinic with multiple (5) skin nodules in the right knee, thoracic region, dorsal aspect of the nose, and right and left thoracic limbs. In the initial clinical examination, the dog was normothermic, bright, alert and responsive, had good body condition and muscle tone, adequate hydration state, normal capillary refill time, and adequate coloration of the mucous membranes.

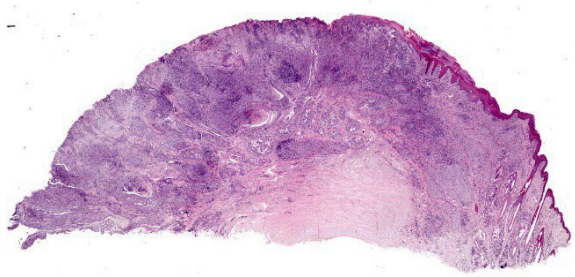

Figure 4-1. Pawpad and haired skin, dog. A single section of pad and adjacent haired skin is submitted for examination. The fat pad and eccrine glands of the pad is effaced by coalescing poorly formed granulomas. (HE, 5X)

The dog was treated empirically and unsuccessfully with enrofloxacin and prednisone. After one month of treatment, the animal was presented again to the clinic with vomiting, diarrhea, and partial loss of vision. The larger mass, located in the left thoracic limb, was surgically biopsied for histologic examination.

Gross Pathology:
A firm, raised skin nodule covered by ulcerated and alopecic epidermis.

Laboratory Results:
No laboratory results reported.

Microscopic Description:
Haired skin. Diffusely expanding the dermis and subcutaneous tissue and elevating the overlying epidermis, there is a dense inflammatory cellular infiltrate composed predominantly of activated and epithelioid macrophages, occasional multinucleated giant cells, lymphocytes, plasma cells, and fewer neutrophils. Admixed with the inflammatory cells, there are numerous extracellular and intrahistiocytic microorganisms and pyknotic and karyorrhectic cellular debris (necrosis). Microorganisms (algae) are mildly pleomorphic, mostly spherical to ovoid, and range between 4 and 17 µm in diameter, with a 2 to 4 µm, often surrounded by a clear halo. Algal cells contain granular flocculent amphophilic material and a distinctly basophilic nucleus. Some algal cells present internal septation with daughter cells (endosporulation). The overlying epidermis is extensively ulcerated or lost, and the superficial dermis covered by extravasated fibrin and necrotic cellular debris, there is extensive fibrosis with perpendicularly-oriented blood vessels lined by plumped epithelium (neovascularization/granulation tissue), scattered fibrin thrombi in small-caliber superficial venules and microhemorrhage.

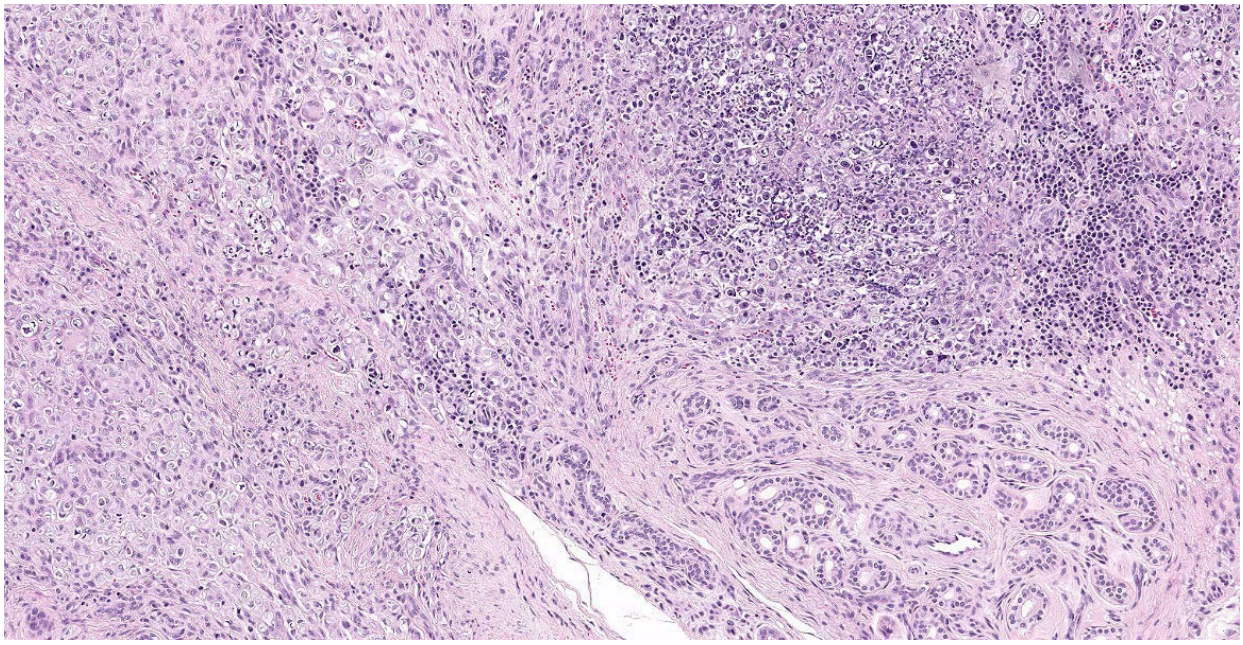

Figure 4-2. Pawpad and haired skin, dog. Poorly formed granulomas efface the pawpad adipose tissue. Eccrine glands are present at lower right. (HE, 126X)

Algal cells are highlighted by GMS stain and PAS reaction.

Contributor's Morphologic Diagnoses:
Haired skin: severe granulomatous and ulcerative dermatitis/panniculitis, with multinucleate giant cells and myriads of intrahistiocytic and extracellular algal microorganisms morphologically resembling *Prototheca* spp., *Canis lupus familiaris*.

Contributor's Comment:
Differential diagnoses on clinical grounds in this case included multifocal/multicentric neoplasia with cutaneous involvement, and granulomatous/pyogranulomatous dermatitis/panniculitis caused by infectious agents, mostly bacterial or fungal infections. The microscopic examination of the biopsy with HE, GMS and PAS stains revealed severe granulomatous dermatitis with intralesional algae morphologically consistent with *Prototheca* spp. as depicted in the submitted slides. Additionally, as part of the diagnostic investigation, formalin-fixed paraffin-embedded skin was processed for molecular identification of *Prototheca* spp. at the Centers for Disease Control and Prevention (CDC) in Atlanta, Georgia. For molecular confirmation and speciation, a polymerase chain reaction-restriction fragments length polymorphism (PCR-RFLP) was performed as previously described.[14] The agent was identified as *P. zopfii* genotype 1.

Thus, the diagnostic investigation in this case allowed for unequivocal confirmation of *P. zopfii* genotype 1 infection in a dog, by a combination of morphological and molecular methods.

Protothecosis is a rare disease caused by environmental algae of the genus *Prototheca*, saprophytes of worldwide distribution that can infect mammals, and result in either localized or systemic, life-threatening disease, particularly in immunocompromised individuals.[15,21] *Prototheca* spp. is a non-photosynthetic, achlorophyllic (colorless), aerobic alga in the family *Chlorellaceae*. Seven *Prototheca* species have been described to date,[11] of these *P. zopfii* and *P. wickerhamii* have

been more commonly implicated in pathogenic infections in humans and animals,[21,2,16] while the novel species *P. miyajii* was isolated recently from a human patient with systemic protothecosis.[11] Within *P. zopfii* species, two different genotypes (1 and 2) are currently recognized; genotype 2 is the most commonly involved in different clinical forms.[2,13]

Prototheca spp. have been associated with various syndromes in different species. The most commonly recognized forms of human protothecosis are disseminated, cutaneous, and olecranon bursitis.[12] In cattle, mastitis is the more common manifestation,[13] while rhinitis and sinusitis have been described in horses.[18] In dogs, protothecosis is usually associated with colitis and/or disseminated disease, sometimes with ocular,[19] or central nervous system involvement.[3,10] The infection restricted only to the skin is rare in this species,[5] although it appears to be the most common form in the cat.[7] The cutaneous form in the dog is usually associated with *P. wickerhamii* infection,[21,16,4] although it has recently been described in a case of *P. zopfii* genotype 2 infection.[2] The case presented here represents the first documentation of *P. zopfii* genotype 1 infection in a dog.[20]

The pathogenesis of protothecosis in dogs is not yet fully elucidated. Ingestion has been regarded as the most likely route of transmission in most cases of disseminated protothecosis by *P. zopfii*;[21] however, cutaneous entrance through skin trauma or penetration through mucosal surfaces have also been documented.[15,21,3,10]

Reports on genotypic characterization of *P. zopfii* strains infecting dogs in South America were limited to one description of the genotype 2 in Brazil,[17] which had also been implicated in cases of bovine mastitis in this country.[14] This genotype has also been detected in diseased dogs in Italy,[2] and the USA.[9] A large epidemiological, phenotypic and molecular analysis of 350 clinical *Prototheca* isolates, including 342 bovine strains from around the world, 6 canine strains (3 from Germany, 2 from Brazil and 1 from USA) and 2 human

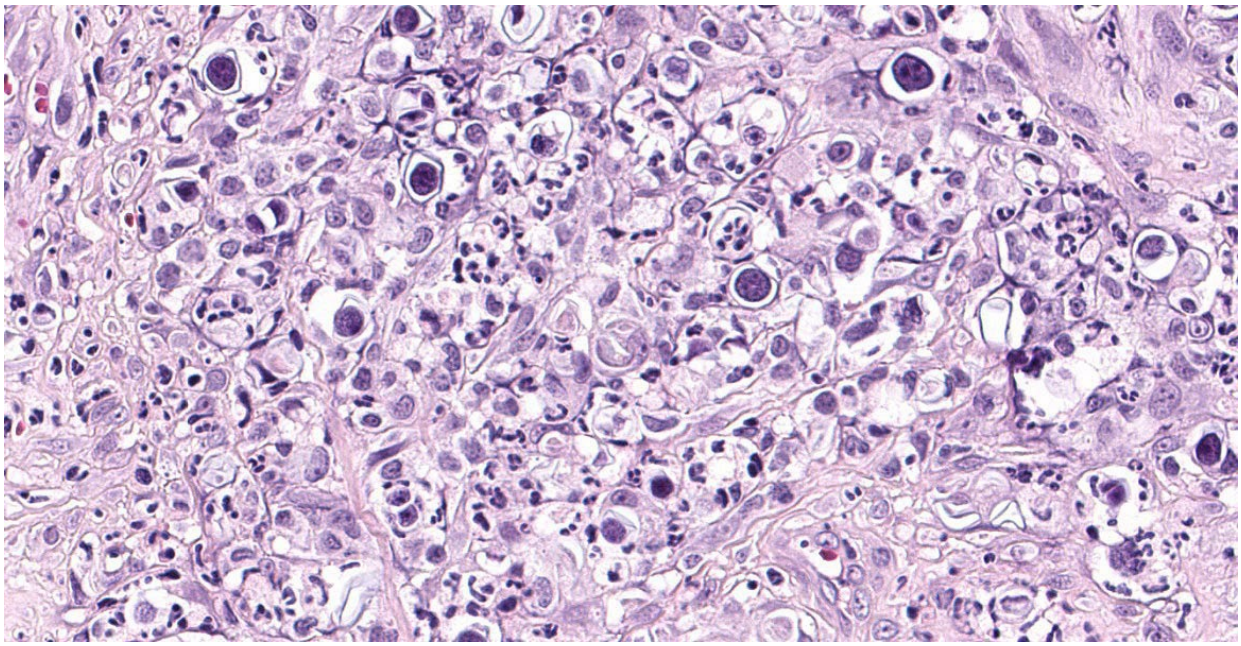

Figure 4-3. Pawpad and haired skin, dog. Numerous algae, including endosporulating forms and empty cell walls are phagocytized by epithelioid macrophages and multinucleated giant cells. (HE, 400X)

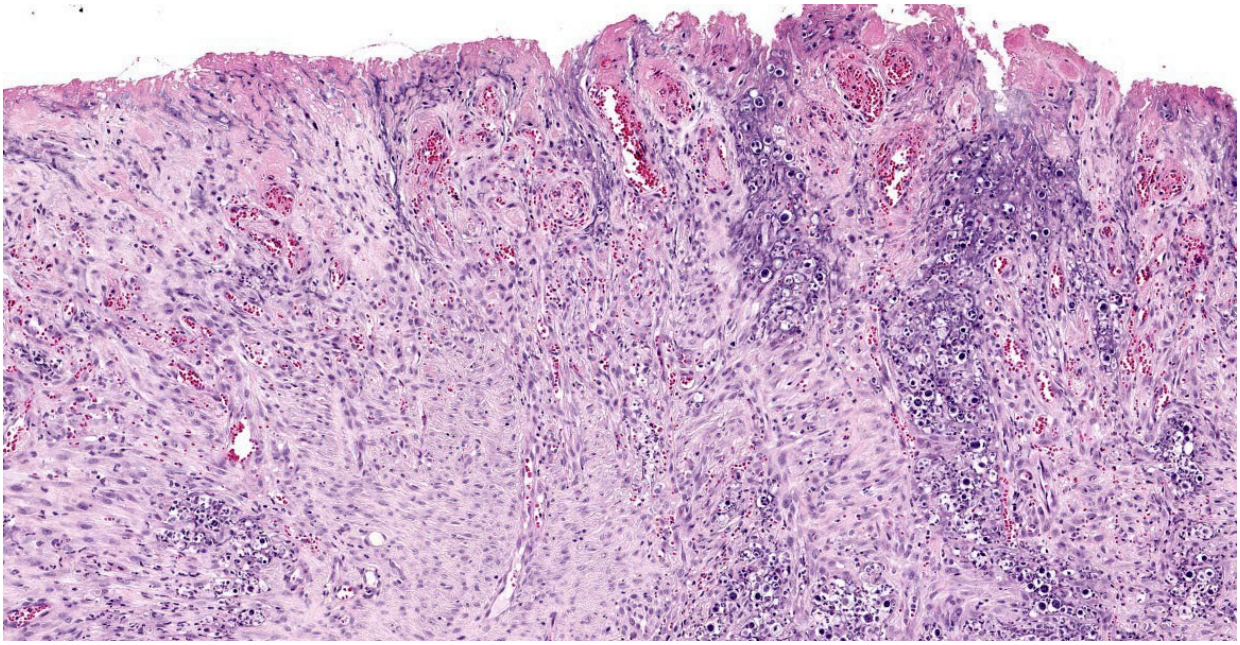

Figure 4-4. Pawpad and haired skin, dog. There is granulation tissue and fibrosis subjacent to the ulcerated pad, and algae-laden macrophages reach up to the ulcerated surface. (HE, 123X)

strains (1 from Austria and 1 from China), revealed that 90.6% of the bovine isolates and 100% canine and human isolates were *P. zopfii* genotype 2.[1] *P. zopfii* genotype 1 was only found in 2 (0.5%) of the 342 bovine isolates, both from Germany.[1] Despite this overall low frequency of detection in clinical cases, *P. zopfii* genotype 1 has recently been linked to human protothecosis,[6] which opposes to previous knowledge that considered this genotype as non-pathogenic.[8]

Contributing Institution:
Plataforma de Investigación en Salud Animal, Instituto Nacional de Investigación Agropecuaria (INIA), Uruguay, www.inia.uy

JPC Diagnosis:
Pawpad and haired skin: Pododermatitis, ulcerative and granulomatous, focally extensive, severe, with numerous intrahistiocytic and extracellular algae.

JPC Comment:
Since this case was submitted in 2018, *Prototheca* taxonomy has expanded to include 15 species, 6 of which are known to cause disease in humans or animals.[12] Additionally, *Prototheca zopfii* genotypes 1 and 2 have been established as their own species: *P. ciferrii* and *P. bovis*, respectively.[12]

In addition to the species described above, *P. wickerhamii* can infect the nose and face of goats causing proliferative and ulcerative nodules of pyogranulomatous inflammation admixed with sporangia which may extend into the nose or underlying bone.[19] Disseminated infection in goats has not been reported, and it appears sheep are either extremely rarely infected or not infected by *Prototheca*.[19]

In contrast, sheep can be infected by a related chlorophyll-containing green algae, *Chlorella*.[19] Infection may be limited to the liver and mesenteric lymph nodes or may be systemic, and the algae produces characteristic green discoloration that persists during formalin fixation but is lost during processing.[19] *Chlorella* sporangia also contain PAS-positive cytoplasmic granules (chloroplasts) that *Prototheca* lacks. *Chlorella* infection has

also been documented in humans, cattle, a dromedary camel, and a dog.[19]

References:

1. Ahrholdt J, Murugaiyan J, Straubinger RK, Jagielski T, Roesler U. Epidemiological analysis of worldwide bovine, canine and human clinical *Prototheca* isolates by PCR genotyping and MALDI-TOF mass spectrometry proteomic phenotyping. *Med Mycol*. 2012;50(3):234–243.
2. Carfora V, Noris G, Caprioli A, Iurescia M, Stravino F, Franco A. Evidence of a *Prototheca zopfii* genotype 2 disseminated infection in a dog with cutaneous lesions. *Mycopathologia*. 2017; 182:603–608.
3. Font C, Mascort J, Marquez M, Esteban C, Sanchez D, Durall N, Pumarola M, Lujan-Feliu-Pascual A. Paraparesis as initial manifestation of a *Prototheca zopfii* infection in a dog. *J Small Anim Prac.* 2014; 55:283–286.
4. Ginel PJ, Perez J, Molleda JM, Lucena R, Mozos E. Cutaneous protothecosis in a dog. *Vet Rec*. 1997;140: 651–653.
5. Gross TL, Ihrke PJ, Walder EJ, Affolter VK. Infectious nodular and diffuse granulomatous and pyogranulomatous diseases of the skin. In: Gross TL, Ihrke PJ, Walder EJ, Affolter VK, editors. Skin diseases of the dog and cat. Oxford, UK: Blackwell Publishing Inc;2005:272–319.
6. Hirose N, Hua Z, Kato Y, Zhang Q, Li R, Nishimura K, Masuda M. Molecular characterization of *Prototheca* strains isolated in China revealed the first cases of protothecosis associated with *Prototheca zopfii* genotype 1. *Med Mycol.* 2018; 56(3):279–287.
7. Huth N, Wenkel RF, Roschanski N, Rösler U, Plagge L, Schöniger S. *Prototheca zopfii* genotype 2-induced nasal dermatitis in a cat. *J Comp Pathol*. 2015; 152:287–290.
8. Irrgang A, Murugaiyan J, Weise C, Azab W, Roesler U. Well-known surface and extracellular antigens of pathogenic microorganisms among the immunodominant proteins of the infectious microalgae *Prototheca zopfii*. *Front Cell Infect Microbiol*. 2015; 5:67.
9. Lane LV, Meinkoth JH, Brunker J, Smith SK 2nd, Snider TA, Thomas J, Bradway D, Love BC. Disseminated protothecosis diagnosed by evaluation of CSF in a dog. Vet Clin Pathol. 2012;41(1):147–152.
10. Marquez M, Rodenas S, Molin J, Rabanal RM, Fondevila D, Añor S, Pumarola M. Protothecal pyogranulomatous meningoencephalitis in a dog without evidence of disseminated infection. *Vet Rec.* 2012; 171:100.
11. Masuda M, Hirose N, Ishikawa T, Ikawa Y, Nishimura K. *Prototheca miyajii* sp. nov., isolated from a patient with systemic protothecosis. *Int J Syst Evol Microbiol*. 2016; 66:1510–1520.
12. Masuda M, Jagielski T, Danesi P, et al. Protothecosis in Dogs and Cats – New Research Directions. *Mycopathologia*. 2021;186:143-152.
13. Mayorga J, Gómez JFB, Martínez APV, Estrada VFM, Welsh O. Protothecosis. *Clin Dermatol*. 2012; 30:432–436.
14. Moller A, Truyen U, Roesler U. *Prototheca zopfii* genotype 2-the causative agent of bovine protothecal mastitis? *Vet Microbiol*. 2007; 120:370–374.
15. Morandi S, Cremonesi P, Capra E, Silvetti T, Decimo M, Bianchini V, Alves AC, Vargas AC, Costa GM, Ribeiro MG, Brasca M. Molecular typing and differences in biofilm formation and antibiotic susceptibilities among *Prototheca* strains isolated in Italy and Brazil. *J Dairy Sci*. 2016; 99(8):6436–6445.
16. Pal M, Abraha A, Rahman MT, Dave P. Protothecosis: an emerging algal disease of humans and animals. *Int J Life Sci Biotechnol Pharm Res*. 2014; 3:1–13.

17. Papadogiannakis EI, Velonakis EN, Spanakos GK, Koutinas AF. Cutaneous disease as sole clinical manifestation of protothecosis in a boxer dog. *Case Rep Vet Med*. 2016;1–4.
18. Ribeiro MG, Rodrigues de Farias M, Roesler U, Roth K, Rodigheri SM, Ostrowsky MA, Salerno T, Sigueira AK, Fernandes MC. Phenotypic and genotypic characterization of *Prototheca zopfii* in a dog with enteric signs. *Res Vet Sci.* 2009;87(3):479–481.
19. Riet-Correa F, do Carmo PMS, Uzal FA. Protothecosis and chlorellosis in sheep and goats: a review. *Jour Vet Diag Invest.* 2021; 33(2): 283-287.
20. Schöniger S, Roschanski N, Rösler U, et al. *Prototheca* species and *Pithomyces chartarum* as causative agents of rhinitis and/or sinusitis in horses. *J Comp Pathol*. 2016; 155:21–125.
21. Shank AM, Dubielziq RD, Teixeira LB. Canine ocular protothecosis: a review of 14 cases. *Vet Ophthalmol.* 2015; 18:437–442.
22. Silveira C, Cesar D, Keating K, DeLeon-Carnes M, Armién AG, Luhers M, Riet-Correa F, Giannitti F. A case of *Prototheca zopfii* genotype 1 infection in a dog (C*anis lupus familiaris*). *Mycopathologia*, 2018, in press.
23. Stenner VJ, Mackay B, King T, et al. Protothecosis in 17 Australian dogs and a review of the canine literature. *Med Mycolo.* 2007; 45:249–266.

WSC 2022-2023 Self-assessment.
Conference 8

1. True or false? Oligodontia-hypotrichosis is primarily seen in bull calves.
    a. True
    b. False

2. Which of the following is not a cause of non-genetic alopecia in calves?
    a. Maternal iodine deficiency
    b. Adenohypophyseal hypoplasia
    c. Maternal Vitamin A deficiency
    d. Transplacental bone pestivirus infection

3. *Trichophyton erinacei* is previously a subspecies of which of the following dermatophytes?
    a. *Trichophyton mentagrophytes*
    b. Microsporum canis
    c. Trichophyton verrucosum
    d. Microsporum gypseum

4. True or false? The histologic findings of sebaceous adenitis vary between affected breeds.
    a. True
    b. False

5. Which of the following is the most common form of protothecosis in cattle??
    a. Mastitis
    b. Olecranon bursitis
    c. Enteritis
    d. Rhinitis

Please email your completed assessment for grading to Dr. Bruce Williams at bruce.h.williams12.civ@mail.mil. Passing score is 80%. This program (RACE program 33611) is approved by the AAVSB RACE to offer a total of 0.5 CE Credits, with a maximum of 12.5 CE Credits being available to any individual Veterinary Medical Professionals for the 2019-2020 Wednesday Slide Conference. This RACE approval is for the subject matter categories of: SCIENTIFIC using the delivery method of NONINTERACTIVE DISTANCE. This approval is valid in jurisdictions which recognize AAVSB RACE.

Joint Pathology Center
Veterinary Pathology Services

WEDNESDAY SLIDE CONFERENCE 2022-2023

Conference #9 2 November 2022

CASE I:

Signalment:
11½ -year-old, spayed female, American Bulldog, canine (*Canis lupus familiaris*)

History:
Two years ago, this canine presented for routine examination and recent increased urination. Ultrasound confirmed mass-like lesions at the trigone and the neck of the urinary bladder. The attending veterinarian suspected transitional cell carcinoma at the time. The owners elected for conservative treatment, so the canine was started on nonsteroidal anti-inflammatory drugs (NSAIDs), famotidine, omeprazole, and gabapentin.

Four months ago, the canine started coughing intermittently. Radiographs revealed multiple chest masses with metastatic pattern and osteophytes of the left distal humerus, suspicious of an early metastatic lesion.

A month later, the canine presented with lameness on the right front paw. Radiographs revealed periosteal reaction and sclerosis in the 2nd metacarpal bone. Not long after, euthanasia was elected due to pain on the right front limb and poor quality of life.

Gross Pathology:
This is the carcass of a 31 kg spayed overconditioned female canine with no autolysis. The lungs have a dozen variable-sized firm masses, ranging from 1 cm scattered throughout to a large 12x10 cm obliterating 50% of the caudal left lobe. The masses are bulging, well demarcated and off-white pale to reddish in color. They are distending and replacing the normal pulmonary parenchyma. The mediastinal lymph nodes are enlarged (1 cm x 5 cm) and flat in shape. On cut section, there are small white nodules (0.3 cm).

The kidneys are within normal limits. The urinary bladder mucosa at the level of the trigone has a soft, 1 cm thick, off-white, fuzzy irregular layer that covers 5 cm around the trigone extending into the urethra. The fundus of the bladder has three masses up to 1.5 cm in diameter that are firm, nodular and protruding.

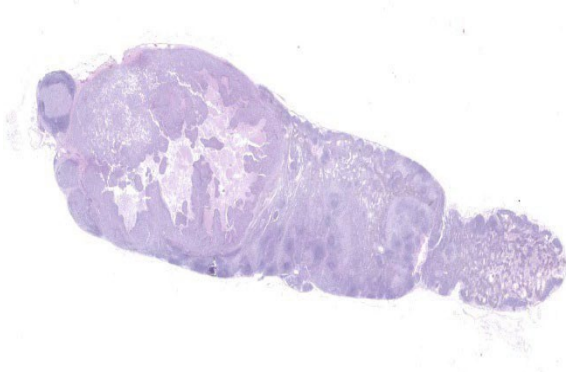

Figure 1-1. Lymph node, dog. A section of lymph node is submitted for examination. There is a large neoplasm which effaces 50% of the node (left). (HE, 6X)

Other lymph nodes, right axillary, mesenteric and retroperitoneal, are firm and slightly enlarged.

The liver has a diffuse, mild reticular pattern with occasional white pale well-demarcated foci (up to 0.5 cm).

The free edges of the left atrioventricular valve have multiple variable-sized nodules (1 mm) with a smooth surface.

The second right metacarpal bone has a 3 cm in diameter hard mass that extends into the proximal phalanx and the distal carpal bone. Upon opening the bone, the mass is necrotic and extends and effaces the carpal bone.

Laboratory Results:
No findings reported.

Microscopic Description:
Lymph node- mediastinal: There is a well-demarcated unencapsulated expansile nodule that effaces the normal follicular lymphoid architecture. The nodule is composed of fronds of thick undulating ribbons of tightly packed neoplastic cells supported by a fine fibrovascular stroma.

Neoplastic epithelial cuboidal to polyhedral cells with abundant pale eosinophilic cytoplasm. The cells show moderate anisokaryosis and anisocytosis with occasional megalokaryosis. There are areas where the cells are less compacted and the cytoplasm has variable-sized empty vacuoles. Occasionally, the large vacuoles displace the nucleus to the periphery. Some of the vacuoles occasionally contain a homogenous granular material. The core of the neoplastic nodule has a large necrotic area.

There are 20 mitotic figures in 10HPF (40x), with a moderate number of aberrant mitotic figures.

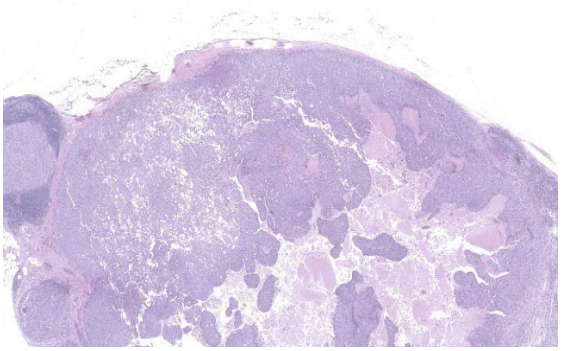

Figure 1-2. Lymph node, dog. There are large areas of necrosis within the metastatic neoplasm. (HE 18X)

There are small nodules of neoplastic cells in the subcapsular sinuses. These nodules are present only in some of the sections.

Contributor's Morphologic Diagnoses:
Lymph node: metastatic transitional cell carcinoma/urothelial carcinoma

Contributor's Comment:
Transitional cell carcinoma (TCC), or urothelial carcinoma (UC), is a malignant tumor that originates in the transitional epithelium of the urinary tract. Squamous and glandular carcinomas can also occur. The urinary bladder is the most common site of the lesion, but it can occur anywhere form the renal pelvis to the distal urethra. Within the urinary bladder, TCC is most commonly diagnosed in the trigone area. TCC mostly occurs in cats and dogs. Bladder neoplasms are rare in horses, sheep, goats, and pigs.

Carcinomas in the urinary bladder can be classified in broad groups: Urothelial carcinoma, squamous cell carcinoma, adenocarcinoma, or undifferentiated carcinoma. This is based on the predominant cell type or the organization of the lesion. Urothelial carcinomas (UC) can be further classified based on their patterns of growth as papillary (project into the lumen), flat, degree of anaplasia (graded on a scale of 1-4), and degree of infiltration (infiltrating or noninfiltrating).

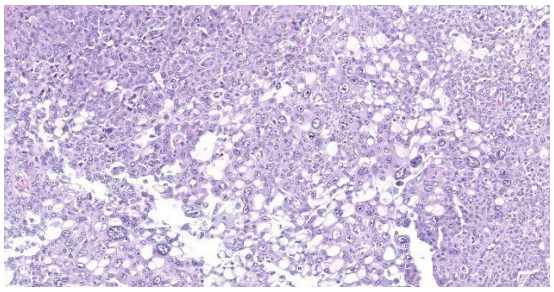

Figure 1-3. Lymph node, dog. In some areas of the tumor, closely-packed tubules lend a "sieve-like" appearance. (HE, 162X)

Most TCCs are intermediate to high-grade papillary infiltrative tumors.

TCC/UC tend to occur in older dogs (average 9-11 years). There is an approximate 2:1 ratio of female: male for bladder neoplasm but this is not always a consistent finding. However, neutered dogs seem to be predisposed to bladder neoplasms. Some breeds, like Scottish terriers. Airedales, Shetland sheepdogs, West Highland white terriers, fox terriers or beagles, have a high risk for TCC/UC than other dogs.

Of all the canine cases of TCC/UC, 90% demonstrate clinical signs. These signs include hematuria, pollakiuria, cystitis or dysuria. These urinary system clinical signs are not unique to neoplasms. Other clinical signs that are not related to the urinary system are mostly due to metastasis. These can include lameness due to bone metastasis or hypertrophic osteopathy, or dyspnea due to pulmonary metastasis.

Most of the literature suggests that tumors of the urinary bladder are less common in cats than in dogs. Cats with TCC/UC are usually older (6-18 years). Most of the clinical signs relate to the lower urinary tract: hematuria, stranguria, dysuria, and pollakiuria. Current urinary tract infection is present in over 70% of the cats with TCC.

If TCC/UC is suspected, the diagnostic work-up should include complete blood count, serum biochemistry profile, urinalysis, urine culture, radiographs (thorax and abdomen), and bladder imaging. Urine should be collected only by free catch or bladder catheterization. Ultrasound is useful to assess the bladder wall thickness but also for viewing regional lymph nodes and other abdominal organs for metastases. A diagnosis of TCC/UC requires histopathologic confirmation.

It can be difficult to differentiate tumors in the prostatic region of male dogs as urothelial origin or prostatic origin. About 30% of TCC/UCs are in the prostate and in neutered dogs it is the most common prostatic tumor. This should be carefully considered when determining the origin of a neoplasia in the prostatic region. Factors that favor TCC/UC Melamed-Wolinska bodies, UPIII immunoreactivity, CK7 immunoreactivity, desmoplasia, and widespread metastasis.

High grade, invasive TCC/UCs are among the most malignant neoplasms and cause death via metastasis and cachexia. Upon diagnosis in canine patients, about 20% have detectable pulmonary metastases, 15% have lymph node metastases, and 6% have lumbar or pelvic bone metastases. In addition, squamous or glandular metaplasia may be important in the prediction of metastases.

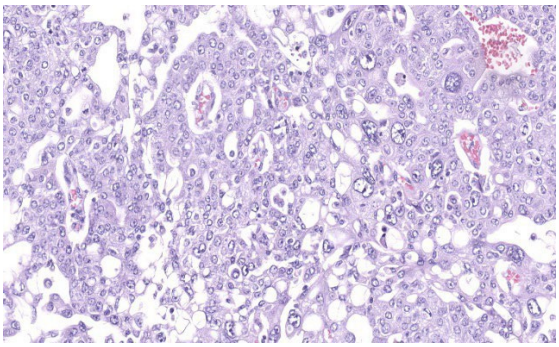

Figure 1-4. Lymph node, dog. There is multifocal nuclear pleomorphism and gigantism scattered throughout the tumor. (HE, 284X)

Prognosis of dogs with TCC/UC is grave. Less than 20% of treated dogs live more than one year.

In humans, most of the cancer associated death, approximately 90%, are caused by metastatic disease rather than primary tumor. The effort to further characterize the neoplastic dissemination has expanded the research in carcinogenesis. First, to understand the metastatic dissemination behind this process, a sequence of a multi-step process of invasion is proposed: the metastatic cascade: 1) epithelial primary neoplastic cell invasion into the surrounding stroma tissue and extra cellular matrix; 2) epithelial cell intravascular invasion; 3) neoplastic epithelial cells need to survive during circulatory transit. 4) neoplastic cell arrest and extravasation through vascular walls and into the parenchyma or distant tissue; 5) formation of microneoplastic colonies. Second, in addition to the metastatic cascade, the neoplastic cells need to be transformed and the concept of epithelial mesenchymal transition (EMT) has been expanded to further characterize carcinogenesis. EMT is a complex biological process where the epithelial cells acquire new properties to successfully invade tissue. These properties include 1) increased motility invasion and 2) ability to degrade extracellular matrix. These EMT properties show at different levels depending on the tissue site and the degree of malignancy. EMT is orchestrated by different tissue transcription factors starting with EMT-inducing transcription factors (EMT-TFs) such as SNAIL, SLUG, or ZEB1. There is still controversial evidence about how much these biological process are involved in metastasis. The other current metastatic process is the dormant niche, where dormant disseminated tumor cells will reside within the site of stem cells and somehow will be protected.

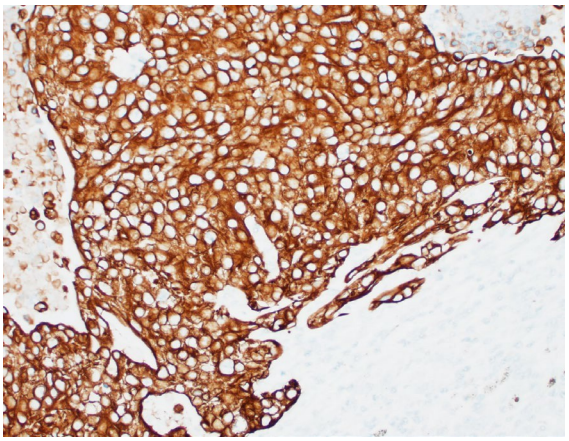

Figure 1-5. Lymph node, dog. Neoplastic cells demonstrate strong cytoplasmic immunopositivity for cytokeratin. (anti-AE1/AE3, 284X)

Primary and metastatic tumors of the bladder occur in dogs and rarely in cats; several tumor types have been reported. Hematuria is a common sign. Metastatic bladder neoplasia is rare but some of the signs listed below are

due to metastases. It has been associated with hypertrophic osteoarthropathy. Systemic signs of urinary obstruction are seen if urine flow at the trigone is blocked. Tumor cells might be present in the urine. Benign polyps of the urinary bladder induce clinical, laboratory and radiographic characteristics similar to neoplasia of the bladder.

Transitional cell carcinoma (TCC) is the most common cancer of the bladder in dogs. Tumors most commonly originate in the trigone, but they can also occur or extend through the urethra. The most common metastatic sites are the iliac and other abdominal lymph nodes, liver and lung. Ultrasonography of the abdomen is done to measure the size of the tumor and look for metastases within the abdomen. When the tumor is accessible, surgery is the best option to prolong survival for dogs with TCC when followed by chemotherapy. Regardless of whether surgery is possible or not, chemotherapy has been shown to alleviate symptoms and prolong survival for many dogs with TCC.

Contributing Institution:
https://www.westernu.edu/veterinary/

JPC Diagnosis:
Lymph node: Urothelial carcinoma, metastatic.

JPC Comment:
Recently, a urine assay measuring the $BRAF^{V595E}$ mutation was developed that provides clinicians with a non-invasive means of differentiating cystitis from neoplasia.[3,8] The BRAF assay has a high sensitivity and sensitivity for the mutation, which affects approximately 70% of dogs with urothelial carcinoma.[3,8] The $BRAF^{V595E}$ mutation in dogs is analogous to the $BRAF^{V600E}$ mutation in many human cancers. The mutation causes constituent activation of the MAPK pathway, preventing apoptosis of neoplastic cells and increasing invasiveness and metastasis.[8] A few recent studies found no significant difference in survival times in UCs with and without the $BRAF^{V595E}$ mutation; the mutation does, however, make the neoplasm more amenable to treatment. Dogs with $BRAF^{V595E}$ mutation treated with chemotherapy or both chemotherapy and surgery had double or triple the survival times, respectively, compared to dogs treated with NSAID therapy alone.[5]

In dogs, the BRAF mutation has also been associated with increased CCL17 expression, which is significantly higher than levels in healthy dogs or dogs with non-neoplastic urinary disease.[8] This is due to overexpression of COX-2 by neoplastic cells, which stimulates production of PGE-2 and upregulation of CCL17. [8] The end effect of CCL17 elevation is infiltration of Foxp3+ regulatory T cells (T-reg) within and surrounding the neoplasm.[8] In many cancers, T-regs are associated with a poor prognosis, possibly due to inhibition of antitumor immune activity.[8]

The overproduction of COX-2 by neoplastic cells has made NSAIDs, such as peroxicam, one of the main therapeutic agents used to prolong UC survival times.[4,8] A recent study found LOX-5 was similarly overproduced by comparing immunohistochemistry scores of UC, cystitis, and normal bladder mucosa.[4] These results suggest that NSAIDs with anti-LOX-5 activity may provide another target for prolonging survival times and should be investigated further.[4]

References:

1. Anesi S, Parry AT, Monti P, Elliott J. Radiographic appearance of an osseous metastasis to the distal radius from a transitional cell carcinoma of the urinary bladder. *Veterinary Record Case Reports*. 2017; *5*(4): p.e000474.
2. Epstein JI, Lotan TL. The Lower Urinary Tract and Male Genital System. In: Kumar V, Abbas AK, Aster JC, eds: *Robbins and Cotran Pathologic Basis of Disease.* Philadelphia, PA: Elsevier Saunders. 2015: 976-981.
3. Ettinger S. Urine luck: A new test for canine bladder and prostate cancer. *DVM360.* July 29, 2019. Accessed October 16, 2020. https://www.dvm360.com/view/urine-luck-new-test-canine-bladder-and-prostate-cancer
4. Finotello R, Schiavo L, Ressel L, Frohmader A, Sivlestrini P, Verin R. Lipoxygenase-5 Expression in Canine Urinary Bladder: Normal Urothelium, Cystitis and Transitional Cell Carcinoma. *J Comp Path*. 2019; 170:1-9.
5. Gedon J, Kehl A, Aupperle-Lellbach H, von Bomhard W, Schmidt JM. BRAF mutation status and its prognostic significance in 79 canine urothelial carcinomas: A retrospective study (2006-2019). *Vet Comp Oncol.* 2022; 20(2):449-457.
6. Knapp DW, McMillan SK. Tumors of the Urinary System. In: Withrow SK, Vail

DM, Page RL, eds: Withrow & MacEwen's Small Animal Clinical Oncology. St. Louis, MO: Elsevier Saunders. 2013; 572-582.
7. Lambert AW, Pattabiraman DR, Weinberg RA. Emerging biological principles of metastasis. *Cell*. 2017; 168(4): 670-691.
8. Maeda S, Yoshitake R, Chambers JK. $BRAF^{V595E}$ Mutation Associates CCL17 Expression and Regulatory T Cell Recruitment in Urothelial Carcinoma of Dogs. *Vet Pathol.* 2021; 58(5): 971-980.
9. Marvel SJ, Séguin B, Dailey DD, Thamm DH. Clinical outcome of partial cystectomy for transitional cell carcinoma of the canine bladder. *Veterinary and Comparative Oncology*. 2017; 15(4): 1417-1427.
10. Meuten DJ, Meuten TLK. Tumors of the Urinary System. In: Meuten DJ, ed: *Tumors in Domestic Animals*. 5th edition. Ames, IO: John Wiley & Sons, Inc. 2017; 666-675
11. Mittal V. Epithelial mesenchymal transition in tumor metastasis. *Annual Review of Pathology: Mechanisms of Disease*. 2018; 13: 395-412.
12. Valastyan S, Weinberg RA. Tumor metastasis: molecular insights and evolving paradigms. *Cell*. 2011; 147(2): 275-292.

CASE II:

Signalment:
10 year-old, male, castrated, German wirehaired pointer (*Canis lupus familiaris*)

History:
During the CT scan of the cervical vertebra, a mass in the thyroid was seen

Gross Pathology:
Excision of a beige-brown egg-shaped tissue fragment measuring 3.3 x 2.1 x 1.9 cm. This one appears to be encapsulated. In cross section, the fragment has a beige-brown aspect.

Laboratory Results:
No findings reported.

Microscopic Description:
Thyroid gland: There is a predominantly solid, locally infiltrative and encapsulated, moderately cellular epithelial neoplasm. Focally, the neoplastic infiltrate appears to extend into the surgical excision margin. The majority of the neoplastic cells grow in contiguous fields, nests and trabeculae and have a rounded to polygonal shape with a very substantial amount of eosinophilic and finely granular cytoplasm with a moderately sized, slightly varying rounded nucleus. In addition to the neoplastic cell component, varying sizes of fields and trabeculae, neoplastic cells with no apparent eosinophilia of the cytoplasm with predominantly larger, hypochromatic nuclei are also observed. In some places, both cell populations are found in close proximity to each other. In several areas, the neoplastic infiltrate shows growth through the surrounding connective tissue capsule with bulging fields of neoplastic cells in vascular lumens. In addition, in several places in the periphery, incisions of pre-existent, inactive thyroid tissue are seen. Mitoses

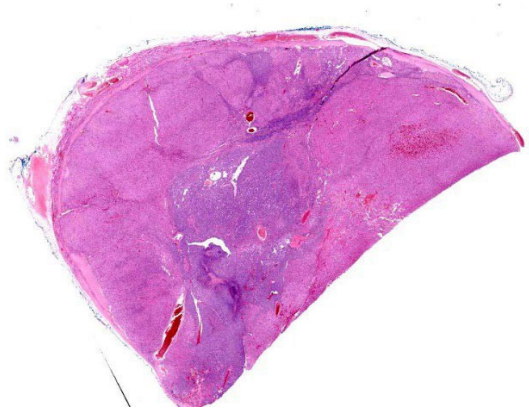

Figure 2-1. Thyroid gland, dog. A section of bisected thyroid gland is submitted for examination. The gland is markedly enlarged and the architecture is effaced by a multilobular neoplasm. (HE, 5X)

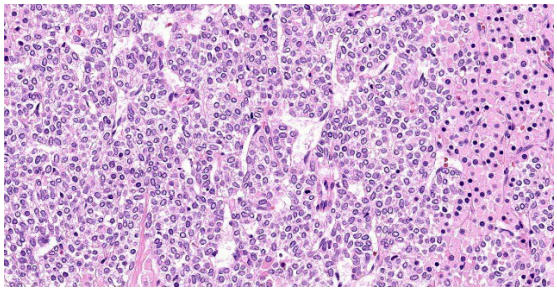

Figure 2-2. Thyroid gland, dog. The neoplasm is composed of polygonal cells which are arranged in nests and cords. At right, neoplastic cells transition into a separate morphology with abundant finely granular eosinophilic cytoplasm (Hurthle cells). (HE, 363X)

are rare and there is mild anysokaryosis and anysocytosis.

Contributor's Morphologic Diagnoses:
Thyroid, Hurtle-cell carcinoma

Contributor's Comment:
Between 10 and 15% of the neoplasms located in the head and neck in dogs are originating from the thyroid.[3] Those neoplasms can be unilateral (most frequent) or bilateral and are often palpable near the larynx as a firm or soft mass.[8,10] Most thyroid carcinomas are nonfunctional.[8] Thyroid carcinoma is the most common and most frequently diagnosed[15] endocrine malignancy in dogs[8] representing 19% of thyroid tumors with up to 38% of metastasis, most of them are already present by the time of diagnosis.[15] Some breeds are thought to be predisposed as Boxers, Beagles, Siberian Huskies and Golden retrievers[10,15] although in one study mixed breeds tend to be more affected.[15] The age ranges from 9 up to 15 years[8,15] without sex prevalence.[10]

Differences between carcinomas and adenomas are essentially based on the size of the neoplasm, adenoma being usually smaller. Thyroid carcinomas are fixed due to local invasion, whereas thyroid adenomas are subcutaneously freely movable.[10] Carcinomas are usually multinodular and often show central necrosis and hemorrhages.[15] Early carcinomas tend to be well demarcated and later carcinomas lead to vascular invasion in 45% of the cases[8], essentially into the branches of the cranial and caudal thyroid veins forming large tumor cell thrombi[10] and resulting in an impossible surgical resection.[8] Dogs and humans show similarities in the spontaneous development of thyroid carcinoma with metastases to the lungs although the incidence of metastases in dogs is higher by the time of the diagnosis.[8] Risks of metastasis are likely to increase with the size of the neoplasm.[8] Pulmonary metastases will often precede retropharyngeal and caudal cervical lymph nodes involvement.[8]

Thyroid tumors, in dogs, are classified according to the World Health Organization (WHO) based on the morphological features.[7,15] Thyroid tumors can arise from either thyroid follicular cells or thyroid C-cells (parafollicular cells, chief cells). The latter cell type is considered to represent less than 5% of thyroid neoplasms in dogs.[8]

Thyroid follicular cell carcinomas are subdivided in different subtypes:
-- cells are forming follicular structures consisting of cubic or columnar epithelial with or without colloid[3,7], the so-called compact cellular (solid) showing cells with centrally localized nuclei and pale eosinophilic and granular cytoplasm.

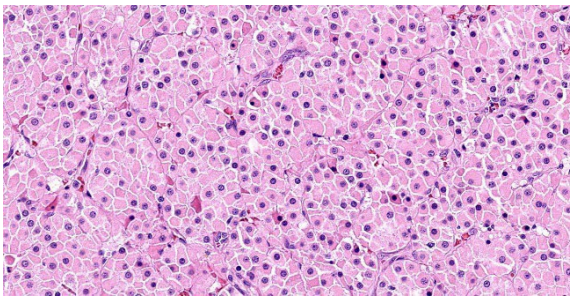

Figure 2-3. Thyroid gland, dog. Some lobules of the neoplasm are completely composed of Hurthle cells. (HE, 381X)

-- the presence of both follicular and solid areas refers to follicular-compact cellular carcinoma.[3,7]
-- papillary structures made of multiple lines of cubic cells extending into cystic spaces surrounded by fibrovascular stroma are so called papillary carcinoma.[3,7]

Follicular thyroid carcinoma can be also classified as well-differentiated, poorly differentiated, undifferentiated or carcinosarcoma.[3]

In the dog, tumors with granular cytoplasm staining brightly eosinophilic with hematoxylin and eosin (HE) include granular cell tumors, rhabdoid tumors, neuroendocrine tumors, and oncocytomas. Oncocytomas are rare, usually benign, tumors composed of oncocytes. Oncocytes[2] also called Hurthle cells or oxyphilic cells, are large, polygonal cells originating from metaplastic transformation of mature glandular or non-glandular cells. The high number of mitochondria present give the appearance of the abundant eosinophilic cytoplasm. Additionally, the cells composing the neoplasm can show a granular eosinophilic cytoplasm will refer to the Hurthle cell tumor and are rarely seen in dogs.[7] In the dog, oncocytomas have been reported originally in the larynx but also in the thyroid gland and in the kidney. Specific immunohistochemical markers are helpful in making a differential diagnosis. Oncocytomas specifically express cytokeratin. Additionally granular cell tumors are positive for vimentin and are negative for epithelial cell markers.[2]

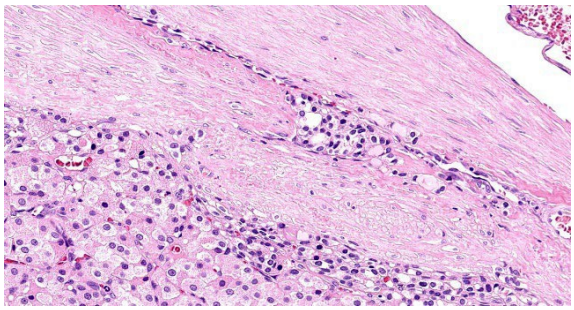

Figure 2-4. Thyroid gland, dog. Neoplastic cells invade the surrounding capsule. (HE, 361X)

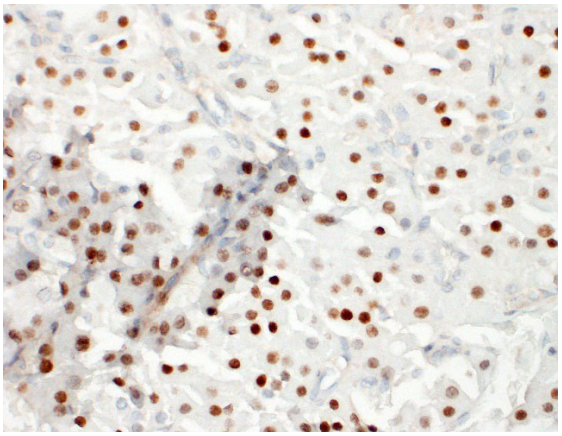

Figure 2-5. Thyroid gland, dog. Neoplastic cells demonstrate moderate nuclear positivity for thyroid transcription factor -1. (anti-TTF-1, 400X)

This is a phenomenon of metaplasia that occurs in inflammatory disorders, such as thyroiditis, or other situations that result in cellular stress. The proliferation of oncocytes gives rise to hyperplastic and neoplastic nodules. Oncocytic cells in the thyroid are often called “Hürthle” cells; however, this is a misrepresentation because they were initially described by Askenazy, and the cells that Hürthle described were in fact C cells.[1]

Numerous studies indicated that the criteria that apply to follicular tumours of the thyroid also distinguish malignant from benign Hürthle cell lesions. These included capsular and vascular invasion.[1]

To differentiate follicular cell carcinoma from C-cell carcinoma immunohistochemistry (IHC) might be necessary. In general, C-cell thyroid carcinomas exhibit strong immunoreactivity to calcitonin, calcitonin gene-related peptide (CGRP), and napsin A or markers of neuroendocrine tissue (Hassan, Campos). While follicular cell thyroid carcinomas show positivity for thyroglobulin, Pax8, and thyroid transcription factor (TTF-1 or NKX2). With the Papanicolau stain, the cytoplasm may be orange, green, or blue. By electron microscopy, the cytoplasmic granu-

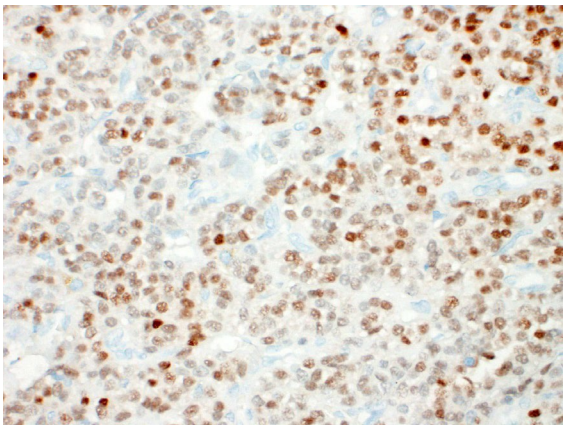

Figure 2-6. Thyroid gland, dog. Neoplastic cells demonstrate moderate nuclear positivity for PAX-8. (anti-PAX-8, 400X)

larity is produced by large mitochondria filling the cell, consistent with oncocytic transformation.[1]

The metastatic rate of thyroid carcinoma in dogs is highly related to the volume of the tumor (>20 cm^3), bilateral and cervical vascular invasion[3]. More recently other factors the presence of estradiol in cells expressing estrogen receptors[15] and to a greater protein expression of factors related to proliferation and angiogenesis (TTF-1, PCNA and VEGF).[13]

Thyroid cancers in dogs can either be inherited or spontaneous. In some breeds as the Dutch German longhaired pointers, two deleterious recessive mutations in the TPO gene have been highly associated with the familial follicular cell carcinoma[16]. Other studies suggest that overexpression of VEGFR-1, VEGFR2, PDPK-1, AKT1, and AKT2 in canine follicular thyroid carcinoma and VEGFR-1, EGFR, and PIK3CA in canine medullary thyroid carcinoma suggests that the PI3K/Akt signaling pathway is activated and increased in the pathogenesis of thyroid cancer in dogs for both follicular thyroid carcinoma and medullary thyroid carcinoma. Missense mutations in K-RAS were occasionally identified in a follicular thyroid carcinoma and a medullary thyroid carcinoma which are likely to be relevant for thyroid gland tumorigenesis.[4]

In cats, thyroid carcinomas tend to be rare and occur much less frequently than adenomas or multinodular hyperplasia[10]. Metastases to regional lymph nodes and distant sites, unlike in dogs, are rarely reported in cats.[8]

Contributing Institution:
Informatie voor dierenartsen - Veterinair Pathologisch Diagnostisch Centrum - Universiteit Utrecht (uu.nl)

JPC Diagnosis:
Thyroid gland: Hurthle cell tumor.

JPC Comment:
The contributor provides a thorough review of thyroid neoplasia and a slightly more nebulous entity – the oncocytoma. The unique dual morphology of neoplastic cells drove spirited discussion amongst conference participants, with some initially considering the possibility of a collision tumor or parathyroid origin. A collision tumor was ruled out by the areas of gradual transition between the two morphologies and the lack of a capsule separating them.

This week's moderator, Dr. Donald Meuten, explained the criteria for lymphovascular invasion in the Veterinary Cancer Guidelines and Protocols reference guide: (1) intravascular tumor with a thrombus adhered, (2) neoplastic cells invading the wall and endothelium, (3) neoplastic cells surrounded by endothelium, and (4) neoplastic cells in a vessel confirmed by vascular immunohistochemistrical stains, with the first two criteria supported by more firm evidence in the literature. Traditionally, infiltration and capsular invasion have also been considered criteria of malignancy in thyroid follicular neoplasms. In this case, the moderator and conference

participants did not favor a diagnosis of malignancy and opted to diagnose a tumor instead of a carcinoma.

As the contributor mentions, in the dog, oncocytomas have been reported in the larynx, thyroid, and kidney, and are most commonly found in the salivary gland.[12] In cats, oncocytomas have been found in the salivary glands and periocular tissues.[5] Additionally, there are rare reports in the nasopharynx and choroid plexus.[5,6,17]

Histologically, the main differential diagnoses for oncocytomas are granular cell tumors and rhabdomyomas. Granular cell tumors have been documented in the oral cavity, lung, pharynx, and brain, and are generally benign.[11] Cytoplasmic granules in both oncocytomas and granular cell tumors are PAS positive; however, electron microscopy reveals them to be different structures; mitochondria in the former, and probably secondary lysosomes in the latter.[11] Differentiation of rhabdomyomas may require immunohistochemical staining to confirm muscle origin.[11] Another differential diagnosis in the kidney is a chromophobe renal cell carcinoma.[11] This rare neoplasm is believed to originate from the intercalated cells of the collecting ducts; is negative for pancytokeratin and PAS; and is positive for vimentin, colloidal iron, and CD117.[12]

References:

1. Asa SL. My Approach to Oncocytic Tumours of the Thyroid. *J Clin Pathol.* 2004; 57(3): 225-232.57, no. 3 (1 March 2004): 225–32.
2. Buergelt CD, Adjiri-Awere A. Bilateral Renal Oncocytoma in a Greyhound Dog. *Vet Pathol.* 2020; 37(2):188-192.
3. Campos M, Ducatelle R, Rutteman G, Kooistra HS, Duchateau L, de Rooster H, Peremans K, Daminet S. Clinical, Pathologic, and Immunohistochemical Prognostic Factors in Dogs with Thyroid Carcinoma. *Jour Vet Intern Med.* 2014;28(6):1805-1813.
4. Campos M, Kool MMJ, Daminet S, Ducatelle R, Rutteman G, Kooistra HS, Galac S, Mol JA. Upregulation of the PI3K/Akt Pathway in the Tumorigenesis of Canine Thyroid Carcinoma. *Jour Vet Intern Med.* 2014; 28(6):1814-1823.
5. Cossic B, Silver G, Kent M, et al. Surgical removal of a choroid plexus oncocytoma in an adult cat. *J Small Anim Pract.* 2017; 58(10):589-592.
6. Doughty RW, Brockman D, Neiger R, McKinney L. Nasal Oncocytoma in a Domestic Shorthair Cat. *Vet Pathol*. 2006; 43:751-754.
7. Gulcubuk A, Erdogan O, Bozkurt ER, Gurel A, Arıkan N, Cat H. Case Report: Compact Cellular (Solid) Carcinoma Containing Hurthle Cell Areas in the Thyroid Gland of a Dog. *Revue de Médecine Vétérinaire.* 2013; 164(10). n.d.
8. Hassan BB, Altstadt A, Dirksen WP, Elshafae SM, Rosol TJ. Canine Thyroid Cancer: Molecular Characterization and Cell Line Growth in Nude Mice. *Vet Path.* 2020;57(2):227-240.
9. Kido N, Itagaki I, Ono K, Omiya T, Matsumoto R. FOLLICULAR CELL CARCINOMA OF THE THYROID GLAND IN THREE CAPTIVE AGED RACCOON DOGS (*NYCTEREUTES PROCYONOIDES*). *J Zoo Wildl Med.* 2015;46(4):889-894.
10. Maxie MG, ed. *Jubb, Kennedy, and Palmer's Pathology of Domestic Animals*. Sixth edition. St. Louis, Missouri: Elsevier, 2016.
11. Meuten DJ, Meuten TLK. Tumors of the Urinary System. In: Meuten DJ, ed: *Tumors in Domestic Animals.* 5th edition. Ames, IO: John Wiley & Sons, Inc. 2017; 640.

12. Munday JS, Lohr CV, Kiupel M. Tumors of the Alimentary Tract. In: Meuten DJ, ed: *Tumors in Domestic Animals.* 5th edition. Ames, IO: John Wiley & Sons, Inc. 2017; 511-512.
13. Pessina P, Castillo V, Sartore I, Borrego J, Meikle A. Semiquantitative Immunohistochemical Marker Staining and Localization in Canine Thyroid Carcinoma and Normal Thyroid Gland: Dog Thyroid Carcinoma Markers. *Vet Comp Oncol.* 2016; 14(3): e102-112.
14. Ramos-Vara JA, Miller MA, Johnson GC, Pace LW. Immunohistochemical Detection of Thyroid Transcription Factor-1, Thyroglobulin, and Calcitonin in Canine Normal, Hyperplastic, and Neoplastic Thyroid Gland. *Vet Pathol.* 2002; 39(2):480-487.
15. Soares LMC, Pereira AHB, de Campos CG, Rocha LS, dos Santos TA, Souza MA, Jark PC, Pescador CA. Histopathological and Immunohistochemical Characteristics of Thyroid Carcinoma in the Dog. *J Comp Path.* 2020; 177: 34-41.
16. Yu Y, Bovenhuis H, Wu Z, Laport K, Groenen MAM, Crooijmans Richard PMA. Deleterious Mutations in the TPO Gene Associated with Familial Thyroid Follicular Cell Carcinoma in Dutch German Longhaired Pointers. *Genes*. 2021; 12(7): 997.
17. You M, Kim Y, Woo G, et al. Nasopharyngeal oncocytoma in a cat. *J Vet DIagn Invest.* 23:391-394.

CASE III:

Signalment:
10-year-old, female, Shiba dog, *Canis lupus familiaris*.

History:
In echo examination at regular checkup, enlarged gall bladder and extrahepatic bile duct enlargement was found. Computed tomography revealed a 1cm-sized mass proximal to the common bile duct. The mass was surgically removed by blunt dissection.

Gross Pathology:
The rounded mass had about 1 cm in diameter, well defined, with a firm consistency and a red brown color.

Laboratory Results:
No findings reported.

Microscopic Description:
A tumor formed beneath the luminal epithelium of the common bile duct. Tumor cells formed continuously from small diverticula and invaginations of the mucosa beneath luminal epithelium of the common bile duct. A partial demarcated, encapsulated, and infil trative tumor composed of nests, cords, acinar, and trabecular of epithelial cells supported by fibrovascular stroma. The tumor cells were polygonal, round to small spindle with distinct cell borders. Cells have moderate amounts of a finely granular, lightly eosinophilic cytoplasm, and round to oval, basilar nuclei with finely stippled chromatin and one small nucleolus. Mitoses were rare (2 per 10 HPF, 400X magnification). There was vascular invasion, but no evidence of necrosis.

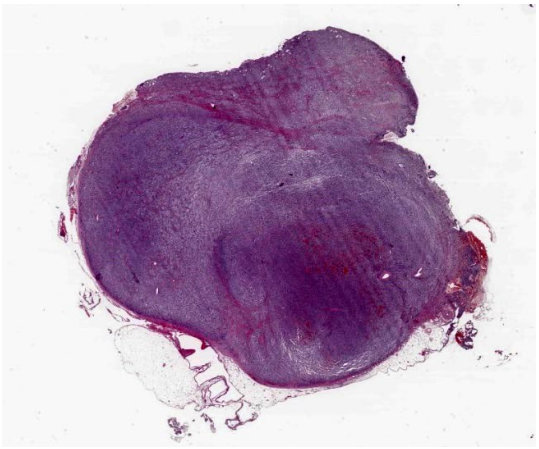

Figure 3-1. Extrahepatic bile duct, dog. One section of a nodular mass arising from an extrahepatic bile duct is submitted for examination. (HE, 6X)

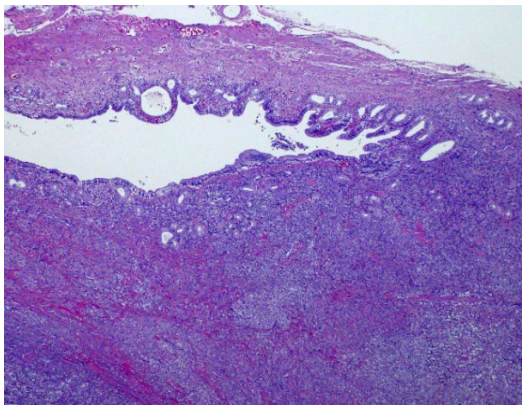

Figure 3-2. Extrahepatic bile duct, dog. The neoplasm arises from the mucosa of the bile duct and effaces the wall. (HE, 40X) (Photo courtesy of: S Laboratory of Pathology Faculty of Pharmaceutical Sciences, Setsunan University, 45-1 Nagaotohge-cho, Hirakata, Osaka, Japan)

Immunohistochemical investigation showed tumor cells strongly positive for neuroendocrine markers (synaptophysin, Insulinoma-associated1(INSM1)) and cytokeratin (AE1/AE3, CK19). Chromogranin A was negative.

Contributor's Morphologic Diagnoses:
Extrahepatic bile duct: Carcinoid (neuroendocrine tumor)

Contributor's Comment:
Carcinoid tumors are thought to arise from embryonal neural crest cells, or so-called argentaffin cells (Kulchitsky cells), which migrate to sites within the respiratory and gastrointestinal tracts during neonatal development. Most cases of neuroendocrine tumors have been reported in the gastrointestinal tract, the respiratory tract, liver, pancreas, and central or peripheral nervous system. It has also been confirmed to occur in the skin. In humans, extrahepatic bile duct carcinoid is extremely rare and accounts for 0.1-0.21% of all carcinoids of the gastrointestinal tract, with most reported cases arising from within

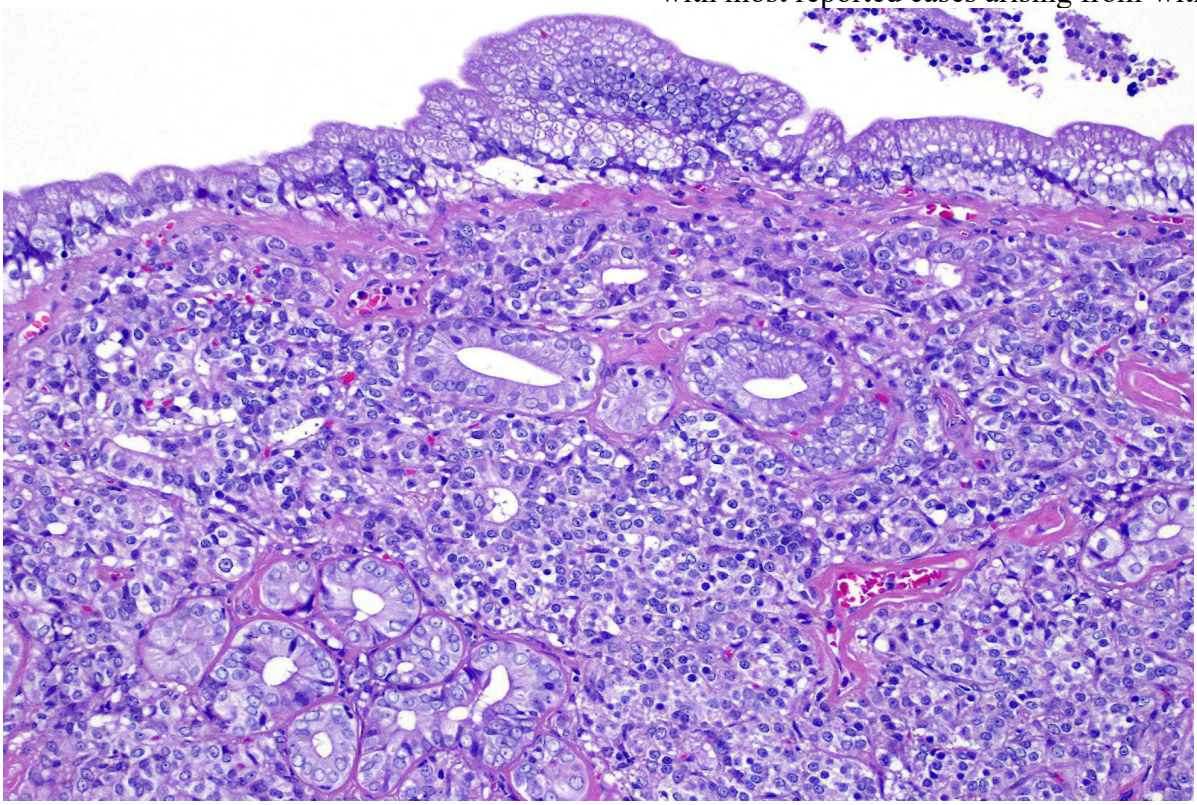

Figure 3-3. Extrahepatic bile duct, dog. Glands within the mucosa are surrounded and separated by nests of neoplastic cells. (HE, 40X) (Photo courtesy of: S Laboratory of Pathology Faculty of Pharmaceutical Sciences, Setsunan University, 45-1 Nagaotohge-cho, Hirakata, Osaka, Japan)

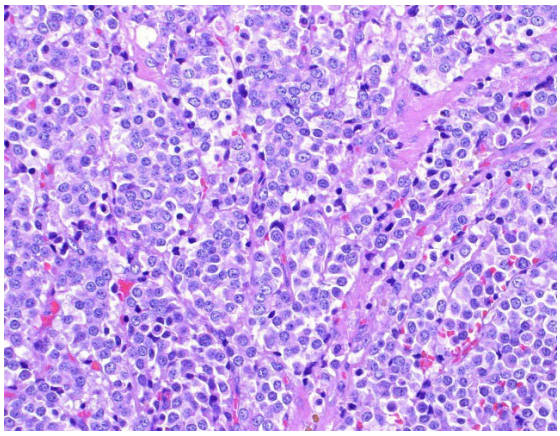

Figure 3-4. Extrahepatic bile duct, dog. High magnification of neoplastic cells. (HE, 40X) (Photo courtesy of: S Laboratory of Pathology Faculty of Pharmaceutical Sciences, Setsunan University, 45-1 Nagaotohge-cho, Hirakata, Osaka, Japan)

the gallbladder.[1,5] In domestic animals, primary gallbladder neuroendocrine carcinomas of cats, dog, and cow are reported in only a few cases.[2,6,8] To the best of our knowledge, there are no reports of primary extrahepatic bile duct carcinoid in dogs.

An important differential diagnosis was cholangiocarcinoma and metastatic tumor. The definitive diagnosis of neuroendocrine tumor is based on histologic features associated with immunohistochemical staining. A relevant panel including chromogranin A, synaptophysin and NSE is recommended to diagnose hepatic carcinoid.[1,5] Recently, INSM1 was identified as a useful specific marker of neuroendocrine differentiation in neuroendocrine neoplasms. The immunoreactivity for INSM1 is greater than conventional cytoplasmic NE markers (chromogranin A, synaptophysin).[1,5] In this case, as INSM1 was strongly diffusely positive. Thus, the morphology of this tumor and the positivity of synaptophysin and INSM1 can eliminate cholangiocarcinoma. Direct infiltration by peripheral organs like liver, pancreas and small intestine or metastasis from other organs was eliminated as a possible diagnosis by no adhesion with surrounding organs and by the gross and morphologic characteristics of the tumor.

The clinicopathologic spectrum of neuroendocrine tumors ranges from the benign carcinoid to the aggressive neuroendocrine carcinoma.[1,5] The malignancy of neuroendocrine tumors is based on the following: 1) tumor size (>2 cm), 2) invasion into adjacent tissues, 3) invasion beyond the submucosa and into adjacent tissues, 4) presence of necrosis, 5) overt cell atypia with more than two mitotic cells per 10 high-power fields, 6) hormone expression and loss of chromogen immunoreactivity, and 7) nuclear P53 protein accumulation. [1,5] However, biologic behavior of neuroendocrine tumor is difficult to predict on histological features, since anaplastic features and mitotic counts are not reliable to determine the malignancy grade. The evidence of tumor invasion into adjacent tissue could reflect criteria of malignancy. So, it is recommended to consider these tumors as potentially malignant. Hepatic carcinoid has been described as aggressive tumor associated with a common metastatic potential to the peritoneum and draining lymph nodes, however it is suggested that in case of gallbladder carcinoid without evidence of intraperitoneal or distant metastasis, the prognosis is considered as good after a surgical treatment. In this case, carcinoid originated in

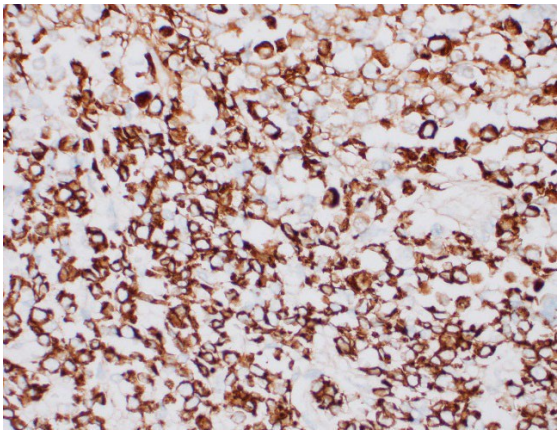

Figure 3-5. Extrahepatic bile duct, dog. Neoplastic cells demonstrate strong cytoplasmic immunoreactivity for cytokeratin. (AE1/AE3, 400X)

extrahepatic bile duct has not been reported previously in dog, so its biological behavior is unknown.

Contributing Institution:
Laboratory of Pathology, Faculty of Pharmaceutical Sciences, Setsunan University, 45-1 Nagaotohge-cho, Hirakata, Osaka 573-0101, Japan

JPC Diagnosis:
Bile duct: Neuroendocrine tumor (carcinoid).

JPC Comment:
Neuroendocrine tumors were first described in 1907 by Siegfried Oberndorfer, a pathologist at the University of Munich.[3] He coined the term "Karzinoide Tumor" (car cinoid) to describe a special cancer of the gastrointestinal system that was typically benign and not related to an adenocarcinoma.[3] Subsequent work throughout the 20th century revealed the neuroendocrine nature of the cells, which were ultimately determined to be entodermal in origin.[3] It is now recognized that neuroendocrine tumors, though they may have similar immunohistochemical staining properties, are diverse in their morphology, biologic behavior, and hormone content.[3]

A recent study described the features of gall bladder neuroendocrine tumors in 13 dogs.

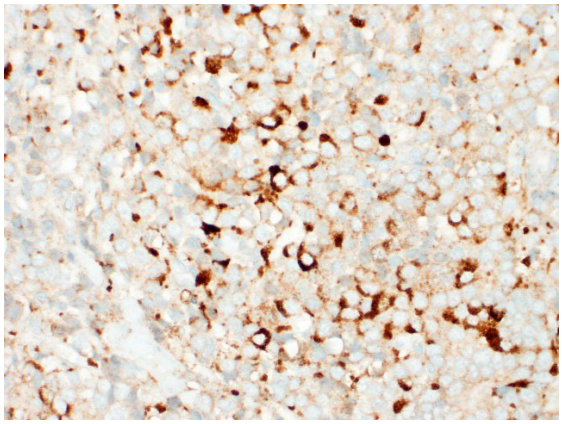

Figure 3-6. Extrahepatic bile duct, dog. Neoplastic cells demonstrate strong scattered cytoplasmic immunoreactivity for chromogranin A. (anti-chromagranin A, 400X)

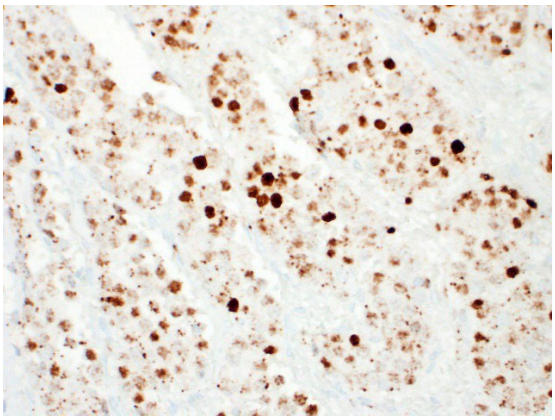

Figure 3-7. Extrahepatic bile duct, dog. Neoplastic cells demonstrate strong scattered cytoplasmic immunoreactivity for INSM-1. (anti-INSM-1400X)

Brachycephalic breeds, particularly the Boston terrier, were overrepresented, and the most common presenting complaint was vomiting.[7] Six of the animals had evidence of metastasis to the liver, with two others metastasizing to the lung and one to the mesentery.[7] Eight animals had vascular invasion, but the vast majority (12) were removed with clean margins.[7] The median survival time for the eight patients which died prior to the end of the study was 3.7 years, and the cause of death in 5 of those patients was neuroendocrine carcinoma.[7]

In contrast to the fair to good prognosis implied in the previous report of gall bladder neuroendocrine tumors, hepatic neuroendocrine tumors appear to have a very poor prognosis, with a median survival time of 3 days in one study of 10 dogs.[8] Hepatic carcinoids typically affect all liver lobes, and in one study from 1981, 14 of 15 cases metastasized, with 13 cases resulting in carcinomatosis and 14 cases of lymph node metastasis.[8,9] These findings indicate that hepatic neuroendocrine carcinomas are potentially aggressive neoplasms.

Another recent study demonstrated that neuroendocrine carcinomas are the most common gastric neoplasm in bearded dragons, ac-

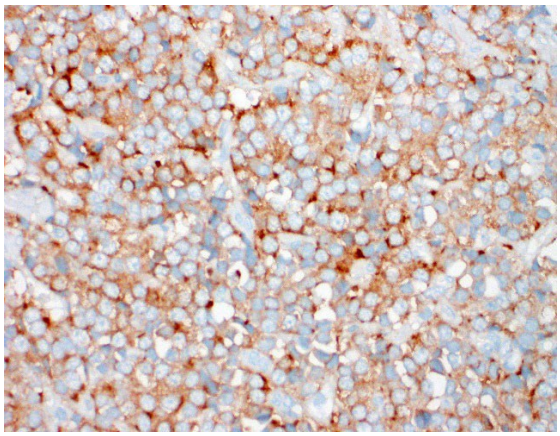

Figure 3-8. Extrahepatic bile duct, dog. Neoplastic cells demonstrate strong scattered cytoplasmic immunoreactivity for synaptophysin. (anti-synaptophysin, 400X)

counting for 16 of 26 gastric and 51 total gastrointestinal tract neoplasms.[4] In an earlier study on bearded dragons, the most common clinical sign was anorexia, and somatostatin was the only immunohistochemical marker expressed in the neoplasms, suggesting they are somatostatinomas.[10] In 6 of 10 of these cases, metastasis occurred to other abdominal organs, and 1 metastasized to the lung, indicating aggressive behavior in this species as well.[10]

References:

1. Fujino K, Yasufuku K, Kudoh S, et al. INSM1 is the best marker for the diagnosis of neuroendocrine tumors: comparison with CGA, SYP and CD56. *Int J Clin Exp Pathol* 2017;10**:** 5393-5405.
2. Johnson LK, Nunez A, Bracegirdle JR, Dwyer JR, Konold T. Neuroendocrine carcinoma of the liver and gallbladder in a cow. *J Comp Pathol*. 2008;138**:** 165-168
3. Kloppel G. Oberndorfer and His Successers: From Carcinoid to Neuroendocrine Carcinoma. *Endocr Pathol*. 2007; 18: 141-144.
4. LaDouceur EB, Argue A, Garner MM. Alimentary Tract Neoplasia in Captive Bearded Dragons (Pogona spp). *J Comp Pathol*. 2022; 194: 28-33.
5. McHugh KE, Mukhopadhyay S, Doxtader EE, Lanigan C, Allende DS. INSM1 Is a Highly Specific Marker of Neuroendocrine Differentiation in Primary Neoplasms of the Gastrointestinal Tract, Appendix, and Pancreas. *Am J Clin Pathol*. 2020;153**:** 811-820.
6. Morrell CN, Volk MV, Mankowski JL. A carcinoid tumor in the gallbladder of a dog. *Vet Pathol*. 2002;39**:** 756-758.
7. O'Brien KM, Bankoff BJ, Rosenstein PK et al. Clinical, histopathologic, and immunohistochemical features of 13 cases of canine gallbladder neuroendocrine carcinoma. *Jour Vet Diag Invest*. 2021; 33(2): 294-299.
8. Patnaik AK, Lieberman PH, Erlandson RA, Antonescu C. Hepatobiliary neuroendocrine carcinoma in cats: a clinicopathologic, immunohistochemical, and ultrastructural study of 17 cases. *Vet Pathol*. 2005;42**:** 331-337.
9. Patnaik AK, Newman SJ, Scase T, et al. Canine Hepatic Neuroendocrine Carcinoma: An Immunohistochemical and Electron Microscopic Study. *Vet Pathol.* 2005; 42:140-146.
10. Ritter JM, Garner MM, Chilton JA, Jacobson ER, Kiupel M. Gastric Neuroendocrine Carcinomas in Bearded Dragons (*Pogona vitticeps*). *Vet Pathol*. 2009; 46:1109-1116.

CASE IV:

Signalment:
9-year-old, male castrated, Shepherd Mix dog (*Canis lupus familiaris*)

History:
Presented to the hospital with a history of lethargy, decreased appetite, unwilling to walk and vomiting. The patient was alert, responsive and with cold distal extremities. On physical examination, the temperature was

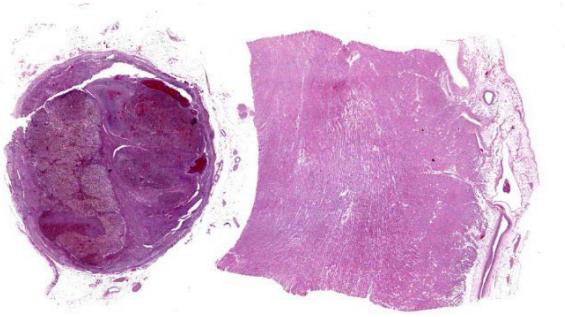

Figure 4-1. Adrenal gland and heart, dog. At subgross magnification, a neoplasm has effaced normal architecture of the adrenal gland. Myocardial fibrosis is also visible at this magnification. (HE, 5X)

97.0 F, heart rate was 76 beats/min and respiratory rate was 56 breaths/min. Left ventricle not contracting appropriately and an enlarged left adrenal gland extending into the phrenicoabdominal vein were identified on ultrasound. In addition, the patient had muffled heart sounds and weak femoral pulses.

Gross Pathology:
The right atrium and the right ventricle had multiple linear, flat dark red 2-cm to 4-cm long streaks around multiple blood vessels. The right and left free ventricular wall ratio was 1:3, and the heart weighed 472-g, which was 1.23% of the body weight (normal range in adult dog is 0.7-1.2%).

The left adrenal gland was enlarged (3.2-cm x 2.5-cm x 1.6-cm), multinodular, and firm. On cut surface, the corticomedullary ratio was 1:10 with a red to dark red, 2.5-cm in diameter mass expanding and replacing the medullary and markedly compressing the cortex. This adrenal gland was firmly attached and penetrated to the adjacent caudal vena cava. The affected caudal vena cava was segmentally and extensively dilated and completely occluded by a dark red, 3.5-cm x 1.5-cm x 1.2-cm cylindrical, firm tumor embolus firmly attached to the vascular intima. The right adrenal gland was 2.5-cm x 1-cm x 0.5-cm, with a distinct corticomedullary junction, yet medulla expanded by ill-defined light brown nodules.

Laboratory Results:
No findings reported.

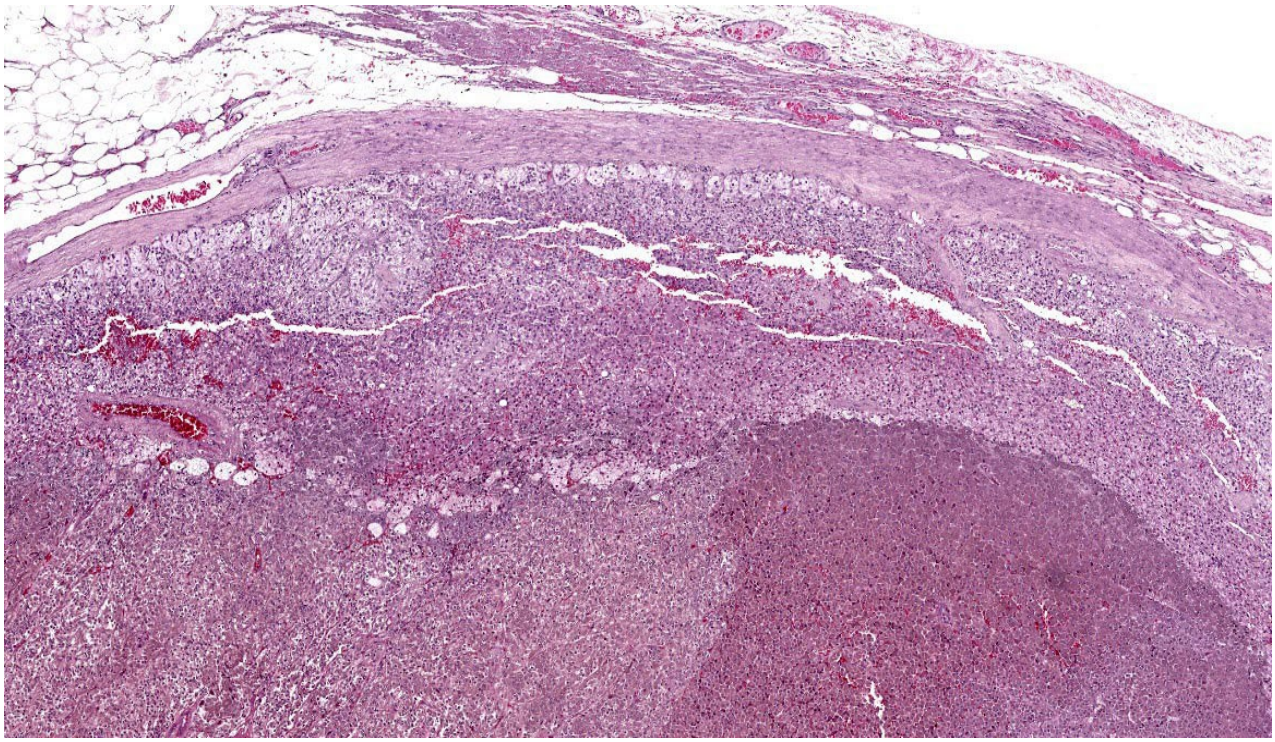

Figure 4-2. Adrenal gland, dog. The adrenal cortex is compressed by an expansile medullary tumor. (HE, 55X)

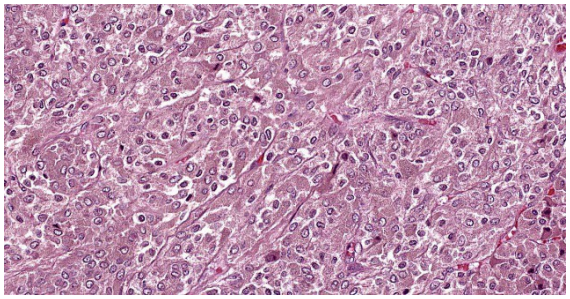

Figure 4-3. Adrenal gland, dog. High magnification of neoplastic cells from the adrenal medulla. (HE, 381X)

Microscopic Description:
Left adrenal gland (not included in this submission's slide): Markedly effacing and expanding the medulla and compressing the cortex is a nonencapsulated, infiltrative, highly cellular neoplasm, composed of round to polygonal cells arranged in dense sheets, nests and packets, supported by delicate fibrovascular stroma. There are extensive areas of necrosis, hemorrhage, fibrin and moderate numbers of degenerate neutrophils along with large clusters of neoplastic cells that invade the caudal vena cava wall and form an intravascular tumor cell thrombus. The neoplastic cells have distinct cell borders, moderate amounts of faintly granular cytoplasm, and a round to oval nucleus with finely stippled chromatin and 1-2 nucleoli. Anisocytosis and anisokaryosis are mild and there are 5 mitotic figures in ten 400x fields (2.37 mm-2). The associated celiac ganglion is focally infiltrated by lymphocytes and plasma cells.

Right adrenal gland (included in this submission's slide): Markedly expanding the medulla and compressing the cortex are multifocal to coalescing nodules comprised by neoplastic cells with similar arrangement and cytonuclear features as those described in the left adrenal gland.

Heart: Diffusely, the myocardial interstitium of the left ventricle is mildly expanded by edema and mildly increased numbers of fibrocytes and fibroblasts. Multifocally, individualized or clusters of cardiomyocytes exhibit pale sarcoplasm (degeneration) or bright eosinophilic sarcoplasm with loss of cross striations and fragmentation, and a pyknotic or karyolytic nucleus (necrosis). Often adjacent to or surrounding these myocytes are infiltrates of histiocytes and rare lymphocytes. Within patchy regions of denser fibrosis, myocytes are separated and atrophied. The tunicas media and adventitia of the multiple epicardial branches of the coronary artery are circumferentially expanded and effaced by hyalinized eosinophilic material (fibrin), and hemorrhage accompanied by perivascular edema and infiltrates of moderate numbers of macrophages, plasma cells and nuclear debris. Occasionally, the blood vessels have plump medial smooth muscle cells and endothelium.

Contributor's Morphologic Diagnoses:
Adrenal glands: Bilateral adrenal pheochromocytomas with caudal vena cava invasion

Heart: Moderate, multifocal, myocardial degeneration and necrosis with coronary arterial fibrinoid necrosis

Contributor's Comment:
Pheochromocytoma is the most common neoplasm of the canine adrenal medulla, arising from chromaffin cells, which physiologically

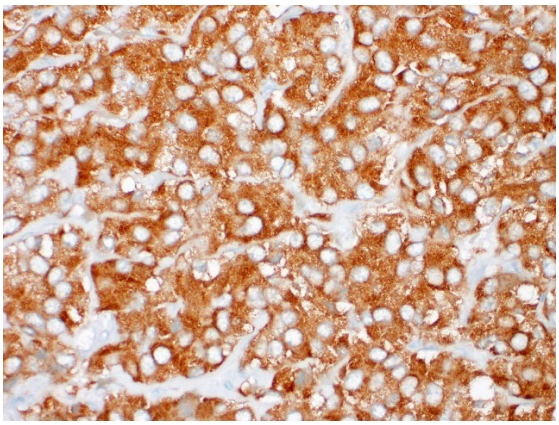

Figure 4-4. Adrenal gland, dog. Neoplastic cells demonstrate strong cytoplasmic immunoreactivity for chromogranin A. (anti-chromagranin A, 400X)

release catecholamines.[3,7,10] Although pheochromocytomas are generally unilateral, they can involve both adrenal glands. These tumors can be benign or malignant, the latter associated with invasion beyond its capsule and, in some instances, to the vena cava and/or phrenicoabdomminal vein as well as adjacent vessels. Metastasis to lung, spleen, liver, heart, bone or regional lymph nodes can also occur.[14] Pheochromocytomas can be nonfunctional or functional. Those tumors with functional activity can secrete catecholamines, being norepinephrine the most frequently reported.[6]

Catecholamines include epinephrine (adrenaline), norepinephrine (noradrenaline) and dopamine.[12] These amines are synthesized from the amino acid tyrosine, which are derived from food or formed from phenylalanine in the liver. Acting as postsynaptic neurons, chromaffin cells release secretory products when triggered by nerve impulses carried by the sympathetic fibers. The secretory products then bind to the G-protein coupled receptors located on targeted organs. Two broad receptor classifications, α and β, have been described, and they can further expand into nine receptor subtypes. Both epinephrine and norepinephrine can bind and act on adrenergic α and β receptors. The catecholamines have a profound physiology effect on blood

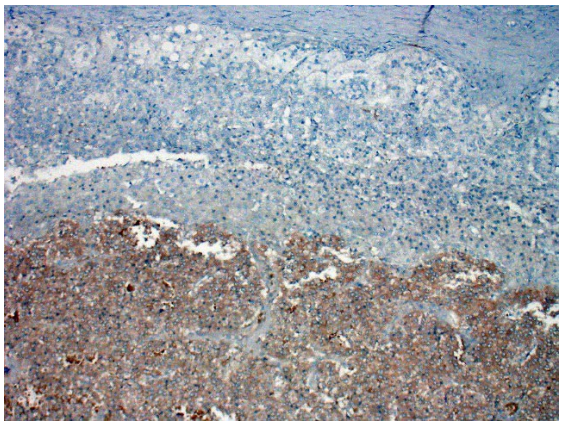

Figure 4-5. Adrenal gland, dog. Neoplastic cells demonstrate strong scattered cytoplasmic immunoreactivity for synaptophysin. (anti-synaptophysin, 400X)

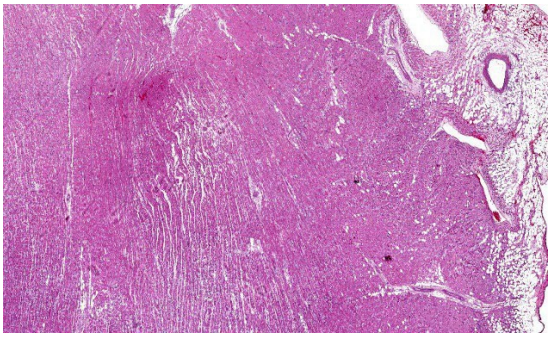

Figure 4-6. Heart, left ventricle, dog. There is diffuse interstitial fibrosis within the myocardium. (HE, 15X)

vessels and heart. Different concentration of epinephrine can elicit opposite reactions on the vasculature. At low concentration, epinephrine can lead to vasodilation by binding to β2; while at higher concentration, mainly stimulates α1 receptor and triggers vasoconstriction. In addition, increased force and rate of contraction of myocardium can occur with binding to β1 receptor.[7,12] Clinical signs are often the result of excessive catecholamine secretion from the pheochromocytoma; however, the amount of secretion is variable, sporadic and unpredictable.[7] Therefore, approximately half of the cases are incidental findings at necropsy or during surgery.

In human and animals, weakness, tachypnea, lethargy, anorexia, vomiting, high blood pressure or cardiac arrhythmias are the most frequently reported clinical signs in pheochromocytoma-affected patients.[4,12,13] Regarding myocardial changes, the theory of pheochromocytoma-associated catecholamine cardiomyopathy has been introduced.[6] However, the mechanism of the cardiomyopathy is multifactorial.[3] Myocardial injuries from circulating catecholamines have been observed in several animal models. The proposed pathogenesis of myocardial damage includes excessive stimulation of adrenergic amines that induce vasoconstriction and vasospasms in the coronary artery, leading to

myocardial hypoxia and/or infarction. In addition, the aberrant concentration of catecholamines has been shown to increase permeability of the sarcolemmal membrane and lead to increased intrasarcoplasmic calcium influx that directly causes cardiomyocyte toxic damage. Moreover, the excessive catecholamine-induced systemic hypertension as well as overloaded pressure contribute to cardiomyocyte hypertrophy and secondary hypertrophic cardiomyopathy. Histologic changes include multifocal cardiomyocyte necrosis with contraction bands, cardiomyocyte degeneration, myocardial hemorrhage, myocarditis and interstitial fibrosis.[6]

In the present case, not only similar histologic changes are present in the cardiomyocytes and interstitium, but coronary arteries exhibit vasculitis / fibrinoid change. Mechanisms leading to vasculitis and fibrinoid change are variable, including systemic hypertension, stress-induced, idiopathic, as well as primary or secondary to inflammatory responses or immune-mediated diseases.[15] No profound inflammation or immune-mediated disease were seen in this case. In addition, hyperthyroidism, diabetes mellitus and hyperaldosteronism were less likely based on clinical and pathologic examination. In cases of pheochromocytomas or hypertension, patients can have adaptive mural thickening, arteriolosclerosis or fibrinoid necrosis in heart, kidney, lung or spleen.[6] It is intriguing that the vasculitis was confined to the coronary arteries in this patient, and the cause is highly suspected to be pheochromocytoma-related.

Contributing Institution:
Auburn University
166 Greene Hall
Pathobiology
College of Veterinary Medicine
Auburn, AL
36849-5519

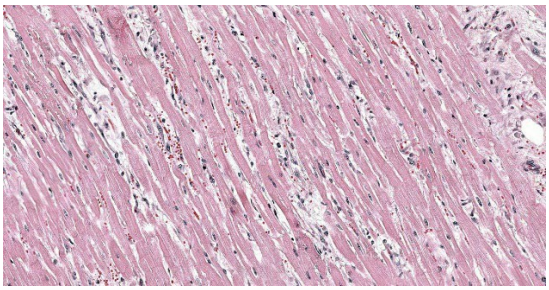

Figure 4-7. Heart, left ventricle, dog. The myocardial interstitium is expanded by loosely arranged collagen, plump fibroblasts, and there is multifocal atrophy of skeletal muscle fibers. (HE, 200X)

JPC Diagnosis:
1. Adrenal gland: Pheochromocytoma.
2. Heart: Arteriolar fibrinoid necrosis, multifocal, moderate with myocardial degeneration, loss, and fibrosis.

JPC Comment:
The contributor provides an excellent overview of adrenal pheochromocytomas and the systemic effects of excessive catecholamine production. Pheochromocytomas occur in many veterinary species, and in clouded leopards specifically they are the most common neoplasm, occurring in 1% of animals in one study of 271 animals.[16] In a separate review, pheochromocytomas accounted for 36% of reported cases of neoplasia in clouded leopards (41 of 144 cases).[9]

Other neoplasms which may originate from the adrenal medulla include neuroblastomas and ganglioneuromas, both of which are rare tumors of neuroectoderm origin.[14] Neuroblastomas originate from primitive neuroectodermal cells and can arise anywhere in the sympathetic nervous system.[1] Adrenal neuroblastomas occur in children, and are rare in dogs, ferrets, and cows.[1,2] Histologically, neuroblastomas are infiltrative, densely cellular neoplasms composed of small cells resembling lymphocytes with scant cytoplasm.[1,14] Occasionally, neoplastic cells form Homer-Wright rosettes and pseudorosettes.[1] There is limited information on the biologic behavior of this neoplasm, but in dogs, it is

likely malignant and may metastasize within the abdomen.[1]

Ganglioneuromas, on the other hand, are benign tumors which have been diagnosed in humans, dogs, cows, rats, and a cotton top tamarin.[5,8,11] The neoplasms are composed of ganglia cells admixed with satellite cells and Schwann cells in a neurofibrillary matrix with prominent fibrous connective tissue.[11,14] The ganglion cells have significant anisocytosis, abundant finely granular cytoplasm, and large round heterochromatic nuclei.[11] Occasionally, ganglioneuromas occur alongside pheochromocytomas, and in one study of rats, all 9 ganglioneuromas were associated with pheochromocytomas.[11]

References:

1. Arenas-Gamboa AM, Tanabe M, Edwards J, Storts R. Peripheral Neuroblastomas in Dogs: A Case Series. *J Comp Path.* 2014; 150: 361-365.
2. Bakthavatchalu V, Muthupalani S, Marini RP, Fox JG. Endocrinopathy and Aging in Ferrets. *Vet Pathol*. 2016; 53(2): 349-365.
3. Barthez PY, Marks SL, Woo J, Feldman EC, Matteucci M. Pheochromocytoma in dogs: 61 cases (1984-1995). *J Vet Intern Med*. 1997:11(5):272-278.
4. Dagartzikas MI, Sprague K, Carter G, Tobias JD. Cerebrovascular event, dilated cardiomyopathy, and pheochromocytoma. *Pediatr Emerg Care*. 2002 Feb;18(1):33-5.
5. Dias JLC, Montali RJ, Strandberg JD, Johnson LK, Wolff MJ. Endocrine neoplasia in New World primates. *J Med Primatol*. 1996; 25: 34-41.
6. Edmondson EF, Bright JM, Halsey CH, Ehrhart EJ. Pathologic and cardiovascular characterization of pheochromocytoma-associated cardiomyopathy in dogs. *Vet Pathol.* 2015;52(2):338-343.
7. Feldman E, Nelson R. Pheochromocytoma and multiple endocrine neoplasia. In: *Canine and Feline Endocrinology and Reproduction.* 3rd ed. Philadelphia, PA: WB Saunders;2003:440-463.
8. Grossi AB. Leifsson PS. Jensen HE. Vainer B. Iburg T. Histologic and Immunohistochemical Classification of 41 Bovine Adrenal Gland Neoplasms. *Vet Pathol*. 2012; 534-542.
9. Mathieu A, Garner MM. A Retrospective Study of Neoplasia in Non-domestic Felids in Human Care, with a Comparative Literature Review. *J Zoo Wildl Med.* 2021; 52(2): 413-426.
10. Miller MA. Endocrine system. In: Zachary JF, ed. *Pathologic Basis of Veterinary Disease*. 6th ed. St. Louis, MO: Elsevier; 2017:709.
11. Pace V, Perentes E, Germann PG. Pheochromocytomas and Ganglioneuromas in the Aging Rat: Morphological and Immunohistochemical Characterization. *Tox Pathol.* 2002; 30(4):492-500.
12. Reusch CE. Pheochromocytoma and multiple endocrine neoplasia. In: Scott-Moncrieff, CR, ed. *Canine and Feline Endocrinology*. 4th ed. Saunders; 2015: 521-551.
13. Rosol TJ, Grone A. Endocrine glands. In: Maxie MG, ed. *Jubb, Kennedy, and Palmer's Pathology of Domestic Animals.* Vol. 3. 6th ed. St. Louis, MO: Elsevier; 2016:343-344, 349-352.
14. Rosol TJ, Meuten DJ. Tumors of the endocrine glands. In: Meuten DJ, ed. *Tumors in Domestic Animals.* Ames, IA: John Wiley and Sons, Inc.; 2017:787-791.
15. Stone JR. Diseases of small and medium-sized blood vessels. In: Buja LM, ed. *Cardiovascular Pathology*. 4th ed. Academic press; 2016: 125-168.
16. Thorel M, Pignon C, Arne P, Donnelly TM, Riviere J. Clouded Leopard (*Neofilis nebulosa*) Morbidity and Mortality in

Captive-Bred Populations: A Comprehensive Retrospective Study of Medical Data from 271 Individuals in European, Asian, and Australian Zoos. *J Zoo Wildl Med.* 2020; 51(1); 150-158.

WSC 2022-2023 Self-assessment.
Conference 9

1. True or false? Less than 20% of dogs with urinary bladder urothelial cell carcinoma survive one year.
    a. True
    b. False

2. The metastatic rate of thyroid carcinoma in the dog is most closely related to which of the following?
    a. Mitotic rate
    b. Volume of tumor
    c. Nuclear gigantism
    d. Lymphvascular invasion

3. Which of the following breeds have a genetic predisposition for development of thyroid carcinoma ?
    a. Dutch shepherd
    b. German shorthaired pointer
    c. Belgian Malinois
    d. Dutch German longhaired pointer

4. INSM-1 is a marker for which type of cell
    a. Neuron
    b. Neuroendocrine
    c. Smooth muscle
    d. Urothelium

5. At low concentration, norepinephrine binding to which of the following causes vasodilation?
    a. Alpha-1
    b. Alpha-2
    c. Beta-1
    d. Beta-2

Please email your completed assessment for grading to Dr. Bruce Williams at bruce.h.williams12.civ@mail.mil. Passing score is 80%. This program (RACE program 33611) is approved by the AAVSB RACE to offer a total of 0.5 CE Credits, with a maximum of 12.5 CE Credits being available to any individual Veterinary Medical Professionals for the 2019-2020 Wednesday Slide Conference. This RACE approval is for the subject matter categories of: SCIENTIFIC using the delivery method of NONINTERACTIVE DISTANCE. This approval is valid in jurisdictions which recognize AAVSB RACE.

Joint Pathology Center
Veterinary Pathology Services

WEDNESDAY SLIDE CONFERENCE 2022-2023

Conference #10 9 November 2022

CASE I:

Signalment:
Unknown gestational age*, intact female, aborted dairy goat fetus (*Capra aegagrus hircus*)

*The animal appears to be nearly full-term on gross examination and measures 46 cm from crown to rump.

History:
None provided with the submission. This animal was submitted with a male twin. No placenta was submitted with the fetuses.

Gross Pathology:
The female twin was grossly unremarkable. The lungs of the male twin had hundreds of disseminated, smooth, white, and flat pinpoint to 2.0 mm nodules within the lung parenchyma and on the pleural surfaces. Lung sections from both twins sank in formalin.

Laboratory Results:
An in-house real time reverse transcriptase multiplex rRT-PCR test using pooled liver had the following result: infectious bovine rhinotracheitis (IBR) was suspect positive, with a Ct of 38; tissues were negative for bovine respiratory syncytial virus (BRSV) and parainfluenza-3 (PI3). Aerobic bacterial culture of lung yielded no growth of pathogens.

Caprine herpesvirus (CapHV-1) PCR testing of a lung sample at Colorado State University Veterinary Diagnostic Laboratory detected nucleic acids (positive).

The viral inclusions did not stain using bovine herpesvirus-1 (infectious bovine rhinotracheitis) antibody (immunohistochemistry).

Figure 1-1. Presentation, twin goats. Two twin goats were submitted for examination. Lesions were seen only in the male twin (top).(Photo courtesy of: University of Illinois at Urbana-Champaign, Veterinary Diagnostic Laboratory, http://vetmed.illinois.edu/vet-resources/veterinary-diagnostic-laboratory/)

Microscopic Description:
Lung: Multiple random foci of necrosis that measure up to 1 mm wide disrupt the pulmonary parenchyma. The alveolar septa are markedly expanded by flocculent pink cell debris, karyorrhectic material and fibrin (coagulative necrosis). Few macrophages, neutrophils, and erythrocytes are admixed. Alveoli are filled with fine pink fibrillar material (fibrin) and pale pink fluid. At the periphery of these foci are degenerating cells with usually a single, eosinophilic intranuclear inclusion that measures approximately 5 um and peripheralizes the chromatin.

Liver: Multiple random foci of hepatic necrosis disrupt the parenchyma and are composed of globular hypereosinophilic cell fragments and karyorrhectic debris admixed with small numbers of macrophages. Hepatocytes along the periphery often have eosinophilic intranuclear inclusions that peripheralize chromatin. Macrophages in and around these nodules have small amounts of globular, dark brown, intracytoplasmic pigment (presumably hemosiderin)

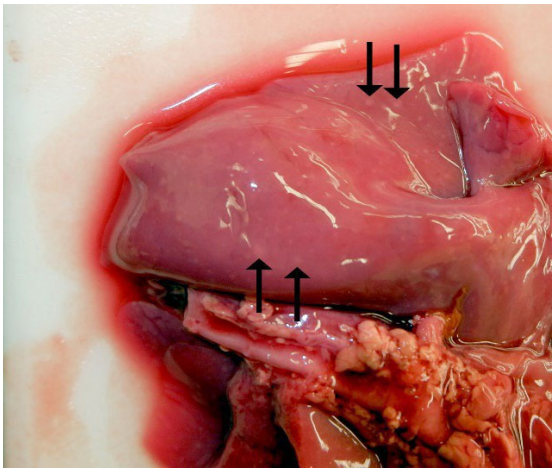

Figure 1-2. Lung, goat kid. There are multiple areas of necrosis scattered through the lungs (arrows). Photo courtesy of: University of Illinois at Urbana-Champaign, Veterinary Diagnostic Laboratory, http://vetmed.illinois.edu/vet-resources/veterinary-diagnostic-laboratory/)

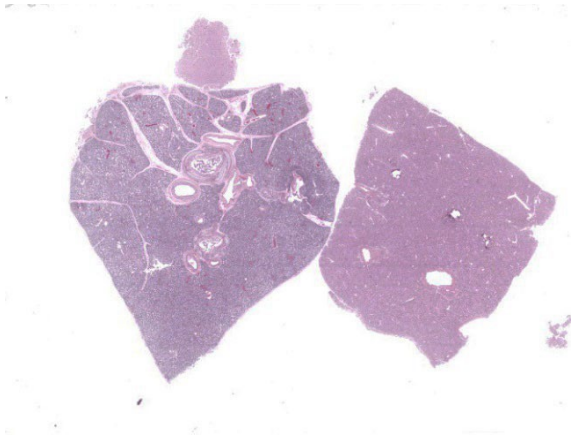

Figure 1-3. Lung, liver, goat kid. One section of lung (left) and liver (right) are submitted for examination. There are no visible lesions at subgross magnification.

Contributor's Morphologic Diagnoses:
1. Lung: multifocal, random, moderate, necrotizing pneumonia with intranuclear viral inclusion bodies
2. Liver: multifocal, random, mild, necrotizing hepatitis with intranuclear viral inclusion bodies

Contributor's Comment:
Caprine herpesvirus 1 (CpHV-1) is globally distributed alphaherpesvirus that occasionally causes disease and is less-commonly implicated as a cause of infectious abortion.[2,6,7,10,11] Clinical manifestation of disease depends on the age of the infected animal. In 1- to 2-week-old kids, a generalized disease with severe gastrointestinal lesions predominates.[1,3,4,6] In contrast, infected adults are often clinically silent or have genital tract infections characterized by vulvovaginitis or balanoposthitis; more rarely do respiratory tract infections and abortions occur. [2,6,7,10,11] Typically, does that abort are subclinically infected; the only manifestation of infection can be late term abortions, stillbirths, or even abortion storms at a herd level. [2,7,10,11] Transmission is thought to be from direct contact during coitus.[10] The source of infection can be challenging to determine, as alphaherpesviruses can remain latent in the trigeminal ganglia or other tissues.[2]

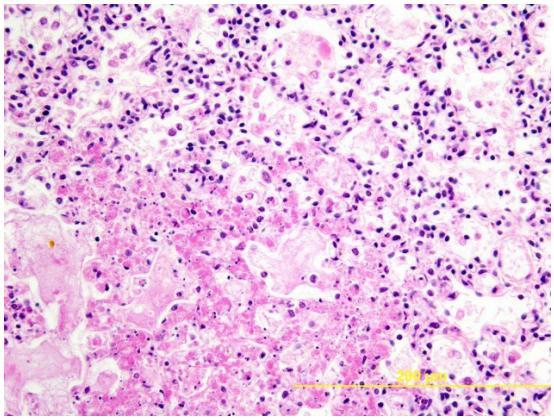

Figure 1-4. Lung, goat kid. There are areas of lytic necrosis scattered throughout the lung. (HE 400X) (Photo courtesy of: University of Illinois at Urbana-Champaign, Veterinary Diagnostic Laboratory, http://vetmed.illinois.edu/vet-resources/veterinary-diagnostic-laboratory/).

The observed herpetic inclusions are consistent with typical Cowdry type A inclusions, which are characterized by large, intranuclear, and eosinophilic to amphophilic inclusions that marginalize the chromatin.[2,3,7] With CpHV-1, inclusions are often at the periphery of necrotic foci.[7] The adrenal glands, liver, lungs, and kidneys are the organs that most commonly contain inclusions.[7] With advanced autolysis, inclusions can be challenging to identify; however, examination of the adrenal gland appears to be a reliable site of inclusion identification.[12] In this case, inclusions were found in the lung, liver, thymus, and adrenal glands but were most numerous within the lung and liver, as submitted.

The other distinguishing histopathologic feature for this infectious abortigenic agent is widespread necrotic foci that are most common within the lungs, adrenal gland, and thymus.[2,7,12] Other affected organs can include the kidney, intestine, lymph nodes, and spleen.[7,12] Thymic necrosis is associated with clusters of macrophages containing the typical Cowdry type A inclusion bodies, which, interestingly, is similar to what is observed in infected neonatal kids.[3,11]

The pathogenesis has yet to be completely elucidated, but it is thought to be associated with viremia of the dam after respiratory or genital colonization.[2,11,12] This results in leukocyte trafficking or hematogenous spread to the uterus where placental endothelium, mesenchyme, and trophoblasts become infected.[12] Death is due to tissue destruction within the fetus and placenta.[12] Viremic potential varies with individual strain, which may further contribute to the rarity of these abortions.[11,12]

Other, more common, causes of caprine abortion should be considered first when presented with a late term caprine abortion, including: *Chlamydophila abortus*, *Coxiella burnetii*, *Toxoplasma gondii*, and *Listeria monocytogenes*.[2,7] In this case, however, these agents were not identified via histologic examination or ancillary testing.

The "suspect" result of the rtPCR for infectious bovine rhinotracheitis suggests that this causative virus has genetic homology with bovine herpes virus-1 (BHV-1). It has been previously shown that CpHV-1 and BHV-1 are closely related and often antibodies will often cross-react on fluorescent antibody or

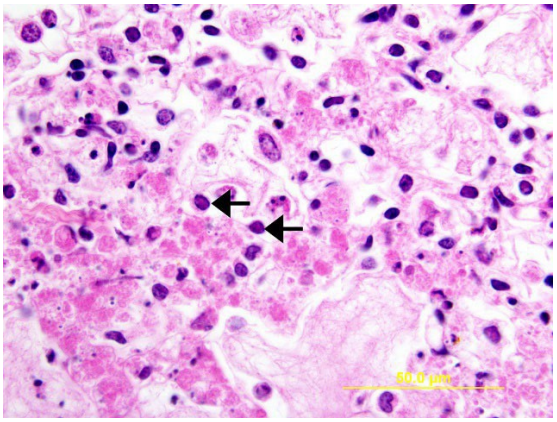

Figure 1-5. Lung, goat kid. Cells at the edge of the areas of necrosis contain intranuclear viral inclusions. (HE 400X) (Photo courtesy of: University of Illinois at Urbana-Champaign, Veterinary Diagnostic Laboratory, http://vetmed.illinois.edu/vet-resources/veterinary-diagnostic-laboratory/)

immunohistochemical assays.[2,6,7] Furthermore, goats can seroconvert against bovine herpesvirus 1, although no BHV-1 induced abortions have been identified in goats, to the author's knowledge.[12] The fetal lesions of CpHV-1 and BHV-1 are essentially identical.[12] Bovine herpesvirus-1 abortions tend to consistently have a necrotizing vasculitis within small vessels of the placental villi.[12] Unfortunately, the placenta was not submitted with this case for evaluation.

The male twin had histologically similar lesions in the lungs, adrenal glands, and thymus.

Contributing Institution:
University of Illinois at Urbana-Champaign, Veterinary Diagnostic Laboratory

JPC Diagnosis:
1. Lung: Pneumonia, necrotizing, multifocal, mild to moderate, with intranuclear viral inclusions.
2. Liver: Hepatitis, necrotizing, multifocal, mild to moderate, with intranuclear viral inclusions.

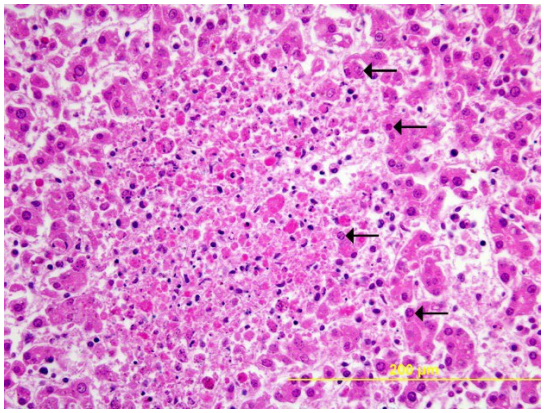

Figure 1-6. Liver, goat kid. There are multifocal areas of necrosis within the liver; hepatocytes at the edges of necrosis contain eosinophilic intranuclear viral inclusions (arrows). (HE 400X) (Photo courtesy of: University of Illinois at Urbana-Champaign, Veterinary Diagnostic Laboratory, http://vetmed.illinois.edu/vet-resources/veterinary-diagnostic-laboratory/)

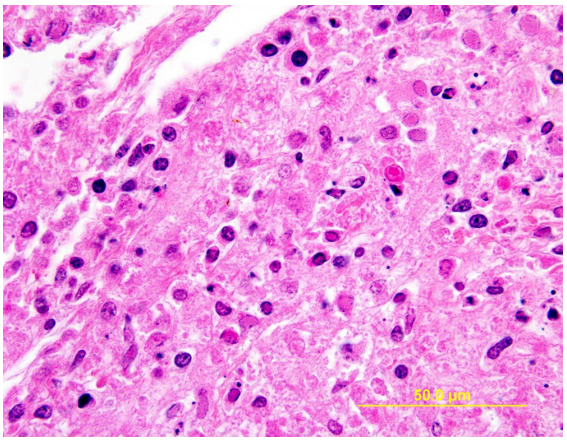

Figure 1-7. Adrenal gland, goat kid. Necrotic cells within the adrenal cortex contain eosinophilic intranuclear viral inclusions (arrows). (HE 400X) (Photo courtesy of: University of Illinois at Urbana-Champaign, Veterinary Diagnostic Laboratory, http://vetmed.illinois.edu/vet-resources/veterinary-diagnostic-laboratory/)

JPC Comment:
This week's moderator, LTC Joseph Anderson, described a few of the histologic features which can indicate that lung samples originated from fetal or neonatal animals. In neonatal rats, the terminal bronchiolar epithelial cells are vacuolated due to intracytoplasmic glycogen accumulations, a feature which was also present in this case.[5] Additionally, developing lung in the saccular stage has thickened airway walls with a large amount of stroma.[5] In this case, there are also squamous epithelial cells within the alveolar lumina which were introduced by amniotic fluid.

Caprine herpesvirus-1 is a double-stranded DNA virus that was first isolated in California and Switzerland in the 1970s and has subsequently achieved a world-wide distribution.[9] Serologic testing for CpHV-1 involves measuring BoHV gB and gE ELISA reactivity; positive gB and negative gE results indicate CpHV-1 infection.[1,13] Serologic studies have elucidated risk factors for CpHV-1 infection, which include large herd size, meat or mixed production breeds, older age, and caprine arthritis-encephalitis viral co-infection.[1] A separate study in France confirmed

that larger herds were more likely to be seropositive, and in these herds, up to 51% of animals were seropositive.[13] The correlation of older age with seropositivity suggestive of prolonged exposure and viral re-circulation within the herd.[1,13]

CpHV-1 has been the subject of recent research on therapeutic oncolytic viruses, which can replicate in and destroy neoplastic cells without harming normal cells. A few viruses, such as adenoviruses, herpesviruses, and reoviruses, have been investigated for their oncolytic properties.[4] Oncolytic herpes simplex virus 1 (oHSV-1) is the first approved oncolytic virus and targets advanced stage, non-resectable melanomas in humans.[4] As it is based on a naturally-occurring human virus, oSHV-1 can cause disease in non-neoplastic tissue as well; thus there is interest in using wild-type viruses that do not normally infect humans. Additionally, humans do not have pre-existing immunity to this virus and thus may be more susceptible to therapeutic infection.[4] Several alpha herpesviruses, including BoHV-1, equine herpesvirus 1, and now CpHV-1 have demonstrated oncolytic properties.[8] CpHV-1 can replicate in and increase apoptosis in several human cancer cell lines.[8] CpHV-1 has promising effects in the treatment of mesothelioma, which has an average survival time of less than 12 months in humans.[4] A recent study showed that the virus induced apoptosis in neoplastic cell cultures, halted cell cycle progression, and had synergistic effects with cisplatin, the current chemotherapeutic of choice for mesothelioma, with minimal effects on normal mesothelial cells.[4]

References:

1. Bortelini S, Rosamilia A, Caruso C. A cross-sectional study to identify a set of risk factors for caprine herpesvirus 1 infection. *BMC Veterinary Research.* 2108; 14(94):1-7.
2. Chénier S, Montpetit C, Hélie P. Caprine herpesvirus-1 abortion storm in a goat herd in Quebec. *Can Vet J*. 2004;**45**:241-243.
3. Cowdry, EV. The problem of intranuclear inclusions in viral diseases. *Arch Pathol*. 1934;**18**(4):527-542.
4. Forte IM, Indovina P, Montagnaro S. The Oncolytic Caprine Herpesvirus 1 (CpHV-1) Induces Apoptosis and Synergizes with Cisplatin in Mesothelioma Cell Lines: A New Potential Virotherapy Approach. *Viruses*. 2021; 13:2458-2472.
5. Greeley MA. Respiratory System. In: Parker GA, Picut CA, eds. *Atlas of Histology of the Juvenile Rat.* Cambridge, MA: Elsevier; 2016. 90-91.
6. Hao F, Mao L, Li W, et al. Epidemiological investigation and genomic characterization of Caprine herpesvirus 1 from goats in China. *Infect Genet Evol.* 2020;**79**:104168.
7. Moeller RB. Chapter 3: Disorders of Sheep and Goats. In: Njaa BL, ed. Kirkbride's Diagnosis of Abortion and Neonatal loss in Animals. 4th ed. West Sussex, UK: Wiley-Blackwell. 2012; 51-52, 55-57.
8. Montagnaro S, Damiano S, Ciarcia R. Caprine herpesvirus 1 (CpHV-1) as a potential candidate for oncolytic virotherapy. *Cancer Biology and Therapy.* 2019; 20(1): 42-51.
9. Osterreider K. Herpesvirales. In: MacLachlan NJ, Dubovi EJ, eds. *Fenner's Veterinary Virology*. 5th ed. Cambridge, MA: Elsevier. 2017; 189-191, 202.
10. Pollock JM, Schofield MJ, Porter C, Miner K, Blash S, Gavin WG. *Caprine herpesvirus* 1: A successful eradication program in dairy goat herd. *Small Ruminant Res*. 2019;**170**:8-11.
11. Roperto F, Pratelli A, Guarino G, et al. Natural Caprine Herpesvirus 1 (CpHV-1)

Infection in Kids. *J Comp Path*. 2000;**122**:298-302.
12. Schlafer DH, Foster RA. Chapter 4: Female Genital System. In: Maxie MG, ed. Jubb, Kennedy, and Palmer's Pathology of Domestic Animals, Volume 3. 6th ed. St. Louis, MO, USA. Elsevier; 2016:433-435.
13. Suavet F, Champion JL, Bartolini L. First Description of Infection of Caprine Herpesvirus 1 (CpHV-1) in Goats in Mainland France. *Pathogens.* 2016; 5(17):1-13.

CASE II:

Signalment:
5-year-9-month-old neutered female Domestic Shorthair cat, *Felis catus*

History:
A 5-year-old neutered female Domestic Shorthair cat was presented to our institution following a two-week history of pollakiuria and urinating in the house, which progressed to ataxia and tetraparesis. Neurologic examination localized the clinical signs to multiple spinal cord segments and an MRI of the spinal cord revealed multifocal intramedullary lesions. The cat was euthanised due to the acute onset, progressive clinical signs and was submitted for necropsy.

Gross Pathology:
Gross examination revealed multifocal, intramedullary, grey-beige areas throughout the spinal cord. The brain was grossly unremarkable. The only other findings were those of splenic congestion and pulmonary reddening (congestion), which were attributed to barbiturate euthanasia.

Laboratory Results:
One year prior to presentation, the submitted cat was tested for FIV, FeLV and *Toxoplasma spp.* (testing method not provided) and was revealed to be positive for FIV and negative for FeLV and *Toxoplasma spp.* At the time of presentation, serology for *Toxoplasma spp.* revealed a high IgG titre (equal to or greater than 800, which is consistent with, though does not confirm active infection) and an IgM titre of <20.

Microscopic Description:
Cervical spinal cord:
Unilaterally, the grey and white matter are focally extensively replaced by large numbers of infiltrating lymphocytes, plasma cells, and fewer macrophages. Neurons in this area are lost and there is amorphous eosinophilic material (necrosis). Within this area are multiple variably sized, approximately 30-60 µm diameter, eosinophilic protozoal cysts bordered by a thin (0.5 µm) capsule and containing numerous 1 µm elongate basophilic bradyzoites (presumptive *Toxoplasma gondii* cysts). Multifocally, there are bands of eosinophilic, fibrillar material (glial scars) and increased numbers of glial cells including gemistocytic astrocytes characterized by large, swollen, eosinophilic cytoplasm, and peripheral round nuclei and gitter cells with foamy cytoplasm and pyknotic nuclei. The adjacent white matter is rarefied and degenerate with distended axon sheaths, occasionally containing swollen, rounded and eosinophilic axons (spheroids) or associated with gitter cells (ellipsoids). Endothelial cells are lined by prominent (reactive) nuclei and Virchow-Robin

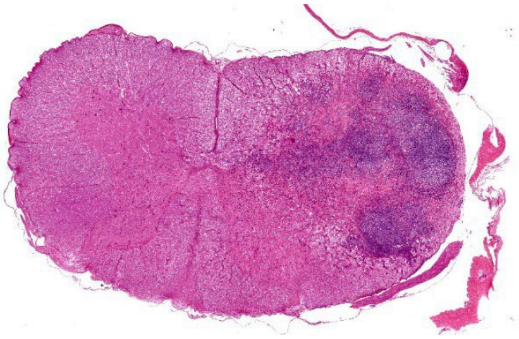

Figure 2-1. Spinal cord, cat. A section of the cervical spinal cord is submitted for examination. There is a large unilateral focus of necrosis, and cellular infiltration at subgross magnification. (HE, 6X)

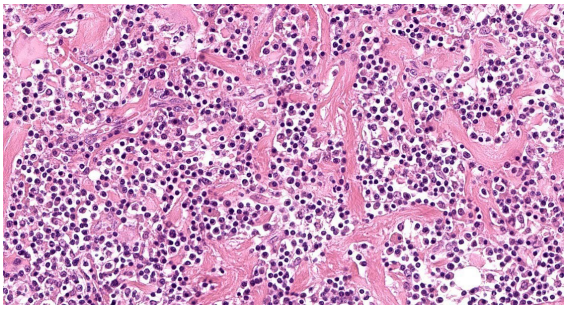

Figure 2-2. Spinal cord, cat. The neuropil (in this case, the white matter) is effaced by innumerable inflammatory cells, with lymphocytes predominating, but there are also large numbers of neutrophils, histiocytes, and plasma cells. (HE, 381X)

spaces are expanded by lymphocytes and plasma cells (perivascular cuffing).

Contributor's Morphologic Diagnoses:
Spinal cord, cervical; focally extensive necrotizing and lymphoplasmacytic myelitis with protozoal cysts (*Toxoplasma gondii*)

Contributor's Comment:
The histologic features in this case are consistent with protozoal necrotizing myelitis due to *Toxoplasma spp.*

Toxoplasma spp. are protozoan parasites able to infect a diverse range of species including humans, nonhuman primates, birds and a large number of mammals[12]. Domestic and non-domestic cats are the definitive host of *Toxoplasma spp.* and become infected following ingestion of asexual stages in tissue or oocysts, or less frequently, congenitally[12]. Organisms then undergo asexual development in intestinal epithelium and can disseminate to a range of other tissues, including the lungs, liver, heart, and nervous system as free organisms or via leukocyte trafficking in lymphocytes or macrophages[11]. Tachyzoites are responsible for the acute presentation of toxoplasmosis and can continue to replicate indefinitely[12].

Typical histologic changes in the central nervous system of cats with active toxoplasmosis include non-suppurative meningoencephalitis and necrosis. Infection in utero can cause placentitis, myocardial injury or systemic inflammation, which in turn lead to necrosis in the brainstem and cerebrocortical white matter[12]. Cell necrosis also occurs directly as a result of intracellular replication of tachyzoites in target cells and subsequent cell lysis or as a consequence of the host immune response. T-cell lymphocytes kill infected cells directly or via interferon-gamma-mediated activation of microglia and astrocytes[11].

Chronic toxoplasmosis is characterized by a dormant stage in which bradyzoites are enclosed within cyst walls and divide slowly. Such bradyzoite-containing cysts are typically found in the brain, skeletal muscle, and myocardium in chronically infected cats[12]. Cyst walls are poorly immunogenic and protect bradyzoites from the host's immune system, allowing them to remain dormant. Thus, there is usually little, if any, associated inflammation. However, in this case, areas of necrosis and inflammation in the spinal cord were associated with bradyzoite-containing cysts.

The finding of bradyzoite cysts within areas of inflammation and necrosis in feline spinal cords has been documented in several case reports of *Toxoplasma* or *Toxoplasma*-like

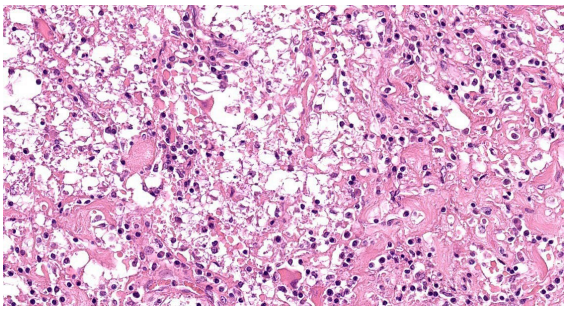

Figure 2-3. Spinal cord, cat. Within the affected white matter, there is necrosis, inflammation and edema (right), dilated myelin sheaths with spheroids (left), and gemistocytic astrocytes (bottom center). (HE, 381X)

infection.[1,6] It is thought that the inflammation in these reports was the result of cyst rupture and zoite release following reactivation of latent infection. From their findings, Lyndsay et al. suggest that when toxoplasmosis in cats manifests as neurologic signs alone, without concurrent systemic signs, it is more frequently due to reactivation than acute infection.[10]

Reactivation of *Toxoplasma* has been reported in immunodeficient or immunosuppressed cats infected with Feline Immunodeficiency Virus (FIV) (as in this case) or receiving immunosuppressive therapy.[2] However, the relationship between concurrent FIV infection and toxoplasmosis is not clear. A recent study by Dubey et al. did not find a correlation between naturally infected cats that were seropositive for FIV and *T. gondii*.[8]

Contributing Institution:
Pathobiology and Population Sciences
Royal Veterinary College
Hawkshead Lane, North Mymms
Hertfordshire
AL9 7TA
United Kingdom

JPC Diagnosis:
Cervical spinal cord: Myelitis, histiocytic and lymphoplasmacytic, unilateral, focally extensive, severe, with gliosis and intracellular protozoal cysts.

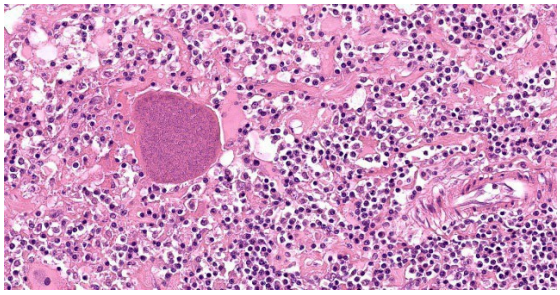

Figure 2-4. Spinal cord, cat. The grey matter is similarly effaced by necrosis and inflammation. Scattered throughout the grey matter are few large protozoal cysts. (HE, 381X)

JPC Comment:
Toxoplasma gondii was first described in 1908 by researchers investigating *Leishmania* in gundis, a type of rodent native to Tunisia.[5] The name was derived from the words *Toxo-*, which means arc and refers to the crescentic shape of zoites; *-plasma*, meaning life; and *gondii*, referring to the species it was first identified in.[5] The first congenital case of *T. gondii* was described in 1938 in a human neonate who died after developing encephalitis and retinitis, and the first case of infection in a cat was diagnosed in 1942.[4,5] In the 1950s, it was discovered to be the causative agent of abortion in ewes in New Zealand (referred to as "type II abortions").[5] Around this time, researchers also discovered links between *T. gondii* infection and the consumption of raw meat and exposure to cat feces, but it wasn't until 1970 that the key to *T. gondii* spread was uncovered: sexual reproduction and shedding of oocysts by felids.[4]

Our knowledge of *T. gondii* has expanded drastically since its initial discovery, and the protozoa is now known to have a worldwide distribution and a wide host range.[5] Felids, both domestic and wild, are the definitive hosts and become infected after ingesting meat infected with bradyzoite-laden cysts.[4] Cats can also be infected by ingesting infected oocytes in feces, but this is less common.[4] There are a wide range of intermediate hosts with significant inter-species variability in morbidity. Australian marsupials and New World monkeys are particularly susceptible to infection, while horses, cattle, and rats seem resistent.[4,11] Other species which can be infected include other mammals, birds. fish, amphibians, and reptiles.[11] Outbreaks in humans have been linked to drinking contaminated water, and it has been speculated that runoff may be the cause of recent infections documented in marine mammals.[8,11]

In cats, acute systemic infections most commonly result in pulmonary, nervous, hepatic, cardiac, and ocular lesions, and, as the contributor mentions, reactivated infections are more commonly restricted to the nervous or ophthalmic systems.[8] *Neospora caninum* and *Sarcocystis neurona* are less common causes of encephalitis and myeloencephalitis in cats.[3,7] These organisms are difficult to impossible to distinguish using light microscopy and should be considered as differential diagnoses in this case. PCR, immunohistochemistry, and serology (as conducted in this case) are generally used to differentiate between these protozoa.[13]

References:

1. Alves L, Gorgas D, Vandevelde M, Gandini G, Henke D. Segmental meningomyelitis in 2 cats caused by *Toxoplasma gondii*. *J Vet Intern Med*. 2011;25:148-152.
2. Barrs VR, Martin P, Beatty JA. Antemortem diagnosis and treatment of toxoplasmosis in two cats on cyclosporine therapy. *Aust Vet J*. 2006;84:30-35.
3. Cantile C, Youssef S. Nervous System. In: Maxie MG, ed. *Jubb, Kennedy, and Palmer's Pathology of Domestic Animals*. Vol 1. 6th ed. 386-389.
4. Dubey JP. History of the discovery of the life cycle of *Toxoplasma gondii. I Journ Parasit*. 2009; 39: 887-882.
5. Dubey JP. The History of *Toxoplasma gondii* – The First 100 Years. *J Eukaryot Microbiol*. 2008; 55(6): 467-475.
6. Dubey JP, Fenner, WR. Clinical segmental myelitis associated with an unidentified Toxoplasma-like parasite in a cat. *J Vet Diagn Invest.* 1993;5:472-480.
7. Dubey JP, Greene CE. Enteric Coccidiosis. In: Greene CE, ed. *Infectious Diseases of the Dog and Cat*. 4th ed. St. Louis, MO : Elsevier; 2012:837.
8. Dubey JP, Lappin MR. Toxoplasmosis and neosporosis. In: Greene CE, ed. *Infectious Diseases of the Dog and Cat*. 4th ed. St. Louis, MO: Elsevier; 2012:806-821.
9. Dubey JP, Lappin MR, Kowk OCH, et al. Seroprevalence of Toxoplasma gondii and concurrent Bartonella spp., Feline Immunodeficiency Virus, and Feline Leukemia Virus Infections in Cats from Grenada, West Indies. *J Parasitol.* 2009;95(5):1129-1133.
10. Lindsay SA, Barrs VR, Child G, Beatty JA, Krockenberger MB. Myelitis due to reactivated spinal toxoplasmosis in a cat. *J Fel Med Surg*. 2010;12:818-821.
11. Miller AD, Zachary, JF. Nervous System. In: Zachary, JF ed. *Pathologic Basis of Veterinary Disease.* 6th ed. St Louis: Elsevier; 2017: 844-845.
12. Uzal FA, Plattner BL, Hostetter JM. Alimentary System. In: Maxie GM, ed. *Jubb, Kennedy & Palmer's Pathology of Domestic Animals*. 6th ed. St. Louis, MO: Elsevier; 2016: 117-243.
13. Vadnevelde M, Higgins RJ, Oevermann A. *Veterinary Neuropathology: Essentials of Theory and Practice.* 1st ed. Ames, IO: John Wiley & Sons, LTD. 2012; 69.

CASE III:

Signalment:
5.5 year old, Female, New Zealand White Rabbit (*Oryctolagus cuniculus*)

History:
2 month history of "red urine". Initial urinalysis was within normal limits, with no RBCs detected. Radiographs revealed urinary blad

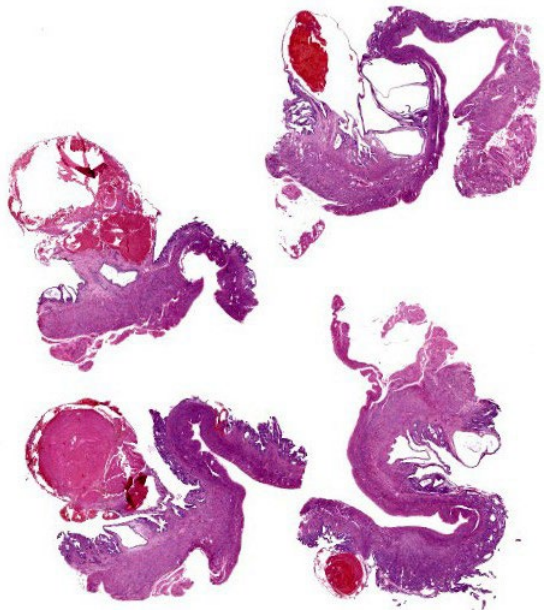

Figure 3-1. Uterus, rabbit. Multiple section of uterus are submitted for examination. A cross section of a large thrombosed endometrial vein and numerous endometrial cysts are evident at subgross magnification. (HE, 6X)

der sludge, which was resolved after subcutaneous fluids. The rabbit was then reported for "red urine" again one month later. Another free-catch urinalysis was submitted which came back positive for red blood cells (too numerous to count) with high protein (100mg/dL) and 1+ cocci. CBC/Chemistry was within normal limits. The rabbit was euthanized at endpoint (for an ocular study) and submitted for necropsy.

Gross Pathology:

An adult female New Zealand White rabbit presents for necropsy several hours post euthanasia via intravenous euthasol. The carcass is in good post-mortem and adequate body condition with adequate subcutaneous and mildly increased visceral adipose stores. Externally, there is an intravenous catheter present in the left ear. There is mild focal yellow staining of the fur surrounding the perineum (urine). The bladder contains a mild amount of thick, moist, white to yellow sediment. The uterus is mildly enlarged, and there are multifocal raised nodules along the uterine horns bilaterally. On cut section, these nodules correspond to semi firm, papillary to polyploid masses that protrude into the uterine lumen, ranging from 1-3 cm in length and 0.5-1.5 cm in diameter. The endometrial surface between the polyploid masses contains numerous variably sized cysts and occasional foci of loosely adhered dark red gelatinous material (clotted blood) ranging from 1-2.5 cm in length. There are no other significant lesions.

Laboratory Results:

CBC/Chemistry: Within normal limits.
Urinalysis (free catch from pan): Red blood cells TNTC; protein 100 mg/dL; 1+ cocci

Uterus: Moderately expanding the endometrium and projecting into the uterine lumen are multifocal dilated veins which contain circular concentric lamellations of red blood cells and fibrin with scattered admixed leukocytes and plump fibroblasts (thrombus). Adjacent endometrium contains macrophages with intracellular brown pigment (hemosiderin, presumptive), mildly dilated blood vessels (congestion), and increased clear space (edema). Endometrial glands are mildly to moderately ectatic and hyperplastic, with attenuated or hyperplastic columnar epithelium occasionally thrown into papillary

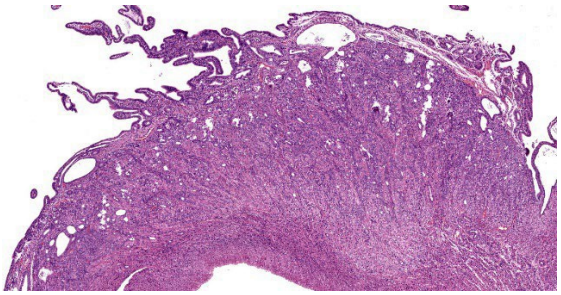

Figure 3-2. Uterus, rabbit. Neoplastic cells forming glands infiltrate the underlying smooth muscle. (HE, 45X)

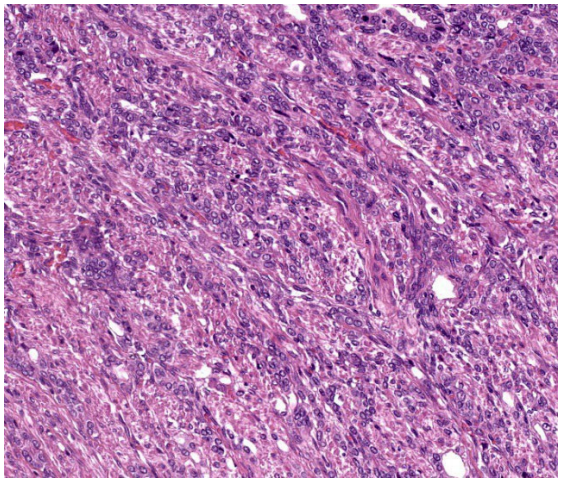

Figure 3-3. Uterus, rabbit. A neoplasm arising in the endometrium infiltrates the underlying uterine mural smooth muscle. (HE, 233X)

folds, and contain low numbers of histiocytes, erythrocytes, and basophilic acellular material. Dysplastic endometrial glands are also present with loss of nuclear polarity, angular glands projecting towards the myometrium, or intraluminal atypical endometrial cells. In other sections of uterus, multifocal uterine adenocarcinoma is present.

Contributor's Morphologic Diagnoses:
Uterus: Endometrial venous aneurysms.
Uterus: Papillary adenocarcinoma, multicentric, with mild multifocal necrosis.
Uterus: Mild multifocal cystic endometrial hyperplasia.

Contributor's Comment:
Hematuria in rabbits may be due to blood originating in the renal system or the reproductive system. Specific causes include neoplasia (uterine adenocarcinoma), uterine or bladder polyps, pyelonephritis or cystis, and urolithiasis.[4,5] An additional cause of hematuria that appears to be unique to lagomorphs is endometrial venous aneurysms. This condition has been reported in multiple species of rabbit, including New Zealand White rabbits and a Holland Lop rabbit.[4,7] The red urine in this case is reproductive in origin and associated with the uterine lesions. Histology of the lesion depicted on this slide was consistent with endometrial venous aneurysm. This rabbit also had multicentric uterine adenocarcinoma, which is not as well represented on this slide.

Grossly, endometrial aneurysms present as dark red, ovoid structures protruding into the uterine lumen from the endometrium, which corresponds microscopically to dilated venous structures containing blood or thrombi.[5] Endometrial venous aneurysms are thought to be a congenital lesion and are characterized by localized venous dilation which may be fusiform or saccular in shape.[7] In humans, congenital aneurysmal lesions of myometrial, cervical, and vaginal vessels but not endometrial veins have been reported.[7] It has also been proposed that prolonged pseudopregnancy, which is common in rabbits and results in prolonged exposure to estrogen and progesterone, may also pay a role in increased vascularity or other vascular changes of the rabbit uterus.[5] In a previous study, endometrial venous aneurysm was identified in 14/854 necropsy cases and 5/150 biopsy cases, with a median age of 32 months.[3]

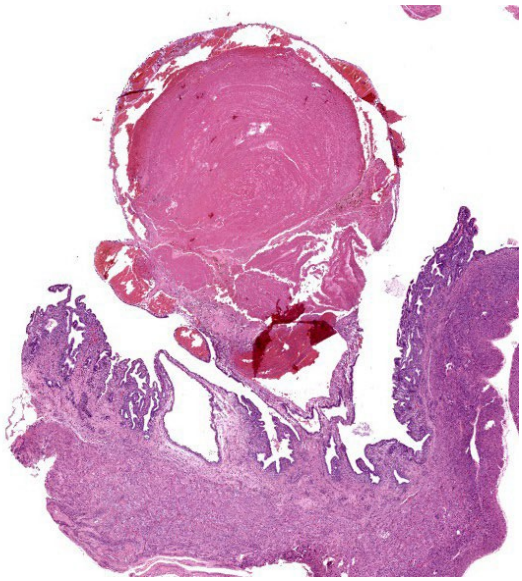

Figure 3-4. Uterus, rabbit. A large thrombosed thin-walled vein measuring 3mm in diameter extends from the endometrium into the uterine lumen. (HE, 45X)

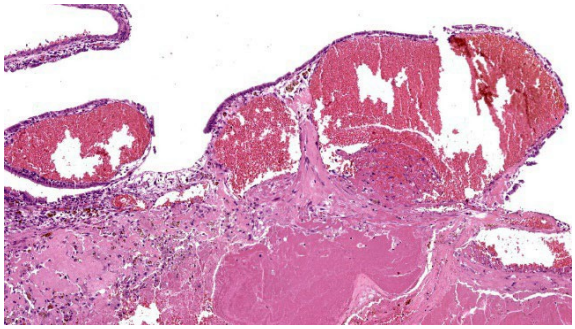

Figure 3-5. Uterus, rabbit. There are smaller vascular lumina at the periphery of the thrombosed vein. The thrombus is attached to the wall and there are siderophages scattered throughout the thrombus. (HE, 96X)

For rabbits that present with hematuria secondary to endometrial venous aneurysms, ovariohysterectomy is recommended because of the risk of life-threatening hemorrhage.[7] Ovariohysterectomy is curative in these cases.[7]

Contributing Institution:
University of Washington
Department of Comparative Medicine
Health Science Center
Seattle, WA 98105

JPC Diagnosis:
1. Uterus: Uterine adenocarcinoma.
2. Uterus: Endometrial venous aneurysms with thrombi.
3. Uterus: Cystic endometrial hyperplasia, diffuse, moderate.

JPC Comment:
The contributor mentions several potential causes of hematuria originating from the reproductive tract in rabbits, including adenocarcinomas and endometrial hyperplasia. Several large-scale studies of neoplasms and uterine lesions in rabbits have demonstrated the relative frequency that these occur. According to several studies, uterine adenocarcinomas are the most frequently diagnosed uterine lesion in rabbits and the third most common neoplasm in rabbits in general, with only mammary carcinomas (20.2% of submissions) and trichoblastomas (18%) occurring with higher frequency in a study of 1238 rabbits.[2,6,9] Most rabbits with uterine adenocarcinoma present with hematuria or serosanguinous vaginal discharge; anorexia is a less common clinical sign.[9] The neoplasm is typically multicentric and nodular and may involve both uterine horns.[1] The average age for diagnosis is 5-6 years of age, and the neoplasm tends to metastasize within 1-2 years to the lungs, liver, bone, or brain.[9]

Endometrial hyperplasia is the second most commonly diagnosed lesion of the rabbit uterus and outnumbers adenocarcinomas in some smaller scale studies.[2,6,8,9,10] Endometrial hyperplasia occurred in 44% of 1928 rabbits with uterine lesions, and the most common clinical signs were similar to adenocarcinoma, with approximately half having hematuria or serosanguinous vaginal discharge and fewer having anorexia. The median age for endometrial hyperplasia is slightly younger, around 4 years.[9,10] Additionally, it is common for adenocarcinoma to develop within areas of endometrial hyperplasia in rabbits, as was described in this case.[2]

In rabbits, hematuria must be differentiated from pigmented urine due to nonpathogenic

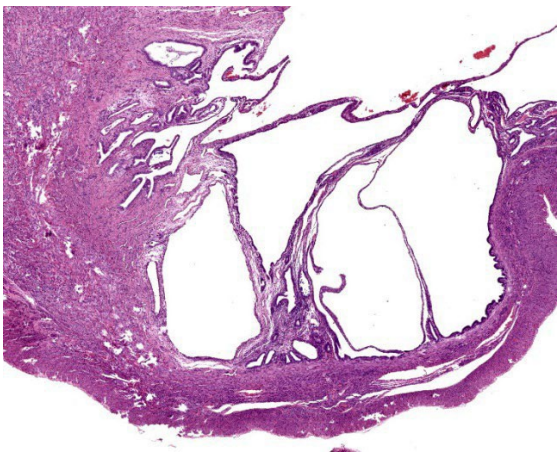

Figure 3-6. Uterus, rabbit. There is marked cystic endometrial hyperplasia of the endometrium. (HE, 26X)

crystals, porphyrins, or bilirubin by conducting a urinalysis, as was done in this case.[1]

References:

1. Barthold SW, Griffey SM, Percy DH. *Pathology of Laboratory Rodents and Rabbits.* 4th ed. Ames, IO: John Wiley and Sons, Inc. 2016: 256, 310, 320.
2. Baum B. Not Just Uterine Adenocarcinoma – Neoplastic and Non-Neoplastic Masses in Domestic Pet Rabbits (*Oryctolagus cuniculus*): A Review. *Vet Pathol.* 2021; 58(5): 890-900.
3. Bertram, CA, Müller K, and Klopfleisch R. Genital tract pathology in female pet rabbits (Oryctolagus cuniculus): a retrospective study of 854 necropsy examinations and 152 biopsy samples. J Comp Path 2018; 164: 17-26.
4. Bray MV, Weir EC, Brownstein DG, and Delano ML. Endometrial venous aneurysms in three New Zealand White rabbits. Lab Anim Sci 1992; 42(4): 360-2.
5. Diagnosis: Uterine Hemorrhage due to Endometrial Venous Aneurysms. Lab Anim 2003; 32(2): 24-25.
6. Kunzel F, Grinniger P, Shibly S. Uterine Disorders in 50 Pet Rabbits. *J Am Anim Hosp Assoc*. 2015; 51(1): 8-14.
7. Reimnitz L, Guzman D, Alex C, et al. Multiple Endometrial Venous Aneurysms in a Domestic Rabbit (Oryctolagus Cuniculus). J Exotic Pet Med 2017; 26: 230–237.
8. Saito K, Nakanishi M, Hasegawa A. Uterine Disorders Diagnosed by Ventrotomy in 47 Rabbits. *J Vet Me Sci.* 2002; 64(6): 495-497.
9. Settai K, Kondo H, Shibuya H. Assessment of reported uterine lesions diagnosed histologically after ovariohysterectomy in 1,928 pet rabbits (*Oryctolagus cuniculus*). *J Am vet Med Assoc.* 2020; 257(10): 1045-1050.
10. Walter B, Poth T, Bohmer E, Braun J, Matis U. Uterine disorders in 59 rabbits. *Vet Rec*. 2010; 166: 230-233.

CASE IV:

Signalment:
A 3-year-old female (intact) Mastiff dog (*Canis familiaris*)

History:
The dog presented with a two-day history of lethargy, inappetence, pyrexia, coughing and a brown/red vaginal discharge. She had been previously diagnosed with a steroid-responsive cough (one year prior to current presentation).

On clinical presentation, the dog was dehydrated, pyrexic and had a thick vaginal discharge. Digital examination of the reproductive tract revealed an open cervix. Abdominal radiographs and ultrasonography showed a fetus with no heartbeat in the uterus. Abortion and pyometra were diagnosed, and an ovariohysterectomy was performed. To further investigate the respiratory disease, thoracic radiographs and bronchoalveolar lavage (BAL) were performed. Radiographs revealed a bronchointerstitial pattern with bronchiectasis and BAL showed a differential count of 40-45% eosinophils, 40-45%

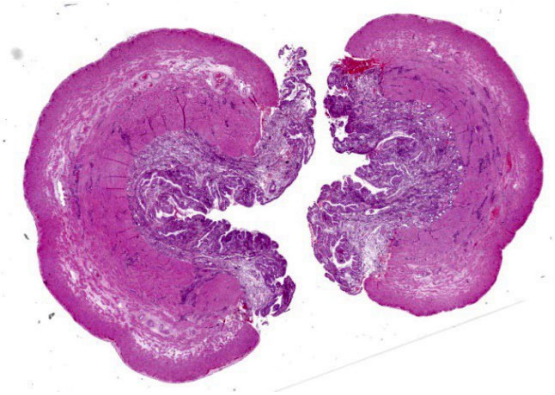

Figure 4-1. Uterus, dog. Two sections of uterus with hyperplastic endometrium are submitted for examination. At subgross, there is a prominent cellular infiltrate. (HE, 5X)

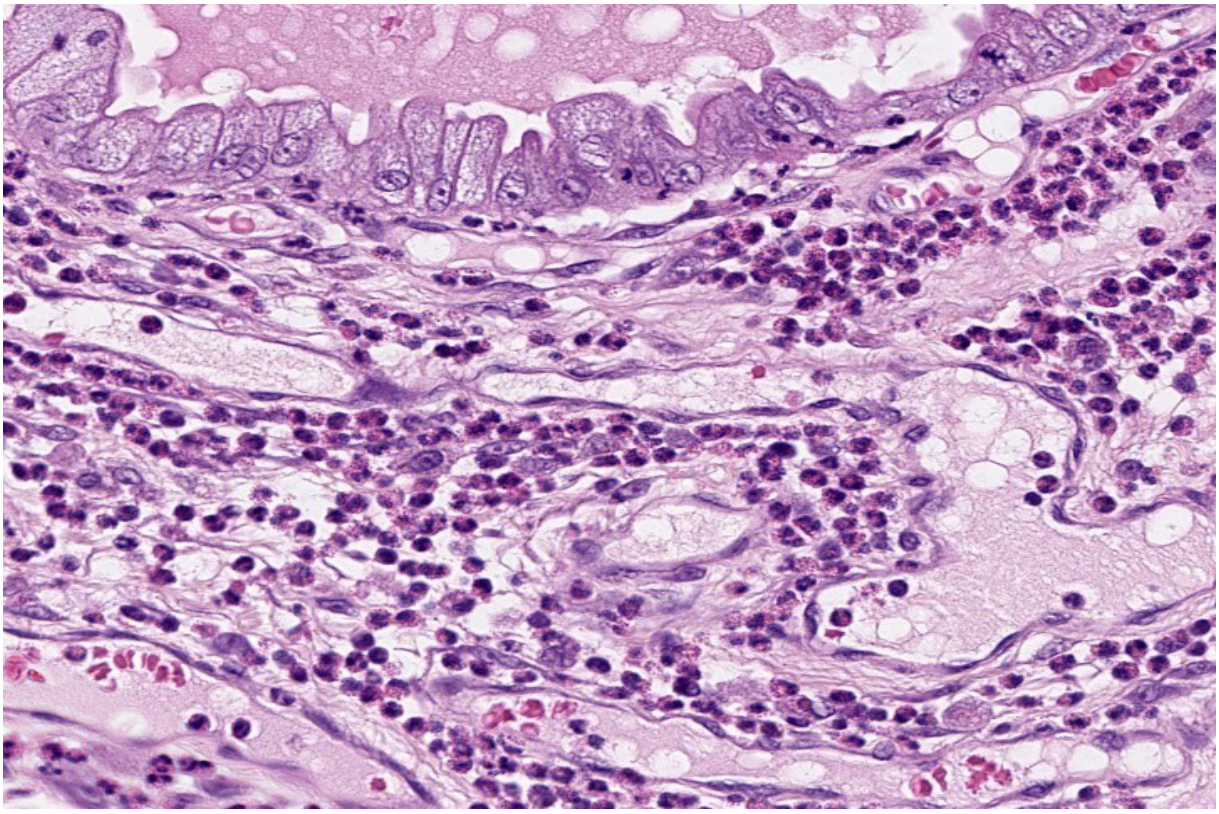

Figure 4-2. Uterus, dog. The edematous stroma is expanded by an infiltrate of large number of eosinophils and fewer foamy macrophages. The endometrial epithelium contains numerous cytoplasmic vacuoles (progesterone change). (HE, 380X)

neutrophils, 10-15% macrophages, and rare lymphocytes in a lightly mucinous background.

Following surgery, the dog presented twice (11 days and 2 months post-surgery) with a cough and labored breathing. On both occasions the dog responded to corticosteroid treatment. Thoracic radiographs taken at two months post-surgery revealed a bronchointerstitial pattern and a 3 cm opaque mass in the caudal lung lobe. Based on clinical and clinico-pathological findings a diagnosis of canine eosinophilic bronchopneumopathy (EBP) was proposed. Unfortunately, there was no repeat bloodwork and the dog was lost to follow up.

Gross Pathology:
The uterus, the placenta and the aborted fetus were submitted for microscopic examination. The uterine mucosa was pale tan to green, irregular and thickened.

Laboratory Results:
CBC showed a marked eosinophilia (11.86 x 10^9/L), neutrophilia (14.35 x 10^9/L), basophilia (1.01 x 10^9/L), and a mild regenerative anemia (HCT 37%). Biochemistry showed a mild increase in creatinine 166 µmol/L (range: 44-159 µmol/L). A Baermann test for lungworm larvae was negative.

Microscopic Description:
Uterus: The endometrium is circumferentially expanded by the presence of large numbers of eosinophils and lesser numbers of foamy macrophages that diffusely infiltrate the interstitium and separate endometrial glands. Multifocally, eosinophils and rare neutrophils are seen migrating through the endometrial epithelial lining. The endometrial glands are mildly dilated, occasionally

tortuous, and mostly lined by cuboidal epithelium. Rare granulocytes are present in the lumen of the glands. In the surface epithelium, cells are arranged in a single layer or are pseudostratified. Endometrial epithelial cells vary from low cuboidal, to tall columnar with eosinophilic foamy cytoplasm and vesiculate nuclei (progestational epithelium). Endometrial blood vessels are moderately congested and lymphatics are ectatic. There are multifocal areas where the endometrial stroma is distended with numerous clear spaces separating blood vessels and endometrial glands (edema). In the lumen of the uterus, there are scattered, multifocal aggregates of erythrocytes, eosinophils and neutrophils admixed with cellular debris. There is moderate to marked edema in the stratum vasculare causing separation of the inner and outer layers of the myometrium with multifocal, dense aggregates of eosinophils infiltrating and separating interconnecting bundles of smooth muscle and surrounding vessels.

Special stains: Luna and Congo red stains demonstrated bright orange to red granules in the cytoplasm of the numerous eosinophils present throughout the endometrium and myometrium.

Tissue autolysis prevented optimal examination of the fetus and the placenta.

Contributor's Morphologic Diagnoses:
Uterus: Eosinophilic endometritis and myometritis**.**

Contributor's Comment:
This case is unique in presenting with eosinophilic endometritis and myometritis, eosinophilic bronchopneumopathy (EBP), and peripheral blood eosinophilia. It is unclear whether the eosinophilic endometritis and myometritis, and the EBP are separate entities or whether these conditions may be part of the multisystemic disorder termed hypereosinophilic syndrome. An eosinophilic leukemia, characteristically presenting with a peripheral eosinophilia count greater than 25 to 30 eosinophils × 10^9/L,[16] was excluded based on a peripheral count of 11.86 x 10^9/L in this patient.

Eosinophilic endometritis and myometritis, representing an abundant eosinophilic infiltration of the endometrium and myometrium respectively, are occasionally reported in dogs. In a recent study, 7.3% of endometrial biopsies in subfertile dogs were classified with eosinophilic endometritis.[12] Despite the surprisingly common incidence of this condition, the pathogenesis and clinical significance remains poorly understood. A significant relationship between eosinophilic endometritis and fetal loss has been established. However, it is unclear if eosinophilic infiltrates result in fetal loss, or if eosinophils infiltrate secondarily to tissue responses associated with placental maturation and late pregnancy.[12] It has been previously reported that high numbers of eosinophils may be present in the uterus of healthy post-partum doges, whereas low numbers of eosinophils may be seen during pro-estrus, estrus, diestrus, early pregnancy and early to mid-anestrus post-partum.[27]

Eosinophilic endometritis has been reported in several other species including ferrets,[11] horses,[23] donkeys,[24] and elk.[4] In ferrets, eosinophilic endometritis was attributed to fetal death resulting from suspected "single kitten syndrome."[11] A similar entity termed "single pup syndrome" has been reported in dogs, where a single-fetus pregnancy results in failure of parturition.[19] It is believed that the single puppy produces insufficient cortisol and ACTH to initiate parturition, and if the birth process is not initiated, the placental supply of oxygen and nutrients diminishes leading to fetal death and mummification or maceration

in utero. A diagnosis of "single pup syndrome" could be potentially considered in the present case. In horses, a causal association between pneumovagina and pneumouterus leading to eosinophilic endometritis has been suggested.[23]

The failure of a single pup to initiate the onset of parturition on or around the expected date has been postulated to be due to the concentration of cortisol secreted by one pup being insufficient to adequately initiate luteolysis via prostaglandin release.

Eosinophilic bronchopneumopathy is a disease characterized by eosinophilic infiltration into the bronchi, terminal bronchioles, alveoli and blood vessels. Siberian Huskies and Alaskan Malamutes appear overrepresented. In some cases, blood peripheral eosinophilias are reported concurrently.[9] Affected dogs usually present with a corticosteroid responsive cough, similar to the patient from the case described here. Eosinophilic bronchopneumopathy is typically diagnosed by cyto logical examination of bronchoalveolar lavage fluid or histologic examination of the bronchial mucosa, combined with radiographic and bronchoscopic findings and exclusion of known causes of eosinophilic infiltration into the airways. In dogs, the most common causes of eosinophilic pneumonitis include heartworm disease caused by *Dirofilaria immitis* and migration of *Angiostrongylus vasorum* larvae through the pulmonary parenchyma.[6,17] *Dirofilaria immitis* is a reportable disease in New Zealand and there are no reports of canine infection with *A. vasorum*, and thus infection with these parasites was considered unlikely in the present case. Less commonly, *Oslerus osleri, Filaroides hirthi, Crenosoma vulpis, Paragonimus kellicotti* and neoplasia (lymphoma and mast cell tumors) have been implicated with pulmonary eosinophilic infiltrates in dogs.[7,18] Other possible causes have been described in the human literature (idiopathic pulmonary fibrosis, medications, mycobacteria or fungi) and could potentially cause this clinical syndrome in dogs, but no reported cases were found in the literature. While the etiology of EPB remains unclear, hypersensitivity to aeroallergens is suspected, however most cases are still considered idiopathic.[7]

Little is known about the cytokines and chemokines involved with EBP. Flow cytometric analysis of BAL samples from dogs with EPB demonstrated an increase of CD4+ T-cells and a decrease of CD8+ T-cells, and resolution of clinical signs with corticosteroid treatment normalized the CD4:CD8 ratio.[8] It was proposed that CD4+ T-cells are at least in part responsible for the infiltration of eosinophils, which has also been shown in asthmatic humans[21] and rodents.[15]

Alternatively, the underlying cause of the multi-organ eosinophilic infiltrates in the present case may be due to idiopathic hypereosinophilic syndrome (HES). This is a rare systemic illness of unknown cause and presents as a sustained peripheral eosinophilia ($>5\times10^9$/L) with multi-organ infiltration causing dysfunction.[16] In humans, peripheral eosinophilia must be present for at least 6 months to be considered HES.[5] Although the cause of HES is still considered idiopathic, it has been proposed that generalized immune

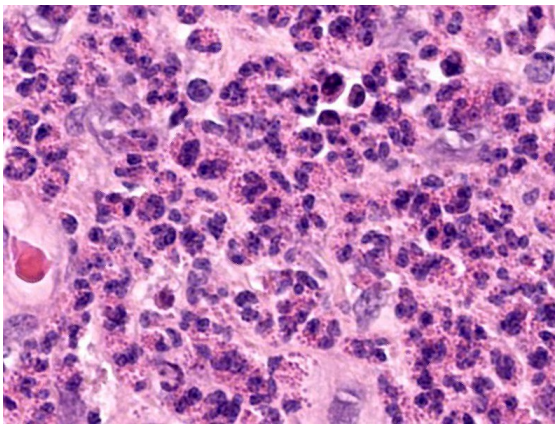

Figure 4-3. Uterus, dog. Higher magnification of the eosinophilic endometrial infiltrate. (HE, 1180X)

dysregulation may lead to increased maturation and recruitment of eosinophils from the bone marrow that enter the circulation and target tissues and organs. Several cytokines, particularly IL-5 and eotaxin, which prime, activate and enhance eosinophilic migration into tissues, have been implicated with HES.[16] In dogs, Rottweilers appear overrepresented,[25] and the condition has been reported in cats,[26] humans,[5] and an owl monkey.[13] In horses, multisystemic eosinophilic epitheliotropic disease is considered the equivalent to HES. Affected horses present with a peripheral eosinophilia of unknown primary origin with multi-organ infiltration.[22]

In dogs with HES, eosinophilic infiltrates have been reported in several organs including the liver, spleen, lung parenchyma, myocardium, lymph nodes, skeletal muscle and bone marrow.[1,14,20,25] Although pulmonary eosinophilic infiltrates are common in dogs with HES, the case presented here could be the first description of uterine infiltrates in an HES dog.

In the human literature, few reports of pregnant women with HES appeared to have minimal complications with no mention of eosinophilic uterine infiltrates. One baby was delivered with a transient hypereosinophilia and there was a single report of a premature twin delivery, however these and all other cases resulted ultimately in the delivery of healthy infants.[2,3]

In this case, the concurrent EBP, eosinophilic myometritis, endometritis and blood peripheral eosinophilia raise the question whether this case should be considered an unusual presentation of HES. A similar report of two Cavalier King Charles Spaniels presenting with eosinophilic stomatitis, peripheral eosinophilia and eosinophilic disease in other body systems also questioned if these cases

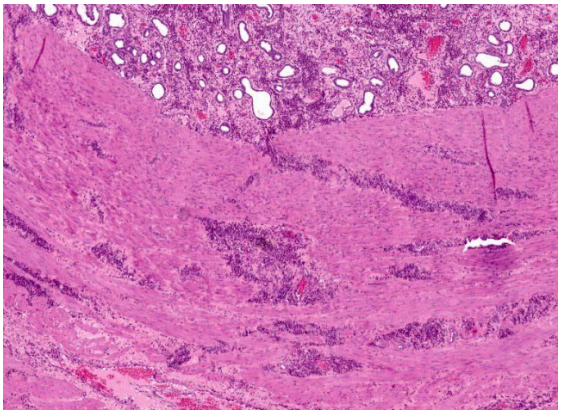

Figure 4-4. Uterus, dog. The eosinophilic infiltrate extends along perivascular connective tissue within the uterine smooth muscle. (HE, 35X)

were unusual presentations of HES.[10] Unfortunately, this case was lost to follow up and a definitive diagnosis could not be established. The persistence and worsening of a corticosteroid responsive cough following ovariohysterectomy, and the presence of similar clinical signs one year prior to presentation, suggests at least EBP. Alternatively, the likelihood of HES with pulmonary and uterine infiltrates is also equally considered.

Contributing Institution:
IVABS
Massey University
Palmerston North, New Zealand
http://www.massey.ac.nz

JPC Diagnosis:
1. Uterus: Endometritis, eosinophilic, diffuse, severe, with edema.
2. Uterus, endometrium: Hyperplasia, diffuse, moderate, with progestational change.

JPC Comment:
The contributor provides a great overview of eosinophilic bronchopneumopathy, eosinophilic endometritis, and the possible link with hypereosinophilic syndrome (HES) in this patient. As the contributor states, HES is a rare and life-threatening disease in dogs and information regarding pathogenesis and

treatment is extrapolated from the human literature.

One common sequela in humans with HES is a thromboembolic event.[17,21] In HES patients, several proteins, cytokines, and chemokines produced by eosinophils create a hypercoagulable state.[17,21] Major basic protein damages endothelial cells, causing endothelial cell and platelet activation, while eosinophil cationic protein activates factor XII (Hageman factor).[21] Eosinophils also release both tissue factor and plasminogen activator inhibitor 2 and separately inhibit fibrinolysis.[17] The net result is a hypercoagulable state, and in humans this manifests as microvascular thrombi in multiple organs and large thrombi within the heart.[17] A case of HES-induced thromboembolism was recently reported in a 3 year old boxer dog. The animal presented with respiratory distress, marked eosinophilia, and a thrombus in the left atrium visible on echocardiography.[17] Increased D-dimer levels and tissue-factor-activated thromboelastography confirmed that the dog was hypercoagulable, and the dog was euthanized after it developed acute aortic thromboembolism and paraplegia.[17] On necropsy, eosinophils infiltrated the lungs, liver, spleen, and lymph nodes and accounted for 90% of the myeloid cells in the bone marrow.[17] This was the first case to be thoroughly documented in a dog; however a similar case was reported in an 11 year old mixed breed dog with HES and a possible intracardiac thrombus on echocardiography.[21] This patient was unique in that it responded well to treatment with hydroxyurea and prednisolone, and the thrombus was not apparent 3 months later.[21] These case reports illustrate that hypercoagulability may be a consequence of HES in dogs, and thromboembolism may be prevented with rapid treatment and resolution of hypereosinophilia, as has been shown in human medicine.[17]

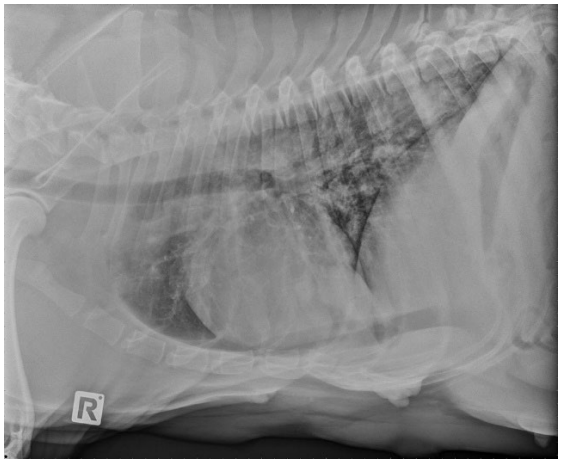

Figure 4-5. Thoracic radiograph, dog. There was a diffuse interstitial pattern and a single nodule within the caudodorsal lobe at presentation. (Photo courtesy of: IVABS, Massey University, Palmerston North, New Zealand, http://www.massey.ac.nz)

In addition to the differentials listed by the contributor, another differential diagnosis for hypereosinophilia is paraneoplastic syndrome. In dogs, cats, horses, and humans, lymphomas can rarely cause hypereosinophilia.[20] It is believed that lymphocytes elaborate products like IL-3, IL-5, and GM-CSF which inhibit eosinophil apoptosis and result in eosinophilia.[20]

References:

1. Aroch I, Perl S & Markovics A. Disseminated eosinophilic disease resembling idiopathic hypereosinophilic syndrome in a dog. *Vet Rec*. 2001;149(13):386-389.
2. Albrecht AE, Hartmann BW, Kurz C, Cartes F & Husslein PW. Idiopathic hypereosinophilic syndrome and pregnancy. *Acta Obstet Gynecol Scand*. 1997;76(5):485-486.
3. Ault P, Cortes J, Lynn A, Keating M & Verstovsek S. Pregnancy in a patient with hypereosinophilic syndrome. *Leuk Res*. 2009;33(1):186.
4. Bender LC, Schmitt SM, Carlson E, Haufler JB & Beyer Jr DE. Mortality of Rocky Mountain elk in Michigan due to meningeal worm. *J Wildl Dis.* 2005;41(1):134-140.

5. Brigden M L. A practical workup for eosinophilia: you can investigate the most likely causes right in your office. *Postgrad Med.* 1999;105(3):193-210.
6. Calvert CA & Losonsky JM. Pneumonitis associated with occult heartworm disease in dogs. *J Am Vet Med Assoc*. 1985;186(10):1097-1098.
7. Clercx C & Peeters D. Canine eosinophilic bronchopneumopathy. *Vet Clin North Am Small Anim Pract.* 2007;37(5):917-935.
8. Clercx C, Peeters D, German AJ, et al. An immunologic investigation of canine eosinophilic bronchopneumopathy. *J Vet Intern Med*. 2002;16(3):229-237.
9. Clercx C, Peeters D, Snaps F, et al. Eosinophilic bronchopneumopathy in dogs. *J Vet Intern Med.* 2000;14(3):282-291.
10. German AJ, Holden DJ, Hall EJ & Day MJ. (2002). Eosinophilic diseases in two Cavalier King Charles spaniels. *J Small Anim Pract*. 2002;43(12):533-538.
11. Garrigou A, Huynh M, & Pignon C. Dystocia in a young ferret (Mustela putorius furo) with a possible "single kitten syndrome". *Rev Vét Clin.* 2004;49(2):63-66.
12. Gifford AT, Scarlett JM, & Schlafer DH. Histopathologic findings in uterine biopsy samples from subfertile doges: 399 cases (1990–2005). *J Am Vet Med Assoc*. 2014;244(2):180-186.
13. Gozalo AS, Rosenberg HF, Elkins WR, Montoya EJ & Weller RE. Multisystemic eosinophilia resembling hypereosinophilic syndrome in a colony-bred owl monkey (*Aotus vociferans*). *J Am Assoc Lab Anim Sci*. 2009;48(3):303.
14. James FE & Mansfield CS. Clinical remission of idiopathic hypereosinophilic syndrome in a Rottweiler. *Aust Vet J*. 2009;87(8):330-333.
15. Lee JJ, McGarry MP, Farmer SC, et al. Interleukin-5 expression in the lung epithelium of transgenic mice leads to pulmonary changes pathognomonic of asthma. *J Exp Med*. 1997;185(12):2143-2156.
16. Lilliehöök I & Tvedten H. Investigation of hypereosinophilia and potential treatments. *Vet Clin North Am Small Anim Pract.* 2003;33(6):1359-1378.
17. Madden VR, Schoeffler GL. Idiopathic hypereosinophilic syndrome resulting in distal aortic thromboembolism in a dog. *J Vet Emerg Crit Care*. 2016; 0(00):1-6.
18. Martin MWS, Ashton G, Simpson VR, & Neal C. Angiostroneylosis in Cornwall: clinical presentations of eight cases. *J Small Anim Pract*. 1993;34(1):20-25.
19. McLean L. Single pup syndrome in an English Bulldog: failure of luteolysis. *Companion Anim.* 2012;17(9):17-20.
20. McNaught KA, Morris J, Lazzerini K, Millins C, Jose-Lopez R. Spinal extradural T-cell lymphoma with paraneoplastic hypereosinophilia in a dog: clinicopathological features, treatment, and outcome. *Clin Case Report.* 2018; 6(6):999-1005.
21. Perkins MC & Watson ADJ. Successful treatment of hypereosinophilic syndrome in a dog. *Aust Vet J*. 2001;79(10):686-689.
22. Robinson DS, Bentley AM, Hartnell A, Kay AB, & Durham SR. Activated memory T helper cells in bronchoalveolar lavage fluid from patients with atopic asthma: relation to asthma symptoms, lung function, and bronchial responsiveness. *Thorax*. 1993;48(1):26-32.
23. Singh K, Holbrook TC, Gilliam LL, Cruz RJ, Duffy J & Confer AW. Severe pulmonary disease due to multisystemic eosinophilic epitheliotropic disease in a horse. *Vet. Pathol*. 2006;43(2):189-193.
24. Slusher, S. H., Freeman, K. P., & Roszel, J. F. Eosinophils in equine uterine cytology and histology specimens. *J Am Vet Med Assoc*. 1984;184(6):665-670.
25. Sokkar SM, Hamouda MA & El-Rahman SM. Endometritis in she donkeys in

Egypt. *J Vet Med Series B*. 2001;48(7):529-536.
26. Sykes JE, Weiss DJ, Buoen LC, Blauvelt MM & Hayden D W. Idiopathic hypereosinophilic syndrome in 3 Rottweilers. *J Vet Intern Med*. 2001;15(2):162-166.
27. Taboada J. Pulmonary diseases of potential allergic origin. *Semin Vet Med Surg (Small Anim)*. 1991;6(4):278-285.
28. Takeuchi Y, Matsuura S, Fujino Y et al. Hypereosinophilic syndrome in two cats. *J Vet Med Sci*. 2008;70(10):1085-1089.
29. Watts J, Wright P, Lee C. Endometrial cytology of the normal dog throughout the reproductive cycle. *J Small Anim Pract.* 1998;39(1):2-9.

WSC 2022-2023 Self-assessment.
Conference 10

1. In adult goats infected with caprine herpesvirus-1, disease is most commonly seen in which of the following systems?
    a. Respiratory
    b. Reproductive
    c. Endocrine
    d. Nervous

2. True or false? Tachyzoites are responsible for the acute presentation of toxoplasmosis and can continue to replicate indefinitely.
    a. True
    b. False

3. True or false? Endometrial venous aneurysms are thought o be congenital in origin.
    a. True
    b. False

4. Which of the following is considered to be the driving cell type in eosinophilic bronchopneumopathy?
    a. B-cells
    b. CD-8 T-cells
    c. Macrophages
    d. CD-4 T-cells

5. “Single puppy syndrome” is thought to be the result of which of the following?
    a. Placental insufficiency
    b. Excessive size at parturition
    c. Uterine inflammation at parturition
    d. Insufficient cortisol at parturition

Please email your completed assessment for grading to Dr. Bruce Williams at bruce.h.williams12.civ@mail.mil. Passing score is 80%. This program (RACE program 33611) is approved by the AAVSB RACE to offer a total of 0.5 CE Credits, with a maximum of 12.5 CE Credits being available to any individual Veterinary Medical Professionals for the 2019-2020 Wednesday Slide Conference. This RACE approval is for the subject matter categories of: SCIENTIFIC using the delivery method of NONINTERACTIVE DISTANCE. This approval is valid in jurisdictions which recognize AAVSB RACE.

Joint Pathology Center
Veterinary Pathology Services

WEDNESDAY SLIDE CONFERENCE 2022-2023

Conference #11 30 November 2022

CASE I:

Signalment:
Adult female giant Pacific octopus (*Enteroctopus dofleini*)

History:
Octopus arrived to the National Aquarium in Baltimore bright, alert, and responsive, but missing multiple distal limb pieces, suspected to be traumatic in nature. Two weeks after capture, this octopus was noted to be hyporexic. Fecal examination was concerning for cystic structures, possibly *Aggregata sp*. Octopus was noted to be dark in color and posturing strangely the next morning, reportedly standing on its limbs. The animal was found deceased after lunch; lack of heartbeat was confirmed via Doppler and ultrasound. Prior to death, water temperature was noted to be within normal limits and dissolved oxygen content at 99%.

Gross Pathology:
The submitting institution performed the gross examination which identified partial traumatic amputation of the distal arms of R1-3, L2, and L4, as well as marked gill pallor. Hemolymph drawn after death was clear when drawn, but turned deep blue (aerated) after 1 minute in the collection tube. The kidneys were also said to contain multiple pinpoint white spots of unknown significance.

Laboratory Results:
Below are values from the aforementioned post-mortem sample; published reference intervals (RI) for hemolymph in octopus are not available.
Hemocyte count: 2.255k/uL (empirically low)
Copper: 174.925 mcg/dL (likely appropriate, RI unknown)
Chemistry: Glu 20 mg/dL (empirically low), *Na 376.2 mmol/L (likely appropriate, RI unknown), K 12.6 mmol/L (empirically high), Cl 402 mmol/L (empirically high)*, TP 11.4 g/dL (empirically very high)

Microscopic Description:
Gill: Moderate numbers of macrogametes are embedded in the connective tissue of the gill lamellae. These round to ovoid cystic structures, with a central nucleus and a large, darkly staining nucleolus, measure up to 100

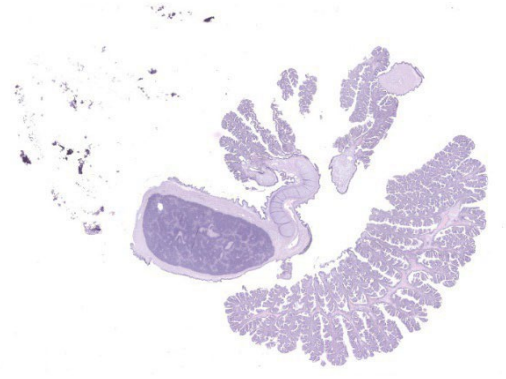

Figure 1-1. Gill lamellae, octopus. A cross section of the gill is submitted for examination. There is no abnormality at subgross magnification. The branchial gland is at left. (HE, 5X)

μm in diameter and frequently invade the gill epithelium. Cysts contain abundant finely granular or vacuolated basophilic cytoplasm. Hemocytic infiltration of the affected gill lamellae is variable, with some areas of severe hemocytic inflammation noted in the interstitium of the gill lamellae. Hypertrophy of infected epithelial cells is quite prominent in some regions. The centralized branchial gland is unaffected. In some sections, low numbers of flagellate protozoa are noted adherent to the apical surface of gill epithelial cells, consistent with *Ichthyobodo sp.*

Contributor's Morphologic Diagnoses:
Gill lamina: coccidiosis, multifocal, moderate with intralesional macrogametes.

Contributor's Comment:
The eimeriorin coccidian protozoal organisms of the genus *Aggregata* and the greater phylum Apicomplexa are frequently found to infect the digestive tract of a diverse number of cephalopods. These parasites can cause damage to the host tissue including direct mechanical injury, as well as indirect enzymatic and innate immune effects.[2] This leaves cephalopods under considerable stress, most commonly those housed in fishery or aquaculture situations, vulnerable to secondary infections. Additionally, it has been reported

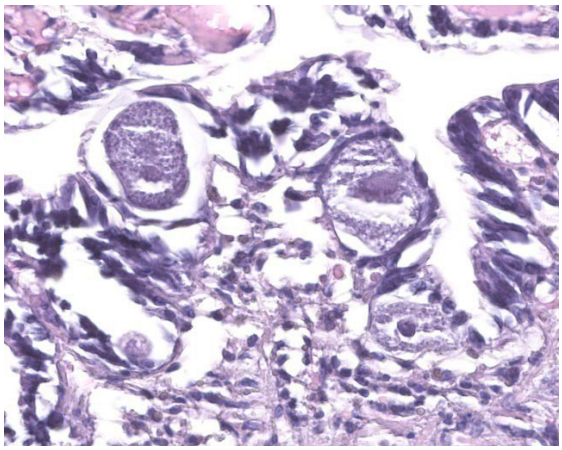

Figure 1-2. Gill lamellae, octopus. Apicomplexan gametocytes with granulated cytoplasm and a single homogenous nucleus are embedded within the hyperplastic epithelium. (HE, 574X)

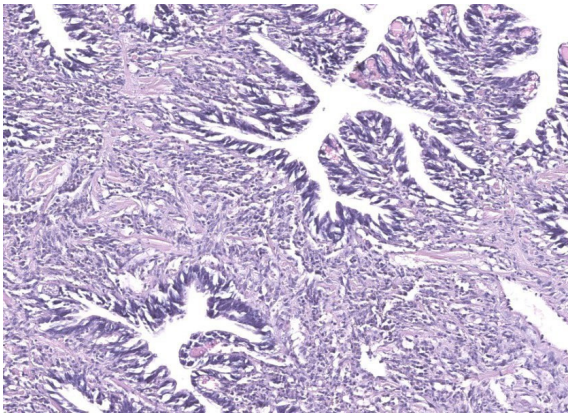

Figure 1-3. Gill lamellae, octopus. The connective tissue of the gill lamella is infiltrated by large numbers of hemocytes. (HE,144X)

that the enzymatic disturbances that occur in octopods result in malabsorption, producing a gradual decline in protein levels, emaciation, and even death.[3] In the past 25 years, *Aggregata spp.* organisms have been considered the most important disease-producing infectious agent in both wild and cultured populations of the common octopus (*Octopus vulgaris*), a major protein source in many fish-eating countries.[4] Infections have previously been described in the intestinal tracts of giant Pacific octopuses (*Enteroctopus dofleini*) from this colony as the result of a newly identified species, *Aggregata dobelli*.[8]

Aggregata spp. coccidia have heteroxenous development with the asexual stages (merozoites, meronts) invading the intestinal epithelial cells of crustaceans, the intermediate host, until subsequent ingestion by cephalopods.[2] These merogonial stages can then infect the digestive tract of the definitive host, as well as the epithelial cells of other tissues, such as the gill lamellae. To gain access to these extraintestinal sites of infection, the invasive oocysts are able to migrate through tissues, causing hypertrophy of invaded cells, hemocytic infiltration, and, consequently, phagocytosis by these hemocytes.[5] Oocyst and macrogamete stages are frequently observed embedded in the connective tissue and surrounded by a thin cyst wall or a multi

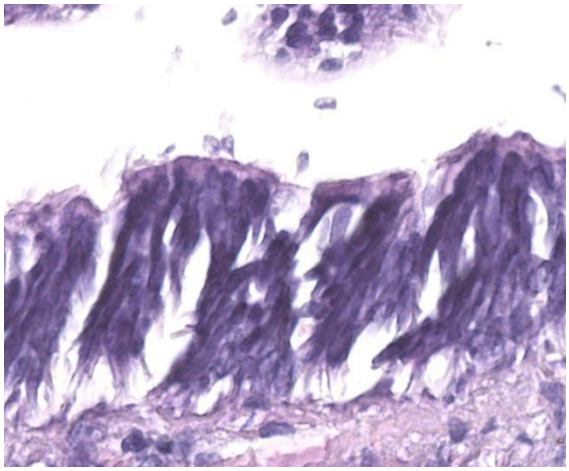

Figure 1-4. Gill lamellae, octopus. Ichthyobodo sp. are attached to the hyperplastic gill epithelium. (HE, 890X)

layered dark membrane. In some cases, abundant developmental stages may be accompanied by desquamation and necrosis of the gill epithelium.

Detection of coccidiosis may be particularly important in octopods caught from the wild for rearing in aquaculture or exhibition in aquariums. Fecal oocyst count is the most common method of detection, although there are no standardized ranges of normal recognized in cephalopods. Determination of the species relies on the morphological characterization of the size, shape, and number of sporozoites in each sporocyst, as well as the ornamentation.[2] For example, *Aggregata dobelli* has a smooth-surfaced sporocyst containing 9-22 sporozoites. The positive identification of this developmental stages requires histological examination of the digestive tract, which cannot be performed in living animals. Treatment also presents a significant dilemma. While protozoan infections in aquarium species are typically controlled through the addition of ionic or chelated copper, high concentrations of formalin, or chloroquine diphosphate solutions to closed tanks, these methods are unsuitable for use on octopods.[1] Thus, the ongoing study of coccidiosis in cephalopods requires new methods of both molecular detection and eradication of these parasites.

Contributing Institution:
Johns Hopkins School of Medicine Department of Molecular & Comparative Pathobiology (https://mcp.bs.jhmi.edu/)

JPC Diagnosis:
Gill: Branchitis, hemocytic, diffuse, moderate, with numerous intraepithelial macrogametocytes (etiology consistent with *Aggregata* sp.) and few surface flagellates (etiology consistent with *Ichthyobodo* sp.).

JPC Comment:
The contributor provides an excellent overview of *Aggregata,* a very important pathogen of octopuses. Another organism featured in this case is *Ichthyobodo*, a free swimming flagellate which can infect freshwater and marine fish and octopuses.[7] The flagellate, which measures 6-10 µm, attaches to and penetrates epithelial surfaces, especially the gills.[7] Gross lesions are typically minimal, and histologic lesions range from absent to severe bronchitis with epithelial degeneration and necrosis.[6,9] The parasites may not be seen histologically as they quickly depart the host after it dies.[9] In a recent survey of 19 wild-caught giant Pacific octopuses which died captivity, ten of the animals had *Ichthyobodo* infections, nine of which had severe bronchitis.[6] In this case, *Ichthyobodo* is present in low levels and was probably not pathogenic to the patient.

References:

1. AZA Aquatic Invertebrate Taxon Advisory Group (AITAG). *Giant Pacific Octopus (Enteroctopus dofleini) Care Manual.* Association of Zoos and Aquariums; 2014.
2. Castellanos-Martínez S, Gestal C, Pascual S, Mladineo I, Azevedo C. Protist (Coccidia) and Related Diseases. In: Gestal C, Pascual S, Guerra Á, Fiorito

G, Vieites J, eds. *Handbook of Pathogens and Diseases in Cephalopods*. 1st ed. Springer, Cham; 2019.
3. Gestal C, Páez de la Cadena M, Pascual S. Malabsorption syndrome observed in the common octopus *Octopus vulgaris* infected with *Aggregata octopiana* (Protista: Apicomplexa). *Diseases of Aquatic Organisms,* 2002; 51: 61–65.
4. Gestal C, Guerra A, Pascual S. *Aggregata octopiana* (Protista: Apicomplexa): a dangerous pathogen during commercial *Octopus vulgaris* ongrowing. *ICES Journal of Marine Science*, 2007; 64: 1743–1748.
5. Mladineo I, Bočina I. Extraintestinal gamogony of *Aggregata octopiana* in the reared common octopus (*Octopus vulgaris*) (Cephalopoda: Octopodidae). *Journal of Invertebrate Pathology*, 2007; 96: 261-264.
6. Newton AL, Smolowitz R. Invertebrates. In: *Pathology of Wildlife and Zoo Animals.* Cambridge, MA: Elsevier. 2018: 1043.
7. Noga EJ. *Fish Disease Diagnosis and Treatment.* 2nd ed. Ames, IO: Wiley Blackwell. 2010; 148-150.
8. Poynton SL, Reimschuessel R, Stoskopf MK. *Aggregata dobelli* N. Sp. and *Aggregata millerorum* N. Sp. (Apicomplexa: Aggregatidae) from Two Species of Octopus (Mollusca: Octopodidae) from the Eastern North Pacific Ocean. *Journal of Protozoology*, 1992; 39(1): 248-256.
9. Seeley KE, Clayton LA, Hadfield CA, et al. Retrospective review of mortality in giant Pacific octopus (*Enteroctopus dolfeini*).

CASE II:

Signalment:
An adult, captive, female giant spider crab (*Macrocheira kaempferi*; Temminck, 1836).

History:
This giant spider crab (*Macrocheira kaempferi*) was found deceased after a short period of anorexia. Other decapods in the tank had shown signs of "shell disease syndrome".

Gross Pathology:
At necropsy, the main gross pathologic findings were multifocal, variably sized, dark brown to black, depressed skin foci in the apron, limb, and carapace

Laboratory Results:
Multiple bacterial cultures of skin and internal organs from other similarly affected and deceased crabs yielded *Vibrio* sp. (1+), *Shewanella putrefaciens* (1+), and *Corynebacterium* sp. (1+).

Microscopic Description:
Apron, Carapace, Limb: Multifocally, the epi-, exo- and endo-cuticle as well as the membranous layer are eroded and ulcerated. Variable amounts of proteinaceous material and hemocyte debris expand and disrupt the cuticle, membranous layer, and epidermis. Multifocally, the epidermis and dermis are infiltrated by granular and reactive agranular hemocytes, occasional melanized cells, karyorrhectic cellular debris and extracellular and intraphagocytic bacteria. Inflammatory

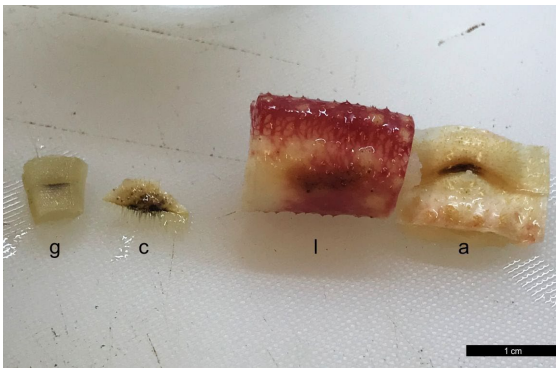

Figure 2-1. Carapace, spider crab. There are multifocal, dark brown to black, depressed skin foci in the apron, limb, and carapace. (Photo courtesy of: Texas A&M Veterinary Medical Diagnostic Laboratory (TVMDL), 483 Agronomy Rd, College Station, TX 77843, USA. https://tvmdl.tamu.edu/)

infiltrates are often more prominent at the setae. Some of these hemocytes infiltrate the connective tissue amid myocytes and variably infiltrate and disrupt vascular structures, more prominently within the deep soft tissue in the apron. Rare hemocyte nodule formation is noted. Hemolymph sinuses exhibit occasional eosinophilic globules.

Gill: Multifocally, the gills are infiltrated and disrupted by granular and agranular hemocytes, cellular debris, proteinaceous fluid, and intraphagocytic and intravascular bacteria.

Contributor's Morphologic Diagnoses:
Apron, Carapace, Limb: Mild to marked, multifocal, subacute erosivo-ulcerative hemocyte epidermitis and dermatitis/hypodermitis with intralesional and intravascular gram-negative bacteria, melanization, and vasculitis.

Gill: Moderate, multifocal, subacute hemocyte branchitis with intralesional and intravascular gram-negative bacteria.

Contributor's Comment:
Based on the clinical history and bacterial culture results from similarly affected and deceased conspecifics, the gross and histopathologic findings in this crab are strongly suggestive of black spot shell disease syndrome (SDS) and hemocoelic bacterial invasion (septicemia).[3,12,15]

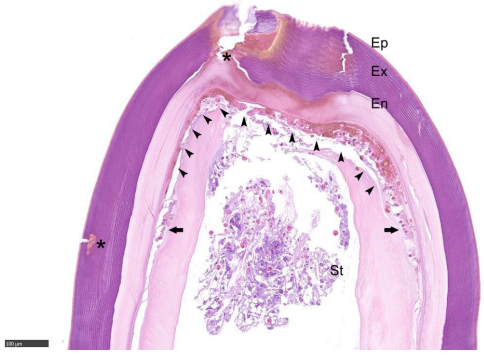

Figure 2-2. Carapace, spider crab. Multifocally, the epi-, exo- and endo-cuticle as well as the membranous layer are eroded and ulcerated. (Photo courtesy of: Texas A&M Veterinary Medical Diagnostic Laboratory (TVMDL), 483 Agronomy Rd, College Station, TX 77843, USA. https://tvmdl.tamu.edu/)

Macrocheira kaempferi (infraorder Brachyura, order Decapoda) is the largest of extant Arthropoda. This species occurs along the Pacific coast of Japan, at depths ranging from 50 to 400 m.[5] Although *M. kaempferi* has been introduced into aquaria worldwide, knowledge on health and disease aspects in the species is very limited.[1,8]

SDS is regarded as a multifactorial syndrome and is one of the main concerns on crabs newly introduced into aquaria.[1,9] Two potential forms of SDS have received attention. These include a) the "classic" form, which is centered around chitin degradation and has been reported in many crustaceans, including lobsters, crabs and shrimp,[7,13] and b) an "epizootic" form, in which chitin degradation is of less significance and primarily affects lobsters.[2] Various environmental stressors[14] and opportunistic chitinolytic bacteria (particularly in the classic form), such as *Vibrio* sp, *Photobacterium* sp, *Aeromonas* sp, *Alteromonas* sp, *Pseudoalteromonas* sp, *Clostridium* sp, *Cytophaga* sp, *Chromobacteria* sp., protozoans and/or fungi play central roles.[4,14,10] High occurrence is linked to polluted environments.[14]

Grossly, SDS is characterized by exoskeletal erosions, pitting, and discoloration, including typical black spots resulting from melanization.[4] Lesions vary from mild (restricted to the exoskeleton), to severe, where injury may extend through the entire shell and into the soft tissues, often resulting in extensive ulcers, fractures, and autotomy.[6] Lesions may initiate via destruction of the epicuticular layer, by proteolytic and lipolytic microbial activities, predatory or cannibalistic attacks,

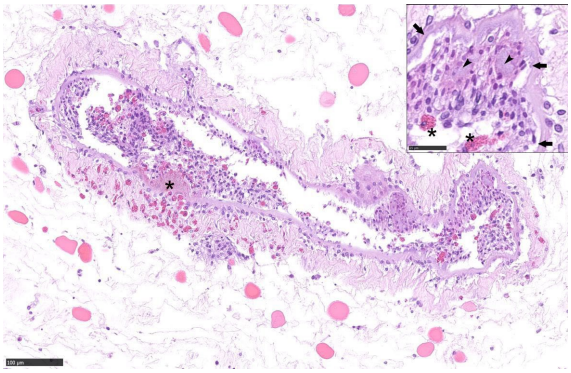

Figure 2-3. Carapace, spider crab. Hemocytes infiltrate the connective tissue, myocytes vascular structures, more prominently within the deep soft tissue in the apron. (Photo courtesy of: Texas A&M Veterinary Medical Diagnostic Laboratory (TVMDL), 483 Agronomy Rd, College Station, TX 77843, USA. https://tvmdl.tamu.edu/)

chemical injury or the abrasive action of sediment and/or articulated body parts; the setal pores are often affected first and may favor internal invasion.[7] Microscopically, there is progressive erosion, ulceration and disruption of the exoskeleton and epidermis. The inflammatory response may include exudation of proteinaceous material, hemocyte debris, infiltration of granular and reactive agranular hemocytes, melanized cells, and extracellular and intraphagocytic bacteria; these changes were observed in the present case. In severe cases, bacteria may extend into the internal viscera and mortality can ensue as result of primary or secondary infection.[12] In the present case, traumatic skin injury by conspecific males likely predisposed to opportunistic bacterial colonization, resulting in eventual hemocoelic bacterial invasion, septicemia, and death.[11,12]

SDS is difficult to control and eradicate, despite occasional remission after molting.[3] Although fallible, treatment methods have been proposed to contain disease progression.[1] In conclusion, the diagnosis of SDS relies upon visualization of typical gross findings combined with histopathology and microbiologic analysis.

Contributing Institution:
Texas A&M Veterinary Medical Diagnostic Laboratory (TVMDL), 483 Agronomy Rd, College Station, TX 77843, USA. https://tvmdl.tamu.edu/

JPC Diagnosis:
Exoskeleton and gills: Dermatitis and branchitis, ulcerative, hemocytic, chronic, multifocal, moderate, with melanization and cuticular epithelial hyperplasia, vasculitis, and intraphagocytic and extracellular bacteria.

JPC Comment:
This week's moderator, Dr. Elise LaDouceur, editor of the recently published textbook *Invertebrate Histology*, described the invertebrate immune system, which lacks an adaptive arm and features hemocytes as the effector cell in most species. In crustaceans and other arthropods, hemocytic recognition of pathogen- or damage-associated molecular patterns leads to adhesion, degranulation, and phagocytosis, or for larger pathogens, encapsulation or nodulation with subsequent melanization. The last step leads to formation of reactive oxygen and nitrogen species and is the underlying cause of the eponymous "black spots" in this syndrome.

Chitin is a biopolymer which makes up 70% of the organic fraction of crustacean exoskeletons and is rapidly degraded by microbes after crustacean molting or death.[14] Chitinolytic bacteria travel along a chitin oligosaccharide gradient, adhere to and form biofilms on chitinous surfaces, express chitin catabolic cascade genes, and produce chitinase and beta glucosaminidases responsible for chitin breakdown.[14] These mechanisms allow the bacteria to use chitin as a source of nitrogen and carbon, which are absorbed through chitoporins.[14]

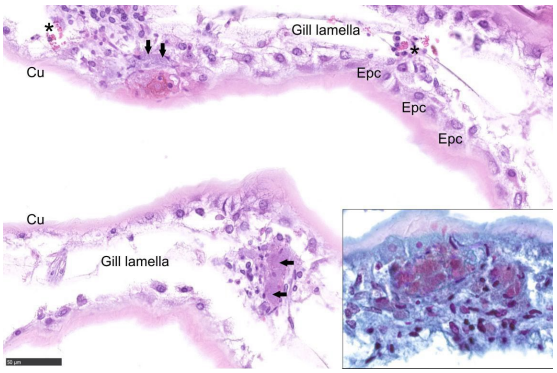

Figure 2-4. Carapace, spider crab. Gills are infiltrated by granular and agranular hemocytes, cellular debris, proteinaceous fluid, and intraphagocytic and intravascular bacteria. (Photo courtesy of: Texas A&M Veterinary Medical Diagnostic Laboratory (TVMDL), 483 Agronomy Rd, College Station, TX 77843, USA. https://tvmdl.tamu.edu/)

The healthy cuticle of crustaceans is resistant to such chitinolytic activity because the most superficial layer – the epicuticle – is nonchitinous and composed primarily of proteolipid material.[12] Disruption of the epicuticle may be mediated by trauma or abrasion, as mentioned by the contributor, or by lipolytic actions of other microbes.[12] Older crustaceans are more susceptible to degradation as they molt and replace their exoskeleton less frequently.[14] Once the epicuticle is disrupted, the chitinous pro-cuticle is exposed and can be colonized by chitinolytic bacteria, which are usually part of a mixed population of microbes which may produce other enzymes, scavenge liberated nutrients, or prey on other microbes.[14]

As the contributor describes, severe lesions can lead to secondary hemocoelic invasion and septicemia. Internal lesions associated with SDS were previously described in a study of shell-disease affected edible crabs, *Cancer pagarus*.[12] In the gills, there were hemocytic infiltrates and nodules which frequently occluded the hemal sinuses, the thin epithelium was occasionally breached and sealed by melanized hemocytic plugs, and nephrocytes at lamellar tips were swollen with abundant dark brown material within a central cytoplasmic vacuole.[12] Hepatopancreatic tubules exhibited variable necrosis and hemocytic nodules in hemal spaces.[12] Hemocytic nodules were also observed in the heart.[12] In general, the severity of the internal lesions mirrored the extent of the shell lesions.[12]

References:

1. AZA Aquatic Invertebrate Taxon Advisory Group. Japanese spider crab care manual. Silver Spring, MD. 2014; Association of Zoos and Aquariums.
2. Chistoserdov AY, Smolowitz R, Mirasol F, Hsu A. Culture-dependent characterization of the microbial community associated with epizootic shell disease lesions in American lobster, Homarus americanus. J Shellfish Res. 2005;24: 741-747.
3. Noga EJ, Hancock AL. Crustaceans. In: Lewbart GA, ed. Invertebrate medicine. John Wiley & Sons; 2011.
4. Noga EJ, Smolowitz R, Khoo LH. Pathology of shell disease in the blue crab, Callinectes sapidus Rathbun (Decapoda: Portunidae). J Fish Dis. 2000;23:389-399.
5. Nonaka M, Iwahashi Y. Some aspects and problems on fisheries of giant spider crab Macrocheira kaempferi (Temmick). Aquac Sci. 1987;35:21-26.
6. Smolowitz R, Chistoserdov AY, Hsu A. A description of the pathology of epizootic shell disease in the American lobster, Homarus americanus, H. Milne Edwards 1837. J Shellfish Res. 2005;24:749-756.
7. Smolowitz RM, Bullis RA, Abt DA. Pathological cuticular changes of winter impoundment shell disease preceding and during intermolt in the American lobster, Homarus americanus. Biol Bull Woods Hole. 1992;183:99-112.

8. Stegeman N, Allender M, Arnold J, Bonar CJ. Aquatic Invertebrates. Exot Anim Lab Diagn. 2020:383-408.
9. Stewart JE. Infectious diseases of marine crustaceans. In: Couch JA, Fournie JW, eds. Pathobiology of marine and estuarine organisms. Boca Raton, FL, USA: CRC Press; 1993.
10. Tlusty MF, Smolowitz RM, Halvorson HO, DeVito SE. Host susceptibility hypothesis for shell disease in American lobsters. J Aquat Anim Health. 2007;19: 215-225.
11. Ueda R, Yasuhara T, Sugita H, Deguchi Y. Gut microflora of the Japanesese giant crab Macrocheira kaempferi. Nippon Suisan Gakki. 1989;55:181.
12. Vogan CL, Costa-Ramos C, Rowley AF. A histological study of shell disease syndrome in the edible crab Cancer pagurus. Dis Aquat Organ. 2001;47:209-217.
13. Vogan CL, Llewellyn PJ, Rowley AF. Epidemiology and dynamics of shell disease in the edible crab Cancer pagurus: a preliminary study of Langland Bay, Swansea, UK. Dis Aquat Organ. 1999;35:81-87.
14. Vogan CL, Powell A, Rowley AF. Shell disease in crustaceans - just chitin recycling gone wrong? Environ Microbiol. 2008;10:826-835.
15. Wang W. Bacterial diseases of crabs: a review. J Inverteb Pathol. 2011;106:18-26.

CASE III:

Signalment:
5 year old, female, African spurred tortoise, *Geochelone* (*Centrochelys*) *sulcata*, *C. sulcata*

History:
Animal kept as pet by a private. No information regarding general state of health, past medical history and gross *post mortem* findings were given by the referring private veterinary practitioner. Only a formalin fixed liver was submitted for histology.

Gross Pathology:
The liver was moderately increased in volume, with rounded margins and diffusely brown to yellow in color. On the surface and in cross-section, multiple to confluent, round and white to yellow lesions was present (multifocal necrotizing hepatic foci). The lesions are smooth with moderately irregular margins and are surrounded by a hyperemic halo. In cross section, hemorrhages are present in the center of the necrosis. The consistency of the liver is markedly reduced, and the organ is friable to the manipulation.

Laboratory Results:
No findings reported.

Microscopic Description:
Liver: Approximately 30% of the hepatic parenchyma is characterized by multifocal, random, 1-3 mm in diameter, irregularly nodular, areas of necrosis and heterophilic-histiocytic inflammation.

The centre of the lesions is composed of abundant basophilic granular karyorrhec-

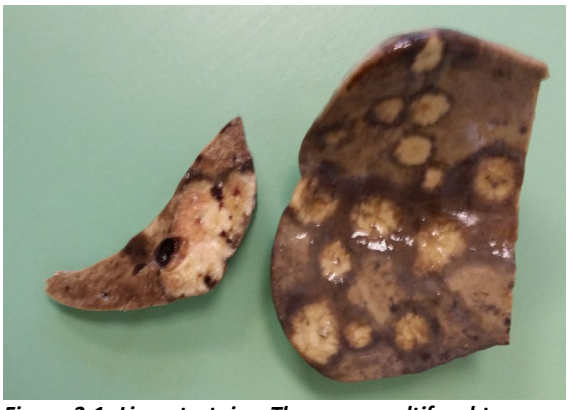

Figure 3-1. Liver, tortoise. There are multifocal to coalescing areas of necrosis within the liver. (Photo courtesy of: DIMEVET-Anatomical Pathology Section, University of Milan.)

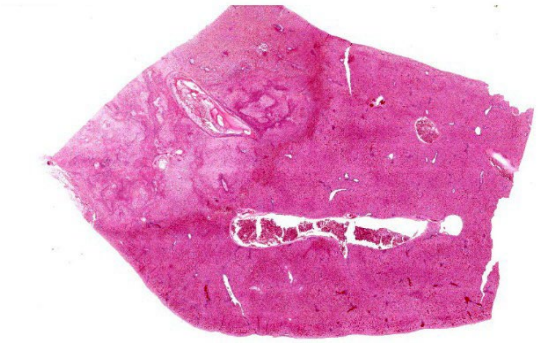

Figure 3-2. Liver, tortoise. A large area of coagulative necrosis rimmed by an area of hemorrhage and necrosis is present at left. (HE, 5X)

tic/necrotic debris with complete loss of cellular details (lytic necrosis) admixed to intensely eosinophilic, shrunken hepatocytes with lysed nuclei (coagulative necrosis). Elevated numbers of both viable and degenerated heterophils with karyolitic nuclei can be seen admixed with the necrosis and at the periphery of the necrotic foci that are multifocally also associated at the periphery with a lightly eosinophilic fibrillary, finely beaded, meshwork (fibrin).

At the periphery of the necrotic foci, surrounding and invading vessel walls and occasionally in the cytoplasm of macrophages variable numbers of oval (15-30 µm in diameter) protozoal structures can be seen. Parasites have a distinct cell membrane, a finely granular to vacuolated cytoplasm, and a single nucleus with marginated chromatin and a lightly basophilic central karyosome (amoebic trophozoites).

The hepatic parenchyma is multifocally characterized by swollen hepatocytes, with granular to clear cytoplasm (vacuolar/hydropic degeneration). Multifocally in the cytoplasm of hepatocytes, yellow-greenish granular pigment (bile stasis) is evident.

Fibrin thrombi occasionally entrapping trophozoites are visible in vascular lumens with endothelial cell necrosis. Diffusely sinusoidal hyperemia is present.

Contributor's Morphologic Diagnoses:
Liver: severe, multifocal to coalescing, random, acute to subacute necrotizing hepatitis and vasculitis with perivascular and intralesional trophozoites consistent with *Entoamoeba* spp.

Contributor's Comment:
Entamoeba invadens is the most important amoeba species infecting reptiles.[6,14,18] This protozoan parasite belongs to the phylum *Sarcomastigophora*, subphylum *Sarcodina (Rhizopoda)*, order *Amoebida*, family *Entamoebidae*, genus *Entamoeba* and is similar morphologically to *Entamoeba histolytica*. Although, *E. invadens* may be the main parasite involved in reptile pathology, other *Entamoeba* species, such as *E. terrapinae, E. insolita, E. barreti, E. testudini*s and *E. ranarum,* can also infect reptiles[8].

E. invadens is a common commensal parasite of different free-ranging reptiles including snakes, crocodilians, turtles, tortoises, and lizards.[18] Turtles, tortoises, and crocodiles are considered reservoir species for *E. invadens*. Herbivorous tortoises harbor the parasite and only occasionally demonstrate clinical signs.[6,11] The mechanism of this resistance is unknown. Based on data available for *Acanthamoeba*, it is possible that some types of sugars (mannitol and glucose) can prevent the adhesion of the trophozoite to the mucosal surface. Among tortoises, giant tortoises (*Geochelone* spp.)[11] and the northern map turtle (*Graptemys geographica*)[17] seem to be more susceptible. Snakes which develop amebiasis are *Boidae* (boas), *Pythonidae* (pythons), *Crotalidae* (crotalids), *Elapidae* (colubrids), and *Viperidae* (vipers). Snakes resistant are greater snake and northern black racers. All the crocodile seems to be immune to *E. invadens*.[4] The presence of carnivorous reptiles resistant to the infection has been associated with the evolutionary strategy to feed with snakes.[4] Among lizards,

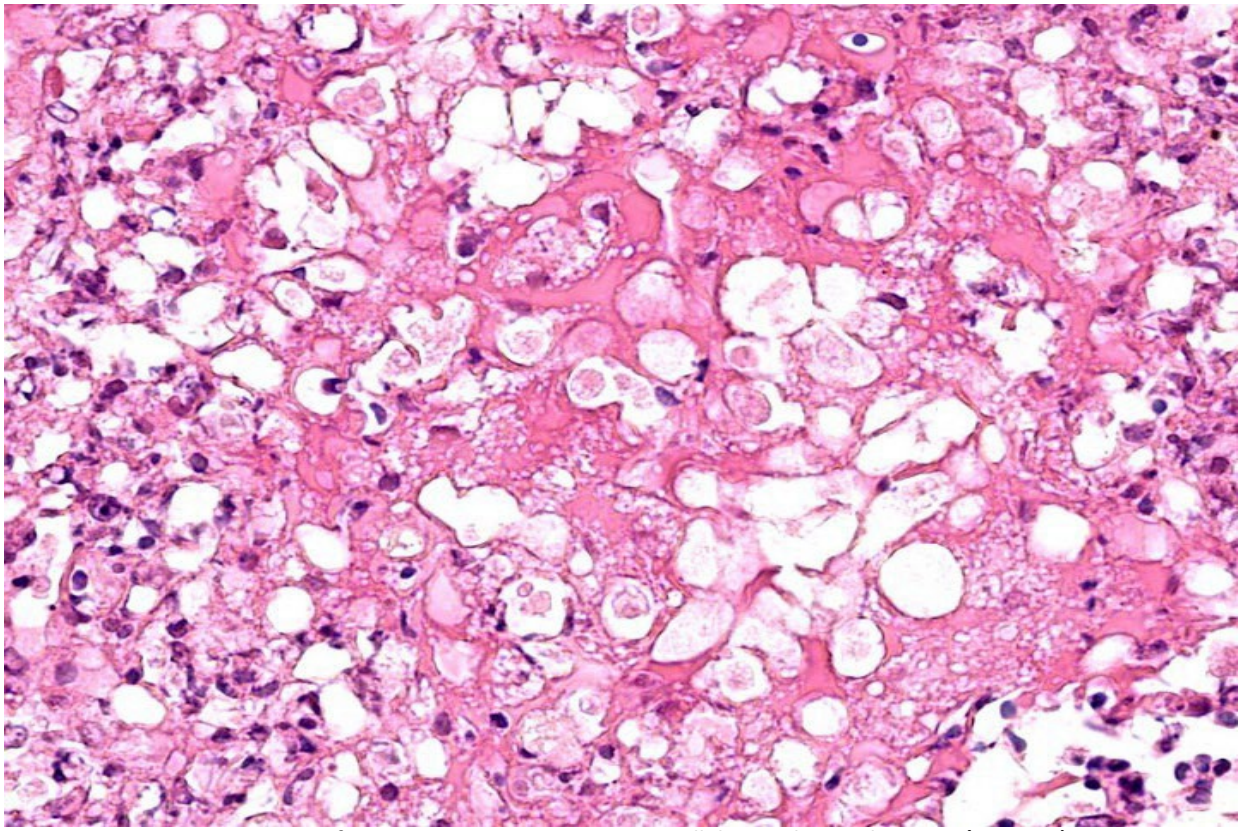

Figure 3-3. Liver tortoise. Areas of necrosis contain numerous extracellular amebic trophozoites. (HE, 280X)

Varanidae (monitor lizard) seems to be the most susceptible species. The onset of clinical signs in resistant animals has been correlated with stress, age and immunosuppression.[8]

Hepatic amoebiasis in tortoises is rare and an outbreak of severe entero-hepatic disease with duodenal involvement seems to have been reported once.[9] In snakes and lizards, *E. invadens* is responsible for a severe epizootic disease characterized by necro-hemorrhagic gastroenteritis, colitis, or entero-hepatitis. Occasionally, the parasite can invade the bloodstream and reach other organs causing extraintestinal complications. Atypical amebiasis manifesting as myositis and ulcerative dermatitis has been reported in a common water monitor lizard (*Varanus salavtor*).[2]

E. invadens has a worldwide distribution[2], with a life cycle characterized by two morphologically different stages, a motile trophozoite stage (vegetative form) and a cystic stage (resistant form). Because of the protection conferred by their walls, amebic cystic forms can survive days to weeks in the environment. In asymptomatic carriers, trophozoites are confined to the intestinal lumen (non-invasive infection). In some animals, trophozoites acquire invasiveness, infiltrating the intestinal wall and the biliary ducts, inducing the enteric form (intestinal disease) or the systemic form (extraintestinal disease). In snakes and lizards, the liver is considered the major extraintestinal target organ.[7] In snakes, invasion of lungs, spleen, pancreas, kidneys, and subcutaneous tissues occurs via hematogenous route.[9]

The èathogenic transformation of the trophozoite into an invasive parasitic form has not been elucidated for *E. invadens*. Although a parallel with the pathogenesis of *E. histolytica* in human beings has been hypothesized

explaining the different forms via the recognition of different parasite strains.[19]

The parasite has an oro-fecal cycle, mature amoebal cyst are ingested with contaminated water, food or arthropod vectors (flies, roaches). Excystation occurs in the small intestine with the release of a trophozoite characterized by four nuclei that after division produce four trophozoites with a single nucleus. Each of these 4 zoites divides in 2, producing a total of 8 trophozoites (amebulae). Trophozoites are the mobile and labile form of the parasite and are capable of migrating in the large intestine. Proteolytic enzymes (glycosidases such as galactosidase, mannosidase, fucosidase and others) produced by trophozoites disrupt the mucous barrier and parasites are able to attach to the gastrointestinal epithelium. The trophozoite first adheres to the intestinal mucin layer and to epithelial cells by a surface Gal/GalNAc-specific lectin (adhesin), and releases pore-forming polypeptides called amoebapores that are small potent peptides able to induce lysis of host cell membrane resulting in intracellular calcium elevation and eventual cell death.

After the epithelial cells are lysed, there is colonic gland invasion and cysteine proteases degrade the extracellular matrix so that trophozoites burrow into lamina propria invading the submucosa[5.] In the large intestine trophozoites start dividing by binary fission producing cysts released in the environment. In humans, amoebic liver abscess (amoeboma, ALA=Amebic liver abscess) is the most frequent extraintestinal manifestation of *E. histolytica* infection. The liver can be infected by two ways, by common biliary duct invasion (continuity ascending route), or by portal vein invasion (thromboembolic route).

Virulence factors involved in ALA development include those necessary for complement resistance (PPGs), ROS resistance (peroxiredoxin), lysis (CPs and amoebapores), and cell adherence (notably, KERP1 and the Gal/GalNAc lectin).[17]

In a recent study on *E. histolytica* pathogenesis, amoebae were demonstrated to kill by biting off and ingesting distinct fragments of viable cells. The internalization of bites of living human cells is reminiscent of trogocy-

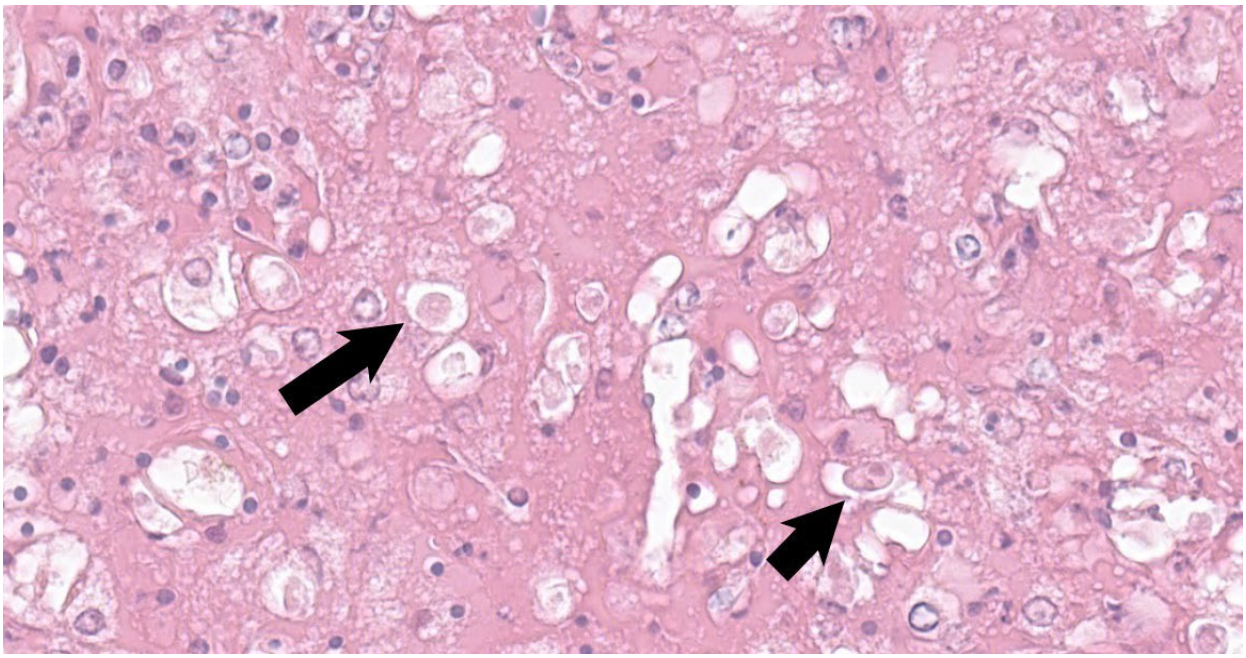

Figure 3-4. Liver, tortoise. Higher magnification of trophozoites (arrows). (HE, 527X)

tosis (Greek *trogo–*, nibble) observed between immune cells, but amoebic trogocytosis differs since it results in death.[13]

Clinical signs associated with amoebiasis in reptiles include anorexia, weight loss, mucoidal or hemorrhagic diarrhea, dehydration, and death after weeks or month of illness. Sudden death is also commonly reported.[4,16,11]

Typical gross findings are thickening of the gastrointestinal wall, with ulcerative and necrotizing colitis in snakes and duodenitis in turtles. Lesions can extend to other parts of the gastrointestinal tract.[2,9] Tubular organs can have transmural ulceration. Ulcers may be flask shaped, with a narrow neck and broad base. The lumen of the intestine is filled with blood, necrotic debris, and mucus. Extraintestinal lesions are secondary to the intestinal infection, and all organ systems can potentially be affected. The lesions start as abscesses evolving in necrotizing lesions centered on blood vessels.[2] Secondary bacterial infections are commonly found in liver and gastrointestinal tract.

Typical histological findings are necro-hemorrhagic lesions in all organs affected. Usually, amoebae can be found admixed to the necrotic debris. *E. invadens* trophozoites range from 10 to 21 µm (intestine: 12-19 x 10-13 µm, liver: 13-21 x 11-18 µm).[9] Nucleus is 3-5 µm in diameter, round and periphery located. A single central endosome is present, and it is 0.6-1 µm. *E. invadens* cysts range from 11 to 20 µm and have four nuclei.

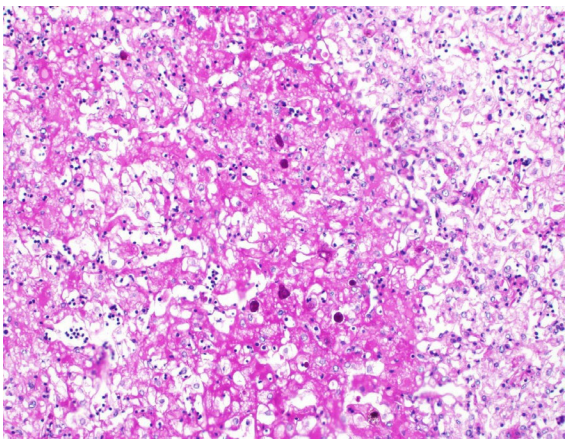

Figure 3-5. Liver tortoise. Amebic trophozoites are densely PAS-positive. (PAS, 200X)

Ultrastructurally,[3] trophozoite cytoplasm is filled by numerous, variably sized vacuoles. Vacuoles are surrounded by an electron dense membrane and contain starch granules and bacteria (food vacuoles). Cytoplasmic, irregularly shaped, electron dense aggregates of 200 nm are associated with the food vacuoles and the nucleus (chromatoid particles). Inside the nucleus, a single electron dense nucleolus is usually present. Cyst cytoplasm can be divided into two areas, one electrondense adjoining the nuclei and around the cell wall and containing vacuoles, and one electrolucent, in between, containing glycogen. The chromatoid particles present in the cyst, are usually aggregated in large crystalline structures (chromatoid bodies).[3]

Gross and histopathological finding are distinctive and mostly diagnostic, additional diagnostic tools are: fecal flotation, histochemical stains (PAS staining-purple, GMS staining-black, and Heidenhain's iron strain for chromatin), immunohistochemistry, indirect immunofluorescence and PCR.[1,18]

Other infectious agents causing hepatic necrosis and hepatitis in tortoises include: Herpes viruses[10] (i.e. tortoise herpesvirus type 1 and 2- responsible for sudden death, upper respiratory disease, hepatic disseminated necrosis and intranuclear eosinophilic inclusion bodies; siadenovirus[16] (systemic infection, intranuclear basophilic to amphophilic inclusion bodies in hepatocytes and non suppurative hepatitis), Iridoviruses (i.e. gen. Ranavirus: disseminated hepatic necrosis, basophilic inclusion bodies, vasculitis)[10]; Bacteria, mostly in septicemic infections or following a primary viral disease (i.e. *Aeromonas*

spp. Escherichia coli, Pasteurella testudinis, Morganella morganii, Serratia marcescens Chlamydophila spp.[10] and Fungi causing sistemic mycoses such as *Aspergillus, Paecilomyces,* and *Penicillium* spp. can sporadically induce hepatic lesions.[10]

Contributing Institution:
DIMEVET-Anatomical Pathology Section
Via Celoria 10
20133 Milano, Italy

JPC Diagnosis:
Liver: Hepatitis, necrotizing and embolic, focally extensive, marked, with vasculitis and numerous amoebic trophozoites.

JPC Comment:
A variety of pathogenic and commensal *Entamoeba* spp. infect the gastrointestinal tract of vertebrates and invertebrates, and the contributor provides a thorough summary of *Entamoeba* infection in reptiles. In addition to *E. invadens,* snakes may rarely be susceptible to another *Entamoeba* species – *Entamoeba ranarum*, which typically infects but rarely causes disease in amphibians.[12,14] There have been two published reports of *E. ranarum* infection causing necrotizing colitis in snakes; one in a ball python, and one in a boa. While both cases had colitis similar to that caused by *E. invadens,* neither featured spread to other organs, such as the liver.[12,14] In one case, the snake had previously been housed with frogs, so fecal-oral transmission is hypothesized. [12]

Another *Entamoeba* afflicting amphibians has recently been identified in invasive cane toads (*Rhinella marina*) in Australia. These amphibians were introduced in 1935 as an unsuccessful means to control beetles consuming sugar cane crops and now inhabit a range of over 1 million square kilometers.[16] In 2014, researchers discovered the novel *Entamoeba* during an outbreak of severe colitis and high mortality in cane toads in one region of northern Australia. PCR and subsequent sequencing illustrated its close relation to both *E. ranarum* and *E. invadens* and lead to its classification is *Entamoeba* sp. CT1.[20] Affected toads had either no gross lesions or mild prominence of vasculature and thickenning of intestinal walls. Histologically, all affected toads had some degree of colitis, with the most severe cases featuring deep ulcers with edema and fibrosis. *Entamoeba* trophozoites were associated with the affected mucosal epithelium and ulcers, but there was no evidence of spread outside the gastrointestinal tract.[20] Subsequent research to evaluate the impact on native frog species has demonstrated a prevalence of approximately 24% in cane toads in the same region and no identification of the parasite in any of the 11 tested native frog species.[16] While the authors acknowledge that intermittent shedding, sample degradation, and testing limiations may have affected the abiilty to isolate the parasite, the results are encouraging for native species and anuran conservationists.[16]

References:

1. Bradford CM. Denver M and Cranfield MR. Development Of A Polymerase Chain Reaction Test For Entamoeba invadens. *J Zoo Wild Med*. 2008; 39(2): 201–207.
2. Chia M.Y., Jeng C.R., Hsiao S.H., Lee A.H., Chien C.Y., and Pang V.F. Entamoeba invadens Myositis in Common Water Monitoring Lizard (Varanus salvator). *Vet Path*. 2009; 46:673-676.
3. Deutsch K, Zaman V. An Electron Microscopic Study of Entamoeba Invadens Rodhain 1934. *Exp Cell Res*. 1959;17(2): 310-319.
4. Divers SJ. Parasitic diseases of the Reptiles. The Merck Veterinary Manual

http://www.merckvetmanual.com/mvm/exotic_and_laboratory_animals/reptiles/parasitic_diseases_of_reptiles.html
5. Espinosa-Cantellano M, Martínez-Palomo A. Pathogenesis of intestinal amebiasis: from molecules to disease. *Clin Microbiol Rev*. 2000;13(2):318-31.
6. Flannagan J. P. Chapter 4. *Fowler's Zoo and Wild Animals Medicine*. Vol 8. 70.
7. Garate M, Cubillos I, Marchant J., and Panjwani N. Biochemical Characterization and Functional Studies of Acanthamoeba Mannose-Binding Protein. *Infect Immun*. 2005; 73(9):5775-81.
8. García G, Ramos F, Pérez RG, Yañez J, Estrada MS, Mendoza LH, Martinez-Hernandez F, Gaytán P. Molecular epidemiology and genetic diversity of Entamoeba species in a chelonian collection. *J Med Microbiol*. 2014;63(Pt 2):271-83.
9. Jacobson E, Clubb S, Greiner E. Amebiasis in red-footed tortoise. *JAVMA*. 1983; 183(11): 1192-1194
10. Jacobson ER. Infectious Diseases and Pathology of Reptiles: Color Atlas and Text. Boca Raton, FL: CRC/Taylor & Francis; 2007: pp. 398, 404, 531.
11. Klingenberg RJ. Understanding Reptile Parasites, 2nd edition. Chapter 11, Amoebiasis.
12. Michaely LM, von Dornberg K, Molnar V. *Entamoeba ranarum* Infection in a Ball Python (*Python regius*). *J Comp Path*. 2020; 179: 74-78.
13. Ralston KS, Solga MD, Mackey-Lawrence NM, Somlata, Bhattacharya A, Petri WA Jr. Trogocytosis by *Entamoeba histolytica* contributes to cell killing and tissue invasion. *Nature.* 2014; 24;508(7497):526-30.
14. Richter B., Kübber-Heiss A., Weissenböck H. Diphtheroid colitis in a Boa constrictor infected with amphibian *Entamoeba* sp. *Vet Parasitol*. 2008;153(1-2):164-7.
15. Rivera S, Wellehan JF Jr, McManamon R, Innis CJ, Garner MM, et al. Systemic adenovirus infection in Sulawesi tortoises (Indotestudo forsteni) caused by a novel siadenovirus. *J Vet Diagn Invest*. 2009;21(4):415-26.
16. Rivory P, Brown G, Shilton C, Shine R, Slapeta J. Apparent lack of spill-over of parasites from an invasive anuran: PCR detects *Entamoeba*in cane toads (*Rhinella marina*) but not in sympatric Australian native frogs. *Int J Parasitol Parasites Wildl*. 2020(12):207-213.
17. Santi-Rocca J, Rigothier MC, Guillén N. Host-microbe interactions and defense mechanisms in the development of amoebic liver abscesses. *Clin Microbiol Rev*. 2009 ;22(1):65-75.
18. Scullion F.T., M. Scullion G. Gastrointestinal Protozoal Diseases in Reptiles. *J. Exot. Pet Med.* 2009; 18(4), 266–278.
19. Sehgal D., Bhattacharya A., Bhattacharya S.. Pathogenesis of infection by Entamoeba histolytica. J Biosci. 1996; 21(3): 423-432.
20. Shilton CM, Slapeta J, Shine R, Brown GP. Pathology Associated with an Outbreak of Entamoebiasis in Wild Cane Toads (*Rhinella marina*) in Tropical Australia. *Vet Pathol.* 2019; 56(6):921-931.

CASE IV:

Signalment:
9-year-old, female, Crawl Cay Boa (*Boa imperator*)

History:
This animal was the only affected animal from a small, multi-species, zoological collection which presented with anorexia for the preceding 7 months, with gradually progressive weight loss resulting in a thin body condition at presentation.

Gross Pathology:
There was a 20cm x 10cm fluid filled structure within distended the mid-coelomic cavity which corresponded to an approximately 20cm long segment of jejunum which was markedly dilated up to approximately 10cm diameter. At this site, on the intestinal mucosal surface were numerous, white, raised nodules measuring up to approximately 1mm x 5mm which were interspersed by multifocal, firm, larger masses measuring up to 2cm diameter and forming multifocal papilliform projection which protruded into the intestinal lumen. At the aboral end of this segmental dilation there was an approximately 10 cm long segment of the intestine which was distorted and had 'telescoped' into the more distal intestine, forming an intussusception.

Laboratory Results:
Immunohistochemistry: CD3 negative, CD20 negative and Iba-1 positive. In-situ hybridisation: Boa CD20 negative.

Microscopic Description:
The intestine at the level of the intussusception was markedly expanded and transmurally effaced by an expansile, multilobulated, unencapsulated and poorly demarcated proliferation of neoplastic, monomorphic round cells forming sheets supported by a fine fibrovascular stroma. These variably formed frond like projections, coalescent polypoid masses or locally expanded the lamina propria. These cells were up to approximately 25 µm diameter (3-4 x the diameter of an erythrocyte), with distinct borders and a large amount of eosinophilic cytoplasm. The nuclei were round to oval, central to eccentrically positioned, with euchromatic and stippled to vesicular chromatin and frequent large nucleoli. There was moderate anisocytosis and anisokaryosis with 10 mitotic figures per 2.37 mm² (equivalent to 10 high power fields; hpf; x400 magnification), some of which were bizarre in form. Occasionally, in multifocal areas, these cells were expanded by increased, clear intercellular spacing (intercellular oedema). The epithelium was multifocally ulcerated with replacement by eosinophilic, homogenous material (fibrin), degenerate heterophils, sloughed necrotic epithelial cells, eosinophilic and karyorrhectic debris, and swathes of basophilic. In other areas, there was slight piling up of epithelial nuclei (hyperplasia; attempted regeneration).

Contributor's Morphologic Diagnoses:
Intestinal histiocytic sarcoma with secondary intussusception.

Contributor's Comment:
The features in this consisted of a coelomic dilation corresponding to a large intestinal dilation and associated intussusception. Microscopic examination revealed extensive effacement of the intestinal mucosa by sheets of neoplastic round cells, which were strongly Iba-1 positive, indicative of a histiocytic sarcoma at this site. Considering the lack of additional lesions, this intussusception was most likely secondary to this neoplasm.

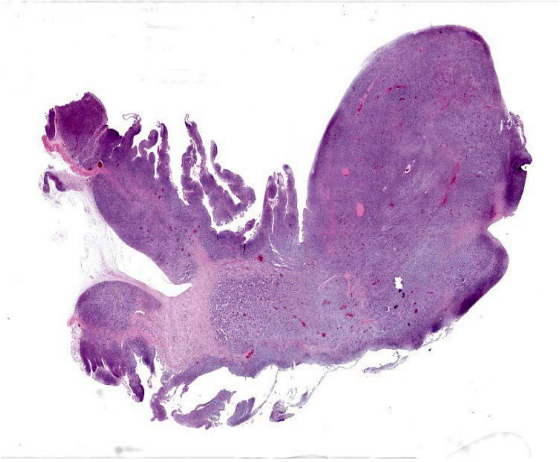

Figure 4-1. Intestine, boa. One section of intestine, markedly expanded by a round cell neoplasm, is submitted for examination. (HE, 5X)

Intestinal intussusception is clinically defined as the telescoping of one segment of digestive tract into the lumen of an adjacent segment, forming an inner intussusceptum and surrounding intussuscipiens. This forms a distended segment of intestine, with significant vascular compression resulting in progression to ischaemic necrosis of both the intussusceptum and intussuscipiens

Histiocytic sarcoma itself has only been rarely reported in boa species, with a single case identified in both a rosy boa (*Lichanura trivirgata*) and a boa constrictor (*Boa constrictor*), whilst an additional single histiocytoma was identified in a rainbow boa (*Epicrates cenchria*).[4,5] Similarly, histiocytic neoplasms have been only rarely identified in other snake species including single reports in a common garter snake (*Thamnophis sirtalis*) and bull snake (*Pituophis catenifer sayi*), though it was not stated in these cases if any additional confirmation such as immunohistochemistry was performed.[5,15]

Only a small number of published case reports have described intussusception secondary to other neoplasms in snakes, including T-cell lymphoma and myeloid leukaemia in boa constrictors and a non-characterised round cell tumor in an Australian sea snake (*Hydrophis major*).[6,8,13] Similarly, only small numbers of published reports describe non-neoplastic causes of intussusception in snakes, including idiopathic intussusception in a pine snake (*Pituophis melanoleucus*) and intussusception secondary to cryptosporidiosis in a corn snake (*Pantherophis guttatus*).[1,16]

Differentiation of histiocytic tumors from other round cell lineages is often challenging in snakes, particularly in comparison to lymphoid proliferations, which often share similar morphological features.[5] Furthermore, consistent immunohistological phenotyping of neoplasms is challenging in reptiles due to the lack of established antibody markers, preventing accurate and reliable immunophenotyping.[13]

Intussusception is a rare but recognized complication of round cell tumors in other species, including humans.[2,9] Similarly to veterinary species, there are only limited individual case reports in human medical literature

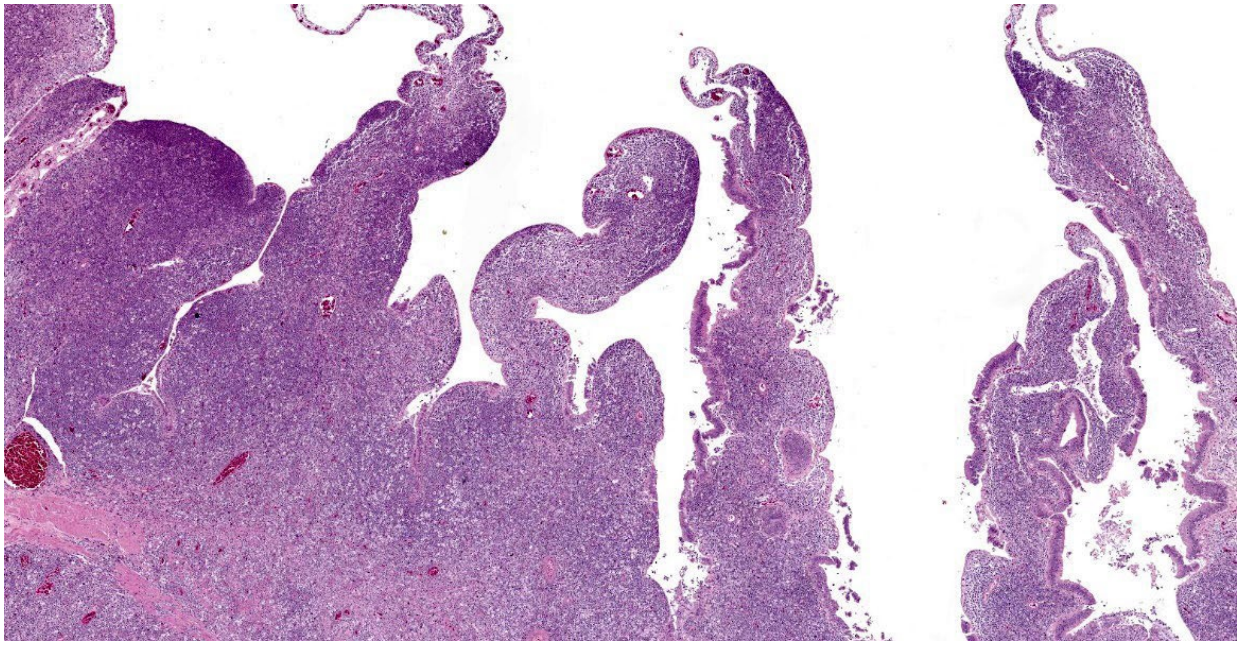

Figure 4-2. Intestine, boa. Villi are markedly expanded by sheets of neoplastic round cells. (HE, 29X

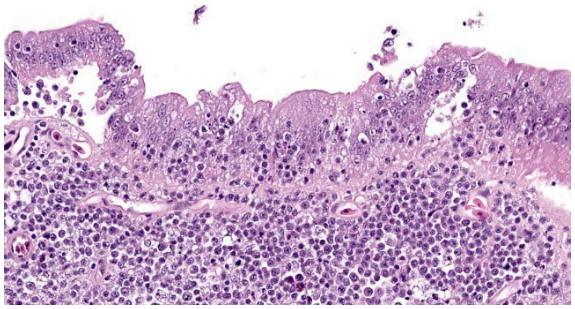

Figure 4-3. Intestine, boa. Small to moderate numbers of neoplastic cells infiltrate the overlying remnant mucosal epithelium. (HE, 381X)

of histiocytic sarcoma associated intussusception.[12]

Contributing Institution:
Easter Bush Pathology – Royal (Dick) School of Veterinary Studies. https://www.ed.ac.uk/vet/services/easter-bush-pathology

JPC Diagnosis:
Intestine: Lymphoma.

JPC Comment:
While a less specific diagnosis of round cell tumor was considered, conference participants ultimately favored a diagnosis of lymphoma based on the histologic appearance of neoplastic cells which had scant cytoplasm and a generally round nucleus. Immunohistochemical evaluation conducted by the JPC was consistent with B-cell lymphoma. Most neoplastic cells had strong neoplastic immunoreactivity for PAX-5, a B cell marker, with few infiltrating T cells positive for CD-3 and IBA-1 highlighting few cells with dendritic morphology, consistent with tumor associated macrophages. Dr. LaDouceur, this week's moderator and author of the Reptile Neoplasia chapter in *Noninfectious Diseases and Pathology of Reptiles,* explained that successful B cell markers are difficult to find in reptiles, and PAX-5 and BLA-36 provide the most utility. The presence of few cells with basophilic cytoplasmic granules lead to brief consideration for a metastatic chromatophoroma; however, there was metachromatic staining to the granules on Giemsa, identifying the cells as mast cells and likely part of inflammation secondary to mucosal ulceration.

In several studies of neoplasms in snakes, malignancies far outnumber benign tumors, ranging from 70 to 80% of all diagnosed neoplasms.[3,10,15] In general, hematopoietic neoplasia, specifically lymphoma, is the most common neoplasm in snakes, though there is some variation between reports, presumedly due to variation in species composition in various collections.[7,10,15] As in other species, lymphoma in snakes may be multicentric and form discrete masses or diffuse organomegaly with or without a leukemic component.

The histomorphology may appear plasmacytoid or histiocytoid, making immunohistochemical often necessary to confirm an uncommon diagnosis of histiocytic sarcoma.[7] Other common neoplasms in snakes include soft tissue sarcomas, renal adenocarcinomas, fibrosarcomas, and melanomas.[5]

Another differential to consider cases of histiocytic or granulomatous inflammation in

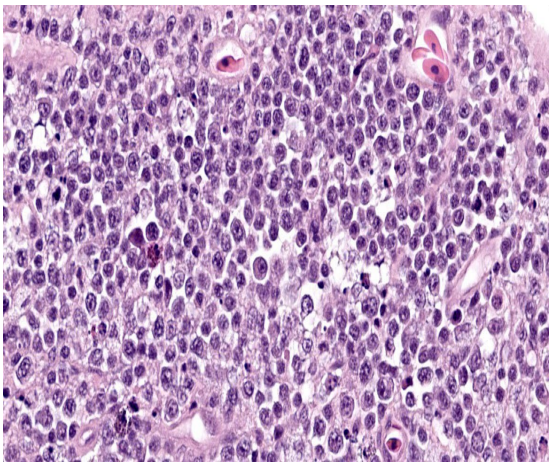

Figure 4-4. Intestine, boa. High magnification of neoplastic round cells. (HE,648X)

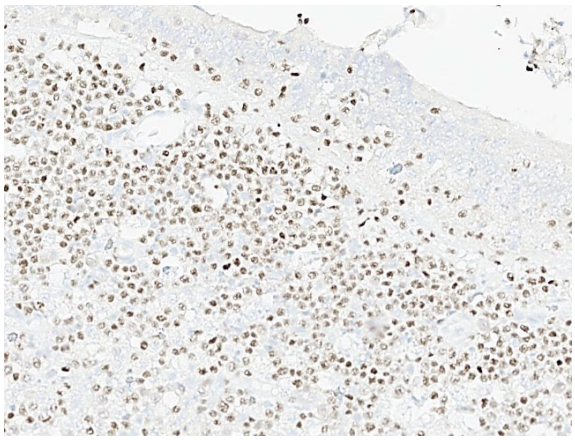

Figure 4-5. Neoplastic cells demonstrate strong nuclear immunoreactivity for PAX-5. (anti-PAX-5, 276X)

snakes is atypical or nontuberculous *Mycobacterium* infection, which causes histiocytic, granulomatous, or occasionally heterophilic inflammation in snakes.[11,14] Estimates of the prevalence of *Mycobacterium* in snake collections vary based on management practices from 0.1% to up to 30%.[11] Mycobacterial infections cause diffuse or multifocal inflammatory infiltrates which can appear as gray to white masses in the subcutaneous tissue and visceral organs, with the pulmonary system most commonly affected.[11] Acid fast staining, such as Ziehl-Neelson and Fite Farraco, can be used to identify the organisms,

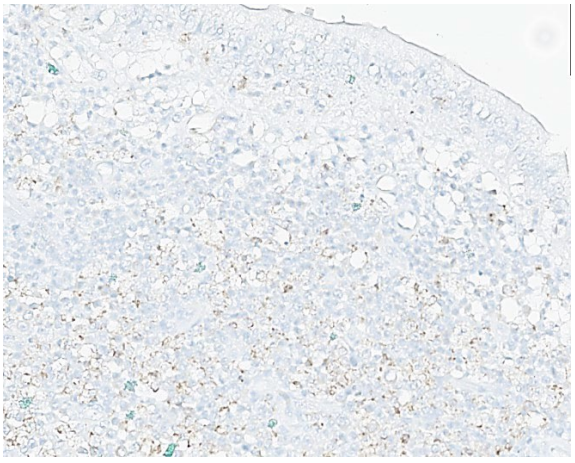

Figure 4-6. Few cells stain for IBA-1, including tingible body macrophages and infiltrating histiocytes. The neoplastic population is non-staining. (anti-IBA-1, 244X)

which may be rare or abundant, though occasionally the bacteria can be visualized on H&E or Gram staining.[14]

References:

1. Bercier M, Zoll W, Rosenberg JF, et al. Gastric intussusceptions in a red corn snake (*Pantherophis guttatus*) associated with cryptosporidiosis. *Case Reports Vet Med*. 2017; 1-5.
2. Bussell HR, Kroiss S, Tharakan SJ, Meuli M, Moehrlen U. Intussusception in children: lessons learned from intestinal lymphoma as a rare lead-point. *Pediatr Surg Int*. 2019;35(8):879–885.
3. Catao-Dias JL, Nichols DK. Neoplasia in snakes at the National Zoological Park, Washington, DC (1978-1997). *J Comp Pathol.* 1999; 1290(1): 89-95.
4. Duke EG, Harrison SH, Moresco A, et al. A Multi-Institutional Collaboration to Understand Neoplasia, Treatment and Survival of Snakes. *Animals (Basel).* 2022;12(3):258-275.
5. Garner MM, Hernandez-Divers SM, Raymond JT. Reptile neoplasia: a retrospective study of case submissions to a specialty diagnostic service. *Vet Clin Exot Anim*. 2004; 7:653-671.
6. Gillett AK, Ploeg R, Flint M, Mills PC. Postmortem examination of Australian sea snakes (Hydrophiinae): Anatomy and common pathologic conditions. *Jour Vet Diagn Invest.* 2017; 29:593–611.
7. LaDouceur EEB. Reptile Neoplasia. In: Garner MM, Jacobson ER, eds. *Noninfectious Diseases and Pathology of Reptiles*. Boca Raton, FL: CRC Press. 2020:16-17.
8. Máté LK, Simard J, Ducatelle R, Hellebuyck T. Ileocolic Intussusception Associated with a Multicentric Round Cell Tumor in a Red-Tailed Boa (Boa constrictor constrictor). *J Herpetol Med Surg*. 2021;32(1):11–19.

9. Özant A, Arslan K, Özçay N, Besim H. Adult multicentric burkitt lymphoma with bowel obstruction due to intussusception. *Turkish J Gastroenterol*. 2018;29(3):361–364.
10. Page-Karjian A, Hahne m, Leach K, et al. Neoplasia in Snakes at Zoo Atlanta during 1992-2012. *Jour Zoo Wildl Medicine.* 2017; 48(2): 521-524.
11. Page-Karjian A, Knowles S, Howerth EW, et al. Pathology in Practice. *Jour Am Vet Med Assoc.* 2012; 241(9): 1159-1161.
12. Speelman A, Kolbe J. A case report of histiocytic sarcoma of the hepatic flexure: peer reviewed case report. *South African Radiogr*. 2012;50(1):27–29.
13. Summa NM, Guzman DS-M, Hawkins MG, et al. Tracheal and Colonic Resection and Anastomosis in a Boa Constrictor (Boa constrictor) with T-Cell Lymphoma. *J Herpetol Med Surg*. 2015;25(3–4):87.
14. Stacy BA, Pessier AP, Ossiboff RJ. Host Response to Infectious Agents and Identification of Pathogens in Tissue Sections. In: Jacobson ER, Garner MM, eds. *Infectious Diseases and Pathology of Reptiles.* Volume I. 2nd ed. Boca Raton, FL: CRC Press. 2021: 383.
15. Sykes IV JM, Trupkiewicz JG. Reptile neoplasia at the Philadelphia Zoological Garden, 1901-2002. *J Zoo Wildl Med*. 2006;37(1):11–19.
16. Wosar MA, Lewbart GA. Ileocolic intussusception in a pine snake (Pituophis melanoleucus). *Vet Rec*. 2006;158(20):698–699.

WSC 2022-2023 Self-assessment.
Conference 11

1. True or false? *Aggregata* sp. infections most commonly affect the gills of octopi.
    a. True
    b. False

2. Which of the following anatomic sites are often affected first with black shell disease?
    a. Gills
    b. Joints
    c. Setal pores
    d. Ocular stalks

3. Which of the following lizards is most susceptible to infection with Entamoeba invadens?
    a. Monitor lizard
    b. Tuatara
    c. Green iguana
    d. Bearded dragon

4. *Entamoeba invadens* results in necrosis of cells as a result of the liberation of?
    a. Perforins
    b. Galactosidase
    c. Nitric oxide
    d. Lipopolysaccharide

5. True or false? The receiving intestinal segment in an intussusception is called the intussuscipiens.
    a. True
    b. False

Please email your completed assessment for grading to Dr. Bruce Williams at bruce.h.williams12.civ@mail.mil. Passing score is 80%. This program (RACE program 33611) is approved by the AAVSB RACE to offer a total of 0.5 CE Credits, with a maximum of 12.5 CE Credits being available to any individual Veterinary Medical Professionals for the 2019-2020 Wednesday Slide Conference. This RACE approval is for the subject matter categories of: SCIENTIFIC using the delivery method of NONINTERACTIVE DISTANCE. This approval is valid in jurisdictions which recognize AAVSB RACE.

Joint Pathology Center
Veterinary Pathology Services

WEDNESDAY SLIDE CONFERENCE 2022-2023

Conference #12 7 December 2022

CASE I:

Signalment:
4 years-old, female, goat (*Capra hircus*), unspecified breed.

History:
The sample was submitted by a general practitioner and little information is available regarding the clinical history. This goat was pregnant and was one month away from parturition. Anorexia was reported.

Gross Pathology:
Kidneys are described by the practitioner as pale and swollen, with irregular white foci. Other reported findings are mesenteric lymph nodes with a caseous and mineralized content. Only kidneys were submitted for histopathological analysis.

Laboratory Results:
No findings reported.

Microscopic Description:
Almost all glomeruli are affected by one or more of the following changes:

- Variable thickening of the glomerular capsule with fibroblastic proliferation;
- Marked thickening of glomerular basement membrane with moderate increased in mesangial cellularity (membranoproliferative glomerulonephritis);
- Adhesions between the glomerular tufts and the capsule (glomerular synechiae);
- Extraglomerular proliferation of spindle cells admixed with fibrin around glomerular tufts, resembling glomerular crescents;
- Glomerular congestion and/or hemorrhages;
- Eosinophilic granular materiel (protein exudation) and/or hemorrhages within the urinary space;
- Shrunken and fibrotic glomeruli (global glomerulosclerosis).

These changes affect almost all glomeruli (diffuse changes) and usually the entire glomerular tuft (global changes).

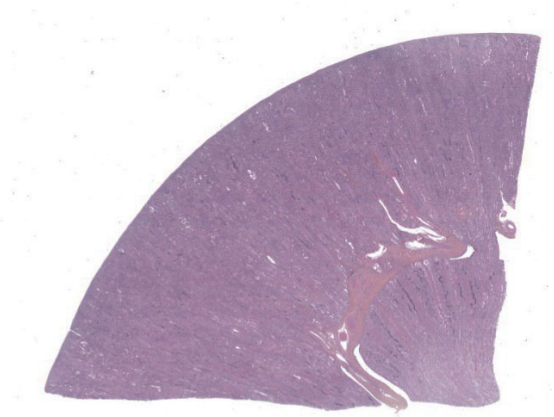

Figure 1-1. Kidney, goat. A single section of kidney is submitted for examination. Tubular dilation and luminal hypercellularity. (HE, 5X)

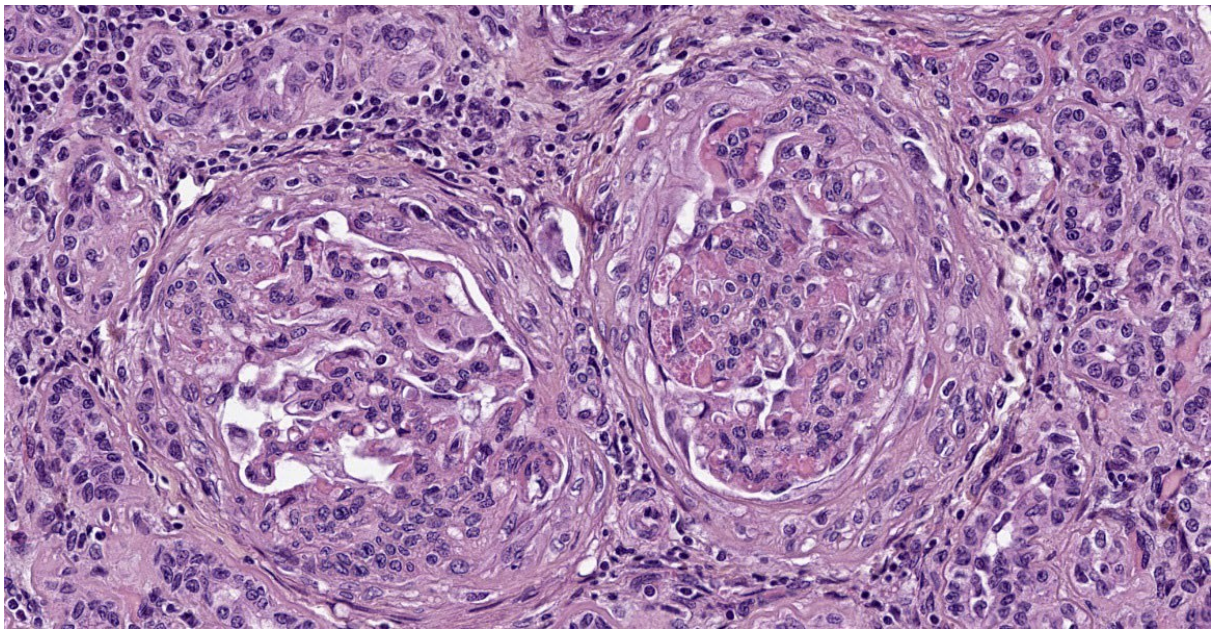

Figure 1-2. Kidney, goat. Glomeruli exhibit expansion of capillary walls and mesangium, mesangial hypercellularity, synechiation, crescent formation, and marked periglomerular fibrosis. The surrounding interstitium is expanded by fibrosis, tubules are mildly atrophic and there is interstitial lymphoplasmacytic inflammation. (HE, 364X)

Also affected are tubules showing a combination of changes: thickened basement membrane; epithelial atrophy; tubular dilation with eosinophilic protein casts, degenerate neutrophils and/or eosinophilic granular debris; mineralization of basement membranes, especially in the medulla; rare crystals (likely calcium oxalate crystals).

The interstitium is moderately expanded by fibrosis and/or infiltration by lymphocytes and plasma cells.

Contributor's Morphologic Diagnoses:
Glomerulonephritis, membranoproliferative, diffuse, global, marked, chronic, with global glomerulosclerosis, lymphoplasmacytic interstitial nephritis, tubular atrophy and tubular casts.

Contributor's Comment:
The case is interesting as it shows a constellation of renal elementary lesions. Glomerulonephritides can be defined as primary glomerular diseases with secondary tubulointerstitial and vascular changes.[2, 4] In this case, the proportion of affected glomeruli (more than 50%), the proportion of the glomerular tuft affected (entire glomerular tuft) and the type of glomerular change (thickening of glomerular basement membrane with mesangial proliferation) favor a diagnosis of diffuse, global, membranoproliferative glomerulonephritis[1]. An interesting feature is the presence of crescent-like structures around glomerular tufts that are reminiscent of crescentic glomerulonephritis in humans. Such crescents have been described in cases of glomerulonephritis in ruminants.[2, 3]

Among glomerular diseases, glomerulonephritis is frequent in veterinary medicine and are the subject of a rather complex nomenclature, based on human renal pathology that can be difficult to apply routinely to veterinary pathology cases especially when additional techniques (immunofluorescence, electron microscopy) are not available. The exact cause is generally unknown but immune-complex deposition secondary to infections is a likely cause in most cases. In ruminants, Maedi-Visna virus and Bovine Viral Diarrhea virus are suspected to initiate immune-mediated glomerulonephritis.[2]

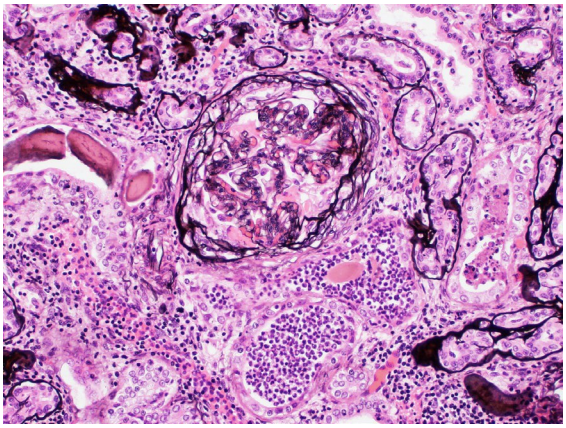

Figure 1-3. Kidney, goat. A periodic acid methenamine silver stain demonstrates the excessive amount of basement membrane within the mesangium, capillarywalls and Bowman's capsule crescents. (PAMS, 400X)

Despite showing marked renal changes of glomeruli, tubules and interstitium, there was no clinical sign or gross lesion suggestive of renal failure in this animal. Clinically silent glomerulonephritis appears to be common in ruminants with the exception of the membranoproliferative glomerulonephritis of Finnish landrace sheep that is present at birth and caused by deficiency in complement component C3. Affected lambs die of renal failure around 1-3 months.[2]

Contributing Institution:
Ecole Nationale Vétérinaire d'Alfort
Unité d'Histologie et d'Anatomie Pathologique, BioPôle Alfort
Département des Sciences Biologiques et Pharmaceutiques
7 avenue du Général De Gaulle
94704 Maisons Alfort Cedex
FRANCE
www.vet-alfort.fr

JPC Diagnosis:
1. Kidney: Glomerulonephritis, membranoproliferative, chronic, diffuse, severe with crescent formation and periglomerular and interstitial fibrosis.
2. Kidney: Tubular degeneration and necrosis, multifocal, moderate with numerous tubular casts and intratubular crystals.

JPC Comment:
Immune complex deposition can cause different types of glomerular disease depending on where they are deposited. In general, deposition of immune complexes in the glomerulus leads to complement activation, membrane attack complex formation, mast cell degranulation, and leukocyte chemotaxis.[2] Activated monocytes and neutrophils cause secondary enzymatic and oxidative damage to podocytes, endothelial cells, and the mesangium.[2] Mesangial cells can also produce inflammatory mediators such as IL1 and arachidonic acid metabolites, initiating inflammation and cause self-induced proliferation.[2] The end result is an amplifying loop of inflammation and proliferation.[2]

As the contributor mentions, electron microscopy and/or immunofluorescence are necessary for confirming immune complex deposition and differentiating it from other conditions with similar histologic appearances. Special stains such as silver stains (i.e. Jones methenamine silver), PAS, and Masson's trichrome may be helpful for visualizing glomerular basement membrane changes.[1]

Deposition of immune complexes between podocytes and the glomerular basement

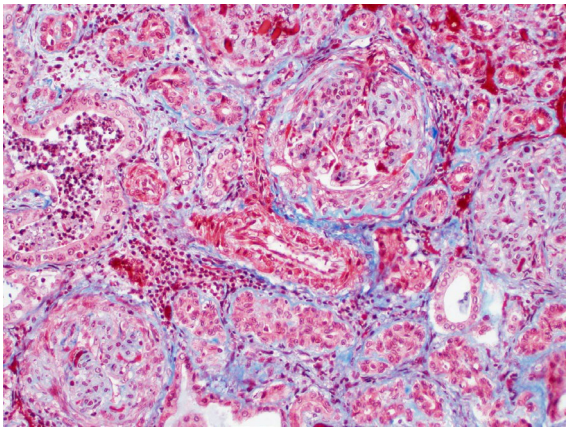

Figure 1-4. Kidney, goat. A Masson's trichrome demonstrates collagen within the glomerular mesangium, capillary walls, crescents, and the surrounding interstitium. (Masson's trichrome, 400X)

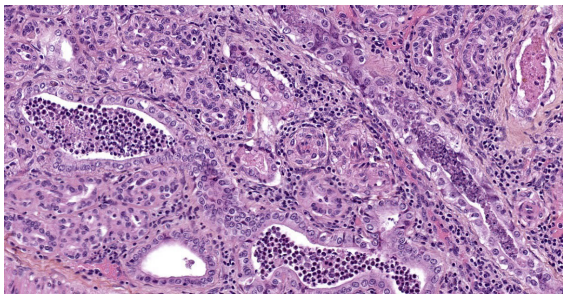

Figure 1-5. Kidney, goat. There is a variety of tubular changes in the midst of interstitial fibrosis and lymphoplasmacytic inflammation, to include ectasia, cellular and protein casts, tubular epithelial degeneration, and tubular atrophy with loss of visible lumina.

membrane leads to membranous glomerulonephropathy.[1] Changes are minimal early in the disease. Later in disease, glomerular basement membranes are thickened, and in advanced stages, there may be secondary glomerulosclerosis.[1] Remodeled glomerular basement membrane features spikes and holes which can be visualized with silver stains such as JMS.[1]

Immune complex deposition on the luminal surface of capillaries leads to membranoproliferative glomerulonephritis.[1] Subsequent endothelial hypertrophy, mesangial hypertrophy, and/or the presence of leukocytes which characteristic hypercellularity of the endocapillary and mesangial compartments.[1] Glomerular basement membranes may be thickened or duplicated, which JMS staining demonstrates in this case.[1] Secondary changes that may occur with membranoproliferative glomerulonephritis include glomerular synechiae and crescents, as seen in this case.[1]

Immune complex deposition within the mesangium leads to mesangioproliferative glomerulonephritis, and resulting hypercellularity is limited to the mesangium.[1]

While low levels of calcium oxalate crystals in the kidney may be an incidental finding in any species, the moderator, Dr. Alicia Moreau, and conference participants remarked about the prevalence of crystals within the section. Ruminants may ingest oxalates in plants such as halogeton, greasewood, rhubarb, and sorrel/dock, or as a mycotoxin in moldy feed.[5] In general, metabolism of oxalate in the rumen makes ruminants resistant to formation of oxalate calculi, but both low magnesium diet and low calcium diets can favor formation of oxalate urolithiasis.[5] Oxalate crystals form in renal vessels and tubules and can cause obstruction, trauma, and necrosis of tubular epithelium, which conference participants suspected in this case.[5] Proximal convoluted tubules are most susceptible to injury due to their high metabolic activity.[5]

References:

1. Cianciolo R, Brown C, Mohr C, et al. *Atlas of Renal Lesions in Proteinuric Dogs*. The Ohio State University; 2018.
2. Cianciolo RE, Mohr FC. Urinary System. In: Maxie MG, ed. *Jubb, Kennedy, and Palmer's Pathology of Domestic Animals.* Vol 2. 6th ed. Elsevier, 2017; 401-413, 456-457.
3. Ohnuki T. Crescentic glomerulonephritis induced in the goat by immunization with homologous or heterologous glomerular basement membrane antigen. *Acta Pathol Jpn*. 1975;25(3):319–331.
4. Slauson DO, Lewis RM. Comparative Pathology of Glomerulonephritis in Animals. *Vet Pathol*. 1979;16(2):135–164.
5. Sula M, Lane LV. The Urinary System. In: Zachary JF, ed. *Pathologic Basis of Veterinary Disease.* 7th ed. Elsevier, 2022; 721,734, 736

CASE II:

Signalment:
9-year-old, spayed female, Welsh Corgi dog (*Canis lupus familiaris*)

History:
The patient presented for lethargy, anorexia, and labored breathing with 2 days duration. On physical examination, the submandibular lymph nodes were enlarged and the lungs sounded harsh on auscultation. Radiographs were unremarkable. The patient's condition worsened and the patient passed away overnight.

Gross Pathology:
Necropsy was performed by the rDVM and multiple fixed tissue samples were submitted for diagnostic evaluation (necropsy-in-a-bottle). Gross findings were not provided.

Laboratory Results:
Results from a complete blood count, blood chemistry, and T4 on the day of presentation for clinical signs was provided by the rDVM. The following abnormalities were noted:

Analyte	Result	Reference Range	Units
WBC	14.4	4.0-15.5	10^3/uL
Neutrophils	12096 (high)	2060-10600	/uL
Monocytes	864 (high)	0-840	/uL
ALP	256 (high)	5-131	IU/L
BUN	187 (high)	6-31	mg/dL
Creatinine	11.4 (high)	0.5-1.6	mg/dL
Phosphorus	23.6 (high)	2.5-6.0	mg/dL
Glucose	65 (low)	70-138	mg/dL
Calcium	13.0 (high)	8.9-11.4	mg/dL
Corrected Ca	13.2		
Magnesium	3.3 (high)	1.5-2.5	mEq/L
Sodium	143	139-154	mEq/L
Potassium	7.2 (high)	3.6-5.5	mEq/L
Na/K ratio	20 (low)	27-38	
Amylase	1145 (high)	290-1125	IU/L
PrecisionPSL	364 (high)	24-140	U/L
T4	<0.5 (low)	0.8-3.5	ug/dL

Microscopic Description:
Kidney: The glomeruli are markedly, diffusely, and globally enlarged by pale, smudgy to amorphous, faintly fibrillar, extracellular eosinophilic material expanding the mesangial matrix and obliterating the glomerular tufts. Glomerular capillaries are compressed, and the glomerular architecture is obscured by the extracellular deposits. Bowman's capsule is occasionally and mildly thickened by similar material and rarely surrounded by a few concentric thin bands of eosinophilic fibrous connective tissue (fibrosis). Renal tubules are characterized by various changes, including: 1) lumina distended by clear space and lined by normal epithelium, 2) lumina containing granular debris and lined by markedly flattened (attenuated) epithelium mixed with a few angular and hypereosinophilic epithelial cells, 3) thinned tubules lined by plump epithelial cells with an open nucleus (regeneration), and 4) epithelial cells that are mildly vacuolated and contain numerous small eosinophilic protein droplets. The interstitium is multifocally infiltrated by small to modest numbers of lymphocytes and plasma cells. While less distinct and severe, the medullary interstitium is mildly expanded by similar eosinophilic material described in the glomeruli.

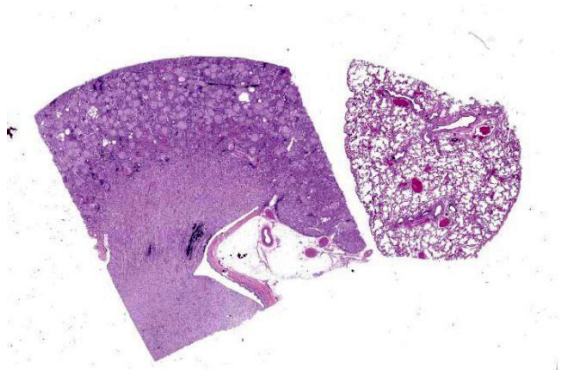

Figure 2-1. Kidney and lung, dog. A section of kidney and lung are submitted for examination. At this magnification, glomeruli and enlarged and hypocellular, and there is a focal area of mineralization within the medulla. There are no discernable lesions in the lung at this magnification. (HE 5X)

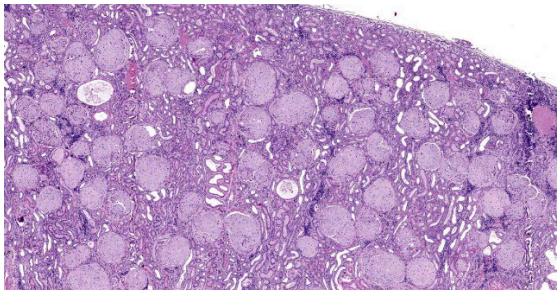

Figure 2-2. Kidney, dog. Glomeruli are markedly enlarged and hypocellular (HE, 33X)

Lung: Alveolar and parenchymal vessels are diffusely congested. The alveolar spaces are often mildly expanded by clear space and contain low numbers of extravasated erythrocytes and fine fibrillary material. In some areas, there is a very faint, thin blue and granular hue to the lining of the alveolar septa (mineralization).

Special staining of the kidney with Congo Red and the lung with von Kossa is performed. Within the kidney, the glomeruli are expanded by orange to red material that rarely exhibits apple-green birefringence under polarized light. The presence of Congophilic material expanding the glomeruli is consistent with amyloid. Within the lung, multifocally lining alveolar septa and partially lining small-caliber parenchymal vessels are thin linear bands of material that stain black, consistent with mineral.

Contributor's Morphologic Diagnoses:
Kidney: Severe glomerular amyloidosis with mild renal tubular degeneration and atrophy, and lymphoplasmacytic interstitial nephritis with fibrosis
Lung: Acute pulmonary congestion with alveolar mineralization and damage

Contributor's Comment:
Amyloidosis is a disease condition that results when amyloid, a proteinaceous material, is deposited intercellularly in a variety of tissues, including the kidneys.[3] Amyloid refers to a group of insoluble, fibrillary proteins with diverse origins but similar structures and properties. [10]

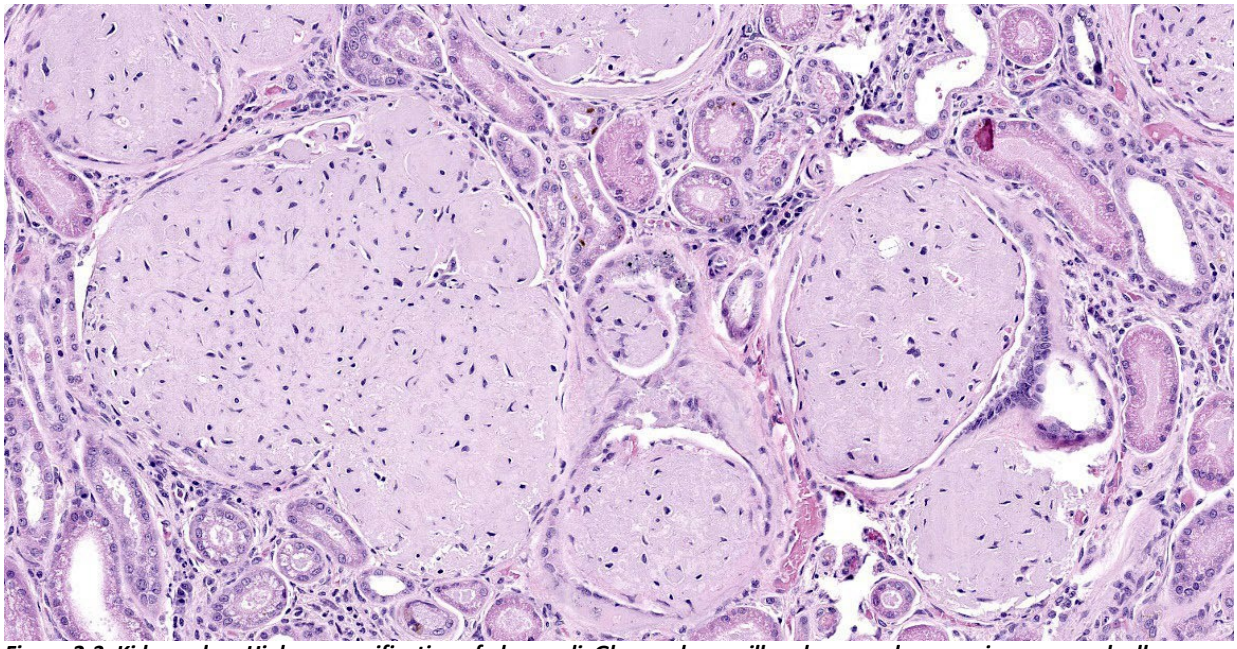

Figure 2-3. Kidney, dog. Higher magnification of glomeruli. Glomerular capillary loops and mesangium are markedly expanded by amyloid, effacing normal architecture. Parietal epithelium is markedly hypertrophic and Bowman's capsule. There is mild fibrosis of the cortical interstitium, tubular degeneration and atrophy, and small aggregates of lymphocytes and plasma cells in the interstitium. (HE, 33X)

Three of the most prominent forms of amyloidosis in animals include reactive, immunoglobulin-derived, and familial amyloidosis. The most common form of amyloidosis is reactive systemic amyloidosis, also called secondary amyloidosis. It results from AA-amyloid being derived from serum amyloid A (SAA), an acute-phase lipoprotein. AA-amyloidosis is often associated with chronic inflammatory disease, persistent infections, or neoplasia. Immunoglobulin-derived amyloidosis, also called primary amyloidosis, is the most common form in humans but less common in domestic animals. It involves AL-amyloid, which is derived from immunoglobulin light chains. [3,10] Familial amyloidosis is another form of amyloidosis that is most commonly seen in Shar Pei dogs and Abyssinian cats.[9]

Amyloidosis occurs when there is misfolding of the progenitor protein. [10] Amyloid proteins are arranged in a β-pleated sheet structure. This renders amyloid insoluble and resistant to proteolysis, allowing it to permanently accumulate in tissues.[7] In the case of AA-amyloidosis, increased SAA due to inflammation coupled with a defect in SAA degradation result in the accumulation of misfolded protein fibrils. [10] Amyloid damages tissues by causing pressure atrophy to adjacent cells. [3] The most common site of amyloid accumulation in dogs is the kidney where it usually affects glomeruli.[9] Amyloid is often also deposited in the liver, spleen, lymph nodes, and adrenal glands. [10]

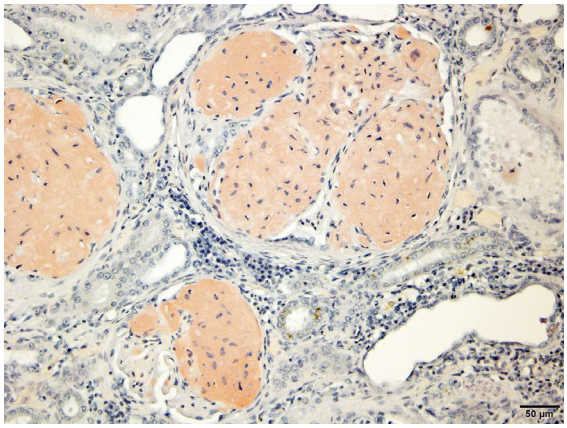

Figure 2-4. Kidney, dog. Glomerular amyloid demonstrates marked congophilia. (Unfortunately, the unstained sections submitted to JPC were too thin to demonstrate birefringence when stained with Congo Red.) (Congo Red, 200X) (Photo courtesy of: University of Illinois at Urbana-Champaign, Veterinary Diagnostic Laboratory, http://vetmed.illinois.edu/vet-resources/veterinary-diagnostic-laboratory/)

Gross changes associated with renal amyloidosis include mild renomegaly, pallor, and a waxy consistency. [3] Microscopically, amyloid is deposited extracellularly.[10] In the kidneys, these deposits are within the mesangial area of the glomerulus.[3] This results in expansion of the mesangium, compressing the adjacent capillary loop.[4] As amyloid accumulates, the glomeruli become enlarged and homogeneous in appearance.[3] In the case of familial amyloidosis in Shar Pei dogs, amyloid often accumulates in the renal medullary interstitium.[9] In order to differentiate amyloid from other extracellular deposits, Congo red stain is used. Congo red stains amyloid deposits orange to red with apple-green birefringence under polarized light.[10]

As renal amyloidosis is irreversible, it often leads to chronic kidney failure. In this case, the dog's serum biochemistry profile indicated severe azotemia, consistent with kidney disease. Additional biochemical findings in this case that are likely attributed to chronic renal failure include hyperkalemia and hyperphosphatemia. Other clinicopathologic abnormalities of renal failure that were either not reported or normal in this case included non-regenerative anemia and metabolic acidosis. Importantly, results of a urinalysis were not provided in this case and so proteinuria, a hallmark of renal amyloidosis, in addition to other common urinalysis findings seen with chronic renal disease cannot be excluded.

A common finding associated with chronic kidney failure and renal azotemia is alveolar

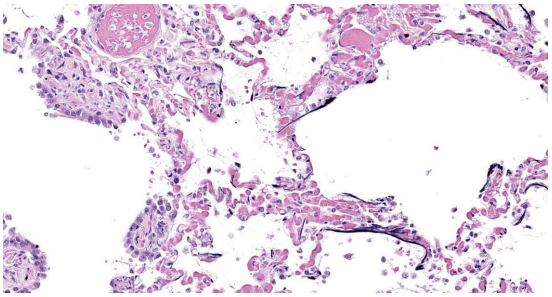

Figure 2-5. Kidney, dog. Alveolar septa are multifocally expanded by deeply basophilic crystalline mineral, mature collagen, and small amounts of edema. There is patchy type II pneumocyte hyperplasia and increased numbers of alveolar macrophages. (HE, 273X)

mineralization within the lungs.[6] Often called uremic pneumonopathy, mineralization occurs within the pulmonary interstitium, specifically the smooth muscle and connective tissue fibers of alveolar septa, veins, and bronchioles.[2] Although uremic mineralization can be multisystemic, mineral deposition often occurs in sites affected by degenerative or necrotic tissue damage. Due to this characteristic and since uremic mineralization can occur regardless of serum calcium concentration, it is most consistent with dystrophic mineralization, as opposed to metastatic mineralization.[1] Other alveolar changes associated with mineralization include pulmonary edema and histiocytosis. Dogs with mineralization of alveoli may or may not exhibit clinical signs of respiratory disease.[2]

Contributing Institution:
University of Illinois at Urbana-Champaign, Veterinary Diagnostic Laboratory
http://vetmed.illinois.edu/vet-resources/veterinary-diagnostic-laboratory/

JPC Diagnosis:
1. Kidney: Amyloidosis, glomerular, global, diffuse, severe, with tubular degeneration, proteinosis, and chronic lymphocytic interstitial nephritis.
2. Lung: Mineralization, subpleural, septal, and vascular, multifocal, moderate.

JPC Comment:
The contributor provides an excellent and succinct comment in this classic condition. Amyloidosis is a subject of frequent research due to its prevalence, diverse presentations, and varied composition in multiple species, including humans. Differentiating the type of amyloid being deposited is critical for understanding the pathogenesis. Traditionally, light-chain amyloidosis (AL) has been differentiated from AA using special stains: AL retains congophilia when pretreated with potassium permanganate, while AA loses congphilia.[5] An additional method to identify AL is immunohistochemical staining for kappa and lambda light chains.[5] Recently, laser microdissection-liquid chromatography-tandem mass spectrometry (LMD-MS) has been used to identify the amyloid precursor proteins in humans, and a study in dogs and cats identified immunoglobulin light chains in 17 of 17 extramedullary plasma cell tumors with amyloid deposition.[5] In the same study, only 12 of 17 cases showed potassium permanganate resistant congophilia, and light chains were only detected in 6 of 17 cases.[5] This study demonstrated that LMD-MS may be more sensitive than traditional methods for identifying light-chain amyloidosis.[5]

Amyloid signature proteins (ASPs) are proteins that are deposited with amyloid fibrils and are likely involved in the pathogenesis of amyloidosis.[8] ASPs studied in man include serum amyloid P component, which protects amyloid fibrils from proteolysis, and various apolipoproteins, including ApoE, which affects the stability and deposition of beta-amyloid.[8] ASPs have yet to be studied thoroughly in veterinary species. Recently, immunohistochemistry and LMD-MS were used to investigate which ASPs are present in three types of amyloidosis in cats; ApoE was identified using both methods in 16 of 16 cases, while SAP was not identified in any cases.[8] In the previously mentioned study of

extramedullary plasma cell tumors, IHC appeared to be more sensitive than LMD-MS, which only identified ASPs in 10 of 15 dogs.[5]

References:

1. Cardoso PGS, Pinto MPR, Moroz LR, et al. Dystrophic Mineralization in Uremic Dogs: An Update. *Pesqisa Veterinária Brasileira*. 2019;**39**: 889-899.
2. Caswell JL, Williams KJ. Respiratory System. In: Maxie MG ed. *Jubb, Kennedy, and Palmer's Pathology of Domestic Animals.* Vol. 2. 6th ed. Philadelphia, PA: Elsevier Saunders. 2016: 494
3. Cianciolo RE, Mohr FC. Urinary System. In: Maxie MG ed. *Jubb, Kennedy, and Palmer's Pathology of Domestic Animals.* Vol. 2. 6th ed. Philadelphia, PA: Elsevier Saunders. 2016: 413-415.
4. Cianciolo RE, Mohr FC, Aresu L, et al. World Small Animal Veterinary Association Renal Pathology Initiative: Classification of Glomerular Diseases in Dogs. *Veterinary Pathology.* 2016;**53**: 113-135.
5. Kadota A, Iwaide S, Miyazaki S, et al. Pathology and Proteomics=Based Diagnosis of Localized Light-Chain Amyloidosis in Dogs and Cats. *Vet Pathol.* 2020: 57(5); 658-665.
6. Le Boedec K, Heng HG, Snyder PW, Pressler BM. Pulmonary Abnormalities in Dogs with Renal Azotemia. *J Vet Intern Med.* 2012;**26**: 1099-1106.
7. Mason NJ, Day MJ. Renal Amyloidosis in Related English Foxhounds. *Journal of Small Animal Practice.* 1996;**37**: 255-260.
8. Miyazaki S, Kadota A, Mitsui I, Murakami T. Amyloid Signature Proteins in Feline Amyloidosis. *J Comp Path.* 2020; 117:10-17.
9. Segev G, Cowgill LD, Jessen S, Berkowitz A, Mohr CF, Aroch I. Renal Amyloidosis in Dogs: A Retrospective Study of 91 Cases with Comparison of the Disease between Shar-Pei and Non-Shar-Pei Dogs. *J Vet Intern Med.* 2012;**26**: 259-268.
10. Woldemeskel M. A Concise Review of Amyloidosis in Animals. *Veterinary Medicine International.* 2012; 2012: 427296.

CASE III:

Signalment:
3-month-old castrated male Angus Cross (*Bos taurus*) bovine.

History:
6 out of 30 calves showed acute clinical signs including: bruxism, rapid breathing, dehydration, difficulty rising, and difficulty passing manure. All animals were normothermic (99.5-99.9 F). The herd was pastured in a native grass meadow with oak trees. The area recently received 3 feet of snow, during which the herd sheltered under the oak trees. The submitted animal died shortly after being tubed with fluids. The referring veterinarian submitted kidney, liver and ruminal contents to the diagnostic laboratory for evaluation.

Laboratory Results:
Gallic acid was strongly positive in the submitted rumen contents, confirming exposure to gallotannins.

Microscopic Description:
Kidney: Approximately 30% of the cortical tubular epithelium is necrotic, characterized by loss of cellular detail, rounding of cell borders, separation from the basement membrane, pyknotic nuclei and cytoplasmic hypereosinophilia. Affected tubules are often expanded by brightly eosinophilic granular

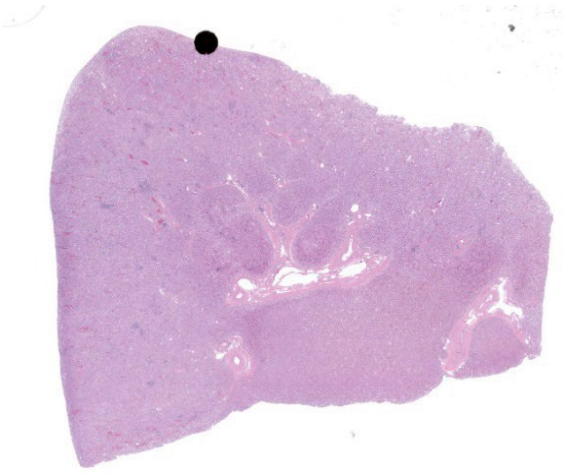

Figure 3-1. Kidney, calf. A wedge-shaped section of kidney is submitted for examination. (HE, 5X)

casts composed of cellular debris and mild amounts of hemorrhage. Occasionally the tubular epithelium is attenuated, mildly vacuolated (degeneration), or hypertrophied with moderate anisokaryosis and rare mitotic figures (regeneration). Few Bowman's spaces and tubules contain high protein fluid. Multifocally the interstitium is expanded by mild fibrosis with infiltration by small aggregates of lymphocytes and plasma cells with fewer neutrophils. The tunica media of large and medium-caliber vessels are mildly vacuolated.

Contributor's Morphologic Diagnoses:
Kidney: Moderate acute/subacute multifocal cortical tubular necrosis.

Contributor's Comment:
The history, histologic lesion, and presence of gallic acid in the rumen are diagnostic for oak toxicosis. Multiple species are potentially susceptible to oak toxicosis including: cattle, sheep, goats, llamas, moose, rabbits, horses, and pigeons.[4, 5, 6, 9, 12, 17, 19] Suspected oak toxicosis has been reported in one dog.[3] Tannins leached from oak leaves that fall into aquatic habitats are known to be toxic to some tadpole species.[10] Pigs appear to be resistant as ingestion increases production of tannin-binding salivary proteins.[17]

Cattle are the most susceptible and most commonly reported species. Cattle develop acute tubular necrosis after ingestion of blossoms, buds, leaves, stems or acorns from oak shrubs and trees (*Quercus spp*) which grow worldwide with case reports in North America, Brazil, Spain, Israel and Africa.[6, 14, 15, 18, 20] Consumption of large quantities of young oak leaves typically occurs in the spring and ingestion of bark or green acorns occurs in the fall. Toxic levels vary between plant species, plant component, and stage of plant maturity.[1] The toxicity of the leaf decreases with maturity, while the opposite occurs with the acorns which are most toxic when mature and freshly fallen.[16] Cattle frequently forage oak components without issue if the oak products represent less than 50% of their diet, therefore feed restriction plays a crucial role, as in this case with snow coverage removing availability of the herd's regular pasture diet.[8] Oak is also not considered to be generally palatable, reinforcing the importance of other feed availability to avoid toxicosis. The toxic substances are metabolites of tannins which are believed to include: tannic acid, gallic acid and pyrogallol.[2,5] Toxicosis is dose-dependent and the exact mechanism of renal tubular damage is unknown. The binding of tannins

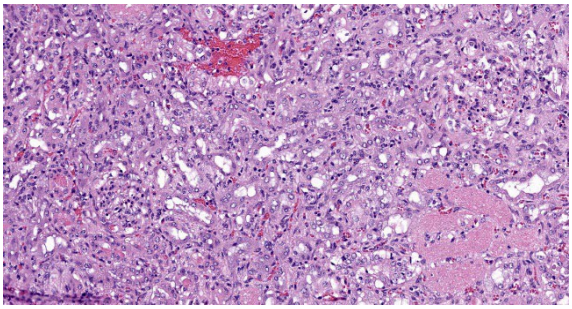

Figure 3-2. Kidney, calf: Due to the numerous and diverse tubular changes, there is loss of normal tubular architecture in the cortex. There is multifocal interstitial hemorrhage and a cluster of tubules containing granular protein casts (lower right). (HE, 228X)

to endothelial cells results in widespread endothelial damage and can lead to perirenal edema, hydrothorax, ascites and disseminated intravascular coagulation.[5]

Clinical signs occur 3-7 days after ingestion and mortality can be as high as 80%.[20] Clinical signs related to endothelial damage and renal failure are typical and can include polyuria, polydipsia, hematuria, dehydration and sternal edema. Animals may also experience abdominal pain, mucoid to hemorrhagic diarrhea, tenesmus, icterus, rumen stasis, anorexia and depression. Malformed calves and abortions have been reported in cows that consume acorns during the second trimester of pregnancy.[11] Clinical pathology findings may include increased BUN and creatinine concentrations, proteinuria, glucosuria, hyperbilirubinuria, hyperphosphatemia, hypocalcemia, and hyposthenuria. Other findings reported include elevated AST, GGT, CK, and lactate dehydrogenase, hypoalbuminemia, hypocalcemia and hypoproteinemia.[2, 5, 6, 14, 16, 20]

Typical gross findings include swollen, pale kidneys with pinpoint hemorrhages on the capsular and cortical surfaces, perirenal edema and hemorrhage, hydrothorax, ascites, and alimentary tract ulceration. Histopathological findings within the kidney are characterized by acute proximal tubular necrosis with casts and intratubular hemorrhage. Chronic cases develop chronic interstitial nephritis with fibrosis, atrophy, thinned cortex and a finely pitted surface. [2, 5, 6, 14, 15, 16, 20]

The diagnosis of oak poisoning is typically based on clinical and gross findings, provided history and histopathological examination of the kidneys. Commercial diagnostic testing for tannin metabolites is available for confirmation. Additional differentials for acute tubular necrosis in cattle include: pigweed (*Amaranthus spp*) toxicity, aminoglycoside antibiotic toxicity, oxalate poisoning, urolithiasis, heavy metal exposure, and ochratoxicosis, yet tubular necrosis with intratubular hemorrhage distinguishes this nephrotoxicity from most other causes.[5]

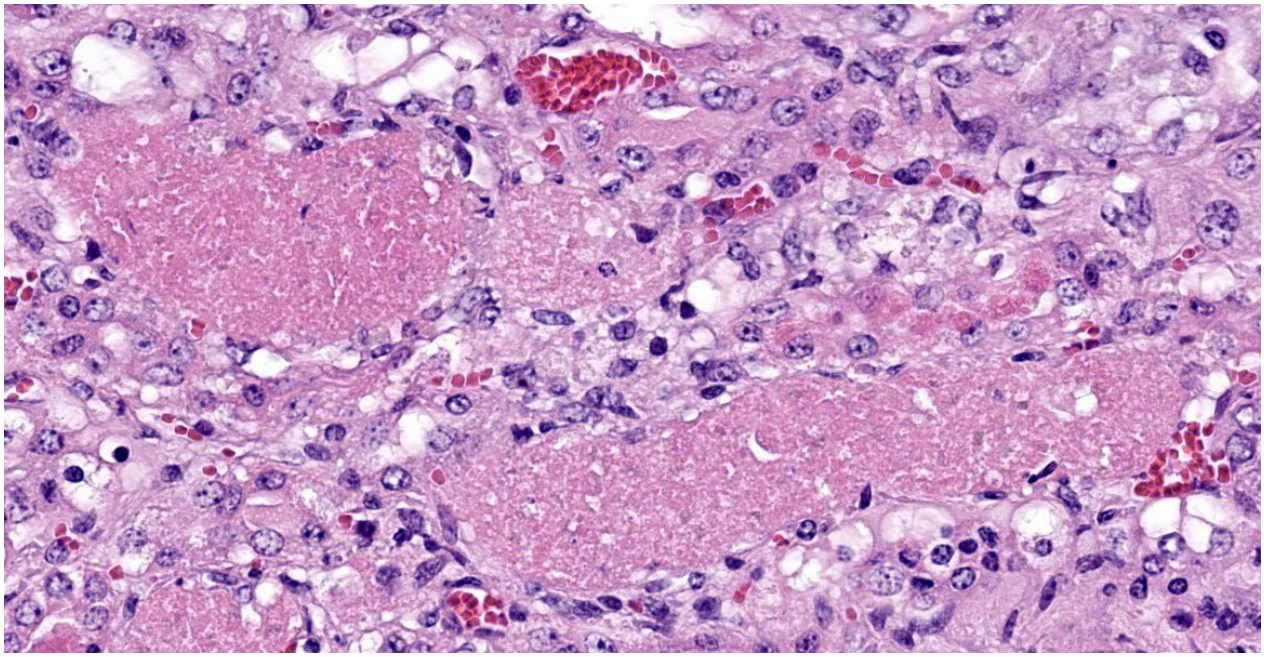

Figure 3-3. Kidney, calf. There is multifocal necrosis and loss of tubular epithelium lining proximal convoluted tubules. Tubular lumina are filled with granular casts. (HE, 560X)

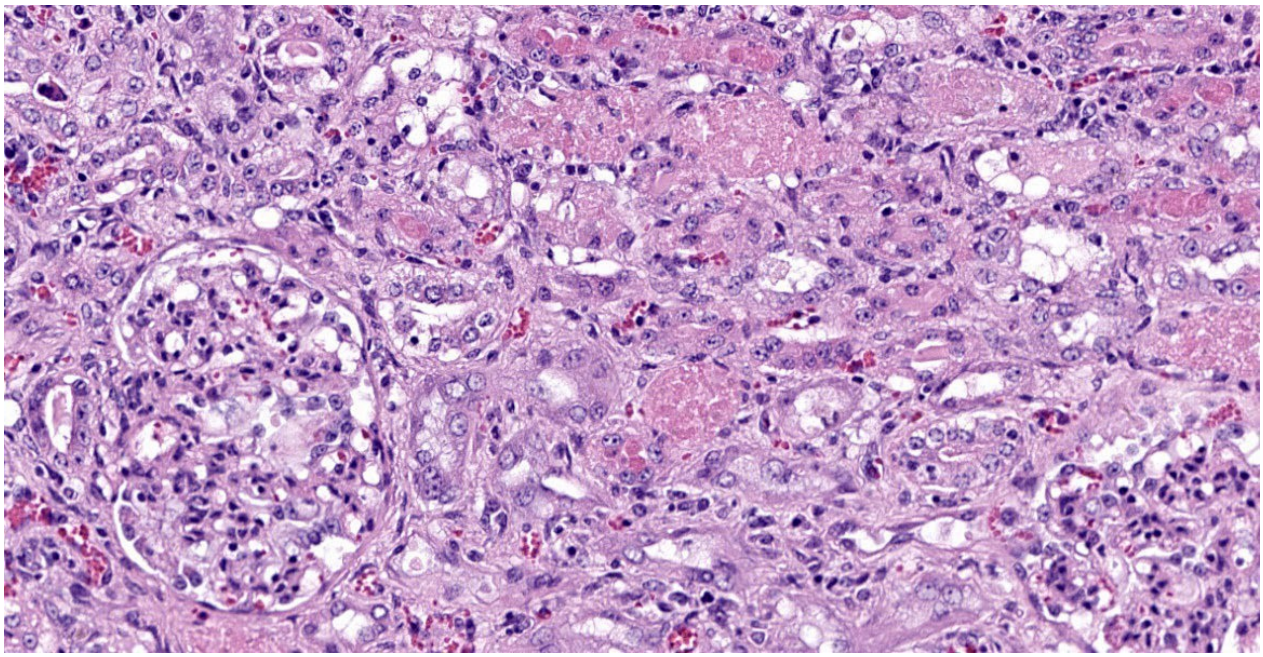

Figure 3-4. Kidney, calf. In additional to necrotic tubules (top center), there are less dramatic changes including numerous regenerating tubular epithelial cells with mildly basophilic cytoplasm and open-faced nuclei, and mildly hypercellular glomeruli. (HE, 350X)

Contributing Institution:
Veterinary Diagnostic Laboratory, Colorado State University Fort Collins, CO, USA
http://csu-cvmbs.colostate.edu/vdl/Pages/default.asp

JPC Diagnosis:
Kidney: Tubular degeneration, necrosis, and regeneration, diffuse, with intratubular granular casts, hemorrhage, and proteinosis.

JPC Comment:
This is a classic case of oak toxicosis. In addition to exogenous toxins so thoroughly described by the contributor, acute tubular injury (ATI) can also be caused by endogenous toxins.[5] Massive release of hemoglobin or myoglobin from hemolysis or rhabdomyolysis can cause pigmentary nephrosis. Tubular injury in these cases may stem from the toxic effects of pigments and secondary factors, such as anemia.[5] Bile is also nephrotoxic in domestic animals.[5] In humans, hepatic cirrhosis causes systemic hypotension and renal hypoperfusion which lead to tubular injury, and bile pigments build up in tubular epithelium and form bile casts in tubules.[5]

Acute tubular injury also occurs as part of renal cortical necrosis; in this condition, all cortical structures, including glomeruli, are damaged. Differentials for renal cortical necrosis include hypoperfusion, ischemia, endotoxemia, disseminated intravascular coagulation, and certain gastrointestinal disease.[5] In some cases, distinguishing ATI and renal cortical necrosis may be difficult as edema may decrease perfusion and cause concurrent ischemia.[5]

The ability to recover from ATI is dependent on preservation of basement membranes.[5] Jones periodic methenamine silver staining and other stains can provide valuable prognostic information in biopsy cases.

References:
1. Basden KW, Dalvi RR. Determination of total phenolics in acorns from different species of oak trees in con-

junction with acorn poisoning in cattle. Veterinary and Human Toxicology. 1987;29.4:305-306.
2. Breshears MA, Confer AW. The urinary system. In: Zachary JF, ed. Pathological Basis of Veterinary Disease. 6th ed. Philadelphia, PA: Mosby Elsevier Inc.; 2017: 672-673.
3. Camacho F, Stewart S, Tinson E. Successful management of suspected acorn (Quercus petraea) toxicity in a dog. The Canadian Veterinary Journal. 2021;62.6: 581.
4. Chamorro MF, Passler T, Joiner K, et al. Acute renal failure in 2 adult llamas after exposure to Oak trees (Quercus spp.). The Canadian Veterinary Journal. 2013; 54.1:61.
5. Cianciolo RE, Mohr FC. Urinary system. In: Maxie MG, ed. Jubb, Kennedy, and Palmer's Pathology of Domestic Animals. 6th ed. Vol 2. St. Louis, MO: Elsevier; 2016:439-441.
6. Cortinovis C, Caloni F. Epidemiology of intoxication of domestic animals by plants in Europe. The Veterinary Journal. 2013;197(2):163-8.
7. Díez MT, del Moral PG, Resines JA, et al. Determination of phenolic compounds derived from hydrolysable tannins in biological matrices by RP-HPLC. Journal of separation science. 2008; 31.15:2797-2803.
8. Doce RR, Belenguar A, Toral PG, et al. Effect of the administration of young leaves of Quercus pyrenaica on rumen fermentation in relation to oak tannin toxicosis in cattle. Journal of Animal Physiology and Animal Nutrition. 2013;97.1: 48-57.
9. Dollahite JW, Pigeon RF, Camp, BJ. The toxicity of gallic acid, pyrogallol, tannic acid, and Quercus havardi in the rabbit. American journal of veterinary research. 1962;23:1264-1267.
10. Earl JE, Semlitsch RD. Effects of tannin source and concentration from tree leaves on two species of tadpoles. Environmental toxicology and chemistry. 2015;34.1:120-126.
11. James LF, Nielsen DB, Panter KE. Impact of poisonous plant on the livestock industry. Rangeland Ecology & Management/Journal of Range Management Archives. 1992:45.1: 3-8.
12. Meiser H, Hagedorn HW, Schulz R. Pyrogallol poisoning of pigeons caused by acorns. Avian diseases. 2000:205-209.
13. Meiser H, Hagedorn HW, Schulz R. Pyrogallol concentrations in rumen content, liver and kidney of cows at pasture. Berliner und Munchener Tierarztliche Wochenschrift. 2000;113.3:108-111.
14. Neser JA, Coetzer JAW, Boomker J, Cable H. Oak (Quercus rubor) poisoning in cattle. Journal of the South African Veterinary Association. 1982;53.3:151-155.
15. Pérez V, Doce RR, García-Pariente C, et al. Oak leaf (Quercus pyrenaica) poisoning in cattle. Research in Veterinary Science. 2011;91.2:269-277.
16. Plumlee KH, Johnson B, Galey FD. Comparison of disease in calves dosed orally with oak or commercial tannic acid. Journal of veterinary diagnostic investigation. 1998;10.3:263-267.
17. Smith S, Naylor RJ, Knowles EJ, et al. Suspected acorn toxicity in nine horses. Equine Veterinary Journal. 2015;47(5):568-572.
18. Spier SJ, Smith BP, Seawright AA, Norman BB, Ostrowski S, Oliver MN. Oak toxicosis in cattle in northern California: clinical and pathologic findings. Journal of the American Veterinary Medical Association. 1987;191.8:958-964.

19. Vikøren T, Handeland K, Stuve G, Bratberg B. Toxic nephrosis in moose in Norway. Journal of wildlife diseases. 1999;35(1):130-3.
20. Yeruham I, Avidar Y, Perl S, et al. Probable toxicosis in cattle in Israel caused by the oak Quercus calliprinos. Veterinary and human toxicology. 1998;40(6):336-40.

CASE IV:

Signalment:
A 1.6 year-old, female, domestic short hair, cat (*Felis catus*)

History:
Acute death with no prior clinical signs.

Gross Pathology:
This is the body of a 4.5 kg, reportedly 1.6 year-old female domestic short hair with a body condition score 6/9 and minimal autolysis. The apex of the heart is slightly rounded. Multiple coronary vessels, especially those in the paraconal groove, are segmentally thickened. There are multiple irregular, depressed areas scattered on the renal cortical surfaces (chronic infarctions/tubulointerstitial nephritis). On section, arcuate renal vessels appear up to 3mm thick. There are no other significant findings.

Laboratory Results:

Special stains	Result
GMS staining	Negative
PAS staining	Negative
Acid-fast staining	Negative

Microscopic Description:
Kidney: Multiple small to large sized arteries are circumferentially obliterated, partially to completely occluded and markedly expanded by a moderately cellular proliferation of spindle shaped cells (presumptive smooth muscle cells and fibroblasts cells) within the tunica intima and media admixed with the pale basophilic extracellular matrix. Occasionally, there are also foci of myointimal necrosis. Multiple dense lymphoid aggregations surround within the tunica adventitia of these affected vessels, and there are moderate lymphocytic, histiocytic and neutrophilic infiltrates transmurally. Multifocally, the endothelial lining of the vessels is plump reactive, infrequently sloughed off from the basement membranes, and lost. The vascular lumens also contain numerous lymphocytes, plasma cells, and infrequent basophilic karyorrhectic debris. Multifocally, the inflammatory reactions that surrounded the vessels extent to the renal interstitial spaces. Multifocally, there is a well-delineated regional infarction involving the renal cortex to the renal medulla.

Contributor's Morphologic Diagnoses:
Kidney: Severe, multifocal, chronic, necrotizing and pyogranulomatous vasculitis

Contributor's Comment:
Histopathology has confirmed severe multisystemic vascular disease that is most pronounced in the kidney, heart and a mesenteric artery. Our primary differential is a ster-

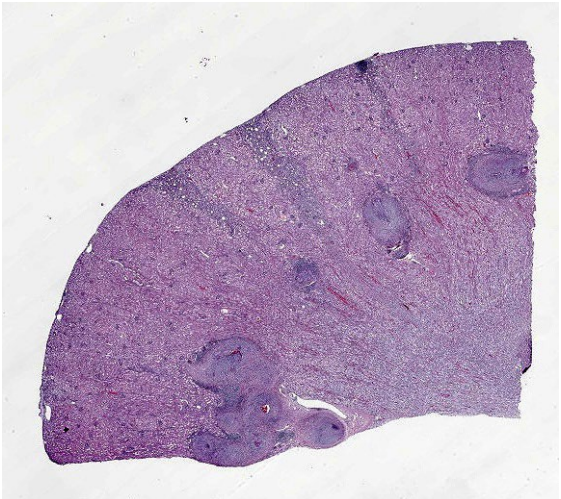

Figure 4-1. Kidney, cat. A wedge-shaped section of kidney is submitted for examination. There is marked increase in the size of the arcuate arteries at the corticomedullary junction. (HE, 5X)

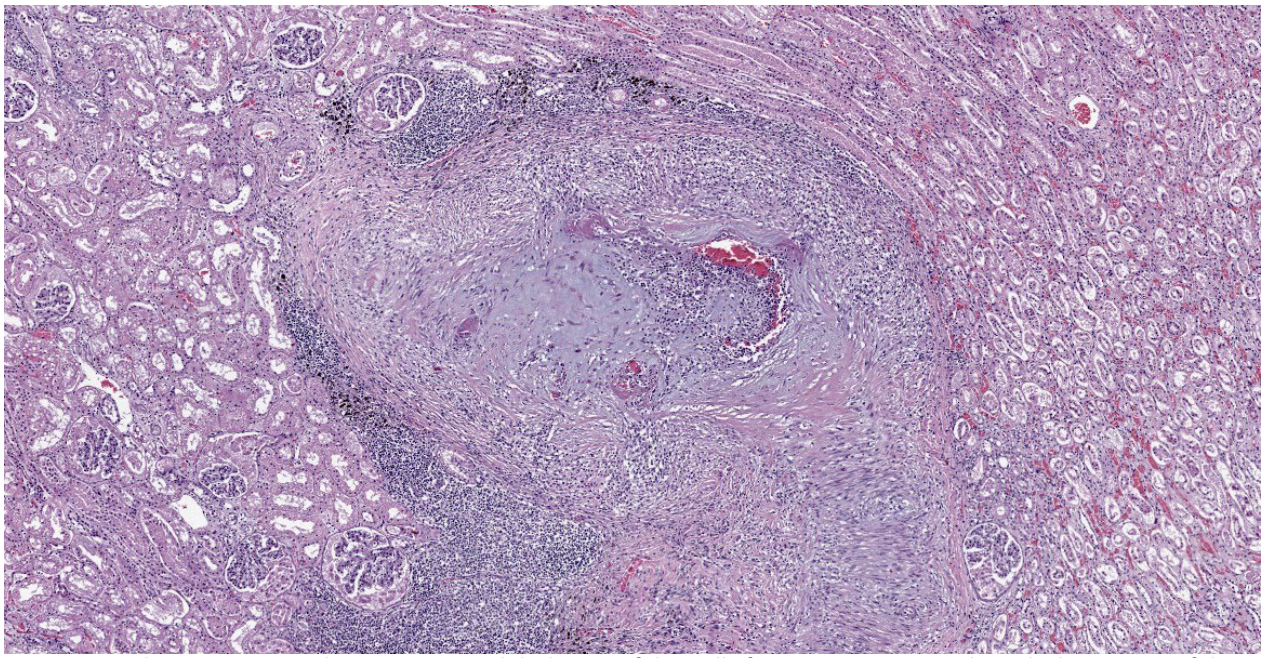

Figure 4-2. Kidney, artery, cat. There is transmural thickening of the wall of an arcuate artery with marked expansion of the tunica intima, media, and adventitia. (HE, 53X

ile/immune mediated arteritis, perhaps resembling polyarteritis nodosa (syn. juvenile polyarteritis) as seen in other species (ie. dogs, cynomolgus macaques, human, rat, others).

Polyarteritis nodosa (PAN) is a systemic necrotizing vasculitis mainly involving small- and medium-sized muscular arteries of visceral organs.[11, 12] The pathogenesis of PAN is still poorly understood.[11,12] In human, PAN has been associated with some virus infections including hepatitis B and C viruses, human immunodeficiency virus, parvovirus B19 and hairy cell leukemia.[5,6] An immune-mediated vasculopathy is highly suggestive due to the infiltrates of histiocytes and CD4+ T lymphocytes within the vascular walls.[3,5] In veterinary medicine, most cases of PAN have not been associated with infectious agents. However, there are some reports described in many species including blue foxes associated with encephalitozoonosis, in sheep infected with ovine herpesvirus 2 and a streptococcal infection has been suspected in pigs.[7,8,9]

PAN has been recently reported in a cat and in our case, the histopathological findings and gross findings resemble to recently described in the cat which includes systemic necrotizing vasculitis involved the small, medium and large arteries of the heart, kidneys, mesentery.[11] In addition to the recent report, our case demonstrates intense neutrophilic infiltration of the vascular walls.[11]

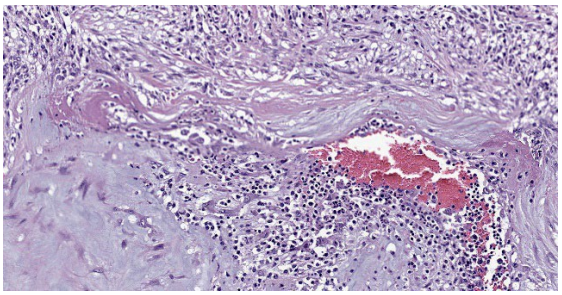

Figure 4-3. Kidney, artery, cat. Higher magnification of the artery in 4-2. There is partial occlusion of the lumen, and at left, pink proteinaceous extruded protein just beneath the remnant endothelium. There is no visible lamina intima, with thickening of the tunica intima by maloriented infiltrating smooth muscle, abundant ground substance, few fibroblasts and collagen and numerous inflammatory cells. The tunica media and adventitia is markedly expanded by fibrosis and inflammatory cells. (HE, 193X)

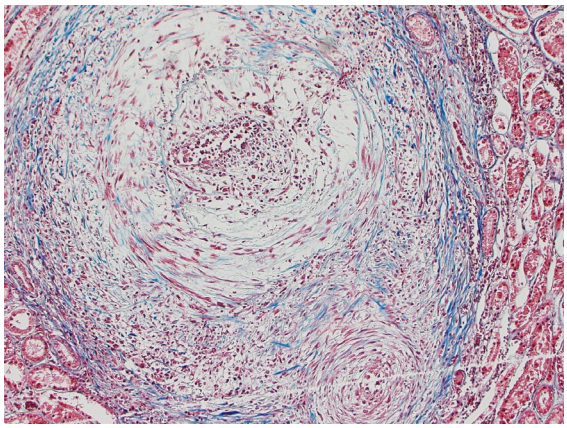

Figure 4-4. Kidney, artery, cat. A Masson's trichrome demonstrates the amount of collagen in the wall of the artery (which should be minimal in the normal state). (Masson's trichrome, 200X)

Some other diagnostic considerations are discussed below. Perhaps the best recognized vasculopathy in the cat is feline infectious peritonitis. Although we have not definitively excluded this pathogen, we suggest that the histologic picture is not entirely typical of this syndrome (ie. morphologic pathology, distribution of lesions). Another possibility might be severe systemic hypertension, but we note that some organs typically affected by hypertension are not involved (ie. meninges, eye).

Contributing Institution:
Oregon State University Magruder Hall Rm. 134 700 SW 30th Street Corvallis, OR 97331
https://vetmed.oregonstate.edu/diagnostic

JPC Diagnosis:
Kidney: Arteritis, proliferative and necrotizing, chronic, diffuse, severe, with cortical infarcts.

JPC Comment:
While relatively uncommon in cats, systemic necrotizing vasculitis is a common background lesion in laboratory species, specifically mice, rats, beagle dogs, and Gottingen minipigs.[1,2,4] In mice, polyarteritis can affect multiple organ systems and tends to occur in strains predisposed to autoimmune diseases, such as MRL and NZB strains. In the kidneys, it can cause segmental infarction, similar to what was seen in this case.[1] Other organs that may be infected include the tongue, pancreas, mesentery, and heart.[1] Polyarteritis may also affect medium sized vessels around the inner and middle ear, causing vestibular signs.[1] Polyarteritis nodosa is a chronic progressive disease of rats and occurs more commonly in rats that are older, male, or Sprague Dawley or spontaneous hypertensive strains.[1,4] Many organ systems can be affected, including the mesentery, kidneys, and testis; however, the lung is spared.[1,4] In beagles, polyarteritis occurs in small to medium caliber arteries of the leptomeninges, cranial mediastinum, and heart and is characterized by lymphoplasmacytic and histiocytic inflammation with fibrinoid necrosis and possible hemorrhage.[2,4] Previously known as beagle pain syndrome for the primary breed affected, this condition is now referred to as steroid responsive meningitis-arteritis and is known to affect other medium and large breeds as well.[2,4] Affected animals have fever and severe spinal pain.[2] Spontaneous polyarteritis also occurs occasionally in Gottingen minipigs, most commonly in small to medium caliber vessels in a single or multiple organs. Affected sites include the heart, reproductive tract (epididymis, oviduct, vagina), kidney, rectum, stomach, urinary

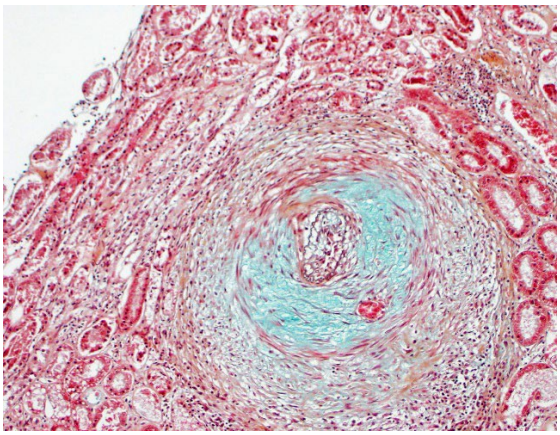

Figure 4-5. Kidney, artery, cat. The internal and external elastic lamina are not visible on a Movat's pentachrome. (Movat, 200X)

bladder, and spinal cord.[4] An important differential to consider in laboratory species used in pre-clinical drug safety studies is drug-induced vasculopathy, which may be induced by vasodilators (minoxidil, endothelin receptor antagonists), bronchodilators (phosphodiesterase inhibitors), and immunomodulatory agents (hydrocortisone, betamethasone).[4]

References:

1. Barthold SW, Griffey SM, Percy DH. *Pathology of Laboratory Rodents and Rabbits.* 4th ed. John Wiley & Sons, Inc: 2016; 98, 99, 156.
2. Cantile C, Youssef S. Nervous System. In: Maxie MG, ed. *Jubb, Kennedy, and Palmer's Pathology of Domestic Animals.* Vol 1. 6th ed. Elsevier; 2016: 395.
3. Cid MC, Grau JM, Casademont J, Campo E, Coll-Vinent B, López-Soto A, Ingelmo M, Urbano-Márquez A. Immunohistochemical characterization of inflammatory cells and immunologic activation markers in muscle and nerve biopsy specimens from patients with systemic polyarteritis nodosa. *Arthritis Rheum.* 1994;37(7):1055-1061.
4. Dincer Z, Picciuto V, Walker UJ, Mahl A, McKeag S. Sponatneous and Drug-Induced Arteritis/Polyarteritis in the Gottingen Minipig-Review. *Tox Pathol.* 2018; 46(2):121-130.
5. Forbess L, Bannykh S. Polyarteritis nodosa. *Rheum Dis Clin North Am*. 2015;41(1):33-46.
6. Ishiguro N, Kawashima M. Cutaneous polyarteritis nodosa: a report of 16 cases with clinical and histopathological analysis and a review of the published work. *J Dermatol*. 2010;37(1):85-93.
7. Liu CH, Chiang YH, Chu RM, Pang VF, Lee CC. High incidence of polyarteritis nodosa in the brains of culled sows. *J Vet Med Sci*. 2005;67(1):125-7.
8. Nordstoga K, Westbye K. Polyarteritis nodosa associated with nosematosis in blue foxes. *Acta Pathol Microbiol Scand A*. 1976;84(3):291-6.
9. Pesavento PA, Dange RB, Ferreras MC, et al. Systemic necrotizing vasculitis in sheep is associated with ovine herpesvirus 2. *Vet Pathol*. 2019: 56(1):87-92.
10. Robinson WF, Robinson NA. Cardiovascular System. In: Maxie MG, ed. *Jubb, Kennedy, and Palmer's Pathology of Domestic Animals.* Vol 3. 6th ed. Elsevier; 2016.
11. Salvadori C, Vezzosi T, Marchetti V, Cantile C. Polyarteritis Nodosa in a Cat with Involvement of the Central and Peripheral Nervous Systems. *J Comp Path.* 2019;167:6-11.
12. Wessels M, Strugnell B, Woodger N, Peat M, La Rocca SA, Dastjerdi A. Systemic necrotizing polyarteritis in three weaned lambs from one flock. *Jour Vet Diagn Invest.* 2017;29(5):733-7.

WSC 2022-2023 Self-assessment
Conference 12

1. Which of the following viruses have been reported to cause glomerulonephritis in ruminants .
    a. Ovine herpesvirus-2
    b. Bovine pestivirus
    c. Bovine herpesvirus-1
    d. Bovine leukemia virus

2. True or false? AA-amyloidosis is the most common form in the dog.
    a. True
    b. False

3. Familial amyloidosis is seen in which breed of dog?
    a. Welsh Corgi
    b. Shar Pei
    c. Dalmatian
    d. Portuguese water dog

4. Pigs are resistant to oak toxicosis due to which of these?
    a. High levels of hepatic cytochrome oxidases
    b. Tannin-degrading gatric mucus
    c. Tannin-binding salivary proteins
    d. Pyrogallol-resistant tubular epithelium

5. True or false? Most cases of polyarteritis nodosa in veterinary medicine result from infectious agents.
    a. True
    b. False

Please email your completed assessment for grading to Dr. Bruce Williams at bruce.h.williams12.civ@mail.mil. Passing score is 80%. This program (RACE program 33611) is approved by the AAVSB RACE to offer a total of 0.5 CE Credits, with a maximum of 12.5 CE Credits being available to any individual Veterinary Medical Professionals for the 2019-2020 Wednesday Slide Conference. This RACE approval is for the subject matter categories of: SCIENTIFIC using the delivery method of NONINTERACTIVE DISTANCE. This approval is valid in jurisdictions which recognize AAVSB RACE.

Joint Pathology Center
Veterinary Pathology Services

WEDNESDAY SLIDE CONFERENCE 2022-2023

Conference #13 14 December 2022

CASE I:

Signalment:
Two, 8 month old female entire Boer goats (*Capra hircus)*

History:
A herd of nine goats were kept with a flock of sheep in a paddock associated with a school agricultural program. The goats gained access to an adjacent paddock of shrubbed land through a hole in the fence which the sheep did not find, and had been foraging in this adjacent paddock for approximately one week. Two goats were found dead initially, and a further two became acutely lethargic and depressed, and died early the following day (these two were submitted for necropsy). Within 24 hours, a further three goats had died, leaving one remaining goat from the herd that was also exhibiting acute clinical signs. One dead goat was found underneath a *Trema tomentosa* (poison peach) tree, and a further two that were observed beneath the *Trema tomentosa* subsequently died. A video was submitted of an affected goat, which showed a standing goat with a wide-based stance, salivation/foam around the mouth, and twitching of the upper lip and eyelids, with apparent unawareness of the surroundings.

Plants within the shrubbed area accessed by the goats included *Trema tomentosa* (Poison peach), *Acacia fimbriata* (Brisbane wattle), *Solanum mauritianum* (Wild tobacco), *Schinus terebinthifolius* (Broad-leaf pepperina), and an unknown species of wattle, (*Acacia* sp.) as identified by a botanist with the Queensland Herbarium.

Gross Pathology:
In one goat, the liver had a generalized, exaggerated reticular pattern, interpreted as periacinar necrosis. The same goat also had a mild pleural effusion and petechial hemorrhages in the subcutaneous tissues of the ventral neck and serosal surfaces of the rumen and small intestine. The second goat appeared slightly more autolyzed than the first, and had no grossly observed pathology. The rumen of both goats contained fragments of foliage from multiple plants species.

Figure 1-1. Presentation, goat. The affected individual demonstrated facial twitching and hypersalivation. (Photo courtesy of: The School of Veterinary Science, The University of Queensland, Gatton Campus, Queensland, Australia 4343, https://veterinary-services.lab.uq.edu.au/).

Laboratory Results:
No findings reported.

Microscopic Description:
Liver: Diffusely, there is submassive to massive necrosis spanning periacinar, midzonal and frequently periportal regions. Necrosis is characterized by disruption and loss of normal hepatic sinusoidal architecture; shrunken, fragmented, hypereosinophilic hepatocytes with pyknotic, karyorrhectic or karyolytic nuclei; or complete loss of hepatocytes, replaced by extravasated erythrocytes (hemorrhage) and small amounts of cellular and karyorrhectic debris. Multifocal intact hepatocytes in periportal areas are swollen with vacuolated pale cytoplasm (degeneration), and rare limiting plate hepatocytes are normal.

Contributor's Morphologic Diagnoses:
Liver: Severe acute submassive to massive hepatic necrosis

Contributor's Comment:
Trema tomentosa, formerly known as *Trema aspera*, and colloquially known as poison peach, is an evergreen shrub to small tree of the family Ulmaceae, which is characterised by alternately attached leaves that are elliptical- to spearhead-shaped and dark green, with finely-toothed edges and hairy upper surfaces; small clusters of greenish-white flowers in the leaf-stem junctions; and round, fleshy, black, 3-4 mm berries.[7] Poison peach is located on the east and north coasts of Australia, in the states of Victoria, New South Wales, Queensland, Northern Territory and the north coast of Western Australia.[7]

Figure 1-3. Leaves and fruit of poison peach (Trema tormentosa). (Photo courtesy of: The School of Veterinary Science, The University of Queensland, Gatton Campus, Queensland, Australia 4343, https://veterinary-services.lab.uq.edu.au/).

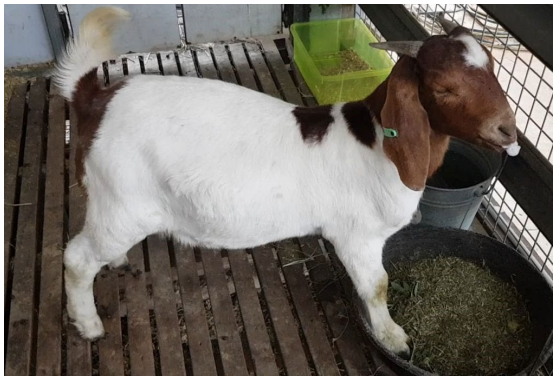

Figure 1-2. Presentation, goat. The affected individual demonstrated a wide-based stance, and its tail was curled over its back. (Photo courtesy of: The School of Veterinary Science, The University of Queensland, Gatton Campus, Queensland, Australia 4343, https://veterinary-services.lab.uq.edu.au/).

The leaves of poison peach contain a toxin known as trematoxin, which is an uncharacterised hepatotoxic glycoside, and is reported to cause fatal poisoning in cattle, sheep, goats, horses, and camels.[4,6,9,10] Clinical signs of trematoxicosis can include recumbency, anorexia, muscle fasciculations, rigid posture, reluctance to move, dyspnoea, rapid weak pulse, and salivation.[5,8,10] On post mortem examination, all reported cases have hepatic necrosis as the main feature, characterised as coagulative, periacinar to massive, and frequently with extensive hemorrhage.[5,7,8,10] Further pathology described in

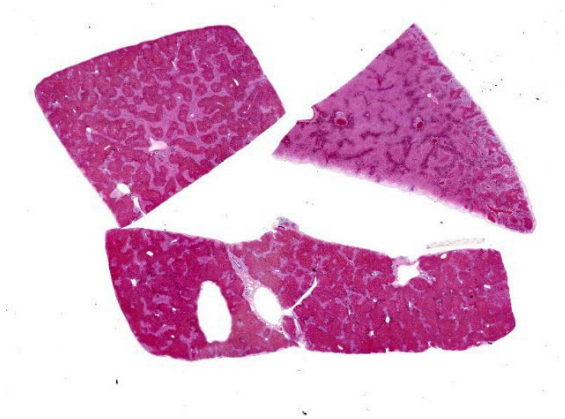

Figure 1-4. Liver, goat. Three sections of liver are submitted for examination. At subgross magnification, there is centrilobular to massive hepatic necrosis, depending on the section. (HE, 7X)

the literature is predominately hemorrhage, including subcutaneous hemorrhages of the neck, chest and abdomen; petechial hemorrhages on the serosa of the rumen, abomasum and duodenum; and subepicardial and endocardial hemorrhages.[6,8]

Another species of the same genus, *Trema micrantha*, is located in the tropical to subtropical Americas, particularly South and Central America, and Florida in North America; and is reported to cause a similar disease in horses and goats.[1,3] Additionally, there is evidence that ingestion of *Trema micrantha* by sheep can cause a fatal pneumotoxicosis, with the documented pathology including mediastinal emphysema, interalveolar septal thickening, and diffuse type II pneumocyte hyperplasia.[11]

As trematoxin is uncharacterized, definitive diagnosis of toxicity is difficult. Diagnosis is generally based on known exposure to the plant in combination with acute periacinar to massive hepatic necrosis. Differential diagnoses for acute hepatotoxicity in goats include amatoxins, cyanobacteria, *Xanthium* spp, green cestrum, cycads, gossypol, iron, polycyclic aromatic hydrocarbons, and carbon tetrachloride.[4,7] Further, intoxication with *Xanthium*, green cestrum and *Trema* spp. cause very similar gross and microscopic changes, and therefore differentiating the three syndromes may involve isolation of the specific toxin where possible, or demonstration of ingestion of the plant species.[3]

In this case, no poison peach leaves or other toxic plant leaves were identified in the rumens of the two goats necropsied. It is hypothesized by the authors and submitting veterinarian that as the leaves are fine and palatable, they were well masticated and digested quickly, or were unidentifiable within the other ingesta of the rumen. There was no known exposure to other hepatotoxins aside from poison peach, and thorough examination of the pasture by the farm hand and submitting veterinarian did not reveal further hepatotoxic plants. Additionally, the sheep that were housed with the goats were not affected. Therefore, it was concluded that ingestion of poison peach was the most likely cause of hepatic necrosis and death in this herd of goats.

Contributing Institution:
The School of Veterinary Science
The University of Queensland, Gatton Campus
Queensland
Australia 4343
https://veterinary-services.lab.uq.edu.au/

JPC Diagnosis:
Liver: Necrosis, massive.

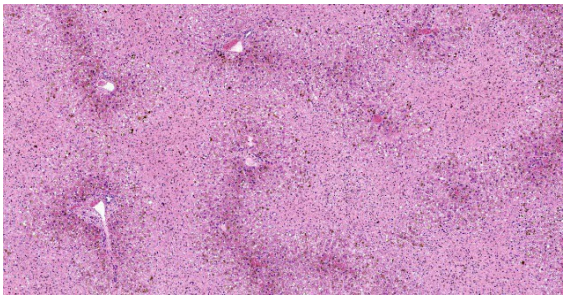

Figure 1-5. Liver, goat. There is necrosis of centrilobular and midzonal hepatocytes characterized by loss of differential staining. (HE, 76X)

JPC Comment:

This case is a classic example of centrilobular hepatocellular necrosis. Centrilobular hepatocytes are particularly susceptible to toxic injury due to their high concentration of cytochrome P450 (CYP450) and susceptibility to hypoxia due to the location furthest downstream of the hepatic artery. [3] During phase I biotransformation and detoxification, CYP450 metabolism of toxins may cause formation of reactive intermediates with local toxic effects.[3] Other examples of toxins which cause centrilobular necrosis are acetaminophen, microcystin, amanita, and *Xanthium* spp.[3] Other less common patterns of hepatocellular necrosis are periportal hepatocellular necrosis, caused by direct acting toxins like yellow phosphorous, and midzonal necrosis, which is the least common.[3]

This week's moderate, Dr. John Cullen, described the variability in histologic appearance between the different sections of liver on the slide. One possible explanation is a phenomenon called portal streaming, where blood from a specific portion of the gastrointestinal tract may be routed to specific areas of the liver through laminar flow, thus delivering different amounts of pathogens (whether toxic, infectious, or neoplastic). Other possible explanations include the different volume of each load, some regulation of flow which redirects blood flow, or sampling technique. Dr. Cullen explained that similar variation between lobes is seen in copper deposition and this variation demonstrates why sampling all hepatic lobes is critical for accurate surgical biopsies.

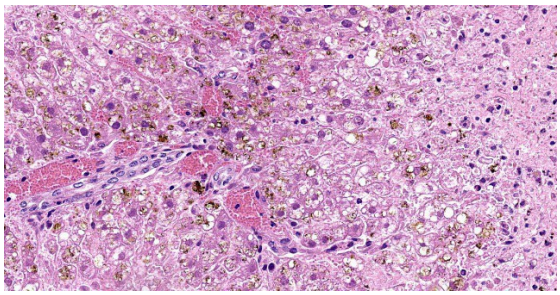

Figure 1-6. Liver, goat. Periportal hepatocytes (left) are degenerate, characterized by cellular swelling and lipidosis. There is abundant brown pigment within the cytoplasm of hepatocytes and Kupffer cells. (HE, 381X)

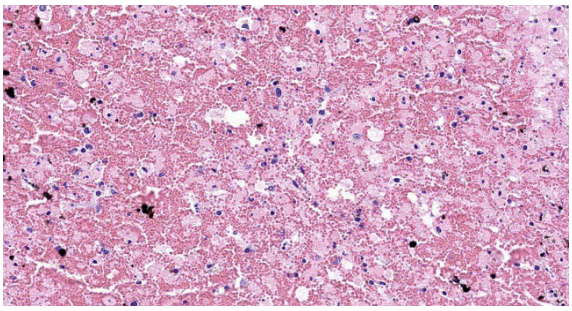

Figure 1-7. Liver, goat. Areas of hepatocellular necrosis demonstrate hemorrhage and stomal collapse. (HE, 381X)

The contributor described a related plant, *Trema micrantha* (Jamaican nettletree or capulin), which causes centrilobular necrosis in horses, goats, and sheep, and also causes pneumotoxicity in sheep. Ingestion of the plant, which appears to be highly palatable, can also cause acute neurotoxicosis without hepatotoxicosis in horses.[2,6] A recent report described *T. micrantha* ingestion by 14 horses in Brazil with primary neurotoxicosis.[6] Horses ingested the plant after being food restricted or having access to fresh trimmings and were ataxic with progressive neurologic signs resulting in death within one week. [6] On necropsy, the brains were diffusely yellow with scattered foci of hemorrhage and necrosis, and the pons most severely affected. [6] Three horses had similar spinal cord lesions. On histology, there was multifocal fibrinoid necrosis of vessels, thrombosis, and liquefactive necrosis in the brainstem, cerebellum, and, less frequently, in the spinal cord. [6] Centrilobular hepatocellular necrosis was present in only five cases and was characterized as mild. [6] Horses with *T. micrantha* toxicity may also develop neurologic signs secondary to hepatotoxicity and hepatic encephalopathy.[6] Histologically, these cases feature perivascular edema and Alzheimer type II astrocytes.[2,6] These were not observed in the recent report, and the hepatic lesions were mild to absent, so hepatic

encephalopathy was not suspected in these horses.[6] The authors speculate that there may be intermediate metabolites which have species-specific toxic effects.[6]

References:

1. Bandarra P, Bezerra P, De Oliveira L, et al. Experimental Trema micrantha (Cannabaceae) poisoning in horses. *Pesqui Vet Brasil*. 2011; **31**(11): 991-996.
2. Bandarra PM, Pavarini SP, Raymundo DL, Correa AMR, Pedroso PMO, Driemeier D. *Trema micrantha* toxicity in horses in Brazil. *Equine Vet J.* 2010; 42(5):456-459.
3. Cullen JM, Stalker MJ. Liver and Biliary System. In: Maxie MG, ed. *Jubb, Kennedy and Palmer's Pathology of Domestic Animals. Vol 2*. 6th Ed. St. Louis, Missouri: Elsevier, 2016:258-352.
4. Haschek WM, Rousseaux CG, Wallig MA. *Fundamentals of toxicologic pathology.* 2nd ed. Amsterdam, NL: Elsevier/Academic Press, 2010.
5. Hill B, Wills L, Dowling R. Suspected poisoning of horses by Trema aspera (poison peach). *Aust Vet J.* 1985; 62(3): 107-108.
6. Lorenzett MP, Pereira PR, Bassuino DM, et al. Neurotoxicosis in horses associated with consumption of *Trema micrantha*. *Equine Vet J.* 2018; 50: 192-195.
7. McKenzie, RA. *Australia's Poisonous Plants, Fungi and Cyanobacteria: a Guide to Species of Medical and Veterinary Importance*. Collingwood, Vic: CSIRO Publishing; 2012. 635-637.
8. Mulhearn C. POISON PEACH (TREMA ASPERA): A PLANT POISONOUS TO STOCK. *Aust Vet J.* 1942; **18**(2): 68-72.
9. Oelrichs P. Isolation and purification of trematoxin from Trema aspera. *Phytochemistry*. 1968; **7**(9); 1691-1693.
10. Trueman K, Powell M. Suspected poisoning of camels by Trema tomentosa (poison peach). *Aust Vet J.* 1991; **68**(6): 213-214.
11. Wouters F, Wouters ATB, Watanabe TTN, et al. Pneumotoxicosis in Sheep Caused by Ingestion of Trema Micrantha. *Vet Pathol*. 2013; **50**(5), 775-778.

CASE II:

Signalment:
20-month-old, female Droughtmaster, ox (*Bos Taurus x indicus*)

History:
Inappetence and weakness; pale mucous membranes; black, watery feces and reduced gut sounds.

Gross Pathology:
Jaundice. Subcutaneous and interstitial pulmonary edema. Pale and yellow liver, marked distention of the gall bladder with mucoid bile.

Laboratory Results:
No findings reported.

Microscopic Description:
There is diffuse hepatocellular disassociation. Hepatocytes are often enlarged and many are multinucleated, containing 2-4 nuclei. The cytoplasm of hepatocytes if often distended with fine vacuolation. Multifocally and often in centrilobular areas, there is mild

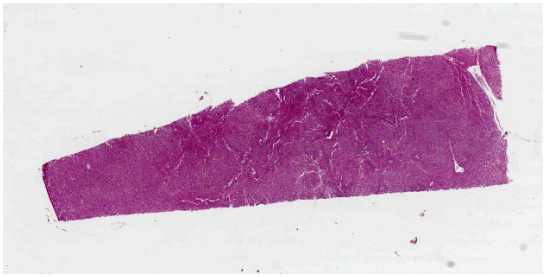

Figure 2-1. Liver, ox. A single section of liver is submitted for examination. There is a homogeneity to the section at subgross magnification resulting from loss of hepatocellular plate architecture. (HE 8X)

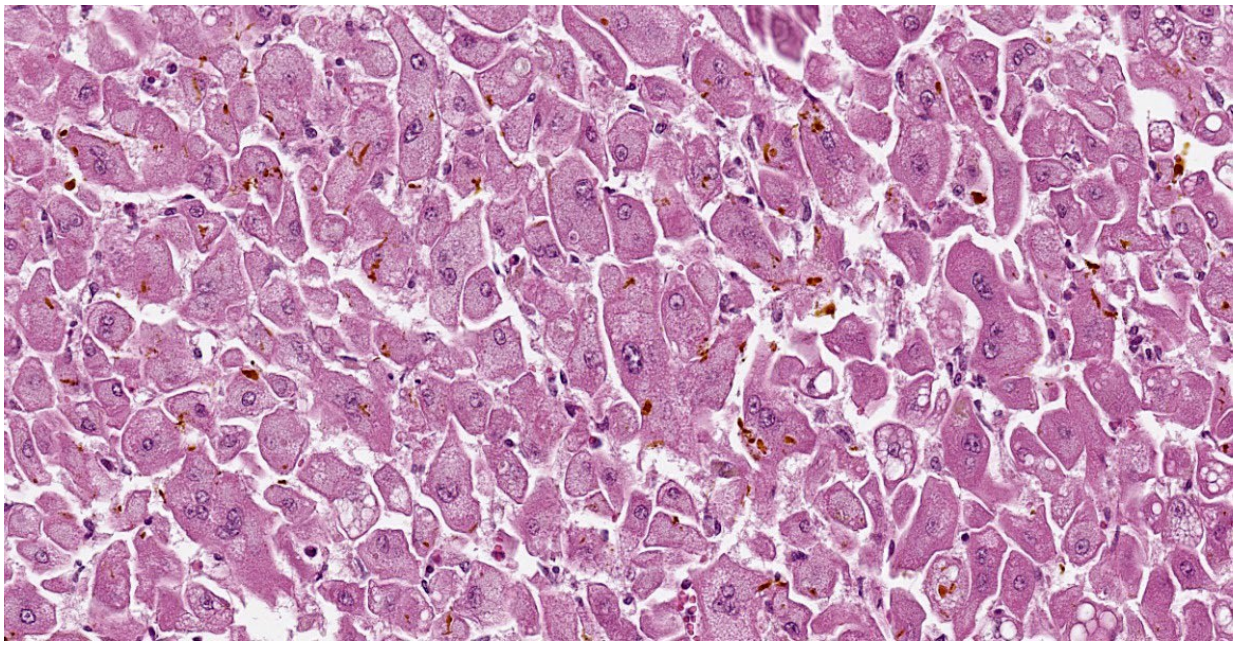

Figure 2-2. Liver, ox. Hepatocytes are diffusely swollen, vacuolated, individualized, and there is loss of normal sinusoidal architecture. There is canalicular cholestasis. (HE, 300X)

to moderate distension of bile canaliculi with bile, this is also present within the cytoplasm of hepatocytes. Multifocally, there is moderate biliary ductule hyperplasia. Multifocally, there is a mild, periportal population of lymphocytes and plasma cells with mild associated fibroplasia.

Contributor's Morphologic Diagnoses:
Liver: Hepatopathy with hepatocellular dissociation, cytoplasmic vacuolation and megalocyte formation; cholestasis and biliary hyperplasia.
Cholangiohepatitis, chronic, mild

Contributor's Comment:
These findings are consistent with lantana toxicity. Lantana (family Verbenaceae) is an ornamental shrub that grows to a height of 2-3 meters and has red, pink or white flowers. It is native to the tropical and subtropical areas of Central and South America and is considered a pest in many parts of the world. The family contains species such as *L. camara, L. indica, L. crenulata, L. trifolia, L. lilacina, L. involuerata* and *L. sellowiance* however *L. camara* is the most widespread and of greatest toxicity to livestock.[6] Its toxicity was first reported in Australia in 1910, this has subsequently been reported in many other countries. Livestock that are familiar with lantana rarely consume it voluntarily, toxicity mostly occurs in times of drought or when feed is otherwise scarce or in animals that have been brought in from lantana free areas.[6] Cattle are most commonly affected; it is rarely noted in sheep and goats as they are less likely to eat the plant.[7]

The significant toxins in lantana are triterpene acids, lantadene A (rehannic acid), lantadene B and their reduced forms; lantadene A appears to be the most toxic of these. The toxic dose depends on the toxin content of the species of lantana.[7] Clinical signs include jaundice, photosensitisation, inappetence and depression, ruminal stasis, constipation or diarrhoea with black, fluid faeces, dehydration and polyuria.[1,6,7] Cattle ingesting a large dose of the toxin can die within 2 days however most cases are more chronic with clinical signs being evident for 2 weeks before death.[7] The rumen can act as a toxin reservoir even after access to the lantana is prevented. Natural or experimental exposure to lantana results in increased bilirubin and globulins,

there can be either a decrease or an increase in PCV. Decreased albumin and increased gamma glutamyl transpeptidase, sorbital dehydrogenase and arginase levels have been variably noted.[1,6]

Gross findings include jaundice; an enlarged, pale and yellow/orange or green-grey liver and a gall bladder that is distended, sometimes with mucoid bile; enlarged, mottled, wet kidneys and blood-stained fluid in the abomasum and small intestine.[7] Histological findings include enlarged hepatocytes and fine hepatocellular cytoplasmic vacuolation which can be more evident in periportal areas and bile accumulation which is often more pronounced in periacinar zones. There is also often bile duct proliferation and, in some cases, periportal apoptosis or necrosis of hepatocytes.[7] The gall bladder can demonstrate mucoid metaplasia of the epithelium with hemorrhage, ulceration, inflammation and necrosis.[1] The kidneys often demonstrate mild to severe vacuolar change or necrosis of the tubular epithelium with extensive tubular cast formation.[1,7] There can also be ulceration of the abomasal mucosa.[1]

The toxin is thought to cause collapse, distension or microvilli damage in bile canaliculi. The mechanism of cholestasis is still unknown however damage to the contractile pericanalicular cytoskeleton or the cell adhesion molecules is possible.[7] The role of hyperbilirubinaemia in the nephropathy is unknown. Myocardial necrosis has been noted in sheep and may be responsible for death in animals that die early in the course of the disease.[7]

Contributing Institution:
Dr Mirrim Kelly-Bosma, School of Veterinary Science, University of Queensland, Gatton campus, Gatton, Queensland, Australia, 4343. (https://veterinary-science.uq.edu.au/)

JPC Diagnosis:
Liver: Hepatocellular dissociation, megalocytosis, multinucleation, rarefaction, lipidosis, diffuse, severe, with ductular reaction, and canalicular cholestasis.

JPC Comment:
This case illustrates a different pattern of hepatotoxicity compared to the centrilobular

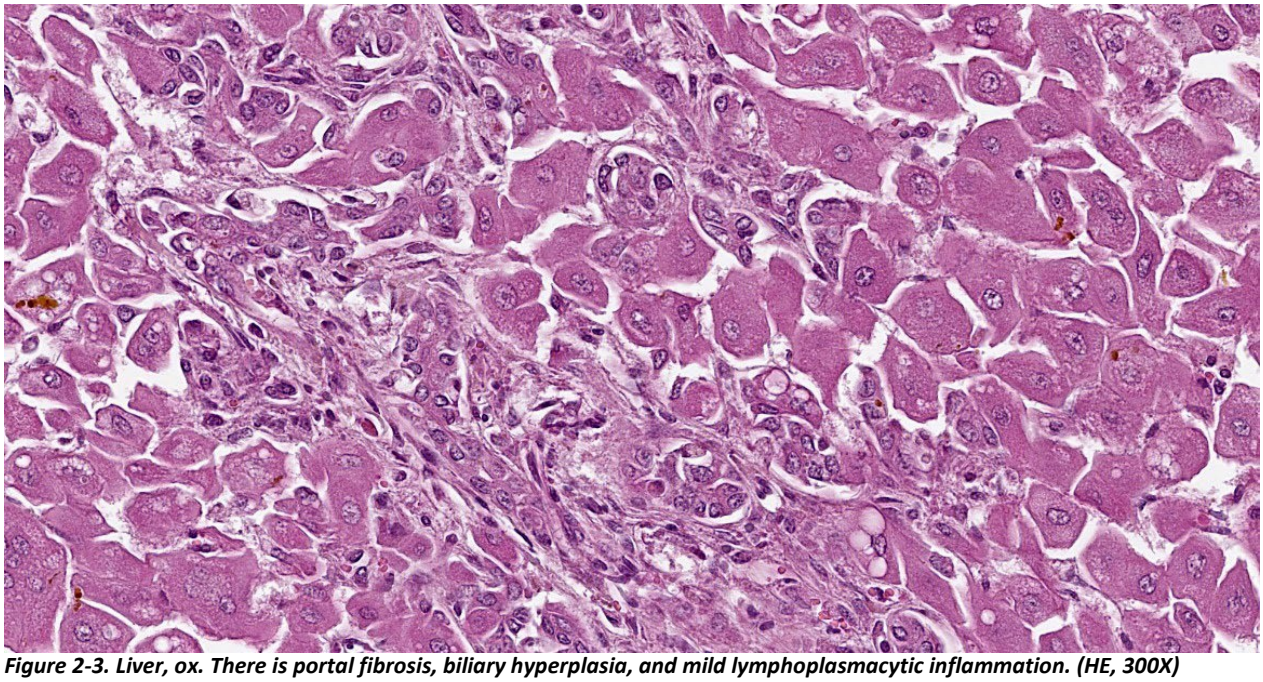

Figure 2-3. Liver, ox. There is portal fibrosis, biliary hyperplasia, and mild lymphoplasmacytic inflammation. (HE, 300X)

necrosis in Case 1 of this conference. In addition to the mechanisms of toxicity mentioned by the contributor, studies in rats have suggested that metabolites inhibit mitochondrial respiration and that reduced lantadene A may be more toxic than lantadene A.[4] The toxin targets the bile canalicular plasma membrane, causing impaired hepatobiliary excretion and intrahepatic cholestasis. The toxins inhibit neural impulses and ruminal stasis.[3,4] Hepatocellular megalocytosis is speculated to be due to enlargement of the rough endoplasmic reticulum.

Key histologic findings, as covered by the contributor, include hepatocellular megalocytosis with cytoplasmic vacuolization and canalicular cholestasis. Dr. Cullen also remarked on the pronounced individualization of hepatocytes, a phenomenon which is also seen in leptospiral infections.

Other hepatotoxins which cause megalocytosis are pyrrolizidine alkaloids and aflatoxin.[2] Repeated exposure to pyrrolizidine alkaloids causes megalocytosis with hepatic atrophy, while ingestion of large quantities causes acute centrilobular necrosis.[2] Similarly, prolonged exposure to low levels of aflatoxin can cause megalocytosis during with scattered necrosis.[2] Acute aflatoxin toxicosis in large animals has only been documented in experimental settings because there are insufficient quantities in moldy feed to induce acute injury.

Another key clinical and histologic feature for lantana toxicosis is cholestasis, and in herbivores, cholestasis can quickly lead to type III (hepatogenous) photosensitization due to the lack of biliary excretion of chlorophyll breakdown products (phylloerythrins) in the blood.[2] When deposited in the skin and exposed to UV light these pigments cause reactive oxygen species formation and tissue damage.[5] Hepatogenous photosensitization is usually caused by mycotoxins and hepatotoxic plants, including sporidesmin and lantana, although it has been associated with a wide range of plants, including normal forage crops like Bermuda grass.[5] Grossly, photosensitization manifests as erythema, edema, and necrosis in sparsely haired or unpigmented skin, and affected animals are pruritic. Histologically, there is edema of the dermis and coagulative necrosis and vesicles in the epidermis.[5]

References:

1. Black H and Carter RG. Lantana poisoning of cattle and sheep in New Zealand. *N Z Vet J*. 1985; 33: 136-137.
2. Cullen JM, Stalker MJ. Liver and Biliary System. In: Maxie MG. *Jubb, Kennedy, and Palmer's Pathology of Domestic Animals. Vol 2.* 6th ed. Elsevier: 2016; 329-339.
3. Kumar R, Sharma R, Patil RD, et a. Subchronic toxicopathological study of lantadenes of *Lantana camara* weed in guinea pigs. *BMC Veterinary Research*. 2018; 14(129):1-13.
4. Manthorpe EM, Jerret IV, Rawlin GT, Woolford L. Plant and Fungal Hepatotoxicities of Cattle in Australia, with a Focus on Minimally Understood Toxins. *Toxins*. 2020; 12(707):1-25.
5. Mauldin EA, Peters-Kennedy J. Integumentary System. In: Maxie MG. *Jubb, Kennedy, and Palmer's Pathology of Domestic Animals. Vol 1.* 6th ed. Elsevier: 2016; 577-580.
6. Sharma OP, Makkar HPS, Dawra RK, et al. A review of the toxicity of Lantana camara (Linn) in animals. *Clin Toxicol*. 1981; 18; 1077-1094.
7. Stalker MJ and Hayes MA. Liver and biliary system In: Maxie MG ed. *Pathology of Domestic Animals*. Fifth ed. Elsevier, 2007: 297-388.

CASE III:

Signalment:
The canine puppies are a mixture of German shepherd, Alaskan malamute, and Norwegian elkhound. It is unknown how large the litters were, but all puppies had clinically healthy littermates. The breeder also reports that a single puppy from a previous litter (also with the same parentage), died at four weeks old.

History:
Three female mixed-breed canine puppies from two sequential litters with the same parents, died at home at less than 5 weeks of age. All animals had a history of poor weight gain, and pale grey, waxy, odorless feces. Puppy #1 (from litter "A") was approximately 3 weeks old and weighed 555 g. Puppy #2 and #3 (both from litter "B") were both approximately 4 weeks old and weighed 1235 g and 2000 g, respectively.

Gross Pathology:
All puppies were in thin body condition, with reduced internal fat stores. The distal small intestine and colon contained thick, pale grey-tan digesta (interpreted as acholic). Puppies #2 and #3 were also noted to be mildly icteric. There was no evidence of extrahepatic portal shunt vessels, and the external anatomy of the livers was normal. In all puppies, at the location of the expected gall bladder and common bile duct, there was a firm tubular structure with no bile content on cut section. It was not recorded in the gross post mortem reports for puppy #1 or #2 whether the major duodenal papilla was present, but the opening of the major duodenal papilla was not grossly appreciable in puppy #3. Puppy #1 had dark black mucous over the rugal folds of the stomach, and similar dark tarry content in some areas of the small intestine and within the colon.

Laboratory Results:
No findings reported.

Microscopic Description:
There is abnormal liver architecture, with no appreciable portal triads, as no biliary epithelium was evident. Portal veins were irregularly spaced, and frequently accompanied by small, reduplicated arterioles, often oriented along the limiting plate and occasionally branching out within the hepatic parenchyma. Hepatocytes were arranged in disorganized cords up to three hepatocytes thick, and occasionally in a more sheet-like formation. Where present, sinusoids were often dilated or ectatic, and adjacent hepatocytes

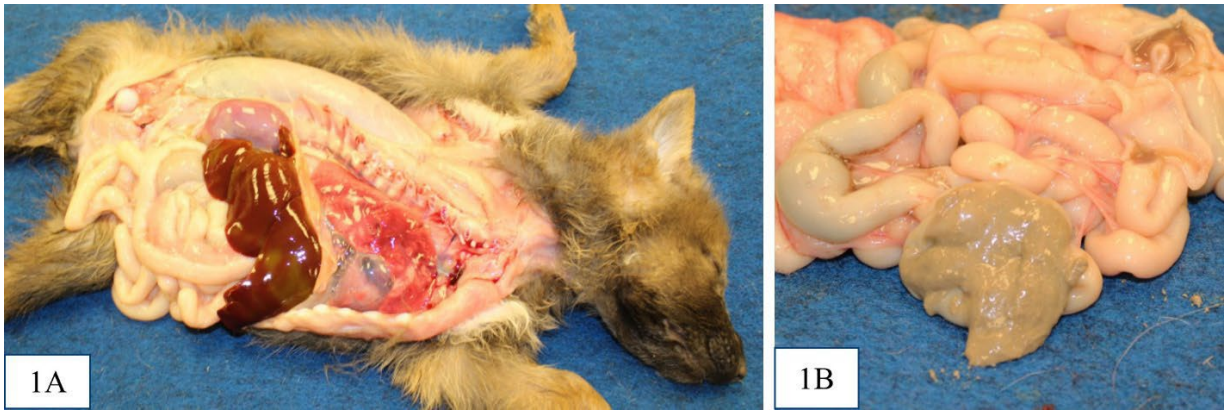

Figure 3-1. Presentation, dog. (From Puppy #3) A) On post mortem external assessment, all animals were in poor body condition. B) The distal small intestine and colon contained light grey-tan digesta (interpreted as acholic and confirmed using Hall's bile stain). (Photo courtesy of: Ontario Veterinary College, Department of Pathobiology, Guelph https://ovc.uoguelph.ca/pathobiology/)

were thin and atrophic. There were innumerable bile plugs in canaliculi throughout the parenchyma. Frequently, Kupffer cells and up to 30% of hepatocytes contained scant fine brown granular pigment.

Contributor's Morphologic Diagnoses:
Congenital atresia of the biliary tract and intrahepatic cholestasis.

Contributor's Comment:
The three puppies had absence of the gall bladder and intrahepatic bile ducts, with intrahepatic cholestasis. The lack of CK7 positive cells forming distinct tubules throughout the liver confirms the diagnosis of complete absence of intrahepatic bile ducts.

In broad categories, the absence of intrahepatic bile ducts and a gall bladder could be because they never formed or that they had partially or completely formed, and then were later lost. During organogenesis of the liver and biliary system, a part of the endoderm forms the hepatic diverticulum, which subdivides into a cranial portion (pars hepatica) and a caudal portion (pars cystica).[4] The gall bladder develops from the pars cystica, and the timing of this development and the precise pathways involved have not been well characterized.[15,23] In contrast, the common bile duct, intrahepatic biliary system, and hepatocytes differentiate from bipotential progenitor hepatoblast cells that differentiate in the pars hepatica– the hepatoblasts within the liver parenchyma become hepatocytes, and those at the interface between the parenchyma and the portal mesenchyme surrounding portal veins strongly express biliary-specific cytokeratins and become biliary epithelial cells that form a single layer referred to as the ductal plate.[3] In the development of intrahepatic bile ducts, just after day 16.5 of embryogenesis in mice when the ductal plate becomes partially bilayered, small focal dilations appear between the two cells layers, giving rise to bile ducts.[7] As the puppies in this case series lacked both a gall bladder and intrahepatic biliary structures, the deviation from normal organ development may have happened at the level of the diverticulum before the subdivision into the pars cystica and pars hepatica, or less likely, there may have been issues in both developmental pathways after the division.

There are a variety of conditions characterized by intrahepatic biliary maldevelopment in humans, which in the literature is referred to as paucity of interlobular bile ducts, intrahepatic biliary hypoplasia or aplasia, intrahepatic biliary atresia, ductular paucity, ductopenia, and ductular hypoplasia.[1,9] Complete congenital absence of the intrahepatic bile ducts has been reported in ten children, many of whom died in early childhood. Unlike these puppies, none of the human cases were reported to have an abnormal extrahepatic biliary system except for one child that had fibrotic cystic and common bile ducts (not observed in any of the canine cases).[12]

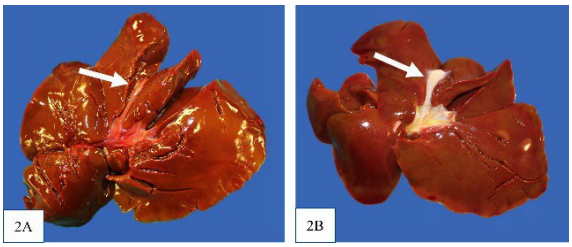

Figure 3-2. Liver, dog. All puppies had livers with unremarkable gross architecture, and no evidence of extrahepatic shunts. All three puppies also had very small, thin tubular structures in the location of the gall bladders (indicated by the arrow) that lacked bile content. A) Liver from Puppy #2. B) Liver from Puppy #3. (Photo courtesy of: Ontario Veterinary College, Department of Pathobiology, Guelph https://ovc.uoguelph.ca/pathobiology/)

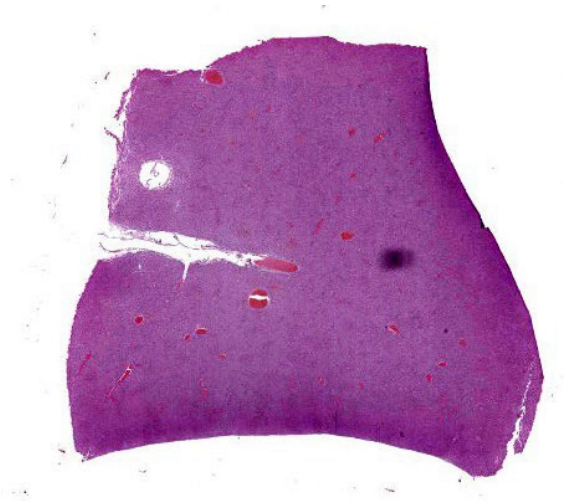

Figure 3-3. Liver, dog. A single section of liver is submitted for examination. (HE, 8X)

Extrahepatic biliary atresia has also been reported in humans, and also rarely in domestic species including dogs, lambs, cats, monkeys, calves and horses.[8,13,14,18,20,22,25] The pathogenesis suggested in all species involves progressive fibrosis resulting in disconnection of the common bile duct from the intrahepatic biliary tree, occurring anywhere from the duodenum to the porta hepatis.[14,16] Extrahepatic biliary atresia in some affected animals was considered naturally occurring, and in others, occurred following toxin exposure (e.g. experimentally induced with fetal trypan blue exposure in piglets, plant toxins in sheep and calves).[14,19] In the two reported cases in young dogs, a distended gall bladder was appreciated, with bile duct obstruction. Cholecystoduodenostomy was performed to surgically circumvent the obstruction in both cases, reportedly with a good short-term clinical outcome in one case.[25] In the other case, involving a border collie puppy, the dog died 6 weeks after the cholecystoduodenostomy was performed due to biliary and hepatic toxocariasis, and histology of the common bile duct at the site of the atresia demonstrated replaced of the bile duct by solid fibrous tissue.[22] Based on the literature, the extrahepatic biliary atresia previously reported in dogs is different from the puppies described in this case series, as there was no evidence of normal gall bladder or common bile duct structures. Additionally, extrahepatic biliary atresia in all species and humans eventually leads to increased connective tissue within portal areas and surrounding proliferating biliary ductules – as we had no intrahepatic biliary structures or increased connective tissue in our cases, the condition affecting these puppies is distinctly different.[2]

Congenital absence of a gall bladder has also been reported in dogs, most often affecting small breed dogs, including Chihuahuas (10 of 17 reported cases), toy poodles (3 of 17 reported cases) and Jack Russell terriers (1 of 17 reported cases), and most often accompanied by hypoplasia or absence of some hepatic lobes.[21] Histologically, all dogs with gall bladder agenesis had similar findings to extrahepatic biliary atresia, with biliary hyperplasia and portal fibrosis, which does not fit with our case series.[21]

Very little literature exists on gall bladder development, but there have been a few key pathways identified in intrahepatic biliary epithelium development which may be abnormal in these puppies. The most common cause of intrahepatic biliary maldevelopment in humans is Alagille syndrome, an autosomal dominant disorder with variable expressivity which is also characterized by at least three of the five main clinical manifestations, including chronic cholestasis, vertebral arch defects, pulmonary artery hypoplasia or stenosis, posterior embryotoxon, and a particular set of facial features.[10] This syndrome does not include absence of a gall bladder, and these puppies lack the other clinical manifestations of the syndrome, but knowledge of this human condition provides some insight into potential genes and signalling pathways that could be abnormal in this case series.[1]

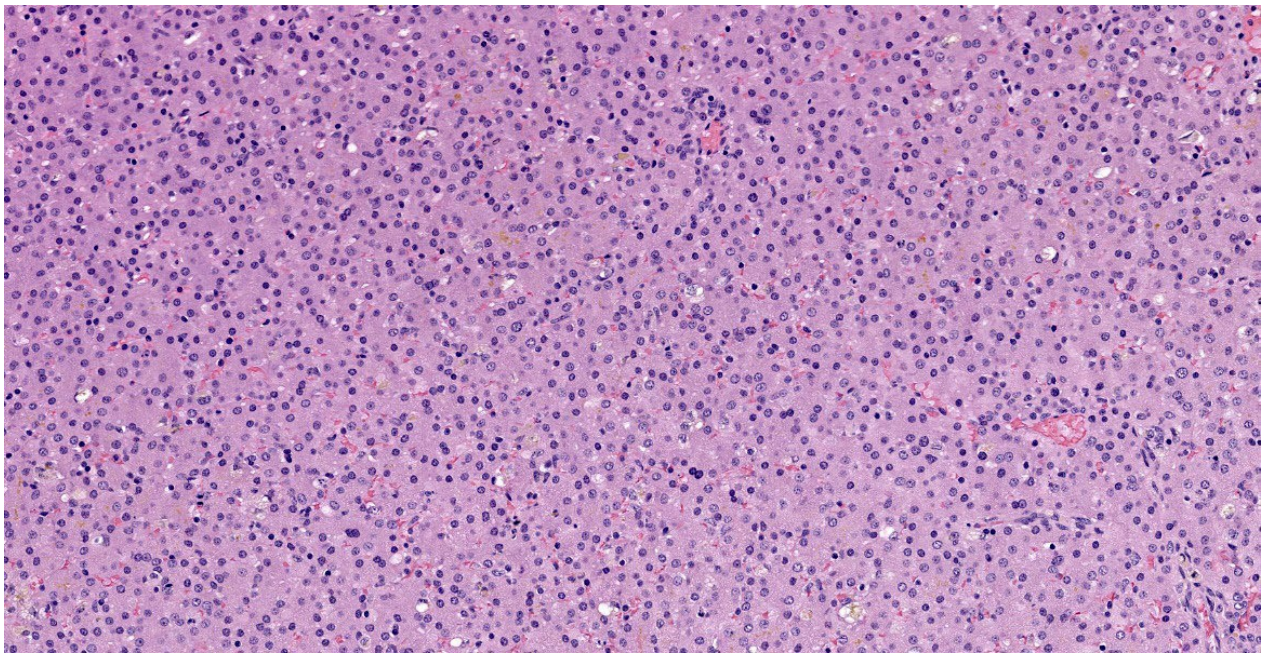

Figure 3-4. Liver, dog. There is diffuse loss of hepatic plate architecture with hepatocytes arranged in thick trabeculae or sheets, and portal areas are markedly reduced or absent. (HE, 8X)

Genetically, Alagille syndrome has been characterized by a duplication of exon 6 of the JAG1 gene on chromosome 20, which encodes a Notch1-signalling pathway with importance in embryogenesis.[26] Notch signalling has been demonstrated to be required for intrahepatic bile duct and ductal plate formation in mice, and loss of Notch signalling in mouse hepatoblast progenitor cells results in reduction of peripheral intrahepatic bile duct branches postnatally.[11,16,24,27] Research of Alagille syndrome has also led to the discovery of transcription factor protein hepatocyte nuclear factor (HNF)-6, which appears to regulate the number of cells that are stimulated to transition from a hepatoblast to a biliary epithelial cell.[7] It is suspected that the levels of this protein influence and are influenced by the hepatic mesenchyme, which also plays a vital role in the transition to biliary epithelium.[23]

Lastly, to explore the possibility that these puppies had biliary trees that had partially or completely formed, and then were later lost, drug-induced "vanishing bile duct syndrome" was briefly considered, which is a human condition that develops following toxin-induced damage to bile ducts.[9] Over thirty drugs are implicating this syndrome, which in its chronic form is clinically characterized by prolonged jaundice or chronic cholestasis for more than one year following administration of one of these drugs, and is histologically characterized by a bile to portal tract ratio of less than 0.5.[8,9] Although these dogs meet the defined criteria for "ductopenia" as described by the literature, these dogs have no known history of drug exposure, and the canine cases in this series lack portal tracts infiltrated by mononuclear cells (which is commonly seen in the human condition).[9] Lastly, again, this phenomenon has also not been reported in association with absence of a formed gall bladder.[9]

In summary, the present case report demonstrates the existence of a novel canine condition characterized by congenital absence of both intrahepatic bile ducts and the gall bladder and extrahepatic biliary tree. According to medical dictionaries, atresia is defined as "abnormal closing or absence of a tube in the body" whereas aplasia is defined as "lack of growth of tissue".[6] Using this nomenclature, arguably both "extrahepatic and intrahepatic biliary atresia" and "extrahepatic and intrahepatic biliary aplasia" could be appropriate when describing these puppies. However, considering that we were unable to unequivocally characterize the CK7 positive duct in the submucosa of the duodenum as being pancreatic or hepatopancreatic in origin, and leaving open the possibility that it may reflect a small portion of an intact common bile duct (which would imply that there is a regionally extensive absence of the extrahepatic biliary tree), "extrahepatic and intrahepatic biliary atresia" may be more appropriate in this case. As multiple litters with the same parentage were affected, we suspect an underlying genetic cause.

Contributing Institution:
Ontario Veterinary College, Department of Pathobiology, Guelph
https://ovc.uoguelph.ca/pathobiology/

JPC Diagnosis:
Liver: Biliary aplasia.

JPC Comment:
The contributor provides an excellent review of embryologic development of the liver and gallbladder as well as the existing literature on gall bladder agenesis and biliary atresia. Another novel presentation of gall bladder agenesis was recently reported by Mestrinho et al in a 1-year-old male French bulldog. In addition to gall bladder agenesis, the dog had an umbilicobiliary fistula that resulted in persistent yellow discharge from the umbilicus.[17] A duct-like structure connected the umbilicus to the common bile duct; histopathologic examination of the resected structure revealed similar features to a gall bladder or bile duct.[17] The authors speculated that the pars cystica of the hepatic diverticulum became trapped during invagination of umbilical cord structures and subsequently formed a cutaneous fistula.[17]

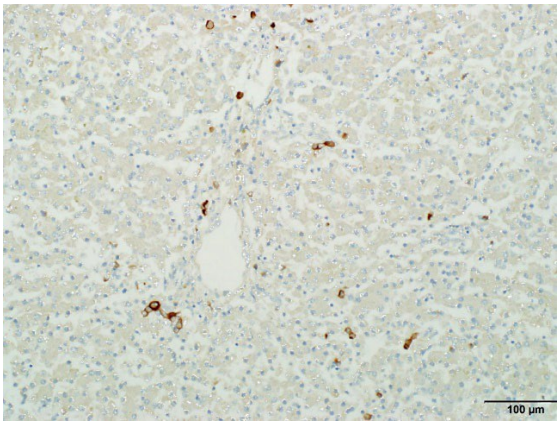

Figure 3-5. Liver, dog. In Puppy #3, immunohistochemistry for cytokeratin 7 (CK7) showed rare individual and paired cells along the limiting plate adjacent to portal veins, but no organized ductular structures. In the other two cases, there were no CK7 positive cells in the liver. (Photo courtesy of: Ontario Veterinary College, Department of Pathobiology, Guelph https://ovc.uoguelph.ca/pathobiology/)

Dr. Cullen and conference participants discussed the greater amount of bile but lesser degree of hepatocellular damage in this case compared to case 2 (lantana toxicity in a goat), in whic bile canaliculi are injured, and liberated bile salts caused damage to hepatocellular membranes. Participants elected to use "aplasia" as a morph due to the complete lack of biliary profiles; most other forms of biliary atresia which frequently feature small CK7 positive biliary profiles.

References:
1. Alagille D, Estrada A, Hadchouel M, Gautler M, Odievre M, Dommergues JP. Syndromic paucity of interlobular bile

ducts (Alagille syndrome or arteriohepatic dysplasia): review of 80 cases. *J Pediatr*. 1987;110(2):195-200.
2. Bassett MD, Murray KF. Biliary atresia: recent progress. *J Clin Gastroenterol*. 2008;42(6):720.
3. Bastianello SS, Nesbit JW. The pathology of a case of biliary atresia in a foal. *J S Afr Vet Assoc*. 1986;57(2):117-120.
4. Bedi N, Bond-smith G, Kumar S, Hutchins R. Gallbladder agenesis with choledochal cyst—a rare association: a case report and review of possible genetic or embryological links. *BMJ Case Rep*. 2013;2013:bcr2012006786.
5. Bouwens L. Cytokeratins and cell differentiation in the pancreas. *J Pathol A J Pathol Soc Gt Britain Irel*. 1998;184(3):234-239.
6. Collin PH, ed. *Dictionary of Medicine*. 2nd ed. New York: Routledge, Taylor & Francis Group; 2014.
7. Clotman F, Lannoy VJ, Reber M, et al. The onecut transcription factor HNF6 is required for normal development of the biliary tract. *Development*. 2002;129(8):1819-1828.
8. Degott C, Feldmann G, Larrey D, et al. Drug-induced prolonged cholestasis in adults: a histological semiquantitative study demonstrating progressive ductopenia. *Hepatology*. 1992;15(2):244-251.
9. Desmet VJ. Vanishing bile duct syndrome in drug-induced liver disease. *J Hepatol*. 1997;26:31-35.
10. Emerick KM, Rand EB, Goldmuntz E, Krantz ID, Spinner NB, Piccoli DA. Features of Alagille syndrome in 92 patients: frequency and relation to prognosis. *Hepatology*. 1999;29(3):822-829.
11. Geisler F, Nagl F, Mazur PK, et al. Liver-specific inactivation of Notch2, but not Notch1, compromises intrahepatic bile duct development in mice. *Hepatology*. 2008;48(2):607-616.
12. Haas L, Dobbs RH. Congenital absence of the intrahepatic bile ducts. *Arch Dis Child*. 1958;33(171):396.
13. Hampson E, Filippich LJ, Kelly WR, Evans K. Congenital biliary atresia in a cat: a case report. *J Small Anim Pract*. 1987;28(1):39-48.
14. Harper PAW, Plant JW, Ungers DB. Congenital biliary atresia and jaundice in lambs and calves. *Aust Vet J*. 1990;67(1):18-22.
15. Lemaigre F. Development of the biliary tract. *Mech Dev*. 2003;120(1):81.
16. Lozier J, McCright B, Gridley T. Notch signaling regulates bile duct morphogenesis in mice. *PLoS One*. 2008;3(3):e1851.
17. Mestrinho LA, Monteiro C, Sobral C, Travancinha J, Niza MM. A case of a congenital umbilicobiliary fistula associated with gallbladder agenesis in a dog. *Rev Bras Med Vet*. 2022; 44:1-5.
18. Rosenberg DP, Morecki R, Lollini LO, Glaser J, Cornelius CE. Extrahepatic biliary atresia in a rhesus monkey (Macaca mulatto). *Hepatology*. 1983;3(4):577-580.
19. Rosenkrantz JG, Lynch FP, Frost WW. Congenital anomalies in the pig: Teratogenic effects of trypan blue. *J Pediatr Surg*. 1970;5(2):232-237.
20. Ruíz-Ramírez JA, García-Márquez LJ, Bedolla-Alva MA, et al. Congenital biliary atresia in a Beefmaster calf. *Brazilian J Vet Pathol*. 2016;9(3):93-97.
21. Sato K, Sakai M, Hayakawa S, et al. Gallbladder Agenesis in 17 Dogs: 2006–2016. *J Vet Intern Med*. 2018;32(1):188-194.
22. Schulze C, Rothuizen J, Sluijs FJ van, Hazewinkel HAW, Van Den Ingh T. Extrahepatic biliary atresia in a border collie. *J Small Anim Pract.* 2000;41(1):27-30.
23. Shiojiri N. Development and differentiation of bile ducts in the mammalian liver. *Microsc Res Tech*. 1997;39(4):328-335.

24. Sparks EE, Perrien DS, Huppert KA, Peterson TE, Huppert SS. Defects in hepatic Notch signaling result in disruption of the communicating intrahepatic bile duct network in mice. *Dis Model Mech*. 2011;4(3):359-367.
25. Thiel C, Steinbach S, Schmidt M, et al. Extrahepatic biliary atresia in a 4-week-old pug. *Vet Surg*. 2015;44(1):35-40.
26. Uberos J, Moreno L, Muñoz-Hoyos A. Hypertension and Biliary Ductopenia in a patient with Duplication of exon 6 of the JAG1 Gene. *Clin Med Insights Pediatr*. 2012;6:CMPed-S9621.
27. Zong Y, Panikkar A, Xu J, et al. Notch signaling controls liver development by regulating biliary differentiation. *Development*. 2009;136(10):1727-1739.

CASE IV:

Signalment:
3-year-old, intact male, Syria Hamster, *Mesocricetus auratus*

History:
It was reported by the owner that the patient had been progressively ailing over a three-month period and that a small mass had been present on his right eye for at least 6 months. On October 14th, 2020, he was found to be cold, trembling, and weak for several hours, but aware of his surroundings. The slight trembling of his hind limbs continued to the next day. Later, the abdominal organs became progressively enlarged and visible through his skin. Four months later the patient became lethargic and began open mouth breathing. The left eye became proptosed and unable to be closed. Patient progressed to teeth grinding and lateral recumbency, with closed mouth, but labored breathing. Patient was euthanized shortly after.

Gross Pathology:
The left lateral, left medial, and right medial liver lobes are fully to partially effaced by soft, multilobular masses that measure 1cm x 3cm x 1.5cm to 2cm x2cm x1cm. The masses are black to red, soft, fluid filled.

Laboratory Results:
No findings reported.

Microscopic Description:
Liver: In multifocal areas the hepatic parenchyma is replaced by large cystic structures lined primarily by a single layer of cuboidal epithelial cells; occasionally there are up to three layers of cells. The lining cells occasionally form variably sized papillae that project into the lumen of the cysts. The lumen of the cystic structures contains an amphophilic, homogenous, vesiculated fluid substance. Portal regions frequently are infiltrated with mild to moderate numbers of lymphocytes and plasma cells. Most portal regions have mild to marked bile duct hyperplasia. In areas of severe bile duct hyperplasia, the surrounding hepatocellular parenchyma contains multifocal areas of hemorrhage with distortion of

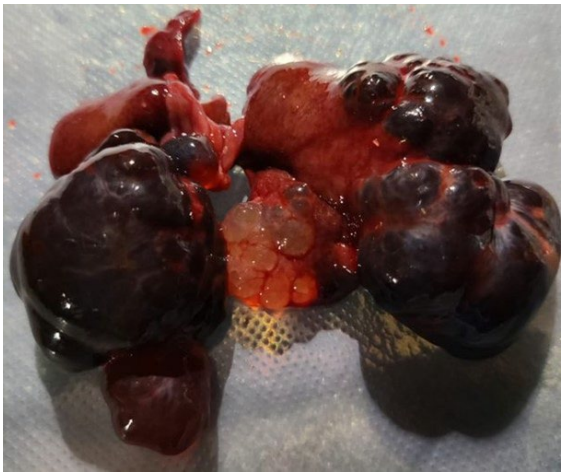

Figure 4-1. Liver, hamster. Tissue from a 3-year-old Syrian hamster. The liver is markedly enlarged and the majority of the hepatic parenchyma of all lobes has been replaced or expanded by fluid filled cysts. (Photo courtesy of: Tuskegee University, College of Veterinary Medicine, Department of Pathobiology, https://www.tuskegee.edu/programs-courses/colleges-schools/cvm)

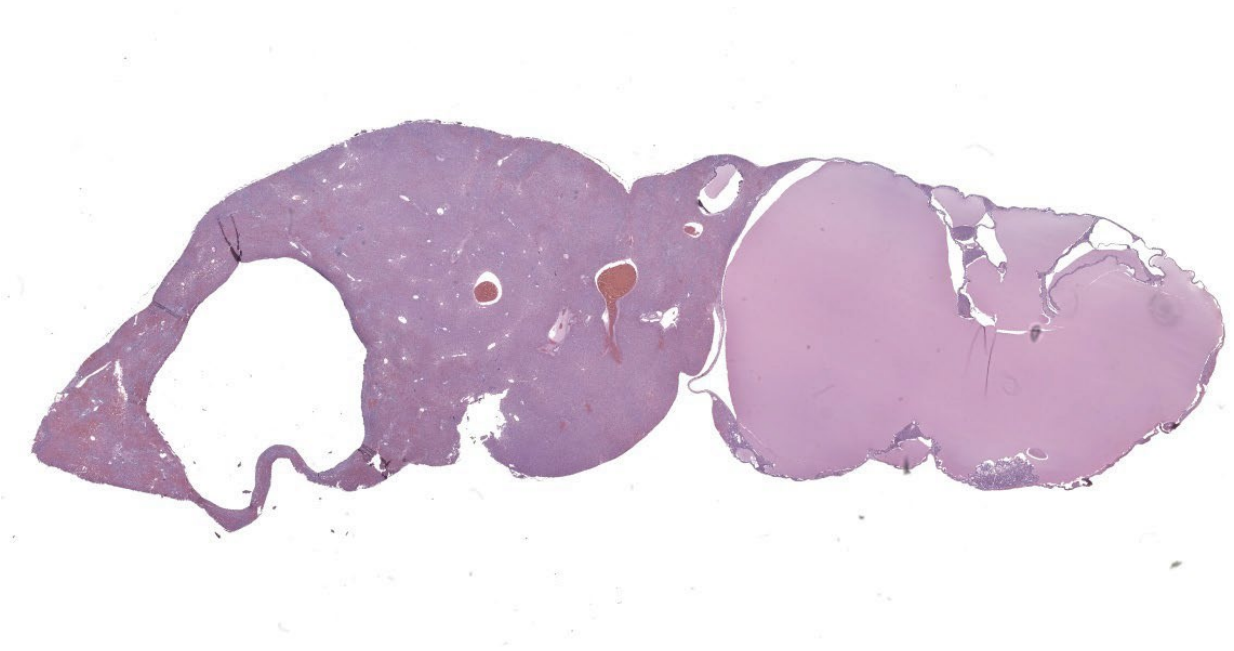

Figure 4-2. Liver, hamster. A single section of liver with multiple large, occasionally fluid filled cysts is submitted for examination. (HE, 6X)

hepatic cord architecture and individual hepatocyte necrosis.

Contributor's Morphologic Diagnoses:
Multifocal hepatic cysts (polycystic liver disease)

Multifocal moderate to marked bile duct hyperplasia and lymphoplasmacytic periportal hepatitis with multifocal hemorrhage and individual cell necrosis

Contributor's Comment:
This Syrian hamster had many of the common findings in aged hamsters including severe glomerulonephropathy, an atrial thrombus, and marked hepatic disease.[14] Although hepatic cysts are very common in older hamsters, they are thought to be the result of disconnected biliary structures present during hepatic development.[3] Ductal structures become disconnected from the biliary tree through loss or defects in genes signaling.[5] Affected animals remain asymptomatic until cyst growth initiates in adulthood.

Polycystic liver disease (PLD) is very well characterized in humans and is subdivided into three distinct entities.[3] The diseases are categorized by both the genetic mechanism and the gross and histological appearance of the lesions. The first is Von Meyenburg complexes (VMC) also called biliary hamartoma or hepatic cystic hamartoma.[9] These lesions have characteristic small, nonhereditary nodular cystic lesions which histologically appear as discrete fibrotic areas with small, irregular bile ducts. The second is isolated polycystic liver disease (autosomal dominant PLD) with presence of innumerable hepatic cysts and autosomal dominant heredity. The final category of PLD is polycystic kidney disease (PKD) where cysts are present in both the kidneys and liver.[19]

Polycystic liver disease in hamsters is characterized by multiple hepatic cysts that eventually lead to the replacement of normal liver parenchyma.[10,13] The etiology of PLD in hamsters has not been completely elucidated but much research has been done to understand PLD in isolation and PLD in association with polycystic kidney disease (PKD) in

humans. Non PKD associated PLD is the result of mutations in several genes including LRP5, PRKCSH, and SEC63 which are in charge of making the proteins sec-63 and hepatocystin.[16] These gene are also responsible for fluid transportation and epithelial cell growth. In polycystic liver disease associated with PKD, renal complications such as renal failure are more common.[16] PKD1 and PKD 2 are the genes are responsible for making polycystin 1 and polycystin 2 and mutation leads to dysregulation of fluid secretion and abnormal growth, ultimately leading to cyst formation.[4]

Hepatic cysts associated with PLD must be differentiated from cysts that might be seen in association with hepatic neoplasms in which cysts may develop such as cholangiocarcinoma or cystadenoma. Syrian hamsters, in general, have a low prevalence of spontaneous tumors of the liver.[8] Kondo et al examination of 15 Syrian hamsters found a single hepatic hemangioma.[8] The epithelial cell papillary projections, hepatic degeneration, necrosis, and leukocyte infiltration seen in this case is not typically seen in PLD but are common findings in neoplastic disease of the liver.[16] True cysts are usually multiple and lined by a single layer of epithelium, whereas tumors can be single or multiple, uni- or bilateral, and may have a complex arboriform pattern. The lack of cellular pleomorphism, stromal invasion, and mitotic figures suggest a non-malignant process. Cysts and cyst-like

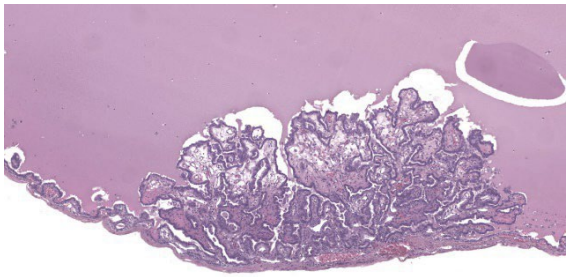

Figure 4-3. Liver, hamster. Epithelium lining the largest of the biliary cysts forms papillary and micropapillary structures into the lumen. (HE, 76X)

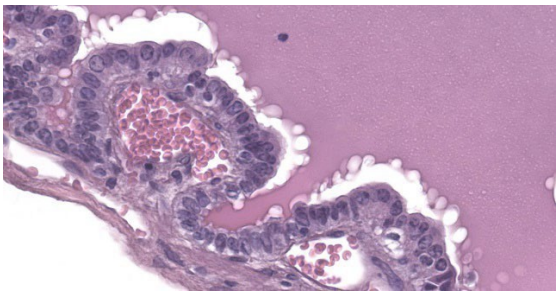

Figure 4-4. Liver, hamster. A single layer of columnar biliary epithelium lines the cysts. (HE, 7X)

structures that develop from parasites, abscesses, or hematomas must also be differentiated from PLD.[1,15]

Contributing Institution:
Tuskegee University, College of Veterinary Medicine, Department of Pathobiology, https://www.tuskegee.edu/programs-courses/colleges-schools/cvm

JPC Diagnosis:
Liver: Biliary cysts, multiple, with bridging ductular reaction and focal intraductal biliary papillary hyperplasia.

JPC Comment:
In hamsters, this relatively common incidental lesion observed in older animals may be accompanied by cysts in the epididymis, seminal vesicles, pancreas, and endometrium.[15] Infrequently, there may be clinically detectable hepatomegaly and ascites with straw colored fluid. The surrounding hepatic parenchyma typically shows pressure atrophy, necrosis, and congestion with possible hemorrhage.[18] Adjacent hepatocytes may demonstrate vacuolar change and there may be biliary ductular reaction within periportal regions.[18]

Conference participants discussed the presence of focal papillary projections into the cyst lumen, and considered the possibility that ductal plate anomalies may evolve into a neoplastic process (biliary cystadenoma), or a neoplasm may spontaneously occur in the

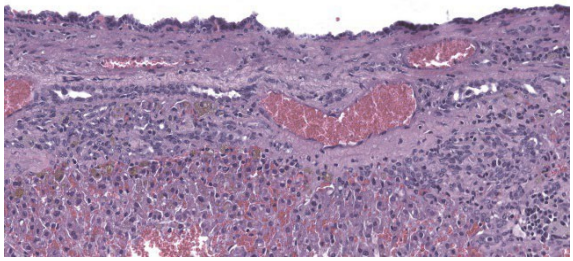

Figure 4-5. Liver, hamster. There is loss of subcapsular hepatocytes, mild biliary hyperplasia, and mild mesothelial hyperplasia. (HE, 267X)

same tissue. Dr. Cullen explained that because the genetic mechanism for polycystic liver disease has not been elucidated in this species, the specific pathogenesis creating papillary projections cannot be distinguished. Participants decided that the inflammation in the section is a secondary reactive hepatitis and elected not to include it in the morphologic diagnosis.

Polycystic liver has been documented in many species, including dogs, cats, pigs, mice, several deer species, chamois, llamas, alpacas, and various fish species.[6,7,12,18,20] Spontaneous polycystic liver has recently been documented in seven K14-LacZ transgenic mice; cysts were lined with cuboidal epithelium that was occasionally ciliated.[12] Affected males also had seminiferous tubular degeneration and a spermatogenesis, while two of the three females had ovarian cysts; affected mice appeared to be infertile.[12]

In veterinary medicine, cystic liver lesions may also be a component of adult or juvenile polycystic diseases.[2] Adult polycystic kidney disease, which has a higher prevalence in bull terriers and Persian cats, is a slowly progressive disease which may include cysts in other organs, such as the liver.[2] In humans, the disease is linked to autosomal dominant mutations in PKD1 and 2, and in dogs and cats, it has been linked to PKD1.[2,17] The mutation causes modification of the polycystin-1 protein in the primary cilia, which forms the centriole during mitosis, serves as a mechanoreceptor, and plays a role in fluid transport. Ciliary dysfunction appears to decrease fluid absorption during cyst development.[17] This disease may feature cysts in the liver and pancreas as well as hepatic fibrosis.[2] An autosomal recessive form of polycystic kidney disease in humans has been associated with a mutation causing dysfunction of fibrocystin, another component of the cilia.[2] This has been documented in West Highland white and Cairn terriers and some breeds of sheep and may also feature cysts in the liver.[2]

References:

1. Brown, Cynthia, and Thomas M. Donnelly. "Disease Problems of Small Rodents." *Ferrets, Rabbits, and Rodents.* 2012: 354–372.
2. Cianciolo RE, Mohr FC. Urinary System. In: Maxie MG. *Jubb, Kennedy, and Palmer's Pathology of Domestic Animals. Vol 2.* 6th ed. Elsevier: 2016; 395-396.
3. Cnossen, W.R., Drenth, J.P. Polycystic liver disease: an overview of pathogenesis, clinical manifestations and management. *Orphanet J Rare Dis.* 2014; 9, 69.
4. Cullen JM, Stalker MJ. Liver and Biliary System. In: Maxie MG. *Jubb, Kennedy, and Palmer's Pathology of Domestic Animals. Vol 2.* 6th ed. Elsevier: 2016; 265-266.
5. Drenth JP, Chrispijn M, Bergmann C: Congenital fibrocystic liver diseases. *Best Pract Res Clin Gastroenterol.* 2010; 24:573–584.
6. Foster A, Duff P, Boufana B, Acaster E, Schock A. Adult polycystic liver disease in alpacas. *Vet Rec.* 2013; 172(25):666-667.
7. Glaswischnig W, Bago Z. Polycystic Liver Disease in Senile Chamois. *J Wildl Disease.* 2010; 46(2):669-672.

8. Kondo H, Onuma M, Shibuya H, Sato T. Spontaneous Tumors in Domestic Hamsters. *Veterinary Pathology*. 2008; 45(5):674-680.
9. Lev-Toaff AS, Bach AM, Wechsler RJ, Hilpert PM, GatalicaZ, RubinR: The radiologic and pathologic spectrum of biliary hamartomas. *American Journal of Roentgenology.* 1995; 165(2): 309-313
10. Lewis J. Pathology of Fibropolycystic Liver Diseases. *Clinical Liver Disease*. 2021; 238-243
11. Longergan GJ, Rice RR, Suarez ES. Autosomal recessive polycystic kidney disease: radiologic-pathologic correlation. *Radiographics* 2000; 20:837-855.
12. Lovaglio J, Artwohl JE, Ward CJ, Diekwisch GH, Ito Y, Fortman JD. Case Study: Polycystic Livers in a Transgenic Mouse Line. *Comp Med.* 2014; 64(2):115-120.
13. Miao Jinxin, Chard Louisa S., Wang Zhimin, Wang Yaohe Syrian Hamster as an Animal Model for the Study on Infectious Diseases. *Frontiers in Immunology.* 2019; 10:2329--3224
14. Miedel, Emily L, Hankenson FC. "Biology and Diseases of Hamsters." *Laboratory Animal Medicine.* 2015: 209–245.
15. Percy DH, Barthold SW. *Pathology of Laboratory Rodents and Rabbits.* Iowa State University Press, 2016: 191–196.
16. Perugorria MJ, Masyuk TV, Marin JJ, et al. Polycystic liver diseases: Advanced insights into the molecular mechanisms. *Nat Rev Gastroenterol Hepatol.* 2014; 11:750-761.
17. Schirrer L, Marin-Garcia PJ, Llobat L. Feline Polycystic Kidney Disease: An Update. *Vet Sci*. 2021; 8(11): 269-279.
18. Somvanshi R, Iyer PKR, Biswas JC, Koul GL. Polycystic Liver Disease in Golden Hamsters. *J Comp Path.* 1987; 97:615-618.
19. Torres VE, Harris PC, Pirson Y: Autosomal dominant polycystic kidney disease. *Lancet*. 2007; 369:1287–1301.
20. Watanabe TTN, Chaigneau FRC, Adaska JM, Doncel-Diaz B, Uzal FA. Polycystic liver in two adult llamas. *J Vet Diagn Invest.* 2019; 31(2): 280-283.

WSC 2022-2023 Self-assessment
Conference 13

1. Which of the following histologic lesions are associated with poison peach toxicosis in ruminants?
    a. Massive hepatocellular necrosis
    b. Bridging portal fibrosis
    c. Marked biliary hyperplasia
    d. Crystal hepatopathy

2. *Trema micrantha* toxicosis in sheep may cause toxic changes in which of the following systems?
    a. Nervous
    b. Urinary
    c. Gastrointestinal
    d. Respiratory

3. The primary hepatic target of action of landatene is theorized to be: ?
    a. Sinusoidal lining cells
    b. Biliary epithelium
    c. Oval cells
    d. Hepatocytes

4. Which of the following does not arise from bipotential hepatoblasts?
    a. Gall bladder
    b. Common bile duct
    c. Intrahepatic biliary system
    d. Hepatocytes
5. Polycystic liver disease in hamsters may be associated with cystic disease in which of the following organs?
    a. Gallbladder
    b. Lung
    c. Kidney
    d. Brainstem

Please email your completed assessment for grading to Dr. Bruce Williams at bruce.h.williams12.civ@mail.mil. Passing score is 80%. This program (RACE program 33611) is approved by the AAVSB RACE to offer a total of 0.5 CE Credits, with a maximum of 12.5 CE Credits being available to any individual Veterinary Medical Professionals for the 2019-2020 Wednesday Slide Conference. This RACE approval is for the subject matter categories of: SCIENTIFIC using the delivery method of NONINTERACTIVE DISTANCE. This approval is valid in jurisdictions which recognize AAVSB RACE.

Joint Pathology Center
Veterinary Pathology Services

WEDNESDAY SLIDE CONFERENCE 2022-2023

Conference #14 **4 January 2023**

CASE I:

Signalment:
14 years old, female-neutered, domestic shorthair cat, feline, *Felis catus*

History:
The owner noted a 3 x 4 x 3 cm subcutaneous mass on the left ventral aspect of the mandible and cranial aspect of the neck. On clinical examination, an enlarged mandibular lymph node was diagnosed. The other palpable lymph nodes were normal in size and no other symptoms or lesions were detectable. Laboratory parameters were unremarkable. Serologic tests for FeLV and FIV were negative. The owner opted for surgical removement, and histopathologic examination was initiated.

The postoperative interval was initially unremarkable; there was no evidence of metastasis or recurrence. Three months after surgery, the animal developed deteriorated general condition, inappetence, and vomiting. Multiple cranial lymph nodes were moderately swollen. Radiologically, an intrathoracic mass associated with the trachea was detected, and both kidneys were enlarged. Progression of malignancy was feared. Brief palliative therapy with prednisolone and antibiotics for several days was given. Due to the deteriorating condition, the owner opted for euthanasia. At postmortem examination, multiple lymph nodes on the head and neck were similarly enlarged. A firm white mass 1 x 2 x 1 cm in diameter was noted on the intrathoracic aspect of the trachea. Both kidneys were enlarged and soft, and the cortex was diffusely pale white in color with some hemorrhages.

Histopathologically and immunohistochemically, the enlarged lymph nodes showed the same neoplastic cell population as in the initially removed lymph node, and both kidneys and the tracheal mass showed the same neoplastic infiltration.

Gross Pathology:
A 4.5 x 3.5 x 2 cm firm lymph node was processed, and the cut surfaces were homogeneously yellow-white in color.

Laboratory Results:
See table 1.1

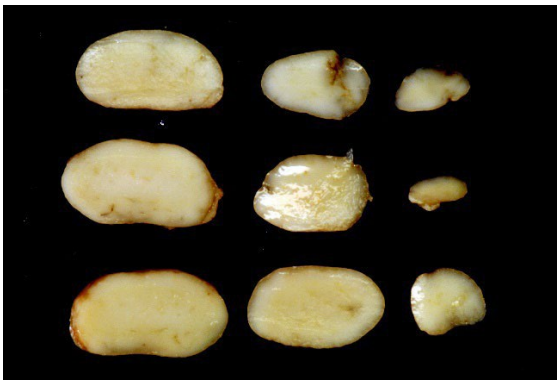

Figure 1-1. Lymph node, cat. The mandibular lymph node is large and there is diffuse loss of nodal architecture. (Photo courtesy of: Institut fuer Veterinaer-Pathologie, Justus-Liebig-Universitaet Giessen, Frankfurter Str. 96, 35392 Giessen, Germany http://www.uni-giessen.de/cms/fbz/fb10/institute_klinikum/institute/pathologie).

Marker	Normal cell type	T7562/21: multinucleated cells (H-RS cells)	T7562/21: monomorphic lymphatic cells (bystander cells)	Other findings
CD3 (polyclonal)	T cells	-	+++	Residual perifollicular cells/T cells ++
CD3 (monoclonal)	T cells	-	+++	Residual perifollicular cells/T cells ++
CD45R (B220)	Feline B cells	-	+	Residual cortical lymphoid follicles/B cells ++
CD20	B cells	-	-	No reactivity
Pax-5	B cells	-	-	Residual cortical lymphoid follicles/B cells ++
BLA.36	B cells	+++	+++	Residual cortical lymphoid follicles/B cells ++
IBA-1	Macrophages, monocytes, histiocytes	-	-	Single dendritic cells +
CD30	H-RS cells	+++	-	No reactivity
CD15	H-RS cells	-	-	No reactivity
Ki-67	Proliferating cells	+	++	30-50 positive nuclei/HPF (0.237 mm^2)

Table 1.1

- negative; + few positive cells; ++ more positive cells; +++abundant positive cells; H-RS cells: Hodgkin and Reed-Sternberg cells.

Microscopic Description:
Lymph node: A densely cellular, poorly demarcated, infiltrative, unencapsulated neoplasm composed of moderate numbers of neoplastic cells on a lymphocytic background and a preexisting fibrovascular stroma effaces the lymph node architecture and compresses the remaining follicles. The neoplastic cells are irregularly polygonal and up to 120 micrometer in diameter with distinct cell borders and abundant eosinophilic cytoplasm. The nuclei define two subtypes of neoplastic cells: Hodgkin cells are mononuclear with a single round to oval nucleus. Reed-Sternberg cells have at least two nuclear lobes or nuclei, but can have up to 5 irregular oval to polygonal (multilobulated) nuclei. The chromatin of both cell types is coarsely stippled to clumped, and the nucleoli are variably visible but often multiple. Rarely, the nucleoli are amphophilic and surrounded by a halo. Multifocally, single neoplastic cells have condensed cytoplasm and pyknotic nuclei ("mummified" Hodgkin cells). There is marked anisocytosis and anisokaryosis, and the mitotic count averages 5 mitoses in 10 high-power fields (2.37 mm^2). Often the mitoses are bizarre.

Contributor's Morphologic Diagnoses:
Mandibular lymph node: Hodgkin-like malignant lymphoma, cat, *Felis catus*

Contributor's Comment:
Lymphomas account for approximately 80% of all hematopoietic neoplasms in domestic animals, and both categorization and classification have been revised and changed several times in the past. Oncologists use different treatment strategies, and follow-up data are often limited.[8,9,10] In addition, diagnoses may vary between pathologists and/or hematopathologists. A still very useful first classification tool is tumor topography. In cats, more than 50% are alimentary forms, whereas in dogs multicentric forms predominate.[11]

The epidemiology of feline lymphomas has changed dramatically in the past due to the successful vaccination campaign against

FeLV.[9,10] Previously, approximately 30% of feline neoplasms were malignant lymphomas and 80% of these were associated with FeLV infection.

In animals, most lymphomas resemble human non-Hodgkin lymphomas, but in some species Hodgkin or Hodgkin-like lymphomas have also been described: for example, a well-characterized case in a ferret.[5]

In 1832, Thomas Hodgkin described a series of seven cases of lymph nodes with unusual changes, now known as Hodgkin lymphoma. In humans, the disease shows a bimodal age distribution with peaks in young adults and the elderly in developed countries. In developing countries, the first peak affects children. Often the disease is localized, with only a few cases being widespread. Overall, this type of lymphoma is considered moderately aggressive but curable in most cases. The typical neoplastic cells are CD30+, usually CD15+, negative for most B-cell markers, typically negative for T-cell markers, negative for immunoglobulin, negative for CD45, and negative for anaplastic lymphoma kinase (ALK). Pax5 is usually expressed by the neoplastic cells.[3]

In veterinary medicine, Hodgkin-like lymphoma appears to be a predominately feline entity manifestating in the upper respiratory and alimentary tract.[7,12] One report described an unusual manifestation of Hodgkin-like

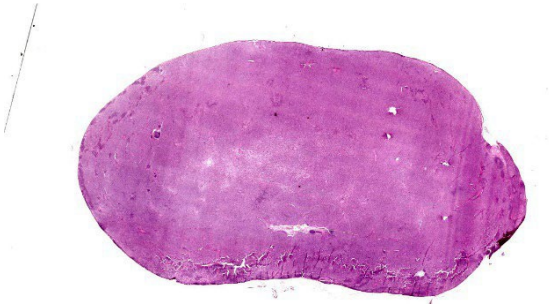

Figure 1-2. Lymph node, cat. There is diffuse loss of nodal architecture. (HE, 7X)

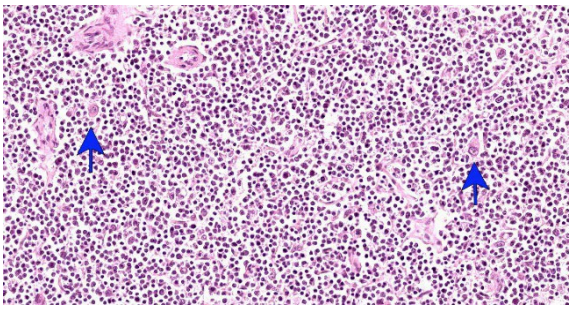

Figure 1-3. Lymph node, cat. Large neoplastic lymphocytes with prominent nucleoli are scattered throughout the section (arrows). (HE, 314X)

lymphoma in the cerebellum of a FeLV-infected cat.[13] Cytologically and histopathologically, the presence of scattered large mononucleated and binucleated to multinucleated cells (Hodgkin and Reed-Sternberg cells, HRS cells) should favor the diagnosis of Hodgkin-like lymphoma. However, immunohistochemistry is required for definitive diagnosis. Many cases appear to be misinterpreted as T-cell-rich B-cell lymphomas.[9,10]

There are some reports of problems with immunohistochemical staining of B cells in cats.[10] CD79-alpha staining, which is well reproducible in dogs, often showed variable results in our laboratory in cats (as did occasionally staining with CD20). Therefore, in the last two decades, the B-cell-specific variant of CD45R (B220) has been preferred by us, as well as by some other laboratories, for B cells in cats. Parallel staining with Pax5 showed reproducible results.[2]

Our case of feline Hodgkin-like lymphoma was well documented clinically, and follow-up examinations including necropsy was performed. Immunohistochemical results (see Table) supported our morphologic diagnosis. The malignant potential in this presented case was obvious.

Contributing Institution:
Institut fuer Veterinaer-Pathologie, Justus-Liebig-Universitaet Giessen
Frankfurter Str. 96, 35392 Giessen, Germany

http://www.uni-giessen.de/cms/fbz/fb10/institute_klinikum/institute/pathologie

JPC Diagnosis:
Lymph node: Lymphoma, large cell, with Hodgkin-like features.

JPC Comment:
Hodgkin lymphoma typically presents as a single enlarged node, or enlargement of multiple contiguous nodes. In humans, these nodes are typically cervical, mediastinal, or para-aortic, and in cats, they are typically mandibular, cervical, or mediastinal.[5,7,12] The neoplasm is thought to arise from germinal or post-germinal center B cells. In humans, neoplastic cells commonly contain increased NF- κB activity, either due to infection by Epstein Barr virus (human herpesvirus 4) or decreased activity of NF-κB suppressors such as IκB.[5] Neoplastic cells produce various cytokines and chemokines which cause influx of a mixed population of leukocytes (lymphocytes, granulocytes, and macrophages); thus neoplastic cells, which are typically giant with abnormal nuclei, account for less than 5% of the cell population within the tumor.[5,12]

The classic neoplastic cell in Hodgkin lymphoma is the Reed-Sternberg cell, as the contributor describes. These cells are up to 45 um in diameter and contain bi-lobed nuclei with large nucleoli up to 7 um in diameter, giving the cell an "owl eye" appearance.[5,12] Mononuclear, multi-nucleated, and lacunar variants of Reed-Sternberg cells also occur. In lacunar variants, the nuclei are folded and surrounded by cytoplasmic clearing due to processing artifact. Reed-Sternberg cells are the predominant neoplastic cell type in classic Hodgkin lymphomas, which can be divided into at four subtypes: nodular sclerosis, mixed cellularity, lymphocyte-rich, and lymphocyte-depletion.[5] These subtypes have similar IHC staining characteristics, but distinct histologic and clinical features.[5]

Another neoplastic cell type, the lymphohistiocytic variant (L&H cell), is seen in a distinct subtype, the nodular lymphocyte-predominance Hodgkin lymphoma. These cells are also known as "popcorn" cells because of

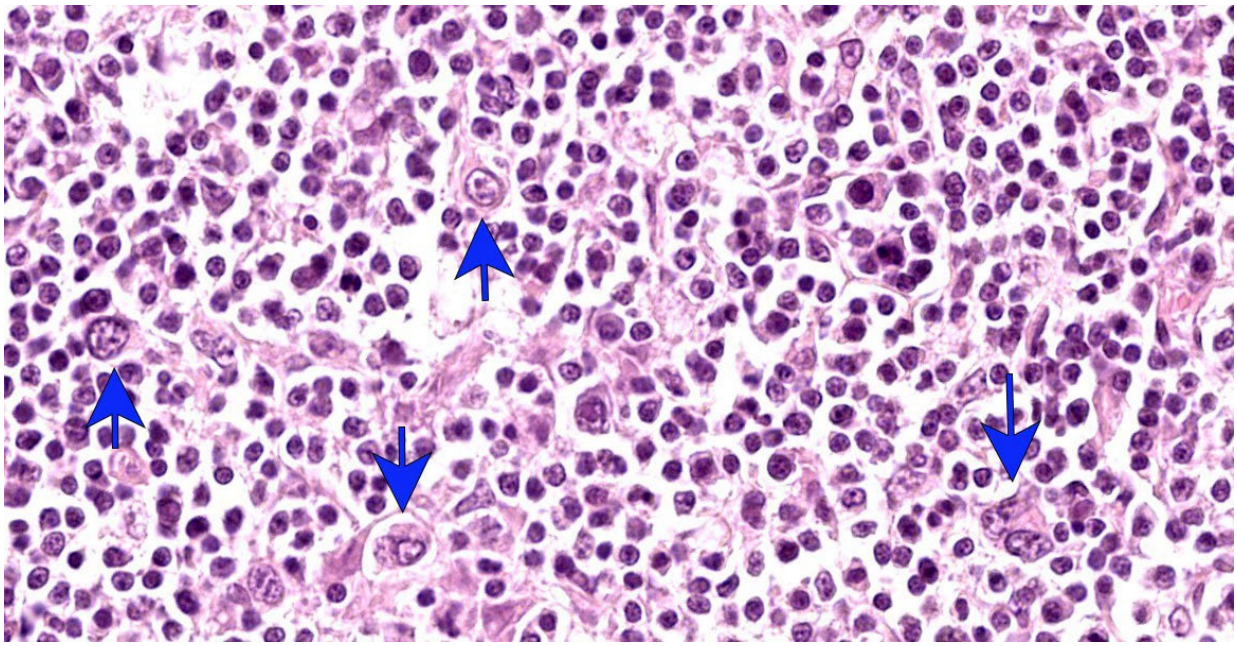

Figure 1-4. Lymph node, cat. Higher magnification of neoplastic cells with large pleomorphic nuclei. (arrows). (HE,750X)

their unique appearance: vesicular, polypoid nuclei with fine chromatin and indistinct nucleoli bear some resemblance to popped popcorn. L&H cells have distinct IHC staining pattern and are generally negative for both CD15 and CD30 and positive for CD20, CD45, and CD79.[5,7]

A report of 20 cases of Hodgkin-like lymphoma in cats provides some insight into this neoplasm, which is uncommon in cats and rare in other veterinary species.[12,14] Unilateral mandibular or cervical lymph node swelling was observed in 18 of 20 cats.[12] Eleven of the cats had classic forms, with nine classified as mixed cellularity and two classified as the nodular sclerosis substype.[12] Nine cats had the lymphocyte-predmoninant Hodgkin lymphoma, with L&H cells predominately surrounded by non-neoplastic small lymphocytes.[12] This study suggested that, as in humans, Hodgkin-like lymphoma is less aggressive than non-Hodgkin lymphoma in cats; however, additional data is needed for statistically significant correlation.[12]

Cases for this week's conference were selected to highlight human-animal correlates in medicine. This week's moderator, Dr. Sarah Cudd, discussed the clinical, pathologic, and historical aspects of the disease in humans. Human MD pathologists at the Joint Pathology center were also consulted on this case, and they favored a diagnosis of malignant B cell lymphoma with Hodgkin-like features, though T-cell/histiocyte-rich large B cell lymphoma could not be ruled out.

References:

1. Carminato A, Tecilla M, Roccabianca P, Zanardello C, Melchiotti E, Capello K, Vascellari M. CD30 Cross-Reactivity and Expression in Feline Normal Tissues and Lymphomas. *Vet Pathol*. 2020; 57: 49-55.
2. Felisberto R, Matos J, Alves M, Cabeçadas J, Henriques J. Evaluation of Pax5 expression and comparison with BLA.36 and CD79αcy in feline non-Hodgkin lymphoma. *Vet Comp Oncol*. 2017;15:1257-1268.
3. Ferry JA. Thomas Hodgkin and Hodgkin lymphoma. *J Hematopathol*. 2014;**7**:123-138.
4. Hodgkin T. On some morbid appearances of the absorbent gland and spleen. *Med Chir Trans*. 1832;17:69–97.
5. Kumar V, Abbas AK, Aster JC, Turner JR. *Robbins and Cotran Pathologic Basis of Disease*. 10th ed. Philadephia, PA: Elsevier: 2021: 611-616.
6. Matsumoto I, Uchida K, Chambers JK, Nibe K, Sato Y, Hamasu T, Nakayama H. Hodgkin's-like lymphoma in a ferret (*Mustela putorius furo*). *J Vet Med Sci*. 2017;79:1660-1663.
7. Steinberg JD, Keating JH. What is your diagnosis? Cervical mass in a cat. *Vet Clin Pathol*. 2008;37:323-327.
8. Valli VE, Jacobs RM, Parodi AL, Vernau W, Moore PF. Histological classification of tumors of hematopoietic tumors of domestic animals. WHO, Washington, DC: Armed Forces Institute of Pathology; 2002, 2nd Series, vol. 8.
9. Valli VEO, Kiupel M, Bienzle D, Wood RD. Hematopoietic system. In: Maxie MG, ed. *Jubb, Kennedy, and Palmer's Pathology of Domestic Animals*. Vol 3. 6th ed. Philadelphia, PA: Elsevier; 2016:102-268.
10. Valli VE, Bienzle, D, Meuten, DJ: Tumors of the hemolymphatic system. In: Meuten DJ, ed. *Tumors in Domestic Animals*. 5th ed. Ames, IA: Wiley Blackwell; 2017: 203-321.
11. Vezzali E, Parodi AL, Marcato PS, Bettini G. Histopathologic classification of 171 cases of canine and feline non-Hodgkin lymphoma according to the WHO. *Vet Comp Oncol*. 2010; 8: 38-49.

12. Walton RM, Hendrick MJ. Feline Hodgkin's-like lymphoma: 20 cases (1992-1999). *Vet Pathol*. 2001; 38: 504-511.
13. Yoshino Y, Chambers JK, Nakamori T, Goto-Koshino Y, Nishigaki K, Tsujimoto H, Matsuki N, Nakayama H, Uchida K. Primary cerebellar lymphoma with Hodgkin lymphoma-like morphology in a cat. *J Vet Diagn Invest*. 2017; 29: 707-710.
14. Vail DM, Pinkerton M, Young KY. Hematopoietic Tumors. In: Vail DM, Thamm DH, Liptak J, eds. *Withrow and MacEwen's Small Animal Clinical Oncology*. 6th ed. Philadelphia, PA: Elsevier. 2019: 715-729.

CASE II:

Signalment:
Rabbit – Lionhead *Oryctolagus cuniculus*; Male neutered, 4.4 years old

History:
Two week history of progressive hyperkeratosis/skin crusting/alopecia. Skin scraping negative for mites. The rabbit clinically had severe otitis externa/media, bilateral corneal ulcers, dyspnea, hypothermia, early GI stasis, severe left sided dental disease, suspected tear duct obstruction, severe pododermatitis, severe urine scalding. Euthanized and submitted for postmortem evaluation.

Figure 2-1. Haired skin, rabbit. There is marked hyperkeratosis and crusting of the skin of the neck, face, and periocular areas. (Photo courtesy of: Dept. of Pathobiology, Ontario Veterinary College, University of Guelph, Guelph Ontario, Canada)

Figure 2-2. Haired skin, rabbit. There is marked hyperkeratosis and crusting of the skin of the perioral area. (Photo courtesy of: Dept. of Pathobiology, Ontario Veterinary College, University of Guelph, Guelph Ontario, Canada)

Gross Pathology:
Submitted is the body of a 2.1 kg, white, male neutered Lionhead rabbit. He is in good body condition with ample subcutaneous fat and symmetrical muscling. There is scaling of the skin over the majority of the body surface, most pronounced on the hocks, the dorsal antebrachia, the dorsal surface of the neck and base of the ears extending over the lateral neck on both sides and ventrally to the level of the sternum. Occasionally, there is hair loss associated with this scaling over the antebrachia and the dorsal and lateral neck. There is marked scaling of the skin around the mouth as well as surrounding the eyes with thick accumulations of dry, yellow to brown crusts in these areas. These areas are also alopecic. There is extensive fecal staining of the perianal area and hindlimbs with alopecia of the medial surface of both proximal hindlimbs. Both eyes have an

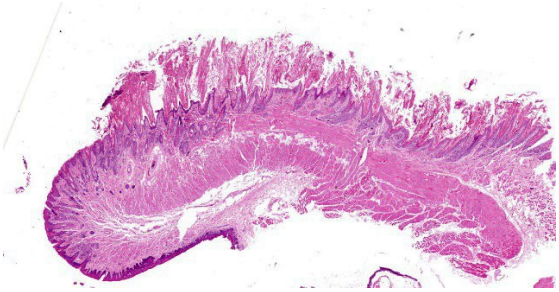

Figure 2-3. Haired skin, rabbit. A section of mucocutaneous junction is submitted for examination. There is a thick 2mm layer of scale over the epidermis. (HE, 10X)

approximately 2.0 mm white opacity centrally on the corneal surface.

There is approximately 2 mL of serosanguineous fluid within the thoracic cavity which contains rare soft, yellow to clear, irregular serous clots. The lungs appear diffusely, mildly atelectatic. The cranial mediastinum is expanded by a dark red to tan, irregular, soft mass measuring approximately 4 cm by 3 cm by 2 cm which displaces the heart caudally and the lungs caudodorsally. This mass is adherent to the ventral thoracic wall and the cranial surface of the pericardial sac. The mass is immediately adjacent to the aorta and cranial vena cava which run over the surface of the mass but are not incorporated into it. On cut section the mass is mottled dark red to tan with multiple cystic spaces containing approximately 1 mL of serosanguineous fluid. There is approximately 1 mL of serosanguineous fluid in the pericardial sac, but the inner surface is intact and there is no association between the mediastinal mass and the heart. The heart appears subjectively enlarged, occupying approximately one quarter of the thoracic cavity. There is subjective dilation of both ventricles but the left: right ventricular ratio is within normal limits. There is an enhanced zonal pattern in the liver which appears diffusely mottled yellow and red. This pattern continues throughout the parenchyma on cut section. The right renal pelvis contains a small amount of red material (rule out hemorrhage vs artifact). The bladder contains a moderate amount of slightly turbid yellow urine. It can be expressed with minimal digital pressure. There are sharp spurs on the lingual aspects of the mandibular cheek teeth and on the buccal aspects of the maxillary cheek teeth, slightly more severe on the left side. There is mild stenosis of the vertical canal of both ears due to thickening and scaling of the skin. There are plugs of white to tan soft exudate within both vertical canals. The tympanic bulla, middle ear, and inner ear appear grossly unremarkable. The nasal sinuses appear grossly unremarkable.

Laboratory Results:
No laboratory results reported.

Microscopic Description:
Individual spinous keratinocytes and basal cells are hypereosinophilic with pyknotic nuclei (cell death) and in some locations there are individual lymphocytes present within the epidermis adjacent to necrotic basal epithelial cells. The epidermis is variably acanthotic (up to 8 cells thick). There is marked, dense compact to basket weave orthokeratotic hyperkeratosis. Occasional nuclei are retained in the some of these keratin layers (parakeratosis). In some sections, there are occasional areas of erosion and thinning of the epidermis with rare areas of complete ulceration extending into the deeper dermis with exposure of the follicular epithelium. These ulcerated areas are covered by an up to 0.7 mm thick serocellular crust with degenerate neutrophils and keratin squames with admixed bacteria.

Lymphocytes are also present within the follicular epithelium (mural folliculitis) and follicles are decreased in size and number and are variably spaced (atrophy/loss). No sebaceous glands are visible in any section.

The superficial dermis has a band of lymphocytes with fewer plasma cells and there is edema of the superficial dermis.

PAS stain: There are rare intracorneal vesicles which contain a pale eosinophilic proteinaceous fluid. No fungal or parasitic organisms are seen in section.

Contributor's Morphologic Diagnoses:
Generalized transepidermal cytotoxic/interface dermatitis, with marked single cell death of epidermis and infundibulum of hair follicles, cell poor lymphocytic dermatitis and mural folliculitis, generalized follicular atrophy, absence of sebaceous glands and marked compact orthokeratotic hyperkeratosis.

Contributor's Comment:
Cytotoxic / interface dermatitis is one of the eight inflammatory reaction patterns in veterinary dermatopathology. It features death of keratinocytes in the epidermis. There are two main subtypes – basal cytotoxic / interface dermatitis (skin manifestation of systemic lupus erythematosus and cutaneous lupus erythematosus) and transepidermal cytoxic / interface dermatitis where all layers are potentially involved – the stratum basale, spinosum and or stratum granulosum. It is called cytotoxic because of death of keratinocytes and the interface terminology is when there is a band of lymphocytes and or plasma cells in the superficial dermis. The primary target of the cytotoxic / interface process is the keratinocyte. The various diseases and syndromes that have the panepidermal or transepidermal pattern of keratinocyte death are either ulcerative or hyperkeratotic. They are ulcerative when the cell death is rapid and severe, and hyperkeratotic (parakeratotic) when the number of dead cells is low.

Transepidermal cytotoxic / interface dermatitis in humans is seen in the syndromes and diseases Stevens-Johnson syndrome, erythema multiforme, and toxic epidermal necrolysis.[9]

In veterinary medicine, separation of different diseases and syndromes is based on clinical findings including extent of the lesions, location, and progression. Because the lesions are similar on histology, diagnosis of individual diseases should be done by clinicians (including dermatologists). Pathologists recognize the reaction pattern.

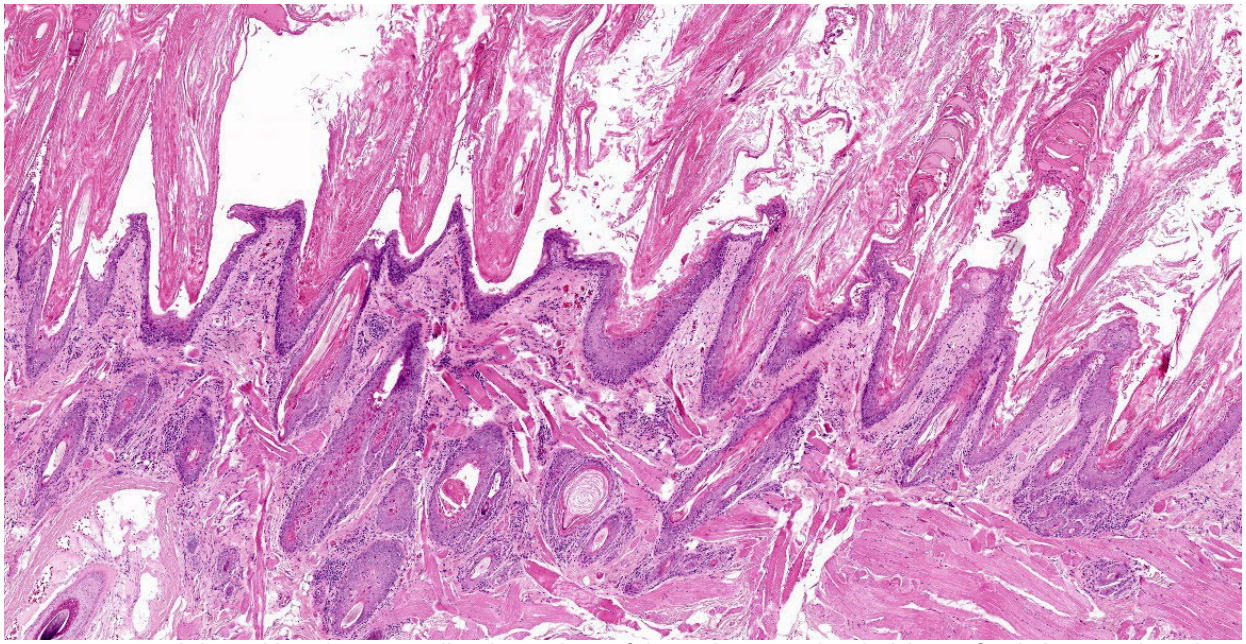

Figure 2-4. Haired skin, rabbit. There is papillary hyperplasia of the epidermis, with a thick layer of orthokeratotic hyperkeratosis. The proliferative and hyperkeratotic change extends into the follicular ostia. (HE, 40X)

This pattern of disease is considered immune-mediated. The trigger is not always identified. In animals, toxic epidermal necrolysis is more likely to be an adverse reaction to a drug; the death of cells is confluent.[9]

This rabbit has a clinically severe scaling or exfoliative dermatitis. The histologic pattern is a transepidermal cytotoxic pattern. The transepidermal pattern is well known in dogs where there are a variety of causes and disease syndromes.[9] This is rare in rabbits, who have a disease profile much like cats. In cats, the diseases are divided into thymoma-associated[7] and non-thymoma-associated exfoliative dermatitis.[4]

The mass in the cranial mediastinum of this rabbit was composed of a mixed population of neoplastic epithelial cells and normal small lymphocytes, thus it was a thymoma. In combination with the scaling dermatitis, the clinical presentation suggests paraneoplastic skin disease that is reported in thymoma in rabbits.[2,6] Overall, studies on exfoliative dermatitis in multiple species both as a paraneoplastic and idiopathic condition provided strong evidence that this is an immune mediated process. There is accumulating evidence that this condition is driven by autoreactive cytotoxic T-cells.

Contributing Institution:
Department of Pathobiology, Ontario Veterinary College, University of Guelph, Guelph Ontario, Canada

JPC Diagnosis:
Mucocutaneous junction, lip: Keratinocyte apoptosis, multifocal, moderate, with lymphocytic satellitosis and marked hyperkeratosis.

JPC Comment:
This is the second example of an integumentary paraneoplastic syndrome reviewed this conference year. Case 2 of conference 4 featured paraneoplastic alopecia in a cat due to a carcinoma in the liver, and the contributor and conference comments provide a general review of paraneoplastic skin lesions in veterinary species. In addition to exfoliative dermatitis, thymomas have also been associated with other paraneoplastic syndromes such as

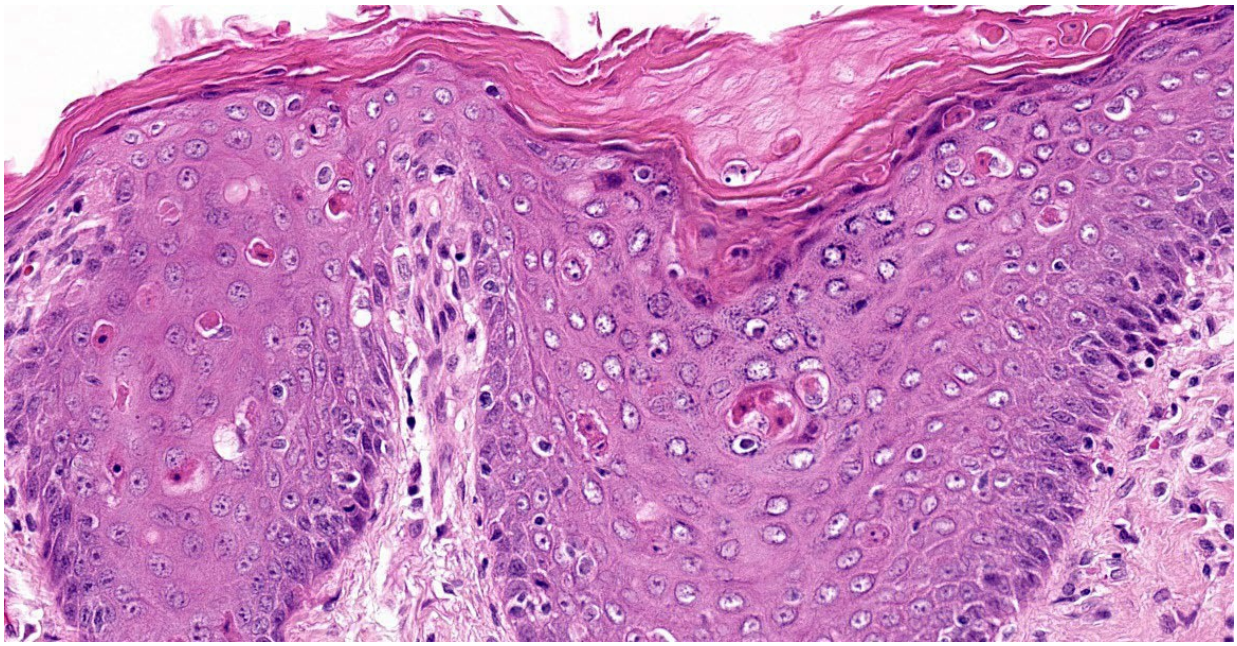

Figure 2-5. Haired skin, rabbit. There are numerous apoptotic keratinocytes within the hyperplastic epidermis. (HE, 381X)

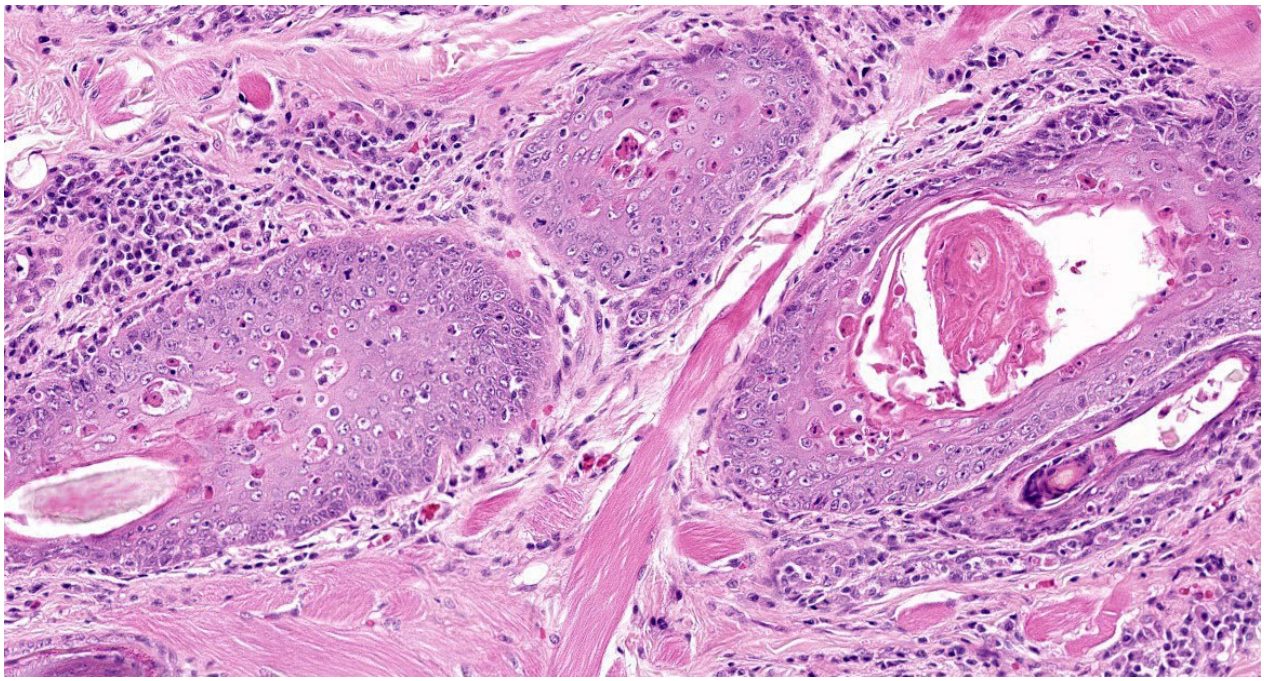

Figure 2-6. Haired skin, rabbit. Similar changes, including epidermal hyperplasia, hyperkeratosis, and keratinocyte apoptosis are present within follicles as well. (HE, 221X)

myasthenia gravis, polymyositis, and granulocytopenia.[1] Additionally, in dogs, thymomas may induce T-cell lymphocytosis, basophilia, or hypercalcemia of malignancy.[8] Exfoliative dermatitis has also recently been reported in a goat with a thymoma.[1]

Thymomas arise from the thymic epithelium and contain variable amounts of lymphocytes. A World Health Organization classification scheme places thymomas in two broad categories based on the histologic appearance of the epithelium. Type B thymomas, the most common type in dogs, have neoplastic cells which are epithelioid in appearance and are further subtyped based on the density of lymphocytes.[5] Type A thymomas have neoplastic cells which are spindloid in shape and accompanied by few lymphocytes.[5] In a study of domestic rabbits, out of 2,970 neoplasms, 48 were thymomas, and the most common subtype was type B1.[5]

In a separate study of thymomas in 13 rabbits, the average age at diagnosis was 6.1 years, and the most common clinical signs were dyspnea, exercise intolerance, and bilateral exophthalmos.[3] These signs were attributed to the mass's space occupying effect in the thorax, and exophthalmos is thought to arise from cranial vena cava syndrome due to decreased venous return to the heart. In some cases, the exophthalmos was transient or accompanied by third eyelid prolapse.[3]

Conference participants discussed two main differential diagnoses in this case: erythema multiforme and exfoliative dermatitis. Given the potentially identical histologic features of these two syndromes, participants could only confidently say exfoliative dermatitis once the clinical history was known. Participants also remarked on the lack of sebaceous glands, a common finding in thymoma-associated exfoliative dermatitis of cats.[7]

References:

1. Byas AD, Applegate TJ, Stuart A, Byers S, Frank CB. Thymoma-associated exfoliative dermatitis in a goat: case report and brief literature review. *J Vet Diagn Invest*. 2019; 31(6):905-908.

2. Florizoone K. Thymoma-associated exfoliative dermatitis in a rabbit. *Vet Dermatol*. 2005; 16: 281-284.
3. Kunzel F, Hittmair K, Hassan J, et al. Thymomas in Rabbits: Clinical Evaluation, Diagnosis, and Treatment. *J Am Anim Hosp Assoc.* 2012; 48(2): 97-104.
4. Linek M, Rüfenacht S, Brachelente C, von Tscharner C, Favrot C, Wilhelm S, Nett C, Mueller RS, Mayer U, Welle M. Nonthymoma-associated exfoliative dermatitis in 18 cats. *Vet Dermatol*. 2015; 26: 40-45.
5. Robson HR, Yanez RA, Magestro LM, French SJ, Kiupel M. Type A thymoma in a pet rabbit. *J Vet Diagn Ivest*. 2022; 34(2): 327-330.
6. Rostaher Prélaud A, Jassies-van der Lee A, Mueller RS, van Zeeland YR, Bettenay S, Majzoub M, Zenker I, Hein J. Presumptive paraneoplastic exfoliative dermatitis in four domestic rabbits. *Vet Rec*. 2013; 172: 155.
7. Rottenberg S, von Tscharner C, Roosje PJ. Thymoma-associated exfoliative dermatitis in cats. *Vet Pathol*. 2004; 41: 429-433.
8. Wikander YM, Knights K, Coffee C, et al. CD4 and CD8 double-negative immunophenotype of thymoma-associated lymphocytes in a dog. *J Vet Diagn Invest.* 2020; 32(6):918-922.
9. Yager JA. Erythema multiforme, Stevens-Johnson syndrome and toxic epidermal necrolysis: a comparative review. *Vet Dermatol.* 2014; 25: 406-e64.

CASE III:

Signalment:
11-month-old male neutered Rottweiler, *Canis lupus familiaris*, canid/domestic dog

History:
An 11-month-old neutered male Rottweiler dog was euthanized 21-days after routine castration under general anesthesia for severe generalized polymyopathy. The dog was reportedly clinically normal prior to the procedure. Ten days following anesthesia the dog presented recumbent, with severe generalized muscle weakness, azotemia, myoglobinuria, and a markedly increased serum creatinine kinase (CK) concentration of 806,080 U/L. With supportive care over the next two weeks the dog's strength and coordination returned, serum CK decreased to 980 U/L, azotemia improved, and myoglobinuria resolved. Twenty-one days post anesthesia/surgery, the dog again became acutely weak and lethargic and was humanely euthanized.

Gross Pathology:
Submitted is the body of a 30 kg brown and black male neutered Rottweiler with adequate fat stores and diffuse decreased symmetrical muscle mass most prominent of the epaxial and gluteal muscles. Mucous membranes are pale pink to white and tacky. There is mild tan/brown tartar on all canines, premolars, and molars. The ventral abdomen from the xiphoid process to the pubis, both antebrachia, the medial aspect of the left and

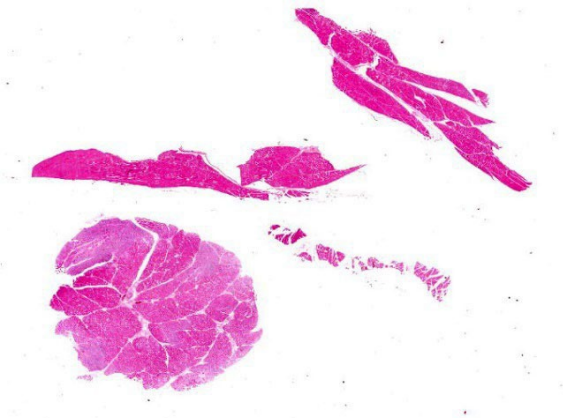

Figure 3-1. Skeletal muscle, dog. Longitudinal and transverse section of skeletal muscle are submitted for examination. (HE, 5X)

right metatarsus, the lateral aspect of the left and right tarsus, and the scrotum have been shaved. There is yellow Vetwrap wrapped circumferentially around the right tarsus. Autolysis is moderate.

External examination:
Paw pad, right forelimb: There is a 3.5 x 0.5-1.0 cm, slightly depressed, well-demarcated, loss of the epidermis with jagged margins that extend the width of the right metacarpal paw pad. The center is mottled tan and pink. There is a similar circular, 1 cm diameter, lesion of the right carpal paw pad. The center is red to brown with serous crusting.

Skin around neck: On either side of the neck there are 2 skin sores that are 4 x 1.5 cm (right-side), and 3.5 x 1 cm (left side). Both sores are well-demarcated with loss of haired skin and a slightly depressed, crusty, pink center. Within the shaved patch of hair on the left antebrachium there is a similar 2.5 x 2.5 cm sore. Scrotum: The skin of the scrotum is light pink. The scrotal incision is intact with little reaction.

Internal Examination:
Skeletal muscle: Throughout the entire body the skeletal muscles are subjectively soft and diffusely pale pink with thin to broad streaks of tan. Most severely affected muscles are within the hindlimbs, epaxial, and serratus muscles, with ~50% of these muscle bundles affected. There are a few small thin streaks of tan in bilateral temporalis muscles, affecting <5% of the tissue. There are a few (~5) tan foci (up to 1 cm in diameter) in bilateral masseter muscles, affecting <5% of the tissue. The diaphragm is diffusely pale and subjectively thickened up to 3 mm.

Heart: In the endocardium of the left atrium there are 4 adjacent raised exophytic nodules. Three of these nodules are small (up to 3 mm), tan to white, firm, with a smooth outer surface. The fourth nodule is larger, ovoid shaped, 8 x 5 mm, 4 mm raised, and red with speckles of tan. It is solid and red on cut section. Surrounding these nodules are multiple (~10) linear to focal, 1-3 mm, hard, raised plaques (suspect jet lesions). Just superior to the pulmonic valve and the aortic valve, there are approximately 2 x 1 cm area that contains multiple previously described hard plaques (suspect jet lesions). The free margins of the right and left atrioventricular valve leaflets are short, white, firm, and mildly thickened. The valve surface remains smooth and glistening.

Kidneys: The kidneys are mottled red/brown to green (suspect autolysis). The cortical surface of both kidneys contains multiple (~50 per kidney) up to 3 mm diameter depressions. On cut section the cortex contains alternating radiating streaks of red/brown and tan.

Spleen: In the capsule at the edge of the head of the spleen there is a dark purple to black 1.0 x 1.0 cm, well demarcated, irregular shaped, depression that is outlined by a 2 mm periphery of tan. This extends slightly into the parenchyma as a tan focus. At the head of the spleen, near the edge, there is also a 0.7 cm x 0.4 cm silver, shiny, plaque adhered to the capsule that does not extend into the parenchyma. Throughout the splenic parenchyma there are hundreds of white foci (0.5 mm to 2 mm in diameter) (suspect lymphoid follicles).

Lungs: The caudal lung lobes are heavy and exude a moderate amount of red-tinged fluid. Subcutaneous tissue: There is a moderate amount of thin light-yellow fluid within the subcutaneous tissues surrounding the hindlimbs.

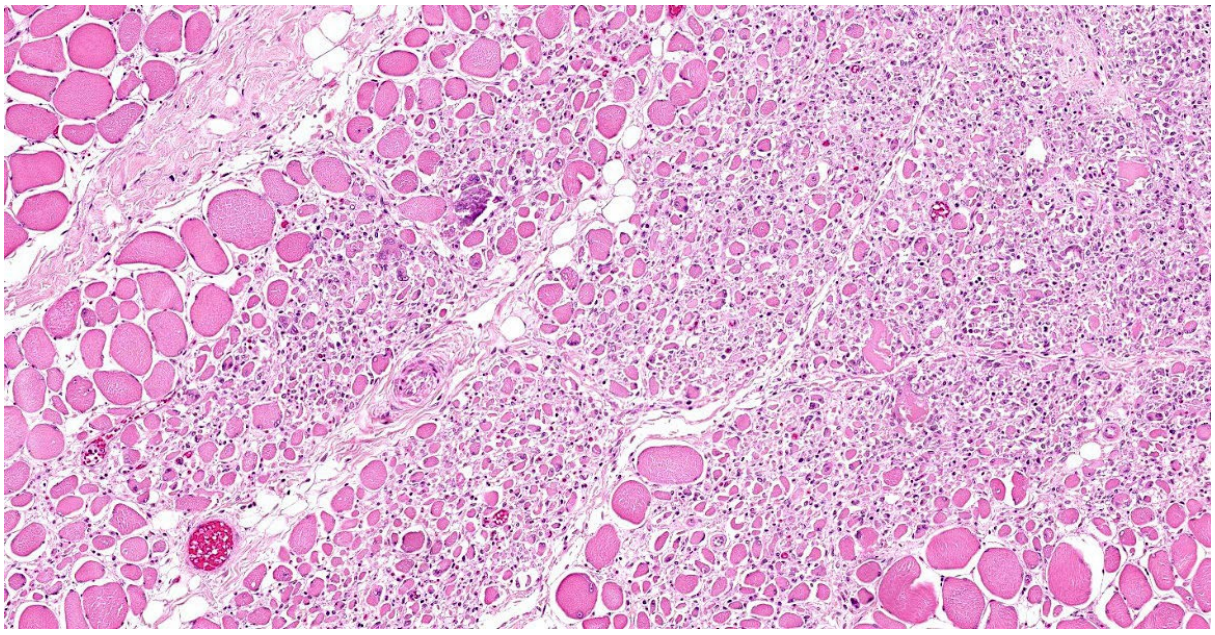

Figure 3-2. Skeletal muscle, dog. There are coalescing areas in which there is marked degenerative changes and atrophy of myofibers. (HE, 129X)

Laboratory Results:
Clinical Pathology:
Day of discharge

Urea 10.6 H mmol/L 3.5-9.0
ALT 317 H U/L 19-107
CK 980 H U/L 40-255
Amylase 1617 H U/L 299-947

Day of readmission before euthanasia Urea: 27.5 mmol/L
ALT 739 U/L
CK 806,080 U/L,
Amylase 1810 U/L

Comparative Neuromuscular Laboratory report:
Cryosection from the epaxial muscle and an archived control muscle were incubated with several polyclonal and monoclonal antibodies against dystrophy associated proteins including the rod and carboxy-terminus of dystrophin, utrophin, spectrin, laminin alpha2 (4F11), dysferlin (hamlet), alpha, beta and delta -sarcoglycans, beta-dystroglycan, caveolin 3, developmental myosin heavy chain (dMHC), MHC-I, collagen VI, emerin, the T cell markers CD3, CD4, and CD8, the B cell marker CD21 and the macrophage/dendritic cell marker CD11c. The staining intensity for rod-domain of dystrophin was normal in appearance. Moderately reduced staining intensity was present with the antibody against the carboxy-terminus of dystrophin and dystrophin associated proteins. Regenerating fibers were highlighted by dMHC staining. Utrophin staining was not increased. Antibody staining for laminin alpha2, dysferlin, caveolin3, collagen VI and emerin were normal in appearance. Several MHC-I and CD11c positive cells were present around necrotic fibers. Sporadic T cells (CD3+, CD4+ & CD8+) were observed. No CD21+ B cells were present. Spectrin2 staining was very weak suggesting partial tissue degradation."
Comment: This may be dystrophin deficient muscular dystrophy with normal staining for rod domain and weak staining for the carboxy terminus. … While I still favor a diagnosis of dystrophin deficient MD, and episode of severe rhabdomyolysis should be ruled out by the clinical history and progression."

Microscopic Description:

Skeletal muscle: All examined skeletal muscles have similar histologic features but vary in severity with up to 50% of myofibers affected. There are large groups of degenerating fibers at different stages of necrosis characterized by: single swollen hypereosinophilic fibers (hypercontraction) with loss of cross-striations, vacuolated cytoplasm and groups of thin, angular fibers with large plump peripheral nuclei. In addition, the cytoplasm of multiple randomly distributed swollen myofibers is replaced by basophilic granular to crystalline matrix (mineral confirmed by Von kossa stain) affecting up to 20% of the affected myofibers in one section (left semimembranosus muscle was most severe). Occasionally there are aggregates of foamy macrophages replacing single myofibers and scattered within the endomysium. Within the large groups of degenerating myofibers there are also single degenerating myofibers characterized by small rounded myofibers with multiple central nuclei (multinucleate muscle giant cells).

Contributor's Morphologic Diagnoses:

Skeletal muscle (generalized): Myonecrosis, degeneration and regeneration, multifocal polyphasic, subacute, severe.

Contributor's Comment:

Differential diagnoses for non-inflammatory canine polymyopathies include, amongst others, congenital or inherited myopathies, rhabdomyolysis, and malignant hyperthermia. Due to the young age of this dog, its breed (Rottweiler), and the gross and histologic findings, an inherited myopathy such as muscular dystrophy was initially suspected.

The most prevalent type of muscular dystrophies are the X-linked dystrophies. Of these, Duchenne's muscular dystrophy (DMD) is the most common followed by Becker muscular dystrophy (BMD. Both dystrophies are caused by a recessive mutation of the large dystrophin gene on the short branch of the X-chromosome encoding the dystrophin protein. Dystrophin is an important protein in stabilization of the myofiber during contraction. Complete loss of dystrophin, as in DMD, or partial loss of dystrophin, as in

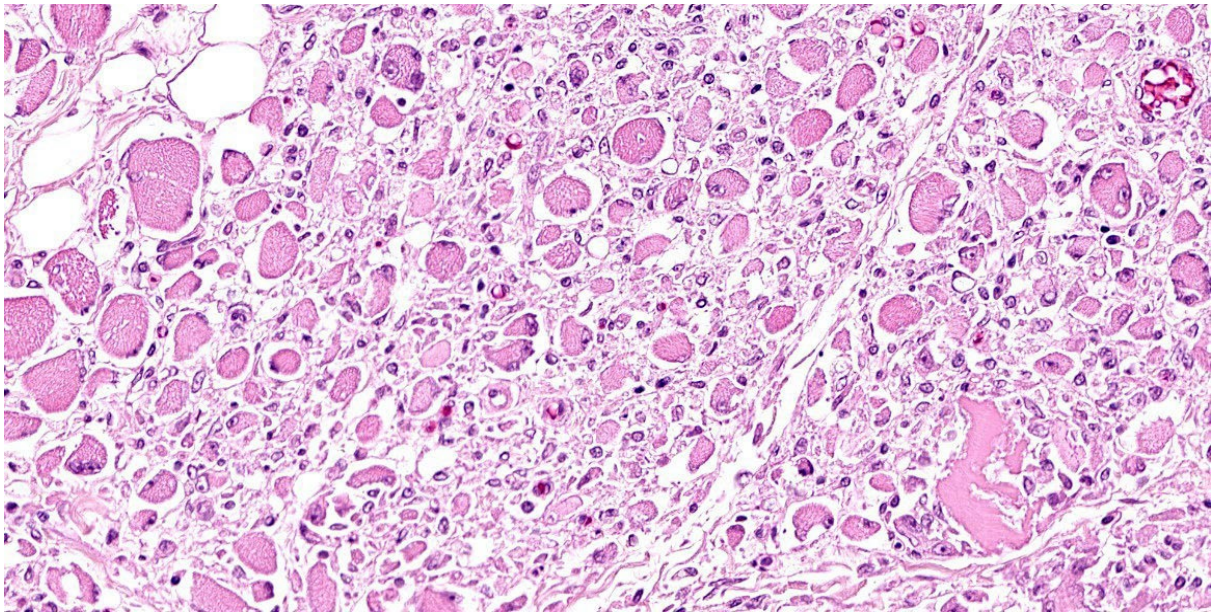

Figure 3-3. Skeletal muscle, dog. Within affected areas, there is marked atrophy of muscle fibers, and fibers display variable signs of degeneration, including loss of cross-striations and vacuolization. Regenerative changes include hypertrophy and internalization of satellite nuclei. A swollen, fragmented necrotic myofiber is at bottom right (arrow). The endomysium is mildly expanded by collagen and fibroblasts. (HE, 349X)

BMD, makes myofibers particularly susceptible to damage. Damaged myofibers leak the muscle-specific enzyme CK which correlates with the often chronically elevated serum CK seen in these cases. Both myofiber necrosis and regeneration within the same muscle is characteristic of the histologic appearance, as a result of repetitive damage.

Canine X-linked muscular dystrophy, specifically DMD, was first described in the Golden retriever in the early 1980s and has since been reported in multiple dog breeds including the Rottweiler. One case of muscular dystrophy resembling BMD in humans was described in a Labrador retriever. In addition, a unique form of muscular dystrophy exists in Rottweilers known as juvenile-onset distal myopathy. This condition has been identified in young dogs with signs of muscle weakness since birth and characterized by skeletal muscle lesions of predominantly the distal limbs. Two dogs in this study had normal immunoreactivity for the dystrophin protein.

Juvenile-onset distal myopathy likely has a different pathogenesis from DMD, and a metabolic defect may play a role. In addition, an inherited non-dystrophin myopathy, known as X-linked myotubular myopathy has also been reported in young Rottweilers, caused by a missense mutation in the MTM1 gene. This inherited condition is characterized by myofibers with central nuclei. Myonecrosis is not a feature.

In this case a diagnosis of muscular dystrophy is supported by the dog's age, breed, gross and histologic findings. However, a defect of the dog's dystrophin protein was not identified by immunohistochemistry and the dog's clinical history is not consistent with past reports of canine muscular dystrophy. Prior to anesthesia/surgery, this dog was reportedly clinically normal with no evidence of muscle weakness.

In addition to muscular dystrophies, a diagnosis of rhabdomyolysis was also considered. Rhabdomyolysis is a condition of acute skeletal muscle necrosis. In dogs it is often associated with painful muscles, limb weakness, markedly increased CK, and myoglobinuria.

Rhabdomyolysis is often attributed to overexertion or trauma but has also been associated with exposure to anesthetic agents, toxin exposure, and drug reaction/overdoses, amongst other things. In this case, a single episode of severe rhabdomyolysis after exposure to inhalant anesthesia is consistent with the myoglobinuria, acute kidney injury, and improved CK. However, rhabdomyolysis does not fit with the histologic findings of multifocal polyphasic myonecrosis and regeneration as rhabdomyolysis is typically characterized by a monophasic pattern of necrosis.

An episode of malignant hyperthermia was also considered. Malignant hyperthermia is an inherited disorder of skeletal muscle characterized by hypermetabolism and contracture and often occurs after exposure to anesthetic agents, exercise, or stress. In humans, pyrexia, hyperkalemia, hypercapnia, systemic acidosis, muscle rigidity, elevated CK levels, and often cardiac arrest are seen. Malignant hyperthermia occurs sporadically in dogs with similar clinical findings. As in humans, canine malignant hyperthermia develops as a result of a mutation of the RYR1 gene, causing uncontrolled calcium-release by skeletal muscles, excessive contraction, and subsequent heat production. Without immediate post-anesthetic bloodwork to support an episode of malignant hyperthermia, evidence of peri-anesthetic pyrexia or cardiac abnormalities, it is difficult to make this diagnosis.

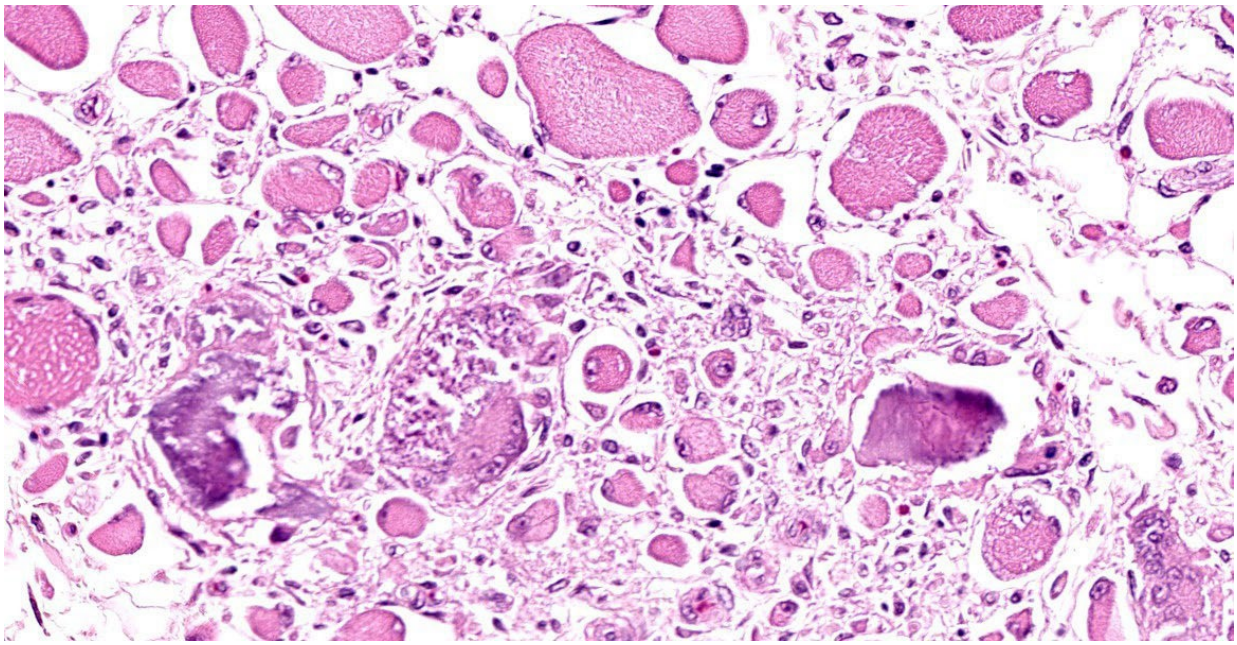

Figure 3-4. Skeletal muscle, dog. There is dystrophic mineralization of necrotic myofibers. (HE, 460X)

Contributing Institution:
Department of Pathobiology, Ontario Veterinary College, University of Guelph
https://ovc.uoguelph.ca/pathobiology/

JPC Diagnosis:
Skeletal muscle, myofibers: Degeneration, necrosis, regeneration and loss, polyphasic, multifocal, with mineralization.

JPC Comment:
The contributor provides good differentials for consideration in this case of polyphasic skeletal muscle necrosis. X-linked muscular dystrophy has been reported in the dog, cat, mouse, and pig.[1,2] The disease, which manifests in adolescents, is characterized by progressive muscle atrophy and weakness, though in the cat, mouse, and rat terrier, marked muscular hypertrophy may be seen.[2] Severely affected animals may die shortly after birth. Older animals may develop dyspnea due diaphragmatic fibrosis and contracture, esophageal dysfunction (and potential regurgitation), exercise intolerance, and a stiff gait. The disease also affects the cardiac muscle and in dogs progresses to degenerative cardiomyopathy. Macroglossia is an interesting feature documented in dogs, cats, humans, and, most recently, a pig. In a recent article, Aihara *et al* described macroglossia in a 6-month-old pig caused by Becker muscular dystrophy. The underlying genetic mutation was pseudoexon insertion in the dystrophin gene, and histologically, the skeletal muscle was replaced by abundant adipose and fibrosis, causing gross enlargement of the tongue (pseudohypertrophy).[1]

Cardiomyopathy is now the leading cause of death in young men with Duchenne's muscular dystrophy (DMD).[5] Gross and histologic lesions of the heart were described in a recent study of 26 dogs with golden retriever muscular dystrophy (GRMD), an animal model for DMD.[5] Gross lesions, seen in dogs over 10 months of age, included myocardial pallor and streaking in both ventricles, papillary muscle fibrosis or mineralization, and dilation of one or both ventricles.[5] Histologically, there was significant fatty infiltration and degeneration, most prominently within the subepicardium and also affecting papillary muscles, and lesion severity correlated positively with age.[5] Affected dogs also had arteriolar medial hypertrophy, and 11 of 26 had aortic

mineralization.[5] Acute coagulative myocardial necrosis was seen in many affected dogs.[5] There was no evidence of thrombosis in histologic sections, and semi-quantitative necrosis scores were correlated with the degree of arteriolar hypertrophy.[5] These findings led the authors to suspect that the necrosis was caused by dysregulation of vascular tone causing functional ischemia coupled with increased susceptibility of dystrophin-deficient cardiomyocytes to hypoxia.[5]

The effects of DMD on vascular smooth muscle was the subject of another recent research article, which evaluated dystrophin expression, nitric oxide synthetase (NOS) activity, and endothelial nitric oxide synthetase (eNOS) expression in large arteries of 16 DMD dogs compared to 15 unaffected dogs.[3] Unlike normal dogs, DMD dogs lacked dystrophin in smooth muscle and endothelial cells of the arteries and vena cava.[2] Additionally, DMD had significantly lower endothelial NOS activity and eNOS expression compared to normal dogs.[3] This is attributed to the fact that dystrophin is used to anchor NOS to the sarcolemma; in cells lacking dystrophin, NOS is delocalized and less effective.[3] Affected arteries had both decreased vasoconstriction and decreased vasodilation in response to endogenous signals, and the arteries were also smaller with decreased wall thickness attributed to tunica media atrophy.[3] This conflicts with the findings of Schneider *et al,* in which arteriolar hypertrophy was seen; however, the type of vessel analyzed differed between the two studies (cardiac arteriole versus femoral artery), and both studies agreed that vascular defects may play a role in DMD pathogenesis.[3,5]

References:

1. Aihara N, Kuroki S, Inamuro R, et al. Macroglossia in a pig diagnosed as Becker muscular dystrophy due to dystrophin pseudoexon insertion derived from intron 26. *Vet Pathol*. 2022: 59(3): 455-458.
2. Cooper BJ, Valentine BA. Muscle and Tendon. In: Maxie MG, ed. *Jubb, Kennedy, and Palmer's Pathology of Domestic Animals.* Vol 1. 6th ed. St. Louis, MO: Elsevier, 2016. 192-196.
3. Hanson SM, Smith MO, Walker TL, Shelton GD. Juvenile-onset distal myopathy in rottweiler dogs. *J Vet Internal Med*.1998; 12: 103.
4. Kodipilli K, Thorne PK, Laughlin MH, Duan D. Dystrophin deficiency impairs vascular structure and function in the canine model of Duchenne muscular dystrophy. *J Pathol.* 2021; 254(5):589-605.
5. Roberts MC, Mickelson JR, Patterson EE, Nelson TE, Armstrong PJ, Brunson DB, Hogan K. Autosomal dominant canine malignant hyperthermia is caused by a mutation in the gene encoding the skeletal muscle calcium release channel (ryr1). *Anesthesiology*. 95: 716-725.
6. Schneider SM, Snsom GT, Guo L, Furuya S, Weeks BR, Kornegay JN. Natural History of Histopathologic Changes in Cardiomyopathy of Golden Retriever Muscular Dystrophy. *Front Vet Sci*. 2022; 8:759585.
7. Shelton GD. 2004. Rhabdomyolysis, myoglobinuria, and necrotizing myopathies. *Vet Clin Small Anim*. 2004; 34: 1469-1482.
8. Shelton GD, Liu LA, Guo LT, Smith GK, Christiansen JS, Thomas WB, Smith MO, Kline KL, March PA, Flegel T, Engvall E. Muscular dystrophy in female dogs. *J Vet Internal Med*. 2001; 15: 240-244.
9. Shelton GD, Rider BE, Child G, Tzannes S, Guo LT, Moghadaszadeh B, Troiano EC, Haase B, Wade CM, Beggs AH. X-linked myotubular myopathy in rottweiler dogs is caused by a missense mutation in exon 11 of the mtm1 gene. *Skeletal Muscle*. 2015; 5: 1

CASE IV:

Signalment:
An adult, male castrated, Golden Retriever, *Canis lupus familiaris*, dog.

History:
The dog presented with reluctance to move and severe pain localized in the cervical spine. Proprioception was decreased in all four legs. MRI showed lytic changes in C2, C7 and T2 vertebral bodies with extension to adjacent musculature and compression of corresponding spinal cord segments. A neoplastic process was suspected and the dog was euthanized due to poor prognosis.

Gross Pathology:
Extending from C2 to T2, the bone marrow of the vertebral bodies, and less frequently the lamina and transverse processes, was gelatinous, dark red to grey-tan and porous with complete effacement of the trabecular bone. Frequently, the process destroyed the cortical bone infiltrating the epaxial and hypaxial muscles and/or protruding into the spinal canal compressing the spinal cord and nerve roots.

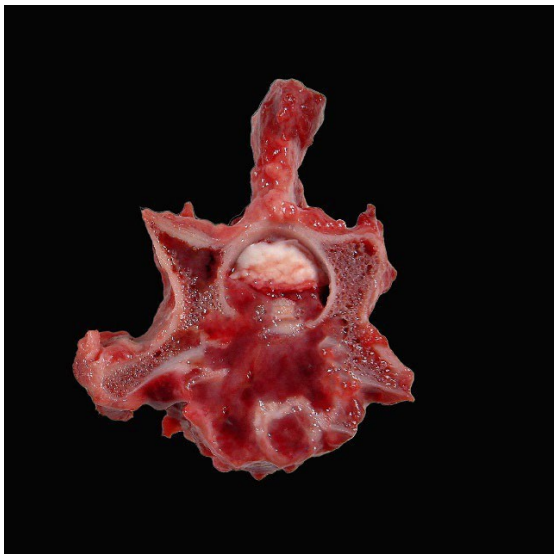

Figure 4-1. 7th cranial vertebra, dog. The bone marrow of the vertebral body, and less affecting the lamina and transverse processes, is multifocally gelatinous, dark red to grey-tan and effacing the adjacent trabecular and cortical bone. The tumor mass is protruding into the spinal canal and compressing the spinal cord. (Photo courtesy of: Department of Veterinary Biosciences, Faculty of Veterinary Medicine, University of Helsinki, https://www.helsinki.fi/en/faculty-veterinary-medicine/research/veterinary-biosciences)

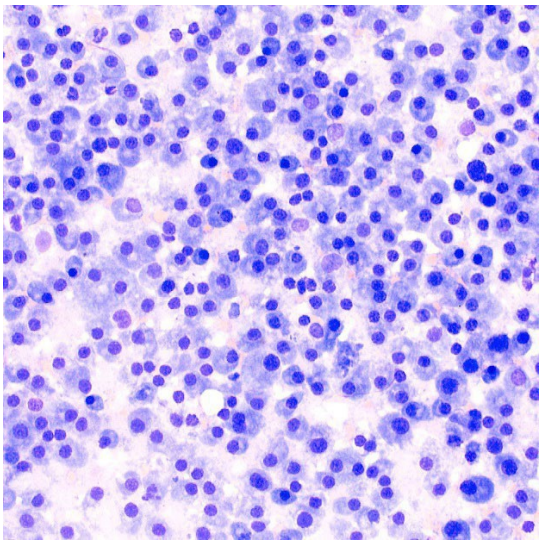

Figure 4-2. Bone marrow (T2 vertebra), dog. Cytologic smear consisting primarily of neoplastic plasma cells with moderate amounts of basophilic cytoplasm, round eccentric nuclei and perinuclear white halo. Neoplastic plasma cells show mild to moderate anisokaryosis and anisocytosis and are occasionally binucleated. (Photo courtesy of: Department of Veterinary Biosciences, Faculty of Veterinary Medicine, University of Helsinki, https://www.helsinki.fi/en/faculty-veterinary-medicine/research/veterinary-biosciences)

Laboratory Results:
Complete blood count revealed mild anemia and serum biochemistry was unremarkable.

Cytologic smear from affected bone marrow of T2: The cytologic smear consists primarily of round cells (neoplastic plasma cells) with moderate amounts of basophilic cytoplasm, round eccentric nuclei and perinuclear white halo. Neoplastic plasma cells show mild to moderate anisokaryosis and anisocytosis and are occasionally binucleated. Mitoses are rare.

Microscopic Description:
Vertebra (T2) and corresponding spinal canal and spinal cord:
Up to 70% of the medullary cavity is effaced by an unencapsulated, poorly demarcated, infiltrative and densely cellular neoplastic process composed of round cells arranged in sheets laying on small amounts of pre-existing fibrovascular stroma. Neoplastic cells have distinct cell borders, moderate amounts of eosinophilic cytoplasm with occasional perinuclear white halo, round to oval, hyperchromatic, eccentric nuclei with up to one basophilic nucleolus. Some cells show large intracytoplasmic pale eosinophilic, homogenous vacuoles pushing the nucleus to the periphery and there are occasional binucleated cells. Mitoses are up to 2 per HPF. Anisocytosis and anisokaryosis are mild to moderate. Necrotic foci composed of eosinophilic cellular debris and karyorrhectic/pyknotic nuclei are observed multifocally. Up to 60 % of trabecular and cortical bone are lytic and/or necrotic and replaced by dense sheets of neoplastic cells and hemorrhages.

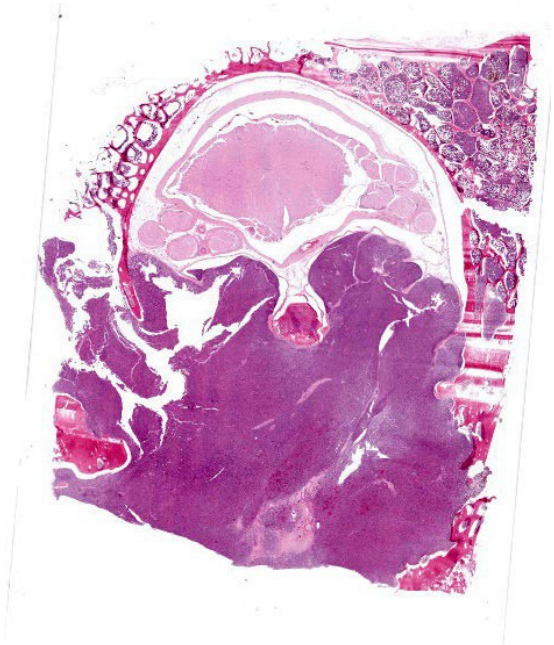

Figure 4-3. 7th cranial vertebra, dog. A multilobular round cell neoplasm has effaced the ventral vertebral body and infiltrated into the spinal canal. (HE, 3X)

Spinal cord (T2): Multifocally, affecting the white matter of the lateral and ventral funiculi, small numbers of axons show evidence of axonal degeneration characterized by dilated myelin sheaths containing glassy, eosinophilic, swollen axons (spheroids) accompanied by increased numbers of activated astrocytes with enlarged, vesicular nucleus (astrocytosis), few astrocytes with large amounts of eosinophilic cytoplasm and large vesicular nucleus (gemistocytes) and activated microglia.

Contributor's Morphologic Diagnoses:
Vertebra (T2): Multiple myeloma with osteolysis and infiltration towards the spinal canal
Spinal cord, T2, white matter: axonal degeneration (ventrolateral funiculi), multifocal, mild, with dilated myelin sheaths and spheroids

Contributor's Comment:
This case represents a classic case of multiple myeloma (MM) affecting the cervical and thoracic vertebrae with multicentric osteolysis and extension towards the spinal canal. MM is a malignant tumor originating from clonal proliferation of plasma cells within the bone marrow. In domestic animals, MM is most commonly reported in dogs, less frequently in cats and occasionally in horses. In dogs, it accounts for approximately 0,5 % of all malignant tumors.[2,11] It is usually diagnosed in middle-aged to old dogs and rarely affects young individuals.[2,11,12] The predilection sites include the vertebrae, ribs, femur, humerus and pelvis, all of which have active hematopoiesis.[2,10,11] The clinical signs are unspecific unless there is tumor-associated bone fracture and spinal cord or nerve roots compression. Generally, affected dogs present with lethargy, weight loss, anorexia, vomiting and fever.[7]

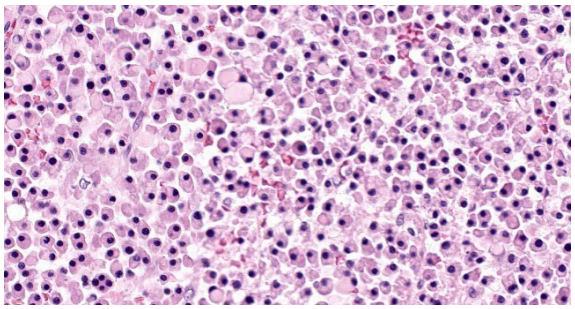

Figure 4-4. 7th cranial vertebra, dog. The neoplasms is composed of sheets of plasma cells. The perivascular hoff that characterizes this cell type occupies almost the entire cytoplasm in some cells. (HE, 589X)

The diagnosis of MM in dogs follows the criteria used for human MM, which is based on detecting ≥2 features including 1) bone marrow with >5 % or >20% of neoplastic plasma cells, 2) lytic bone lesions, 3) presence of clonal immune-globulin paraproteins in the serum (monoclonal gammopathy) and 4) presence of free light-chain immunoglobulins (fLC) in urine (Bence-Jones proteinuria).[5,7,12] Additional clinical findings can include anemia, hyperviscosity syndrome, bleeding disorders and hypercalcemia.[11] Increased numbers of plasma cells in the bone marrow can be also a feature of infectious diseases including ehrlichiosis and leishmaniasis, which should be taken into consideration if other features of MM are not evidenced.[11]

Gross findings in the affected bone are characterized by discrete, irregular, soft to gelatinous, pink-grey foci of tumor tissue replacing trabecular and cortical bone. Secondary pathological fractures may be evidenced.[2,11]

Histologically MM is characterized by dense colonies of well differentiated, monoclonal plasma cells or large, anaplastic plasma cells with high mitotic index, which replace normal hematopoietic and adipose tissue. Multiple myeloma oncogene 1/interferon regulatory factor 4 (MUM1/IRF-4) immunohistochemistry can be used for confirmation of plasma cell tumors in dogs and cats but is often unnecessary due to distinctive histological features of MM.[2,11] Infiltration to the bone with osteolysis is a typical finding mediated by cytokines produced by neoplastic plasma cells leading to decreased numbers of osteoblasts, suppression of their activity and increased numbers of activated osteoclasts. The excess of osteoclastic activity will cause destruction of bone tissue.[1,11]

Metastasis to visceral organs is rarely reported in dogs with the spleen being the most common site. This feature differs from MM in cats, in which metastasis to abdominal organs including spleen, liver, and lymph nodes is frequently observed.[4,6,11] Overall, MM can be additionally accompanied by renal disease or amyloidosis, since light-chain immunoglobulins produced by the neoplastic plasma cells can be deposited in the glomerular membrane resulting in glomerulonephritis, or form amyloid to be deposited in the glomeruli, spleen or liver.[3,4,11] In this case, histological changes observed in the adjacent spinal cord including dilation of the myelin sheaths and spheroid formation are secondary to compression caused by the tumor mass protruding into the spinal canal.

Contributing Institution:
Department of Veterinary Biosciences
Faculty of Veterinary Medicine
University of Helsinki

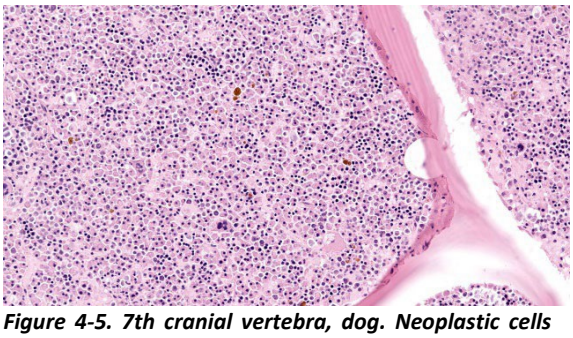

Figure 4-5. 7th cranial vertebra, dog. Neoplastic cells occupy bone marrow spaces in the affected vertebra. (HE, 222X)

https://www.helsinki.fi/en/faculty-veterinary-medicine/research/veterinary-biosciences

JPC Diagnosis:
Vertebra and spinal canal: Myeloma.

JPC Comment:
The contributor provides an excellent review of this classic condition seen in both human and veterinary medicine. All veterinarians and veterinary pathologists are familiar with the condition Bence Jones proteinuria and its neoplastic cause; fewer have knowledge of Dr. Henry Bence Jones and his initial characterization of the phenomenon which bears his name. Dr. Bence Jones was a British physician of the mid-19th century whose initial research focused on chemical chemistry, specifically the analysis of cysteine oxide stones and proteins. He later specialized in the composition of urine in health and disease. Thomas Alexander McBean was a patient afflicted by bone pain and peripheral edema (and who is now known to have suffered from multiple myeloma). His urine contained a protein that produced peculiar results when analyzed using standard laboratory testing at the time. The patient's attending physicians sent a sample to Dr. Bence Jones. After further testing, he dubbed the protein "hydrated deutoxide of albumin" and published the first reports on this unique urinary protein. Bence Jones proteins are now considered to be the first tumor marker discovered, and Dr. Bence Jones the first chemical pathologist.[8]

A recent report described a case of erythrophagocytic multiple myeloma, which is incredibly rare in dogs and cats and slightly more common in humans.[7] A 5 year old female spayed golden retriever dog presented for a severe nonregenerative anemia and thrombocytopenia, and abundant neoplastic plasma cells which occasionally exhibited erythrophagocytosis were observed in the spleen, liver, and bone marrow.[7] Anemia in the patient was likely due to erythrophagia; however, dogs with multiple myeloma commonly have anemia due to erythrocyte destruction in hyperviscosity syndrome, myelophthisis, blood loss, or anemia of chronic disease, so these may have also contributed to the anemia.[7] This week's moderator also explain that anemia is a common presenting complaint in human patients with multiple myeloma.

References:

1. Brigle K, Rogers B. Pathobiology and Diagnosis of Multiple Myeloma. *Semin Oncol Nurs*. 2017;**33**(3).
2. Craig LE, Dittmer KE., Thompson KG. Bones and joints. In: Maxie MG, ed. *Jubb, Kennedy and Palmer's Pathology of Domestic Animals.* Vol 3. 6th ed. Philadelphia, PA: Elsevier Saunders; 2016:123.
3. Kim DY, Taylor HW, Eades SC, Cho DY. Systemic AL amyloidosis associated with multiple myeloma in a horse. *Vet Pathol*. 2005;**42**(1).
4. Mellor PJ, Haugland S, Smith KC, et al. Histopathologic, immunohistochemical, and cytologic analysis of feline myeloma-related disorders: Further evidence for primary extramedullary development in the cat. *Vet Pathol*. 2008;**45**(2).
5. Moore AR, Harris A, Jeffries C, Avery PR, Vickery K. Retrospective evaluation of the use of the International Myeloma Working Group response criteria in dogs with secretory multiple myeloma. *J Vet Intern Med*. 2021;**35**(1).
6. Patel RT, Caceres A, French AF, McManus PM. Multiple myeloma in 16 cats: A retrospective study. *Vet Clin Pathol*. 2005;**34**(4).
7. Romanelli P, Recordati C, Rigamonti P, Bertazzolo W. Erythrophagocytic

multiple myeloma in a dog. *J Vet Diagn Invest*. Published online May 21, 2022. doi:10.1177/10406387221092299

8. Sewpersad S, Pillay TS. Historical perspectives in clinical pathology: Bence Jones protein – early urine chemistry and the impact on modern day diagnostics. *J Clin Pathol.* 2020; 0:1-4.
9. Sung S, Lim S, Oh H, Kim K, Choi Y, Lee K. Atypical radiographic features of multiple myeloma in a dog: A case report. *Vet Med*. 2017;**62**(9).
10. Thompson KG, Dittmer KE. Tumors of bone. In: Meuten DJ, ed. *Tumors in domestic animals.* 5th ed. Ames, IA: John Wiley & Sons; 2017:412,513.
11. Wachowiak IJ, Moore AR, Avery A, et al. Atypical multiple myeloma in 3 young dogs. *Vet Pathol*. Published online April 11, 2022. doi:10.1177/03009858221087637

WSC 2022-2023 Self-assessment
Conference 14

1. Hodgkin-like lymphoma has been most commonly seen in which of the following species?
    a. Dog
    b. Cat
    c. Horse
    d. Pig

2. The primary target of the cytotoxic/interface pattern in the skin is the?
    a. Vasculature
    b. Basement membrane
    c. Keratinocyte
    d. Lymphocyte

3. A defect in which of the following genes is the cause of malignant hyperthermia in dogs ?
    a. Colchicine
    b. Dystrophin
    c. Ryanodine
    d. Endothelin

4. In which of the following species is myeloma most common diagnosed?
    a. Dog
    b. Cat
    c. Horse
    d. Swine

5. Which of the following is the most common site of metastasis of myeloma in the dog?
    a. Spleen
    b. Liver
    c. Lung
    d. Kidney

Please email your completed assessment for grading to Dr. Bruce Williams at bruce.h.williams12.civ@mail.mil. Passing score is 80%. This program (RACE program 33611) is approved by the AAVSB RACE to offer a total of 0.5 CE Credits, with a maximum of 12.5 CE Credits being available to any individual Veterinary Medical Professionals for the 2019-2020 Wednesday Slide Conference. This RACE approval is for the subject matter categories of: SCIENTIFIC using the delivery method of NONINTERACTIVE DISTANCE. This approval is valid in jurisdictions which recognize AAVSB RACE.

Joint Pathology Center
Veterinary Pathology Services

WEDNESDAY SLIDE CONFERENCE 2022-2023

Conference #15 **11 January 2023**

CASE I:

Signalment:
3-month-old, male, Lewis rat (*Rattus norvegicus*)

History:
This rat was part of a study receiving high-dose whole body irradiation daily for six days. Five days after the last exposure, the animal presented quiet, with thin body condition (BSC 1/5), a hunched appearance, and an unkempt haircoat. Due to lack of improvement with supportive care, the animal was euthanized two days later and submitted for necropsy evaluation.

Gross Pathology:
On gross examination, the cecum was slightly distended and doughy, and there was a small amount of fecal staining at the ventral tail base. There were several formed fecal pellets present in the colon. The liver was mildly and diffusely pale.

Laboratory Results:
On CBC analysis, there was mild lymphopenia, mild neutrophilia, and moderate monocytosis. In addition, there was a mild decrease in HCT and MCV, and a mild increase in MCHC, representing a microcytic, hypochromic anemia.

Microscopic Description:
In sections of small intestine, there was loss of normal villus architecture characterized by moderate and multifocal villus blunting and fusion, with replacement of areas of lamina propria with loose collagen and granulation tissue. The deep crypt epithelium was hyperplastic with large, plump crypt epithelial cells that showed piling and disorganization with frequent mitotic figures. Within the ileum, similar changes were present within the lamina propria and crypt epithelium, with the additional finding of severe, locally extensive mucosal ulceration with replacement by granulation tissue. There was diffuse and moderate lymphangiectasia within small intestinal villi and marked depletion of mucosal associated lymphoid tissue. Within the colon, there was marked degeneration and necrosis of the superficial mucosal and deep glandular epithelium with the presence of necrotic debris present within glandular lumens. There was moderate granulation tissue throughout the lamina propria of the colon, with attenuation, loss, and regeneration of colonic glandular epithelium. There was mild edema present within the submucosa, and severe lymphoid depletion within Peyer's patches. In the cecum, there were sporadic areas of glandular degeneration with loss of epithelium and small amounts of granulation tissue within the lamina propria. In other organs, there was

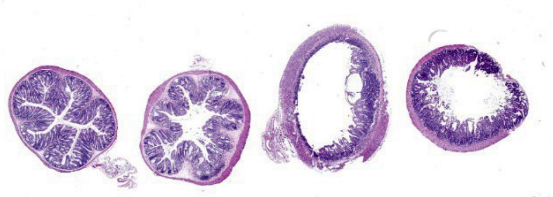

Figure 1-1. Colon, intestine, rat. Three sections of colon (from left) and one section of intestine are submitted for examination. Dilated colonic glands are visible at subgross magnification. (HE, 6X)

minimal and multifocal myofiber degeneration representative of chronic cardiomyopathy in the heart, sporadic clusters of alveolar histiocytes within the lung, and decreased erythroid progenitors within the bone marrow.

Contributor's Morphologic Diagnoses:
Small and large intestine: Enterocolitis, necrotizing and ulcerative, diffuse, with regeneration.

Contributor's Comment:
This case represents lesions which result from radiation toxicity to the intestinal tract. The lesions observed here are a continuum of glandular epithelial necrosis, regeneration, and ultimately, villar blunting, fusion, and granulation tissue proliferation as a result of cytotoxicity of rapidly dividing crypt epithelial cells. In humans, radiation-induced gastrointestinal syndrome (RIGS) occurs secondary to radiation therapy for neoplasia of the abdomen and pelvis and is a major limiting factor and source of morbidity and mortality in patients receiving this therapy.

The detrimental effects of radiation exposure were first described by Walsh (1897) two years after the discovery of X-rays, who concluded that irradiation caused inflammation of the mucosa of the intestinal tract.[2,16] Mechanisms underlying this side effect of radiation are still incompletely understood, and there are still no effective preventions or treatments for this condition. Every year, over 300,000 patients receive abdominal radiation for cancer treatment, and approximately 60-80% of these patients develop some form of bowel toxicity.[2,8] In the process of radiation treatment for intra-abdominal or pelvic neoplasia, healthy bowel is ultimately affected by the radiation treatment, resulting in significant morbidity and mortality.[13] Therefore, it is a significant limiting factor for many patients receiving radiation therapy for abdominal or pelvic neoplasia.[19,26] However, radiation therapy is still a mainstay of cancer treatment, used in approximately half of cancer patients, and is therapeutically critical in ~25% of cancer cures so a better understanding of mechanisms behind RIGS and preventative measures against it are critical.[8]

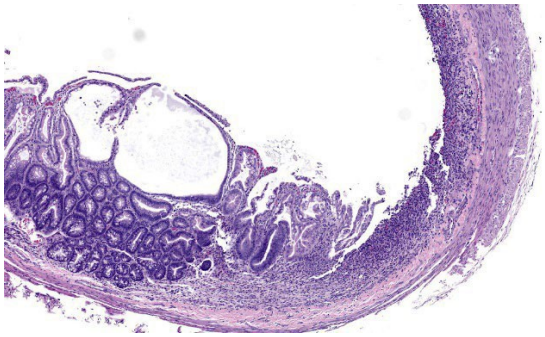

Figure 1-2. Colon, rat. There is a segmental area of ulceration (right), with ectatic glands at the periphery. (HE, 52X)

In acute cases of RIGS, the intestine represents an important organ at early risk, because of the nature of intestinal biology. While the pathophysiology of RIGS is still not fully understood, data suggests that it arises from a complex interaction of epithelial damage, and alterations in the immune, vascular, and enteric nervous systems, influenced by host (co-morbidities such as IBD, diabetes, vascular or collagen disorders, genetic predisposition, body mass index, tobacco smoking, genetic disorders) and therapeutic factors (dose of radiation, length of bowel involved, concurrent chemotherapy, abdominal surgery).[8,13] Intestinal epithelium, particularly intestinal stem cells (ISCs) have a high rate of proliferation and thus make the bowel a sensitive target for radiation toxicity.[13] In acute RIGS, this phase occurs immediately following exposure and may persist for hours to several days, and results from a direct cytotoxic effect of radiation resulting in cytotoxicity of crypt epithelial cells, including stem cells, which results in epithelial cell loss, villus blunting, fusion, and impairment of epithelial barrier function with loss of electrolytes, water, protein, mucosal

ulceration, and increased permeability to luminal pathogens and antigens, resulting in mucosal inflammation and ultimately systemic effects of sepsis.[2,8,13,16] Compromise to the vascular architecture leads to hemorrhage and thrombosis, which precedes ischemic damage; in addition, several animal studies have shown a direct effect on the enteric nervous system, resulting in reduced transit time and intestinal ileus.[13]

As lesions progress, acute RIGS may resolve following cessation of radiation exposure, or in some cases (often months to several years following exposure) may become a chronic condition, secondary to progressive occlusive vasculitis, extracellular matrix remodeling, and collagen deposition resulting in atrophy of the intestinal mucosa, fibrosis, structure formation, fistula development, and intestinal obstruction or perforation; the chronic form of RIGS occurs in up to ~17% of individuals treated with abdominal/pelvic irradiation.[8,13,16] In fact, a latency period of several decades (20-30 years) between radiation therapy and chronic RIGS is not an uncommon clinical phenomenon.[8]

While the pathophysiology of RIGS is poorly understood, a number of studies have shown a relationship between growth factor pathways, cell cycle proteins, DNA damage mediators, and developmental or stem cell pathways in the progression of disease. For example, radiation induced damage to the intestinal tract is associated with upregulation of the JNK-MAPK cell growth and proliferation pathways and decreased expression of stress-activated p38 MAPK pathways which are important for regeneration and repair of intestinal mucosal defects.[26] Inhibition of the cell cycle, either through cyclin/cdk complex inhibition, or modulation of cell cycle regulators and DNA damage checkpoint mediators, appears to protect against or improve response to GI toxicity; CDK4/6 inhibitors

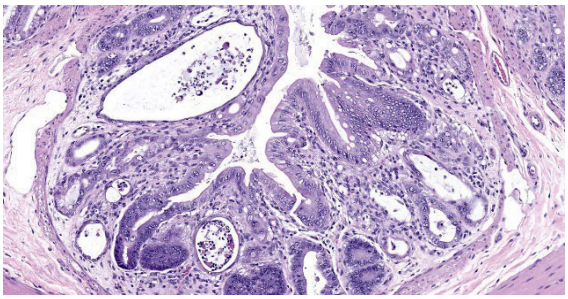

Figure 1-3. Colon, rat. Dilated colonic glands are lined by attenuated epithelium and contain low numbers of necrotic epithelium and cellular debris. (HE, 158X)

improve survival in irradiated mice by blocking crypt epithelial apoptosis and promoting epithelial cell survival and self-renewal through upregulation of stem cell factors (LGF5, BMI-1, Hopx, mTERT, Lrig1) and inhibiting radiation induced P53 apoptotic response.[16,17,18,19,24] Prophylactic therapy with various growth factors and cytokines such as TGFb, IL-11, keratinocyte growth factor (KGF), and Kruppel-like factor (KLF) increases crypt survival following radiation.[1,2,7,15] Radiation induced injury to the intestinal tract is also associated with increased levels of oxidative tissue injury, and studies have shown that certain antioxidants and mediators of oxidative stress play a role in RIGS and its progression. For example, cyclooxygenase induced prostaglandins prevent cytotoxicity of crypt epithelial cells in mice,[16] and alterations in the mTOR-PI3K and NRF2 pathways regulating oxidative stress can protect the intestinal tract through mediation of oxidative stress and upregulation of stem cell factors and growth pathways such as the NF-kB pathway.[5,25] Finally, blockage of the TLR pathway, important in promotion of inflammatory responses to microbial pathogens, protects from lethal radiation induced intestinal injury in mice.[22]

Since intestinal stem cells are a target of radiation induced toxicity, activation of developmental and stem-cell embryonic pathways have shown to be effective in mediating RIGS in animal models, as epithelial regeneration following radiation injury requires

intestinal stem cell repopulation.[12,14,19] For example, activation of the Wnt/beta-catenin pathway or suppression of the adenomatous polyposis coli (Apc) gene function in radiation injury stimulates repair and significantly improves morbidity and mortality in mice following high dose radiation.[19] Notch signaling, another developmental/stem cell pathway, regulates self-renewal of intestinal stem cells and activation of this pathway accelerates reversal of radiation induced damage in the intestinal tract.[14] Mesenchymal stem cells, or stromal progenitor cells (SPCs) have been shown to have regenerative, immune modulatory, angiogenic, and anti-inflammatory properties that promote healing.[3,21] In addition, the recruitment of extra-intestinal and bone marrow-derived cells has been shown to play a role in promotion of intestinal healing and improvement of morbidity and mortality in radiation-induced intestinal injury through secretion of growth factors, stem cell mediators, and inflammatory cytokines in a paracrine fashion.[21]

Lastly, there is a significant role of the microbiome in the response to RIGS.[8,13] Radiation of the intestinal tract results in alterations in normal intestinal microbiota, which is an important factor in the pathogenesis of radiation enteritis; radiation reduces the normal diversity of the gut microbiota and leads to dysbiosis, which aggravates RIGS by weakening intestinal epithelial barrier function and promoting inflammation.[4,9] Changes in the microbiome of the intestine reflect altered diversity reflective of decreased beneficial *Lactobacillus* and *Bacterioides* spp. and increased *E. coli* and *Streptococcus* spp.[23,26] As a further result of altered diversity of microbes, the composition of short-chain fatty acids (SCFAs), the key metabolites generated by large intestinal microbial metabolism, is altered as well; SCFAs play an important role in intestinal repair, inflammation, and homeostasis in the gut.[26] Transplantation of normal fecal microbiota has been shown to improve survival in irradiated animals and improve overall function of the intestinal tract.[4] Dysbiosis also promotes inflammation and alterations in barrier function in the intestinal tract, influenced by enhanced pro-inflammatory cytokine signaling through TNFa and IL1b expression, and rearrangement of important tight junction proteins induced by microbes such as pathogenic E. coli.[9,23] In fact, beneficial effects on intestinal symptoms have been observed using probiotics including *Lactobacillus* in animal models and humans in reducing endotoxin levels, reduction in severity of bowel injury, and reduction in potential bacteremia.[13]

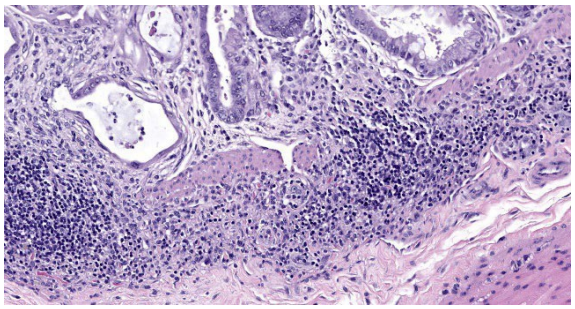

Figure 1-4. Colon, rat. Beneath affected glands, lymphocyte numbers in Peyer's patches are markedly diminished. (HE, 241X)

In summary, a full understanding of the pathophysiology of radiation induced injury in the intestinal tract is still incomplete, but likely involves a complex interplay between epithelial damage and repair, induction of developmental and stem cell pathways, growth factors and cell cycle/DNA damage mediators, the inflammasome, endothelial injury, tissue remodeling, and effects on the enteric nervous system, influenced by alterations in normal gut microbiota to result in the clinical syndrome of RIGS.

Contributing Institution:

In Vivo Animal Core, Unit for Laboratory Animal Medicine
University of Michigan Medicine
North Campus Research Complex, Building 36, Rm G177

2800 Plymouth Road
Ann Arbor, MI 48109

JPC Diagnosis:
1. Colon: Colitis, necrotizing, multifocal to coalescing with glandular regeneration and lymphoid depletion.
2. Small intestine: Enteritis, necrotizing, segmental, moderate, with ulceration, crypt abscesses, and crypt hyperplasia.

JPC Comment:
The contributor provides an excellent description of radiation-induced gastrointestinal syndrome. To see the effects of ionizing radiation on the lung, WSC 2021, Conference 17, Case 4 is a case of radiation pneumonitis in a rhesus macaque exposed to whole thorax radiation, and the contributor described the pathogenesis behind acute and chronic phases of injury.

This week's moderator, Dr. Cory Brayton of Johns Hopkins University School of Medicine, commented on the atypical features of regeneration in this case, including anyisocytosis, anisokaryosis, and presence of goblet cells in the crypts, which provide clues as to pathogenesis of this case. IBA-1 revealed the scattered inflammatory infiltrate in the lamina propria to be composed of abundant macrophages called into clean up necrotic cellular debris.

Additionally, she pointed out a histoanatomic feature which is helpful identifying origin of a colonic section: the mucosal folds in present in the colonic section in this case are more prominent in the proximal section of the colon and correspond to grossly visible diagonal lines on the serosal surface.

Acute radiation syndrome occurs after exposure to a substantial amount of ionizing radiation and may occur as a result of radiotherapy/radiopharmaceuticals, nuclear accidents, or atomic bombings. The effects are dependent on both the dose and type of radiation and regions and proportion of the body exposed. Systems particularly sensitive to acute radiation injury include the hematopoietic, gastrointestinal, integumentary, and nervous systems. The prodrome phase of ARS occurs immediately after exposure and results in nausea, vomiting, fatigue, or loss of consciousness from autonomic stability.[6] This is

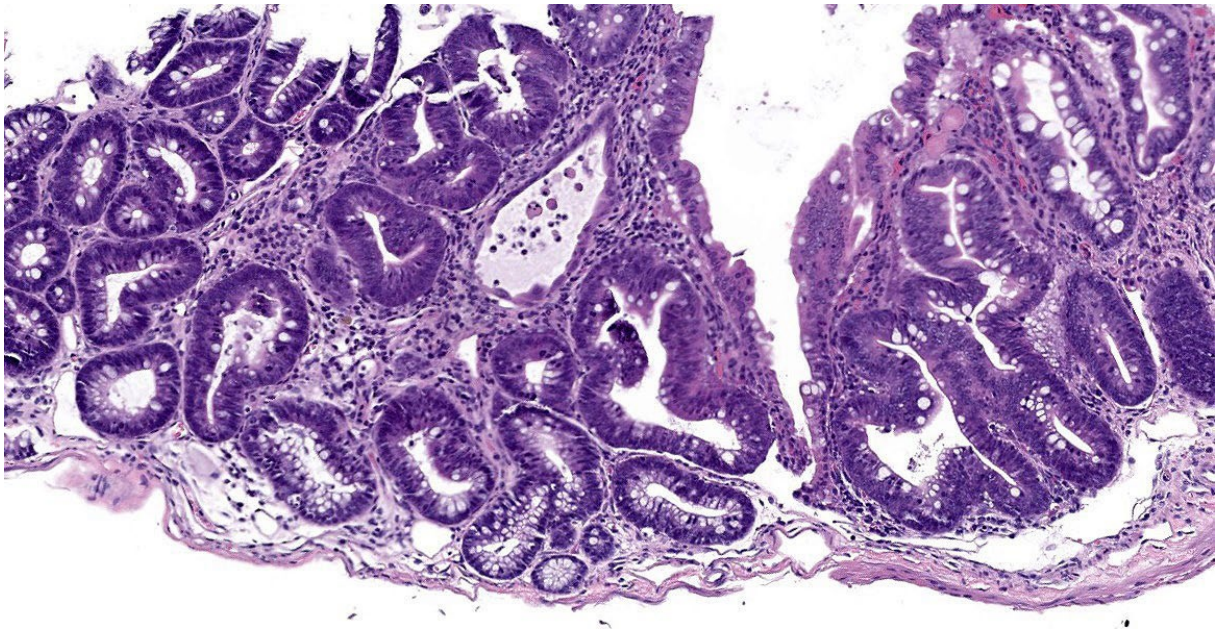

Figure 1-5. Intestine, rat. There are necrotic crypts within the intestinal mucosa as well. (HE, 241X)

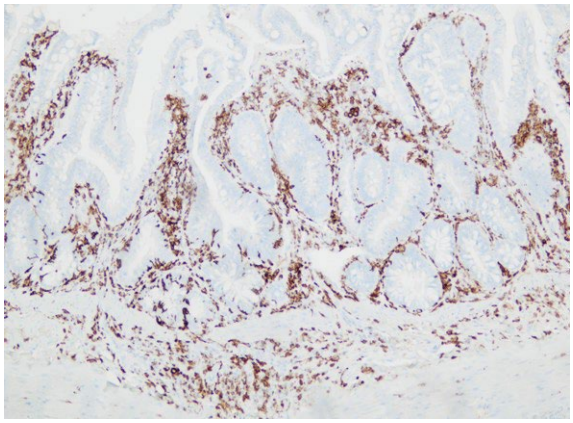

Figure 1-6. There are numerous macrophages infiltrating the lamina propria of irradiated segments of intestine. (IBA-1, 200X)

followed by a variable and dose-dependent latent period followed by manifest illness.[6] Apoptosis of myeloid precursors in bone marrow and peripheral leukocytes (particularly lymphocytes) leads to cytopenias.[6,11] Thrombocytopenia results in hemorrhage, while lymphopenia and neutropenia impair immune function.[6,11] Radiation induced gastrointestinal system leads to transmigration of bacteria and subsequent septicemia.[6] At higher levels of exposure, neurologic injury and hemorrhage injury occurs.[6,11]

The radiation exposure level required to induce clinical signs is variable between species and between individuals. The LD50/30, or the dose where 50% of animals survive 30 days without medical care, varies from as little as 2.5 Gy in swine to up to 10 Gy in Mongolian gerbils.[6] For reference, 1 Gy is approximately 300 times the annual background radiation exposure of a person in the US.[20]

Severity is of radiation injury is compounded when it is followed by or simultaneous with other trauma (i.e. thermal burns, wounds).[6,11] In a canine study, thermal burns covering 20% of the body resulted in minimal mortality, but when combined with 1 Gy exposure, burns of the same extent caused 73% mortality.[6] This compounded effect is attributed, at least in part, to delayed wound healing and acute immunosuppression from radiation injury.[6,11] The likelihood of polytrauma in radiation exposure secondary to nuclear weapon detonation is high: approximately 70% of atomic bomb survivors in Hiroshima and Nagasaki and 10% of Chernobyl nuclear accident survivors experienced combined injuries.[11]

Effects of acute radiation syndrome are considered deterministic, as exposure above a certain threshold produces these injuries consistently as a result of direct cellular damage and tissue reactions.[10] Deterministic effects may occur acutely or have a late onset.[10] Stochastic effects, on the other hand, tend to have a late onset and are the result of genetic damage. These do not occur as consistently as deterministic effects; rather, the incidence of disease increases proportionally with the degree of exposure. An example of a stochastic effect is an increased risk of cancer due to mutations in somatic cell DNA; hereditary effects also occur as a result of mutations in germline cells.[10]

Long term stochastic effects of radiation exposure have been extensively documented in the Life Span Study, a decades-long and ongoing study evaluating the medical outcomes of 93,741 atomic bombing survivors from Hiroshima and Nagasaki and 26,580 unexposed cohorts.[20] The earliest stochastic effect was an increase in rates of leukemia seen within two years of the bombings. Since then, the study has uncovered a significant linear and dose dependent increase in the occurrence of cancers in multiple locations, including the stomach, lung, liver, colon, thyroid, and skin.[20] Risks of death due to solid cancers, stroke, and heart disease are significantly increased in exposed individuals.[20] The study also found a decrease rate of growth in those who were 5-15 years old at the time of the bombings.[20]

References:

1. Boerma M, Wang J, Sridharan V, Herbert JM, Hauer-Jensen M. Pharmacological induction of transforming growth factor-beta1 in rat models enhances radiation injury in the intestine and the heart. *PLoS One*. 2013;8**:** e70479.
2. Booth C, Tudor G, Tudor J, Katz BP, MacVittie TJ. Acute gastrointestinal syndrome in high-dose irradiated mice. *Health Phys*. 2012;103**:** 383-399.
3. Chang PY, Zhang BY, Cui S, et al. MSC-derived cytokines repair radiation-induced intra-villi microvascular injury. *Oncotarget*. 2017;8**:** 87821-87836.
4. Cui M, Xiao H, Li Y, et al. Faecal microbiota transplantation protects against radiation-induced toxicity. *EMBO Mol Med*. 2017;9**:** 448-461.
5. Datta K, Suman S, Fornace AJ, Jr. Radiation persistently promoted oxidative stress, activated mTOR via PI3K/Akt, and downregulated autophagy pathway in mouse intestine. *Int J Biochem Cell Biol*. 2014;57**:** 167-176.
6. DiCarlo AL, Maher C, Hick JL, et al. Radiation Injury After A Nuclear Detonation: Medical Consequences and the Need for Scare Resources Allocation. *Disaster Med Public Health Prep*. 2011; 5 Suppl 1: S32-44.
7. Farrell CL, Bready JV, Rex KL, et al. Keratinocyte growth factor protects mice from chemotherapy and radiation-induced gastrointestinal injury and mortality. *Cancer Res*. 1998;58**:** 933-939.
8. Hauer-Jensen M, Denham JW, Andreyev HJ. Radiation enteropathy--pathogenesis, treatment and prevention. *Nat Rev Gastroenterol Hepatol*. 2014;11**:** 470-479.
9. Jian Y, Zhang D, Liu M, Wang Y, Xu ZX. The Impact of Gut Microbiota on Radiation-Induced Enteritis. *Front Cell Infect Microbiol*. 2021;11**:** 586392.
10. Kamiya K, Ozasa K, Akiba S, et al. Long-term effects of radiation exposure on health. *Lancet*. 2015; 386: 469-478.
11. Kiang JG, Olabisi AO. Radiation: a polytraumatic hit leading to multi-organ injury. *Cell Biosci*. 2019; 9(25):1-15.
12. Kulkarni S, Wang TC, Guha C. Stromal Progenitor Cells in Mitigation of Non-Hematopoietic Radiation Injuries. *Curr Pathobiol Rep*. 2016;4**:** 221-230.
13. Kumagai T, Rahman F, Smith AM. The Microbiome and Radiation Induced-Bowel Injury: Evidence for Potential Mechanistic Role in Disease Pathogenesis. *Nutrients*. 2018;10.
14. Kwak SY, Shim S, Park S, et al. Ghrelin reverts intestinal stem cell loss associated with radiation-induced enteropathy by activating Notch signaling. *Phytomedicine*. 2021;81**:** 153424.
15. Li M, Gu Y, Ma YC, et al. Kruppel-Like Factor 5 Promotes Epithelial Proliferation and DNA Damage Repair in the Intestine of Irradiated Mice. *Int J Biol Sci*. 2015;11**:** 1458-1468.
16. MacNaughton WK. Review article: new insights into the pathogenesis of radiation-induced intestinal dysfunction. *Aliment Pharmacol Ther*. 2000;14**:** 523-528.
17. Metcalfe C, Kljavin NM, Ybarra R, de Sauvage FJ. Lgr5+ stem cells are indispensable for radiation-induced intestinal regeneration. *Cell Stem Cell*. 2014;14**:** 149-159.
18. Pant V, Xiong S, Wasylishen AR, et al. Transient enhancement of p53 activity protects from radiation-induced gastrointestinal toxicity. *Proc Natl Acad Sci U S A*. 2019;116**:** 17429-17437.
19. Romesser PB, Kim AS, Jeong J, Mayle A, Dow LE, Lowe SW. Preclinical murine platform to evaluate therapeutic countermeasures against radiation-induced gastrointestinal syndrome. *Proc Natl Acad Sci U S A*. 2019;116**:** 20672-20678.
20. Sakata R, Grant EJ, Ozasa K. Long-term follow-up of atomic bomb survivors. *Maturitas*. 2012; 72: 99-103.

21. Sung J, Sodhi CP, Voltaggio L, et al. The recruitment of extra-intestinal cells to the injured mucosa promotes healing in radiation enteritis and chemical colitis in a mouse parabiosis model. *Mucosal Immunol*. 2019;12**:** 503-517.
22. Takemura N, Kawasaki T, Kunisawa J, et al. Blockade of TLR3 protects mice from lethal radiation-induced gastrointestinal syndrome. *Nat Commun*. 2014;5**:** 3492.
23. Wang Z, Wang Q, Wang X, et al. Gut microbial dysbiosis is associated with development and progression of radiation enteritis during pelvic radiotherapy. *J Cell Mol Med*. 2019;23**:** 3747-3756.
24. Wei L, Leibowitz BJ, Wang X, et al. Inhibition of CDK4/6 protects against radiation-induced intestinal injury in mice. *J Clin Invest*. 2016;126**:** 4076-4087.
25. Yang W, Sun Z, Yang B, Wang Q. Nrf2-Knockout Protects from Intestinal Injuries in C57BL/6J Mice Following Abdominal Irradiation with gamma Rays. *Int J Mol Sci*. 2017;18.
26. Zhu S, Liang J, Zhu F, et al. The effects of myeloablative or non-myeloablative total body irradiations on intestinal tract in mice. *Biosci Rep*. 2021;41.

CASE II:

Signalment:

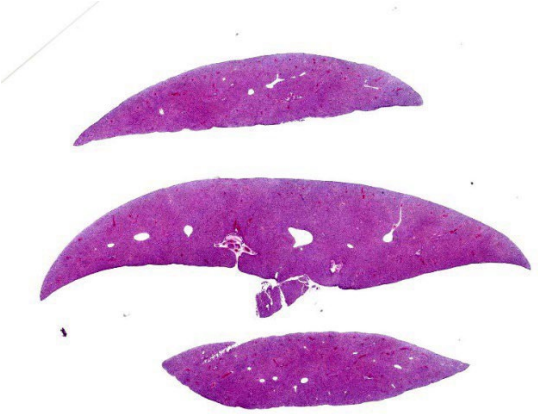

Figure 2-1. Liver, mouse. Three sections of the liver are submitted for examination. There are no changes evident at subgross magnification. (HE, 6X)

Three ~12-week-old male mice (*Mus musculus*) on a C57BL/6J background were evaluated.

History:
Mice were heterozygous knockouts for a gene involved in tRNA modification* and had no clinically detectable phenotype. The mutation had been generated in C57BL/6J mice (B6J) and backcrossed to wild-type B6J.
**The phenotype of this mutation is as yet unpublished, and permission has not been granted to reveal the specific gene.*

Gross Pathology:
Two of the three male mice had small livers at necropsy.

Laboratory Results:
No laboratory findings reported.

Microscopic Description:
In the livers of all three mice, portal veins were diffusely absent or small and slit-like. Portal triads frequently contained multiple hepatic arteriolar profiles (arteriolar reduplication), many of which had thickening of the tunica media. Periportal lymphatics were dilated and prominent and mild dilation of hepatic sinusoids was also present multifocally. Two of the three mice also had multifocal, random and perivascular small aggregates of infiltrating leukocytes, sometimes accompanied by focal loss or degeneration of hepatocytes. Infiltrating leukocytes consisted of mononuclear cells and, less frequently, neutrophils.

Contributor's Morphologic Diagnoses:
Liver:
1. Portal vein hypoplasia, diffuse, severe, with lymphatic ectasia and arteriolar reduplication
2. Mononuclear and neutrophilic infiltration, random and perivascular, mild

Contributor's Comment:

Portal vein hypoplasia is the histologic manifestation of intra or extrahepatic portosystemic shunting (PSS).[1,4] In dogs, the term microvascular dysplasia (MVD) has been used to describe histologic findings of PSS in the absence of a detectable shunt but, because the histology and pathogenesis of MVD overlap with that of congenital PSS, the morphologic diagnosis of portal hypoplasia is now preferred for both conditions according to the World Small Animal Veterinary Association.[4] Portal vein hypoplasia is characterized by absent or slit-like portal vein profiles and increased hepatic arteriolar profiles, or arteriolar reduplication. Arteriolar reduplication can occur with portal hypertension[6], however congenital PSS lacks portal hypertension and, as in this submission, associated changes of portal fibrosis may be absent. In PSS, arteriolar duplication may represent a compensatory response to decreased portal delivery of trophic factors to hepatocytes.[1]

Spontaneous congenital portosystemic shunting (PSS) with a microscopic appearance similar to this submission was recently described in a fairly high (~25%) number of C57BL6/J mice.[2] Affected mice were both transgenic and wild-type and originated from multiple different institutions, thus the finding was believed to be background strain-related. Shunting was not visible grossly and was confirmed by microscopy and by specialized imaging of blood flow through the liver. Based on shunt location (within the left side of the liver), pathogenesis was speculated to involve persistence of the ductus venosus (shunts blood from placenta to vena cava in the fetus). Inheritance was non-Mendelian and epigenetic alterations were suspected. As is typical of PSS in dogs, bilirubin, alanine aminotransferase (ALT), and aspartate aminotransferase (AST) remained within historic reference intervals, although affected

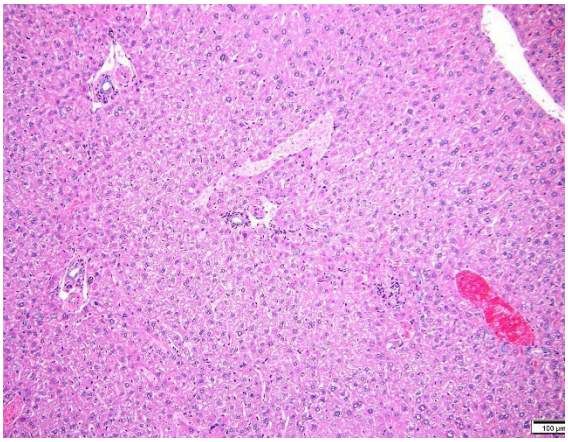

Figure 2-2. Liver, mouse. Hepatic lobules are decreased in size; portal triads are in close proximity. (HE, 100X) (Photo courtesy of: University of Michigan Unit for Laboratory Animal Medicine In Vivo Animal Core (IVAC) https://animalcare.umich.edu/business-services/vivo-animal-core)

mice had greater variation in AST and ALT. Bile acids may be more diagnostic but are not routinely performed in mice. Of note, affected mice were originally identified by an abnormal brain neurochemical profile (elevated glutamine) during screening by proton magnetic resonance spectroscopy. Glutamine is an end-product of ammonia detoxification by astrocytes in hepatic encephalopathy. Although symptoms of hepatic encephalopathy were not described, elevation of brain glutamine levels correlated with portosystemic shunting and may indicate some level of subclinical metabolic encephalopathy.[2] Thus, altered metabolism and/or neurochemistry in B6J mice with this defect may affect their suitability for research.

Based on this previous report, intrahepatic shunting may be more common than typically realized in mice and caution is warranted in specifically ascribing a finding of portal hypoplasia to genetic manipulation. In this submission, it was not possible to determine whether portal vein hypoplasia was related to the knockout gene, but spontaneous occurrence was suspected due to the background strain and the lack of a biologically plausible link between the knockout to the lesion. It is intriguing that the lesion was

present in 3 of 3 male but 0 of 3 female heterozygotes, however the knockout was not restricted to the liver nor was a sex-linked or liver-restricted phenotype expected. Other mice from the strain were not available for evaluation. No clinical signs suggestive of symptomatic portosystemic shunting (neurological symptoms, small size) were seen, although 2 of the male mice were noted to have small livers at necropsy.

Small foci of random or perivascular infiltrating leukocytes as seen in these mice are common murine background findings. Since they were occasionally accompanied by hepatocyte loss, they may have been exacerbated in this case by decreased trophic supply of nutrients to hepatocytes due to portal hypoplasia.

Contributing Institution:
University of Michigan Unit for Laboratory Animal Medicine In Vivo Animal Core (IVAC) https://animalcare.umich.edu/business-services/vivo-animal-core

JPC Diagnosis:
Liver, portal areas: Venous hypoplasia, multifocal.

JPC Comment:
The histologic appearance in this case is characteristic of portal vein hypoperfusion: decreased portal vein profiles, increased numbers of arteriolar profiles due compensatory hyperperfusion, and hepatocellular atrophy with irregularly spaced small portal triads. Portal vein hypoperfusion can also feature periportal fibrosis, biliary ductular reaction, and lipogranulomas.[3,4]

Portal vein hypoperfusion is the non-specific result of several distinct diseases. In many of these conditions, hypoperfusion is the result of portal hypertension, which can result in ascites, a useful distinguishing clinical characteristic. Examples of diseases which produce portal hypertension include arterioportal fistulas, obstruction of the portal vein, and primary portal vein hypoplasia.[4] Obstruction of the portal vein may occur due to thrombosis or neoplasia and leads to decreased portal blood flow and hypoperfusion. In arteriovenous fistulas, blood travels from a higher-

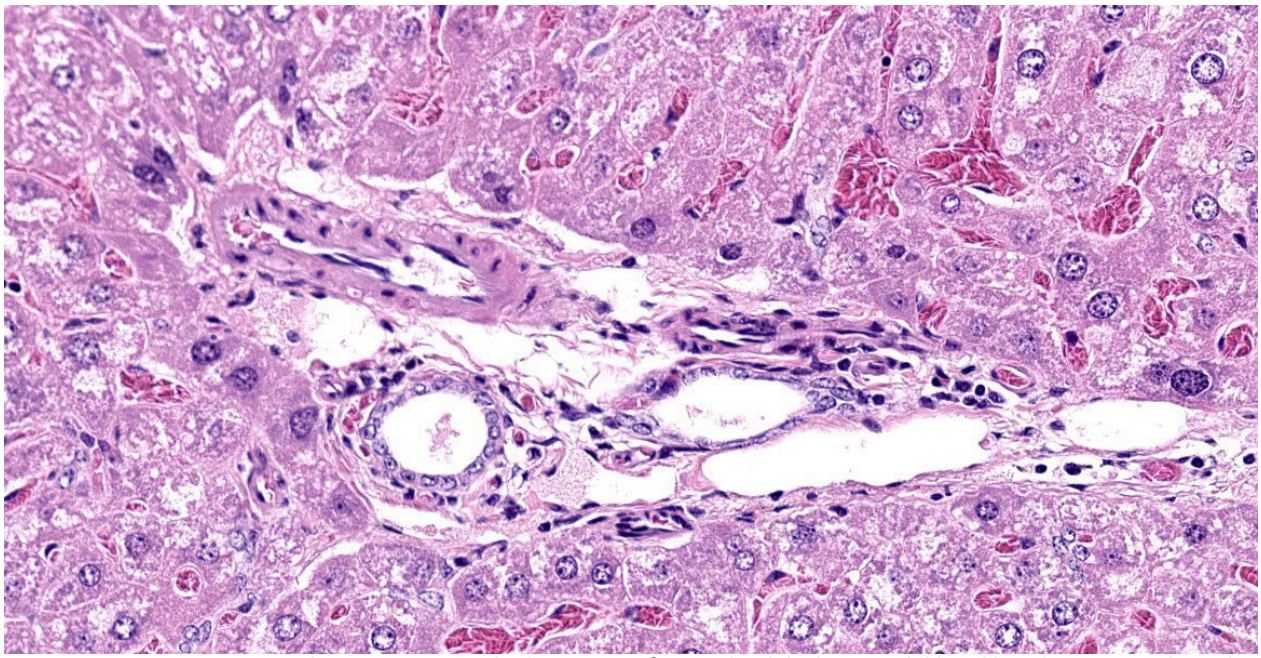

Figure 2-3. Liver, mouse. Portal areas contain multiple sections of arterioles, bile ducts, and dilated lymphatics. Portal venules are not evident. (HE, 381X)

pressure artery into the portal vein, leading to retrograde venous blood flow. While the directly affected lobe contains venous aneurysmal dilations and thick tortuous arteries, subsequent portal hypertension causes characteristic portal vein hypoperfusion in the unaffected lobes. Primary hypoplasia of the portal vein may occur in extrahepatic or intrahepatic locations. Some forms are mild, and histologic lesions are limited to those of hypoperfusion; moderate to severe forms are characterized by portal fibrosis and portal hypertension.

The end result of portal hypertension is acquired portosystemic shunting of blood, where blood flows through numerous enlarged and tortuous collateral veins to reach systemic circulation. Congenital portosystemic shunts, on the other hand, characteristically lack portal hypertension. The flow of blood bypasses the liver, traveling directly from portal vessels to the caudal vena cava or azygous vein and causing portal vein hypoperfusion.

Several features of portosystemic shunts in C57BL/6J mice were described in a recent study evaluating the effect of portal circulation in non-alcoholic fatty liver disease.[5] In PSS mice, the hepatic surface was faintly nodular and dull compared to normal livers.[5] Staining with pimonidazole, a hypoxia marker, revealed strong staining in the centrolobular region but negative staining in the portal regions, illustrating that arteriolar compensation for portal hypoperfusion was not able to fully oxygenate the distant centrolobular zone.[5] When given the hepatotoxin carbon tetrachloride, PSS mice had less hepatic injury than non-PSS mice.[5] This was previously reported to be due to decreased CYP2E1 expression; however, this study found CYP2E1 expression was increased in PSS mice and the authors speculated that decreased oxygen availability from hypoxia may have reduced free radical generation.[5]

The moderator described some of the portosystemic shunts may have on research studies, including smaller livers, altered neurochemical phenotypes, and altered metabolism of drugs and xenobiotics. Participants also discussed the hepatocellular anisokaryosis, particularly in the mid-zonal regions, which is an incidental aging change due to polyploidy.

References:

1. Baade S, Aupperle H, Grevel V, Schoon HA. Histopathological and immunohistochemical investigation of hepatic lesions associated with portosystemic shunting in dogs. *J Comp Pathol*. 2006;134:80-90.
2. Cudalbu C, McLin VA, Lei H, et al. The C57BL/6J mouse exhibits sporadic congenital portosystemic shunts. *PLoS One*. 2013; 8(7): e69782.
3. Cullen JM, Stalker MJ. Liver and biliary system. In: Maxie MG, ed. *Jubb, Kennedy and Palmer's Pathology of Domestic Animals*. Vol 2. 6th ed. St. Louis, MO: Elsevier Ltd; 2016:266-267,289-292
4. Cullen JM, van den Ingh TSGAM, Bunch SE, Rothuizen J, Washabau RJ, Desmet VJ: Morphological classification of the circulatory disorders of the canine and feline liver. In: *WSAVA Standards for Clinical and Histological Diagnosis of Canine and Feline Liver Diseases*. St. Louis, MO: Elsevier. 2006: 41-59, 97-98.
5. Meng L, Goto M ,Tanaka H, et al. Decreased Portal Circulation Augments Fibrosis and Ductular Reaction in Nonalcoholic Fatty Liver Disease in Mice. *Am J Pathol.* 2021; 191(9):1580-1591.
6. Nakhleh RE. The pathological differential diagnosis of portal hypertension. *Clinical Liver Disease*. 2017;10(3):57-62.

CASE III:

Signalment:
13-month-old, female-intact, Sprague-Dawley rat (*Rattus norvegicus)*

History:
Sentinel rat, presented with abdominal distention. On physical examination, the clinician palpated a freely moveable, large, firm mass within the peritoneal cavity.

Gross Pathology:
The animal is underconditioned (2/5 score). The right kidney is 2.834 g, the left kidney is 122.0 g. The mass is surrounded but not adhered to omentum. Approximately 90% of the right kidney is replaced by a 7 x 5.5 x 5 cm, discrete, encapsulated, semi-firm, pale-tan to brown to red, multilobular mass. On cut section, the mass is composed of smooth, homogeneous, pale-tan regions surrounding a friable, dark-red to brown core.

Laboratory Results:
Immunohistochemistry and special stains:
Vimentin: Strong, diffuse, cytoplasmic immunoreactivity of blastemal and stromal neoplastic populations. The primitive tubular epithelial structures are negative.

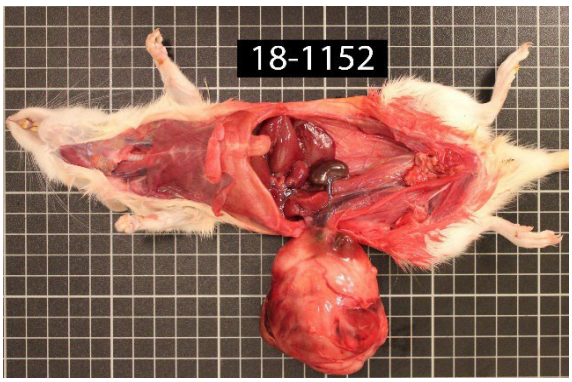

Figure 3-1. Kidney, rat. The right kidney is replaced by a multilobular, pale-tan to red to brown, irregular, smooth mass. Sprague-Dawley rat. (Photo courtesy of Laboratory of Comparative Pathology; Hospital for Special Surgery, Memorial Sloan Kettering Cancer Center, The Rockefeller University, Weill Cornell Medicine. https://www.mskcc.org/research-areas/programs-centers/comparative-medicine-pathology)

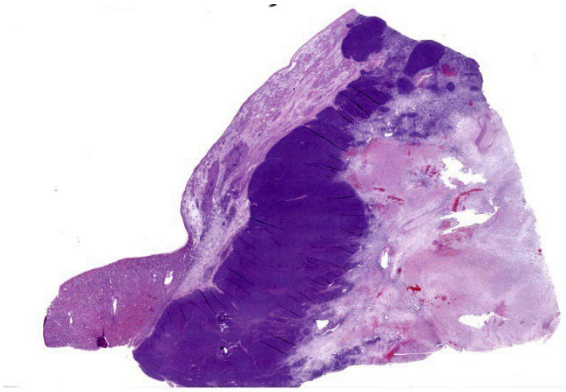

Figure 3-2. Kidney, rat. A section of kidney with a large unencapsulated mass is submitted for examination. (HE, 3X)

Cytokeratin wide-spectrum screening (WSS): Strong, diffuse, cytoplasmic immunoreactivity of tubular epithelial neoplastic cell populations. The blastemal and stromal components negative.

Wilms tumor protein (WT1): Moderate, diffuse, nuclear immunoreactivity of the blastemal with variable immunoreactivity of the stromal neoplastic population and rare, equivocal nuclear immunoreactivity of a few tubular structures.
N.b. Normal renal tubular and glomerular epithelium also has moderate, variable nuclear immunoreactivity.

Masson's Trichrome: Masson's trichrome confirms the presence of collagen within the tumor population (blue staining) and suggests differentiation into muscle (red staining).

Microscopic Description:
Arising from, compressing, and replacing approximately 50% of the renal parenchyma is a partially encapsulated, multilobular, ill-demarcated, expansile and densely cellular neoplasm that extends to cut borders. The neoplasm is composed of three haphazardly organized cell populations: epithelial, stromal and blastemal. The epithelial component is characterized by cuboidal to columnar cells which form tubules rimmed by a few layers of blastemal cells. The stromal population is

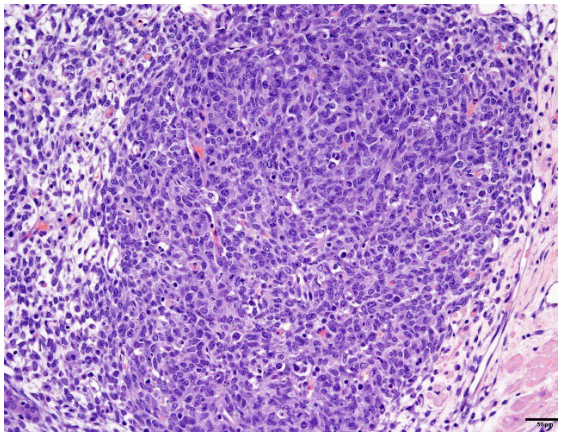

Figure 3-3. Kidney, rat. The blastemal population is composed of dense streams of basophilic polygonal cells with scant cytoplasm, and indistinct cell borders. (HE, 400X) (Photo courtesy of Laboratory of Comparative Pathology; Hospital for Special Surgery, Memorial Sloan Kettering Cancer Center, The Rockefeller University, Weill Cornell Medicine. https://www.mskcc.org/research-areas/programs-centers/comparative-medicine-pathology)

composed of fusiform cells arranged in bundles and are supported by a loose fibrovascular stroma. Multifocally, there is differentiation of the mesenchymal cells into collagen, striated and smooth muscle. The blastemal population is composed of dense streams of basophilic polygonal cells with scant cytoplasm, and indistinct cell borders. Anisocytosis and anisokaryosis are mild. The mitotic count in the blastemal population is high, but low in the other populations. The mass has large lakes of necrosis, hemorrhage, edema, fibrin and rare mineralization, admixed with large numbers of degenerate and non-degenerate neutrophils, macrophages, and lesser numbers of lymphocytes and plasma cells. Multifocally, vessels are partially occluded by fibrin thrombi. At the margins of the mass, scattered within the stromal population, are small numbers of misshapen, partially developed and variably sclerotic glomeruli, occasionally surrounded by an ectatic Bowman's space. Adjacent to these, there are small numbers of variably sized tubules, which are not surrounded by a rim of blastemal cells.

Contributor's Morphologic Diagnoses:

Kidney: Triphasic nephroblastoma with striated and smooth muscle differentiation (syn: Wilms Tumor)

Contributor's Comment:

A nephroblastoma, also known as a Wilms tumor (WT), is an undifferentiated, embryonal, mesodermal tumor with multipotent differentiation capabilities, that is thought to arise from the primitive renal stem cell.[14] It is the most common renal tumor in childhood.[9] In human pediatric patients, it is associated with germline and/or somatic mutations of the WT1 gene, but other genes are thought to be involved as well[3]. Precursor lesions of WT are so called nephrogenic rests and are defined as "a focus of abnormally persistent nephrogenic cells, meaning cells that can be induced to form a Wilms' tumor".[3]

Histologically, WT present with three distinct cell types: epithelial, stromal, and blastemal. All three elements are not required for diagnosis, but when all are present, the term "triphasic" is used. Heterologous components, including collagen, smooth muscle, skeletal muscle, cartilage, and bone may also

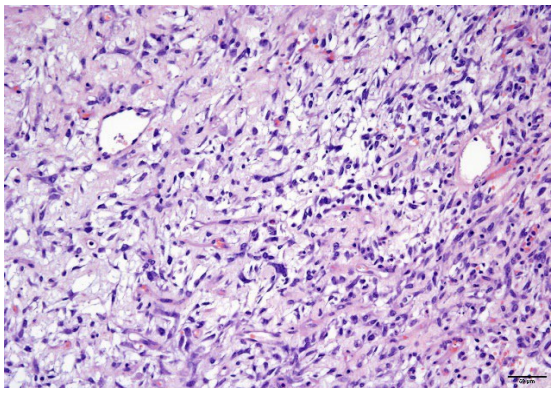

Figure 3-4. Kidney, rat. The stromal population is composed of fusiform cells arranged in bundles and are supported by a loose fibrovascular stroma. (HE, 400X) (Photo courtesy of Laboratory of Comparative Pathology; Hospital for Special Surgery, Memorial Sloan Kettering Cancer Center, The Rockefeller University, Weill Cornell Medicine. https://www.mskcc.org/research-areas/programs-centers/comparative-medicine-pathology)

be present. Zhuang et al. showed that the blastemal, epithelial, stromal, and other heterologous components of WT all have identical genetic changes, suggesting all features of this tumor are neoplastic.[21]

In laboratory animals, nephroblastomas have been frequently reported in rats, but are infrequent in mice and non-human primates.[4,6] In rats, nephroblastomas occur both experimentally and spontaneously. Experimentally, they can be induced by chemical administration of N-ethyl-N-nitrosurea or N-methyl-N-nitrosourea, both alkylating agents.[20] Spontaneously, they have been reported in Sprague-Dawley and F344 rats, with only rare reports of metastases to the lymph nodes and lungs.[5,18] No metastases were identified in our case.

The diagnosis of triphasic WT was based on the presence of blastemal, epithelial, and stromal components. Primitive tubular structures, surrounded by a rim of blastemal cells were identified, however, there was no evidence of primitive glomeruloid structures. In addition, there was widespread differentiation of the stromal components into striated

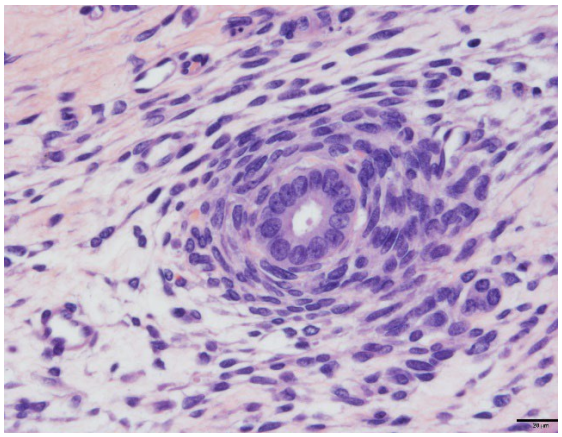

Figure 3-5. Kidney, rat. The epithelial component is characterized by cuboidal to columnar cells which form tubules rimmed by a few layers of blastemal cells. (HE, 400X) (Photo courtesy of Laboratory of Comparative Pathology; Hospital for Special Surgery, Memorial Sloan Kettering Cancer Center, The Rockefeller University, Weill Cornell Medicine. https://www.mskcc.org/research-areas/programs-centers/comparative-medicine-pathology)

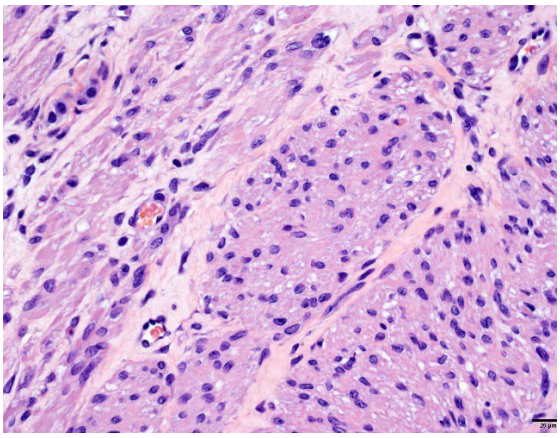

Figure 3-6 Kidney, rat. The stromal population has large areas with heterologous smooth muscle differentiation. (HE, 400X) (Photo courtesy of Laboratory of Comparative Pathology; Hospital for Special Surgery, Memorial Sloan Kettering Cancer Center, The Rockefeller University, Weill Cornell Medicine. https://www.mskcc.org/research-areas/programs-centers/comparative-medicine-pathology)

and smooth muscle, and collagen. The diagnosis of WT was aided by immunoreactivity of both blastemal and stromal populations with WT1, vimentin and immuno-negativity for cytokeratin WSS. The epithelial component was positive for cytokeratin, equivocally immunoreactive for WT1 and negative for vimentin. However, from our search, the veterinary literature is inconclusive regarding immunohistochemical profiles of these tumors, especially regarding the epithelial component. This may in part be due to the challenge in differentiating the epithelial population from the blastemal population, the choice of antibody, or the up/downregulation of certain proteins at different cellular developmental stages. In our case, the identification of epithelial components was simplified by the presence of discrete tubular structures, which were immunoreactive with cytokeratin WSS.

The main differential diagnosis for a WT is a renal mesenchymal tumor (RMT). RMTs arise from multipotential spindle-shaped mesenchymal cells, and, like WTs, can also give rise to heterologous components, such as smooth or skeletal muscle, fibrous tissue, cartilage and/or bone.[17] Further misleading

pathologists, profiles of hyperplastic tubules are frequently found in RMTs, but these are considered preexisting entrapped renal tubules, rather than newly formed. The pathognomonic feature of WTs is the population of blastemal cells, which are immediately apparent in our case.

Finally, the significance of multiple, individual, partially developed, and variably sclerotic glomeruli, as well as variably sized tubules within the stromal population at the margins of the tumor is not determined. We suspect these may represent normal renal structures that were entrapped and separated from the renal parenchyma at the early onset of neoplasia. However, we cannot exclude that they may have arisen *de novo*.

Contributing Institution:
Laboratory of Comparative Pathology; Hospital for Special Surgery, Memorial Sloan Kettering Cancer Center, The Rockefeller University, Weill Cornell Medicine.
https://www.mskcc.org/research-areas/programs-centers/comparative-medicine-pathology

JPC Diagnosis:
Kidney: Nephroblastoma.

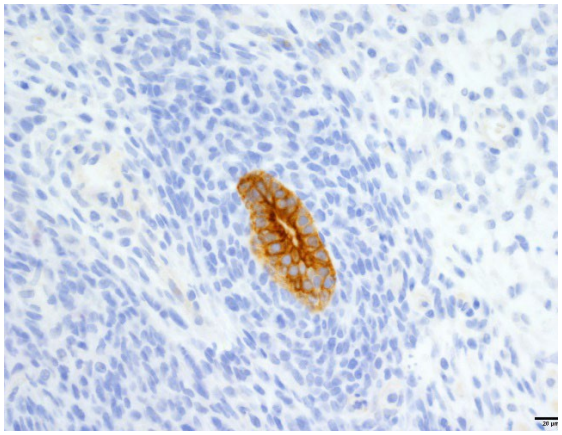

Figure 3-7. Kidney rat. The tubular structures formed by the epithelial population have strong cytoplasmic immunoreactivity, while the surrounding blastemal cells are negative. Cytokeratin WSS IHC.

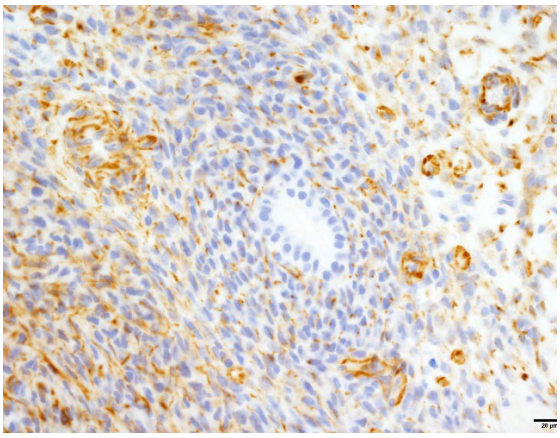

Figure 3-8. Kidney, rat. The blastemal and stromal populations have moderate cytoplasmic immunoreactivity, while the tubular structures of the epithelial population are negative. Vimentin IHC.

JPC Comment:
Nephroblastomas are the most common renal neoplasms in pigs, chickens, and fish.[13] In pigs, they generally exhibit a benign behavior.[13] Nephroblastomas also occur in a variety of other veterinary species, including dogs, cats, bovine fetuses, Japanese eels, guanacos, cottontail rabbits, and budgerigars.[1,8,10,16] In recent literature, a primary nephroblastoma was reported in the nasopharynx of a 3-month-old Boer goat, and unilateral stromal-type nephroblastomas were reported in the kidneys of two hedgehogs.[2,19]

In dogs, nephroblastomas are the third most common renal neoplasm, accounting for approximately 5% of renal neoplasia.[13] Up to 50% of canine nephroblastomas metastasize, and potential sites include the contralateral kidney, lung, liver, mesenteric lymph nodes, and spinal cord.[7] A recent report also described the first documented case of gingival metastasis in an 8 year old miniature Pinscher.[7] Primary spinal nephroblastomas also occur in young dogs, arising from nephrogenic rests between the dura and spinal cord, typically in the thoracolumbar region.[12] A recent report in a 1-year-old male American pitbull terrier documented multifocal spinal nephroblastomas arising in the thoracolumbar region, cervical intumescence, sacral

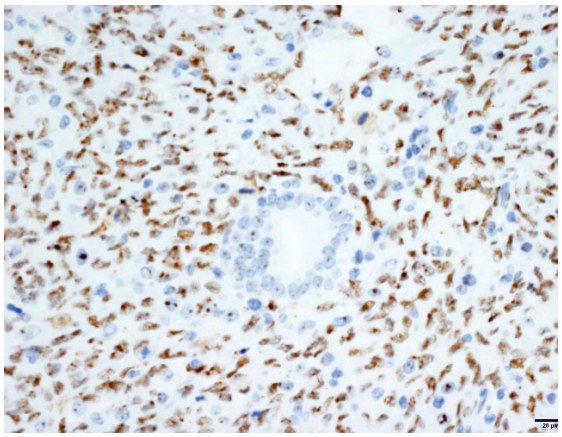

Figure 3-9. Kidney, rat. The blastemal population has moderate, nuclear immunoreactivity, while the nuclear immunoreactivity of tubular structures is equivocal and appears to correspond to reactivity of nucleoli. WT1 IHC.

segment, and cauda equina.[11] The authors believed that neoplastic seeding of the CNS resulted in the multifocal distribution, because vascular invasion was not observed but neoplastic cells expanded Virchow-Robbins spaces (which are continuous with the subarachnoid space).[11]

Differential diagnoses discussed by the contributor included renal cell carcinoma, renal mesenchymal tumor, amphophilic vacuolar tumor, renal sarcoma, and liposarcoma; diagnostic criteria for the tumors can be reviewed on the Global Open Registry Nomenclature Information System at goRENI.org.

References:

1. Agnew D. Camelidae. In: Terio KA, McAloose D, St. Leger J, eds. *Pathology of Wildlife and Zoo Animals.* San Diego, CA: Elsevier. 2018; 193.
2. Athey JM, Rice LE, Harvey AB, Washburn KE, Rodrigues-Hoffman A. Nasopharyngeal nephroblastoma in a 3-month-old Boer goat. *J Vet Diagn Invest.* 2021; 33(1):108-111.
3. Beckwith J, Bruce NB, Bonadio K. Nephrogenic rests, nephroblastomatosis, and the pathogenesis of Wilms' tumor. *Pediatr Pathol*. 1990; 10:1-36.
4. Castiglioni V, De Maglie M, Queliti R. Immunohistochemical characterization of a renal nephroblastoma in a trp53-mutant and prolyl isomerase 1-deficient mouse. *J Toxicol Pathol*. 2013; 26:423-427.
5. Chandra M, Carlton WW. Incidence, histopathologic and electron microscopic features of spontaneous nephroblastomas in rats. *Toxicol lett*. 1992; 62: 179-190.
6. Chandra M, Riley MGI, Johnson DE. Spontaneous renal neoplasms in rats. *J Appl Toxicol*. 1993; 13:109-116.
7. Chen B, Li W, Wang F. A blastema-predominant canine renal nephroblastoma with gingival metastasis: case report and literature review. *J Vet Diagn Invest*. 2018; 30(3): 430-437.
8. Delaney MA, Treuting PM, Rothenburger JL. Lagamorpha. In: Terio KA, McAloose D, St. Leger J, eds. *Pathology of Wildlife and Zoo Animals.* San Diego, CA: Elsevier. 2018; 486.
9. Dumba M, Jawad N, McHugh K. Neuroblastoma and nephroblastoma: an overview and comparison. *Cancer Imaging*. 2014; 14:O15.
10. Frasca Jr S, Wolf JC, Kinsel MJ, Camus AC, Lombardini ED. Osteichthyes. In: Terio KA, McAloose D, St. Leger J, eds. *Pathology of Wildlife and Zoo Animals.* San Diego, CA: Elsevier. 2018; 961.
11. Henker LC, Bianchi RM, Vargas TP, de Olveira EC, Driemer D, Pavarini SP. Multifocal Spinal Cord Nephroblastoma in a Dog. *J Comp Path*. 2018; 158: 12-16.
12. Higgins RJ, Bollen AW, Dickinson PJ, Siso-Llonch S. *Tumors of the Nervous System*. In: Meuten DJ, ed. Tumors in Domestic Animals. 5th ed. Ames, Iowa: Iowa State Press; 2017
13. Meuten DJ, Meuten TLK. Tumors of the urinary system. In: Meuten DJ, ed. *Tumors in Domestic Animals.* 5th ed. Ames, Iowa: Iowa State Press; 2017:646-649.

14. Pritchard-Jones K. Malignant origin of the stromal component of Wilms' tumor. *J Natl Cancer Inst*. 1997; 89:1089–1091.
15. Pritchard-Jones K, Vujanic G. Multiple pathways to Wilms tumor: how much is genetic?. *Pediatr Blood Cancer*. 2006; 47:232-234.
16. Reaville DR, Dorrenstein G. Psittacines, Coliiformes, Musophagiformes, Cuculiformes. In: Terio KA, McAloose D, St. Leger J, eds. *Pathology of Wildlife and Zoo Animals.* San Diego, CA: Elsevier. 2018; 784.
17. Seely JC. Renal mesenchymal tumor vs nephroblastoma: revisited. *J Toxicol Pathol*. 2004; 17: 131-136.
18. Tanaka, N, Takeshi I, Jyoji Y. Spontaneous nephroblastoma with striated muscle differentiation in an F344 rat. *J Toxicol Pathol*. 2017; 30:231-234.
19. Ueda K, Imada T, Ueda A, Imada M, Ozaki K. Stromal-type Nephroblastoma with or without Anaplasia in Two Hedgehogs. *J Comp Path*. 2019; 172: 48-52.
20. Yoshizawa K, Kinoshita Y, Emoto Y. N-Methyl-N-nitrosourea-induced Renal Tumors in Rats: Immunohistochemical Comparison to Human Wilms Tumors. *J Toxicol Pathol*. 2014; 26:141-148.
21. Zhuang Z, Merino MJ, Vortmeyer AO. Identical genetic changes in different histologic components of Wilms' tumors. *J Natl Cancer Inst*. 1997; 89:1148-52.

CASE IV:

Signalment:
Adult, female, Sprague Dawley rat, *Rattus norvegicus*

History:
The animal was in the control group on a 5-week general toxicology study. The animal was dosed with vehicle via oral gavage and had no notable clinical signs.

Gross Pathology:
There were no significant gross lesions.

Laboratory Results:
There were no abnormalities on urinalysis, serum chemistry, or hematology.

Microscopic Description:
In a section of kidney, at the junction of the medulla and cortex are multifocal areas of proliferative stellate to polygonal blastemal cells separating and infiltrating between normal fully developed tubules supported by a small amount of fine fibrovascular stroma. The blastemal cells have a small amount of pale basophilic cytoplasm, have indistinct cell borders, and are arranged in streams, nests, rosettes, and irregular tubules. The tubules are lined by a single layer of epithelial cells or are piled haphazardly. The cells have ovoid nuclei with finely stippled chromatin and 1-3 nucleoli. There are 1-2 mitoses per high power (400x) field. Small numbers of lymphocytes infiltrate these areas. Adjacent areas of the medulla and cortex appear unaffected.

Contributor's Morphologic Diagnoses:
Kidney: Multifocal nephroblastematosis

Contributor's Comment:
Nephroblastematosis is a spontaneous/incidental lesion that can be encountered in rats

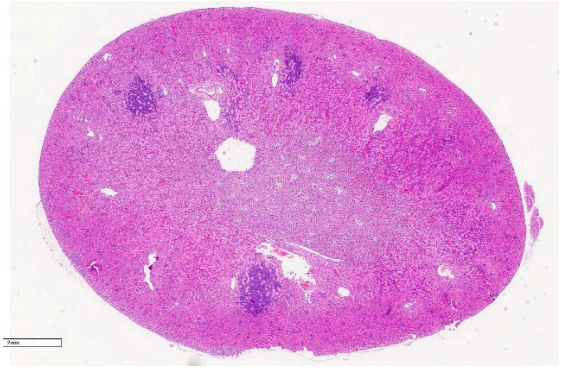

Figure 4-1. Kidney, rat. One section of kidney is submitted for examination. There are multiple hypercellular foci within the cortex. (HE, 5X) (Photo courtesy of: Charles River Laboratories, Mattawan, MI)

in toxicologic studies.[2] This condition is also known as nephroblastomatosis, blastemal rest, nephrogenic rest, or intralobar nephroblastematosis and has been reported in rats, dogs, and human children.[2,5,6,7] Nephroblastematosis can be encountered in any age of rat and may have the potential to develop into nephroblastomas as the lesions enlarge; thus, they are regarded as preneoplastic lesions.[1,2,6,7] These lesions are not grossly apparent, and by the time the lesions are large enough to be observed grossly, they are more consistent with a diagnosis of nephroblastoma.[7]

As described, the lesions are composed of microscopic masses at the corticomedullary junction composed of dense blastemal cells with scant basophilic cytoplasm and basophilic nuclei (Figure 1).[2] There may be rare renal organoid differentiation into rosettes, glomeruloid structures and tubules (Figure 2).[2] Adjacent pars recta tubules may have mitotic figures, which is an autocrine response to the blastema.[1] These lesions usually do not cause severe disruption of the surrounding kidney architecture, though may be associated with dilated tubules.[7]

Nephroblastoma is the main differential for this lesion, though the delineation between these findings appears arbitrary and based on size and degree of organoid differentiation such as more tubules and glomerular structures.[2,7] Nephroblastematosis also usually presents with a multifocal nature, as in this case.[2]

In humans, nephrogenic rests are differentiated into incipient, dormant, involuting, hyperplastic, or neoplastic rests.[1,5] Incipient rests have microscopic evidence of proliferation or maturation and are seen in infants.[5] Dormant rests are present in older people and may remain unchanged for years.[1,5] Involuting, also known as sclerosing or obsolescent, rests are composed of a well-formed tubule lined by a single layer of low-cuboidal epithelium surrounded by dense collagen, and may eventually disappear.[1,5] Hyperplastic rests exhibit proliferation in diffuse or focal areas and may progress to grossly apparent masses.[1] Neoplastic rests are those in which neoplastic transformation occurs within single cells of the rest which go on to produce Wilms tumor.[1] These rests can also be separated into perilobar or intralobar nephrogenic rests.[1] Perilobar nephrogenic rests occur at the periphery of the lobe, whereas intralobar rests occur anywhere within the lobe.[1] In humans, intralobar nephrogenic rests have been associated with loss or mutation of the WT1 gene.[1]

Some authors refer to nephroblastematosis in rats, which have a unilobar kidney, as intralobar nephroblastematosis as the blastemal cells occur within the lobule at the corticomedullary junction.[7] While some authors consider the terms nephroblastematosis and nephroblastomatosis to be synonymous, others consider the terminology nephroblastomatosis to represent multiple grossly apparent nephroblastomas.[2,7] Nephroblastematosis is the preferred terminology by the International Harmonization of Nomenclature and Diagnostic Criteria for Lesions in Rats and Mice (INHAND) Project and Standardization for Exchange of Nonclinical Data (SEND).[2]

Contributing Institution:
Charles River Laboratories, Mattawan, MI

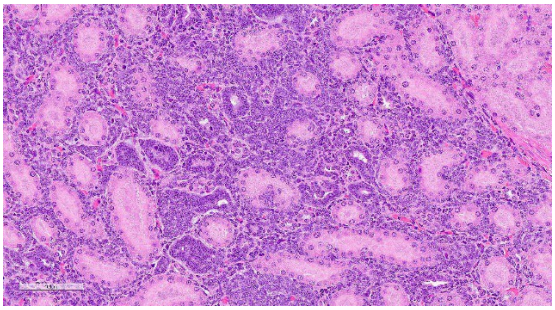

Figure 4-2. Kidney, rat. Tubules are surrounded and separated by blastemal cells. (HE, 200X) (Photo courtesy of: Charles River Laboratories, Mattawan, MI)

JPC Diagnosis:
Kidney: Nephroblastematosis, multifocal.

JPC Comment:
The contributor provides a thorough description of an uncommonly documented lesion in veterinary species, and this case of nephroblastematosis provides a glimpse of pre-neoplastic changes which may have proceeded the nephroblastoma from Case 3 of this conference.

Nephroblastematosis was first described in a 1961 report of a premature human infant at 32 weeks gestation.[4] The cortical surfaces were enlarged and slightly lobulated, and they kidneys were histologically consistent with 14-16-week gestational age, with blastemal cells surrounding areas of stroma, tubules, and glomeruli. [4] In that case, both kidneys were diffusely affected, but it is now known that nephroblastomatosis more commonly occurs focally or multifocally. [4] During normal embryogenesis, migration of the ureteric bud into the metanephric blastema induces development of glomeruli, nephrons, and stroma. [4] Defects earlier in nephrogenesis result in the failure of differentiation in intralobular nephrogenic rests, while later defects result in persistent perilobular rests. [4] Nephroblastematosis occurs when nephrogenic rests persist beyond 34-36 weeks gestation in humans. [4] Nephrogenic rests are found in approximately 1% of all human pediatric autopsies, with perilobar the most common location. [4] All nephrogenic rests

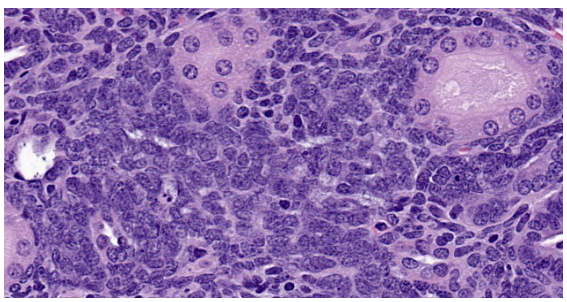

Figure 4-3. Kidney, rat. High magnification of blastemal cells. (HE, 400X)

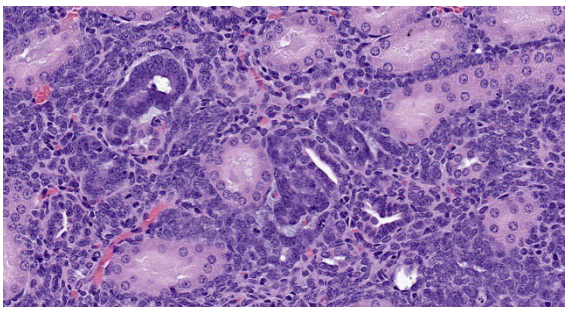

Figure 4-4. Kidney, rat. Blastemal cells multifocal differentiate into tubules. (HE, 400X)

have the potential to become neoplastic, either as adenomas (i.e. metanephric adenoma or adenofibroma) or nephroblastomas. [4] In humans, however, regression is much more common, and only approximately 1% progress to neoplasia. [4]

As the contributor alludes to, differentiating nephroblastomatosis and nephroblastoma is challenging. In humans, nephrogenic rests generally have irregular margins, lack encapsulation, may have foci of sclerosis between rests, whereas nephroblastomas are generally round with pseudoencapsulation and may lack sclerosis.[4] Pre-existing non-neoplastic blastema may be found along the periphery of nephroblastomas.[4] Conference participants remarked about the presence of irregular tubules which could lead a pathologist to diagnose nephroblastoma, but elected to follow criteria from human literature described above.

Reports of nephroblastematosis are very rare in veterinary species, and the contributor covers this condition in rats well. Additionally, nephroblastomatosis has also been described as an incidental finding in a single cynomolgus macaque.[3]

References:

1. Beckwith JB. Nephrogenic rests and the pathogenesis of Wilms tumor: Developmental and clinical consideration. *Am J Med Genet.* 1998;79:268-273.
2. Frazier KS, Seely, JC, Hard GC, et al. Proliferative and nonproliferative lesions

of the rat and mouse urinary system. *Tox Pathol.* 2012;40:14S-86S.
3. Goens SD, Moore CM, Brasky KM, et al. Neprhoblastomatosis and nephroblastoma in nonhuman primates. *J Med Primatol.* 2005; 34: 165-170.
4. Hennigar RA, O'Shea PA, Grattan-Smith JD. Clinicopathologic features of nephrogenic rests and nephroblastomatosis. *Adv Anat Pathol.* 2001; 8(5):276-89.
5. Jackson CB and Kirkpatrick JB. Nephrogenic rest in a Crl:CD (SD)IGS BR rat. *Vet Pathol*. 2002;39:588-589.
6. Kelaiselvan P, Mathur KY, Pande VV, et al. Intralobar nephroblastematosis in a nine-week-old Wistar rat. *Tox Pathol.* 2009;37:819-825.
7. Mesfin GM. Intralobar nephroblastematosis: Precursor lesions of nephroblastoma in the Sprague-Dawley Rat. *Vet Pathol.* 1999;36:379-390.

WSC 2022-2023 Self-assessment
Conference 15

1. True or false? The enteric biome plays a significant role in the intestine's response to radiation injury.
    a. True
    b. False
    c.
2. Spontaneous congenital portosystemic shunting has recently been described in which of the following mouse strains?
    a. C57BlL6/J
    b. 129/J
    c. CD-1
    d. NOD/SCID

3. In animals with microvascular dysplasia, which is the following is either markedly hypoplastic or absent?
    a. Veins in portal triads
    b. Arterioles in portal triads
    c. Lymphatics in portal triads
    d. None of the above

4. Which of the following is not a cell type seen in nephroblastoma?
    a. Mesenchymal
    b. Epithelial
    c. Stromal
    d. Blastemal

5. True or false? Nephroblastematosis is considered a preneoplastic lesion
    a. True
    b. False

Please email your completed assessment for grading to Dr. Bruce Williams at bruce.h.williams12.civ@mail.mil. Passing score is 80%. This program (RACE program 33611) is approved by the AAVSB RACE to offer a total of 0.5 CE Credits, with a maximum of 12.5 CE Credits being available to any individual Veterinary Medical Professionals for the 2019-2020 Wednesday Slide Conference. This RACE approval is for the subject matter categories of: SCIENTIFIC using the delivery method of NONINTERACTIVE DISTANCE. This approval is valid in jurisdictions which recognize AAVSB RACE.

Joint Pathology Center
Veterinary Pathology Services

WEDNESDAY SLIDE CONFERENCE 2022-2023

Conference #16 **18 January 2023**

CASE I:

Signalment:
11-year-old, intact male, snow leopard (*Panthera uncia*)

History:
The animal was diagnosed with COVID-19 via PCR and was doing well until an acute decline. Frank hemorrhage exuded from the nares, and blood was present on rectal.

Gross Pathology:
Gross Description: A moderate amount of dark red, dried blood was adhered to the fur around both nares. The thoracic cavity contained 164 mL of serosanguinous, semi-translucent fluid with few strands of fibrin. The lungs were red to dark red, wet, and edematous. Scattered throughout the lung were few tan to white mottled, nodular to multinodular masses, the largest of which was 4.0 cm x 3.2 cm x 2.7 cm. Similar nodules were present within the heart, bulging from the left atrioventricular endocardium and extending into the myocardium. The cortex and medulla of both kidneys were also expanded by numerous randomly scattered tan, bulging, masses like those within the lung and heart.

Laboratory Results:
1. Thoracic radiographs: Bilateral alveolar pattern of the caudodorsal lung fields
2. Covid-N rRT-PCR: Positive
3. In situ hybridization with v-SARS-CoV-2-N-01 (N gene) probe of lung, nasal, and tracheal sections: Distinct punctate staining in rare sloughed epithelial cells within nasal passages, in cells within alveoli (macrophages and/or sloughed epithelial cells), and within rare pneumocytes lining alveoli. These findings confirm the presence of SARS-CoV-2 RNA within tissue sections, albeit at low levels.

4.18 s rRNA PCR Sequencing of FFPE Lung tissue: 99.70% identity to *Scedosporium apiospermum*

Microscopic Description:
Lung: Scattered throughout the lung parenchyma are multiple large nodules composed of a core of eosinophilic and karyorrhectic cell debris mixed with abundant fibrin, some edema, and hemorrhage. Cores are surrounded by a dense rim of numerous necrotic

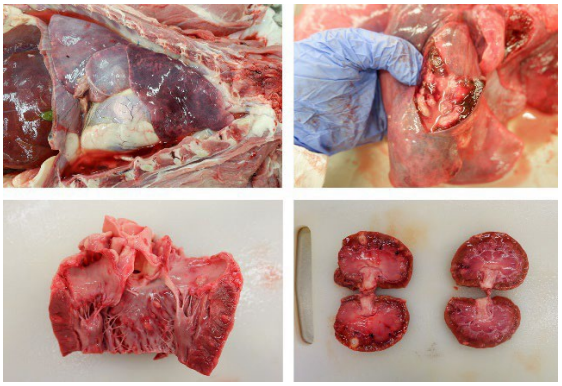

Figure 1-1. Multiple organs, snow leopard. White nodules are scattered throughout the lung, endocardium, and kidneys. (Photo courtesy of: (Photo courtesy of: University of Illinois at Urbana-Champaign, Veterinary Diagnostic Laboratory)

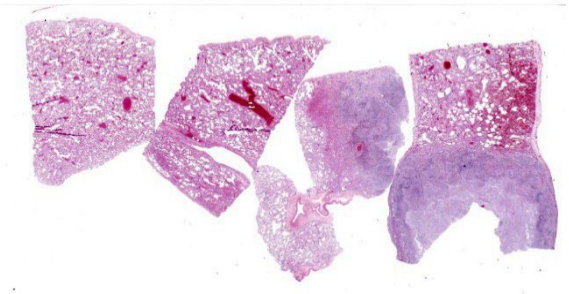

Figure 1-2. Lung, snow leopard. Two sections of lung (right) contain a large nodule of necrosis and inflammation which obscures pulmonary parenchyma. (HE, 7X)

neutrophils and epithelioid macrophages mixed with fewer lymphocytes and plasma cells. Throughout the necrotic cores and extending into the inflammatory rim are numerous fungal hyphae that are 3-6 µm wide with parallel walls, regular septations, dichotomous acute angle branching, and bulbous dilatations (presumptive ascomycete fungus). Throughout these nodules, septal vessels often contain thrombi composed of layers of lamellated fibrin. In many areas, septa are coagulatively necrotic, characterized by maintained architecture with diffuse hypereosinophilic and loss of nuclear detail. Rarely, necrotic debris is mineralized. Many alveolar septa are expanded by congestion, eosinophilic fibrillar material (fibrin), clear and colorless space (edema) and foamy macrophages; some septa contain smooth muscle hypertrophy and hyperplasia. Type 1 pneumocytes are often absent and replaced by deeply eosinophilic lamellar material (hyaline membranes). In some areas type 1 pneumocytes are replaced by cuboidal epithelium which segmentally lines alveolar spaces (type 2 pneumocyte hyperplasia). Alveolar spaces are frequently filled with variable combinations of foamy macrophages, eosinophilic proteinaceous material (edema), extravasated erythrocytes, fibrin, and neutrophils. Similar accumulations are present in many bronchioles and bronchi.

Other histopathology findings that are not included in the provided slide:

- Multifocal, chronic, pyogranulomatous necrotizing encephalitis, myocarditis, nephritis, and bilateral retinitis and choroiditis, with left eye scleritis and posterior uveitis, with intralesional hyphae
- Moderate, diffuse, chronic rhinitis with fibrosis
- Moderate, multifocal to coalescing, lymphoplasmacytic tracheitis with erosions and ulcerations

Contributor's Morphologic Diagnoses:

1. Lung: Marked, subacute interstitial pneumonia with type-2 pneumocyte hyperplasia and hyalin membrane formation, and marked hemorrhage and edema
2. Lung: Marked, multifocal, chronic, pyogranulomatous necrotizing pneumonia with intralesional hyphae.

Contributor's Comment:

Two main processes are identified in this animal, which contributed to death. The first is significant alveolar damage and interstitial inflammation accompanied by abundant pulmonary edema and hemorrhage, which is histologically compatible with SARS-CoV2 infection. The pathophysiologic mechanisms of COVID-19 are incompletely understood, however direct effects are primarily limited to the lung, while systemic disease occurs via

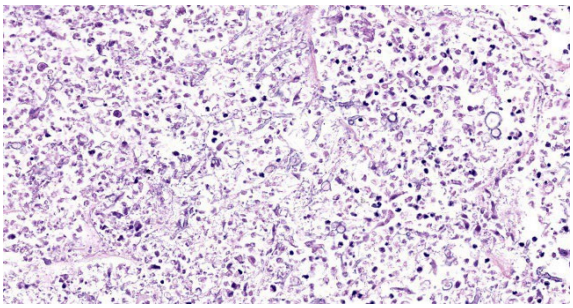

Figure 1-3. Lung, snow leopard. Within the area of necrosis, there are numerous 4-6 µm septate dichotomously branching fungal hyphae with bulbous swelling. (HE, 381X)

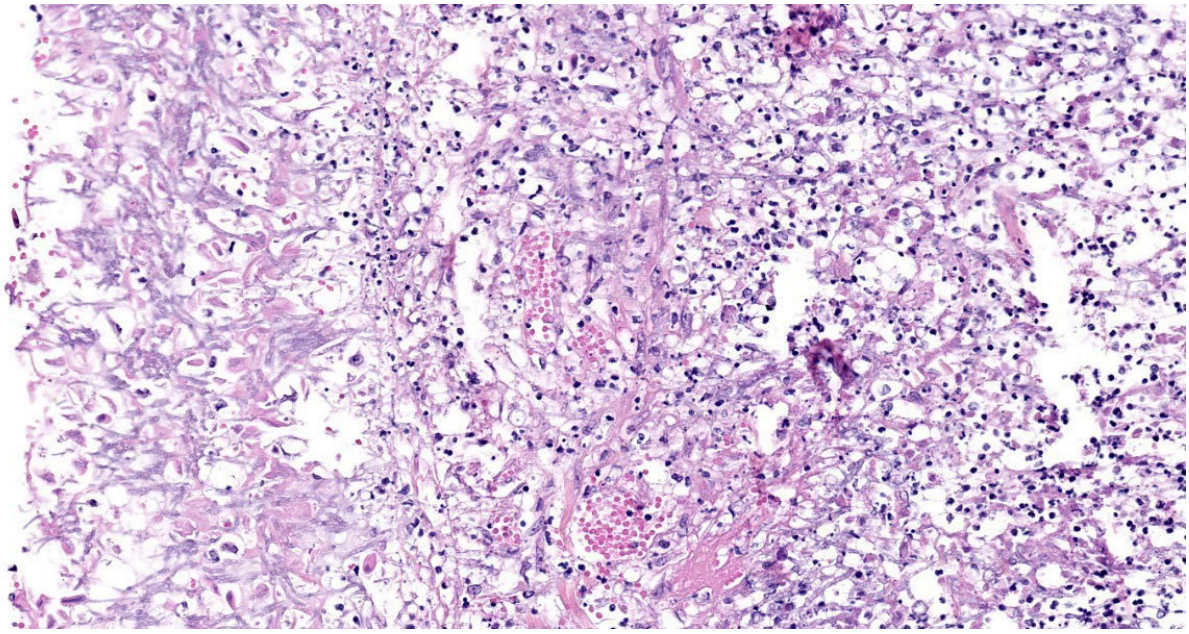

Figure 1-4. Lung, snow leopard. A large mat of fungal hyphae expands the pleura and extends into the pleural space (at left). (HE, 265X)

secondary effects.[2] Within humans, the histopathologic lesions associated with severe COVID-19 are consistent with Diffuse Alveolar Damage (DAD) secondary to Acute Respiratory Distress Syndrome (ARDS). DAD is not specific for COVID-19, and can be induced by various causes, including mechanical ventilation, various pulmonary infections, thermal injury, toxic gas exposure, and septicemia.[3]

The exact appearance of DAD will vary depending on the chronicity. An acute, exudative phase occurs during the first week after pulmonary injury, and is characterized by congested alveolar septa, and alveoli filled with copious protein-rich edema and fibrin. Inflammation is generally low unless DAD is the result of previous pneumonia. The formation of hyalin membranes—aggregates of fibrin, other serum proteins, and cell debris which line alveoli and alveolar ducts, impeding the junction between the airspace and the septum—is an important characteristic histologic finding.[3,10] Over time, DAD will progress into an organizing or proliferative phase, characterized by interstitial proliferation of fibroblasts and myofibroblasts, accompanied by type 2 pneumocyte hyperplasia and squamous metaplasia.[2] Microvascular thrombi are also frequently seen with COVID-19, however it is speculated that this lesion is more associated with ARDS than COVID-19 specifically.[2]

COVID-19 has been seen within multiple animal species, including domestic cats, domestic dogs, tigers, lions, gorillas and snow leopards (USDA Confirmed Cases of SARS-CoV-2 in animals in the United States). A recent study has shown that domestic cats (*Felis catus*) can be utilized as an infection model for COVID-19, displaying similar clinical and histopathologic as in humans.[13] COVID-19 viral infection and replication within a host depends on the presence and distribution of angiotensin-converting enzyme 2 (ACE2) receptors.[2] The ACE2 receptor within cats is similar in structure and distribution to humans, which may contribute to the similarities in clinical and histologic findings.[13] It has not been studied if these same principles apply to large felids such as snow

leopards. Within this case, interstitial and alveolar changes within the lung are consistent with a sub-acute DAD response transitioning between the exudative phase and proliferative phase. While there are multiple differentials for a DAD response within this animal, in situ hybridization confirms COVID-19 infection within the epithelial cells of the nasal passages and rare pneumocytes of the alveoli.

The second process in this case consists of severe pyogranulomatous and necrotizing lesions throughout multiple organs, including the lung, brain, heart, kidneys, and the choroid and retina of both eyes. Sequencing of the fungal organisms within these lesions identifies it as *Scedosporium apiospermum*, an opportunistic filamentous fungus found worldwide.[6] Once considered the asexual form of *Pseudoallescheria boydii,* recent taxonomic changes upon introduction of molecular phylogenetics places *S. apiospermum* within the *Scedosporium* genus, where it is the most pathogenic of the included species.[4,14] *S. apiospermum* is of increasing importance in human medicine, where it can cause severe systemic infections within immunocompromised and immunocompetent patients. Rare cases of both localized and disseminated infections have been reported in various animal species, including the dog, cat, horse, and a stranded northern elephant seal.[1,4,8,9]

Diagnosis of a *Scedosporium* infection is difficult due to clinical and histopathologic similarities to *Aspergillus, Fusarium,* and other hyalin hyphomycetes.[7] Subtle histologic differences between *Scedosporium* and *Aspergillus* do exist, including slightly more irregular branching within *Scedosporium* vs the more regular and dichotomous branching pattern of *Aspergillus*. Additionally, *Scedosporium* will commonly have terminal or intercalary, globose chlamydospores, thick-walled structures up to 20um in diameter which can be confused with yeasts.[7] These differences are subtle, and further testing such as in situ hybridization, culture, or molecular sequencing are important for definitive diagnosis. It is likely that *Scedosporium* is underdiagnosed in veterinary medicine due

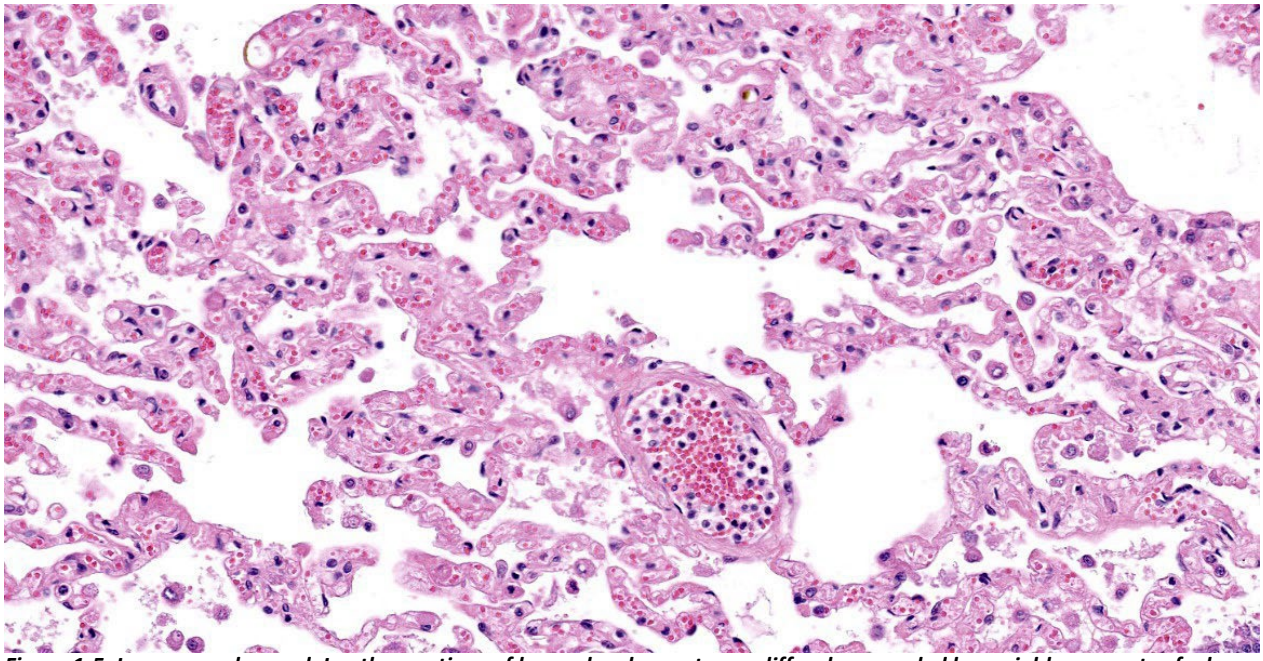

Figure 1-5. Lung, snow leopard. In other sections of lung, alveolar septa are diffusely expanded by variable amounts of edema, congestion, fibrin, and few Type II pneumocytes. There is mild alveolar edema and low numbers of alveolar macrophages (HE, 251X)

to its similarities to other fungal species.[4] Definitive diagnosis of *Scedosporium* is important, due to differences in antifungal resistance profile from *Aspergillus*.[6]

In this case, it is speculated that the primary COVID-19 infection led to immunocompromise of the animal, and systemic opportunistic infection by *Scedosporium apiospermum*, demonstrating both the importance of COVID-19 within the snow leopard species, and the growing importance of *Scedosporium apiospermum* within veterinary medicine.

Contributing Institution:
University of Illinois at Urbana-Champaign, Veterinary Diagnostic Laboratory

JPC Diagnosis:
1. Lung: Pneumonia, interstitial, necrotizing, subacute, diffuse, marked, with septal thrombosis, hemorrhage, and type II pneumocyte hyperplasia.
2. Lung: Pleuropneumonia, pyogranulomatous and necrotizing, multifocal, severe, with innumerable fungal hyphae.

JPC Comment:
A review of recent literature demonstrates that experimental severe acute respiratory syndrome coronavirus 2 (SARS-CoV2) infection in domestic cats can produce a spectrum of clinical disease and histologic lesions. As the contributor describes, one possible outcome is diffuse alveolar damage, as described by Rudd et al in a 2021 *Viruses* article.[13] In Rudd's study, the virus was inoculated directly into the trachea of 12 nine-month-old specific pathogen free (SPF) cats; six cats were used as controls.[13] Inoculated cats developed clinical signs of illness, including lethargy, fever, and dyspnea, and histologic evidence of diffuse alveolar damage.[13]

In a prior study, Gaudreault et al inoculated 6 five-month-old SPF cats with a slightly larger volume of the same strain of virus, but through nasal and oral routes.[5] These animals remained asymptomatic but transmitted the virus to co-housed, uninfected animals.[5] Histopathologic findings were minimal to moderate and localized to conducting airways, with lymphocytic and neutrophilic inflammation of the tracheobronchial seromucous glands which resolved by 21 days post challenge.[5]

Finally, a more recent study published by Patania et al in *Vet Pathol* described a different pattern of interstitial pneumonia with occlusive bronchiolitis in experimentally infected cats.[12] Ten SPF cats, ages 19 to 24 week, were inoculated by a different viral strain through intraocular, intranasal, tracheal, and oral routes.[12] No control cats were used. The cats remained asymptomatic, but on histology, there was patchy interstitial pneumonia, histiocytic bronchiolitis, and persistent interstitial thickening. Most of the cats lacked diffuse alveolar damage.[12] Bronchiolar lumens were often occluded by adherent plugs of epithelioid macrophages.[12] Early in the disease, interstitial and alveolar septal thickening was partially attributed to a mixed inflammatory infiltrate composed of B lymphocytes, T lymphocytes, and macrophages.[12] Once the inflammation resolved, interstitial thickening persisted and was attributed to endothelial hyperplasia, proliferative and disorganized capillaries, and individualized type II pneumocyte hyperplasia only appreciable with cytokeratin IHC; fibrosis was not a feature in thickened septae.[12] One of the three cats evaluated at 28 days post-challenge had more severe changes, including atelectasis, vasculitis, and inflammatory exudates and fibrin within alveoli.[12]

The differences in the results of these studies illustrate the wide range of lesions which may

be induced by experimental SARS-CoV2 infections in cats, and differences in study design (routes of inoculation, challenge dose, viral strain used) and individual host responses may account for these results.

Invasive fungal diseases (IFD) secondary to SARS-CoV-2 infection occur with relative frequency in hospitalized human patients.[11] Up to 7.6% of hospitalized COVID-19 experience pulmonary aspergillosis due to *Apsergillus fumigatus*, and this coinfection has a mortality rate of 56%.[11] Other documented coinfections include candidiaisis and mucormycosis, most commonly due to *Rhizopus.*[11] There are multiple possible reasons why COVID-19 patients are more susceptible to fungal infections, including tissue damage, immune dysfunction, and individual host factors or preexisting conditions. Viral infection impairs mucocilliary clearance and causes local tissue damage, exposing hidden host receptors permissive to fungal invasion.[11] Viral induced lymphopenia, depletion and dysfunction of dendritic cells, and local hypoxia attenuate the immune response to fungal invasion; this can be exacerbated by the use of immunsuppressive agents prescribed for controlling the overwhelming inflammatory response.[11] Chronic viral infection leads to decreased numbers of CD8+ T cells and NK cells, and remaining cells may demonstrate an ineffective and immune-exhausted phenotype (expressing PD1 and NKG2A, respectively) which create risk factors for IFB.[11] COVID-19 may also cause impaired fungicidal activity by neutrophils, leading to impaired innate immunity.[11]

References:

1. Berzina I, Trumble NS, Novicki T, et al. Subconjunctival mycetoma caused by *Scedosporium apiospermum* infection in a horse. *Vet Clin Pathol*. 2011; 40(1):84-88.
2. Caramashi S, Kapp ME, Miller SE, et al. Histopathological findings and clinicopathologic correlation in COVID-19: a systematic review. *Mod. Pathol.* 2021; 34:1614-1633.
3. Caswell JL, Williams KJ. Respiratory System. In: Maxie MG, ed. *Jubb, Kennedy, and Palmer's Pathology of Domestic Animals.* Vol 2. 6th ed. St. Louis, MO: Elsevier; 2016.
4. Di Teodoro G, Averaimo D, Primavera Miria, et al. Disseminated *Scedosporium apiospermum* infection in a Maremmano-Abruzzese sheepdog. *BMC Vet Res*. 2020: 16(2):372.
5. Gaudreault NN, Trujillo JD, Carossino M. SARS-CoV-2 infection, disease and transmission in domestic cats. *Emerg Microbes Infect*. 2020; 9(1): 2322-2332.
6. Goldman C, Akiyama MJ, Torres J, et al. *Scedosporium apiospermum* infections and the role of combination therapy and GM-CSF: A case report and review of the literature. *Med. Mycol Case Rep.* 2016; 11:40-43.
7. Guarro J, Kantarcioglu AS, Horre R, et al. *Scedosporium apiospermum*: a changing clinical spectrum of a therapy-refractory opportunist. *Med. Mycol*. 2006; 44(4):295-327.
8. Haulena M, Buckles E, Gulland FMD, et al. Systemic mycosis caused by *Scedosporium apiospermum* in a stranded northern elephant seal (*Mirounga angustirostris*) undergoing rehabilitation. *J. Zoo Wildl Med. 2002;* 33(2):166-171.
9. Leperlier D, Vallefuoco R, Laloy E, et al. Fungal rhinosinusitis caused by *Scedosporium apiospermum* in a cat. *J Feline Med Surg*. 2010; 12:697-971.
10. Montero-Fernandez MA, Pardo-Garcia R. Histopathology features of the lung in COVID-19 patients. *Diagn Histopathol*. 2021; 27(3):123-127.

11. Morton CO, Griffiths JS, Loeffler J, Orr S, White PL. Defective antifungal immunity in patients with COVID-19. *Front Immunol.* 2022; 13:1-11.
12. Patania OM, Chiba S, Halfmann PJ, et al. Pulmonary lesions induced by SARS-CoV-2 infection in domestic cats. *Vet Pathol*. 2022; 59(4): 696-706.
13. Rudd JM, Selvan MT, Cowan S, et al. Clinical and histopathologic features of a feline SARS-CoV-2 infection model are analogous to acute COVID-19 in humans. *Viruses.* 2021;13(8):1550.
14. Taylor A, Talbot J, Bennett P, et al. Disseminated *Scedosporium prolificans* infection in a Labrador retriever with immune mediated haemolytic anaemia. *Med Mycol Case Rep*. 2014; 6:66-69.

CASE II:

Signalment:
Juvenile, male intact, bobcat (*Lynx rufus*)

History:
The bobcat presented to a wildlife rehabilitation center for right hind lameness, dehydration, and emaciation. The bobcat initially improved with therapy but after a couple of weeks of hospitalization deteriorated rapidly and died.

Gross Pathology:
The spleen was slightly enlarged with a meaty consistency and had multifocal, sparse, pinpoint, white foci throughout the parenchyma. The retropharyngeal, mesenteric and renal lymph nodes were moderately to markedly enlarged and on the cut surface had many white to pale tan foci. The liver was brown and had multifocal, pinpoint to 0.1 cm white foci throughout the parenchyma. The right distal tibia was slightly expanded by a bony proliferation (interpreted as callus). The abdominal cavity contained approximately 40 ml of yellow, transparent, viscous to slightly gelatinous fluid.

Laboratory Results:
Immunohistochemistry:
Feline coronavirus antigen specific immunohistochemistry performed on the section of ileum was negative.

Bacteriology:
Francisella tularensis was isolated from the liver by aerobic culture.

Molecular diagnostics:
The isolated bacteria were confirmed to be *Francisella tularensis* type A based on PCR.

Microscopic Description:
Ileum – Multifocally, Peyer's patches are largely effaced by variably-sized, central areas of eosinophilic cellular and basophilic karyorrhectic debris admixed with degenerate neutrophils (lytic necrosis) which are surrounded by moderate to large numbers of epithelioid macrophages. Multifocally infiltrating the surrounding submucosa are moderate numbers of lymphocytes, plasma cells, neutrophils and macrophages. The outer longitudinal lamina muscularis is multifocally effaced by small areas of lytic necrosis and cellular debris, and within the inner circular lamina muscularis there are multifocal, often perivascular clusters of lymphocytes, plasma

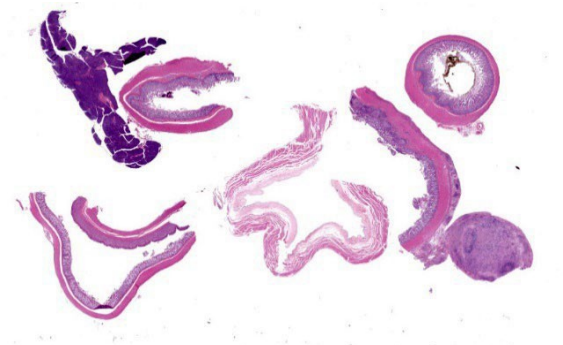

Figure 2-1. Multiple organs, bobcat. A selection of organs is submitted on this individual. The tissue of interest is a section of ileum with attached lymph node (right). (HE, 6X)

cells, neutrophils and macrophages. The attached mesentery is multifocally effaced by large areas of lytic necrosis as well as moderate numbers of lymphocytes, plasma cells and macrophages with fewer neutrophils, admixed with fibrillar, brightly eosinophilic material (fibrin). Within the mucosa there is a reduced density of crypts, with widespread blunting of villi and expansion of the lamina propria with moderate numbers of neutrophils and fewer lymphocytes, plasma cells and macrophages. Within the superficial mucosa and intestinal lumen are multifocal small colonies of mixed bacteria, as well as moderate numbers of apicomplexan coccidian organisms in various developmental stages, including: few schizonts containing numerous basophilic, elongate merozoites; numerous uninucleate, eosinophilic macrogametes; numerous oocysts containing pale eosinophilic granular material; and rare large microgamonts with numerous condensed, basophilic nuclei.

Mesenteric lymph node – The mesenteric lymph node associated with the ileum is markedly expanded and almost completely effaced by a large, central area of lytic necrosis as previously described, admixed with macrophages, neutrophils, and fibrin. Few small to moderately sized aggregates of mature lymphocytes and plasma cells remain scattered throughout the section.

Contributor's Morphologic Diagnoses:
1. Ileum:
a. Ileitis, pyogranulomatous and necrotizing, multifocal, severe, chronic.
b. Intraepithelial coccidian organisms, moderate.

2. Mesenteric lymph node, lymphadenitis, pyogranulomatous and necrotizing, widespread, severe, chronic.

Contributor's Comment:
Francisella tularensis, the causative agent of tularemia, is a gram negative, obligate aerobe, intracellular coccobacillus of the gamma-subclass of Proteobacteria.[10,12] There are currently 4 recognized subspecies: subspecies *tularensis* (type A), which is highly

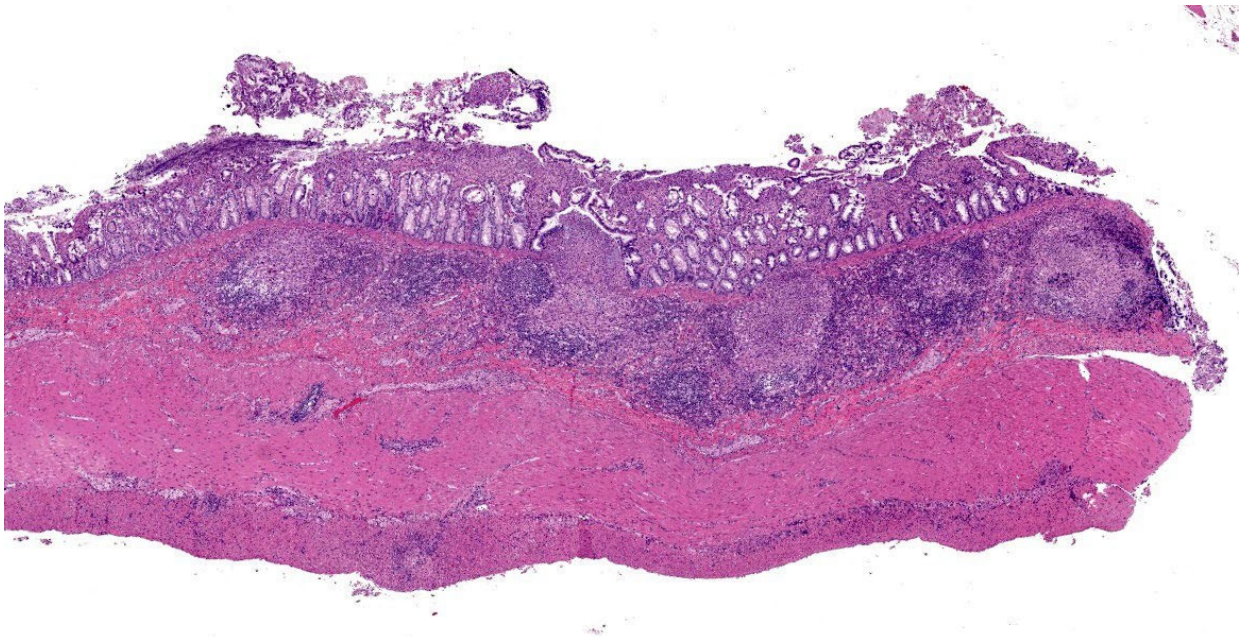

Figure 2-2. Ileum, bobcat. There are changes in all layers of the wall. There is ulceration of the mucosa and marked cellular infiltration of the underlying lamina propria. There is marked necrosis of the submucosal Peyer's patches. There is necrotizing vasculitis and lymphangitis of the muscularis and serosa. (HE, 32X)

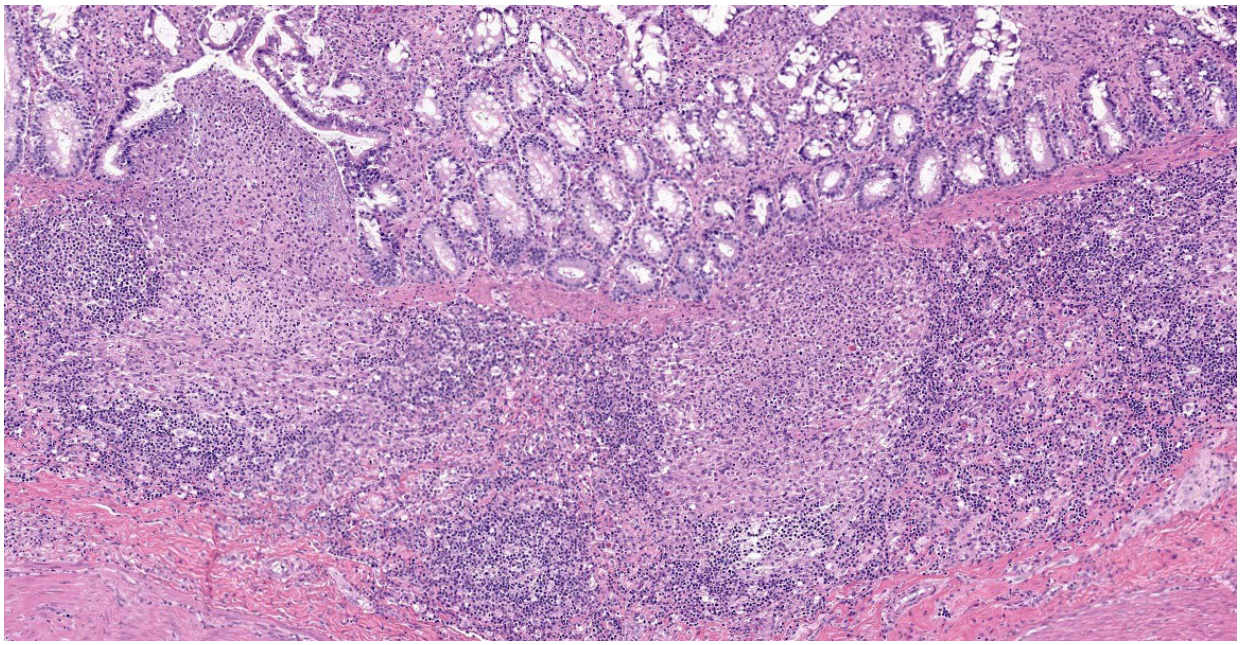

Figure 2-3. Ileum, bobcat. There is marked lymphoid depletion and focal necrosis within the ileal Peyer's patch) (HE, 88X)

virulent in domestic animals and humans, predominantly found in North America, and is most commonly associated with lagomorphs; subspecies *holarctica* (type B), which is less virulent, endemic throughout the Northern Hemisphere, and more frequently associated with rodents and waterborne disease; subspecies *novicida*, which is mostly avirulent in humans and predominantly found in North America; and subspecies *mediasiatica*, which is also considered to be avirulent in humans and predominantly found in Russia and central Asia.[11] The type A subspecies is further divided into 2 distinct subpopulations, A1 and A2. In the USA, A1 subpopulations occur primarily in the eastern half of the country while A2 subpopulations occur primarily in the west.[9]

F. *tularensis* has a wide and varied range of hosts, with a list of known susceptible species including 190 mammals, 88 invertebrates, 23 birds and 3 amphibians, with occasional reports in reptile and fish species.[6] Although lagomorphs and rodents are frequently implicated in the spread and maintenance of this disease, there has been no evidence to suggest that they act as a major reservoir.[7,12] Transmission to humans can occur via a number of different routes, including handling of infected animals, ingestion of improperly cooked infected meat or contaminated water, inhalation of infective aerosols, and arthropod bites.[9] Important arthropod vectors for transmitting *F. tularensis* in the USA include hard ticks, deer flies, stable flies and horseflies. Of those, hard ticks are considered to be the primary vectors for type A strains; ticks of the *Ambylomma* and *Dermacentor* genera are typically responsible for human cases while ticks of the *Ixodes* and *Haemophysallis* genera are more important in maintaining enzootic foci among wildlife.[4,9] Sheep are historically considered to be the domestic mammal most commonly associated with tularemia type A, however, in the past few decades domestic cats have become an increasing source for zoonotic transmission.[4]

Gross lesions in affected animals typically involve miliary white foci within the spleen, liver and lymph nodes, as well as splenomegaly, hepatomegaly and lymphadenopathy.[8] These lesions are grossly indistinguishable from the lesions caused by *Yersinia* species. Histologically, these white foci are composed

of multifocal areas of lytic necrosis, admixed with degenerate neutrophils and/or surrounded by macrophages and fibroblasts in older lesions. *F. tularensis* bacteria are generally difficult to visualize histologically in routine H&E and even Gram-stained sections, whereas *Yersinia* species bacteria tend to be readily visible.

In this bobcat, there was a translucent, straw colored, viscous, serofibrinous abdominal effusion, reminiscent of the effusion which characterizes the wet form of feline infectious peritonitis (FIP). In the submitter's experience, this is an atypical finding for tularemia. Therefore, and because bacteria were not detected within the lesions, immunohistochemistry for feline coronavirus antigen was performed on the section of ileum; however, coronaviral antigen was not detected within any of the cells in the section.

The coccidian organisms within the lumen of this bobcat's ileum were morphologically most similar to *Cystoisospora felis*. In a recent paper, *C. felis*-like organisms were found in feces of 2 bobcats and transmitted to domestic cats.[2] Unlike *C. felis* in domestic cats which develops within the villar epithelium, the schizonts and gamonts of these *C. felis*-like coccidia were located within the lamina propria of the ileum, indicating that they are likely to be a similar but different parasite to *C. felis* of domestic cats. In our

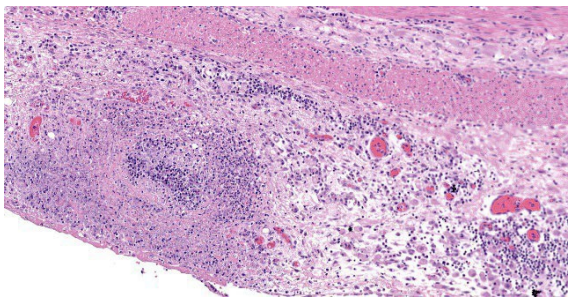

Figure 2-4. Ileum, bobcat. There is necrotizing vasculitis and diffuse inflammation and edema within the serosa. (HE, 173X)

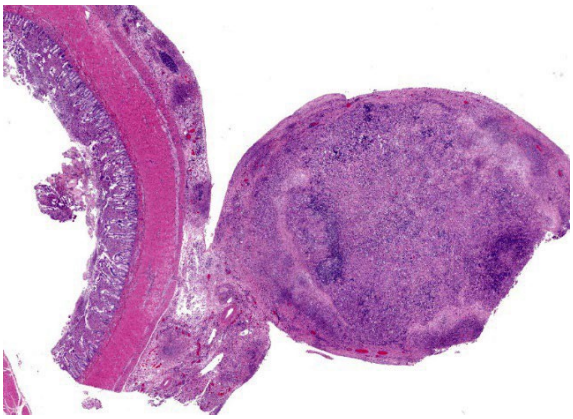

Figure 2-5. Mesenteric lymph node, bobcat. There is diffuse necrosis and loss of nodal architecture. (HE, 15X)

bobcat's case, it is difficult to assess the organisms' location with certainty due to the significant blunting and disruption of the villi. In addition, the significance of the mixed colonies of bacteria within the intestinal lumen is unknown. While they may have contributed to the suppurative ileitis, it is also possible that they represent an intraluminal 'bystander' population.

F. tularensis is a tier 1 agent on the US Department of Health and Human services biological select agents list as it has the potential to pose a severe threat to public health and safety.[3] As a consequence of being on this list, there are strict regulations involved when handling *F. tularensis*. The agent and all tissues that contain the agent must be destroyed, and this destruction must be reported. Appropriate personal protective equipment (PPE) should be worn when this agent is suspected, including gloves and a cut-resistant glove, an impermeable apron, lab boots, a face shield, and a respirator such as a properly fitted N95 mask.

Contributing Institution:
Veterinary Diagnostic Laboratory, University of Minnesota, St Paul, MN.
https://vdl.umn.edu/

JPC Diagnosis:
1. Ileum: Ileitis, necrotizing, diffuse, moderate, with multifocal vasculitis and Peyer's patch necrosis.
2. Mesenteric lymph node: Lymphadenitis, necrotizing, diffuse, severe.
3. Mesentery, vessels: Vasculitis, necrotizing, severe.
4. Ileum: Coccidial gamonts and oocysts, multiple.
5. Pancreas and adipose tissue: Zymogen granule depletion and fat atrophy.

JPC Comment:
During the conference, the participants and moderator, COL(R) Derron (Tony) Alves, remarked on the marked vasculitis along the serosa and within the mesentery and prominent reactive mesothelium suggestive of abdominal effusion. Before knowing the clinical history and laboratory results, participants considered the possibility of FIP based on these histologic lesions, but the contributor ruled this out using immunohistochemical staining. Participants also had spirited discussion regarding inflammation surrounding areas of lymphoid necrosis in Peyer's patches and lymph nodes; some felt this would qualify as pyogranulomatous inflammation, while others felt that the remaining cells represented residual dendritic cells associated with lymphoid follicles.

In 1909, a researcher investigating bubonic plague in squirrels in California discovered a novel bacterium which caused enlarged lymph nodes.[5] The bacteria was dubbed *Bacterium tularense*, reflecting where it was discovered – Tulare county. This new bacterium was not directly contagious but could be transmitted via infected blood, tissue, or fleas. [5] The first confirmed infection in a human occurred in a butcher in Ohio in 1911. [5] In the early 1920s, researchers in Montana conducting wood tick surveillance for Rocky Mountain Spotted Fever discovered that

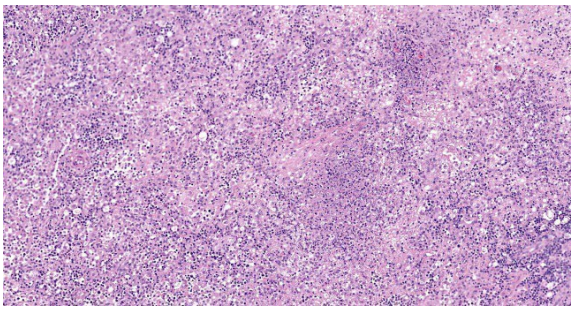

Figure 2-6. Mesenteric lymph node, bobcat. There is marked lymphoid depletion, tingible body macrophages, and multifocal areas of lytic necrosis within the submitted node. (HE, 125X)

some ticks were infected with *B. tularense* and could pass this infection to animals. [5] Furthermore, these ticks could transmit the bacterium transovarially and would remain infected for life. [5]

Around the same time, Edward Francis began his research in Utah on "Deer Fly Fever", a condition in humans caused by *B. tularense* featuring fever, lymphadenitis, and draining tracts from affected nodes.[5] In 1928, Francis published a thorough report on 629 human cases of *B. tularense*, and the bacterium was later renamed *Francisella tularense* in acknowledgement of his extensive research.[5] This rechristening was also fitting in that Francis was frequently affected by the disease himself: he was infected at least five times during his life, likely due to his reluctance to wear gloves during autopsies.[5]

Of the cases reported by Francis, 400 were attributed to contact with rabbits, and 70 were attributed to tick bites.[5] The disease had an incubation period of less than 10 days and resulted in acute fever with two to three months of convalescence.[5] The most common clinical presentation was the ulceroglandular form, as an ulcer formed at the site of exposure and regional lymphadenitis resulted in a draining tract over the inflamed "gland".[5] Other reported forms included oculoglandular (where conjunctival exposure resulted in

conjunctivitis, corneal ulceration, and regional lymphadenitis), glandular form (similar to ulceroglandular form without cutaneous lesions), and typhoidal (systemic disease lacking ocular, cutaneous, and lymph node involvement).[5] Additional forms subsequently described include an oropharyngeal form and pneumonia.[5]

F. tularensis is a facultative intracellular parasite which can survive and replicate in a variety of host cells, including macrophages, dendritic cells, neutrophils, endothelial cells, type II pneumocytes, and hepatocytes.[1] The pathogencity of *Francisella* is associated with intracytoplasmic replication within macrophages.[13] The bacteria induces phagocytosis by binding to mannose receptors; the C3 complement receptor, scavenger receptor A, nucleolin, or lung surfactant protein A once opsonized; or the Fcγ receptor once antibody-opsonized.[1] The microbe survives within the phagosome by delaying phagosome maturation, inhibiting NADPH oxidase activation, and resisting the effects of reactive oxygen species.[1,13] While other bacteria which live in the cytosol use lipid hydrolases or phospholipases to escape the phagosome (such as *Listeria*), *Francisella* is unique in that it likely uses a type VI secretion system for phagosome egress.[1,13] The bacterium then uses "nutritional virulence" to adapt to the cytosolic environment.[13] *Francisella* LPS has low endotoxicity and is not recognized by TLR4; rather, the bacteria triggers TLR2 signaling, activates both the AIM-2 and NLRP3 inflammasomes, and ultimately results in production of proinflammatory cytokines IL1 beta and pro-IL8.[1] Apoptosis or pyroptosis of infected cells leads to liberation of the bacteria, which can then infect new cells.[1,13] The bacteria can also directly penetrate adjacent cells using trogocytosis.[13]

References:

1. Celli J, Zahrt TC. Mechanisms of *Francisella tularensis* Intracellular Pathogenesis. *Cold Spring Harb Perspect Med*. 2013; v.3(4):1-14.
2. Dubey JP, Houk AE, Verma SK, Calero-Bernal R, Humphreys JG, Lindsay DS. Experimental transmission of C*ystoisospora felis*-like coccidium from bobcat (*Lynx rufus*) to the domestic cat (*Felis catus*). *Vet Parasitol*. 2015;211(1-2):35-39.
3. Federal Select Agent Program, US Department of Health and Human Services, accessed May 31, 2022. <https://www.selectagents.gov/>
4. Friend M. *Tularemia*. Circular 1297. U.S. Geological Survey; 2006
5. Hirschmann JV. From Squirrels to Biological Weapons: The Early History of Tularemia. *Am J Med Sci.* 2018; 356(4): 319-328.
6. Keim P, Johansson A, Wagner DM. Molecular epidemiology, evolution, and ecology of *Francisella*. *Ann N Y Acad Sci*. 2007;1105:30-66.
7. Lamps LW, Havens JM, Anders S, Page DL, Scott MA. Histologic and molecular diagnosis of tularemia: a potential bioterrorism agent endemic to North America. *Mod Pathol.* 2004;17:489-495.
8. Maxie MG, Jubb KVF, Kennedy PC, Palmer N. *Jubb, Kennedy, and Palmer's Pathology of Domestic Animals*. Elsevier Saunders; 2007.
9. Petersen JM, Mead PS, Schriefer ME. *Francisella tularensis*: an arthropod-borne pathogen. *Vet Res*. 2009;40(2):7.
10. Quinn PJ, Markey BK, Leonard FC, Fitz-Patrick ES, Fanning S, Hartigan PJ. *Veterinary Microbiology and Microbial Disease*. John Wiley & Sons; 2011.
11. Timofeev V, Titareva G, Bahtejeva I, et al. The comparative virulence of *Francisella tularensis* subsp. *mediasiatica* for vaccinated laboratory animals. *Microorganisms*. 2020;8(9):1403.

12. World Health Organization. *WHO Guidelines on Tularemia*. WHO Press; 2007.
13. Ziveri J, Barel M, Charbit A. Importance of Metabolic Adaptations in *Francisella* Pathogenesis. *Front Cell Infect Microbiol*. 2017; 7(96): 1-8.

CASE III:

Signalment:
2-month-old male entire Domestic Shorthair (*Felis catus)*

History:
A two-month-old kitten owned for 10 days with a history of diarrhoea and vomiting for the past 24 hours, presented with hypoglycaemia and agonal breathing. Arrested, cardiopulmonary resuscitation performed for 20 minutes, and owner consented for cessation.

Gross Pathology:
At postmortem examination, the lungs are mottled pale pink to dark red, spongy, with a bullous appearance to all distal margins (marginal emphysema) and have variably pale pink, approximately 0.8 cm wide linear discolouration (rib impressions, presumed related to CPR noted in history). The stomach contains a small amount of pale brown-green, pasty ingesta. The orad small intestines contain moderate amounts of thin, yellow fluid that transitions to pale cream digesta within the jejunum and scant cream-yellow digesta within the ileum. The colon contains pale brown, flocculent, variably mucoid, and watery faeces, and pale brown pasty faeces are within the rectum. The mesenteric lymph node is enlarged (4.0 x 1.2 x 0.3 cm, within normal limits for a kitten), and the ileocecal and colonic lymph nodes are similarly prominent.

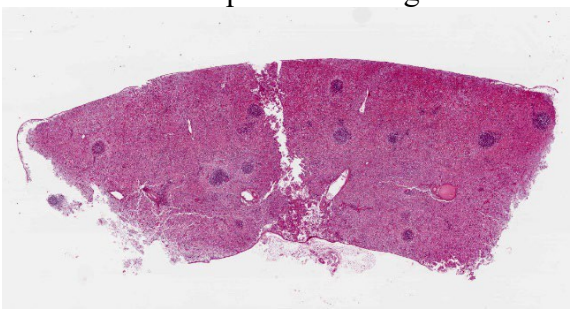

Figure 3-1. Spleen, cat. A section of markedly congested spleen is submitted for examination. White pulp is diffusely and markedly depleted and lacks mantle formation. (HE, 6X)

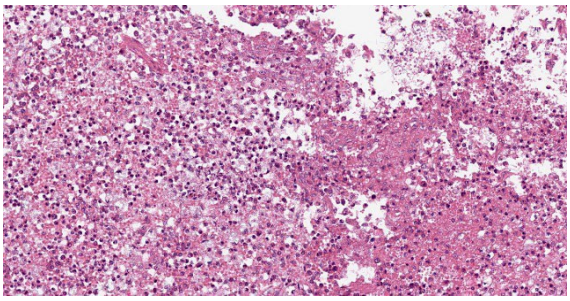

Figure 3-2. Spleen, cat. Scattered throughout the white matter are areas of lytic necrosis. (HE, 240X)

Additional findings included: reduced subcutaneous adipose tissue stores, pale pink oral mucous membranes, a prominent (age-appropriate) thymus, heart measurements within normal ratio, mild lobular pattern on the liver, moderately distended gall bladder, kidney measurements within normal limits, congested meninges, and pale skeletal muscle.

No significant gross abnormalities are detected in the following tissues: sciatic nerve, coxofemoral joints, femur bone, femur bone marrow, thyroid gland, parathyroid glands, tongue, pharynx, larynx, great cardiac vessels, adrenal glands, ureters, eyes, and ears.

Laboratory Results:
Faecal PCR Panel: Negative (below assay detection limits) for the following organisms: *Campylobacter, Salmonella, Giardia duodenalis, Cryptosporidium [C. parvum, C. hominis], Tritrichomonas foetus, Toxoplasma gondii, Dientamoeba fragilis, Neospora*

caninum, *Clostridium perfringens* enterotoxin cpe, Parvovirus, Distemper virus, Feline and Canine Coronavirus.

Faecal flotation: (Saturated sodium chloride, specific gravity 1.2): No evidence of eggs from nematodes or coccidia in the sample provided.

Microbiology: (spleen and liver): Samples of spleen and liver (collected at necropsy and frozen back for ancillary diagnostics if needed) were submitted for aerobic bacterial and fungal culture following initial histopathology review. After 24 hours incubation, cultures of both tissues yielded a pure heavy growth of a large, mucoid, lactose fermenting, non-haemolytic, gram-negative rod with colony morphology that was circular, raised, mucoid, smooth, grey, and approximately 3 mm diameter in size. The IMViC and urease profile for the isolates were as follows: Indole negative, Methyl Red negative, Voges-Proskauer positive, Citrate positive, Urease positive. Microbiology comments: The biochemical profile and colony morphology of the isolates are consistent with *Klebsiella pneumoniae* subsp. *pneumoniae*, and isolate identification has been confirmed by bioMérieux API20E assay.

Microscopic Description:
Spleen: White pulp follicles are smaller than expected and are widely separated by a hypercellular red pulp composed of erythrocytes interspersed with abundant homogenous eosinophilic material (presumed lysed erythrocytes), many macrophages and neutrophils, and myriad extracellular and intrahistiocytic bacterial rods, and scattered cellular debris and haematopoietic precursors. Additionally, throughout the sections, there are regionally extensive aggregates of approximately 2-4 microns round to ovoid discrete faintly eosinophilic structures with central round to elongate internal structures somewhat reminiscent of nuclei; Giemsa and Gram-stained replicate sections reveal a similar staining pattern to the marked proliferations of bacteria elsewhere throughout the parenchyma (suggestive of 'encapsulated' bacteria).

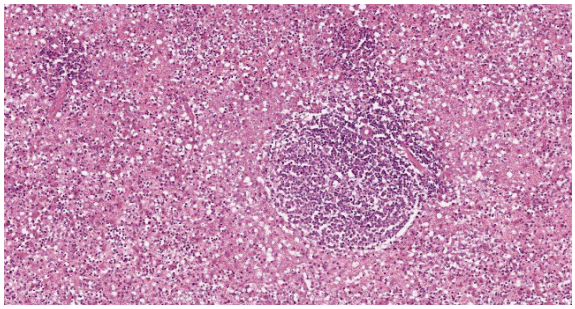

Figure 3-3. Spleen, cat. White pulp is severely depleted. (HE, 116X)

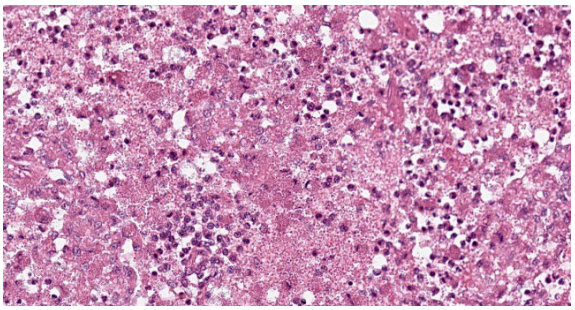

Figure 3-4. Spleen, cat. Throughout the white pulp, there are innumerable encapsulated bacilli which are also present in the cytoplasm of macrophages. (HE, 400X)

Contributor's Morphologic Diagnoses:
Splenitis, diffuse, histiocytic, and neutrophilic, acute to subacute, severe, with myriad extracellular and intrahistiocytic bacteria

Contributor's Comment:
Morbidity and mortality were ascribed to fulminant *Klebsiella pneumoniae* subsp. *pneumoniae* (Kpp) septicaemia and complications which most likely included multiple organ dysfunction syndrome (MODS) and systemic inflammatory response syndrome (SIRS). Numerous encapsulated Gram-negative rods were evident histologically within the vasculature of all evaluated tissues and within the parenchyma of blood filtering organs. While

some of this may be reflective of post-mortem overgrowth, the relatively short post-mortem interval combined with the identification of intracellular bacteria and acute inflammation in many tissues and heavy growth of pure cultures of Kpp isolated from spleen and lung support a diagnosis of severe antemortem bacteraemia. Kpp is an opportunistic bacterium found in the environment and as a commensal in the nasopharynx and alimentary tract of dogs and cats. Kpp can be associated with clinically significant infections of the respiratory, gastrointestinal and genitourinary tracts and systemic bacteraemia in carnivores. In some instances, underlying immunosuppression appears to have played a role in disease development (e.g., drugs, malnutrition, stress, endocrine disease, and other infections, including feline leukaemia virus, feline immunodeficiency virus infection). Kpp-induced enteritis, pneumonia, and sepsis with concurrent MODS has been reported in dogs. The diarrhoea and enteritis in this kitten were presumably related. Pneumonia was of sufficient severity to have resulted in some degree of respiratory compromise which was likely further exacerbated by SIRS, accounting for the clinically noted respiratory distress. In the medical and veterinary microbiology literature, the most common pathogenic bacteria that have capsules linked to virulence include are *Klebsiella pneumoniae, Escherichia coli, Haemophilus influenzae, Streptococcus pneumoniae, Yersinia pestis* and *Bacillus antracis,* where only the first four are gram-negative.[6]

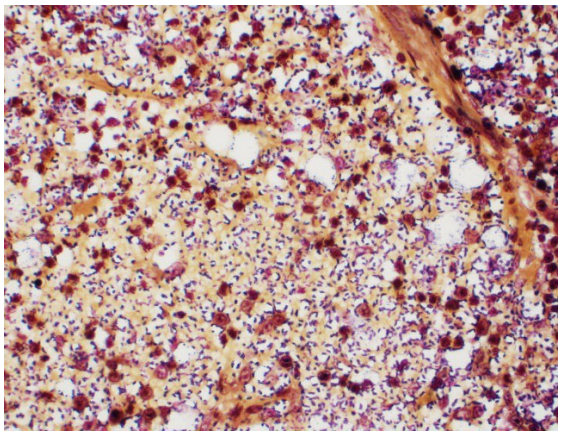

Figure 3-5. Spleen, cat. A gram stain demonstrates the widely spaced encapsulated bacilli characteristic of Klebsiella pneumoniae. (Brown-Brenn, 400X)

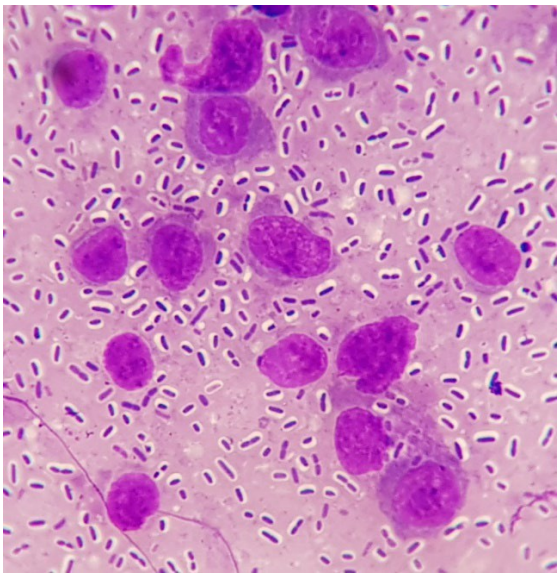

Figure 3-6. Spleen, cat. A rapid Diff-Quik stain on splenic cytology also demonstrates the encapsulated bacilli at the autopsy table. (Diff-Quik, 400X) (Photo courtesy of University of Sydney, https://sydney.edu.au/science/schools/sydney-school-of-veterinary-science/veterinary-science-services.html)

Contributing Institution:
University of Sydney
https://sydney.edu.au/science/schools/sydney-school-of-veterinary-science/veterinary-science-services.html

JPC Diagnosis:
Spleen: Splenitis, histiocytic and neutrophilic, diffuse, severe with lymphoid depletion, congestion, and innumerable extracellular and intrahistiocytic bacilli.

JPC Comment:
Klebsiella pneumoniae is associated with community-acquired, opportunistic, and nosocomial infections in both humans and animals and is one of the leading causes of healthcare-associated infections in humans. There are a wide range of virulence factors which contribute to its pathogenicity. Kpp has 78 distinct capsular serotypes, but K1 and

K2 are the most commonly isolated.[3,4] Its capsule prevents phagocytosis, blocks opsonization, and prevents complement-mediated lysis.[3] To acquire necessary iron, Kpp produces several sidephores, including enterobactin, yersiniabactin, salmochelin, and aerobactin.[3] Adhesins and type 1 and 3 fimbriae facilitate adhesion, invasion, and biofilm formation. Biofilms form on indwelling devices (such as catheters) and facilitate colonization of the gastrointestinal, respiratory, and urinary tracts.[3] Kpp utilizes quorum sensing to coordinate gene expression at certain bacterial densities.[3] Additionally, a hypervirulent strain of *K. pneumoniae* (hvKp) has emerged and is associated with serious community-acquired infections in humans, causing pneumonia, hepatic abscesses, meningoencephalitis, and septic arthritis.[3,4] This strain produces excess capsular material, causing hypermucosity, and higher quantities of siderophores than the classic strains.[3]

K. pneumoniae naturally produces chromosomal penicillinases, conferring resistance to ampicillin, carbenicillin, and ticarcillin; in the past four decades, however, *K. pneumoniae* has also collected additional antibiotic resistance plasmids, expanding its antibiotic resistance repertoire. Some strains are now developing resistance to carbapenem, previously considered a first-line treatment for this infection.[3]

A recent retrospective study of infections in 697 domestic animals in Brazil provides a glimpse of the spectrum of diseases caused by *K. pneumoniae.*[4] The urinary system was the most common system affected in dogs and cats, accounting for 51.9% of 393 canine cases and 63% of 27 feline cases; the infection caused cystitis, pyelonephritis, and urethritis in these species.[4] In cattle, 59.7% of 149 cases were due to mastitis; the majority of these were clinical and considered moderate to severe.[4] In 53.1% of 98 cases in horses, the bacteria was associated with reproductive infection, causing seminal vesiculitis, pyometra, abortion, and orchitis. In pigs, 59.1% of 22 cases were associated with diarrhea.[4]

References:

1. Green CE, Sykes J. *Infectious Diseases of the Dog and Cat.* 4th ed. St. Louis, MO: Elsevier Saunders; 2011:187-188.
2. Koenig A. Gram-Negative Bacterial Infections. In: Green CE, ed. *Infectious Diseases of the Dog and Cat.* 4th ed. St. Louis, MO: Elsevier. 2012: 353-355.
3. Piperaki ET, Syrogiannopoulos GA, Tsouvelekis LS, Daikos GL. *Klebsiella pneumoniae*: Virulence, Biofilm and Antimicrobial Resistance. *The Pediatric Infectious Disease Journal.* 2017; 36(10): 1002-1005.
4. Ribiero MG, de Morais ABC, Alves AC. *Klebsiella*-induced infections in domestic species: a case-series study in 697 animals (1997-2019). *Brazilian Journal of Microbiology*. 2022; 53: 455-464.
5. Roberts DE, McClain, HM, Hansen, DS, Currin P, Howerth, EW. An outbreak of Klebsiella pneumoniae infection in dogs with severe enteritis and septicemia. *J Vet Diagn Invest.* 2000; 12:168-173.
6. Tortora GJ, Funke BR, Case CL. *Microbiology: An Introduction.* 9th ed. San Francisco, CA: Pearson Benjamin Cummings.

CASE IV:

Signalment:

A 23.5-year-old female African green monkey (*Chlorocebus aethiops sabaeus*).

History:

This monkey had a three-year history gradual weight loss and a slow growing cranial abdominal mass.

Gross Pathology:
A 12x8x7 cm mottled tan to red soft multilobular mass extended from the wall of the greater curvature of the body of the stomach into the peritoneum. The omentum was firmly adhered to the mass and the adjacent small intestines, stomach, liver, and left kidney. On sectioned surface, the mass was mottled tan to red with large red to black areas of necrosis.

Laboratory Results:
No laboratory results reported.

Microscopic Description:
A well demarcated, partially encapsulated multilobular mass, expanding the muscularis externa and serosa, is composed of streams and bundles of closely spaced neoplastic mesenchymal cells supported by a fine fibrovascular stroma, and infiltrated by a few

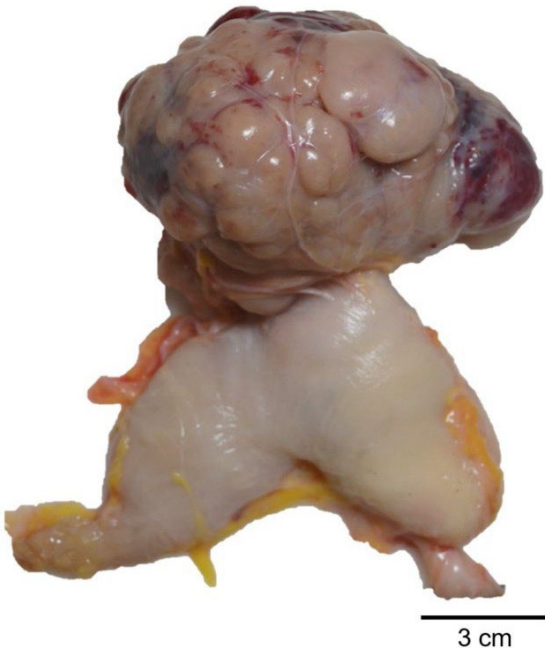

Figure 4-1. Stomach, African green monkey. A 12x8x7 cm mottled tan to red multilobular mass extended from the wall of the greater curvature of the body of the stomach into the peritoneum. (Photo courtesy of: Wake Forest School of Medicine. Department of Pathology, Section on Comparative Medicine, Medical Center Boulevard, Winston-Salem, NC 27157, www.wakehealth.edu)

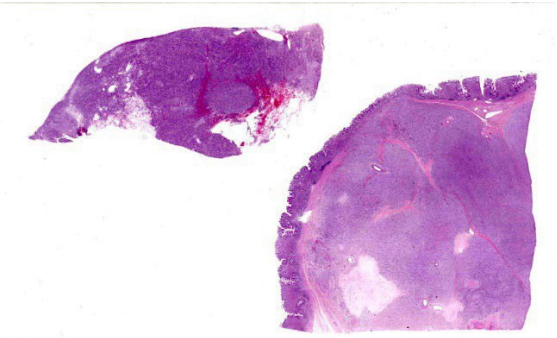

Figure 4-2. Stomach, African green monkey. Two sections of stomach are submitted for examination. In the larger section (with mucosa), the gastric wall is markedly distended by a mesenchymal neoplasm. (HE, 4X)

small aggregates of lymphocytes. The neoplastic cells range from 30x10-50x15 µm, have indistinct cell borders, abundant fibrillar to clear eosinophilic cytoplasm, and central oval to fusiform 10x10 -25x12 µm nuclei with finely stippled chromatin, without nucleoli. Mitoses occur at 0-1 per 10, 40x fields. Macrophages with intracytoplasmic golden-tan pigment (hemosiderin) infiltrate the capsule of the neoplasm. The overlying gastric mucosa is disorganized, thickened up to twice normal, with loss of polarity in the gastric pits and glands. Many of the gastric glands are lined by or have prominent parietal cells, and mitoses are numerous. Small hemorrhages are scattered throughout the lamina propria, and lymphoid aggregates along the deep mucosa are prominent. Few lymphocytes, eosinophils, and neutrophils infiltrate the muscularis mucosa. The smooth muscle of the tunica media of some arterioles in the submucosa are thickened, and the lumina are reduced in size. The neoplastic cells were immunohistochemically negative for smooth muscle actin (SMA) and positive for CD117.

Transmission electron microscopy findings: The elongate neoplastic cells have medium electron-dense to electron lucent cytoplasm with few mitochondria, and fusiform euchromatic nuclei, some with single nucleoli. A few cells have two nuclei. The cells are separated by extracellular matrix containing 20

Table 4.1

Differential Diagnoses	Positive Immunohistochemical Stains
Leiomyoma	Smooth muscle actin (SMA)
Leiomyosarcoma	SMA
Peripheral nerve sheath tumor	CD99 / S100
Schwannoma	S100
Neurofibroma	S100 / CD34+ (focal)

nm wide electron-dense fibrils, electron lucent spaces, and amorphous medium electron dense-material.

Contributor's Morphologic Diagnoses:
Gastric body: Gastrointestinal stromal tumor

Contributor's Comment:
Gastrointestinal stromal tumors (GISTs) are rare mesenchymal tumors of the gastrointestinal tract which are thought to originate from the interstitial cells of Cajal. They have been reported in rhesus macaques, chimpanzees, baboons, and spider monkeys, numerous domestic animals, and humans.[1,2,3,10,13,14] In companion animals they most frequently arise in the intestine, whereas in humans and non-human primates, they primarily occur in the gastric cardia and body.[1,2,13]

Characteristic histologic findings include a herringbone pattern of mesenchymal cell proliferation supported by dense fibrovascular stroma, and in larger tumors necrosis is common. These tumors typically arise from the mucosa or submucosa, and transmural invasion is common.[10] The majority of GISTs are CD117 (c-KIT), CD34, and DOG-1 (discovered on gastrointestinal stromal tumors protein-1) positive.[13]

The majority of GISTs contain a mutation in the *KIT* receptor tyrosine kinase gene, resulting in the overexpression of the KIT protein, which can be identified immunohistochemi-

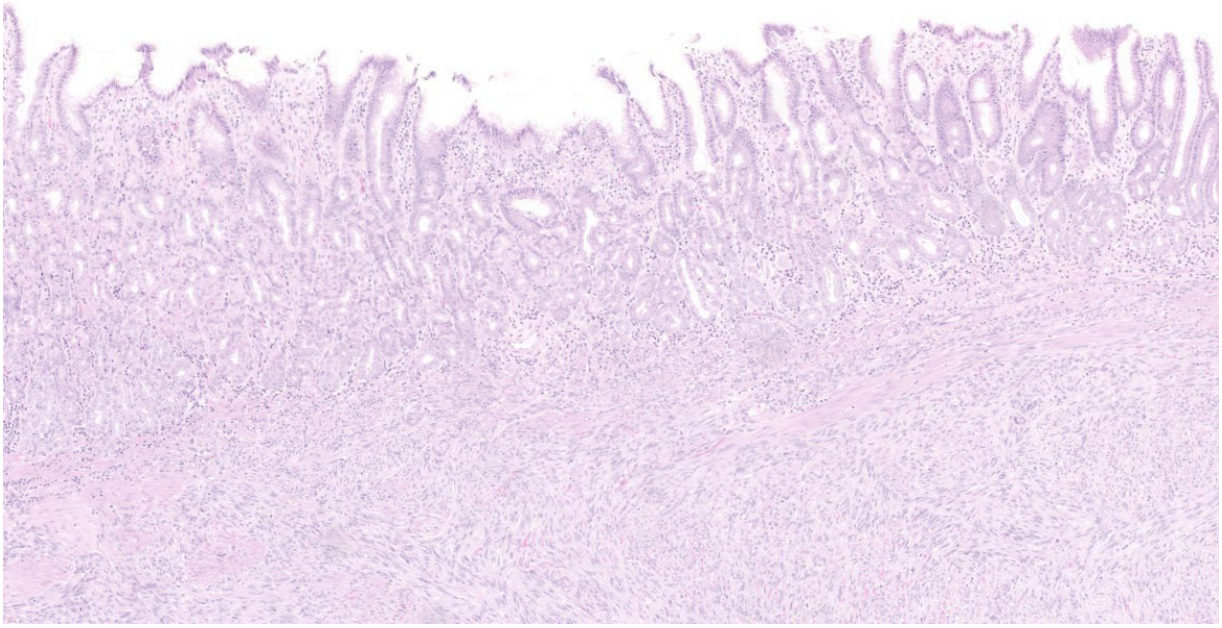

Figure 4-3. Stomach, African green monkey. A spindle cell neoplasm arises from the submucosa, effacing the wall and infiltrating the overlying mucosa. (HE, 73X)

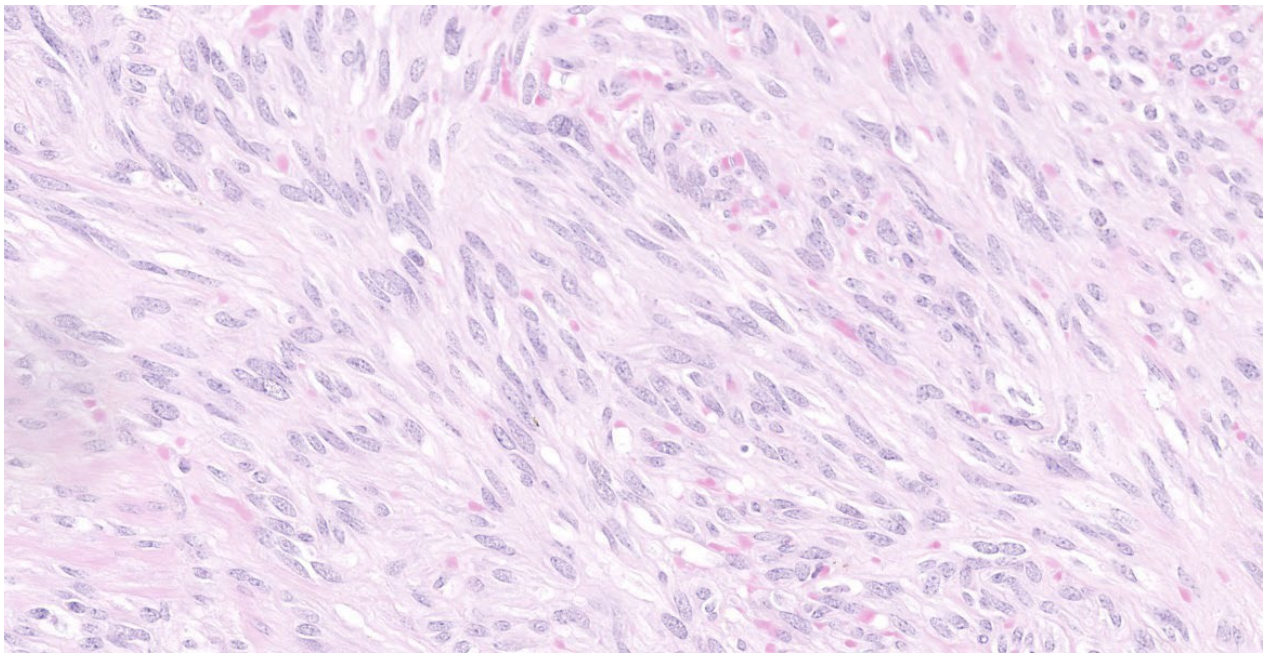

Figure 4-4. Stomach, African green monkey. High magnification of neoplastic cells. (HE, 73X)

cally with CD117 (c-KIT).[12] CD34, an antigen for hematopoietic progenitor and endothelial cells is positive in some interstitial cells of Cajal and in the majority of GISTs in humans and other species.[4,15] In humans and dogs, DOG-1 is a more sensitive and specific marker for GISTs than CD117. DOG-1 is independent of mutations in CD117, and has been documented to stain CD117- and CD34-negative GISTs.[5,8]

Ultrastructurally, GISTs are composed of primitive mesenchymal cells which may have non-membrane-bound electron lucent regions in the cytoplasm. Dense bodies, which are characteristic of smooth muscle, are present in leiomyomas and leiomyosarcomas, and absent in GISTs.[6] Some GISTs, particularly in the intestinal tract and rectum in humans, may have skeinoid fibers, of which the composition is unknown. Histologically they appear as extracellular hyaline globules. Ultrastructurally, skeinoid fibers are composed of medium electron-dense fibrils resembling collagen but with a periodicity of ~43 nm.[11,14] Skeinoid fibers were not identified in this case.

GISTs should be differentiated from leiomyomas, leiomyosarcomas, peripheral nerve sheath tumors, schwannomas, and neurofibromas because of the differences in metastatic potential and prognoses (Table 4.1). In humans, GISTs often arise in the gastric cardia and body, whereas leiomyomas are more common in the esophagus.[9,17]

Contributing Institution:
Wake Forest School of Medicine
Department of Pathology, Section on Comparative Medicine

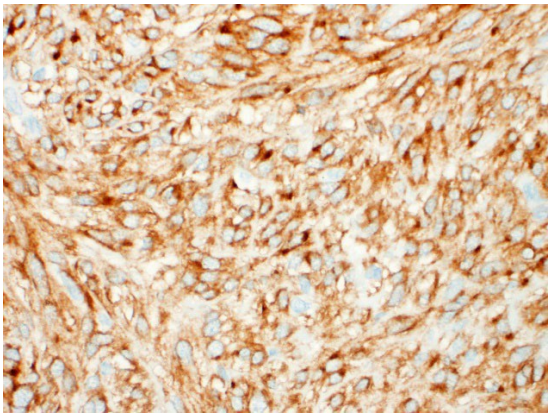

Figure 4-5. Stomach, African green monkey. Neoplastic cells are strongly positive for c-Kit. (anti-C-Kit, 400X)

Medical Center Boulevard, Winston-Salem, NC 27157
www.wakehealth.edu

JPC Diagnosis:
Stomach: Gastrointestinal stromal tumor.

JPC Comment:
As the contributor mentions, one of the differentials for gastrointestinal stromal tumors (GISTs) is a smooth muscle neoplasm, such as leiomyoma and leiomyosarcoma.[7] Historically, human GISTs humans were diagnosed as smooth muscle neoplasms prior to ultrastructural evaluation and the discovery of the CKIT protooncogene marker of these neoplasms.[7] Leiomyomas and leiomyosarcomas have historically been the most common spindle cell neoplasm of the gastrointestinal tract in rats and mice in the National Toxicology Program's two-year bioassays, so researchers recently conducted a retrospective study evaluating CKIT expression in smooth muscle tumors of these species.[7] In B6C3F1/N mice, 22 of 32 tumors (69%) previously diagnosed as leiomyoma/leiomyosarcoma were CKIT positive, indicating they are likely GISTs.[7] Most (16) of these tumors arose in the cecum, with fewer in the colon and stomach. In rats, all of the tumors were negative for CKIT, and most were positive for desmin and smooth muscle actin, confirming their diagnosis as smooth muscle tumors.[7] These surprising results indicate that GISTs are more common than leiomyoma/leiomyosarcomas in mice in the NTP bioassays.[7]

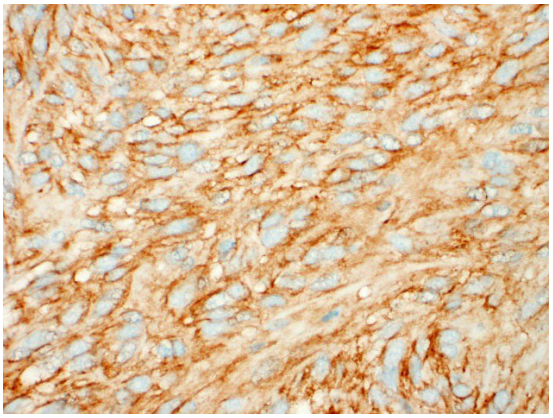

Figure 4-6. Stomach, African green monkey. Neoplastic cells are strongly positive for DOG-1. (anti-DOG-1, 400X)

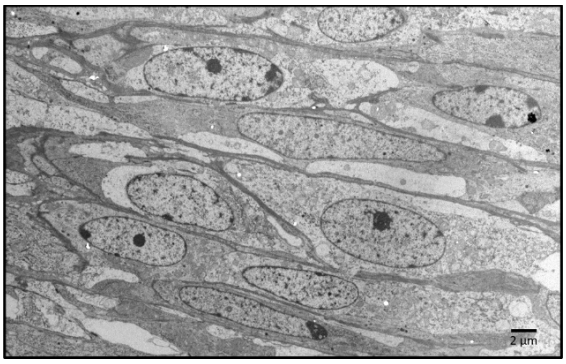

Figure 4-7. Stomach, African green monkey. Transmission electron micrograph of the neoplastic cells. The cells have regions of electron lucency and lack the dense bodies typical for smooth muscle. (Photo courtesy of: Wake Forest School of Medicine. Department of Pathology, Section on Comparative Medicine, Medical Center Boulevard, Winston-Salem, NC 27157, www.wakehealth.edu)

Another recent study described gastrointestinal stromal tumors (GISTs) in four guinea pigs of advanced age.[16] Three animals had neoplasms in the gastric wall at the cardia, while the fourth was in the small intestine.[16] One of the gastric GISTs metastasized to the duodenal and cecal mesentery.[16] The gastric GISTs were positive for c-KIT, DOG-1, and smooth muscle actin.[16] The small intestinal GIST was negative for smooth muscle actin, but positive for c-KIT and DOG-1.[16] In all neoplasms, atypia was mild and mitotic figures were rare. Additionally, all cases had deletion mutations in exon 11 of the *Kit* gene.[16]

References:

1. Banerjee M, Lowenstine LJ, Munn RJ. Gastric stromal tumors in two rhesus macaques (*Macaca mulatta*). *Vet Pathol*. 1991; 28: 30-36.
2. Bommineni YR, Dick EJ, Jr., Hubbard GB. Gastrointestinal stromal tumors in a baboon, a spider monkey, and a chimpanzee and a review of the literature. *J Med Primatol*. 2009; 38: 199-203.

3. Brown SL, Anderson DC, Dick EJ, Jr., Guardado-Mendoza R, Garcia AP, Hubbard GB. Neoplasia in the chimpanzee (*Pan* spp.). *J Med Primatol*. 2009; 38: 137-144.
4. Bure I, Braun A, Kayser C et al. The expression of hematopoietic progenitor cell antigen CD34 is regulated by DNA methylation in a site-dependent manner in gastrointestinal stromal tumours. International Journal of Cancer 141: 2296-2304, 2017
5. Dailey DD, Ehrhart EJ, Duval DL, Bass T, Powers BE. DOG1 is a sensitive and specific immunohistochemical marker for diagnosis of canine gastrointestinal stromal tumors. *J Vet Diagn Invest*. 2015; 27: 268-277.
6. Ferenczy A, Richart R, Okagaki T. A comparative ultrastructural study of leiomyosarcoma, cellular leiomyoma, and leiomyoma of the uterus. *Cancer.* 1971; 28: 1004-1018.
7. Janardhan KS, Venkannagari P, Jensen H, et al. Do GISTs Occur in Rats and Mice? Immunohistochemical Characterization of Gastrointestinal Tumors diagnosed as Smooth Muscle Tumors in the National Toxicology Program. *Toxicol Pathol.* 2019; 47(5):577-584.
8. Jung JH, Im S, Choi HJ, Lee YS, Jung ES. Gastrointestinal stromal tumor with dedifferentiation to undifferentiated pleomorphic sarcoma. *Pathol Int*. 2013; 63: 479-482.
9. Levy AD, Remotti HE, Thompson WM, Sobin LH, Miettinen M. Gastrointestinal stromal tumors: radiologic features with pathologic correlation. *Radiographics*. 2003; 23: 283-304, 456; quiz 532.
10. Meuten DJ. *Tumors in Domestic Animals*. Fifth edition. Ames, IO: Wiley Blackwell. 2017.
11. Min KW: Gastrointestinal stromal tumor: an ultrastructural investigation on regional differences with considerations on their histogenesis. *Ultrastruct Pathol.* 2010; 34: 174-188.
12. Novelli M, Rossi S, Rodriguez-Justo M, Taniere P et al. DOG1 and CD117 are the antibodies of choice in the diagnosis of gastrointestinal stromal tumours. *Histopathology*. 2010; 57: 259-270.
13. Parab TM, DeRogatis MJ, Boaz AM, et al. Gastrointestinal stromal tumors: a comprehensive review. *J Gastrointest Oncol*. 2019; 10: 144-154.
14. Saito T, Ueno M, Ota Y et al. Histopathological and clinical characteristics of duodenal gastrointestinal stromal tumors as predictors of malignancy. *World J Surg Onc.* 2013; 11.
15. Saturday GA, Lasota J, Frost D, Brasky KB, Hubbard G, Miettinen M: KIT-positive gastrointestinal stromal tumor in a 22-year-old male chimpanzee (*Pan troglodites*). *Vet Pathol*. 2005; 42: 362-365.
16. Ueda K, Takanosu M, Kagawa Y, et al. Gastrointestinal stromal tumors with *Kit* gene mutation in 4 guinea pigs (*Cavia porcellus*). *Vet Pathol*. 2022. 59(5): 740-746.
17. Yang DY, Wang X, Yuan WJ, Chen ZH: Metastatic pattern and prognosis of gastrointestinal stromal tumor (GIST): a SEER-based analysis. *Clin Transl Oncol*. 2019.

WSC 2022-2023 Self-assessment
Conference 16

1. COVID-19 viral infection and replication within a host depends on the presence and distribution of which of the following?
    a. E-cadherin receptors
    b. Angiotensin-converting enzyme receptors
    c. Muscarinic receptors
    d. Histamine receptors

2. *Scedosporium apiospermum* was previously considered to be the asexual form of which of the following?
    a. *Aspergillus fumigatus*
    b. *Pseudoallescheria boydii*
    c. *Mortierella polycephala*
    d. *Actinomyces viscosus*

3. Which of the following vectors are considered most important for the transmission of type A strains of *Francisella tularensis* ?
    a. Mosquitoes
    b. Biting flies
    c. Hard ticks
    d. Biting midges

4. True or false? Klebsiella pneumoniae is a commensal organism in the dog and cat ?
    a. True
    b. False

5. Skeinoid fibers, extracellular hyaline globules seen in some GISTs, are composed of:
    a. Amyloid
    b. Elastin
    c. Collagen
    d. Fibrinogen

Please email your completed assessment for grading to Dr. Bruce Williams at bruce.h.williams12.civ@mail.mil. Passing score is 80%. This program (RACE program 33611) is approved by the AAVSB RACE to offer a total of 0.5 CE Credits, with a maximum of 12.5 CE Credits being available to any individual Veterinary Medical Professionals for the 2019-2020 Wednesday Slide Conference. This RACE approval is for the subject matter categories of: SCIENTIFIC using the delivery method of NONINTERACTIVE DISTANCE. This approval is valid in jurisdictions which recognize AAVSB RACE.

Joint Pathology Center
Veterinary Pathology Services

WEDNESDAY SLIDE CONFERENCE 2022-2023

Conference #17 **25 January 2023**

CASE I:

Signalment:
1 day old, female, commercial lineage, *Sus scrofa domesticus*, swine.

History:
Our research group was contacted to investigate a disease that have been affecting neonates piglets in a sow farm located in West of Santa Catarina, Brazil. The farm has 330 sows, in an intensive system. In the period between May 2020 and January 2021, the farm manager have reported the birth of piglets with large and caudally rotated ears ("Dumbo-like piglets"), with weakness, apathy and in most cases, dyspnea. The morbidity rate was 3,4%, the mortality was 3% and the lethality was 86%. Most of the affected piglets was born from gilts (77%), and with a bith average of 4.8 "Dumbo-like piglets" per litter. The piglets died 1 to 5 days after birth. We received 14 piglets for routine diagnosis investigation.

Gross Pathology:
Grossly, the lungs of all piglets did not collapse upon the opening of the thoracic cavity, and also had marked interlobular edema. Also, all piglets had large and caudally rotated ears. No other significant abnormalities were visible in the remaining organs.

Laboratory Results:
PCR:
The samples (pool of CNS, lung, heart, liver, and spleen) tested positive for PCV3 and negative for PCV1, PCV2, PPV 1, 2, 5, and 6, APPV, PRRSV, and OvHV-2.
ISH findings:
Replication of PCV3 was most commonly observed in lymphocytes and plasma cells in perivascular areas and in the smooth muscle of arteries (fig. 3). We also observed PCV3 replication in lungs (fig. 4), heart (fig. 5), and in neurons of the brain.

Microscopic Description:
The slides submitted for this conference contained tissues from only one affected piglet. Vascular plexus and mesenteric lymph node: surrounding and disrupting the wall of vessels (mainly in arteries and arterioles), there is a severe and multifocal inflammatory infiltrate composed of lymphocytes, histiocytes and rare plasma cells. The

Presentation, piglets. Affected piglets had large, caudally rotated ears ("Dumbo piglets"). (*Photo courtesy of:* (*Photo courtesy of:* Faculdade de Veterinária, Universidade Federal do Rio Grande do Sul, Setor de Patologia Veterinária, http://www.ufrgs.br/patologia)

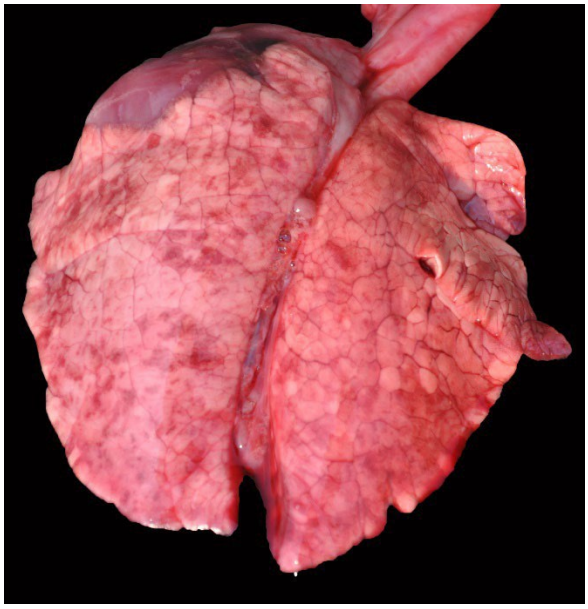

Lung, piglet. The lungs of one affected piglet fail to collapse, and have marked interlobular edema.j.. (*Photo courtesy of:* (*Photo courtesy of:* Faculdade de Veterinária, Universidade Federal do Rio Grande do Sul, Setor de Patologia Veterinária, http://www.ufrgs.br/patologia)

infiltrate is associated with mild fibrinoid degeneration. In the mesenteric lymph node, mild necrosis of the germinal centers is observed, in addition to lymphoid rarefaction and mild infiltrate of macrophages containing brown pigment in their cytoplasm (hemosiderin).

Heart: in the pericardium and myocardium there is a moderate and multifocal inflammatory infiltrate surrounding and disrupting the vessel walls (mainly in arteries and arterioles), composed of lymphocytes, histiocytes, and rare plasma cells. There is also mild fibrinoid degeneration. Some cardiomyocytes present mild necrosis and are surrounded by lymphocytes, macrophages, and plasma cells.
Lung: surrounding and disrupting the wall of vessels (mainly in arteries and arterioles), there is a severe and multifocal inflammatory infiltrate composed of lymphocytes, histiocytes, and rare plasma cells. A similar infiltrate is observed severely expanding the alveolar septa. There is also moderate and diffuse interlobular edema.

The other tissues presented a variable amount of lymphocytes, histiocytes, and plasma cells infiltrating and disrupting the wall of vessels, occasionally with fibrinoid degeneration, mainly in arteries and arterioles. Also, in the brain, there were multifocal areas of gliosis.

Contributor's Morphologic Diagnoses:
Mesenteric plexus: lymphohistiocytic periarteritis and arteritis, multifocal, marked and mild fibrinoid degeneration;
Lymph node: lymphoid rarefaction and necrosis, multifocal, mild, and hemosiderosis, multifocal, mild.
Heart: lymphohistiocytic periarteritis and arteritis multifocal, marked and lymphohistiocytic myocarditis, multifocal, mild.
Lung: lymphohistiocytic interstitial pneumonia, diffuse, marked, with mild lymphohistiocytic periarteritis and arteritis.

Contributor's Comment:
The diagnosis of PCV3-associated clinical disease in neonatal piglets was based on the molecular findings in association with the detection of PCV3 mRNA in microscopic lesions. PCV3 was first detected in 2015 in the United States, related to abortion cases, high mortality in sows, and clinical signs compatible with swine dermatitis and

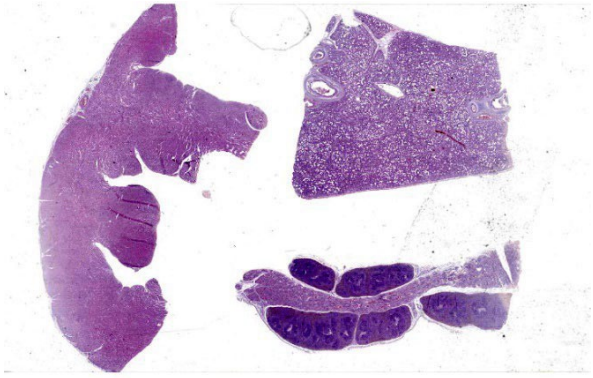

Multiple organs, piglet: Sections of the heart (left) lung (top right), and mesenteric vascular plexus (bottom right) are submitted for examination. (HE, 381X)

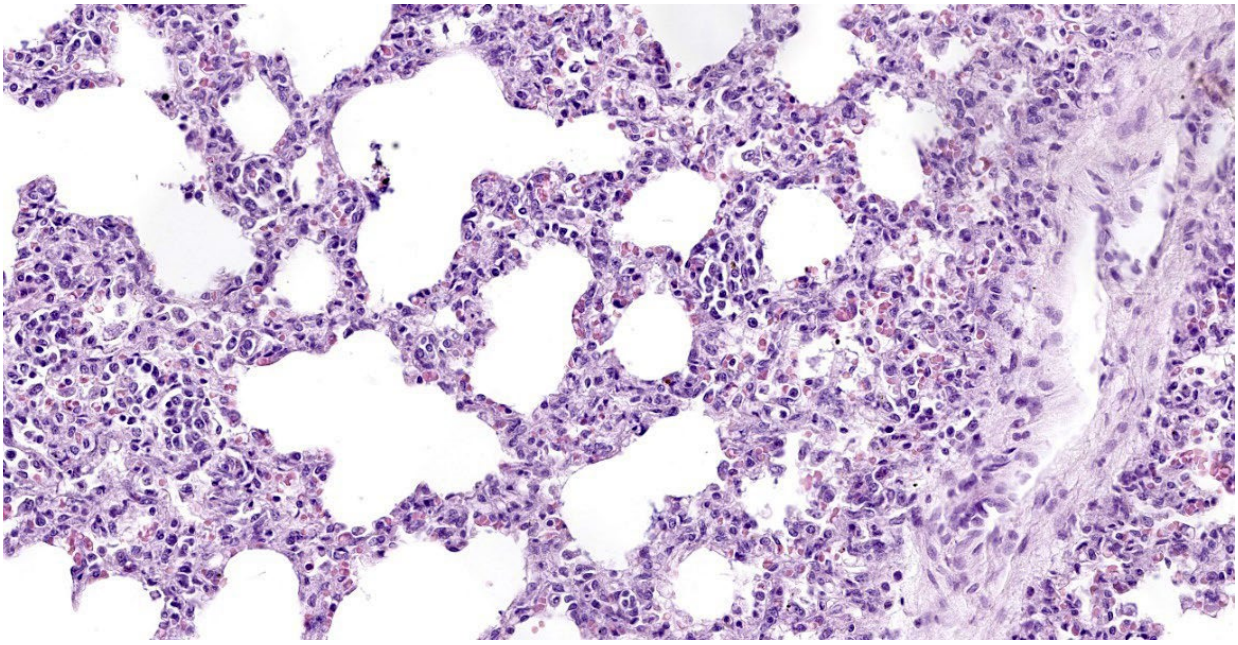

Lung, piglet. Alveolar septa are markedly thickened by macrophages, edema, congestion, and patchy Type II pneumocyte hyperplasia. Interlobular septa are expanded by edema. A large mat of fungal hyphae expands the pleura and extends into the pleural space (at left). (HE, 282X)

nephropathy syndrome.[8] Also, PCV3 was described in three pigs from 3 to 9 weeks old, with multisystemic inflammation and myocarditis.[9] Other clinical/pathological presentations were also associated with PCV3 infection, such as gastrointestinal, respiratory, and neurological disturbances.[10] In most studies, the viral DNA has been detected in different tissues of pigs, however, without the demonstration of the agent in the lesions. PCV3 genetic material was detected through PCR in healthy piglet tissues,[5, 8] which makes it difficult to conclude the real pathogenic potential of the virus and its economic impact on swine production. Therefore, the diagnosis of PCV3 must be confirmed through detecting its DNA in affected swine lesions, using techniques such as ISH, or at least associating the histopathological lesions with qPCR.

The ear malformation was a consistent feature observed in piglets of this farm. This finding was described in PCV3 positive pigs, previously,[1, 6] however, it is necessary to perform more studies to characterize the pathogenesis of the large and caudally rotated ears and their relation to the PCV3 infection.
Multisystem vasculitis, myocarditis, and encephalitis were already PCV3-associated with the death of neonates,[2, 6] and post-weaning piglets.[9] Replication of PCV3 through ISH, was detected in the smooth muscle of arteries and arterioles.[2]

Lymphoplasmahistiocytic interstitial pneumonia was a constant pathological finding in the evaluated piglets, and through ISH it was possible to show the PCV3 viral replication within the lesions. This finding was described in a 19 day old piglet.[9] Interstitial pneumonia is a common finding in viral infections of the inferior respiratory tract. In the maternity phase (usually until 21-25 days old), the main causes of viral pneumonia include the Aujeszky virus and PRRSV. There are no reports of clinical disease related to PRRSV presence in Brazil, and this virus was ex-

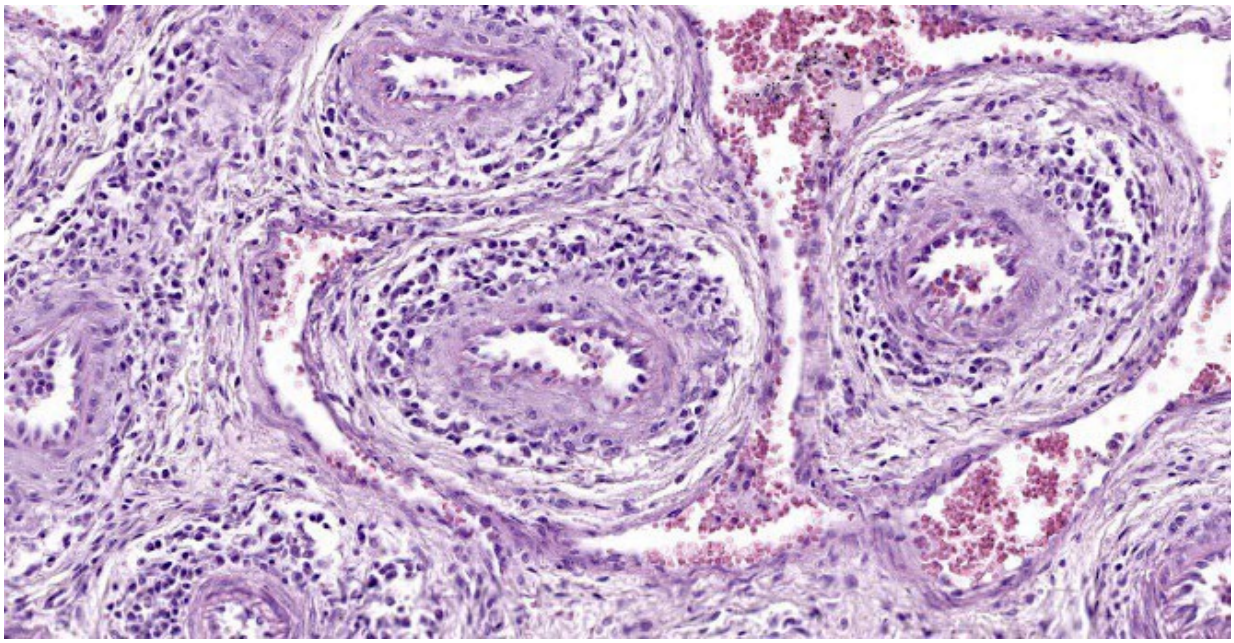

Mesenteric vascular plexus, piglet. The adventitia of arterioles and intervening fibrous connective tissue are infiltrated by moderate numbers of lymphocytes, macrophages, and histiocytes.

cluded through a PCR test. Pneumonia related to the Aujeszky virus can occur in piglets up until 5 days old; however, in this phase, neurologic signs are prominent, while respiratory signs are usually common in growing and finishing pigs.[3] PCV2 is an important cause of interstitial pneumonia, described mainly in nursery and finishing piglets,[4] and the lymphocytic and plasmacytic periarteritis is a common finding between PCV3 and PCV2 infection.[2, 7] All samples tested negative for PCV1, PCV2, PRRSV, APPV, PPV, and OvHV-2, which are other potential causes of myocarditis, vasculitis, and encephalitis in neonatal piglets.

Contributing Institution:
Faculdade de Veterinária
Universidade Federal do Rio Grande do Sul
Setor de Patologia Veterinária
http://www.ufrgs.br/patologia

JPC Diagnosis: 1. Lung: Pneumonia, interstitial, histiocytic, diffuse, severe, with intralobular edema and histiocytic arteritis.

2. Mesenteric vascular plexus, heart: Arteritis, histiocytic, diffuse, moderate.

3. Lymph node, subcapsular and medullary sinuses: Hemosiderosis, moderate.

JPC Comment: As the contributor states, porcine circovirus 3 was first diagnosed in 2015; however, retrospective studies have identified PCV-3 in samples from as early as the 1960s.[7] And even though there is still much to be elucidated regarding this relatively young virus, PCV-3 is no longer the newest circovirus on the block: PCV-4 was discovered in 2019 in 7-week old pigs with respiratory disease, porcine dermatitis and nephropathy syndrome, and diarrhea.[7]

PCV-3 has been detected in a wide range of species and produces viremia in cattle, dogs, and laboratory mice.[7] Wild boar are thought to be a reservoir, with prevalence of up to 61.54%.[7] Mosquitos can also be infected, but studies have failed to support vector-borne transmission.[7] In fact, the precise mode of transmission has not been worked out, and virus has been identified in oral fluids, the salivary glands, colostrum, semen, and testicles.[7]

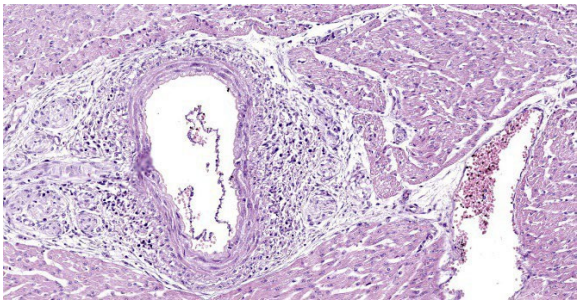

Coronary vessel, piglet: The intima of the coronary vessels is expanded by edema and moderate numbers of lymphocytes, plasma cells and macrophages. (HE, 279X)

The virus can infect a wide variety of cells and has been found in myocardiocytes, vascular smooth muscle, trophoblasts, adipocytes, ependymal cells. This suggests that the virus ligand binds to a widely expressed host receptor, which has yet to be identified.[7] Affected pigs may have a persistent infection with prolonged viremia.[7] Determining the effects of PCV-3 infection is challenging for multiple reasons: as the con- tributor states, there are a wide variety of syn- dromes associated with infection, but the vi- rus has also been isolated in subclinical ani- mals. Additionally, PCV-3 infection regu- larly occurs alongside other infectious agents, including PCV-2, porcine parvovirus, porcine reproductive and respiratory syndrome virus, making attribution of clinical signs with a specific agent difficult.[7]

A recent retrospective study reviewed formalin-fixed paraffin-embedded tissues from 587 pigs free of porcine circovirus 2 in Spain.[4] PCV-3 ISH and qPCR were conducted on a subset of cases which contained lesions reported to be associated with PCV-3, including reproductive disease, congenital tremors, porcine dermatitis and nephropathy syndrome, arteritis or periarteritis, myocarditis, encephalitis, and peri-weaning failure-to-thrive syndrome. [4] All evaluated cases of periarteritis were qPCR positive for PCV3, and most were positive via IHC. [4] The most consistently affected sites for periarteritis were the mesenteric arteries and the kidney, indicating they are likely suitable choices for diagnostic testing. [4] Additionally, PCV-3 was not detected in cases of myocarditis and encephalitis where periarteritis was lacking. [4]

The moderators and conference participants discussed a unique anatomic feature of pigs evident in this slide: the mesenteric arterial plexus. While the exact function is unknown, it may serve as a countercurrent mechanism to help regulate blood pressure. Conference participants also discussed the few foci of histiocytic infiltrates in the myocardium; the significance of these infiltrates is unknown.

References: 1. Alomar J, Saporiti V, Pérez M, Gonçalvez D, Sibila M, Segalés J. Multisystemic lymphoplasmacytic inflammation associated with PCV-3 in wasting pigs. *Transbound Emerg Diseases* 2021; 1-6.

2. Arruda B, Piñeyro P, Derscheid R, Hause B, Byers E, Dion K, Long D, Sievers C, Tangen J, Williams T, Schwartz K. PCV3-associated disease in the United States swine herd. *Emerg Microbes Infect* 2019; 8:684-698.

3. Ciacci-Zanella LR. Doença de Aujeszky. In: Megid J, Ribeiro MG, Paes AC (eds) Doenças infecciosas em animais de produção e companhia, 2016, 1st ed. Roca, Rio de Janeiro, 598-602.

4. Cobos A, Sibila M, Alomar J, Perez M, Huerta E, Segales J. Retrospective assessment of porcine circovirus 3 (PCV-3) in formalin-fixed paraffin-embedded tissues from pigs affected by different clinical-pathologic conditions. *Porcine Health Manag*. 2022; 8(1):51-60.

5. França TN, Ribeiro CT, Cunha BM, Peixoto PV. Circovirose suína. *Pesq Vet Bras* 2005; 25(2):59-72.

6. Franzo G, Delwart E, Fux R, Hause B, Su S, Zhou J, Segalés J. Genotyping porcine circovirus 3 (pcv-3) nowadays: does it make sense? *Viruses* 2020; 12(3):265.

7. Kroeger M, Temeeyasen G, Pineyro PE. Five years of porcine circovirus 3: What have we learned about the clinical disease, immune pathogenesis, and diagnosis. *Virus Res.* 2022; 314: 198764.

8. Molossi FA, Almeida BA, Cecco BS, Silva MS, Mósena ACS, Brandalise L, Simão GMR, Canal CW, Vanucci F, Pavarini SP, Driemeier D. A putative PCV3-associated disease in piglets from Southern Brazil. *Braz J Microbiol* 2022; 53:491–498.

9. Opriessnig T, Janke BH, Halbur PG. Cardiovascular lesions in pigs naturally or experimentally infected with porcine circovirus type 2. *J Comp Pathol* 2006; 134:105-110.

10. Palinski R, Piñeyro P, Shang P, Yuan F, Guo R, Fang Y, Byers E, Hause BM. A novel porcine circovirus distantly related to known circoviruses is associated with porcine dermatitis and nephropathy syndrome and reproductive failure. *Virol J* 2017; 91(1):e01879-16.

11. Phan TG, Giannitti F, Rossow S, Marthaler D, Knutson T, Li L, Deng X, Resende T, Vanucci FA, Delwart E. Detection of a novel circovirus PCV3 in pigs with cardiac and multi-systemic inflammation. *Virol J* 2016; 13(1):184.

12. Zhai SL, Zhou X, Zhang H, Hause BM, Lin T, Liu R, Chen QL, Wei WK, Hong D, Wen XH, Li W, Wang D. Comparative epidemiology of porcine circovirus type 3 in pigs with different clinical presentations. *Virol J* 2017; 14(1):222.

CASE II:

Signalment:
3½ month-old, intact female, Siberian Husky, Canis lupus familiaris, dog.

History:
This puppy was initially presented to our institution's veterinary teaching hospital with a history of anorexia, diarrhea and mild intermittent fever of 10 days duration. It had been vaccinated against CDV, CPV-2, CAV-1, *Leptospira spp.* and *Bordetella bronchiseptica* at 2 and 3 months of age, and administered anthelminthics (fenbendazole). At presentation, moderate dyspnea was observed and treated with antibiotics, anti-inflammatory drugs, IV fluids and oxygen. Hematology revealed moderate lymphopenia. The respiratory signs gradually worsened over the next 5 days, with seizures developing within 3 days after presentation; the seizures were well controlled with diazepam. Considering the progressive deterioration of the animal's condition, the owners elected for euthanasia. Littermates were unaffected.

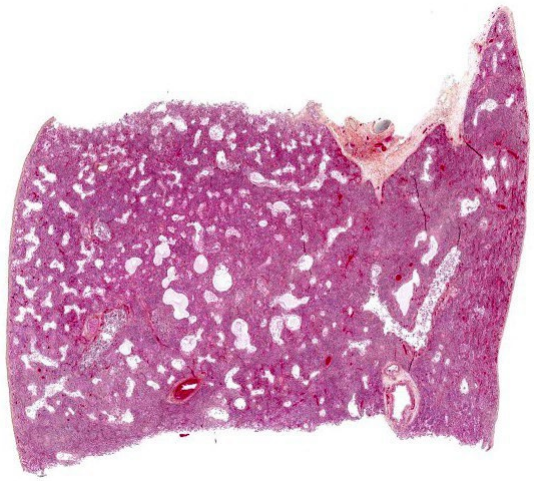

Lung, dog. On subgross magnification, there is diffuse consolidation of the lung. (HE, 6X)

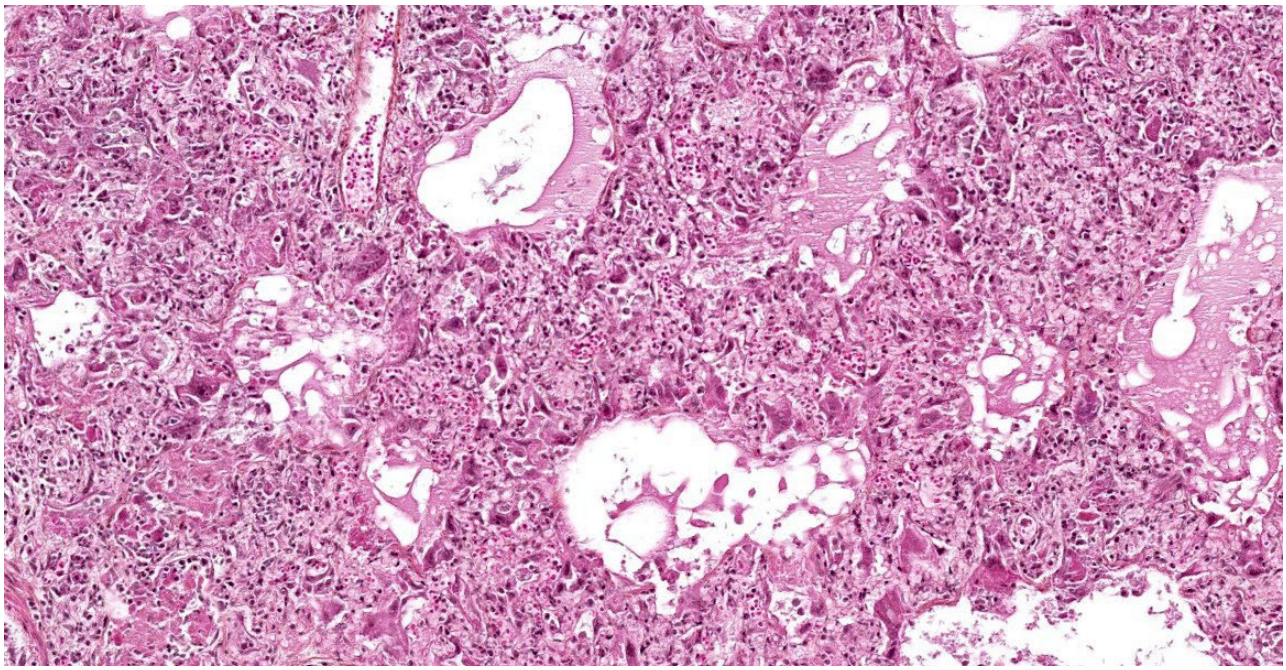

Lung, dog. Normal pulmonary architecture is lost. There is marked expansion of alveolar septa, and alveoli contain brightly eosinophilic hypertrophic Type II pneumoncytes and viral syncytia. Airways are often devoid of epithelium and filled with edema fluid. (HE, 148X)

Gross Pathology:

Body condition was assessed as 3/9. The lungs failed to collapse when the thorax was opened, and they were diffusely pale red to purplish with a rubbery to firm texture (interstitial pneumonia); there was no exudate on cut sections. The only other significant gross lesion was marked thymic atrophy.

Laboratory Results:

PCR for canine distemper virus (CDV) on lung samples was positive (Ct: 17.00)

Microscopic Description:

The lesions are similar in all pulmonary lobes (only one section submitted). Diffusely, the pulmonary alveoli are lined by pleomorphic squamous to polygonal cells (type II pneumocytes), many of them multinucleated (syncytia). Multifocally and to variable degrees within the alveolar lumina, there are macrophages and desquamated pneumocytes with protein-rich edema and, to a lesser degree, fibrin and/or necrotic debris; small numbers of neutrophils are occasionally present. Minimal, mainly lymphoplasmacytic interstitial inflammation is present in the alveolar septa. Although there is significant post-mortem desquamation, some terminal bronchioles and alveolar ducts can be seen to be lined by squamous to cubic epithelial cells often with amphophilic cytoplasm (regeneration). Numerous variably sized, brightly eosinophilic, intracytoplasmic inclusion bodies are present in type II pneumocytes, alveolar macrophages and, to a lesser degree, bronchiolar epithelial cells.

Other relevant lesions observed in this pup were: 1) severe lymphoid depletion in the thymus, spleen and Peyer's patches, 2) inclusion bodies in the renal pelvic and vesical urothelium, 3) mild multifocal, mainly histiocytic cerebral leptomeningitis with intrahistiocytic inclusion bodies, 4) a few syncytial cells (uncertain cell type) with inclusion

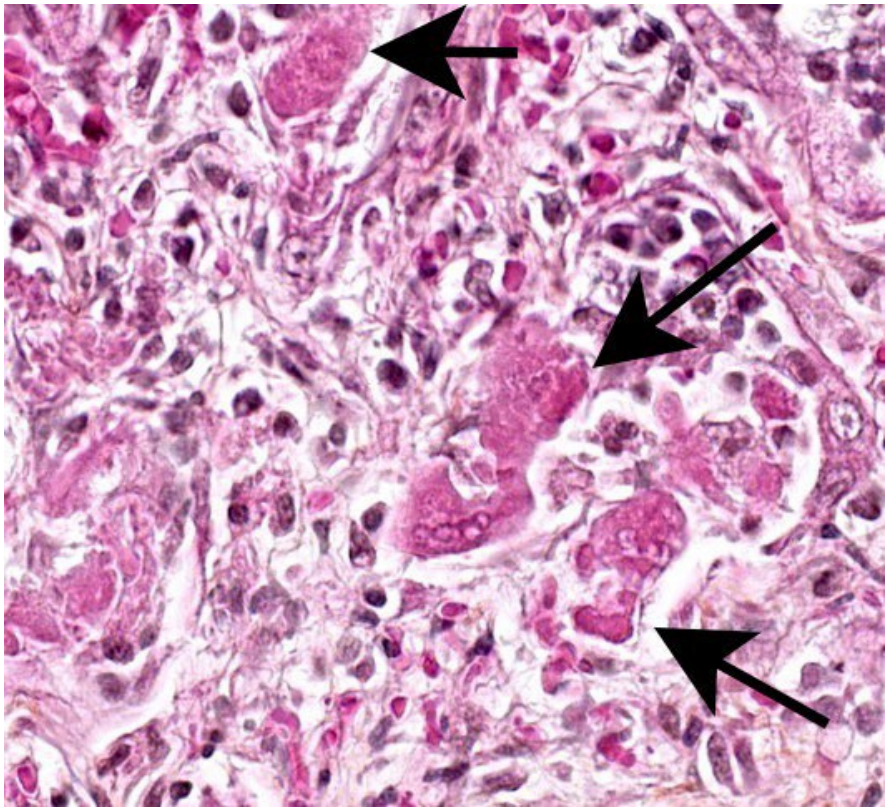

Lung, dog. Viral syncytia contain irregular, brightly eosinophilic intracytoplasmic viral inclusions. (HE, 440X)

bodies in the ocular trabecular meshwork, and 5) a few small foci of myocardial necrosis associated with vascular fibrinoid necrosis and minimal lymphoplasmacytic inflammation. Inclusion bodies were not found in other organs/tissues (e.g. stomach, conjunctiva…), and there were no lesions in the upper respiratory tract and conjunctiva.

Contributor's Morphologic Diagnoses:
Marked, diffuse, subacute, proliferative and bronchointerstitial pneumonia with numerous epithelial syncytia (type II pneumocytes) and intracytoplasmic eosinophilic inclusion bodies, consistent with canine distemper virus (CDV) pneumonia.

Contributor's Comment:
Histopathological observations and PCR results were consistent with systemic canine distemper (CD), characterized by marked pneumonia and lymphoid depletion and minimal CNS and ocular lesions; the myocardial necrosis was also attributed to CDV.[2,5] Testing for other pulmonary pathogens (e.g. CPIV-5 or CAV-1PCR; bacteriology) was not done as the lesions were typical for canine distemper virus (CDV) and there was no evidence of secondary bacterial infection. This case was submitted as an example of a CDV-induced proliferative pneumonia with numerous type II pneumocytes syncytia and inclusion bodies which, when present, are characteristic of the disease.[2] Canine distemper is a systemic disease caused by a single-stranded RNA virus in the family *Paramyxoviridae*, genus *Morbillivirus*. This genus presently includes, in addition to CDV, the *Measles virus* (MeV), the *Phocine distemper virus* (PDV), the *Cetacean morbillivirus* (CeMV), the *Peste des petits ruminants virus* (PPRV), the *Rinderpest virus* (RPV) and the more recently discovered *Feline morbillivirus* (FeMV); the RPV was eradicated in 2011.[3] All morbilliviruses share many virological, clinicopathological and epidemiological characteristics, with the exception of FeMV which is associated with renal tubulointerstitial disease.[3,10] Typical morbillivirus-induced disease is characterized mainly by profound and protracted immunosuppression, with respiratory, neurological and/or gastrointestinal signs, depending on virus/host.[3] As the range of hosts susceptible to MeV infection is very limited (primates),

CDV represents an interesting alternative model for the study of morbillivirus-induced disease such as measles.[3,4] The spectrum of hosts susceptible to CDV-induced disease includes all families of the order Carnivora, several seal species, javelinas and several macaque species;[1,4] CDV has also been isolated from many other terrestrial mammals and CDV is readily transmitted from one species to another.[7] In countries where vaccination is routinely done, CD incidence in dogs is low even though some vaccinated animals can develop the disease (possibly due to different strains).[1] However, CD is still very much a threat to domestic dogs and ferrets from countries where vaccination is not widespread and to wildlife in general. In the last decades, the known host range has expanded and several large outbreaks in different wildlife species have been documented; for instance, the much-publicized 1994 outbreak in large felids in Tanzania's Serengeti National Park killed about a third of its lion's population.[7]

Canine distemper is a highly contagious disease. Transmission of CDV is most frequently by inhalation of aerosols from the respiratory tract or direct contact with oronasal secretions, but all secretions are potentially infective.[1,2,7,9] The virus reaches the upper respiratory tract or pulmonary mucosa where it infects macrophages and monocytes and then reaches the tonsils and regional lymph nodes; it is highly lymphotropic. There is a subsequent first viremia and the virus is disseminated to all lymphoid organs/tissues (~2-6 days P.I.), either free or within leukocytes. The virus induces apoptosis in lymphocytes, mainly CD4+ T cells, resulting in lymphoid depletion, lymphopenia and immunosuppression. There is a second viremia in which the virus spreads to epithelial cells in many organs, mainly in the respiratory, gastrointestinal and urinary tracts and to the CNS (~10 days P.I).[1,2,7,9] The CDV H-protein (hemagglutinin) is considered the key protein in viral attachment to host cells.[3,7,11] It is also essential to cell fusion, responsible for the formation of syncytia which are characteristic of systemic morbilliviral diseases.[11] There are two major receptors, both with an immunoglobulin-like variable domain, for CDV on host cells: 1) CD150 or SLAM (signaling lymphocyte activation molecule) on B and T lymphocytes, dendritic cells and macrophages, and 2) nectin-4 (poliovirus-receptor-like-4) on epithelial cells.[4,7] The pathogenesis, pathology and clinical signs of the neurological form of CD are variable; it will not be discussed further (see reference 1). The severity of CDV-induced disease depends on virus strain (there is only one serotype), host immunity, age and species; in domestic animals, ferrets are considered the most susceptible species.[3] Animals with adequate humoral and cellular immunity will generally clear the infection after the first viremia, within 14 days of infection.[1]

In susceptible dogs, CD is generally a disease of dogs 3-6 months of age, when passive immunity declines.[2,9] The disease can be transmitted *in utero* (transplacental) in CDV-naïve animals, causing abortion, weak puppies and fatal neurological disease in newborn puppies; an unusual case with respiratory, but not neurological disease has been reported in 5-12 days puppies.[9] The pathology of CD in dogs is variable, but lesions are mostly found in the CNS (most frequently demyelinating leukoencephalomyelitis), the lower respiratory tract and lymphoid organs (lymphocytolysis and lymphoid depletion);[1,2] ocular and nasal discharge is relatively frequent and helpful in the clinical diagnosis of respiratory and/or neurological disease (e.g CD vs rabies). In the lungs, CD may cause minimal to no lesions, typical viral bronchitis/bronchiolitis or bronchointerstitial pneumonia with or without type II pneumocyte proliferation. Syncytial formation is variable and observed

in the lungs and occasionally in the CNS;[2] it has been reported that the more a CDV strain is attenuated, the more it will induce syncytial formation.[11] Inclusion bodies can be found in nearly all organs (epithelial cells, histiocytic cells, astrocytes, neurons…), with or without lesions, and are helpful for diagnosis. They are eosinophilic, mostly intracytoplasmic in epithelial and histiocytic cells, and mostly intranuclear in the CNS (astrocytes and neurons); a study found the tonsils to be the most consistently involved cells, which could be of interest for the ante-mortem diagnosis of CD (biopsy).[6] Some dogs have minimal CD-associated lesions, but because of immunosuppression develop opportunistic infections (e.g. bacterial and/or CAV-1 pneumonia, toxoplasmosis, cryptosporidiosis …). Other reported lesions include:

1. Pustular dermatitis and nasodigital hyperkeratosis/parakeratosis ("hardpad disease")[1,2]
2. Enamel hypoplasia/dysplasia[1,2]
3. Conjunctivitis ± keratitis, retinitis, optic neuritis[2]
4. Polioencephalomyelitis (can be concomitant with leukoencephalomyelitis) and "old dog encephalitis"[1,2]
5. Myocardial necrosis[2,5]
6. Growth retardation lattice (metaphyseal osteosclerosis)[1,2]

Contributing Institution:
Faculty of veterinary medicine, Université de Montréal. http://fmv.umontreal.ca/faculte/departements/pathologie-et-microbiologie

JPC Diagnosis: Lung: Pneumonia, bronchointerstitial, proliferative and histiocytic, diffuse, severe, with marked type II pneumocyte hyperplasia and hypertrophy, viral syncytia, and intracytoplasmic and intranuclear inclusions.

JPC Comment:
The contributor provides a thorough review of this classic case of canine distemper virus infection. As previously stated, CDV infects a wide range of host species, and a 2020 *Vet Pathol* report detailed the first documented cases of CDV infections in sloths.[8] The outbreak occurred in Tennessee, and five of eight sloths within the quarantine enclosure died after a short history of lethargy and hyporexia.[8] Crusting and ulceration over the tongue, oropharyngeal mucosa were present in three animals.[8] All cases had lingual and oropharyngeal mucosal erosions and ulcerations, necrotizing bronchointerstitial pneumonia, multifocal splenic necrosis, random hepatic necrosis.[8] Intranuclear and intracytoplasmic inclusions were observed in numerous tissues, including oropharyngeal mucosa, trachea, alveolar macrophages, type II pneumocytes, esophagus, urinary bladder, and hepatocytes.[8] IHC confirmed CDV presence in the epithelial cells of the tongue, hepatocytes, and less frequently in the meningeal vessel walls, ependymal cells, and choroid plexus.[8] The infection also spread to three kinkajous in the same enclosure who died after developing the same clinical signs.[8]

The moderators, Dr. Eric Lee and Dr. Juliana Lee, and conference participants discussed the amount of autolysis in this specimen, as evidenced by sloughing of individualized epithelial cells in the bronchioles, which obscured evidence of epithelial necrosis. Ultimately, the group decided there was enough convincing evidence of bronchiolar involvement to diagnose bronchointerstitial pneumonia.

References:
1. Beineke A, Puff C, Seehusen F, *et al*. Pathogenesis and immunopathology of systemic and nervous canine distemper.

Vet Immunol Immunopathol. 2009;**127**(1-2):1-18.
2. Caswell JL, Williams KJ. Respiratory system. In: *Jubb, Kennedy and Palmer's Pathology of domestic animals*, vol.2. Sixth Edition. Elsevier. St.Louis, Mo, 2016:465-591.
3. da Fontoura Budaszewski R, von Messling V. Morbillivirus Experimental Animal Models: Measles Virus Pathogenesis Insights from Canine Distemper Virus. Viruses. 2016;11;**8**(10). pii: E274.
4. de Vries RD, Ludlow M, Verburgh RJ, *et al*. Measles vaccination of nonhuman primates provides partial protection against infection with canine distemper virus. J Virol. 2014;**88**(8):4423-33.
5. Higgins RJ, Krakowka S, Metzler AE, *et al*. Canine distemper virus-associated cardiac necrosis in the dog. Vet Pathol. 1981;**18**(4):472-86.
6. Kubo T, Kagawa Y, Taniyama H, *et al*. Distribution of inclusion bodies in tissues from 100 dogs infected with canine distemper virus. J Vet Med Sci. 2007;**69**(5):527-9.
7. Loots AK, Mitchell E, Dalton DL, *et al*. Advances in canine distemper virus pathogenesis research: a wildlife perspective. J Gen Virol. 2017;**98**(3):311-321.
8. Nambulli S, Sharp CR, Acciardo AS, Drexler JF, Duprex WP. Mapping the evolutionary trajectories of morbilliviruses: what, where, and whither. *Curr Opin Virol.*2016; 16:95-105.
9. Pandher K, Podell B, Gould DH, *et al*. Interstitial pneumonia in neonatal canine pups with evidence of canine distemper virus infection. J Vet Diagn Invest. 2006;**18**(2):201-4.
10. Park ES, Suzuki M, Kimura M, *et al*. Epidemiological and pathological study of feline morbillivirus infection in domestic cats in Japan. BMC Vet Res. 2016;**12**(1):228.
11. von Messling V, Zimmer G, Herrler G, *et al*. The hemagglutinin of canine distemper virus determines tropism and cytopathogenicity. J Virol. 2001; **75**(14):6418-27.
12. Watson AM, Cushing AC, Sheldon JD, et al. Natural Canine Distemper Virus Infection in Linnaeus's 2-Toed Sloths (*Choloepus didactylus*). *Vet Pathol*. 2020; 57(2): 311-315.

CASE III:

Signalment:
Estimated 3-year-old, spayed-female, Beagle dog (*Canis lupus familiaris*)

History:
The patient was originally adopted from Puerto Rico and was estimated to be 3-years-old. The patient was reportedly up-to-date on routine veterinary care, including vaccination (last vaccination was given Sept 2018 - about 1 year prior to presentation).

Patient initially presented to the Neurology Service for a one-month history of progressive ataxia and lethargy. At that time, neurolocalization included the thalamic cortex and cerebellar vestibular system. MRI did not reveal any abnormalities and CSF analysis showed normal protein levels with a slightly elevated mononuclear cell count. Tick-borne

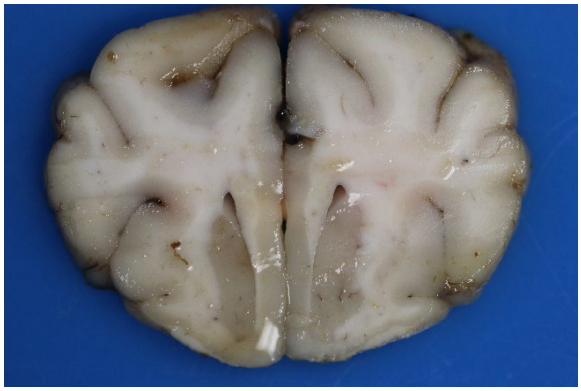

Cerebrum, dog: There is multifocal loss of the sharp linear distinction between grey and white matter (Photo courtesy of: Animal Medical Center, 510 E. 62nd Street, New York, NY 10065.)

disease panel was negative. The patient was managed over one month with doxycycline and corticosteroids. Over the following month, the patient continued to decline with progressive ataxia and mentation changes, resulting in euthanasia.

Gross Pathology:
There is multifocal loss of grey-to-white matter distinction. Randomly the white matter contains poorly demarcated, soft, tan regions/streaks (tinctorial change; decreased parenchymal whiteness), which is more evident in the rostral cerebrum. Throughout the cerebral cortex, the grey and white matter there are dozens of poorly demarcated, soft, light brown-yellow foci. The meninges over the spinal cord are mildly to markedly thickened, mottled tan, brown, and dark red (hemorrhages).

Laboratory Results:
Touch imprints of the meningeal surface are of good cellular and stain quality. Sample is comprised of rafts of cohesive mildly pleomorphic epithelial cells mixed with small numbers of macrophages, lymphocytes, and plasma cells on a hemodiluted background.

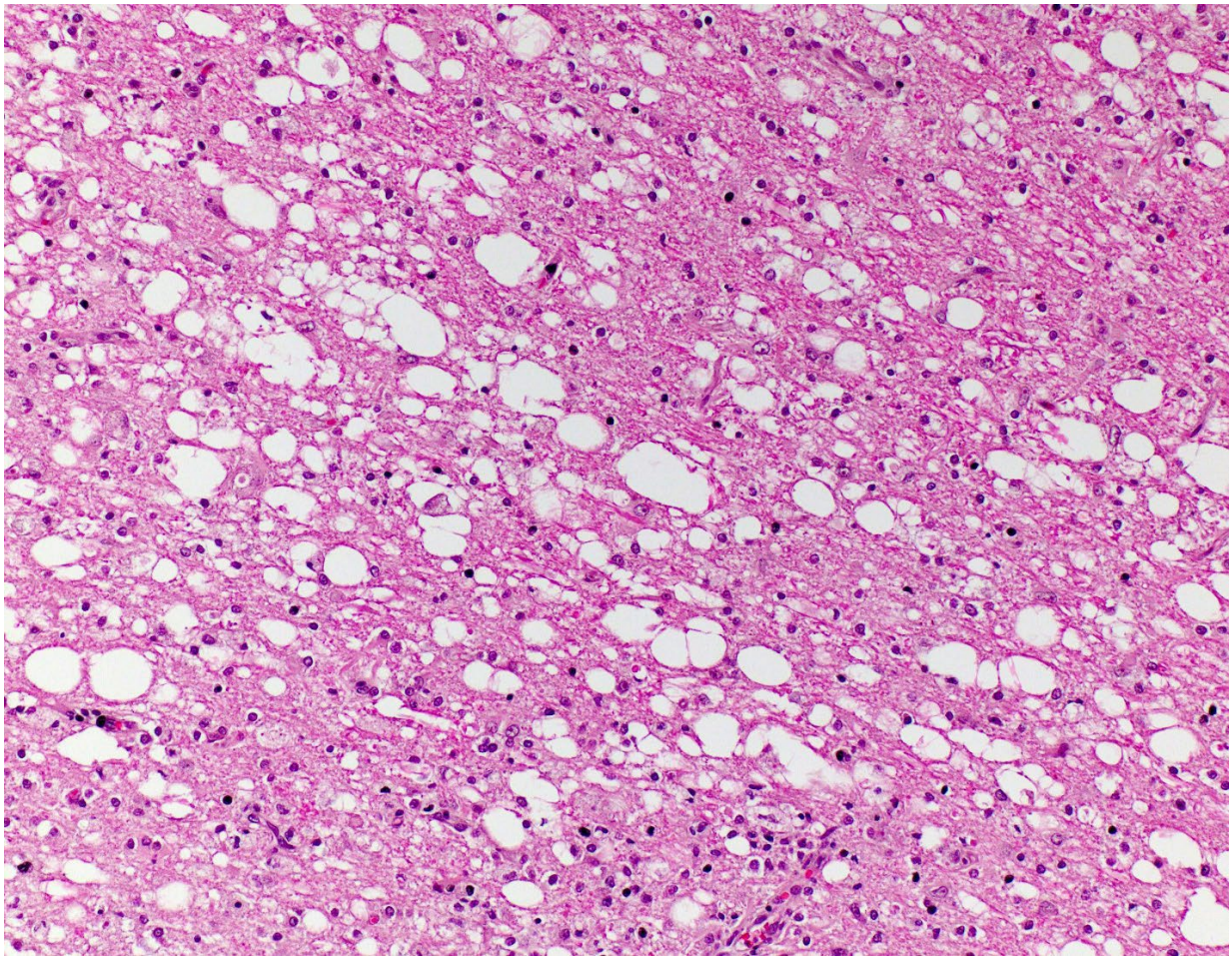

Within the subcortical white matter tracts, white matter tracts of the pons, and interspersed white matter within metencephalon are foci of spongiosis with myelin sheath loss, severely dilated myelin sheaths that infrequently contain macrophages or fragmented myelin (digestion chambers), and multifocal swollen axons (spheroids). (Photo courtesy of: Animal Medical Center, 510 E. 62nd Street, New York, NY 10065.)

Microscopic Description:
Brain, cerebral cortex -or- metencephalon at the level of the cerebellar peduncles: Subcortical white matter tracts, white matter tracts of the pons, and interspersed white matter within metencephalon are multifocally pale and vacuolated (spongiosis). Within these regions, there is myelin sheath loss, severely dilated myelin sheaths that infrequently contain macrophages or fragmented myelin (diges tion chambers), and multifocal swollen axons (spheroids). Affected white matter tracts contain moderately increased numbers of reactive astrocytes. Multiple, inconsistently coalescing, poorly demarcated regions of grey matter display mild neuropil rarefaction and contain moderately to severely increased numbers of activated, reactive glial cells and gemistocytic astrocytes and few infiltrating lymphocytes and plasma cells. Astrocytes are commonly hypertrophied. Regional neurons are degenerate, multifocally display central chromatolysis, and are less frequently are shrunken, angulated, and hypereosinophilic (necrotic neurons). Neurons and astrocytes often contain intranuclear and/or -cytoplasmic 3-7µm, round to oval, hyaline, pink or magenta inclusion bodies that in nuclei are associated with chromatin margination and clearing. There are rare syncytial cells. Regional cerebral blood vessels are occasionally tortuous and are often lined by swollen, hypertrophied endothelial cells. Multifocally, the meninges are mildly infiltrated by lymphocytes, plasma cells, and macrophages. Following along Virchow-Robbin spaces and surrounding multiple cerebral blood vessels are moderate cuffs of lymphocytes, plasma cells, and lesser macrophages.

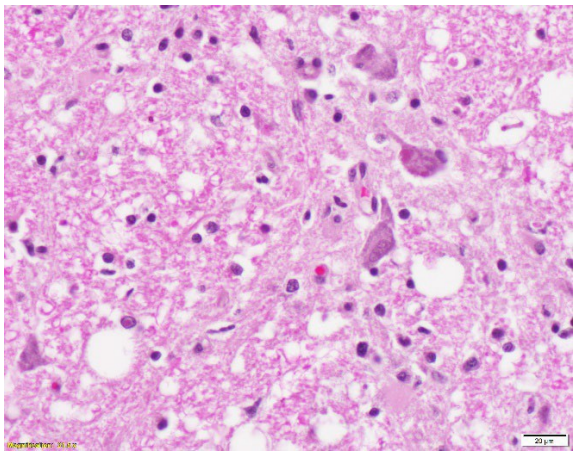

Cerebrum, dog: Affected white matter tracts contain moderately increased numbers of reactive astrocytes. (Photo courtesy of: Animal Medical Center, 510 E. 62nd Street, New York, NY 10065.)

Immunohistochemical stain for canine distemper virus (Animal Health Diagnostic Center/Cornell University) was placed on sections of the brain and revealed strong cytoplasmic immunoreactivity within neurons and astrocytes and highlights axonal projections.

Contributor's Morphologic Diagnoses:
1) Demyelination and axonal degeneration, multifocal to locally extensive, moderate to marked with spongiosis, swollen myelin sheaths with fragmented myelin and macrophages (digestion chambers), and multifocal distended axons (spheroids)
2) Leukoencephalitis, lymphoplasmacytic, histiocytic, chronic, multifocal, moderate with regional moderate to marked gliosis, neuronal degeneration and necrosis with mild neuronophagia, numerous intranuclear and -cytoplasmic inclusions, rare syncytial cells, and moderate lymphoplasmacytic perivascular cuffs

Contributor's Comment:
Histologic features in this case were consistent with a demyelinating leukoencephalitis. Other findings in this dog were a single *Dirofilaria immitis* adult in the pulmonary artery with expected reactive changes in the blood vessel and a single metazoan parasite larva in one kidney. In dogs, differentials for leukoencephalopathy include viral (rabies, CDV, canine herpes virus) and parasitic (*Neospora caninum*) infections, as well as non-

infectious etiologies (e.g., polyneuritis, allergic encephalitis, necrotizing encephalitis).[16] Profound demyelination and the presence of both intracytoplasmic and -nuclear inclusion bodies was suggestive of paramyxovirus infection. Lesions were most prevalent and severe in the cerebral cortex and the caudalmost focus was in the metencephalon at the level cerebellar peduncles. The cerebellum, caudal brainstem, and spinal cord were spared. Immunohistochemistry for CDV confirmed intense immunoreactivity in neurons and astrocytes. Based on this patient's signalment and history, progressive neurologic disease over two months, and histologic lesion distribution, the current case was most consistent with "old dog encephalitis" (ODE). Like other reported cases of ODE, this patient was up-to date on vaccinations.

Canine distemper virus is a highly contagious disease of carnivores with a worldwide distribution.[1-21] Infections and outbreaks have been reported in numerous families within the order Carnivora**,** including Canidae (fox, wolves), Mustelidae (ferret, mink), Hyaenidae (hyena), Procyonidae (raccoon), Ailuridae (red panda), Ursidae (bear), Viverridae (civet, mongoose), Mephitidae (skunks), Odobenidae (walrus), Otariidae, and Felidae.[3, 5, 9-11, 13, 19, 21] Most infections involve carnivores, but infections have been reported in non-carnivore species in the orders Rodentia, Primates, Artiodactyla (pigs, cervids), Pilosa (tamandua and sloth), and Proboscidea (elephants).[5, 9, 10, 11, 17] Outbreaks have been described in multiple wildlife species and hence CDV is a threat to conservation efforts worldwide.[5, 10, 11] CDV can circulate in wildlife species even when infection rates are low in domestic dogs, suggesting that the virus persists in a complex reservoir system[10] and thus both asymptomatic domestic and wildlife reservoirs play an important role in driving epidemics.[5] In one review, the majority of cases outside of domestic dogs were reported

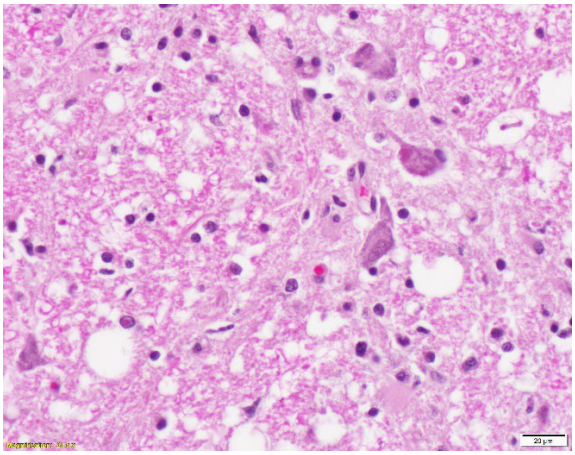

Cerebrum, dog: Affected white matter tracts contain moderately increased numbers of reactive astrocytes. (Photo courtesy of: Animal Medical Center, 510 E. 62nd Street, New York, NY 10065.)

in captive animals, suggesting that conditions of captivity (e.g., housing multiple mammalian species in close proximity) is a risk factor for infection.[10] CDV should be a considered a differential diagnosis of disease and extinction events, even in species outside of the order Carnivora.[10]

Canine distemper virus (CDV) belongs to the family Paramyxoviridae within the morbillivirus genus.[1-3, 5-11, 13, 14, 16, 17, 20, 21] Other important morbilliviruses in veterinary medicine include Rinderpest Virus, Peste des Petits Ruminants Virus, Phocine Distemper Virus, Cetacean Morbillivirus, and Equine Morbilivirus.[8-11, 16, 19, 21] Important veterinary pathogens within the larger Paramyxoviridae family include those of the genera henipavirus (Hendra and Nipah Viruses), avulavirus (Newcastle Disease Virus and other avian paramyxoviruses), rubulavirus (Porcine Rublavirus, mumps), respirovirus (Sendai virus, Bovine Parainfluenza Virus 3), Metapneumovirus (Avian Rhinotracheitis Virus), ferlavirus (Fer-de-lance), and aquaparamyxovirus (Atlantic Salmon Paramyxovirus), as well as several unclassified paramyxoviruses (Bottle-nosed Dolphin paramyxovirus, Salem Virus). [8, 9, 11, 12]

Paramyxoviruses are large (150-300 nm), pleomorphic, enveloped viruses with a negative-sense, single-stranded RNA genome.[3, 5, 6, 8, 9, 11, 14, 17, 20, 21] Viral proteins include two viral envelope glycoproteins (fusion (F) and hemagglutinin (H)), a nucleocapsid (N) protein, two transcription-associated proteins (P protein and viral polymerase (L)), and a membrane (M) protein. [3, 5, 9-12, 20] Infection is initiated through binding of the viral hemagglutinin (H) protein to SLAM (signaling lymphocyte activation molecule) and nectin-4 receptors on host immune and epithelial cells, respectively.[5, 9, 10, 20] A potential 3rd host receptor, GliaR, is suggested on glial cells.[5] Thus, the highly variable H glycoprotein is the main determinant of cellular and host tropism. [5, 9, 10, 12, 20] Virulence is modulated via the fusion (F) glycoprotein, which mediates union between the virus and host plasma membranes allowing for viral penetration.[5, 20] Characteristic syncytial cells due to host cell fusion is likewise facilitated by the F glycoprotein.[9, 20] Replication occurs in the host cell cytoplasm and virions are released by budding from the plasma membrane through interactions with the membrane (M) protein.[5, 11, 12] Infection is cytolytic with the virus killing host cells during replication and release.[11, 20] Virus is shed primarily in respiratory secretions, but other body secretions and fluids are infectious to a lesser extent.[3, 5, 7] The primary modes of transmission include close contact and aerosol.[3, 5-7, 9-11, 20, 21] As this virus is relatively labile in the environment, [9, 11] fomite transmission is less frequent. [3, 5-7, 9-11, 20, 21]

After inoculation, CDV first colonizes the upper respiratory tract mucosa, where it infects local lymphocytes and is phagocytized by local macrophages and dendritic cells.[6, 9, 11, 13, 19-21] Infected immune cells then travel to the regional lymph nodes and tonsils, where viral replication occurs resulting in lymphoid necrosis and depletion.[3, 6, 9, 11, 13, 19-21] Primary viremia results allowing for dissemination through the hemolymphatic system.[3, 6, 9, 11, 13, 19-21]

The resulting immunosuppression facilitates the development of opportunistic infections, [3, 6, 9, 11, 13, 19 21,

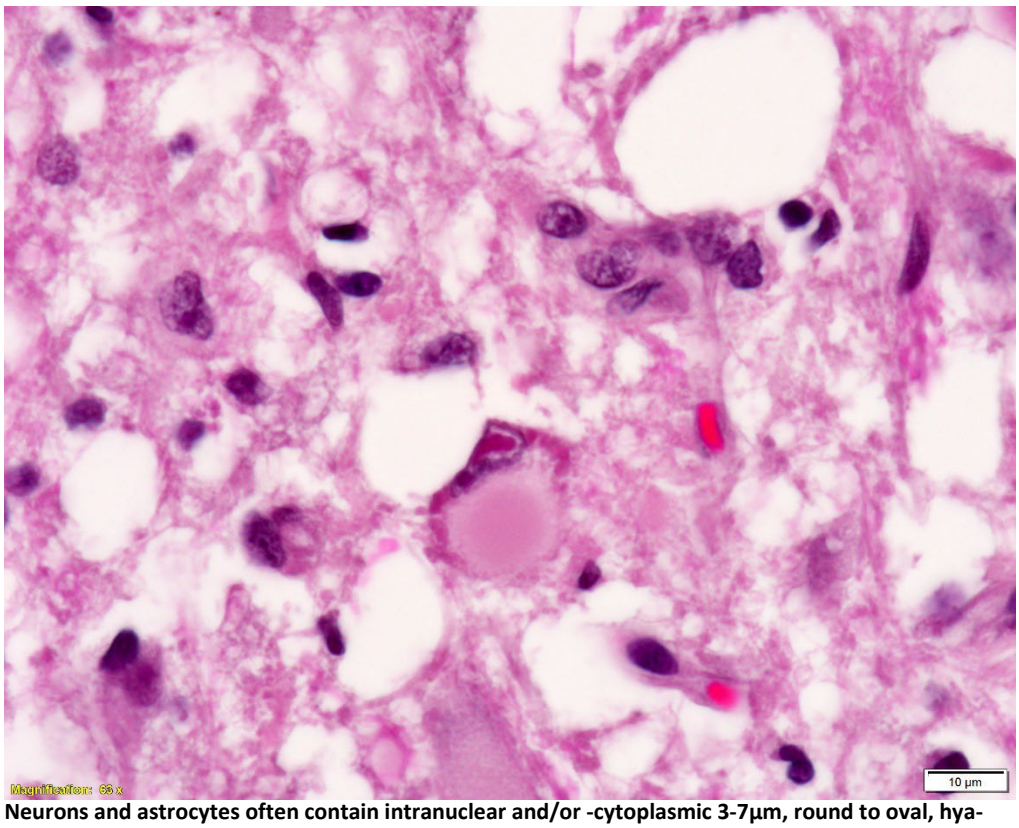

Neurons and astrocytes often contain intranuclear and/or -cytoplasmic 3-7µm, round to oval, hyaline, pink or magenta inclusion bodies. (Photo courtesy of: Animal Medical Center, 510 E. 62nd Street, New York, NY 10065.)

and CDV-associated thymic atrophy further drives immunosuppression.[3, 16] Secondary viremia develops through leukocyte and platelet trafficking and cell free viremia.[5, 6, 9, 11, 13, 19-21] The extent of viral dissemination and thus clinical disease depends on the rapidity and effectiveness of the individual's immune response against the specific viral strain.[3, 9, 11-13, 21] Patients with an adequate immune response will go on to clear infection, while those that mount a poor to absent response display widespread systemic disease with high mortality.[3, 9, 13, 21] With an intermediate immune response, minor to absent mucosal disease and variable neurologic disease may be seen.[3, 9, 13, 21]

Canine distemper virus is pantropic with a high affinity for lymphoid, epithelial, nervous, and ocular tissues.[13, 20, 21] Severity of disease depends on the viral strain, age and immune status of the host, and rapidity of the immune response. [3, 6, 9, 11-13] Clinical disease in dogs is most common in puppies of 12-16 weeks of age when maternally derived, passive immunity wanes. [3, 6, 9, 11-13, 20] In these young naive dogs, clinical disease typically manifests as a combination of CNS, respiratory, and/or gastrointestinal signs. [9, 13, 20] Infection typically starts with fever and conjunctivitis and rapidly progresses to respiratory and gastrointestinal signs.[3, 9] Extra-nervous signs typically develop about a week post inoculation and include pyrexia, oculonasal discharge, pharyngitis, tonsilitis, otitis interna/labyrinthitis, cough, vomit, diarrhea, skin rash and pustules, hyperkeratosis of the nose and foot pads, enamel hypoplasia (due to ameloblast degeneration and necrosis), lower urinary tract signs, ocular disease (due to viral retinitis, non-suppurative optic neuritis, and optic nerve demyelination), and abortion.[3, 5, 6, 9, 11-17, 19-21] Histologic changes in the lungs include necrotizing bronchointerstitial

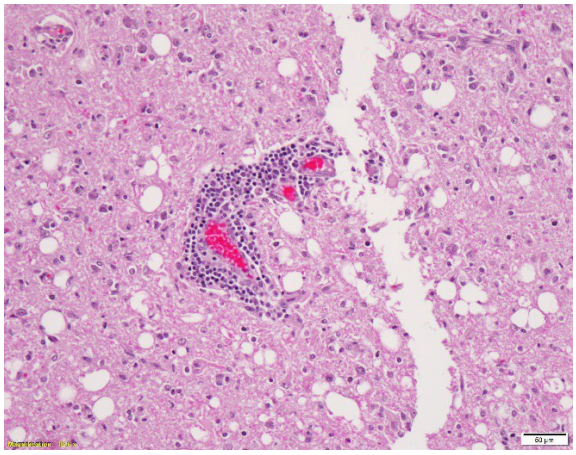

Cerebrum, dog: Regional cerebral blood vessels are occasionally tortuous and are often lined by swollen, hypertrophied endothelial cells and contain 2-3 layers of lymphocytes and plasma cells. (Photo courtesy of: Animal Medical Center, 510 E. 62nd Street, New York, NY 10065.)

pneumonia with type II pneumocyte hyperplasia and syncytial cell formation, pulmonary edema, and inclusion bodies in pneumocytes and alveolar macrophages.[3] Enteric lesions attributable to the gastrointestinal signs are not well described, but virus is thought to infect the intestinal crypt epithelium.[14] CDV less consistently causes an infectious myocarditis, which depending on chronicity can be accompanied by frank myocardial necrosis and/or fibrosis. [3, 19] In both experimental and natural infections growth retardation lattices can be seen in the bones, which in experimental models was related to transient impaired osteoclastic resorption of the primary spongiosis.[4] In an outbreak in Linnaeus's 2-toed sloth (*Choloepus didactylus*), marked hepatic tropism was an atypical striking feature.[17] Affected dogs may die at this stage, recover fully, or go on to develop neurologic signs 1-6 weeks later.[3, 6, 9, 11, 21]

CDV is associated with several distinct nervous system manifestations in dogs[1] that include: 1) canine distemper encephalomyelitis in immature dogs, 2) old dog encephalitis, 3) multifocal distemper encephalomyelitis in mature animals, and 3) post-vaccinal enceph-

alitis.[1, 7] The latter three are uncommon manifestations confined to the CNS only.[1, 2, 7] The syndrome that develops is directly dependent on the viral strain, host age and immune status, and neuroanatomic location of pathologic lesions.[7] The most common CNS manifestation is canine distemper encephalomyelitis in immature dogs that is part of the above-described pantropic infection. [1, 2, 7, 13] In these naive animals, neurologic disease can occur with or without preceding or concurrent gastrointestinal and/or respiratory signs.[9, 13, 16, 20, 21] Approximately 30% of dogs infected with systemic disease ultimately develop neurologic dysfunction observed 1-6 weeks after the onset of initial signs.[6, 9, 20, 21] Hematogenous spread to the CNS allows for initial infection of and viral replication in vascular pericytes and astrocyte foot processes, endothelial cells, microglia, and choroid plexus epithelium.[13, 20, 21] Involvement of the choroid plexus epithelium and ependyma allows for the virus to be shed into and disseminated by the CSF.[3, 20, 21] With dissemination, virtually all cells of the CNS are susceptible to infection.[3, 11, 13, 20, 21] Neurologic signs include cerebellar or vestibular ataxia, "gum chewing", paresis to paralysis, myoclonus, tremors, circling, hyperesthesia, and epileptic seizures. [3, 5, 6, 9, 11, 16, 19-21] In a recent single case report, CDV infection presented as focal lower motor neuron signs and hyperesthesia to one forelimb, which rapidly progressed to diffuse lower motor signs of all limbs and seizures.[6] This unique presentation was related to lesion distribution to the C5 and lumbar spinal cord segments.[6] The main histologic lesion in naïve patients is a demyelinating leukoencephalopathy related to viral-induced injury to the neurons and olidodendroglia.[9, 13, 16, 17, 20, 21] Acute lesions in the CNS are not overwhelmingly inflammatory and are likely related to metabolic dysfunction, decreased myelin synthesis by damaged oligodendrocytes, and microglia activation.[9] With lesion progression CDV-specific immuneresponses and viral persistence induce an inflammatory reaction.[9] Viral-induced damage to oligodendrocytes leads to highly characteristic, primary demyelination predominantly distributed to the cerebellum, periventricular white matter, spinal cord, and optic tracts.[3, 6, 9, 13, 16, 18, 20, 21] Additional white matter changes depend on chronicity and include intra-myelinic edema, vascular proliferation with hypertrophied endothelial cells, infiltrating macrophages associated with myelin debris, white matter necrosis, gliosis.[3, 9, 16, 18, 20, 21] Alterations to the grey matter target the cerebral cortex, cerebellum, brainstem, and spinal cord and include non-suppurative encephalitis with perivascular cuffs.[3, 16, 20, 21] Neuronal injury is demonstrated by central chromatolysis and degenerative neurons that progress to eventual necrosis with inconsistent neuronophagia.[3, 16, 20, 21] Intracytoplasmic and -nuclear inclusions are seen in neurons and astrocytes.[11, 16, 21] Sclerotic astrocyte foci and myelin loss may be seen in survivors.[3, 11, 20, 21]

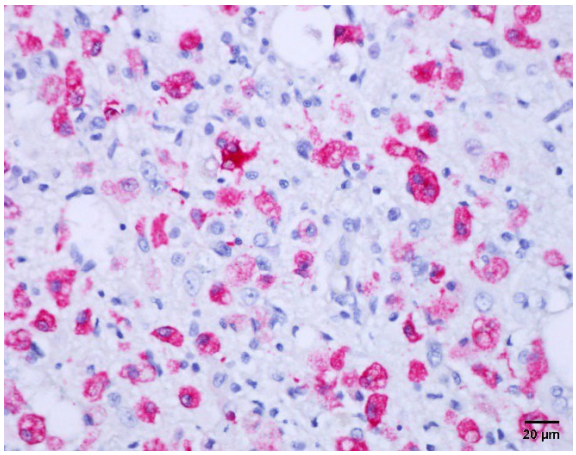

Cerebrum, dog: Immunohistochemistry for CDV antigen reveals strong cytoplasmic immunoreactivity within neurons and astrocytes and highlights axonal projections. (Photo courtesy of: Animal Medical Center, 510 E. 62nd Street, New York, NY 10065.)

This patient's signalment and history (i.e., middle-age, progressive neurologic disease

over two months, and up-to-date vaccination status) and pathologic findings (i.e., lack of findings consistent with systemic CDV infection, histomorphologic features confined to the CNS, and lesion distribution) were most consistent with "old dog encephalitis". Old dog encephalitis (ODE) is a rare, unique, invariably fatal CNS-only presentation in older dogs.[1-3, 7, 9-12, 16, 21] A diagnosis of ODE necessitates a combination of clinical history and findings, typical histologic lesions and distribution, and absence of CDV-induced lesions in other organs.[7] Affected animals are typically completely vaccinated with no evidence of previous systemic CDV infection.[1, 7, 9, 12, 20] Clinical disease is insidious characterized by chronic, progressive cortical disease with motor and behavioral disturbances (i.e., circling, swaying, weaving, compulsive walking, postural reaction deficits, head pressing, and pushing on fixed objects) .[1-3, 7, 11, 21] In one experimentally-induced ODE case, the dog exhibited multiple episodes of relapsing cortical and subcortical signs and epileptic seizures were part of this dog's disease.[1] Gross lesions are non-specific with ODE and include dilation of the ventricles, loss of grey-white matter distinction, and grey-brown regions in the forebrain.[2,7] Histologic changes are confined to the cerebral cortex, thalamus, and mid-brain, with sparing of the caudal brainstem and spinal cord.[1, 2, 7, 16, 21] Histomorphologic features include demyelination; vacuolization of the subcortical white matter, non-suppurative encephalitis with profound perivascular cuffs; astrocytosis and astrogliosis; neuronal loss, degeneration, and necrosis; and neuropil rarefaction.[1, 2, 7, 16, 21] Inclusion bodies are numerous.[1, 2, 7, 16, 21] Ultrastructural changes include mononuclear cuffs, viral nucleocapsids and viral budding in the grey matter, electron-dense granular material in Virchow-Robbins spaces (unclear origin), and white matter changes suggestive of abortive and inadequate axonal remyelination (i.e., naked axons surrounded by astrocyte processes and remyelinated axons with thin myelin sheaths) and chronic demyelination (i.e., loosely arranged demyelinated axons separated by inflammatory cells).[1] The pathogenesis of old dog encephalitis is unclear and the host-to-virus relationship is not understood.[1-3, 7, 9-12, 16, 21] Previously proposed theories have included: 1) wild-type viral persistence in a rare replication-defective state, 2) terminal result of chronic subclinical CDV encephalitis, 3) re-infection, and 4) a viral strain predisposed to persistent infection.[1, 2, 9, 11, 12, 21] At this time, ODE is believed to be the result of virus persistence in the CNS in a replication-defective form.[1-3, 7, 9-12, 16, 21] Evidence to support this theory include: 1) ODE isolates are antigenically similar to the wild-type virus and don't display a mutation rate beyond what is expected for an RNA virus,[1, 7] 2) unique histomorphologic features of ODE that are less consistent with progression of previous infection (i.e., profound angiogenic distribution and atypical lesion localization),[1, 7] 3) difficult post-infection isolation of the inoculating virus (i.e., prolonged culture and coculture with susceptible Vero cell monolayer),[1] and 4) patient histories[1-3, 7, 9-12, 16, 21]. In addition, ODE has some similarities to subacute, sclerosing panencephalitis (SSPE) seen in children with persistent infections with a replication-defective measles virus.[1, 11, 12] SSPE is slightly different from ODE in that SSPE isolates are constitutively replication defective and therefore never produce viral particles, where in ODE virions can be isolated but with significant difficulty.[1, 12]

Other CNS-only manifestations of CDV are similarly uncommon. Multifocal distemper encephalitis in the mature dog is a rare, chronic progressive disease due to infection in middle-aged to senior dogs (4-8-years-old).[2] Clinical signs include slowly progressive head tremors, hindlimb paresis, and in-

coordination.[2] Seizures are not typical.[2] Histologic changes are restricted to the CNS, where lesions are predominantly distributed to the cerebellum and spinal cord, with sparing of the cerebral cortex.[2] Histologic features include a demyelinating leukoencephalitis, multifocal necrotizing, non-suppurative encephalitis, and rare intranuclear inclusion bodies.[2] Post-vaccinal distemper is uncommon and presents as severe, often lethal neurologic decompensation with aggressive behavior in patient who have been recently vaccinated (within 3 weeks) with an attenuated viral strain.[2, 16] Histologic lesions are not well-characterized, but grey matter changes are similar to those described in natural disease with relative sparing of the white matter.[2]

Contributing Institution:
Animal Medical Center
510 E. 62nd Street
New York, NY 10065

JPC Diagnosis: Cerebrum: Encephalitis, lymphohistiocytic, chronic, multifocal, moderate, with spongiosis, gliosis, and neuronal and glial intranuclear and intracytoplasmic viral inclusions.

JPC Comment: The contributor provides an excellent and thorough review of systemic and neurologic manifestations of canine distemper virus infection. This week's moderators, Drs. Eric and Juliana Lee, selected two cases of canine distemper (see Case 2 for CDV-pneumonia in a dog) to demonstrate the spectrum of disease caused by this pancytotropic virus.

CDV is closely related to two other morbilliviruses: rinderpest virus (RPV) and human measles virus (HMV). Rinderpest virus, which was recently eradicated, is the oldest of these viruses, with origins in Asia over three thousand years ago.[11] The virus then spread to the Near East and Europe, and texts from Greece and Rome document rinderpest outbreaks in the fourth century BCE.[15] Human measles virus was first documented around the ninth century CE, and the term morbilli, a diminutive for "morbus" or illness, was coined to differentiate it as a "small" illness compared to smallpox.[11] It is thought that human measles virus originated from RPV or a common morbillivirus precursor of ungulates and phylogenetic analysis suggests that it diverged around 12th century CE.[11,15] Canine distemper virus is much younger than both RPV and HMV, with the first reports in Central and South America in the early 1700s.[11] Two decades years after its first appearance in the New World, CDV was reported in Europe and its initial epizootic spread had a high initial rate of mortality, characteristic of a newly introduced pathogen.[15]

Several hypotheses have been proposed regarding the evolution and first occurrence of CDV in the Americas, including a sylvatic virus that jumped to domestic dogs or a virus of domestic dogs belonging to Paleoindians which spread with their movement.[15] A recent study by Uhl et al evaluated historical records, genetic and epidemiologic characteristics, and paleopathologic data to uncover the origins of CDV, and ultimately, they supported a different theory: that CDV began when HMV jumped from humans to dogs.[15] First, the group evaluated 2335 permanent teeth from 96 dog skeletons from the Weyanoke Old Town (750-1470 CE) site in Virginia and found no evidence of enamel hypoplasia (indicative of in utero CDV infection); additionally, enamel lesions were absent in 42 dogs from South American site dating from 1030-1324 CE.[15] These findings support the fact that CDV arose after the arrival of European explorers and the HMV they carried. Second, the remarkable genetic similarities in sequence, structure, antigenic epitopes, and host receptors they target indicate CDV and HMV likely arose from a common ancestor.[15] Codon usage analysis also indicates that CDV likely evolved from a virus that previously infected humans, as its codon usage bias (which reflects evolutionary host adapta-

tion) favors that of a human over a dog.[15] Finally, the authors used historical records to demonstrate the massive social disruption and upheaval caused by European activities coupled with overwhelming illness and death with the introduction of HMV to naïve populations provided ample opportunity for the virus to jump species and adapt to domestic dogs.[15] While not definitive proof, this interdisciplinary evidence supports the hypothesis that CDV infection in dogs arose from HMV epidemics in native South American populations.[15]

Conference participants debated whether demyelination or encephalitis were the primary lesions. Ultimately, participants felt the inflammation was more significant, and the number of gitter cells and level of myelin debris did not reach a level to support demyelination in the morphologic diagnosis. The term spongiosis was used to describe the white matter vacuolation visible from sub-gross magnification and could be the end-state of either of these two processes.

References

1. Axthelm ML and Krakowka S. Experimental Old Dog Encephalitis (ODE) in a Gnotobiotic Dog. *Vet Pathol*. 1998; 35: 527-534.
2. Cantile C and Youssef S. Nervous System. In: Maxie MG, ed. *Jubb, Kennedy and Palmer's Pathology of Domestic Animals*. Vol 1. 6th ed. Philadelphia, PA: Elsevier Saunders; 2016: 384-385.
3. Caswell JL and Williams KJ. Respiratory System. In: Maxie MG, ed. *Jubb, Kennedy and Palmer's Pathology of Domestic Animals*. Vol 2. 6th ed. Philadelphia, PA: Elsevier Saunders; 2016: 574-576.
4. Craig LE, Dittmer KE, and Thompson KG. Bones and Joints. In: Maxie MG, ed. *Jubb, Kennedy and Palmer's Pathology of Domestic Animals*. Vol 1. 6th ed. Philadelphia, PA: Elsevier Saunders; 2016: 104-105.
5. Duque-Valencia J, Sarute N, Olarte-Castillo XA, et al. Evolution and Interspecies Transmission of Canine Distemper Virus – An Outlook of the Diverse Evolutionary Landscape of a Multi-Host Virus. *Viruses*. 2019; 11: 582.
6. Green L, Cook L, Martinez M, et al. Distemper Encephalomyelitis Presenting with Lower Motor Neuron Signs in a Young Dog. *JAAHA*. 2020; 56: 127-132.
7. Headly SA, Amude AM, Alfieri AF, et al. Molecular detection of *Canine Distemper Virus* and the immunohistochemical characterization of the neurologic lesions of in naturally occurring Old Dog Encephalitis. JVDI. 2009; 21: 588-597.
8. Maclachlan NJ and Dubovi EJ. *Frenner's Veterinary Virology*. 5th eds. Elsevier. 2017: 327-328.
9. Martella V, Elia G, and Buonavoglia C. Canine Distemper Virus. *Vet Clinic Small Anim*. 2008; 38: 787-797.
10. Martinez Gutierrez M and Ruiz-Saenz J. Diversity of Susceptible Hosts in Canine Distemper Infection: A Systemic Review and Data Synthesis. *BMC Veterinary Research*. 2016; 12: 78.
11. Nambuli S, Sharp CR, Acciardo AS, Drexler JF, Duprex WP. Mapping the evolutionary trajectories of morbilliviruses: what, where, and wither. *Curr Opin Virology*. 2016; 16:95-105.
12. Quinn PJ, Markey BK, Carter ME, Donnelly WJ, Leonard FC. *Veterinary Microbiology and Microbial Disease*. Blackwell publishing. Ames Iowa. 2006: 381-389.

13. Rima BK, Baczko K, Imagawa DT, et al. Humoral Immune Response in Dogs with Old Dog Encephalitis and Chronic Distemper Meningoencephalitis. *J Gen Virol*. 1987; 68: 1723-1735.
14. Roody PJ, Singh K, and Basavarajappa MS. Pathology in Practice. *JAVMA*. 2012; 240(10): 1169-1171.
15. Uhl EW, Kelderhouse C, Buikstra J, Blick JP, Bolon B, Hogan RJ. New world origin of canine distemper: Interdisciplinary insights. *Int Jour Paleopathol.* 2019, 24:266-278.
16. Uzal FA, Plattner BL, Hostetter JM. Alimentary System. In: Maxie MG, ed. *Jubb, Kennedy and Palmer's Pathology of Domestic Animals*. Vol 2. 6th ed. Philadelphia, PA: Elsevier Saunders; 2016: 116-117.
17. Valli VEO, Kiupel M, Bienzle, and Wood RD. Hemopoeitic System. In: Maxie MG, ed. *Jubb, Kennedy and Palmer's Pathology of Domestic Animals*. Vol 3. 6th ed. Philadelphia, PA: Elsevier Saunders; 2016: 207, & 145-146.
18. Vandevelde M, Higgins RJ, and Oevermann A. *Veterinary Neuropathology: Essentials of Theory and Practice*. 1st eds. Wiley-Blackwell. 2012: 61-3, 54, & 57.
19. Watson AM, Cushing AC, Sheldon JD, et al. Natural Canine Distemper Virus Infection in Linnaeus's 2-Toed Sloths (*Choloepus didactylus*). Veterinary Pathology. 2020; 57(2): 311-315.
20. Wilcock BP and Njaa BL. Special Senses. In: Maxie MG, ed. *Jubb, Kennedy and Palmer's Pathology of Domestic Animals*. Vol 1. 6th ed. Philadelphia, PA: Elsevier Saunders; 2016: 474.
21. Young Kim D, Zinn MM, Odemuyiwa SO, et al. Myocarditis caused by naturally acquired canine distemper virus infection in 4 dogs. *JVDI*. 2021; 33(1): 167-169.
22. Zachary JF. Mechanisms of Microbial Infections. In: Zachary JF and McGavin MD, eds. *Pathologic Basis of Veterinary Disease*. 5th eds. Elsevier Mosby. St Louis. 2012: 226-227.
23. Zachary JF. Nervous System. In: Zachary JF and McGavin MD, eds. *Pathologic Basis of Veterinary Disease*. 5th eds. Elsevier Mosby. St Louis. 2012: 854-855.

CASE IV:

Signalment:
7-year-old male Alaskan Malamute dog

History:
A 7-year-old male Alaskan Malamute dog was presented with non-specific clinical

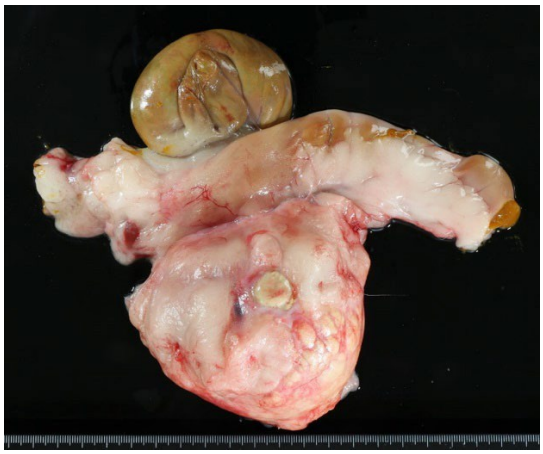

Mesenteric lymph node, dog. The mesenteric lymph node is effaced by encapsulated mass of about 15 cm. in diameter, with a central area of caseous necrosis. (*Photo courtesy of:* Servei de Diagnostic de Patologia Veterinària, Facultat de Veterinària UAB, Bellaterra (Barcelona).)

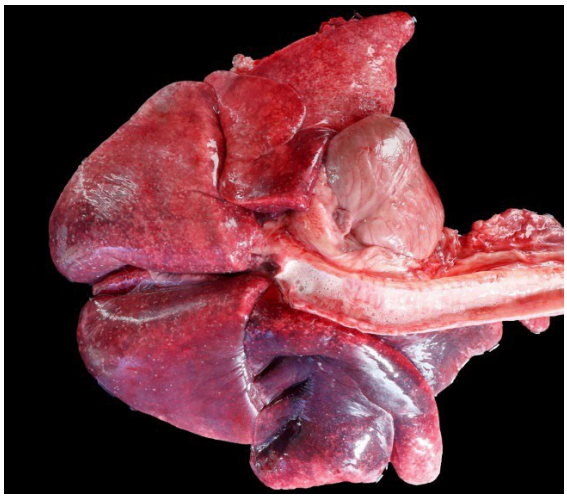

Lung, dog. Multifocal to coalescing, whitish and dense nodules up to 0.5 cm in diameter are randomly scattered through all pulmonary lobules. Moderate amount of white foam in the trachea and bronchial lumen. (*Photo courtesy of:* Servei de Diagnostic de Patologia Veterinària, Facultat de Veterinària UAB, Bellaterra (Barcelona).)

signs (weight loss, apathy and anorexia). Ultrasonography and CT scan revealed the presence of a large mass in the abdominal cavity and multiple smaller masses in the liver. Biopsies of the masses were taken, and a pyogranulomatous hepatitis and lymphadenitis was diagnosed histologically. GRAM, Ziehl-Neelsen (ZN), Grocott and PAS stains did not reveal bacterial or fungal aetiology. Negative results were obtained by PCR for *Leishmania* spp., *Bartonella* spp., atypical Mycobacteria, *Neospora caninum*, *Toxoplasma gondii* and *Cryptosporidium* spp. Because of the poor prognosis the dog was euthanatized.

Gross Pathology:

At postmortem examination, the dog showed loss of body condition. The mesenteric lymph node was replaced by a soft, encapsulated mass of about 15 cm. in diameter, with a central area of caseous necrosis. Also, multiple, randomly distributed granulomas of 0.2 to 0.5 cm in diameter were seen along the serosa and in the parenchyma of lung, heart, liver, kidneys, omentum and brain.

Laboratory Results:

Postmortem: Additional ZN staining were performed on several tissues taken at necropsy. ZN stain showed acid-fast bacilli in the necrotic center of granulomas and also within macrophages. Frozen samples preserved at necropsy were submitted for mycobacterial investigation. Direct PCR for the *Mycobacterium tuberculosis* complex (MTC) yielded a positive result, and a mycobacteria belonging to the MTC was cultured. The isolated mycobacteria was identified as *Mycobacterium tuberculosis* by spoligotyping.

Microscopic Description:

Kidney: Multifocal to coalescing, variably size (0.2 to 0.5 cm in diameter) granulomatous-necrotizing nodular lesions scattered throughout the cortex, medulla and to a lesser extent pelvis, are observed replacing approximately 20-25% of the evaluated parenchyma. The center of some of these nodules is composed of moderate amount of acellular and amorphous hypereosinophilic necrotic material admixed with cellular debris, karyorexis and karyolysis (lytic necrosis). Depending on the section assessed, occasional necrotic glomeruli and tubules are trapped

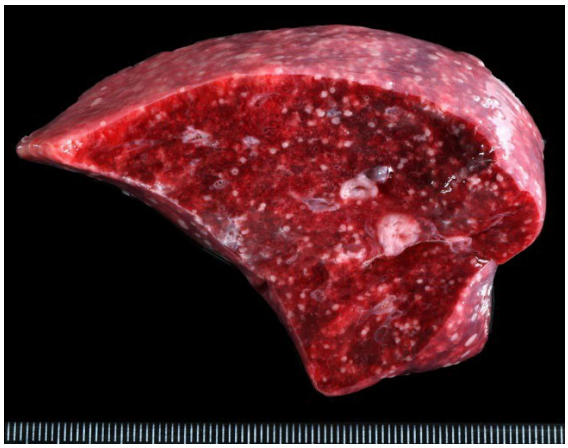

Lung, dog. Transverse section showing the intraparenchymatous and subpleural location of the nodules. (*Photo courtesy of:* Servei de Diagnostic de Patologia Veterinària, Facultat de Veterinària UAB, Bellaterra (Barcelona).)

within the necrotic debris also with mild deposition of granular and basophilic mineral material (dystrophic mineralization). These nodules are demarcated by mild to moderate macrophagic inflammation, mainly epithelioid cells, with scarce multinucleated giant cells (Langhans type), surrounded by a thin capsule of mature connective tissue (fibrosis) at the periphery (Granuloma). Multifocally, other non-encapsulated granulomas are also observed and are composed of moderate amount of viable and degenerated neutrophils and macrophages without obvious areas of lytic necrosis in the center. Acid-fast bacilli were observed in the cytoplasm of macrophages and free within the necrotic material with ZN staining. Diffusely, the glomeruli of non-affected parenchyma showed moderate thickening of the glomerular Bowman capsule and basement membranes due to the presence of acellular and amorphous eosinophilic material.

Contributor's Morphologic Diagnoses:
Nephritis, granulomatous and necrotizing, multifocal to coalescing, severe, chronic.

Contributor's Comment:
Tuberculosis (TB) is a zoonotic disease caused by mycobacteria of the *Mycobacterium tuberculosis* complex (MTC) in a broad range of mammalian hosts. MTC comprises *M. tuberculosis, M. bovis, M. africanum, M. microti, M. canetti, M. caprae, and M. pinnipedii* ([3][16]). Though a significant progress has been made toward the elimination of tuberculosis from humans, this disease remains an important health, social and economic problem ([1][14]).

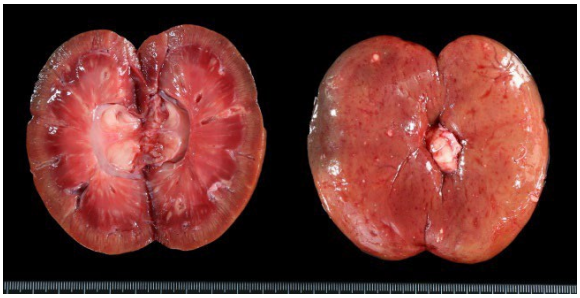

Kidneys, dog. Multifocal to coalescing, prominent white nodules up to 0,3 cm in diameter surrounded by a red halo are randomly distributed through the cortex, affecting both cortex and medulla in the opened section. (*Photo courtesy of:* Servei de Diagnostic de Patologia Veterinària, Facultat de Veterinària UAB, Bellaterra (Barcelona).)

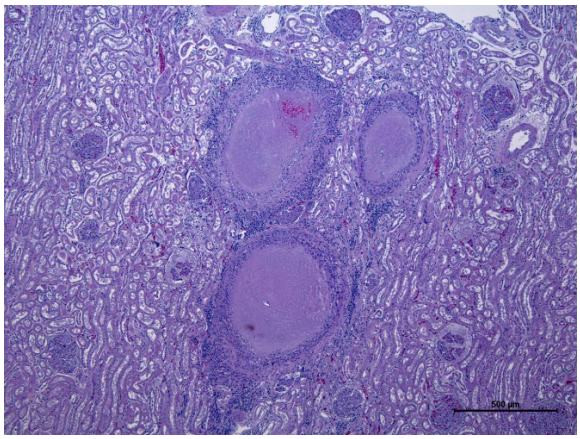

Kidney, dog. Multifocal to coalescing, randomly distributed 500 µm to 600 µm in diameter granulomatous and necrotizing nodules scattered through renal cortex, composed of moderate amounts of central lytic necrosis .. (HE, 100X) (*Photo courtesy of:* Servei de Diagnostic de Patologia Veterinària, Facultat de Veterinària UAB, Bellaterra (Barcelona).)

M. tuberculosis and *M. bovis* occur most frequently in their respective hosts, but may infect many other species. Humans are the only reservoir host for *M. tuberculosis*; however, this bacterium has a wide host range, including dogs, cats, pigs, cattle, captive monkeys, psittacine birds, fish, reptiles and marine animals ([2][7][16][17]).

Dogs and cats have been pointed as potential carriers and as a possible source of tuberculous infection to other species ([1]). The susceptibility of dogs to infection with *M. tuberculosis* is still a matter of debate. Malin (1940) was the first who reported tuberculosis in dogs and their owners. Later on, tuberculosis in dogs was linked to the disease in humans and cattle ([1][13]). Studies on dogs being in contact with people suffering from

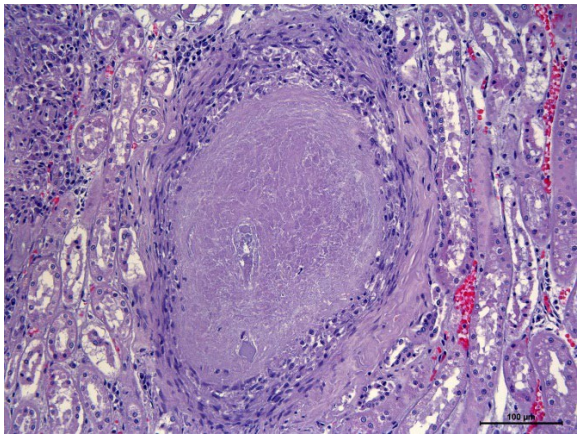

Kidney, dog. Granulomas are surrounded by moderate amounts of inflammatory cells and thin fibrous capsule. (HE, 200X) (*Photo courtesy of:* Servei de Diagnostic de Patologia Veterinària, Facultat de Veterinària UAB, Bellaterra (Barcelona).)

tuberculosis show high levels of *M. tuberculosis* isolated from otherwise healthy-looking animals and, in some cases, dogs infected with *M. tuberculosis* demonstrated the full clinical picture of the disease ([1]).

Canine TB has been caused by *M. tuberculosis, M. bovis*, and *M. microti* ([3]). Although dogs are less susceptible to *M. tuberculosis* than to the other tuberculous mycobacteria, they can become infected after prolonged exposition to infected human respiratory secretions ([1][3][14][16]). Thus, *M. tuberculosis* infection in dogs is considered an anthropozoonosis ([7][11]). Therefore, the incidence of canine TB is closely related to the incidence of human TB, being higher in urban areas, where the human patients are concentrated, or in developing countries ([1][7][16]). Middle Africa and Southern Asia seem to be the parts of the world where human TB is most prevalent ([15]). Evidence indicates that many companion animals infected with *M. tuberculosis* had a history of living in an environment with humans infected by TB, or that the animals had intimate contact with owners affected by TB ([11]). Genotypic comparison of mycobacteria recovered from owners and dogs may confirm the similarity of strains that infected household members and/or their pet ([5][11]).

The inhalation of aerosolized droplets from humans appears to be the primary route of canine TB infections ([12]). In addition, cutaneous and ingestion of contaminated food or sputum are well-recognized sources of *M. tuberculosis* transmission from humans to dogs ([1][11][12]).

Although no clear canine-to-human *M. tuberculosis* transmission has been documented, dogs can discharge organism in the sputum leading to elimination of *M. tuberculosis* into the home environment ([7][11][16]). In addition, experimental infection results led to the assumption that the transmission of *M. tuberculosis* between infected and healthy dogs kept in close contact is possible, suggesting that naturally infected dogs may be a continuous source of infection for humans and other animals ([1][11]).

Natural TB in companion animals is most commonly a subclinical disease. TB-infected dogs with less than two years old rarely exhibit clinical manifestations except when ex-

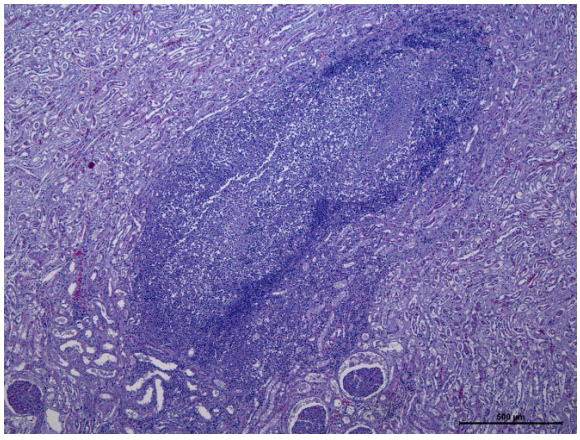

Kidney, dog. Deeper in the cortex and within the medulla, granulomas are forming in areas of tubular and vascular necrosis. (HE, 100X) (*Photo courtesy of:* Servei de Diagnostic de Patologia Veterinària, Facultat de Veterinària UAB, Bellaterra (Barcelona).)

posed to a high number of pathogenic mycobacteria [10]. In dogs that develop clinical signs, the most common primary sites of TB infection are the lungs and the pulmonary lymph nodes, being pneumonia the main clinical manifestation of *M. tuberculosis* [1][4][11]. Nevertheless, occasional cases of canine mycobacterial infection involving primarily the digestive tract have been described worldwide, although some of them caused by non-tuberculous mycobacteria, especially *M. avium* [8][9]. A generalized form of TB is considered rare in dogs infected with *M. tuberculosis* [11]. These cases probably result from hematogenous dissemi- nation of bacilli following erosion of the wall of a blood vessel by an expanding tubercle. In some instances, presumably following substantial release of bacilli into the blood, the presence of innumerable tiny white foci justifies the term "miliary tuberculosis." Embolic lesions are most common in lung, and may involve lymph nodes, bone, liver, kidney, mammary gland, uterus, pleura, peritoneum, pericardium, and meninges. Lesions are rare in salivary gland, pancreas, spleen, brain, myocardium, or muscle [2][3]. Un- like other species, such as bovine, TB in dogs often appears as granulation tissue in which macrophages are scattered at random and giant cells are rare. Small and generalized granulomas are uncommon, and are composed principally of epithelioid cells surrounded by narrow zones of fibrous tissue in which there are scattered small collections of lympho- cytes and plasma cells. Thus, the lack of Langhans cells and demarcation of the gran- ulomas is considered as an essential feature of TB in dogs. In addition, the necrosis is not a feature in these kind of granulomas but is often present in the centers of larger and more chronic ones [2]. In dogs, intrabronchial dissemination within the lungs occurs quite rapidly and can lead to tuberculous bronchitis and bronchiolitis. Pleuritis or peritonitis often accompanies primary infections in the lungs or intestine, respectively, with diffuse or finely nodular pleural thickening by granulation tissue containing few macrophages and bacilli [2].

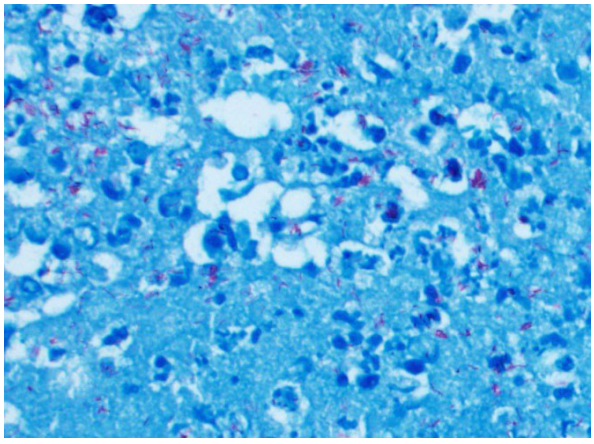

Kidney, dog. Acid fast bacilli are scattered in low numbers throughout areas of granulomatous inflammation. (Fite-Faraco, 400X)

Dogs can also be infected by non-tuberculous mycobacteria which, in contrast, are ubiquitous and potentially pathogenic. Within the nontuberculous mycobacteria group, the Mycobacterium avium complex (MAC) encompasses mycobacterial species considered to be the most likely causative agent of disseminated disease in humans and dogs. Zoonotic transmission of MAC is as likely as environmental acquisition [3]. Dogs are relatively less susceptible to infection with MAC organisms than to MTC pathogens, and despite the ubiquitous and widespread nature of MAC organisms, infections in dogs are rare, owing to their innate resistance [6].

Intradermal tuberculin testing and serological tests in dogs are considered inconsistent and unreliable. The pathomorphological and bacteriological analyses are still the most reliable tests and constitute mainly post-mortem diagnosis. Although PCR techniques are becoming very valuable, mycobacterial culture is considered the reference standard for TB diagnosis [1][3][11]. The use of ZN staining in microscopic examination, cytology, and/or histology samples for the identification of acid-fast organisms is a valuable method for routine mycobacterial diagnosis. In this case, the presence of acid-fast bacteria in the granulomas observed was not homogeneous with ZN stain. Very few or absence

of bacteria were observed in the most chronic granulo- mas in which areas of central necrosis are seen but higher amounts of them were seen in the more incipient granulomas, in which there are not areas of evident central necrosis. This fact can justify that bacteria were not ob- served in biopsies taken antemortem with Zn stain. These results demonstrate the possibil- ity of obtaining false negative results using ZN and show the need for combining meth- ods in the diagnosis of canine TB ([11]).

Contributing Institution:
Servei de Diag- nostic de Patologia Veterinària, Facultat de Veterinària UAB, Bellaterra (Barcelona).

JPC Diagnosis:
Kidney: Nephritis, granu- lomatous, multifocal to coalescing, marked.

JPC Comment:
The hallmark of *Mycobacte- rium tuberculosis* (MTB) infection is the pulmo- nary granuloma; this case illustrates these classi- cal caseous granulomas in an extrapulmonary lo- cation, and the contributor does an excellent job summarizing this disease in dogs.

A recent article by Pereira et al in the *Journal of Comparative Pathology* described the histologic appearance and distribution of MTB lesions in naturally infected fifteen nonhuman primates, and the authors demonstrated that the infection did not always manifest as pulmonary granu- loma.[12] In all nine infected Old World Monkeys (OWMs), granulomas were present in at least one organ, with six having typical pulmonary granu- lomas.[12] These granulomas were either caseous (with a necrotic core), non-necrotizing (solidly- cellular), or suppurative.[12]

In New World Monkeys (NWMs), on the other hand, pulmonary granulomas were only observed in one of six infected animals.12 Four other in- fected NWMs had diffuse interstitial pneumonia with foamy macrophages expanding alveolar sep- tae but without distinct granulomas or necrosis.12 This macrophage morphology may be due to ac- cumulation of MTB lipids in vesicles, and foam cell formation may be induced by oxygenated forms of mycolic acid. Only one NWM, an Uta Hick's bearded saki, had typical pulmonary gran- ulomas.

In this case, conference participants discussed the variable appearance of the lesions in the kidney: some are mature granulomas, while others are poorly organized and likely reflect an earlier change. Conference participants also discussed the spread of these lesions: while arrival at the kidney was likely hematogenous given the multi- systemic distribution, spread within the kidney may have occurred through blood vessels or within affected tubules. Ultimately, participants decided the route of spread could not be deter- mined in this histologic section.

References:

1. Bonovska, M., Tzvetkov, Y., Najden- ski, H., Bachvarova, Y. PCR for de- tection of Mycobacterium tuberculo- sis in experimentally infected dogs. *J Vet Med B Infect Dis Vet Public Health.* 2005; 52(4): 165-170.
2. Caswell JL, Williams KJ. Respiratory System, In: Maxie MG, ed. *Jubb Ken- nedy and Palmer's Pathology of Do- mestic Animals*. Vol 2. 6th ed. St. Louis, MO: Elsevier Press. 2016: 547-551.
3. De la Fuente C, Pumarola M, Ródenas S, Foradada L, Lloret A, Pérez De Val B, Añor S. Imaging diagnosis- magnetic resonance imaging findings of an intracranial epidural tubercu- loma in a dog. *Vet Radiol Ultrasound*. 2012;53: 655-659. Engelmann N, Ondreka N, Michalik J, Neiger R. Intra-abdominal Myco- bacterium tuberculosis infection in a dog. *J Vet Intern Med*. 2014; 28:934- 8.
4. Erwin PC, Bemis DA, Mawby DI, et al. Mycobacterium tuberculosis trans- mission from human to canine. *Emerg Infect Dis*. 2004; 10(12): 2258-2260.
5. Etienne C, Granat F, Trumel C, et al. A mycobacterial coinfection in a dog suspected on blood smear. *Vet Clin Pathol*. 2013; 42:516-21.
6. Greene CE, et al. Mycobacterial in- fections.

In: Greene EC, Gunn-Moore AD, eds. *Infectious Diseases in Dogs and Cats*. Vol 1. 2nd ed. Mexico: McGraw-Hill Interamericana. 2000:246-258.
7. Greene CE, Prescott JF. Mycobacterial infections. In: Greene CE, ed. *Infectious Diseases of the Dog and Cat*. 3rd ed. St. Louis, MO: Elsevier. 2012; 334-335.
8. Horn B, Forshaw D, Cousins D, Irwin PJ. Disseminated Mycobacterium avium infection in a dog with chronic diarrhea. *Aust Vet J*. 2000; 78: 320–325.
9. LoBue PA, Enarson DA, Thoen CO. Tuberculosis in humans and animals: an overview. *Int J Tuberc Lung Dis*. 2010; 14: 1075–1078.
10. Martinho AP, Franco MM, Ribeiro MG, et al. Disseminated Mycobacterium tuberculosis infection in a dog. *Am J Trop. Med Hyg*. 2013; 88:596–600.
11. Pereira AHB, Lopes CAA, Pissinatti TA, et al. Pulmonary Granuloma Is Not Always the Tuberculosis Hallmark: Pathology of Tuberculosis Stages in New World and Old World Monkeys Naturally Infected with the *Mycobacterium tuberculosis* complex. *J Comp Path.* 2022; 199: 55-74.
12. Ribeiro, M. G. et al. Pre−Multidrug-Resistant Mycobacterium tuberculosis Infection Causing Fatal Enteric Disease in a Dog from a Family with History of Human Tuberculosis. *Transbound. Emerg. Dis.* 2016; 64: e4–e7.
13. Snider, WR. Tuberculosis in canine and feline populations. Review of the literature. *Am Rev Respir Dis.* 1971: 104(6), 877–887.
14. Szaluś-Jordanow, O., Augustynowicz-Kopeć, E., Czopowicz, M., et al. Intracardiac tuberculomas caused by *Mycobacterium tuberculosis* in a dog. *BMC Veterinary Res.* 2016; 12(1).
15. Turinelli V, Ledieu D, Guilbaud L, et al. *Mycobacterium tuberculosis* infection in a dog from Africa. *Vet Clin Path*. 2004; 33:177–181.
16. Une Y, Mori T. Tuberculosis as a zoonosis from a veterinary perspective. *Comp Immunol Microbiol Infect Dis.* 30, 415–425.

WSC 2022-2023 Self-assessment
Conference 17

1. Malformation of the following has been associated with PCV-3 infection in piglets?
    a. Tail
    b. Feet
    c. Ears
    d. Nose

2. Canine morbillivirus induces apoptosis in which of the following?
    a. B cells
    b. CD3+ lymphocytes
    c. CD4+ lymphocytes
    d. CD8+ lymphocytes

2. Which of the following paramyxoviruses is not contained within the genus *Morbillivirus* ?
    a. Hendra virus
    b. Distemper
    c. Pestis du petits ruminants
    d. Rinderpest

3. Which of the following proteins is the determination of virulence in canine distemper virus ?
    a. P protein
    b. Hemagglutinin protein
    c. Fusion protein
    d. Membrane protein

4. Which of the following has been identified as a cause of canine tuberculosis?
    a. M. smegmatis
    b. M. microti
    c. M paratuberculosis
    d. M. chelonae

Please email your completed assessment for grading to Dr. Bruce Williams at bruce.h.williams12.civ@mail.mil. Passing score is 80%. This program (RACE program 33611) is approved by the AAVSB RACE to offer a total of 0.5 CE Credits, with a maximum of 12.5 CE Credits being available to any individual Veterinary Medical Professionals for the 2019-2020 Wednesday Slide Conference. This RACE approval is for the subject matter categories of: SCIENTIFIC using the delivery method of NONINTERACTIVE DISTANCE. This approval is valid in jurisdictions which recognize AAVSB RACE.

Joint Pathology Center Veterinary Pathology Services

WEDNESDAY SLIDE CONFERENCE 2022-2023

Conference #18 **1 February 2023**

CASE I:

Signalment:
Goitered gazelle (*Gazella subguttorosa*), adult, gender unknown.

History:
Lung tissue was collected from a carcass found in Darvi soum, Khovd province, Mongolia in January 2017. Formalin-fixed tissue was embedded in paraffin at the State Central Veterinary Laboratory, Mongolia.

Gross Pathology:
The carcass was emaciated.

Laboratory Results:
The lateral flow device penside test for eye swab was positive for Peste-des-petits-ruminants virus antigen.

Microscopic Description:
Mild epithelial desquamation and peribronchial edema are observed in the bronchi. Epithelial necrosis and desquamation are severer in bronchioles. Infiltration of neutrophils, epithelioid macrophages and syncytial cells occurs multifocally in alveolar lumina, which is associated with the proliferation of type II pneumocytes. Bronchial and bronchiolar epithelial cells sometimes contain intracytoplasmic and intranuclear inclusion bodies. Intracytoplasmic and intranuclear inclusion bodies are also frequently observed in epithelioid macrophages and syncytial cells.

By immunohistochemistry, bronchial and bronchiolar epithelial cells, epithelioid macrophages, syncytial cells, and type II pneumocytes reacted weakly with anti-canine distemper virus monoclonal antibody (clone DV2-12).

Contributor's Morphologic Diagnoses:
Lung: Acute necrotizing bronchopneumonia with intracytoplasmic and intranuclear inclusion bodies and syncytial cell formation.

Contributor's Comment:
Peste des petits ruminants (PPR) is a viral disease of goats and sheep characterized principally by stomatitis, diarrhea, oculonasal discharge, and pneumonia. The causative agent is closely related to rinderpest virus and these two are classified along with the measles virus and CDV in the genus Morbillivirus in the Family *Paramyxoviridae.* PPR was reported to the OIE, for the first time in Mongolia, in 2016 and was confirmed to affect sheep, goat and yak in the western part of Mongolia.[2]

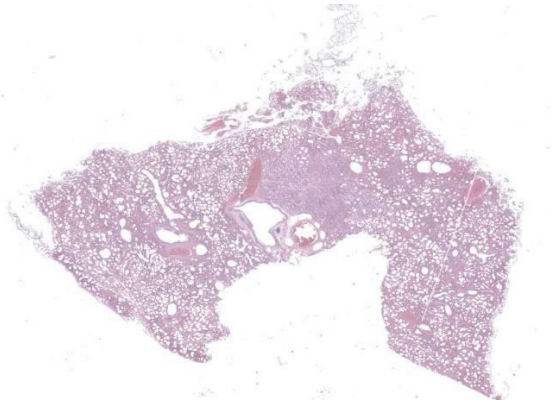

Figure 1-1. Lung, gazelle. A single section of mildly autolytic lung is submitted from examination (HE, 6X)

Death in these domestic animals declined rapidly after extensive vaccination; however, the virus continued to spread to wild animals such as saiga, Siberian ibex and goitered gazelle.[2]

Histopathological findings observed in this case are similar to those in goats and sheep experimentally infected with PPR virus.[1,3] Syncytial cells observed within alveolar spaces were reported to be macrophage origin.[3]

Contributing Institution:
Laboratory of Comparative Pathology
Faculty of Veterinary Medicine, Hokkaido University
Kita 18, Nishi 9, Kita-ku
Sapporo 060-0818, Japan
https://www.vetmed.hokudai.ac.jp/en/

JPC Diagnosis:
Lung: Pneumonia, bronchointerstitial, necrotizing, diffuse, marked, with edema, numerous viral syncytia, and intranuclear and intracytoplasmic eosinophilic viral inclusions.

JPC Comment:
This case of peste des petits ruminants virus infection in a goitered gazelle bears striking similarities to the case of canine distemper virus infection and pneumonia in Conference 17, Case 2, of this year, as they are both morbilliviruses and produce similar diseases. Peste des petits ruminants (PPR), which translates to mean plague of small ruminants, is known by several other names, including kata, stomatitis-pleuropneumonia complex, goat plague, ovine rinderpest.[4,8] Goats and sheep are the primary hosts, with goats typically experiencing more severe disease, and while other animals such as cattle, buffalo, and pigs can be infected, they are considered dead end hosts that do not shed the virus and generally do not develop clinical signs.[5]

PPR was first described in 1942 by Gargadennec and Lalanne in the Ivory Coast, West Africa, though the disease may have been present beforehand and misidentified as rinderpest virus.[5] It is now endemic in Africa,

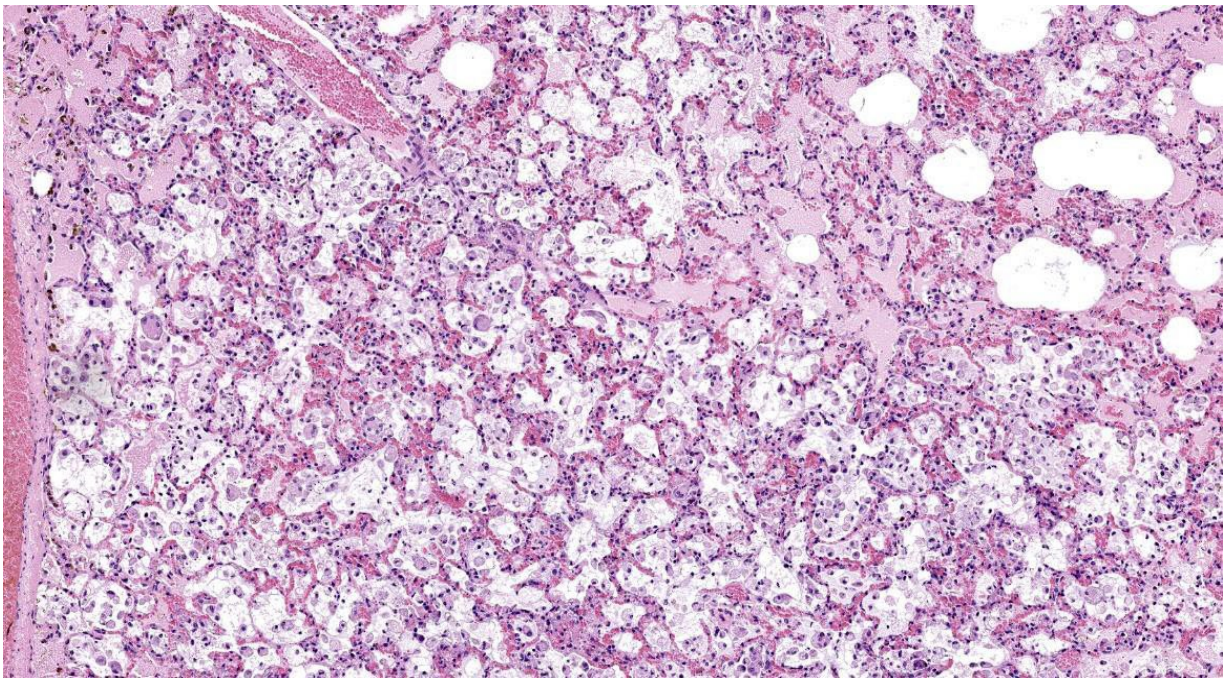

Figure 1-2. Lung, gazelle. Regionally, alveolar septa are markedly expanded, and alveoli are filled with edema fluid and numerous foamy alveolar macrophages. (HE, 109X)

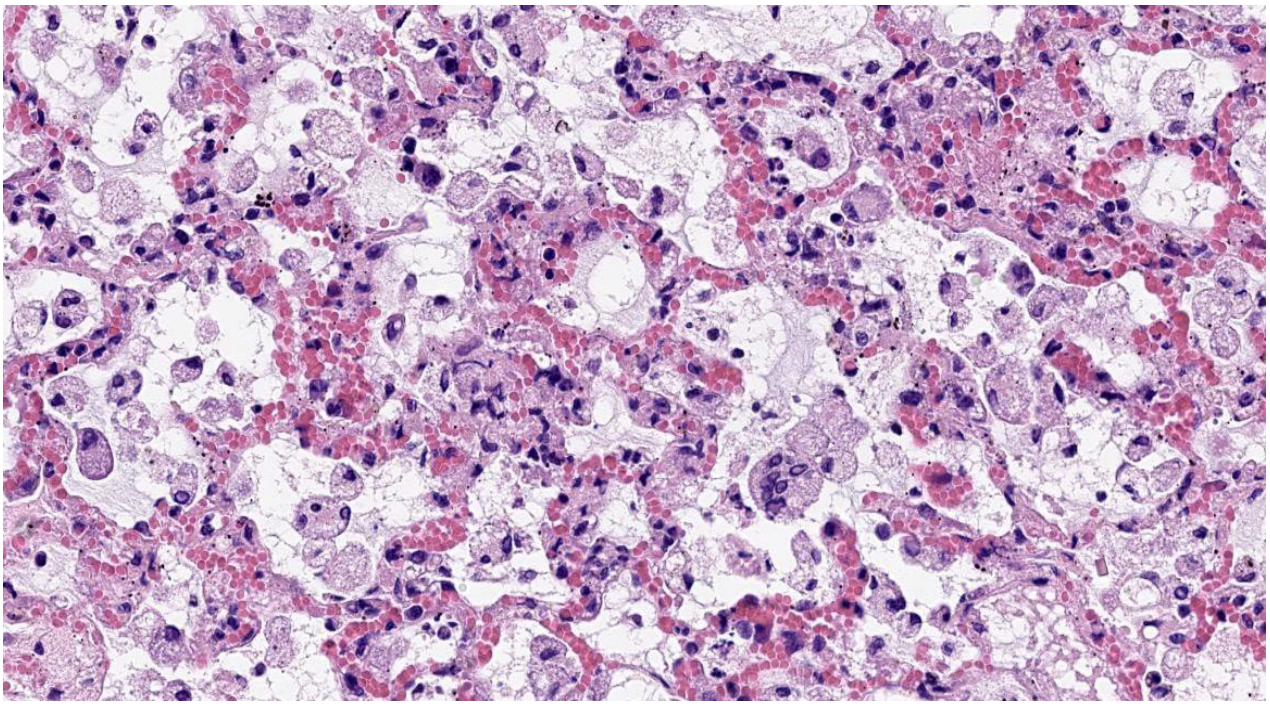

Figure 1-3. Lung, gazelle. Higher magnification of affected areas of lung. Alveolar spaces also contain scattered multinucleated syncytia (arrow). (HE, 381X)

the Middle East, China, India, and south Asia. There are four lineages of the virus, and while historically lineages I, II, and III have been present in Africa and IV present in Asia, lineage IV has now become the dominant strain in Africa.[5] Increased incidence has been associated with the spread of lineage IV, possibly indicating that is more virulent.[5]

PPRV is a non-segmented, single-stranded, negative-sense morbillivirus, and like other morbilliviruses, is highly lymphotropic and epithliotropic.[4,5] The virus uses the hemagglutinin protein H to bind to the typical morbillivirus receptors: signaling lymphocyte activation molecule (SLAM)/CD150 on lymphocytes, macrophages, and dendritic cells; and Nectin-4 on epithelial cells.[4,5] The F protein facilitates fusion of the viral envelop and host cell membrane, and the virus subsequently replicates in the cytoplasm.[5] The M protein facilitates viral egress from host cells via budding.[5]

Infection occurs through direct contact with aerosolized virus or infected bodily secretions. It is presumed that the virus first infects leukocytes in the respiratory mucosa and then spread to local lymphoid tissue where initial replication occurs. After an initial immune cell proliferation, viremia results in systemic spread of the virus, and

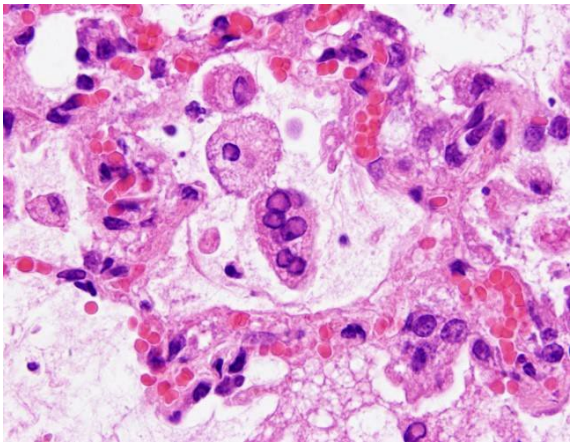

Figure 1-4. Lung, gazelle. Alveoli contain multinucleated viral syncytia with intranuclear and intracytoplasmic inclusions. Intracytoplasmic inclusions are also present within the cytoplasm of uninucleate alveolar macrophages. (HE, 400X) (Photo courtesy of: Laboratory of Comparative Pathology, Faculty of Veterinary Medicine, Hokkaido University, Kita 18, Nishi 9, Kita-ku, Sapporo 060-0818, Japan, https://www.vetmed.hokudai.ac.jp/en/)

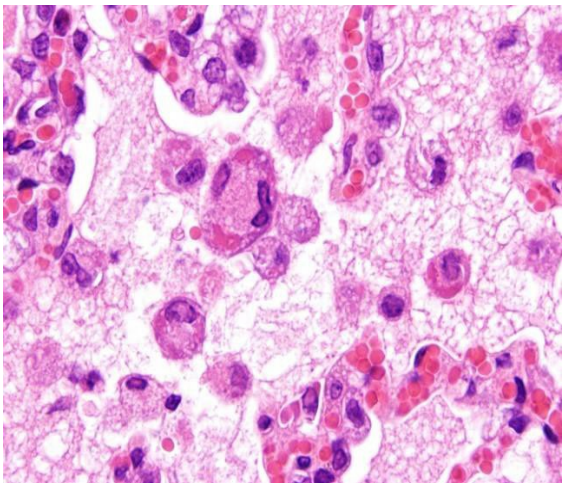

Figure 1-5. Lung, gazelle. Another field more clearly demonstrates intracytoplasmic viral inclusions within alveolar macrophages. (HE, 400X) (Photo courtesy of: Laboratory of Comparative Pathology, Faculty of Veterinary Medicine, Hokkaido University, Kita 18, Nishi 9, Kita-ku, Sapporo 060-0818, Japan, https://www.vetmed.hokudai.ac.jp/en/)

subsequent leukopenia with reduction of CD4+ T cells occurs approximately 4 days post infection. PPRV causes clinically significant immunosuppression by inducing leukopenia and inhibition of type I and II interferon activity due to viral nonstructural proteins.[5]

PPRV has high morbidity and mortality rates, though certain breeds are more resistant and virulence varies by viral strain.[5] The disease has a more rapid onset and clinical progression than rinderpest.[8] Clinical signs begin around 3 days post-infection and initially consist of pyrexia, malaise, and serous to mucopurulent oculonasal discharge, and results in dyspnea.[4] In animals which recover, clinical signs resolve by 14 days post-infection, and these animals generally have life-long immunity.[4]and pseudomembranous ulcerations in the mouth and nose, followed by acute severe gastroenteritis and hemorrhagic colitis.[5,8] Pneumonia occurs late in the disease process

Profound immunosuppression can lead to secondary bacterial infection by microbes such as *Mycoplasma* or *Pasteurella.*[4,8] This week's moderator, Dr. Kali Holder from the Smithsonian's National Zoo, described how morbilliviruses cause immunosuppression by causing leukopenia, by targeting mechanisms of innate immunity, and by inducing immune amnesia by specifically targeting T and B memory cells and dendritic cells.

Histologic features of PPRV infection are typical for morbilliviruses. Syncytia form in leukocytes of the lymph nodes, white pulp, GALT, oral mucosa, pulmonary alveoli, and liver.[4,8] Eosinophilic cytoplasmic and nuclear inclusions occur in the renal pelvis, abomasum, respiratory epithelium, and type II pneumocytes.[8] Histologic lesions in the lung include inflammation and necrosis of airway epithelium, bronchointerstitial pneumonia, and type II pneumocyte hyperplasia, as seen in this case.[1,8]

This week's moderator also described how PPRV has caused massive mortality events in hoofstock in Mongolia, including the Siberian ibex, the goitered gazelle, and in the critically endangered Saiga antelope. Researchers using distance sampling techniques

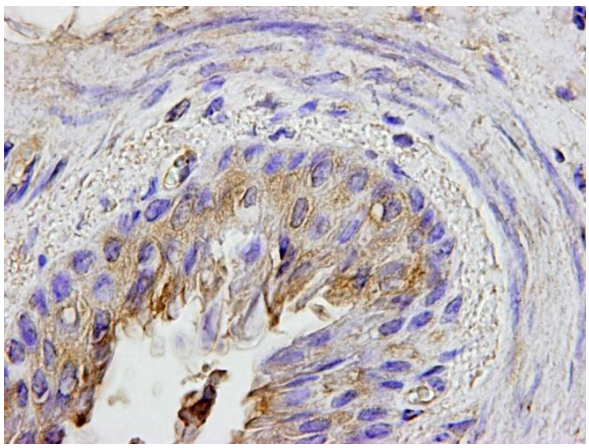

Figure 1-6. Lung, gazelle. Hyperplastic airway epithelium is strongly immunopositive for PRRV antigen. (anti-PPRV, 400X) (Photo courtesy of: Laboratory of Comparative Pathology, Faculty of Veterinary Medicine, Hokkaido University, Kita 18, Nishi 9, Kita-ku, Sapporo 060-0818, Japan, https://www.vetmed.hokudai.ac.jp/en/)

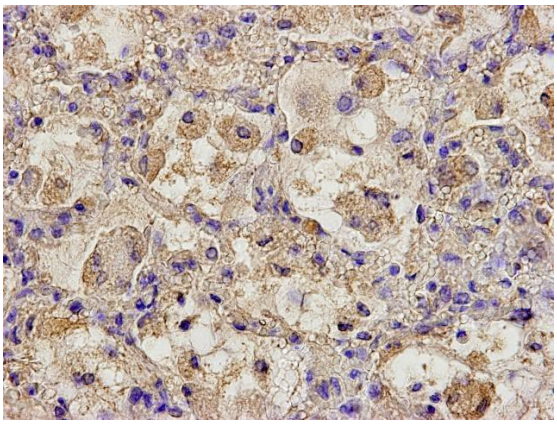

Figure 1-7. Lung, gazelle. Alveolar macrophages are strongly immunopositive for PRRV antigen. (anti-PPRV 400X) (Photo courtesy of: Laboratory of Comparative Pathology, Faculty of Veterinary Medicine, Hokkaido University, Kita 18, Nishi 9, Kita-ku, Sapporo 060-0818, Japan, https://www.vetmed.hokudai.ac.jp/en/)

estimate that PPRV outbreak caused a population decline of up 80% in the Saiga antelope.[6]

References:

1. Brown CC, Mariner JC and Olander HJ. An immunohistochemical study of the pneumonia caused by peste des petits ruminants virus. *Vet Pathol*. 1991;28(2):166-70.
2. Caswell JL, Williams KJ. Respiratory System. In: Maxie MG, ed. *Jubb, Kennedy and Palmer's Pathology of Domestic Animals*. Vol 2. 6th St. Louis, MO: Elsevier Ltd; 2016:557.
3. Kock RA. Mongolia Investigation of Peste des Petits Ruminants (PPR) among wild animals and its potential impact on the current PPR situation in livestock. Mission Report 20th January-1st February 2017. *Crisis Management Centre-Animal Health (CMC-AH)*. 30 March 2017.
4. Kumar N, Maherchandani S, Kashyap SK, et al. Peste Des Petits Ruminants Virus Infection of Small Ruminants: A Comprehensive Review. *Viruses*. 2014;6: 2287-2327.
5. Parida S, Muniraju M, Mahapatra M, Mutchuchelvan D, Buczkowski H, Banyard AC. Peste des petits ruminants. *Vet Microbiol.* 2015; 181(1-2):90-106.
6. Pruvot M, Fine AE, Hollinger C, et a. Outbreak of Peste des Petits Ruminants among Critically Endangered Mongolian Saiga and Other Wild Ungulates, Mongolia, 2016-2017. *Emerg Infect Dis.* 2020; 26(1):51-62.
7. Truong T, Boshra H, Embury-Hyatt C, Nfon C, Gerdts V, Tikoo S, Babiuk LA, Kara P, Chetty T, Mather A, Wallace DB, Babiuk S. Peste des petits ruminants virus tissue tropism and pathogenesis in sheep and goats following experimental infection. *PLoS One*. 2014;9(1):e87145.
8. Uzal FA, Plattner BL, Hostetter JM. Alimentary system. In: Maxie MG, ed. *Jubb, Kennedy and Palmer's Pathology of Domestic Animals*. Vol 2. 6th ed. St. Louis, MO: Elsevier Ltd; 2016:115,130-131.

CASE II:

Signalment:
One-month-old, male intact Grant's gazelle (*Nanger granti granti*)

History:
Acute onset of lethargy, anorexia, and pyrexia (106 F°). After initial supportive care, euthanasia was elected.

Gross Pathology:
An approximately 10 x 10 cm area of the right lobe of the liver surrounding the gallbladder had a roughened, red to tan granular capsular surface. On cut section, the subtending parenchyma was granular and sharply demarcated from the left lobe. The lungs were diffusely dark red, wet, and heavy.

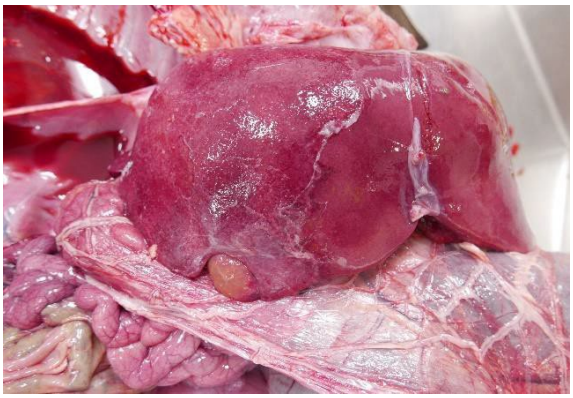

Figure 2-1. Liver, Grant's gazelle. The liver has a regionally extensive area near the gallbladder with a granular capsular surface. (Photo courtesy of: Disease Investigations, San Diego Zoo Wildlife Alliance, http://institute.sandiegozoo.org/disease-investigations)

Laboratory Results:
PCR: A sample of liver was submitted for Chlamydia PCR and was positive. Sequencing identified *Chlamydia pecorum*.

Microscopic Description:
Liver: Within a well-demarcated region of the liver are multifocal distinct and occasionally coalescing foci of neutrophilic inflammation, karyorrhectic debris, and rare multinucleated giant cells that obscure the normal architecture. Neutrophilic aggregates are surrounded by a rim of hepatocytes with a loss of nuclear detail and faint cytoplasmic borders (coagulative necrosis) and acute hemorrhage with fibrin. Kupffer cells adjacent to areas of inflammation and necrosis occasionally have granular amphophilic material in the cytoplasm (coccobacilli). Diffusely, intact hepatocytes have variably sized, well-defined intracytoplasmic vacuoles, and sinusoids are mildly congested. Multiple portal areas have a mild increase in biliary epithelial cells (ductular reaction).

Immunohistochemistry (Chlamydia): Clusters of punctuate, intra-cytoplasmic immunoreactivity is common in areas of necrosis and less common within areas of suppurative inflammation. No immunoreactivity is detected with Coxiella IHC.

Contributor's Morphologic Diagnoses:
1. Liver: Severe, acute, regionally extensive, necrosuppurative hepatitis with intralesional coccobacilli, *Chlamydia pecorum*

Contributor's Comment:
Chlamydia pecorum is one of eleven species within the Chlamydia genus, the only genus in the family *Chlamydiaceae*.[12] It is endemic in many populations of cattle and sheep, as detection in the intestines of clinically normal animals is common.[1,7] The bacterium has been reported to cause disease in a wide range of species, but koalas, various species of domestic and exotic ruminants, and swine appear to be the most commonly affected. In ruminants, particularly lambs and calves, polyserositis including arthritis, encephalomyelitis, keratoconjunctivitis, mastitis, orchitis, placentitis, endometritis, and pneumonia have been reported.[1,6,8,14] Additionally, one study described up to a 48% reduction in gained weight in infected calves suggesting the economic impact extends beyond individuals with clinical disease.[10] While less abortogenic than *C. abortus*, necrotizing placentitis and neutrophilic hepatitis have also been described in goats and sheep that aborted due to *C. pecorum* infection.[5,15] This case is unusual in that the liver was the organ affected in this one-month-old. Most likely, the liver was infected via portal spread from the small intestine. The source of infection in this case is also unknown, as this is the first report of disease caused by *C. pecorum* at the institution. Spread from nearby domestic animals or direct exposure from subclinically infected conspecifics are both possible.

In koalas, *C. pecorum* can result in keratoconjunctivitis as well as disease in the urogenital and respiratory tracts resulting in blindness, infertility, or a condition known as 'wet bottom' or 'dirty tail' due to urine staining of the fur secondary to cystitis and urinary

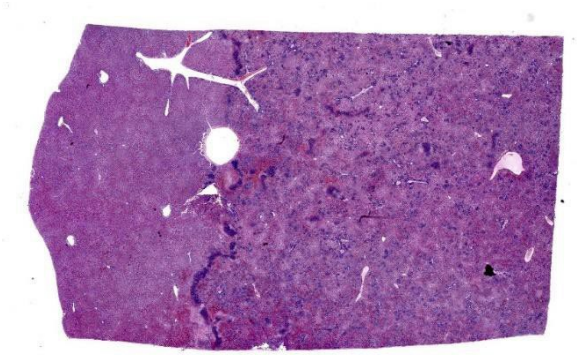

Figure 2-2. Liver, gazelle. At subgross magnification, coalescing areas of necrosis in both sections are visible. (HE, 8X)

incontinence.[1,8] Conjunctivitis due to *C. pecorum* infection in koalas in Southern Australia has been associated with koala gammaretrovirus infection (KoRV-B).[4]

Of the Chlamydia spp. that cause disease in animals, *C. psittaci* is the most well-documented zoonotic species and can be cause mild conjunctivitis (ornithosis) or more severe disease due to myocarditis, encephalitis, or pneumonia.[1,12] The zoonotic potential of *C. pecorum* is less clearly defined.[3]

A recent review describes the challenges of diagnosing chlamydial diseases in animals.[1] While neutrophilic inflammation, necrosis, and basophilic 'chlamydial' inclusion bodies are considered histologically characteristic, many infections lack these features or have less specific inflammatory pattern. As a result, immunohistochemistry, histochemical staining, and molecular tests are considered the mainstays of diagnosis of chlamydial diseases in animals. Histochemical stains to highlight the intracellular bacteria via cytology or histology include modified Macchiavello, Giemsa, Castaneda, modified Ziehl-Neelsen, or modified Gimenez.[11] Molecular techniques are considered the gold standard for diagnosis due to the inability to isolate *Chlamydia* spp. on agar plates as they require a host cell for survival. However, care should be taken not to over interpret a positive PCR test as infection with *C. pecorum* is considered endemic in many ruminants and may be an incidental finding in the absence of associated disease.[7] Fluorescent antibody tests and ELISAs also have been developed but are unable to differentiate between various *Chlamydia* species.[11] Immunohistochemistry and PCR were both used in this case to confirm *C. pecorum* as the causative agent.

Contributing Institution:
Disease Investigations
San Diego Zoo Wildlife Alliance
PO Box 120551
San Diego, CA 92112
http://institute.sandiegozoo.org/disease-investigations

JPC Diagnosis:
Liver: Hepatitis, necrotizing, focally extensive, marked, with intrahepatocytic and intrahistiocytic bacteria.

JPC Comment:
Chlamydia species are obligate intracellular Gram-neagative bacteira with a unique lifecycle which begins as an infectious extracellular elementary body.[1,2] Inside the host cell, the bacteria matures within a vacuole into a slightly larger reticulate body, and after several rounds of replication, the bacteria converts back to an elementary body and lyses the cell.[1,2] During times of stress, the bacteria may take on an aberrant body phenotype, a non-replicative persistent state.[1]

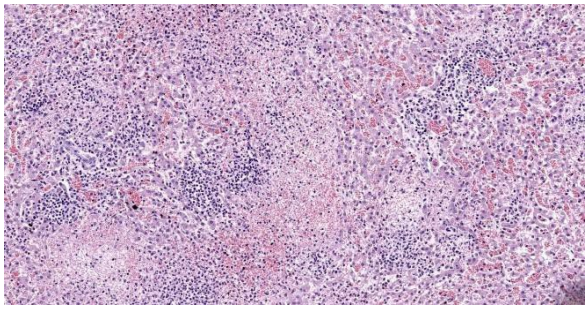

Figure 2-3. Liver, gazelle. Higher magnification of areas of necrosis, showing predominantly lytic foci. (HE, 792X)

While the contributor describes several forms of Chlamydial infection in mammals, the bacteria also causes clinical and subclinical infection in reptiles, amphibians, and fish. In reptiles, clinical disease is characterized by granulomatous inflammation in the heart, lung, liver, and/or spleen.[1,2] A recent article in *Vet Pathol* described an outbreak of *Chlamydia* in farmed American alligators.[2] Over the span of ten days, approximately 100 alligators died acutely. Histologically, these animals had severe necrotizing hepatitis and myocarditis, mild enterocolitis, and splenic lymphoid depletion; most animals also had lymphoplasmacytic interstitial pneumonia and nephritis.[2] Animals which died later during the outbreak also had erosive conjunctivitis, keratoconjunctivitis, and mild uveitis; lesions in other systems were less severe than in the animals that died earlier in the outbreak.[2] Chlamydial antigen was identified using immunohistochemistry and was particularly high in the liver, heart, spleen, and intestine.[2] Based on genetic sequencing and phylogenetic analysis, the authors suspect that the *Chlamydia* species is closely related to *Chlamydia poikilothermis* identified in snakes.[2]

An important differential to consider for this case of well-demarcated, randomly distributed foci of hepatic necrosis in a ruminant is ruminal acidosis with secondary necrobacillosis (rumenitis-liver abscess complex). [13]

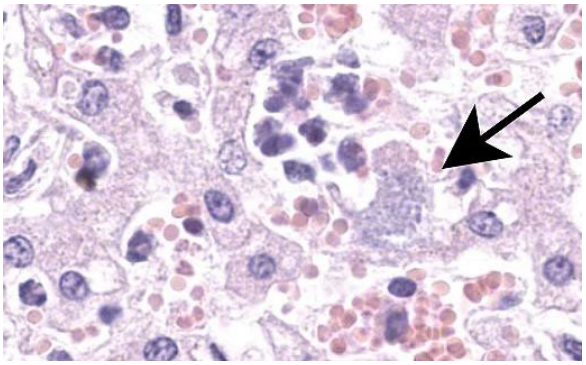

Figure 2-4. Liver, gazelle. Rare hepatocytes and Kupffer cells contain cytoplasmic bacteria (arrow). (HE, 150X)

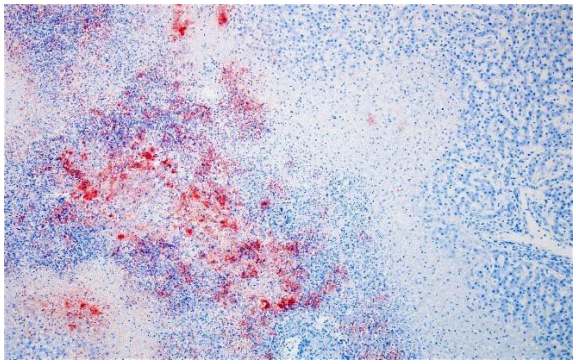

Figure 2-5. Liver, gazelle. There is strong immunoreactivity to antibodies against Chlamydia sp. within areas of necrosis. (anti-Chlamydia sp., 100X) (Photo courtesy of: Disease Investigations, San Diego Zoo Wildlife Alliance, http://institute.sandiegozoo.org/disease-investigations)

Ruminal acidosis is caused initially by carbohydrate overload and leads to alterations of microflora, overgrowth of organisms such as *Streptococcus bovis*, and ruminal atony.[13] High levels of acid within the rumen and intestine cause increased osmotic pressure, fluid influx, and systemic hypovolemia. Ultimately, *Fusobacterium necrophorum*, an opportunistic pathogen which is part of the normal GI flora, invades the ruminal mucosa, causing mucosal necrosis and ulceration, and travels through the portal system causing multifocal random hepatic necrosis.[13] While the pattern of necrosis in this case is consistent with necrobacillosis, this case lacks colonies of filamentous bacteria along the margins of necrosis seen with *F. necrophorum.*

The moderator and conference participants agreed that, while intracellular bacteria were visible on the H&E slide, reaching a definitive diagnosis of *Chlamydia pecorum* is not possible without further testing (such as with PCR and IHC, as completed in this case.) Other differentials for intracellular bacteria discussed by the participants included *Brucella* and *Clostrium piliforme.*

References:

1. Borel N, Polkinghorne A, Pospischil A. A review of Chlamydial diseases in

animals: still a challenge for pathologists? *Vet Pathol.* 2018;55:374-390.
2. Carossino M, Nevarez JG, Sakaguchi K, et a. An outbreak of systemic chlamydiosis in farmed American alligators (*Alligator mississippiensis*).*Vet Pathol*. 2022; 59(5): 860-868.
3. Cheong HC, Lee CYQ, Cheok YY, et al. *Chlamydiaceae*: diseases in primary hosts and zoonosis. *Microorganisms.* 2019;7(5):146.
4. Fabijan J, Sarker N, Speight N, et al. Pathological findings in koala retrovirus-positive koalas (Phascolarctos cinereus) from northern and southern Australia. *J Comp Path.* 2020;176:50-66.
5. Giannitti F, Anderson M, Miller M, et al. *Chlamydia pecorum*: fetal and placental lesions in sporadic caprine abortion. *J Vet Diagn Invest.* 2016;28:184-189.
6. Jelocnik M, Forshaw D, Cotter J, et al. Molecular and pathological insights into *Chlamydia pecorum*-associated sporadic bovine encephalomyelitis (SBE) in Western Australia. *BMC Vet Res.* 2014;10:121.
7. Li J, Guo W, Kaltenboeck B, et al. *Chlamydia pecorum* is the endemic intestinal species in cattle while *C. gallinacea, C. psittaci*, and *C. pneumoniae* associate with sporadic systemic infection. *Vet Microbiol.* 2016;193:93-99.
8. Ostfeld N, Islam MM, Jelocnik M, et al. *Chlamydia-pecorum*-induced arthritis in experimentally and naturally infected sheep. *Vet Pathol*. 2021;58:346-360.
9. Palmieri C, Hulse L, Pagliarani S, et al. *Chlamydia pecorum* infection in the male reproductive system of koalas (*Phascolarctos cinereus*). *Vet Pathol*. 2019;56:300-306.
10. Poudel A, Elasser TH, Rahman KhS, et al. Asymptomatic endemic *Chlamydia pecorum* infections reduce growth rates in calves by up to 48 percent. *PLOS ONE*. 2012;7:e44961.
11. Sachse K, Vretou E, Livingstone M, et al. Recent developments in the laboratory diagnosis of chlamydial infections. *Vet Microbiol.* 2009;135:2-21.
12. Sachse K, Bavoil PM, Kaltenboeck B, et al. Emendation of the family *Chlamydiaceae*: proposal of a single genus, *Chlamydia*, to include all currently recognized species. *Syst Appl Microbiol.* 2015;38:99-103.
13. Uzal FA, Plattner BL, Hostetter JM. Alimentary System. In: Maxie MG, ed. *Jubb, Kennedy, and Palmer's Pathology of Domestic Animals*. Vol 2. 6th ed. St. Louis, MO: Elsevier. 2016; 40-43.
14. Walker E, Lee EJ, Timms P, et al. *Chlamydia pecorum* infections in sheep and cattle: a common and under-recognised infectious disease with significant impact on animal health. *Vet J.* 2015;206:252-260.
15. Westermann T, Jenkins C, Onizawa E, et al. *Chlamydia pecorum*-associated sporadic ovine abortion. *Vet Pathol*. 2021;58:114-122.

CASE III:

Signalment:
A 5-year-old, female, bald eagle (*Haliaeetus leucocephalus*).

History:
The bald eagle was found on the side of the road and looked like it couldn't walk properly. On arrival at the LSU Wildlife Hospital, the bald eagle was emaciated, lethargic, and anemic (PCV: 23%). The left metacarpal joints were swollen and had purulent exudates. She had severe louse infestation, and fecal flotation revealed whipworm eggs and strongyle eggs. The eagle was treated with fluids, Frontline, vitamin B complex, iron dextran, meloxicam, ceftiofur, and piscivore

diet. Over ten days the eagle got more alert and ate fish and rabbit on her own, but then declined and found dead in her kennel, 13 days after admission.

Gross Pathology:
The bald eagle was found on the side of the road and looked like it couldn't walk properly. On arrival at the LSU Wildlife Hospital, the bald eagle was emaciated, lethargic, and anemic (PCV: 23%). The left metacarpal joints were swollen and had purulent exudates. She had severe louse infestation, and fecal flotation revealed whipworm eggs and strongyle eggs. The eagle was treated with fluids, Frontline, vitamin B complex, iron dextran, meloxicam, ceftiofur, and piscivore diet. Over ten days the eagle got more alert and ate fish and rabbit on her own, but then declined and found dead in her kennel, 13 days after admission.

Laboratory Results:
Aerobic bacterial culture (liver): *E. coli* (moderate), *Enterococcus canintestini* (moderate)
Salmonella culture (liver): Negative
Fecal flotation test: No parasites seen

Microscopic Description:

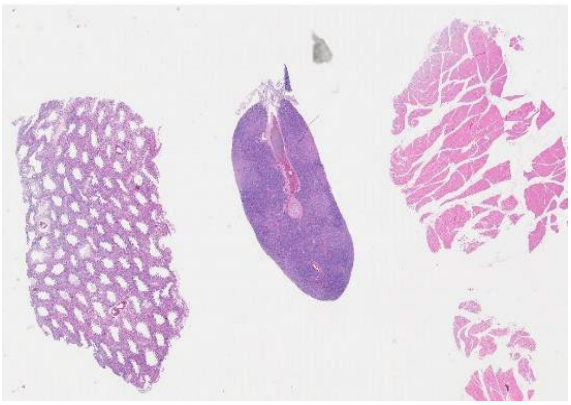

Figure 3-1. Multiple tissues, bald eagle. Lung, pancreas and skeletal muscle are submitted for examination. Loss of normal pulmonary architecture is present at subgross magnification. (HE, 6X)

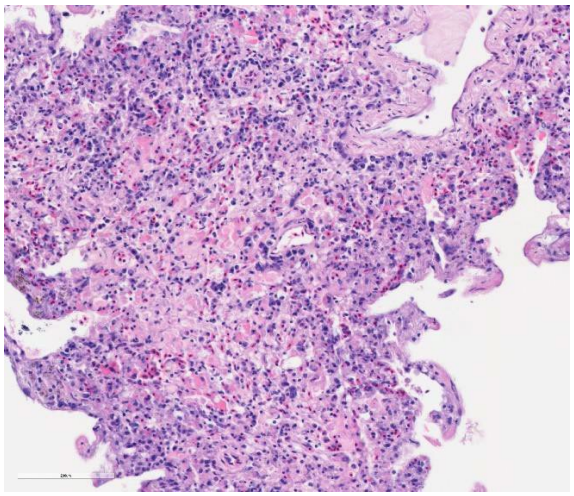

Figure 3-2. Lung, bald eagle. Normal architecture of air capillaries is effaced by a mixed inflammatory infiltrate and lumina contain abundant eosinophilic protein and fibrin. (HE, 166X)

Lung: The parabronchial wall is diffusely infiltrated by large numbers of plasma cells, lymphocytes, fewer Mott cells, and heterophils, narrowing and obliterating the air capillaries. Some air capillaries contain eosinophilic proteinaceous material mixed with fibrin. Frequently within presumed endothelial cells, there are clusters of 1-2 x 3-5 µm, elongated, basophilic, merozoites with a small dark basophilic nucleus. Occasional interatrial septa have small aggregates of macrophages containing brown-black pigment (pneumoconiosis).

Pancreas: There is multifocal to coalescing necrosis associated with multiple clusters of merozoites. Mild fibroplasia and ductular reaction are present adjacent to the necrotic areas. Low numbers of plasma cells and lymphocytes infiltrate the interstitium. The capsule is partially covered by fibrin, and the capsule abutting the necrotic area is thickened by fibroplasia and infiltration of macrophages.

Skeletal muscle: Occasional myofibers contain sarcocysts measuring up to 80 x 150 µm, containing large numbers of bradyzoites. Sporadic myofibers are degenerate and

necrotic, characterized by loss of cross-striation and fragmentation of the sarcoplasm. Occasionally, necrotic myofibers are replaced by infiltration of macrophages and lymphocytes.

Contributor's Morphologic Diagnoses:
Lung: Severe subacute diffuse lymphoplasmacytic interstitial pneumonia with intraendothelial apicomplexan merozoites
Skeletal muscle: Multiple sarcocysts; mild multifocal muscular degeneration and necrosis
Pancreas: Moderate subacute multifocal to coalescing necrotizing pancreatitis with intralesional apicomplexan merozoites

Contributor's Comment:
In this case, merozoites consistent with *Sarcocystis* sp. and associated necrotizing inflammation was noted in multiple organs including the lung, liver, pancreas, cerebellum, and to a lesser extend in the cerebrum, and sarcocysts were noted in the skeletal and cardiac muscle. The final diagnosis on this case was systemic sarcocystosis. Chronic septic arthritis of the left carpal joint was also noted.

Sarcocystis spp. are apicomplexan protozoal parasites that infect mammals, birds, and reptiles. More than 200 species are known in this genus. *Sarcocystis* spp. have an obligate 2-host life cycle. The sexual stages develop in a predator host (definite host), whereas the asexual phases develop in the prey animal (intermediate host). The intermediate host ingests sporocysts or sporulated oocysts through herbage contaminated by the definite host's feces. Sporozoites are released and invade endothelial cells where they undergo schizogony. One or two generations of schizogony take place. The merozoites derived from these generations invade skeletal and cardiac myocytes where they develop into thin-walled cysts initially containing round metrocytes, which repeatedly divide through

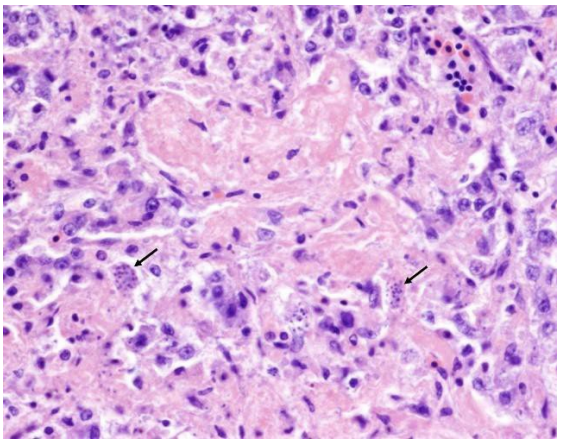

Figure 3-3. Lung, bald eagle. Endothelial cells contain numerous 2-3um apicomplexan merozoites (arrows). (HE, 400X) (Photo courtesy of: Department of Pathobiological Sciences and Louisiana Animal Disease Diagnostic Laboratory, School of Veterinary Medicine, Louisiana State University, Baton Rouge, LA, USA. https://www.lsu.edu/vetmed/laddl/)

a process termed endodyogeny to produce numerous banana-shaped bradyzoites. The definite host consumes the skeletal muscle with the sarcocysts containing bradyzoites. The sexual cycle is developed in the intestinal epithelium of the predatory host.[5,9]

In most cases, sarcocystosis is subclinical in the definitive or intermediate host. In definitive hosts, it causes intestinal sarcocystosis which is often asymptomatic or self-limiting. For intermediate hosts, muscular sarcocystosis is a common incidental finding on postmortem examination. However, certain *Sarcocystis* species can cause serious diseases in intermediate hosts. Those include *Sarcocystic neurona* causing equine protozoal myeloencephalitis in horses and *S. calchasi* causing pigeon protozoal encephalitis in domestic pigeons.

Certain *Sarcocystis* spp. are zoonotic, and Sarcocystosis may be underdiagnosed in humans. Humans are definite hosts of *S. hominis, S. heydorni, and S. suihominis*. Consuming undercooked beef (*S. hominis, S. heydorni*) and pork (*S. suihominis*) is the route of infection, which causes intestinal

sarcocystosis. Humans also serve as intermediate hosts for other *Sarcocystis* spp. by accidental consumption. One example is *S. nesbitti* of which a predatory snake is thought to be the definite host. In these circumstances, muscular sarcocystosis can develop.[2,9]

At least six species of *Sarcocystis* infect birds.[11] Two species are known to cause serious clinical diseases in birds. *Sarcocystis calchasi*, the causative agent of pigeon protozoal encephalitis, has been first described in domestic pigeons and causes sporadic cases of encephalitis in Columbidae. Epizootics associated with *S. calchasi*-induced encephalitis have been reported in wild feral rock pigeons[6], in three different psittacine species in a zoological exhibit[7], and in wild Brandt's cormorants [1], all of which occurred in California. Experimental studies demonstrated a biphasic disease in domestic pigeons: an acute schizogonic phase and a late phase with neurologic signs. According to a study, inflammatory lesions in the cerebrum were identified as early as 20 days post infection (d.p.i.) while the onset of neurologic signs appeared at 47 d.p.i. As the numbers of *sarcocystis* organisms or the amount of DNA did not increase with the increase of cerebral inflammation, a delayed-type hypersensitivity was proposed as the pathogenesis of *S.*

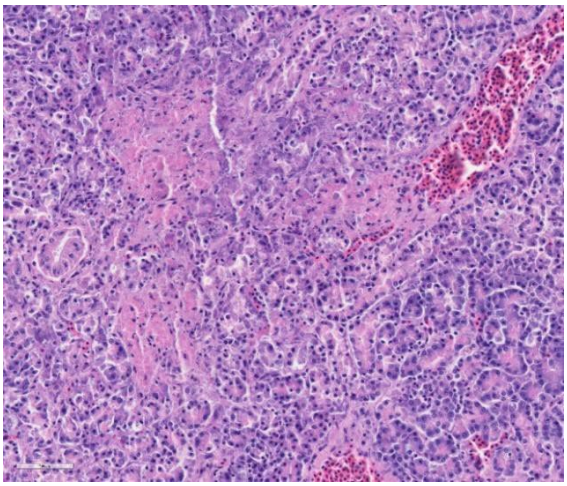

Figure 3-4. Pancreas, bald eagle. There are multifocal areas of lytic necrosis of acinar tissue. (HE, 166X)

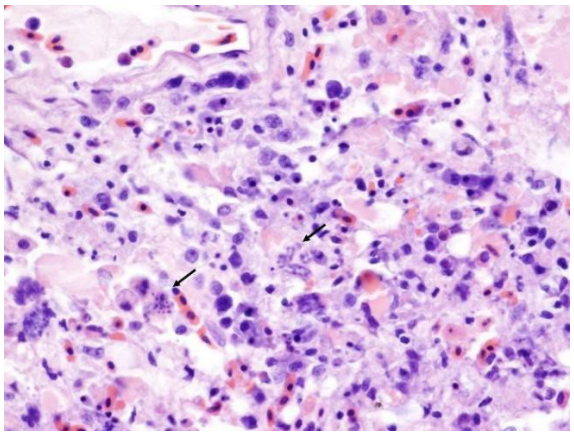

Figure 3-5. Pancreas, bald eagle. Endothelial cells contain numerous 2-3 µm apicomplexan merozoites (arrows). (HE, 400X) (Photo courtesy of: Department of Pathobiological Sciences and Louisiana Animal Disease Diagnostic Laboratory, School of Veterinary Medicine, Louisiana State University, Baton Rouge, LA, USA. https://www.lsu.edu/vetmed/laddl/)

calchasi-induced encephalitis.[4] The definite hosts of *S. calchasi* are northern goshawks (*Accipiter gentilis*) and European sparrowhawks (*A. nisus*) in Europe and Cooper's hawks (*A. cooperii*) and red-tailed hawks (*Buteo jamaicensis*) in North America.[8]

Sarcocystis falcatula, which also can cause fatal sarcocystosis in birds, uses Virginia opossums (*Didelphis virginiana*) as a definite host. Natural intermediate hosts are cowbirds and grackles. Psittacine birds, especially old world psittacine, are known to be susceptible to *S. falcatula* infection. The primary lesion is pulmonary congestion, edema, and hemorrhage with intravascular merozoites, but myositis and encephalitis also occur. Clinical disease also has been reported in Victoria crowned pigeons characterized by sudden death caused by pulmonary sarcocystosis.[10] Birds of prey including free-ranging bald eagles, golden eagles[12], and a great horned owl[13] also have been reported with fatal pulmonary and/or neurologic sarcocystosis caused by *S. falcatula*. *S. ryleyi* affects waterfowls and usually is an incidental finding at necropsy.

According to Wünschmann et al.[12], among three bald eagles and one golden eagle that had fatal *Sarcocystis falcatula* infection, two bald eagles had blood lead concentration consistent with subclinical lead intoxication, and one had lead intoxication. It was not discussed in this article whether the lead intoxication played a role in the disease susceptibility, but we were wondering if lead intoxication make the birds more susceptible to sarcocystosis. In the present case, the infection was disseminated affecting multiple organs, compared to previously reported sarcocystosis cases in raptors. Heavy metal level was not measured in this case, but the chronic septic arthritis may have caused immunosuppression predisposing the fatal systemic sarcocystosis.

In this case, the diagnosis was made based on the morphology and the location (pulmonary endothelium) of the apicomplexan parasites, and further characterization of the organism was not performed. PCR is usually used for confirmation of sarcocystosis and identifying the species.

Contributing Institution:
Department of Pathobiological Sciences and Louisiana Animal Disease Diagnostic Laboratory, School of Veterinary Medicine, Louisiana State University, Baton Rouge, LA, USA
https://www.lsu.edu/vetmed/laddl/
https://www.lsu.edu/vetmed/pbs/index.php

JPC Diagnosis:
1. Lung: Pneumonia, interstitial, lymphoplasmacytic and histiocytic, diffuse, marked with intraendothelial apicomplexan merozoites.
2. Pancreas: Pancreatitis, necrotizing, multifocal to coalescing, moderate with intraendothelial apicomplexan merozoites.
3. Skeletal muscle: Sarcocysts, numerous.

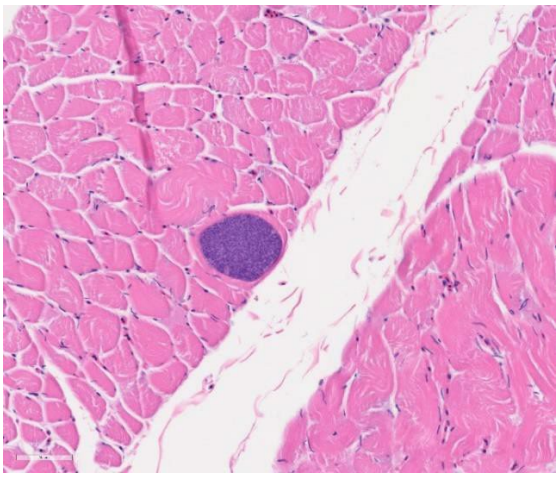

Figure 3-6. Skeletal muscle, bald eagle. Numerous myocytes contain sarcocysts which occupy part of the sarcoplasm. (HE, 166X)

JPC Comment:
As the contributor describes, *Sarcocystis calchasi* is one of the main pathogenic Sarcocystis species in birds and primarily infects Columbiformes and Psittaciformes. The first documented cases of infection in Galliformes were recently reported in a 2022 *Journal of Veterinary Diagnostic Investigation* article.[3] Two captive vulturine guineafowl, ground dwelling birds, developed acute and rapidly fatal infections after having been moved to a new enclosure with other avian species.[3] The first bird presented unable to stand and experienced progressive neurologic signs.[3] The second bird presented shortly after the first with nonspecific signs of lethargy and weight loss, and both animals died despite ponazuril therapy.[3] The animals had nonsuppurative meningoencephalitis with perivascular lymphoid cuffing and glial nodule formation, and one animal had protozoal schizonts in areas of inflammation.[3] Both animals were PCR positive for *Sarcocystis,* and sequencing indicated the species was *S. calchasi*.[3]

References:

1. Bamac OE, Rogers KH, Arranz-Solís D, et al. Protozoal encephalitis associated with *Sarcocystis calchasi* and *S. falcatula* during an epizootic involving Brandt's cormorants (*Phalacrocorax penicillatus*)

in coastal Southern California, USA. *Int J Parasitol: Parasites Wildl*. 2020;12: 185-191.
2. Fayer R, Esposito DH, Dubey JP. Human infections with Sarcocystis species. *Clin Microbiol Rev*. 2015;28: 295-311.
3. Gadsby S, Garner MM, Bolin SR, Sanchez CR, Flaminio KP, Sim RR. Fatal *Sarcocystic calcahsi*-associated meningoencephalitis in 2 captive vulturine guineafowl. *J Vet Diagn Invest*. 2022; 34(3):543-546.
4. Maier K, Olias P, Enderlein D, et al. Parasite distribution and early-stage encephalitis in Sarcocystis calchasi infections in domestic pigeons (Columba livia f. domestica). *Avian Pathol*. 2015;44: 5-12.
5. Maxie MG. *Jubb, Kennedy & Palmer's pathology of domestic animals*. Vol 1. 6th ed. St. Louis, MO: Elsevier. 2015.
6. Mete A, Rogers KH, Wolking R, et al. *Sarcocystis calchasi* outbreak in feral rock pigeons (*Columba livia*) in California. *Vet Pathol*. 2019;56: 317-321.
7. Rimoldi G, Speer B, Wellehan Jr JF, et al. An outbreak of *Sarcocystis calchasi* encephalitis in multiple psittacine species within an enclosed zoological aviary. *J Vet Diagn Invest*. 2013;25: 775-781.
8. Rogers KH, Arranz-Solís D, Saeij JP, Lewis S, Mete A. *Sarcocystis calchasi* and other Sarcocystidae detected in predatory birds in California, USA. *Int J Parasitol: Parasites Wildl.* 2022;17: 91-99.
9. Rosenthal BM. Zoonotic sarcocystis. *Res Vet Science*. 2021;136: 151-157.
10. Suedmeyer W, Bermudez AJ, Barr BC, Marsh AE. Acute pulmonary *Sarcocystis falcatula*-like infection in three Victoria crowned pigeons (*Goura victoria*) housed indoors. *J Zoo Wildl Med*. 2001;32: 252-256.
11. Terio KA, McAloose D, Leger JS. *Pathology of Wildlife and Zoo Animals*. Academic Press. 2018.
12. Wünschmann A, Rejmanek D, Conrad PA, et al. Natural fatal *Sarcocystis falcatula* infections in free-ranging eagles in North America. *J Vet Diagn Invest.* 2010; 22: 282-289.
13. Wünschmann A, Rejmanek D, Cruz-Martinez L, Barr BC. *Sarcocystis falcatula*—associated encephalitis in a free-ranging Great Horned Owl (*Bubo virginianus*).*J Vet Diagn Invest*. 2009;21: 283-287.

CASE IV:

Signalment:
12-year-old male striped hyena (*Hyaena hyaena*)

History:
A firm, non-painful, approximately 3-cm-diameter subcutaneous mass was observed elevating skin over the dorsal cervical region. Skin was intact and freely moveable over the surface of the mass. The mass was monitored for a period of several months with no obvious changes. A diagnosis was first made from punch biopsies, following which the entire mass was excised.

Gross Pathology:
The specimen submitted was an approximately 7 x 7 cm elliptical section of haired skin, extending to panniculus musculature at its deep margin. The skin surface was centrally elevated and surrounding tissue compressed by a well-demarcated, firm, approximately 3-cm-diameter, multilobular mass. On cut surfaces, the mass was homogeneously white to pale pink, with lobules separated by septa of dense connective tissue.

Laboratory Results:
Serum biochemistry:
Within normal limits
CBC:

WBC 13.2x10^3/μL; 1% band neutrophils, 73% segmented neutrophils, 21% lymphocytes, 3% monocytes
HCT: 42.7%

Microscopic Description:
Haired skin: A densely cellular, multilobular, pseudoencapsulated, expansile neoplasm expands the subcutis, elevating the overlying dermis and compressing adjacent tissues. Neoplastic lobules sometimes abut or protrude into large vascular spaces, especially at the periphery, but remain separated from lumina by a thin layer of endothelium. The neoplastic cell population consists of round to polygonal to sometimes spindloid cells arranged in solid sheets, cords, or packets, supported by a fine fibrovascular stroma. The cells have moderate amounts of pale eosinophilic, vacuolated cytoplasm and indistinct cytoplasmic borders. Nuclei are centralized and round to ovoid, sometimes reniform or indented, with vesicular or dispersed chromatin. Anisocytosis and anisokaryosis are moderate. Mitotic figures are infrequent, with 4 mitotic figures seen in ten 400x fields in the most mitotically active regions. Scattered individual tumor cells are hypereosinophilic

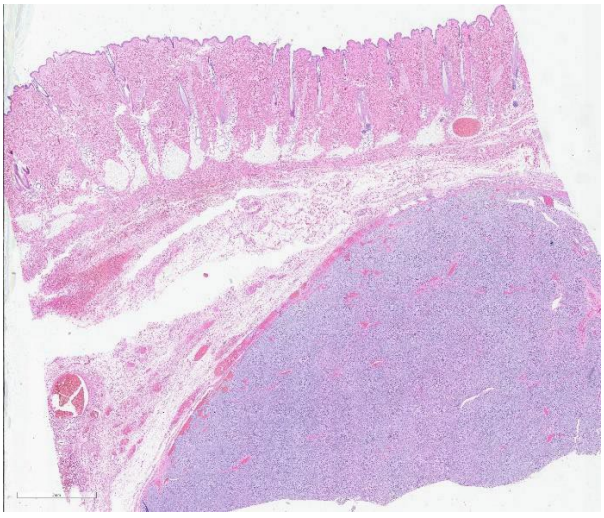

Figure 4-1. Haired skin, hyena. A single section of haired skin is submitted for examination. Within the subcutis, there is an expansile nodular neoplasm with a compression capsule and dilated blood vessels around it. (HE, 5X)

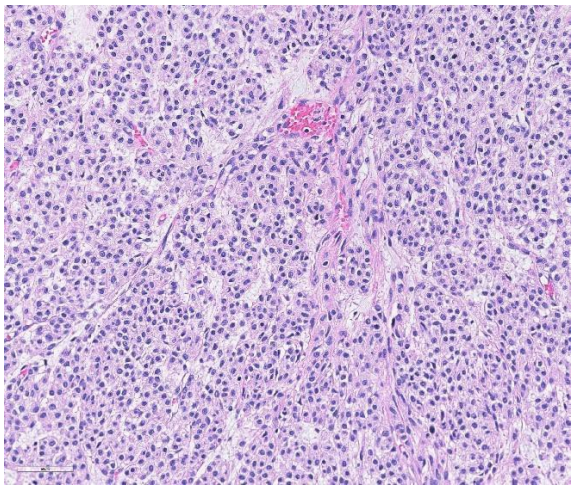

Figure 4-2. Haired skin, hyena. The neoplasm is composed of polygonal cells arranged in nests and packets. (HE, 215X)

and have condensed nuclear material, and there are a few small foci of necrosis and associated hemorrhage within the mass. In a few areas there are aggregates of fibrin and neutrophils adjacent to or partially occluding vascular lumina (thrombosis). In some sections, there is a broad zone of necrosis and regional hemorrhage with moderate numbers of hemosiderin- and hematoidin-laden macrophages (previous biopsy site).

Special stains and immunohistochemistry: Fine basement membranes surrounding individual tumor cells or small clusters of cells are immunoreactive for laminin and are also clearly highlighted with a Periodic acid-Schiff (PAS) stain. Neoplastic cells exhibit strong, punctate, cytoplasmic immunoreactivity for vimentin and α-smooth muscle actin. Immunohistochemical staining for desmin and pancytokeratin is negative.

Contributor's Morphologic Diagnoses:
Subcutis: glomus tumor

Contributor's Comment:
Glomus bodies are specialized arteriovenous shunts that function in thermoregulation by modifying capillary perfusion.[8] They are found most frequently in skin of the distal extremities, particularly in digital skin and

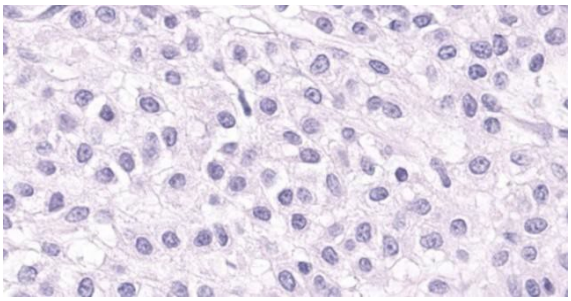

Figure 4-3. Haired skin, hyena. High magnification of neoplastic cells. (HE, 1025X)

subungual regions. In glomus bodies, the branching pre-glomic arterioles blend into arteriovenous anastomoses (Sucquet-Hoyer canals) with surrounding modified smooth muscle cells termed "glomus cells." They are richly invested with small nerves and blood vessels, and are circumscribed by dense, lamellar collagen.

Glomus tumors arise from the modified smooth muscle cells of the glomus body. They are uncommon but well-recognized in humans, where they occur most often as solitary nodules in subungual sites and in the dermis or subcutis of the digits and distal extremities.[8] They occur rarely in other sites, including visceral organs and bone.[8] Glomus tumors are often reported to be exquisitely painful, likely as a consequence of their rich peripheral nerve supply.[8]

Histologically, glomus tumors tend to be well-circumscribed and consist of densely cellular sheets and cords of epithelioid cells surrounding and abutting vascular structures, with fine basement membranes surrounding individual cells or clusters of cells. Several histologic variants are described in humans, including solid tumors, angiomatous glomus tumors (glomangiomas), myxoid glomus tumors, and oncocytic glomus tumors.[7] Malignant glomus tumors (glomangiosarcomas) are exceedingly rare. Even in glomus tumors with focal or regional cytologic features of malignancy, invasive behavior and distant metastases are uncommon.[7-9]

Using immunohistochemistry, the neoplastic cells are routinely positive for α-smooth muscle actin and vimentin. Desmin immunoreactivity is variable, and pancytokeratin immunoreactivity is uniformly negative. Basement membranes surrounding individual cells or clusters of cells can be demonstrated by PAS stains or by positive immunoreactivity for laminin and collagen IV.

Glomus tumors are rare in veterinary species, but have been reported in dogs, cats, horses, bovids, and non-human primates.[1-3,5,6,11,12,14,-16,18,20] Digital/subungual sites (or homologous regions) were affected in two dogs, a cat, and a horse.[2,3,5,20] Glomus tumors of the skin of the head or neck were reported in three equine cases, two of which were diagnosed as malignant variants.[2] In bovids, the two reports of glomus tumors describe neoplasms of the liver and of the urinary bladder.[10,16]

Proposed criteria suggesting malignancy include (1) large size (>2 cm diameter) with deep location (deep to muscular fascia); (2) presence of atypical mitotic figures; or (3) nuclear atypia with relatively high mitotic rate (>5/50 high power fields).[4] Vascular involvement is not reported to be associated with malignancy. In this case, the mass was

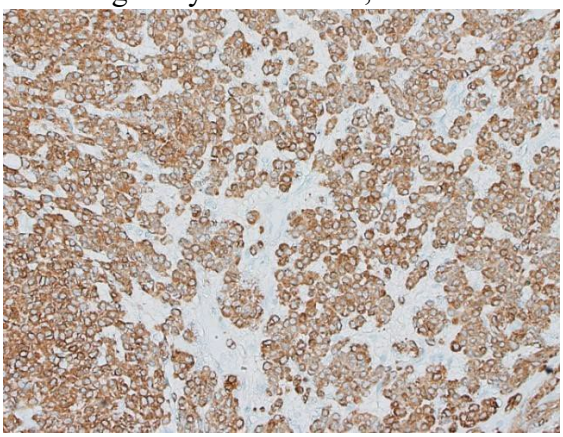

Figure 4-4. Haired skin, hyena. Neoplastic cells are strongly immunopositive for smooth muscle actin. (anti-SMA, 400X) (Photo courtesy of: Disease Investigations, San Diego Zoo Wildlife Alliance, http://institute.sandiegozoo.org/disease-investigations)

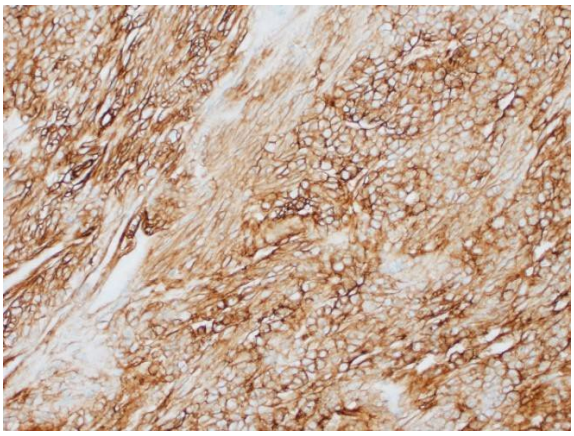

Figure 4-5. Haired skin, hyena. Neoplastic cells demonstrate strong membranous staining for laminin. (anti-laminin, 400X) (Photo courtesy of: Disease Investigations, San Diego Zoo Wildlife Alliance, http://institute.sandiegozoo.org/disease-investigations)

relatively large (~3 cm in diameter) but superficial. Atypical mitotic figures were not a significant feature. There was mild nuclear atypia, but a relatively high mitotic rate in some areas. Based on the criteria suggested above, this mass would warrant the (admittedly non-committal) designation of "glomus tumor of uncertain malignant potential." Radiographs taken at the time of excisional biopsy did not demonstrate metastatic lesions, and no evidence of recurrence or metastasis has been noted in the four months following excision.

Contributing Institution:
Disease Investigations
Institute for Conservation Research
San Diego Zoo Global
PO Box 120551
San Diego, CA 92112
http://institute.sandiegozoo.org/disease-investigations

JPC Diagnosis:
Haired skin: Glomus tumor.

JPC Comment:
This case is a classic example of a glomus tumor in a novel species. Glomus tumors are typically well-demarcated neoplasms composed of densely packed round to spindleloid cells which occasionally form nests.[10,17] Neoplastic cells frequently surround entrapped vascular channels, which may appear as blood-filled clefts, or may surround larger cavernous vessels (glomangiomas).[10,13] As the contributor mentions, the tumor is frequently associated with vessels and nerves, which may be visible along the tumor margin.[10] Differential diagnoses include Merkel cell tumors (arranged in a packet pattern), plasma cell tumors (cells are more pleiomorphic with eccentric nuclei), histocytomas (more top-heavy in distribution), other round cell neoplasms, and leiomyoma (particularly of the arrector pili muscle, or piloleiomyoma).[10] Other differentials considered by the moderator and participants were hidradenoma (as some areas of packeting mimicked tubules), melanoma, and a neuroendocrine tumor. When histologic findings are equivocal, special stains and IHCs may be necessary for differentiation, as described by the contributor.

A potential source for confusion in this uncommon veterinary neoplasm are the human entities glomus jugulotympanicum paraganglioma and glomus tympanicum paraganglioma.[13,19] While they contain the word glomus in the name, they are not associated with the glomus bodies in the dermis and subcutis. Rather, they are paragangliomas arising from neural-crest derived chemoreceptor cells of the paraganglia located along certain cranial nerves and within the jugular foramen.[13,19] As paragangliomas, neoplastic cells are positive for synapthophysin and chromogranin A on immunohistochemistry.[19]

References:

1. Brounts SH, Adams SB, Vemireddi V, Holland CH. A malignant glomus tumour in the foot of a horse. *Equine Vet Educ*. 2008;20:24-27.
2. Burns RE, Pesavento PA, McElliott VR, Ortega J, Affolter VK. Glomus tumours

in the skin and subcutis of three horses. *Vet Dermatol*. 2011;22:225-231.
3. Dagli ML, Oloris SC, Xavier JG, dos Santos CF, Faustino M, Oliveira CM, Sinhorini IL, Guerra JL. Glomus tumour in the digit of a dog. *J Comp Pathol*. 2003;128:199-202.
4. Folpe AL, Fanburg-Smith JC, Miettinen M, Weiss SW. Atypical and malignant glomus tumors: Analysis of 52 cases, with a proposal for the reclassification of glomus tumors. *Am J Surg Pathol*. 2001;25(1):1-12.
5. Furuya Y, Uchida K, Tateyama S. A case of glomus tumor in a dog. *J Vet Med Sci.* 2006;68:1339-1341.
6. Galofaro V, Rapisarda G, Ferrara G, Iannelli N. Glomangioma in the prepuce of a dog. *Reprod Dom Anim*. 2006;41:568-570.
7. Goldblum JR. Soft Tissues. In: Goldblum JR, Lamps LW, McKenney JK, Myers JL, eds. *Rosai and Ackerman's Surgical Pathology, 11th ed.* Philadelphia, PA: Elsevier; 2018:1810-1914.
8. Goldblum JR, Folpe AL, Weiss SW. Perivascular Tumors. In: Goldblum JR, Folpe AL, Weiss SW, eds. *Enzinger and Weiss's Soft Tissue Tumors, 6th ed*. Philadelphia, PA: Elsevier; 2014:749-765.
9. Gould EW, Manivel JC, Albores-Saavedra J, Monforte H. Locally infiltrative glomus tumors and glomangiosarcomas. *Cancer*. 1990;65:310-318.
10. Gross TL, Ihrke PJ, Walder EJ, Affolter VK. Perivascular tumors. In: *Skin Diseases of the Dog and Cat Clinical and Histopathological Diagnosis*. 2nd Ames, IA: Blackwell Science Ltd.; 2005:759-762.
11. Horiuchi N, Komagata M, Shitamura K, Chiba S, Matsumoto K, Inokuma H, Matsui T, Kobayashi Y. Glomus tumor in the liver of a cow. *J Vet Med Sci*. 2015;77(6):729-732.
12. Hubbard GB, Wood DH. Glomangiomas in four irradiated *Macaca mulatta*. *Vet Pathol*. 1984;21:609-610.
13. Miettinen M, Fetsch JF, Antonescu CR, Folpe AL, Wakely Jr PE. Smooth Muscle Tumors. In: *Tumors of the Soft Tissues*. Silver Spring, MD: ARP Press. 2014; 274-278.
14. Park CH, Kozima D, Tsuzuki N, Ishi Y, Oyamada T. Malignant glomus tumour in a German shepherd dog. *Vet Dermatol*. 2009;20:127-130.
15. Peters M, Grafen J, Kuhnen C, Wohlsein P. Malignant glomus tumour (glomangiosarcoma) with additional neuroendocrine differentiation in a horse. *J Comp Pathol*. 2016;154:309-313.
16. Roperto S, Borzacchiello G, Brun R, Perillo A, Russo V, Urraro C, Roperto F: Multiple glomus tumors of the urinary bladder in a cow associated with bovine papillomavirus type 2 (BPV-2) infection. *Vet Pathol*. 2008;45:39-42.
17. Santa Cruz DJ, Gru AA. Tumors of the Skin. In: Fletcher DM, ed. *Diagnostic Histopathology of Tumors*. Vol 2. 5th Ed. Philadelphia, PA: Elsevier. 2021; 1814-1815.
18. Shinya K, Uchida K, Nomura K, Ozaki K, Narama I, Umemura T. Glomus tumor in a dog. *J Vet Med Sci.* 1997;59:949-950.
19. Thompson LDR. Tumors of the Ear. In: Fletcher DM, ed. *Diagnostic Histopathology of Tumors*. Vol 2. 5th Ed. Philadelphia, PA: Elsevier. 2021; 2271.
20. Uchida K, Yamaguchi R, Tateyama S. Glomus tumor in the digit of a cat. *Vet Pathol.* 2002;39:590-592.

WSC 2022-2023 Self-assessment
Conference 18

1. The pestis du petits ruminants virus is most closely related to the virus that causes which of the following?
    a. Ovine progressive pneumonia
    b. Border disease
    c. Bovine viral diarrhea
    d. Measles

2. PPRV utilizes which of the following receptors on epithelial cells?
    a. SLAM
    b. CD150
    c. Nectin-4
    d. Kinesin

3. True or false? *Chlamydia pecorum* is considered endemic in ruminants, complicating diagnosis of infection.
    a. True
    b. False

4. Which of the following causes encephalitis in pigeons?
    a. Sarcocystic falcatula
    b. Sarcocystis neurona
    c. Sarcocystis nesbitti
    d. Sarcocystis calchasi

5. Glomus tumors are strongly immunopositive for which of the following?
    a. Desmin
    b. Smooth muscle actin
    c. Cytokeratin
    d. Myosin heavy chains

Please email your completed assessment for grading to Dr. Bruce Williams at bruce.h.williams12.civ@mail.mil. Passing score is 80%. This program (RACE program 33611) is approved by the AAVSB RACE to offer a total of 0.5 CE Credits, with a maximum of 12.5 CE Credits being available to any individual Veterinary Medical Professionals for the 2019-2020 Wednesday Slide Conference. This RACE approval is for the subject matter categories of: SCIENTIFIC using the delivery method of NONINTERACTIVE DISTANCE. This approval is valid in jurisdictions which recognize AAVSB RACE.

Joint Pathology Center
Veterinary Pathology Services

WEDNESDAY SLIDE CONFERENCE 2022-2023

Conference #19 **8 February 2023**

CASE I:

Signalment:
10-year-old intact male French Bulldog (*Canis familiaris*)

History:
A 10-year-old intact male French Bulldog presented for evaluation of a left cranial cervical mass. One month prior to presentation, the dog was seen by his family veterinarian for weight loss and increased respiratory efforts. A complete blood count and serum biochemical profile were unremarkable. Thoracic radiographs revealed a marked diffuse bronchointerstitial pattern that was interpreted to be pneumonia and a course of antibiotics (doxycycline) was started. The clinical signs worsened, and three weeks later the dog presented to an internal medicine service with coughing, gagging, shallow breathing, and reduced appetite. A nonmobile firm mass in the left craniolateral cervical region near the mandibular angle was palpated; a computed tomography (CT) scan revealed a heterogeneous, contrast enhancing mass that compressed the larynx medially. Cytology of a fine needle aspiration of the mass was diagnostic for neoplasia, and highly suggestive of an epithelial tumor.

On presentation, the dog was bright and alert and mildly overweight (body condition score, 3.5/5). On physical examination, the dog had laborious breathing with increased abdominal effort and increased upper respiratory sounds. The rest of the physical examination and the cardiac auscultation were unremarkable. The dog underwent a head/thorax CT the next day. The CT revealed a diffuse nodular pattern in the lungs, consistent with pulmonary metastases. The cervical mass was interpreted as an enlarged left medial retropharyngeal lymph node, and multiple tracheobronchial, sternal, mediastinal and cervical lymph nodes were rounded. The changes were diagnosed as carcinoma metastases, origin of primary mass uncertain, and the owners elected for human euthanasia.

Gross Pathology:
On gross post-mortem examination, intimately adherent to the outer wall of the left common carotid artery at the bifurcation into the external and internal carotid arteries, was a 3 cm in diameter firm, tan/white nodular mass that was soft to firm and mottled red/white on cut section. Another mass of

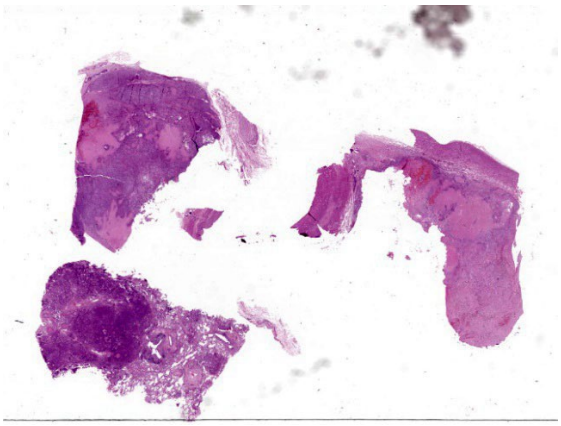

Figure 1-1. Lung, mediastinum, dog. Two sections of mediastinum (top) and one section of lung (bottom left) are submitted for examination. (HE, 5X)

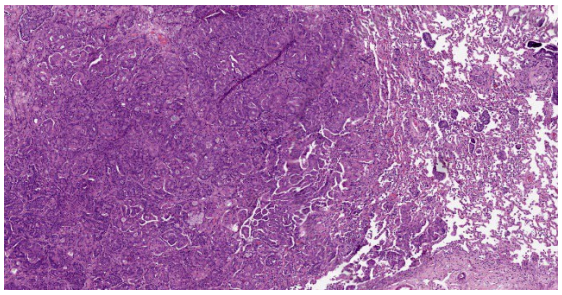

Figure 1-2. Lung, dog. An infiltrative neoplasm is present within the lung and extends into adjacent alveoli. (HE, 66X)

similar size and appearance was identified intimately adherent to the outer wall of the aorta at the heart base. Throughout the parenchyma of the lungs were generalized firm, white to grey nodules, some of which were raised by up to 5 mm, that varied in size from 0.3 to 2.5 cm in diameter, affecting all lung lobes equally and representing approximately 75% of the lungs. Multiple bronchial, cervical, and pancreatic lymph nodes were up to 2 times enlarged and homogeneously pale tan on cut surface. Other gross abnormalities included a 2 mm in diameter, firm, tan focus within the parenchyma of the right testis.

Laboratory Results:
No laboratory findings reported.

Microscopic Description:
Within the connective tissue surrounding the tunica adventitia of the external and internal carotid arteries, is a partially encapsulated, focally infiltrative multilobular neoplastic mass. The mass was predominantly (50%) composed of lobules of polygonal cells separated by dense bands of connective tissue and arranged in nests and packets separated by a fine highly vascular stroma. Neoplastic cells had variably distinct borders, a moderate amount of frequently wispy granular cytoplasm, and a round to oval nucleus with coarsely granular chromatin. There was occasionally karyomegaly (up to 8 times) and rare mitotic figures.

Additionally, multifocally throughout the mass, clusters of neoplastic cells sometimes in a tubular pattern, and represented approximately 30% of the section. These regions have a different cell morphology; cuboidal neoplastic cells with distinct cell borders, moderate amounts of cytoplasm and condensed chromatin were arranged in cords and tubules, sometimes with intraluminal wispy basophilic material. In these areas, there were 11 mitotic figures per 10 high power fields (HPF). The remainder of the mass (20%) was composed of coalescing areas of necrosis, characterized by loss of tissue architecture and replacement by eosinophilic cellular debris. The aortic mass had a similar mixed morphological appearance, but with larger areas (70%) of necrosis.

Within the pulmonary parenchyma, compressing and replacing lung tissue, were multiple poorly circumscribed, infiltrative nodules of neoplastic epithelial cells that are arranged in cords and tubules that sometimes contained necrotic debris, supported and moderate stroma. The cells were cuboidal to columnar, sometimes ciliated, with distinct cell borders, abundant eosinophilic cytoplasm, and a round to oval nucleus with condensed chromatin. There was 2-fold anisocytosis and anisokaryosis and 14 mitotic figures per 10 HPF. Neoplastic cells similar to the ones described in the lung were also found effacing bronchial and pancreatic lymph

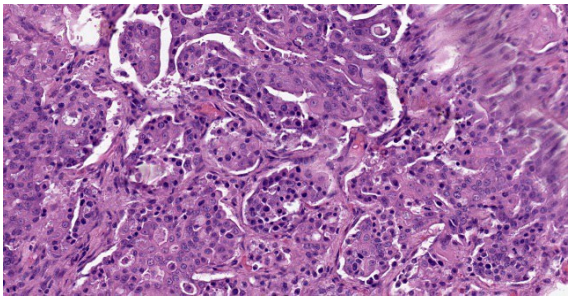

Figure 1-3. Lung, dog. Neoplastic cells are cuboidal to columnar and forms tubules and papillary projections in adjacent alveolar spaces. (HE, 346X)

nodes, and within lumen of blood and/or lymphatic vessels surrounding lungs, aorta, pancreas, and adrenal glands.

Other histological abnormalities included an interstitial cell tumor in the right testis. The cervical lymph nodes were hyperplastic and draining hemorrhage, but no neoplastic cells were present.

Representative sections from the carotid body tumor, the aortic body tumor, a pulmonary adenocarcinoma nodule, and a bronchial lymph node with metastasis were stained for chromogranin A (rabbit polyclonal, dilution 1:400, Dako, Glostrup, Denmark; labels approximately 65% of canine chemodectomas4,9,21), synaptophysin (rabbit monoclonal, ready to use, Ventana Medical Systems, Tucson, USA; labels 65% of canine chemodectomas4), pan-cytokeratin (mouse monoclonal, clone AE1/AE3, dilution 1:100, Dako, Glostrup, Denmark; labels 100% of canine primary pulmonary epithelial tumors [9]), and thyroid transcription factor-1 (TTF-1) (mouse monoclonal, clone 8G7G3/1, dilution 1:50, Dako, Glostrup, Denmark; labels 85% of canine primary pulmonary tumours2). External positive controls for IHC were pancreas, thyroid gland, and parathyroid gland for chromogranin A; pancreas, brain, adrenal gland and thyroid gland for synaptophysin; lung, liver, kidney, and small intestine for pan-cytokeratin; and thyroid gland for TTF-1. Slides incubated with non-immune rabbit serum or with antibody diluent were used as negative controls.

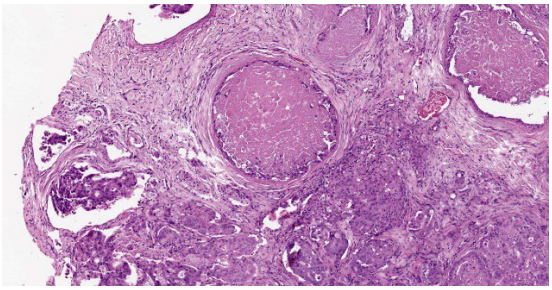

Figure 1-4. Lung, dog. There is lymphovascular invasion of pulmonary vessels and lymphatics by neoplastic cells. Some lymphatic emboli are necrotic. (HE, 200X)

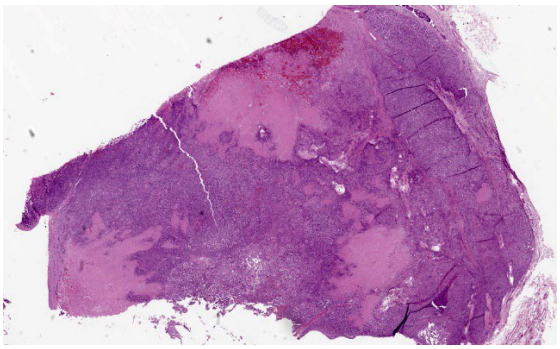

Figure 1-5. Mediastinum, dog. A second, partially necrotic neoplasm effaces mediastinal tissue. (HE, 14X)

The nests of polygonal neoplastic cells showed intense diffuse cytoplasmic immunoreactivity for chromogranin A and synaptophysin in the carotid body and aortic body tumors, while tubule-forming cuboidal neoplastic cells in the chemodectomas, and pulmonary and lymph node neoplastic cells were negative. The neoplastic epithelial cells within the lung and bronchial lymph node, and the tubule-forming cuboidal neoplastic cells in the carotid body and aortic body tumors showed weak to moderate diffuse cytoplasmic and weak to intense membranous immunoreactivity for pan-cytokeratin, while the nests of polygonal cells in the chemodectomas were negative. Immunoreactivity for TTF-1 was negative in all neoplastic cells examined; intense nuclear staining was observed in occasional type II pneumocytes (internal positive control).

Contributor's Morphologic Diagnoses:
Carotid body tumor
Aortic body tumor
Pulmonary adenocarcinoma with metastases to lung, carotid and aortic body tumors, and bronchial and pancreatic lymph nodes

Contributor's Comment:
Based on the locations of the cervical and aortic masses, a preliminary diagnosis of ca-

rotid body and aortic body tumors with metastases to the lungs was made; representative sections of the masses and internal organs were fixed in 10% neutral buffered formalin and processed for histopathological examination. It is also worth noting that the dog is a brachycephalic breed (French bulldog), and chemodectomas have been shown to occur at a higher frequency in brachycephalic breeds such as Boxers, Bulldogs, and Boston Terriers, predominantly in middle-aged to older males.[10,11,16,22] Aortic body tumors are diagnosed 4 to 12 times more often than carotid body tumors in dogs, and multiple chemodectomas are not uncommon, with 14-22% of dogs with carotid body tumors having a concomitant aortic body tumour.[10,11,12, 16,22]

The pulmonary masses were diagnosed as a primary pulmonary adenocarcinoma with metastases to bronchial and pancreatic lymph nodes. Given the two histologically distinct areas within the carotid body and aortic body tumors, immunohistochemistry (IHC) was done to further characterize the neoplasm. Representative sections from the carotid body tumor, the aortic body tumor, a pulmonary adenocarcinoma nodule, and a bronchial lymph node with metastasis were stained for chromogranin A, synaptophysin, pan- cytokeratin, and thyroid transcription factor-1 (TTF-1). (See microscopic description for IHC results). The IHC findings, together with the gross observations, were interpreted as a primary pulmonary acinar adenocarcinoma with metastases to carotid and aortic body tumors, and bronchial and pancreatic lymph nodes. It should be noted, however, that a primary carcinoma of unknown origin with metastases to lung and other tissues could not be ruled out.

Tumor-to-tumor metastasis is a rare phenomenon, with only about 100 human cases reported in the English literature.[14] To the best of our knowledge, this has only been reported

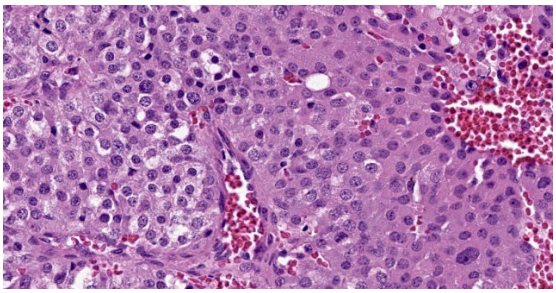

Figure 1-6. Mediastinum, dog. Neoplastic cells are polygonal, arranged in nests and packets, with finely granular to clear cytoplasm, and there is moderate anisokaryosis (bottom right). (HE, 574X)

once in a domestic species; a dog with a mammary gland tumor that metastasized to a right auricular haemangiosarcoma.[13] Tumor-to-tumor metastasis should not be confused with a "collision tumor". The term "collision tumor" refers to two histologically distinct, proximally coexistent, but independent tumors. Criteria have been suggested to define a tumor-to-tumor metastasis, which include the presence of more than one primary tumor, and that the metastatic (or donor) neoplasm is a true metastasis rather than contiguous growth of two tumors (i.e., collision tumor) or embolization of tumor cells without established growth.[7]

In humans, the most frequent donors are lung and breast carcinomas, while the most frequent recipients are renal cell carcinomas, sarcomas, and meningiomas.[17] In general, recipient tumors are slow growing, well vascularized, and can vary from benign to highly malignant. Pulmonary carcinomas have been reported to metastasize to several different types of tumours,[6] with most reported cases metastasizing to renal cell carcinomas[19] and intracranial meningiomas.[3] There are two reports of tumor metastasis to chemodectomas; one intracranial chemodectoma with metastasis from an esophageal carcinoma[15], and a carotid body tumor with metastasis from a poorly-differentiated pulmonary carcinoma.[6]

Concurrent primary neoplasms are not infrequent in dogs with chemodectomas. An investigation into 357 cases of dogs with chemodectomas found that 38% had at least one other microscopically confirmed primary tumour.[10] The most frequent second primary tumors were thyroid carcinomas and interstitial cell tumors. Pulmonary carcinoma, seen in 6 dogs, was the 11th most frequent second primary tumor. There are several possible reasons for the co-occurrence of chemodectomas and second primary tumors. Chemodectomas metastasize infrequently (12-22% of cases), are usually slow growing, non-functional and generally found in older dogs where they can act as space-occupying lesions.[10,16] Therefore, dogs diagnosed with chemodectomas simply have an extended time in which to develop a second primary tumor. There could also be a genetic component, with dogs genetically predisposed to chemodectomas also being at higher risk for other tumors. Indeed, bulldog-related breeds had a higher number of second primary tumors (47%) compared to all other breeds (32%).[10]

Contributing Institution:
University of Guelph
Guelph, Ontario Canada
www.uoguelph.ca

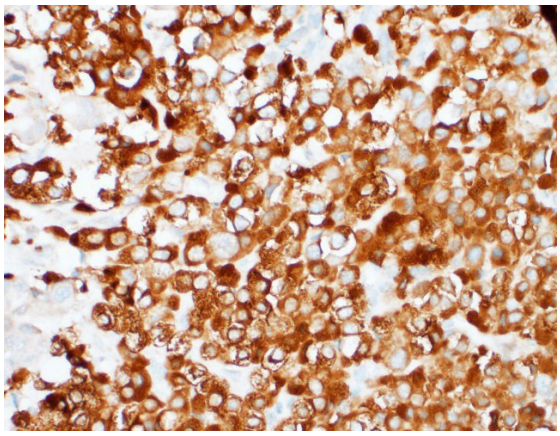

Figure 1-7. Mediastinum, dog. Neoplastic cells are strongly positive for chromogranin A. (anti Chroma-granin-A, 400X)

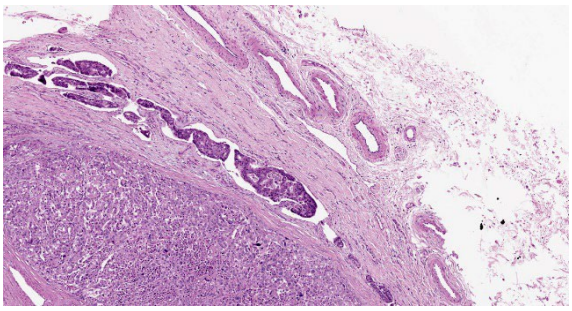

Figure 1-8. Mediastinum, dog. Metastatic cells from the pulmonary carcinoma are present in lymphatics at the periphery of the chemodectoma. (HE, 79X)

JPC Diagnosis:
1. Lung: Pulmonary adenocarcinoma.
2. Fibrovascular tissue (presumed mediastinum) (2): Neuroendocrine carcinoma and metastatic pulmonary adenocarcinoma.

JPC Comment:
This week's moderator, Colonel (Retired) Jo Lynne Raymond, and conference participants discussed whether the adenocarcinoma could be definitively diagnosed as pulmonary adenocarcinoma based on H&E. Conference participants felt the variable patterns of growth, including tubular, acinar, and lepidic patterns, and few visible cilia along the apical aspect of neoplastic cells are strongly suggestive of pulmonary origin.

Pulmonary adenocarcinomas are the most common lung tumor in dogs. Patterns of tumor growth include minimally invasive, lepidic, papillary, acinar, solid, and micropapillary, and the predominant histologic pattern can be predictive of biologic behavior.[8] The first three are the most commonly reported in dogs and have the longest survival times.[8] In the lepidic pattern, neoplastic cells form single-cell layer linings which trace alveolar walls, akin to a row of butterflies resting on a branch.[18] Papillary growths are more cellular than the lepidic pattern, and form exophytic projections into alveolar lumens.[20] In the acinar form, neoplastic cells line tubules and chords.[20] Pulmonary carcinomas may

also form squamous or adenosquamous patterns, with the latter being composed of at least 10% glandular and 10% squamous populations.[18]

In cats, tumor size is correlated with rate of metastasis[8], a finding which was confirmed in a recent retrospective study by Santos et al which described gross and histologic features of pulmonary carcinomas in 39 cats.[18] Tumors larger than 1.9 cm in diameter were more likely to metastasize. While metastasis to the digit has traditionally been the most well recognized in cats[8], this study found metastasis to the skeletal muscle, kidneys, and parietal pleura more common than digital metastasis, reinforcing the use of the MODAL acronym (muscle, ocular, digit, aorta, lung).[18] Additionally, the authors found that pulmonary carcinomas were the cause of death in only 66% of cases; cats frequently had comorbidities related to old age (lymphoma, chronic renal disease) which contributed to mortality.[18]

The study also evaluated P-40 and napsin-A expression in feline pulmonary carcinomas. Nuclear P-40 expression was found in all of the adenosquamous variants (with immunoreactivity in 100% of squamous cells and approximately 30% of the glandular components), which is expected for this basal cell marker expressed in cutaneous squamous cell carcinomas.[18] Napsin-A, on the other hand, was non-contributory in all feline tissues.[18] Napsin A is used in evaluation of human pulmonary tumors and has some utility in canine pulmonary carcinomas: another recent study showed Napsin A expression in 62 of 67 canine pulmonary adenocarcinomas.[1] The specificity is relatively low, however, as it is expressed in 60% of thyroid neoplasms and renal cell carcinomas, which are important differentials to consider for any carcinoma in the lung.[1]

References:

1. Beck J, Miller MA, Frank C, DuSold D, Ramos-Vara JA. Surfactant Protein A and Napsin A in the Immunohistochemical Characterization of Canine Pulmonary Carcinomas: Comparison with Thyroid Transcription Factor I. *Vet Pathol*. 2017; 54(5): 767-774.
2. Bettini G, Marconato L, Morini M, Ferrari F. Thyroid transcription factor-1 immunohistochemistry: diagnostic tool and malignancy marker in canine malignant lung tumours. *Vet Comp Oncol*. 2009; 7: 28-37.
3. Bhargava P, McGrail KM, Manz HJ, Baidas S. Lung carcinoma presenting as metastasis to intracranial meningioma: case report and review of the literature. *Am J Clin Oncol*. 1999; 22: 199-202.
4. Brown PJ, Rema A, Gartner F. Immunohistochemical characteristics of canine aortic and carotid body tumours. *J Vet Med A Physiol Pathol Clin Med*. 2003; 50: 140-144.
5. Burgess HJ, Kerr ME. Cytokeratin and vimentin co-expression in 21 canine primary pulmonary epithelial neoplasms. *J Vet Diagn Invest*. 2009; 21: 815-20.
6. Bury Y, Green R, Jain M, Moor J. Metastasis of carcinoma of the lung to a carotid body paraganglioma. *BMJ Case Rep*. 2012.
7. Campbell LV Jr, Gilbert E, Chamberlain CR Jr., Watne AL. Metastases of cancer to cancer. *Cancer*. 1968; 22: 635-643.
8. Caswell JL, Williams KJ. Respiratory System. In: Maxie MG, ed. *Jubb, Kennedy, and Palmer's Pathology of Domestic Animals*. Vol 2. 6th ed. St. Louis, MO: Elsevier. 2017; 495-496.

9. Doss JC, Grone A, Capen CC, Rosol, TJ. Immunohistochemical localization of chromogranin A in endocrine tissues and endocrine tumors of dogs. *Vet Pathol*. 1998; 35: 312-5.
10. Hayes HM, Sass B. Chemoreceptor neoplasia: a study of the epidemiological features of 357 canine cases. *Zentralbl Veterinarmed A*. 1988; 35: 401-408.
11. Hayes HM. An hypothesis for the aetiology of canine chemoreceptor system neoplasms, based upon an epidemiological study of 73 cases among hospital patients. *J Small Anim Pract*. 1975; 16: 337-43.
12. Hayes HM Jr., Fraumeni JF Jr. Chemodectomas in dogs: epidemiologic comparisons with man. *J Natl Cancer Inst*. 1974; 52, 1455-1458.
13. Hilbe M, Hauser B, Zlinszky K, Ehrensperger F. Haemangiosarcoma with a metastasis of a malignant mixed mammary gland tumour in a dog. *J Vet Med A Physiol Pathol Clin Med*. 2002; 49: 443-444.
14. Lee T, Cha YJ, Ahn S, Han J, Shim YM. A Rare Case of Tumor-to- Tumor Metastasis of Thyroid Papillary Carcinoma within a Pulmonary Adenocarcinoma. *J Pathol Transl Med.* 2015; 49: 78-80.
15. Lu JQ, Khalil M, Hu W, Sutherland GR, Clark AW. Tumor-to-tumor metastasis: esophageal carcinoma metastatic to an intracranial paraganglioma. *J Neurosurg*. 2009; 110: 744-8.
16. Patnaik AK, Liu SK, Hurvitz AI, McClelland AJ. Canine chemodectoma (extra-adrenal paragangliomas) - a comparative study. *J Small Anim Pract*. 1975; 16: 785-801.
17. Petraki C, Vaslamatzis M, Argyrakos T, et al. Tumor to tumor metastasis: report of two cases and review of the literature. *Int J Surg Pathol*. 2003; 11: 127-35.
18. Santos IR, Raiter J, Lamego EC, et al. Feline pulmonary carcinoma: Gross, histological, metastatic, and immunohistochemical aspects. *Vet Pathol.* 2023; 60(1):8-20.
19. Sella A, Ro JY. Renal cell cancer: best recipient of tumor-to-tumor metastasis. *Urology*. 1987: 30; 35-8.
20. Wilson DW. *Tumors of the Respiratory Tract*. In: Meuten DJ, ed. Tumors of Domestic Animals. Ames, IO: Wiley Blackwell. 2017; 487-490.
21. Yamamoto S, Fukushima R, Hirakawa A, Abe M, Kobayashi M, Machida N. Histopathological and immunohistochemical evaluation of malignant potential in canine aortic body tumours. *J Comp Pathol*. 2013; 149: 182-191.
22. Yates WD, Lester SJ, Mills JH. Chemoreceptor tumors diagnosed at the Western College of Veterinary Medicine 1967-1979. *Can Vet J*. 1980; 21: 124-129.

CASE II:

Signalment:
9-year-old, castrated male, Netherland dwarf rabbit (*Oryctolagus cuniculus domesticus)*

History:
This rabbit presented to the rDVM with chronic uveitis which was poorly responsive to treatment with oral and topical non-steroidal anti-inflammatory drugs and antibiotics. The rabbit otherwise appeared to be in good health. The owners opted for enucleation and submission for of the eye for histopathology.

Gross Pathology:
The submitted eye was grossly unremarkable.

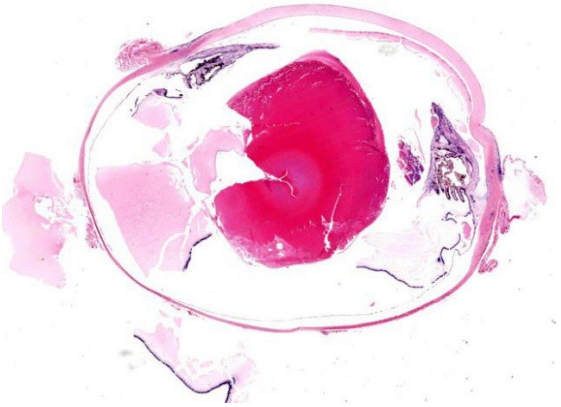

Figure 2-1. Globe, dwarf rabbit. A globe is presented for examination. The cornea is at top. There are areas of pallor within the lens, and eosinophilic protein within the posterior segment. (HE, 6X)

Laboratory Results:
No laboratory findings reported.

Microscopic Description:
The iris contains moderate diffuse infiltrates of plasma cells accompanied by small numbers of lymphocytes and few scattered heterophils. Occasional strands of fine fibrous stroma associated with moderate aggregates of epithelioid macrophages, fewer multinucleated giant cells, occasional heterophils, proteinaceous debris and a few erythrocytes are noted in the anterior and posterior chambers. Thin strands of fibrous tissue rarely extend from the posterior iris near the pupillary margin. There are large areas where subcapsular lens fibers appear fragmented, rounded and are replaced by amorphous pink debris. Small amounts of basophilic, fine mineral, as well as numerous, 1-2 micron long, ovoid, gram positive, spores, are present beneath the lens capsule and within lens epithelial cells. Lens epithelial cells are often vacuolated and rarely form small piled up aggregates. In some areas, subcapsular lens fibers are lost and replaced by sparse cell debris.

Contributor's Morphologic Diagnoses:
Eye: Moderate, chronic, plasmacytic and granulomatous, anterior uveitis with cataracts and numerous intralenticular, gram positive, microsporidial spores (consistent with Encephalitozoon cuniculi)

Contributor's Comment:
The clinical history and microscopic appearance of the ocular lesions in this rabbit are most compatible with cataract formation and phacoclastic uveitis due to the ocular form of *Encephalitozoon cuniculi* infection.

Encephalitozoon cuniculi is a microsporidial pathogen with worldwide distribution. Although previously phylogenetically classified as a protozoa, it is currently considered a fungus.[5,6] There are three major genotypes of *E. cuniculi*. Genotype 1 (or the rabbit strain) is generally associated with disease in pet and commercially raised rabbits. This organism has a direct life cycle. Horizontal transmission is most commonly through the ingestion of spores in urine-contaminated feed, or less commonly via inhalation. Vertical (or transplacental) transmission may also occur and is often hypothesized to be the cause of intraocular infections which facilitates access to, and colonization of lens fibers during fetal development.[6] Typically, in the intestine, the spores primarily infect host cells through extrusion of their polar filament and injection of sporoplasm into a host cell. Phagocytosis

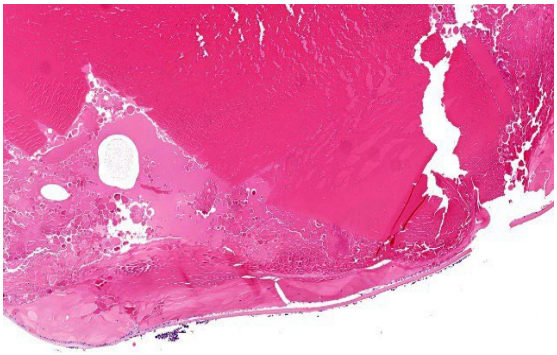

Figure 2-2. Globe, dwarf rabbit. There is degeneration of the posterior lens fibers with formation of Morgagnian globules. (HE, 66X)

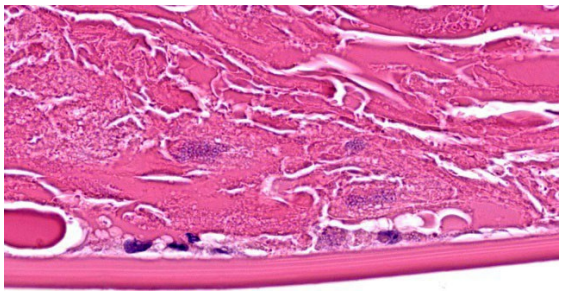

Figure 2-3. Globe, dwarf rabbit. In areas of degeneration, fibers are often swollen by cytoplasmic microsporidial spores. (HE, 857X)

by host cells has also been demonstrated.[6] Initial target organs for infection via horizontal transmission are those with high blood flow such as the lungs, liver and kidney but many sites may be involved. Infection of the central nervous system (CNS) generally occurs later in the course of disease. At tissue sites, sporogony continues and eventually leads to rupture of host cells and the release of spores which induces a localized lymphoplasmacytic to granulomatous inflammatory response. Most immunocompetent animals have subclinical infections with foci of granulomatous inflammation most commonly present in the brain, kidneys, and eye.[5,6] Spores are shed intermittently in the urine of infected rabbits. Clinical disease in rabbits is most often seen in older rabbits as immunocompetency wanes with age or following stressors that may have a negative impact on the host immune response (ie. changes in environment, other illnesses, medications, etc). In rabbits, the most common manifestations of *E. cuniculi* infection are clinical signs of central nervous system disease, uveitis, and chronic renal disease.

Rabbits with encephalitozoonosis most commonly present with a variety of neurologic clinical signs resulting from foci of lymphoplasmacytic to granulomatous meningoencephalitis. Many affected rabbits develop central vestibular disease which presents as head tilt, ataxia, nystagmus, and/or circling movements. More severe clinical signs may include rotation along the body length axis (i.e., rolling) or lateral recumbency which are generally associated with a poorer prognosis.[5] The main clinical differential diagnosis in these rabbits is peripheral vestibular disease due to otitis interna. Other neurologic signs that may be associated with encephalitozoonosis include seizures, paresis, altered mentation and behavioural changes.

Ocular lesions are most frequently reported in young rabbits with no other apparent clinical signs and lesions are most often unilateral. However, bilateral lesions have been documented in rabbits.[5] In some cases (likely largely older individuals), other clinical signs (especially neurologic signs) may also be noted.[8] In the eye, spores infect the lens epithelial cells and when these cells rupture it results in lens fiber degeneration, cataract formation and eventually phacoclastic uveitis.

Rabbits with significant renal disease resulting from chronic encephalitozoonosis often have slightly pale, pitted kidneys that microscopically exhibit lymphoplasmacytic to granulomatous, tubulointerstitial nephritis with fibrosis. These rabbits generally present with non-specific clinical signs of polyuria, polydipsia, weight loss, dehydration, and anorexia.

Figure 2-4. Globe, dwarf rabbit. A Gram stain demonstrates microsporidial spores within lens fibers. (Brown-Brenn, 400X)

In tissue sections, within foci of inflammation, microsporidial organisms are gram-positive which is a useful means of highlighting spores. Immunohistochemistry (IHC) and PCR testing of tissues, especially the eye contents, has been used to try to confirm a diagnosis of encephalitozoonosis. Unfortunately, PCR and IHC testing for diagnostic specimens is not easily accessible. Antemortem diagnosis of *E. cuniculi* remains a challenge. *Encephalitozoon cuniculi* is considered zoonotic, especially in immunocompromised people who are at an increased risk of acquiring infection.

Contributing Institution:
Atlantic Veterinary College, University of Prince Edward Island

JPC Diagnosis:
Eye, globe: Uveitis, phacoclastic, granulomatous, diffuse, moderate, with cataractous change and intralenticular microsporidial spores.

JPC Comment:
This is a classic case of phacoclastic uveitis caused by *E. cuniculi*. These microsporidian parasites have a characteristic coiled polar filament visible on electron microscopy as parallel strips winding around the nucleus, or if viewed in cross section, as regularly spaced circles along the periphery of the organism.[3] As the contributor mentioned, there are several genotypes of *E. cuniculi*, with genotypes II, III, and IV representing murine, canine, and human strains, respectively, though the genotypes are not exclusive to a single host species.[3] *E. cuniculi* can infect a variety of species, including guinea pigs, mice, rats, hamsters, primates, foxes, birds, dogs, and humans.[1,3] Ocular *E. cuniculi* infections have been sporadically documented in other species; for instance, cataracts have been reported in a snow leopard, dogs, mink, and blue foxes.

Two reports have described *E. cuniculi* cataracts in domestic cats in Austria and California. In a 2011 report by Benz et al, positive *E. cuniculi* titers were found in 11 cats (total of 19 eyes) with uveitis and cataracts in Austria.[2] In 18 of the eyes, *E. cuniculi* was identified on PCR of lens material.[2] In 11 of the eyes, histopathology with acid-fast trichrome of the anterior lens capsule revealed *E. cuniculi* spores in the lens epithelial cells.[2] The authors concluded that a positive *E. cuniculi* titer in conjunction with cataracts is strongly indicative of active infection in cats.[2] Similarly, *E. cuniculi* infection was diagnosed in three cats with immature cataracts and uveitis in California based on lens histopathology (hematoxylin and eosin or Ziehl-Neelsen) or PCR, and serologic testing was positive in the two tested cats.[7] These reports illustrate that *E. cuniculi* can induce similar ocular lesions in cats as in rabbits.

Control of the infection appears to be linked to the Th1 immune response and IFN-gamma production.[3] Studies have shown an initial CD4+ T-cell proliferation in the spleen followed by CD8+ T-cell proliferation, and high levels of IFN-gamma can be detected in the spleen, mesenteric lymph nodes, and Peyer's patches.[3] Humoral immunity does not appear to offer sufficient protection against infection

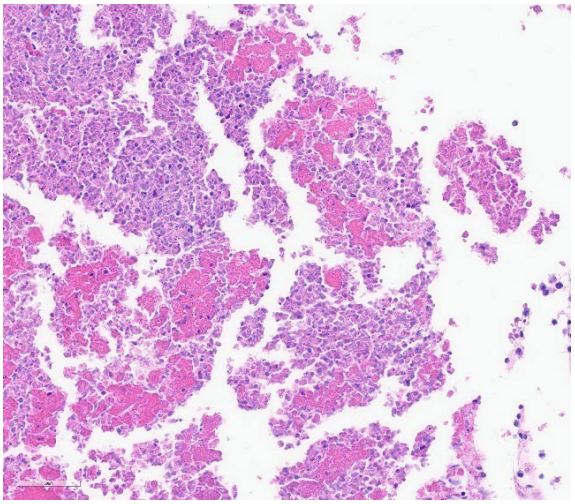

Figure 2-5. Globe, dwarf rabbit. There is extruded lens protein in the posterior chamber with aggregates of degenerate macrophages. (HE, 381X)

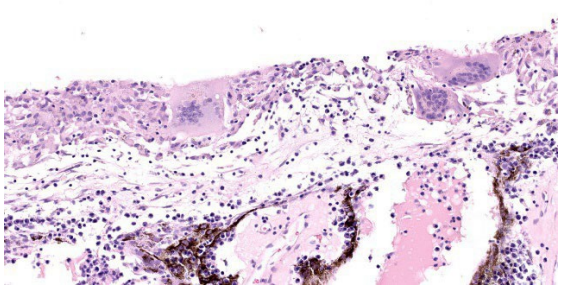

Figure 2-6. Globe, dwarf rabbit. The ciliary body is lined by a fibrovascular membrane lined by epithelioid macrophages and multinucleated giant cells. (HE, 246X)

but may aid in diagnosis as serologic testing is one of the few antemortem tests available.[3] Antibody titers initially rise by 4 weeks post infection and are high by 9 weeks.[1] Infected animals have an initial spike in IgM followed in a few weeks by an IgG spike.[3] Since a single positive titer cannot differentiate active infection from previous exposure, serial sampling to evaluate the titer differences is crucial. Perhaps the most helpful test is a negative titer: while a single negative test may happen in acute infections, paired negative titers spaced three weeks apart can rule out *E. cuniculi* infection.[3]

Spontaneous and congenital cataracts also occur in domestic rabbits and should be considered as a differential diagnosis for *E. cuniculi*-induced cataracts.[1] The incidence of cataracts in New Zealand white rabbits is suggestive of an inherited autosomal recessive defect in this breed.[1] As the contributor mentions, intra-ocular infection by *E. cuniculi* in rabbits is speculated to be due to in utero infection of the developing lens; however, a recent study in specific-pathogen free rabbits demonstrated lens after experimental oral infection with *E. cuniculi*, indicating other routes of infection may be possible.[4]

References:

1. Barthold SW, Griffey SM, Percy DH. *Pathology of Laboratory Rodents and Rabbits.* 4th ed. Ames, IO: John Wiley & Sons, Inc. 2016; 79, 146, 186, 234, 293-295, 318.
2. Benz P, Maas G, Csokai J, et a. Detection of *Encephalitozoon cuniculi* in the feline cataractous lens. *Vet Ophthalm.* 2011; 14 (Suppl 1) 37-47.
3. Dobosi AA, Bel LV, Pasitu AI, Pusta DL. A Reivew of *Encephalitozoon cuniculi* in Domestic Rabbits (*Oryctolagus cuniculus*)-Biology, Clinical Signs, Diagnostic Techniques, and Prevention. *Pathogens*. 2022; 11: 1486-1500.
4. Jeklova E, Leva L, Kummer V, Jekl V, Faldyna. Immunohistochemical Detection of *Encephalitozoon cuniculi* in Ocular Structures of Immunocompetent Rabbits. *Animals (Basel)*. 2019; 9(11): 988-995.
5. Kunzel F, Fisher PG. Clinical signs, diagnosis, and treatment of *Encephalitozoon culiculi* infection in rabbits. *Vet Clin Exot Anim.* 2018; 21:69-82.
6. Latney LV, Bradley CW, and Wyre NR. *Encephalitozoon cuniculi* in pet rabbits: diagnosis and optimal management. *Vet Med Res.* 2014; 5:169-180.
7. Lin J, Nell B, Horikawa T, Zarfoss. Feline intraleunticular *Encephalitozoon cuniculi:* three cases from California. *JFMS Open Rep.* 2022; 8(2): 1-9.
8. Morsy EA, Salem HM, Khattab MS, Hamza DA, and Abuowarda MM. *Encephalitozoon cuniculi* infection in farmed rabbits in Egypt. *Acta Vet Scand.* 2020; 62:11

CASE III:

Signalment:

13 Years, male, indoor only cat (*Felis catus)*

History:

The cat presented at the vet because the owner had realized that the right eye seemed "bigger", accompanied by a widened pupil. The clinical examination revealed normal pulse, mucosal surfaces, abdomen andlymph

nodes as well as nondescript auscultation of heart and lung.

The intraocular pressure in the right eye was 59 mm Hg initially, and the intraocular pressure was 25 mmHg in the left eye. After one week of treatment with Azopt three times per day, the intraocular pressure of the right eye was reduced to 21 mmHg at the second consultation.

Values of the clinical examination at the second consultation:
Blood pressure: 160/120 (5 measurements)
Glucose: 6.4 mmol/l
T4: within the normal range
Renal values: within the normal ranges

Clinical examination of the right eye: eye is open; reflexes are negative apart from a minimal pupil reflex; eye lids and their position are in within normal range; the conjunctiva is pink; the cornea is clear; the anterior eye chamber is clear; iris is in mydriasis; the lens demonstrates mild nucleosclerosis; the corpus vitreous with partly ablated retina in nasal area with a pigmented mass in the temporal area extending into the corpus vitreous.

Ultrasound of the right eye: temporal mass in the area of the ciliary body /periphery of the fundus lead to a suspicion of intraocular melanoma or mass of the ciliary body.

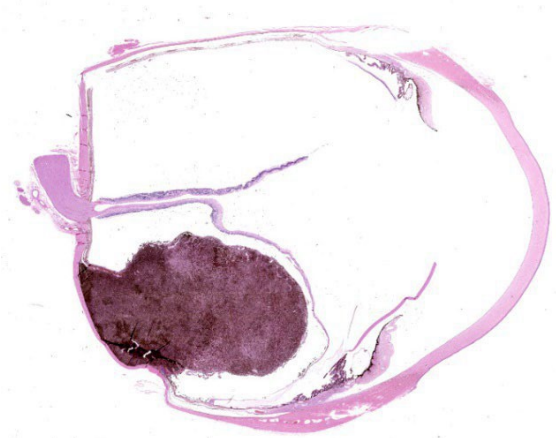

Figure 3-1. Globe, cat. A large, pigmented neoplasm arises from the subretinal choroid. The retina is detached and only a fragment of lens capsule is present in this section. (HE, 6X)

Two weeks after the first presentation, transpalpebral enucleation of the right eye with a continuous closure with Vicryl 5/0 suture material was performed. The suture material of the cutaneous suture was removed 10 days after surgery.

Gross Pathology:
Oculus dexter: Conjunctiva bulbi, cornea, anterior eye chamber, iridicorneal angle, iris, lens, ciliary body, the retinal pigment epithelium, the papilla nervi optici, n. opticus and the sclera did not show any macroscopical changes.

The vitreous was only partially present between a pigmented chorioidal mass and the completely ablated, cup shaped retina, that was only attached at the papilla nervi optici and focally attached to the posterior side of the lens.

Within the chorioidea, partly covered by the ablated retina, there was a nodular round to oval shaped endophytic protruding soft mass (about 10 mm in diameter) located between the pars ciliaris of the ciliary body and the papilla nervi optici with a homogenously black colored cut surface.

Laboratory Results:
Urea: 1.499 mmol/l
Creatinin: 12906.692 µmol/l
Urea/Creatinin: 16
Alanin-amino-transferase (ALT): 500.1 nkat/l
Aspartat-amino-transferase (AST): 316.73 nkat/l
Alkaline phosphatase (ALKP): 316.73 nkat/l
Thyroxin: 25 nmol/l
Serum chemistry profile values were within normal limits.

Microscopic Description:
The conjunctiva bulbi, cornea, anterior eye chamber, irido-corneal angle, the lens and the nervus opticus / optic cup do not show any histological changes.

Limbus: The limbal cornea shows a mild infiltration by pigmented cells (melanosis oculi).
Iris: There is moderate mydriasis, the facies posterior contains multifocal single cysts.
Ciliary body: The outer non-pigmented epithelium reveals a mild to focally moderate atrophy.
Vitreous body: There is focal evidence of scattered plump melanin containing cells (questionable RPE).
Retina: A total retinal ablation with moderate to severe atrophy of all retinal layers (neuronal - inner/outer granular-and photoreceptor layer) is present.
Retinal pigmentary epithelium (RPE): There is focally mild hypertrophy.
Choroid: Located between ciliary body and papilla nervi optici, within the chorioid, there is a round to oval shaped, about 1 cm in diameter large chorioidal mass with focally infiltrative growth, partly covered by a thin layer of RPE and regular chorioidal pigmented cells (cream brown pigment). The cells are moderately densely packed, well demarcated and demonstrate solid to nodular growth pattern. The moderately pleomorphic cell population appears disordered, divided by a fine fibrovascular stroma. The cells are plump, round to weakly elongated with a diameter of about 25 µm, with eosinophilic cytoplasm with a variable content of cytoplasmatic granular, partly clumped brownish material (melanin granules) and often indistinct cell borders. Where discernible, the nuclei are about 10 µm in diameter and contain little condensed chromatin and one central nucleolus. Anisocytosis and anisokaryosis is high. Only few binucleated cells are visible, the bleached specimens show 0-1 mitotic figures per high power field. Focally, in the periphery of the cell proliferate there is a small area of osseous metaplasia.
Sclera: Opposing the tumor, the sclera is focal mildly thinned. There is no evidence of the neoplastic cells infiltrating the sclera.

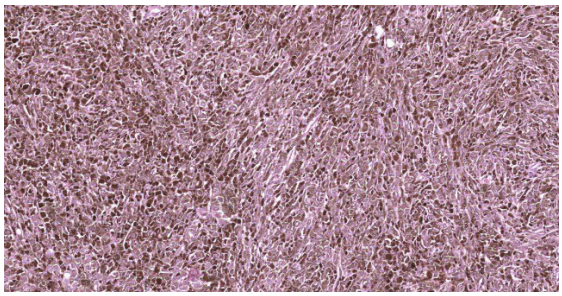

Figure 3-2. Globe, cat. Both polygonal to round and spindled melanocytes comprise the neoplasm. (HE, 132X)

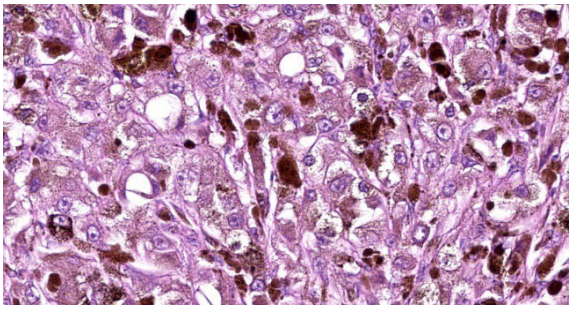

Figure 3-3. Globe, cat. Higher magnification of neoplastic in less pigmented areas demonstrate bland nuclei. (HE, 600X)

Contributor's Morphologic Diagnoses:

- Choroid: endophytic choroidal plump cellular melanoma
- Ciliary body: atrophy of outer non-pigmented epithelium, mild to focally moderate
- Retina: total retinal ablation and atrophy, moderate to severe
- RPE: hypertrophy, focal mild
- Iris: iridial mydriasis with focal cyst formation (facies posterior), focal, moderate
- Melanosis oculi, focal, mild

Contributor's Comment:
The most common melanocytic tumor in the eye of the cat is the feline diffuse iris melanoma.[2] In the present case the neoplastic cell proliferate was not involving the iridociliary body and it was only focal, protruding into the vitreous. Additionally, iridociliary epithelial tumor can also be pigmented, but have been ruled out in this case due to same reasons as mentioned above.[2]

According to Parul Singh and Abhishek Singh`s Paper in 2012, choroidal melanoma is the most common malignant primary neoplasia in humans with most often metastasis in liver, frequent the lung and bone.[6] Whereas canine choroidal melanomas are common, being usually benign and never metastasize[2], a choroidal melanoma has been reported in a cat the first time in 2011.[5] In the current case, no X-ray was performed to check for metastasis and no history of further locations with potential cell proliferates is known. The large cell proliferate led to ablation and atrophy of the retina with consecutive atrophy of the outer epithelium of the ciliary body and focal RPE hypertrophy, interpreted as secondary glaucomatous alterations.

Iridal cysts can be congenital or occur spontaneously, due to trauma or inflammatory processes.[3] In the current case, it is seen as an incidental finding just as the mild melanosis oculi.

Contributing Institution:
Institute of Veterinary Pathology Zuerich (IVPZ)
www.vetpathology.uzh.ch

JPC Diagnosis:
1. Eye: Choroidal melanocytoma.
2. Eye: Iridal cysts.

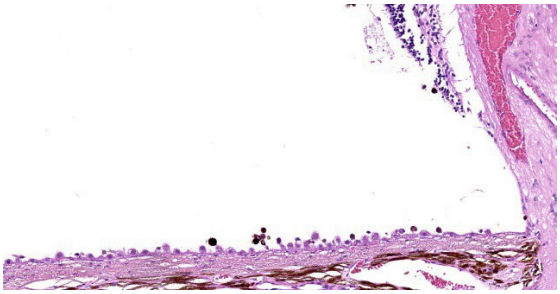

Figure 3-4. Globe, cat. There is hypertrophy of retinal pigmented epithelium. (HE, 1900X)

JPC Comment:
While iris melanoma is the most common intraocular tumor of cats, this case is an example of melanoma originating from extra-iridal structures, which is uncommon to rare in cats.[1,4] Only four cases of choroidal melanocytic neoplasms have been reported in the English literature. In two cases, neoplastic melanocytes infiltrated into the adjacent iris, and in a third case, there was a high mitotic rate (24 per 10 high power fields) with significant anisocytosis and anisokaryosis.[1] These three cases were diagnosed as choroidal melanoma.[1] The remaining case was diagnosed as a melanocytoma.[5]

Melanocytic neoplasms more commonly arise from the iris and are termed feline diffuse iris melanoma (FDIM).[4] These neoplasms start as iris melanosis, characterized as a non-neoplastic focus of proliferative and dysplastic melanocytes up to 3 layers thick.[4] Iris melanosis may remain static or rapidly progress to FDIM with infiltration of the subjacent iris stroma.[4] Early FDIM and iris melanosis are grossly indistinguishable, but as FDIM progresses, the iris becomes thickened and the pupil may be irregularly shaped and less mobile.[4] Features of malignancy for FDIM include a high mitotic rate (not well established and cut-off varies between studies), high nuclear to cytoplasmic ratio, significant nuclear pleomorphism, and multinucleation.[1,4] Survival for cats with FDIM is cor-

related with histologic invasion, with neoplasms confined to the iris or trabecular meshwork producing survival times similar to control cats, and neoplasms extending into the sclera associated with decreased survival time.[4] While cellular morphology can vary significantly and include patterns such as spindle cell, anaplastic, and giant cell variants, there is no correlation between morphology and metastasis.[4] Rates of FDIM metastasis vary from 19 to 63%, and the liver is the most common site of metastasis.[4] While some aggressive FDIMs metastasize quickly, others may metastasize late in the disease, sometimes years after the initial diagnosis.[4]

References:

1. Bourguet A, Piccicuto V, Donzel E, Carlus M, Chahory S. A case of primary choroidal malignant melanoma in a cat. *Vet Ophthalm*. 2015; 18(4): 345-349.
2. Dubielzig RR. Tumors of the Eye. In: Meuten DJ, ed. *Tumors in Domestic Animals*. 5th ed. Ames, IO: Wiley-Blackwell; 2017:892-911.
3. Gemensky-Metzler AJ, Wilkie DA, Cook CS. The use of semiconductor diode laser for deflation and coagulation of anterior uveal cysts in dogs, cats and horses a report of 20 cases. *Vet Ophthalmol*. 2004;7(5):360-8.
4. Kayes D, Blacklock B. Feline Uveal Melanoma Review: Our Current Understanding and Recent Research Advances. *Vet Sci.* 2022; 9(2): 46-59.
5. Semin MO, Serra F, Mahe V, Deviers A, Regnier A, Raymond-Letron I. Choroidal melanocytoma in a cat. *Vet Ophthalmol*. 2011;14(3):205-8
6. Singh P, Singh P. Choroidal melanoma. *Oman J Ophthalmol*. 2012; 5(1):3-9.

CASE IV:

Signalment:
1 year-old, intact female, Cavalier King Charles Spaniel, dog (*Canis familiaris*)

History:
This dog was a normal active puppy up until 4 weeks prior when the owner noted the puppy acting lethargic and had labored breathing. The puppy was brought to the vet and was diagnosed with a respiratory infection. Fungal cultures were negative. The puppy was started on an antibiotic, prednisone, and another medication (unknown). Clinical signs improved but then worsened and the puppy quickly died. All other puppies in the litter and dogs in the home were all normal with no clinical signs.

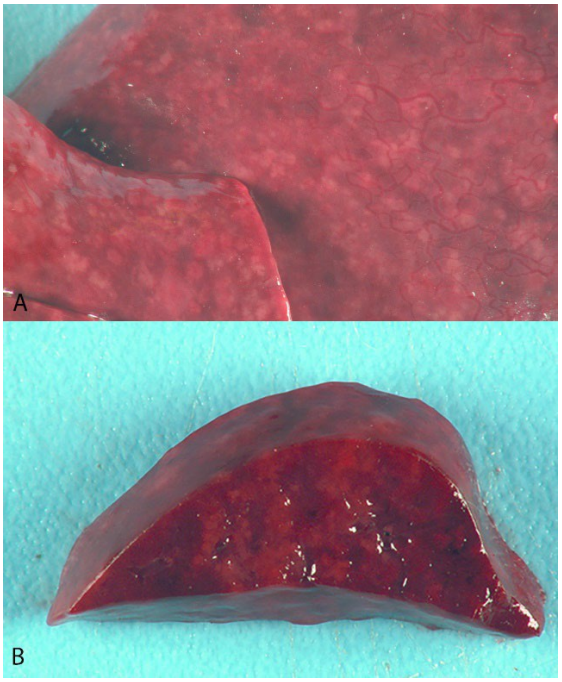

Figure 4-1. Lung, dog. The pulmonary parenchyma was diffusely dark red, rubbery, and did not collapse. There were hundreds of randomly scattered, 1-2 mm in diameter, tan to white, firm raised foci throughout all lung lobes. (Photo courtesy of: Michigan State University Veterinary Diagnostic Laboratory. Department of Pathobiology and Diagnostic Investigation - https://cvm.msu.edu/vdl) (HE, 5X)

Gross Pathology:
The pulmonary parenchyma was diffusely dark red, rubbery, and did not collapse. There were hundreds of randomly scattered, 1-2 mm in diameter, tan to white, firm raised foci throughout all lung lobes.

Laboratory Results:
No laboratory findings reported.

Microscopic Description:
Approximately 90% of alveolar spaces are multifocally expanded by eosinophilic, foamy, amorphous material with numerous approximately 7µm in diameter, teardrop-shaped, yeast structures that have variably thick walls highlighted by a Grocott's Methenamine Silver (GMS) stain. Moderate numbers of histiocytes are associated with these regions. The adjacent alveoli are lined by plump cuboidal type II pneumocytes. The remaining pulmonary parenchyma is extensively autolytic and contains multifocal mats of cadaver bacilli.

Contributor's Morphologic Diagnoses:
Lung: Severe, multifocal, histiocytic alveolitis with intralesional yeasts and type 2 pneumocyte hyperplasia

Contributor's Comment:
Pneumocystis sp., is a commensal yeast-like fungal organism, in the class Pneumocystidomycetes, found in the lungs of adult animals. Initial colonization with *Pneumocystis sp*. is thought to occur during the birthing process but can also be horizontally transmitted between the same species as an airborne organism[5,8]. Essentially every mammal has a unique strain of *Pneumocystis sp*. and interspecies transmission is not thought to occur. There are five host-specific *Pneumocystis sp*. that have been formally described in the literature and include: *P. carinii/wakefeldii* in rats, *P. murina* in mice, *P. oryctolagi* in rabbits, and *P. jirovecii* in humans[1]. Pneumocystis pneumonia (PCP) can occur in any species of animal, especially if immunocompromised. In humans, PCP and secondary airway obstruction are serious consequences in immunocompromised individuals, especially in those individuals that are infected with human immunodeficiency virus (HIV). *Pneumocystis* sp. are fastidious organisms and cannot be grown in continuous culture, leading researchers to heavily rely on animal models of disease[2,5,8]. *P. carinii* infections in rats were the original study models; however, due to host-specific genotypic and phenotypic variations, it was difficult to make comparisons to *P. jirovecii* infections in humans[2]. Additionally, due to the inability to recreate an HIV model in rats, rat models to study PCP infections were not ideal. Studies utilizing macaques infected with simian immunodeficiency virus (SIV) then became the most relevant animal model not only due to macaques developing clinical signs similar to

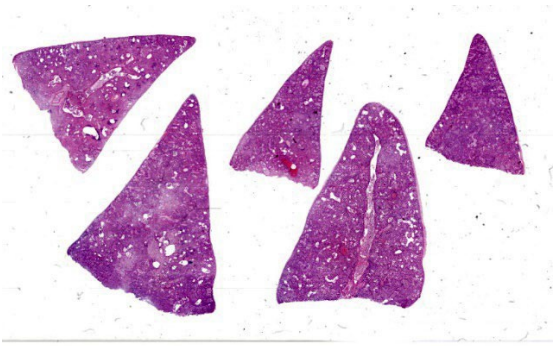

Figure 4-2. Lung, dog. Multiple sections of lung are submitted for examination. At subgross examination, all are consolidated with abundant foamy alveolar exudate. (HE, 5X)

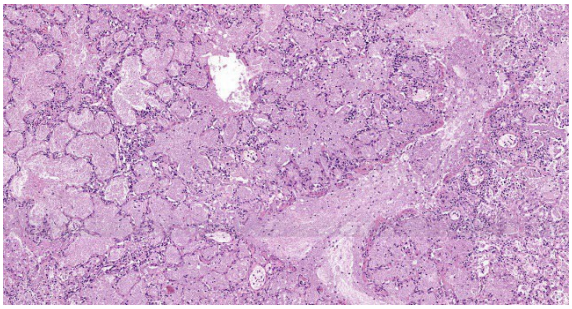

Figure 4-3. Lung, dog. Alveoli are filled with a foamy "soap-bubble" exudate; alveolar septa are expanded by macrophages, fibrin, and edema. (HE, 100X)

those in humans with AIDS, but *P. carinii* derived from humans and non-human primates are evolutionarily more related than *P. carinii* derived from rats[2].

Pneumocystis pneumonia, suspected to be caused by *Pneumocystis carinii f sp. canis*[6] is uncommon in dogs. Young to middle-aged Cavalier King Charles Spaniels and Miniature Dachshunds are overrepresented and may have inheritable immunodeficiency predisposing them to over colonization[3,9]**.** In a study that evaluated IgG, IgM, and IgA serum concentration in Cavalier King Charles Spaniels diagnosed with Pneumocystis pneumonia compared to breed and age-matched nonaffected dogs, it was found that affected dogs had significantly lower IgG concentrations[9]. These dogs tend to respond to medical treatment if treated early in the course of the disease.

Pneumocystis infects hosts by direct attachment to the alveolar epithelium via surface antigen glycoprotein A (gpA). The life cycle is composed of two morphologically distinguished forms, a trophic form and a cystic form which undergo binary fission and sexual replication, respectively. The trophic form is the predominant form during infection and is characterized by 1-4µm, thin-walled, uninucleate organisms[8]. The cystic form is 5-8 µm in diameter, thick-walled, and contains 8 intracystic nuclei/bodies. The intracystic bodies are released, attach to type I pneumocytes, and are thought to develop into the trophic form[4].

Pneumocystis can evade host immunity due to its cell wall composed of mannose-rich polysaccharides and heavily glycosylated surface antigens[4]. gpA is the key surface antigen responsible for attachment to the host epithelium as well as evasion of host immunity via interactions with macrophages, surfactant proteins, and fibronectin[4]. Multiple genes encode this protein; however, during infection only one isoform is expressed[3]. The expression of this isoform is unique to the associated organism adapted to each host species. Pneumocystis causes disease by expanding alveoli as well as possibly altering surfactant homeostasis. Infection is controlled by macrophages and cell-mediated immunity[4].

Gross lesions can be multifocal to diffuse and are often characterized by red to brown areas of consolidation that may be variably nodular[4]. Histologically, lesions are characterized by foamy eosinophilic material and variable numbers of foamy macrophages that fills alveolar spaces. Organisms are difficult to identify on routine hematoxylin and eosin staining. Special staining with methenamine sliver highlights the walls of the organism. Secondary, variably prominent findings include, increased interstitial lymphocytes, plasma cells, and type II pneumocyte hyperplasia[4]. The number of organisms within alveolar spaces can greatly vary, thus PCR is the most sensitive detection method.

Contributing Institution:
Michigan State University Veterinary Diagnostic Laboratory. Department of Pathobiology and Diagnostic Investigation - https://cvm.msu.edu/vdl

JPC Diagnosis:
Lung: Pneumonia, interstitial, histiocytic and necrotizing, diffuse, marked, with type II

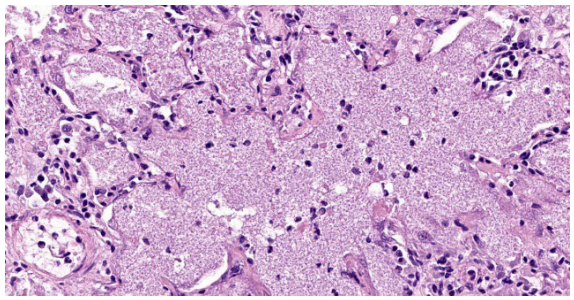

Figure 4-4. Lung, dog. High magnification of the characteristic alveolar exudate characteristic of infection with Pneumocystis carinii. (HE, 450X)

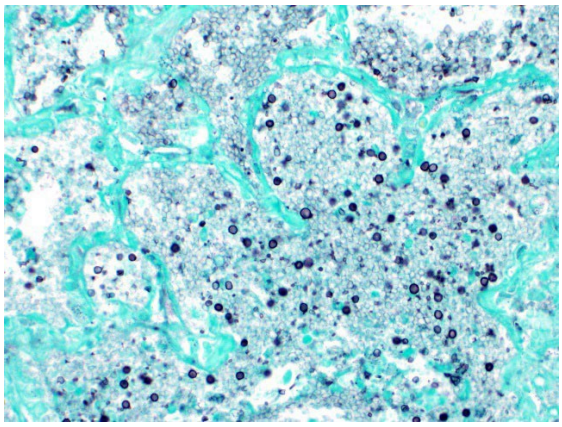

Figure 4-5. Lung, dog. A silver stain demonstrates cysts of Pneumocystis carinii within the alveolar exudate. (HE, 450X)

pneumocyte hyperplasia and many intra-alveolar yeasts.

JPC Comment:

The contributor provides a great overview of this ubiquitous fungus which can infect a wide variety of hosts. A recent meta-analysis evaluated the clinical and diagnostic features of 43 dogs with pneumocystosis.[10] Miniature dachshunds and cavalier King Charles spaniels were predisposed.[10] Clinical signs were nonspecific and included weight loss, cough, dyspnea, and cyanosis, but, interestingly, most dogs had normal body temperature. [10] Hemogram changes include leukocytosis and neutrophilia.[10] The authors found that hypogammaglobulinemia was useful in the diagnosis and reflects the inability of infected dogs to class-switch from IgM to IgG production.[10] On necropsy, the lungs were firm or rubbery and discolored or pale. [10] Pneumothorax was uncommonly seen in these dogs but is a common finding in human infections.[10] Cytologic examination of bronchoalveolar lavage fluid, the mainstay of diagnosis in humans, was insensitive and unreliable in this report; more sensitive antemortem diagnostics included fine needle aspirates of the lung and cytologic examination of tracheal swabs.[10] Histologic findings included lymphohistiocytic interstitial pneumonia with type II pneumocyte hyperplasia and foamy to granular eosinophilic material filling alveolar lumens containing poorly-staining extracellular and intracellular trophozoites and cysts.[10] GMS and PAS highlighted the cyst walls and confirmed the diagnosis.[10] Advanced diagnostics that were useful in the meta-analysis include PCR, electron microscopy, and immunohistiochemistry.[10]

An uncommon complication of pneumocystis infection is disseminated spread, which was recently reported in a young adult toy poodle.[7] In addition to the alveolar lumen, the fungus was found in the pulmonary interstitium and had spread to multiple lymph nodes, the liver, heart, spleen, pancreas, kidneys, and gastrointestinal tract.[7] There was marked lymphoid depletion in multiple lymph nodes and the spleen.[7] Based on the distribution pattern, the authors speculated that the fungus spread through lymphatics.[7] The dog may have been immunodeficient due to a prolonged course of corticosteroids or due to a underlying immunodeficiency.[7]

Conference participants discussed the gross photograph from this case; the pale patchy discoloration combined in an immunosuppressed animal (i.e. in a severe combined immunodeficiency in an Arab foal, or an NHP infected with SIV) is strongly suggestive of *Pneumocystis* pneumonia.

References:

1. Alanio A, Bretagne S. Pneumocystis jirovecii detection in asymptomatic patients: what does its natural history tell us? *F1000 Research*. 2017; 6.
2. Board KF, Patil S, Lebedeva I, et al. Experimental Pneumocystis carinii pneumonia in simian immunodeficiency virus–infected rhesus macaques. *J Infect Dis.* 2003;187(4): 576-588.
3. Farrow, BRH, Watson, ADJ, Hartley, WJ, and Huxtable, CRR. Pneumocystis

pneumonia in the dog. *J Comp Path*. 1972; 82(4): 447-453.
4. Maxie, MG. *Jubb, Kennedy & Palmer's Pathology of Domestic Animals*. Vol 2. Elsevier. 2015; 535-536.
5. Morris A, Sciurba FC, Norris KA. Pneumocystis: a novel pathogen in chronic obstructive pulmonary disease? *COPD*. 2008;(1)5: 43-51.
6. Ralph E, Reppas G, Halliday C, Krockenberge M, Malik R. Pneumocystis canis pneumonia in dogs. *Microbiology Australia*. 2015; 36:79-82.
7. Sakashita T, Kaneko Y, Izzati U z, et al. Disseminated Pneumocystosis in a Toy Poodle. *J Comp Pathol.* 2020; 175: 85-89.
8. Thomas C, Limper A. Current insights into the biology and pathogenesis of Pneumocystis pneumonia. *Nat Rev Microbiol*. 2007;5: 298–308.
9. Watson PJ, Wotton P, Eastwood J, Swift ST, Jones B, Day MJ. Immunoglobulin deficiency in Cavalier King Charles spaniels with Pneumocystis pneumonia. *J Vet Intern Med*. 2006; 20(3): 523-527.
10. Weissenbacher-Lang C, Fuchs-Baumgartiner A, Guija-De-Arespocachaga, Klang A, Weissenbock H, Kunzel F. Pneumocystosis in dogs: meta-analysis of 43 published cases including clinical signs, diagnostic procedures, and treatment. *J Vet Diagn Invest*. 2018; 30(1): 26-35.

WSC 2022-2023 Self-assessment
Conference 19

1. True or false. "Collision tumor" and "tumor to tumor metastasis" are synonymous.
    a. True
    b. False

2. Dwarf rabbits infected with encephalitozoon will manifest disease in all but WHICH of the following?
    a. Eye
    b. Brain
    c. Kidney
    d. Lung

3. True or false? Most rabbits infected with *Encephalitozoon cuniculi* have subclinical disease.
    a. True
    b. False

4. Which is the most common site for ocular melanoma in cats?
    a. Choroid
    b. Ciliary body
    c. Iris
    d. Cornea

5. *Pneumocystis sp.* are currently considered to be which of the following?
    a. Fungus
    b. Microsporidian
    c. Bacteria
    d. Alga

Please email your completed assessment for grading to Dr. Bruce Williams at bruce.h.williams12.civ@mail.mil. Passing score is 80%. This program (RACE program 33611) is approved by the AAVSB RACE to offer a total of 0.5 CE Credits, with a maximum of 12.5 CE Credits being available to any individual Veterinary Medical Professionals for the 2019-2020 Wednesday Slide Conference. This RACE approval is for the subject matter categories of: SCIENTIFIC using the delivery method of NONINTERACTIVE DISTANCE. This approval is valid in jurisdictions which recognize AAVSB RACE.

Joint Pathology Center
Veterinary Pathology Services

WEDNESDAY SLIDE CONFERENCE 2022-2023

Conference #20 **15 February 2023**

CASE I:

Signalment:
14-week-old, male, Saanen kid

History:
One of five kids from a herd of 60 goats that developed progressive onset hindlimb ataxia and sternal recumbency terminally.

Gross Pathology:
No specific findings. CNS appeared normal.

Laboratory Results:
Liver copper 0.01 mmol/kq, (normal range 0.06 – 2.5 mmol/kg – values for sheep)
Liver molybdenum 9.54 µmol/kq,(normal range 15.6 – 62.0 µmol/kg – values for sheep)

Microscopic Description:
Cerebellum: multifocally, Purkinje cells are lost, and a small number are shrunken/angulated with cytoplasmic eosinophilia and karyopyknosis. Ectopic Purkinje cells noted within an irregularly thinned granular layer. Concurrent prominence of reactive Bergmann glial cells. Occasional light perivascular cuffs of admixed lymphocytes and plasmacytes noted in cerebrum. No significant changes noted elsewhere in brain or in spinal cord.

Contributor's Morphologic Diagnoses:
Cerebellum: degeneration and dysplasia (particularly affecting Purkinje cells), multifocal, moderate

Contributor's Comment:
A diagnosis of delayed enzootic ataxia (swayback) in this goat kid was based on: signalment, clinical signs, the microscopically visible cerebellar lesions and low liver copper concentrations. This neurological disease of sheep and goats is generally accepted to result from a primary deficiency in the intake of copper or a secondary deficiency caused the reduced absorption/availability of copper during pregnancy.[3] In the secondary form dietary molybdenum, zinc, iron and cadmium can interfere with copper absorption.[1,6] Molybdenum is an important antagonist for copper as (in combination with sulfate), it forms thiomolybdates in the rumen which can complex with copper, limiting its absorption.[3] All three affected kids had liver copper concentrations below the normal range. There was no history of swayback in this goat herd and the dams' diet consisted of grass, hay and sheep concentrate (unknown quantity). The

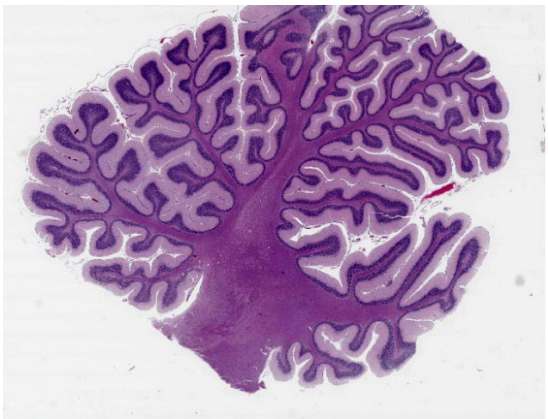

Figure 1-1. Cerebellum, goat kid. A section of cerebellum is submitted for examination. The granular cell layer is diffusely and mildly thinned. (HE, 7X)

goats had access to mineral licks/blocks and were being housed at night.

Clinically, two forms of enzootic ataxia in goat kids and lambs are described: a congenital form, more commonly reported in lambs develops in utero and manifests in the first few days of life; and a delayed form in both lambs and kids up to six months of age.[1,2] Affected animals develop progressive neurologic signs such as ataxia (swaying), hindlimb paralysis, and blindness. Lesions are found in the cerebrum, brainstem, and spinal cord in the congenital form, but are limited to the brainstem and cord in the delayed form. Cerebral lesions may be found in approximately 50% of congenitally infected lambs but rarely in kids: these consist of bilaterally symmetrical cavities in the white matter.[3,6] Microscopically visible lesions in both white and gray matter regions of the brainstem and spinal cord in both congenital and delayed forms are similar in both goats and sheep. Neurons in the medullary reticular, red, and lateral vestibular nuclei in the brainstem and in the lateral and ventral spinal cord exhibit degenerative changes: chromatolysis, cytoplasmic eosinophilia and pyknosis/margination of nuclei. Wallerian-type axonal degeneration is observed in dorsolateral and ventromedial spinal cord funiculi.[3,6] Ultrastructural observations in the goat and the particular involvement of neurons having long processes within the CNS or extending into peripheral nerves, suggest that the neuraxon rather than its myelin sheath is targeted in delayed enzootic ataxia.[14] While myelin degradation in this eventuality would then be expected as a secondary event, myelin in this context is qualitatively abnormal and therefore potentially unstable.[3] Accompanying astrogliosis is mild.[3,6] Cerebellar cortical lesions, particularly targeting Purkinje cells as described here are reported more commonly in goats than in sheep.[2,14]

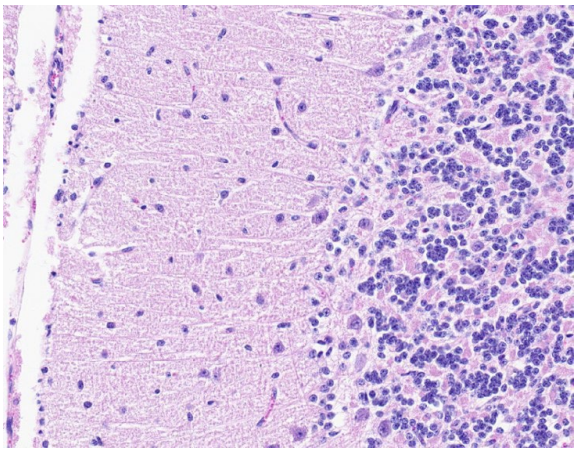

Figure 1-2. Cerebellum, goat kid. There is segmental loss of Purkinje cells and proliferation of Bergmann's glial cells within the molecular layer (HE, 400X)

Copper is required for the activity of several enzymes essential for neural function, including cytochrome oxidase (mitochondrial respiration) and copper-zinc superoxide dismutase (antioxidant activity). Suggested mechanisms contributing to the development of these lesions include altered function of cytochrome oxidase in mitochondria leading to suppression of mitochondrial respiration and reduced phospholipid synthesis. This energy failure is likely to result in axonal/neuronal degeneration. The generation of excessive reactive oxygen species as a consequence of inadequate function of superoxide dismutase ultimately results in oxidative injury within the CNS.[3,6]

Copper deficiency is more commonly encountered in grazing animals because of the poor availability of this element in grass. Foodstuffs from which copper is more readily absorbed are those low in fiber such as cereals. Preservation of grass in the form of hay or silage improves copper availability.[2] The fact that goats have a lower capacity to store copper in the liver than do sheep[10,14] would suggest this species requires a higher daily intake. In previous instances of enzootic ataxia in goats, sheep concentrate, low in copper, had been used as supplementary food. No

further cases occurred following the replacement of sheep concentrate by concentrate appropriate for cattle and horses.[14]

Differential diagnoses in this case would include white muscle disease, spinal trauma/vertebral body abscess, caprine arthritis encephalitis, meningoencephalitis, and possible toxicity (lead, organophosphate). Enzootic ataxia may be prevented through adequate copper supplementation of the dam during the latter half of pregnancy.[2]

Contributing Institution:
Room 012, Veterinary Sciences Centre,
School of Veterinary Medicine, University College Dublin, Belfield, Dublin 4, Ireland
http://www.ucd.ie/vetmed/

JPC Diagnosis:
Cerebellum: Purkinje and granular cell loss, segmental, moderate.

JPC Comment:
The contributor provides a good overview of the gross lesions, histologic findings, and pathogenic features of this classic entity in small ruminants. Another example of copper deficiency in a young goat was seen in WSC 2021 Conference 2 Case 1. Readers are encouraged to review that case which also demonstrated neuroaxonal degeneration in the spinal cord secondary to copper deficiency. Copper deficiency has also been implicated as a cause of laryngeal neuropathy in adult goats. In a 2017 *Veterinary Pathology* study, researchers described goats with severe copper deficiency that had both ataxia and stridor, while moderately affected goats had ataxia without stridor.[12] The severely affected goats demonstrated atrophy of laryngeal muscles appreciable both grossly and histologically, with Wallerian degeneration of the recurrent laryngeal nerve.[12] Interestingly, both sets of goats also had increased serum iron levels, with the more severely affected goats having higher levels, indicating that high dietary iron may have led to copper deficiency.[12]

As the contributor describes, copper is an essential cofactor in the activity of many enzymes in the body. Copper is an essential component of tyrosinase, which is involved in the rate-limiting step in melanin synthesis, and deficiency results in depigmentation of the hair or wool, causing a rusty brown discoloration and the formation of spectacles in the fur around the eyes (periocular achromotrichia).[5,13] Copper is also important for oxidation of sulfhydryl groups during keratinization, and deficiency causes hair shafts in sheep to be straighter with less

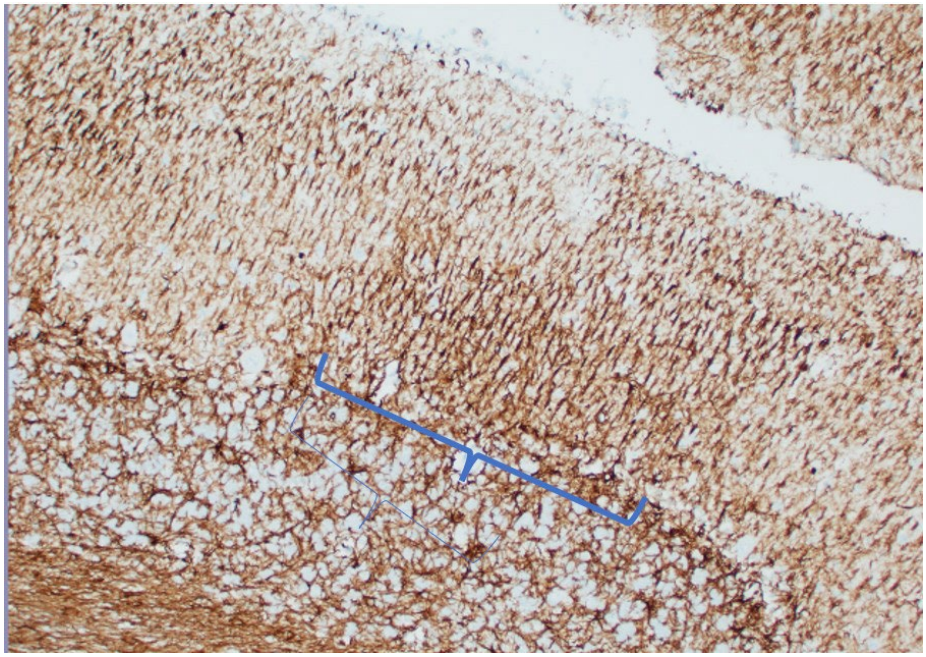

Figure 1-3. Cerebellum, goat kid. A GFAP stain demonstrates the proliferation of Bergmann's astocytic fibers in areas of Purkinje cell loss (bracket). (GFAP, 200X)

crimp ("string" or "steely" wool).[5,13] Alterations in coat color and texture due to copper deficiency have been reported in dogs, cattle, sheep, and moose.[5]

Copper is also a component of lysyl oxidase and is required for the proper crosslinking of collagen and elastin.[4] Copper deficiency can lead to fragile bones and cartilage in dogs, lambs, foals, calves, and pigs.[4] In dogs, copper deficiency is associated with decreased osteoblast activity and can produce metaphyseal lesions similar to the scorbutic lattice of vitamin C deficiency.[4] In foals, copper deficiency may cause the articular epiphyseal cartilage complex to lyse which may resemble osteochondrosis.[9]

Prolonged copper deficiency has been associated with sudden death and myocardial scarring in cattle in Australia and Florida ("falling disease").[11] In a recent study on the effect of prolonged copper deficiency on cardiac function, researchers found histologically apparent fibrosis in the ventricular myocardium, severe decrease in copper-zinc superoxide dismutase activity, and significantly increased levels of lipid peroxidation byproducts.[8]

This week's moderator, LTC Keith Koistinen, Chief of Diagnostic Pathology at the Joint Pathology Center, described the function of Bergmann glial cells (specialized radial glia astrocytes) which are prominent in this case: to provide scaffolding for the migration of Purkinje cells. Bergmann glial cells are difficult to distinguish solely on H&E. In this case, the molecular layer looks slightly denser in the areas of Purkinje cell loss, suggesting proliferation of Bergmann glial cells; however, definitive identification of Bergmann glial cells requires GFAP immunohistochemistry. The moderator and participants also remarked on the fact that Purkinje cells were present in the granular layer, reflective of defective migration referenced in the contributor's morphologic diagnosis of Purkinje cell dysplasia. The moderator also described that the best tissue for submission for copper analysis is brains for neonates and liver for adults.

References:

1. Allen AL, Goupil BA, Valentine BA. A retrospective study of spinal cord lesions in goats submitted to 3 veterinary diagnostic laboratories. *Can Vet J.* 2012;53:639–642.
2. Banton MI, Lozano-Alarcon F, Nicholson SS, Jowett PLH, Fletcher J, Olcottet BM. Enzootic ataxia in Louisiana goat kids. *J Vet Diagn Invest.* 1990;2:70–73.
3. Cantile C, Youssef S. Nervous system. In: Maxie MG, ed. *Jubb, Kennedy and Palmer's Pathology of Domestic Animals*. 6th Vol. 1. St. Louis, MO:Elsevier Ltd; 2016:328–329.
4. Craig LE, Dittmer KE, Thompson KG. In: Maxie MG, ed. *Jubb, Kennedy and Palmer's Pathology of Domestic Animals*. 6th Vol. 1. St. Louis, MO:Elsevier Ltd; 2016:66.
5. Mauldin EA, Peters-Kennedy J. Integumentary System. In: Maxie MG, ed. *Jubb, Kennedy and Palmer's Pathology of Domestic Animals*. 6th Vol. 1. St. Louis, MO:Elsevier Ltd; 2016:558.
6. Miller AD, Zachary JF. Copper deficiency. In: Zachary JF, ed. *Pathologic Basis of Veterinary Disease*. 6th ed. St. Louis, MO: Elsevier Ltd; 2017:887–888.
7. Miller AD, Porter BF. Nervous system. In: Zachary JF, ed. *Pathologic Basis of Veterinary Disease*. 7th ed. St. Louis, MO: Elsevier; 2022:973-974.
8. Olivares RWI, Postma GC, Schapira A, et al. Biochemical and Morphological Alterations in Hearts of Copper-Deficient Bovines. *Biol Trace Elem Res.*2019; 189(2):447-455.

9. Olson EJ, Dykxtra JA, Armstrong AR, Carlson CS. Bones, Joints, Tendons, and Ligaments. In: Zachary JF, ed. *Pathologic Basis of Veterinary Disease*. 7th ed. St. Louis, MO: Elsevier; 2022:1060.
10. Papachristodoulou C, Stamoulis K, Tsakos P, Vougidou C, Vozikis V, Papadopoulou C, Ioannides, K. Liver concentrations of copper, zinc, iron and molybdenum in sheep and goats from northern Greece, determined by energy-dispersive x-ray fluorescence spectrometry. *Bull Environ Contam Toxicol* 2015;94:460–467.
11. Robinson WF, Robinson NA. Cardiovascular System. In: Maxie MG, ed. *Jubb, Kennedy and Palmer's Pathology of Domestic Animals*. 6th Vol. 1. St. Louis, MO:Elsevier Ltd; 2016:34.
12. Sousa RFA, Almeida VM, Neto JE, et al. Laryngeal Neuropathy in Adult Goats with Copper Deficiency. *Vet Pathol.* 2017; 54(4): 676-682.
13. Welle MM, Linder KE. The Integument. In: Zachary JF, ed. *Pathologic Basis of Veterinary Disease*. 7th ed. St. Louis, MO: Elsevier; 2022:1201.
14. Wouda W, Borst GHA, Gruys E. Delayed swayback in goat kids, a study of 23 cases, *Vet Q.* 1986; 8 (1):45-56.

CASE II:

Signalment:
6-month-old, Hereford steer (*Bos taurus*)

History:
A 6-month-old Hereford steer presented to the Texas A&M Large Animal Food Animal Medicine and Surgery with a history of acute onset of being unable to rise. At presentation, the steer was recumbent and experiencing seizures. On neurological examination, he was ataxic, head-pressing and appeared blind. His condition was unresponsive to medical intervention, and the decision was made to humanely euthanize and perform a necropsy.

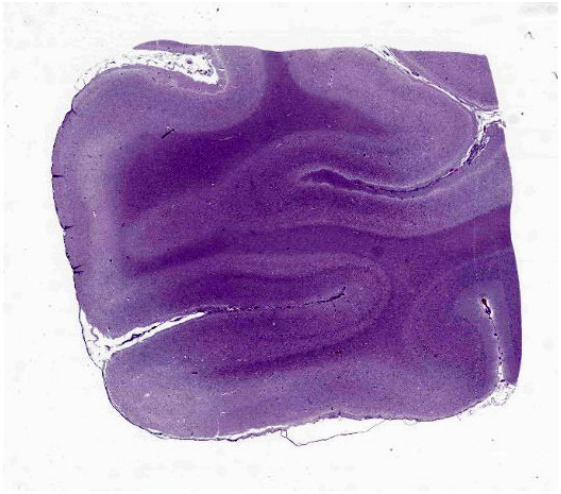

Figure 2-1. Cerebrum, ox. A section of cerebrum is submitted for examination. There are segmental areas of pallor beneath the meninges. (HE 6X)

Gross Pathology:
Flared metaphyses of the ribs with retained calcified cartilage and mild cerebral edema.

Laboratory Results:
Blood lead level= 0.71 ppm (lab normal=0-0.3 ppm); Post-mortem analysis of renal tissue (after formalin fixation) = 6.2 ppm (>3 ppm indicative of toxicity). Radiographs of ribs revealed a flared physis and a radiodense band at the metaphysis.

Microscopic Description:
Cerebrum. The deep cerebrocortical interface has a laminar zone of rarefaction (edema), and many neurons are diffusely hypereosinophilic, shrunken/polygonal with pyknotic nuclei (neuronal necrosis) or are lost. Endothelial cells are swollen. Reactive astrocytes are numerous (gliosis). Occasional vessels have a few surrounding neutrophils. Rarely, the nuclei of neurons have 2-4 µm, round, eosinophilic (lead) inclusions.

Contributor's Morphologic Diagnoses:
Severe, diffuse, laminar cortical neuronal necrosis with gliosis, edema and rare intraneuronal intranuclear eosinophilic inclusions (lead inclusions).

Contributor's Comment:
The clinical signs related to lead poisoning are predominantly neurologic and include depression, inappetence, staggers, muscle tremors, bruxism, head pressing, convulsions, blindness, and death.[1,14] Acute poisoning in cattle often results in death within 12-24 hours.[1] Gross lesions are not striking in cases of lead poisoning but may include brain swelling, hemorrhage, or meningeal and cerebrovascular congestion.[14] Microscopic lesions in acute cases may be confused with early autolysis.[1] In subacute cases, microscopic lesions of laminar cortical necrosis of the cerebrocortical gyri, astrocytosis, perivascular edema or hemorrhage.[14] Other differentials for bovine laminar cerebrocortical neuronal necrosis include, thiamine deficiency and consuming diets or water containing high sulphate (both causing ruminant polioencephalomalacia), or as a residual lesion of cyanide poisoning.[1] This case is remarkable for the number of mitotic figures along with the significant neuronal necrosis. The mitotic population is presumably glial cells responding to the neuronal necrosis, but the population is negative with GFAP.

While multiple species may be affected with lead intoxication, cattle are 10 times more likely to be affected than dogs, cats, or horses.[10] The disease is often acute in cattle and chronic in horses.[1] Sheep are less commonly affected and swine are rarely affected.[1] A retrospective, case-controlled study of cattle at North American veterinary school hospitals revealed a seasonality to lead intoxication cases with the most being reported in the late spring and summer months and an association between age and likelihood of exposure to lead with cattle less than four years of age at an increased risk.[8] The highest risk age group are cattle between 2 and 6 months of age.[8] Calves have higher exposure than adults, which is often from licking painted troughs, walls, etc. while confined. Adult cattle on pasture are often exposed through accidental ingestion of discarded car batteries, old lead paint on farm

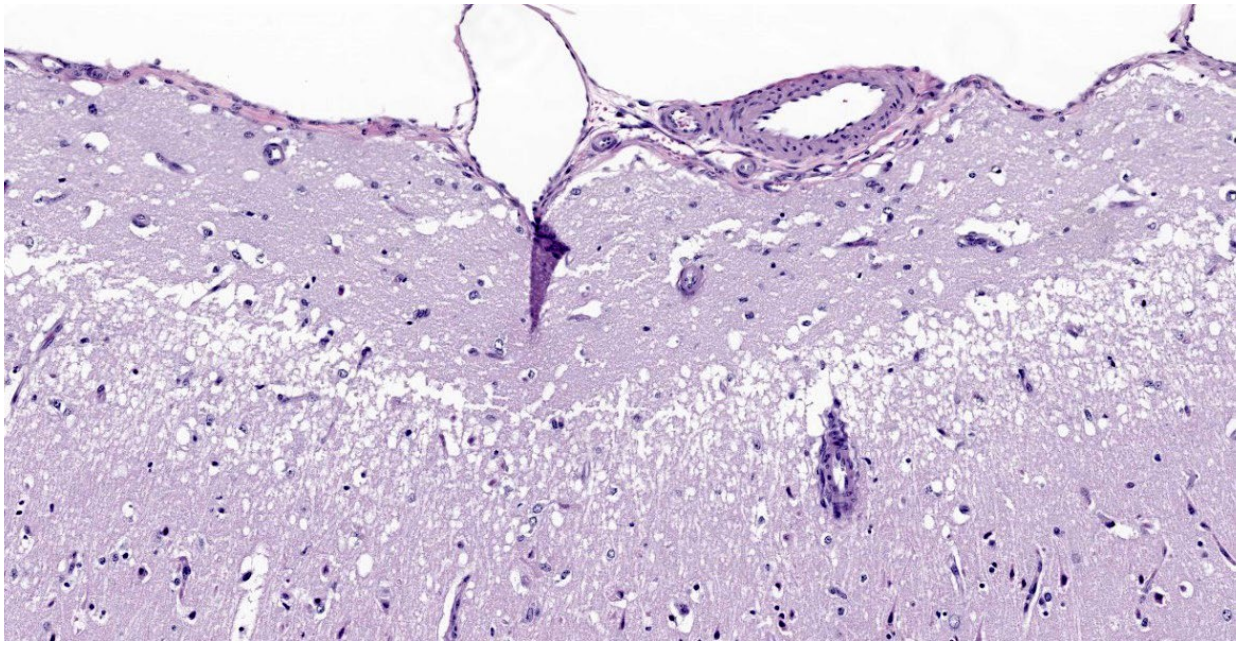

Figure 2-2. Cerebrum, ox. Higher magnification of a laminar area of rarified submeningeal grey matter. (HE 150X)

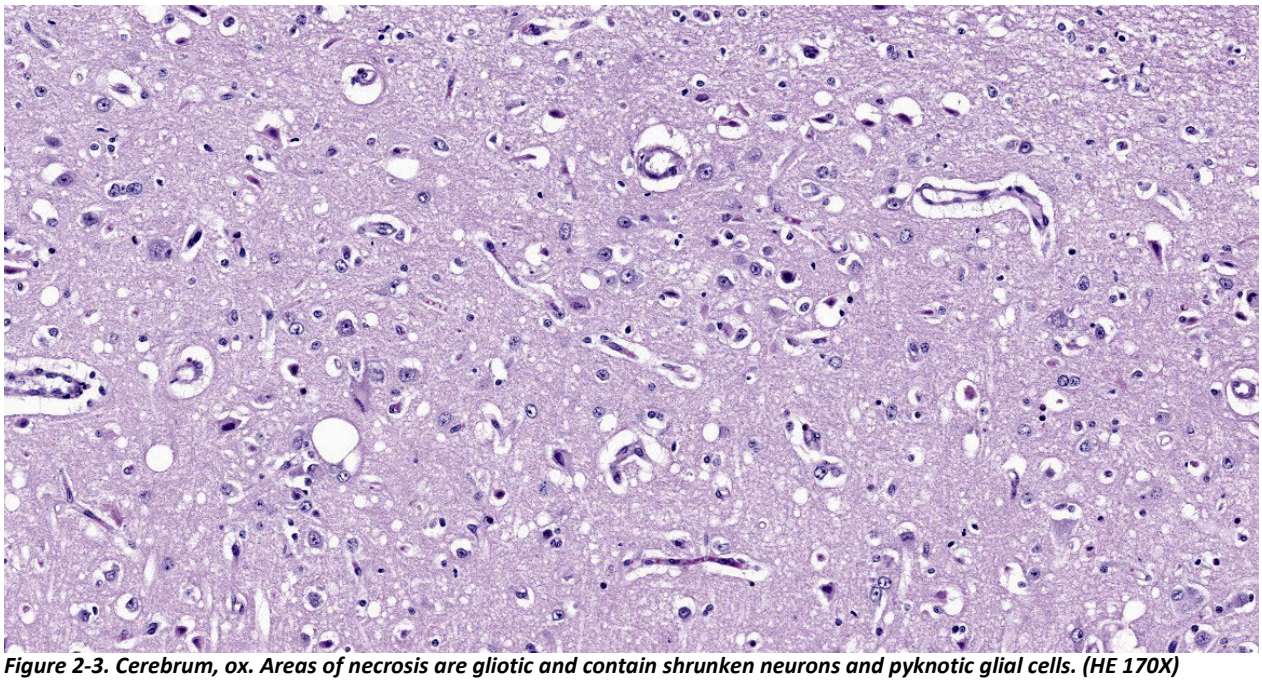

Figure 2-3. Cerebrum, ox. Areas of necrosis are gliotic and contain shrunken neurons and pyknotic glial cells. (HE 170X)

buildings or fences, or old asphalt shingles.[4,14] Experimental models of lead intoxication do not reach the levels of naturally acquired lead intoxication, which may be due to the formation of lead salts that increases ingestion of lead contaminated objects.[1] Other sources of environmental contamination include land near highways with historical lead accumulation in the soil from leaded gasoline exhaust, land near clay pigeon shooting ranges, industrial pollution, accumulation in plants, or fertilizers and pesticides.[5,9,12]

In lead intoxication the laminar necrosis does not autofluoresce under UV-light, suggesting a different pathogenesis from thiamine-related necrosis. The mechanism of action in lead intoxication is not well defined. The two theories of lead toxicosis are ionic mechanism and an oxidative stress mechanism. [2] The ionic mechanism proposes that lead metal ions cross the blood brain barrier using cationic transporters and replace other bivalent ions like Ca^{2+}, Mg^{2+} or Fe^{2+}.[5,14] The direct neuronal toxicity is presumed to be due to altered function of the dopaminergic, cholinergic and glutamatergic neurotransmitter systems.[14] Lead accumulates within neurons and astrocytes by utilizing a calcium transporter channel and disrupts calcium homeostasis, which leads to calcium release from the mitochondria with a subsequent increase in apoptosis. The oxidative stress mechanism proposes that lead toxicosis causes the levels of reactive oxygen species to increase while concurrently decreasing the antioxidant levels of proteins such as glutathione.[5]

Contributing Institution:

Dr. John Edwards and Dr. Martha Hensel
(jedwards@cvm.tamu.edu; mhensel@cvm.tamu.edu)
Department of Veterinary Pathobiology
College of Veterinary Medicine and Biomedical Sciences
Texas A&M University
College Station, TX 77843-4467
http://vetmed.tamu.edu/vtpb

JPC Diagnosis:

Cerebrum: Neuronal necrosis and loss, cortical, laminar, multifocal, with gliosis and edema.

JPC Comment:
This entity was last seen in Wednesday Slide Conference during Conference 10, Case 2 of 2021-2022. That case demonstrated lead toxicosis in the kidney of an African penguin, and readers are encouraged to review that case which details the features of disease in avian species and a brief review of the history of lead toxicity. During that conference, a recent *Vet Pathol* article was discussed which described lead intoxication in bald eagles; in this species, lead toxicosis leads to fibrinoid necrosis in arterioles of the heart, brain, and eyes leading to petechia, hemorrhagic necrosis, and ischemia in these organs.[7]

In the gross findings of this bovine case, the contributor describes flared metaphyses of the ribs and retained calcified cartilage, reflecting the effect of lead toxicity on bone. Lead inhibits the function of osteoclasts, which in growing animals normally resorb mineralized cartilage and woven bone of the primary spongiosa, making way for lamellar bone of the secondary spongiosa during endochondral ossification. [3] In lead toxicosis, osteoclasts fail to resorb bone and, histologically, osteoclasts are detached from the surface of trabeculae and may contain characteristic acid-fast eosinophilic occlusions.[2] Grossly, there is a band of sclerosis and flaring of the metaphysis due to retained mineralized cartilage, and radiographically, this produces a characteristic lead line.[2]

Lead toxicosis can affect other systems as well. During erythropoiesis, lead inhibits heme synthesis and causes a nonregenerative, hypochromic, microcytic anemia with circulating sideroblasts. Lead also causes retention of RNA, leading to basophilic stippling.[11] Lead quickly accumulates in the kidney and concentrates in the tubular epithelium nucleus, where inclusions are readily apparent (the moderator noted that eosinophilic intranuclear inclusions can be normal findings in healthy dogs). Lead inhibits mitochondrial respiration and in acute toxicosis can cause apoptosis of proximal tubular epithelium.[6] In rabbits, lead toxicosis causes outer retinal degeneration secondary to lipofuscin buildup, and in rats, it causes necrosis of the photoreceptor cells and inner nuclear layer of the retina.[13]

Conference participants and the moderator debated on the presence of eosinophilic intranuclear inclusions and could not reach a consensus on whether they were present. Acid-fast staining by JPC did not confirm the presence in this case.

References:

1. Cantile C, Youssef S. Nervous system. In: Maxie MG, ed. *Jubb, Kennedy & Palmer's Pathology of Domestic Animals*. 6th ed. Philadelphia, PA: Elsevier; 2016; 250-406.
2. Craig LE, Dittmer KE, Thompson KG. Bones and Joints. In: Maxie MG, ed. *Jubb, Kennedy, and Palmer's Pathology of Domestic Animals*. Vol 1. 6th ed. St. Louis, MO: Elsevier. 2016; 23, 86.
3. Gunson D, Groppe KE, Varela A. Bones and Jones. In: Wallig MA, Haschek WM, Rosseaux CG, Bolon Brad, eds. *Fundamentals of Toxicologic Pathology.*3rd ed. 2018; 773.
4. Hoff B, Boermans HJ, Baird JD. Retrospective study of toxic metal analyses requested at a veterinary diagnostic toxicology laboratory in Ontario (1990-1995). *Can Vet J.* 1998; 39(1)**:**39-43.
5. Jaishankar M, Tseten T, Anbalagan N, Mathew BB, Beeregowda KN. Toxicity, mechanism and health effects of some heavy metals. *Interdiscip Toxicol.* 2014;7(2)**:**60-72.
6. Khan KNM, Hard GC, Li X, Alden CL. Urinary System. In: Wallig MA, Haschek WM, Rosseaux CG, Bolon Brad, eds.

*Fundamentals of Toxicologic Pathology.*3rd ed. 2018; 250.
7. Manning LK, Wünschmann A, Armién AG, et al. Lead Intoxication in Free-Ranging Bald Eagles (*Haliaeetus leucocephalus*). *Vet Pathol*. 2019;56(2):289-299.
8. Mavangira V, Evans TJ, Villamil JA, Hahn AW, Chigerwe M, Tyler JW. Relationships between demographic variables and lead toxicosis in cattle evaluated at North American veterinary teaching hospitals. *J Am Vet Med Assoc.* 2008; 233(6)**:**955-959.
9. Payne JH, Holmes JP, Hogg RA, van der Burgt GM, Jewell NJ, Welchman Dde B. Lead intoxication incidents associated with shot from clay pigeon shooting. *Vet Rec.* 2013;173(22)**:**552.
10. Priester WA, Hayes, HM. Lead poisoning in cattle, horses, cats and dogs as reported by colleges of veterinary medicine in the United States and Canada from July, 1968, through June, 1972. *Am J Vet Res.*1974:35**:**567-569.
11. Ramiah L, Bounous DI, Elmore SA. Hematopoietic System. In: Wallig MA, Haschek WM, Rosseaux CG, Bolon Brad, eds. *Fundamentals of Toxicologic Pathology.*3rd ed. 2018; 329-334.
12. Steuerwald AJ, Blaisdell FS, Geraghty CM, Parsons PJ. Regional distribution and accumulation of lead in caprine brain tissues following a long-term oral dosing regimen. *J Toxicol Environ Health A.* 201; 77(12)**:**663-678.
13. Teixeira L, Dubielzig RR. Special Senses - Eye. In: Wallig MA, Haschek WM, Rosseaux CG, Bolon Brad, eds. *Fundamentals of Toxicologic Pathology.*3rd ed. 2018;725.
14. Zachary JF. Nervous System *Pathologic Basis of Veterinary Disease*. 5th ed. St. Louis, MO: Elsevier. 2012: 771-870.

CASE III:

Signalment:
Male, Sprague-Dawley rat (*Rattus norvegicus)*

History:
This rat was administered a test article to induce seizures in order to evaluate the effectiveness of anticonvulsant therapeutics.

Laboratory Results:
No laboratory findings reported.

Microscopic Description:
Cerebrum at the level of the thalamus and hippocampus: Multifocally within the cerebral cortex, piriform cortex, amygdala, hippocampus, thalamus, caudate nucleus, and putamen, there is neuronal degeneration and necrosis characterized by shrunken, angular, hypereosinophilic cytoplasm of neuron cell bodies. There is rarefaction of the white matter immediately adjacent to affected neuron cell bodies.

Contributor's Morphologic Diagnoses:
Cerebrum at the level of the thalamus and hippocampus: Neuronal degeneration and necrosis, multifocal, severe, with rarefaction.

Contributor's Comment:
Due to low cost and ease of manufacturing of chemical warfare agents, there is an increased likelihood of use of chemical warfare agents by terrorists, as well as, by various governments. Relatively recent examples of chemical attacks include the use of chlorine gas by Al Qaeda in 2006 and 2007, the use of various chemicals by ISIS in 2015 and 2016, and the poisoning of a former Russian agent in 2018. One of the most notable examples of a chemical warfare agent being deployed is the use of the nerve agent sarin by members of the Aum Shinrikyo religious cult in Japan in 1995 that killed 12 and sickened 5,000 others.

In order to decrease the likelihood of future chemical warfare agent use there is a focus on strategies to research and mitigate the negative physiologic effects of various agents so that their deployment is useless as effective antidotes are readily available.

Mechanism of Action of Nerve Agents. The chemical warfare (CW) nerve agents include the anticholinesterase nerve agents tabun (GA), sarin (GB), soman (GD), cyclosarin (GF), and VX, all of which are, or have been, part of the US domestic munitions inventories.[8] These agents are potent anticholinesterase compounds deliberately formulated to induce debilitating effects or death during wartime hostilities and have been used by military authorities of several nations to develop munitions (e.g., Germany during the Nazi era, the USA, and the former Soviet Union).[8]

All of the listed nerve agents are anticholinesterase compounds and induce accumulation of the neurotransmitter acetylcholine (ACh) at neural synapses and neuromuscular junctions by of nerve agents can result in excessive bronchial, salivary, ocular and intestinal secretions, sweating, miosis, bronchospasm, intestinal hypermotility, bradycardia, muscle fasciculations, twitching, weakness, paralysis, loss of consciousness, convulsions, depression of the central respiratory drive, and death.[8]

Nerve Agent-Associated Injury to the Nervous System. Nerve agents exert their neuropathologic effects through binding and irreversible inactivation of acetylcholinesterase (AChE), the enzyme that hydrolyzes ACh, leading to a toxic accumulation of ACh at nicotinic (skeletal muscle and preganglionic autonomic) receptors, muscarinic (mainly postganglionic parasympathetic) receptors, and central nervous system synapses.[9]

Historically, this has been of concern in organophosphate and carbamate insecticide exposure among farm workers; however, it is likely that use of nerve agents in civilian populations or against military personnel would result in a range of exposures that stem from both the proximity of various groups to the site of deployment and the persistence of residues of some agents in the environment.[9]

Common nerve agents developed for chemical warfare purposes include the G-series (so names because they were first developed by German scientists in the mid-1930s) and V-series (a designation of more ambiguous origin) weapons.[9] As previously mentioned, the G-series includes tabun (GA), sarin (GB), soman (GD), and cyclosarin (GF), while the V-series includes VX, first synthesized by the British in 1954.[9] The G-series compounds are volatile liquids at room temperature, are soluble in both fat and water, and are absorbed readily through the eyes, respiratory tract, and skin.[9] V-series agents are viscous and toxic mainly via skin exposure, and therefore pose a lower inhalation hazard than the G-agents; however, they are notoriously persistent in the environment.[9]

Acute exposure to nerve agents is associated with a range of clinical symptoms, varying from abnormal movements and salivation to limb tremor and muscle fasciculations, to convulsions.[9] In a variety of animal and especially rodent models, animals that survived

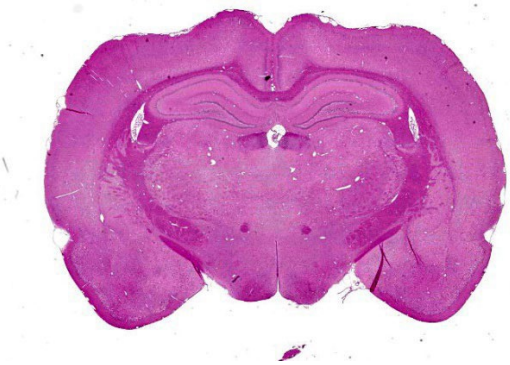

Figure 3-1. Diencephalon, rat. A transverse section of brain at the level of the diencephalon. (HE, 6X)

seizures tended to manifest extensive bilateral brain neuronal necrosis that affected predominantly the forebrain, thalamus, tegmentum, and spinal cord.[9] Acute injury may be attributable to several mechanisms.[9]

Ischemic hypoxia may derive from respiratory insufficiency during prolonged seizures, and evidence of cellular ischemia is present in brains of exposed animals.[9] This consists of shrinkage of the cell soma and proximal dendrites, cytoplasmic microvacuolation due to mitochondrial swelling, dispersion of Nissl substance (cytoplasmic RNA), increased cytoplasmic eosinophilia, nuclear changes including displacement of the nucleus to an eccentric position in the neuron, shrinkage, and darkening.[9] Generally, these nerve agent-associated lesions were described as indistinguishable from those associated with brain ischemia or anoxia.[9]

Within minutes after exposure to nerve agents, there is a marked decrease in AChE activity and associated rise in ACh.[9] The earliest seizure activity begins in the absence of other significant neurotransmitter alterations and is prevented by anticholinergic drugs.[9] These observations suggest that seizure-associated neuropathologic findings that occur upon nerve agent exposure are caused primarily by a mechanism of cholinergic toxicity.[9]

However, if seizures progress untreated, other neurotransmitter systems display secondary alterations, and the involvement of these has been invoked in models of injury to cerebrum that involve mechanism of "excitotoxic" injury.[9] Specifically, these refer to the involvement of the excitatory amino acid transmitter glutamate, which increases intracellular calcium mobilization.[9]

In excitotoxicity, overstimulation of glutamatergic synapses leads to marked neuronal calcium dyshomoeostasis that in turn leads to neuronal injury.[9] Importantly, pretreatment or early post-exposure treatment of experimental animals with anticonvulsants (e.g., benzodiazepines such as diazepam), blocks nerve agent-associated seizures which in turn prevents or diminishes neuropathologic effects.[9] This occurs in the absence of a direct effect on cholinergic processes.[9] These observations, taken together, suggest strongly that excitotoxic mechanisms contribute largely to the structural changes observed in the cerebrum upon nerve agent exposures.[9]

Abrogation of these mechanisms by anticholinergic drugs within 20-40 min of the onset of seizures is sufficient in most cases to significantly diminish neuropathologic lesions.[9] The failure of anticholinergic drugs to prevent nerve agent-associate pathologic changes after this time period has been attributed to the recruitment and dominance of non-cholinergic mechanisms of excitotoxicity and perhaps to secondary loss of the integrity of the blood-brain barrier.[9]

Technical Considerations for Toxicologic Neuropathology. Cost-effective, high-quality neuropathologic evaluations require teamwork involving the recording and assessment of detailed clinical signs and gross postmortem observations, careful and timely collection and processing of tissues, and a working knowledge of both neuroanatomy and neuropathology.[4] The process begins well before the necropsy.[4] It is important for the pathologist to have knowledge of the likely target effects (distribution, biochemistry, secondary changes) of the compound so that tissue collections and evaluations can be optimized.[4]

Evaluation of murine brain tissue requires considerable expertise in the preparation of

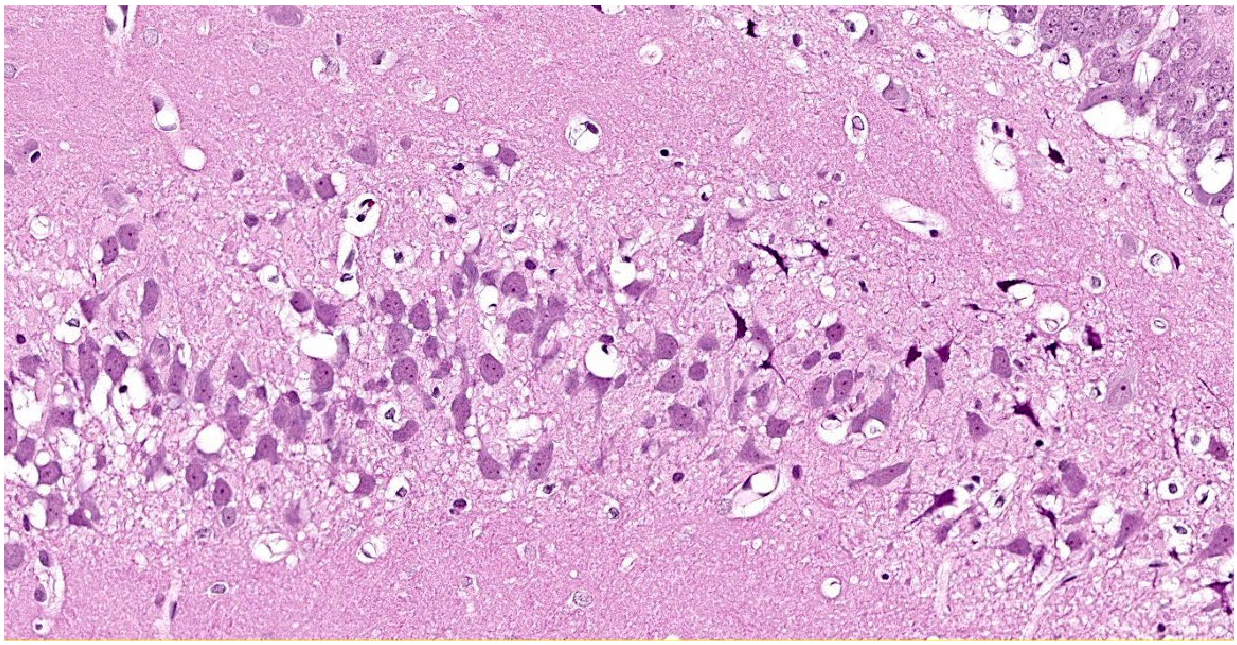

Figure 3-2. Diencephalon, rat. There are numerous degenerating and necrotic neurons within CA3 of the hippocampus. Astrocytes associated with degenerating neurons are markedly swollen by cytosolic edema (HE, 276X)

tissue samples prior to examination by a neuropathologist. The use of whole-animal perfusion techniques and specialized grossing implements (such as brain matrices) are practical and effective tools which can help ensure that virtually identical brain regions are collected and prepared from each animal within a large study.

As with many other organ systems, the most common way for nervous tissue to be fixed is by direct immersion in an aldehyde fixative solution.[3] However, whole body perfusion via the vascular system is preferred, particularly if any degree of special detail is necessary in the study.[3] Once mastered, perfusion yields reproducible, high-quality preparations of nervous tissue.[3] However, this approach requires technical dedication and practice before mastery.[3] The technique cannot simply be written and given to an inexperienced technical specialist for execution without proper instruction and training.[3] An excellent summary of the practical aspects of whole body perfusion is provided in the below referenced article by Fix and Garman.[3]

Investigators seeking to evaluate brain injuries will select a region of interest using a standard brain atlas which localizes the desired coronal section by its relationship to the sutures of the skull. By definition, the Bregma level refers to the junction of the coronal and sagittal sutures on the skull, and a coronal brain section at this level corresponds to a Bregma level of 0.0 mm.[4] Bregma coordinates represent the number of millimeters rostral (positive numbers) or caudal (negative numbers) to this plane.[4]

Rat brain atlases are developed using rats of a particular sex, strain, and weight class (e.g., adult, male, medium-sized [270 to 310 g], Wistar rats were used for Paxinos and Watson's *The Rat Brain in Stereotaxic Coordinates*, 5th edition).[6] For this reason, if rats of a different sex, strain, or weight class are used, stereotaxic accuracy will be affected.[6] In other words, if the rat brain is smaller than the medium-sized rat used for the reference atlas, the distance from the Bregma to the desired coronal section will need to be proportionately scaled down to acquire the region of interest.

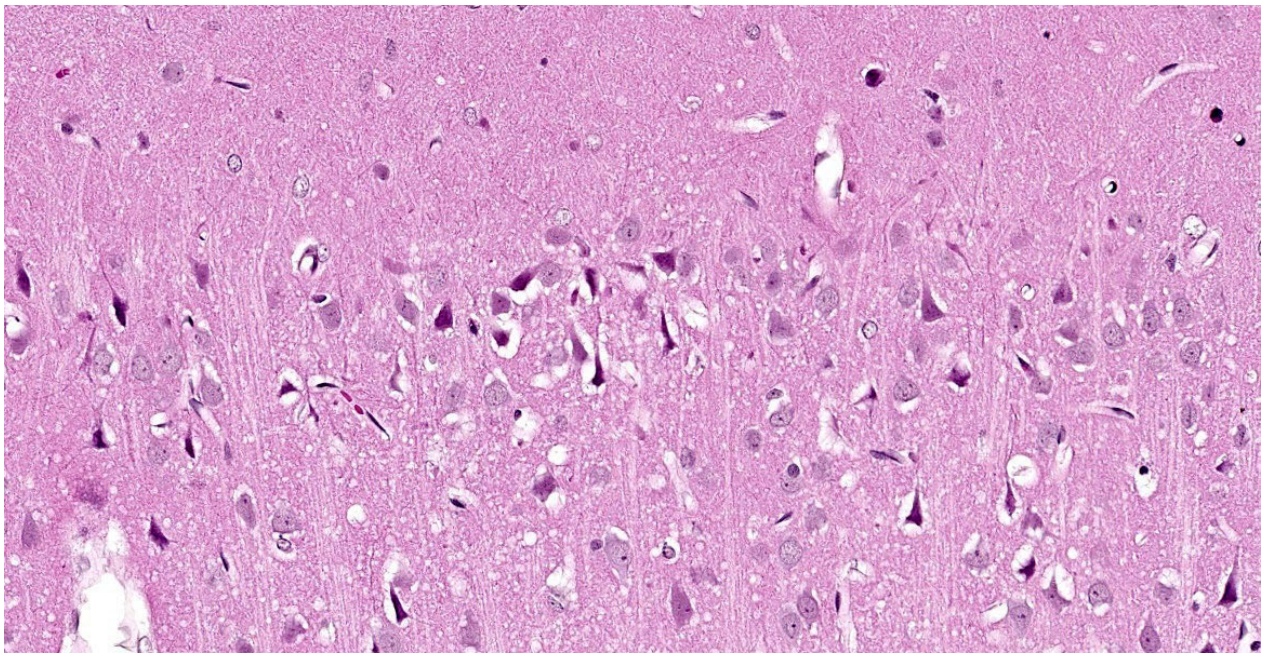

Figure 3-3. Diencephalon, rat. There are scattered degenerating and necrotic neurons within throughout the neocortex, but far fewer than in the hippocampus. (HE, 298X)

Even with a good brain atlas, the process of actually matching slides on the microscope with sites depicted in the atlas can be challenging.[4] Since histologic sections rarely match the exact plane of section depicted in an atlas, the pathologist must have a basic working knowledge of neuroanatomy and the ability to envision how the landmarks will be shifted when sections are tilted or skewed from the true coronal planes typically presented in the atlases.[4] A series of atlases coauthored by Paxinos and Watson provides good neuroanatomic references for rodents, and is available in both hard copy and in electronic format.[4]

Once the target tissue within the brain has been fixed, grossed, and embedded, the technical skill in the histology laboratory is perhaps the most important factor in arriving at a mounted section of the specific region of interest. The target tissue must be embedded with sufficient excess tissue to allow for block facing and sectioning through the block until the desired serial section is mounted on the glass slide.

The skill level of the histology technician cannot be overstated in murine brain research. First, the individual must have a detailed understanding of murine neuroanatomy. Second, he or she must possess the academic interest to study reference brain atlases and understand where the region of interest is located relative to other structures. Third, the technician must be able to recognize detailed brain structures in unstained paraffin-embedded tissue sections. Finally, the technician must be able to make adjustments if the animal's size or gender do not match the reference atlas. Microtomy is, by its nature, a destructive process since the technician must section through the block until the desired section is exposed. Because of this, the technician must know when to stop sectioning so that the region of interest is not inadvertently consumed.

For pathologists with an interest in toxicologic neuropathology, there is an excellent compilation of resources, designed to consolidate a broad range of useful neurobiology, neuropathology, and neurotoxicology resources in a single reference.[1]

Contributing Institution:
https://usamricd.apgea.army.mil/

JPC Diagnosis:
Cerebrum, hippocampus and thalamus: Neuronal degeneration and necrosis, multifocal and segmental, with rarefaction.

JPC Comment:
The moderator remarked on the remarkable preservation of this tissue achieved by perfusion and described the histologic evidence of perfusion: dilated (non-retracted) empty blood vessels and reduced dark neuron artifact.

This case illustrates the classic but nonspecific lesion of acute eosinophilic (acidophilic) neuronal degeneration and necrosis. In this case, neuronal necrosis is due to the effects of a nerve agent, which, as the contributor describes, works in a few ways: by causing direct neuronal acetylcholine toxicity by inhibiting acetylcholinesterase, by causing excitatory nerve injury, and by causing ischemia due to respiratory depression secondary to prolonged seizure activity. Acute eosinophilic neuronal necrosis can occur in other conditions as well, including ischemia or hypoxia, thiamine deficiency, heavy metal toxicosis (including lead and organic mercury), hypoglycemia, and inflammation.[5,7] Neurons are acutely sensitive to ischemic and hypoxic injury because they maintain minimal energy stores.[2] When deprived of oxygen due (i.e. ischemia or cardiac arrest), the most sensitive neurons in the cerebral cortex die within 10 minutes due to decreased ATP generation.[2] Neurons in the cerebral cortex, Purkinje cells, and the hippocampus are the most sensitive to ischemic injury; this phenomenon is referred to as selective neuronal vulnerability.[2,5] Other causes of decreased ATP generation leading to neuronal necrosis include cyanide, which interferes with mitochondrial cytochrome oxidase activity during cellular respiration, and carbon monoxide, which prevents oxygenation of peripheral tissues. [2,5] For the same reason, hypoglycemia (i.e. due to a functional insulinoma) also causes neuronal necrosis, and, in general, neurons display the same sensitivity to hypoglycemia as ischemia (with the exception of Purkinje cells, which are more resistant to hypoglycemic injury).[2]

References:

1. Bolon B, Bradley A, Garman RH, Krinke GJ. (2011). Useful toxicologic neuropathology references for pathologists and toxicologists. *Toxicol Pathol* 2011;39(1): 234-239.
2. Cantile C, Youssef S. Nervous system. In: Maxie MG ed. *Jubb, Kennedy, and Palmer's Pathology of Domestic Animals*. Vol 1. 6th ed. Philadelphia, PA: Elsevier Saunders; 2016:253-254.
3. Fix AS, Garman RH. Practical aspects of neuropathology: a technical guide for working with the nervous system. *Toxicol Pathol.* 2000;28(1):122-131.
4. Jordan WH, Young JK, Hyten MJ, Hall DG. Preparation and analysis of the central nervous system. *Toxicol Pathol.* 2011;39(1):58-65.
5. Miller AD, Porter BF. Nervous System. In: Zachary JF, McGavin MD, eds. *Pathologic Basis of Veterinary Disease*. 7th ed. St. Louis, MO: Elsevier Mosby; 2022: 904-905,934.
6. Paxinos G, Watson C. *The Rat Brain in Stereotaxic Coordinates, 5th ed*. San Diego, CA: Elsevier Academic Press; 2005.
7. Vandevelde M, Higgins RJ, Oevermann A. *Veterinary Neuropathology: Essentials of Theory and Practice.* 1st ed. Ames, IO: John Wiley & Sons, Ltd. 2012: 108-116.
8. Watson A, Opresko D, Young R, Hauschild V, King J, Bakshi K. Organophosphate Nerve Agents. In: Gupta RC,

ed. *Handbook of Toxicology of Chemical Warfare Agents.* London, UK: Academic Press; 2009:43-49.
9. Woltjer RL. Neuropathologic Effects of Chemical Warfare Agents. In: Gupta RC, ed. *Handbook of Toxicology of Chemical Warfare Agents.* London, UK: Academic Press; 2009:653-659.

CASE IV:

Signalment:
5-month-old, intact male, Labrador, C*anis familiaris,* canine

History:
This dog was presented to the emergency service of a veterinary clinic. Owners reported that he was alert in the morning and ate well. He suddenly became lethargic, and they rapidly brought him to the clinic. On arrival, his temperature was elevated (39,4 ºC), but returned to normal values within an hour. He was in a lethargic state that gradually worsened. Blood parameters revealed only slightly decreased hematocrit (32) and potassium (3.4) values. Blood pressure was normal. He received intravenous fluids and intralipids, but his general state rapidly deteriorated and he was in cardiopulmonary arrest a few hours after his arrival at the clinic. Cardiopulmonary resuscitation was performed unsuccessfully.

Gross Pathology:
The dog weighed 20 kg and was in good body condition. Lungs were diffusely edematous, and the pericardial sac contained a small amount (5-6 ml) of blood-tinged fluid. The heart weighed 174 g (within normal values) and showed no anomaly. Approximately 20 to 25 ml of uncoagulated blood was present in the abdominal cavity. No lesion explaining this blood was found in the abdominal organs. The stomach was full of undigested dry food, amongst which two small blue particles (size of blueberries) were noted. No diarrhea was present. Considering the rapid onset of clinical signs and the fact the dog was healthy and up to date on his vaccination schedule, an intoxication was suspected.

Laboratory Results:
Routine bacteriological culture of the lung, liver and kidney revealed only rare hemolytic *E.coli* and few contaminants. A PCR for canine herpesvirus was negative. Stomach content was sent for toxicological analysis and results showed a large amount of phenethylamine detected by GCMS.

Microscopic Description:
Histological changes are limited to the cerebrum; they are multifocal, present in all lobes, but most severe in the right frontal lobe. There is marked and extensive vasogenic edema involving mainly the white matter, variably extending into the adjacent cerebral cortex, associated with vascular fibrinoid degeneration/necrosis and mostly perivascular hemorrhages. The wall of affected blood vessels is effaced by fibrinoid material, sometimes with pycnotic nuclei, and eryhrocytes and/or fibrin are present in the Virchow-Robin spaces. In affected areas, there are numerous reactive astrocytes and microgliocytes and, multifocally a few to several neutrophils. There are numerous microgli-

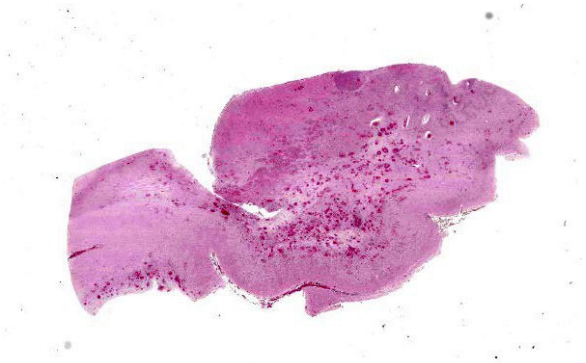

Figure 4-1. Cerebrum, dog. A section of cerebrum is submitted for examination. At subgross magnification, there are numerous areas of perivascular hemorrhage, predominantly within the white matter. (HE, 7X)

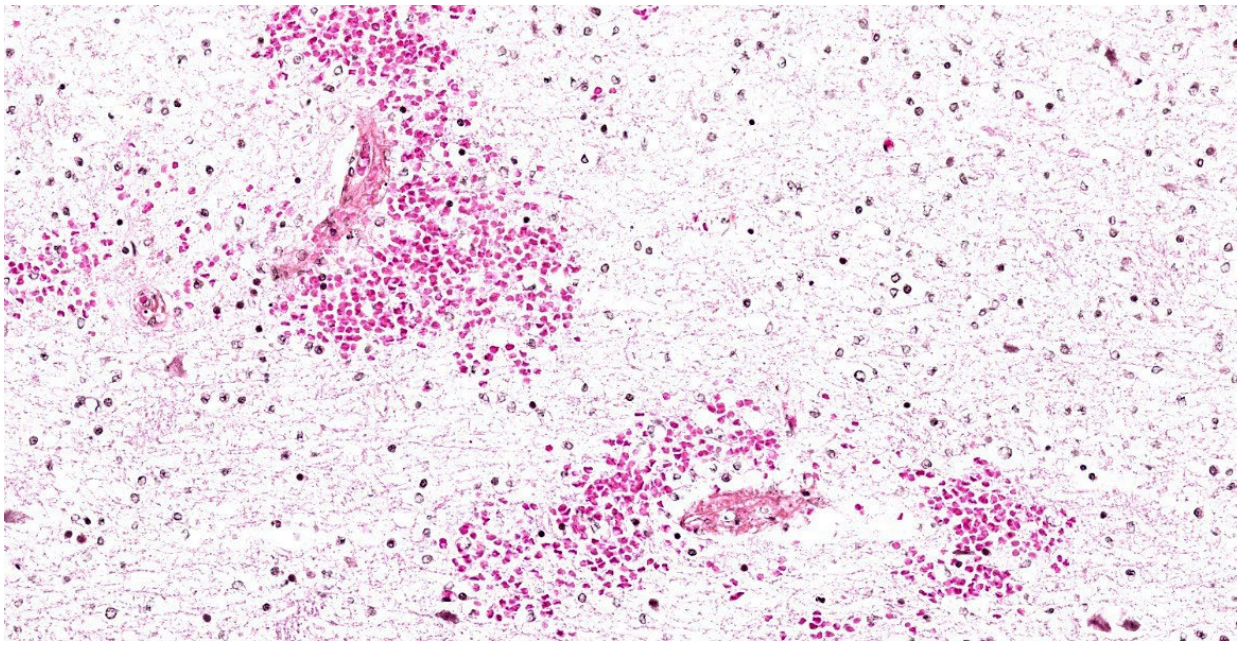

Figure 4-2. Cerebrum, dog. There is fibrinoid necrosis of vessel walls with perivascular hemorrhage. (HE, 248X)

ocytes/macrophages and occasional neutrophils in the perivascular (Virchow-Robin) and subarachnoidal spaces. Neuronal changes are interpreted as artefactual ("dark neurons").

Contributor's Morphologic Diagnoses:
Marked and extensive vasogenic cerebral edema associated with vascular fibrinoid degeneration/necrosis and perivascular hemorrhages (mainly white matter)

Contributor's Comment:
Phenethylamine is an organic compound, natural monoamine alkaloid, and trace amine, which acts as a central nervous system stimulant. It represents the core structure of numerous drugs with stimulant-like properties such as amphetamines and methamphetamines.[8] It is also the major component of stimulant drugs used to treat attention-deficit/hyperactivity disorder (AD/HD) by improving brain levels of serotonin and norepinephrine.[10] In the present case, the exact substance containing phenethylamine that was ingested by the dog could not be identified. The owners suspected that the dog had eaten an illegal substance, possibly from a neighbor's gathering that took place the night before. To the best of their knowledge, the dog did not have access to other possible sources of phenethylamine-containing substances.

Very few reports have documented intoxication of dogs by amphetamines or by drugs prescribed for the management of AD/HD.[2,4,9,11] The principal mechanisms of toxicity in amphetamine poisoning are the release of catecholamine with stimulation of the nervous system and a marked increase in the release of norepinephrine, dopamine, and serotonin. Clinical signs most commonly reported are cardiovascular signs such as hypertension and tachycardia and central nervous system signs such as hyperactivity, agitation, and tremors. Hyperthermia is also often present. Lethargy, depression, and coma have been reported in the latter course of intoxication. Peak plasma concentrations of amphetamine occur 1-3 hours after ingestion.[1] The median lethal dose (LD50) for orally administered amphetamine sulfate in dogs is 20 to 27 mg/kg.[1] Full recovery can be achieved when a rapid diagnosis is made together with an aggressive intervention. In the present

case, lethargy and depression were the principal clinical signs displayed. The very young age of the dog (4 months) and the presence of a large amount of phenethylamine as determined by GCMS analysis could have both contributed to the rapid deterioration of the animal leading to coma and death.

Histological lesions in the present case were present only in the brain and were centered around blood vessels (principally cerebral edema with a marked exudation of fibrin and perivascular hemorrhages). These changes are consistent with a significant increase in vascular permeability. In humans, it is generally assumed that death following a methamphetamine overdose results from heart attack or stroke. Central nervous system alterations are difficult to precisely determine in humans since polysubstance abuse is seen in the majority of cases.[3] Arterial or venous infarcts and subarachnoid or parenchymal hemorrhages have been reported as neuropathological complications.[5] A necrotizing vasculitis, predominantly of small blood vessels, but larger arteries and veins may be involved has also been observed in few cases.[5]

Recent studies using a rat model of acute methamphetamine intoxication showed the development of a temperature-dependent leakage of the blood-brain barrier and the development of vasogenic edema that could finally result in decompensation of vital functions and death. [6,7] More specifically, the authors found the leakage of albumin in the neuropil (reflecting alterations in vascular endothelium), an increased number of glial cells and the presence of several pyknotic neurons in rats that had received 9 mg/kg of methamphetamine.[6,7] These changes were temperature dependent, being more severe in rats that were maintained under warm (29°C) compared to standard (23° C) ambient temperature. Histological changes in the brain of dogs following an intoxication by amphetamines have not been reported. However, the histological lesions observed in the present case are consistent with a severe alteration of the blood-brain barrier following intoxication with a phenethylamine-containing substance.

Contributing Institution:
Département de pathologie et microbiologie
Faculté de médecine vétérinaire
Université de Montréal

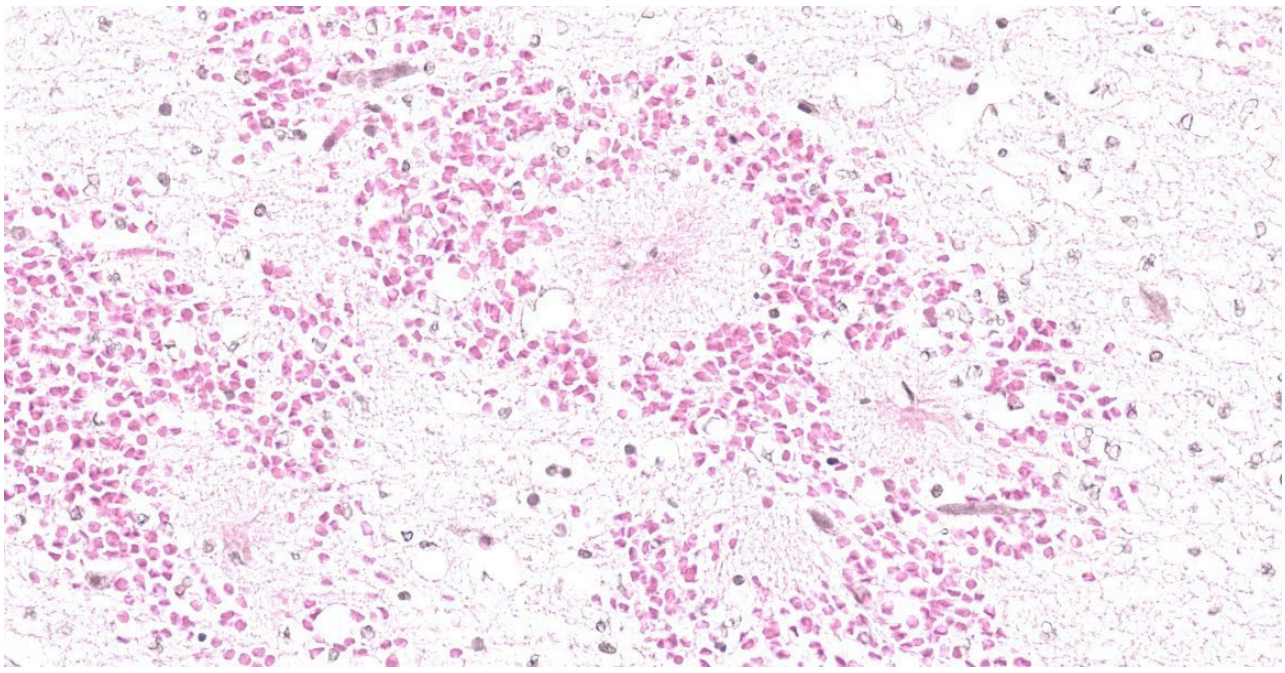

Figure 4-3. Cerebrum, dog. Effete vessels are replaced by polymerized fibrin and surrounded by ring hemorrhage. (HE, 351X)

www.umontreal.ca

JPC Diagnosis:
Cerebrum: Fibrinoid vascular degeneration and necrosis, acute, multifocal to coalescing, with, hemorrhage, edema, and gliosis.

JPC Comment:
Prior to reviewing the clinical history and gross necropsy findings of this case, the moderator and participants discussed possible differentials for fibrinoid vascular degeneration in the cerebrum of a dog, including infectious agents (i.e., endotoxemia, *Rickettsia rickettsia,* and *Ehrlichia canis*), accidental ingestion of illicit substances, and hypertension.

In a nine year retrospective study evaluating 241,261 cases of suspected poisoning events reported to the ASPCA's Animal Poison Control Center in the United States, exposure to human medications accounted for 40% and 32% of canine and feline cases, respectively, and recreational or elicit medications accounted for 1.83% and 0.44% of exposures, respectively.[12] Exposure to prescribed amphetamines and illicit methamphetamine comprised a small portion of these toxicities, accounting for 1.16% and 1.44% of total canine and feline exposures.[12] Human pharmaceuticals more commonly referenced as a source of exposure included analgesics and medications treating CNS, gastrointestinal, and cardiovascular disorders.[12] These results indicate that amphetamine toxicity is an uncommon toxicosis in dogs and cats, but one that clinicians and pathologists should be cognisant of.[12]

Amphetamines are lipid-soluble drugs rapidly absorbed in the gastrointestinal tract and which cross the blood-brain barrier.[1] Clinical signs begin within 20 minutes of ingestion.[1] Peak plasma concentration occurs within 3 hours, and, in dogs, the drug is cleared within 6 hours.[1]

Amphetamines continuously stimulate muscle activity causing energy depletion, calcium overload in the sarcoplasmic reticulum, and constant muscle fasciculations, exacerbating energy demands.[10] Rhabdomyolysis is a common consequence of amphetamine toxicosis in humans and is occasionally reported in dogs.[1,10] Some cases may progress to myoglobinuria and acute kidney injury.[10] Hyperthermia and respiratory failure can lead to disseminated intravascular coagulation, a potential cause of death in intoxicated dogs.[1] Other reported cause of death include cerebral hemorrhage secondary to hypertension and heart failure.[1] Metarubricytosis, hypersegmentation of neutrophil nuclei, and thrombocytopenia presumedly due to hyperthermia have been reported secondary to amphetamine toxicosis in a Boxer.[13]

References:

1. Bischoff K. Toxicity of drugs of abuse. In: Gupta R, ed. *Veterinary toxicology: basic and clinical principles*. 3rd ed. Amsterdam: Elsevier, 2007.
2. Bischoff K, E. Beier 3rd and WC Edwards. Methamphetamine poisoning in three Oklahoma dogs. *Vet Hum Toxicol* 40: 19-20, 1998
3. Büttner A. The neuropathology of drug abuse. Neuropathology and applied neurobiology. Neuropathol Appl Neurobiol. 2011;**37(2)**:118-134.
4. Diniz PP, Sousa MG, Gerardi Dg et al. Amphetamine poisoning in a dog : case report, literature review, and veterinary medical perspectives. *Vet Hum Toxicol* 2003:45:315-317
5. Ellison D, Love S, Chimelli L, et al. *Neuropathology. A reference text of CNS pathology.* 3rd ed. Elsevier, 2013.
6. Kiyatkin EA, Sharma HS. Acute methamphetamine intoxication: brain hyperthermia, blood-brain barrier and brain

edema. *Int Rev Neurobiol* 2009;**88**:65-100.
7. Kiyatkin EA, Sharma HS. Leakage of the blood-brain barrier followed by vasogenic edema as the ultimate cause of death induced by acute methamphetamine overdose. *Int Rev Neurobiol* 2019;**146**:189-207.
8. Pei Y, Asif-Malik A, Canales AJ. Trace amines and the trace amine-associated receptor 1: pharmacology, neurochemistry and clinical implications. *Front. Neurosci*. 2016;**10**: 1-17 (article 148).
9. Pei Z, Zhang X. Methamphetamine intoxication in a dog: case report. *BMC Vet Res.* 2014;**10**:139-145.
10. Smith MR, Wurlod VA. Severe Rhabdomyolysis Associated with Acute Amphetamine Toxicosis in a Dog. *Case Rep Vet Med.* 2020; 2816373.
11. Stern LA, Schell M. Management of attention-deficit disorder and attention-deficit/hyperactivity disorder drug intoxication in dogs and cats. *Vet Clin North Am Small Anim Pract* 2018;**48**: 959-968.
12. Swirski AL, Pearl DL, Berke O, O'Sullivan TL. Companion animal exposures to potentially poisonous reported to a national poison control center in the United States in 2005 through 2014. *J Am Vet Med Ass*. 2020; 257(5): 517-530.
13. Wilcox A, Russell KE. Hematologic changes associated with Adderall toxicity in a dog. *Vet Clin Pathol.* 2008; 37(2): 184-189.

WSC 2022-2023 Self-assessment
Conference 20

1. Which of the following has been identified in adult goats with copper deficiency?
    a. Cataracts
    b. Hoof cracks
    c. Laryngeal neuropathy
    d. Cauda equina demyelinatio

2. True or false? Cerebral lesions are most prominent in delayed forms of enzootic ataxia.
    a. True
    b. False

3. Which of the following is true?
    a. Lead accumulates in both neurons and astrocytes.
    b. Lead enters the cell via a sodium transporter channel.
    c. White matter lesions predominate in the cerebral cortex.
    d. Calves less than 4 months are primarily affected as a result of concentration in the dam's milk.

4. Common nerve agents degrade which of the following?
    a. Acetylcholinesterase
    b. Glutamine
    c. Sphingosine
    d. Norepinephrine

5. The release of which of the following is NOT seen in amphetamine toxicosis?
    a. Norepinephrine
    b. Serotonin
    c. Dopamine
    d. Acetylcholine

Please email your completed assessment for grading to Dr. Bruce Williams at bruce.h.williams12.civ@mail.mil. Passing score is 80%. This program (RACE program 33611) is approved by the AAVSB RACE to offer a total of 0.5 CE Credits, with a maximum of 12.5 CE Credits being available to any individual Veterinary Medical Professionals for the 2019-2020 Wednesday Slide Conference. This RACE approval is for the subject matter categories of: SCIENTIFIC using the delivery method of NONINTERACTIVE DISTANCE. This approval is valid in jurisdictions which recognize AAVSB RACE.

Joint Pathology Center
Veterinary Pathology Services

WEDNESDAY SLIDE CONFERENCE 2022-2023

Conference #21 **29 March 2023**

CASE I:

Signalment:
12-year-old, male neutered, Havanese dog (*Canis familiaris*)

History:
A 12-year-old, male neutered Havanese dog has been managed through the Neurology Service over the course of 2 years for a right forebrain mass and cluster seizures. The dog was treated with radiation therapy 2 years ago and continued to have seizures. More recently, the dog started showing progressive neurologic signs consistent with regrowth of the mass (more frequent seizures, circling to the right, dull mentation, decreased menace OS). The dog presented to the Neurology service for cluster seizures and was hospitalized for seizure management. The seizures could only be controlled with a valium CRI. His owners elected euthanasia given the persistent breakthrough seizure activity and progressive neurologic dysfunction.

Gross Pathology:
The right frontal lobe has a focal, firm, tan, irregular mass that is adhered to the regional dura and measures 2.3 x 3 x 3.3 cm. The regional cerebral gyri are expanded (edema). Impression smears are obtained.

The fixed brain is sectioned. In the right frontal lobe, there is an irregular, firm, tan mass with a midline shift and regional parenchymal expansion.

Laboratory Results:
Impression smear cytology of brain mass: Smears are highly cellular and contain large numbers of round, oval and polygonal cells with abundant cytoplasm and well-defined cell borders. Cells contain large amounts of finely granulated, eosinophilic to amphophilic or basophilic cytoplasm. Nuclei are frequently eccentrically placed, round to oval and monomorphic with single or indistinct nucleoli. There is marked anisocytosis and mild anisokaryosis.

Microscopic Description:
One section of rostral cerebrum is examined. Extending from and expanding the leptomeninges, infiltrating into the regional cerebral cortex, there is a plaque-like, irregular, unencapsulated, mildly infiltrative neoplasm measuring approximately 1.8 x 1.0 cm. The neoplasm is comprised of large round, oval and polygonal cells forming sheets and supported by a scant, fibrovascular stroma. Neoplastic cells have well defined cell borders and contain abundant cytoplasm with densely packed eosinophilic granules. Nuclei are frequently eccentric, round, oval and sometimes angular, exhibiting mild pleomorphism (up to 2-fold) with finely stippled chromatin and an indistinct or single central nucleolus. There are zero mitoses in ten 40x (2.37 mm^2) high power fields. The leptomeninges within and around the tumor undergoes fibrosis, with multifocal regions of chondroid metaplasia. The regional infiltrated cortex exhibits parenchymal rarefaction, vacuolation, increased

numbers of small caliber vessels lined by hypertrophied endothelial cells, increased numbers of glial cells comprised of microglial (including Gitter cells) and astrocytes. Multifocally, dilated, eosinophilic axons are observed (spheroids). Occasional foci of karyorrhectic debris, amorphous eosinophilic material and hemorrhage are present (necrosis). Rare perivascular aggregates of inflammatory cells are observed throughout the parenchyma and leptomeninges, comprised of lymphocytes, plasma cells and fewer macrophages containing golden brown, granular pigment (hemosiderin). Small vessels are infrequently mineralized.

Contributor's Morphologic Diagnoses:
Brain (rostral cerebrum): Granular cell tumor with regional infiltration, edema, gliosis, and leptomeningeal fibrosis with chondroid metaplasia

Special stains: Cytoplasmic granules are PAS positive and diastase resistant

Contributor's Comment:
Granular cell tumors (GCTs) are most common in the meninges of the cerebrum in dogs.[2] In dogs, these tumors are typically supratentorial and extra-axial, plaque-like and infiltrative, however, can also cause diffuse

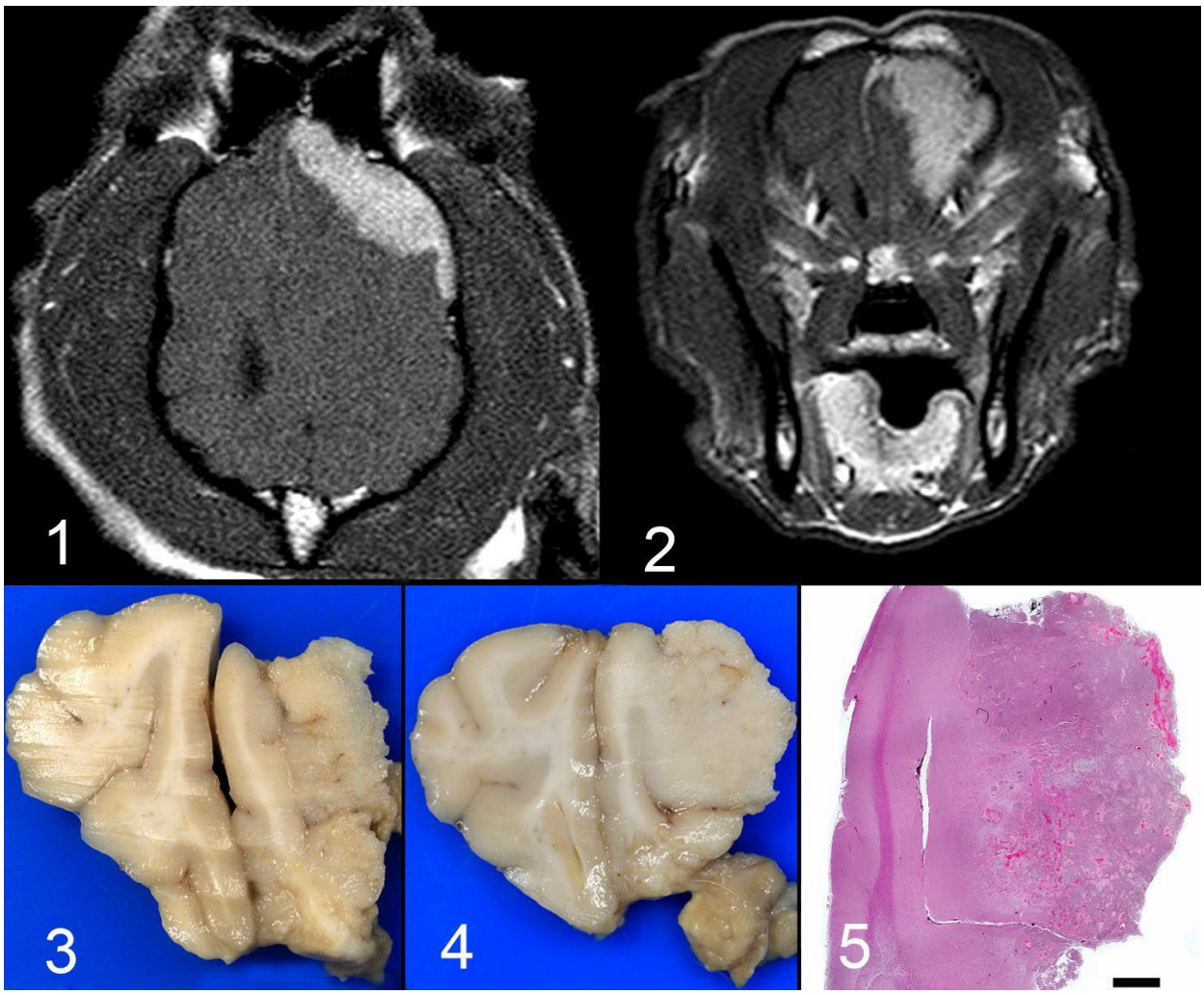

Figure 1-1. Cerebrum, dog. A plaque-like mass centered on the rostral surface of the right frontal lobe extends caudally along the parietal lobe and medially along the falx cerebri (Fig 1,2). The right frontal lobe has a firm tan, mass that is adhered to the dura and measures 2.3 x 3 x 3.3 cm. The regional cerebral gyri are expanded (edema). (Fig 3-5).

thickening of the meninges.[2] GCTs are typically unilateral, which can result in midline shifts caused by cerebral edema (as in this case). There are few reports of GCTs in the peripheral nervous system of dogs.[4] These tumors are characteristically comprised of large cells with abundant, granular eosinophilic cytoplasm.[2] The granular appearance of the cytoplasm is thought to be due to the presence of abundant lysosomes.[2] The cell of origin is unknown and is disputed in the literature.[2,5] It has been suggested that GCTs represent a common phenotype expressed by a variety of tumor cells.[1,3] Tumors that can exhibit granu lar changes are many and include meningiomas and other primary tumors of the CNS, paragangliomas, schwannomas, neurofibromas, leiomyomas, hibernomas, fibroxanthomas and rhabdomyomas.[4] In humans, peripheral GCTs are of Schwann cell origin, while intracranial GCTs are derived from astrocytes and pituicytes,[5] commonly occurring within the infundibulum or neurohypophysis.[3] Granular cells are frequently observed in other types of primary brain tumors,[2] which may reflect a nonspecific metabolic transformation.[3] A granular cell component has been reported in some human astrocytomas, meningiomas, and oligodendrogliomas.[3,5]

The imaging appearance of this tumor is characterized by strong, uniform, contrast enhancement and T1 weighted hyperintensity, as observed in this case.[2] The presence of T1 weighted hyperintensity in GCTs is considered a useful diagnostic feature.[2] These tumors can also be hyperintense on T2 weighted and FLAIR images,[1,2] however, this mass was predominantly T2 isointense to faintly hypointense with patchy FLAIR hyperintensities. Additional useful imaging features include a plaque-like distribution pattern, peritumoral edema with a mass effect, meningeal involvement and an absence of bone involvement.[1] These characteristics are not unique to the GCT, thus must be interpreted with caution, as GCT represents an extremely rare neoplasm of the canine central nervous system.[1]

Granular cell tumors typically stain strongly with PAS and are diastase resistant.[1-5] With immunohistochemistry, the granules are immunoreactive for ubiquitin,[2,3] with variable immunoreactivity for Vimentin, S-100, α 1-antichymotrypsin and α 1-antitrypsin.[2,3] GCTs are consistently negative for GFAP, pancytokeratins, leukocyte and macrophage markers.[3] The uniform positive ubiquitin staining may indicate cytosolic proteosome degradation activated by ubiquitin dependent

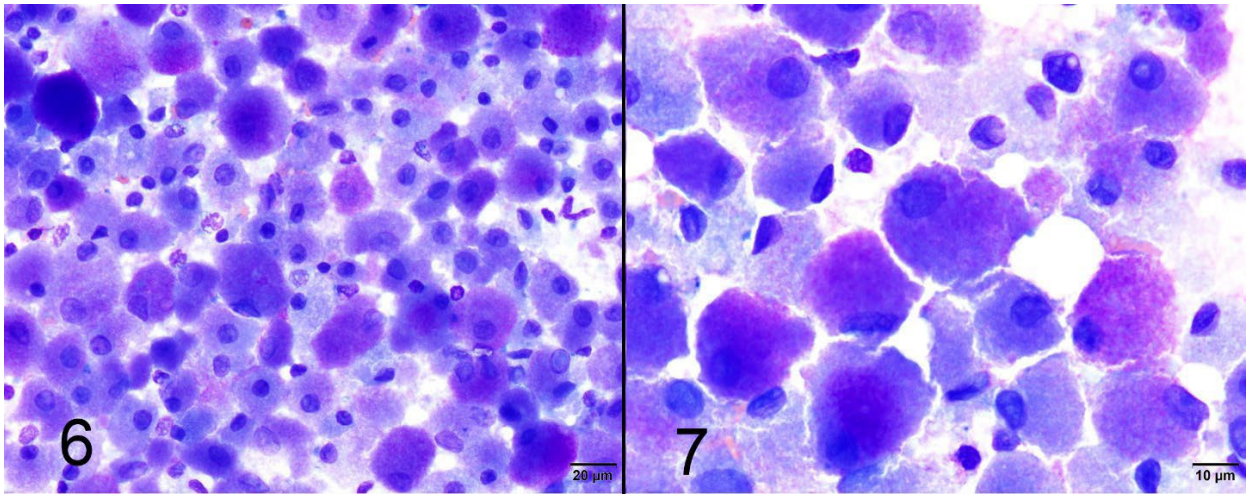

Figure 1-2. Cerebrum, dog. Impression smears of the mass. (Photo courtesy of: Animal Medical Center, 510 East 62nd St. New York, NY 10065. http://www.amcny.org)

processes or breakdown of proteins facilitated by protein-ubiquitin conjugates mediated by the endosome-lysosome system.[3] Staining of granules with anti-proteinases (α-1 antitrypsin and chymotrypsin) was initially thought to reflect a possible histiocyte origin, however, these findings are of limited specificity and histiocytic origin is not considered likely.[3] Ultrastructural evaluation reveals that the granular cytoplasm contains densely packed autophagosomes containing residual and dense bodies, irregular and membrane bound granules, multivesicular bodies, empty vesicles and membrane-like whorls.[2,3] Lysosomal accumulation is thought to be secondary to cellular degeneration, lysosomal enzyme defects and autophagy.[5] Schwann or meningeal cell origin is considered less likely due to the lack of desmosomal or gap junctions as well as peripheral basal lamina.[2]

Fibrosis was prominent in the regional leptomeninges in this case, and the presence of abundant collagenous tissue has been previously reported in canine GCTs.[3] In one case series, spindle shaped cells entrapped within collagenous tissue were hypothesized to transition to the large granular cells outside of the collagenous extracellular matrix.[3] GCTs grow slowly and rarely metastasize,[4] and in this case, the tumor was documented to be present for a period of 2 years following radiation therapy. These tumors are described in numerous other species, including people,

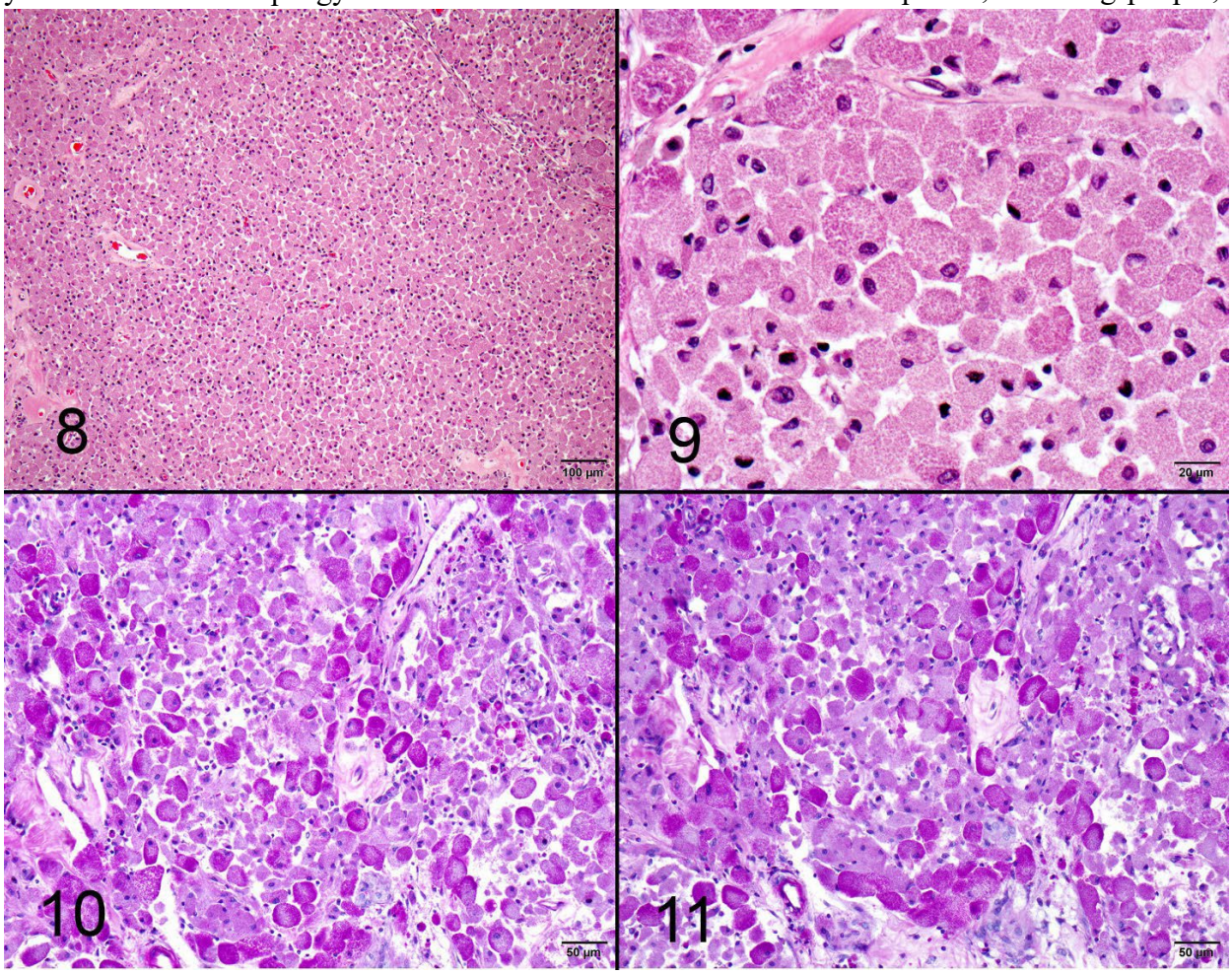

Figure 1-3. Cerebrum, dog. The neoplasm is comprised of large round, oval and polygonal cells in sheets. (Figs. 8,9) Cytoplasmic granules are PAS positive (Fig 10) and diastase resistant (Fig 11) (Photo courtesy of: Animal Medical Center, 510 East 62nd St. New York, NY 10065. http://www.amcny.org)

horses, rats, cats, ferrets and birds.[5] Common locations include the lungs in horses, the tongue in dogs and the meninges in rats.[5] In rats, GCTs are the most common primary CNS tumor.[1,3,4] Ultrastructural and morphological evidence in rats suggests that intracranial GCTs originate from arachnoid cells of the meninges.[1,3]

Contributing Institution:
Animal Medical Center, 510 East 62nd St.
New York, NY 10065.
http://www.amcny.org

JPC Diagnosis:
Leptomeninges and cerebrum: Granular cell tumor.

JPC Comment:
There are a few recent publications on this uncommon neoplasm in novel species. This week's moderator, MAJ Daniel Finnegan, described a meningeal granular cell tumor in a green tree python.[2] Reifinger et al. documented another case of granular cell tumor in the abdominal cavity of a snake.[6] These cases both had PAS positive and diastase resistant cytoplasmic granules, confirmed to be phagolysosomes on electron microscopy. These were the first two documented granular cell tumors in snakes, and granular cell tumors are rarely reported in non-mammalian species.

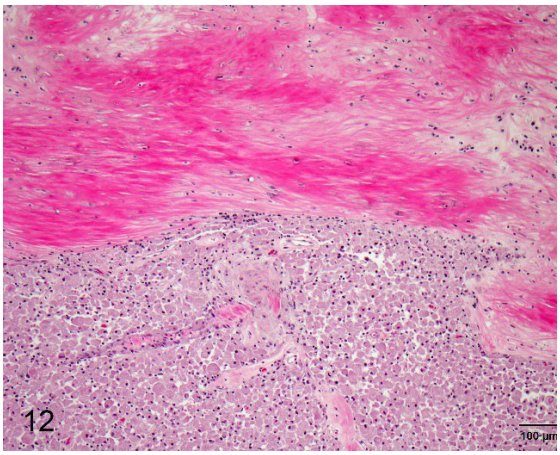

Figure 1-4. Cerebrum, dog. There is fibrosis of the leptomeninges which extends into the neoplasm (Fig. 12) (HE, 400X) (Photo courtesy of: Animal Medical Center, 510 East 62nd St. New York, NY 10065. http://www.amcny.org)

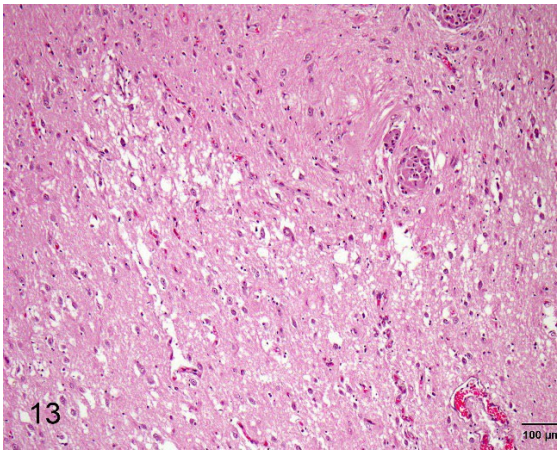

Figure 1-5. Cerebrum, dog. At the advancing edge of the neoplasm, there is parenchymal rarefaction and gliosis. (HE, 400X) (Photo courtesy of: Animal Medical Center, 510 East 62nd St. New York, NY 10065. http://www.amcny.org)

Granular cell tumors are characteristically compressive and non-infiltrative neoplasms. This case is unique in its infiltrative growth pattern; the moderator and participants discussed that this might be due to the chronicity or size of the neoplasm.

The contributor described the common presentations of granular cell tumors in mammalian species. A recent study demonstrated the propensity for rabbits to develop testicular granular cell tumors.[7] In 52 rabbits with testicular tumors, 63% were granular cell tumors, and 11 of 36 had bilateral granular cell tumors.[7] While other studies cite interstitial cell tumors as the most common testicular tumor in rabbits, this study suggests that granular cell tumors may be more common.

References:
1. Anwer, C.C., Vernau, K.M., Higgins, R.J., et al. Magnetic resonance imaging features of intracranial granular cell tumors in six dogs. *Vet Radiol Ultrasound* 2013; **54**:271–277.

2. Finnegan DK, Cartoceti AN, Hauck AM, LaDouceur EEB. Meningeal Granular Cell Tumor in a Green Tree Python (*Morelia viridis*). *J Comp Path.* 2020; 174: 54-57.
3. Higgins RJ, Bollen AW, Dickinson PJ, Siso-Llonch, S. Tumors of the Nervous System. In: *Tumors in Domestic Animals*, 5th Ed. Ames, IA: John Wiley & sons, Inc; 2017:870-872.
4. Higgins, R.J., LeCouteur, R.A., Vernau K.M., et al. Granular cell tumors of the canine central nervous system: two cases. *Vet Pathol* 2001; **38**:620–627.
5. Rao, D., Rylander, H., Drees, R., et al. Granular cell tumor in a lumbar spinal nerve of a dog. *J Vet Diagn Invest* 2010; **22**:638–642.
6. Reifinger M, Dinhopl N, Gumpengberger M, Konecny M, Cigler P. Granular Cell Tumour in a California Kingsnake. *J Comp Path.* 2020; 175: 24-28.
7. Reineking W, Seehusen F, Lehmbecker A, Wohlsein P. Predominance of Granular Cell Tumors among Testicular Tumours of Rabbits (*Oryctolagus cuniculi* f. dom.). *J Comp Path*. 2019; 153: 24-29.
8. Spoor MS, Kim DY, Kanazono S. et al. What is your diagnosis? Impression smears of a cerebral mass from a dog. *Vet Clin Pathol* 2013; **42**(2):240-241.

CASE II:

Signalment:
7-month-old, female spayed, boxer dog (*Canis familiaris*)

History:
The patient presented to their veterinarian for a 3-month history of pollakiuria characterized by voiding small volumes of urine every 30-60 minutes. Cystocentesis of the patient's bladder yielded small quantities of foul-smelling urine which upon urinalysis, contained markedly increased numbers of leukocytes (pyuria) and erythrocytes (hematuria). Aerobic bacterial culture of the urine isolated large numbers of *Escherichia coli*. Despite antibiotic therapy for several weeks, pollakiuria persisted. Ultrasonographic and radiographic assessment of the urinary bladder revealed a severely and irregularly thickened bladder mucosa; there was no overt evidence of cystoliths. An incisional biopsy of the urinary bladder was taken and submitted for histopathology.

Gross Pathology:
The bladder mucosa was markedly thickened by multifocal-to-coalescing, poorly demarcated, firm, pale tan, polypoid masses.

Laboratory Results:
No laboratory results reported.

Microscopic Description:
Urinary bladder: Expanding the superficial aspect of the urinary bladder lamina propria and elevating the overlying urothelium is a large, poorly demarcated, densely cellular, plaque-like mass composed of dense sheets of large macrophages. These large macrophages have abundant cytoplasms that are packed with innumerable coarse eosinophilic granules and frequently contain one to three, 5-15 μm, pale eosinophilic, finely granular intracytoplasmic inclusions. Multifocally scattered throughout the dense sheets of macrophages are small aggregates of lymphocytes, plasma cells, and neutrophils. The

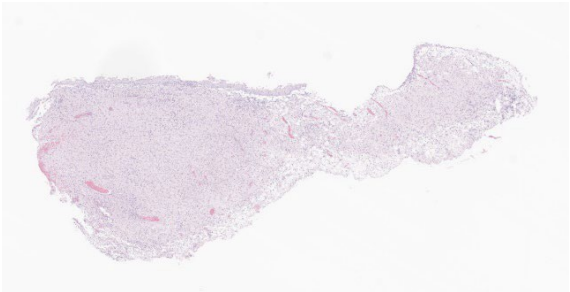

Figure 2-1. Urinary bladder, dog. A section of urinary bladder contains a mildly hyperplastic mucosa overlying a markedly expanded submucosa. (HE 6X)

urothelium overlying the mass is multifocally eroded and has small-to-moderate numbers of lymphocytes and neutrophils percolating throughout. The lamina propria underlying the mass is moderately expanded by clear to pale eosinophilic wispy fluid (edema).

100% of the large macrophages comprising the plaque-like mass exhibit strong cytoplasmic and membranous immunolabelling with Iba1.

The intracytoplasmic granules and inclusions within the macrophages are all strongly PAS-positive. The granules and inclusions do not stain positively with Toluidine blue, Luxol fast blue, Giemsa, Von Kossa, or Prussian blue stains. There is no overt evidence of acid-fast organisms within these macrophages upon application of Ziehl-Neelsen and Fite-Faraco stains.

Contributor's Morphologic Diagnoses:
Urinary bladder: Severe, locally extensive, chronic, granulomatous cystitis with myriad intracytoplasmic PAS-positive granules and inclusions, lamina propria edema, and multifocal epithelial erosion

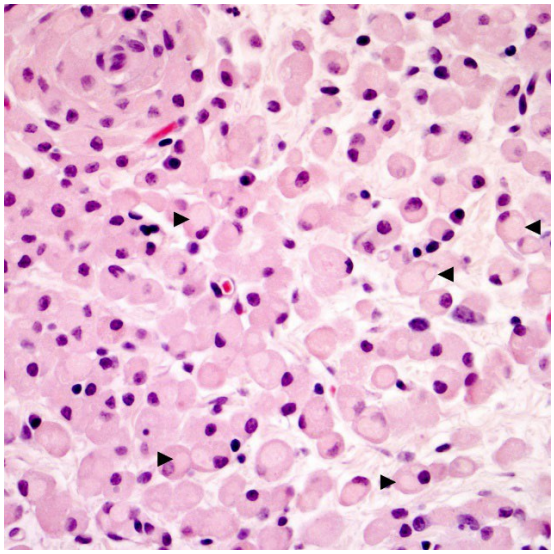

Figure 2-2. Urinary bladder, dog. The submucosal infiltrate is composed of numerous macrophages (HE, 400X). (Photo courtesy of: Cornell University School of Veterinary Medicine; https://www.vet.cornell.edu/departments/biomedical-sciences/section-anatomic-pathology).

Contributor's Comment:
Histopathology of the submitted urinary bladder mass revealed expansion of the lamina propria by a large plaque-like aggregate of large macrophages filled with abundant intracytoplasmic PAS-positive granules and inclusions. These microscopic findings, when viewed in conjunction with the signalment of the patient and the submitted clinical history, were deemed most consistent with a diagnosis of malakoplakia. Granular cell tumor and mycobacteriosis were also considered differential diagnoses prior to positive immunohistochemistry results for Iba1 (discounting a granular cell tumor) and the absence of overt acid-fast organism upon application of additional histochemical stains (discounting mycobacteriosis).

Malakoplakia is an uncommon granulomatous disease that has been reported in several veterinary species including dogs[2,3,6,123] cats[1,4,10], pigs[7,14], and a Cynomolgus macaque (*Macaca fascicularis*)[11]. Malakoplakia typically manifests within the genitourinary tract (particularly the urinary bladder) but has been reported in a variety of other body systems[7,14,15]. In humans, most cases of malakoplakia occur in middle-aged women, with infrequent cases reported in children[15]. In the seven previously reported cases of malakoplakia in dogs, all seven cases occurred in females with ages ranging from 6-weeks-old to 8-months-old[2,3,6,13]. In all of the other spontaneously occurring veterinary cases in which the full signalment was reported, all animals were female[4,9,14].

While the exact etiopathogenesis of malakoplakia is still unclear, it has been putatively associated with recurrent bacterial infections, with the most commonly isolated bacteria be-

ing *E. coli* (as in the present case)[15]. It is postulated that females are over-represented in the current literature as they are more susceptible to urinary tract infections than males [5]. Immunosuppression has also been implicated as a contributing factor in the development of this disease as many human patients with malakoplakia are ailed by concurrent conditions that debilitate the immune system (e.g. acquired immunodeficiency syndrome and neoplasia) or are receiving immunosuppressive therapy[15].

Grossly, malakoplakia appears as firm tan to yellow-brown masses that vary in morphology from focal plaques to multifocal-to-coalescing nodules to locally extensive thickenings of the affected organ(s). The typical histological appearance of malakoplakia is exuberant granulomatous inflammation characterized by dense sheets of large macrophages filled with abundant intracytoplasmic PAS-positive granules and inclusions (so-called 'von Hansemann-type macrophages')[15]. Many have postulated that the PAS-positive granules and inclusions within these macrophages are the result of defective macrophage phagolysosome function and subsequent accumulation of bacterial breakdown products within the cytoplasm[15]. While not present in all cases, small numbers of 3-8 µm basophilic intracellular and/or extracellular targetoid concretions termed 'Michaelis-Gutmann bodies' are scattered throughout regions of granulomatous inflammation; these concretions are thought to be pathognomonic for malakoplakia[9]. 'Michaelis-Gutmann bodies' stain positively with both Von Kossa and Prussian blue stains and are postulated to represent concretions of organic matter, iron, and calcium derived from bacterial breakdown products[9]. Von Kossa and Prussian blue stains did not highlight the presence of 'Michaelis-Gutmann bodies' in the present case.

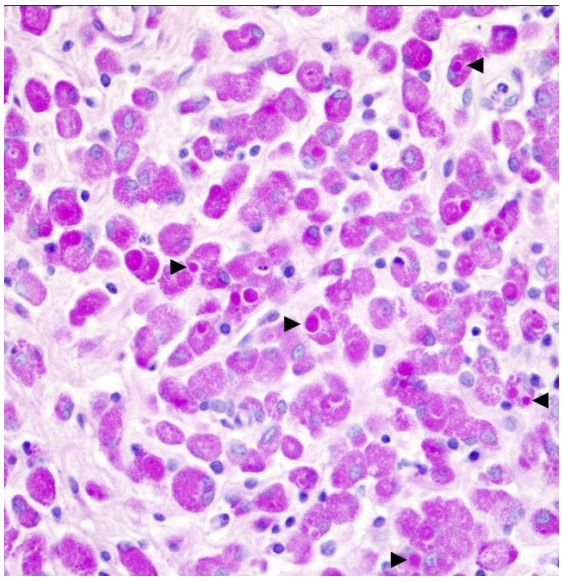

Figure 2-3. Urinary bladder, dog. Macrophages contain numerous PAS-positive granules and inclusions (arrows). (PAS, 400X). (Photo courtesy of: Cornell University School of Veterinary Medicine; https://www.vet.cornell.edu/departments/biomedical-sciences/section-anatomic-pathology).

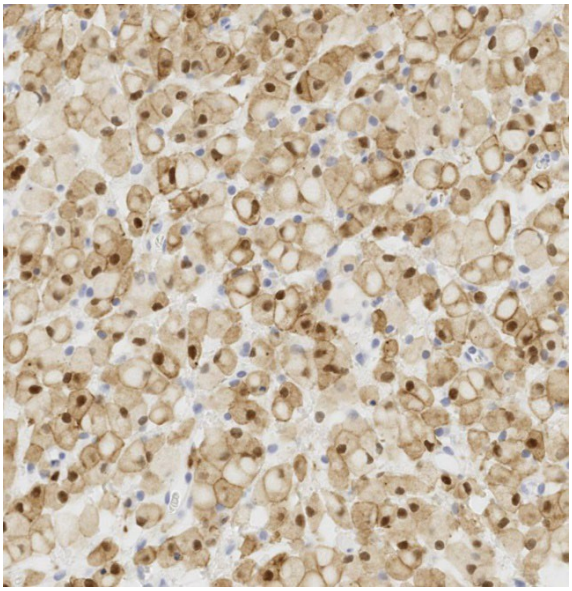

Figure 2-4. Urinary bladder, dog. Macrophages demonstrate strong immunopositivity for IBA-1. (anti-IBA-1, 400X). (Photo courtesy of: Cornell University School of Veterinary Medicine; https://www.vet.cornell.edu/departments/biomedical-sciences/section-anatomic-pathology).

The histological appearance of the macrophages within malakoplakia lesions are strikingly similar to those found in cases of granulomatous colitis of boxer dogs (GCB; also

known as histiocytic ulcerative colitis. GCB, similar to malakoplakia, is also associated with an exuberant granulomatous inflammatory response to *E. coli* [11]. It is salient to note that all seven reported cases of malakoplakia in dogs (including the present case) occurred in brachycephalic breeds that have been known to develop GCB (Boxer, Pug, English Bulldogs, Staffordshire Bull Terrier, and French Bulldog) [2,3,6,13]. The similarities between GCB and malakoplakia are intriguing and certainly strengthen the hypothesis that malakoplakia may arise in individuals that possess macrophages that are unable to eliminate certain *E. coli* pathotypes, resulting in persistent infections and macrophages becoming laden with PAS-positive bacterial products.

In summary, malakoplakia is an uncommon granulomatous disease that typically affects the genitourinary tract. Females, brachycephalic dog breeds, and young animals are over-represented in cases of malakoplakia within the current veterinary literature. While the exact etiopathogenesis of malakoplakia is unclear, both bacterial infection (namely *E. coli*) and immunosuppression are putatively associated with the development of this disease. Given the various similarities between malakoplakia and granulomatous colitis of boxer dogs (GCB), a genetic deficit that renders macrophages unable to eliminate certain *E. coli* pathotypes may also be involved in the development of malakoplakia. Malakoplakia should be considered a differential diagnosis for urinary bladder masses, especially in young female dogs with a history of bacterial cystitis.

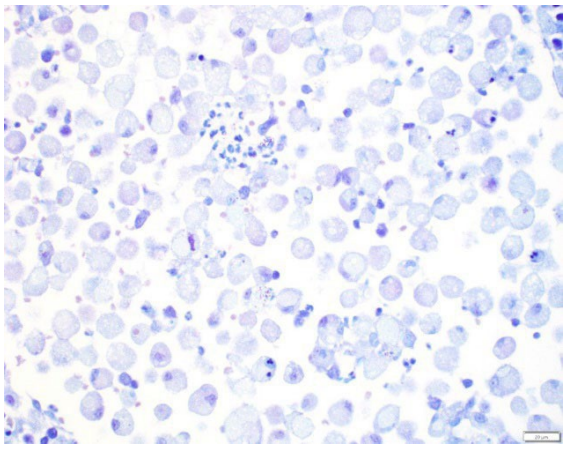

Figure 2-5. Urinary bladder, dog. Rare histiocytes contain aggregates of bacilli in their cytoplasm. (Giemsa, 300X)

Contributing Institution:
Department of Biomedical Sciences, Section of Anatomic Pathology
College of Veterinary Medicine
Cornell University
Ithaca, NY
USA

https://www.vet.cornell.edu/departments/biomedical-sciences/section-anatomic-pathology

JPC Diagnosis:
Urinary bladder, lamina propria: Cystitis, granulomatous, diffuse, severe.

JPC Comment:
The contributor provides an excellent comment on this uncommon condition in humans and select animal species. The term malakoplakia is derived from the Greek words for soft (*malacos*) and plaques (*placos*). The condition was first described by Michaelis, Gutmann, and von Hansemann in 1902-1903, and the key histologic features of this condition still bear their names.[8] Malakoplakia occurs more commonly in humans than in animals, though it is still rare. In humans, the condition has been documented in the urinary tract, gastrointestinal tract, gall bladder, pancreas, skin, reproductive tract (prostate, testes, cervix, vulva), lungs, and other tissues.[15] In the gastrointestinal system, the most commonly affected sites are the colon and rectum, and its occurrence in the colon has been associated with colon cancer.[15] Cutaneous malakoplakia more commonly occurs in adult

males and in organ transplant recipients on an immunosuppressive regimen.[8] Cutaneous lesions may present as papules, nodules, ulcers, or abscesses with draining tracts; occasionally, cutaneous lesions are associated with nonhealing surgical wounds.[8] While *E. coli* is the most commonly isolated organism in humans, certain types of patients may be prone to developing malakoplakia with a different organism. *Rhodococcus equi*, for instance, is commonly found in patients with acquired immunodeficiency syndrome.[15]

References:

1. Bayley C, Slocombe R, Tatarczuch L. Malakoplakia in the urinary bladder of a kitten. *J Comp Pathol*. 2008;139(1):47-50.
2. Benzimra C, Job C, Pascal Q, Bureau S, Combes A, Bongrand Y, R. Faucher M. Malakoplakia of the bladder in a 4-month-old puppy. *J Am Anim Hosp Assoc. 2019*;55(5):261-5.
3. Brückner M. Malakoplakia of the urinary bladder in a young French Bulldog. *J Am Vet Med Assoc.* 2022;260(5):543-8.
4. Cattin RP, Hardcastle MR, Simpson KW. Successful treatment of vaginal malakoplakia in a young cat. *J Feline Med Surg Open Rep.* 2016;2(2). doi:10.1177/2055116916674871
5. Cianciolo RE, Mohr FC. Urinary system. In: Maxie GM, ed. *Jubb, Kennedy, & Palmer's Pathology of Domestic Animals*. 6th ed. Elsevier; 2015:459–461.
6. Davis KL, Cheng L, Ramos-Vara J, Sánchez MD, Wilkes RP, Sola MF. Malakoplakia in the urinary bladder of 4 puppies. *Vet Pathol*. 2021;58(4):699-704.
7. Gelmetti D, Gibelli L, Gelmini L, Sironi G. Malakoplakia with digestive tract involvement in a pig. *Vet Pathol*. 2014;51(4):809-11.
8. Kohl SK, Hans CP. Cutaneous Malakoplakia. *Arch Pathol Lab Med*. 2008; 132: 113-117.
9. Lewin KJ, Fair WR, Steigbigel RT, Winberg CD, Droller MJ. Clinical and laboratory studies into the pathogenesis of malacoplakia. *J Clin Pathol*. 1976;29(4):354-63.
10. Rutland BE, Nimmo J, Goldsworthy M, Simcock JO, Simpson KW, Kuntz CA. Successful treatment of malakoplakia of the bladder in a kitten. *J Feline Med Surg*. 2013;15(8):744-8.
11. Simpson KW, Dogan B, Rishniw M, Goldstein RE, Klaessig S, McDonough PL, German AJ, Yates RM, Russell DG, Johnson SE, Berg DE. Adherent and invasive Escherichia coli is associated with granulomatous colitis in boxer dogs. *Infect Immun.* 2006;74(8):4778-92.
12. Taketa Y, Inomata A, Sonoda J, Hayakawa K, Nakano-Ito K, Ohta E, Seki Y, Goto A, Hosokawa S. Granulomatous nephritis consistent with malakoplakia in a cynomolgus monkey. *J Toxicol Pathol*. 2013;26(4):419-22.
13. Tang KM, Serpa PB, Santos AP. What is your diagnosis? Urine from a dog. *Vet Clin Pathol.* 2022. doi:10.1111/vcp.13139.
14. Taniyama H, Ono T, Matsui T. Systemic malacoplakia in a breeding pig. *J Comp Pathol*. 1985;95(1):79-85. (9)
15. Yousef GM, Naghibi B. Malakoplakia outside the urinary tract. *Arch Pathol* Lab Med. 2007;131(2):297-300. (11)

CASE III:

Signalment:
9-year-old spayed female canine (*Canis familiaris*)

History:
Patient presented 6 months before for a mass in the ventral neck. It was diagnosed as a possible abscess and Clavamox and Baytril were prescribed.

Today, patient presented for recheck with no improvement noted. She has difficulty walking, generalized weakness and is hesitant to move. She is painful (4/5) and anxious (4/5). Differential diagnosis includes IVDD.

Gross Pathology:
The submandibular lymph nodes are enlarged bilaterally and asymmetrically. The left lymph node (7 x 3 x 2 cm) starts at the mandibular ramus, is firm, movable and dark red in color. The right lymph node (4 x 1.5 x 1 cm) has the same appearance. The cranial mediastinal lymph nodes are dark red in color, firm and enlarged (3 x 1, 5 x 4 cm nodules). On cut section, all the affected lymph nodes are solid, firm, and diffusely red. The lymph node architecture is partially effaced. Severe degree of spondylosis T13-L1, L2-L3, L4-L5 and L-S junction, extending into the vertebral canal. The ventral thoracic vertebrae also show a mild degree of spondylosis. No IVDD was found.

Laboratory Results:
No laboratory results reported.

Microscopic Description:
Lymph node, one section. Approximately 90% of the entire architecture is effaced by an expansile area characterized by locally extensive proliferation of anastomosing, variable sized and dilated slit openings resembling vascular channels. These channels are lined by plump endothelial cells. There are small areas of necrosis, characterized by intense eosinophilic, amorphous material, admixed with scattered macrophages, rare lymphocytes and plasma cells. These vascular channels are filled with RBCs and scattered clusters of neutrophils and macrophages. Pigment-laden macrophages are common throughout (hemosiderin). The remaining normal nodal architecture is compressed with cortex and paracortex characterized by coalescing lymphoid follicles with starry sky appearance (tingible body macrophages). The lymphoid follicles have prominent germinative centers.

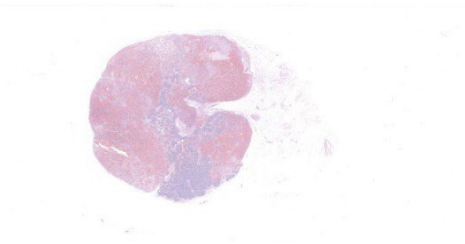

Figure 3-1. Mandibular lymph node, dog. A single transverse section of lymph node is submitted for examination. Approximately 50% of the node is effaced and markedly congested. (HE, 6X)

Contributor's Morphologic Diagnoses:
DDX: Lymph node: locally extensive vascular proliferation with lymphoid atrophy compatible with nodal plexiform vasculopathy.

Contributor's Comment:
Benign, non-neoplastic and neoplastic vascular proliferations in the lymph nodes have been described in different animal species.

The differential diagnosis for vascular proliferations in a lymph node includes nodal angiomatosis, plexiform vasculopathy, nodal hemangioma, nodal vascular hamartoma, and nodal telangiectasis. All of them are of unknown cause and usually present as incidental, benign proliferations that will efface and replace the normal lymphoid architecture.

Plexiform vasculopathy, also known as vascular transformation of lymph nodes, is an endothelial proliferation within lymph nodes and has been reported in humans, cats, and one dog with thyroidal carcinoma.[5] It is an uncommon lesion, and it is still unknown whether the proliferating endothelial cells are of lymphatic or blood origin. The literature describes it as a lymphadenopathy with vasoproliferation and lymphoid atrophy.[7] The lesions are usually focal but can involve most

of the lymphoid tissue. The lesions are distinct from more common findings such as lymphosarcoma, reactive lymphadenopathies, and normal lymph nodes.

The pathogenesis of this disease is unclear in both the human and animal literature.
The description of plexiform vasculopathy has been limited to cats. The human equivalent to this disease is nodal angiomatosis. There is one paper that describes a lymphadenopathy in a dog associated with thyroid carcinoma. The histological description was similar to that of nodal angiomatosis and plexiform vasculopathy.[3]

Clinical signs are nonspecific and generally present as secondary signs to some sort of lymphadenopathy in the cervical or inguinal region. Lymph nodes are enlarged and in cross section they have a fleshy tan to purple appearance.[7] Some of these signs include dyspnea, nonpainful masses, and difficulty swallowing. Histopathology shows severe loss of lymphoid tissue distributed throughout the lymph node and replaced by accumulations of erythrocytes within a capillary-like proliferation of endothelial cells. The endothelial cells are characterized by small, elongated, basophilic nuclei and inconspicuous cytoplasm. Mitotic figures were rare throughout.[5,7]

Cytoplasmic expression of CD31 and factor VIII-related antigens were found via immunohistochemistry in all proliferated intranodal endothelial cells. A recent study used the lymphendothelial-specific marker, Prox-1, to determine the origin of the intranodal endothelial cells. The results of this study determined that the proliferative endothelial cells were of lymphatic origin.[5]

There are a variety of possible pathogenic explanations for plexiform vasculopathy including disturbances in drainage caused by tumors in the lymph node, thrombosis, severe congestive heart failure, or angiogenic factors released by a neoplastic process. A similar lesion of lymphatic proliferation has been experimentally induced in rabbits via incomplete occlusion of veins combined with complete obstruction of lymphatics, or just by the complete obstruction of lymphatics.[5] The

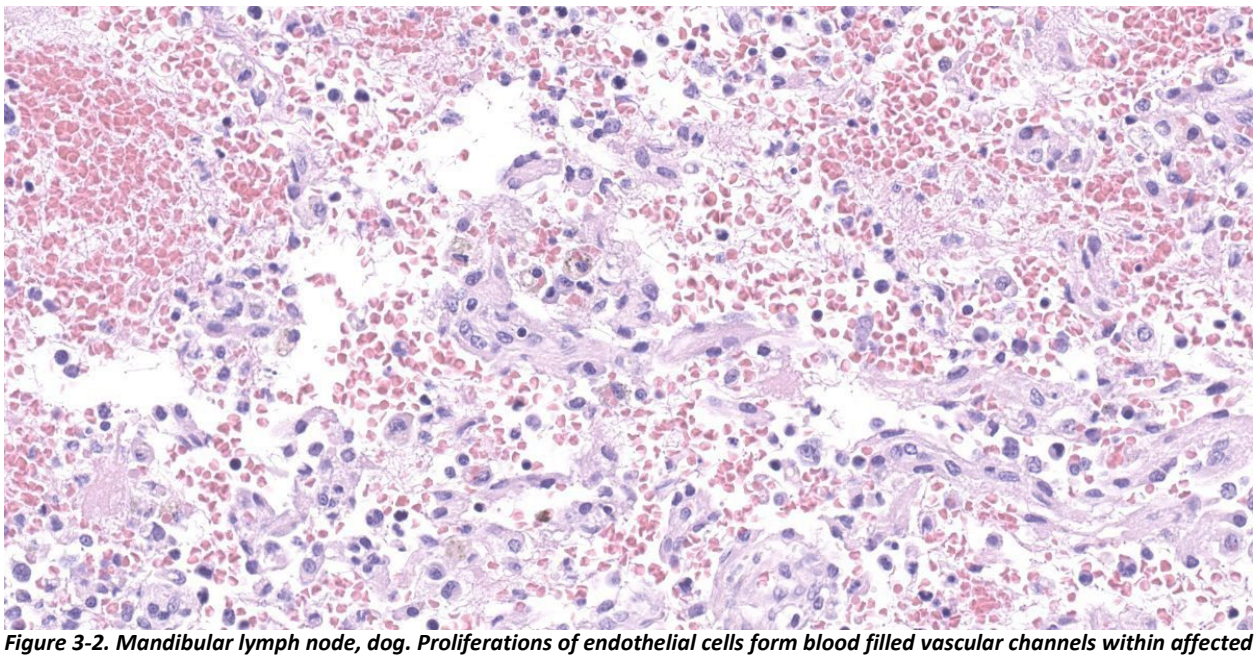

Figure 3-2. Mandibular lymph node, dog. Proliferations of endothelial cells form blood filled vascular channels within affected areas of the node. (HE, 372X)

later stages of human Acquired Immune Deficiency Syndrome (AIDS) is characterized by progressive lymphoid atrophy with vascular proliferation. However, the vascular proliferation associated with AIDS involves post-capillary venules with subsequent severe immune deficiency which does not occur in plexiform vasculopathy.[7]

Differentials should include other intranodal vascular proliferations such as angiomatous hamartoma, nodal lymphangiomatosis, hemolymph nodes, and nodal hemangiomas. However, none of these have been described in dogs.

Welsh et al. (1999) reported that complete excision of a retropharyngeal lymph node appears curative. Post-operative complications appeared to be limited to edema in the region of the excised lymph node.

Contributing Institution:
College of Veterinary Medicine, Western University of Health Sciences, 309 E. Second street
Pomona, California 91766

http://www.westernu.edu/xp/edu/veterinary/staff.xml

JPC Diagnosis:
Lymph node: Vasculopathy and hemorrhage, severe, with marked fibrin deposition and extramedullary hematopoiesis.

JPC Comment:
Two major categories of non-neoplastic vascular proliferations within lymph nodes are angiomyomatous hamartoma and vascular transformation of sinuses.[8] In vascular transformation of sinuses, there is capillary proliferation within subcapsular and intermediate sinuses accompanied by variable amounts of fibrosis and lymphoid atrophy.[8] Variants of vascular transformation of sinuses include plexiform vasculopathy, nodal angiomatosis in humans, and angiomatous hyperplasia in Wistar rats.[8] While not completely known, vascular transformation of sinuses is thought to occur due to occlusion of lymphatic or efferent veins which causes edema in the draining region. Plexiform vasculopathy is most commonly documented in the cervical lymph nodes of cats,[5,9] and in some cases, has been associated with malignant transformation to angiosarcoma.[9]

Angiomyomatous hamartoma, which has been documented in humans, a cynomolgus macaque, and a dog, involves proliferation of vessels with muscular walls within the cortex of the lymph node. The pathogenesis of angiomyomatous hamartoma is unknown. A recent report described the incidence of both angiomyomatous hamartoma within the hilus and vascular transformation within the subcapsular and medullary sinuses in the cranial mediastinal lymph nodes of a 1-year-old beagle in a toxicity study.[8]

This case generated significant discussion among the moderator and conference participants. In some regions of the node, the presence of well-defined plexiform channels is consistent with nodular plexiform vasculopathy. In other regions, collagen and smooth muscle actin within vascular walls (confirmed via histochemical and immunohistochemical staining) are more prominent than would be expected in plexiform vasculopathy

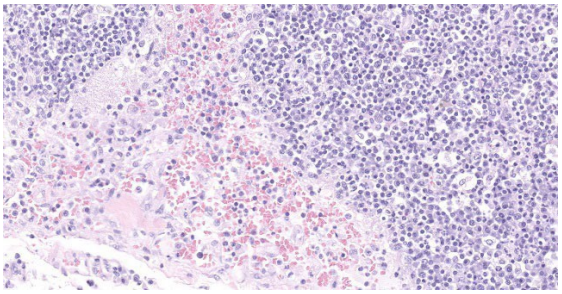

Figure 3-3. Mandibular lymph node, dog. Vascular proliferation expands the subcapsular sinus. The adjacent cortex is moderately hyperplastic with numerous tingible body macrophages. (HE, 311X)

but not enough to be consistent with a diagnosis of angiomyomatous hamartoma. The moderator and conference participants also discussed another prominent feature of this case: hemorrhage and fibrin thrombi. Participants discussed how polymerized fibrin can induce endothelial proliferation and fibrosis, and in this case, might serve as a potential cause for secondary vasculopathy within the node. Thus, hypercoagulability (i.e. due to protein losing nephropathy) was discussed as a potential differential.

Another differential considered less likely by the moderator and participants is neoplastic transformation. Hemangiomas are generally well circumscribed and expansile,[8] features which are lacking in this case. Hemangioendothelioma and hemangiosarcoma also feature a high mitotic rate, cellular atypia, and invasion.[8] Additionally, primary vascular neoplasia within lymph nodes is uncommon; in a study of 439 vascular tumors in dogs, only one primary tumor occurred in a lymph node, and only 2 of 63 angiosarcomas metastasized to lymph nodes.[2] In a separate study of 175 beagles that were controls in a toxicology study, however, hemangiomas were found incidentally in 9 popliteal and 1 hepatic lymph node, demonstrating that these may not be as uncommon as the literature suggests.[4]

Another feature discussed by the moderator and participants in this case is extramedullary hematopoiesis, consisting of lymphoid and erythroid precursors, megakaryocytes, and nurse cells.

References:

1. Fuji RN, Patton KM, Steinbach TJ, Schulman FY, Bradley GA, Brown TT, Wilson EA, Summers BA. Feline systemic reactive angioendotheliomatosis: eight cases and literature review. *Vet Pathol*. 42: 608-17.
2. Gamlem H, Nordstoga K, Arnesen K. Canine vascular neoplasia – a population based clinicopathologic study of 439 tumors and tumour-like lesions in 420 dogs. *APMIS*. 2018; Suppl 125: 41-54.
3. Gelberg HB, Valentine BA. Diagnostic exercise: Lymphadenopathy associated with thyroid carcinoma in a dog. *Vet Pathol*. 2011; 48(2), 530-534.
4. HogenEsch H, Hahn FF. Primary vascular neoplasms of lymph nodes in the dog. *Vet Pathol.* 1998; *35*(1): 74-76.
5. Jungwirth N, Junginger J, Andrijczuk C, Baumgärtner W, Wohlsein P. Plexiform vasculopathy in feline cervical lymph nodes. *Vet Pathol.* 2018; 55 (3),453-456.
6. Karim MS, Ensslin CJ, Dowd ML, Samie FH. Angiomyomatous hamartoma in a postauricular lymph node: A rare entity masquerading as a cyst. *JAAD Case Reports*. 2021; *7*:131.
7. Lucke V, Davies JD, Wood CM, Whitbread TJ. Plexiform vascularization of lymph nodes: an unusual but distinctive lymphadenopathy in cats. *J Comp Pathol*. 1987; 97: 109-119.
8. Nelissen S, Chamanza R. An Angiomyomatous Hamartoma With Features of Vascular Transformation of Sinuses in the Mediastinal Lymph Node of a Beagle Dog. *Toxicol Pathol.* 2020; *48*(8), 1017-1024.
9. Roof-Wages E, Spangler T, Spangler WL, Siedlecki CT. Histology and clinical outcome of benign and malignant vascular lesions primary to feline cervical lymph nodes. *Vet Pathol*. 2015; 52(2), 331-337.
10. Welsh EM, Griffon D, Whitbread TJ. Plexiform vascularization of a retropharyngeal lymph node in a cat. *J Small Anim Pract*. 1999; 40(6):291.

CASE IV:

Signalment:
An 8-month-old spayed female Boxer dog (*Canis familaris*)

History:
The dog was referred by a practitioner to a specialist veterinary center for management of acute spontaneous pneumothorax. On presentation to the specialist clinic the dog was tachypneic (64 bpm), hypoxemic (pulse oximetry 66% without oxygen supplementation, 92% with oxygen supplementation), and had increased respiratory effort with an abdominal component to the respiration. Lung sounds on the right side were dull on auscultation. Initial bloodwork revealed a mixed acidosis (pH 7.299; normal 7.35 – 7.45), with mild hemoconcentration (57%) and normal total solids (6.6 g/dl). Blood glucose was normal (4.7 g/dl), with no evidence of lactic acidosis (1.9 mmol/L; normal < 2.5 mmol/L).

Computed tomography (CT) showed multiple variably sized bullae in the right middle lung lobe, and partial or complete atelectasis of all remaining lung lobes. The dog was anesthetized for surgery but died from cardiopulmonary arrest during pre-surgical thoracocentesis.

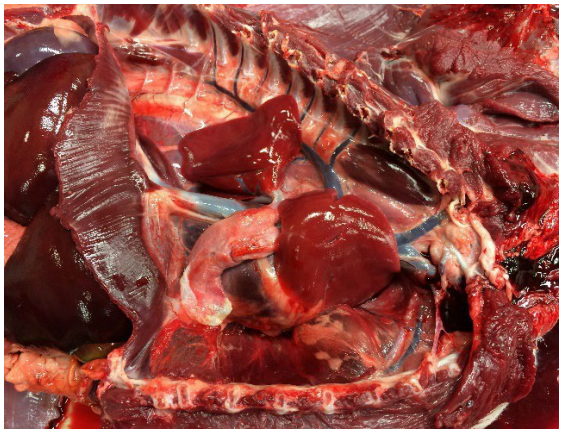

Figure 4-1. Right lung, dog. There was bilateral pneumothorax at autopsy, with atelectasis of all lung lobes. (Photo courtesy of: Department of Veterinary Clinical and Diagnostic Sciences, Faculty of Veterinary Medicine, University of Calgary, 3280 Hospital Dr. NW, Calgary, Alberta T2N 4Z6, Canada, http://vet.ucalgary.ca)

Gross Pathology:
Necropsy examination revealed severe bilateral pneumothorax, with marked atelectasis of all lung lobes. The right middle lung lobe was small, pale and flaccid, with numerous collapsed, coalescing pleural bullae along its ventral and ventrocaudal margins; rupture of these bullae was presumed to be the source of the pneumothorax. The cartilage of the lobar bronchus supplying the right middle lung lobe was thin, flimsy and easily compressed when compared with bronchi supplying other lobes. In transverse section its lumen was slit-shaped rather than circular. In addition, an aberrant right subclavian artery arose in common with the left subclavian artery, forming a bisubclavian trunk. The right subclavian artery passed dorsal to the esophagus and compressed it.

Laboratory Results:
No laboratory results reported.

Microscopic Description:
This section from the right middle lung lobe is severely malformed and difficult to recognize as lung. It consists predominantly of a thick fibrovascular trabecular network outlining collapsed; empty spaces lined by a simple cuboidal to simple squamous epithelium. The lining epithelium is multifocally lost (autolytic artifact), and cystic spaces frequently contain rafts of sloughed epithelial cells. The fibrovascular trabeculae are variably thick, ranging in width from 20 to 300 microns, and contain many thin-walled blood vessels lined by mature endothelial cells, numerous mineralized areas, and scattered lymphoplasmacytic foci.

Multifocally, recognizable bronchiole-like structures are present. These are lined by simple cuboidal epithelium and have irregular bundles of smooth muscle in their walls. They are frequently adjacent to profiles of large arteries and veins (pulmonary vessels).

The section also contains a malformed bronchus surrounded by a nearly continuous layer of smooth muscle. Cartilage plates in this bronchus are irregular and present only around one half of the airway's circumference. The cartilage is immature, with small chondrocytes, less chondroid matrix and smaller lacunae (when compared with other lung sections from this dog and an age-matched control dog). Bronchial glands are fewer in number (when compared with other lung sections from this dog and the control dog).

Contributor's Morphologic Diagnoses:
Lung: Congenital pulmonary airway malformation (CPAM)-like lesion

Contributor's Comment:
The differential diagnosis for a single malformed lung lobe in a dog includes congenital

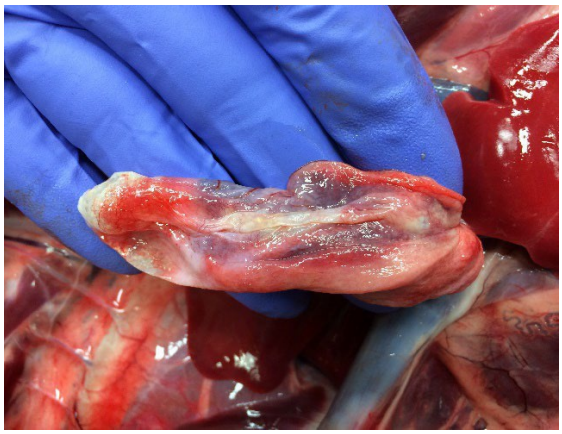

Figure 4-2. Right lung, dog. The right middle lung lobe was small, pale and flaccid. (Photo courtesy of: Department of Veterinary Clinical and Diagnostic Sciences, Faculty of Veterinary Medicine, University of Calgary, 3280 Hospital Dr. NW, Calgary, Alberta T2N 4Z6, Canada, http://vet.ucalgary.ca)

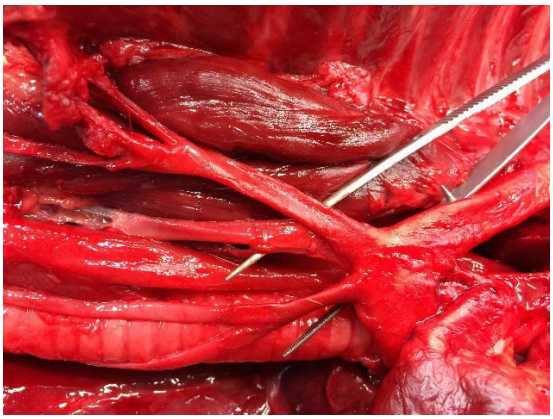

Figure 4-3. Right subclavian artery, dog. The right subclavian artery passes dorsal to and compresses the esophagus. (Photo courtesy of: Department of Veterinary Clinical and Diagnostic Sciences, Faculty of Veterinary Medicine, University of Calgary, 3280 Hospital Dr. NW, Calgary, Alberta T2N 4Z6, Canada, http://vet.ucalgary.ca)

lobar emphysema (CLE), a congenital pulmonary sequestration, and congenital pulmonary airway malformation (CPAM). Based on gross and histologic findings, the first two potential diagnoses can be ruled out in this dog. CLE requires overinflated alveoli or hyperplastic alveoli, whereas the affected lobe in this dog lacks alveoli. A congenital pulmonary sequestration lacks, by definition, any connection with the tracheobronchial tree. In this dog the affected lobe had a lobar bronchus, although it was flattened. Therefore, a presumptive diagnosis of CPAM-like lesion was made based on the similarity of this dog's lesions to described human lesions of CPAM and exclusion of other potential diagnoses.

The term CPAM refers to a spectrum of human airway malformations characterized by abnormal development of various portions of the tracheobronchial tree.[16] Formerly called congenital cystic adenomatoid malformations, CPAMs are well-recognized and relatively common in people. All types of CPAM are characterized by multiple irregular pulmonary cystic structures lined by varying types of epithelium. CPAMs in people are generally subdivided into five types based

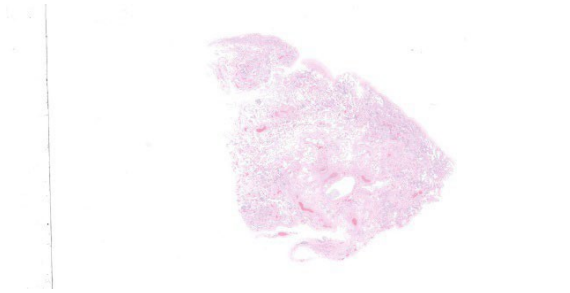

Figure 4-4. Right lung, dog. One section of the right lung is submitted for examination. Normal alveolar architecture is not present. (HE, 7X)

on the anatomic site of the malformation.[16] These are the: proximal tracheobronchial tree (type 0); bronchial/proximal bronchiolar region (type 1); bronchiolar region (type 2); terminal bronchiolar/alveolar duct region (type 3); and alveoli (type 4). There may be overlap between different types, and other classification systems have been proposed.[11,13]

The malformations in the dog in this case report shared overlapping features of human CPAM types 2 and 4. Type 2 CPAM is characterized by the presence of numerous 2-15 mm diameter parenchymal cysts. These consist of dilated bronchiole-like structures lined by cuboidal to columnar epithelium but with mucus-producing cells generally absent. Other congenital abnormalities, including cardiovascular and renal malformations may be present in humans. (Interestingly, this dog had a malformation of the right subclavian artery, although the clinical significance of this was uncertain.) Type 4 CPAM is characterized by larger cysts, typically found toward the periphery of the lobe. These are lined by a mixture of flattened or rounded alveolar lining cells, and occasionally a low cuboidal epithelium. Both type 2 and type 4 human CPAMs typically affect a single lung lobe, as in this dog, and have a good prognosis after surgical resection.[16,17]

Like CPAM, congenital lobar emphysema (CLE) is also a well-recognized congenital lung malformation in humans.[7,8,17] It is characterized by overinflation of a single lung lobe due to partial obstruction of the bronchus supplying that lobe.[10] This obstruction can result from numerous causes, including malformation of the bronchus, external compression of the bronchus by masses or vascular anomalies, or internal obstruction of the

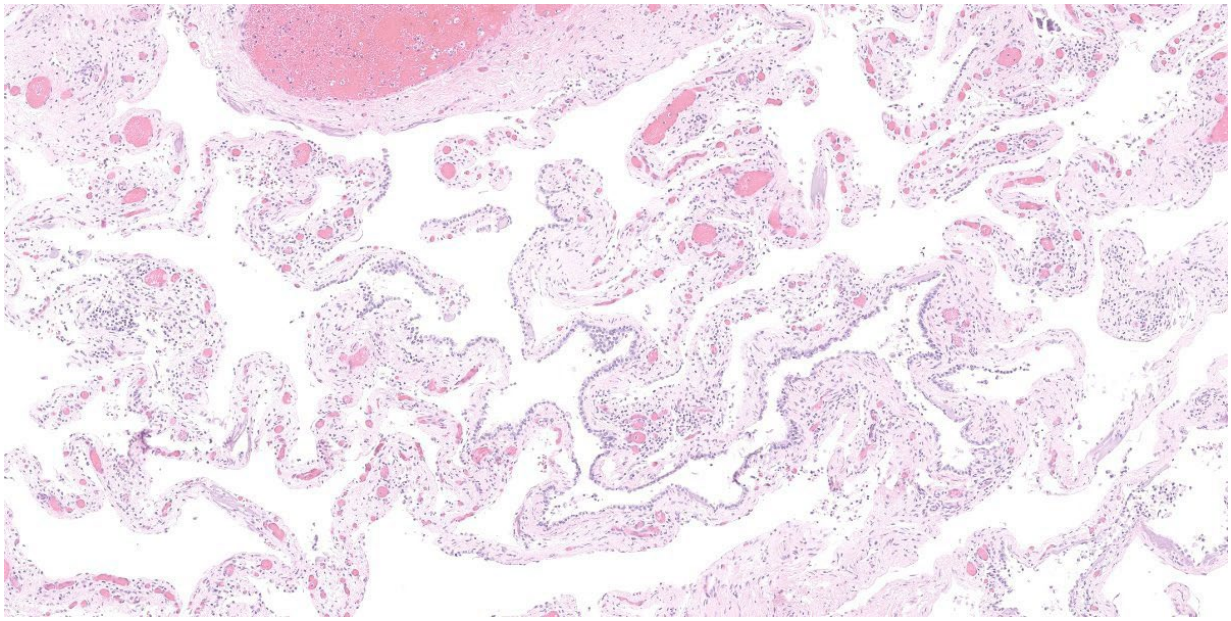

Figure 4-5. Right lung, dog. The lobe is composed of airway-like structures lined by cuboidal epithelium separated by dense fibrous stroma. There is no alveolar parenchyma. (HE, 85X)

bronchial lumen by mucus plugs or granulation tissue.[8] Regardless of the cause, the result is significant lobar overinflation as the partially obstructed bronchus acts as a one way valve and traps air. In the dog described in this case report the lobar bronchus was malformed and partially collapsed, consistent with one cause of CLE. However, in human CLE, alveoli are distended but are otherwise histologically normal, and fibrosis, inflammation or necrosis are rarely seen.[8] This is significantly different from the histologic lung changes in the dog described in this case report.

CLE has been previously reported several times in dogs,[1,5,6,11,12,14,15,19,20] and the dog described in this report has several features in common with many reported canine cases of CLE: the right middle lung lobe was affected; a bronchial structural abnormality was present; bullae and pneumothorax were a feature; and the dog was less than six months old. However, this dog's most significant histologic lesions (absence of recognizable alveolar architecture, with marked interstitial fibrosis) were incompatible with the simple alveolar hyperinflation expected in CLE. Seven human pediatric pathologists were consulted on this case and all agreed that this dog did have a congenital lung malformation and that it was not CLE.

This case highlights that there are multiple types of congenital lung malformations in dogs. It is possible that some reported canine cases of CLE may, in fact, represent CPAM-like lesions. Among published canine CLE reports, two describe histologic features that are suggestive of CPAM type 2[4] or type 4.[11] It may be that these were cases of CPAM-like lesions that were interpreted to be CLE, or that forms of pulmonary disease that share features of both diseases exist in dogs. There are numerous reports of human congenital lung lesions fulfilling criteria for both CPAM and other congenital lung lesions,[7] and this may also prove to be the case in dogs.

It is important to recognize that not all congenital lung malformations in dogs are CLE, and that this diagnosis should not be made based solely on imaging or the gross appearance of an affected lung lobe; CPAM and CLE must be distinguished histologically. In humans there are practical clinical reasons for making an accurate diagnosis of congenital lung lesions. Most importantly, CPAM may progress to malignant neoplasia while CLE does not.[5,7] Lobectomy is generally indicated for CPAM lesions, while CLE may resolve spontaneously and can often be managed conservatively unless it causes mediastinal displacement or severe dyspnea.[7] Because CPAM-like disease in dogs has not been reported previously it is not possible to compare its treatment or prognosis with those of CLE.

Contributing Institution:
Department of Veterinary Clinical and Diagnostic Sciences
Faculty of Veterinary Medicine
University of Calgary
3280 Hospital Dr. NW
Calgary, Alberta T2N 4Z6
Canada
http://vet.ucalgary.ca/

JPC Diagnosis:
Lung: Congenital pulmonary airway malformation with mineralization.

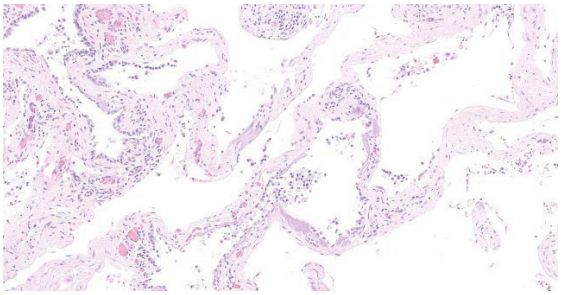

Figure 4-6. Right lung, dog. There is multifocal mineralization of the stroma surrounding airway-like spaces. (HE, 7X)

JPC Comment:
The contributor provides an excellent review of congenital pulmonary airway malformations, congenital lobar emphysema, and the differences between the two diagnoses.

This week's moderator described the six stages of development of the lung: embryonic, pseudoglandular, canalicular, saccular, alveolar, and vascular maturation. Additionally, the moderator described that TTF-1 and HNF-3 are important transcription factors for early lung development.

Congenital pulmonary abnormalities in veterinary species are rare, and one of the more common conditions is accessory lung development in ruminants.[2,9] Accessory lungs are found in extrapulmonary locations, such as in the abdomen and subcutis.[2,9] These lobulated masses consist of haphazardly arranged and variably differentiated pulmonary elements, including bronchi lined by ciliated respiratory epithelium, alveoli, cartilage, and blood vessels.[2,9] While composed of similar elements, pulmonary hamartomas are different in that they are located within the lung. Pulmonary hamartomas are the most commonly diagnosed benign lung tumor in humans, typically discovered as incidental findings on radiographs, and are also occasionally seen in ruminants.[2,3] A recent article described a pulmonary hamartoma in a captive-bred, full-term elk calf found dead. The mass replaced the left caudal lung lobe, encompassed approximately half of the thorax, and compressed the remaining lungs.[2]

The moderator and conference participants also remarked on the presence of mineralization in this case; an explanation for mineralization was not readily apparent on H&E examination.

References:

1. Billet JPHG, Sharpe A. Surgical treatment of congenital lobar emphysema in a puppy. *J Small Anim Pract.* 2002; 43: 84-87.
2. Boggiatto PM, Steven SC, Palmer MV. Pulmonary hamartoma in an elk calf. *J Vet Diagn Invest.* 2023; 3; 5(2): 193-195.
3. Caswell JL, Williams KJ. Respiratory System. In: Grant MG, ed. *Jubb, Kennedy, and Palmer's Pathology of Domestic Animals.* Vol 2. 6th ed. St. Louis, MO: Elsevier. 484-485.
4. Gopalakrishnan G, Stevenson GW. Congenital lobar emphysema and tension pneumothorax in a dog. *J Vet Diagn Invest. 2007;* 19: 322-325.
5. Hancock BJ, Dilorenzo M, Youssef S, Yazbeck S, Marcotte JE, Collin PP. Childhood Primary Pulmonary Neoplasms. *J Pediatr Surg.* 1993; 28: 1133-1136.
6. Herrtage ME, Clarke DD. Congenital lobar emphysema in 2 dogs. *J Small Anim Pract.* 1985; 26: 453-464.
7. Laberge J-M, Puligandla P, Flageole H. Asymptomatic congenital lung malformations. *Semin Pediatr Surg.* 2005; 14: 16-33.
8. Langston C. New concepts in the pathology of congenital lung malformations. *Semin Pediatr Surg.* 2003; 12: 17-37.
9. Lopez A, Martinson SA. Respiratory System, Thoracic Cavities, Mediastinum, and Pleura. In: Zachary JF, ed. *Pathologic Basis of Veterinary Disease.* 7th ed. St. Louis, MO: Elsevier. 2022; 570.
10. Mani H, Suarez E, Stocker JT. The morphologic spectrum of infantile lobar emphysema: a study of 33 cases. *Paediatr Respir Rev.* 2004; 5: S313-S320.
11. Matsumoto H, Kakehata T, Hyodo T, Hanada K, Tsuji Y, Hoshino S, Isomura H. Surgical correction of congenital lobar emphysema in a dog. *J Vet Med Sci*. 66: 217-219.

12. Moon H-S, Lee M-H, Han J-H, Kim S-K, Lee S-G, Lee L, Hyun C. Asymptomatic congenital lobar emphysema in a Pekinese dog. *Journal of Animal and Veterinary Advances*. 2007; 6: 556-558.
13. Puligandla PS, Laberge JM: Congenital Lung Lesions. *Clin Perinatol.* 2012; 39: 331-347.
14. Ruth J, Rademacher N, Ogden D, Rodriguez D, Gaschen L. Imaging diagnosis—congenital lobar emphysema in a dog. *Vet Radiol Ultrasound.* 20111 52: 79-81.
15. Stephens JA, Parnell NK, Clarke K, Blevins WE, DeNicola D. Subcutaneous emphysema, pneumomediastinum, and pulmonary emphysema in a young schipperke. *J Am Anim Hosp Assoc*. 2002; 38: 121-124.
16. Stocker J. Congenital pulmonary airway malformation: a new name for and an expanded classification of congenital cystic adenomatoid malformation of the lung. *Histopathology*. 2002; 41: 424-431.
17. Stocker JT. Congenital and Developmental Diseases. In: Tomashefski Jr JF, ed. *Dail and Hammar's Pulmonary Pathology*. 3rd ed. New York: Springer Science. 2008.
18. Tennant BJ, Haywood S. Congenital bullous emphysema in a dog - a case report. *J Small Anim Pract.* 1987; 28: 109-116.
19. Voorhout G, Goedegebuure SA, Nap RC. Congenital lobar emphysema caused by aplasia of bronchial cartilage in a Pekingese puppy. *Vet Pathol.* 1986; 23: 83-84.
20. Yun S, Lee H, Lim J, Lee K, Jang K, Shiwa N, Boonsriro H, Kimitsuki K, Park C, Kwon Y. Congenital lobar emphysema concurrent with pneumothorax and pneumomediastinum in a dog. *J Vet Med Sci*. 2016; 78: 909-912.

WSC 2022-2023 Self-assessment
Conference 21

1. Granular cell tumors are universally positive for which of the following?
    a. IBA-1
    b. Ubiquitin
    c. S-100
    d. GFAP

2. True or false? Malakoplakia is most commonly seen in female dogs.
    a. True
    b. False

3. Malakoplakia is most commonly seen in which organ in dogs?
    a. Oral cavity.
    b. Vagina
    c. Urinary bladder
    d. Stomach

4. True or false? The large numbers of mitotic figures seen in nodal plexiform vasculopathy hinders its differentiation from metastatic hemangiosarcoma.
    a. True
    b. False

5. Which of the following may progress to malignant neoplasia?
    a. Congenital pulmonary airway malformation
    b. Congenital lobar emphysema
    c. Both
    d. Neither

Please email your completed assessment for grading to Dr. Bruce Williams at bruce.h.williams12.civ@mail.mil. Passing score is 80%. This program (RACE program 33611) is approved by the AAVSB RACE to offer a total of 0.5 CE Credits, with a maximum of 12.5 CE Credits being available to any individual Veterinary Medical Professionals for the 2019-2020 Wednesday Slide Conference. This RACE approval is for the subject matter categories of: SCIENTIFIC using the delivery method of NONINTERACTIVE DISTANCE. This approval is valid in jurisdictions which recognize AAVSB RACE.

Joint Pathology Center
Veterinary Pathology Services

WEDNESDAY SLIDE CONFERENCE 2022-2023

Conference #22 **14 April 2023**

CASE I:

Signalment:
Adult, male, Belgian blue, Ox (*Bos taurus)*

History:
An adult Belgian blue bull was severely depressed, with severe bilateral keratoconjunctivitis, mucopurulent oculo-nasal discharge, and multifocal to coalescing erosive lesions on the muzzle. As the animal's condition started to deteriorate rapidly, the decision to euthanize was taken by the owner.

Gross Pathology:
The animal was in poor body condition. There was bilateral conjunctivitis and multifocal, scattered, round, alopecic cutaneous lesions on the head. The oral mucosa exhibited multifocal, irregular to linear erosions, which were most pronounced on the tongue and the hard palate. The esophageal mucosa exhibited severe multifocal longitudinally oriented linear erosion and ulceration, with scattered multifocal hemorrhage. Generalized lymphadenomegaly and hyperemia of the vertebral rete mirabilis were also observed.

Laboratory Results:
PCR targeting the polymerase gene of AlHV-2 and OvHV-2 was carried out on samples from the tongue and lymph node. Both samples yielded a positive result for OvHV-2 DNA.

Microscopic Description:
Oral mucosa. Diffusely, affecting both small and larger vessels (both arteries and veins), there is mild to moderate perivascular inflammation, composed of lymphocytes, plasma cells and fewer macrophages. The endothelial cells are often hypertrophic with plump nuclei which protrude in the vascular lumen. The tunica media of medium and large-sized arteries is expanded by moderate to large numbers of inflammatory cells and, in some arteries, there is multifocal accumulation of bright eosinophilic material (fibrinoid necrosis). The overlying oral mucosa shows focally extensive moderate intracellular and intercellular edema and necrosis, with erosion

Figure 1-1. Presentation, ox. A Belgian blue bull was severely depressed, with severe bilateral keratoconjunctivitis, mucopurulent oculo-nasal discharge, and multifocal to coalescing erosive lesions on the muzzle. (Photo courtesy of: Department of Veterinary Pathology and Public Health, Institute of Veterinary Science, University of Liverpool, Leahurst campus, CH64 7TE, UK. https://www.liverpool.ac.uk/vetpathology/)

of the epithelial layer and sloughing of the epithelial cells and eosinophilic necrotic cellular debris. There is also mild to moderate multifocal lymphoplasmacytic infiltration of the epithelium. Inflammation and severe hyperemia are present in the superficial lamina propria, particularly extending between rete pegs.

Contributor's Morphologic Diagnosis:
Oral mucosa: Moderate to severe diffuse subacute lymphoplasmacytic vasculitis with erosive stomatitis.

Contributor's Comment:
Malignant catarrhal fever (MCF) is a viral disease which affects many different species of the order *Artiodactyla*, predominantly ruminants. Currently, several different viruses are considered causative agents of MCF; those which have been classified all belong to the genus *Macavirus* (malignant catarrhal virus), subfamily *Gammaherpesvirinae* and include *Alcelaphine gammaherpesvirus 1* (AlHV-1), *Alcelaphine gammaherpesvirus 2* (AlHV-2), *Ovine gammaherpesvirus 2* (OvHV-2) and *Caprine gammaherpesvirus 2* (CpHV-2) (https://talk.ictvonline.org/taxonomy/). These viruses, and others, including Ibex-MCF virus and another uncharacterized

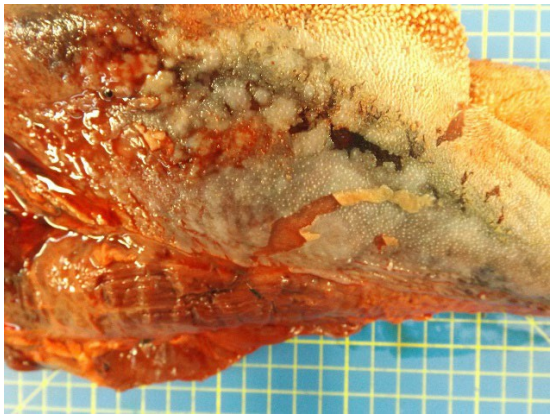

Figure 1-2. Tongue, ox. There are extensive ulcers on the tongue. (Photo courtesy of: Department of Veterinary Pathology and Public Health, Institute of Veterinary Science, University of Liverpool, Leahurst campus, CH64 7TE, UK. https://www.liverpool.ac.uk/vetpathology/)

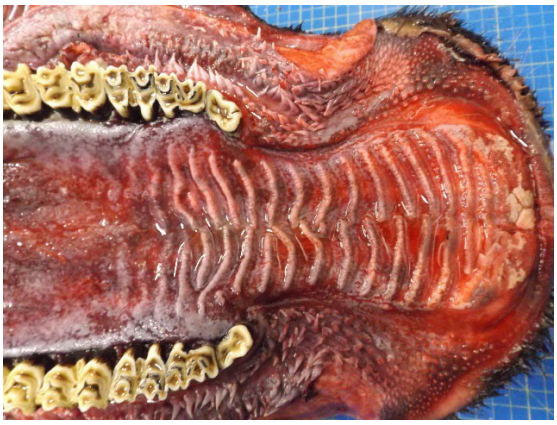

Figure 1-3. Palate, ox. There are extensive ulcers on the palate. (Photo courtesy of: Department of Veterinary Pathology and Public Health, Institute of Veterinary Science, University of Liverpool, Leahurst campus, CH64 7TE, UK. https://www.liverpool.ac.uk/vetpathology/)

virus isolated from clinically affected white-tailed deer (WTD-MCFV) are responsible for natural outbreaks of MCF.[4,8,13] Under experimental conditions, *Hippotragine gammaherpesvirus 1* (HipHV-1) induced MCF in rabbits, although naturally occurring infections are not reported in this species.[17] Gammaherpesviruses of ruminants are highly cell-associated lymphotropic herpesviruses. The key features shared among all the macaviruses, is the presence of the 15-A antigen epitope and high degree of similarity of the polymerase gene.[13]

The MCF-associated viruses have a recognized reservoir host, for example, sheep and wildebeest for OvHV-2 and AlHV-1, respectively. In the reservoir host, these viruses are usually clinically silent in contrast to susceptible species, in which infection causes clinical disease. The severity of the clinical signs varies greatly according to the species affected; some animals, for example bison (*Bison* spp.) or Pere's David deer (*Elaphurus davidianus*), show a high susceptibility to disease, while others such as the white-tailed deer (*Odocoileus virginianus*), appear to be more resistant.[11] The main source of infection

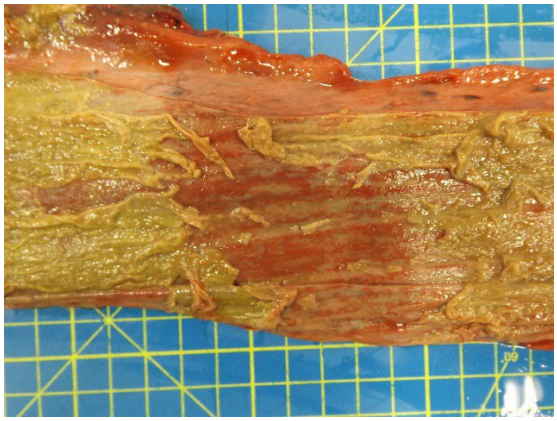

Figure 1-4. Tongue, ox. There are large areas mucosal ulceration in the esophagus. (Photo courtesy of: Department of Veterinary Pathology and Public Health, Institute of Veterinary Science, University of Liverpool, Leahurst campus, CH64 7TE, UK. https://www.liverpool.ac.uk/vetpathology/)

is the reservoir host, in which infection is transmitted from adults to young animals at 2-3 months of age, while clinically susceptible species usually act as dead-end hosts; in the latter, however, vertical transmission and abortion has sporadically reported.[5] Similar to other herpesvirus infections, the virus is shed through ocular and nasal discharges, which can then be inhaled or ingested via contaminated water or food. Even though the virus remains viable for only relatively brief periods outside the host animal, long distance transmission of OvHV-2 has been reported, causing MCF in bison.[9]

Clinical signs of MCF are similar, regardless of the causative gamma herpesvirus, but can be highly variable between individual animals. The most common and well-known expression of clinical disease is the "head and eye" form, in which the main clinical signs comprise depression, fever, keratoconjunctivitis, oral ulceration, lymphadenopathy and rhinitis with nasal discharge. However, gastro-intestinal, urinary, and neurological signs can be observed.[18]

Postmortem examination can reveal a wide range of lesions; bilateral keratoconjunctivitis, erosion of the nares with adhered crusts, and bilateral oculo-nasal discharge are typical gross findings. Cutaneous lesions consisting of exanthemata with overlying crusting are described on the thorax, abdomen, inguinal regions, perineum, and, less often, on the head.[13] In the gastrointestinal system the most common lesions are observed in the oral cavity. Erosive lesions develop first on the lips, especially close to labial commissure, then develop on the tongue before extending over the oral mucosa, from the gingiva to the palate.[13] Similar lesions can be observed also in the esophagus, the forestomachs and abomasum. The liver may show mild diffuse enlargement with multifocal pinpoint foci of white discoloration. Petechiae and erosions have also been described on the gall bladder mucosa. Respiratory lesions may be present, especially in the upper airway, ranging from mild congestion to fibrinous tracheobronchitis. Lesions in the urinary system are very characteristic and specific but are not always present; these consist of multifocal interstitial nephritis with infarcts giving a mottled appearance to the kidneys. In the lower urinary tract, erosion and hemorrhage are reported on the mucosa of the renal pelvis and the urinary bladder. Lymphadenomegaly is very common in most hosts and may be generalized or grossly affecting only a proportion of lymph nodes. Likewise, hemolymph nodes are affected and appear swollen. Edema of the meningeal vessels is also reported.[18]

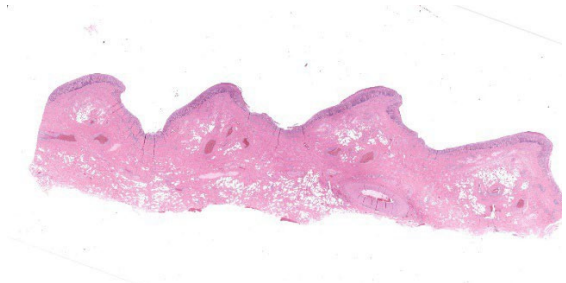

Figure 1-5. Oral mucosa, ox. A section of multifocally ulcerated oral mucosa is submitted. (HE, 6X)

The gross findings may be variable in distribution and severity, depending on the progression of the disease: acute MCF with rapid mortality is more likely to be associated with fewer grossly-evident lesions. In these cases, histopathology is an invaluable key diagnostic tool. Histologically, diffuse accumulation of mononuclear inflammatory cells around arteries and veins with fibrinonecrotizing vasculitis constitutes the hallmark of the disease; the distribution of these changes can be variable, affecting some tissues more severely than others, but are always present.[13,18] The infiltrate is mainly composed of lymphoid cells with large, open nuclei and prominent nucleoli, with occasional plasma cells and small lymphocytes.[18] Alongside these lesions, lymph nodes exhibit diffuse hyperplasia of the paracortical areas and necrosis and/or apoptosis can be observed in the skin, urinary and gastrointestinal tracts. Autolysis, accelerated by hyperthermia which occurs before death, can hamper diagnosis, especially in those cases where the lesions are mild.[13]

The gross and histopathological features are well recognized, however, the pathogenesis of MCF is not fully understood.[7] Viral infection of susceptible hosts induces a lymphocytic proliferation, mainly targeting vessels, with the development of severe arteritis/phlebitis and consequent necrosis affecting several organs. The majority of these lymphocytes show a CD8+ immunophenotype, but only a small fraction show evidence of viral infection.[13] Furthermore, large granular lymphocyte-like morphology and non-MHC restricted killing activity is observed in infected lymphocytes;[1] *in vitro* experiments indicated that the cells are resistant to concanavalin A while responsive to cyclosporin A.[7] Taken together, these findings seem to indicate that viral infection causes an autoimmune disease provoked by lymphocytic dysregulation, rather than a direct effect of the viral infection of lymphocytic cells. However, in experimental infection of bison an unexpectedly large number of virus-infected T cells was detected, suggesting that both direct viral effects and indirect immune responses may play a role in MCF pathogenesis.[2,7,12] Further studies are needed in order to solve this discrepancy. Recently, the role of AlHV-1 sema, a member of the semaphorin protein family, has been studied. An immune-escaping activity has been shown *in vitro*; however, absence of viral AlHV-1 sema had did not impair MCF induction and associated lymphoproliferative lesions in experimentally infected rabbits.[11]

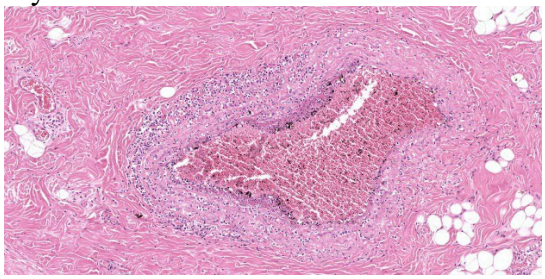

Figure 1-6. Oral mucosa, ox. There is a moderately dense cellular infiltrate within the adventitia and to a lesser extent, the media of affected vessels. (HE, 114X)

Contributing Institution:
Department of Veterinary Pathology and Public Health, Institute of Veterinary Science, University of Liverpool, Leahurst campus, CH64 7TE, UK
https://www.liverpool.ac.uk/vetpathology/

JPC Diagnosis:
Hard palate mucosa: Arteritis, lymphocytic and necrotizing, multifocal to coalescing, moderate, with ulceration.

JPC Comment:
This contributor provides a great description of this classic case of OvHV-2 malignant catarrhal fever in an ox. This week's contributor, Dr. Patricia Pesavento of the University of California at Davis, discussed that when there is mucosal or epithelial ulceration with-

out an evident cause on the surface, it is important to examine the arteries subjacent the ulcer in a search for vascular lesions. In this case, there is subtle vacuolation to the endothelium of the large artery within the section, and, more superficially, the medium caliber arteries are more severely affected with transmural, predominantly T-cells disrupting the arterial wall and lifting the intima, presumably arising from the capillary bed of the adventitia. The moderator also stressed the importance of being specific in vascular lesions: in this case, the lesion specifically affects medium caliber arteries, thus arteritis was included in the morphologic diagnosis as opposed to vasculitis. This localization is important in sorting other potential causes.

The moderator and conference participants discussed bovine viral diarrhea virus as a differential which would cause vascular lesions, and for that the gross images of the palate and esophagus, these would be reasonable differentials. The moderator also described how the herpesviruses which contribute to MCF are characteristically lymphoproliferative, so a pleomorphic population of lymphocytes may weigh more in favor of MCF. Aside from PCR for OvHV2 (which was conducted in this case and is the most common cause of MCF in the United States), IHC for BVDV or ISH for the MCF agent would allow for differentiation of these two entities.

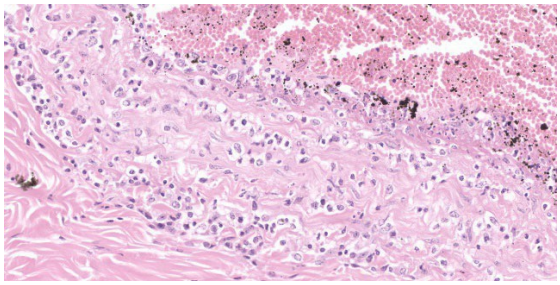

Figure 1-7. Oral mucosa, ox. The arteriolar mural infiltrate is a mixed cellular population of large and small lymphocytes and macrophages. (HE, 374X)

There are some histologic features which point to a location more specific than oral mucosa: the distribution of submucosal adipose, the presence of an elastic artery close to the mucosal surface, and especially the undulating surface point to the hard palate.

While OvHV-2 typically does not cause clinical signs in the host-adapted species, in a 2018 *Vet Pathol* report, Dr. Pesavento et. al showed that OvHV-2 is associated with systemic necrotizing vasculitis and can sporadically cause arteritis in sheep similar to MCF in cattle.[14] This study included a collection of cases previously diagnosed as idiopathic polyarteritis ("polyarteritis nodosa") and using the in-situ hybridization probe specific for OvHv-2, demonstrated viral nucleic acid in lymphocytes associated with vasculitis in small to medium caliber arteries in all cases.[14] This work showed that OvHv-2 driven MCF may occur in the adapted host.[14]

OvHV-2 associated MCF in cattle is generally fatal, and chronic infection and recovery are both considered rare.[10,16] A histologic hallmark of chronic MCF in cattle is neointimal hyperplasia characterized by proliferation of spindle (myofibroblast) cells between the endothelium and internal elastic lamina; this may be accompanied by obliterative arteriopathy due to luminal narrowing.[10,16] Other arterial lesions described in chronic MCF include disruption of the internal elastic lamina and attenuation or loss of the tunica media. A 2022 report in the *Journal of Veterinary Diagnostic Investigation* also reported lymphocytic hypophysitis in a chronic case of OvHV-2 associated MCF, and the lymphocytes positively labeled for OvHV-2 ISH.[10]

T-cells are described as the predominant inflammatory cell in the vascular lesions of

MCF; however, a recent study evaluating rete mirabile lesions of 34 cases of OvHV-2 MCF in cattle, water buffalo, and bison found that macrophages were present in equal or greater numbers to T cells in all cases.[16] This raises the possibility that the pathogenesis of vascular damage and necrosis may be secondary to macrophage activity.[16] This study also evaluated the expression of viral protein oLANA and ov-IL10 mRNA, products of latency-associated genes, and demonstrated that the virus infects many more cells than just T-cells: endothelial cells, smooth muscle cells, and macrophages all demonstrated immunohistiochemical staining for oLANA and in-situ hybridization for ov-IL10 mRNA.[16]

As the contributor describes, there are a group of MCF viruses from the genus Macavirus, sub-family Gammaherpesvirinae, family Herpesviridae, that cause MCF disease in susceptible hosts, and a recent report described an Ibex-MCF virus outbreak in captive duikers (small antelope).[2] The virus was presumed to be spread indirectly from captive ibex in an enclosure 35 meters away, and cases in duikers were associated with times of parturition in the ibex.[2] The disease was fatal, and clinical signs included anorexia, ataxia, and diarrhea or sudden death.[2] On necropsy, mucosal ulceration was lacking, however, most of the animals had pulmonary ecchymoses, lymphadenomegaly, renomegaly, mucosal hemorrhage in the urinary bladder, and ascites.[2] Half of the cases also had hydrothorax and hepatomegaly.[2] Histologically, there were dense and wide perivascular lymphocytes and scattered (rare) fibrinoid vascular necrosis in multiple organs, demonstrating remarkable and chronic lymphoproliferation, with ibex-MCF identified in all cases using PCR and demonstrated in lymphocytes using ISH.[2] Most of the animals were deficient in copper, and the authors raised the possibility of copper deficiency

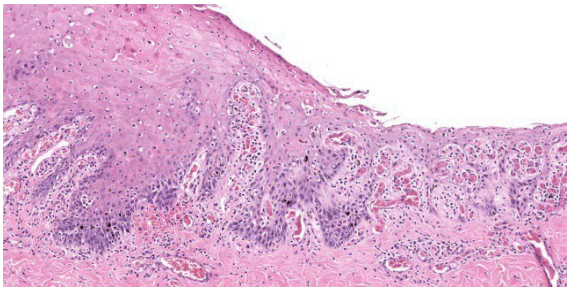

Figure 1-8. Oral mucosa, ox. There is ulceration of the mucosa overlying affected vessels. (HE, 340X)

compromising the duikers' immune responses, predisposing the animals to overwhelming viral infection.[2] Clinically normal but infected ibex were culled and lacked any gross or histologic lesions associated with the virus.[2]

References:

1. Burrells C, Reid HW. Phenotypic analysis of lymphoblastoid cell lines derived from cattle and deer affected with "sheep-associated" malignant catarrhal fever. *Vet Immunol Immunopathol*. 1991;29(1-2):151-161.
2. Carvallo FR, Uzal FA, Moore JD, et al. Ibex-Associated Malignant Catarrhal Fever in Duikers (*Cephalophus Spp*). *Vet Pathol.* 2020; 57(4): 577-481.
3. Cunha CW, Gailbreath KL, O'Toole D, et al. Ovine herpesvirus 2 infection in American bison: virus and host dynamics in the development of sheep-associated malignant catarrhal fever. *Vet Microbiol*. 2012;159(3-4):307-319.
4. Gasper D, Barr B, Li H, et al. Ibex-associated malignant catarrhal fever-like disease in a group of bongo antelope (Tragelaphus eurycerus). *Vet Pathol*. 2012;49(3):492-497.
5. Headley SA, Pimentel LA, Oliveira VH, et al. Transplacental Transmission of Ovine Herpesvirus 2 in Cattle with Sheep-associated Malignant Catarrhal Fever. *J Comp Pathol*. 2015;153(4):206-211.

6. Hierwerger MM, Boujon CL, Kauer RV, et al. Cerebral Ovine Herpesvirus 2 Infection of Cattle is Associated with a Variable Neuropathological Phenotype. *Vet Pathol*. 2020; 58(2): 384-395.
7. Li H, Cunha CW, Taus NS, Knowles DP. Malignant catarrhal fever: inching toward understanding. *Annu Rev Anim Biosci*. 2014;2:209-233.
8. Li H, Dyer N, Keller J, Crawford TB. Newly recognized herpesvirus causing malignant catarrhal fever in white-tailed deer (Odocoileus virginianus). *J Clin Microbiol*. 2000;38(4):1313-1318.
9. Li H, Karney G, O'Toole D, Crawford TB. Long distance spread of malignant catarrhal fever virus from feedlot lambs to ranch bison. Can Vet J. 2008;49(2):183-185.
10. Milliron SM, Stranahan LW. Rivera-Velez AG, et al. Systemic proliferative arteriopathy and hypophysitis in a cow with chronic ovine herpesvirus 2-induced malignant catarrhal fever. *J Vet Diagn Invest.* 2022; 34(5): 905-908.
11. Myster F, Palmeira L, Sorel O, et al. Viral semaphorin inhibits dendritic cell phagocytosis and migration but is not essential for gammaherpesvirus-induced lymphoproliferation in malignant catarrhal fever. *J Virol.* 2015;89(7):3630-3647.
12. Nelson DD, Taus NS, Schneider DA, et al. Fibroblasts express OvHV-2 capsid protein in vasculitis lesions of American bison (Bison bison) with experimental sheep-associated malignant catarrhal fever. *Vet Microbiol*. 2013;166(3-4):486-492.
13. O'Toole D, Li H. The pathology of malignant catarrhal fever, with an emphasis on ovine herpesvirus 2. *Vet Pathol*. 2014;51(2):437-452.
14. Pesavento PA, Dange RB, Ferreras C. Systemic Necrotizing Vasculitis in Sheep is Associated with Ovine Herpesvirus 2. *Vet Pathol.* 2018; 56(1): 87-92.
15. Russell GC, Stewart JP, Haig DM. Malignant catarrhal fever: a review. *Vet J*. 2009;179(3):324-335.
16. Saura-Martinez H, Al-Saadi M, Stewart JP, Kipar A. Sheep-Associated Malignant Catarrhal Fever: Role of Latent Virus and Macrophages in Vasculitis. *Vet Pathol.* 2020. 58(2): 332-345.
17. Schock A, Reid HW. Characterisation of the lymphoproliferation in rabbits experimentally affected with malignant catarrhal fever. *Vet Microbiol*. 1996;53(1-2):111-119.
18. Uzal FA, Plattner BL, Hostetter J. Malignant catarrhal fever. In: Maxie MG, ed. *Jubb, Kennedy and Palmer's Pathology of Domestic Animals*. 6th ed. St. Louis, Missouri: Elsevier; 2016:131-136.

CASE II:

Signalment:
1-year-old, male, Domestic Shorthair Cat (*Felis catus*)

History:
A 1-year-old indoor male Domestic Shorthair cat was found deceased with no premonitory signs. The history indicated a prolapsed rectum had been surgically repaired in the past.

Gross Pathology:
Grossly, the lungs were diffusely edematous, mildly consolidated, and mottled dark red to red with petechial hemorrhages. The distal trachea and bronchi contained moderate amounts of yellow mucus and foamy fluid. There were two 4-5 cm long white worms in the right cardiac ventricle, located at the tricuspid valve. An oval 1 cm area of intimal hemorrhage was present in the base of the pulmonary artery. The heart was within normal limits for size and shape.

Laboratory Results:
No laboratory findings reported.

Microscopic Description:
Multifocally, the tunica intima of the small and medium-sized pulmonary arteries are markedly thickened and have villous-like proliferations that protrude into the lumens, partially or completely occluding the arteries. The intimal proliferations are often lined by hypertrophied endothelial cells and consist of fibrous connective tissue with hyperplastic fibroblasts and smooth muscle cells. Moderate to marked infiltration by eosinophils, macrophages, fewer lymphocytes, and plasma cells are present in the affected tunica intima, occasionally associated with minimal hemorrhage. In some arteries, the lumen is completely obliterated by endothelial proliferation, with a few small blood vessels lined by hypertrophied endothelial cells. Often, the internal elastic lamina is effaced and obscured by the intimal proliferation and inflammation. Most of the pulmonary arteries and arterioles, with or without intimal changes, are narrowed and have moderate hypertrophy of the tunica media. The alveolar septa adjacent to the affected arteries are moderately thickened by infiltration by eosinophils, macrophages, and fewer lymphocytes. Occasionally, the alveoli contained increased numbers of foamy macrophages, fewer eosinophils, hemorrhage, rare edema, and minimal

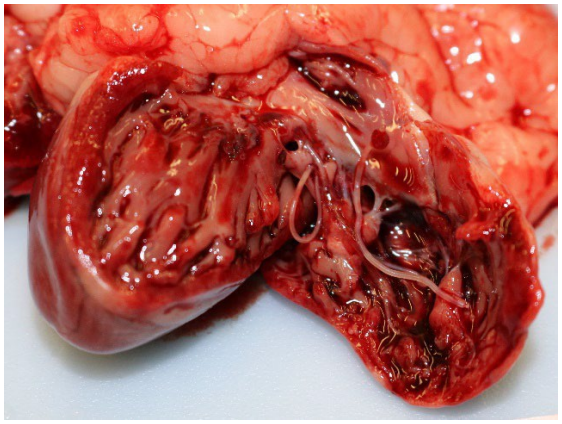

Figure 2-1. Heart, cat. Two heartworms were in the right ventricle. (Photo courtesy of: Connecticut Veterinary Medical Diagnostic Laboratory, http://cvmdl.uconn.edu/)

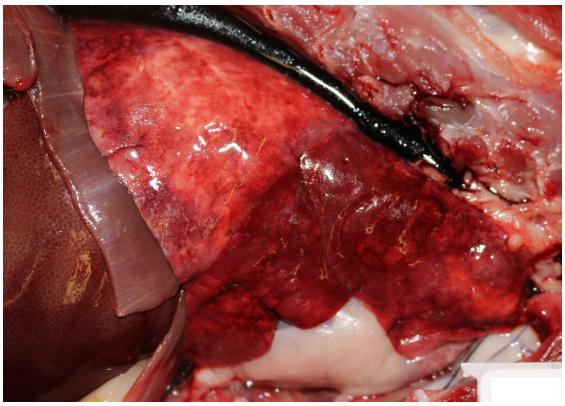

Figure 2-2. Lung, cat. Grossly, the lungs were diffusely edematous, mildly consolidated, and mottled dark red to red with petechial hemorrhages. (Photo courtesy of: Connecticut Veterinary Medical Diagnostic Laboratory, http://cvmdl.uconn.edu/)

amounts of fibrin. There are multiple granular, linear, or round concentric basophilic mineralized deposits in the pulmonary capillaries, bronchiolar smooth muscles, and arterial media. Round concentric deposits, some resembling corpora amylacea, are 15-20 microns in diameter and often located in the connective tissue around arteries and bronchi. The pulmonary capillaries are diffusely congested.

Contributor's Morphologic Diagnoses:
Lung, arteries: (1) Endarteritis, proliferative and eosinophilic, chronic, multifocal, moderate to marked, with occasional luminal occlusions and re-canalizations; (2) Medial hypertrophy, diffuse, mild to moderate.

Lung: (1) Interstitial pneumonia, eosinophilic and histiocytic, multifocal, mild; (2) Mineralization, multifocal, moderate

Contributor's Comment:
Dirofilaria immitis commonly causes clinical diseases in dogs, but can infect other mammals including cats, wild felids, wild canids, and rarely humans.[15] Typical histological lesions in lungs in both dogs and cats caused by

D. immitis are villous proliferation of the arterial intima with medial hypertrophy and eosinophilic infiltrates.[12,15]

Mosquitoes play the main role in the heartworm lifecycle. The first, second, and early third stage larvae of *D. immitis* are obligate parasites of mosquitoes of the genera *Aedes, Culex* or *Anopheles*. In mosquitoes, larvae develop to the infective stage in the malpighphian tubules and then migrate to the proboscus. When mosquitoes feed on hosts, the infective third stage larvae deposit on the skin and enter through the bite wound. The third stage larvae molt to the fourth stage and become immature adults in the connective tissue. Finally, immature adults enter the veins and migrate to the pulmonary arteries, 70-90 days postinfection. The immature adults mature in 3 months to adults, after which time female worms produce microfilariae. The average pre-patent period is 6-8 months for *D. immitis*.[10,11,15]

Dogs are the natural definitive host of *D. immitis*, and canine dirofilariasis occurs when heartworms become adults and produce microfilariae. In dogs, the most common clinical presentation is a chronic congestive right

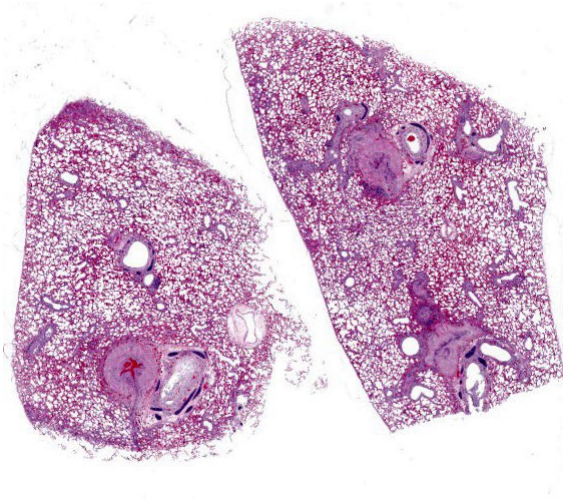

Figure 2-3. Lung, cat. Two sections of lung are submitted for examination. Multifocally, pulmonary arteries are markedly thickened and tortuous. (HE, 6X)

cardiac failure with more than 30 adult worms, and it is usually seen in dogs older than 5 years with continuous or multiple infections. Mechanical irritation by adult worms and microfilariae can cause pulmonary arterial sclerosis and hypertension, leading to chronic heart failure. Also, large numbers of adult *D. immitis* (usually more than 100) infecting the right atrium and vena cava can result in acute venous obstruction and shock, known as vena cava syndrome.[15]

The prevalence and pathogenesis of feline dirofilariasis is somewhat different from dogs.[10,11] The distribution of feline dirofilariasis parallels that of dogs, but the overall prevalence is between 5-10 % of that in dogs in any given area.[16] Mosquitos feeding preferences and the poor suitability of cats as definitive hosts may be reasons for this low prevalence.[10] Since cats are atypical hosts for *D. immitis*, the majority of worms are cleared in the immature adult stage, and there are typically only 2-4 adult worms infect the heart. Due to low numbers of adult worms and poor suitability, cats tend to be amicrofilaremic or have only a short (2-3 months) microfilaremic period.[6,10,11] Vena cava syndrome caused by a large burden of *D. immitis* infection has been described rarely in cats.[12] Similar to dogs, chronic heartworm disease with adult worms occurs in cats, but congestive right cardiac failure or pulmonary hypertension are rare.[17]

Chronic feline dirofilariasis caused by adult worm infection can cause death,[10,11] as seen in this case. Cats may be asymptomatic or show chronic respiratory signs such as coughing or intermittent dyspnea during the infection.[1,6] Vomiting is also a relatively common finding, reported in about half of the cases with unknown pathogenesis [1]. Unlike most cases of canine dirofilariasis, acute respiratory distress and sudden death with adult

heartworms in cats are attributed to embolization of dead worms causing pulmonary arterial infarction and circulatory collapse.[6,10,11] Adult heartworms are believed to secrete a product that suppresses the activity of the pulmonary intravascular macrophage (PIM), the main component of the reticuloendothelial system in cats; PIM are not present in normal dogs.[8] Decreased PIM activity results in an anti-inflammatory reaction and minimizes the clinical signs of cats having adult worms, but the death of adult worms triggers an intense inflammatory reaction.[8,10]

Additionally, there is a condition known as heartworm-associated respiratory disease (HARD) in cats, that is caused by the death of larvae in caudal pulmonary arteries before they migrate into the heart.[7,10,15,] Clinical respiratory signs associated with HARD are similar to chronic feline dirofilariasis, but occur around 3-6 months post-infection without any adult worms.[7,10] The strong inflammatory response induced by larval death is also hypothesized to be due to the activity of PIM only seen in cats.[8,10]

Histological presentation of chronic feline dirofilariasis and HARD is similar, but HARD has less severe lesions.[3,17] The fibromuscular intimal proliferation has been considered a reaction to heartworms, but a response to intracellular bacteria *Wolbachia* harbored by *D. immitis* may be involved.[10,12,14] Arterial medial hypertrophy is another common finding in both cats and dogs infected with *D. immitis*.[12,15] In cats, this change can be spontaneous, and also can be caused by other parasites such as *Aelurostrongylus abstrusus* and *Toxocara cati*.[12,14] However, a recent experimental study revealed a strong association of smooth muscle hypertrophy of arteries, bronchi, and bronchioles in cats infected with *D. immitis*.[7] Without any adult heartworms, pulmonary proliferative and/or eosinophilic endarteritis is suggestive for larval *D. immitis* infection. As with hypertrophy of the arterial tunica media, migration of other larval worms (including *Toxocara* spp), is known to cause eosinophilic endarteritis in feline lungs.[14]

Aberrant migration of *D. immitis* occurs with greater frequency in cats than in dogs.[9,14] Aberrant migration of larvae to body cavities, eyes, and central nervous system are more common in cats, inducing an inflammatory response at the site of migration.[9,10] Recently, aberrant migration of heartworms to the femoral artery causing hind limb paresis was described in a cat.[13] Migrating *D. immitis* should be considered for any nematodes found anywhere in cats.

There was conversation about concentric mineral deposits in the pulmonary connective tissues in this cat as to whether they were dead larvae or spontaneous mineralization. Some of deposits had fragmented or concentric structures but were not associated with any inflammation, and there were no histologically identifiable larvae. It is known that dead *D. immitis* tend to induce strong inflammation.[9] No other cause for arterial mineralization was identified on anatomic examination, and antemortem bloodwork was not available. The cause of this widespread mineralization was not identified.

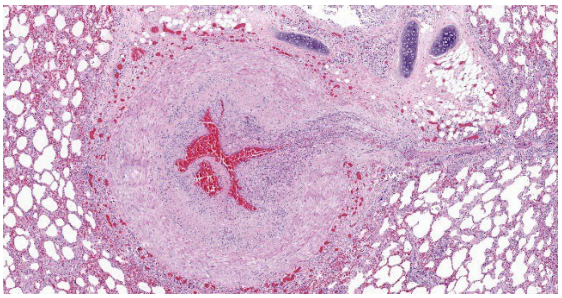

Figure 2-4. Lung, cat. A cross section of a pulmonary artery shows a recanalized lumen with marked intimal hyperplasia, mural thickening, and marked inflammation of the intima and adventitia. (HE, 42X)

Contributing Institution:
Connecticut Veterinary Medical Diagnostic Laboratory
http://cvmdl.uconn.edu/

JPC Diagnosis:
Lung, arteries, and arterioles: Endarteritis, proliferative and eosinophilic, diffuse, severe, with marked smooth muscle hypertrophy.

JPC Comment:
The fundamental histologic finding in this case is neointimal proliferation of pulmonary arteries. During the conference, the moderator and conference participants discussed presence of visible small caliber blood vessels in the expanded region of the tunica inwhich represents either neovascularization or hypertrophy of existing, penetrating vasa vasorum. Indeed, immunohistochemical and special stains were helpful to evaluate the character of the intimal proliferation: negative reactivity to smooth muscle actin and abundant factor 8 immunoreactivity confirmed that the majority of the proliferation is from small caliber vessels. Conference participants also discussed the presence of interstitial pneumonia, but felt the changes were mild and did not warrant morphologic diagnosis. The fatal outcome of such a low parasite load in cats is enigmatic, in this case there were no filaria, nor evidence of emboli (in sections examined)

The contributor provides a good summary of the histologic lesions of the pulmonary vasculature in cats, as well as the parasite life cycle, clinical signs, and pathogenesis of this disease. Heartworm infection may also lead to membranoproliferative glomerulonephritis due to deposition of antigen-antibody complexes, or to glomerular damage fraying and thickening glomerular basement membrane, both of which lead to proteinuria.[5,15]

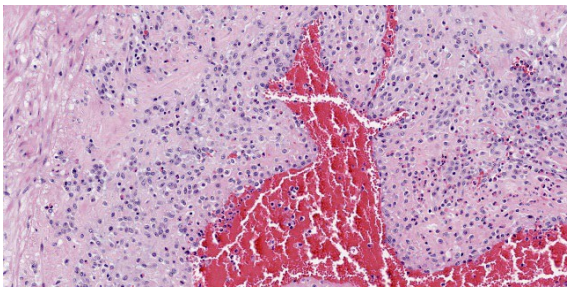

Figure 2-5. Lung, cat. Higher magnification of the pulmonary artery show marked intimal hyperplasia with segmental loss of the endothelium, and infiltration of the markedly thickened intima by moderate numbers of macrophages and eosinophils. (HE, 215X)

Dirofilaria can cause similar lesions in dogs. Dogs also can harbor *Angiostrongylus vasorum*, which can cause proliferative endarteritis, intimal proliferation, and medial hypertrophy in the lung.[4] This metastrongyle differs from *D. immitis* in both life cycle and pathogenesis. The intermediate host of *A. vasorum* is a mollusk (snail or slug), which is ingested by a dog. Larvae migrate through the lymph nodes, where they molt, and adults reside in the pulmonary arteries and right ventricle.[2,4] Eggs pass into the pulmonary vessels, hatch, and penetrate into alveolar lumen, eventually to be coughed up, swallowed, and passed into the feces. These eggs and larvae can cause granulomatous pneumonia, occasionally forming larger granulomas containing mixed inflammatory cells, while the adult worms cause characteristic proliferative endoarteritis.[4]Histologically, the presence of eggs in the granulomatous inflammation and within adult female nematodes is a helpful differentiating feature between *A. vasorum* and *D. immitis*; other differences include a thin coelomyarian musculature and a large intestine in *A. vasorum* compared to tall coelomyarian musculature and a small intestine in *D. immitis*.[4]

References:

1. Atkins CE, DeFrancesco TC, Coats JR, et al. Heartworm infection in cats: 50 cases (1985-1997). *J Am Vet Med Assoc*. 2000; 217(3):355-8.
2. Bowman DD. Helminths. In: *Georgis' Parasitology for Veterinarians*. 11th ed. St. Louis, MO: Elsevier. 2021; 203.
3. Browne LE, Carter TD, Levy JK, et al. Pulmonary arterial disease in cats seropositive for *Dirofilaria immitis* but lacking adult heartworms in the heart and lungs. *Am J Vet Res*. 2005; 66(9):1544-1549.
4. Caswell JL, Williams KJ. Respiratory System. In: Maxie MG, ed. *Jubb, Kennedy, and Palmer's Pathology of Domestic Animals.* Vol 2. 6th ed. St. Louis, MO: Elsevier; 2016: 586-587.
5. Cianciolo RE, Mohr FC. Urinary System. In: Maxie MG, ed. *Jubb, Kennedy, and Palmer's Pathology of Domestic Animals.* Vol 2. 6th ed. St. Louis, MO: Elsevier; 2016: 418.
6. Dillon R. Feline Dirofilariasis. *Vet Clin North Am Small Anim Prac*t. 1984; 14(6): 1185–1199.
7. Dillon AR, Blagburn BL, Tillson M, et al. Heartworm-associated respiratory disease (HARD) induced by immature adult *Dirofilaria immitis* in cats. *Parasit Vectors*. 2017; 10(suppl 2):514.
8. Dillon AR, Warner AE, Brawner W, et al. Activity of pulmonary intravascular macrophages in cats and dogs with and without adult *Dirofilaria immitis*. *Vet Parasitol*. 2008; 158(3):171-6.
9. Donahoe JM. Experimental infection of cats with *Dirofilaria immitis*. *J Parasitol*. 1975; 61:599-605.
10. Lee AC, Atkins CE. Understanding feline heartworm infection: disease, diagnosis, and treatment. *Top Companion Anim Med*. 2010; 25(4):224-230.
11. Lister AL, Atwell RB. Feline heartworm disease: a clinical review. *J Feline Med Surg*. 2008; 10:137-144.
12. McCracken MD, Patton S. Pulmonary arterial changes in feline dirofilariasis. *Vet Pathol*. 1993; 30:64-69.
13. Oldach MS, Gunther-Harrington CT, Balsa IM, et al. Aberrant migration and surgical removal of a heartworm (Dirofilaria immitis) from the femoral artery of a cat. *J Vet Intern Med*. 2018; 32(2):792-796.
14. Parsons JC, Bowman DD, Grieve RB. Pathological and haematological responses of cats experimentally infected with Toxocara canis larvae. *Int J Parasitol*. 1989; 19(5):479-488.
15. Robinson WF, Robinson NA. Cardiovascular system. In: Maxie MG, ed. *Jubb, Kennedy, and Palmer's Pathology of Domestic Animals.* Vol 3. 6th ed. St. Louis, MO: Elsevier; 2016: 83-85.
16. Ryan W, Newcomb K. Prevalence of feline heartworm disease - a global review. *Proceedings of the Heartworm Symposium '95, Auburn, Alabama*. Batavia, Illinois: American Heartworm Society.
17. Winter RL, Ray Dillon A, Cattley RC, et al. Effect of heartworm disease and heartworm-associated respiratory disease (HARD) on the right ventricle of cats. *Parasit Vectors*. 2017; 10 (Suppl 2):492.

CASE III:

Signalment:
8-week-old, male intact, Australian Heeler dog (*Canis familiaris*)

History:
This puppy presented with seizures and was euthanized on the same day. The puppy was unvaccinated, and the vaccination status of the dam was unknown.

Gross Pathology:
Unremarkable

Laboratory Results:

Sample	Test	Results
Brain (unfixed)	Direct fluorescent antibody testing for rabies virus	Negative
Lung (unfixed)	Aerobic culture	No growth

Microscopic Description:
Brain (cerebrum, hippocampus, and thalamus): Widespread throughout the white and gray matter of the cerebrum, hippocampus, and thalamus, there is mild gliosis. Many distinct glial nodules composed of aggregates of mononuclear cells including oligodendroglial cells and astrocytes are present. Many glial cells within these nodules have karyorrhectic or pyknotic nuclei. Multifocally, there are occasional neurons that are surrounded by small numbers of glial cells (satellitosis). Rare neurons are hypereosinophilic and shrunken with pyknotic nuclei (neuronal necrosis) and surrounded by small numbers of glial cells (neuronophagia). Occasional neuroparenchymal and meningeal blood vessels are surrounded and partially obscured by a variably thick layer of lymphocytes, plasma cells, fewer macrophages, and rare neutrophils (perivascular cuffing). Affected blood vessels are lined by hypertrophied endothelial cells. Throughout the section, there are rare, small, randomly distributed foci of hemorrhage. Occasional endothelial cells, rare glial cells, and rare intravascular mononuclear cells have chromatin margination and a solitary, large, approximately 4-6µm in diameter, intranuclear, basophilic inclusion body that often fills the entire nucleus. The leptomeninges, typically adjacent to blood vessels, are multifocally infiltrated by small to moderate numbers of plasma cells and lymphocytes.

Brain (cerebellum and brainstem) [not provided]: The histological changes are similar to those described in the cerebrum, hippocampus, and thalamus.

Liver [not provided]: There are many widely disseminated hepatocytes and rare, scattered Kupffer cells with chromatin margination and intranuclear inclusion bodies similar to those described in the brain. There are scattered small aggregates of lymphocytes with rare plasma cells and neutrophils, some of which are concentrated around blood vessels. There are rare hepatocytes with individual cell necrosis and/or apoptosis characterized by hypereosinophilia and karyorrhectic nuclei.

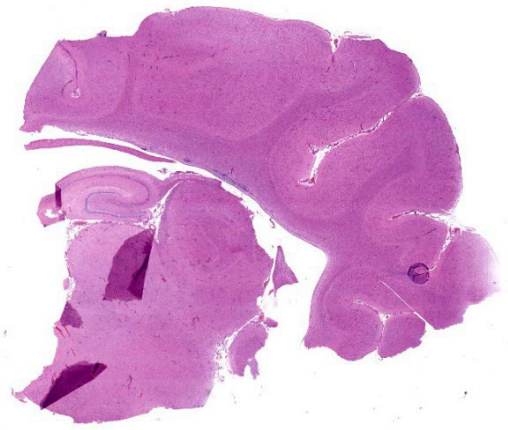

Figure 3-1. Diencephalon, dog. A single section of thalamus, hippocampus, and overlying cerebral cortex is submitted for examination. There are no apparent lesions at subgross magnification. (HE, 6X)

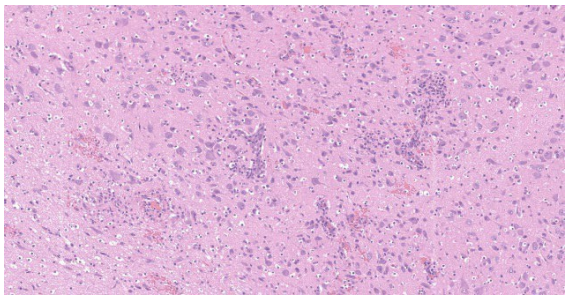

Figure 3-2. Diencephalon, dog. Predominantly in the thalamus, there is perivascular hypercellularity and hemorrhage, and diffuse gliosis of the intervening neuroparenchyma. (HE, 140X)

Immunohistochemistry:

1. Brain:
   a. Canine adenovirus-type 1 (CAV-1): There are scattered rare endothelial cells that have strong intracytoplasmic and occasional intranuclear immunoreactivity.
   b. Adenovirus: There are scattered rare endothelial cells that have strong intracytoplasmic and occasional intranuclear immunoreactivity.
   c. Canine distemper virus: There is no immunoreactivity.
2. Liver:
   a. CAV-1: There are occasional Kupffer cells, hepatocytes, and rare endothelial cells, with strong intracytoplasmic and occasional intranuclear immunoreactivity.
   b. Canine herpesvirus: There is no immunoreactivity.

Contributor's Morphologic Diagnoses:

1. Brain (cerebrum, thalamus, hippocampus, brainstem, and cerebellum) - encephalitis, lymphohistiocytic, multifocal, moderate to marked, subacute, with gliosis, glial nodules, perivascular cuffing, lymphoplasmacytic vasculitis, endothelial and glial cell intranuclear basophilic inclusion bodies, and mild lymphoplasmacytic leptomeningitis
2. Liver [not provided] - hepatitis, lymphocytic, multifocal and random, mild, subacute, with individual cell necrosis/apoptosis and intranuclear basophilic inclusion bodies

Contributor's Comment:

Canine adenovirus type-1 (CAV-1) is a non-enveloped DNA virus, and is the causative agent of infectious canine hepatitis. The virus affects various canids, including domestic dogs, foxes, coyotes, and wolves, as well as skunks and bears.[1,3,4,9] Clinical signs are typically more severe in younger animals (<1-2 years of age), ranging from asymptomatic to severe, and may include pyrexia, inappetence, lethargy, vomiting, diarrhea, abdominal pain, corneal edema, or death often without premonitory clinical signs.[1,3,4] The virus has affinity for endothelial cells, hepatocytes, and mesothelium, resulting in edema, serosal hemorrhage, and hepatic necrosis.[1-3] The neurological manifestation of CAV-1 infection in domestic dogs has rarely

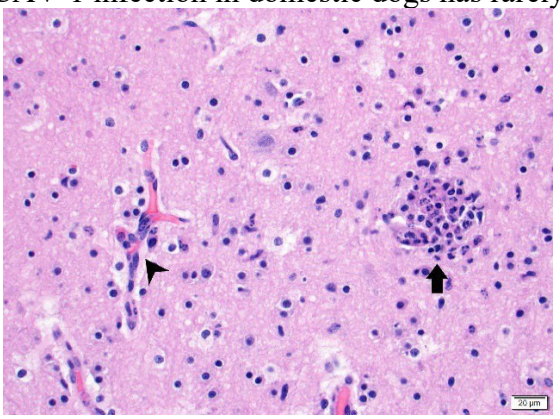

Figure 3-3. Diencephalon, dog. There is mild gliosis and ran-domly distributed glial nodules (arrow). Blood vessels are surrounded by perivascular cuffs of variable thickness, with as many as three layers of lymphocytes, fewer macrophages, and plasma cells. Affected blood vessels are often lined by re-active/ hypertrophic endothelial cells (arrow-head). (Image courtesy of: The University of Minnesota, College of Veterinary Medicine, Veterinary Diagnostic Laboratory. https://www.vdl.umn.edu) (HE, 400X)

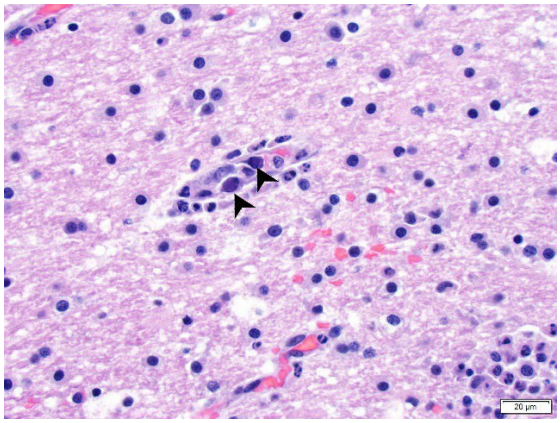

Figure 3-4. Diencephalon, dog. Affected endothelial cells (as well as rare intravascular leukocytes and mono-nuclear cells within glial nodules) have large, 4-6 µm in diameter, basophilic, intranuclear inclusion bodies that often fill the entire nucleus (arrow-heads). (Image courtesy of: The University of Min-nesota, College of Veterinary Medicine, Veteri-nary Diagnostic Laboratory. https://www.vdl.umn.edu) (HE, 400X)

been reported, and is most commonly seen in non-domestic animal species.[6,10]

In this case, a diagnosis of CAV-1 infection was made based on the characteristic histologic changes and immunohistochemical results involving the liver and brain. In previously reported CAV-1 cases in domestic dogs involving the brain, characteristic lesions included hemorrhage, vasculitis, and perivascular accumulation of mononuclear cells.[2,6,10] The lesions are typically seen in the brainstem, thalamus, and caudate nuclei, often sparing the cerebral and cerebellar cortices,[8] although in one report, the changes were most commonly observed in the corona radiata, caudate nucleus, thalamus, pons, and leptomeninges.[6]

CAV-1-associated encephalitis has been more commonly associated with foxes.[5,10] Under experimental conditions, the foxes developed hemorrhage predominantly affecting the brainstem and spinal cord, and variable mononuclear meningoencephalitis with perivascular cuffing.[5] In the present case, the lesions differed slightly from those previously reported in dogs and foxes, with evidence of encephalitis with gliosis and glial nodules, in addition to the previously reported vascular changes. In addition, the lesions were more widespread, involving the cerebral cortex, thalamus, hippocampus, brainstem, and cerebellum.

Neurological signs associated with CAV-1 have been attributed to vascular damage within the central nervous system,[3,4,10,11] although other possibilities include hepatic encephalopathy and/or concurrent infection with canine distemper virus (CDV).[11] It has been suggested that different CAV-1 strains may have tropism for the endothelium of the central nervous system.[2,10] However, to our knowledge, sequence analysis has not been performed to confirm this hypothesis. In this case, the cause of the reported seizures likely involved a combination of encephalitis and central nervous system vascular involvement. Although speculative, it is possible that the differences in the lesions and distribution of

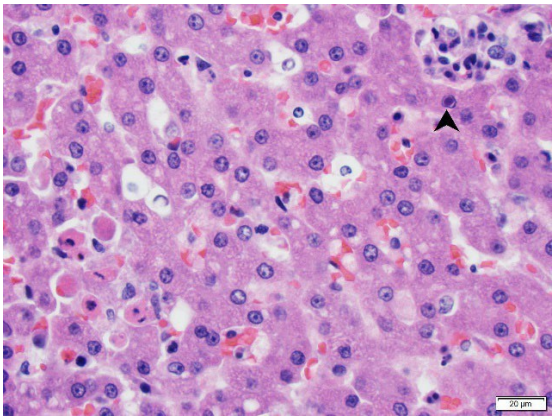

Figure 3-5. Liver, dog. There is individual hepatocyte necrosis, and scattered hepatocytes, Kupffer cells, and endothelial cells have intranuclear inclusion bodies similar to those observed in the brain (arrowhead). (Image courtesy of: The University of Minnesota, College of Veterinary Medicine, Veterinary Diagnostic Laboratory. https://www.vdl.umn.edu) (HE, 400X)

the lesions from the previously reported cases may have been due to the characteristics of the CAV-1 strain and/or the host immune response.

Susceptible dogs are exposed to CAV-1 via oronasal route through contact with infectious saliva, feces, urine, or respiratory secretions, or through direct animal-to-animal contact.[1,4,10,11] The virus initially replicates in the tonsillar crypts resulting in tonsillitis, followed by spread to the local lymph nodes and systemic circulation.[1,3,8] Viremia typically lasts 4-8 days and the virus spreads to the liver, endothelial cells, and mesothelial cells.[1,3,10] The virions exit the cells by cell lysis, resulting in cell death and tissue injury.[1,9] Characteristic histological lesions typically involve the liver, and range from randomly scattered foci of hepatocellular necrosis to widespread centrilobular necrosis.[1,3] Intranuclear inclusion bodies are often found in hepatocytes, vascular endothelium, and Kupffer cells.[1,3] Other lesions that may be seen include corneal edema/iridocyclitis (typically between 14 to 21 days post infection), gallbladder wall edema, interstitial nephritis, hemorrhagic enteritis, laryngitis, tracheitis, pneumonia, and ecchymotic and petechial hemorrhages.[1-4,6,11]

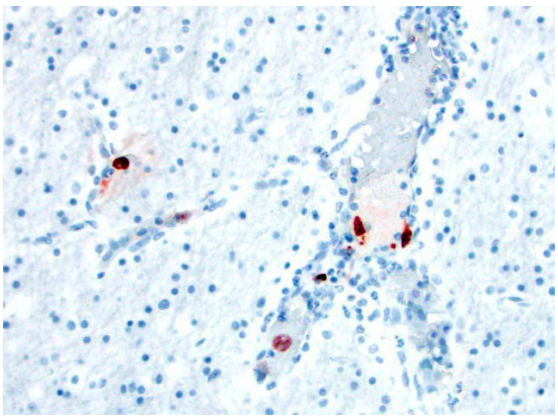

Figure 3-6. Brain (cerebral cortex), dog. Canine adenovirus type-1 immunohistochemistry. Scattered endothelial cells have strong intracytoplasmic and rare intranuclear immunoreactivity. (Image courtesy of: The University of Minnesota, College of Veterinary Medicine, Veterinary Diagnostic Laboratory. https://www.vdl.umn.edu) (anti-CAV-1, 400X)

Differential diagnoses for viral encephalitis in dogs include CDV, rabies virus, and canine herpesvirus. Coinfection is possible, with reports of CDV and CAV-1 resulting in an increased mortality rate.[6] CDV infection may be characterized by both intranuclear and intracytoplasmic inclusion bodies. CDV infection was excluded in this case based on the negative immunohistochemistry results. Rabies was considered unlikely based on negative direct fluorescent antibody testing result for rabies antigen. Canine herpesvirus (CHV)-associated meningoencephalitis has been reported in natural and experimental conditions.[7] In one case series involving natural canine herpesvirus encephalitis, lesions were characterized by randomly distributed glial nodules throughout the white and gray matter of the cerebrum, brainstem, and cerebellum, as well as lymphocytic meningitis and cerebellar cortical necrosis.[7] Although CHV immunohistochemistry was not performed on the brain in this case, the liver was immune-negative, and CHV infection was considered unlikely.

Contributing Institution:
The University of Minnesota, College of Veterinary Medicine, Veterinary Diagnostic Laboratory. https://www.vdl.umn.edu

JPC Diagnosis:
Thalamus and cerebrum: Vasculitis, lymphocytic, multifocal to coalescing, moderate, with glial nodules and intraendothelial intranuclear viral inclusions.

JPC Comment:
The moderator and conference participants discussed the presence of glial nodules, which are multifocal proliferation of microglial cells in reaction to injury in the CNS and neuronal necrosis. Canine adenovirus 1 is not

apparently associated with the glial nodule formation, and glial nodule formation is not an expected finding in canine adenovirus-1 infection. All agreed that the contributor did an excellent workup to rule out canine distempervirus and canine herpesvirus-1. Both viruses can cause neuronal necrosis with glial nodule formation and would be top differentials based on this H&E section.

Two helpful histologic features which indicate that this animal is juvenile are the diffuse high concentration of glial cells and the prominence of the undifferentiated glial and neuronal precursors ("rests") in the periventrular tissue. Both of these findings are normal in puppies.

Most vertebrate species can be infected by viruses of the Adenovirus family, but individual viruses have narrow host ranges, are persistent, and generally are subclinical or associated with mild respiratory infections.[8] There are notable exceptions such as CAV-1, deer adenovirus, and several avian adenoviruses, which cause important diseases in their host species.[8] There are five genera in the *Adenoviridae* family: *Mastadenovirus, Aviadenovirus, Atadenovirus, Siadenovirus,* and *Ichtadenovirus.* The name adenovirus is derived from how the virus was initially identified: as a cause of cellular degeneration in human adenoid cultures.[8]

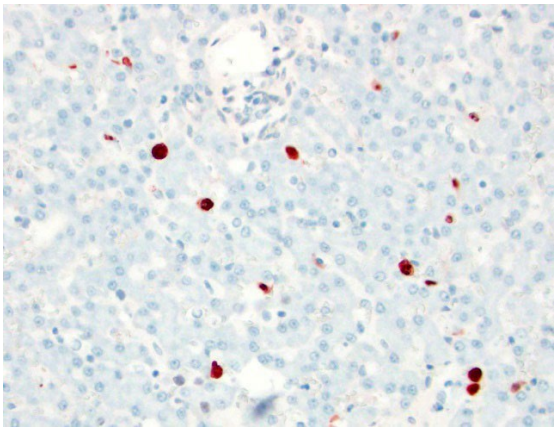

Figure 3-7. Brain (cerebral cortex), dog. Canine adenovirus type-1 immunohistochemistry. Occasional Kupffer cells, hepatocytes, and rare endothelial cells have strong intracytoplasmic and occasional intranuclear immunoreactivity. (Image courtesy of: The University of Minnesota, College of Veterinary Medicine, Veterinary Diagnostic Laboratory. https://www.vdl.umn.edu) (anti-CAV-1, 400X)

Canine adenovirus 1, which affects domestic and wild canids, skunks, coatis, and bears, was discovered in 1954 as the causative agent of fox encephalitis.[8,9] The contributor provides an excellent overview of CAV-1 infection in dogs and non-domestic animals. A recent report by Pereira et al described natural CAV-1 infection and death in captive maned wolf puppies.[9] On necropsy, findings mirrored those seen in dogs, with nonsuppurative meningoencephalitis, necrotizing hepatitis and splenitis, and intranuclear inclusion bodies in hepatocytes (1 of 2 pups) and kidneys (2 of 2 pups).[9]

Canine adenovirus 2, another virus in the *Mastadenovirus* family, is a member of the canine respiratory disease complex and infection is limited to the respiratory system.[9]

Significant adenoviruses in avian species fall within the *Aviadenovirus, Atadenovirus,* and *Siadenovirus* genera.[9] Fowl adenovirus 1, a member of *Aviadenovirus* genus, causes quail bronchitis and is characterized by necrotizing tracheitis, air sacculitis, conjunctivitis, and gastrointestinal disease, with a high mortality in young quail.[9] Another member of the *Aviadenovirus* genus is fowl adenovirus 4, which causes hydropericardium syndrome in chickens, with the most severe disease occurring around one month of age.[9] In addition to the pericardial effusion, pulmonary edema and enlargement of the kidneys and liver may be seen.[9] Within the *Siadenovirus* genus, turkey adenovirus 3 causes hemorrhagic enteritis in turkeys over a month of age, and two

closely related (serologically indistinguishable) viruses cause marble spleen disease in pheasants and avian adenovirus splenomegaly in chickens.[9]

References:

1) Brown DL, Van Wettere AJ, Cullen JM. Hepatobiliary system and exocrine pancreas. In: Zachary JF, ed. *Pathologic Basis of Veterinary Disease*. 6th ed. Elsevier Mosby; 2017.
2) Caudell D, Confer AW, Fulton RW, et al. Diagnosis of infectious canine hepatitis virus (CAV-1) infection in puppies with encephalopathy. *J Vet Diagn Invest*. 2005; 17: 58-61.
3) Cullen JM, Stalker MJ. Liver and biliary system. In Maxie MG, ed. *Jubb, Kennedy and Palmer's Pathology of Domestic Animals.* 6th ed., vol. 2. Saunders Elsevier; 2016.
4) Decaro N, Martella V, Buonavoglia C. Canine adenoviruses and herpesvirus. *Vet Clin Small Anim*. 2008; 38: 799-814.
5) Green RG, Ziegler NR, Green BB, Dewey ET. Epizootic fox encephalitis. I. General description. *Am J Epidemiol*. 1930; 12: 109-129.
6) Hornsey SJ, Philibert H, Godson DL, Snead ECR. Canine adenovirus type 1 causing neurological signs in a 5-week-old puppy. *BMC Vet Res*. 2019; 15: 418.
7) Jager MC, Sloma EA, Shelton M, Miller AD. Naturally acquired canine herpesvirus-associated meningoencephalitis. *Vet Path*. 2017; 54: 820-827.
8) MachLachlan NG, Dubovi EJ. *Adenoviridae.* In: MacLachlan NJ, Dubovi EJ, eds. *Fenner's Veterinary Virology*. 5th ed. San Diego, CA: Elsevier. 2017; 217-227.
9) Pereira FMAM, de Oliveira AR, Melo ES, et al. Naturally Acquired Infectious Canine Hepatitis in Two Captive Maned Wolf (*Chrysocyon bracyurus*) puppies. *J Comp Path.* 2021; 182: 62-68.
10) Pintore MD, Corbellini D, Chieppa MN, et al. Canine adenovirus type 1 and Pasteurella pneumotropica co-infection in a puppy. *Vet Ital.* 2016; 52: 57-62.
11) Sykes JE. Infectious canine hepatitis. In Sykes JE, ed. *Canine and Feline Infectious Diseases*. Saunders; 2014.

CASE IV:

Signalment:
8-month-old male American mink (*Neogale vison*) (non-Aleutian)

History:
This mink was a non-inoculated experimental control animal. All mink were acclimated to the facility after arrival for a period of 3 weeks prior to initiation of the experiment. No clinical signs were observed in this mink.

Gross Pathology:
Bright red lungs that did not collapse normally.

Laboratory Results:
Other mink from this cohort were PCR positive for Aleutian Mink Disease Virus (AMDV) in lung and spleen samples. Frozen samples from this case were not immediately available for molecular testing at the time of conference submission.

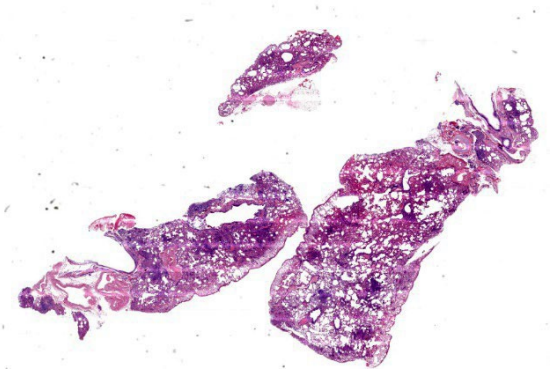

Figure 4-1. Lung, mink. Foci of hypercellularity can be seen even at subgross magnification. (HE, 6X)

Immunohistochemistry for B cell, T cell, and macrophage markers. Most perivascular mononuclear cells stained with CD3 antibody with immunohistochemistry.

Microscopic Description:
Lung: The alveolar septa are diffusely thickened due to increased numbers of lymphocytes and enlarged round to cuboidal epithelium (type II pneumocyte hyperplasia) lining the alveoli. There are many lymphocytes with fewer plasma cells around pulmonary vasculature. There are multifocal areas of low numbers of neutrophils within alveoli and alveolar septa along with numerous alveolar macrophages. Alveolar macrophages have two distinct morphologies. The first type is 20-35 microns in diameter with a round to reniform 10-20 microns in diameter; the cytoplasm is amphophilic with an eosinophilic perinuclear clear zone. The second population of macrophages have prominent 2–3-micron intracytoplasmic vacuoles. There are occasionally multinucleated macrophages. Alveolar lumens also contain sloughed epithelial cells multifocal areas of eosinophilic proteinaceous fluid. Alveolar septa are lined by a curved cup-shaped eosinophilic material. Capillaries are congested with red blood cells and occasionally filled with dense eosinophilic material that expands the capillary. Near the lung periphery, capillaries are largely devoid of red blood cells.

Pneumocytes occasionally have vacuolated cytoplasm. Rarely within intra-alveolar cells, there are oval to round magenta intranuclear inclusion bodies 3-4 µm in diameter with peripheralized chromatin. There are multifocal areas where alveolar septal walls are absent, and alveoli conjoin (microbullae).

Contributor's Morphologic Diagnoses:
Interstitial pneumonia, lymphohistiocytic, diffuse, moderate, chronic with perivascular lymphocytes.

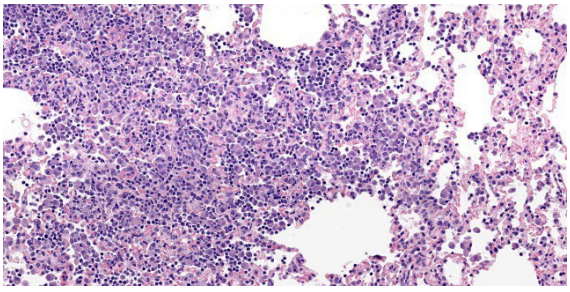

Figure 4-2. Lung, mink: Hypercellular foci consist of alveoli filled by numerous macrophages with basophilic cytoplasm, fewer neutrophils and lymphoplasmacytic infiltrate of peribronchial and perivascular connective tissue. There is also Type 2 pneumocyte hyperplasia contributing to the mix. (HE, 200X)

Contributor's Comment:
The microscopic findings are consistent with Aleutian Mink Disease Virus (AMDV). Previous mink from this shipment died acutely upon arrival and were positive for AMDV by PCR in the spleen and lungs and had concomitant severe hepatic lipidosis.

Aleutian mink disease virus (AMDV) is the archetype and prototype member of Amdoparvoviruses that infects domesticated and wild mink. Individual cases of infection with AMDV in other species is reported, but some historic reports did not include evaluation of sequence. The viral family within the carnivores has recently grown, with distinct, host-specific *amdoparvoviruses* (APVs) discovered in fishers, grey foxes, red foxes, raccoon dogs, red pandas, and striped skunks.[8] In AMDV infected mink, the host age and immune status affects the clinical outcome. In mink kits, the disease classically manifests with interstitial pneumonia and viral replication is predominantly within type II pneumocytes.[3,7] In adult mink, the virus is found in macrophages in lymphoid tissue. Plasma cells proliferate and infiltrate the liver, spleen, kidneys, and lymph nodes. The disease has also been called mink plasmacytosis because of this. Mink have a hypergammaglobulinemia and develop renal disease char-

acterized by glomerulonephritis and interstitial nephritis. Glomerulonephritis and vasculitis are due to viral-antibody complexes (type III hypersensitivity) in affected mink.[3,6]

Aleutian mink are named for a hair coat color dilution due to a genetic mutation. The mutation, termed Chédiak-Higashi syndrome, results in defective lysosomes, melanosomes, cytolytic granules, and platelet rich granules.[6] Aleutian mink are more susceptible to AMDV and appear to be affected by all isolates or strains; whereas, non-Aleutian mink, may be less susceptible to some virus strains resulting in non-progressive persistent infections.[3]

Contributing Institution:
National Animal Disease Center
https://www.ars.usda.gov/midwest-area/ames/nadc/

JPC Diagnosis:
Lung: Pneumonia, interstitial, lymphohistiocytic, diffuse, moderate, with type II pneumocyte hyperplasia, peribronchial and perivascular lymphoplasmacytic infiltrates, and intranuclear viral inclusion bodies.

JPC Comment:
As the contributor mentions, a critical component of the pathogenesis of Aleutian mink disease is the exuberant production of antibodies by plasma cells leading to a type III hypersensitivity reaction (immune complex hypersensitivity). These reactions occur when immune complexes (typically containing IgM and IgG) accumulate in tissues, activate complement, and recruit neutrophils, leading to local damage.[6] Type III hypersensitivity reactions generally occur when there is slightly more antigen than antibody; if antibody is present in large quantities, the insoluble complex is easily cleared by tissue macrophages and hypersensitivity does not develop.[5,6] Complexes may deposit in vessels, joints, glomeruli, or choroid plexus.[4,6] Type III hypersensitivity reaction typically occur in diseases that are the result of persistent infection (i.e. Aleutian mink disease), autoimmunity (i.e. systemic lupus erythematosus), or inhalation of environmental antigens (chronic obstructive pulmonary disease).[6] The Arthus reaction is a localized, cutaneous version of a type III hypersensitivity reaction that can be induced experimentally via intracutaneous injection of antigen into an animal with a preformed antibody; the resulting reaction produces fibrinoid necrosis in vessel walls and subsequent thrombosis.[4]

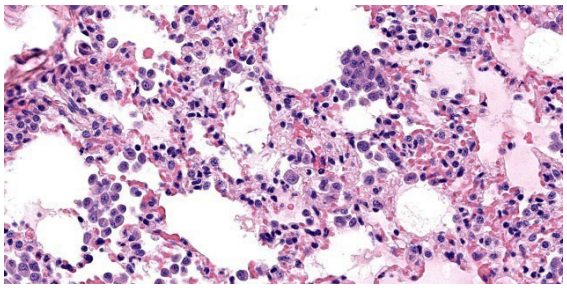

Figure 4-3. Lung, mink: There is diffuse expansion of alveolar septa by congestion, edema, macrophages, lymphocytes and scattered hyperplastic Type II pneumocytes. (HE, 580X)

Aleutian mink disease virus is single stranded, negative-sense DNA virus of the genus *Amdoparvovirus*.[2,5] Dr. Pesavento described that diseases associated with other carnivore APVs (Red Panda and Skunk) share many of the features of AMDV in mink, including tissue distribution, but the well described immune complex disease of the infected mink is not present with other APV infections so far.

The *amdoparvovirus* isolated from endangered red pandas (RPAV) is widespread in captive populations in the United States, with the virus isolated from at least 50% of 104 animals tested.[1] Infection appears to be persistent, as well: the virus was consistently isolated from 6 animals serially sampled for up to 6 years.[1,2] In the index case, the red

panda had virus associated by ISH with significant pyogranulomatous inflammation in multiple sites, including the peritoneum, pancreas, and heart.[1] It appears that a subset of pandas is susceptible to viral associated disease, with heavy loads of virus, and lesions consistently in kidneys, but also variably in other tissues (lung, heart, brain, eggs). In pandas positive for the virus, but dead from other causes, virus was identified in normal lymphoid tissues and within normal gastrointestinal mucosa. The intestinal tract, given the consistent shedding and the ISH results, is a likely site of persistence in Red Pandas.

Classically, parvoviruses are thought to infect cells only which are actively replicating (in S-phase, i.e. crypt enterocytes), since the virus requires cellular machinery to replicate, as the contributor mentions. Dr. Pesavento described, however, that human parvovirus B19, the causative agent of fifth disease in humans, induces a DNA damage response (DDR) that facilitates viral DNA replication.

In addition to AMDV, mink are susceptible to another parvovirus, mink enteritis virus, which is closely related to feline panleukopenia virus and an important disease of farmed mink.[5,8] Similar to feline panleukopenia, mink enteritis virus targets the enterocytes, causing crypt epithelial necrosis; lymphocytes, causing lymphoid necrosis; and bone marrow progenitor cells, causing leukopenia.[8] Curiously, mink enteritis virus is not associated with cerebellar hypoplasia.[5]

Conference participants discussed euthanasia artifact due to barbiturate salt precipitation as a possible cause for the thickening and eosinophilic debris in the pleura.

References:

1. Alex CE, Kubiski SV, Jackson KA, Wack RF, Pesavento PA. Amdoparvovirus infections are prevalent, persistent, and genetically diverse in zoo-housed red pandas (*Ailurus fulgens)*. *J Zoo Wildl Medicine.* 2022; 53(1): 83-91.
2. Alex CE, Kubiski SV, Li L, et al. Amdoparvovirus Infection in Red Pandas (*Ailurus fulgens). Vet Pathol.* 2018; 55(4): 552-561.
3. Bloom ME, Kanno H, Mori S, Wolfinbarger JB. Aleutian mink disease: puzzles and paradigms. *Infect Agents Dis*. 1994;3: 279-301.
4. Kumar V, Abbas AK, Aster JC. Diseases of the Immune System. In: *Robbins & Cotran Pathologic Basis of Disease.* Philadelphia, PA: Elsevier. 2021; 210-212.
5. MacLachland NJ, Dubovi EJ, eds. Parvoviridae. In: *Fenner's Veterinary Virology.* San Diego, CA: Elsevier. 2017; 251-255.
6. Snyder PW. Disease of Immunity. In: Zachary JF, ed. *Pathologic Basis of Veterinary Disease*. 7th ed. Philadelphia, PA: Elsevier, Inc. 2022: 320.
7. Turner P. Viral Diseases of Mink. *The Merck Veterinary Manual 11*. Retrieved 6/6/2022, from https://www.merckvetmanual.com/exotic-and-laboratory-animals/mink/viral-diseases-of-mink.
8. Williams BH, Burek Huntington KA, Miller M. Mustelids. In: Terio KA, McAloose D, St. Lger J, eds. *Pathology of Wildlife and Zoo Animals*. San Diego, CA: Elsevier. 2018; 296.

WSC 2022-2023 Self-assessment
Conference 22

1. Which of the following species are very susceptible to malignant catarrhal fever?
    a. Cattle
    b. White-tailed deer
    c. Bison
    d. Sheep

2. In malignant catarrhal fever, the largest pool of proliferating lymphocytes are which of the following?
    a. CD3+
    b. CD4+
    c. CD8+
    d. CD20+

3. The strong inflammatory response to embolization of dead heartworms in cats is mediated by?
    a. Pulmonary intravascular macrophages
    b. Interstitial mast cells
    c. Eosinophils
    d. Alveolar macrophages

4. True or false? The large numbers of mitotic figures seen in nodal plexiform vasculopathy hinders its differentiation from metastatic hemangiosarcoma.
    a. True
    b. False

5. Aleutian mink disease is characterized by the accumulation of which of the following in a variety of tissues?
    a. Eosinophils
    b. Mast cells
    c. Hypersegmented neutrophils
    d. Plasma cells

Please email your completed assessment for grading to Dr. Bruce Williams at bruce.h.williams12.civ@mail.mil. Passing score is 80%. This program (RACE program 33611) is approved by the AAVSB RACE to offer a total of 0.5 CE Credits, with a maximum of 12.5 CE Credits being available to any individual Veterinary Medical Professionals for the 2019-2020 Wednesday Slide Conference. This

RACE approval is for the subject matter categories of: SCIENTIFIC using the delivery method of NONINTERACTIVE DISTANCE. This approval is valid in jurisdictions which recognize AAVSB RACE.

Joint Pathology Center
Veterinary Pathology Services

WEDNESDAY SLIDE CONFERENCE 2022-2023

Conference #23 **19 April 2023**

CASE I:

Signalment:
16-years old, female spayed, French bulldog, (*Canis lupus familiaris) canine*

History:
The dog was presented to the animal hospital for mass of the right eye that had grown from two months ago. Marked exophthalmos was observed in the right eye and enucleation was performed.

Gross Pathology:
Most of formalin fixed material was neoplastic tissue and normal ocular structures were unclear. On cut surface, there was scattered bleeding and necrosis in the tumor tissue.

Laboratory Results:
No laboratory findings reported.

Microscopic Description:
The nonencapsulated and poorly demarcated mass surrounded the optic nerve behind the globe. The mass consisted of spindle or epithelioid polygonal cell arranged in whorls, bundles or sheets, and often formed tumor islands of variable size and lobules separated by fibrovascular stroma. These tumor cells had various amounts of pale eosinophilic cytoplasm with slightly distinct cell margins. The cells had ovoid nuclei with stippled chromatin and occasional clear nucleoli. Anisocytosis and anysokaryosis was mild. 11 mitotic figures were observed under 10 high-magnification fields of view. Several large to small foci of necrosis and hemorrhage were also seen. Although no tumor invasion was observed into the eye tissue, the neoplastic cells extensively invaded into peripheral adipose and muscle tissues. Clusters of neoplastic cells were seen in some lymphatic or blood vessels. The ocular structures markedly compressed by the tumor. In other specimens submitted, the corneal epithelium showed hyperplastic thickening with some small pustules and ulcer. In the substantia propria of cornea, severe fibrosis with mild hemorrhage, edema and infiltration of lymphocytes can be seen. The structures of the iris and ciliary body were collapsed, the lens and retinae were obscure.

Contributor's Morphologic Diagnosis:
Eye: Orbital meningioma, right eye, dog

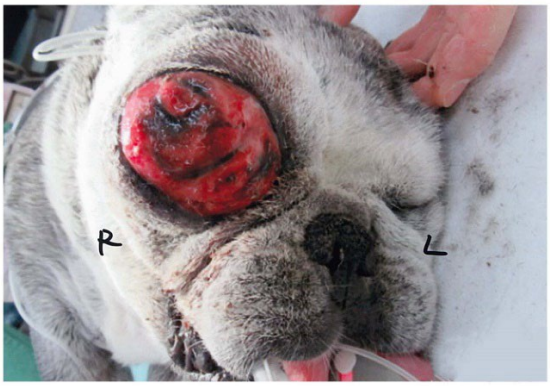

Figure 1-1. Presentation, dog. Marked exophthalmos was observed in the right eye (Photo courtesy of: Department of Veterinary Pathology and Public Health, Institute of Veterinary Science, Univ Laboratory of Pathology, Faculty of Pharmaceutical Sciences, Setsunan University, 45-1 Nagaotohge-cho, Hirakata, Osaka 573-0101, Japan)

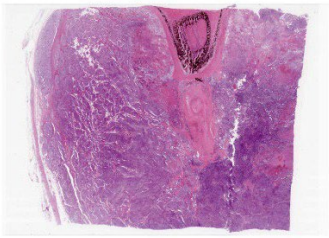

Figure 1-2. Orbit, dog. A single section of orbit containing a compressed phthitic globe and the optic nerve projecting downward (top center). An infiltrative mass effaces the orbital skeletal and periorbital fat. (HE

Contributor's Comment:

Meningioma is a common primary brain tumor in dogs (up to 45%) and cats (60%), and most intracranial meningiomas occur as well-demarcated solitary masses. However, meningioma in the retrobulbar site accounts for only 2 to 3 % of all meningiomas and develops surrounding optic nerve area with invasion into peripheral tissue.[14,15] Meningioma is derived from arachnoidal cap lining arachnoid villi. In veterinary medicine, orbital meningioma is considered a primary lesion originating in meninge covering intraorbital or intracanalicular optic nerve, while in human medicine, some are observed as secondary lesion occurring intracranially and extend along the optic nerve.[6,7]

Orbital meningioma is characterized by proliferation in sheets or cluster of various sized epithelioid cells with glassy eosinophilic cytoplasm and may form whorls or bundles as is the intracranial cases, but psammoma bodies are rare. While chondro-osseous metaplasia is rare in intracranial meningioma, it is frequently observed in orbital meningiomas and is useful for diagnosis.[13,14,18] In 3 previous cases in the Wednesday Slide Conference, epithelioid or spindle cells arranged in small lobules and whorls in 2 cases (Conference 19, 2013, Case 2; Conference 20, 2015; Case 4) , epithelioid cells arranged in nests and sheets predominated in 1 case (Conference 7, 2018, Case 4), and chondro-osseous metaplasia was seen in all cases. This case is thought to be typical orbital meningioma at the point of location and histological morphology except for the lack of chondro-osseous metaplasia.

Although immunohistochemistry is not always necessary in typical cases, it may be useful for excluding other differential diagnosis such as carcinoma. In general, neoplastic cells show positive reaction for vimentin, S100 and neuron specific enolase in varying degree, and negative for pancytokeratin and glial fibrillary acidic protein, however, cytokeratin expression was detected in few cases on a report .[2,11,13,15]

Orbital meningioma is slow growing and malignant variants are rarely reported. One study of 22 canine orbital meningiomas revealed that 6 of 17 recurred and furthermore 2 of them presented subsequent central blindness suggesting intracranial invasion of the tumor.[10] In addition, two other reports showed distant metastasis to lung.[12,16] These aggressive biologic behaviors of this tumor might be associated with stage and progression at the time of excision.

Malignancy of human orbital meningiomas are assessed by WHO grading system for intracranial meningioma, which depends on histologic subtypes and specific cytological features.[6,7] In canine intracranial meningioma, application of the system has been proposed because they are likely to exhibit biological similarities to their human

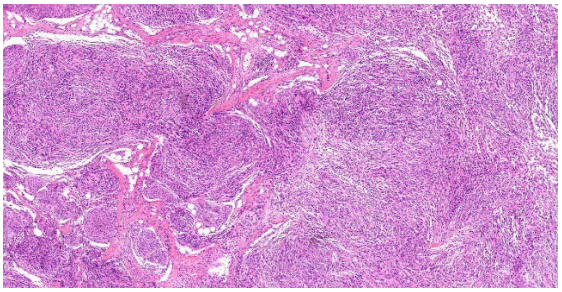

Figure 1-3. Orbit, dog. The neoplastic cells are arranged in long streams, bundles, and frequent whorls. (HE, 39X)

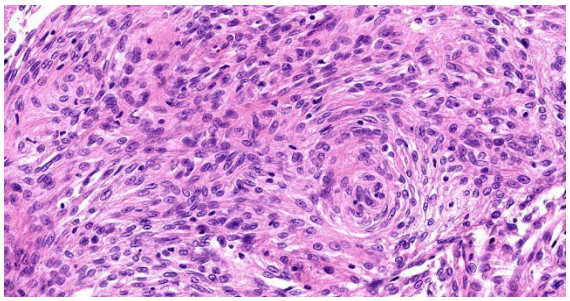

Figure 1-4. Orbit, dog. High magnification of neoplastic cells. (HE, 388X)

counterparts, but it is not yet used for orbital lesions. The number of cases of canine orbital meningioma is small and correlation be tween grading and prognosis with both types of meningioma has not been validated, therefore the standardization of grading system in canine meningioma needs further studies using larger caseloads.[1,11]

This case might have poor clinical outcome such as recurring and/or extension into cranium because of the histopathological features including prominent local invasion, lymphovascular invasion and frequent mitotic figures. It was suggested that loss of the eye structure was due to compression by the neoplastic tissue and secondary inflammatory change.

Contributing Institution:
Laboratory of Pathology, Faculty of Pharmaceutical Sciences, Setsunan University,
45-1 Nagaotohge-cho, Hirakata, Osaka 573-0101, Japan

JPC Diagnosis:
Globe, right: Orbital meningioma.

JPC Comment:
Meningioma was last seen in the Wednesday Slide Conference in 2021-2022, conference 7, case 2: this case was an intracranial neoplasm in a cat, and the contributor and conference comments delineate the pathologic and historical aspects of this common neoplasm.

Non-orbital canine meningiomas are classified according to the 2007 WHO human grading system. The two most common types of meningioma, the meningotheliomatous (epithelioid) and transitional (mixed) types, are both considered grade I, as are fibrous, psammomatous, angiomatous, microcystic, and myxoid types.[3] Grade II meningiomas include choroid and atypical meningiomas, which have a higher mitotic rate ($\geq$ 4 per 10 high power fields) and hypercellularity.[3] Grade III meningiomas include papillary, rhabdoid, and anaplastic forms, which have cytologic features of malignancy and greater than 20 mitotic figures per 10 high power fields.[3,17] While orbital meningiomas are not graded, this week's moderator, Dr. Jey Koehler from Auburn University, described several concerning features which could *potentially* be indicative of a more aggressive behavior (and would be characteristic of malignancy in a non-orbital meningioma): large areas of necrosis and regions with significant anisokaryosis and high mitotic rate.

A recent study described four cases of the uncommon rhabdoid meningioma in dogs.[17] In all cases, the neoplasms were located in the olfactory or frontal lobes and were locally invasive.[17] Rhabdoid cells comprised >70% of the tumor population, were arranged in

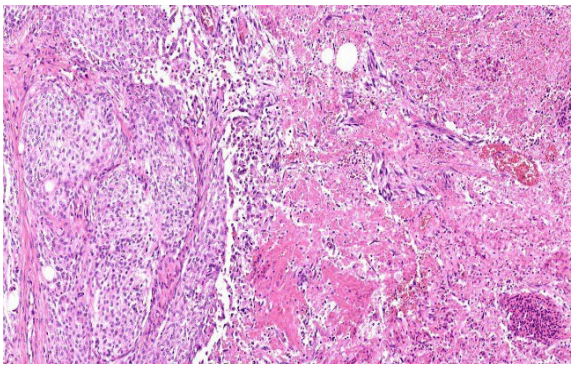

Figure 1-5. Orbit, dog. There are large areas of necrosis scattered throughout the neoplasm. (HE, 108X)

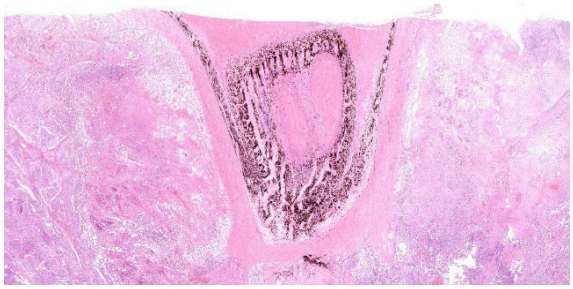

Figure 1-6. Orbit, dog. The compressed globe is phthitic – there is remnant pigment outlining the position of the ciliary body, uvea and choroid, but the anterior and posterior chamber are replaced by mature collagen (HE, 11X)

sheets, and had well-delineated cell borders, abundant eosinophilic cytoplasm, and hyaline to fibrillar inclusions which peripheralized the nucleus.[17] On electron microscopy, these inclusions were composed of whirling intermediate filaments (consistent with a rhabdoid morphology), a network of extensive cell process interdigitations (consistent with a rhabdoid-like morphology), or abundant mitochondria (consistent with an oncocytic meningioma).

In humans, expression of Ki-67, a marker of proliferation, and osteopontin, a cytokine with multiple activities important in tumor progression, are highly correlated to the histologic grade and recurrence rate of meningiomas.[8] Janssen et al recently evaluated 35 canine meningiomas and found that neither Ki-67 nor osteopontin were correlated with histologic grading according to the WHO classification system for human meningiomas.[8]

Meningiomas have a characteristic cytologic appearance, and samples may be obtained via impression smears or crush preparations of biopsy or by fine needle aspirate.[4,5] As on histology, samples from meningiomas may demonstrate whirling or acini formation and psammoma bodies on cytology. Additionally, neoplastic cells may have intracytoplasmic nuclear invaginations or an elongate nucleus with a longitudinal, dark blue linear bar imparting a "coffee bean" appearance to the nucleus.[4,5] These characteristic nuclei can be seen on histology throughout the neoplasm in this case as well.

Another primary neoplasm of the optic nerve described in dogs is an ocular astrocytoma.[9] This may arise in the optic nerve or within the retina and can lead to retinal detachment.[9]

References:

1. Avallone G, Rasotto R, *et al*. Review of Histological Grading Systems in Veterinary Medicine. *Vet Pathol*. 2021;58(5):809-828.
2. Barnhart KF, Wojcieszyn J, *et al*. Immunohistochemical staining patterns of canine meningiomas and correlation with published immunophenotypes. *Vet Pathol*. 2002;39(3):311-21.
3. Cantile C, Youssef S. Nervous system. In: Maxie, MG, ed. *Jubb, Kennedy, and Palmer's Pathology of Domestic Animals*, Vol I. 6th ed. Philadelphia, PA: Elsevier Ltd; 2016:396-398, 494.
4. DeLorenzi D, Mandara MT. The Central Nervous System. In: Raskin RE, Meyer DJ, eds. *Canine and Feline Cytology*. 3rd ed. St. Louis, MO: Elsevier. 2016: 396-400.
5. Gould A, Naskou MC, Brinker E. What is your diagnosis? Impression smear from a dog with an intracranial mass. *Vet Clin Pathol.* 2022; 00:1-5.
6. Grossnilaus HE, Eberhart CG, Kivelä TT. The 2016 World Health Organization Classification of Tumors of the Eye. 139.
7. Jain D, Ebrahimi KB, et al. Intraorbital meningiomas: a pathologic review using current World Health Organization criteria. *Arch Pathol Lab Med.* 2010;134(5):766-70.
8. Janssen J, Oevermann A, Walter I, Tichy A, Kummer S, Gradner G. Osteopontin and Ki-67 expression in World Health Organization graded canine meningioma.

9. Labelle P. The Eye. In: Zachary JF, ed. *Pathologic Basis of Veterinary Disease*. 7th ed. St. Louis, MO: 2022. 1423.
10. Mauldin EA, Deehr AJ, et al. Canine orbital meningiomas: a review of 22 cases. *Vet Ophthalmol*. 2000;3(1):11-16.
11. Montoliu P, Añor S, et al. Histological and immunohistochemical study of 30 cases of canine meningioma. *J Comp Pathol*. 2006;135(4):200-7.
12. Pérez V, Vidal E, et al. Orbital meningioma with a granular cell component in a dog, with extracranial metastasis. *J Comp Pathol.* 2005;133(2-3):212-7.
13. Regan DP, Kent M, *et al*. Clinicopathologic findings in a dog with a retrobulbar meningioma. *J Vet Diagn Invest.* 2011; 23(4):857-62.
14. Richard RD. Tumors of the Eye. In: Meuten DJ, ed., *Tumors in Domestic Animals.* 5th ed. Ames, IA. Wiley Blackwell. 915-916.
15. Robert JH, Andrew WB, *et al*.: Tumors of the Nervous System. In: Meuten DJ, ed., *Tumors in Domestic Animals.* 5th ed. Ames, IA. Wiley Blackwell. 864.
16. Schulman FY, Ribas JL, *et al*. Intracranial meningioma with pulmonary metastasis in three dogs. *Vet Pathol.* 1992;29(3):196-202.
17. Tabaran AF, Armien AG, Pluhar GE, O'Sullivan MG. Meningioma with rhabdoid features: Pathologic findings in dogs. *Vet Pathol*. 2022; 59(5): 759-762.
18. Wilcock BP: Special Senses. In: *Jubb Kennedy and Palmer's Pathology of Domestic Animals.* 6th ed. Vol 3. St. Louis, US: Elsevier; 2016:487-488.

CASE II:

Signalment:
14-year-old neutered male Persian cat (*Felis catus*)

History:
The cat had an acute onset of difficulty walking on the hind limbs, with a progressive worsening. The cat urinated and defecated in inappropriate places with sagging of the limbs during urination / defecation; had difficulty in jumping and appeared depressed. Palpation of the thoraco-lumbar spine caused discomfort. The cat underwent hospitalization and a complete diagnostic workflow. Due to a severe worsening of the symptoms and the health status, the cat was euthanized, and a necropsy was performed.

Gross Pathology:
An intramedullary neoformation was present in the thoraco-lumbar spinal cord (approximately T7).

Laboratory Results:
Hematobiochemistry: mild leucopenia; hyperazotemia.

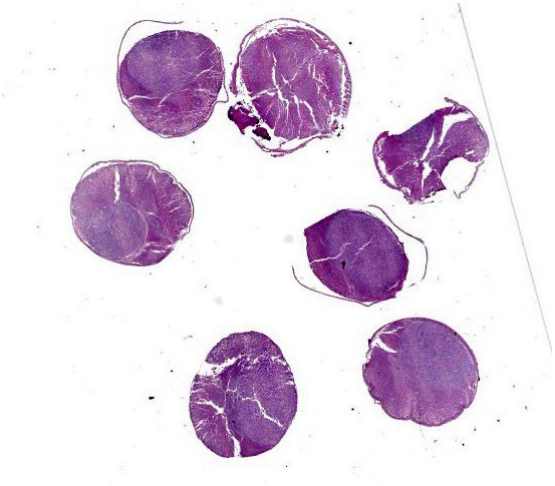

Figure 2-1. Spinal cord, cat. Multiple sections of spinal court are submitted for examination. At subgross magnification, an infiltrative neoplasm effaces 50-60% of the normal architecture. (HE, 6X)

Serology for FIV, FeLV, *Toxoplasma gondii*: negative.
PCR for Feline coronavirus, *Neospora caninum*, Feline parvovirus, *Toxoplasma gondii* (liquor): negative.
Liquor cytology: mixed pleocytosis, mainly monocytoid and neutrophilic.
Liver and spleen cytology: mild hepatocellular degeneration; splenic extramedullary hemopoiesis.

Microscopic Description:
Spinal cord. Focally effacing and replacing about 60% of the grey and white matter compressing the adjacent tissue, there is a nodular neoplasm of 4 mm that is moderately cellular, multifocally infiltrative, moderately demarcated and unencapsulated.

Neoplastic cells are variably arranged in interlacing streams, short bundles, and sheets with scant amounts of supporting fibrovascular stroma. A mixed cell population is present. The predominant neoplastic cells are round to angular, 20-50 microns large, with low nucleus/cytoplasm ratio, variably distinct cell borders and abundant eosinophilic cytoplasm that multifocally forms stout processes. Nuclei are 5-15 microns large, round to elongated to pleomorphic, eccentric, with open-faced chromatin and mostly single prominent nucleolus. Rare binucleated neoplastic cells and multifocal megakaryosis are observed. Anisokariosis and anisocytosis are severe (gemistocyte-like cells; 60%). The predominant population is admixed with spindle to stellate cells, 10-15 microns large, with high nucleus/cytoplasm ratio, indistinct cell borders and scant eosinophilic cytoplasm. Nuclei are oval to elongated, 6-8 micros large, central with finely stippled chromatin and rarely evident nucleoli. Anisokariosis and anisocytosis are mild (astrocytes; 40%). Mitoses are less than 1 in 2.37mm^2.

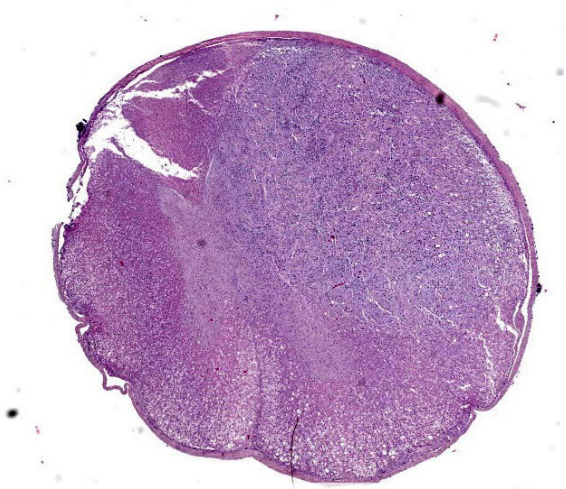

Figure 2-2. Spinal cord, cat. Slightly higher magnification of one section of spinal cord demonstrating the neoplasm (HE, 17X)

In the surrounding white matter axonal sheaths are moderately vacuolized (spongiosis). Vessels are hyperemic.

Immunohistochemistry: neoplastic cells are diffusely and strongly GFAP-positive, diffusely and moderately S100-positive; negative to CNPase.

Contributor's Morphologic Diagnosis:
Spinal cord. Gemistocytic astrocytoma, grade II

Contributor's Comment:
Gliomas are primary neoplasms of the central nervous system originating from glial cells.[18] Astrocytomas are common in dogs, whereas they are rare in cats. In cats, astrocytomas represent about 2.8% of intracranial neoplasms and 3.5% of spinal ones; the most common tumors of the spinal cord in cats are lymphoma and osteosarcoma.[1,8,18] The most frequent location of astrocytomas in cats, according to the literature, is telencephalon, with rarer reports in the brainstem, cerebellum and spinal cord.[8,9,12,18]

Astrocytomas have variable macroscopic appearance, although their presence might be hard to assess grossly. They can be firm,

palpable masses, ranging from white to gray, with ill-defined borders and possible areas of necrosis, especially with larger and more malignant tumors.[3]

Histologically, astrocytomas are neuroepithelial tumors classified in different histological subtypes which correlate to the grade. Based on the 2007 World Health Organization (WHO) classification of tumors of the central nervous system, there are:
• Low-grade astrocytomas (grade I), with the variants fibrillary astrocytoma, protoplasmic astrocytoma, pilocytic astrocytoma, and subependymal giant cell astrocytoma;
• Medium grade astrocytomas (grade II), with the gemistocytic variant;
• Anaplastic astrocytomas (grade III);
• High-grade astrocytomas (grade IV) or glioblastoma.[3,6]

Low-grade astrocytomas are mostly scarcely or moderately cellular, unencapsulated, expansile, with round to oval neoplastic cells replacing the pre-existing tissue. On the other hand, the medium grade astrocytomas usually are more densely cellular, showing more nuclear atypia. Anaplastic astrocytomas are characterized by cells with the greater extent of atypia and higher mitotic index. In high-grade astrocytomas there are frequent areas of haemorrhages and necrosis, around which neoplastic cells are pseudopalisading. Proliferation of the endothelium of blood vessels is present. In this entity high pleomorphism and atypia of the neoplastic cells are expected.[3]

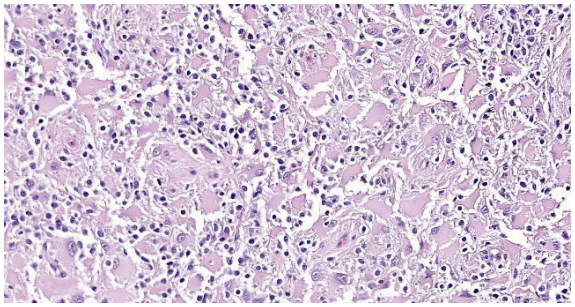

Figure 2-3. Spinal cord, cat. The neoplasm is composed of large polygonal gemistocytes which are separated by bundles of astrocyte process, numerous microglia, and fewer Schwann cells and non-neoplatic astrocytes. (HE, 337X)

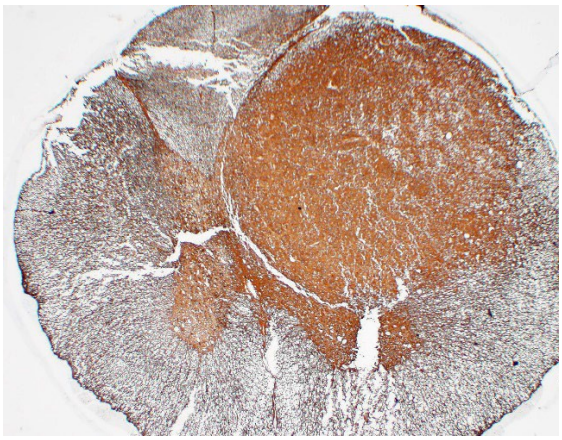

Figure 2-4. Spinal cord, cat. The neoplasm (and adjacent compressed grey matter) demonstrates strong immunopositivity for glial fibrillary acidic protein. (HE, 40X)

Alongside the well differentiated astrocytomas reported in cats, the rarer subtypes eg. pilocytic astrocytoma, granular cell astrocytoma, angiocentric astrocytoma and anaplastic gemistocytic astrocytoma are also described.[8,9,15,18] There are few reports of gemistocytic astrocytoma in cats. Gemistocytic astrocytoma is considered a medium-grade (grade II) tumor that is histologically characterized by the prevalence of large cells with abundant eosinophilic cytoplasm and eccentric oval nuclei (gemistocytic cells).[3] Nevertheless, in human pathology gemistocytic astrocytomas are no longer recognized as a histological subtype but rather as a pattern ("gemistocytic tissue pattern"), according to 2021 World Health Organization classification of tumors of the central nervous system.[7] A threshold of 20% gemistocytes in the neoplastic population is suggested to adopt this definition.[7]

On immunohistochemistry, neoplastic cells in gemistocytic astrocytomas are immunoreactive for glial fibrillar acidic protein (GFAP), S100, vimentin, whereas they do not stain for CNPase and epidermal growth factor receptor (EGFR), in contrast to

oligodendrolioma or glioblastoma, respectively.[1,3] Variable immunoreactivity for p53 was also described in one study, suggesting a possible abnormal biological behavior of this protein in the pathogenesis of feline astrocytoma.[1]

We classified the lesion we submitted as a gemistocytic astrocytoma taking into consideration the prevalence of gemistocytic cells observed on histology in association with the immunohistochemical positivity for S100 and GFAP and negativity for CNPase.

Contributing Institution:
San Marco Veterinary Clinic and Laboratory Pathology division
Viale dell'Industria 3, 35030
Veggiano (PD), Italy
https://www.clinicaveterinariasanmarco.it/

JPC Diagnosis:
Spinal cord: Gemistocytic astrocytoma.

JPC Comment:
A recent *Vet Pathol* review article by Rissi details the clinical, pathologic, diagnostic, and behavioral features of primary central nervous system neoplasms in cats. Most intracranial neoplasms in cats are primary brain tumors, and the most common primary brain tumor is the meningioma, representing 60%

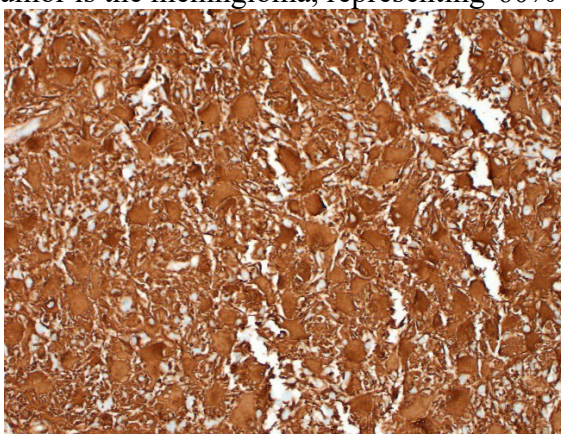

Figure 2-5. Spinal cord, cat. Neoplastic cells and their processes demonstrated strong immunopositivity for glial fibrillary acidic protein. (HE, 40X)

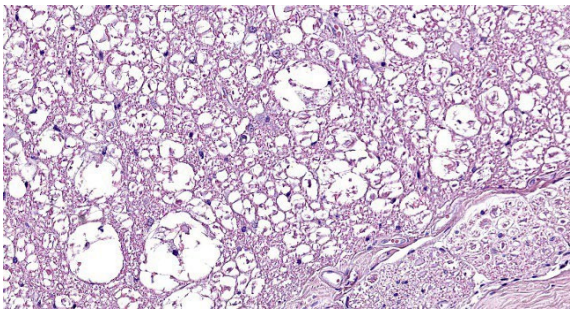

Figure 2-6. Spinal cord, cat. Adjacent to the neoplasm, there are few markedly dilated myelin sheaths continuing axonal debris and Gitter cells. (HE, 314X)

of all intracranial tumors and 85% of all primary brain tumors. [12] Gliomas are the second most common primary CNS tumor of the cat but, in the spinal cord and vertebral column, gliomas are slightly more common (8%) than meningiomas (7%).[12] The most commonly reported type of glioma in the cat is the astrocytoma; ependymoma and oligodendroglioma are reported at lower rates.[12]

Astrocytomas have variable staining for GFAP and OLIG-2, whereas oligodendrogliomas have strong labeling for OLIG-2 and variable reactivity for GFAP.[13] Round cell markers may also be useful to rule out lymphoma in neoplasms that lack OLIG-2 staining, as lymphoma is the most common spinal cord tumor of cats.[13] Recently, Elbert and Rissi reported on doublecortin immunolabeling in 11 feline gliomas. Doublecortin (DCX) is a protein of neuronal precursor cells. [13] DCX expression along the periphery of invasive human gliomas is suggestive of more invasive behavior. [13] In this study on feline gliomas, DCX was expressed in all 4 astrocytomas, with more intense staining along the margins of the neoplasms. [13] Neuronal nuclear protein (NeuN), expressed by mature neurons, was negative in all four astrocytomas of this study. [13]

Gliosarcoma is a rare subtype of the grade IV astrocytoma (glioblastoma), and the first documented case in a cat was reported by Alvarez et al in 2019. Gliosarcomas are composed

of bimorphic cell populations: a glial component and a sarcomatous component; both components are thought to arise from a common progenitor cell due to their similar genetic alterations.[2] This case was in a 5-year-old cat with 1.5-year history of mild neurologic signs that acutely progressed, and a gliosarcoma was discovered in the septum pellucidum. Within the glial component, neoplastic cells histologically resembled astrocytes and were positive for GFAP and negative for OLIG-2.[2] This case also contained all four types of structures of Scherer, which are histologic features of invasiveness in glial tumors.[2] Types of Scherer structures include spread within the subpial space, perivascular infiltration, and perineuronal and perivascular satellitosis.[2]

The glioma entity was first described over 200 years ago, and several notable pathologists have contributed to our knowledge of the entity. Rudolf Virchow coined the term glioma and provided the first histologic description of the neoplasm,[11] and Howard Tooth, Percival Bailey, and Harvey Cushing later expanded the knowledge of glioma histology. German pathologist Hans Joachim Scherer (1906-1945), the namesake for Scherer structures, also conducted extensive landmark research on gliomas.[11] One of the many observations made by Scherer that shape our understanding of gliomas is the pseudopalisading of neoplastic cells around areas of necrosis in glioblastoma multiforme (high grade astrocytoma).[17] As a researcher in Germany during the first half of the 20th century, Scherer's work was both influenced and interrupted by Nazi activities and World War II. After being arrested by the Gestapo in 1933, Scherer fled to Belgium, where published numerous studies on human gliomas while employed at the Institute Bunge in Antwerp.[10] In 1941, the German military ordered Scherer to return to Germany, and he began working at the Neurologic Institute in Breslau (now Poland).[10] There, he conducted post-mortem examinations on at least 209 euthanized children, most with neurologic disabilities.[5] Whether his work in this program was voluntary or conducted under coercion is still unknown, but his prior arrest, his exodus from Germany after Hitler rose to power, and personal accounts from his acquaintances suggest that he was not sympathetic to the Nazi party.[16] Scherer died in 1945 in a railway station attacked during one of the last Allied bombings.[11]

Readers are encouraged to review Case 1, Conference 7, 2021-2022, a grade IV astrocytoma in the dog. The contributor and conference comments provide an excellent review of features of canine astrocytoma, including a recently published grading scheme for canine gliomas.

References:

1. Aloisio F, Levine JM, Edwards JF. Immunohistochemical features of a feline spinal cord gemistocytic astrocytoma. *J Vet Diagn Invest*. 2008 Nov;20(6):836-8.
2. Alvarez P, Wessmann A, Pascual M, Comas O, Pi D, Pumarola M. Cerebral gliosarcoma with perivascular involvement in a cat. *JFMS Open Reports.* 2019; 5(2): 1-6.
3. Cantile C, Youssef S. Nervous System. In: Grant Maxie M, ed. *Jubb, Kennedy and Palmer's Pathology of Domestic Animals*. 6th ed. St. Louis, USA: Elsevier. 2016; 250-406.
4. Elbert JA, Rissi DR. Doublecortin immunolabeling and lack of neuronal nuclear protein immunolabeling in feline gliomas. *J Vet Diagn Invest.* 2022; 34(4):757-760.
5. Kleiheus P. Reply to Marc Scherer. *Brain Pathol.* 2013; 23(4): 488.
6. Louis DN, Ohgaki H, Wiestler OD, et al. The 2007 WHO classification of tumours

of the central nervous system. *Acta Neuropathol*. 2007; 114(2):97-109.
7. Louis DN, Perry A, Wesseling P, et al. The 2021 WHO Classification of Tumors of the Central Nervous System: a summary. *Neuro Oncol*. 2021 Aug 2;23(8):1231-1251.
8. Marioni-Henry K. Tumors affecting the spinal cord of cats: 85 cases (1980–2005). *J Am Vet Med Assoc*. 2008; 232: 237–243.
9. Murthy VD, Liepnieks ML, Roy MA, et al. Diagnosis and clinical outcome following surgical resection of an intracranial grade III anaplastic gemistocytic astrocytoma in a cat. *JFMS Open Rep*. 2020; 6(2): 2055116920939479.
10. Peiffer J, Kleiheus P. Hans-Joachim Scherer (1906-1945), pioneer in glioma research. *Brain Pathol.* 1999; 9(2): 241-245.
11. Reuter G, Lombard A, Molina ES, Scholtes F, Bianchi E. Hans Joachim Scherer: an under-recognized pioneer of glioma research in Belgium. *Acta Neurol Belg.* 2021; 121(4): 867-872.
12. Rissi DR. Feline glioma: a retrospective study and review of the literature. *J Feline Med Surg*. 2017; 19:1307–1314.
13. Rissi DR. A review of primary central nervous system neoplasms of cats. *Vet Pathol.* 2023. Online First.
14. Rissi DR, McHale BJ, Armién AG. Angiocentric astrocytoma in a cat. *J Vet Diagn Invest*. 2019; 31(4): 576-580.
15. Sant'Ana FJ. Pilocytic astrocytoma in a cat. *Vet Pathol*. 2002; 39: 759–761.
16. Scherer M. Some comments on the paper: Hans-Joachim Scherer (1906-1945), a pioneer in glioma research. *Brain Pathol*. 2013; 23(4):485-487.
17. Stoyanov GS, Petkova L, Dzenkov DL.Hans Joachim Scherer and His Impact on the Diagnostic, Clinical, and Modern Research Aspects of Glial Tumors. *Cureus.* 2019; 11(11): e6148.
18. Troxel MT. Feline intracranial neoplasia: retrospective review of 160 cases (1985–2001). *J Vet Intern Med*. 2003; 17: 850–859.

CASE III:

Signalment:
2-year-old, female-neutered domestic short hair cat (*Felis catus)*

History:
The cat was presented in a veterinary practice with acute back pain and mild ataxia after a jump from a cupboard. The clinical examination revealed no specific findings, and the cat was treated with non-steroidal anti-inflammatory drugs (NSAIDs) for a suspected traumatic injury of the vertebral bone and spinal cord. After 2 days without clinical improvement, blood work was performed and displayed mild hypophosphatemia (3.1 mg/dl, reference range: 3.4 – 8.5 mg/dl) and monocytosis (6.6%, reference range: 1 – 3%). The radiological examination showed no abnormalities in the skeleton or spinal cord but a mildly increased interstitial pattern in the

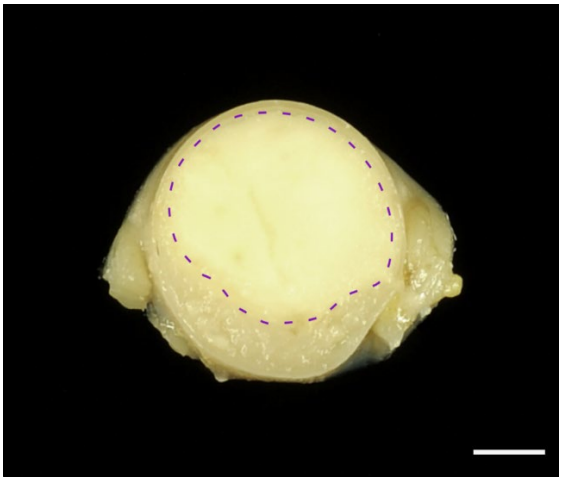

Figure 3-1. Spinal cord, cat. Cross-section with a leptomeningeal, circumferential, grey, solid neoplasm compressing the spinal cord (dashed line: junction tumor – spinal cord). Scale bar: 2 mm. (Photo courtesy of: Department of Pathology, University of Veterinary Medicine, Hannover, Buenteweg 17, 30559 Hannover, Germany. http://www.tiho-hannover.de/kliniken-institute/institute/institut-fuer-pathologie/)

craniodorsal lung. The cat was treated further with NSAIDs, antibiotics and vitamin B. Four days after initial presentation, the cat showed mild apathy and severe ataxia with markedly reduced proprioceptive reactions in all four limbs and reduced segmental reflexes in the thoracic limbs. The suspected neuroanatomical localization was the brain or the spinal cord cranially to Th2. No cells were found in the cerebrospinal fluid (CSF). Infection with feline coronavirus, bornavirus, *Toxoplasma gondii* and *Bartonella henselae* within the CSF was excluded via PCR. Computed tomography (CT) of the entire body was performed but showed no abnormalities of the central nervous system. During hospitalization, further progressive clinical decline and irresponsiveness to treatment resulted in lateral recumbency and spontaneous death within 6 days after initial presentation. The cat was subsequently submitted for necropsy.

Gross Pathology:
Leptomeninges were diffusely prominent, mostly pronounced within cervical segments with rostral extension to the medulla oblongata. After formalin fixation, cross sections revealed a well demarcated, gray-beige, soft, subdural thickening within the whole circumference of the spinal cord, involving primarily the cervical part, and the medulla oblongata with partial compression of the neuroparenchyma. No intraaxial mass was found in coronal sections of the brain and spinal cord.

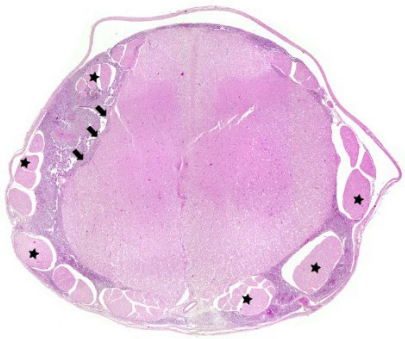

Figure 3-2. Spinal cord, cat. The neoplasm is highly cellular and restricted to the subarachnoidal space with compression of the adjacent neuroparenchyma (arrows) and omission of the spinal nerves (asterisks). HE, bar: 2 mm. (Photo courtesy of: Department of Pathology, University of Veterinary Medicine, Hannover, Buenteweg 17, 30559 Hannover, Germany. http://www.tiho-hannover.de/kliniken-institute/institute/institut-fuer-pathologie/)

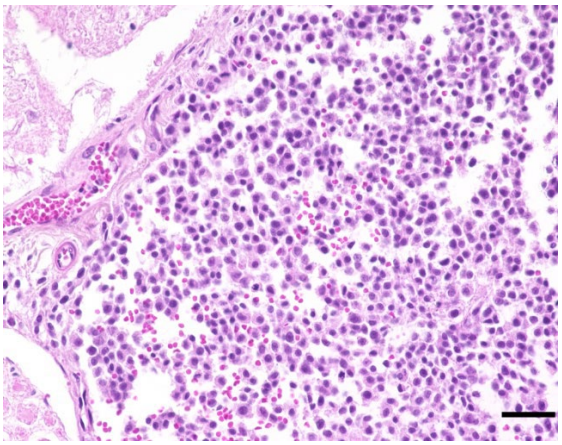

Figure 3-3. Spinal cord, cat. The leptomeningeal neoplasm is composed of numerous round cells arranged in sheets and containing a large hyperchromatic nucleus. HE, bar: 50 µm. (Photo courtesy of: Department of Pathology, University of Veterinary Medicine, Hannover, Buenteweg 17, 30559 Hannover, Germany. http://www.tiho-hannover.de/kliniken-institute/institute/institut-fuer-pathologie/)

Laboratory Results:
The mass was immunostained using the ABC method with commercially available antibodies. Neoplastic cells showed a diffuse, intranuclear expression of oligodendrocyte transcription factor 2 (OLIG2) and doublecortin. Moreover, tumor cells exhibited a diffuse cytoplasmic expression of microtubule-associated protein 2 (MAP2), CNPase and synaptophysin. Some of the neoplastic cells displayed a cytoplasmic vimentin expression. Ki-67 as a proliferation marker protein was detected in more than 50% of the neoplastic cells. Scattered ionized calcium-binding adapter molecule 1 (Iba1)-positive cells and few scattered glial fibrillary acid protein (GFAP)-positive cells were present within the neoplasm (interpreted as reactive

macrophages/microglia and astrocytes, respectively). Neoplastic cells lacked immunoreactivity for neurofilament (NF), S100 protein, neuron specific enolase (NSE), myelin basic protein, p75 neurotrophin receptor, neuronal nuclear protein (NeuN), periaxin, pan-cytokeratin, CD3, CD20, CD79a, paired box 5 transcription factor (PAX5) and multiple myeloma oncogene 1 (MUM1).

Microscopic Description:
Spinal cord: Expanding the subarachnoidal space, there is a solid, non-encapsulated, cell-rich, circumferential accumulation of neoplastic cells extending from the arachnoidea to the margins of the spinal cord. The neoplasm is composed of closely packed, round, mononuclear cells arranged in sheets, accompanied by low amounts of fine fibrovascular stroma. The medium-sized cells possess variably distinct cell borders and contain low amounts of finely granular eosinophilic cytoplasm. Nuclei measure 10–15 µm in diameter, are centrally to eccentrically located, round to oval and frequently hyperchromatic with one distinct small nucleolus. Multifocally, large necrotic areas with complete loss of cytological details are present. Tumor cells exhibit mild anisocytosis and –karyosis with a mitotic count of 10 mitoses per 2.37 mm² (with variation throughout the samples). Occasionally, mild hemorrhages are present. The neuroparenchyma adjacent to the tumor multifocally shows compression and marked degenerative changes including spheroid formation and vacuolation of the white and gray matter.

Contributor's Morphologic Diagnosis:
Spinal cord: Leptomeningeal oligodendrogliomatosis, feline.

Contributor's Comment:
The presented findings relate to a rare case of primary diffuse leptomeningeal oligodendrogliomatosis, which represents an oligodendroglioma-like tumor with an unusual distribution.

In contrast to other glial tumors, which mostly arise intracranially within the neuroparenchyma and may secondarily infiltrate the leptomeninges, primary diffuse leptomeningeal gliomatosis (PDLG) is defined as a diffuse infiltration of the subarachnoidal space by neoplastic glial cells without evidence of a primary intraaxial tumor.[27] Having been described in humans and in dogs before, this entity has recently been reported in an older cat.[1,10,21,28] The presented case is the second report of feline PDLG.[2]

Histologically, oligodendroglial tumors are typically characterized by uniform, densely packed cells with vacuolated or eosinophilic cytoplasm, a round hyperchromatic nucleus and distinct cell borders with variable patterns of cell arrangement. Delayed formalin fixation often causes a perinuclear halo, resulting in a "honeycomb pattern" appearance.[25] However, these tumors can vary in their appearance and origin, which requires distinction from other neoplasms (such as lymphomas and neurocytomas) by

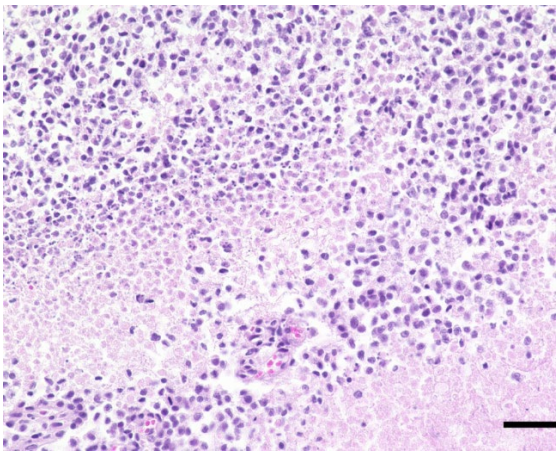

Figure 3-4. Spinal cord, cat. There are large necrotic areas within the neoplasm. HE; bar: 50 µm. (Photo courtesy of: Department of Pathology, University of Veterinary Medicine, Hannover, Buenteweg 17, 30559 Hannover, Germany. http://www.tiho-hannover.de/kliniken-institute/institute/institut-fuer-pathologie/)

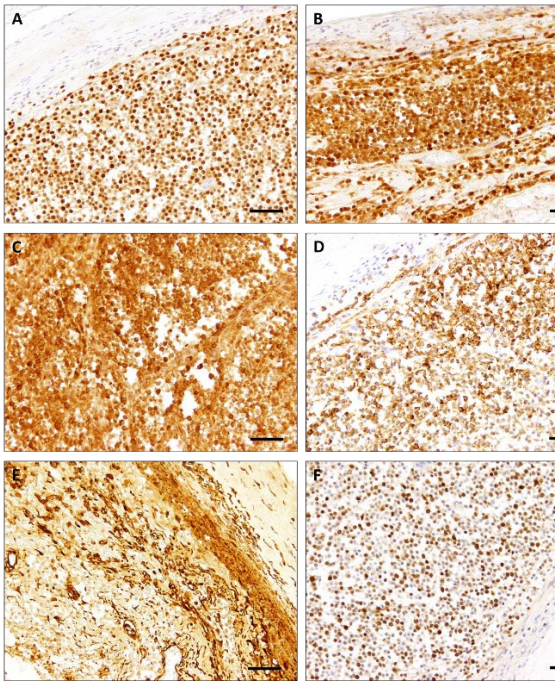

Figure 3-5. Spinal cord, cat. The tumor shows diffuse immunopositivity for OLIG2 (A), doublecortin (B) and MAP2 (C). Most tumor cells were also immunopositive for synaptophysin (D). Tumor-associated vasculature stained positive for vimentin (E). Positive nuclear staining for Ki-67 demonstrates high proliferation activity (F). bars: 50 µm. (Photo courtesy of: Department of Pathology, University of Veterinary Medicine, Hannover, Buenteweg 17, 30559 Hannover, Germany. http://www.tiho-hannover.de/kliniken-institute/institute/institut-fuer-pathologie/)

immunohistochemistry, as performed in the present case. Tumor cells in the present case exhibited an expression of oligodendrocyte transcription factor 2 (OLIG2), doublecortin, microtubule-associated protein 2 (MAP2), CNPase and synaptophysin. Some of the neoplastic cells displayed a cytoplasmic vimentin expression.

Further differentials in humans and domestic animals for leptomeningeal cell infiltrates include secondary leptomeningeal gliomatosis, ependymoma, pilocytic astrocytoma, or multicentric neoplasia and meningitis of autoimmune or infectious etiology.[1,5,11,27] In felines, the most frequently reported extraparenchymatous tumors of the spinal cord are lymphomas and osteosarcomas.[14] An infectious disease that needs to be considered in cats for this localization is feline infectious peritonitis (FIP).[7,22]

To date, the exact origin of PDLG remains unknown. Several authors postulated that PDLG arises from so-called heterotopic glial cell nests, which represent small aggregates of glial cells within the subarachnoid space arising from protrusions of mature glia cells from the neuraxis, but this hypothesis remains controversial.[4,5,19] Occasional simultaneous immunopositivity for OLIG2 and neuronal markers like synaptophysin or doublecortin, as also observed in the present case, suggests a histiogenesis from a common progenitor cell.[15,16,18]

In humans, the incidence of diffuse leptomeningeal oligodendroglioma-like neoplasms is higher in children and young adults when compared to other age groups.[20] Several genetic abnormalities have been attributed to oligodendroglial neoplasms in humans including a 1p/19q deletion.[26] Concerning domestic animals, brachycephalic dog breeds are predisposed to develop oligodendroglioma with a suspected defect on chromosome 26.[23,24] The exclusive representation of brachycephalic dogs (4 boxer dogs, 1 Staffordshire bull terrier, 1 Cane Corso) in published cases of canine diffuse leptomeningeal gliomatosis may propose a similar breed disposition to PDLG.[1,8,10,12] However, further case data need to be obtained to confirm this assumption. No specific genetic alterations have been determined so far for PDLG in domestic animals.

Intravital diagnosis of PDLG, which is predominantly based on MRI findings and exclusion of other diseases, is challenging due to relatively unspecific clinical and CSF findings and requires histopathological confirmation.[1,5,6,8,10,12,27,28] In most cases, final diagnosis is made at necropsy due to the rapid progression and poor prognosis of the tumor.[5]

Contributing Institution:
Department of Pathology,
University of Veterinary Medicine,
Hannover,
Buenteweg 17,
30559 Hannover, Germany.

http://www.tiho-hannover.de/kliniken-institute/institute/institut-fuer-pathologie/

JPC Diagnosis:
Leptomeninges, spinal cord: Oligodendrogliomatosis.

JPC Comment:
The moderator and conference participants had a spirited discussion over the morphologic diagnosis in this case. As the contributor mentions, it is impossible to determine whether the oligodendrogliomatosis is a primary lesion, or if it arose secondary to a small primary tumor not in section. Due to this uncertainty, some participants favored a broader diagnosis of oligodendroglioma; however, most felt that the term oligodendrogliomatosis would provide valuable information for the clinicians, as a focal oligodendroglioma would not be consistent with the neurologic signs, advanced imaging patterns (MRI with contrast), and gross lesions produced by a diffuse leptomeningeal lesion.

In this section, there is a small focus of fibrosis within the meninges, and some participants considered a second morphologic diagnosis of fibroma. The moderator explained that focal fibrosis within the meninges and in the nerve sheath is a common aging change in geriatric animals and is not considered abnormal in this case.

In a 2020 *Vet Pathol* article, Kauer et al described leptomeningeal olgodendrogliomatosis in a 4.5 year old cow which died after progressive neurologic signs, including ataxia,

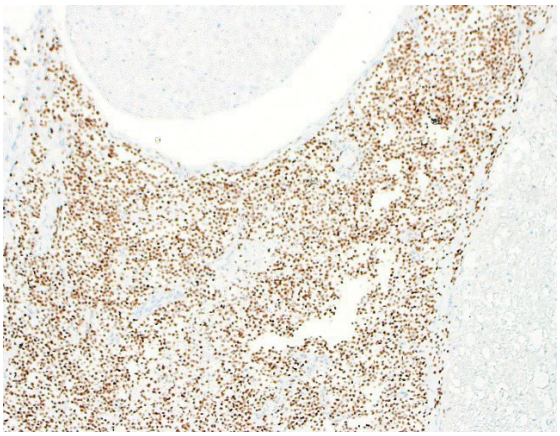

Figure 3-6. Spinal cord, cat. Neoplastic cells stain demonstrates strong nuclear immunopositivity for Olig-2. (anti-Olig-2, 200X)

circling, and tremors.[9] Grossly, the leptomeninges spanning the cerebellum, ventral occipital lobe, and first cervical spinal cord segment were expanded by a gelatinous, tan to gray mass that protruded into the third and fourth ventricles and extended into the thalamus.[9] Histologically, the neoplastic cells were uniformly round and hyperchromatic, arranged in sheets, nests, and cords, and surrounded by a myxoid matrix.[9] There were multifocal microcysts filled with mucin. Multifocal areas of necrosis, microvascular proliferation, and a high mitotic rate were indicative of malignancy.[9] The vast majority of tumor cells had strong nuclear immunoreactivity for Olig-2.[9] These features were consistent with a diffuse high-grade leptomeningeal oligodendrogliomatosis.[9] While this is the first documented bovine case of diffuse leptomeningeal oligodendrogliomatosis, two previously documented cases of oligodendrogliomas in cows also featured this diffuse leptomeningeal growth without identification of a primary neoplasm. The authors suggest that these prior cases may also be instances of diffuse leptomeningeal oligodendrogliomatosis.[9]

Two other rare proliferative lesions of the leptomeninges have recently been reported in cats: angiocentric astrocytoma and

meningiomatosis.[3,17] In a 2019 *Vet Pathol* article, Rissi et. al described the first veterinary case of angiocentric astrocytoma in a 15 year old cat with seizures refractory to medical therapy.[17] On necropsy examination, the leptomeninges surrounding the olfactory bulbs were swollen and firm with multifocal hemorrhage.[17] Histologically, blood vessels within the leptomeninges of the olfactory bulb and extending caudally to the thalamus were surrounded by polygonal to elongate, sometimes palisading neoplastic cells.[17] No primary neoplasm was identified. On IHC, these cells had strong reactivity for GFAP, S100, and vimentin.[17] The histologic morphology, IHC staining, and ultrastructure features of this case were all consistent with a diagnosis of astrocytoma, and this case bears many similarities to human angiocentric astrocytoma, a rare entity in children and young adults.[17]

The first documented case of meningioangiomatosis in a cat was recently reported by Corbett et al.[3] Previously, this rare entity has been described in humans and dogs. Corbett's report details a 13 year old cat with history of acute behavioral changes, open mouth breathing, and facial twitching that progressed to generalized seizures.[3] The animal died despite 5 days of hospitalization, and on necropsy, a unilateral hemorrhagic plaque expanded the meninges over the right pyriform, temporal, and ventral aspect of the occipital lobes and extended into the subjacent cerebral cortex.[3] Histologically, the leptomeninges were thickened by proliferations of vimentin-positive spindle cells streaming and whirling around blood vessels.[3] The histomorphology and IHC profile were consistent with the cases of meningioangiomatosis documented in humans and dogs.[3]

References:

1. Canal S, Bernardini M, Pavone S, et al. Primary diffuse leptomeningeal gliomatosis in 2 dogs. *Can Vet J*. 2013;**54:** 1075–1079.
2. Chludzinski E, Puff C, Weber J, et al. Case Report: Primary diffuse leptomeningeal oligodendrogliomatosis in a young adult cat. *Front Vet Sci*. 2021;**8:** 795126.
3. Corbett MP, Kopec BL, Kent M, Rissi DR. Encephalic meningioangiomatosis in a cat. *J Vet Diagn Invest.* 2022; 34(5): 889-893.
4. Cooper IS, Kernohan JW. Heterotopic glial nests in the subarachnoid space; histopathologic characteristics, mode of origin and relation to meningeal gliomas. *J Neuropathol Exp Neurol*. 1951;**10:** 16–29.
5. Debono B, Derrey S, Rabehenoina C, et al. Primary diffuse multinodular leptomeningeal gliomatosis: case report and review of the literature. *Surg Neurol*. 2006;**65:** 273–282; discussion 282.
6. Dietrich PY, Aapro MS, Rieder A, et al. Primary diffuse leptomeningeal gliomatosis (PDLG): a neoplastic cause of chronic meningitis. *J Neurooncol*. 1993;**15:** 275–283.
7. Fondevila D, Vilafranca M,Pumarola M. Primary central nervous system T-cell lymphoma in a cat. *Vet Pathol*. 1998;**35:** 550–553.
8. Giron C, Paquette D, Culang D, et al. Diffuse meningeal oligodendrogliomatosis characterized by spinal intra-parenchymal nodules on magnetic resonance imaging in a dog. *Can Vet J*. 2020;61**:** 1312–1318.
9. Kauer RV, Bagatella S, Oevermann A. Diffuse Leptomeningeal Oligodendrogliomatosis in a Cow. *Vet Pathol*. 2020; 57(2): 253-257.
10. Kovi RC, Wünschmann A, Armién AG, et al. Spinal meningeal oligodendrogliomatosis in two boxer dogs. *Vet Pathol*. 2013;**50:** 761–764.

11. Lee JK, Ko HC, Choi JG, et al. A Case of diffuse leptomeningeal glioneuronal tumor misdiagnosed as chronic tuberculous meningitis without brain biopsy. *Case Rep Neurol Med*. 2018;**2018:** 1391943.
12. Lobacz MA, Serra F, Hammond G, et al. Imaging diagnosis – magnetic resonance imaging of diffuse leptomeningeal oligodendrogliomatosis in a dog with "dural tail sign". *Vet Radiol Ultrasound*. 2018;**59:** E1–e6.
13. Louis DN, Perry A, Reifenberger G, et al. The 2016 World Health Organization classification of tumors of the central nervous system: a summary. *Acta Neuropathol*. 2016;**131:** 803–820.
14. Marioni-Henry K, Van Winkle TJ, Smith SH, et al. Tumors affecting the spinal cord of cats: 85 cases (1980-2005). *J Am Vet Med Ass*. 2008;**232:** 237–243.
15. Perry A, Scheithauer BW, Macaulay RJ, et al. Oligodendrogliomas with neurocytic differentiation. A report of 4 cases with diagnostic and histogenetic implications. *J Neuropathol Exp Neurol*. 2002;**61:** 947–955.
16. Rissi DR, Levine JM, Eden KB, et al. Cerebral oligodendroglioma mimicking intraventricular neoplasia in three dogs. *J Vet Diagn Invest*. 2015;**27:** 396-400.
17. Rissi DR, McHale BJ, Armien AG. Angiocentric astrocytoma in a cat. *J Vet Diagn Invest.* 2019; 31(40: 576-580.
18. Rissi DR, Miller AD. Feline glioma: a retrospective study and review of the literature. *J Feline Med Surg*. 2017;**19:** 1307–1314.
19. Riva M, Bacigaluppi S, Galli C, Citterio A, Collice M. Primary leptomeningeal gliomatosis: case report and review of the literature. *Neurol Sci*. 2005;**26:** 129–134.
20. Rodriguez FJ, Perry A, Rosenblum MK, et al. Disseminated oligodendroglial-like leptomeningeal tumor of childhood: a distinctive clinicopathologic entity. *Acta Neuropathol*. 2012;**124:** 627–641.
21. Roussy G, Cornil L, Leroux R. *Tumeur meningee a type glial*. vol. 30. Paris: Rev. Neurologique.1923:**30**: 294–298.
22. Shrader S, Lai S, Cline K, et al. Gliomatosis cerebri in the brain of a cat. *Vet Sci*. 2016;**3** (3): 13. doi: 10.3390/vetsci3030013.
23. Snyder JM, Shofer FS, Van Winkle TJ, et al. Canine intracranial primary neoplasia: 173 cases (1986-2003). *J Vet Intern Med*. 2006;**20:** 669–675.
24. Truvé K, Dickinson P, Xiong A, et al. Utilizing the dog genome in the search for novel candidate genes involved in glioma development - genome wide association mapping followed by targeted massive parallel sequencing identifies a strongly associated locus. *PLoS Genet*. 2016;**12** (5)**:** e1006000. doi: 10.1371/journal.pgen.1006000.
25. Vandevelde M, Higgins R, Oevermann A. Neoplasia. In: *Veterinary Neuropathology: Essentials of Theory and Practice*. Ames, IA, USA: Wiley-Blackwell; 2012:137–139.
26. Wesseling P, van den Bent M, Perry A. Oligodendroglioma: pathology, molecular mechanisms and markers. *Acta Neuropathol*. 2015;**129:** 809–827.
27. Yomo S, Tada T, Hirayama S, et al. A case report and review of the literature. *J Neurooncol*. 2007;**81:** 209–216.
28. Zoll WM, Miller AD, Bandt C, et al. Primary leptomeningeal gliomatosis

in a domestic shorthaired cat. *J Vet Diagn Invest*. 2019;**31:** 94–97.

CASE IV:

Signalment:
1-year and 4-month-old, male entire, Lagotto Romagnolo dog (*Canis lupus familiaris).*

History:
The dog was presented with a 4-month progressive history of intention head tremors, head bobbing, hypermetria in all limbs, indicating a cerebellar disease, which were slowly progressing in severity. The clinical signs started to be present at 4 months of age. Magnetic Resonance Imaging (MRI) was performed and revealed a diffuse cerebellar cortical atrophy, characterized by a moderately and diffusely reduced in size cerebellum, accompanied by prominent cerebellar folia and sulci. Based on the clinical sings and MRI findings, the main clinical differential diagnosis was a neurodegenerative disease, such as altered autophagy and cerebellar storage disease of the Lagotto Romagnolo due to an unidentified mutation, or another form of cerebellar abiotrophy.

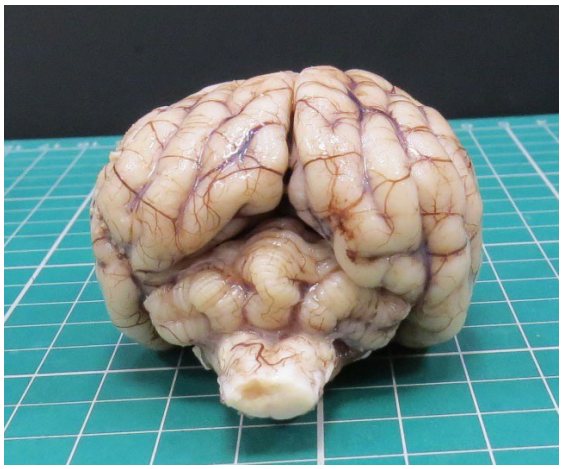

Figure 4-1. Cerebellum, dog. The cerebellum was diffusely reduced in size. (Photo courtesy of: Veterinary Pathology Service, School of Veterinary Medicine and Science, University of Nottingham, College Road, Sutton Bonington, Loughborough, LE12 5RA, United Kingdom https://www.nottingham.ac.uk/vet/service-for-business/veterinary-pathology-service/index.aspx)

The dog was humanely euthanized and submitted for a post-mortem examination (PME).

Gross Pathology:
At PME, macroscopic lesions were restricted to the cerebellum, which was diffusely and moderately reduced in size. Upon sectioning of the formalin-fixed cerebellum, the cortical cerebellar folia appeared markedly thinned.

Laboratory Results:
The genetic test LSD for the ATG4D gene mutation, as a specific DNA test for cerebellar storage disease in Lagotto Romagnolo, was negative.

Microscopic Description:
Cerebellum**:** Diffusely, the cerebellar folia are markedly flattened and there is diffuse, marked thinning and hypocellularity of the granular cell layer with marked loss of granular cells, leading to almost complete absence of this layer accompanied by moderate to marked vacuolation of the neuropil (spongiosis). Rarely, remaining granular cells are either swollen with a vacuolated cytoplasm (degeneration), or shrunken with pyknotic nucleus (necrosis). Glial and microglial cells are diffusely observed replacing the granular layer.

The Purkinje cell layer appears rarely affected with occasional loss of Purkinje cells which are often replaced by large, irregularly round, clear areas (empty baskets). Multifocally, scattered Purkinje cells are either shrunken with angular cellular profile, have a hypereosinophilic cytoplasm and pyknotic nucleus (necrosis) or are rarely swollen with central chromatolysis (degeneration). Rarely, swollen, pale eosinophilic proximal Purkinje

cell axons (torpedoes) are observed extending into the granular cell layer.

Diffusely, the molecular layer appears reduced in thickness, but is otherwise unremarkable.

Contributor's Morphologic Diagnosis:
Cerebellum**:** Diffuse, severe, granular cell degeneration and loss, with spongiosis, and mild, multifocal Purkinje cell loss

Contributor's Comment:
Detailed macroscopic examination in a 1-year and 4-month-old Lagotto Romagnolo dog revealed a severe, diffuse, and symmetric cerebellar atrophy, histologically characterized by a diffuse depletion of the cerebellar granular cell layer neurons, with relative sparing of the Purkinje cell layer, compatible with a cerebellar granuloprival degeneration (CGD). CGD is a type of cerebellar cortical degeneration, also termed cerebellar atrophy or abiotrophy.

Cerebellar cortical abiotrophies (CCAs) are a group of rare diseases characterized by premature or accelerated and progressive degeneration and loss of fully developed neurons, secondary to a presumed intrinsic metabolic defect.[2] CCA has been described as a hereditary defect in various species, such as various dog breeds[7,-9,12,18], Arabian horses[14,17], rabbits[16], goats[10], and rarely in cats[2,18].

Animals with CCA are usually neurologically normal at birth and then start to develop progressive signs of cerebellar disease in weeks, months or less commonly years after birth. Histologically, there is a characteristic degeneration and loss of Purkinje cells, which could be accompanied by secondary loss of granule cell neurons, as a retrograde degeneration.[4,6]

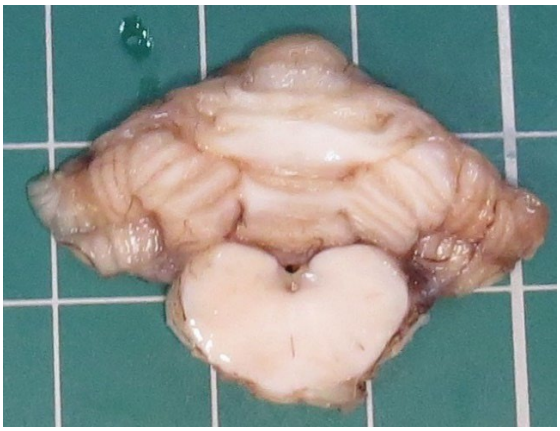

Figure 4-2. Cerebellum, dog. The cortical cerebellar folia appeared markedly thinned (Photo courtesy of: Veterinary Pathology Service, School of Veterinary Medicine and Science, University of Nottingham, College Road, Sutton Bonington, Loughborough, LE12 5RA, United Kingdom https://www.nottingham.ac.uk/vet/service-for-business/veterinary-pathology-service/index.aspx

The case presented herein, represents an unusual presentation of cerebellar cortical degeneration/abiotrophy in a Lagotto Romagnolo dog, characterized by marked degeneration and loss of granular cell neurons with relative sparing of Purkinje cells. Based on these histopathological features, this condition has been named cerebellar granuloprival degeneration (CGD).

The main differential diagnosis based on the breed, clinical signs, and MRI findings was altered autophagy and cerebellar storage disease of the Lagotto Romagnolo. This disease is characterized by progressive cerebellar ataxia and cerebellar atrophy as the main MRI finding, as observed in this case. However, the characteristic histopathological changes of the cerebellar storage disease of the Lagotto Romagnolo, consisting of widespread neuronal cytoplasmic vacuolization within both the central and peripheral nervous system, marked progressive Purkinje cell loss accompanied by reduction of granular cell neurons, as well as spheroid formation and cytoplasmic vacuolation in extra-neural tissues (e.g., pancreatic acinar cells, prostate, mammary gland)[11], were not observed in the

reported case, excluding this disease as a definitive diagnosis.

CGD has been occasionally reported in various dog breeds, including an Australian kelpie and a Labrador retriever, an Italian hound, a Chihuahua, and Border collies, Bavarian mountain and Lagotto Romagnolo dogs.[3,7-9,12,15]

The etiology and pathogenetic mechanisms leading to CGD are still not completely understood, and, although the development of CCA in some dog breed has been attributed to a genetic abnormality, no specific genetic mutation has been yet identified for canine CGD. Inflammatory and infectious diseases have been considered as differential causes for CGD. In Coton de Tulear dogs, two forms have been recognized: the neonatal cerebellar ataxia (aka Bandera's neonatal ataxia) caused by a mutation of the GRM1 gene [4], and a suggested immune-mediated form where the destruction of granular cell neurons results from an immune system defect.[19]

In the presented case, the pathogenetic mechanism leading to CGD was unclear although the histopathological features were not consistent with an inflammatory/infectious etiology. Therefore, a genetic origin was considered more likely. Further studies are needed to elucidate the pathogenesis of this condition in dog breeds.

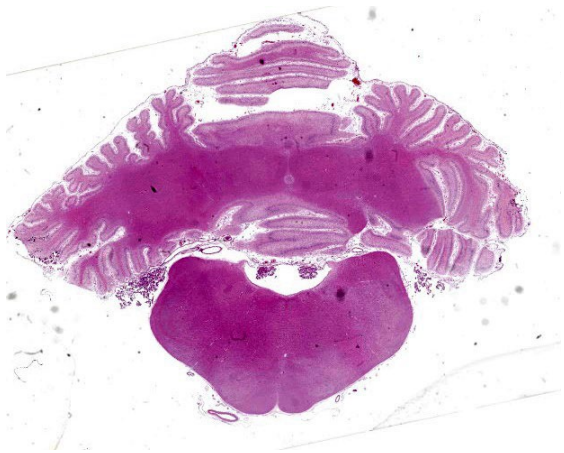

Figure 4-3. Cerebellum, dog. Cerebellar folia are markedly thinned and hypocellular. (HE, 5X)

Contributing Institution:
https://www.nottingham.ac.uk/vet/service-for-business/veterinary-pathology-service/index.aspx

JPC Diagnosis:
Cerebellum: Granule neuron degeneration and loss, diffuse, severe, with mild multifocal Purkinje cell loss.

JPC Comment:
The contributor provides an interesting and uncommon presentation for cerebellar degeneration which was last seen in case 1, conference 12, 2016, in a Coton de Tulear dog.

The moderator explained that granule cells receive most of their stimulation from Purkinje cells, thus are quite susceptible to transsynaptic degeneration during Purkinje cell injury. In the case of granule cell injury, however, Purkinje cells continue to receive stimulation from other neurons (such as the climbing fibers from the olive nucleus), making them more resistant to transsynaptic degeneration. This explains why the secondary Purkinje cell loss was less severe than the primary granule cell loss in this case.

Certain viruses can infect and destroy neuroblast precursors of granule cells in the cerebellum, so an important differential for cerebellar degeneration in young animal to consider is in utero viral infection.[20] In addition to granule cell loss, immature Purkinje cells may be fewer in number or malpositioned in the molecular layer, as granule cells to form the scaffolding for migration.[13,20] Viruses associated with cerebellar dysplasia include feline and rat parvoviruses; porcine and bovine pestiviruses (classical swine fever virus and bovine viral diarrhea virus), and certain bunyaviruses (Akabane virus, Cache valley

virus, and Ainovirus).[1,20] Kilham's rat parvovirus and minute virus of mice (mouse parvovirus) cause cerebellar hypoplasia in rats and mice, respectively, and both of these rodent parvoviruses can also cause cerebellar hypoplasia in experimentally infected Syrian hamsters.[1] In pigs, cerebellar hypoplasia can also be induced in utero when sows are treated with certain organophosphates late in gestation.[20]

Purkinje cells are named after their discoverer, 19th century Czech physiologist Jan Evangelista Purkinje (1787-1869).[5] Purkinje conducted extensive research and contributed to the advancement of multiple disciplines, including histology, embryology, and anatomy. The abundance of his research is evidenced in the variety of histoanatomic structures and physiologic phenomena that bear his name. In ocular physiology, Purkinje described dark adaptation, now known as the Purkinje phenomenon, where the perceived intensity of the color red decreases faster than green and blue as light intensity increases. He also described how a bright light in dim surroundings produces four images (Purkinje-Sanson images). These images are generated by the planes of transition as light passes through the eye: the anterior corneal surface, posterior corneal surface, anterior lens surface, and posterior lens surface. With the benefit of improved microscope technology, Purkinje also provide the first description of cells in the cerebellum. Camillo Golgi (with his newly developed silver stain) and

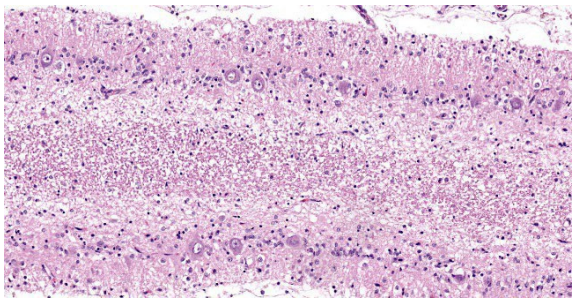

Figure 4-4. Cerebellum, dog. There is almost total depletion of the granular cell layer. (HE, 180X)

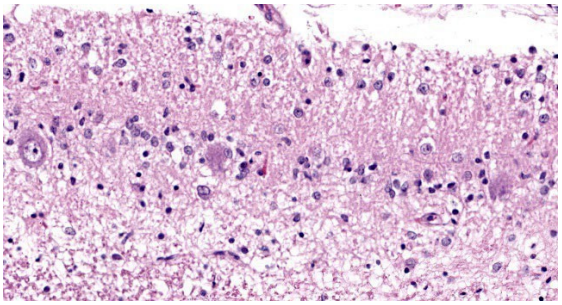

Figure 4-5. Cerebellum, dog. There is multifocal loss of Purkinje cells with proliferation of Begmann's astocytes. (HE, 370X)

Santiago Ramon y Cajal later described structure and processes of these cells, and Cajal recommended the cells be dubbed Purkinje cells. Purkinje's pursuit of knowledge did not stop with the external world; he also conducted pharmacologic experiments on himself, investigating the effects of agents such as digitalis extract, belladonna, camphor, and turpentine. There is some irony in the long list of discoveries which bear Purkinje's name, as Purkinje himself stated, "Science is not about names but discoveries."[5]

References:

1. Barthold SW, Griffey SM, Percy DH. *Path,ology of Laboratory Rodents and Rabbits.* Ames, IO: John Wiley & Sons, Inc. 2016; 18, 124, 175.
2. Biolatti C, Gianella P, Capucchio MT, et al. Late onset and rapid progression of cerebellar abiotrophy in a domestic shorthair cat. *J Small Anim Pract.* 2010;51:123–126.
3. Cantile C, Salvadori C, Modenato M, et al. Cerebellar Granuloprival Degeneration in an Italian Hound. *J Vet Med*. A 49, 523–525 (2002).
4. Cantile C, Youssef S. Nervous system. Maxie MG ed. In: Jubb Kennedy and Palmer's Pathology of Domestic Animals. Vol 1. 6th ed. Philadelphia, PA: Elsevier Saunders; 2016:276, 318-320.
5. Cavero I, Guillon JM, Holzgrefe HH. Reminiscing about Jan Evangelista

Purkinje: a pioneer of modern experimental physiology.
6. Coates JR, O'Brien DP, Kline KL, et al. Neonatal Cerebellar Ataxia in Coton de Tulear Dogs. *J Vet Intern Med*. 2002;16:680–689.
7. Flegel T, Matiasek K, Henke D, et al. Cerebellar cortical degeneration with selective granule cell loss in Bavarian mountain dogs. *J Small Anim Pract*. 2007;48, 462–465.
8. Huska J, Gaitero L, Heindrich N Snyman, et al. Cerebellar granuloprival degeneration in an Australian kelpie and a Labrador retriever dog. *Can Vet J*. 2013;54:55–60.
9. Jokinen TS, Rusbridge C, Steffen F, et al. Cerebellar cortical abiotrophy in Lagotto Romagnolo dogs. *J Small Anim Pract*. 2007;48:470–473.
10. Koehler JW, Newcomer BW, Holland M, et al. A Novel Inherited Cerebellar Abiotrophy in a Cohort of Related Goats. *J Comp Path*. 2015;153:135-139.
11. Kyöstilä K, Syrjä P, Jagannathan V, et al. A Missense Change in the ATG4D Gene Links Aberrant Autophagy to a Neurodegenerative Vacuolar Storage Disease. *PLoS Genet*. 2015;11(4): e1005169.
12. López Betran M, Mascort J, Pumarola M, et al. Cerebellar granuloprival and transsynaptic degeneration in a Chihuahua. *Vet Rec Case Rep*. 2020;8:e000873.
13. Miller AD, Zachary JF. Nervous System. In: Zachary JF, ed. Pathologic Basis of Veterinary Disease. 7th ed. Saint Louis, MO: Elsevier; 2022: 964.
14. Sabada SA, Madariaga GJ, Cobi Botto CM, et al. First report of cerebellar abiotrophy in an Arabian foal from Argentina. *Open Vet J.* 2016; 6(3): 259–262.
15. Sandy JR, Slocombe RF, Mitten RW, et al. Cerebellar Abiotrophy in a Family of Border Collie Dogs. Vet Pathol. 2002;39:736–738.
16. Sato J, Sasaki S, Yamada N, et al. Hereditary Cerebellar Degenerative Disease (Cerebellar Cortical Abiotrophy) in Rabbits. *Vet Pathol*. 2012;49(4):621-8.
17. Scott EY, Penedo MCT, Murray JD, et al. Defining Trends in Global Gene Expression in Arabian Horses with Cerebellar Abiotrophy. *Cerebellum*. 2017;16(2):462-472.
18. Taniyama H, Takayanagi S, Izumisawa Y, et al. Cerebellar Cortical Atrophy in a Kitten. *Vet Pathol.* 1994;31:710-713.
19. Tipold A, Fatzer R, Jaggy A, et al. Presumed immune-mediated cerebellar granular degeneration in the Coton de Tuléar breed. *J Neuroimmunol*. 2000;10(1-2):130-133.
20. Vandevelde M, et al. *Veterinary Neuropathology.* Ames, IA: Wiley-Blackwell; 2012: 96-98.

WSC 2022-2023 Self-assessment
Conference 23

1. Which of the following is very characteristic of orbital meningiomas in the dog?
    a. Sparing of the orbital muscles
    b. Chondro-osseus metaplasia
    c. Their location behind the optic chiasm
    d. Psammoma body formation

2. Which of the following is the most common location for astrocytoma in cats?
    a. Brainstem
    b. Thalamus
    c. Telencephalon
    d. Cerebellum

3. In addition to humans and cats, primary leptomeningeal oligodendrogliomatosis has been reported in which species?
    a. Baboons
    b. Horses
    c. Dogs
    d. Cattle

4. True or false? Animals with cerebellar cortical abiotrophy are typically clinically normal at birth.
    a. True
    b. False

5. True of false. Cerebellar granulomprival degeneration demonstrates relative sparing of neurons.?
    a. True
    b. False

Please email your completed Asessment for grading to Dr. Bruce Williams at bruce.h.williams12.civ@mail.mil. Passing score is 80%. This program (RACE program 33611) is approved by the AAVSB RACE to offer a total of 0.5 CE Credits, with a maximum of 12.5 CE Credits being available to any individual Veterinary Medical Professionals for the 2019-2020 Wednesday Slide Conference. This RACE approval is for the subject matter categories of: SCIENTIFIC using the delivery method of NONINTERACTIVE DISTANCE. This approval is valid in jurisdictions which recognize AAVSB RACE.

Joint Pathology Center
Veterinary Pathology Services

WEDNESDAY SLIDE CONFERENCE 2022-2023

Conference #24 **26 April 2023**

CASE I:

Signalment:
13-day old male Holstein calf (*Bos taurus).*

History:
This male Holstein calf was unable to stand since birth. There were increased lung sounds and bilateral nasal discharge. There was asymmetry in the right tuber coxae. Radiographic changes suggested congenital unilateral hip dysplasia.

Gross Pathology:
The calf was in good body condition with symmetrical muscle mass but was smaller than normal. The umbilical stump is dry.

The joint capsule of the right coxofemoral joint is thickened up to 2 cm by tough white fibrous tissue and gelatinous or clear to yellow fluid. Within the joint capsule are thick mats of yellow-tan friable material resembling fibrin. The synovial fluid is yellow and less viscous than normal. The cartilage of the femoral head is dull and irregular with a punctate to moth-eaten appearance. There is gelatinous thin strands of fibrin with focal hemorrhage within the left stifle and right tarsal joint. The rest of the body was normal.

Laboratory Results:
No aerobic or anaerobic bacteria were isolated from the hip joint. The joint capsule was positive for *Ureaplasma* sp by PCR

Microscopic Description:
The tissue on this slide includes joint capsule with synovial membrane, femoral head with articular epiphyseal cartilage complex, epiphysis, physeal cartilage and metaphysis. Within the wall of the joint capsule are aggregates of neutrophils and macrophages with high-protein fluid including fibrin. There is fibrous tissue surrounding these areas. The synovial membrane has villus formation and synoviocytes are hypertrophied and up to 3 cells thick.

There is fibrin with neutrophils beneath the synovial membrane at the transition zone, the junction between joint capsule and perios-

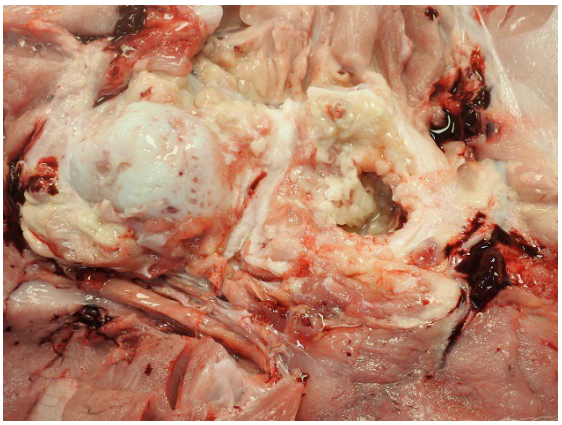

Figure 1-1. Joint, calf. The joint capsule of the right coxofemoral joint is thickened and fibrotic up to 2 cm. and contains thick mats of fibrin. The synovial fluid is yellow and less viscous than normal. The cartilage of the femoral head is dull and irregular with a punctate to moth-eaten appearance. (Photo courtesy of: Department of Pathobiology, Ontario Veteirnary College, University of Guelph, Guelph, Ontario, Canada; https://ovc.uoguelph.ca/pathobiology).

Figure 1-2. Joint, calf. One section of markedly thickened joint capsule (left) and the femoral head are submitted (right). (HE, 5X)

teum. The articular epiphyseal cartilage complex is mostly normal however within the epiphysis is a region of fibrosis and connective tissue replacement of hematopoietic marrow of the intertrabecular spaces. Some of this fibrous tissue has mature collagen.

Contributor's Morphologic Diagnoses:
Osteomyelitis of femoral head, neutrophilic and histiocytic fibrosing joint capsulitis/periarthritis and synovial hyperplasia.

Contributor's Comment:
The history, diagnostic imaging findings, gross pathology findings and histopathology indicates this is a congenital infectious arthritis and osteomyelitis. The identification of *Ureaplasma* confirms this as fetal infection and arthritis with *Ureaplasma diversum*. This is an uncommon manifestation of *Ureaplasma* infection, which is better known for inducing amnionitis and fetal pneumonia with large lymphoid follicles around bronchi. The location of the reaction in the coxofemoral joint is typical of this entity.

Contributing Institution:
Department of Pathobiology, Ontario Veterinary College, University of Guelph,
Guelph, Ontario, Canada
https://ovc.uoguelph.ca/pathobiology/

JPC Diagnosis:
Coxofemoral joint: Arthritis, pyogranulomatous and proliferative, diffuse, severe, with osteomyelitis and articular cartilage necrosis and erosion.

JPC Comment:
In large animals, neonatal polyarthritis is commonly the result of systemic infection secondary to omphalophlebitis and/or failure

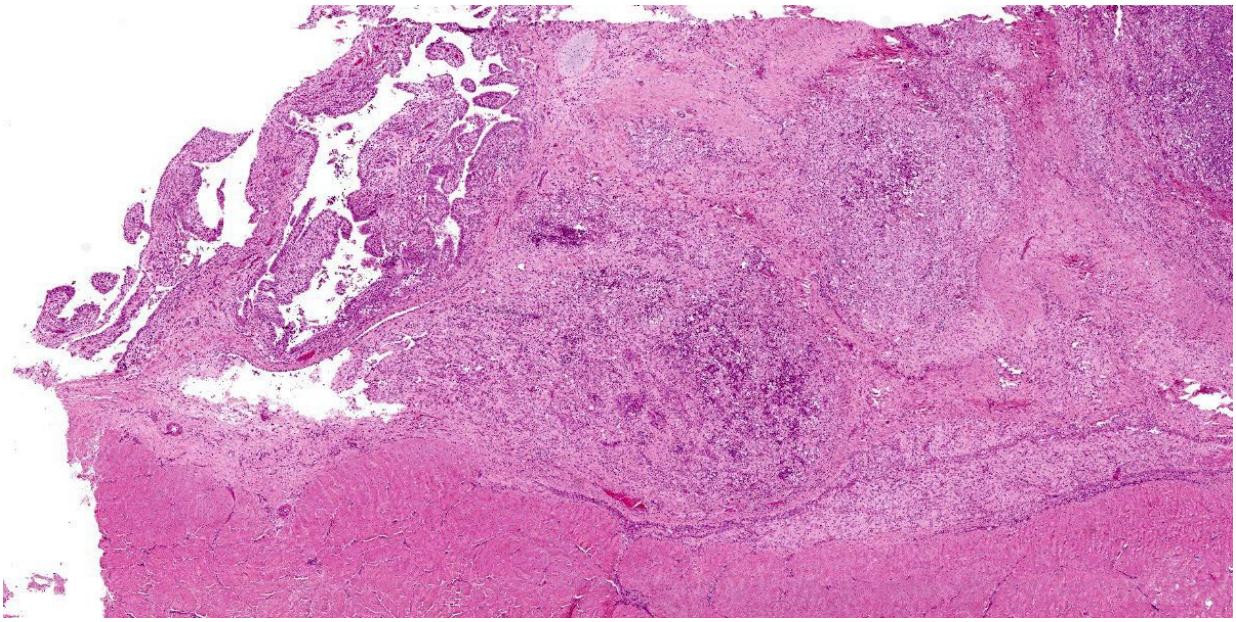

Figure 1-3. Joint capsule, calf. There are prominent synovial villi (left) and the joint capsule is expanded by marked inflammation and fibrosis (right). (HE, 25X)

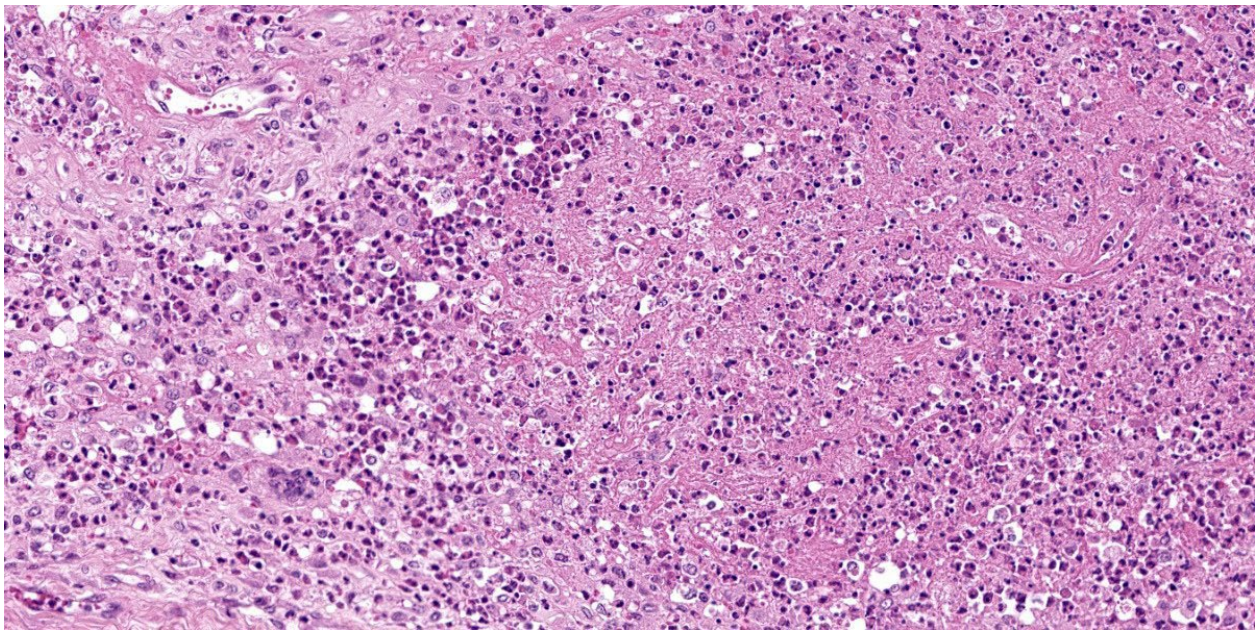

Figure 1-4. Joint capsule, calf. Areas of necrosis within the joint capsule are infiltrated by large number of viable and necrotic neutrophils, macrophages, and rare multinucleated giant cell macrophages. (HE, 272X)

of passive transfer with subsequent immunodeficiency. In calves, the most common organisms associated with neonatal polyarthritis are coliforms and streptococcus. Both agents result in systemic lesions, including fibrinosuppurative meningitis and polyarthritis. *Streptococcus* septicemia also characteristically causes embolic iridocyclitis with hypopyon and corneal clouding.[3]

Another important differential for polyarthritis in calves is *Mycoplasma bovis*¸ which belongs to the same order as *Ureaplasma*.[3] *M. bovis* causes a variety of diseases in cattle including pneumonia, mastitis, otitis media in calves, and polyarthritis.[3] Calves are infected by consuming the bacterium in the milk of infected cows and often develop concurrent pneumonia. Histologically, affected joints have fibrinosuppurative and erosive arthritis with synovial hyperplasia.[3]

Ureaplasma diversum differs from these neonatal infections as infection in calves begins *in utero*. *U. diversum* is a common commensal organism found in the nasal passage and male and female reproductive tracts of cattle.[6] The bacteria is transmitted by coitus and as a major cause of reproductive loss in cattle.[5] It causes urogenital infections such as vaginitis and endometritis in cows and seminal vesiculitis in bulls.[6] Pregnant cows infected with virulent strains may have third trimester abortions or give birth to weak or stillborn calves.[5] The bacterium causes necrotizing placentitis and mild arteritis which affect the amnion more severely than the chorioallantois.[5] Aborted calves are well preserved and fetal membranes may be retained. Calves may have erosive conjunctivitis and

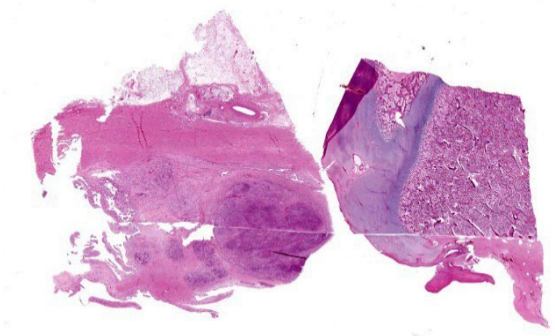

Figure 1-5. Femoral head, calf. There is a focal area of medullary fibrosis within the femoral epiphysis. (HE, 72X)

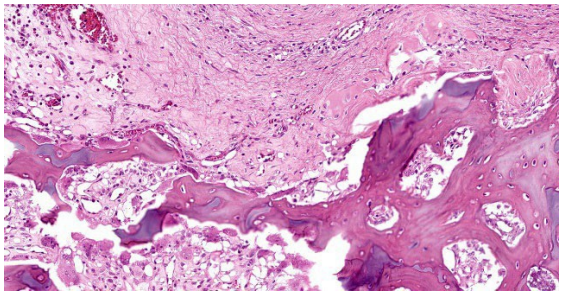

Figure 1-6. Femoral head, calf. There is osteoclastic remodeling of boney trabeculae at the edge of the area of epiphyseal fibrosis. (HE, 72X)

nonsuppurative alveolilis.[5] Interstitial pneumonia in a calf due to *U. diversum* was recently seen in WSC, year 2021-2022, Conference 24, Case 2; readers are encouraged to review that case for a full histologic picture of the infection in calves.

This case illustrates another sequela to *U. diversum* infection in utero: severe erosive polyarthritis[3,4]. The infection may affect one or multiple joints and tends to target the coxofemoral joint, shoulders, elbows, stifle, and carpal and tarsal joints.[3,4] In affected joints, articular surfaces are deformed, with irregularly thinned cartilage and extensive granulation tissue that extends into the subchondral bone.[3,4]

One last differential to consider for severe polyarthritis in calves is *Chlamydia pecorum.* Infection may occur due to ingestion of the bacteria or in-utero infection.[3] Virulent strains of this obligate intracellular bacteria spread from the intestine via portal circulation to the liver and then systemically were it ultimately finds the joints.[3] Affected animals are febrile, depressed, and reluctant to move.[3] In addition to severe polyserositis and meningoencephalitis, there is severe serofibrinous arthritis with edema and petechiation in the adjacent soft tissue.[1,3]

Conference participants discussed the quality of the primary and secondary spongiosa in this section. The thin, delicate spicules that with retained cartilage cores led some conference participants to consider osteogenesis imperfecta as a secondary process. According to the history provided by the contributor, this animal was never able stand, so participants also considered disuse osteopenia as a potential cause for these findings.

References:

1. Cantile C, Youssef S. The nervous system. In: Maxie MG, ed. *Jubb, Kennedy and Palmer's Pathology of Domestic Animals*. Vol 1. 6th ed., Philadelphia, PA: Elsevier Ltd.; 2016:391-392.
2. Carli SD, Dias ME, da Silva M, Breyer GM, Siqueira FM. Survey of beef bulls in Brazil to assess their role as source of infectious agents related to cow infertility. *J Vet Diagn Invest.* 2022;34(1): 54-60.
3. Craig LE, Dittmer KE, Thompson KG. Bones and Joints. In: Maxie MG, ed. *Jubb, Kennedy, and Palmer's Pathology of Domestic Animals.* Vol 1. 6th ed. St. Louis, MO: Elsevier; 2016: 154.
4. Himsworth CG, Hill JE, Huang Y, Waters EH, Wobeser GA. Destructive polyarthropathy in aborted bovine fetuses: a possible association with Ureaplasma diversum infection? *Vet Pathol*. 2009; 46(2): 269-72.
5. Schlafer DH, Foster RA. Female Genital System. In: Maxie MG, ed. *Jubb, Kennedy, and Palmer's Pathology of Domestic Animals.* Vol 3. 6th ed. St. Louis, MO: Elsevier; 2016:399-402, 411-416.
6. Strait EL, Madsen ML. Mollicutes. In: McVey DS, Kennedy M, Chengappa MM, eds. *Veterinary Microbiology.* 3rd ed. Ames, IO: Wiley Blackwell. 283-292.

CASE II:

Signalment:

12-year-old, male, mixed breed, dog (*Canis familiaris*)

History:
Left shoulder pain for 1 year. Radiographs show marked proliferation of bone around the shoulder joint involving, among other, the glenoid cavity, the head of the humerus and the greater tubercle. The limb was amputated.

Gross Pathology:
The specimen received was approximately 15cm in diameter. It was rigid and consisted of bone covered with muscle, tendons and connective tissue. Normal anatomic landmarks, including the joint, were not identified. The specimen was sliced transversely and sampled in several areas.

Laboratory Results:
No laboratory findings reported.

Microscopic Description:
Near the outer surface of the bone there is an elongate cystic structure in the wall of which there are several variably sized nodules of low cellularity composed of spindle and stellate cells with small hyperchromatic nuclei and thin and long cytoplasmic processes floating in optically empty spaces. The nodules are surrounded by fibrous tissue and/or more densely packed neoplastic tissue. In

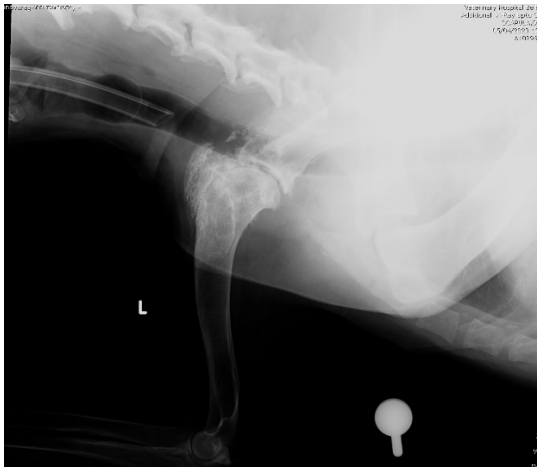

Figure 2-1. Scapulohumeral joint, dog. Pre-amputation radiographs demonstrate marked proliferation of bone around the shoulder joint involving, among other, the glenoid cavity, the head of the humerus and the greater tubercle. (Photo courtesy of: The Weizmann Institute of Science; http://www.weizmann.ac.il/)

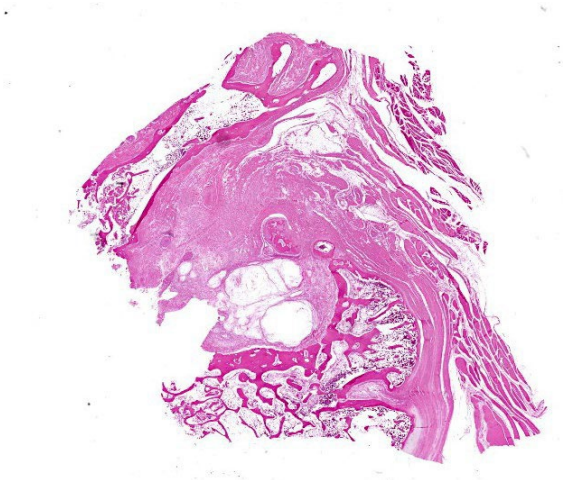

Figure 2-2. Scapulohumeral joint, dog. One section of the scapulohumeral joint with the joint capsule and humeral head is submitted for examination. (HE, 6X)

The nodules form an aggregate near the outer surface of the bone. Mitotic figures are rare. In both slides, the undulant contour of adjacent bone suggests compression by the proliferative tissue and there is probable osteophyte formation (bone islands away from the bulk of the bone). Polygonal cells of uncertain identity are attached to the inner aspect of the pseudocyst.

Contributor's Morphologic Diagnoses:
Synovial myxoma

Contributor's Comment:
Synovial myxoma is the most common benign neoplasm in the joints of dogs.[3] Its microscopic appearance is characteristic but because it is an uncommon tumor 86% of cases in one report were initially diagnosed as malignant.[1] The tumor typically consists of variably sized nodules composed of a low number of stellates to spindle cells surrounded by abundant hypovascular myxoid matrix.[1,3]

The findings in a series of 39 cases indicate that large breed, middle-aged dogs, especially Doberman Pinschers and Labrador retrievers were commonly affected, and the stifle and digits were the most common sites. Survival times were long (average >2.5

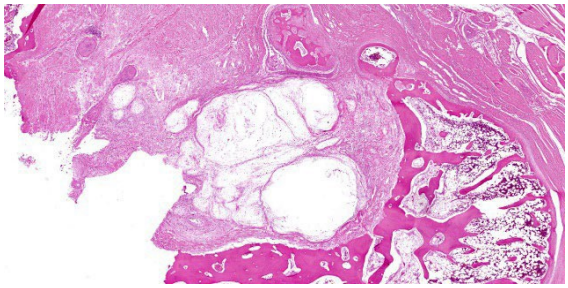

Figure 2-3. Scapulohumeral joint,dog. The joint space and is expanded by a multilobular mass with abundant clear myxomatous stroma. (HE, 6X)

years) even with incomplete excision. Three of 39 cases had local recurrence, but none metastasized or directly resulted in death.[1] Whilst some cases are confined to the joint capsule, others are infiltrative and grow along fascial planes. This appears to be the case in the submitted slides in which the tumor is located near bone and not within the joint. In the series of 39 cases, bone invasion was seen in 8 dogs. The authors concede that bone invasion is not typical of benign tumors, but their rationale to use the same diagnosis for all cases was the similarity of the histologic features of the tumors, irrespective of the presence of bone invasion.[1] Cases without bone lysis or expansion outside the joint capsule can be treated with synovectomy. Of cases confined to the joint capsule and treated with synovectomy, 10% recur.[3] Cases with bone lysis cause significant pain and usually require amputation.[3]

The viscous fluid produced by these tumors suggests that they originate from type B (fibroblast-like) synoviocytes which produce synovial fluid,[1] but this remains unproven as there are no reliable markers for this cell[2] and the IHC results in the case series cited above showed significant positive staining for CD18, which is a marker for type A synoviocytes.[1]

Previous designations of this entity include myxoma of the synovium – the term used for this entity when it was first described by RR Pool in 1990 (in the 3rd edition of Meuten's *Tumors in Domestic Animals*), myxosarcoma and nodular synovial hyperplasia.[3]

The submitted case is unusual in involving the shoulder, which was not affected in any case of the large case series.

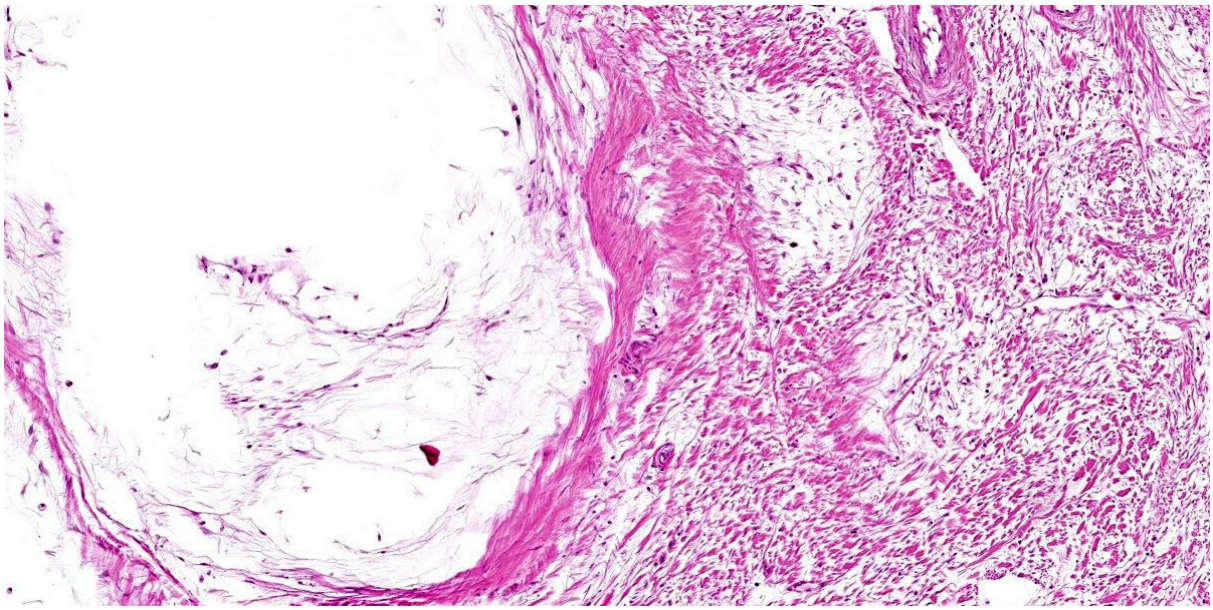

Figure 2-4. Scapulohumeral joint, dog. There is a large lobule of the neoplasm, a smaller developing nodule, and more diffuse infiltration of the joint capsule (right). (HE, 17X)

The three most common tumors of the canine synovium are histiocytic sarcoma, synovial cell sarcoma, and synovial myxoma, with widely divergent prognosis. Because bone invasion may be present in synovial myxoma, the 3 tumors cannot be differentiated radiographically. Synovial myxoma can be identified by its characteristic histologic appearance. Immunohistochemistry can be used to differentiate synovial histiocytic sarcoma (cytokeratin negative, CD18 positive) – the most common malignant tumor from the synovial cell sarcoma (cytokeratin positive, CD18 negative), which is a controversial entity in animals.[1,2]

Contributing Institution:
The Weizmann Institute of Science
http://www.weizmann.ac.il/

JPC Diagnosis:
Joint capsule: Synovial myxoma.

JPC Comment:
A few reports of synovial myxomas with atypical presentations in dogs have been reported. Izawa et al describe a synovial myxoma with intramuscular infiltration as an incidental finding in a 16-year-old dog that was euthanized due to progressive renal failure. The dog had no clinical signs of lameness, and the tumor was only described when a jelly-like substance was discovered between skeletal muscles of the hind limb on necropsy.[4] There were also multiple small translucent nodules in the stifle. Histologically, the nodules had the classic appearance of a synovial sarcoma, with few spindle to stellate cells embedded in abundant myxoid matrix, and similar nodules were identified in the jelly-like areas between muscles.[4]

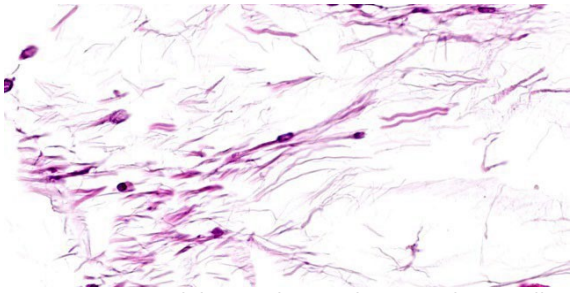

Figure 2-5. Scapulohumeral joint, dog. Neoplastic cells are spindled with long processes and pink vacuolated cytoplasm. (HE, 710X)

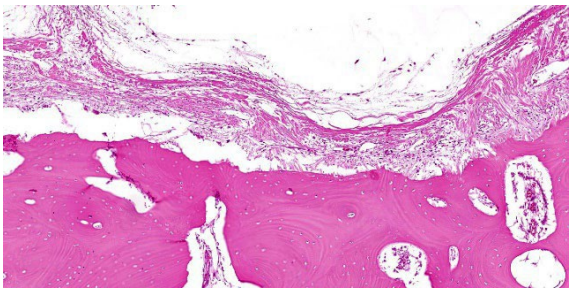

Figure 2-6. Scapulohumeral joint, dog. There is scalloping of the humeral cortex in apposition to the neoplasm as a result of remodeling due to pressure. (HE, 103X)

Neary et al described a synovial myxoma associated with the cervical articular facet in a 12-year-old mixed breed dog. The animal presented with a two-week history of progressive neurologic deficits and tetraparesis, and the dog was successfully treated with a dorsal hemilaminectomy and facetectomy.[6]

Synovial myxomas were recently described in cats as well. In a 2020 *Vet Pathol* article, Craig et al described synovial cystic and myxomatous lesions in 16 cats. Most (12) of the masses were located in the elbow, and in all cases, the masses were unilateral. Three cats had masses composed of cysts; two cats had masses composed of spindle cells on myxomatous matrix (myxoma); and 11 cats had a combination of cysts and myxoma. While most of the lesions increased with time, the lesion was not the cause of natural death or euthanasia in any of the cats. Since the majority of the cats in this study also had bilateral degenerative joint disease, the authors hypothesized that synovial cysts initially form due to increased articular pressure and herniation of synovium; myxomas then

form when there is subsequent neoplastic transformation.[2]

A single report of a synovial myxoma has been published in a 5-year-old rabbit. The affected hind limb was amputated, and grossly, the neoplasm partially effaced the femur and stifle joint, elevating the patella and extending into the fascia between muscles. Histologically, the neoplasm had the classic features of myxoma and was frequently surrounded by reactive bone, fibrosis, or cartilage. The authors recommended using the term "infiltrative" as part of the diagnosis for such invasive tumors to provide a better description of the biologic behavior.[5]

References:

1. Craig LE, Kirmer PM, Colley AJ: Canine Synovial Myxoma: 39 Cases. *Vet Pathol.* 2010, 47:931-936.
2. Craig LE, Kirmer PM, O'Toole AD. Synovial Cysts and Myxomas in 16 Cats. *Vet Pathol.* 2020; 57(4): 554-558.
3. Craig LE, Thompson KG: Tumors of Joints. In: Meuten DJ, ed. *Tumors in Domestic Animals.* 5th ed. Wiley Blackwell. 2017; 345-347.
4. Izawa T, Tanaka M, Aoki M, Ohahshi F, Yamate J, Kuwamura M. Incidental Synovial Myxoma with Extensive Intermuscular Infiltration in a Dog. *J Vet Med Sci.* 2012; 74(12):1631-3.
5. Lohr CV, Hedge ZN, Pool RR. Infiltrative myxoma of the stifle joint and thigh in a domestic rabbit (*Oryctolagus cuniculus)*. 2012; 147(2-3):218-222.
6. Neary CP, Bush WW, Tiches DM, Durham AC, Gavin. Synovial myxoma in the vertebral column of a dog: MRI description and surgical removal. *J Am Anim Hosp Assoc.* 2014; 50(3):198-202.

CASE III:

Signalment:
2 years and 6 months old female Holstein Friesian Cow (*Bos taurus).*

History:
The cow was euthanized due to a large (41.5cm circumference), round, firm, ulcerated mass with embedded incisors at the rostral aspect of the mandible. Whilst the cow was unable to hold saliva, she was still able to eat and drink with some adaptation.

Gross Pathology:
A very large (160x140x160 mm), expansile, broad based, firm, pink to red mass extends from the dorsolingual aspect of the rostral mandible, displacing teeth 301, 302, 401, 402, 403 and 404 laterally. Approximately 70% of the surface of the mass is ulcerated. On cut surface, the mass exhibits a central 60x24x16 mm cavity which contains approximately 15 ml of clear, yellow tinged, watery fluid surrounded by cream to yellow to pale pink, variably soft to very firm, gelatinous to fleshy tissue. Where the mass merges with

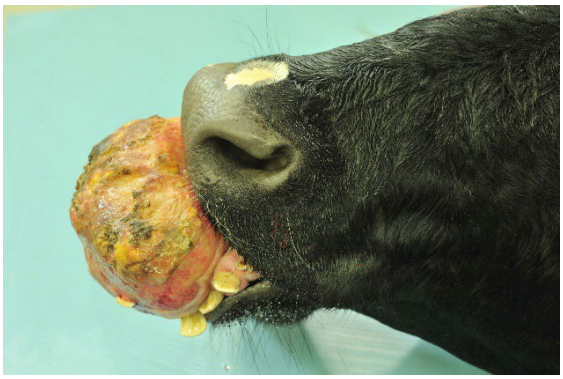

Figure 3-1. Mandible, ox. A 1.6 cm expansile, broad based neoplasm extends from the dorsolingual aspect of the rostral mandible, displacing teeth 301, 302, 401, 402, 403 and 404 laterally. (Photo courtesy of: Division of Pathology, Public Health and Disease Investigation Veterinary Diagnostic Services, School of Veterinary Medicine, College of Medical, Veterinary and Life Sciences, University of Glasgow (Garscube Campus) 464 Bearsden Road, Glasgow G61 1QH, Scotland, https://www.gla.ac.uk/schools/vet/cad/)

regular mandible, the mandible is thickened to a maximum thickness of 69 mm.

The forage in the forestomaches, particularly the rumen, is excessively long.

Laboratory Results:
No laboratory findings reported.

Microscopic Description:
Mandibular mass: The section contains parts of a large and moderately cellular mass which comprises loosely to moderately densely and haphazardly arranged, very vague bundles and streams of neoplastic cells, situated in and supported by a moderate to large amounts of multifocally mildly oedematous, fine collagenous stroma, interspersed with numerous elongated, partially anastomosing bony spicules and trabeculae arranged in parallel to one another and perpendicular to the superficial surface. The bone trabecules are lined by a largely one cell (ranging up to three cells) thick layer of polygonal to elongate cells with eosinophilic/mildly basophilic cytoplasm and round to oval nuclei with finely stippled to clumped and marginated chromatin (osteoblasts). The neoplastic cells are

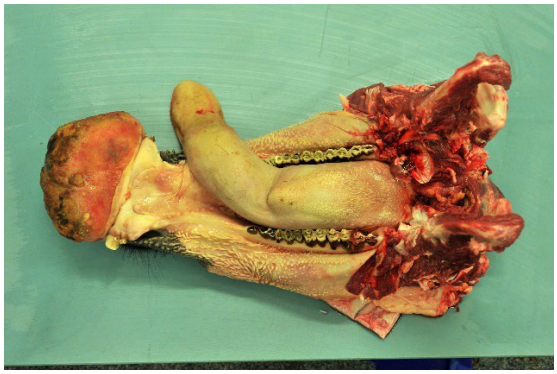

Figure 3-2. Mandible, ox. Dissected specimen of this mandibular neoplasm (Photo courtesy of: Division of Pathology, Public Health and Disease Investigation Veterinary Diagnostic Services, School of Veterinary Medicine, College of Medical, Veterinary and Life Sciences, University of Glasgow (Garscube Campus) 464 Bearsden Road, Glasgow G61 1QH, Scotland, https://www.gla.ac.uk/schools/vet/cad/)

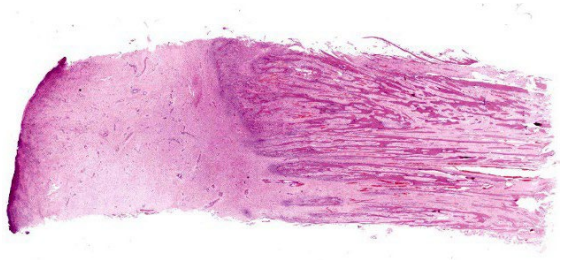

Figure 3-3. Mandible, ox. One section of undecalcified maxilla is submitted for examination. The mass is composed of spindle cells and fibrous matrix separated by parallel trabeculae of unmineralized mature woven bone. (HE, 6X)

spindle-shaped to stellate-shaped with moderately defined cell boundaries and small amounts of eosinophilic cytoplasm. Their nuclei are irregularly oval with finely stippled to mildly clumped, commonly also marginated chromatin and one or two, small basophilic nucleoli. Anisocytosis and anisokaryosis are mild, very small numbers of binucleated cells are present and less than one mitotic figure is seen in 10 high power fields. Mitotic figures, however, are more evident in those regions close to bone formation and at the interface between bone and collagenous tissue, where also a substantial increase in cellularity is evident.

The mucosa is diffusely ulcerated, and covered by fibrin, eosinophilic and basophilic cellular debris and large numbers of viable and degenerate neutrophils, in deeper levels admixed with small numbers of macrophages, lymphocytes and plasma cells which in turn are situated amongst plump fibroblasts vaguely orientated parallel to the surface and small vessels lined by hypertrophied endothelial cells orientated perpendicular to the superficial surface (granulation tissue formation).

Very small numbers of lymphocytes, plasma cells and macrophages are diffusely distributed throughout the neoplastic population and commonly also seen forming very small aggregates in perivascular location.

Contributor's Morphologic Diagnoses:
Mandible, rostral aspect: Ossifying fibroma, bovine, *Bos taurus.*

Contributor's Comment:
Ossifying fibromas (OF) are benign, proliferative, intraosseous lesions with a rapid growth rate and strong predilection for the mandible.[3,17] OF are most frequently recognized in human beings and young horses (<1 year old)[8], but have also been described in dogs[2,3,6,7], cats[3], sheep[3], and rarely cattle.[13,19] Additionally, individual cases of OF are published in a range of other species including a canary[14], a rabbit[19], a llama[5], roe deer[21] and a cynomolgus monkey[15].

In humans OF are most commonly found in the posterior mandible, although maxillary and zygomatic lesions are also recognized.[4] The rostral mandible represents a clear predilection site in young horses (where the condition also is known as *equine juvenile mandibular ossifying fibroma*)[8], and also in ruminants and domestic carnivores[3,13,14]. Additional reported sites include long bones[3,14], equine paranasal sinuses[12], the equine proximal phalanx[1], the canine os penis[7] and the canine zygomatic arch.[2] Reported cases in cattle are restricted to the mandible (although paucity of cases may underlie a lack of recognition of atypical locations).[13,14]

In humans, a predilection for ossifying fibromas has been established in females in their

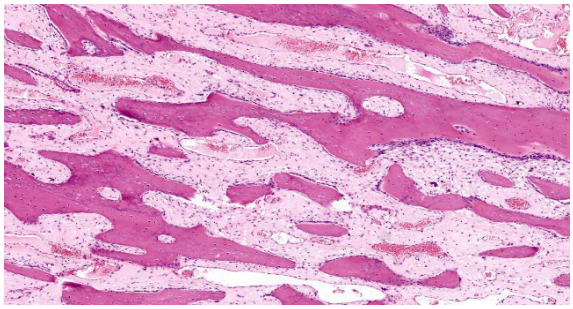

Figure 3-4. Mandible, ox. Higher magnification of trabeculae of mature woven bone lined by a single layer of quiescent osteoblasts. (HE, 117X)

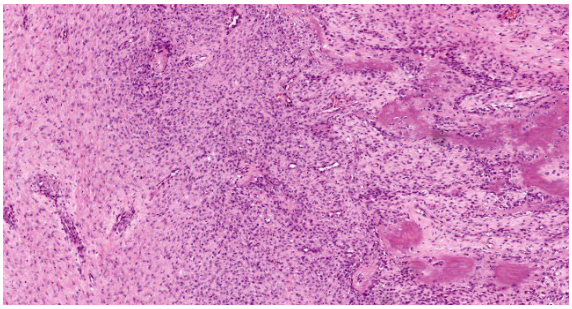

Figure 3-5. Mandible, ox. The leading edge of the mass is densely cellular. (HE, 57X)

30s or 40s.[4] In contrast to this, equines exhibit such lesions most commonly in young animals (<12 months)[8], whilst no clear age-related predilection is reported for other species at present (possibly again due to paucity of cases). No sex predisposition is currently reported in animals.

Human OF are reported to be non-painful. Their most significant effects are of malocclusion and cosmetic impairment.[4] Similarly, the primary effects of OF in domestic animals are impaired occlusion and/or prehension as well as a predisposition to pathologic fractures.[3,8,13,14] The further effects of OF in atypical locations are largely due to their space-occupying behavior and specific effects dependent on the location in question, for example urethral obstruction in the case of an OF in the os penis.[1,2,7,12]

Histologically ossifying fibromas are characterized by spindle shaped fibroblasts interspersed with trabeculae of woven bone which are surrounded by a rim of osteoblasts.[17] Historical miscategorisation and underreporting of OF in the literature is suspected, owing to the similarity between osteoma and OF and the disagreement about the existence of a disease continuum between fibrous dysplasia (FD) and OF.[17,18] Currently, histological differentiation of OF from FD is largely based on the presence of a rim of osteoblasts surrounding foci of woven bone.[7,8,10,18,19,20] Osteomas can be distinguished from OF by their grossly sessile or pedunculated appearance

arising from the surface of the bone, their containment within the periosteal membrane, relative hypocellularity and the presence of lamellar bone with bone marrow, whilst osteosarcomas can be differentiated from OF by the pleomorphism and a considerably higher mitotic rate of the neoplastic population with osteoblasts typically also filling the intertrabecular spaces rather than only lining the bony trabecules.[7,8,12,18,19,20]

Contributing Institution:
Division of Pathology, Public Health and Disease Investigation
Veterinary Diagnostic Services
School of Veterinary Medicine
College of Medical, Veterinary and Life Sciences
University of Glasgow (Garscube Campus)
464 Bearsden Road
Glasgow G61 1QH, Scotland
https://www.gla.ac.uk/schools/vet/cad/

JPC Diagnosis:
Bone, mandible: Ossifying fibroma.

JPC Comment:
As the contributor describes, ossifying fibromas are rare in cattle, and since this case was submitted to WSC, another report of three cases of mandibular ossifying fibromas in cattle was published in *Journal of Comparative Pathology.* All cases were characterized as well demarcated and projected from the rostral mandible, where they replaced or displaced multiple incisors. Histologically, the neoplasms had the characteristic features of ossifying fibroma: trabeculae of bone lined by osteoblasts surrounded by haphazardly arranged neoplastic spindle cells with invasion, degeneration, and necrosis of adjacent bone.[11] In one case, the neoplastic spindle cells were confluent with the periodontal ligament, and some have speculated that ossifying fibroma of the mandible may originate from pluripotent stem cells of the periodontal ligament.[11]

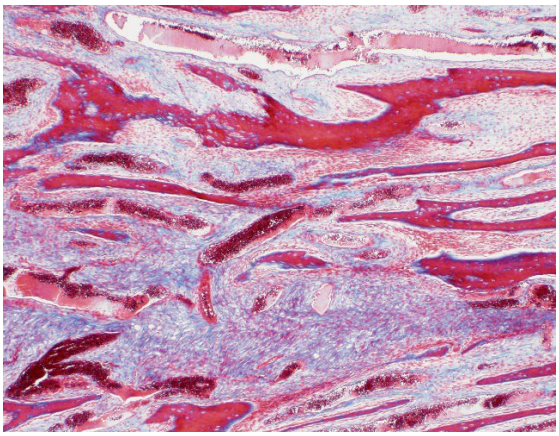

Figure 3-6. Mandible, ox. A Masson's trichrome highlights the collagen in the intertrabecular spaces. (Masson's trichrome, 400X)

Ossifying fibroma is also rarely reported in marine (striped mullet) and freshwater fish (sauger and walleye). The freshwater fish cases were linked to pollution from a mining operation. A single case of cutaneous osseous fibroma was more recently reported in the caudal peduncle of a tetra.[10] The neoplasm contained dysplastic ctenoid scales, and the authors theorize that the neoplasm may have originated from the bone in these scales, a theory which is in line with central ossifying fibromas in humans, which also originate from bone.[10]

Historically the presence or absence of a rim of osteoblasts around trabeculae of woven bone was used to differentiate ossifying fibroma (OF) from fibrous dysplasia (FD). Recent work, however, has demonstrated that both OF and FD can have osteoblasts around trabeculae. Alternatively, both OF and FD may lack an osteoblastic rim around trabeculae. For these reasons, the presence or absence of an osteoblastic rim is no longer considered diagnostically useful. The degree of bone differentiation histologically, and the sharpness of demarcation radiographically are generally considered the most useful features in distinguishing OF and FD. OF has

well differentiated woven bone histologically, and sharply defined margins radiographically. FD may have poorly differentiated bone that is difficult to recognize as bone (ie "proto-bone") histologically, and is poorly delineated with ill-defined margins radiographically. Both OF and FD arise from the intra-osseous region and can have multinucleated giant cells (osteoclasts). As these represent a spectrum of benign, fibro-osseous lesions, it may be challenging to impossible to definitively differentiate OF from FD without the use of radiographs.[8,16]

References:

1. Balducci J, Selberg K, Pool R and Radue RP. Primary ossifying fibroma of the proximal phalanx in a horse. *Equine Vet Educ.* 2019;**32**:40-44.
2. Best E. Ossifying fibroma of the zygomatic arch in a 20-month-old male corgi. *Vet Times.* 2011.
3. Craig LE, Dittmer KE and Thompson KG. Chapter 2 Bones and Joints. In: Jubb, Kennedy and Palmer's Pathology of Domestic Animals. Volume 1. Maxie MG. 6th ed. Ames, Iowa; Wiley Blackwell; 2015:109.
4. da Silveira DT, Cardoso FO, Silva BJ, Alves Cardoso CA and Manzi FR. Ossifying fibroma: report on a clinical case, with the imaging and histopathological diagnosis made and treatment administered. *Rev Bras Ortop.* 2015;**51**(1):100-104.
5. McCauley CT, Campbell GA, Cummings CA and Drost WT. Ossifying fibroma in a llama. *J Vet Diagn Invest.* 2000;**12**:473–476.
6. Miller MA, Towle HAM, Heng HG, Greenberg CB and Pool RR. Mandibular Ossifying Fibroma in a Dog. *Vet Pathol.* 2008;**45**(2):203–206.
7. Mirkovic TK, Schmon CL and Allen AL. Urinary obstruction secondary to an ossifying fibroma of the os penis in a dog. *J Am Anim Hosp Assoc.* 2004; **40**:152-156.
8. Morse CC, Saik JE, Richardson DW and Fetter AW: Equine juvenile mandibular ossifying fibroma. *Vet Pathol*. 1988;**25**:415–421.
9. Murphy B, Imai DM. Cuatneous Ossifying Fibroma in a Neon Tetra (*Paracheirodon innesi)*. *J Comp Pathol.* 2016; 155(2-3): 272-275.
10. Murphy BG, Bell CM, Soukup JW. *Veterinary Oral and Maxillofacial Pathology*. Hoboken, NJ: John Wiley & Sons. 2020; 243.
11. De Oliveira Freitas DC, Melo FG, de Melo Ocarino N, Abreu DM, Araujo FR, Serakides R. Three Cases of Ossifying Fibroma in Cattle. *J Comp Pathol.* 2022; 198: 16-21.
12. Orsini JA, Baird DK and Ruggles AJ. Radiotherapy of a recurrent ossifying fibroma in the paranasal sinuses of a horse. *JAVMA.* 2004;**224**(9):1483-1454.
13. Raval SH, Joshi DV, Patel BJ, Patel J, Sutariya P, Soni M and Rathod AS. Bovine dental tumors: A report of four cases. *Indian J Vet Pathol.* 2017:**41**:119-122.
14. Razmyar J, Dezfoulian O and Peighambari S. Ossifying Fibroma in a Canary (*Serinus canaria*). *J Avian Med Surg.* 2008;**22**(4):320-322.
15. Schmelting B, Zöller M, Kaspareit J. Peripheral ossifying fibroma and juxtacortical chondrosarcoma in cynomolgus monkeys (*Macaca fascicularis*). *J Am Assoc Lab Anim Sci*. 2011;**50**(1):98-104.
16. Soltero-Rivera M et al. Benign and malignany proliferative fibro-osseous and osseous lesions of the oral cavity of dogs. *Vet Pathol*. 2015; 52(5):894-902.
17. Thompson KG, Dittmer KE. Tumors of Bone. In: Meuten DG, ed. *Tumors in Domestic Animals.* 5th ed. Ames, Iowa: Wiley Blackwell; 2017:362-363.

18. Toyosawa S, Yuki M, Kishino M, Ogawa Y, Ueda T, Murakami S, Konishi E, Iida S, Kogo M, Komori T and Tomita Y. Ossifying fibroma vs fibrous dysplasia of the jaw: molecular and immunological characterization. *Mod Pathol.* 2007;**20**:389–396.
19. Whitten KA, Popielarczyk MM, Belote DA, McLeod GC and Mense MG. Ossifying fibroma in a miniature rex rabbit (*Oryctolagus cuniculus*). *Vet Pathol.* 2008;**43**:62–64.
20. Yayla S, Kiliç E, Özen H, Dağ S, Baran V and Aydin U. A case of osteofibroma on the symphysis mandible in a cow. *J Hell Vet Med Soc.* 2018;**69**(1):879-882.
21. Zürcher-Giovannini S, Ruder TD, Pool R, Erdelyi K and Origgi FC. Mandibular Ossifying Fibroma and Multiple Oral Papillomas in a Roe Deer (*Capreolus capreolus*). *Front Vet Sci.* 2020;**7**:166.

CASE IV:

Signalment:
19 months old, female, mixed-breed (*Sus scrofa domesticus*) domestic pig.

History:
The pig was from a small farm housing pigs and other animals, including one boar and four sows that farrowed 23 piglets. After birth, the piglets were divided into four pens containing piglets of the same size from different sows. The number of piglets in each pen were as follows: pen 1, 8 piglets; pen 2, 4 piglets; pen 3, 9 piglets; and pen 4, 2 piglets. All pigs were fed a diet of boiled corn bran and millet; however, only the piglets in pen 3 became ill. At 10 months old, the first clinical signs appeared in the piglets, and their condition progressively worsened. Initially, the piglets presented with respiratory distress and underdevelopment. Later, they developed bilateral swollen face, mainly in

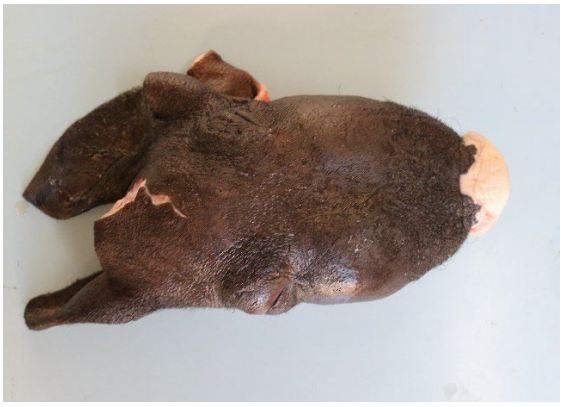

Figure 4-1. Maxilla, pig. There is marked bilaterally symmetrical expansion of the maxilla. (Photo courtesy of: Laboratório de Patologia Veterinária, Faculdade de Medicina Veterinária, Universidade Federal de Mato Grosso, Brazil)

the maxilla, partial mouth opening and protruding tongue, difficulty in food retention and mastication, loss of general body condition, and dyspnea. Subsequently, all pigs in pen 3 died under these conditions.

Gross Pathology:
One piglet was euthanized and underwent necropsy. Marked bilateral enlargement of the facial bones, predominantly in the maxilla, was observed. These were easily sliced using a knife and the section surfaces were observed to be pale. The nasal cavity lumen decreased due to thickening of the maxillary bones. The teeth were loose, and the molars were lingually tipped. In addition, the ribs were soft and broke effortlessly under pressure. Most of the long bones showed epiphyseal plate thickening, and the trabecular structure was poorly visible.

Laboratory Results:
No laboratory findings reported.

Microscopic Description:
Histopathological examination of the mandible and maxilla revealed accentuated diffuse proliferation of soft and irregular fibrous conjunctive tissue, which was evaluated by Masson's trichrome staining around the osteoid trabeculae, many of which were

partially or completely demineralized, as observed on von Kossa staining. Osteoclasts forming multinucleated cells were observed in the surface grooves (Howship's lacunae) in the mineralized trabeculae or clustered within the connective tissue. Histological changes were not observed in the renal parenchyma or parathyroid gland.

Contributor's Morphologic Diagnoses:
Face bones, maxilla: osteolysis, diffuse, severe fibroplasia (fibrous osteodystrophy), domestic pig (*Sus scrofa domesticus*)

Contributor's Comment:
Bone growth and maturation are complex processes involving an interaction between genetic factors, local and systemic hormones, dietary nutrients, and mechanical forces. Any factors interfering with the synthesis of proteoglycans or collagen by chondroblasts or osteoblasts, differentiation of precursor cells, or resorption of bone by osteoclasts can result in skeletal abnormalities. The expression of an abnormality depends on many factors, including the phase of skeletal development that is altered, severity of the defect, age of the animal at the time of insult, and persistence of the influencing factor. Thus, the range of possible skeletal defects is large and a single cause can develop several different manifestations[5].

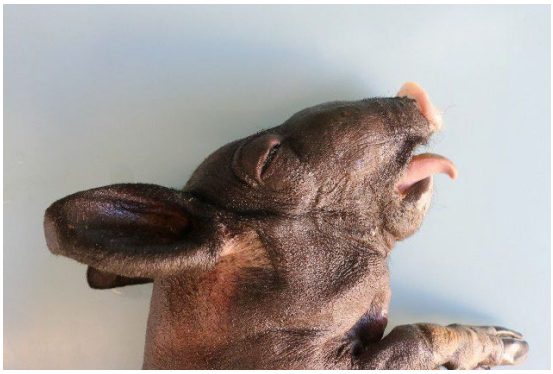

Figure 4-2. Maxilla, pig. There is marked bilaterally symmetrical expansion of the maxilla. (Photo courtesy of: Laboratório de Patologia Veterinária, Faculdade de Medicina Veterinária, Universidade Federal de Mato Grosso, Brazil)

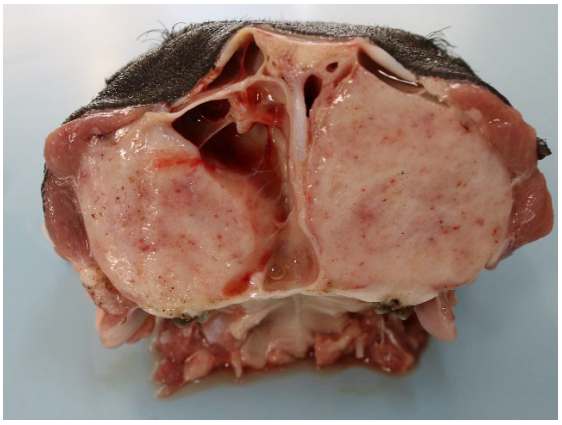

Figure 4-3. Maxilla, pig. The maxilla cut easily with a knife. There is marked bilaterally symmetrical expansion of the maxilla with encroachment on the nasal cavity. (Photo courtesy of: Laboratório de Patologia Veterinária, Faculdade de Medicina Veterinária, Universidade Federal de Mato Grosso, Brazil)

Understanding the regulation of phosphorus and calcium levels in the animal body is necessary to comprehend the pathogenesis of bone lesions. Most mediators involved in calcium phosphorus homeostasis have evolved in fish, although their roles are repurposed during adaptation to land environments. Thus, while susceptibility to vitamin D deficiency in vertebrates can be traced back to fish, the specifics of its manifestation as a disease show both similarities and differences to what is observed in humans. Calcium and phosphorus are strictly regulated in all animals because of their vital roles in numerous cellular functions. During the colonization of land, vertebrates transitioned from a sea environment that was comparatively richer in calcium than phosphorus to a land environment, with a six- fold higher gravity force, that was poor in calcium and relatively richer in phosphorus. This led to the evolutionary changes involving major adaptations in bone structure and calcium/phosphorus regulation. These adaptations included a highly efficient system for intestinal calcium absorption and flexible bone remodeling, which allowed the use of bones as an internal reservoir of calcium to compensate for variations in dietary intake[14].

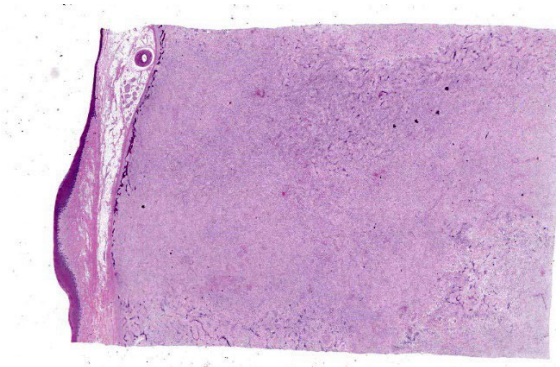

Figure 4-4. Maxilla, pig. A single section of the mass is submitted for examination. There is marked resorption of the cortex of the bone. (HE, 6X)

Deficiencies in calcium, phosphorus, and vitamin D disrupt bone conditions, resulting in a group of diseases known as osteodystrophies or metabolic bone disease. In the field of veterinary medicine, this is a broad term denoting pathological conditions affecting multiple bones. Osteodystrophies are most frequently caused by genetic, nutritional, and/or hormonal abnormalities that affect bone growth, modeling, or remodeling, typically through disruptions in calcium/phosphorus metabolism. Calcium and phosphorus are required for a variety of essential bodily functions in addition to those involved in skeletal development. The skeleton is composed of approximately 99% of calcium and 85% of phosphorus in the body. There are three distinct forms of calcium and phosphorus in the body: ionized, protein-bound, and complex atoms in extracellular fluids (including plasma). The ionized fractions of these minerals (Ca2+ and HPO42-) are physiologically active and are strictly regulated by the parathyroid hormone (PTH), 1,25- dihydroxyvitamin D (1,25[OH]2D3), calcitonin, and phosphatonin system[5,6,9,14].

PTHs are secreted by the parathyroid gland when calcium-sensing receptors on chief cells detect low serum ionized calcium concentrations. The net effect of PTH increases plasma ionized calcium levels and reduces plasma phosphate concentrations. The PTH induces the renal tubules to open the calcium channel, allowing increased resorption of calcium from the renal filtrate and increased breakdown of phosphate channels. Consequently, the resorption of phosphorus from the renal filtrate decreases. In the bone, high PTH concentration results in the recruitment and activation of osteoclasts, leading to increased osteoclastic bone resorption and release of calcium and phosphorus in the circulation[5].

Vitamin D exists in two forms: vitamin D2 (ergocalciferol), obtained from yeasts and plants and vitamin D3 (cholecalciferol), obtained from the diet or as an end product of the skin photochemical reaction of 7-dehydrocholesterol, which explains why sun exposure increases vitamin D levels in most species. Latitude, time of day, season, and level of skin pigmentation can affect the vitamin D3 production in the skin. At lower angles, the sun does not have the requisite intensity to produce vitamin D in the skin. Furthermore, high levels of melanin in the skin absorb ultraviolet photons, making it unavailable for vitamin D synthesis. A dense hair/wool coat also reduces cutaneous vitamin D3 synthesis. Dogs and cats are an exception in mammals in that they do not produce vitamin D in the skin, owing to the presence of an enzyme that breaks down 7-dehydrocholesterol, making it unavailable for conversion to vitamin D. Therefore, cats and dogs are reliant on dietary vitamin D.

Vitamin D2 from the diet and vitamin D3 from the skin/diet are transported to the liver, where they form 25-hydroxyvitamin D (25OHD), the major form of vitamin D in the circulation. Therefore, serum 25OHD concentration reflects the level of cutaneous vitamin D3 formation and/or dietary levels of vitamin D. Serum 25OHD levels are measured to determine whether an individual has

adequate or deficient vitamin D status. The most active form of vitamin D is 1,25-dihydroxyvitamin D, which is formed in the renal proximal tubular epithelial cells. This step is closely regulated and 1,25(OH)2D3 production is directly stimulated by high PTH and low phosphorus levels, and indirectly by low ionized calcium, which acts via PTH. When plasma phosphorus and ionized calcium concentrations are adequate and PTH levels are low, 25OHD is converted to inert metabolites during the initial step of the degradation pathways. Active vitamin D binds to the nucleus of the renal tubular and intestinal epithelial cells, resulting in increased absorption of calcium and phosphorus from the kidneys and intestine, inhibition of PTH production in the parathyroid gland, and negative feedback to decrease its own production[5,6,14].

Calcitonin is secreted by thyroidal C cells in response to increased serum ionized calcium concentrations. It inhibits osteoclast action leading to decreased osteoclastic bone resorption, and subsequent decrease in the release of calcium and phosphorus into the blood, allowing normalization of serum ionized calcium levels[5].

Recently, many phosphatonins have been found to be involved in phosphorus metabolism, the most important of which is the fibroblast growth factor 23 (FGF23). FGF23 is produced by osteocytes in the bone and its production is increased by either hyperphosphatemia or increased 1,25(OH)2D3. The kidney is the main target organ of FGF23; together with its cofactor klotho, FGF23 downregulates phosphorus channels in the kidney, resulting in decreased resorption of phosphorus from the renal tubules. FGF23 also decreases the production of 1,25(OH)2D3 by inhibiting the enzyme that acts in its formation and activates the enzyme that catabolizes 1,25(OH)2D3. in the parathyroid gland, FGF23 decreases secretion of PTH. FGF23 activity results in decreased plasma phosphorus concentration[5].

Metabolic bone diseases can occur when these regulatory mechanisms do not work in harmony. Metabolic bone diseases include rickets, osteomalacia, fibrous osteodystrophy, or osteoporosis; these distinct morphological entities have characteristic pathogenesis and lesions. Nonetheless, specific diagnosis is difficult in many cases, as multiple conditions may be present, especially in those induced by nutritional deficiencies. This means that cases reported in the literature should be scrutinized, and only those confirmed by histopathology should be considered definitive[5,6,14].

Fibrous osteodystrophy (osteodystrophia fibrosa, osteitis fibrosa cystica) is a relatively common metabolic bone disease characterized by extensive osteolysis, accompanied by proliferation of fibrous tissue and poor mineralization of the immature bone. The pathogenesis involves primary or secondary hyperparathyroidism with persistently elevated

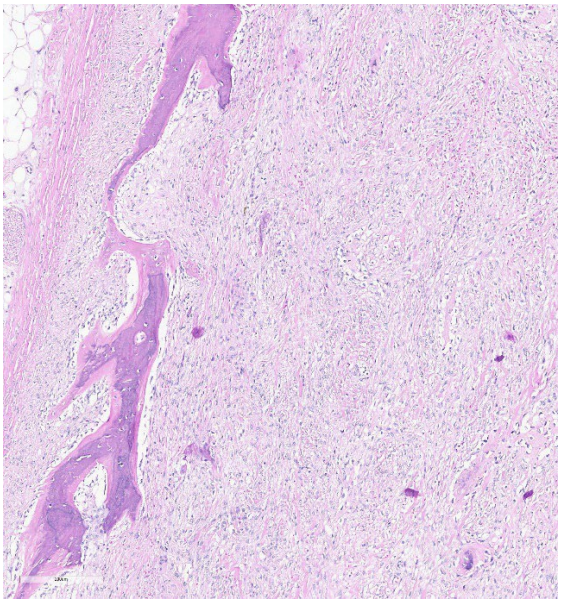

Figure 4-5. Maxilla, pig. Higher magnification of the resorbed cortex. (HE, 110X)

plasma PTH levels causing bone resorption, resulting in skeletal alterations. The susceptibility of different animal species to fibrous osteodystrophy varies, as does the distribution of lesions. Horses, pigs, dogs, cats, ferrets, dromedary camels, guinea pigs, reptiles, New World nonhuman primates, and goats are commonly affected, but the disease is rare in sheep and cattle[1,4,5,6,9,12,13].

Primary hyperparathyroidism, typically caused by functional parathyroid gland adenoma, leads to an increase in PTH levels. Parathyroid gland adenocarcinoma and hyperplasia, although reported, are rare[3,5]. Generalized bone resorption can also occur because of paraneoplastic syndrome (pseudohyperparathyroidism or hypercalcemia of malignancy) when tumors produce calcitropic hormones that act similarly to parathyroid hormones[2].

Secondary hyperparathyroidism is a much more frequent cause of fibrous osteodystrophy in animals than primary hyperparathyroidism and may stem from either chronic renal disease, or a dietary imbalance of calcium and phosphorus. PTH secretion is stimulated by a reduction in plasma ionized calcium, whatever the cause, and if the stimulus persists, generalized bone resorption results[5].

Renal hyperparathyroidism occurs predominantly in small animals as a complication of chronic renal failure, most often in dogs and occasionally in cats. This alteration often referred as renal osteodystrophy, has recently been renamed "chronic renal failure–mineral and bone disorder" (CKD-MBD) in humans and veterinary medicine. Renal osteodystrophy may occur in dogs with CKD; however, the manifestations of uremia are usually more severe than those of skeletal lesions. Impaired glomerular filtration in renal failure leads to progressive hyperphosphatemia

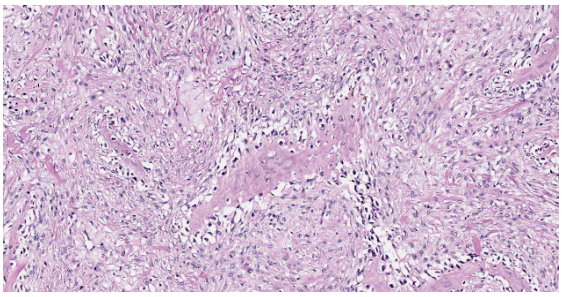

Figure 4-6. Maxilla, pig. Within the fibrous matrix replacing the bone, there are irregular trabeculae of woven bone lined by a single layer of vacuolated osteoblasts. (HE, 400X)

caused by reduced renal clearance of phosphate, causing hypocalcemia because of the inverse relationship between plasma ionized phosphate and calcium concentrations. Hyperphosphatemia also triggers the production of FGF23 by osteocytes, exacerbating hypocalcemia, as FGF23 functions to decrease the production of 1,25(OH)2D3 due to inhibition of the enzyme that acts in the formation and activates the enzyme that catabolizes 1,25(OH)2D3. Persistent hypocalcemia stimulates PTH release, resulting in osteoclastic bone resorption[4,5,7].

Nutritional hyperparathyroidism while frequently noted in horses, is reported sporadically in other species, mainly in young, rapidly growing animals. This condition is generally caused by diet containing low calcium and a relatively high concentration of phosphorus, or in association with vitamin D deficiency. Vitamin D deficiency alone can cause rickets or osteomalacia, but reduced calcium absorption from the intestine in animals combined with vitamin D deficiency often results in concurrent fibrous osteodystrophy. Excess dietary phosphorus may cause fibrous osteodystrophy even in animals receiving adequate dietary calcium. Increased plasma phosphate concentrations, resulting from increased intestinal absorption of phosphorus, depresses plasma ionized calcium and indirectly stimulates the release of PTH. In all species, several factors influence the

development and severity of lesions in secondary hyperparathyroidism. These include the degree to which dietary calcium is deficient and, perhaps more importantly, the degree to which dietary phosphorus is in excess. This condition usually occurs after ingesting unsupplemented diets consisting largely of grain, corn, and grain byproducts, such as bran, for some months, hence the term bran-disease[1,5,8,9]. In dogs and cats, nutritional hyperparathyroidism is often caused by diets that consist largely or entirely of meat or offal, as the calcium content of such diets is low, and the calcium to phosphorus ratio is very high. Additionally, in horses, fibrous osteodystrophy occurs in animals grazing on tropical grasses high in oxalate; even though dietary calcium and phosphorus are normal, oxalate binds calcium making it unavailable for absorption. Several grasses, including *Setaria sphacelata, Cenchrus ciliaris, Brachiaria mutica, B. humidicola, Digitaria decumbens, Pennisetum clandestinum, P. purpureum, and Panicum spp.,* contain sufficient oxalate to produce clinical disease[5,14].

The clinical signs and gross lesions of fibrous osteodystrophy generally develop more rapidly in young, growing animals because of their increased rates of bone synthesis and remodeling. Early signs include minor changes in gait, stiffness, transient and shifting lameness, and lassitude. Loss of appetite with progressive cachexia and decreased growth develops later. Affected animals frequently show bilateral enlargement of the bones of the skull, affecting both the maxillae and mandibles, hence the term big-head. Bony enlargement begins along the alveolar margins of the mandible, producing cylindrical thickening and reducing the intermandibular space. The molar margins of the maxillae subsequently begin to enlarge, and the enlargement spreads to involve the palate, remainder of the maxillae, and lacrimal and zygomatic bones. Initially, the enlargements were soft and could be cut using a knife. Involvement of the palate reduces the nasal passage and may cause dyspnea. Palatine and mandibular thickening causes a reduction in the buccal cavity, impairing mastication. This causes teeth to loosen and get partially buried or exfoliate, and the softened bone causes pressure, further impairing prehension and mastication[1,5,9].

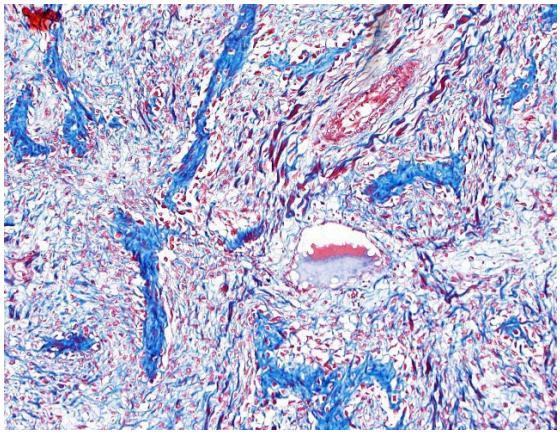

Figure 4-7. Maxilla, pig. A Masson's trichrome demonstrates the loosely arranged collagen in the intertrabecular spaces, and the collagen within trabeculae of woven bone. (HE, 100X)

The microscopic features of fibrous osteodystrophy are similar in all domestic animal species, and characterized by increased osteoclastic bone resorption, marked fibroplasia, and increased osteoblastic activity with the formation of immature woven bone. In early lesions, the increase in bone resorption is reflected by an increased number of active osteoclasts, often within Howship's lacunae along the surface of the trabeculae. Osteoblastic activity is also prominent, and it is not unusual to observe bone trabeculae resorption on one side, while new bone is being added to the other. Under physiological conditions, once osteoclasts have completed their required phase of resorption, they undergo apoptosis and disappear from the resorption sites. However, in fibrous osteodystrophy, groups of osteoclasts are fre-

quently found mixed with fibroblastic elements as PTH enhances osteoclast survival[1,5,9].

Contributing Institution:
Laboratório de Patologia Veterinária, Faculdade de Medicina Veterinária, Universidade Federal de Mato Grosso, Brazil.

JPC Diagnosis:
Jaw bone: Osteopenia, diffuse, severe, with marked fibroplasia (fibrous osteodystrophy).

JPC Comment:
The contributor provides an excellent review of the physiologic regulation of calcium and phosphorous and the pathologic manifestations of dysregulation of these minerals. Our scientific understanding of calcium and phosphorous metabolism began just over a century ago, but the descriptions of rickets date back millenia, with Roman physicians in the first and second century C.E. describing bowed legs and curved spines.[11] Beginning in the 17th century, there was a steady increase in the number of children afflicted by rickets (or English disease, as it was known at the time). In 1634, rickets was listed as the cause of death in 14 of 10,900 deaths in London, and extensive texts describing the clinical and gross features of rickets were published around 1650.[10,11] The association with lack of sunlight was first suspected by Polish physician Sniadecki in 1822, and in 1889, a map of cases in England revealed its association with industrialized cities, whose tall buildings and narrow streets blocked sunlight, and the seasonality of the affliction.[8,10] In the 20th century, it was estimated that up to 90% of the urban-dwelling children in Boston and Leiden suffered from rickets.[10,11]

In the early 20th century, our understanding of calcium and phosphorous metabolism began to grow. The first histopathologic description of rachitic bones was published by

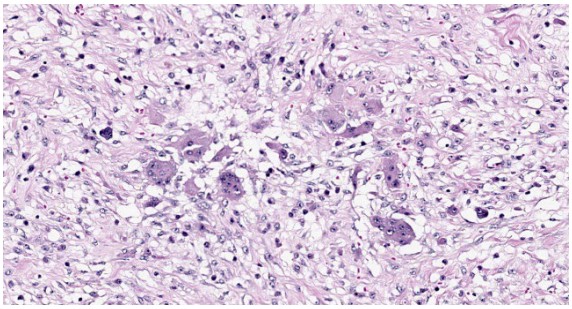

Figure 4-8. Maxilla, pig. Aggregates of osteoclasts are present in areas of previous mineralized bone resorption. (HE, 400X)

German physician and pathologist Christian Georg Schmorl in 1909, and in 1918, British biochemist Edward Mellanby successfully induced rickets in beagle puppies by feeding an oatmeal diet.[8,10] He further went on to cure the affliction by administering cod liver oil, a remedy used to prevent rickets in fishing villages.[8,10] Many suspected that the curative agent within cod liver oil was the fat soluble vitamin A. Elmer McCollum, who discovered vitamin B, hypothesized that a novel vitamin in cod liver oil possessed antirachitic properties; he proved this theory by demonstrating that cod liver oil still cured rickets even after aeration and heat destroyed the notoriously labile vitamin A.[8,10,11] Around the same time, it was demonstrated that UV light exposure prevented and treated rickets; and exposure of certain foods to the same UV radiation endowed that food with antirichitic properties.[8,10] Vitamin D2 and D3 were synthesized in the 1930s, and soon after, vitamin D supplementation of commercial foods and public awareness campaigns to increase sunlight exposure virtually eliminated rickets in industrialized nations.[8,10] It was not until 2004 that FGF23 was discovered, which filled in many of the gaps in our knowledge of phosphorous metabolism.[8]

References:

1. Bandarra PM, Pavarini SP, Santos As, et al. Nutritional fibrous osteodystrophy in

goats. Pesp Vet Bras. 2011;(31):10, 875-878.
2. Bergman PJ. Paraneoplastic hypercalcemia. Top Companion Anim Med. 2012;27(4):156-158.
3. Bonczynski J. Primary hyperparathyroidism in dogs and cats. Clin Tech Small Anim Pract. 2007;22(2):70-74.
4. Chacar FC, Kogika MM, Zafalon RVA, et al. Vitamin D Metabolism and Its Role in Mineral and Bone Disorders in Chronic Kidney Disease in Humans, Dogs and Cats. Metabolites. 2020;10(12):499.
5. Craig, LE, Dittmer, KE, Thompson, KG. Bones and joints. In: Maxie, MG, ed. Jubb, Kennedy, and Palmer's Pathology of Domestic Animals. 6th ed. St Louis, MO: Elsevier; 2016:16-163
6. Dittmer KE, Thompson KG. Vitamin D metabolism and rickets in domestic animals: a review. Vet Pathol. 2011;48(2):389-407.
7. Foster JD. Update on Mineral and Bone Disorders in Chronic Kidney Disease. Vet Clin North Am Small Anim Pract. 2016;46(6):1131-1149.
8. Gallagher JC, Rosen CJ. Vitamin D: 100 years of discoveries, yet controversy continues. Lancet Diabetes Endocrinol. 2023; 11(5): 362-374.
9. Hines ES, Stevenson VB, Patton ME, et al. Fibrous osteodystrophy in a dromedary camel. J Vet Diagn Invest. 2021;33(1):144-148.
10. Holick MF. The One-Hundred-Year Anniversary of the Discovery of the Sunshin Vitamin D3: Historical, Personal Experience, and Evidence-Based Perspectives. Nutrients. 2023; 15(3): 593.
11. Miller WL, Imel EA. Rickets, Vitamin D, and Ca/P Metabolism. Horm Res Paediatri. 2022; 95: 579-592.
12. Schwarz T, Störk CK, Megahy IW, et al. Osteodystrophia fibrosa in two guinea pigs. J Am Vet Med Assoc. 2001;219(1):63-66.
13. Tokarnia CH, Döbereiner J, Peixoto PV. Poisonous plants affecting livestock in Brazil. Toxicon. 2002;40(12):1635-1660.
14. Uhl EW. The pathology of vitamin D deficiency in domesticated animals: An evolutionary and comparative overview. Int J Paleopathol. 2018;23:100-109.

WSC 2022-2023 Self-assessment
Conference 24

1. Which of the following organs is most commonly affected in fetuses infected with *Ureaplasma* sp?
    a. Lung
    b. Liver
    c. Kidney
    d. Brain

2. Which of the following is the most common location for synovial myxoma in dog?
    a. Scapulohumeral joint
    b. Tibiotarsal joint
    c. Femorotibial joint
    d. Humeroradial joint

3. True or false? PTH increased the presence of ionized calcium in the blood and decreases serum phosphorus
    a. True
    b. False

4. True or false? Dogs and cats are unable to convert vitamin D in their skin.
    a. True
    b. False

5. Which of the following bones is a predilection site for the development of ossifying fibroma in young horses?
    a. Radius
    b. Metacarpal
    c. Mandible
    d. Basisphenoid

Please email your completed Assessment for grading to Dr. Bruce Williams at bruce.h.williams12.civ@mail.mil. Passing score is 80%. This program (RACE program 33611) is approved by the AAVSB RACE to offer a total of 0.5 CE Credits, with a maximum of 12.5 CE Credits being available to any individual Veterinary Medical Professionals for the 2019-2020 Wednesday Slide Conference. This RACE approval is for the subject matter categories of: SCIENTIFIC using the delivery method of NONINTERACTIVE DISTANCE. This approval is valid in jurisdictions which recognize AAVSB RACE.

Joint Pathology Center
Veterinary Pathology Services

WEDNESDAY SLIDE CONFERENCE 2022-2023

Conference #25 **10 May 2023**

CASE I:

Signalment:
A 2-year-old, male, mixed breed dog (*Canis familiaris*)

History:
This dog was presented to the clinic with one-week history of firm and multicentric swelling of the face and muzzle, acute vision loss, generalized lymphadenomegaly, fever, and asymmetric testicular swelling. The dog was neutered, and the testicles were submitted for histopathology with a presumptive diagnosis of neoplasia. After neutering, the dog was treated with steroids and doxycycline, facial swelling and lymphadenomegaly decreased after treatment. Once therapy was discontinued, facial swelling and lymphadenomegaly waxed and waned for approximately two months. Three months after neutering, the dog developed multiple nodules over the thigh region and stertorous respiration was noticed on physical exam. Skin nodules were submitted for histopathology (slides not included in this WSC submission).

Gross Pathology:
Both testicles (3.5 and 4.5 cm in greatest dimension) were received in 10% buffered formalin for histopathology. Diffusely and bilaterally, the epididymis was markedly enlarged by multiple, expansile, pale tan, firm masses. Similar masses expanded the testicular parenchyma, and elevated and effaced the visceral vaginal tunic. White bar = 1 cm.

Laboratory Results:

Clinical Pathology
Thrombocytopenia and leukopenia were documented. Cytologic examination of FNA material from the submandibular lymph nodes and swollen skin of the muzzle revealed histiocytic inflammation.

Serology
Serum samples were submitted to different laboratories to test for Rocky Mountain spotted fever, ehrlichiosis, brucellosis, Lyme disease, bartonellosis, and leishmaniasis. All serologic tests came back negative.

Microbiology
Fungal and aerobic bacterial cultures of fresh samples of skin (nodules from thigh region) and popliteal lymph node failed to detect microorganisms.

Microscopic Description:
Testicle: Broad, coalescing, areas of angiocentric and interstitial inflammation obliterate the testicular parenchyma and visceral vaginal tunica, and obscure and efface approximately 40% of the epididymal ducts. Inflammatory cells are composed of numerous epithelioid macrophages and lesser numbers of degenerate neutrophils, plasma cells, and lymphocytes. Macrophages are often arranged in concentric collections (granulomas) that, in some areas, encompass aggregates of degenerate neutrophils admixed with necrotic cellular debris (pyogranulomas). In addition, multiple macrophages contain a

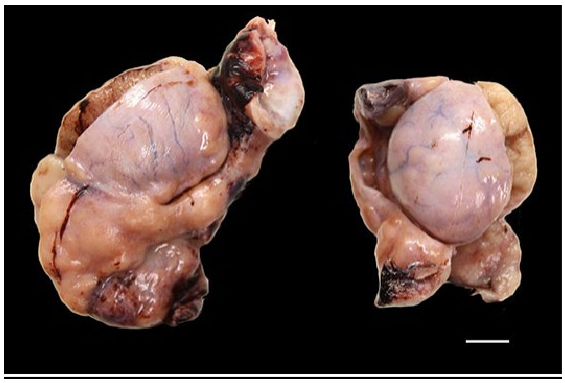

Figure 1-1. Testes, dog. The epididymis and to a lesser extent, the testis is expanded by numerous yellow-tan nodules. (Photo courtesy of: Wyoming State Diagnostic Laboratory www.uwyo.edu/wyovet/)

large, 4 to 7 µm, cytoplasmic, clear vacuole. Macrophages often display mitotic figures and cytological atypia, including pleomorphic nucleus and anisokaryosis. There are low numbers of binucleate and multinucleate cells among inflammatory leukocytes. A few areas of lytic necrosis are scattered among inflammatory foci. The lumen of seminiferous tubules and epididymal ducts lacks spermatids and spermatozoa.

The following special stains (not submitted) failed to highlight microorganisms in replicate and appropriately controlled sections: GMS, PAS, Brown & Hopps, Giemsa, Steiner's, acid fast, and Gimenez.

Haired skin (thigh nodules) and popliteal lymph node (not submitted): The dermis, subcutaneous tissue, and lymph node parenchyma were effaced by coalescing areas of inflammation with similar microscopic features as those described above in the testicles. Immunohistochemical staining for CD1a, CD4, and CD11c of frozen skin sections (thigh nodules) was performed. Dermal infiltrates of round cells were positive for CD11c and CD4. The immunoreactivity for CD1a was reported as ambiguous.

Contributor's Morphologic Diagnoses:
Testicle: Epididymitis and orchitis, angiocentric and interstitial, granulomatous, pyogranulomatous, and lymphoplasmacytic, severe, multifocal with histiocytic atypia and testicular atrophy

Haired skin (thigh nodule, not submitted): Dermatitis and panniculitis, angiocentric to interstitial, granulomatous, pyogranulomatous, and lymphoplasmacytic, moderate to severe, diffuse with histiocytic atypia

Popliteal lymph node (not submitted): Lymphadenitis, pyogranulomatous, severe, diffuse with histiocytic atypia

Contributor's Comment:
The dog in the present case had granulomatous and pyogranulomatous inflammation with histiocytic atypia in the skin, draining lymph nodes, and testes. Based on the immunohistochemical results from skin nodules and negative results from ancillary tests, the final diagnosis was systemic reactive histiocytosis. The initial presentation of this case was strongly suggestive of infectious disease and infection by either *Leishmania* sp or *Brucella* sp was suspected. Multiple infectious diseases were ruled out with a combination of

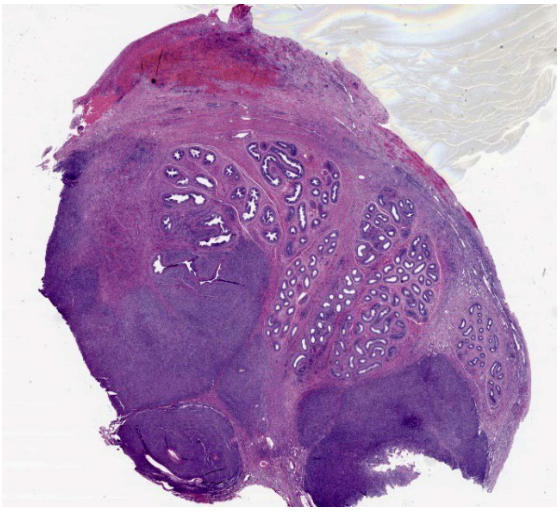

Figure 1-2. Epididymis, dog. There are nodular infiltrates effacing approximately 50% of epididymal tubules. (HE, 7X)

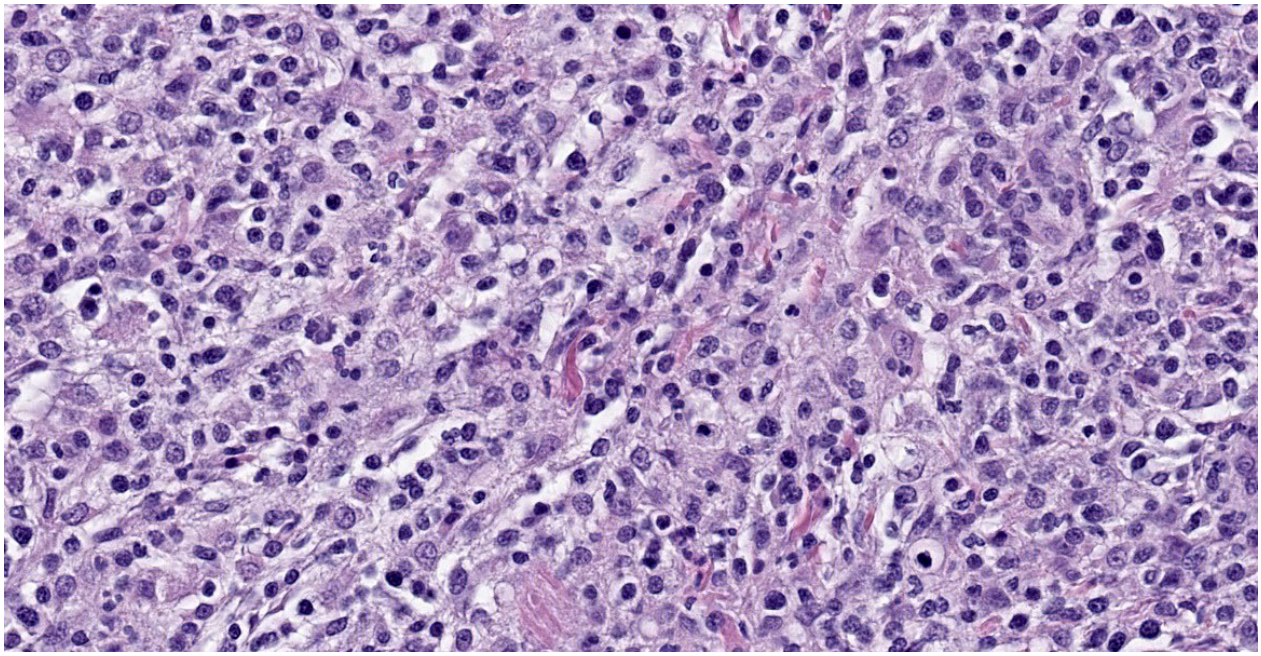

Figure 1-3. Epididymis, dog. The cellular infiltrate is composed of large numbers of macrophages with fewer lymphocytes and neutrophils. (HE, 450X)

special stains, bacteriology, and serology. No immunohistochemistry for dendritic cell markers was done on sections of testis (i.e., they were received in formalin), but immunohistochemistry of frozen haired skin samples was considered sufficient for the diagnosis of systemic reactive histiocytosis.

Reactive histiocytosis is a proliferative disorder of interstitial dendritic cells that has been well characterized in dogs,[3] and is uncommonly reported in other veterinary species.[1] In dogs, reactive histiocytosis has two clinical manifestations: cutaneous and systemic. While cutaneous reactive histiocytosis is confined to skin and draining lymph nodes, systemic reactive histiocytosis involves extracutaneous sites such as nasal and ocular mucosa, and internal organs. Involvement of the testicles, however, is less common than other extracutaneous sites. In the present case, intraocular and pulmonary involvement was suspected due to acute vision loss and stertorous respiration.[4] Systemic reactive histiocytosis was first described in the Bernese Mountain dog but has now been reported in multiple dog breeds. The diagnosis of reactive histiocytosis is based on immunohistochemistry for dendritic cell markers. Histiocytes in both cutaneous and systemic reactive histiocytoses express markers of dendritic cells (CD1a, CD11c/CD18, CD90, and MHC class II) and a marker of dendritic cell activation (CD4).[3] In addition, macrophages lack expression of E-cadherin. It is important to bear in mind that most of these markers are assessable in frozen tissue sections only (CD90, MHC class II, and E-cadherin are the exceptions).

After the diagnosis of systemic reactive histiocytosis was made, the dog of the present case has been on an anti-inflammatory dose of steroids and, according to the practitioner, the dog has shown great improvement.

Contributing Institution:
Wyoming State Diagnostic Laboratory
www.uwyo.edu/wyovet/

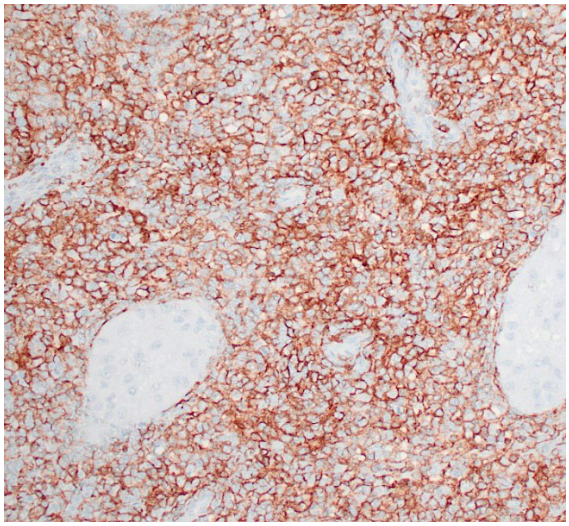

Figure 1-4. Epididymis, dog. The macrophages within the infiltrate stain strongly positive for IBA-1 (as you know, macrophages do.) (anti IBA-1, 400X)

JPC Diagnosis:
Epididymis: Epididymitis, lymphohistiocytic, chronic, multifocal to coalescing, moderate.

JPC Comment:
This case illustrates the challenge of diagnosing proliferative histiocytic diseases in dogs, which often require immunohistochemical staining for a definitive diagnosis.

Proliferative histiocytic diseases in dogs are typically of dendritic cell origin.[5] Dendritic cells arise from CD34+ precursors in the bone marrow and differentiate into *interstitial dendritic cells* or epidermal dendritic cells (*Langerhans cells*). Proliferative diseases of interstitial dendritic cells include cutaneous and systemic reactive histiocytoses and histiocytic sarcoma. The main proliferative diseases of canine Langerhans cells are cutaneous histiocytoma and cutaneous Langerhans cell histiocytosis.

Since these diseases all originate from dendritic cells (excepting the hemophagocytic form of histiocytic sarcoma), they express common dendritic cell markers: CD1a, CD11c, CD18, and MHCII.[3,5] Dendritic cells, which are professional antigen presenting cells, use CD1a and MHCII for antigen presentation for T cells. CD11c and CD18 are components of the beta-2 integrin heterodimer CD11c/18, one of the adhesion molecules expressed by leukocytes.[3]

A few additional immunohistochemical stains can assist in differentiating the diseases under the dendritic cell umbrella. Langerhans cells express E-cadherin, which they use to bind homotypically to the epithelium, so canine cutaneous histiocytoma and Langerhans cell histiocytosis are both expected to have E-cadherin immunoreactivity. Canine cutaneous and systemic reactive histiocytosis are diseases of activated interstitial dendritic cells and thus express CD4, a marker for activation. They also express CD90 (Thy-1), which is not expressed by Langerhans cells.[3]

In this section, the main histologic differentials are histiocytic sarcoma, histiocytic inflammation (i.e from dimorphic fungus), and systemic reactive histiocytosis. The relatively bland cellular population lacks atypia and bizarre nuclei, making histiocytic sarcoma less likely. Differentiating between primary inflammation and reactive histiocytosis is not possible based solely on this H&E section, so conference participants decided to morph

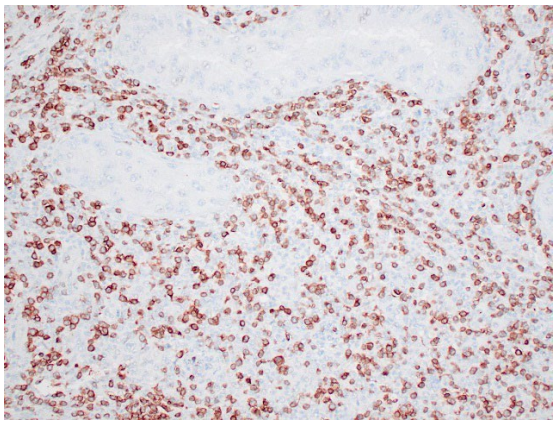

Figure 1-5. Epididymis, dog. Lymphocytes within the infiltrate stain strongly positive for CD3 within the (anti-CD3, 400X)

lymphohistiocytic epididymitis. The clinical history, CD4 immunoreactivity of cutaneous lesions noted by the contributor, and lack of infectious agents on special stains, microbiologic, and serologic testing, however, are consistent with the diagnosis of systemic reactive histiocytosis.

In the multifocal cutaneous lesions of reactive histiocytosis, another differential to consider is canine cutaneous Langerhans cell histiocytosis, which is histologically similar to a histiocytoma but multifocal in distribution. These can generally be differentiated on H&E sections by their growth patterns: they are "top heavy" lesions, with the base of the tumor smaller than the top and tend to track adnexal structures.[2] Reactive histiocytosis lesions are generally bottom-heavy, extend into the subcutis, and are oriented along vasculatures.[2]

This week's moderator, Dr. Rachel Neto from Auburn University, explained that even though Langerhans cells live within the epithelium, they are thought to arise from precursors within the dermis, and cellular proliferations in Langerhans cell histiocytosis and cutaneous histiocytoma occur in the superficial dermis. She also explained that Langerhans cells are dependent on epidermal growth factors, and the closer they are to the epidermis, the stronger their expression of E-cadherin.

References:

1. Helie P, Kiupel M, Drolet R: Congenital cutaneous histiocytosis in a piglet. *Vet Pathol.* 2014:51(4):812-815.
2. Mauldin EA, Peters-Kennedy J. Integumentary system. In: Maxie MG, ed. *Jubb, Kennedy, and Palmer's Pathology of Domestic Animals*. Vol 1. 6th ed. Philadelphia, PA: Elsevier Ltd. 2016:728-730.
3. Moore PF. A review of histiocytic diseases of dogs and cats. *Vet Pathol*. 2014;51:167-184.
4. Pumphrey SA, Pizzirani S, Pirie CG, Sato AF, Buckley FI: Reactive histiocytosis of the orbit and posterior segment in a dog. *Vet Ophthalmol*. 2013:16(3):229-233.
5. Valli VEO, Kiupel M, Bienzle D. Histiocytic proliferative diseases. In: Maxie MG, ed. *Jubb, Kennedy, and Palmer's Pathology of Domestic Animals.* Vol 3. 6th ed. Philadelphia, PA: Elsevier Ltd. 2016:247-250.

CASE II:

Signalment:
12-year-old neutered male European Shorthair cat (*Felis catus*)

History:
The cat had a clinical history of respiratory dyspnea and cough.

Gross Pathology:
The entire pulmonary lobe was submitted for histopathology.

Laboratory Results:
No laboratory findings reported.

Microscopic Description:
Lung. About 70% of the parenchyma is effaced by a multifocal to coalescing, severe proliferative process. Alveolar spaces are filled with numerous round cells of 25 micrometer in diameter, with distinct cell borders, high nuclear-to-cytoplasmic ratio, and small to moderate amounts of finely granular eosinophilic cytoplasm. Nuclei are round, central, with finely stippled chromatin and one or more visible nucleoli. Anisocytosis and anisokaryosis are mild and occasional mitoses with atypical features are present. Admixed to these cells, there are multifocal

aggregates of large alveolar macrophages with foamy cytoplasm, or scant cell debris and hypersegmented neutrophils. In about the 20% of the section and mainly the periphery of the lesions, the alveolar spaces are multifocally dilated and merged, with disrupted and blunted septae (emphysema). Lining the alveoli there are plump and cuboidal pneumocytes (type II pneumocyte hyperplasia). Smooth muscle fibers of terminal bronchioles are diffusely increased in size (hypertrophy). The interstitium is multifocally and markedly expanded by haphazardly arranged eosinophilic collagen fibers embedding fibrocytes (fibrosis), small caliber capillaries and rare macrophages containing coarsely granular brown-black pigment (anthracosis), and numerous lymphocytes; bronchial glands are increased in number (hyperplasia) and bronchial walls are collapsed multifocally. Blood vessels are multifocally engorged with erythrocytes (hyperemia) and the tunica media of medium and small arteries is moderately thickened by several layers of smooth muscle cells (arteriolar hypertrophy).

Immunohistochemistry (slides not submitted, pictures submitted as supporting material on DVD): vimentin+, Iba+, e-cadherin+, CK-.

Contributor's Morphologic Diagnosis:
Lung. Multifocal to coalescing, alveolar histiocytosis with emphysema and smooth muscle hyperplasia, with fibrosis and arteriolar hypertrophy.

ND. Feline Pulmonary Langerhans cell Histiocytosis

Contributor's Comment:
Feline pulmonary Langerhans cell histiocytosis (FPLCH) is a rare disease of older cats (>10 years) that causes progressive respiratory insufficiency that leads to death secondary to pulmonary parenchymal infiltration with Langerhans cells (LCs).[1,7,9,13] Clinical signs vary from acute respiratory distress, including tachypnea, labored breathing, and open mouth-breathing, to prolonged chronic pulmonary disease.[7,9,13] FPLCH is thought to represent a neoplastic process because of cellular morphological characteristics and extrapulmonary invasion, reported in pancreas and kidney[2,6], and the pulmonary one is the only form of Langerhans cells proliferation described in this species, with no cutaneous manifestation reported.[1]

Similar to the pulmonary lesions in canine LCH, histiocytic proliferations affect first the peribronchial parenchyma, causing multinodular-to- diffuse proliferations that vary from 2-5 mm in diameter and affect all lung lobes.[1] As the disease progresses, nodules coalesce, and lesions extend to the pleural surface. In advanced cases, the whole lungs tend to be affected, and all lobes appear diffusely firm.[13] However, there is a higher degree of cellular and nuclear pleomorphism. Aggregates of histiocytes are usually cohesive, and proliferating cells extend from the peribronchial parenchyma into the surrounding alveolar septa and alveoli, eventually effacing the pulmonary parenchyma.

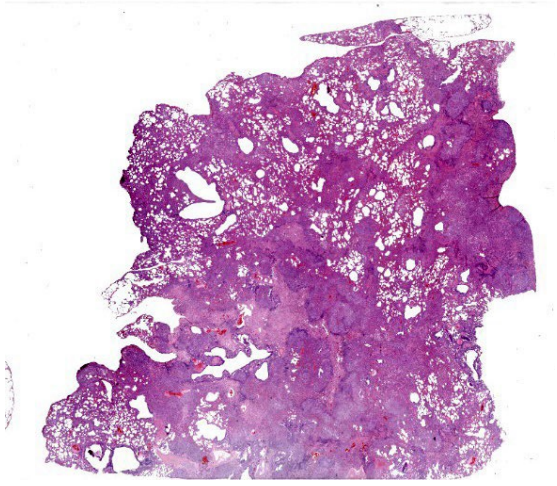

Figure 2-1. Lung, cat. A single section of consolidated lung is submitted. There are areas of emphysema and dilated airways. (HE, 7X)

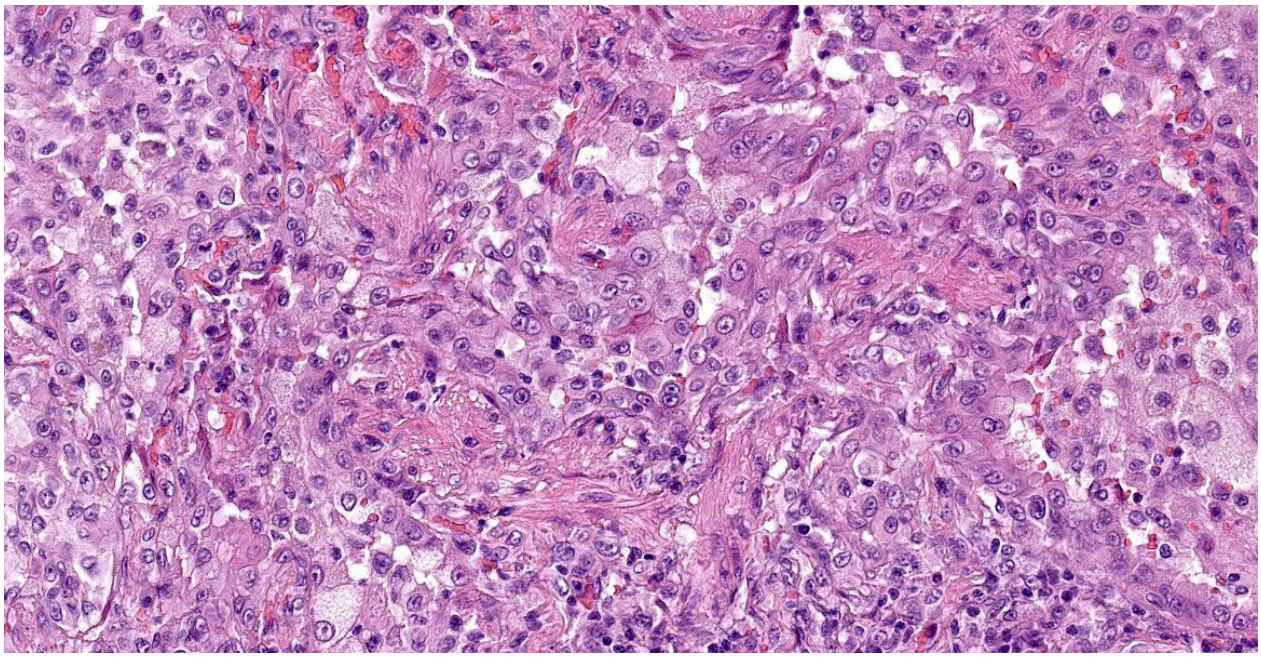

Figure 2-2. Lung, cat. Alveoli are filled with numerous histiocytes with prominent nuclei and nucleoli. There is marked smooth muscle hyperplasia. (HE, 381X)

Ultrastructurally, Birbeck granules, which represent the internalized cell surface receptor langerin (CD207) cross-linked by an antibody, have been reported in the cytoplasm of proliferating histiocytic cells, confirming a Langerhans cell origin. This is in contrast to canine Langerhans cells, which do not have Birbeck granules.[7,13]

Immunohistochemically, histiocytic cells of feline LCH are positive for CD18 and E-cadherin and negative for CD204 in formalin-fixed tissues.[9] In the current case, FPLCH was diagnosed on the basis of E-cadherin positive neoplastic cell, with variable pattern and intensity of immunolabeling among pulmonary lobes (see attached figures: 1, e-cadherin, 2 Iba1).

In a recent work by Hirabayashi et al., that accurately characterized histiocytic cell types of cats by immunohistochemistry and immunofluorescence, non-neoplastic histiocytes were mostly positive for Iba-1 and HLA-DR, while the immunoreactivity of other antibodies varied among histiocytes that resided in different organs. Dermal interstitial Dendritic Cells (iDCs) and macrophages were positive for CD204 and negative for E-cadherin. Epidermal LCs were negative for CD204 and positive for E-cadherin. However, antibodies for CD1a, langerin/CD207, and S100, which are regarded as specific markers of human LCs, were not available for detecting LCs on formalin-fixed, paraffin-embedded tissue sections of the cat, as well as those of the dog.[9,12] Double-labeling immunohistochemistry of the lymph nodes revealed E-cadherin-positive CD204-negative histiocytes and E-cadherin and CD204-double positive histiocytes in the sinus, which may be veiled cells and LC-like cells, respectively.[6] Neoplastic histiocytic cells were immunohistochemically positive for Iba-1 and HLA-DR in all cases of Feline Progressive Histiocytosis (FPH) and Histiocytic Sarcoma (HS). Immunoreactivity for CD204, CD163, and E- cadherin varied among cases. Of the HS cases, the neoplastic cells of more than half of cases presented with the iDC/macrophage immunophenotype (CD204+/E-cadherin-), while a minor number presented with the LC immunophenotype (CD204-/E-cad-

herin+), and with the LC-like cell immunophenotype (CD204+/E-cadherin+). Feline HS with the LC immunophenotype may correspond to Langerhans cells histiocytosis (LCH) or LC sarcoma (LCS) in humans.[1] Among FPH cases of the study, the neoplastic cells of the majority of cases presented with the iDC/macrophage immunophenotype (CD204+/E-cadherin-) and a minor part with the LC immunophenotype (CD204-/E-cadherin+). Moreover, the epitheliotropism of neoplastic cells was reported in some E-cadherin-positive cases. In a previously reported case of FPLCH, E-cadherin expression by ne oplastic cells was decreased in extrapulmonary metastatic lesions, while in one of the HS cases in the Hirabayashi study, the E-cadherin immunoreactivity of neoplastic cells varied in different organs.[2,6] These results suggest that the expression of E-cadherin by feline neoplastic histiocytes could be altered by their microenvironments.

PLCH in humans has been associated with tobacco smoke, especially in young adults.[1,3] Tobacco smoke supposedly causes damage to the bronchial epithelium, which prompts the release of peptides that stimulate alveolar macrophages to secrete cytokines that activate resident antigen-presenting LCs.[3] Genetic and other factors, such as prior treatment with chemo-therapeutic agents, may also be involved in the pathogenesis of PLCH.[1]

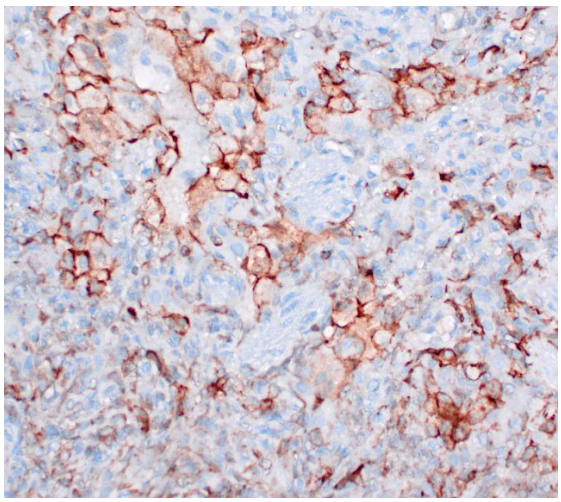

Figure 2-3. Lung, cat. Cells within alveoli demonstrate strong immunopositivity for IBA-1. (anti-IBA-1, 400X)

Contributing Institution:
San Marco Veterinary Clinic and Laboratory Pathology division
Viale dell'Industria 3, 35030
Veggiano (PD), Italy
https://www.clinicaveterinariasanmarco.it/

JPC Diagnosis:
Lung: Histiocytosis, alveolar, chronic, diffuse, severe, with fibrosis, type II pneumocyte hyperplasia, and smooth muscle hyperplasia.

JPC Comment:
This case of feline pulmonary Langerhans cell histiocytosis provided participants with an opportunity to review proliferative histiocytic disease in cats and complements the first case in this week's conference, a case of canine systemic reactive histiocytosis.

As in dogs, proliferative histiocytic disease of cats generally arises from dendritic cells – either interstitial dendritic cells or epidermal dendritic cells (Langerhans cells). Feline pulmonary Langerhans cell histiocytosis is the only proliferative disease of Langerhans cells in cats, as a feline equivalent canine cutaneous histiocytoma has not been documented. Proliferative diseases of interstitial dendritic cells include feline progressive histiocytosis and histiocytic sarcoma (except the hemophagocytic form, which likely arises from macrophages).

Feline progressive histiocytosis and histiocytic sarcoma can both affect the lung and are histologic differentials for this section. FPH occurs in older cats and starts as single to multiple raised, alopecic, nonpainful and

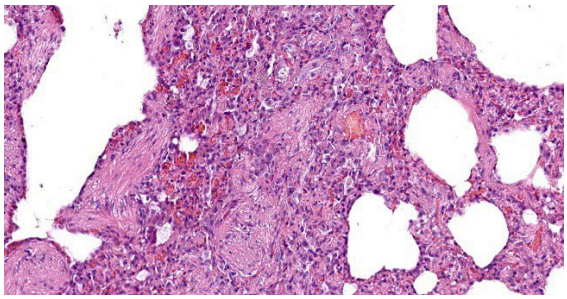

Figure 2-4. Lung, cat. There is marked airway smooth muscle hyperplasia. (HE, 460X)

nonpruritic nodules in the skin. The lesions do not regress, but wax and wane, and in advanced cases, can spread to internal organs, such as the lungs, liver, and spleen.[4,8,9] Histiocytic sarcoma can occur as a primary (localized) or metastatic (disseminated) neoplasm in the lung of cats, though it is less common in cats than in dogs.[9] Histiocytes of both FPH and histiocytic sarcoma are expected to be negative for E-cadherin, which is normally expressed by Langerhans cells, and allows these differentials to be ruled out in this case.[8,9]

Langerhans cells were first discovered by German physician Paul Langerhans (1847-1888) while working in Rudolf Virchow's laboratory at the Berlin Pathologic Institute. Langerhans was also the first to describe the pancreatic islets, now known as the islets of Langerhans, which he discovered nestled among pancreatic acini in the rabbit pancreas. Langerhans did not discover the function of these cells which bear his name; his academic career ended early after a pulmonary infection drove him to relocate to Portugal and return to medical practice. In this coastal location, he also developed a keen interest in marine biology, and several species of marine worms bear his name. Langerhans died when he was only 41 due to a severe kidney infection.[11]

References:

1. Argenta FF, de Britto FC, Pereira PR, Rissi DR, Gomes C, da Costa FVA, Pavarini SP. Pulmonary Langerhans cell histiocytosis in cats and a literature review of feline histiocytic diseases. *J Feline Med Surg*. 2020 Apr;22(4):305-312.
2. Busch MD, Reilly CM, Luff JA, Moore PF. Feline pulmonary Langerhans cell histiocytosis with multiorgan involvement. *Vet Pathol*. 2008 Nov;45(6):816-24.
3. Casolaro MA, Bernaudin JF, Saltini C, et al. Accumulation of Langerhans'cells on the epithelial surface of the lower respiratory tract in normal subjects in association with cigarette smoking. *Am Rev Respir Dis* 1988; 137: 406–411.
4. Caswell JL, Williams KJ. Respiratory System. In: Maxie MG, ed. *Jubb, Kennedy, and Palmer's Pathology of Domestic Animals*. Vol 1. 6th ed. Philadelphia, PA: Elsevier Ltd. 2016:498-499.
5. Coste M, Prata D, Castiglioni V, et al. Feline progressive histiocytosis: a retrospective investigation of 26 cases and preliminary study of Ki67 as a prognostic marker. *J Vet Diagn Invest*. 2019;31(6):801–808.
6. Hirabayashi M, Chambers JK, Sumi A, Harada K, Haritani M, Omachi T, Kobayashi T, Nakayama H, Uchida K. Immunophenotyping of Nonneoplastic and Neoplastic Histiocytes in Cats and Characterization of a Novel Cell Line Derived From Feline Progressive Histiocytosis. *Vet Pathol.* 2020 Nov;57(6):758-773.
7. Lopez A, Martinson SA. Respiratory system, mediastinum and pleurae. In: Zachary JF ed. *Pathologic Basis of Veterinary Disease,* 6th St. Louis, MO: Elsevier; 2017:554.
8. Mauldin EA, Peters-Kennedy J. Integumentary system. In: Maxie MG, ed. *Jubb, Kennedy, and Palmer's Pathology of Domestic Animals*. Vol 1. 6th ed. Philadelphia, PA: Elsevier Ltd. 2016:728-730.

9. Moore PF. A review of histiocytic diseases of dogs and cats. Vet Pathol. 2014 Jan;51(1):167-84.
10. Rissi DR, Brown CA, Gendron K, Good J, Lane S, Schmiedt CW. Pancreatic Langerhans cell histiocytosis in a cat. *J Vet Diagn Invest*. 2019 Nov;31(6):859-863.
11. Sakula A. Paul Langerhans (1847-1888): a centenary tribute. *J R Soc Med.* 1988; 81(7): 414-415.
12. Son NV, Uchida K, Thongtharb A, et al. Establishment of cell line and in vivo mouse model of canine Langerhans cell histiocytosis. *Vet Comp Oncol.* 2019; 17(3):345–353.
13. Valli VEO, Kiupel M, Bienzle D. Hematopoietic system. In: Maxie MG, ed. *Jubb, Kennedy, and Palmer's Pathology of Domestic Animals*. Vol 3. 6th ed. St. Louis, MO: Elsevier Limited; 2016:243.

CASE III:

Signalment:
11-month-old female spayed Golden Retriever (*Canis lupus familiaris*)

History:
Female, spayed, Golden Retriever presented with chronic anterior uveitis, possible vitritis, possible iris mass, and secondary glaucoma in the right eye. The right eye is blind; thus, removal with histopathology of the right eye was elected.

Gross Pathology:
Uveitis with secondary glaucoma

Laboratory Results:
No laboratory findings reported.

Microscopic Description:
Right eye: Within the cornea, there is a small number of small-caliber vessels originating from the limbus and coursing through the peripheral stroma (neovascularization). The anterior chamber contains a large amount of hemorrhage (hyphema) admixed with eosinophilic homogeneous to polymerized material (proteinaceous fluid) and small numbers of polymorphonuclear cells. The iris, iridiocorneal angle, and ciliary body are markedly expanded and almost completely effaced by an unencapsulated, poorly demarcated, infiltrative, densely cellular mass. The mass is composed of pleomorphic neoplastic spindle to oval cells arranged in extensive sheets supported by a moderate amount of fibrous to collagenous matrix. Multifocally, the neoplastic cells are separated and lined upon, small, thin trabecula composed of deeply eosinophilic granular to glassy extracellular material (osteoid) that is variably mineralized. Multifocally, neoplastic cells are present in lacuna and are embedded within a basophilic matrix (cartilage matrix). Neoplastic cells have a moderate amount of cytoplasm, variably discernible cell boundaries, a large oval nucleus with stippled chromatin, and 1-4 prominent nucleoli. Neoplastic cells

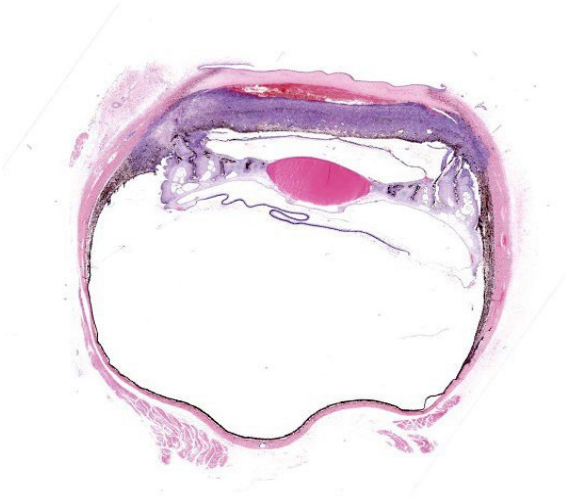

Figure 3-1. Globe, dog. A neoplasm infiltrates and expands the iris, ciliary body, anterior uvea, sclera, and bilaterally effaces the filtration angle. There is hemorrhage within the anterior segment. (HE, 6X)

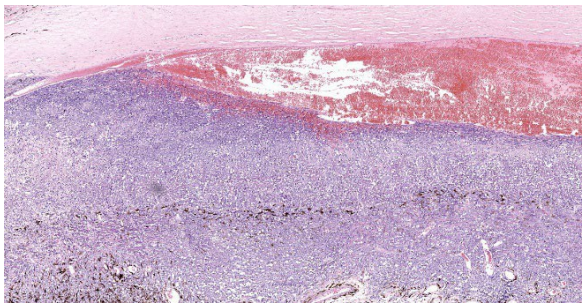

Figure 3-2. Globe, dog. The neoplasm is composed of short, haphazardly arranged bundles of plump spindle cells. The cornea is at top. There is hemorrhage between the cornea and the neoplasm. (HE, 37X)

demonstrate marked anisocytosis, anisokaryosis, and have a high mitotic index (20 per ten 0.237mm^2 fields). 50-60% of the mass is lack differential staining (coagulative necrosis) or a complete loss of cellular architecture with replacement by eosinophilic karyorrhectic and cytolytic cellular debris (lytic necrosis). The iris is multifocally adhered to the anterior lens capsule (posterior synechia). The iridocorneal angle is collapsed and effaced by neoplastic cells. The ciliary body is mostly effaced by neoplastic cells and neoplastic cells are observed extending up the zonules of Zinn to the lens capsule. There is a distinct layer of fibrous connective tissue extending from the surface of the ciliary body over the posterior lens capsule (cyclitic membrane). The non-tapetal retina is diffusely thin with marked hypocellularity of all layers, especially the ganglion and inner nuclear layers (retinal degeneration). The tapetal retina is somewhat spared, but there is hypocellularity of the ganglion and inner nuclear layer (ganglion cell layer degeneration). There are aggregates or emboli of neoplastic cells and necrotic cell debris within the scleral veins (vascular invasion).

Contributor's Morphologic Diagnosis:
Right eye: Osteoblastic osteosarcoma, anterior uvea, with neovascularization, hyphema, cyclitic membrane, secondary glaucoma, and retinal degeneration, Golden Retriever, *Canis lupus familiaris*, canine

Contributor's Comment:
Osteosarcoma is the most common tumor of the appendicular skeleton in dogs and cats.[10] They are locally invasive and readily metastasize to the regional nodes and elsewhere, especially lungs. Extraskeletal osteosarcomas are less common and occur in soft tissue and visceral organs, without any primary bone involvement.[9] Organs commonly affected are the adrenal gland, kidney, mesentery, ileum, liver, spleen, reproductive organs, and the eye.[8] Osteosarcoma in the eye, as a primary process, occurs with even more rarity in dogs and cats.[1,5] This ocular tumor has been reported most in large breed dogs between the age of 9 – 11.5 years.[5] Common clinical signs include exophthalmos[5], hyphema, and blepharospasm.[11]

Histologically, extraskeletal osteosarcomas appear similar to other skeletal osteosarcoma.[7] Within the eye, the tumors are observed in the iris and ciliary body. Tumors are composed of pleomorphic spindle cells or stellate cells, with occasional multinucleated cells resembling osteoclasts, in an abundant extracellular collagenous matrix (osteoid).[5,11] Anaplastic osteoblasts are characteristic of osteoblastic osteosarcoma[2], such as in this case. Other nuclear characteristics include hyperchromic, often eccentric nuclei with varying amounts of basophilic cytoplasm.[3]

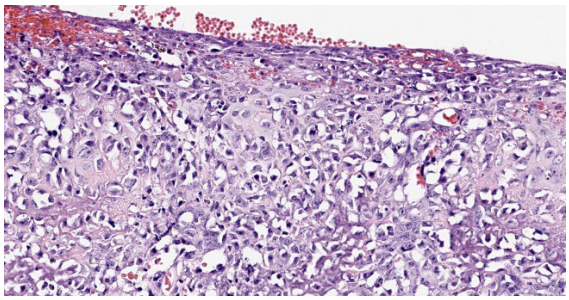

Figure 3-3. Globe, dog. Neoplastic cells are separated and surrounded by pink osteoid matrix. (HE, 318X)

Osteoblastic osteosarcomas are further characterized into 'productive' or 'non-productive' osteosarcoma to indicate the amount of bone production: minimal, lacy strands, irregular islands, and larger accumulation.[3] In dogs, the most common subcategory of skeletal osteosarcoma is moderately productive osteoblastic osteosarcoma.[3] Only one small scale study noted osteoblastic osteosarcoma as being the most frequent type of extraskeletal osteosarcoma in the dog, but was not further subcategorized.[8]

Similar to humans, extraskeletal osteosarcomas are highly malignant, and metastasis is common. However, this occurs less often to the lungs when compared to skeletal osteosarcomas.[9] Decreased survival times result from late detection of tumors and restricted surgical resection of tumors from some sites.[9]

In comparison, ocular osteosarcomas in cats can arise after trauma to the eye.[12] Feline post-traumatic osteosarcoma can occur several months to several years after penetrating injury to the eye. The tumor starts at the lens and progresses towards lining the interior of the eye. It then extends to the scleral venous plexus or optic nerve[10], to diffusely affect the globe.[4,11] The lining of the eye by the tumor is a key feature in differentiating metastatic osteosarcoma vs. primary ocular osteosarcomas. Metastatic rates in these feline cases have occasionally been documented to be 60% with metastasis reaching the brain even post enucleation.[12]

Contributing Institution:
Department of Veterinary Pathology
College of Veterinary Medicine
Iowa State University
Ames, Iowa 50010-1250
https://vetmed.iastate.edu/vpath

JPC Diagnosis:
Eye, anterior uvea and sclera: Osteosarcoma.

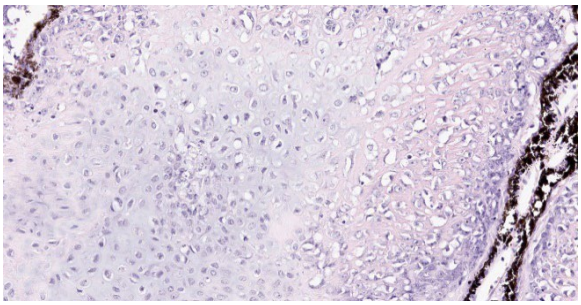

Figure 3-4. Globe, dog. In some areas of the neoplasm, neoplastic cells are entrapped by cartilaginous matrix (HE, 256X)

JPC Comment:
As the contributor mentions, primary intraocular osteosarcoma is rare in veterinary species and has been reported in dogs, cats, a cockatoo, and most recently, a rabbit. Makishima et al. described a primary intraocular osteosarcoma in an 8-year-old lop-eared rabbit. The animal had a history of cataracts, glaucoma, and posterior lens luxation in the left globe several years prior to the development of osteosarcoma. The neoplasm created significant exophthlamos and effaced almost the entire globe, extended beyond the sclera in the retrobulbar space, but did not invade the optic nerve or surrounding tissues. There was no evidence of metastasis, and the animal died due to respiratory failure caused by pulmonary neuroendocrine tumors.[8]

Primary appendicular osteosarcoma can be difficult to differentiate histologically from other primary bone tumors, including chondrosarcoma and fibrosarcoma. One key histologic feature considered diagnostic for osteosarcoma is the presence of osteoblasts producing osteoid. In equivocal cases, immunohistochemistry may be required to differentiate these bone tumors, and a recent study evaluated several markers with varying historical utility in osteosarcoma: alkaline phosphatase (ALP), runx2, osteonectin (ON), and osteopontin (OP). All four markers were found to be very sensitive for osteosarcoma, but specificity varied. The study authors

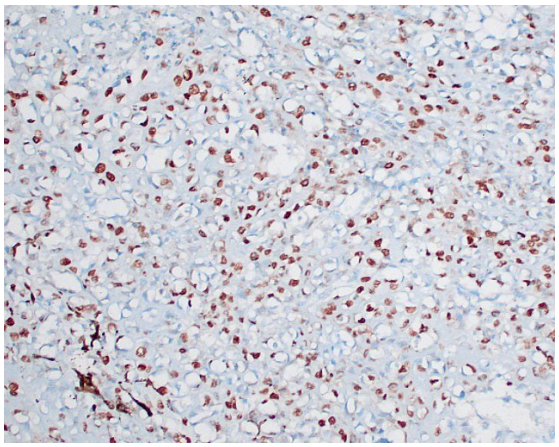

Figure 3-5. Globe, dog. Neoplastic cells, embedded in matrix, demonstrate immunopositivity for SABT2 (anti-SATB2, 400X)

found that ALP, which has the highest sensitivity but low specificity, is best used as an initial screening test, and runx2, an osteoblast transcription factor with highest specificity of the four markers, should be run on ALP-positive sections. Combining these two tests in parallel provided 87% sensitivity and 85% specificity in canine appendicular osteosarcomas.[2]

The moderator discussed how the presence of neoplastic cells within the scleral vessels adjacent to the trabecular meshwork is likely due to passive drainage and not necessarily indicative of primary vascular invasion. Additionally, differentiation between primary and metastatic neoplasia in this case cannot be done histologically and requires correlation with clinical findings. Historically, the lung has been the most common site for osteosarcoma metastasis, but the moderator also discussed that, anecdotally, oncologists are seeing an increased number of osteosarcoma metastasis to atypical sites. This may be due to prolonged survival times with advances in tumor treatment.

References:

1. Attali-Soussay K, Jegou JP, Clerc B. Retrobulbar tumors in dogs and cats: 25 cases. *Vet Ophthalmol*. 2001;4**:** 19-27.
2. Barger A, Baker K, Driskell E, et al. The use of alkaline phosphatase and runx2 to distinguish osteosarcoma from other common malignatn bone tumors in dogs. *Vet Pathol.* 2022. 59(3): 427-432.
3. Craig LE, Dittmer KE, Thompson KG. Bones and Joints: Tumors and Tumor-Like Lesions of bones. In: Jubb K, Kennedy P, Palmer N, eds. *Pathology of Domestic Animals*. 6th ed. St. Louis, Missouri: Elsevier; 2016:110-116.
4. Dubielzig RR, Ketring K, McLellan GJ, Albert DM. Non-surgical trauma. In: Dubielzig RR, Ketring K, McLellan GJ, Albert DM, eds. *Veterinary Ocular Pathology*. Edinburgh: W.B. Saunders; 2010:103,111.
5. Heath S, Rankin AJ, Dubielzig RR. Primary ocular osteosarcoma in a dog. *Vet Ophthalmol*. 2003;6**:** 85-87.
6. Hendrix DV, Gelatt KN. Diagnosis, treatment and outcome of orbital neoplasia in dogs: a retrospective study of 44 cases. *J Small Anim Pract*. 2000;41**:** 105-108.
7. Labelle AL, Labelle P. Canine ocular neoplasia: a review. *Veterinary Ophthalmology*. 2013;16**:** 3-14.
8. Makishima R, Kondo H, Naruke A, Shibuya H. Intraocular extraskeletal osteosarcoma in a rabbit (*Oryctolagus cuniculus*). *J Vet Med Sci.* 2020; 82(8): 1151-1154.
9. Patnaik AK. Canine extraskeletal osteosarcoma and chondrosarcoma: a clinicopathologic study of 14 cases. *Veterinary pathology*. 1990;27**:** 46-55.
10. Thompson KG, Dittmer KE. Tumors of Bone. In: Meuten DJ, ed. *Tumors in Domestic Animals*. 5th ed. Ames,

IA: John Wiley & Sons, Inc.; 2017:329.
11. van de Sandt RROM, Boevé MH, Stades FC, Kik MJL, Kirpensteijn J. Intraocular osteosarcoma in a dog. *Journal of Small Animal Practice*. 2004;45**:** 372-374.
12. Wilcock BP, Njaa BL. Special Senses. In: *Jubb K*, K*ennedy P*, P*almer N*, eds. *Pathology of Domestic Animals*. 6th ed. St. Louis, Missouri: Elsevier; 2016.

CASE IV:

Signalment:
4.8-years-old, female, Limousin, (*Bos taurus*) bovine.

History:
Presented to the Institute of Veterinary Pathology with a history of thickened skin, hypotrichia, alopecia and signs of lameness.

Gross Pathology:
The skin displayed generalized thickening with folding and wrinkling. The peripheral lymph nodes were enlarged. Multiple white miliary foci were disseminated in the respiratory and vaginal mucosa, fasciae and scleral conjunctivae. The claws revealed rotation of the distal phalanges.

Laboratory Results:
No laboratory findings reported.

Microscopic Description:
Eye (anterior part): Multifocal expansion and bulging of the conjunctiva, iris and sclera by many interstitial mature protozoal cysts. The multi-layered protozoal tissue cysts are 150-350 µm in diameter with an outermost 15-30 µm pale eosinophilic, hyaline capsule. Next is a greenish intermediate layer (5 µm, not in all cysts), followed by a 5-15 µm rim of host cell cytoplasm containing 2-5 giant but flattened nuclei. The majority of the cyst is composed of the central parasitophorous vacuole containing numerous, tightly packed, crescent-shaped, 2x7 µm bradyzoites. Occasionally, a thin concentric layer of spindle-shaped cells with flattened nuclei (fibrocytes) and eosinophilic fibers (mature collagen) surrounds cysts. Some cysts are concentrically surrounded by small to moderate numbers of macrophages, multi-nucleated giant cells, lymphocytes and fewer plasma cells and eosinophils. Occasionally, cysts are directly beneath and bulging iridal anterior and posterior pigment layers and corneal endothelium (not on all slides).

Contributor's Morphologic Diagnosis:
Eye: Conjunctivitis and iritis, multifocal, granulomatous, mild, chronic with intralesional protozoal cysts.

Cause: *Besnoitia besnoiti*

Etiologic diagnosis: Protozoal conjunctivitis

Contributor's Comment:
Bovine besnoitiosis is a chronic debilitating disease of cattle, caused by the cyst-forming

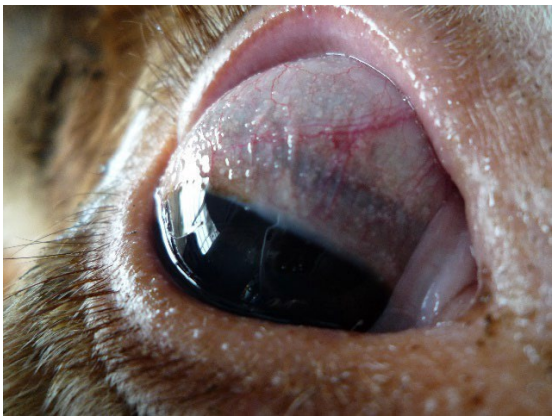

Figure 4-1. Globe, ox. Numerous Besnoitia cysts ae present within the sclera of the globe. (Photo courtesy of: Institute of Veterinary Pathology, Faculty of Veterinary Medicine, LMU Munich, Veterinaerstr. 13, 80539 Muenchen, http://www.patho.vetmed.uni-muenchen.de/index.html)

Figure 4-2. Globe, ox. Multiple sections of the anterior segment of the globe are submitted for examination. (HE, 3X)

apicomplexan parasite *Besnoitia besnoiti*. The disease is re-emerging in Europe and showed rapid spread to Germany, Italy, Switzerland, Hungary, Belgium, and Ireland within eight years.[11] The genus *Besnoitia* has 10 species (Table 4.1).[6] *B. besnoiti*, the type species mainly affects cattle, and wild ungulates may represent a natural reservoir of infection.[10] The life cycle of bovine besnoitiosis is incompletely understood. Cattle represent intermediate hosts, where cyst-formation takes place but the definitive hosts, where intestinal sexual reproduction is thought to occur are unknown. In analogy to the four species with complete knowledge of life cycle (*B. darling, B. neotomofelis, B. oryctofelisi, B. wallacei*) a heteroxenous life cycle is assumed.

In cattle, acute besnoitiosis is characterized by fast proliferation of tachyzoites in endothelial cells and cells of macrophage lineage. Clinical signs include pyrexia, anorexia, nasal and ocular discharge, peripheral lymphadenopathy, lameness and subcutaneous edema. Histological alterations in this stage consist of microcirculatory and vascular lesions like vasculitis, thrombosis, hemorrhage, and edema. Tachyzoites are few in naturally acquired bovine besnoitiosis and are difficult to identify in FFPE-tissues.[1,10]

In the chronic stage, pathognomonic parasitic cysts develop in various tissues. Preferentially affected are non-intestinal mucosa, scleral conjunctiva, skin and fasciae. For unknown reasons and in contrast to peripheral tissues, visceral organs harbor markedly reduced parasite load. Severe chronic bovine besnoitiosis leads to thickening and wrinkling of the skin, sole ulcers and – in bulls – orchitis and sterility.[3,6,13,14] Cysts consist of a central, cytoplasmic, single-membraned parasitophorous vacuole harboring numerous slow-replicating bradyzoites. The host cell cytoplasm surrounding the parasitophorous vacuole is usually thin and contains several enlarged, but flattened hots cell nuclei. The next layer (intermediate layer, inner cyst wall) is not present in every mature cyst but is readily visible in developing cysts. The outermost layer of the cyst is a pale-eosinophilic, hyaline layer, consisting of interwoven collagen fibrils.13 The host cell of B. besnoiti is immunohistochemically positive for vimentin and smooth muscle actin suggesting myofibroblast origin.5 Usually, at

Table 4.1

Species	Target organs	Intermediate host	Definitive host
B. akodoni	Internal organs	Grass mouse	Unknown
B. bennetti	Non-intestinal mucosa, skin, SC	Donkey, burro, horse, mule	Unknown
B. besnoitii	Non-intestinal mucosa, skin, SC	Cattle, wild ungulates, antelopes	Unknown
B. caprae	Non-intestinal mucosa, skin, SC	Goat, sheep	Unknown
B. darlingi	Ear, internal organs, SC	Virginia opossum, (lizard)	Cat, bobcat
B. jellisoni	Internal organs	Deer mouse	Unknown
B. neotomofelis	Internal organs	Woodrat	Cat
B. oryctofelisi	Internal organs, muscle	Rabbit	Cat
B. tarandi	Non-intestinal mucosa, skin, SC	Caribou, reindeer, mule deer, muskox	Unknown
B. wallacei	Internal organs	Rat	Cat

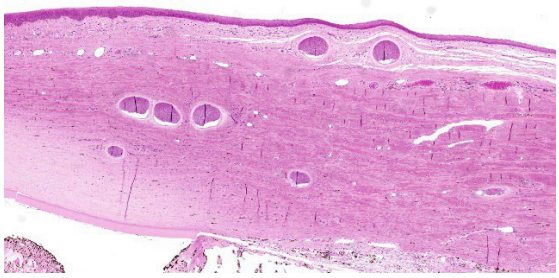

Figure 4-3. Sclera, ox. Cysts of Besnoitia benoitii are present within the sclera. (HE, 47X)

least some cysts are surrounded by pericystic inflammation, which mainly consists of T-cells, macrophages, multinucleated giant cells and eosinophils. Destruction of cysts is evident in subacute and chronic cases.[14]

In animals with obvious lesions, the diagnosis is made via clinical findings and histology. Because most of the chronic cases are mildly clinical or subclinical, diagnosis of bovine besnoitiosis on the herd level requires serology and/or PCR.[7,18,19] Epidemiology of bovine besnoitiosis is incompletely understood. Animals are infected via direct contact, biting arthropods or mechanical vectors. Transmission occurs mainly in the summer months when insect activity is high. In endemically infected herds, there is variable seasonal serological and clinical incidence and prevalence.[9,10]

Contributing Institution:
Institute of Veterinary Pathology
Faculty of Veterinary Medicine
LMU Munich
Veterinaerstr. 13
80539 Muenchen
http://www.patho.vetmed.uni-muenchen.de/index.html

JPC Diagnosis:
Eye, conjunctiva, sclera, and iris: Multiple apicomplexan cysts.

JPC Comment:

This represents a classic case of ocular *Besnoitia* in a cow, and this protozoan produces characteristic cysts which can reach up to 5 mm in diameter and are visible on gross examination. Protozoal cysts appear as small white nodules on the haired skin of the face, ears, scrotum, and conjunctiva, where they are called scleral pearls.[2] Other classic signs of chronic *B. besnoitii* infection include alopecia, thickening, and wrinkling of the periocular skin, the scrotum, and other areas of the body due to scleroderma.[17] Gross differentials for the skin lesions include dermatophytosis and photosensitization, both of which can cause blepharitis, and *Moraxella bovis* and *Listeria monocytogenes*, both of which are important causes of conjunctivitis in cattle. None of these differentials would have pearlescent nodules.[3]

The acute phase of *Besnoitia* infection has less specific clinical signs (i.e. fever), lasts less than a month, and often goes undetected. The underlying lesion is vasculitis and thrombosis of small caliber vessels, which some authors have speculated is due to replication of tachyzoites within endothelial cells.[17] The acute phase may result in death due to nephrotic syndrome or respiratory distress.[17] A recent review article found that bulls are likely more susceptible than females to infection, and in the acute phase they can develop significant orchitis and infertility.[17]

This review article also found that infection of animals less than 6 months of age is rare,

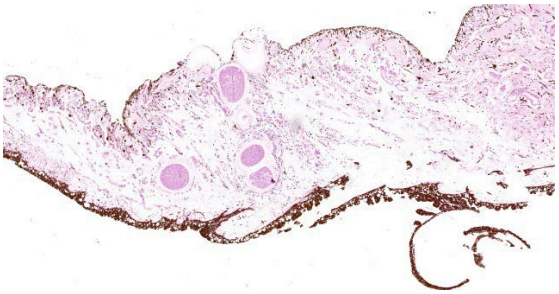

Figure 4-4. Iris, ox. Cysts of Besnoitia benoitii are present within the iris. (HE, 59X)

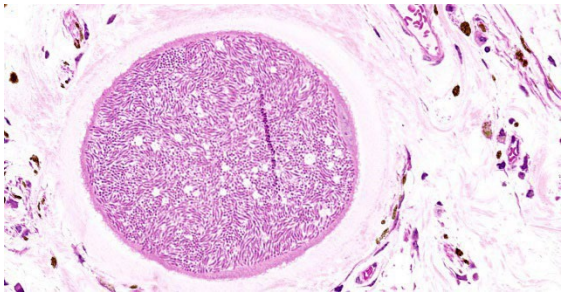

Figure 4-5. Iris, ox. High magnification of Besnoitia cysts demonstrating the thick hyaline wall and numerous enclosed bradyzoites. (HE, 562X)

and that the incidence of infection increased with advancing age.[17]

Besnoitia is an economically important disease in many areas of the world. Most cases are subclinical or have scleral cysts as the only clinical sign. When infection is introduced into a naïve herd, it is expected that 10% to 50% of animals will develop clinical signs and lose economic value within the next three years.[17] In endemically infected herds, the proportion of animals showing clinical signs is expected to increase with time.[17] A recently developed modified live vaccine controls clinical signs but does not appear to be effective in preventing subclinical infection.[17]

Some of the conference participants described the vacuolation of the corneal endothelium in this section as a pathologic change; the moderator, who has a special interest in ocular pathology, explained that this is a normal and expected finding. Unless coupled with attenuation or other corroborating evidence, it should not be considered abnormal.

The moderator discussed other protozoa which can be found in the eye, including *Trypanosoma, Toxoplasma, Leishmania* (25% of systemic cases involve the eye)*, and Neospora caninum; Encephalitozoon cuniculi* can also cause phaecoclastic uveitis in rabbits.

References:

1. Basson PA, McCully RM, Bigalke RD. Observations on the pathogenesis of bovine and antelope strains of *Besnoitia besnoiti* (Marotel, 1912) infection in cattle and rabbits. *Onderstepoort J Vet Res.* 1970;37(2): 105-126.
2. Bowman DD. Protists. In: *Georgis' Parasitology for Veterinarians.* St. Louis, MO: Elsevier. 2021; 116.
3. Buergelt CD, Clark EG, Del Piero F. *Bovine Pathology.* Boston, MA: CABI. 2017: 371-372.
4. Cortes H, Leitao A, Vidal R, et al. Besnoitiosis in bulls in Portugal. *Vet Rec.* 2005;157(9): 262-264.
5. Dubey JP, Wilpe E, Blignaut DJC, Schares G, Williams JH. Development of early tissue cysts and associated pathology of *Besnoitia besnoiti* in a naturally infected bull (*Bos taurus*) from South Africa. *J Parasitol.* 2013;99(3): 459-466.
6. Dubey JP, Yabsley MJ. *Besnoitia neotomofelis* n. sp. (Protozoa: Apicomplexa) from the southern plains woodrat (*Neotoma micropus*). *Parasitology.* 2010;137(12): 1731-1747.
7. García-Lunar P, Ortega-Mora LM, Schares G, Diezma-Díaz C, Álvarez-García G. A new lyophilized tachyzoite based ELISA to diagnose *Besnoitia* spp. infection in bovids and wild ruminants improves specificity. *Vet Parasitol.* 2017;244: 176-182.
8. Gollnick NS, Scharr JC, Schares G, Langenmayer MC. Natural *Besnoitia besnoiti* infections in cattle: chronology of disease progression. *BMC Vet Res.* 2015;11: 35.
9. Gollnick NS, Scharr JC, Schares S, Barwald A, Schares G, Langenmayer MC. Naturally acquired bovine besnoitiosis: Disease frequency, risk and outcome in an endemically infected beef herd. *Transbound Emerg Dis.* 2018.

10. Gutierrez-Exposito D, Arnal MC, Martinez-Duran D, et al. The role of wild ruminants as reservoirs of Besnoitia besnoiti infection in cattle. *Vet Parasitol.* 2016;223: 7-13.
11. Gutiérrez-Expósito D, Ferre I, Ortega-Mora LM, Álvarez-García G. Advances in the diagnosis of bovine besnoitiosis: current options and applications for control. *Int J Parasitol.* 2017;47(12): 737-751.
12. Gutiérrez-Expósito D, Ortega-Mora LM, García-Lunar P, et al. Clinical and serological dynamics of *Besnoitia besnoiti* infection in three endemically infected beef cattle herds. *Transbound Emerg Dis.* 2017;64(2): 538-546.
13. Kumi-Diaka J, Wilson S, Sanusi A, Njoku CE, Osori DI. Bovine besnoitiosis and its effect on the male reproductive system. *Theriogenology.* 1981;16(5): 523-530.
14. Langenmayer MC, Gollnick NS, Majzoub-Altweck M, Scharr JC, Schares G, Hermanns W. Naturally acquired bovine besnoitiosis: histological and immunohistochemical findings in acute, subacute, and chronic disease. *Vet Pathol.* 2015;52(3): 476-488.
15. Langenmayer MC, Gollnick NS, Scharr JC, et al. *Besnoitia besnoiti* infection in cattle and mice: ultrastructural pathology in acute and chronic besnoitiosis. *Parasitol Res.* 2015;114(3): 955-963.
16. Lucio-Forster A, Lejeune M. Diagnostic Parasitology. In: Bowman DD, ed. *Georgis' Parasitology for Veterinarians.* St. Louis, MO: Elsevier. 2021: 443.
17. Malatji PM, Tembe D, Mukaratirwa S. An update on epidemiology and clinical aspects of besnoitiosis in livestock and wildlife in sub-Saharan Africa: A systematic review. *Parasite Epidemiol Control*. 2023; 21:e00284.
18. Schares G, Langenmayer MC, Scharr JC, et al. Novel tools for the diagnosis and differentiation of acute and chronic bovine besnoitiosis. *Int J Parasitol.* 2013;43(2): 143-154.
19. Schares G, Maksimov A, Basso W, et al. Quantitative real time polymerase chain reaction assays for the sensitive detection of *Besnoitia besnoiti* infection in cattle. *Vet Parasitol.* 2011;178(3-4): 208-216.

WSC 2022-2023 Self-assessment
Conference 25

1. Systemic histiocytosis was first identified in which of the following breeds?
    a. German Shorthaired pointer
    b. Bernese Mountain dog
    c. Jack Russell terrier
    d. Pomeranian

2. True or false. Langerin is found in canine Birbeck granules?
    a. True
    b. False

3. True or false? Pulmonary Langerhans cell in humans is associated with alcohol dependency.
    a. True
    b. False

4. True or false? Extraskeletal osteosarcomas have a higher rate of pulmonary metastasis than skeletal osteosarcomas.
    a. True
    b. False

5. The host cell of the *Besnoitia* cysts in chronic infection is most likely?
    a. Myofibroblast
    b. Endotheliuml
    c. Macrophage
    d. Sensory neuron

Please email your completed Asessment for grading to Dr. Bruce Williams at bruce.h.williams12.civ@mail.mil. Passing score is 80%. This program (RACE program 33611) is approved by the AAVSB RACE to offer a total of 0.5 CE Credits, with a maximum of 12.5 CE Credits being available to any individual Veterinary Medical Professionals for the 2019-2020 Wednesday Slide Conference. This RACE approval is for the subject matter categories of: SCIENTIFIC using the delivery method of NONINTERACTIVE DISTANCE. This approval is valid in jurisdictions which recognize AAVSB RACE.